



International Conferences on
Wind Turbine Noise

11th Edition of the

International Conferences on
Wind Turbine Noise

Copenhagen, Denmark – 10th to 13th June 2025

**CONFERENCE
PROCEEDINGS**

International Conferences on Wind Turbine Noise

WTN2025
11th edition of the International Conferences on
Wind Turbine Noise
June 10-13, 2025
Copenhagen, Denmark

Editor: Franck Bertagnolio

Publisher: DTU Wind Energy (Technical University of Denmark)

All views and claims expressed in the articles
are the sole responsibility of the respective authors

Copyright © 2025, DTU Wind
All rights reserved by
DTU Wind and Energy Systems

DTU Wind Energy E-0258

ISBN: 978-87-87335-86-7

DOI: <https://doi.org/10.11581/08042886-dea0-4511-b4bd-6c5403125735>

Foreword

This document is reporting the 11th edition of the International Conferences on Wind Turbine Noise series, including all final articles as proceedings.

The conferences has been running every second year since 2005 with INCE/Europe as the organising institution. Starting this year, DTU Wind is taking over the organisation. The host city for this 2025 edition is naturally Copenhagen.

Each edition of the conferences has been a central point for people from over the world to discuss this topic sensitive to the public, and thereby the deployment of wind energy in the landscape.

A total of 44 articles and oral presentations spanning a variety of research, industrial and societal topics are presented this year. In addition, 4 Open Forums in the form of a panel discussion followed by interaction with the audience, are organized. These should provide a better status of our knowledge – or lack thereof – on specific aspects of wind turbine noise. The conference is concluded by a technical visit of the Poul La Cour wind tunnel at DTU-Risø campus.

We hope that you enjoyed your time in Copenhagen and gained a comprehensive overview of current knowledge and on-going activities in the field of wind turbine noise, which are the primary goals of the conference.

Hopefully, see you at the next edition in 2017!

Franck Bertagnolio
Chair of the Organizing Committee

Table of Contents

Organization	p. 5
Conference program	p. 6
Conference summary	p. 11
List of participants	p. 12
Proceedings' content	p. 15
List of authors in alphabetic order	p. 16
List of conference articles	p. 17

Organization

Executive Committee

- Franck Bertagnolio, Denmark
- Marianne Arbik, Denmark

Advisory Committee

- Dick Bowdler, UK
- Geoff Leventhall, UK
- Jean Tourret, France
- Cathy MacKenzie, UK

Scientific Committee

- Mark Bastasch, USA
- Dick Bowdler, UK
- Norm Broner, Australia
- Sylvia Broneske, UK
- Matthew Cand, UK
- Damiano Casalino, Netherlands
- David Ecotière, France
- Luca Fredianelli, Italy
- Duncan Halstead, Canada
- Malcolm Hayes, UK
- Michaela Herr, Germany
- Cordula Hornung, Germany
- Brian Howe, Canada
- David Michaud, Canada
- Lars Søndergaard, Denmark
- Frits van den Berg, Netherlands

Technical and Organizational Support

- DIS Congress Service A/S

Conference endorsed by ICA

International Commission for Acoustics



Conference organized by DTU Wind

Department of Wind and Energy Systems
Technical University of Denmark



Conference program

The conference spanned over four days. The first three days took place at the Scandic Kødbyen hotel (Copenhagen). The last day took place at DTU-Risø campus (Roskilde) in the Niels Bohr auditorium in the morning, followed by the technical visit of the Poul la Cour wind tunnel in the afternoon.

The following four pages contain the full conference schedule.

DAY 1**Tuesday 10 (morning)****Registration desk opens at 09:00****Conference start**

09:00-10:15

09:00-09:50	Registration and Coffee
09:50-10:15	Foreword: Dick Bowdler Welcome speech: Christian Bak (DTU, Professor, Head of the Poul la Cour Wind Tunnel, Head of Section)

Session 1 - Blade and airfoil noise I (Chair: Michaela Herr)

10:20-12:00

10:20-10:40	On the detection of vortex generator noise influence using beamforming in a large aeroacoustic wind tunnel Gelot, Matthieu <i>Abstract #5 (ID: 337)</i>
10:40-11:00	Aeroacoustic investigation of leading edge erosion in a wind tunnel Lylloff, Oliver <i>Abstract #13 (ID: 347)</i>
11:00-11:20	Multi-Scale Turbulence Structures in Grid-Generated Turbulence for Leading Edge Noise Prediction Sharma, Sparsh <i>Abstract #31 (ID: 365)</i>
11:20-11:40	Investigation of acoustics inside wind turbine blades and how it effects the outside Schneider, Lukas <i>Abstract #21 (ID: 355)</i>
11:40-12:00	Modifications to BPM model to incorporate trailing edge noise reduction by porous add-ons Caboni, Marco <i>Abstract #15 (ID: 349)</i>

Lunch Break

12:00-13:00

DAY 1**Tuesday 10 (afternoon)****Session 2 - Blade and airfoil noise II (Chair: Oliver Lylloff)**

13:00-13:40

13:00-13:20	A Native GPU CFD solver to predict trailing edge noise of wind turbine blades Reese, Hauke <i>Abstract #36 (ID: 371)</i>
13:20-13:40	Turbulent boundary layer trailing-edge noise reduction with permeable blade extensions at full-scale conditions Hartog, Friso <i>Abstract #44 (ID: 387)</i>

Session 3 - Rotor noise models I (Chair: Oliver Lylloff)

13:45-14:45

13:45-14:05	A High-Fidelity, Multi-Disciplinary Framework for Wind Turbine Aero-acoustic and Vibro-acoustic Noise Reduction van der Velden, Wouter <i>Abstract #3 (ID: 333)</i>
14:05-14:25	Aeroacoustic investigation into the X-Rotor vertical-axis wind turbine using lattice-Boltzmann very large eddy simulation (LB-VLES) Wu, Yan <i>Abstract #27 (ID: 361)</i>
14:25-14:45	Design and Validation of Trailing-Edge Serration to achieve 3dB Reduction of Wind Turbine Noise Kamruzzaman, Mohammad <i>Abstract #10 (ID: 344)</i>

Coffee Break

14:45-15:15

Session 4 - Rotor noise models II (Chair: Cordula Hornung)

15:15-16:15

15:15-15:35	Validation of a wind turbine noise high-frequency prediction tool Gimeno Garcia, Andres <i>Abstract #24 (ID: 358)</i>
15:35-15:55	Investigation of individual pitch control for infrasound noise reduction from wind turbines Shah, Anik Hirenkumar <i>Abstract #17 (ID: 351)</i>
15:55-16:15	Blade-tower interaction noise prediction using a simplified 2D vortex model Bertagnolio, Franck <i>Abstract #37 (ID: 372)</i>

Session 5 - Tonalities (Chair: Cordula Hornung)

16:20-17:00

16:20-16:40	Comparing Narrow-Band and 1/3-Octave Band Methods for Detecting Tonal Wind Turbine Noise Boon, Jaap <i>Abstract #12 (ID: 346)</i>
16:40-17:00	A feasibility study on Neural Networks for Rating Prominent Tones in Noise Søndergaard, Lars Sommer <i>Abstract #19 (ID: 353)</i>

Reception at Copenhagen City Hall

18:00-19:00

DAY 2**Wednesday 11 (morning)****Registration desk opens at 08:30****Session 6 - Low-frequency noise (Chair: Carlo Di Napoli)**

09:00-10:20

09:00-09:20	Wind turbine infrasound propagation over long distance Crozier, Steven	<i>Abstract #1 (ID: 331)</i>
09:20-09:40	Long term low frequency noise measurements near wind park Dijkstra, Mike	<i>Abstract #6 (ID: 338)</i>
09:40-10:00	The effects of low frequency noise considering the real complainants and real sites, and methodology for surveys of residents and development of mobile devices for good understanding on sound at wind turbine sites. Yamada, Shinji	<i>Abstract #8 (ID: 342)</i>
10:00-10:20	Acoustic Profiling of Infrasound and Audible Emissions from Wind Turbines: Field Measurements in Northern Sweden Chilo, José	<i>Abstract #43 (ID: 385)</i>

Coffee Break

10:20-11:00

Session 7 - Noise mitigation (Chair: Mark Bastasch)

11:00-12:00

11:00-11:20	Production Optimized Noise Curtailment on Wind Farms Sørensen, Thomas	<i>Abstract #4 (ID: 335)</i>
11:20-11:40	Impact of a Novel Flexible Serrated Trailing Edge in the Reduction of Far-Field Wind Turbine Noise Church, Ryan	<i>Abstract #25 (ID: 359)</i>
11:40-12:00	A comparison of turbine mitigation methods to achieve an 'n' decibel reduction in sound power level Marshall, Kira	<i>Abstract #29 (ID: 363)</i>

Lunch Break

12:00-13:00

DAY 2**Wednesday 11 (afternoon)****Session 8 - Noise assessment I (Chair: David Ecotièrre)**

13:00-14:40

13:00-13:20	Frequency Content of Measured Wind Farm Noise Levels and Band-Limited Regressions Levet, Tom	<i>Abstract #28 (ID: 362)</i>
13:20-13:40	Experimental validation of a prediction model of wind turbine noise variability Kayser, Bill	<i>Abstract #33 (ID: 367)</i>
13:40-14:00	Long-term Wind Farm Noise assessment over different meteorological conditions Lowe, Krispian	<i>Abstract #39 (ID: 375)</i>
14:00-14:20	Unwanted event removal and background noise characterization in wind turbine noise Fredianelli, Luca	<i>Abstract #40 (ID: 376)</i>
14:20-14:40	Procedure for predicting noise impact of new and repowered wind farms Bernardini, Marco	<i>Abstract #41 (ID: 380)</i>

Coffee Break

14:40-15:10

Session 9 - Propagation (Chair: Luca Fredianelli)

15:10-15:50

15:10-15:30	Numerical investigation of noise propagation in wind farms and the influence of wind turbine layouts Colas, Jules	<i>Abstract #18 (ID: 352)</i>
15:30-15:50	Developing a coastal sound speed profile for propagation models McKeown, Eugene	<i>Abstract #42 (ID: 382)</i>

Open forum #1 - Wind Turbine Noise Prediction: Status and What needs to be improved

16:00-17:00

16:00-16:10	Moderator/Introduction by: Damiano Casalino (TU Delft)
16:10-17:00	Panelists: Michaela Herr (DLR), Fabrice Junker (EDF renouvelables), Mohammad Kamruzzaman (Enercon), Stefan Oerlemans (Siemens Gamesa), Erik Sloth (Vestas)

DAY 3**Thursday 12 (morning)**

Registration desk opens at 09:00

Session 10 - Noise assessment II (Chair: Krispian Lowe)

09:00-10:40

09:00-09:20	Examining the Effects of Atmospheric Parameters on Sound Power Level Measurements from Wind Turbines: Findings from Parallel Measurements in the IEC 61400-11 Reference Position and Extended Distances Christensen, Niels Frederik <i>Abstract #34 (ID: 368)</i>
09:20-09:40	An investigation of immission spectrum resulting from increasing turbine rotor diameter Garnett, Merlin <i>Abstract #30 (ID: 364)</i>
09:40-10:00	Estimating wind turbine noise in Swedish national noise map over green areas Ögren, Mikael <i>Abstract #16 (ID: 350)</i>
10:00-10:20	Measurement of directivity patterns of a commercial wind turbine under yaw offset Finez, Arthur <i>Abstract #20 (ID: 354)</i>
10:20-10:40	Acoustic and SCADA data for the wind turbine noise level estimation Rkhiss, Abdelazyz <i>Abstract #26 (ID: 360)</i>

Coffee Break

10:40-11:10

Session 11 - Perception and annoyance I (Chair: Eoin King)

11:10-12:10

11:10-11:30	Perceived noise impact of transitioning towards larger wind turbines using auralisations Pockelé, Josephine Siebert <i>Abstract #9 (ID: 343)</i>
11:30-11:50	Psychological and physiological responses to amplitude-modulated low-frequency sounds Matsuda, Hiroshi <i>Abstract #32 (ID: 366)</i>
11:50-12:10	How do Residents Experience Wind Turbine Noise? The Results of a Two-Year Study Koppen, Erik <i>Abstract #11 (ID: 345)</i>

Lunch Break

12:10-13:10

DAY 3**Thursday 12 (afternoon)****Session 12 - Perception and annoyance II (Chair: Lars Søndergaard)**

13:10-14:10

13:10-13:30	Influence of Ambient Noise in Sound Quality Assessment of Auralised Wind Turbine Noise Pockelé, Josephine Siebert <i>Abstract #23 (ID: 357)</i>
13:30-13:50	Estimating the effects of Wind Turbine Noise on annoyance and cognitive performance O'Hora, Denis <i>Abstract #7 (ID: 340)</i>
13:50-14:10	The role of the planning process for wind turbine noise annoyance – results from multiple cross-sectional and longitudinal field studies Müller, Florian J. Y. <i>Abstract #38 (ID: 374)</i>

Session 13 - Planning (Chair: Lars Søndergaard)

14:10-14:50

14:10-14:30	Prediction Based Noise Limits and Why They Should Not Be Used When Consenting Wind Farms Baldwin, Jason <i>Abstract #22 (ID: 356)</i>
14:30-14:50	Planning conditions - what should they cover? Mackay, James <i>Abstract #35 (ID: 369)</i>

Coffee Break

14:50-15:20

Session 14 - General aspects (Chair: Gavin Irvine)

15:20-16:00

15:20-15:40	Overview of the results of the PIBE project (Predicting the Impact of wind turbine noise) Ecotiere, David <i>Abstract #14 (ID: 348)</i>
15:40-16:00	20 Years of Turbine Noise Bowdler, Dick <i>Abstract #2 (ID: 332)</i>

Open forum #2 - Wind Turbine Noise: What the Industry Needs, What Science Knows, and What the Public Hears

16:05-17:05

16:05-16:15	Moderator/Introduction by: Christophe Delaire (Marshall Day Acoustics)
16:15-17:05	Panelists: Jason Baldwin (TNEI), Calum Cais (OnPath Energy), Madelon Ekelschot-Smink (Arcadis), Duncan Halstead (Aercoustics), Colin Le Bourdat (ENGIE Green)

Conference dinner at DGI Byen

18:00-22:00

DAY 4**Friday 13 (morning)****Copenhagen to Risø Campus (Niels Bohr auditorium)**

9:00-10:00

9:00-10:00	Bus from Scandic hotel area to Risø Campus PICK-UP will be in the street in front of hotel - Departure at 9AM SHARP!
------------	---

**Open forum #3 - Sound Characteristics:
Amplitude Modulation and Tonalities**

10:00-11:00

10:00-10:10	Moderator/Introduction by: Matthew Cand (Hoare Lea) & Lars S. Søndergaard (FORCE Technology)
10:10-11:00	Panelists: Niels Frederik Christensen (Sweco), Bernd Hellmich (Nordex), Oliver Lyloff (DTU), David Puertollano (Encon/WRD), Seth Roberts (Hayes McKenzie Partnership)

Coffee break

11:00-11:30

**Open forum #4 - The Noise We Hear, the Feelings We Hold:
Exploring the Complexity of Wind Turbine Noise Reactions**

11:30-12:30

11:30-11:40	Moderator/Introduction by: Denis O'Hora (University of Galway)
11:40-12:30	Panelists: Birgit Junker (Statkraft), Florian Müller (MSH Hamburg), Lars S. Søndergaard (FORCE Technology)

Lunch break

12:30-13:30

DAY 4**Friday 13 (afternoon)****Technical visit of the Poul La Cour wind tunnel**

13:30-14:45

13:30-13:45	Introduction by: Christian Bak
13:45-14:00	Walk from Niels Bohr auditorium to PLC wind tunnel
14:00-14:45	Visit of the Poul La Cour wind tunnel

Return to Copenhagen

15:00-17:00

15:00-16:30	Bus from Risø Campus to Copenhagen First stop will be at CPH Airport with an ETA at 16:30!
16:30-17:00	CPH Airport to Scandic hotel/Kødbyen area

Conference summary

A total of 44 research articles and 4 open forums provided insight into topics such as technological noise reduction methods, low-frequency noise, noise assessment, public acceptance, annoyance, health implications, and the regulatory landscape.

Significant attention was given to technological innovations aimed at reducing noise emissions. These include refined blade designs (e.g. trailing-edge modifications), and better predictive models and measurements (e.g. in wind tunnel) to estimate noise sources and sound propagation. Experts emphasized that quieter turbine technologies and scientific knowledge related to it can enhance community acceptance without sacrificing efficiency. However, the fact that the size of wind turbines is continuously growing, inevitably affecting their overall environmental impact, was also pointed out several times during the conference.

Infrasound exposure and its potential health effects on nearby residents are still regarded as an ongoing concern. Researchers presented new studies on how low-frequency noise travels, affects sleep patterns, and possibly contributes to stress or other health symptoms.

Assessment and measurement of wind turbine noise remain complex scientific and regulatory challenges. Noise is not just about volume: factors such as frequency content, modulation, tonalities, and weather conditions all influence how noise can be measured and perceived. Presenters examined various methods used to assess sound levels around wind farms, including real-time monitoring, modeling tools, and newly developed measurement technologies. These assessments are critical to setting safe noise limits and ensuring wind farms compliance with local regulations.

Importantly, several researchers discussed the limitations of current noise standards, which often focus on average A-weighted sound levels and may overlook short-term variations or low-frequency components (or other aspects) that can potentially be more disturbing for residents. This relates to the above-mentioned importance of assessing noise correctly according to its actual impact on the environment and humans. There was a growing support for moving toward a more holistic soundscape approach that includes not only decibel levels but also the overall human experience of noise in a given environment.

The issues of public engagement and policy, recognizing the importance of transparency during planning and evidence-based noise immission levels were discussed. The role of non-acoustic factors, such as visual impact, trust in developers, and possible financial involvement (although this can also have an opposite effect on acceptance) was also acknowledged in influencing public perception and annoyance levels.

To sum up, WTN2025 reaffirmed the need for a balanced development: expanding wind energy to combat climate change while ensuring that its implementation respects local communities. As wind turbines grow in size and their deployment scales up, the conference underscored the importance of sound science and technology, thoughtful design, and public dialogue in achieving a sustainable energy future.

List of participants

First Name	Last Name	Organization
Assia	Achhibat	ENGIE GREEN
Marianne	Arbirk	DTU
Ivan	Asin Cruz	Vestas Deutschland GmbH
Helena	Axelsson	Multiconsult Norge AS
Jason	Baldwin	TNEI Services Ltd
Andrea	Bartolazzi	Sr International
Mark	Bastasch	Jacobs
Linda	Baten	dBa-Plan bv
Andrea	Bauerdorff	German Environment Agency (UBA)
Marco	Bernardini	iPOOL S.r.l.
Franck	Bertagnolio	DTU
Andrew	Birchby	TNEI Services Ltd
Jaap Cornelis	Boon	Arcadis Nederland B.v.
Lennart Johannes	Bouma	RIVM
Dick	Bowdler	The Haven
Sylvia	Broneske	RWE Renewables UK Ltd
Nicolas	Bureau	EDP Renewables
Jacques	Burillier	NTI AUDIO
Markus	Busse	RWE Renewables Europe & Australia GmbH
Calum Michael	Cais	Onpath Energy
Matthew	Cand	Hoare Lea
Leonardo	Cardoso	Texas A&M University
Damiano	Casalino	TU-Delft
Jose	Chilo	University Of Gavle
Niels Frederik	Christensen	Sweco Danmark A/S
Ryan	Church	Biome Renewables
Conor	Coady	BrightWind
Patrick	Cordes	Vestas Deutschland GmbH
Michael Thomas	Craven	Res
Steven	Crozier	Medcroz AS
Pawel	Cwiek	Iberdrola Renewables Polska Sp. Z O.o.
Christophe	Delaire	Marshall Day Acoustics
Carlo	Di Napoli	AFRY Finland Oy
Mike	Dijkstra	Lbpsight
Didier	Dragna	Centrale Lyon
David	Ecotièrè	Cerema
Arthur	Finez	ENGIE GREEN
Luca	Fredianelli	Italian National Council Of Research
Merlin S	Garnett	Green Cat Renewables
Tjeu Andries	Gehlen	Tu Delft/ Mutech
Andres V.	Gimeno-Garcia	RWTH Aachen
Maria	Glukhova	WRD GmbH
Christian	Grundmann	UKA Umweltgerechte Kraftanlagen GmbH & Co. KG

First Name	Last Name	Organization
Tomas Rosenberg	Hansen	Siemens Gamesa
Friso	Hartog	MuTech B.V.
Bernd	Hellmich	Nordex Energy Se & Co Kg
Mark	Hempel	Vestas
Iris	Hensen	DbA-plan
Michaela	Herr	German Aerospace Center, DLR
Moritz	Hildemann	EMD International A/s
Ann	Himpens	Arcadis
Cordula	Hornung	Enercon / WRD GmbH
Sean Gerard	Horsman	University Of Galway
Gavin	Irvine	Ion Acoustics Ltd
Simon	Jekosch	Vestas
Sonja	Jeram	National Institute Of Public Health
Fabrice	Junker	EDF Renouvelables
Mohammad	Kamruzzaman	Enercon/WRD GmbH
Bill	Kayser	Cerema
Erik Vilhelm	Kildemark	DTU
Eoin Anthony	King	University Of Galway
Akshay	Koodly Ravishankara	TNO
Erik	Koppen	Arcadis Nederland B.V.
Ewout	Lagerweij	Enercon R&D (WRD)
Colin	Le Bourdat	Engie Green
Justin (Hui)	Lee	Green Cat Renewables Canada
Tom	Levet	Hayes McKenzie Partnership
Magnus	Lindqvist	Swedish environmental protection agency
Angela	Lorenzo Del Moral	EDP Renewables
Krispian Tom Edward	Lowe	RWE Renewables UK Limited
Oliver	Lylloff	Technical University of Denmark (DTU)
Douglas	Manvell	DMdB
Kira	Marshall	Green Cat Renewables Ltd
Hiroshi	Matsuda	Nihon University
Eugene Patrick	Mckeown	University Of Galway
Florian	Müller	MSH Medical School Hamburg
Lasse Christner	Månsson	Danish EPA
Dharmaraju	Nalliboyana	Vestas Nacelles Deutschland GmbH
Juliette Anna	Naumann	Vestas Deutschland GmbH
Sharath Kodi	Navada	DTU
Stefan	Oerlemans	Siemens Gamesa Renewable Energy
Denis	O'Hora	University Of Galway
Signe Lynge	Olsson	Statkraft
Irene	Ortega	Sweco
Patrick	Pannwitt	Nordex Group
Gustav Juul Lind	Pedersen	Sweco
Prakyath	Pindi Nataraj	DTU
Lucas	Pinthon	ENGIE GREEN
Felix	Plagemann	Nordex Energy SE & Co. KG
Josephine Siebert	Pockelé	Delft University Of Technology, Faculty Of Aerospace Engineering
David	Puertollano	WRD GmbH
Guy	Putzeys	dBA-Plan bv
Nicola	Quaia	DTU

First Name	Last Name	Organization
Paul	Radons	UKA Umweltgerechte Kraftanlagen GmbH & Co. KG
Hauke	Reese	Ansys Germany GmbH
Abdelazyz	Rkhiss	ENGIE GREEN
Seth	Roberts	Hayes McKenzie Partnership Ltd
Oier	Saldana	Nordex SE
Ashwin	Saraf	Vestas Wind Systems
Lukas	Schneider	ESM GmbH
Anik Hirenkumar	Shah	TU Munich - Wind Energy Institute
Spارش	Sharma	German Aerospace Center (DLR)
Jonathan James	Sims	Noise Consultants Ltd
Jim	Singleton	TNEI Services Ltd
Erik	Sloth	Vestas
Madelon Maria Elisabeth	Smink	Arcadis Nederland B.V.
Philipp	Spelten	University Siegen
Steve	Summers	Mr. S M Summers
Lars Sommer	Søndergaard	FORCE Technology
Thomas	Sørensen	EMD International A/s
Carsten	Thomsen	CTXI Aps
Conor James	Tickner	Hayes Mckenzie
Emily	Tilbury	Metrica Environmental Consulting Ltd
Vincent Louis	Tréfois	I.C.A. Srl
Ric	van Poll	National Institute for Public Health and the Environment RIVM, Netherlands
Bieke	von den Hoff	MuTech B.V.
Brian Victor	Wilfred	B Hez Group
Shinji	Yamada	University of Yamanashi
Mikael	Ögren	University Of Gothenburg

Proceedings' content

The present document contains the collected articles corresponding to the oral presentations delivered at the conference. The articles are arranged in the order of their original abstract submission on the conference website.

A list of authors in alphabetical order is provided on the next page. Note that a dynamic link should be visible for each article (if using a standard PDF file reader). By clicking it, you should be automatically redirected to the first page of the article transcript in the proceedings. Otherwise, refer to the 'List of conference articles' starting on p. 17 for finding the page number corresponding to the beginning of each article transcript.

Note that the author names provided in the 'List of authors' and 'List of conference articles' do not necessarily reflect the actual main author of each article. These names are those that were used initially to upload the abstract on the conference website. The main author is the first one mentioned in the article transcript itself.

There is no full article (but an extended abstract) for Florian Müller.

Finally, note that these conference proceedings can be referenced using a DOI (Digital Object Identifier). The latter can be found at the very beginning of this document. The identifier applies to the whole conference proceedings. Unfortunately, it proved not practically possible to create individual DOI's for each article.

List of authors in alphabetic order

Author name	Paper #	Paper ID
Baldwin	22	356
Bernardini	41	380
Bertagnolio	37	372
Boon	12	346
Bowdler	2	332
Caboni	15	349
Chilo	43	385
Christensen	34	368
Church	25	359
Colas	18	352
Crozier	1	331
Dijkstra	6	338
Ecotièrre	14	348
Finez	20	354
Fredianelli	40	376
Garnett	30	364
Gelot	5	337
Gimeno García	24	358
Hartog	44	387
Kamruzzaman	10	344
Kayser	33	367
Koppen	11	345
Levet	28	362
Lowe	39	375
Lylloff	13	347
Mackay	35	369
Marshall	29	363
Matsuda	32	366
McKeown	42	382
Müller	38	374
O'Hora	7	340
Pockelé	9	343
Pockelé	23	357
Reese	36	371
Rkhiss	26	360
Schneider	21	355
Shah	17	351
Sharma	31	365
Søndergaard	19	353
Sørensen	4	335
Wu	27	361
Yamada	8	342
van der Velden	3	333
Ögren	16	350

List of conference articles

- Paper #1 - ID: 331 - Crozier, Steven
Wind turbine infrasound propagation over long distance p. 20
- Paper #2 - ID: 332 - Bowdler, Dick
20 Years of Turbine Noise p. 34
- Paper #3 - ID: 333 - van der Velden, Wouter
A High-Fidelity, Multi-Disciplinary Framework for Wind Turbine Aero-acoustic and Vibro-acoustic
Noise Reduction p. 44
- Paper #4 - ID: 335 - Sørensen, Thomas
Production Optimized Noise Curtailment on Wind Farms p. 57
- Paper #5 - ID: 337 - Gelot, Matthieu
On the detection of vortex generator noise influence using beamforming in a large aeroacoustic
wind tunnel p. 70
- Paper #6 - ID: 338 - Dijkstra, Mike
Long term low frequency noise measurements near wind park p. 77
- Paper #7 - ID: 340 - O'Hora, Denis
Estimating the effects of Wind Turbine Noise on annoyance and cognitive performance p. 86
- Paper #8 - ID: 342 - Yamada, Shinji
The effects of low frequency noise considering the real complainants and real sites, and methodol-
ogy for surveys of residents and development of mobile devices for good understanding on sound
at wind turbine sites. p. 96
- Paper #9 - ID: 343 - Pockelé, Josephine Siebert
Perceived noise impact of transitioning towards larger wind turbines using auralisations .. p. 111
- Paper #10 - ID: 344 - Kamruzzaman, Mohammad
Design and Validation of Trailing-Edge Serration to achieve 3dB Reduction of Wind Turbine Noise
..... p. 130
- Paper #11 - ID: 345 - Koppen, Erik
How do Residents Experience Wind Turbine Noise? The Results of a Two-Year Study p. 151
- Paper #12 - ID: 346 - Boon, Jaap
Comparing Narrow-Band and 1/3-Octave Band Methods for Detecting Tonal Wind Turbine Noise
..... p. 170
- Paper #13 - ID: 347 - Lylloff, Oliver
Aeroacoustic investigation of leading edge erosion in a wind tunnel p. 190
- Paper #14 - ID: 348 - Ecotièrre, David
Overview of the results of the PIBE project (Predicting the Impact of wind turbine noise) p. 204

Paper #15 - ID: 349 - Caboni, Marco
Modifications to BPM model to incorporate trailing edge noise reduction by porous add-ons p. 210

Paper #16 - ID: 350 - Ögren, Mikael
Estimating wind turbine noise in Swedish national noise map over green areas p. 227

Paper #17 - ID: 351 - Shah, Anik Hirenkumar
Investigation of individual pitch control for infrasound noise reduction from wind turbines p. 236

Paper #18 - ID: 352 - Colas, Jules
Numerical investigation of noise propagation in wind farms and the influence of wind turbine lay-
outs p. 247

Paper #19 - ID: 353 - Søndergaard, Lars Sommer
A feasibility study on Neural Networks for Rating Prominent Tones in Noise p. 255

Paper #20 - ID: 354 - Finez, Arthur
Measurement of directivity patterns of a commercial wind turbine under yaw offset p. 270

Paper #21 - ID: 355 - Schneider, Lukas
Investigation of acoustics inside wind turbine blades and how it effects the outside p. 286

Paper #22 - ID: 356 - Baldwin, Jason
Prediction Based Noise Limits and Why They Should Not Be Used When Consenting Wind Farms
..... p. 300

Paper #23 - ID: 357 - Pockelé, Josephine Siebert
Influence of Ambient Noise in Sound Quality Assessment of Auralised Wind Turbine Noise p. 314

Paper #24 - ID: 358 - Gimeno García, Andrés
Validation of a wind turbine noise high-frequency prediction tool p. 326

Paper #25 - ID: 359 - Church, Ryan
Impact of a Novel Flexible Serrated Trailing Edge in the Reduction of Far-Field Wind Turbine
Noise p. 341

Paper #26 - ID: 360 - Rkhiss, Abdelazyz
Acoustic and SCADA data for the wind turbine noise level estimation p. 358

Paper #27 - ID: 361 - Wu, Yan
Aeroacoustic investigation into the X-Rotor vertical-axis wind turbine using lattice-Boltzmann
very large eddy simulation (LB-VLES) p. 369

Paper #28 - ID: 362 - Levet, Tom
Frequency Content of Measured Wind Farm Noise Levels and Band-Limited Regressions . p. 386

Paper #29 - ID: 363 - Marshall, Kira
A comparison of turbine mitigation methods to achieve an ‘n’ decibel reduction in sound power
level p. 401

Paper #30 - ID: 364 - Garnett, Merlin
An investigation of immission spectrum resulting from increasing turbine rotor diameter .. p. 414

Paper #31 - ID: 365 - Sharma, Sparsh Multi-Scale Turbulence Structures in Grid-Generated Turbulence for Leading Edge Noise Prediction	p. 429
Paper #32 - ID: 366 - Matsuda, Hiroshi Psychological and physiological responses to amplitude-modulated low-frequency sounds ..	p. 441
Paper #33 - ID: 367 - Kayser, Bill Experimental validation of a prediction model of wind turbine noise variability	p. 450
Paper #34 - ID: 368 - Christensen, Niels Frederik Examining the Effects of Atmospheric Parameters on Sound Power Level Measurements from Wind Turbines: Findings from Parallel Measurements in the IEC 61400-11 Reference Position and Extended Distances	p. 456
Paper #35 - ID: 369 - Mackay, James Planning conditions - what should they cover?	p. 469
Paper #36 - ID: 371 - Reese, Hauke A Native GPU CFD solver to predict trailing edge noise of wind turbine blades	p. 479
Paper #37 - ID: 372 - Bertagnolio, Franck Blade-tower interaction noise prediction using a simplified 2D vortex model	p. 492
Paper #38 - ID: 374 - Müller, Florian J. Y. The role of the planning process for wind turbine noise annoyance – results from multiple cross-sectional and longitudinal field studies	p. 505
Paper #39 - ID: 375 - Lowe, Krispian Long-term Wind Farm Noise assessment over different meteorological conditions	p. 507
Paper #40 - ID: 376 - Fredianelli, Luca Unwanted event removal and background noise characterization in wind turbine noise	p. 518
Paper #41 - ID: 380 - Bernardini, Marco Procedure for predicting noise impact of new and repowered wind farms	p. 527
Paper #42 - ID: 382 - McKeown, Eugene Developing a coastal sound speed profile for propagation models	p. 545
Paper #43 - ID: 385 - Chilo, José Acoustic Profiling of Infrasound and Audible Emissions from Wind Turbines: Field Measurements in Northern Sweden	p. 554
Paper #44 - ID: 387 - Hartog, Friso Turbulent boundary layer trailing-edge noise reduction with permeable blade extensions at full-scale conditions	p. 562

Paper #1 - ID: 331

Title: Wind turbine infrasound propagation over long distance

Author: Steven Crozier

11th Edition of the
International Conferences on
Wind Turbine Noise

Copenhagen, Denmark – 10th to 13th June 2025

Infrasound with large peak to trough blade pass harmonics in two houses between three large wind turbine farms - WTFs on the northwest coast of Norway and two single health cases and a health survey near the WTF in Tysvær, Norway

Steven Crozier, MD, Specialist in Family Medicine and retired Municipal Chief Medical Officer on the island of Frøya

Member of the Public Health Committee in Motvind Norge

Sistranda, Trøndelag, 7260, Norway stevenfroya@gmail.com

Summary

The handling of sound pollution was to be transferred from the county governors in Norway to the municipalities in 2020. As chief medical officer on the small island of Frøya, pop. 5.500, that was to become my responsibility. The decision was made in late 2018 to complete the planned WTF with 14 Vestas V136 turbines on Frøya. This brought on many local protests, one being the claim that infrasound from WTFs cause health problems. This seemed somewhat absurd to me, how could any low frequency, non-audible air pressure waves cause havoc on humans and animals?

I decided to look into the available information on any health issues around WTFs. A steep learning curve ensued and resulted in the procurement of the Atkinson & Rapley SAM Scribe II [\[1\]](#) equipment for making null point recordings in homes near the planned WTF on Frøya, before it came into commission in 2021.

In late 2019 I was contacted by concerned citizens on the neighbouring island of Hitra, where Norway's first full scale WTF Hitra 1 with 24 Siemens SWT 2.3 CS turbines with 5.800m² sweep areas had been in commission since 2004. [\[2\]](#) It wasn't until the Hitra 2 WTF, with 26 Vestas V117 turbines with twice the sweep area 10.745m², started their production in the autumn of 2019 that health issues arose. [\[3\]](#)

Simultaneous 2 channel sound recordings were made in the bedrooms and outside of two houses on Hitra in December 2019 and in February 2021. Both houses are located ten kilometres to the northwest and to the north, northwest of Hitra 1&2 WTFs.

Sound measurements and the health issues of the residents are presented.

Norway's second health survey of residents near Tysvær WTF performed in 2023 is touched.

Public health's approach to infrasound from WTFs, a coda on infrasound effects in human and animal physiology at a cellular level and a short discussion on infrasound monitoring and setting limits in homes.

1. Introduction

Proceedings from the Conference on Low Frequency Noise and Hearing, Aalborg, Denmark, May 7-9, 1980: *“The first international colloquium concerned only with infrasound was held in Paris 1973. At this colloquium several effects of infrasound on human beings were presented and reviewed. An effort was also made to suggest some very preliminary criteria for infrasonic exposure. In the following years a number of new results were published, and several of them indicated that the limits for acceptable infrasonic exposure should be lowered considerably, if psychological effects were to be taken into account. Several countries have started more systematically to investigate infrasonic sources and to registrate complaints from people being disturbed by infrasound.”* [4]

Dr. Neil Kelley’s work from 1982: *“A Methodology for Assessment of Wind Turbine Noise Generation”* [5] and the 1987 presentation: *“A Proposed Metric for Assessing the Potential of Community Annoyance from Wind Turbine Low-Frequency Noise Emissions”* [6] set me on a quest to find out more.

The Danish Environmental Protection Agency - DEPA proposed limits on infrasound emissions from WTFs into residential homes in 2011.

Vestas, a large wind turbine company and economic provider in Denmark, had made it very clear that the distances required to comply with the set limits would seriously compromise their business model both nationally and internationally. DEPA reneged on their proposed infrasound limits. [7]

2. Recordings

The recordings on Hitra were supplemented with recordings four hours later in a house on the neighbouring island of Frøya for comparison. The Frøya house is located sixteen kilometres from the Hitra house and twenty kilometres from Hitra 1&2 WTFs. The outdoor microphone for channel wav-1 was placed two metres above the ground and two metres from the house facing Hitra 1&2. The indoor microphone for channel wav-2 was placed 15 centimetres above the pillow in the bedroom, also facing Hitra 1&2. Calibration tone 1 kHz, 94 dB. Ten minutes recordings with 16bit resolution and 11.025 kHz sampling rate. The sound files are 25 MB and are time, date and GPS location tamper-proof embedded. Weather conditions: Cloud overcast 7/8 with no precipitation. Wind 6-7 m/s with gusts up to 10m/s from E-N-E 60° Temperature between 0° and +1°C with temperature inversion over a large body of water. Air pressure 1003 hPa and humidity 99 percent. The meteorological conditions were similar at the Hitra and Frøya houses 16 kilometres and 4 hours apart. Analysis Signal Lab e.K Sigview 7.1 program. [8]

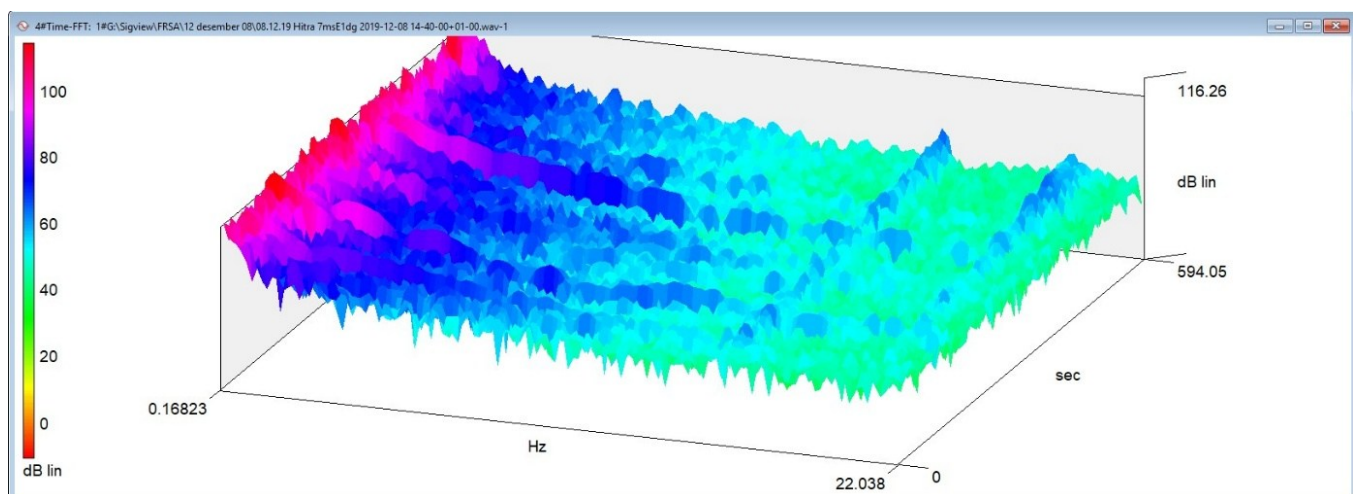


Figure 1 Hitra outdoor X axis 0.17-22 Hz, Y axis 0-596 seconds, Z axis dB lin. 1340-1350 UTC

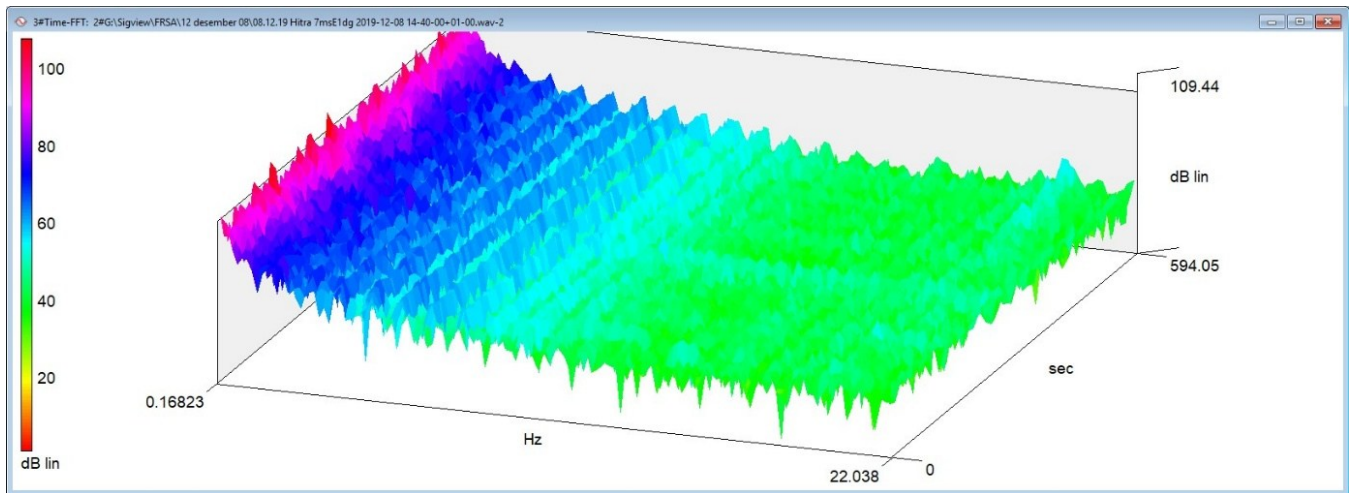


Figure 2 Hitra bedroom X axis 0.17-22 Hz, Y axis 0-596 seconds, Z axis dB lin. 1340-1350 UTC

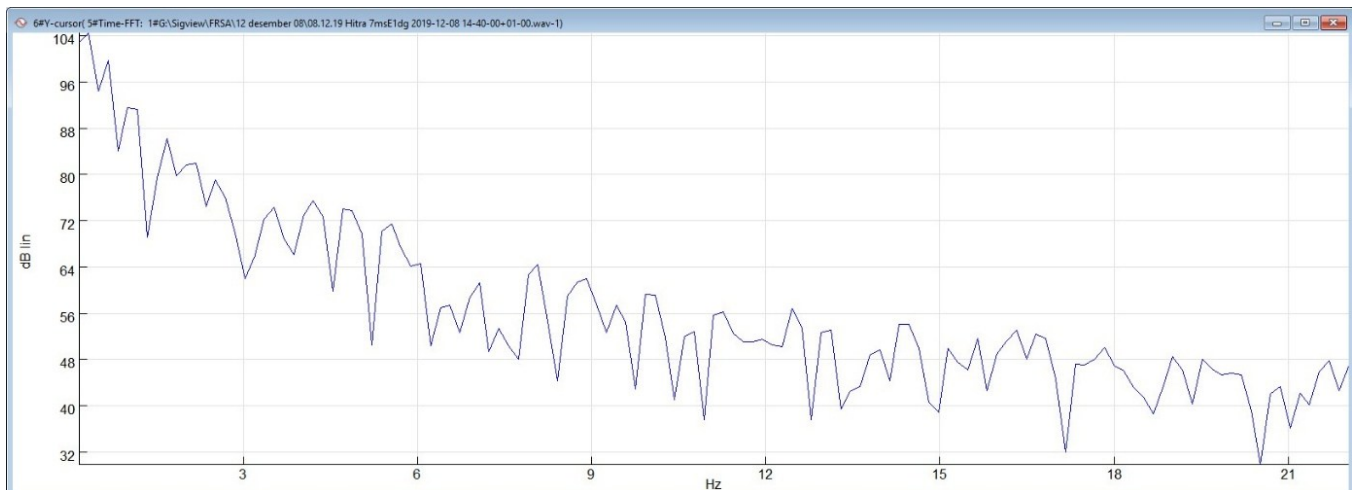


Figure 3 Hitra outdoor X axis 0.17-22Hz, Y axis dB lin. 1340-1350 UTC

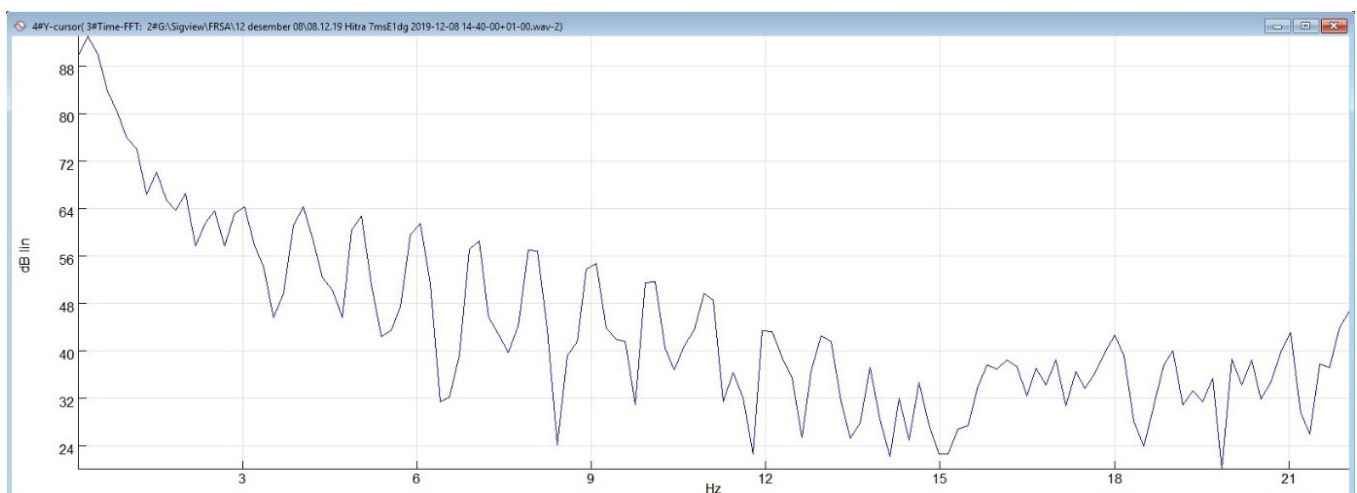


Figure 4 Hitra bedroom X axis 0.17-22Hz, Y axis dB lin. 1340-1350 UTC

Figures 5,6,7 and 8 show the corresponding recordings in the house on Frøya

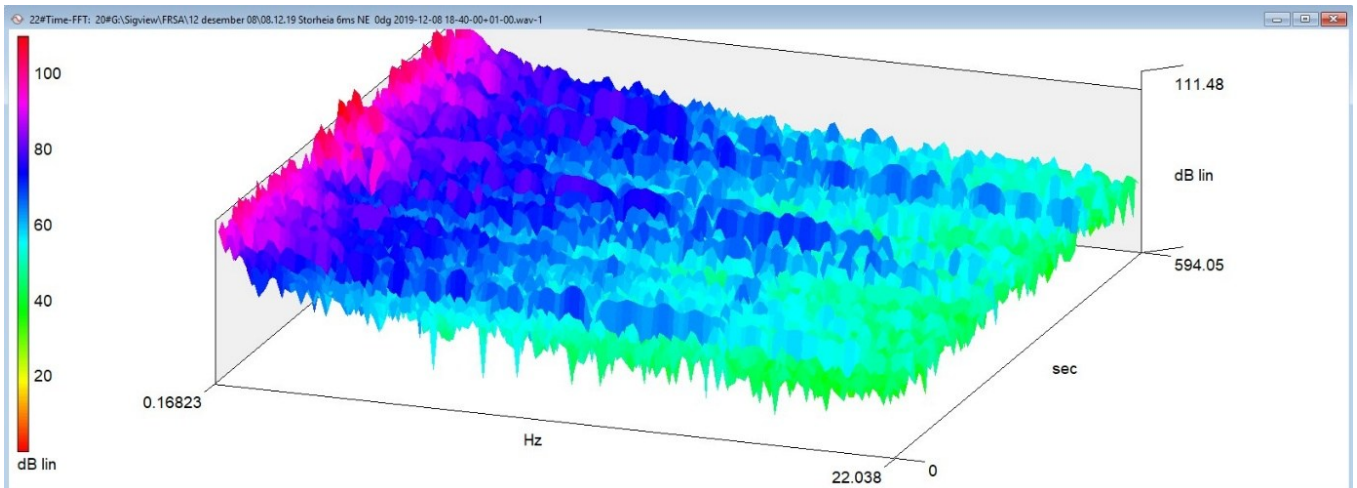


Figure 5 Frøya outdoor X axis 0.17-22 Hz, Y axis 0-596 seconds, Z axis dB lin. 1740-1750 UTC

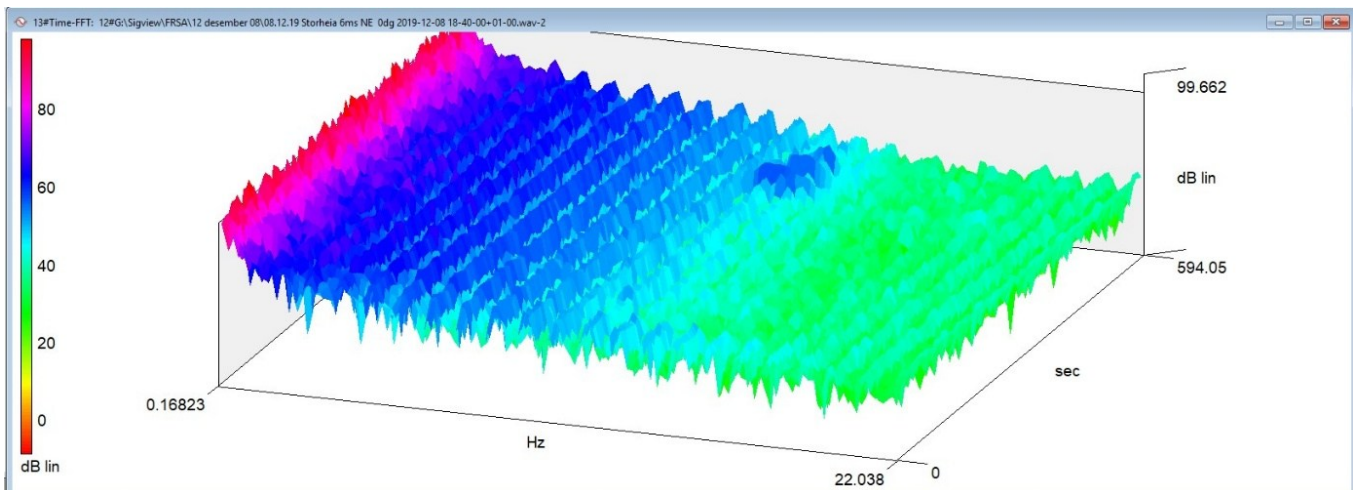


Figure 6 Frøya bedroom X axis 0.17-22 Hz, Y axis 0-596 seconds, Z axis dB lin. 1740-1750 UTC

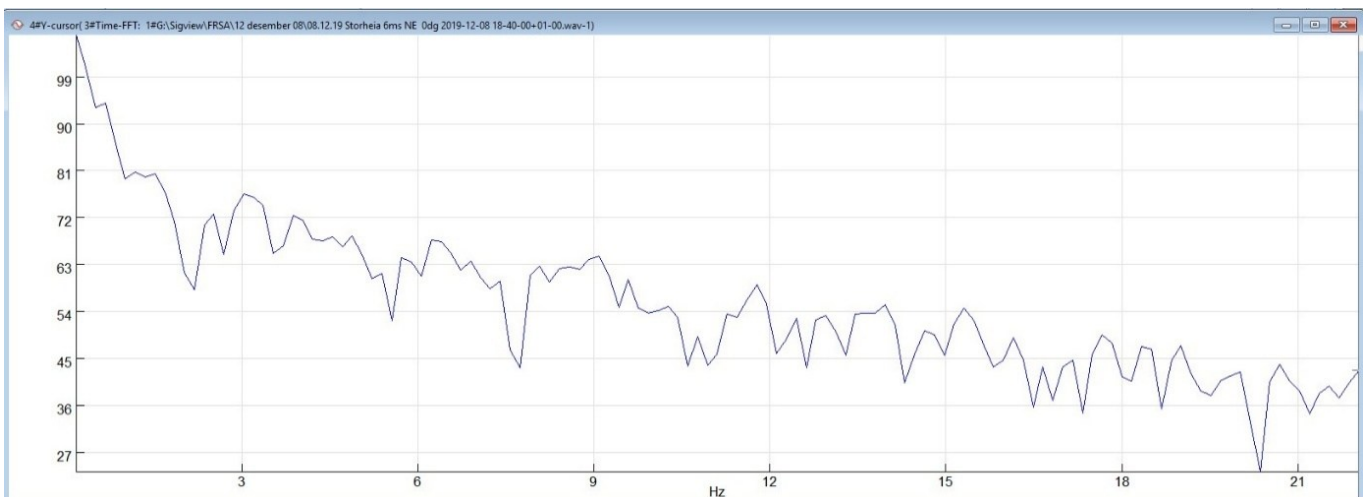


Figure 7 Frøya outdoor X axis 0.17-22Hz, Y axis dB lin. 1740-1750 UTC

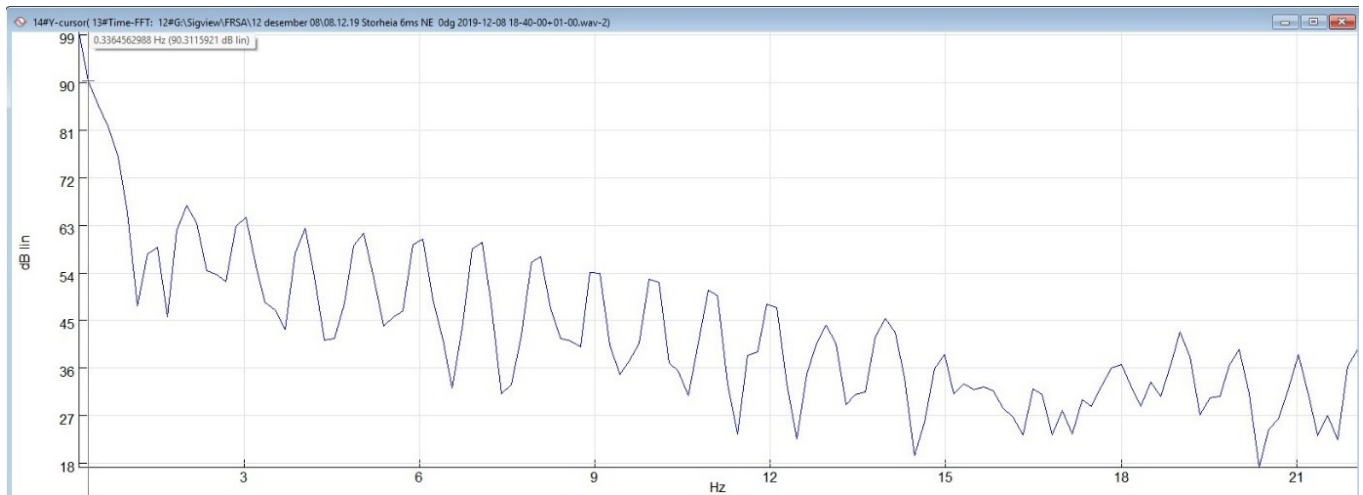


Figure 8 Frøya bedroom X axis 0.17-22Hz, Y axis dB lin. 1740-1750 UTC

Table 1 Outdoor peak to trough values

Outdoor	3 Hz	6 Hz	9 Hz	12 Hz	15 Hz	18 Hz	21 Hz
Hitra	12 dB	14 dB	9 dB	6 dB	11 dB	9 dB	7 dB
Frøya	11 dB	6 dB	10 dB	7 dB	9 dB	9 dB	9 dB

Table 2 Bedroom peak to trough values

Bedroom	3 Hz	6 Hz	9 Hz	12 Hz	15 Hz	18 Hz	21 Hz
Hitra	18 dB	29 dB	23 dB	21 dB	8 dB	19 dB	16 dB
Frøya	20 dB	28 dB	19 dB	25 dB	28 dB	7 dB	20 dB

The indoor harmonic patterns displayed in the spectrum and in the graphs show similar patterns in the Hitra house and Frøya house for comparison.



Figure 9 Fosen area in Trøndelag, Norway

Hitra 1&2 with 24 SWT2.3 and 26 V117 to the bottom left and Storheia and Roan with 80 and 71 Vestas V117 turbines respectively. Frøya with 14 Vestas V136 started production autumn 2021. The house with the 2021 recordings is not marked on the map. It is located ten kilometres north, northwest of the Hitra 1&2 WTFs

3. Discussion

The Hitra 1&2 wind turbines located ten kilometres away from the Hitra house were the prime suspected cause for the newly arisen noise and sleep disturbances starting in the autumn of 2019 after Hitra 2 came into commission. However, it is likely that the Roan and Storheia WTFs also contribute to the infrasound signature as they consist of 151 of the same Vestas V117 turbines and the wind coming from the east-northeast.

The upper levels recorded in the Hitra house were 116 dB outdoors and 109 dB in the bedroom. The Frøya house had 111dB outdoor and 99 dB indoor upper levels.

The twenty kilometres distance from Hitra 1&2 to the Frøya house explain an attenuation, yet it is not calculated how much the meteorological conditions contributed that day.

Note that the Frøya house has a ten kilometres closer proximity to the Storheia and Roan WTFs which are seventy and ninety kilometres away, versus eighty and hundred kilometres for the Hitra house.

Comparing data from the two houses, the wind turbines 70/90 and 80/100 kilometres away are likely contributors to the sound pattern. The temperature inversion over the large body of water between Hitra and Frøya and the Fosen region of Trøndelag and the downwind that day facilitate the transmission of infrasound over these long distances.

Further recordings and analysis are required to determine how much the Roan and Storheia WTFs contribute to the infrasound and blade pass harmonics on Hitra and Frøya. Without any connection to the topic of infrasound propagation, these are the same WTFs that the Norwegian Supreme Court ruled against in October 2021 for breaching the Sápmi's human rights by limiting their reindeer herding possibilities. [\[9\]](#)

4. Two cases concerning newly arisen health issues in persons living ten kilometres from the Hitra 1&2 WTFs

A person with a serious sleep disturbance

In December 2019 a person contacted me for help to map newly arisen noise in their house. The spectrograms and graphs in figures 1,2,3 and 4 are from this person's house.

They had lived ten kilometres from the Hitra 1 WTF for nine years without any health issues and were favourable to wind power generation.

After Hitra 2 WTF, also ten kilometres away started production, the rooms in their house started to rumble and boom when the windspeed rose above 5 m/s and came from certain directions.

Occupancy had become a burden and more time was spent out of the house. They would go out and about at night looking for the source of the noise, without any success. Sleep had become seriously affected and they often had to abandon the house to get sufficient rest.

A person with recurring atrial fibrillation

In 2021 a person in their late fifties also living ten kilometres from the Hitra 1&2 WTFs developed atrial fibrillation and received DC conversion five times due to relapses within a week after returning to the house. After an ablation, a procedure to break up or insulate the electrical signals in the heart that cause irregular heartbeats, the atrial fibrillation can still recur when in the house, yet abates within a day after vacating the house, see graphs in figures 10 and 11.

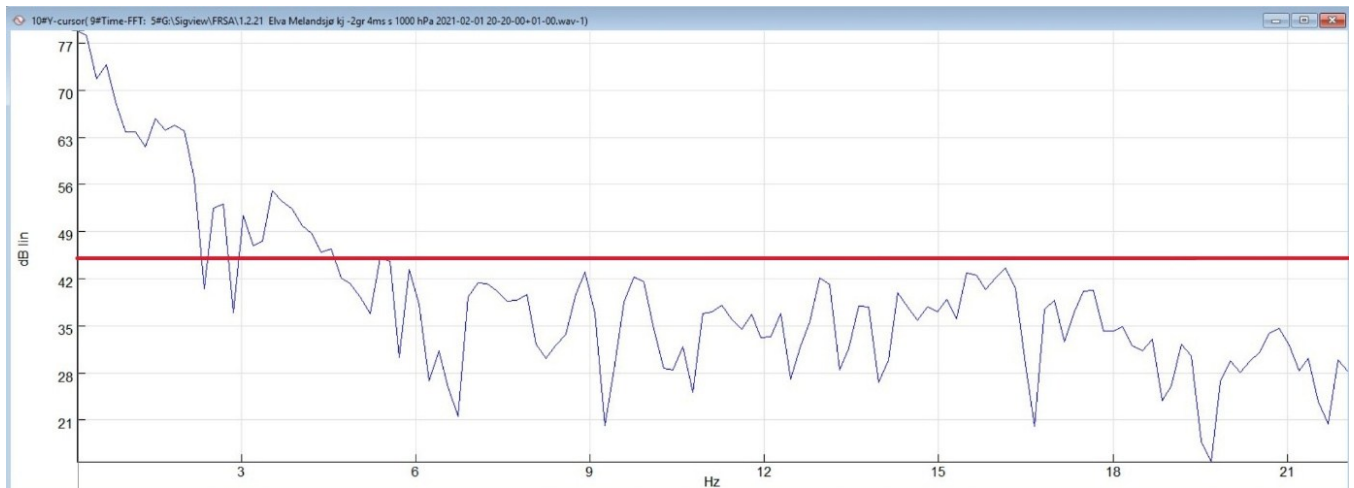


Figure 10 Hitra outdoor X axis 0.17-22Hz, Y axis dB 1910-1920 UTC Feb. 1st 2021

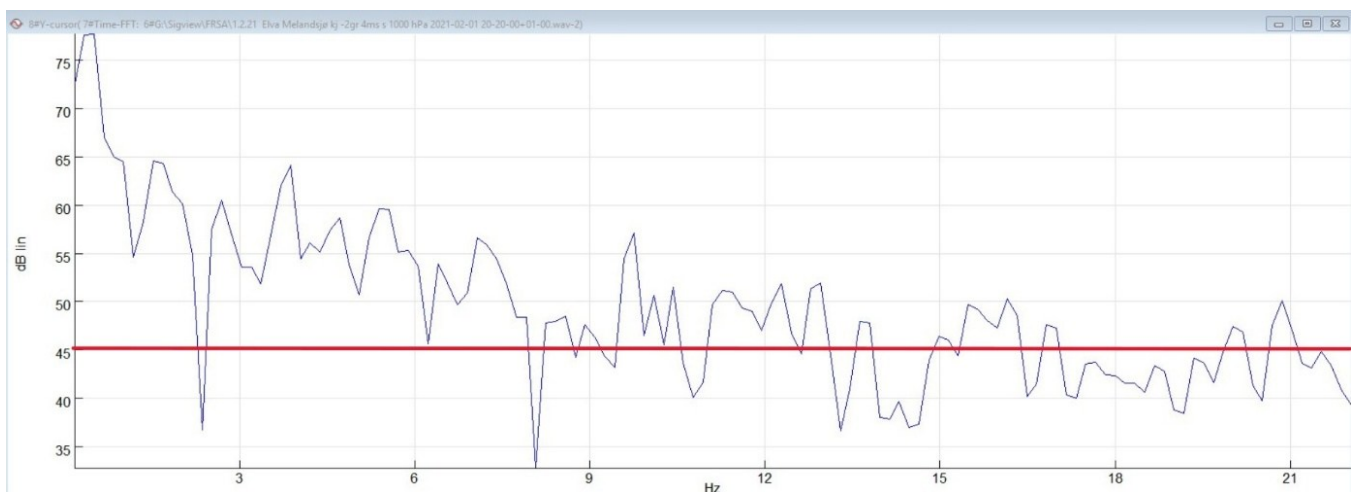


Figure 11 Hitra bedroom X axis 0.17-22Hz, Y axis dB 1910-1920 UTC Feb. 1st 2021

The sound mapping in both houses with affected persons shows a similar pattern in the spectrograms and graphs with large bedroom peak to trough levels in the blade pass harmonics. The person with heart arrhythmia had substantially higher levels of infrasound in their bedroom than outdoors, see figure 11. The two persons describe themselves as highly sensitive - HSP. Approximately one out of five people are HSP.

It is notable that health issues started when turbines with larger blades that produce a higher level of infrasound were added to the WTFs. These two health cases prove nothing about any cause and effect from rhythmic infrasound emissions generated by wind turbines.

However, they give reason for further health studies of residents living within ten kilometres from wind turbine factories.

5. Health Survey amongst residents within two kilometres from Tysvær WTF

A health survey was commissioned by the Tysvær municipality in 2023 after having received a number of health complaints after the Tysvær WTF started production in 2021. This is the second health survey of residents living near a WTF in Norway. [\[10\]](#)

Table 3 Health issues reported in the Tysvær health survey

Numbers in percent	Norway n=1000	Reference community n=200	Tysvær n=140	Total percentage over the reference community
Sleep disturbances	63	51	89	37
Muscle pain	56	53	70	17
Dizziness	33	39	55	16
Headache- migraine	24	21	41	20

Forty-seven percent of the 140 responders in the survey were severely annoyed by the audible noise from the WTF. Sixty-three percent were non-favourable to the WTF as opposed to seventeen percent in favour of them.

One notable feature is the high incidence of migraine in Tysvær, almost double of the national and reference community.

The low rate of participants in the health survey, fifty-three percent of the 262 persons living within a two kilometres radius of the WTF, could have given higher relative numbers of health complaints. Assuming that persons without any health issues were less inclined to participate in the survey.

6. Infrasound from WTFs

Often the wind power industry, and even the Ministry of Energy in 2021, refer to a 2020 study: *“Infrasound Does Not Explain Symptoms Related to Wind Turbines”* [11]

In the study twenty neighbours to a WTF with noise complaints were invited to a ten minutes long listening test of a years recorded and compiled sound taken 2.5 kilometres from the WTF. When they could not discern the sound, nor had a rise in blood pressure or pulse, the conclusion was that WTFs are not the cause of any health problems for residents living near WTFs. The problems could be in their heads and self-inflicted.

The sound levels in the study are way below the 95dB or higher levels of infrasound people living near WTFs are exposed twenty-four-seven whenever the wind blows.

You can compare the design of the study to one that shows that smoking is not detrimental to your health by letting twenty non-smokers smoke two cigarettes in ten minutes and them not getting sick.

7. Public health’s dealing with health issues presumed to be caused by living near a WTF

Conflict of interests: None, other than a fine for civil disobedience in September 2020 which was upheld in a lower court ruling February 2021.

The disobedience was to set focus on the lack of following the precautionary principle, prescribed in the Norwegian Public Health Act of 2011, in the concession given for the wind turbine factory on Frøya in 2016. [12]

I am aware of how both physical and psychological bias influence research and analysis. I have tried to approach and discuss my findings with an open mind.

However, I do have strong opinions on how health issues from affected neighbours near WTFs are met by the Norwegian Institute of Public Health - NIPH.

We had a meeting with them in January 2020 presenting recordings with high levels of infrasound in a house five hundred metres from a WTF in Egersund, Norway. The parents were having adverse health reactions, very likely attributable to the WTF.

We appealed for health surveys and monitoring of persons living near WTFs, yet were brushed off citing lack of funds. Likewise, an appeal for legislation to make the industry prove the safety of their products, ever larger wind turbines that produce ever higher levels of infrasound, was dismissed.

The NIPH website updated in May 2022 states: *“Although neither infrasound nor low-frequency sound are **specific** to wind turbines, there has been particular concern about the health consequences of infrasound from wind turbines”* [13]

Infrasound from WTFs is **specific** with signatures comprised of blade pass harmonics with high peak to trough levels, as opposed to randomly generated broad band infrasound from traffic and in nature.

The 2 channel recordings show how resonance and perchance interference increase the infrasound’s peak to trough levels in the house

The health survey from Tysvær is not mentioned in NIPH’s chapter on WTFs and health. However, the one other health survey from Lista in 2015 is noted. 2/3 of the residents living within 1 kilometre from the WTF in Lista experience strong noise annoyance.

8. Infrasound effects in human and animal physiology at a cellular level

Recent knowledge of how infrasound affects cell physiology is presented by Ursula Maria Bellut-Staeck in the 2023 study: *“Impairment of the Endothelium and Disorder of Microcirculation in Humans and Animals Exposed to Infrasound due to Irregular Mechano-Transduction.”* [14]

Her study adds to the work of Vladimir Stepanov et al from 2003. They presented increasingly lower recommended Maximum Pressure Limits- MPLs in the workplace and residences from 1973 and on to 2000. [15]

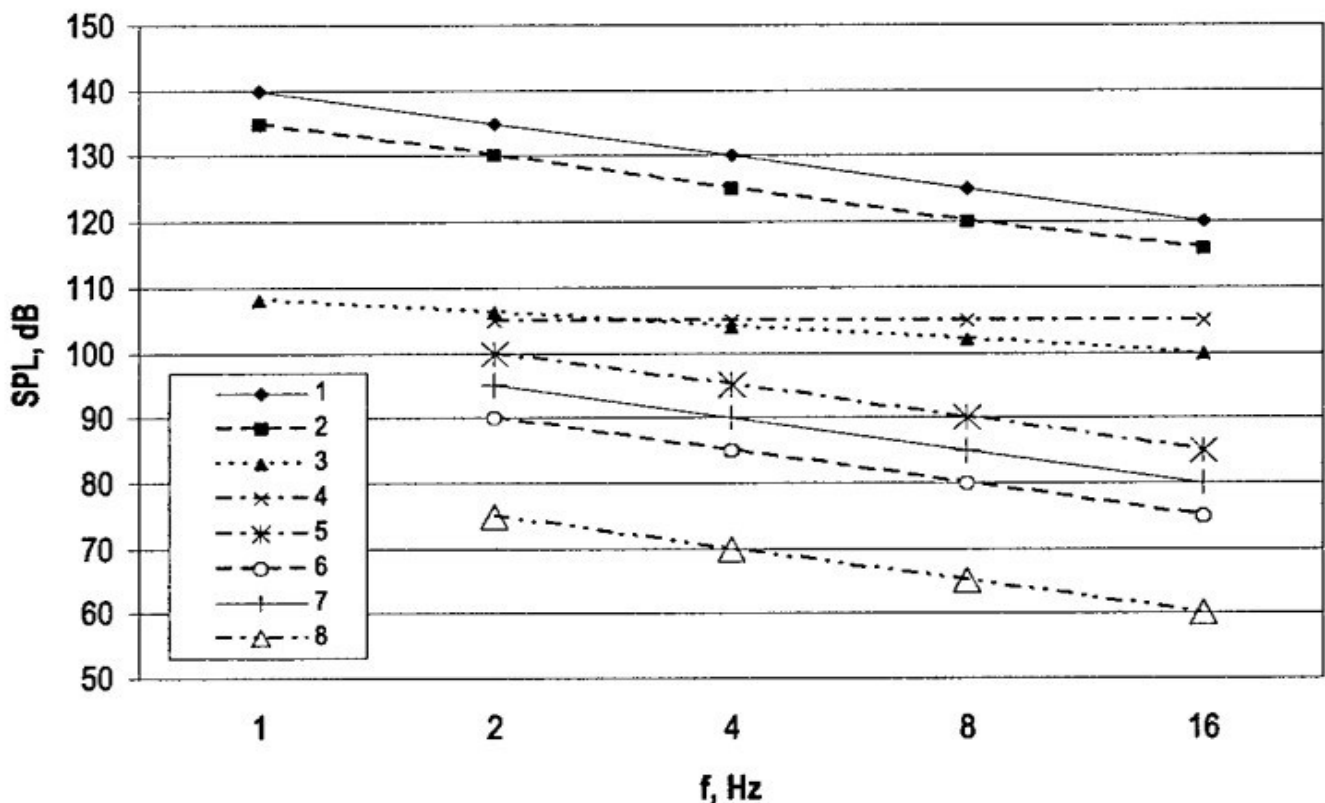


Figure 12 - MPLs dynamics for Low Frequency Acoustic Oscillations and infrasound in 1973-2000

- 1- MPLs recommended by D.Johnson and C.Nixon (1973)
- 2- MPLs recommended by Paris International colloquium (CNRS) (1973)
- 3- MPLs recommended by Institute of Biophysics (1979)
- 4- MPLs recommended by Research Institute of Labour Hygiene and Occupational Diseases of the USSR Academy of Medical Sciences et al (1980)
- 5- Modern MPLs recommended by Labour Medicine Research Institute of Russian Academy of Medical Sciences et al (1996) jobs of different intensity inside industrial premises and at the industrial territory
- 6- Intellectual and emotional jobs
- 7- Populated areas
- 8- Living and public premises

An assumption could be proposed that the large peak to trough levels in blade pass harmonics generate more hysteresis in cells and organs than a constant high level of infrasound with lower peak to trough levels and thereby have a greater disruptive effect at the cellular level.

The descriptions in: “*Examples of hysteresis phenomena in biology*” [16] may explain how myocardial cells are affected by rhythmic infrasound with pronounced harmonics causing atrial fibrosis and arrhythmias.

The study from 2021: “*Infrasound exposure promotes development of atrial fibrosis in rats*” discusses this issue. [17]

9. Conclusions

Working on a small island community as a General Practitioner since 1985 and as Municipal Chief Medical Officer on a rotational basis, sharing the position with my wife Eli, gave me the challenge of having to deal with noise pollution from 2020. As I delved into the literature on infrasound from WTFs, I came across an abundance of studies with no clear conclusions on health impacts.

Proprietors of WTFs do not have to conduct any post erection measurements of the 45 dBA Lden adopted and calculated standard, nor record any infrasound inside nearby houses.

Any measured results are not divulged due to proprietary and competitive issues amongst the industry.

Were they to be shared the results would most likely not be dealt with, as there are no set limits for infrasound in Norway and fellow Municipal Chief Medical Officers most often have limited knowledge of sound pollution.

The wind power industry has not yet been forced to prove that their products, which are ever larger turbines which generate ever higher levels of infrasound, are not harmful to humans and animals.

Where the Norwegian Water Resources and Energy Directorate, that issues concessions, lacks in public health expertise, they have to rely on the NIPH’s lacklustre approach to the issue, and the wind turbine industry gets to maintain the calculated 45 dBA Lden limit.

Without having to deal with infrasound pollution from their products.

Suppose the same lack of certification standards were applied to the licencing of automobiles or with the introduction of new pharmaceuticals?

How come some countries after the Paris 1973 infrasound colloquium adopted ever stringent band specific limits for permitted infrasound in the workplace and in homes, whereas other countries have chosen to not set any limits for infrasound or vibrations?

As it seems that highly sensitive persons are the first to report health issues from living in the vicinity of a WTF, is the eighty percent normo-sensitive population not directly affected by WTFs reason enough to not pursue the issue of suspected health problems related to WTFs?

Were up to twenty percent of the population stricken by a suspected agent, one would certainly push to elucidate the matter.

“The wind industry is relatively new in Norway. The likelihood that there may be errors or shortcomings in both the guidelines and regulations is therefore present, something that Norwegian health authorities should take into account. If more wind industry is to be developed, thorough studies should be carried out by independent actors before licenses are awarded. Furthermore, it should be ensured that the people working on the study have the necessary professional expertise in subjects such as acoustics, environmental hygiene, occupational hygiene, public health and occupational medicine. Negative health effects should be assessed both in isolation and collectively, for the best possible overview.” [18]

The Public Health Committee in Motvind Norge has had meetings with The Norwegian Water Resources and Energy Directorate, The Norwegian Environment Agency and The Norwegian Directorate of Health to discuss guidelines for evaluating the **sum effects** of audible and uneven amplitude modulated noise, infrasound, high-intensity flashes of light at night, shadows cast by -and the sight of moving turbine blades, Bisphenol-A and PFAS spread in nature and drinking water, grief of nature loss and property value loss. They all give kudos to the group’s efforts and agree that these are issues that need to be addressed.

Yet, they admit that they do not have the competence to make any sound evaluations or recommendations, AKA passing the buck. The Norwegian Institute of Public Health does not respond.

Are we up against a similar problem as those that were encountered when dealing with the exposure to asbestos particles and tobacco smoke? Knowledge of the hazards to their exposure was allowed to fester for decades before regulations were signed into law.

Could proceeds from the wind turbine industry be a step to take for the regulatory bodies to fund independent research and set guidelines?

Until then my advice for guarding the public health is to invoke the precautionary principle and mandate infrasound measurements in homes near WTFs, set limits on infrasound in residences as DEPA intended back in 2011 and impose a moratorium on erecting any WTF closer than ten kilometres to residential areas.

Acknowledgements

Being an avid high-fidelity buff chasing the holy grail of perfect sound recording, I bought a pair of Bruel & Kjaer 4004 studio microphones back in 1988 to record performances of the choir Havdur, which Eli has been singing with since then. This has offset any looming annoyance for the time I have spent on performing infrasound recordings in and out of houses around Norway pro bono.

Kind thoughts for my parents who encouraged my curiosity since early childhood. This is a trait our children also seem to share, and since we’re not cats, the going has been pretty good - so far.

Championing peace cuts it down to the maxim: ***“Justice for troubled wind farm neighbours won't happen until those who aren't affected become as outraged as those who are”.***

References

- 1) [H.H.C. Bakker, B.Rapley, R.Summers, M.Alves-Pereira and P.Dickinson "An Affordable Recording Instrument for the Acoustical Characterisation of Human Environments" 2017](https://www.researchgate.net/publication/317702715_An_Affordable_Recording_Instrument_for_the_Acoustical_Characterisation_of_Human_Environments)
https://www.researchgate.net/publication/317702715_An_Affordable_Recording_Instrument_for_the_Acoustical_Characterisation_of_Human_Environments
- 2) [NVE- Hitra vindkraftverk 2004](https://www.nve.no/konsesjon/konsesjonssaker/konsesjonssak/?id=10&type=A-6)
<https://www.nve.no/konsesjon/konsesjonssaker/konsesjonssak/?id=10&type=A-6>
- 3) [NVE-Hitra-2-vindkraftverk](https://www.nve.no/konsesjon/konsesjonssaker/konsesjonssak/?type=A-6&id=34)
<https://www.nve.no/konsesjon/konsesjonssaker/konsesjonssak/?type=A-6&id=34>
- 4) [H.Møller, P.Rubak, "Proceedings of Conference on Low Frequency Noise and Hearing", Aalborg, Denmark, 1980"](https://vbn.aau.dk/ws/portalfiles/portal/227874366/1980_M_ller_and_Rubak_Proceedings_LF_conference.pdf)
https://vbn.aau.dk/ws/portalfiles/portal/227874366/1980_M_ller_and_Rubak_Proceedings_LF_conference.pdf
- 5) [N. Kelley, "A Methodology for Assessment of Wind Turbine Noise Generation" 1982](https://docs.wind-watch.org/kelley_ASME_1982.pdf)
https://docs.wind-watch.org/kelley_ASME_1982.pdf
- 6) [N.Kelley, "A Proposed Metric for Assessing Potential of Community Annoyance from Wind Turbine Low Frequency Noise Emissions" 1987](https://docs.wind-watch.org/Kelley_Proposed-metric-assessing-potential-annoyance-wind-turbine-LF.pdf) https://docs.wind-watch.org/Kelley_Proposed-metric-assessing-potential-annoyance-wind-turbine-LF.pdf
- 7) [D. Engel, "Letter from Vestas CEO to the Danish Environmental Protection Agency - DEPA" June 29th 2011](https://stopthesethings.com/wp-content/uploads/2015/02/engel-ditlev-vestas-letter-to-danish-environment-minister-in-english.pdf) <https://stopthesethings.com/wp-content/uploads/2015/02/engel-ditlev-vestas-letter-to-danish-environment-minister-in-english.pdf>
- 8) [SIGVIEW is a powerful signal analysis software package that supports both real-time and offline processing.](https://www.sigview.com/?gad_source=1&gclid=Cj0KCQiA2oW-BhC2ARIsADSIAWrZ2ToFvfw87IF9QAwIYRsPbD9PdwUD5gugGYkURkZKY_oKpUNXgIYaAvpVEALw_wcB)
https://www.sigview.com/?gad_source=1&gclid=Cj0KCQiA2oW-BhC2ARIsADSIAWrZ2ToFvfw87IF9QAwIYRsPbD9PdwUD5gugGYkURkZKY_oKpUNXgIYaAvpVEALw_wcB
- 9) [Norwegian Human Rights Institution: "About the wind farms on Fosen and the Supreme Court judgment "](https://www.nhri.no/en/2023/about-the-wind-farms-on-fosen-and-the-supreme-court-judgment/)
<https://www.nhri.no/en/2023/about-the-wind-farms-on-fosen-and-the-supreme-court-judgment/>
- 10) [Opinion AS "Health Survey among residents near Tysvær wind turbine factory" 2023](https://www.tysver.kommune.no/_f/p1/i9820ceda-3d74-4805-a06b-a76b09bd8b4a/rapport_helsekartlegging-blant-beboere-nar-tysvar-vindpark_20122023.pdf)
https://www.tysver.kommune.no/_f/p1/i9820ceda-3d74-4805-a06b-a76b09bd8b4a/rapport_helsekartlegging-blant-beboere-nar-tysvar-vindpark_20122023.pdf
- 11) [P. Maijala, A.Turunen, I.Kurki et al. "Infrasound Does Not Explain Symptoms Related to Wind Turbines" - VTT 2020](https://julkaisut.valtioneuvosto.fi/handle/10024/162329) <https://julkaisut.valtioneuvosto.fi/handle/10024/162329>
- 12) [C.Fjeldavli "The enemy of the people on Frøya" - Bergensia from Harvest Magazine March 2021](https://bergensia.com/the-enemy-of-the-people-on-froya/)
<https://bergensia.com/the-enemy-of-the-people-on-froya/>
- 13) [Norwegian Institute of Public Health "Low-frequency sound, infrasound and health" May 2022](https://www.fhi.no/kl/stoy/stoy--fra-vindturbiner-helseskadelig/#lavfrekvent-lyd-og-infralyd-og-helse)
<https://www.fhi.no/kl/stoy/stoy--fra-vindturbiner-helseskadelig/#lavfrekvent-lyd-og-infralyd-og-helse>
- 14) [U.M. Bellut-Staek "Impairment of the Endothelium and Disorder of Microcirculation in Humans and Animals Exposed to Infrasound due to Irregular Mechano-Transduction" 2023](https://www.researchgate.net/publication/368111111_Impairment_of_the_Endothelium_and_Disorder_of_Microcirculation_in_Humans_and_Animals_Exposed_to_Infrasound_due_to_Irregular_Mechano-Transduction)
https://www.researchgate.net/publication/368111111_Impairment_of_the_Endothelium_and_Disorder_of_Microcirculation_in_Humans_and_Animals_Exposed_to_Infrasound_due_to_Irregular_Mechano-Transduction

https://www.researchgate.net/publication/371517232_Impairment_of_the_Endothelium_and_Disorder_of_Microcirculation_in_Humans_and_Animals_Exposed_to_Infrasound_due_to_Irregular_Mechano-Transduction

- 15) [V. Stepanov et al. "Biological Effects of Low Frequency Acoustic Oscillations and their Hygienic Regulation" 2003](#)
<https://apps.dtic.mil/sti/pdfs/ADA423963.pdf>
- 16) [H.R.Noori, "Examples of hysteresis phenomena in biology - 2014](#)
https://www.researchgate.net/publication/319991355_Examples_of_hysteresis_phenomena_in_biology
- 17) [A.Lousinha, M.J.R. Oliveira, G.Borrecho et al."Infrasound exposure promotes development of atrial fibrosis in rats" - Annals of Medicine Sept. 28th 2021](#)
<https://pmc.ncbi.nlm.nih.gov/articles/PMC8480765/>
- 18) [S.Crozier, C.Fjeldavli, "Turbinstøy og folkehelse" - Harvest Magazine May 2021](#)
<https://www.harvestmagazine.no/artikkel/turbinstoy-og-folkehelse>

Paper #2 - ID: 332

Title: 20 Years of Turbine Noise

Author: Dick Bowdler

11th Edition of the

International Conferences on Wind Turbine Noise

Copenhagen, Denmark – 10th to 13th June 2025

20 Years of Wind Turbine Noise

An immediate end to business as usual is a precondition for planetary survival. [1]

Dick Bowdler.

Acoustic Consultant Scotland

Summary

In 2005, the first conference of this series was held in Berlin. This paper looks at the advances in knowledge and technique in the generation, propagation and impact of wind turbine noise over the last 20 years and tentatively looks at where we might be in another 20 years in 2045. Most turbines operating in 2005 were stall controlled but about this time pitch-controlled turbines were taking over. Since then we have seen increases in turbine size and power output, particularly since 2015, but there are various reasons why that may not continue at the current rate. A big advance has been our knowledge of source noise generation. This allowed better predictions of noise and the development of STEs and other noise mitigating developments. We have better knowledge of propagation, amplitude modulation, the impact of noise on people. Overall, there have not been dramatic breaks-through but a steady improvement in our knowledge and practice over the last 20 years which is to be welcomed. But our way of work has changed with the overall rapid advance of technology - particularly computer power and storage and connectivity. Will this advance of new technology continue at the same rate? Will there be more remote operation, more accurate smartphone apps? Will we have much more of a soundscape approach to noise limits and to assessment by 2045? And, of course, how can we harness AI to help?

1. Introduction

20 years ago, in 2005, the first conference of this series was held in Berlin. In another 20 years it will be 2045. Will we have achieved Net-Zero? Whatever 2045 brings, life will be very different from now, just as now is different from 2005. On the one hand I want to look back at what we have achieved in terms of knowledge about wind turbine noise and how it affects people, what we haven't achieved and what our priorities need to be for the future.

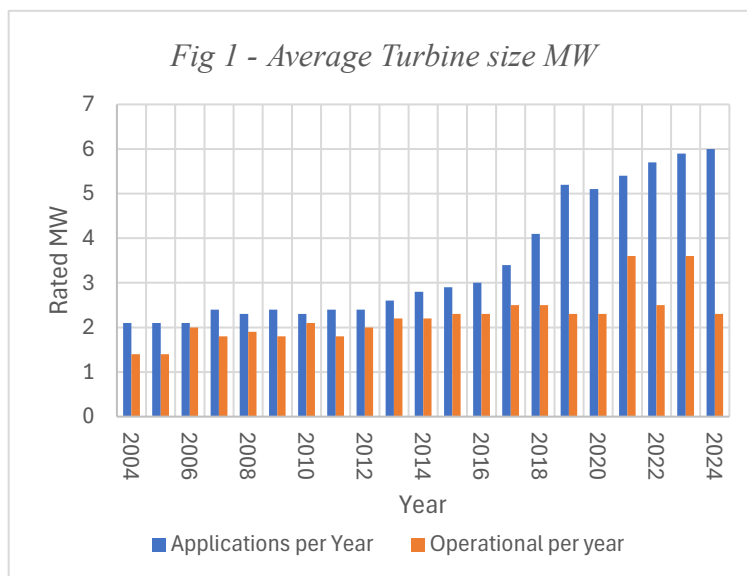
Inevitably, because I work mostly in the UK, these thoughts are UK centred. Some will apply widely to most other countries but others will vary from nation to nation. This paper is my opinion but enabled by all those that have contributed to the last 10 conferences. I hope some of it might be proved right!

The conferences have been, at their core, about spreading knowledge about wind turbine noise and its effects whether we are researchers or consultants or wind farm developers. There are many things that drive our work but perhaps two in particular. The first is demand; is someone willing to pay for the work? The second is technology and knowledge; on the one hand, do we have or can we obtain the technology to and knowledge to carry out a task.

2. Turbines

Turbines have increased in size in the last 20 years but there is a big lag between planning and operation. In 2005 the time between a planning application and turbines coming into operation for larger wind farms in the UK was about 3 years. It rose to a peak of over 8 years in about 2016 and has now dropped to about 5 or 6 years. And there will likely be two years preparation before planning applications are submitted.

In the year leading up to the 2005 conference the average tip height of turbines installed and becoming operational in the UK was 88m and the rotor average diameter was 63m. The power output was 1.5MW. There was only a slight increase in the size of those turbines starting operation each year, shown by the orange bars in Fig 1, reaching an average of about 2MW in 2012 and not quite 2.5MW by 2020. Since then there has been a bigger rate of increase – though erratic. Those starting operation in the 4 years 2021 – 2024 had an average rating of 3.3MW and tip height of 130m. That is the ones that were operational. As the blue bars in Fig 1 below show, applications for wind farms show power per turbine gradually increasing over more than 10 years from an average of 2MW in 2005 to 3MW in 2016. Then there was a rapid increase in 3 years from 3MW to 5MW in 2019 and to 6MW by 2023 [2]. There will be others reading this who can explain the reason for this sudden increase better than I but clearly blade technology and blade transportation technology must have played a part.



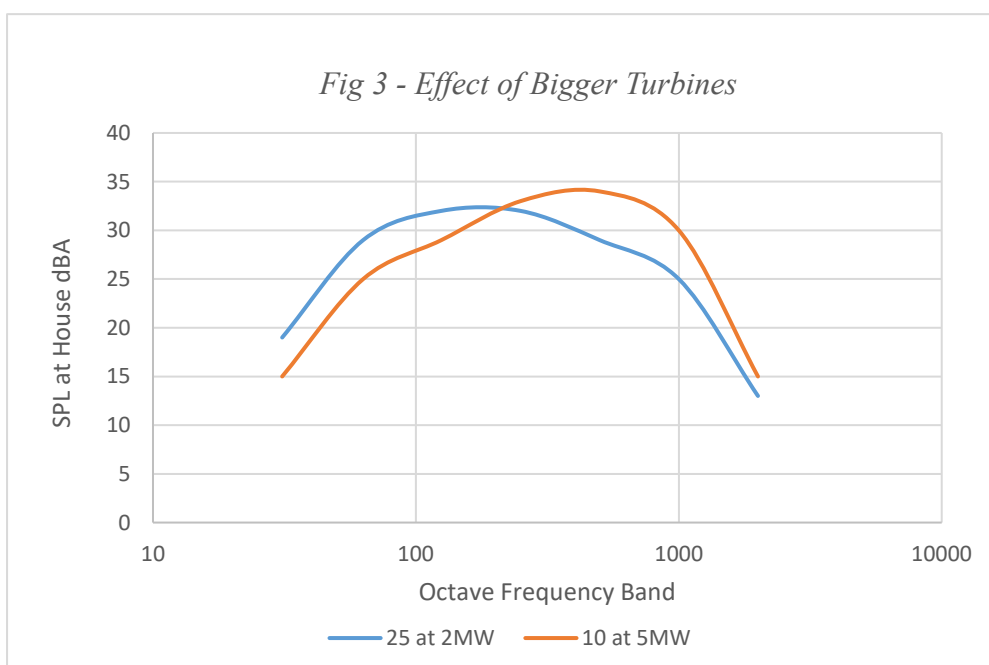
Will this increase in size continue? Undoubtedly turbines coming on stream in the next 4 or 5 years will be in the 5 to 6MW range with a height of up to 250m to blade tip because the applications being submitted and those consented but not yet built are in this range. Beyond that, is there a demand for still bigger turbines? It probably is, and technically, as far as the turbines themselves are concerned, there seems to be no reason why not, as much bigger turbines are becoming available for offshore. In most cases they would have to be run at much quieter modes onshore to meet noise limits. On the other hand there are good reasons why we might have reached a limit of size for onshore wind. There is increasing resistance to larger turbines for visual reasons and transportation of blades and other components becomes more difficult and more disruptive. There are a lot of other factors of course such as improvements in transportation techniques and perhaps we will see airships brought in to deliver turbines to site.

Fig 2 - Airship delivering turbine tower and base.



What of turbine noise itself? How has that changed? Only 3 years before the Berlin conference, IEC 61400-11 had standardised the method of measuring sound power levels of turbines to more or less the method we have now. Prior to that sound power was presented as a value at 8m/s and a slope of dB against wind speed. That suited stall regulated machines whose sound power increased steadily with wind speed but was no use for pitch regulation where sound power levelled off at 7 – 8m/s.

As pitch-controlled turbines have got bigger, unsurprisingly, they have become noisier, but the sound power level per MW seems to have stayed much the same. Perhaps counter-intuitively and certainly in contradiction to turbine sceptics, the increase has been concentrated more to the mid frequencies around 500 and 1k. And as the turbines got bigger less were needed on a particular site. So overall, for moderate sized wind farms, turbine noise at neighbours has not changed much in dBA terms but has shifted up in frequency rather than down. The figure here shows two turbine schemes for the same site fifteen years apart. The first one was 25 turbines at 2MW each and the second was 10 turbines at 5MW each. The



noise level at a neighbouring house about 1.4km away has gone up slightly from 35 to 36dBA but, as the figure shows, the increase is in the 500 to 1000Hz region and low frequency noise in the 31.5, 63 and 125Hz bands is significantly lower by 4-5dB. On the other hand the bigger turbine reaches its maximum sound level at 6m/s while the earlier one did not reach it's maximum until 8m/s (all wind speeds standardised). This is just one example but there does not seem to be any significant evidence that low

frequency noise has increased in the last 20 years and there does not seem to be any reason why it should do in the future.

3. SOURCE NOISE GENERATION

The modelling and testing of turbine noise sources was reported in Berlin where we saw the arrival of the now ubiquitous image by Stefan Oerlemans and Beatriz Méndez López in their paper about the SIROCCO project.

Fig 4 - Turbine Noise Sources



Thanks to Stefan and Beatriz for this iconic picture.

An EU funded project called DATA, had already looked at the acoustic design of blades in the few years before using a model turbine in a wind tunnel. The intention of the SIROCCO project was to extend this work to a full-size turbine. The turbine noise calculated by the model was validated using a measurement technique that would localise and quantify noise sources on the rotating blade. The aim of the project was to lower the level of noise by improving the aerodynamic flow at the trailing edge of the blades.

The EU Research and Development Information Service says that “The work carried out by the SIROCCO project has enabled silent, high performance airfoil sections to be developed for the wind turbine industry”. I don’t think that is quite the right story but it formed the basis of future work on airfoil noise.

Schepers in the next conference in 2007 brought us more information about SIROCCO and in 2009 there were four papers dealing with source noise, mainly design of airfoil shape to reduce noise. By 2011 there were 8 papers on source noise with more complex computational models. Significantly there was the first paper (by Petitjean and others) with some results for serrated trailing edges though the effect of serrations was discussed by 4 presenters in the 2005 conference and had been presented elsewhere by Oerlemans and others in 2001. The number of papers on source noise generation peaked in 2015 and 2017 in Glasgow and Rotterdam at 17 and 14 respectively. Recent conferences have seen fewer papers.

It might seem a stupid question but why do we want to reduce turbine noise? Of course it depends on whom you ask. If you ask the windfarm neighbour they will say that it is because it will reduce the noise and improve their amenity. If you ask the developer they will say that that it allows them to get more turbines on a site without breaching the noise limit. In a discussion in Lisbon in 2019, whilst consultants and regulators found trailing edge mitigation research interesting and sometimes helpful, developers saw it as essential to drive down the cost of renewable energy. The fact of the matter is that noise levels at neighbours is determined by regulations; quieter turbines don’t mean quieter residences they mean more turbines.

So the pressure for more work on reducing turbine source noise will come from developers (and hence manufacturers as well). Much of this, if it happens, is likely to stay outside the public domain. There still seems to be some pressure but on the other hand, have we got almost as far as we can go in reducing turbine noise? There are other solutions that have been discussed at several conferences but not yet progressed as far as TES; for example, porous trailing edges, vortex generators and brushes.

We seem to have reached a peak in publicly available work on the reduction of turbine noise but perhaps technological advances will favour development of active noise reduction in some form.

4. Propagation

In 2005, we had no properly validated propagation methodology for wind farms, though there had been quite a bit of work done in the late 1990s to develop methodologies in individual countries and at a European level. Propagation of wind turbine noise often used “Danish Statutory Order on Noise from Windmills (Nr. 304, Dated 14 May 1991)” as produced by The Danish Ministry of The Environment. Hemispherical propagation and octave band absorption or 5dB per km air absorption. In 2005 Kragh, Plovsing and Bo Søndergaard from Delta reported using Nord2000 for wind farms and they were back in 2009 at Aalborg to report on the validation of Nord2000 for wind turbines. In the UK in 2009 the use of ISO 9613 became largely accepted with a set of defined inputs. By the time we met in Glasgow ten years ago, we thought we had got as far as we could – and perhaps we had. But the question of accuracy of propagation calculations would not go away.

One of the striking points that came out of the 2019 conference was the difference in research requirements between the consultants and regulators on the one hand and developers and manufacturers on the other. The former were generally happy with the quality of the models available. Models such as ISO 9613 and Nord2000, if used with care, were able to provide the answer within a couple of decibels and by being conservative, that was good enough for an environmental assessment. For developers and manufacturers, however, two decibels might make the difference between a viable or non-viable wind farm, so more accurate propagation methods and, importantly, verification of the methodology was important.

These pressures are likely to continue and the advance in technology is favourable so I can see that we will hear more about this in the next 20 years. It is likely that weather conditions and topography will be incorporated in more detail.

5. Amplitude Modulation

Frits Van den Berg gave two papers in 2005. The second one dealt with the difference between turbine noise in the day in an unstable atmosphere and at night in a stable one. In particular he concluded that the reason for amplitude modulation (though he did not call it that) was the difference between the angle of attack at the top and the bottom of the rotation due to the difference in wind speed because of wind shear, and that was often more at night. That explanation for AM has been developed and there is a consensus that this may be at least one cause. There are other possibilities though, including those associated with atmosphere – such as at a location upwind of a turbine which is in the shadow zone of the bottom of the rotor but not in the shadow zone when the rotor is at the top. Similar shadowing can be created by topography. All these have been discussed at conferences from time to time but not in great depth.

It is certainly a complicated issue and highly dependent on meteorological and topographical conditions. Most of the work that has been done has been theoretical and we do not really know how it occurs and so when it might happen. We also know little about how common and how severe it is.

AM seems to be a rather “British thing”. Of the roughly 30 papers on AM in the last 10 years, 50% have been from Britain. In Britain – and in Ireland where there have been a number of court cases where AM has been a factor in overturning planning consents – there is a perception among wind farm objectors that AM is a problem. It is a character of the noise unique to wind turbines and identifies in people’s minds, rightly or wrongly, why wind turbine noise is subjectively different from other noise and so more annoying.

Although several of the theories would suggest that bigger turbines would produce more AM than smaller ones there is not any compelling evidence that that is the case, but that may be because we do not yet have enough of the 150m plus high turbines in operation to have the evidence.

It is difficult to know whether there is significant demand for more work on AM. Wind farm neighbours are not in a position to drive research. Developers are not going to be interested in investing in research unless they are going to be penalised if their wind farm produces AM. Source noise is clearly the domain of the manufacturer. So one difficulty is that no-one has complete ownership of AM. There will be advances in our knowledge of the mechanism of AM in the future but how big those advances are, depends on what the next generation of turbines brings and on how much pressure there is from those who consider it a major issue.

6. Background Noise, Noise Limits and Compliance Testing

Some countries set noise limits relative to background noise – or at least as part of a hybrid limit. The UK has ETSU-R-97 which is a hybrid limit – 5dB above background noise or a fixed limit whichever is the greater.. Whether or not it was intentional, or whether it was based on precedent from other noise controls is not clear but relating turbine noise to background was a logical thing to do in the 1990s. Most turbines at the time were stall controlled so the sound power level continued rising with wind speed continuously in the same way as background noise. At about the time of our first conference, as I mentioned earlier, pitch-controlled turbines were taking over from stall control. When pitch control became dominant it might be argued that, because the turbine noise levelled off a point around 7 or 8m/s a fixed limit might be the better way of control. But none of that has actively driven the setting of limits anywhere as far as I know. Few limits have significantly changed in most countries over the last 20 years.

The turbines we have now are much more flexible pitch-controlled turbines that can, or might shortly be able to, be controlled in such a way as to shape the turbine noise level to the required noise limit. A turbine with 14 sound modes could presumably be controlled to run at the same sound power level in all winds or to follow a background noise curve.

So background noise data is still going to be needed at present. In any case it would arguably be required in the preparation of an Environmental Impact Statement under European and most other regulations as a statement of baseline conditions. Improvements in the measurement of background noise in the last 20 years have mostly come about through technological developments becoming available rather than driven by any specific demand. For example longer battery life and remote monitoring. It is often forgotten that the data processing is as important as data collection and it is increased speed and flexibility of data analysis and accumulated experience that have advanced. These have made it easier to recognise anomalies in the data such as water noise and the dawn chorus of birds and to evaluate topography more quickly.

It is difficult to see any great change coming in the measurement of background noise other than more automation and remote monitoring and in particular coordination of all the elements of the analysis. There is no driver for big improvements in accuracy. By 2045 perhaps we shall have much more of a soundscape approach to noise limits and to assessment methodology. I can see this as much more of a public awareness of soundscape generally.

The subject of compliance testing was a late starter in the conference series, perhaps because in the early days there were relatively few complaints. As time went on, more turbines were built and social media facilitated the setting up of residents and objectors groups complaints rose and there were more compliance measurements. Well before 2045, it should be possible for wind farm operators to get live feedback of the subjective and objective impact of their wind farm.

7. Impact on People

Of course, if there were no impact of wind turbine noise on people then we would not need to hold these conferences. In 2005, Eja Pedersen and Kerstin Persson Waye presented a paper which gave the results of a survey to establish the likelihood of being annoyed (rather and very annoyed) by wind turbine noise and concluded that there was little annoyance where turbines were designed to be below 35dB at a wind speed of 8m/s and about 10% of people were annoyed around 38 to 40dB. Equally important was that they looked at the way in which other factors moderated the reaction to noise. For example hardly anyone who was unconcerned with the change in the landscape brought about by turbines was annoyed by the noise. Pedersen, with others, did further work over the years which generally confirmed her first research and these, together with a few others were used by WHO in the 2018 Environmental Noise Guidelines for the European Region. David Michaud's extensive work in Canada which he reported in 2015 was too late for the WHO cut-off date but again was broadly supportive of earlier work including the influence of non-acoustic factors. It took longer for work on sleep disturbance to get going. Other than a clutch of papers in the 2011 conference which were largely inconclusive, there has been little reporting of the subject until the last 3 conferences.

By 2015 it had been established in several studies that there are no significant direct health effects on people. The notable impact that had been observed was on a segment of the population who experience health issues related to stress induced by annoyance. The implication of non-acoustic factors within the complaints about noise has been well known for over 50 years in the case of aircraft noise. In 2023, in Dublin, Hübner reported a previous paper [3] that the strongest predictor of annoyance in wind farm neighbours is the planning process. However, its not clear whether it is the process itself or the result of the process (to allow the wind farm to be built) that is the problem. Whilst there has been more research and some useful work, our overall knowledge of the situation has not changed much in the last 20 years though it does show signs of changing now. We can predict the proportion of the population annoyed at a particular noise level but we cannot get anywhere near predicting the impact on any individual because the level of noise is only one factor.

We have always had one or two delegates and contributors from the field of medicine – David Michaud, has been with us most conferences since 2005 and David Colby has been another regular. The last few conferences, and in particular the last one, have seen a welcome rise in other delegates with medical or associated expertise to bring more into the debate. The 2023 conference also saw a small shift of emphasis with a look at different perceptions stakeholders have of noise, and indeed of wind farms in general. It also looked in more detail at what conditions of turbine operation people were most annoyed. This, together with the possibility of getting feedback through Apps in real time, opens up new possibilities for control of wind farm noise.

Apps that allow residents to report their reaction to turbine noise and other aspects of turbines are possible. The apps allow people to feel they have more control if they can report annoyance easily. Also they give operators a better understanding of conditions under which annoyance occurs. The app can provide each residence with information about predicted noise levels and other factors such as shadow flicker. Combined with monitoring of weather conditions such an arrangement could provide very powerful information. But how could that possibly be converted into action. It is clearly not going to be acceptable to operators for the wind farm to be controlled solely by the views of the neighbours. In any case, though it is used by WHO, it has not been established that annoyance is the best measure to judge the impact of noise.

One problem is that we don't really know what the incidence of complaints is in the UK, and I'm not clear whether other countries have figures or not. It is clear that the number of people likely to be affected is a small proportion of the population because nearly all turbines are located in areas where population density is low.

8. Technology and Knowledge

I have discussed individual aspects of technology advances in wind turbines which have played key roles in advancing our knowledge of wind turbine noise and its effect on people. However, it is the general rather than the specific advance in technology and knowledge that, arguably, has made most of the difference in the last 20 years and almost certainly will in the next twenty unless perhaps Politics, which I discuss briefly in the next section, intervenes. It seems extremely unlikely that the progress of technology will diminish as we move forward in the next two decades. It maybe difficult, even for those who were working 20 years ago to remember how things have moved on since 2005. There was no Twitter/X, no Netflix, no significant mobile internet, no iphone though we did have the Blackberry. Less than half homes in the UK were on broadband, though probably more than half of businesses were. Speeds of 0.5 to 1Mbs were around the maximum for most people.

Fig 5 – Phone from 2005



Apart from a few people ahead of the game, we could not receive data remotely and in real time. LIDAR and SODAR were available but I am not aware of anyone using them for wind farm developments until about 2011. Sound Level Meter batteries needed a lead acid battery back-up to run for more than a week

When we look at the technological advances in the last 20 years, there is no reason why the next 20 years should not bring equally big advances. In fact it seems to me more likely that we will have a faster advance. Perhaps we could predict a few of these but most will evolve over time. There is little evidence of a major break with the current technology of three-bladed HAWTs. No doubt there is plenty of work going on in the background but it seems unlikely at present that we are suddenly going to discover that VAWTs or Multi-rotors some other innovation can be more efficient or profitable.

I suggest the most predictable advances will be with artificial intelligence. AI is already making inroads into acoustics. The writing of field notes to incorporate photographs, measurements, topography and weather automatically. Noise source identification and sound source location are all using AI now, though in early stages. It is inevitable that AI will be able to help us in the analysis of data and identify anomalies. I would expect individual companies and people regularly to write their own apps for targeted tasks – using AI to help with the software writing.

But, while AI will certainly be used to help develop turbine technology I do not see that, of itself, AI will change the direction in which technology moves - it is likely to have more influence, for the time being at least, on the way we work rather than the way hardware develops. More accurate propagation predictions will undoubtedly involve variations with weather, that means that real time weather information may be required on a wind farm site; the presence of amplitude modulation may be alerted by neighbours with smartphone apps (this already happens in pilot studies). Perhaps we will have AI driven AM monitoring stations; all these will be brought together and processed by AI, perhaps directly to modify the operation of the turbines but more likely to inform controllers in the first place. Things go together – if we can measure compliance more accurately then there is an incentive to make propagation calculations more accurate.

9. Conclusions

Demand over the last 20 years has been driven by our knowledge about climate change and how that will affect our futures. A consensus has built over a broad range of political views that we need to take action to mitigate the effects of climate change. But there is a spectrum of views on the urgency with which we need to do this – and of course some who do not believe the climate is changing at all. In an Irish High Court case [1] the interplay between local planning decisions and national climate obligations was tested. The developer sought permission to construct a 13-turbine wind farm and ABP, Ireland's national planning authority, denied the application, citing visual impacts and that the County Development Plan said the area was unsuitable for wind farms. The developer challenged this decision, and the High Court ruled that ABP had not adequately considered its obligations under the Climate Action and Low Carbon Development Act 2015. The judge said that climate goals should take precedence over concerns like visual impacts, stating, "An immediate end to business as usual is a precondition for planetary survival."

Similarly there is strong political pressure to build wind farms in most jurisdictions though with varying enthusiasm. But political pressures change happens. Since 2005, there have been four presidents of France, four presidents of the USA and eight Prime Ministers of the UK! Though things change more slowly elsewhere - Angela Merkel became chancellor of Germany just two months after our first conference in Berlin in 2005 and has not long ago been replaced.

Nevertheless, even if there is a dramatic change in technology or a dramatic change in world politics, I think we shall still building wind farms and assessing noise from them in 2045.

Acknowledgments

Thanks to Wikipedia, ChatGPT and Microsoft Co-Pilot for their assistance.

References

- [1] Coolglass Windfarm Limited v. An Bord Pleanála [2025] IEHC 1
- [2] <https://www.gov.uk/government/publications/renewable-energy-planning-database-monthly-extract>
- [3] Pohl, J., Hübner, G., Liebig-Gonglach, M., & Hornberg, C. (2020). Verbundvorhaben: Objektive Kriterien zu Erschütterungs- und Schallemissionen durch Windenergieanlagen im Binnenland (TremAc); Schlussbericht zu den Teilvorhaben Umweltpsychologische Analyse der Windenergie-Immissionswirkungen auf Akzeptanz und Wohlbefinden der Anwohner (MLU) und Umweltmedizinische Analyse der Wirkung von Windenergieanlagen auf Gesundheit und Wohlbefinden von Anwohnern/innen (UBI).

Paper #3 - ID: 333

Title: A High-Fidelity, Multi-Disciplinary Framework for Wind Turbine Aero-acoustic and Vibro-acoustic Noise Reduction

Author: Wouter van der Velden

11th Edition of the
International Conferences on
Wind Turbine Noise

Copenhagen, Denmark – 10th to 13th June 2025

**A High-Fidelity, Multi-Disciplinary Framework for Wind Turbine
Aero-acoustic and Vibro-acoustic Noise Reduction**

W.C.P. van der Velden

Dassault Systèmes B.V. , 's-Hertogenbosch, the Netherlands

S. Mulski, M. Fries, D. Casalino

Dassault Systèmes Deutschland GmbH, Stuttgart, Germany

D. Singh

Dassault Systèmes Solutions Lab Private Ltd, Pune, India

Summary

Wind energy, led by wind power's rapid global growth is advancing in both scale and technology. However, increasing turbine size and density has raised concerns about noise emissions. This paper outlines practical workflows for predicting and mitigating both broadband (aero-acoustic) and tonal (vibro-acoustic) noise using Dassault Systèmes tools. Aero-acoustic noise, primarily from blade trailing edges, is addressed through optimized serration designs, achieving up to 4 dB reduction. Tonal noise from drivetrain components is analyzed through multibody and vibro-acoustic simulations to identify dominant noise paths. The study emphasizes high-fidelity modeling, simulation efficiency, and IP-protected collaboration, while highlighting the need for ongoing research to refine mitigation strategies and improve simulation accuracy with real-world data.

1. Introduction

Renewable energy has become one of the fastest-growing and most affordable energy sources globally. Wind power is currently the cheapest source of electricity [1], which has seen a 12.5% global growth in 2023, equaling 116 Gigawatts of added capacity. Installations in China made up over 65% of the global market and saw a 19.2% growth in 2023, with 75 Gigawatts being added [2]. As a result of this massive expansion, not only is technology advancing rapidly—evidenced by the world's largest turbine with a rotor diameter of 310 meters and a 26 MW rating, capable of powering 55,000 homes with an average wind speed of 10 m/s [3]—but wind energy capacity density is also increasing. As wind turbines proliferate, concerns over their acoustic footprint (Fig 1), especially in densely populated and environmentally sensitive areas, have intensified.

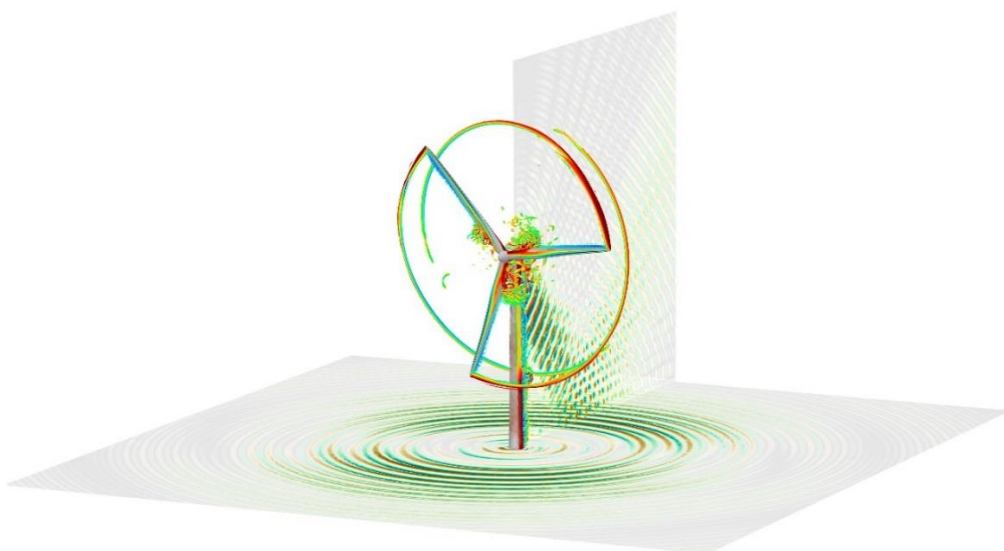


Figure 1 This visualization displays the near-wake aerodynamics and acoustics of the NREL 5MW.

Although court cases in which local residents sue wind turbine operators because of noise issues are extremely rare, stricter regulations have come into effect. In Germany, wind turbines are regulated like other technical installations, with nighttime total cumulative noise limits set at 35 dB(A) in residential areas, 40 dB(A) in small urban areas, and 45 dB(A) in villages and mixed-use zones [4]. Wind parks are sometimes forced to operate at reduce capacity in order to comply with regulations, leading to a loss of revenue.

The noise spectrum of wind turbines can be decomposed into broadband and tonal contributions as illustrated in Fig 2. Broadband noise is caused by flow-induced noise generation mechanisms when the blades pass through the air. In contrast, tonal noise is associated with the drivetrain vibrations that propagate through the nacelle, tower and blades, from where noise is radiated. It is characterized by the distinct, narrow-band frequencies and becomes particular intrusive when exceeding the broadband aero-acoustic noise. Predicting the noise emitted by a wind turbine therefore requires calculating both the broadband aero-acoustic and the tonal vibro-acoustic contributions. This paper outlines two workflows for calculating both contributions in a practical way, using tools and methods from Dassault Systèmes available to all. In addition, noise mitigation techniques are discussed which provide a competitive edge and can enhance the availability of clean and inexpensive sustainable energy.

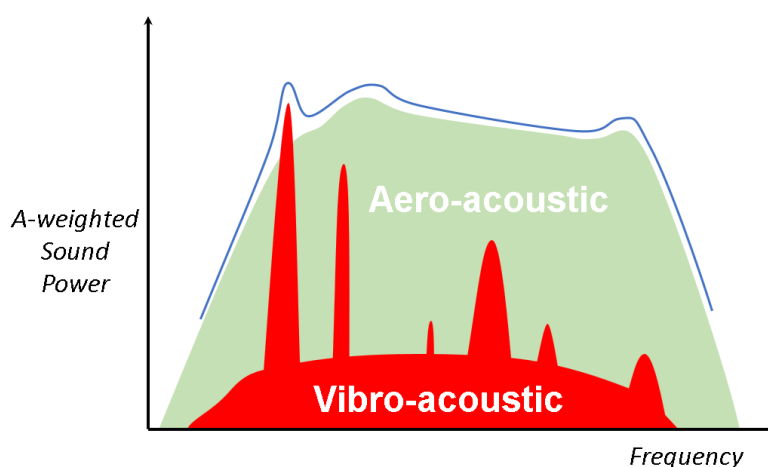


Figure 2 Radiated sound power spectrum of a wind turbine. Tonal mechanical noise, in red, becomes noticeable with decreasing aero-acoustic levels, in green [10]

2. Aero-acoustic noise

As rotor diameters increase, prototyping costs rise, making digital simulations essential. Larger blades also amplify flow-induced noise, impacting nearby communities. While some noise can be reduced through blade design, minimizing trailing-edge noise remains a challenge. Optimizing aerodynamics and aeroacoustics is key to efficiency and cost reduction. This section explores how aerodynamic simulations can optimize blade serrations to reduce trailing-edge noise. Serrations are a proven noise reduction method, achieving up to 7 dB in wind tunnels and 3 dB in real-world applications. The discrepancy stems from differences in noise propagation and local aerodynamic conditions, highlighting the need for accurate 3D modeling.

2.1 Methodology

The 3DS wind-turbine aerodynamic noise simulation framework integrates blade design, aerodynamic analysis, and noise prediction. Blade geometry is designed and optimized using CATIA® and a BEMT tool, with shape optimization managed by SIMULIA Process Composer. This process is conducted on the 3DEXPERIENCE® platform.

The framework begins with geometry preparation, which converts an unstructured mesh into a structured blade mesh. BEMT calculations determine lift and drag, followed by SIMULIA PowerFLOW® simulations using two workflows: (i) 2.5D trailing-edge noise (TENoise), or (ii) 3D rotor aeroacoustics (MAAS). The 2.5D method is about ten times less computationally demanding than 3D simulations, with radial strips selected based on prior low-fidelity results. Results were validated in past publications [5,6,7,8].

In the final step the wind-turbine noise spectra at ground-level microphones is computed using a FW-H solver. In summary, the methodology can handle three different fidelity levels:

- Low-fidelity: Semi-analytical airfoil noise model based on wall-pressure data.
- Mid-fidelity: Sectional noise spectra using FW-H on 2.5D PowerFLOW simulations.
- High-fidelity: One-blade noise spectra via FW-H.

Virtual microphone arrays capture noise across multiple rotor revolutions, applying Doppler and atmospheric absorption corrections. In lower fidelity cases, the 3D-to-2D transformation matrix adjusts microphone positions before noise calculations. Further details on the physical models are in Casalino et al [5].

2.2 Baseline results

This paper uses the NREL 5MW demonstration wind turbine as a reference. Fig 3 presents a typical far-field noise spectrum at a 100 m downwind distance, emphasizing the broadband nature of turbulent boundary layer trailing edge noise. Additionally, Fig 4 displays the Overall Sound Pressure Level (OSPL) map, illustrating how noise changes with blade rotation. Maximum noise radiation occurs approximately 45° before the blade reaches its lowest position, consistent with trailing-edge noise patterns observed in earlier field tests by Oerlemans et al. [9].

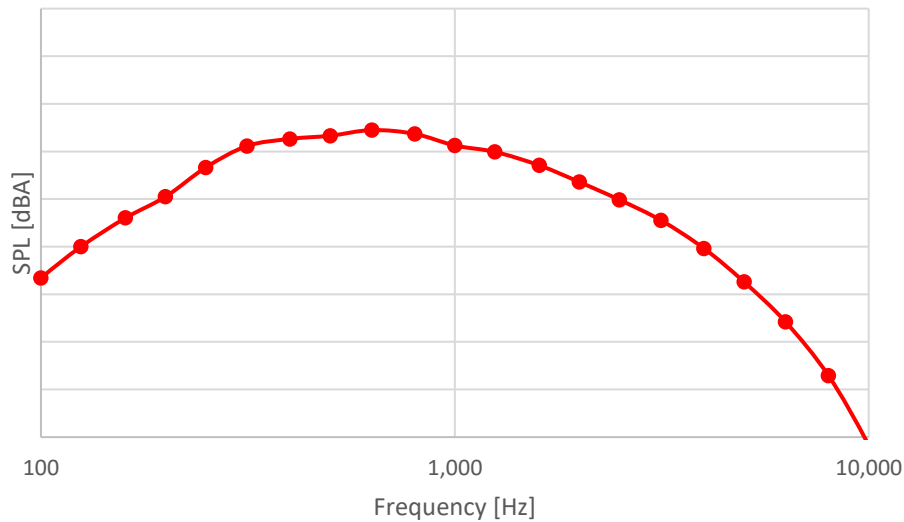


Figure 3 Far-field noise 1/3-octave band spectrum at a downwind distance of 100m on the rotor axis, no ground reflection.

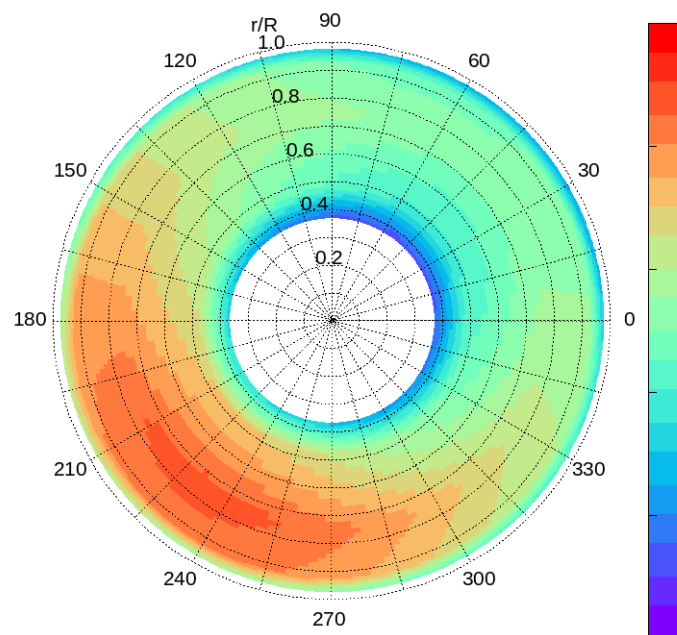


Figure 4 OSPL [dB] map for a baseline single blade, over one rotation along the blade's radius. Microphone is placed at a 100-meter downwind location on ground. Blade rotation is counter-clockwise, with 90 and 270 deg indicating sky position ground position respectively.

2.3 Serration location definition

This framework aims to optimize serrations for full-scale wind turbines, as wind tunnel tests and simulations alone cannot reliably predict certification noise levels. The 2.5D methodology offers accuracy comparable to 3D simulations at a lower computational cost, making it ideal for this process. Since designers typically create planar serrations and current semi-analytical trailing-edge noise models lack strong predictive capabilities, the study focuses on 2.5D PowerFLOW simulations (mid-fidelity branch).

Low-fidelity BEMT analysis identifies key radial sections for high-fidelity 2.5D simulations. As shown in Fig 5, the sections at 45 m and 55.5 m ($r/R = 0.75$ and 0.925) dominate noise levels for the 60 m radius blade. These sections (green dots) and their local flow conditions from BEMT are used for serration modeling, while baseline 2.5D results are reused for other sections (blue dots).

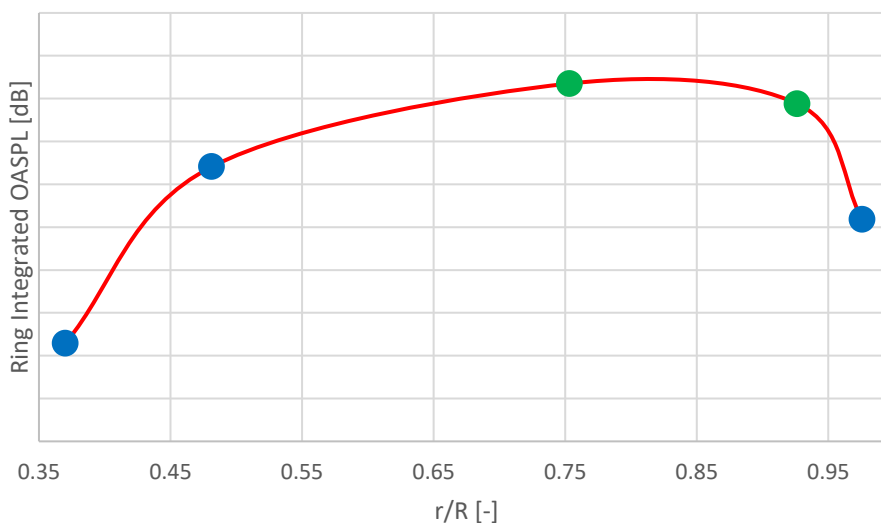


Figure 5 Integrated far-field noise along radial position, together with the 5 radial sections of 2.5D calculations. The green points indicated the sections where serrations have been applied.

Two serration designs are tested: type A (sharp tip/root) and type B (rounded tip/root). Serration length is set at 10% of the local chord, with flap angles from -11° to -5.5° , aligning with the suction side profile and wake, respectively. To model full-scale wind turbine noise, results from five sections (green and blue dots) are interpolated along the blade radius to estimate total acoustic energy.

2.4 Full-scale far-field noise results

The 2.5D methodology enables noise evaluation of a three-bladed serrated wind turbine without full 3D simulations. Fig 6 compares serrated blade configurations to the baseline, with measurements taken 100 m downwind and 1.2 m above ground per IEC certification. Ground reflection and atmospheric absorption are included.

The delta plot shows that all serration configurations reduce noise below 500 Hz, while the moderate flap angle (-5.5°) further lowers noise up to 1 kHz without significant increases elsewhere. The largest reduction (~ 4 dB) occurs at 200 Hz for the moderate angle, whereas the -11° flap angle increases noise by 4 dB at 1 kHz. This confirms the moderate angle's effectiveness, aligning with Romani et al. [9]. Type A and B serrations show minor differences, with type A performing interestingly slightly better at low frequencies in particular.

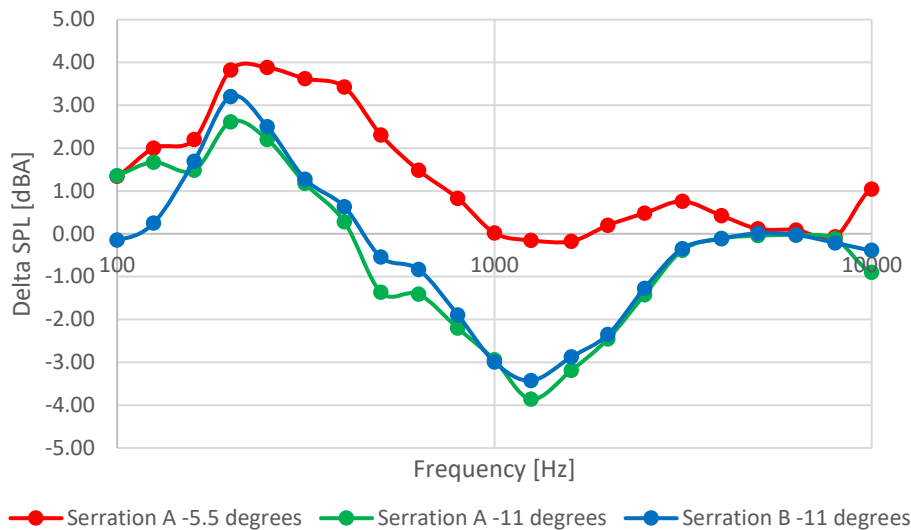


Figure 6 Far-field noise 1/3-octave delta band spectrum with respect to baseline at a downwind distance of 100m at 1.2 m from ground, with reflection.

3. Vibro-acoustic noise

As aero-acoustic levels continue to decrease through the application of advanced simulation methods, previously concealed tonal noise become increasingly prominent. Its high perceptibility makes tonal noise particularly intrusive, which necessitates new mitigation strategies, as traditional noise reduction approaches that are effective for broadband noise may not adequately address tonal noise. This section presents a combined workflow of multibody and vibro-acoustic simulations for calculating the tonal noise of wind turbines efficiently. It offers powerful insights on the dominant transfer path along which noise mitigation measures will be most effective. The workflow uses Simpack® [11] to predict the vibrations induced by drivetrain excitations and their propagation through the wind turbine to the sound radiating bodies such as the tower. The subsequent radiation of noise is then governed by the vibroacoustic software wave6® [12].

3.1 Excitations

The most common sources of tonality in a wind turbine systems stems from gearboxes and generators, which are illustrated in Fig 7. Within the gearboxes, the excitations are primarily caused by the non-constant load transfer between the meshing gears. Likewise in generators, the vibration commonly arises from the electromagnetic interactions between the poles of the rotor and stator. For this work, we focused on the gear pairings as our vibrations source.

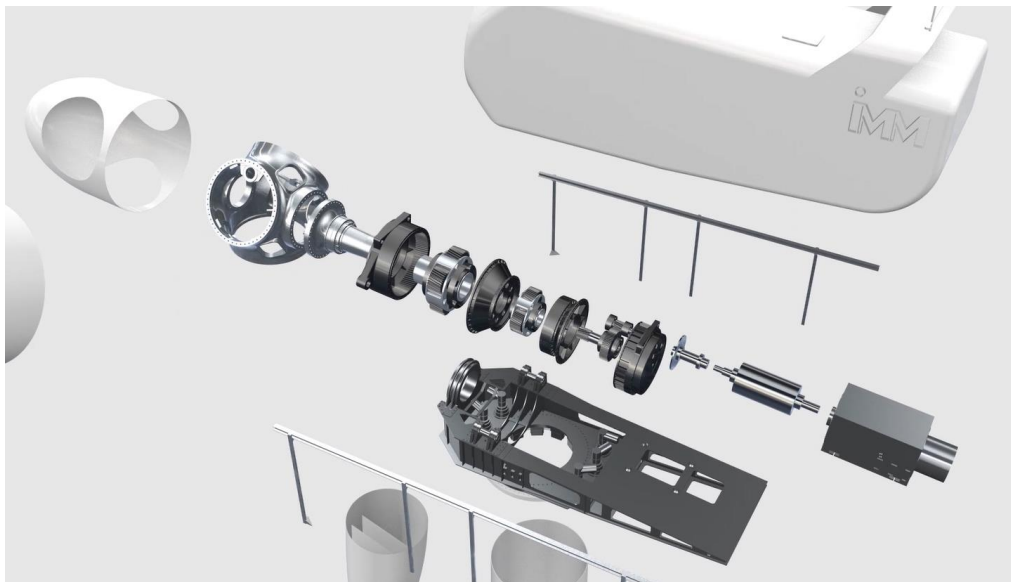


Figure 7 Exploded view of 5MW wind turbine drivetrain components consisting of two planet stages and one helical stage.

As gear wheels engage, the number of gear teeth in contact is continually changing, for example, continually jumping between three and four teeth being in contact. This changing stiffness is the main source of vibration within gearboxes and results in Transmission Error (TE). Generally, wind turbines employ helical gears, as opposed to spur gears in order to reduce noise (reversing in a car is often noticeably louder than driving forward, as spur ‘reverse’ gears are used to reduce manufacturing costs). See Fig 8. Additionally, micro-geometry corrections on the tooth flanks are applied in order to reduce TE. Under ideal conditions, micro-geometry can be optimized and can almost completely eliminate TE. However, this optimization is only valid for one specific load. Since micro-geometry must be optimized over a wide range of loading scenarios that a wind turbine is subjected to, TE can only be mitigated and not completely eliminated.

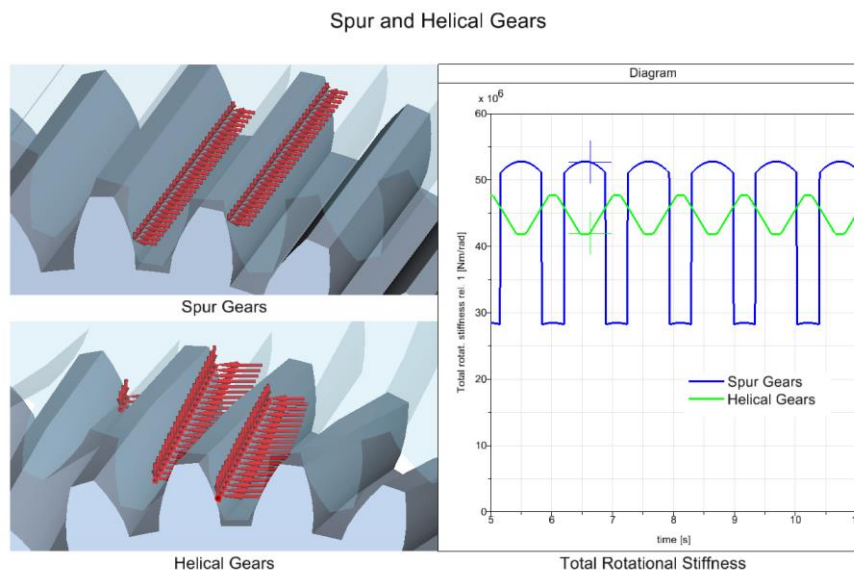


Figure 8 Changes in rotational stiffness due to gear meshing, spur gears (blue curve) and helical gears (cyan curve)

3.2 Multibody system simulation

In order to correctly generate and predict the excitations and vibrations within a wind turbine, Finite Element (FE) models are used within high fidelity holistic Multibody System (MBS) simulations. The FE models must accurately capture deformations and high frequency vibrations of not only the major components, such as the tower, blades, bedplate and gearbox housing, but also smaller components, e.g.

shafts, planet carriers and gearwheels. These components are assembled within MBS along with many other detailed necessary components, for example non-linear bearings, bushings and gear wheel pairings (non-linear refers to the non-linear changing stiffness under different loading conditions, Fig 9). These highly specific, and not unduly burdened, elements enable very efficient system simulation over the complete range of necessary simulation scenarios. In addition, MBS, combined with imported FE models, significantly simplifies understanding of complex vibration phenomena due to the many various abstraction levels that can be easily employed and compared.

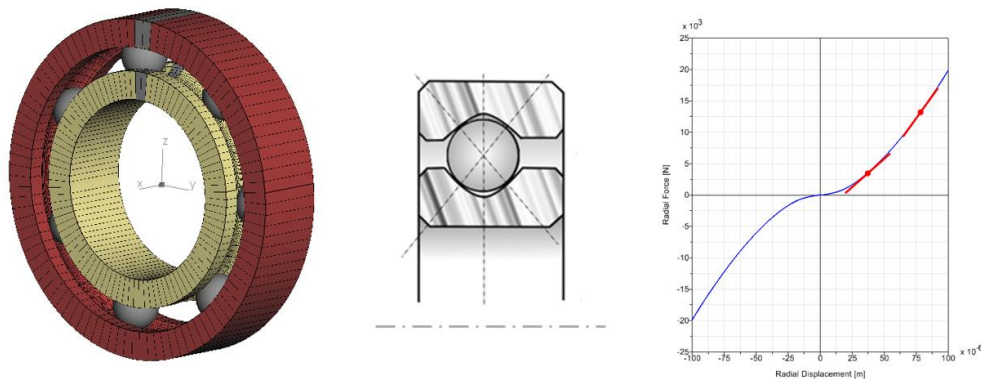


Figure 9 Four point rolling bearing. Blue curve shows non-linear radial stiffness. Depending upon state of model during linearization, different linear stiffnesses are achieved, highlighting the need to investigate a range of loading conditions as these different linear stiffnesses will affect results

The high-fidelity holistic MBS cannot only describe the drivetrain performance but also how drivetrain vibrations propagate through various paths to the sound radiating components, such as the tower, where the vibrations become audible as mechanical noise. Typically, three main transfer paths are distinguished as illustrated in Fig 10: First, the structure-borne transmission through the bearings and mainframe to the nacelle cover and tower, which subsequently radiate sound. Second, the structure-borne transmission through the gears and main shaft to the blades that radiate sound. Third, the radiation of sound by the gearbox housing and the subsequent airborne transmission through the nacelle cover and louver. The relevance of each transfer path to the perceived noise depends on the excitation, which is affected by the specific loading condition, the frequency and the vibro-acoustic design of a wind turbine. Large forces and moments on the drivetrain cause transvers and angular misalignments of the gearwheels effecting TE. Large thrust force and torque on the rotor significantly affect the distributed loading between the flexible bedplate and tower via the yaw bearing, which in turn excite different tower modes and magnitudes thereof. In addition, a significant component of the transfer path can sometimes be through the yaw drives systems around the top of the tower.

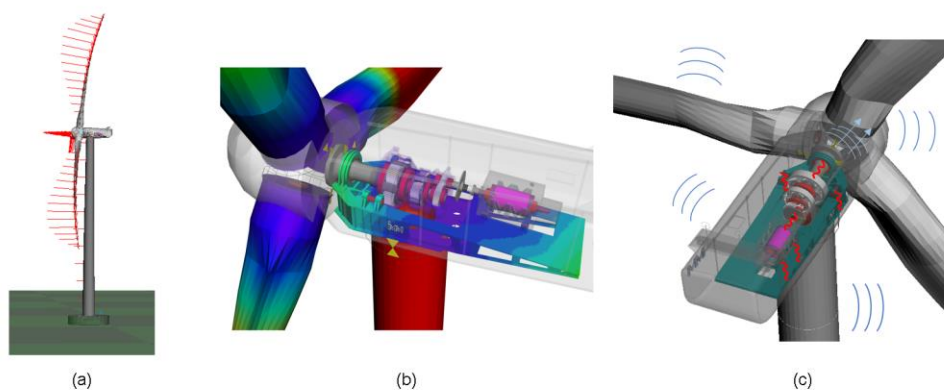


Figure 10 Large thrust forces and torque causes extreme and uneven loading and deformation on many components (a, b). Transfer paths, from gear meshing to radiating surfaces, highlighted in red (c), are dependent upon loading

Particular attention should be given to the modelling of the yaw bearing to ensure accurate predictions. The yaw bearing commonly consists of two rows of four-point ball bearings or a combination of ball and roller bearings, see Fig 11. Correct modelling with attention to the prestress forces is essential for accurate transfer of forces between the bedplate and tower.

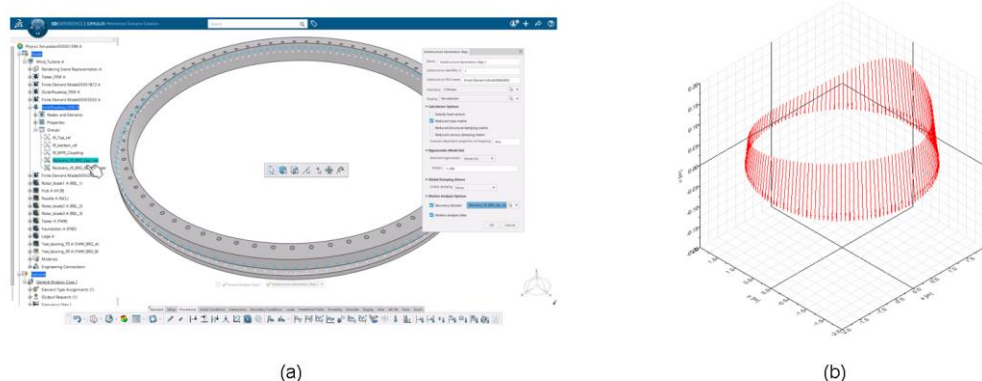


Figure 11 Yaw bearing. Detailed design in the 3DEXPERIENCE® Platform (a) and distributed loading from the bedplate through to the tower top via the yaw bearing in Simpack (b)

The MBS simulations can be carried out in either time or frequency domain. For tonality investigations we are mainly concerned with high frequency, low amplitude, and quasi-static vibrations. By linearizing the non-linear holistic model at specific states, efficient analyses can be carried out in the frequency domain using Linear System Analysis. It is important to note that a very large range of different linearization states, with appropriate corresponding excitations, is necessary to correctly generate a realistic meaningful scatter of results. This poses high demands on the computational efficiency of the MBS simulation, as well as the subsequent vibro-acoustic analysis. Due to the numerous nonlinearities in wind turbine models, some simulations are conducted in the time domain to ensure that certain effects are not unintentionally neglected and to simplify overall workflows.

3.3 Noise Radiation and Ground Measurements

The vibro-acoustic model of the wind turbine covers the second part of the transmission paths and accounts for the sound radiation, the subsequent transmission through other bodies as well as the scattering by other objects and the ground. Its inputs are the surface vibrations of the sound radiating bodies calculated in the MBS simulation. These bodies are commonly represented by flexible bodies in modal coordinates, see Fig 12 for an example of four mode shapes of the tower. Using modal reduction allows to express the surface vibration as a linear combination of mode shapes and modal participation factors (MPF). This offers significant benefits compared to a nodal representation. Variations within the MBS model such as different linearization states or gear meshing excitations typically do not change the modes of the sound radiating bodies but only the MPF. Solving the vibro-acoustic model for a different set of MPF can leverage information of previous solves allowing for a rapid assessment of the radiated noise. An additional advantage lies in the possibility to calculate how individual modes contribute to the sound pressure level at the IEC locations. This provides insights on the relevance of individual modes, which is particularly valuable for developing noise mitigation strategies.

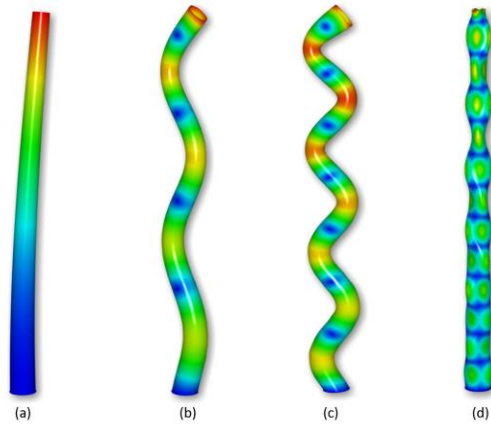


Figure 12 Mode shapes of the tower. Natural frequencies are increasing from (a) to (d)

The vibro-acoustic model consists of a finite element model of the interior acoustic cavity within the nacelle, a structural finite element model of the nacelle cover and a boundary element model of the exterior acoustic half-space surrounding the wind turbine. Surface vibrations of the gearbox housing, the nacelle and the tower are taken into consideration. The sound radiation from the blades is neglected for simplicity but could be included within the workflow. The reflecting ground is assumed flat and receivers are located at the IEC locations and at multiple planes inside and outside the nacelle. An illustration of the absolute sound pressure field at 50Hz is shown in Fig 13. Evaluating the sound pressure level at the IEC locations for frequencies of up to 200Hz yields the narrowband spectrum presented in Fig 14.

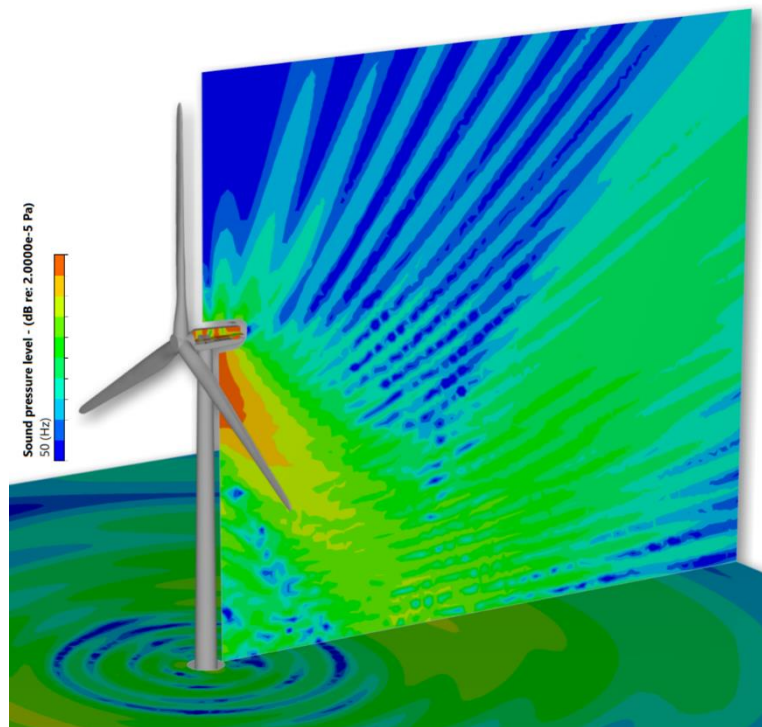


Figure 13 Absolute sound pressure field at 50Hz due to sound radiation of the gearbox housing transmitted through the nacelle and the structure-borne noise radiated by the tower.

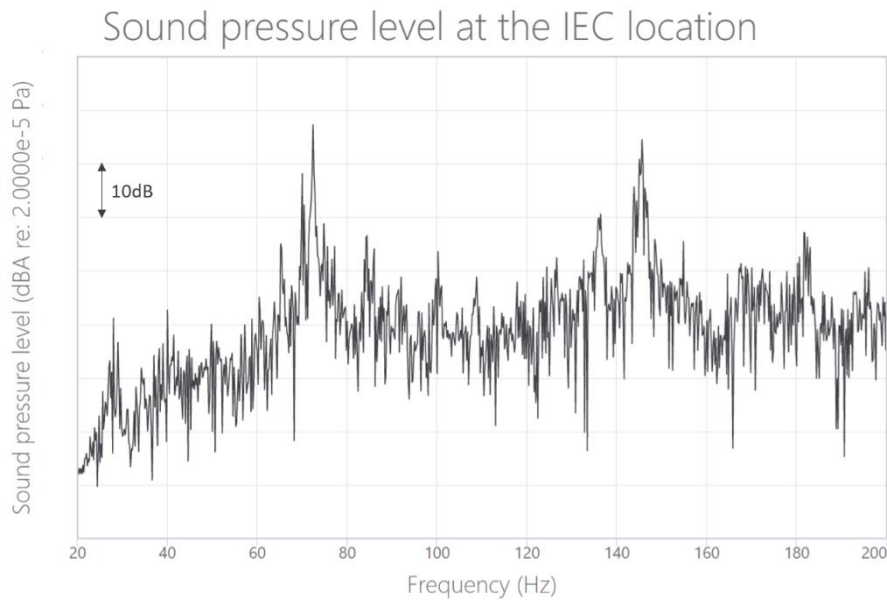


Figure 14 Sound pressure level at the IEC locations for a given gear meshing excitation

3.4 IP Protected Collaboration

The illustrated high fidelity holistic system models commonly consist of an assembly of sub-systems from suppliers and original equipment manufacturers (OEMs). All involved parties require simulation tools that enable model sharing and integration, with the ability to retain proprietary technology, as collaborations are rarely exclusive. Companies can overcome this Intellectual property (IP) protection issue by only exchanging state-space matrices (SSM) of the sub-systems. However, these matrices are only valid for one static, or quasi-static state, and can only be used for frequency domain analysis methods. The required number of SSMs for each sub-system increases significantly with model fidelity and size of the system and non-linearities therein, in order to accurately cover the extensive range of loading conditions.

Another viable solution, which is software specific and available in Simpack, enables users to export a sub-system, as a ‘BlackBox’ model, which can then be subsequently imported and assembled into holistic system models. See Fig 15 for a graphical illustration. Apart from protecting any sensitive model data, this method has the advantage that it can be used with any solver method, either in the frequency or time domain. In addition, the user who generates the BlackBox model can make specific model parameters and data modifiable by the BlackBox model user. For example, users of BlackBox models can carry out system DoE by varying the location of a bearing or exchange a flexible body data file, within the protected subsystem. The choice of which data to protect or enable access to, is completely up to the creator of the BlackBox.

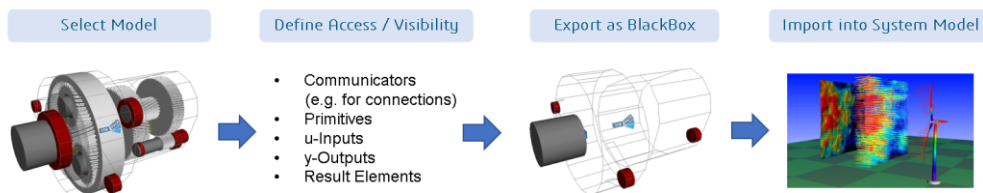


Figure 15 Blackbox workflow, which enables protection of sensitive data during collaboration

4. Conclusion

As wind energy expanded rapidly, addressing noise emissions became increasingly critical for regulatory compliance and public acceptance. This paper presented a practical framework for predicting and mitigating both broadband aero-acoustic and tonal vibro-acoustic noise in wind turbines. The aerodynamic noise reduction workflow leveraged 2.5D to optimize blade serrations, achieving up to 4 dB noise reduction in critical frequency ranges. The vibro-acoustic workflow combined multibody and finite element

simulations to assess tonal noise transmission paths, providing key insights into the dominant contributors to tonal emissions.

The findings demonstrated that targeted serration designs effectively reduced low-frequency broadband noise, while drivetrain modeling identified key vibration sources influencing tonal noise propagation. However, further research is needed to refine noise mitigation strategies, particularly in optimizing serration geometries for varying wind conditions and developing advanced materials to dampen structural vibrations. Additionally, integrating real-world operational data with high-fidelity simulations could enhance predictive accuracy and support adaptive noise control strategies.

Vibro-acoustic analysis requires high-fidelity system simulations that integrate multiple disciplines, including finite element analysis (FEA), multibody simulation (MBS), and acoustic analysis. To accurately understand system behavior and facilitate noise mitigation, simulations must encompass the full range of loading conditions. The detailed modeling of components within the holistic system models requires close collaboration between suppliers and OEMs, for which the disclosure of sensitive data is no longer necessary. However, further research and development in this field remain essential. For example, methodologies for accurately predicting gear-pairing transmission error—a primary source of vibro-acoustic noise—across the entire load spectrum are continually being further developed and enhanced to improve efficiency and performance.

As wind turbines continue to grow in size and efficiency, addressing noise challenges will remain a crucial aspect of sustainable energy development.

References

- [1] Levelized cost of electricity by source https://en.wikipedia.org/wiki/Cost_of_electricity_by_source
- [2] WWEA Annual Report 2023: Record Year for Windpower <https://wwindea.org/AnnualReport2023>
- [3] World's First 26 MW Offshore Wind Turbine Rolls Off Production Line <https://www.offshorewind.biz/2024/10/14/worlds-first-26-mw-offshore-wind-turbine-rolls-off-production-line/>
- [4] M.Marini, C.C.Mastino, R.Baccoli, A. Frattolillo, A. Di Bella, "Implementation of the Issue of Noise from Wind Turbines at Low Frequencies", *23rd International Congress on Acoustics, September 2019 Aachen, Germany* <https://pub.dega-akustik.de/ICA2019/data/articles/001517.pdf>
- [5] D. Casalino, W.C.P. van der Velden, and G. Romani, "A Framework for Multi-Fidelity Wind-Turbine Aeroacoustic Simulations," *28th AIAA/CEAS Aeroacoustics 2022 Conference*, June 2022, doi: <https://doi.org/10.2514/6.2022-2892>
- [6] W.C.P. van der Velden, D. Casalino, and G. Romani, "Full-Scale Serrated Wind Turbine Trailing Edge Noise Certification Analysis Based on the Lattice-Boltzmann Method," *AIAA SCITECH 2023 Forum*, Jan. 2023, doi: <https://doi.org/10.2514/6.2023-0970>
- [7] "LM Wind Power," *Dassault Systèmes*, Apr. 15, 2024. <https://www.3ds.com/insights/customer-stories/lm-wind-power> (accessed Jan. 31, 2025).
- [8] A.F. Ribeiro, W.C.P. van der Velden, D. Casalino and G. Wang, "Aeroacoustic Simulations of a Wind Turbine: Validation With Field Tests, Including Trailing-Edge Serrations", *30th AIAA/CEAS Aeroacoustics 2024 Conference*, June 2024, doi: <https://doi.org/10.2514/6.2024-3287>
- [9] S. Oerlemans, P. Sijtsma and B.M. Lopez., "Local and quantification of noise sources on a wind turbine," *Journal of Sound and Vibration*, Vol. 299, 2006, pp. 869–883. doi: <https://doi.org/10.1016/j.jsv.2006.07.032>
- [10] C. Schwarz, "Simulation-Based Wind Turbine Gearbox Tonality Analysis and Risk Assessment", *5th Wind & Drivetrain Conference*, SIMULIA Wind Turbine Community, <https://www.3ds.com/products-services/simulia/solutions/infrastructure-energy-materials/wind/>
- [11] Simpack MBS software, <https://www.3ds.com/products/simulia/multibody-system-dynamics-motion-simulation>
- [12] wave6, Advanced Noise and Vibration Analysis software <https://www.3ds.com/products/simulia/wave6>

Paper #4 - ID: 335

Title: Production Optimized Noise Curtailment on Wind Farms

Author: Thomas Sørensen

11th Edition of the
International Conferences on
Wind Turbine Noise

Copenhagen, Denmark – 10th to 13th June 2025

Production Optimized Noise Curtailment on Wind Farms

Thomas Sørensen, ts@emd.dk and Moritz Hildemann
EMD International A/S, Aalborg Ø, 9220, Denmark

Summary

Wind farm operators face the challenge of balancing noise regulation compliance with energy production goals. When wind farms are already installed or the planned positions are decided upon, the remaining option is to control the operation modes of the turbines, also referred to as curtailment. The curtailment of wind turbine modes or stopping them completely comes with reduced noise emission but also reduced energy production. The purpose of noise curtailment optimization in the context of wind farm planning is to satisfy acoustic constraints while maximizing the usual benefits, e.g. energy production or profit. This study presents a flexible curtailment optimization method designed to address this complex issue. The method's key strengths lie in its adaptability to different noise propagation models, consideration of multiple environmental variables, and ability to handle non-linear wake interactions. By employing a heuristic optimization approach, the algorithm effectively navigates the np-hard problem of wind farm curtailment. It successfully generates optimal operational strategies that meet noise regulations while maximizing energy production. The algorithm is designed for easy adaptation to evolving regulatory landscapes, such as Germany's "area of influence" concept, and efficiency. Results demonstrate the method's capability to find optimal curtailment plans even when initial noise levels significantly exceed permitted levels. The improved algorithm resulted in production gains of 5.2% compared to a common industrial approach due to improvements of the proposed optimization method. Furthermore, the ability to optimize under varying meteorological conditions contributed an additional 2.7% increase in energy production. Finally, the integration of the 'area of influence,' yielded another relative production gain of 4.9%. This research contributes a valuable and flexible solution to wind farm noise modellers, offering a solution that enables wind farm noise compliance in various conditions with minimal impact on production. The proposed optimization tool overcomes both theoretical and practical implications, providing a significant contribution to the wind energy industry. The work was executed within the DECOWIND project, which was supported by Innovation Fund Denmark and included participation by the Technical University of Denmark (DTU), Siemens Gamesa Renewable Energy, FORCE Technology and EMD International A/S.

1. Introduction

Wind farms must comply with noise regulations, and two approaches are being used to ensure compliant noise emission levels at noise receptors emitted by wind turbines: control the turbine position [1] or control the turbine operation modes [2]. When wind turbines are already installed or the planned positions are decided upon, the remaining option is, therefore, curtailing the operation modes of the turbines. The curtailment of wind turbine modes comes with reduced noise emission but also reduced energy production

[3]. The purpose of noise curtailment optimization in the context of wind farm planning is to satisfy acoustic constraints while maximizing the usual benefits, e.g., energy production or profit.

The strategic curtailment of wind turbines to comply with noise regulations while maximizing energy production presents a critical challenge in wind farm operations. This optimization problem exhibits inherent complexity due to its NP-hard nature, stemming from non-linear wake interactions and discrete operational constraints across multi-dimensional meteorological conditions. At its core lies a fundamental dependency: the calculated noise emission and immission levels at noise receptors directly depend on the acoustic propagation model mandated by regional regulations, which vary substantially across jurisdictions. It is important to carefully define the noise propagation model, such as the general ISO 9613-2 [4] noise model or the NORD2000 model.

Current regulatory frameworks prescribe specific implementations of standardized models like ISO 9613-2 and NORD2000, including receiver height specifications, tone correction procedures, atmospheric absorption coefficients, ground impedance models, reflection handling.

Moreover, the noise varies with meteorological conditions. This allows defining highly granular turbine control if the regulations account for it. For maximum production, a curtailment scheme is calculated for the set of turbines and every set of meteorological conditions that is considered in the applying noise regulation of the location of the time for getting the permission for the wind farm. However, even for a single set of meteorological conditions the number of combinations increase exponentially dependent on the number of turbines and the number of operation modes. This prohibits an evaluation of all combinations. Due to non-linearities in the objective and constraint functions from wake interactions, it is not possible to construct a linear problem [1] that could be solved exactly. Meta-heuristic algorithms have been tackled to solve the problem but are often not able to find the global optimum and the results often differ due to the inherent stochasticity. While meta-heuristics such as genetic algorithms (GA) or particle swarm optimization (PSO) are effective in exploring complex solution spaces, their stochastic nature can lead to inconsistent results, including suboptimal solutions and high computational overhead, particularly in problems where sufficient knowledge about the problem's nature is available [5].

We introduce a two-phase optimization framework combining a greedy global search heuristic based on a noise violation per production gradient that identifies promising solutions. The local neighbourhood of these solutions is then explored to refine it in a second step.

The proposed optimization framework implemented in windPRO can be configured to exactly match the noise regulations. The research questions we address is:

1. How does the performance of the proposed optimization algorithm compare to standard approach of derating the highest noise contributing turbine?
2. How do optimal production losses change with different granularities of ISO 9613-2 noise model configurations?

To tackle the research questions, the optimization is tested on four realistic noise model setups with different fidelities, from a simple setup with few meteorological bins to an advanced setup that includes a recent addition that is applicable in multiple German counties, called the area of influence.

2. Methods

Initially, the noise propagation models and their application in regional noise regulation are briefly outlined. Following this, the various meteorological and temporal conditions are introduced as dimensions of the optimization problem that is subsequently defined. Then, a standard default approach and innovative algorithms to address the issues are described. Finally, the experimental design is explained.

2.1 Noise propagation models and regulatory specifications

Noise propagation models translate the sound emission from the noise sources, in this case wind turbines, to the noise immission points, typically the surrounding dwellings. In the present study the ISO 9613-2 propagation model is used but in principle any propagation model could be considered, such as the NORD2000 model. The ISO 9613-2 model [4] is considered an industry standard model and went through

a revision in 2024. It is used as the basic propagation model in many countries and regions with local variations, both for wind turbine sound and other industrial sound modelling. One such country is Germany where the use of the ISO 9613-2 model is described in the TA-Lärm guideline [6].

Propagation models, whether it is the ISO 9613-2, the NORD2000 model or other propagation models, include several meteorological parameters that change over time, such as wind direction, temperature, humidity or shear, each resulting in a different translation of source noise level to impact noise level at the receptor.

Some noise regulations consider the wind speed uniform across the wind farm and although wind speed may be referred to at 10 m height, the International Electrotechnical Commission (IEC) wind profile translates the wind speed to hub height and a particular wind speed in the noise constraint translates to a fixed wind speed at hub height. In reality, however, wind speed can vary considerably inside the wind farm, partly due to terrain and partly due to the wakes of the wind turbines, so asking that the wind farm must be curtailed at x m/s at y m height, requires a reference location and an individual wind speed bin for each wind turbine. Even if the propagation model assumes downwind conditions from every turbine to every receptor, the translation of wind speed will need to take into account wind direction.

2.2 Dimensions and binning for curtailment

The curtailment matrix can inhibit multiple dimensions, such as wind speed, direction and time, and be limited by the granularity in which curtailments can be applied. A minimum bin size can be required by the original equipment manufacturer (OEM), or a limited number of operation modes is available. An example is shown in Figure 1 where a curtailment matrix is defined for three dimensions, wind speed, wind direction and time (day, evening and night). Within each bin, the turbine is set to use a particular operation mode with its own noise curve.

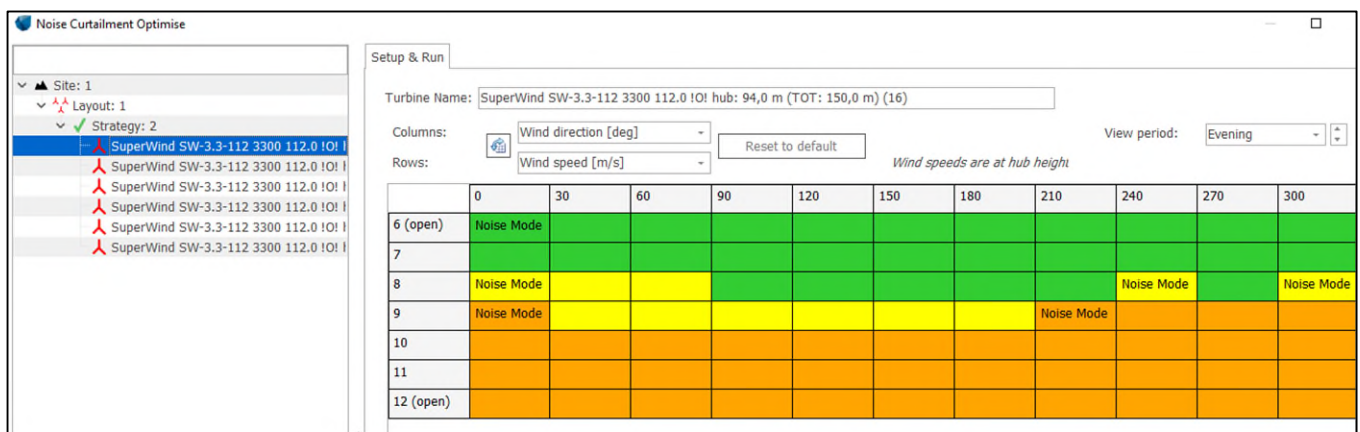


Figure 1. Example of a noise curtailment matrix, presenting two dimensions, wind speed and direction, within the time dimension bin “evening”.

The binning of dimensions is more complex than it might seem. In a system with uniform wind speed across the wind farm, there would be a match between the bins tested against a threshold and the bins in the curtailment matrix (Figure 2). However, actual wind speed translation may result in untested bins or bins with multiple tests (Figure 2), both of which require some decision-making.

A threshold based on maximum noise impact is independent of wind speed, requiring the curtailment to ensure that the combined noise impact at any wind speed stays within the threshold. In contrast, a threshold conditioned on a particular wind speed necessitates curtailment to ensure the threshold is not exceeded at that specific wind speed. However, what occurs at wind speeds that are not constrained by a threshold? In such cases, the turbine may be allowed unrestricted operation or must remain in the operation mode of the closest test wind speed. This situation becomes more complex if the test is not based on the wind speed at the wind turbine but on a reference location.

Decisions regarding granularity and the translation of wind speed across the wind farm significantly influence the outcome of noise curtailment. While not fully explored in this paper, the consequences on the curtailment plan and calculated benefit are substantial.

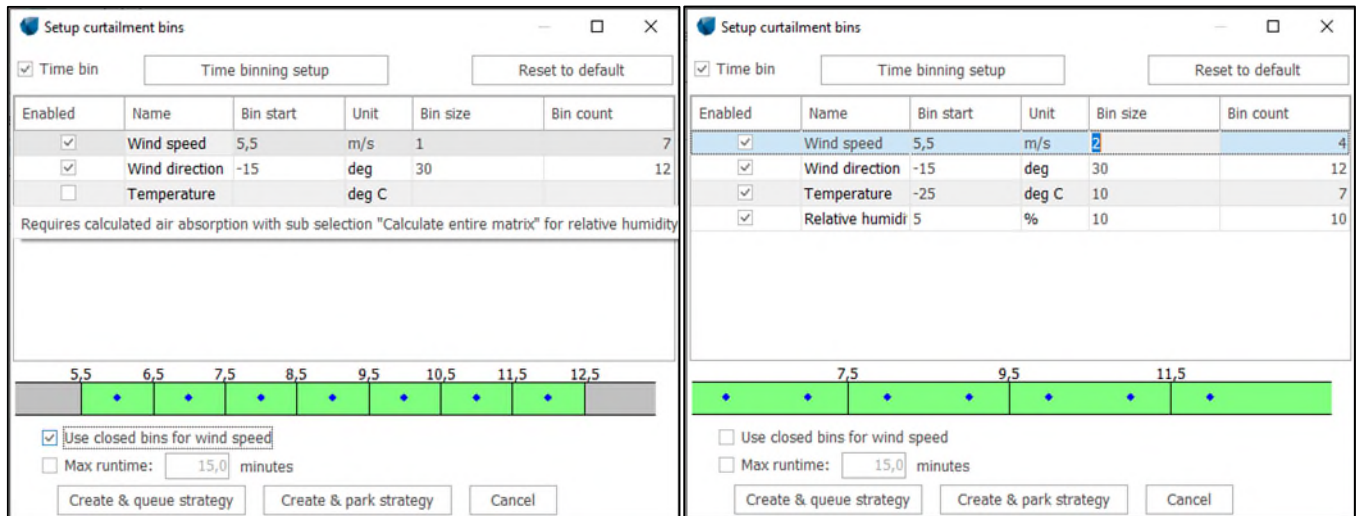


Figure 2. Left: Binning in the curtailment matrix (boxes) with a test in each bin(dots). Right: Large bins with multiple tests.

The goal of any noise curtailment strategy is to ensure compliance with the noise receptor thresholds. Therefore, the success of the curtailment plan is highly dependent on the structure of these thresholds. Consequently, a noise curtailment matrix must be established for each turbine, in alignment with the noise constraints and regulatory requirements.

2.3 Optimization problem

The decision variables of the optimization problem are the operation modes of all turbines of the wind farm. The objective of the optimization is to maximize the energy production of the wind farm, and the constraint is to maintain the noise level at all noise receivers below a certain noise level for all meteorological conditions. Without the wake effects of turbines, the problem could be categorized as a multi-dimensional knapsack problem. However, the wake effects add interactions between the decision variables: The production mode of the wake influences the wind speed and with it in energy production and noise outputs at the positions of the wake receiving turbines, and that interaction applies to all wind turbines within the wind park. This makes it a non-linear knapsack problem with non-separable objectives and constraints [7]. The notion of non-separable objective and constraint functions refers to the interaction of the decision variables. This problem quickly becomes intractable and cannot be solved exactly due to the exponentially increasing complexity of the problem with the number of variables, i.e. the number of turbines and the number of operation modes. Moreover, the optimization problem is independent between each binned set of meteorological conditions [8].

2.4 Optimization algorithms

2.4.1 Reference algorithm

A typical standard approach is to iteratively reduce the noise emission of the wind turbine that contributes the largest share of the noise impact at the receptor with the largest exceedance above threshold. This procedure is typically applied on each turbine uniformly instead of derating the turbine in certain meteorological conditions. The argument for this approach is that derating the biggest contributing turbine provides the largest reduction in noise impact at the receptor. This approach is widely adopted and has been part of industrial solutions such as windPRO for decades. In the context of this paper, it is labelled the classic method.

The main weakness of this model is that it ignores the power production of the wind turbines and is not performed on binned meteorological condition that match the control variables from the specified noise

model. Derating the largest noise contributing turbine will often result in a large noise reduction, but it can result in drastic losses of energy production. The second weakness is that the curtailments are not adjusted to the meteorological conditions that influence the received noise. It is simply not necessary to derate the individual turbines equally at all wind speeds, wind directions, temperatures and air pressures to comply with thresholds.

2.4.2 Greedy global search heuristic

The objective is not just to comply with receptor noise thresholds but to do so with a minimal loss of energy production. If a turbine is exceptionally well producing or the needed reduction to comply with the permitted noise level can be achieved by reducing another less energy producing turbine, this is often preferable.

We suggest a deterministic greedy approach to tackle the knapsack problem on binned meteorological conditions. The decisions of which turbine to derate now depends on the relative energy production contributions of wind turbines to noise exceedance levels above permitted noise at noise receptors.

First, all turbines are set into the highest possible operation mode. As long as the noise impact exceeds the permitted noise level, the noise receptor with the highest noise exceedance is identified. Then, a metric is computed for each turbine that quantifies the relation of produced power to the noise exceedance at the receptor. The turbines are sorted reversely according to that metric, and the turbine with the worst relative power per noise contribution gets derated into the next possible production mode. This loop is continued until all noise levels at the noise receptors meet the permitted noise level of the current meteorological and temporal bin. It continues with identifying and solving the problem for the next bin, until all bins are optimized. The result is a multidimensional curtailment matrix with optimized operation modes for turbines across all bins. The algorithm proved to be the right balance between accuracy and computation time [8].

2.4.3 Step model - Local Neighbourhood Search

The greedy global search heuristic described above often ends up in a local optimum. However, we found that it generally finds a high-quality solution that only differs in a few decisions made when compared to the global optimum. For this reason, a local search phase is performed that systematically explores the neighborhood of the greedy solution. This phase is controlled by an exploration depth parameter, which controls how far the search can deviate from the current solution. The method is inspired by Large Neighborhood Search [9], which emphasizes systematic exploration of increasingly distant solution neighborhoods to overcome local optimality.

Step 1. Global Upgrading:

First, the algorithm attempts to further increase the operation mode of each turbine, one at a time, up to a fixed number of levels above its current setting (as defined by the exploration depth). If any such upgrade leads to an improvement in total energy production, the new configuration is immediately accepted.

Step 2. Downgrade-Compensation Cycle:

If no improvement is found through upgrades alone, the algorithm then explores more complex adjustments. For each turbine, it considers temporarily reducing its operation mode by up to the exploration depth. For every such downgrade, the algorithm then attempts to compensate by increasing the operation modes of the other turbines, again within the allowed depth. If this combination results in a net improvement in total energy production, the new solution is accepted. This approach allows the algorithm to escape local optima by making coordinated changes that the greedy strategy overlooked. The search continues until a complete pass through all turbines fails to yield any further improvement.

The main parameter controlling the breadth of the local search is the exploration depth. A higher value increases the chances of finding a better solution but also raises computational demands, the complexity is $O(\text{number of decision variables}^2 \cdot \text{exploration depth}^2)$. In practice, the algorithm is efficient for moderate-sized problems. The default value is set to 3.

2.5 Design of experiment

The difference between the classic optimization algorithm and the production conditioned algorithm plus the possibilities of using a detailed curtailment matrix, can be demonstrated with a fictional wind farm example. This example is located in hilly terrain and consists of 10 wind turbines and 4 receptors (Figure 3). The wind turbines are Siemens Gamesa SG 6.6-170, hub height 175 m [10], with 9 operation modes available as listed in Table 1. Decreasing noise means decreasing production as demonstrated in Figure 4.

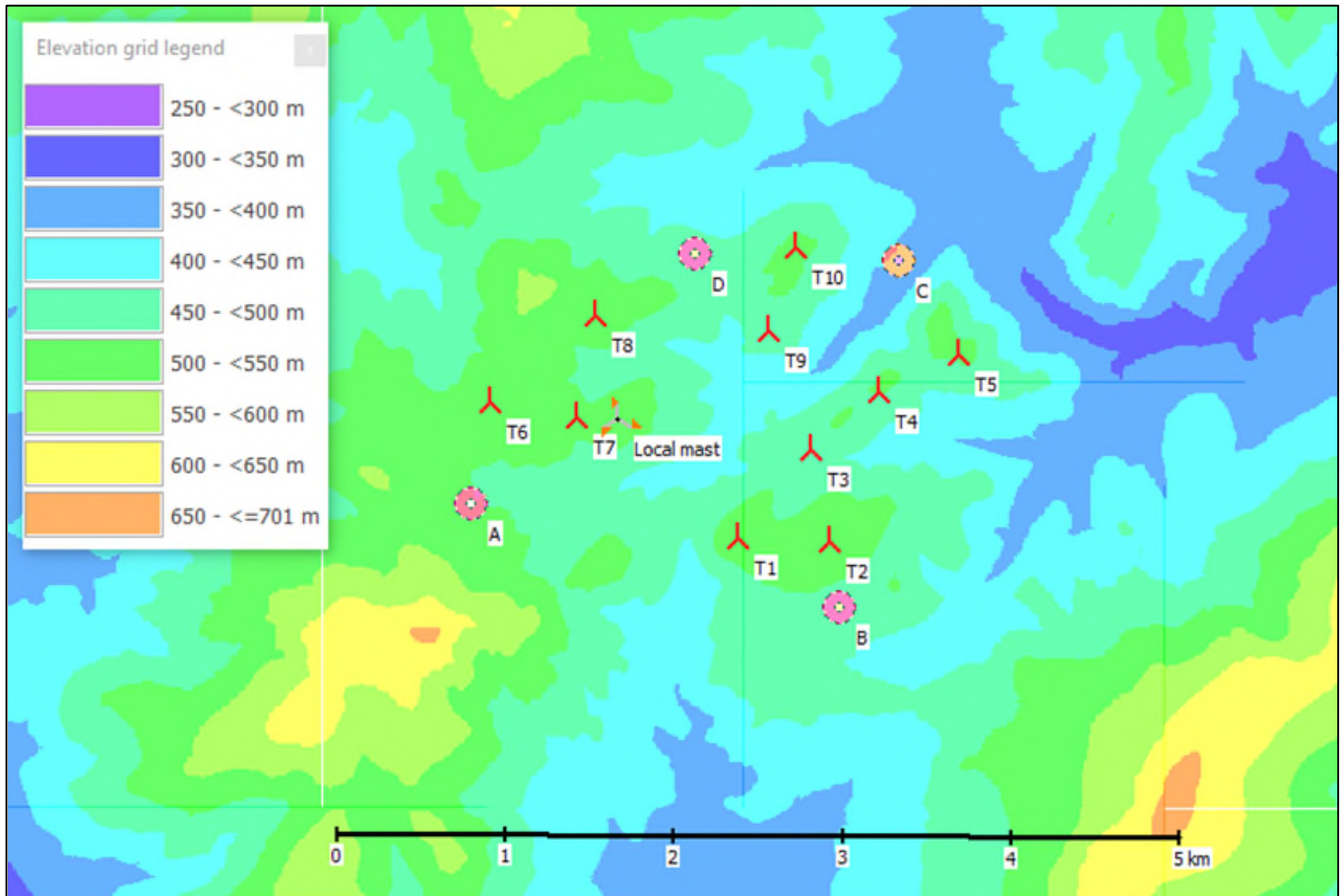


Figure 3. Test case wind farm consisting of 10 wind turbines (red rotor symbol and 4 receptors (pink circles). The site is hilly with considerable terrain differences within the wind farm. The “Local mast” is a suggested reference point.

Table 1. Operation modes for the Siemens Gamesa SG 6.6-170 used in this test.

Name	Power curve	Noise data
AM 0	(AM 0, 6.6MW) - 1.225 kg/m ³	AM 0 - 2022-08
N1	N1 - 105.5dB(A) - 1.225 kg/m ³	N1 - 2022-08
N2	N2 - 104.5dB(A) - 1.225 kg/m ³	N2 - 2022-08
N3	N3 - 103dB(A) - 1.225 kg/m ³	N3 - 2022-08
N4	N4 - 102dB(A) - 1.225 kg/m ³	N4 - 2022-08
N5	N5 - 101dB(A) - 1.225 kg/m ³	N5 - 2022-08
N6	N6 - 100dB(A) - 1.225 kg/m ³	N6 - 2021-12
N7	N7 - 99dB(A) - 1.225 kg/m ³	N7 - 2021-21
N8	N8 - 98dB(A) - 1.225 kg/m ³	N8 - 2021-12

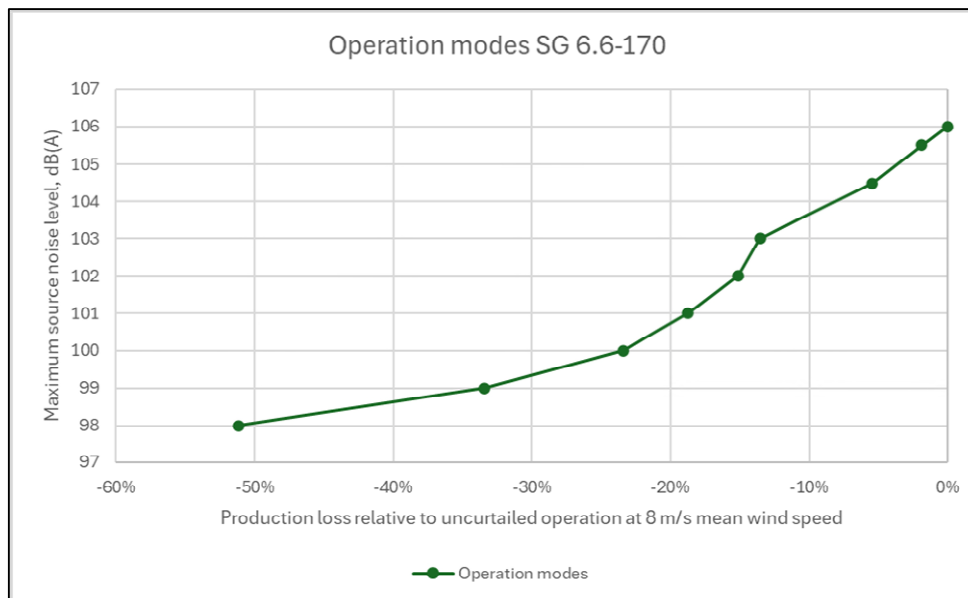


Figure 4. Production loss for each operation mode relative to uncurtailed operation (at 8 m/s mean wind speed) for the SG 6.6-170 used in the case examples.

Four cases are presented in the following, demonstrating the potential benefit allowing for bin-wise curtailment schemes and applying the optimizer. The cases all use the ISO 9613-2 model as propagation model with parameter settings as listed in Table 2. The dimensions focused on in the tests are wind speed, wind direction and time, though any variable in the propagation model could potentially be used.

Each test case is compared to the classic algorithm. The classic algorithm uses the same propagation model as the production conditioned algorithm but with no binning (except for time). Therefore, the improvements are directly related to the algorithm and the use of a curtailment matrix.

Case 4b introduces the use of the Area of influence clause in TA-Lärm [6]. The Area of influence clause, also known as an irrelevance criterion, limits the noise sources to take into account at a given receptor. The clause (2.2) states that noise sources that contribute less than 10 dB below the receptor threshold can be excluded from the calculation of noise impact. This clause is implemented differently across Germany. The implementation applied in test case 4b is that individual wind turbines in the planned wind farm are excluded if the individual contribution is less than 10 dB below threshold. All tests are run in windPRO 4.2.

Table 2. Study case settings.

Parameters	Case 1	Case 2	Case 3	Case 4a	Case 4b
Wind speed	Maximum source noise	4 -12 m/s, step 2 m/s	4 -12 m/s, step 2 m/s, actual wind speed in wind farm	Maximum source noise	Maximum source noise
Wind direction	Downwind	12 directions, ISO derived	12 directions, ISO derived	Downwind	Downwind
Ground attenuation	General, G=0.5	General, G=0.5	General, G=0.5	Agr = -3 dB	Agr = -3 dB
Receptor height above	4 m	4 m	4 m	5 m	5 m
Uncertainty	0 dB	0 dB	0 dB	2.1 dB	2.1 dB
Air absorption	T: 10 °C, RH: 70%	T: 10 °C, RH: 70%	T: 10 °C, RH: 70%	TA-Lärm	TA-Lärm
Time domain	Uniform	Uniform	Uniform	day and night (22-6)	day and night (22-6)
Other	-	-	-	-	Area of influence: 10 dB

3. Study cases

3.1.1 Case 1

Case 1 is a simple case where the noise level thresholds are a uniform dBA values across all bins, with 35 dBA at receptor A, and 40 dB at receptor B – D. The curtailment scheme, therefore, results in a uniform operation mode setting for each turbine. The parameters of the case are presented in Table 2.

The resulting curtailment strategies with presented reference approach described in Sect. 2.4.1. and the proposed search algorithm in 2.4.2 are presented in Table 3. Moreover, the operation modes from the

classic strategy and the production conditioned strategy are listed for all the turbines and it is clear that the more advanced model found a different strategy, particularly in avoiding the very expensive mode N8.

Using the proposed search algorithms, the improvement across the wind farm is 5.2% in annual production output compared to the annual production modes from the reference algorithm.

Table 3. Results of study cases 1, 2 and 3, quantifying improvements in production relative to reference algorithm.

Wind turbine	Classic strategy	Case 1 strategy	Case 1 improvement	Case 2 improvement	Case 3 improvement
T1	N2	N1	3.1%	3.0%	1.9%
T2	N6	N4	10.1%	10.5%	8.1%
T3	AM 0	N6	-19.3%	-3.9%	-2.4%
T4	AM 0	AM0	1.4%	-1.4%	-5.3%
T5	N3	N1	11.2%	8.4%	8.8%
T6	N8	N6	41.2%	35.3%	31.8%
T7	N8	N6	41.1%	48.6%	48.3%
T8	N3	N4	-3.3%	0.7%	-1.2%
T9	N3	N6	-10.1%	2.3%	-0.2%
T10	N3	N4	-1.3%	1.0%	1.1%
Total			5.2%	8.2%	6.9%

3.1.2 Case 2

Case 2 maintains the same receptor thresholds as Case 1, but allows the turbines to be curtailed along two dimensions: wind speed with a binning size of 2 m/s and wind direction with a binning size of 30 degrees. The wind speed bins range from 4 to 12 m/s. Above 12 m/s, the turbines are unrestricted and can run freely. The wind direction component is derived from the ISO 9613-2 model and excludes source directivity.

The greater granularity in the curtailment scheme results in a more intricate curtailment matrix for each wind turbine. Figure 5 presents an example with T5. Due to this complexity, a simple mode, as seen in Cases 1 and 2, cannot be presented.

Compared to the classic algorithm without binning, the improvement in annual production output is 8.2%, with the more granular binning adding 2.7% of production compared to the uniform case 1 (Table 3). Some of this increase is due to unrestricted operation outside the tested bins. Clearly, both the advanced algorithm and the curtailment matrix contribute to the production gain.

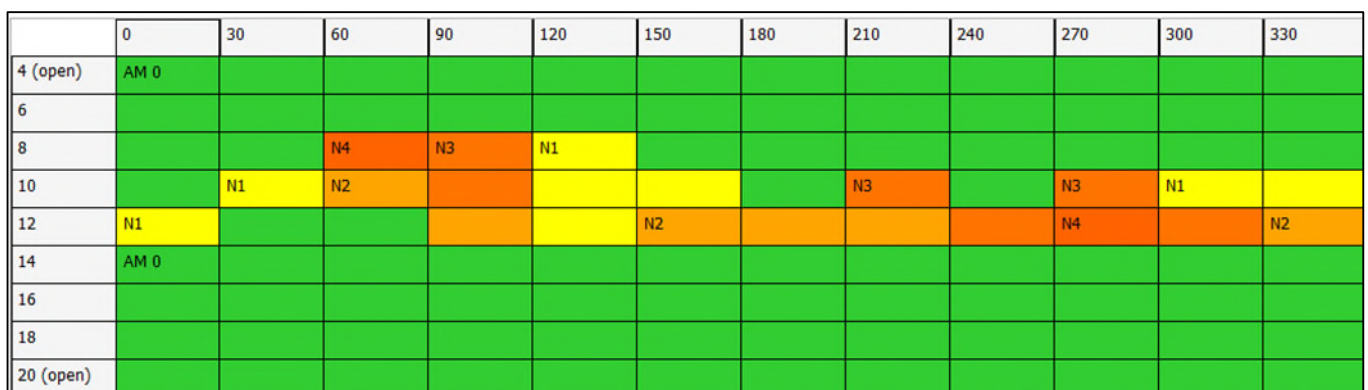


Figure 5. The curtailment matrix of turbine T5. The matrix consists of vertical wind speed bins and horizontal wind direction bins. The colour coding represents bin settings.

3.1.3 Case 3

Case 3 extends Case 2 by considering variable wind speeds across a wind farm. Each turbine's SCADA data determines its operation mode, requiring the curtailment plan to factor in actual wind speeds at individual turbines. Tests are conducted at fixed wind speeds, using a central meteorological mast at 100.7

m as the reference point. Wind speeds are adjusted for each turbine, accounting for terrain and wake effects, with the reference location unaffected by wake.

The resulting curtailment matrix looks different from Case 2 (example with T5 in Figure 6). Because the wind turbines generally are experiencing higher wind speed than the reference location and height, the turbines will be higher on the noise curve and need to be curtailed more. The overall improvement compared to the simple classic case is in this setup 6.9% on annual production (Table 3).

Adding the actual wind speed differences across the wind farm is not therefore necessarily a gain to production output, but an acceptance of reality, that if we want to control our wind turbines with high granularity, we must also accept that the wind turbines at any given time will experience different wind speed.

	0	30	60	90	120	150	180	210	240	270	300	330
4 (open)	AM 0											
6												
8											N1	
10		N2			N1						N3	
12	N1	N3		N3	N2		N4	N2		N3		
14	AM 0			N2		N3		AM 0	N3	N4	N2	
16		N2										
18												
20 (open)												

Figure 6. The curtailment matrix of turbine T5 using actual wind speed within the wind farm. The bins continue to be the wind speed experienced by the wind turbine, but the test wind speeds are now determined by the wind speed at the reference location, which translates to different wind speeds at the wind turbines.

3.1.4 Case 4

In Case 4, an actual noise code is applied, specifically adapting the German noise code as described by TA-Lärm [6]. In this scenario, Receptor A is set to 35 dB(A) at night and 50 dB(A) during the day, while Receptors B-D are set to 40 dB(A) at night and 55 dB(A) during the day. Nighttime is defined as the period from 22:00 to 06:00.

The parameters of the propagation model are set according to Table 1, which includes an uncertainty penalty of 2.1 dB on the source noise levels of the turbines as a typical (maximum) value.

During daylight hours, the wind farm can operate without curtailment, but significant curtailment is required at night. Table 4 lists the resulting curtailment modes for both the classic approach and the production-conditioned approach. In both cases, two wind turbines need to shut down at night, but the production-conditioned approach still gains 2.8% in production.

This case is expanded with the option of applying the area of influence principle, which is allowed in some German regions [6] as explained in section 2.5. As applied here, turbines that individually contribute less than 10 dB below the receptor threshold can be ignored for that receptor. From a curtailment optimization perspective, the challenge is that reducing a turbine with a small partial contribution can have a large impact on the energy production, and the classic approach does not consider this fact.

Applying this option in Case 4b results in a 7.6% improvement in production for the wind farm relative to the classic reference algorithm. This gain is largely due to avoiding the shutdown of turbine T2 and the costly mode N8.

Table 4. Results of case 4, quantifying improvements in production relative to reference algorithm.

	Night time curtailments				
	Classic	Case 4 strategy	Improvement	Case 4b: including area of influence	Improvement
T1	N3	N3	-0.1%	N5	-2.5%
T2	Shutdown	Shutdown	0.0%	N6	46.3%
T3	N5	N6	-1.9%	N7	-5.6%
T4	N5	N5	-0.1%	N4	1.0%
T5	N7	N5	5.8%	N5	5.5%
T6	Shutdown	Shutdown	0.0%	Shutdown	0.0%
T7	N7	N7	-0.1%	N5	5.5%
T8	N8	N6	11.1%	N5	12.9%
T9	N8	N7	6.3%	N6	9.8%
T10	N8	N7	6.7%	N6	10.5%
Total			2.8%		7.6%

4. Discussion

The test cases are examples of the use of the optimization algorithm and are by no means exhaustive. There are many variations of noise codes and wind farm sites differ in how they are constrained. The test cases exemplify the fundamental benefit of considering production loss when optimizing noise curtailment, as seen in Case 1 where there was a 5.2% production gain. Additionally, allowing a curtailment matrix has proven valuable, though strongly connected to the noise code of the region or country of the wind farm in terms of both dimensions and granularity. This option will therefore not always be available, yet the production benefit may be an argument for revising noise codes to allow for detailed curtailment matrices. In Case 2, the curtailment matrix added 2.7% production to the wind farm.

The potential complexity of connecting a noise code to an actual wind farm with differences in wind speed among the wind turbines for different flow cases is evident. Requiring the wind farm to comply with specific dB levels at certain wind speeds necessitates both a reference location and a transformation of that wind speed to the individual wind turbine, as demonstrated in Case 3. Moreover, the algorithm can be applied to specific noise codes with particular requirements or opportunities and help make them beneficial. In the German case (Case 4), this led to a 7.6% improvement relative to just using a common industrial optimization algorithm that merely addresses not violating constraints without a focus on the objective.

The initial case presented in the study, where meteorological and temporal conditions were not binned, demonstrated a production gain of 5.2% purely from the algorithm's improvement. Addressing the first research question, "How does the performance of the proposed optimization algorithm compare to the standard approach of derating the highest noise contributing turbine?", it's evident that further gains were achieved by efficiently optimizing all individual bins separately, adding another 2.7% to the production. While this is specific to the site studied, it illustrates the significant performance enhancement offered by the proposed algorithm. Although not presented in this study, it is worth noting that the two-step heuristic approach outperformed both the meta-heuristic and dynamic programming approaches tested on the same problem, excelling in both solution quality and computation time.

For the second research question, "How do optimal production losses change with different granularities of ISO 9613-2 noise model configurations?", the flexibility to tailor the optimization algorithm to new and advanced regulations, such as the area of influence principle, leads to considerable gains. Implementing this principle allowed the continued operation of a turbine that would otherwise have been shut down, resulting in a relative gain of 4.9% compared to an approach that did not incorporate this rule.

5. Conclusion

The study explores the efficacy of an advanced noise curtailment optimization algorithm in enhancing wind farm production while adhering to noise constraints. The research highlights the significance of balancing production efficiency with environmental considerations, particularly in regions with stringent noise regulations, and the importance of tailoring wind farm control to the noise regulations in place.

The methodology involved detailed analysis and application of the optimization algorithm across various test cases. The two step heuristic search algorithm with a global and a local search approach is designed to efficiently account for noise constraints while optimizing production despite a highly non-linear optimization problem due to wake interactions within the wind farm. The study cases demonstrated the algorithm's ability to improve production by considering factors such as meteorological conditions and temporal variations, and by implementing principles like the area of influence.

The discussion section elaborated on the substantial production gains achieved through the optimization algorithm. For instance, Case 1 exhibited a 5.2% increase in production by optimizing individual bins separately. Case 2 showcased an additional 2.7% production gain through the implementation of a curtailment matrix. Case 3 highlighted the complexities of connecting noise codes to actual wind farm operations, emphasizing the need for specific dB levels at certain wind speeds. The German test case (Case 4) demonstrated a 7.6% improvement in production by incorporating advanced regulations like the area of influence principle.

In conclusion, the study highlights the importance of selecting the most appropriate approach with an efficient and flexible optimization algorithm that is tailored to regional noise regulations.

Acknowledgments

The work was executed within the DECOWIND project, which was supported by Innovation Fund Denmark and included participation by the Technical University of Denmark (DTU), Siemens Gamesa Renewable Energy (SGRE), FORCE Technology and EMD International A/S. DTU and SGRE were project coordinators.

References

- [1] J. F. Cao, W. J. Zhu, W. Z. Shen, J. N. Sørensen and Z. Y. Sun, "Optimizing wind energy conversion efficiency with respect to noise: A study on multi-criteria wind farm layout design," *Renewable Energy* 159, pp. 468-485, 2020.
- [2] C. M. Nyborg, A. Fischer, P.-E. Réthoré and J. Feng, "Optimization of wind farm operation with a noise constraint," *Wind Energy Science* 8, pp. 255-276, 2023.
- [3] M. Steurer, U. Fahl, A. Voss and P. Deane, "Curtailment," *Europe's Energy Transition - Insights for Policy Making: Elsevier*, pp. 97-104, 2017.
- [4] International Organization for Standardization (ISO), ISO 9613-2:2024 Acoustics - Attenuation of sound during propagation outdoors - Part 2: Engineering method for the prediction of sound pressure levels outdoors., 2024.
- [5] S. Shabir and R. Singla, "A Comparative Study of Genetic Algorithm and the Particle Swarm Optimization," *International Journal of Electrical Engineering*, vol. 9, no. 2, 2016.
- [6] Bundesministeriums für Umwelt, Naturschutz, Bau und Reaktorsicherheit , "Technische Anleitung zum Schutz gegen Lärm – TA Lärm," 2017.
- [7] K. Bretthauer and B. Shetty, "The nonlinear knapsack problem - algorithms and applications," *European Journal of Operational Research* , vol. 138, pp. 459-472, 2002.
- [8] R. Slot, T. Sørensen, T. R. Hansen, S. Oerlemans, J. Feng, C. M. Nyborg and E. Thysell, "Optimal noise curtailment of modern wind farms," in *WindEurope Techworkshop 2022*, 2022.

- [9] P. Shaw, *Using Constraint Programming and Local Search Methods to Solve Vehicle Routing Problems*, New York: Springer, 1998.
- [10] Siemens Gamesa Renewable Energy, “Acoustic Emission for 0, SG-6.6-170, Rev. 0,” 2022.

Paper #5 - ID: 337

Title: On the detection of vortex generator noise influence using beamforming in a large aeroacoustic wind tunnel

Author: Matthieu Gelot

11th Edition of the

International Conferences on Wind Turbine Noise

Copenhagen, Denmark – 10th to 13th June 2025

On the detection of vortex generator noise influence using beamforming in a large aeroacoustic wind tunnel

Matthieu B. R. Gelot¹

Vestas Technology UK, Stag Lane, Newport PO30 5TR, United Kingdom

Erik Sloth

Vestas Wind Systems A/S, Hedeager 42, Aarhus 8200, Denmark

Oliver A. Lylloff

DTU Wind Energy, Frederiksborgvej 399, 4000 Roskilde, Denmark

Luis D. C. G. S. Cruz

Vestas Design Center Porto, R. de Asprela 162, Porto 4200-072, Portugal

Summary

The present work aims to report some wind tunnel findings while testing vortex generators (VG) on aerofoils dedicated to wind turbine generators in the Poul La Cour tunnel (PLCT), using an aeroacoustic setup with Kevlar side walls. It consisted of testing Vestas proprietary aerofoil designs fitted with vortex generators and serrated trailing-edge add-on (STE) at three different flow speeds and a wide range of negative and positive geometrical angles of attack (AoA). Aerofoil noise was investigated using a microphone array and a classical frequency-domain beamforming approach to generate acoustic images. To suppress wind tunnel background noise and spurious sources, several integration zones were used. The results suggest that no major VG noise influence was detected while focusing on the sole trailing-edge (TE). Hence, two more beamforming integration strategies were created where a VG only configuration integrates mainly around the VG strip and a TE&VG configuration englobes both TE and VG. The relative difference between the TE&VG and the TE only configurations showed a potential significant noise increase detected at high angle of attack (AoA) when the beamforming integration zone includes the VGs. This observation seems independent of flow speed. The trend also shows a slight noise reduction in the low AoA region. This study showed, that VGs influence on noise is not detected unless one looks for it.

1. Introduction and setup description

The present study reports on the influence of vortex generators (VG) on noise from aerofoils dedicated to wind turbine generators. The wind tunnel campaign was led in the Poul La Cour tunnel (PLCT) [1], using an aeroacoustic setup with Kevlar side walls. It consisted of testing Vestas proprietary aerofoil designs fitted with vortex generators and serrated trailing-edge add-on (STE) at three different flow speeds and a wide range of negative and positive geometrical angles of attack (AoA).

¹ Corresponding author – Email: mtege@vestas.com

The different geometry configurations (airfoil, VG, STE) were tested at three different wind tunnel speeds – which will be labelled as low, mid and high speeds respectively – and for a wide range of negative and positive geometrical angles of attack (AoA). Aerofoil noise was investigated using a microphone array consisting of 84 microphones positioned 2.3m from the aerofoil trailing edge. The aerofoil was mounted vertically in the test section (2m x 3m x 6m [H x W x L]) and a classical frequency-domain beamforming approach [2] was used to generate acoustic images. In order to suppress wind tunnel background noise and spurious sources, several integration zones were used. Figure 1 illustrates the beamforming approach where sound sources are detected on the aerofoil surface. On this figure’s subplots, the observer stands on the suction side of the aerofoil model; the leading edge (LE) and trailing edge (TE) are highlighted in orange and lie respectively at $x=0.6\text{m}$ and $x=0\text{m}$ with the flow directed from the right-hand to the left-hand side. The span of the model is 2m long, but the beamforming integration is performed on a reduced spanwise region to discard wall effects from the resulting signal as much as possible. The beamforming integration zone is highlighted for each configuration in purple.

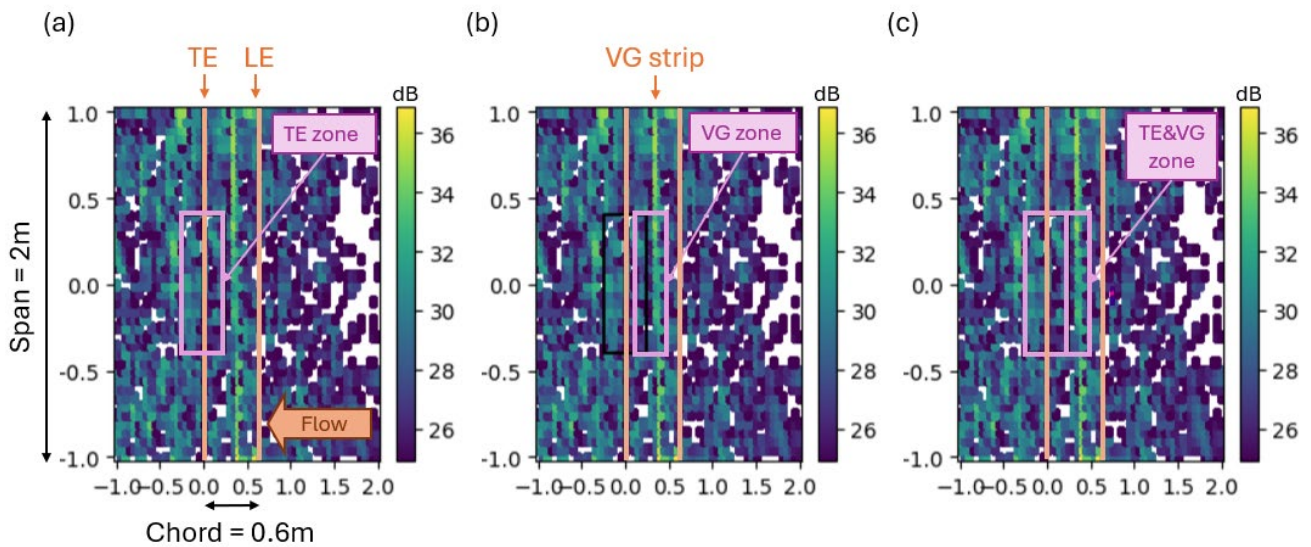


Figure 1 - Diagram of the classical beamforming integration zone (top view; flow from right to left). (a) the TE only configuration; (b) the VG only configuration; (c) the TE&VG configuration. Acoustic image is provided for a given 1/12th octave central frequency. Geometrical scale not respected.

The present study derives from the observation that no major VG noise influence was detected while focusing on the sole trailing-edge (TE) i.e. in the Figure 1(a) configuration. Hence, two more beamforming integration strategies were created as depicted in Figure 1(b) and (c) where a VG only configuration integrates mainly around the VG strip and the TE&VG configuration englobes both TE and VG via a logarithmic sum.

2. Results

2.1 Overall Sound Pressure Levels

The resulting integrated OASPL are shown in Figure 2 where configurations of beamforming integration zones and flow speeds are compared. The overall SPL is summed from 350 to 6000 Hz (as recommended by DTU for the tunnel) and the y-axis is rescaled with the nearest integer level to the maximum measured level (labelled as LVL). The x-axis is centred on AoA_e corresponding to the angle of attack where suction side displacement thickness equals pressure side one for the concerned aerofoil.

The relative difference between the TE&VG and the TE only configurations is exhibited in Figure 3 where one can see that the inclusion of the VG line in the analysis yields a noise increase at all angles of attack. However, the noise increase generated by the VGs is the lowest at very negative angles. It rebounds in the region from -10 to -5 degrees before lowering again for angles close to AoA_e . The peak noise increase is detected at high angles of attack. This peak looks independent of flow speed.

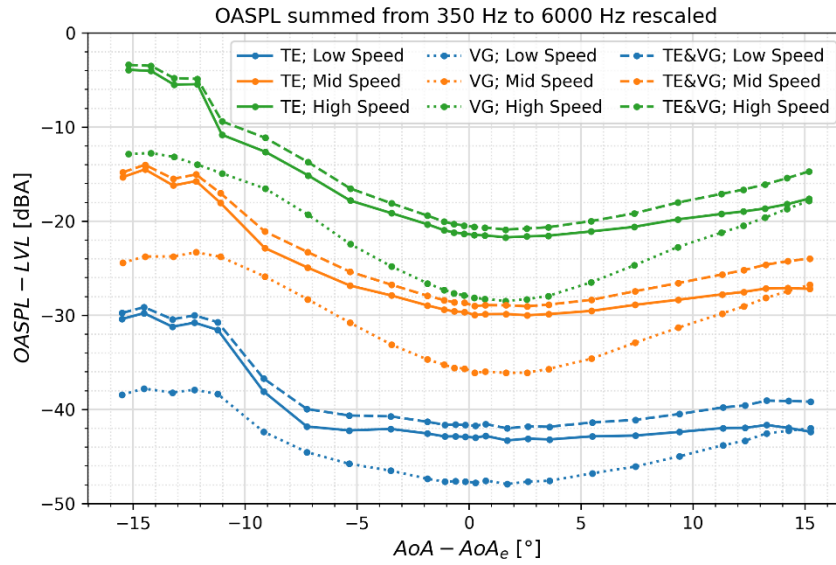


Figure 2 – Rescaled OASPL comparison between TE; VG and TE&VG configurations at three different flow speeds.

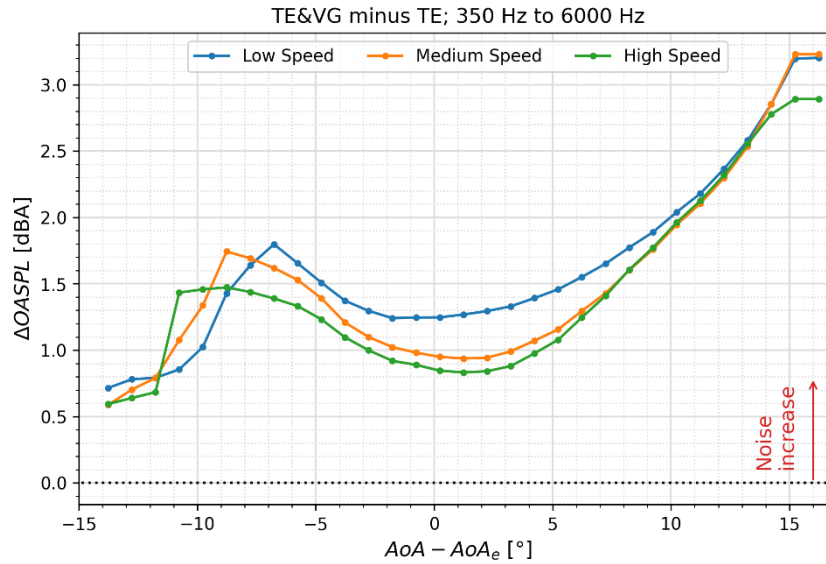


Figure 3 - OASPL difference (TE&VG minus TE) at three flow speeds showing noise increase in the presence of VG in the zone of analysis.

2.2 Sound Pressure Level spectra

Figure 4 to Figure 7 show the comparison of normalised SPL spectra between the three different analysis zones (VG, TE and TE&VG) for the three different speeds at four angles of attack. Like in the previous section, the SPL is normalised using the arbitrary level. The four normalised angles of attack, computed with

$$AoA_n = AoA - AoA_e$$

where AoA_e is the angle of attack of equal displacement thickness on suction and pressure sides, are chosen such that the range covers low to near stall AoA . Low speed is in blue, mid in orange and high in green. The spectra are shown from 200 to 6000 Hz but the region between 200 and 350 Hz is shaded to emphasise that it is a discarded region for the OASPL summation. The right-hand side plots show the SPL difference between TE and VG beamforming integration zones on a narrower frequency range for better visualisation.

The reader can see – more so with the difference plots on the right hand-side – that the level of noise provided by the VG strip integration progressively increases with AoA_n in the 300 to 600 Hz region and in the region above 4 kHz. At $AoA_n = 14.2^\circ$, the level of noise from the sole VG strip integration can

locally exceed the one from the TE strip integration by 3-5 dBA. This directly supports the observation made on the overall SPL in the previous section: the summed integration area yields louder noise than the classical sole TE integration as the VG noise becomes more prominent. The impact of VG on aerofoil noise is not negligible and should carefully be considered in wind tunnel studies. In other words, “one will not find VG noise unless one looks for it”.

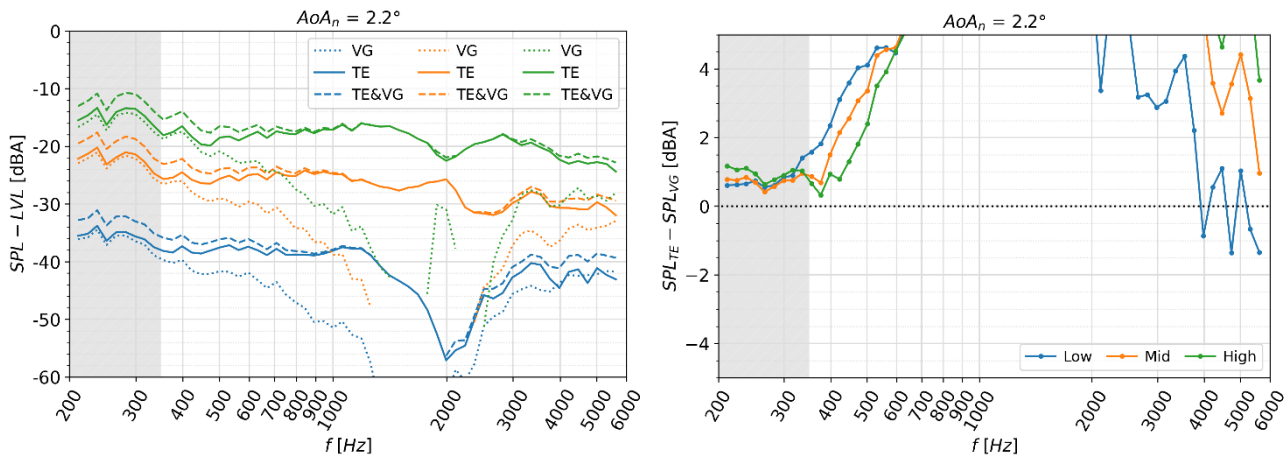


Figure 4 - Comparison of normalised SPL spectra between the beamforming integration zones (VG, TE and TE&VG) for the three different speeds (low in blue, mid in orange and high in green) at $AoA_n = 2.2^\circ$

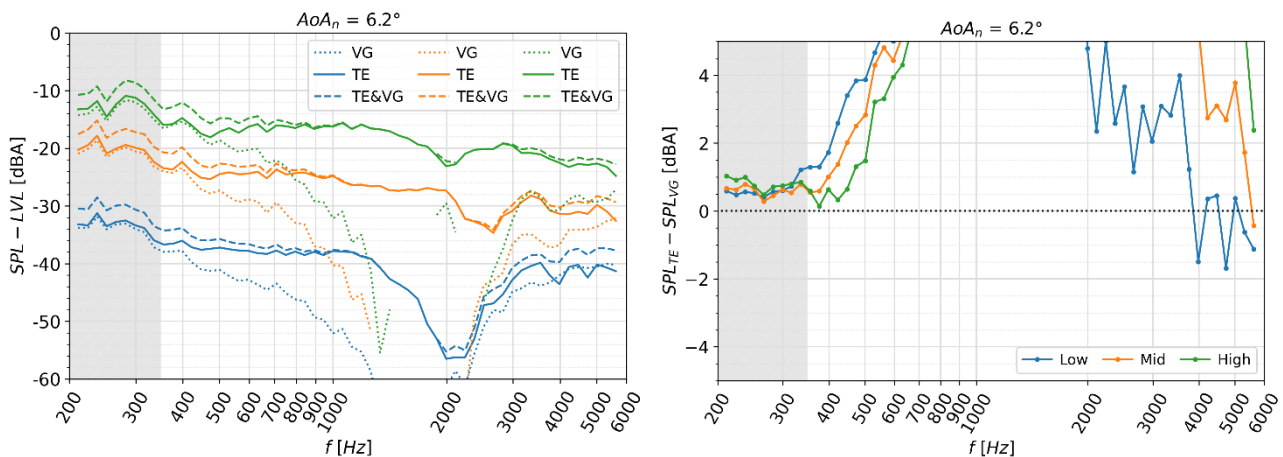


Figure 5 - Comparison of normalised SPL spectra between the beamforming integration zones (VG, TE and TE&VG) for the three different speeds (low in blue, mid in orange and high in green) at $AoA_n = 6.2^\circ$

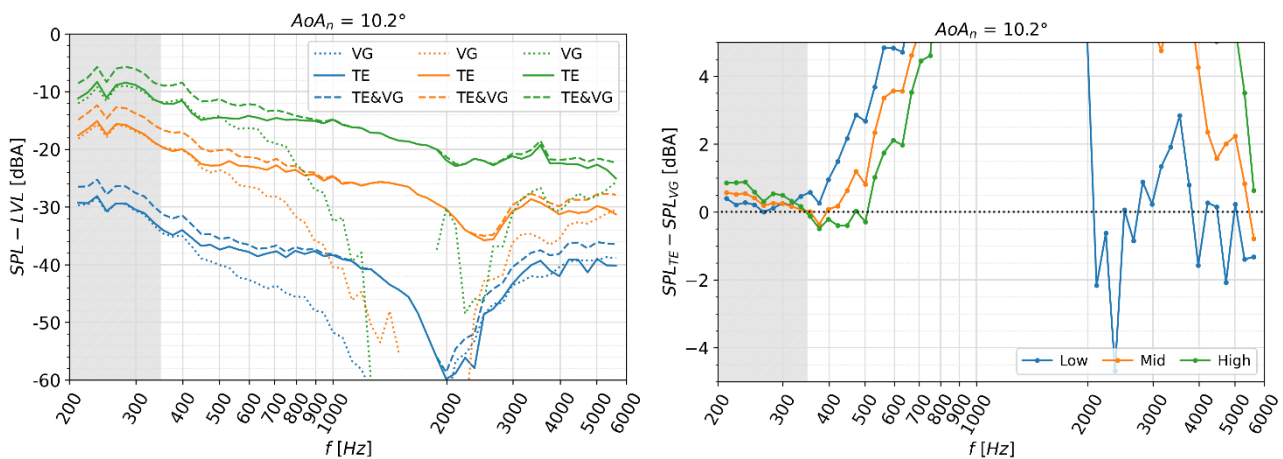


Figure 6 - Comparison of normalised SPL spectra between the beamforming integration zones (VG, TE and TE&VG) for the three different speeds (low in blue, mid in orange and high in green) at $AoA_n = 10.2^\circ$

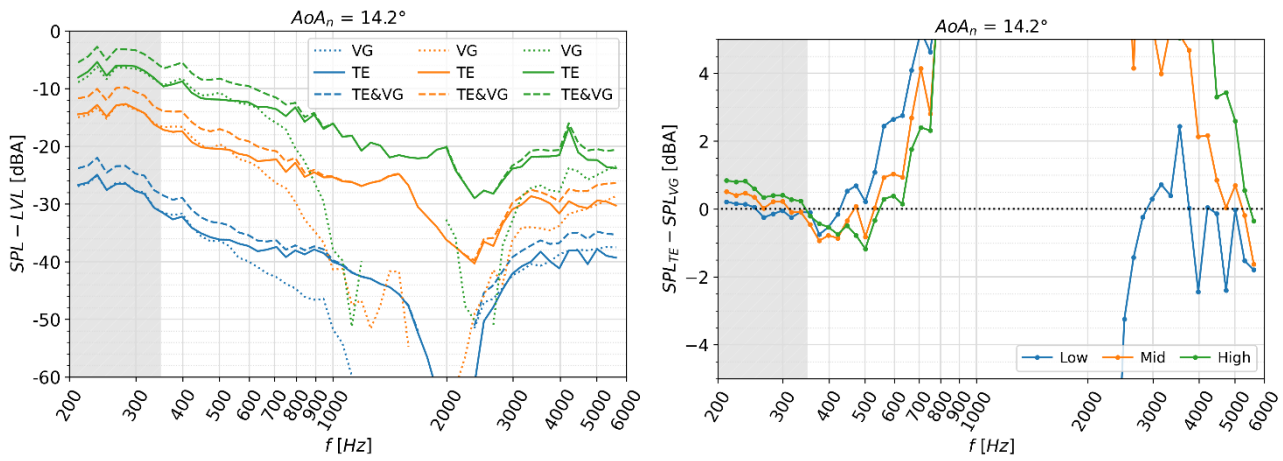


Figure 7 - Comparison of normalised SPL spectra between the beamforming integration zones (VG, TE and TE&VG) for the three different speeds (low in blue, mid in orange and high in green) at $AoA_n = 14.2^\circ$

2.3 Acoustic images

Figure 8 below displays a matrix of acoustic images (see section 1 for details on the processing) at $AoA_n = 2.2, 6.2, 10.2, 14.2^\circ$ for $1/12^{th}$ octave bands between 5 and 6 kHz. The table of pictures exhibits a significant increase of noise source strength at the VG line as the frequency increases and as the angle of attack increases. The reader can see that the bottom right hand-side corner shows the VG region around 5-10 dBA louder than top left hand-side corner.

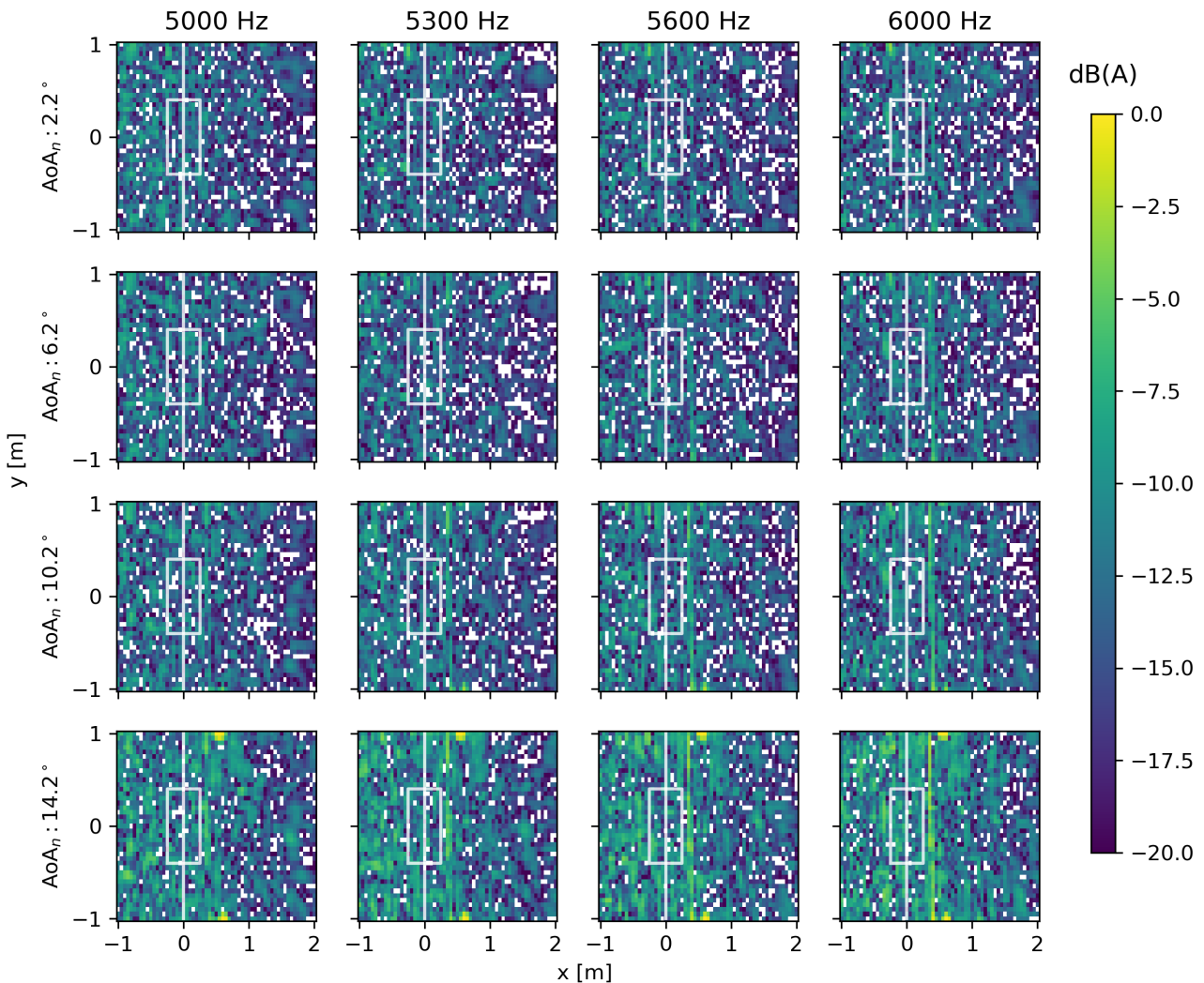


Figure 8 - Acoustic images at normalised angles of attack 2.2, 6.2, 10.2, 14.2 degrees at four different $1/12^{th}$ octave between 5 and 6 kHz. Flow direction is right to left and the aerofoil trailing edge is located at the vertical white line. The TE integration region is denoted by a white square.

A clear conclusion can be drawn: 6 kHz as the maximum frequency captured is too low for this kind of application. Thus, it is impossible to determine if the peak of noise sources observed at 6 kHz grows even further beyond that frequency band and hence contribute more prominently to the overall sound pressure level. The authors therefore recommend the community to capture the largest frequency range possible especially while testing vortex generators.

3. Conclusions

To conclude, we can summarize the findings of this short study as follows:

- A non-negligible noise increase is detected at high angle of attack when the beamforming zone of analysis includes the VG line compared to a zone that does not
- The above conclusion is moreover supported by the investigation of spectra which shows that the low frequency noise generated by the VG region is of similar strength to the one generated by the TE region alone as the angle of attack increases
- Acoustic images reveal that the noise generated in the vicinity of the VGs drastically increases at high angle of attack and frequencies above 5 kHz

Therefore, the authors would like to propose a set of recommendations for future wind tunnel campaigns:

- When testing different types of add-ons placed at various locations along the chord, multiple beamforming regions should be considered to get the “big picture”
- One should always seek to extract the largest frequency range possible to not risk missing some potential significant contributions (from higher frequencies in particular)

References

- [1] C. Bak, A. S. Olsen, A. Fischer, O. Lylloff, R. Mikkelsen, M. Gaunaa, J. Beckerlee, S. Ildvedsen, T. Vronsky, F. Grasso, A. Loeven, L. Broersma, B. Akay, J. Madsen, R. Hansen and R. Kommer, “Wind tunnel benchmark tests of airfoils,” *Journal of Physics: Conference Series*, vol. 2, no. 2265, 2022.
- [2] D. H. Johnson and D. E. Dudgeon, *Array signal processing: concepts and techniques*, Englewood Cliffs: PTR Prentice Hall, 1993.

Paper #6 - ID: 338

Title: Long term low frequency noise measurements near wind park

Author: Mike Dijkstra

11th Edition of the

International Conferences on Wind Turbine Noise

Copenhagen, Denmark – 10th to 13th June 2025

Long term low frequency noise measurements near a large wind farm

M.T. Dijkstra¹

LBP|SIGHT, Nieuwegein, the Netherlands

Summary

Long term noise measurements have been carried out at a wind farm consisting of 45 turbines with a hub height of 145 m and rotor diameter of 131 m. The measurements were performed at the location of nine dwellings during a period of two years. This period contains several months where the wind farm was not in operation and several months where the wind farm was nearly in full operation. The analysis is made of three consecutive months of data from the same season of different years (with and without wind farm activity). By analysing the difference, the sound levels from the wind turbines can be separated from the ambient sound levels. This is done by comparing the results in the form of a histogram. The aim of the measurements was to evaluate the low frequency noise. The results show that low frequency noise emitted by the turbines can be measured and that an increase in low frequency sound level occurs at dwellings near the wind farm. The levels are below limit values for low frequency noise and are mostly in agreement with expected values. For four of the nine measurement locations a 3 to 7 dB higher than expected noise level was measured at 100 and 125 Hz third octave bands. Also noise emission was measured of a few turbines according to the IEC61400-11 method, to measure the sound power level. These measurements show good agreement with the specifications of the turbines but do not confirm the higher measured levels at 100 and 125 Hz.

1. Introduction

From 2020 to 2022 measurements have been carried out near a large wind farm in the Netherlands. The measurements started in 2020 when the wind farm was not yet built or in operation. The measurements were continued during the construction of the wind farm until the farm was in full operation. The aim of the measurements was to assess the low frequency noise caused by the wind farm at dwellings near the wind farm.

The measurements were carried out by DGMR and LBP|SIGHT by order of the municipalities Aa and Hunze and Borger-Odoorn.

2. The wind farm

Wind farm ‘De Drentse Monden en Oostermoer’ is located in the northeast of the Netherlands near the town of Stadskanaal and consists of 45 turbines in six lines. The turbines are of the type Nordex N131 with a hub height of 145 m and rotor diameter of 131 m.

¹ Corresponding author – Email: m.dijkstra@lbsight.nl

3. Measurement setup

Measurements were carried out at nine dwellings surrounding the wind farm. Most microphones (apart from N227 and Z71 which were mounted on a pole) were mounted close to the facades of the dwellings causing a reflection of 3 to 6 dB. The measurement height was between 3 and 4 m above ground level.

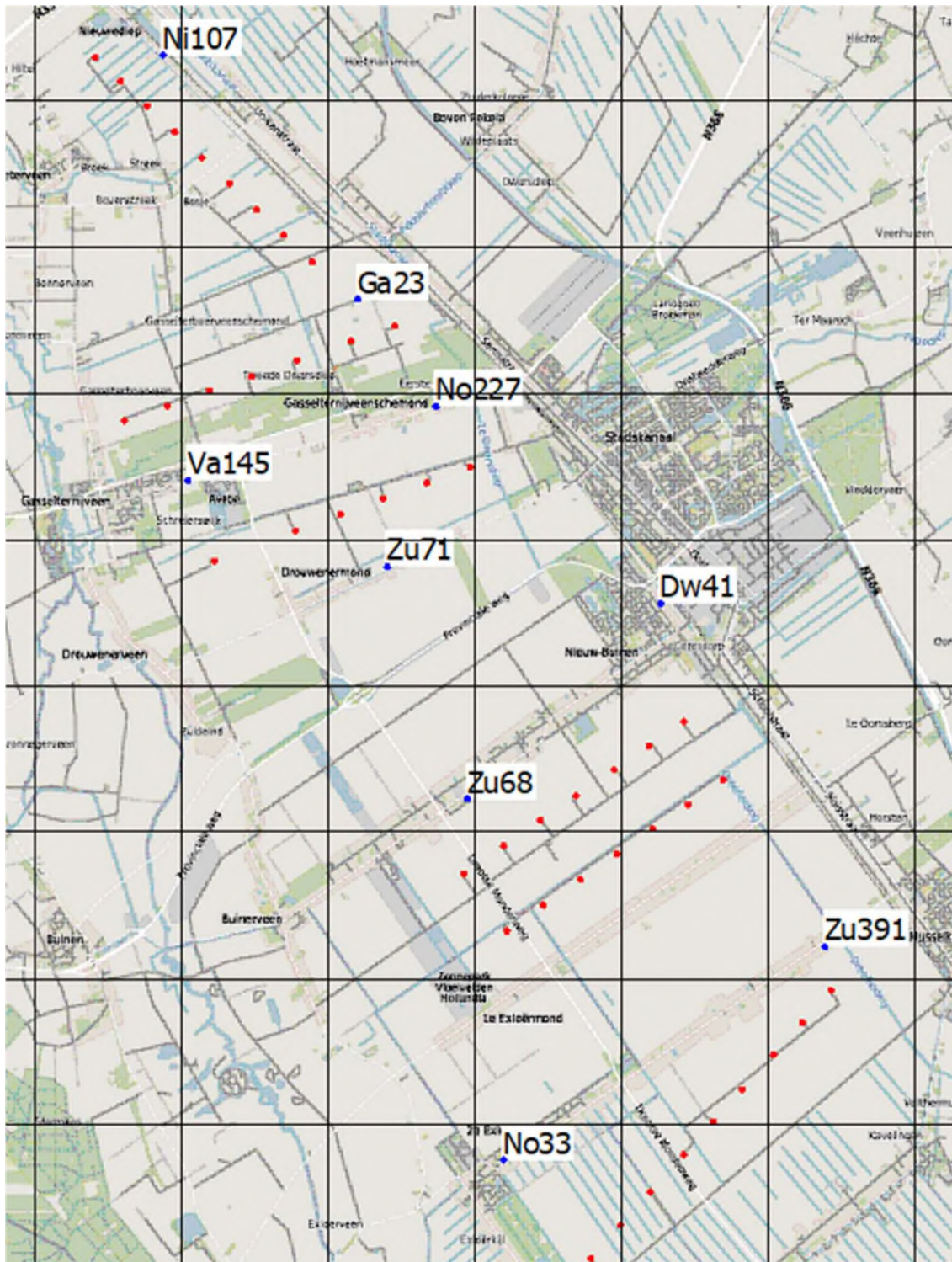


Figure 1 The measurement locations in blue, turbines of the wind farm in red. The grid is 2 km.

At measurement point Z71 and N33 the meteorological conditions were also measured. The shortest distance to a turbine is location Ga23 and Zu391 with a distance of approximately 600 m. The longest distance to the closest turbine is location Dw41 and No33 with a distance of approximately 1700 m.

At each measurement point the average sound pressure level was measured of the overall A-weighted sound level and of the unweighted sound level in the third octave bands of 6,3 to 125 Hz. The sampling

and averaging time was 10 minutes. The equipment was measuring the whole period from start to finish and was not removed during construction of the farm.

The data from May, June and July of 2020 and the data from May, June and July of 2022 was used in the analysis. The first dataset is from the period when the wind farm was not yet built, the second dataset is from the period when the wind farm was (almost) in full operation. The same months of the year have been used to minimise the effect of vegetation. A period of three months was used to obtain results at a broad range of meteorological conditions.

Only the data in the evening and night periods (between 7.00 pm and 7.00 am) was used in the analysis. The levels during the day were considerably higher than during the night and were mostly influenced by traffic noise.

4. Results

The effect of the wind farm can be assessed by comparing the time equivalent sound levels of all evening and nights of the data set from 2020 with the data from 2022. If the level in 2022 is substantially higher (i.e. more than 3 dB), then the effect of the wind farm can be calculated by subtracting the levels from each other. In figure 2, the results of point zu68 are given. This is one of three measurement locations where an effect on the average noise level was found. At six locations (see example in figure 3) the effect on the average sound level is minimal.

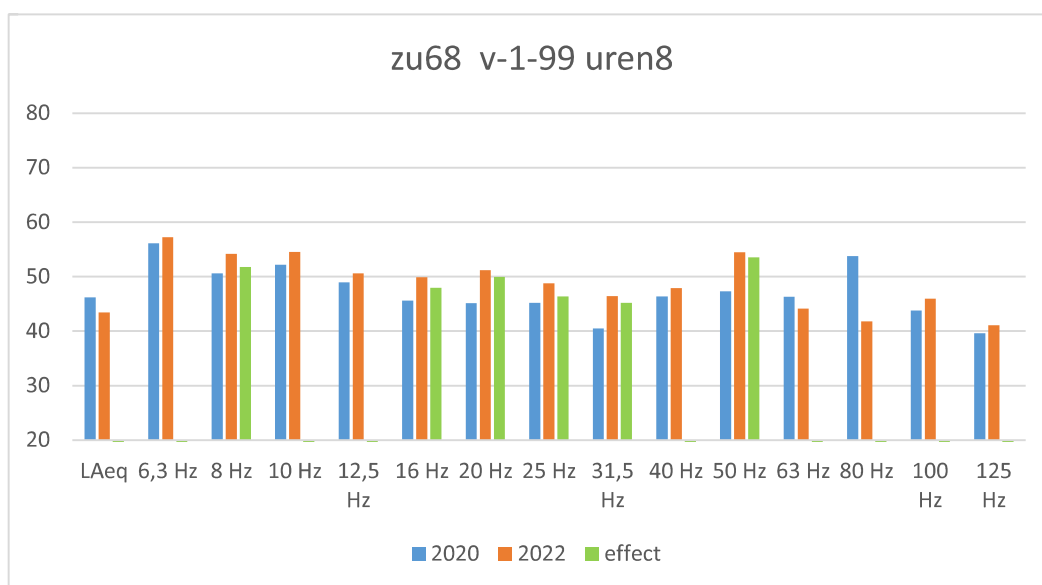


Figure 2 The average sound level at location zu68 of all nights from the data set.

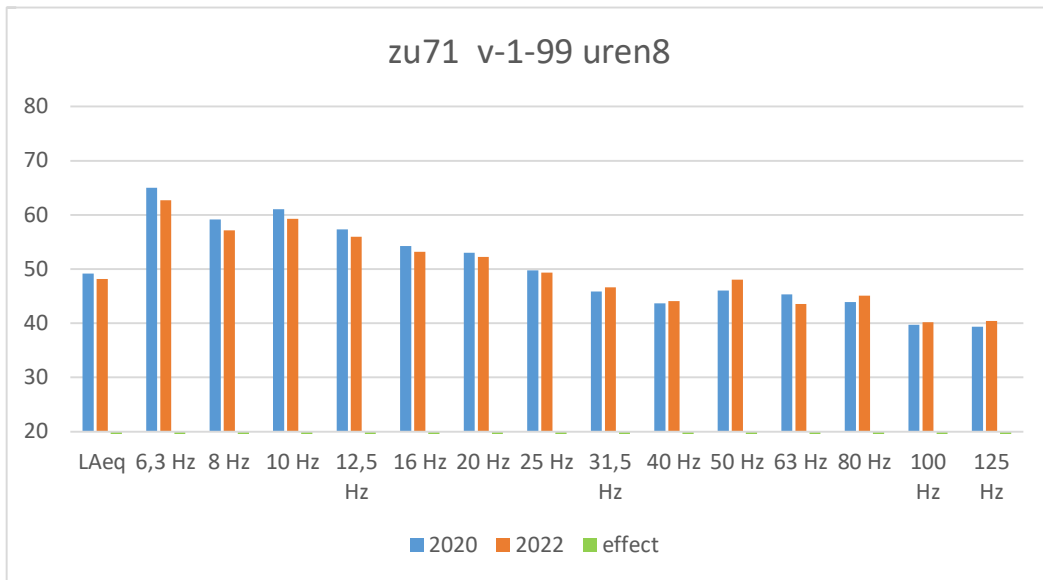


Figure 3 The average sound level at location zu71 of all nights from the data set.

The effect of the wind farm can also be assessed by using a histogram to present the data. By binning the data according to 10 minute sound levels of 1 dB and counting the number of samples in each bin, a histogram is obtained. Figure 4 shows the results for location zu68. The data from 2020 show quite a symmetric distribution of sound levels between 25 and 60 dB(A). The data from 2022 show that including the wind farm, most levels are in the region of 33 to 43 dB(A).

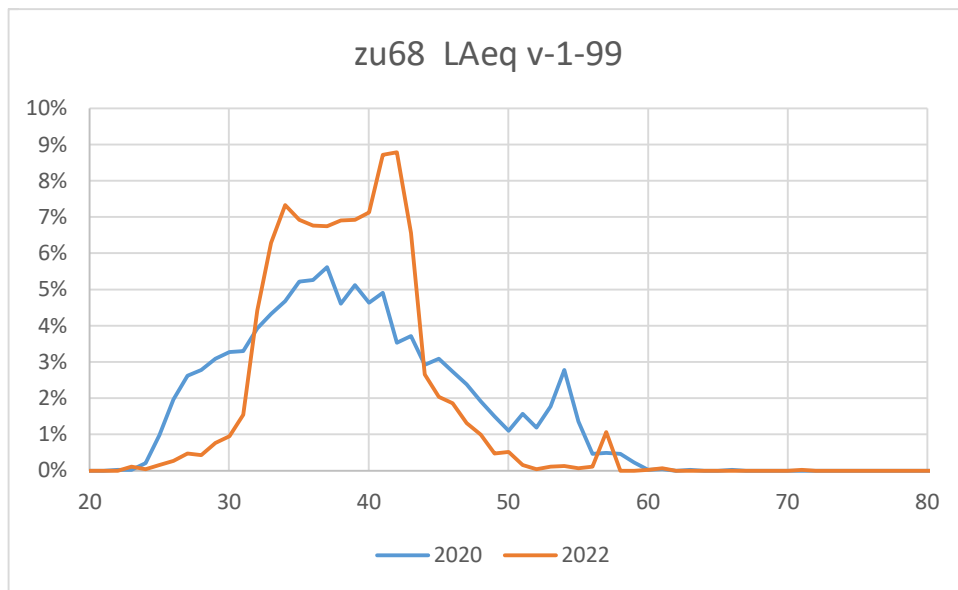


Figure 4 Histogram of location zu68 of all nights from the data set.

For location zu71, the histograms of 2020 and 2022 appear to be almost identical, apart from an increase in the occurrence of sound levels at 41 and 42 dB(A). The increase becomes more distinct when only comparing data at wind speeds higher than 1 m/s (see figure 6).

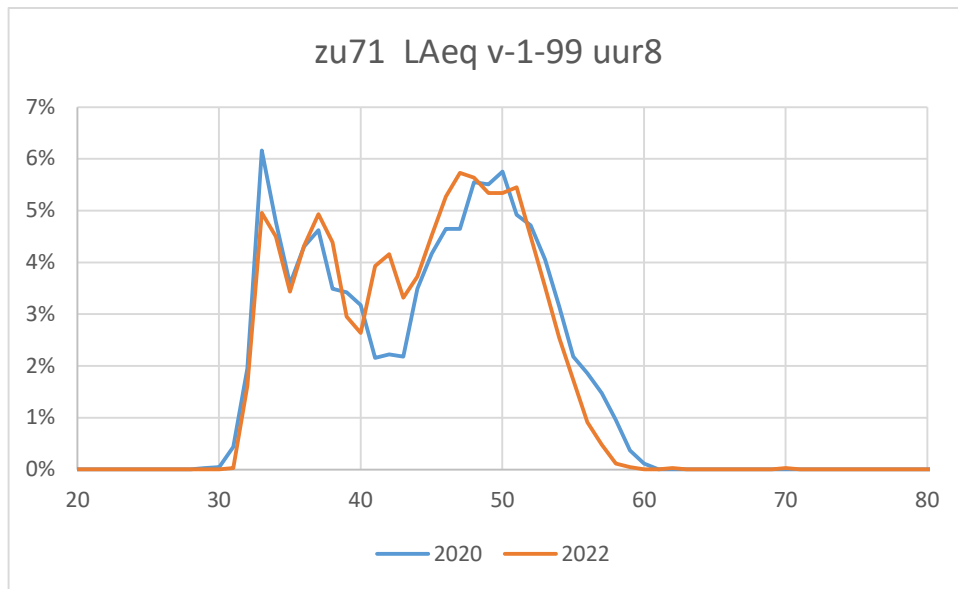


Figure 5 Histogram of location zu71 of all nights from the data set.

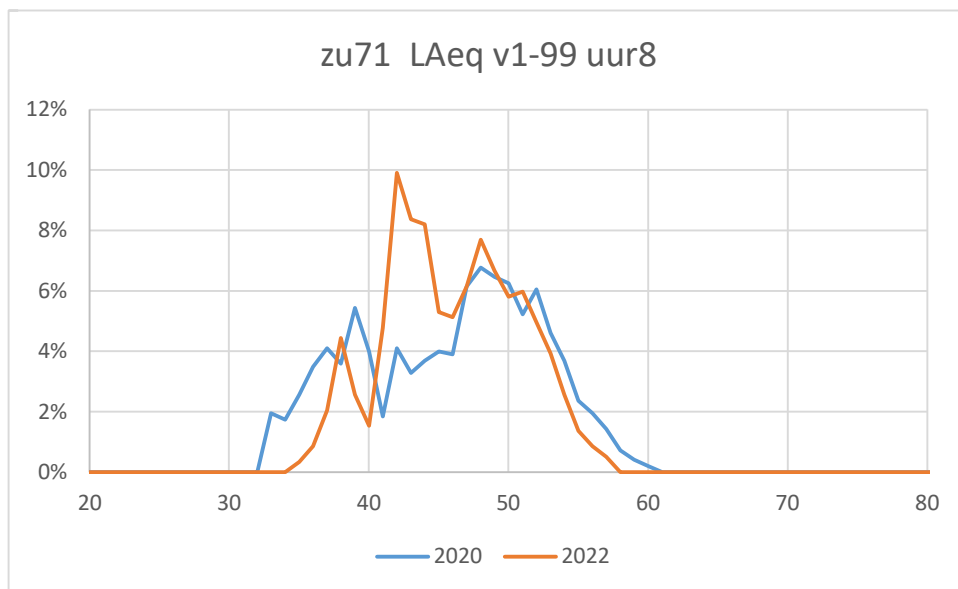


Figure 6 Histogram of location zu71 of all nights from the data set with wind speed > 1 m/s.

A histogram was made of all measured third octave bands. Most low frequencies show a clear increase in noise level when data is used with sufficient wind (> 1 m/s) (see the example in figure 7).

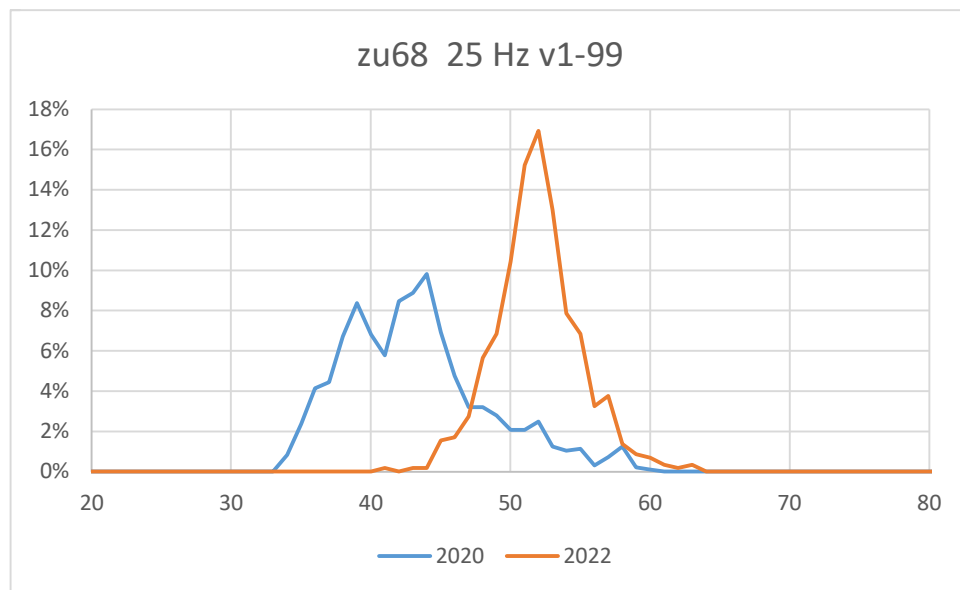


Figure 7 Histogram of third octave band 25 Hz of location zu68 of all nights from the data set with wind speed > 1 m/s.

From all histograms [1] of the third octave bands, the unweighted sound levels of figure 8 are obtained. The levels are from the samples when the wind farm is almost in full operation. The graph in figure 8 also shows two curves to assess the low frequency levels outside dwellings. The NSG-curve [2] can be understood as the level at which low frequency can be heard by humans. The VROM-curve [3] can be assumed as the level when annoyance occurs.

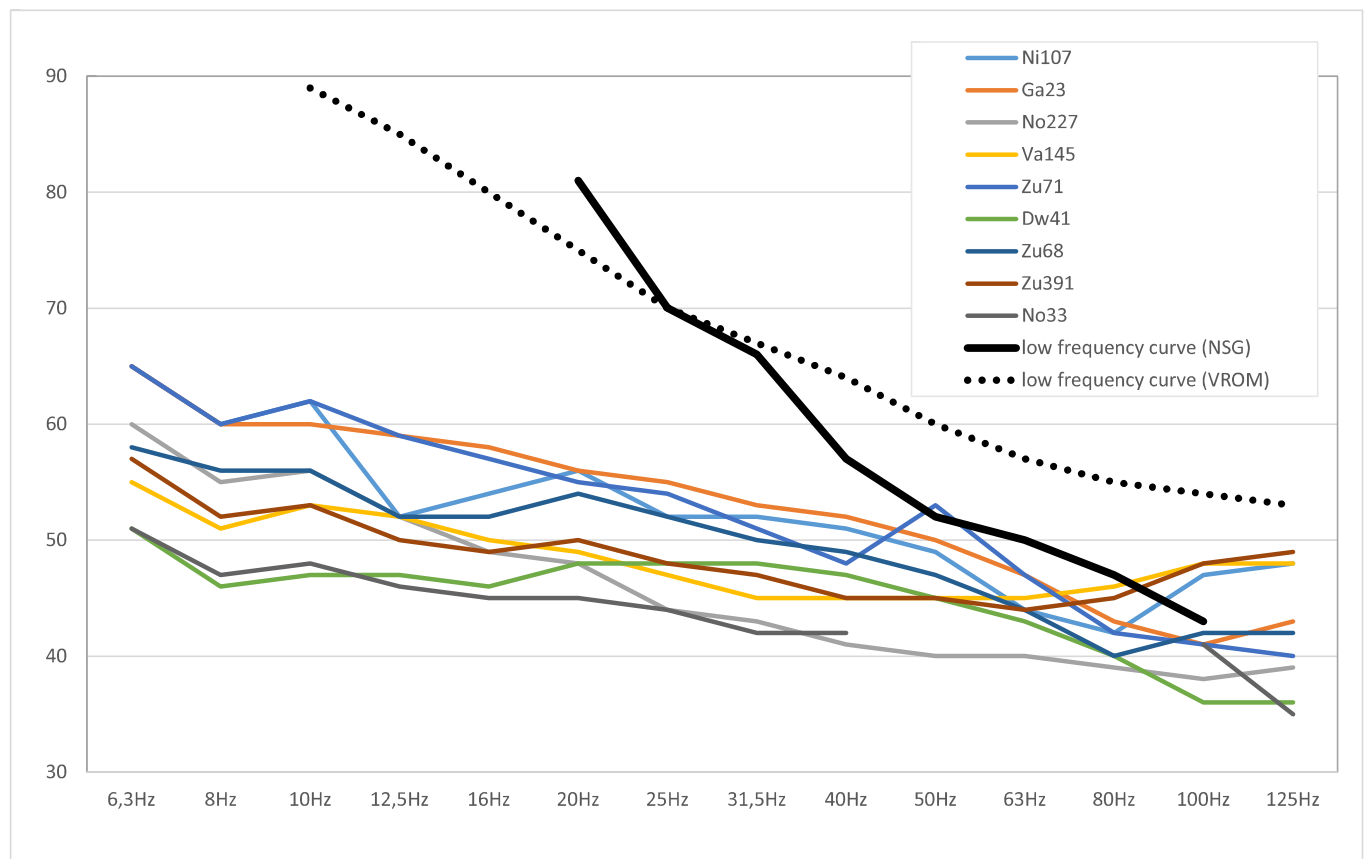


Figure 8 Unweighted low frequency sound level in windy conditions compared to NSG and VROM curves to assess outdoor low frequency sound.

The sound levels at dwellings are also calculated according to the Dutch method (similar to ISO 9613-2) based on the specifications from Nordex. In table 1 the measured levels are compared to the calculated levels.

Table 1 A-weighted levels in octave bands

Point	Measured					Calculated		
	8Hz	16Hz	31,5Hz	63Hz	125Hz	31,5Hz	63Hz	125Hz
Ni107	-8	6	18	24	33	23	32	29
Ga23	-9	7	19	25	28	25	34	31
No227	-14	-1	9	19	24	19	28	24
Va145	-17	0	12	25	34	21	30	27
Zu71	-8	6	17	26	26	18	27	24
Dw41	-23	-2	14	21	22	17	26	23
Zu68	-13	4	16	22	28	22	31	28
Zu391	-17	0	13	24	34	22	31	28
No33	-22	-4	9	--	24	15	25	21

Table 1 shows that the measured levels for the 31,5 and 63 Hz octave bands are lower than expected. For the 125 Hz octave band the measured levels are up to 7 dB higher than expected at four of the nine locations (Ni107, Va145, Zu71 and Zu391).

5. IEC61400-11 emission measurement

In addition to the long term measurement of the sound emission at dwellings, short term measurements of the emission of three of the 45 turbines were performed according to the IEC61400-11 method. Additional indicative short term measurements were also performed at 12 other turbines to check if the spectral distribution is the same as the three turbines measured according to the IEC-method.

The results of the three turbines measured according to the IEC-method show that the overall sound power level are similar or lower than the specifications. No relevant tonality was found.

In figure 9 the spectral results in octave bands are given. The results show that the measured spectral distribution is similar to the specifications. The measured levels at high frequencies are notably lower. For one of the measured turbines, the emission at 31,5 and 63 Hz is 1 to 2 dB higher. At the 125 Hz octave band the measured levels are not higher than expected.

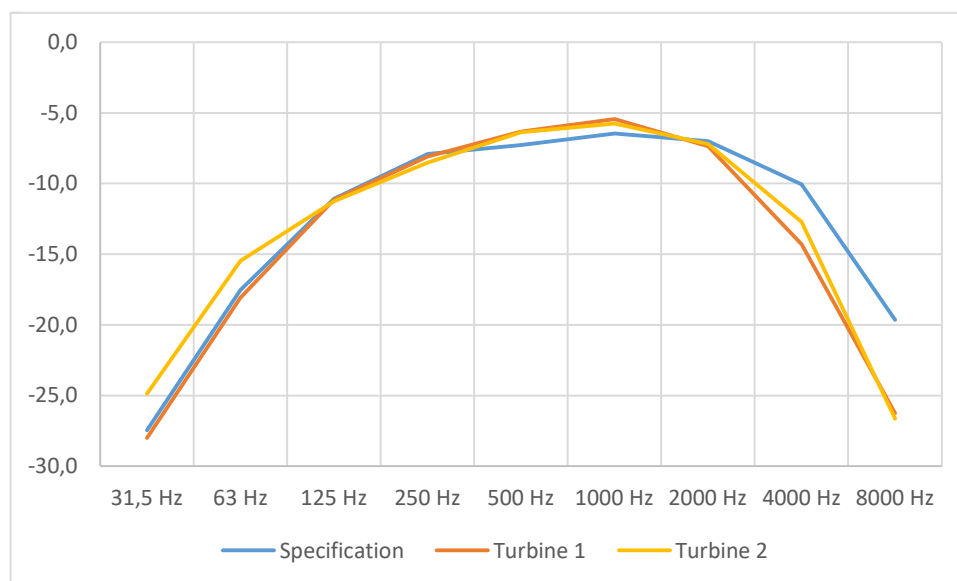


Figure 9 Sound spectrum of measured emission of 2 turbines compared to the specifications

6. Conclusions

Long term sound measurements have been performed before and after the wind farm was built. By analysing a period of several months, a clear difference can be found in the sound emission levels with and without the wind farm. Histograms have been used to analyse the difference in sound levels. The histograms show the number of 10 minute samples for each discrete sound level value. The analysis shows that low frequency sounds were measured at dwellings surrounding the wind farm.

For most measurement locations and most frequencies, a clear effect of the low frequency sound of the wind farm can be seen. Figure 8 shows that for the lowest frequencies (6 to 40 Hz) the sound levels are not relevant and probably will not be perceived.

The higher frequencies (50 to 125 Hz) can be heard but are not significantly higher than expected and annoyance due to low frequency sound is not expected.

The measured levels for the 31,5 and 63 Hz octave bands are lower than expected. For the 125 Hz octave band the measured levels are higher than expected at four of the nine locations (Ni107, Va145, Zu71 and Zu391). The higher levels at the 125 Hz octave band were not found in the measured emission at the turbines. The cause of these higher levels at the dwellings was not found.

Acknowledgements

The long term noise measurements were carried out by DGMR, Drachten together with LBP|SIGHT, Nieuwegein. The author wishes to thank G. van Kempen from DGMR.

References

- [1] LBPSIGHT, Akoestisch onderzoek Windpark De Drentse Monden en Oostermoer. R068502aa.22CH7TH.md, *Gemeente Borger-Odoorn*, Jan. 30, 2023. Accessed: Mar. 24, 2025. [Online]. Available: www.borger-odoorn.nl/geluid-gezondheidsonderzoek
- [2] NSG (Nederlandse Stichting Geluidhinder), "NSG-richtlijn laagfrequent geluid," Delft, Apr. 1999. Accessed: Mar. 24, 2025. [Online]. Available: static.nsg.nl/NSG-Richtlijn-rlfg.pdf
- [3] M.L.S. Vercammen, "Low-frequency noise limits," *Journal of Low frequency noise and vibration*, vol. 11, no. 1, Mar. 1992. Accessed: Mar. 24, 2025. [Online]. Available: <https://doi.org/10.1177/026309239201100102>

Paper #7 - ID: 340

Title: Estimating the effects of Wind Turbine Noise on annoyance and cognitive performance

Author: Denis O'Hora

11th Edition of the
International Conferences on
Wind Turbine Noise
Copenhagen, Denmark – 10th to 13th June 2025

Estimating the effects of Wind Turbine Noise on Annoyance and Cognitive Performance: The Role of Noise Sensitivity

Denis O’Hora¹, Eoin King, Santiago Garcia-Guererro, and Manish Manohare
University of Galway, Galway, Ireland

Summary

Despite growing public concerns about the cognitive impacts of wind turbine noise exposure, empirical evidence examining its effects on cognitive functioning remains limited. This study investigated whether wind turbine sound affects memory performance and subjective experience through potential interference with neural processing. In a within-subjects design, 46 participants completed a recognition memory task (304 trials) under systematically varied wind turbine sound conditions. We manipulated memory load and acoustic properties while measuring recognition accuracy and subjective annoyance ratings. Memory performance showed the expected load-dependent decrements in accuracy, but critically, showed no significant impairment from wind turbine sound exposure. Analysis of subjective responses revealed that while overall annoyance ratings were modest, they systematically correlated with specific acoustic parameters and were elevated in noise-sensitive participants. Annoyance ratings increased across blocks suggesting potential cumulative effects of prolonged exposure and this increase was exacerbated in noise-sensitive participants. However, these elevated annoyance levels did not predict memory performance decrements. These findings challenge popular concerns about wind turbine noise’s impact on cognitive function while highlighting the importance of distinguishing between subjective discomfort and objective performance effects in environmental psychology.

1. Introduction

The global transition towards sustainable energy will depend on the exploitation of wind energy [1–3]. Wind turbine noise (WTN) is a concern for communities residing near wind farms [4] and, thus, understanding the effects of WTN on the population is necessary for sensitive and sensible deployment of wind turbines.

Wind turbines produce a variety of sounds during operation, including tonal, broadband, low-frequency, and impulsive components [5, 6]. This complexity may be part of the reason that WTN tends to be reported as more annoying compared to other environmental noises at the same sound pressure level. For example, WTN that sounds like “swishing,” “lapping,” or “whistling” has been found to elicit greater annoyance than WTN described as “grinding” and “low frequency” [7]. The irregular rhythmic attributes of WTN (lacking in patterns and symmetry) can make WTN more difficult to ignore and intrusive [8]. Consequently, addressing WTN may not simply require noise level reduction, but interventions focused on the specific acoustic characteristics that affect noise annoyance [9].

¹Corresponding author - Email: denis.ohora@universityofgalway.ie

"Noise annoyance" is formally recognised by the World Health Organization (WHO) as an "environmental health burden" [10]. Annoyance is, however, a difficult construct to measure. It is inherently complex and highly subjective, varying significantly between individuals. A noise that is considered moderately annoying by one person could be extremely annoying to another. Individual differences in noise sensitivity are also recognised as an important antecedent to noise annoyance. WTN annoyance includes negative feelings such as dissatisfaction, disturbance, displeasure, irritation, and nuisance [11]. Associations between WTN exposure and various health outcomes have been investigated, including mental health indicators such as sleep disturbance, anxiety, and noise sensitivity, as well as physical factors like cardiovascular and metabolic effects [9, 12, 13]. There is no evidence of direct, harmful physical effects on people from WTN exposure [9, 14], but annoyance and sleep disturbance have been associated with WTN [12].

When attempting to measure a subjective response such as annoyance, there are a number of response biases that can be observed in addition to the variations in sensitivity. For instance, in any affective report, peak and recency effects can be observed in self-reports. In addition, one's attitude to wind energy or the planning processes that preceded the installation of a wind farm might colour one's experience of the sounds of wind energy being generated. To one person, it might be an imposition and to another, a reminder of their commitment to a greener future. To attenuate these response biases, researchers have proposed alternative measures of annoyance that include physiological or other stress indicators [3].

Despite the absence of evidence of direct physiological effects of WTN, it remains a salient concern of wind farm communities. When considering how noise might affect the human body, one vector worth considering is the human auditory system. The human auditory system is highly sensitive to fluctuations in air pressure, and neural activity that is induced in this system is what enables the perception of sound. Sympathetic oscillations within the system are entrained through contact with the sound. The brainwave entrainment hypothesis posits that external rhythmic stimuli can induce the brain to synchronise its neural activity to the frequency of the external stimulation [15, 16]. This mechanism is argued to underpin the perception of complex stimuli like music.

Specific neural oscillations, such as those in the theta and alpha frequency bands, are known to be linked to attention and memory processes [17–19]. External rhythmic stimulation has the potential to either enhance or interfere with cognition by facilitating or disturbing these endogenous neural frequency patterns. Given the aerodynamic nature of wind turbine noise, there is a direct relationship between the frequencies at which wind turbines produce sound and the potential influence of these frequencies on brain activity.

Two recent studies have explored the effects of WTN on memory. In an experiment by Yu et al. [20], participants completed a backward digit span (working-memory) task in the presence of wind farm recordings in a virtual environment. No significant differences in memory recall scores were found across experimental conditions. Ruotolo et al. [21] also employed a virtual environment to investigate the effects of WTN on short-term verbal memory and semantic memory. They found that accuracy of short-term verbal memory was not influenced by their experimental factors, such as distance to the noise source. Verbal fluency (how quickly and easily participants responded), on the other hand, was lower when participants were closer to the noise source.

Previous work from our laboratory has assessed the effects of WTN on cognitive performance and annoyance. It was observed that annoyance increased across blocks of trials in a cognitive experiment when controlling for acoustic features of WTN. In addition, noise sensitivity moderated the effects of acoustic features. Noise-sensitive individuals exhibit greater sensitivity to WTN than noise tolerant individuals [22, 23]. The current experiment explores whether annoyance effects due to exposure to WTN are exacerbated for noise sensitive participants.

2. Method

2.1 Participants

Forty-six participants (mean age = 26, range 18–65, 23 females) participated in the study. Participants were screened to exclude those with hearing issues, psychological disorders, or cardiovascular problems. Participants were exposed to 304 trials, so the sample size was sufficient for the use of mixed effect models with repeated measures [24]. Exclusion criteria included hearing-related issues, psychological disorders (e.g., depression, stress, post-traumatic stress disorder, anxiety), or cardiovascular problems.

2.2 Measures

Prior to the experimental task, participants completed questionnaires assessing demographics, noise sensitivity using the Weinstein Noise Sensitivity Scale (WNSS) [25], and attitudes toward wind turbines using a scale reported by Schäffer et al., [26]

2.3 WTN Stimuli

Auditory stimuli were extracted from an available dataset collected at Knocknalour, Gibbet Hill, Ballynancoran and Ballycadden wind farms in County Wexford, Ireland [27]. Audio recording (24-bit rate) of 10 min each were conducted at various intervals during different periods. The recordings used for this study were recorded at an average distance of 500 metres from the source.

From this collection of 10-minute recordings, eighteen 90-second audio tracks were presented during the memory task. In order to effectively sample the range of acoustic parameters within the whole set, clusters of recordings were derived to effectively sample the range of loudness, sharpness, roughness, and fluctuation strength in the overall dataset.

2.4 Working Memory Task

The Working-Memory Task (WMT) was based on tasks by Vogel et al [28] and Sausaeng et al [29] and was conducted in a sound chamber. Visual stimuli, consisting of slides with coloured squares, were presented on a monitor, while auditory stimuli, 90-second audio tracks of WTN, were played through a speaker.

The visual stimuli were displayed on a 22-in digital monitor (1920 x 1080 resolution, refresh rate 60 Hz), located in front of the user (60 cm). Also, a single speaker (Genelec 8330) was used to reproduce the auditory stimuli, located further behind the computer screen (1.40 cm). The exact sound pressure levels produced by the speaker were calibrated at the listener's position using a calibrated class-1 sound level meter. The task was programmed using PsychoPy® (v2023.2.3; [30]), and run from a standard laptop.

Participants completed 19 blocks of 16 trials during the experiment. 18 blocks were accompanied by WTN and one was not. Each trial block started and finished with five seconds of WTN with no visual stimulation. On each trial, a fixation dot was briefly presented in the centre of the screen (1600 ms), immediately after which an arrow (presented for 200 ms) cued participants to attend to either the left or right (50% of trials towards each direction). Next two arrays of visual stimuli appeared for 200 ms. The screen then cleared for a retention interval lasting one second. Finally, a second pair of arrays of visual stimuli were presented for two seconds.

If the a square on the cued side changed colour, participants were required to press the spacebar to indicate the change (Go). If they did not see a change, they did not respond (No Go). Changes were present in 50% of the trials. During practice, participants responses were provided with feedback on their responses, but there was no feedback during the 304 experimental trials.

At the end of each block of 16 trials, the following question appeared at the top of the screen: “Thinking about the sound you heard during the last block of trials, how much did it bother, disturb or annoy you?”. Participants then pressed a button on the keyboard to respond on the following scale: 1(Not all all), 2(Slightly),

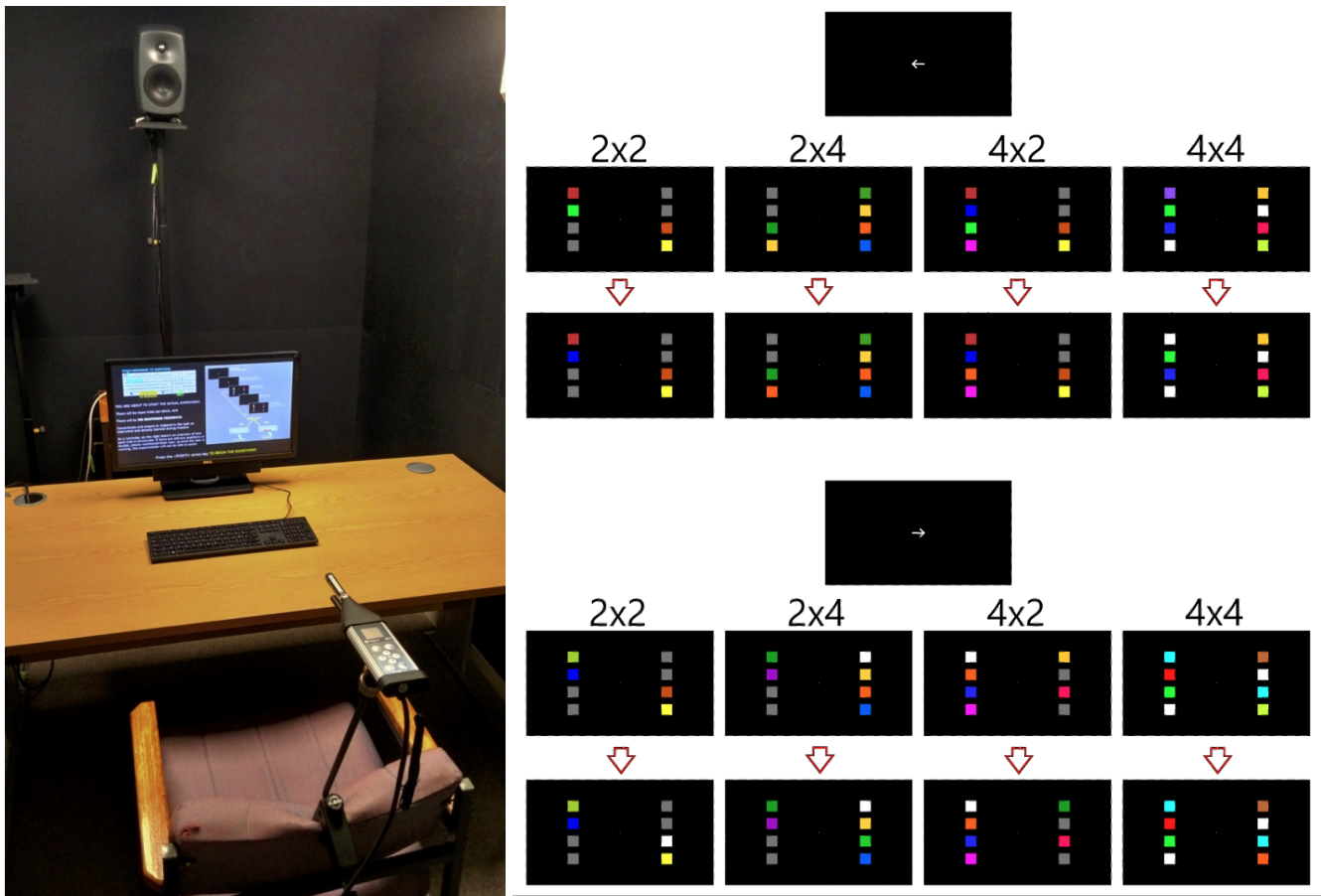


Figure 1 Laboratory set up and examples of the trials in the working memory experiment

3(Moderately), 4(Strongly), 5(Extremely).

3. Results

Participants completed 304 trials each, and 88% of the ratings of the WTN samples were rated as "not at all" annoying. Median noise sensitivity in the sample was 76.5 indicating a relatively noise-sensitive sample and attitudes towards wind turbines were quite positive (median response 41 out of 50). Noise sensitivity and wind turbine attitudes were not significantly correlated ($r = -0.25$, 95% CI = $-.50, .04$, $p = .09$)

3.1 Cognitive Performance

A mixed-effects binomial logistic regression model was employed to assess influences on cognitive performance. Participant was included as a random variable. The expected cognitive load effects were observed in the experiment (see Table 1), with increased relevant stimuli ($b = -0.81$, $p < .001$) and increased distractor stimuli ($b = -0.15$, $p < .05$) reducing accuracy. There was a significant interaction indicating that increased distractors reduced performance for easier probes to a greater extent ($b = 0.72$, $p < .001$); see Figure 2). Noise sensitivity and annoyance were included in the model but did not significantly influence accuracy, despite visual trends that suggested interference (Figure 2). Acoustic parameters did not improve the model of cognitive performance.

3.2 Annoyance

Annoyance responses on the 5 point likert scale were dichotomised into two variables. An annoyed response was coded for any response above "Not Annoyed" (2 or above). A highly annoyed response was coded for any response equal to or above "Highly Annoyed" (4 or 5). A mixed-effects binomial logistic regression model (see Table 2) identified a significant effect of noise sensitivity (WNSS) on annoyance, indicating that

Table 1 Binomial Mixed Effects Model Predicting Cognitive Performance

Term	<i>b</i>	SE	<i>z</i>	<i>p</i>	
1 (Intercept)	2.70	0.10	25.99	0.00	
2 Relevant	-0.81	0.07	-11.91	0.00	***
3 Distractors	-0.15	0.07	-2.15	0.03	*
4 Noise Sens	-0.15	0.10	-1.54	0.12	
5 Block	0.41	0.12	3.49	0.00	***
6 No Go Trial	-0.28	0.06	-4.50	0.00	***
7 Annoyed	-0.12	0.09	-1.39	0.16	
8 Rel x Dist	0.72	0.14	5.29	0.00	***
9 Rel x Noise Sens	0.04	0.06	0.67	0.51	
10 Dist x Noise Sens	-0.00	0.06	-0.00	1.00	
11 Rel x Block	0.09	0.23	0.39	0.70	
12 Dist x Block	0.13	0.23	0.53	0.59	
13 Noise Sens x Block	0.09	0.11	0.80	0.42	
14 Rel x Dist x Noise Sens	0.07	0.13	0.57	0.57	
15 Rel x Dist x Block	-0.32	0.47	-0.69	0.49	
16 Rel x Noise Sens x Block	0.02	0.22	0.07	0.94	
17 Dist x Noise Sens x Block	0.08	0.22	0.34	0.73	
18 Rel x Dist x Noise Sens x Block	0.49	0.44	1.10	0.27	
19 sd__(Intercept)	0.60				

Note. Significance *p* levels at .05*, .01**, .001***

Block is proportion of total blocks. Remaining continuous variables *z* scored.

Binary Variables scored -.5, +.5.

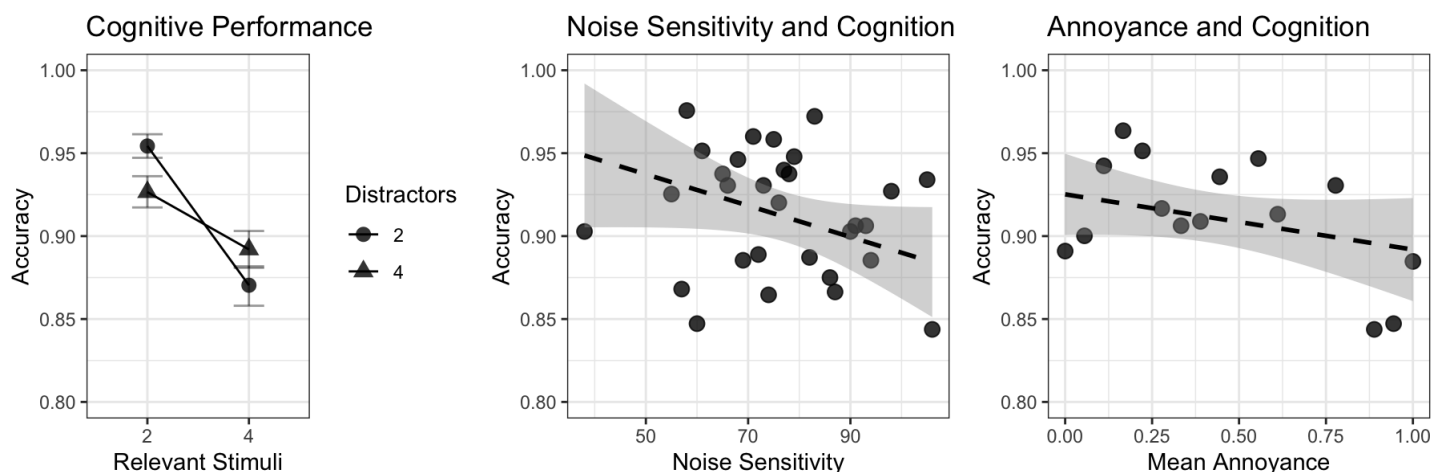


Figure 2 Accuracy during the Cognitive Task. Column 1 depicts the relationship between the visual stimuli presented and accuracy. Columns 2 and 3 depict the effects of noise sensitivity and annoyance on accuracy

individuals with higher noise sensitivity perceived the WTN samples as more annoying. Exposure to WTN increased annoyance across blocks of the experimental session. In addition, noise sensitivity moderated the effects of exposure such that those who were more sensitive to noise exhibited greater increases in annoyance across the session.

Of the acoustic characteristics of WTN, sharpness was excluded from the analyses due to very high negative correlations with roughness in our WTN samples. The remaining acoustic measures, loudness, roughness, and fluctuation strength, all significantly predicted participants' annoyance ratings. Notably, the effects of loudness and roughness on annoyance were stronger for individuals with high noise sensitivity. Amplitude modulation depth significantly increased annoyance, but frequency was associated with lower annoyance.

Table 2 Binomial Mixed Effects Model Predicting Annoyance

Term	<i>b</i>	SE	<i>z</i>	<i>p</i>	
1 (Intercept)	-0.50	0.57	-0.88	0.38	
2 Noise Sens	1.33	0.57	2.34	0.02	*
3 Loudness	0.78	0.03	25.79	0.00	***
4 Roughness	0.44	0.03	12.74	0.00	***
5 Fluctuation Str	0.17	0.03	5.55	0.00	***
6 Mod. Depth (200-800 dB)	0.33	0.03	10.80	0.00	***
7 Mod. Frequency (200-800 Hz)	-0.19	0.03	-6.53	0.00	***
8 Block	0.40	0.09	4.35	0.00	***
9 Noise Sens x Block	0.53	0.09	5.90	0.00	***
10 Noise Sens x Loudness	0.10	0.03	3.55	0.00	***
11 Noise Sens x Roughness	0.10	0.03	3.37	0.00	***
12 Noise Sens x F Str	-0.01	0.03	-0.48	0.63	
13 sd__(Intercept)	3.75				

Note. Significance *p* levels at .05*, .01**, .001***

Block is proportion of total blocks. Remaining continuous variables *z* scored.

Binary Variables scored -.5, +.5.

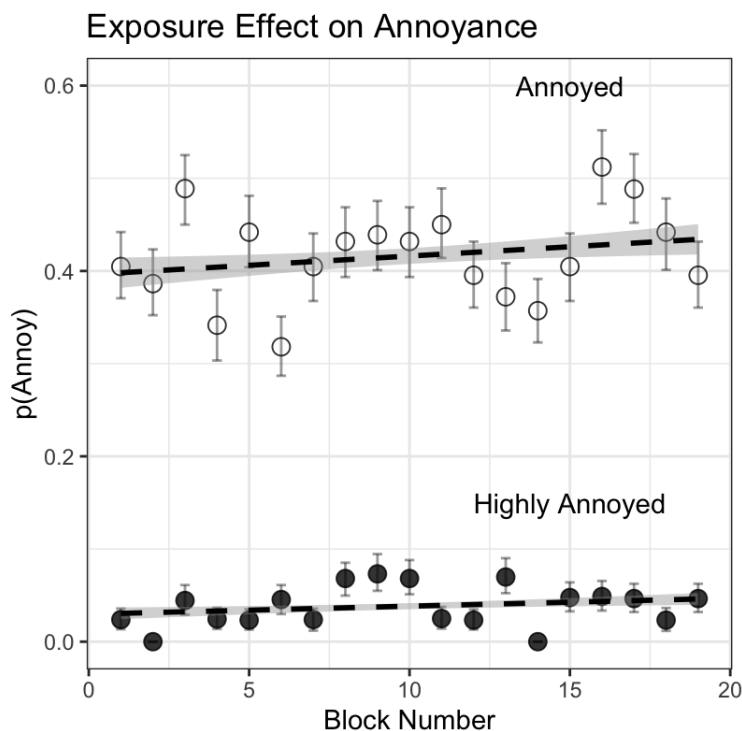


Figure 3 The effect of WTN Exposure on Annoyance

4. Conclusion

The current study addressed the effects of noise sensitivity and exposure to WTN on cognitive performance and annoyance by WTN. Noise-sensitive individuals were more prone to perceive WTN as annoying, but it did not significantly impair visual working memory. Noise-sensitive people attend more to sounds, display lower noise discrimination thresholds and evaluate noises out of their control as more threatening, compared to noise-tolerant people [31]. In the current study, noise-sensitive individuals were also more susceptible to exposure effects. So, not only are noise-sensitive individuals more likely to find a given noise annoying, but their annoyance is likely to increase more over time.

Immediate annoyance in the presence of WTN is not the same as the chronic annoyance that community members report in field studies. Our experiment was of significant duration, but it does not compare with living near a source of WTN. In addition, our participants were required to attend closely to the memory task to complete it. Anecdotal evidence suggests that environmental noise may be more annoying when individuals are attempting to relax and when attention is drawn to the WTN source without significant competition. Despite these limitations, our study did show that exposure to WTN increases annoyance by WTN and that noise sensitivity exacerbates this effect. Since WTN may become increasingly annoying over time, this should be considered when positioning wind farms and working with communities.

The working memory tasks employed in the current study focused on the visual modality or sense. This was intentional to prevent any physical interference between WTN and an auditory paradigm. However, it remains to be seen whether such sound might interfere with processing of visual stimuli that evoke phonological responses (e.g., words, nonsense words). There is somewhat mixed evidence on this issue based on the work of Yu et al [20] and Ruotolo et al. [21] and the current paradigm would be easily modified to include such tasks.

Acknowledgments

Our thanks to Dr. Sean Horsman for his help with sound calibration during the experimental setup.

Funding: The research conducted in this publication was funded by Research Ireland under grant number COALESCE/2022/1739.

References

- [1] F. Dincer, "The analysis on wind energy electricity generation status, potential and policies in the world," *Renewable and Sustainable Energy Reviews*, vol. 15, no. 9, pp. 5135–5142, 2011.
- [2] J. K. Kaldellis and D. Zafirakis, "The wind energy (r)evolution: A short review of a long history," *Renewable Energy*, vol. 36, no. 7, pp. 1887–1901, 2011.
- [3] F. J. Y. Müller, V. Leschinger, G. Hübner, and J. Pohl, "Understanding subjective and situational factors of wind turbine noise annoyance," *Energy Policy*, vol. 173, p. 113361, Feb. 2023.
- [4] R. Horbaty, S. Huber, and G. Ellis, "Large-scale wind deployment, social acceptance," *WIREs Energy and Environment*, vol. 1, no. 2, pp. 194–205, 2012.
- [5] E. A. King, F. Pilla, and J. Mahon, "Assessing noise from wind farm developments in Ireland: A consideration of critical wind speeds and turbine choice," *Energy Policy*, vol. 41, pp. 548–560, 2012.
- [6] S. Oerlemans, "Effect of wind shear on amplitude modulation of wind turbine noise," *International Journal of Aeroacoustics*, vol. 14, no. 5–6, pp. 715–728, 2015.
- [7] K. P. Waye and E. Öhrström, "Psycho-acoustic characters of relevance for annoyance of wind turbine noise," *Journal of Sound and Vibration*, vol. 250, no. 1, pp. 65–73, 2002.
- [8] S. Large and M. Stigwood, "The noise characteristics of "compliant" wind farms that adversely affect its neighbours," 2014.

- [9] I. Van Kamp and F. Van Den Berg, "Health effects related to wind turbine sound, including low-frequency sound and infrasound," *Acoustics Australia*, vol. 46, no. 1, pp. 31–57, 2018.
- [10] L. Fritschi, A. L. Brown, R. Kim, D. Schwela, and S. Kephelopoulos, eds., *Burden of disease from environmental noise: Quantification of healthy life years lost in Europe*. World Health Organization, Regional Office for Europe, 2011.
- [11] World Health Organization, Regional Office for Europe, *Environmental noise guidelines for the European Region*. World Health Organization, Regional Office for Europe, 2018.
- [12] E. Karasmanaki, "Is it safe to live near wind turbines? reviewing the impacts of wind turbine noise," *Energy for Sustainable Development*, vol. 69, pp. 87–102, 2022.
- [13] L. D. Knopper and C. A. Ollson, "Health effects and wind turbines: A review of the literature," *Environmental Health*, vol. 10, no. 1, p. 78, 2011.
- [14] I. Van Kamp and F. Van Den Berg, "Health effects related to wind turbine sound: An update," *International Journal of Environmental Research and Public Health*, vol. 18, no. 17, p. 9133, 2021.
- [15] U. Will and S. Makeig, "Eeg research methodology and brainwave entrainment," in *Music, science, and the rhythmic brain*, pp. 86–107, Routledge, 2012.
- [16] R. M. Ingendoh, E. S. Posny, and A. Heine, "Binaural beats to entrain the brain? a systematic review of the effects of binaural beat stimulation on brain oscillatory activity, and the implications for psychological research and intervention," *PLOS ONE*, vol. 18, no. 5, p. e0286023, 2023.
- [17] P. Lakatos, G. Karmos, A. D. Mehta, I. Ulbert, and C. E. Schroeder, "Entrainment of neuronal oscillations as a mechanism of attentional selection," *Science*, vol. 320, no. 5872, pp. 110–113, 2008.
- [18] C. S. Herrmann, D. Strüber, R. F. Helfrich, and A. K. Engel, "Eeg oscillations: From correlation to causality," *International Journal of Psychophysiology*, vol. 103, pp. 12–21, 2016.
- [19] D. Henao, M. Navarrete, M. Valderrama, and M. Le Van Quyen, "Entrainment and synchronization of brain oscillations to auditory stimulations," *Neuroscience Research*, vol. 156, pp. 271–278, 2020.
- [20] T. Yu, H. Behm, R. Bill, and J. Kang, "Audio-visual perception of new wind parks," *Landscape and Urban Planning*, vol. 165, pp. 1–10, 2017.
- [21] F. Ruotolo, V. P. Senese, G. Ruggiero, L. Maffei, M. Masullo, and T. Iachini, "Individual reactions to a multisensory immersive virtual environment: The impact of a wind farm on individuals," *Cognitive Processing*, vol. 13, no. S1, pp. 319–323, 2012.
- [22] R. J. McCunney, K. A. Mundt, W. D. Colby, R. Dobie, K. Kaliski, and M. Blais, "Wind turbines and health: A critical review of the scientific literature," *Journal of Occupational & Environmental Medicine*, vol. 56, no. 11, pp. e108–e130, 2014.
- [23] T. R. Haac, K. Kaliski, M. Landis, B. Hoen, J. Rand, J. Firestone, D. Elliott, G. Hübner, and J. Pohl, "Wind turbine audibility and noise annoyance in a national u.s. survey: Individual perception and influencing factors," *The Journal of the Acoustical Society of America*, vol. 146, no. 2, pp. 1124–1141, 2019.
- [24] M. Brysbaert and M. Stevens, "Power analysis and effect size in mixed effects models: A tutorial," *Journal of Cognition*, vol. 1, no. 1, p. 9, 2018.
- [25] N. D. Weinstein, "Individual differences in reactions to noise: A longitudinal study in a college dormitory," *Journal of Applied Psychology*, vol. 63, no. 4, pp. 458–466, 1978.
- [26] B. Schäffer, R. Pieren, U. Wissen Hayek, N. Biver, and A. Grêt-Regamey, "Influence of visibility of wind farms on noise annoyance – a laboratory experiment with audio-visual simulations," *Landscape and Urban Planning*, vol. 186, pp. 67–78, 2019.

- [27] RPS group, “Knocknalour wind farm noise monitoring report,” Tech. Rep. MGE0552RP0005; Noise Monitoring Services (Wexford Wind Farms) – Lot 1, Wexford County Council, 2017.
- [28] E. K. Vogel, G. F. Woodman, and S. J. Luck, “Storage of features, conjunctions, and objects in visual working memory,” *Unknown Journal*, vol. 27, no. 1, p. 92, 2001.
- [29] P. Sauseng, W. Klimesch, K. F. Heise, W. R. Gruber, E. Holz, A. A. Karim, M. Glennon, C. Gerloff, N. Birbaumer, and F. C. Hummel, “Brain oscillatory substrates of visual short-term memory capacity,” *Current Biology*, vol. 19, no. 21, pp. 1846–1852, 2009.
- [30] J. W. Peirce, “Psychopy—psychophysics software in python,” *Journal of Neuroscience Methods*, vol. 162, no. 1–2, pp. 8–13, 2007.
- [31] S. A. Stansfeld, “Noise, noise sensitivity and psychiatric disorder: Epidemiological and psychophysiological studies,” *Psychological Medicine. Monograph Supplement*, vol. 22, pp. 1–44, 1992.

Paper #8 - ID: 342

Title: The effects of low frequency noise considering the real complainants and real sites, and methodology for surveys of residents and development of mobile devices for good understanding on sound at wind turbine sites.

Author: Shinji Yamada

11th Edition of the
International Conferences on
Wind Turbine Noise

Copenhagen, Denmark – 10th to 13th June 2025

The effects of low frequency noise considering the real complainants and real sites, and methodology for surveys of residents and development of mobile devices for good understanding on sound at wind turbine sites

Shinji YAMADA¹ and Toshiya KITAMURA

University of YAMANASHI, Takeda 4-3-11, Kofu, Yamanashi, 400-8511, Japan

Hiroaki OCHIAI, Tetsuya DOI and Keiichiro IWANAGA

Kobayasi Institute of Physical Research, Higashimotomachi 3-20-41, Kokubunji, Tokyo, 185-0022, Japan

Summary

Regarding the low frequency noise problem, we carefully analysed the situation at the real site and did experiments. These results can be used for good understanding for wind turbine sites.

At the real complain sites, the sound is normally continuous wave. The hearing thresholds by continuous sound are larger than those of the intermittent sound (ISO method).

The thresholds of complainants and university students were no essential differences on low frequency noise.

When complainants and university students were exposed to low-frequency noise, some complainants experienced the increase in breathing rate but there was no change in the university students. At the lower level than the hearing threshold, there was no effect.

The reference value on low frequency noise in Japan was created by drawing a line that distinguishes between real complainants, who have a corresponding relationship to machine operation time and unpleasant time, and complainants, who do not.

The thresholds (by vibration feeling and hearing) of deaf persons were very high comparing to ordinary persons. So, infrasound or low frequency noise are perceived in ordinary persons by hearing system. At the wind turbine site, no effect occurs except very near area scientifically.

From the experience of many sites, we will describe how to conduct surveys in areas where wind turbines are installed. We also created devices that can be carried to the site. The residents can have the real experiences on low frequency noise. We will describe how to use these devices to obtain appropriate good understanding of residents.

¹ Corresponding author – Email: shinji-yamana@ae.auone-net.jp

1. Introduction

When complaints about low-frequency noise occur, the authors have carefully listened to the complainant's complaint, measured the sound at the complaint site, and made an effort to resolve the problem. Authors have visited about 50 complaint sites and provided support to the complainants. Authors valued the complainants and the complaint sites, but in order to maintain objectivity, authors also tried to interview the sound source as much as possible. In the process, authors also felt the importance of human relations between the sound source and the sound receiver.

The author, Yamada, was a certified counsellor of the Japanese Association of Counselling Science. His experience in providing psychological counselling was also useful for psychological analysis of the complainants.

In this study, authors would like to present the experiences gained from many years of research on low-frequency noise, regarding the good method of research, the way of approaching subjects, and the way of approaching complainants. It is important to harmonize scientific thinking with respect for humanity, which is the philosophical aspect of academic studies that deal with human beings. In dealing with complainants of low-frequency noise, we would like to show the importance of individuality in the way research is conducted. We would also like to use these experiences to talk about wind turbines and wind turbine noise.

2. Low-frequency noise problems in Japan

2.1 Classification of low-frequency noise complainants

When a complaint about low-frequency noise occurred, an author visited the site and listened and measured for at least three hours. If the complainant(s) said that the low-frequency noise woke them up, the author measured continuously throughout the night and observed and recorded the complainant's condition. The author listened carefully to the complaint, measured the sound at the complaint site, and made efforts to resolve the issue. During the visit to the complaint site, the author noticed that there were cases where the complainant's expression did not match the reality.

Complaints were classified into cases where the complaints were clearly related to the operating status of the noise source, and cases where the complaints were thought to be unrelated to the operating status of the sound source. Although the number was small, there were also cases where the causal relationship between the complaint content and the operating status of the sound source could not be clearly determined. The author classified the complaints into three categories: corresponding, without corresponding, and ambiguous corresponding. With the exception of some experiments, we asked complainants with correspondence to cooperate in the experiments.

2.2 Cases where there is a correspondence

- The operating time of the sound source matches the time when the complaint occurred.

Later we say "complaint with correspondence".

2.3 Cases where the occurrence of a complaint does not match the operating status of the sound source (without correspondence).

- Cases where the measured sound change and the complaint record do not match at all in terms of time
- Cases where the complained-about machine is stopped but the complainant says the sound is still there, or the complaint does not go away.
- There are also cases where it seems to be tinnitus. It is difficult for the complainant to confirm whether it is tinnitus or not. The author has low-frequency tinnitus like the low-frequency sound that he often heard in experiments.
- Some complainants say that they are troubled by low-frequency noise and electromagnetic waves. About 40 years ago, the media broadcast that people are suffering from infra-sound that they cannot hear. Nowadays, there are people who believe similar articles on the Internet.
- It is claimed that it is the oil water heater of the neighbouring house, but after staying together for a few hours, the sound of an airplane is claimed to be the noise coming from the neighbouring house. The room is surrounded by lead plates. It is too quiet inside the room, and it feels unnatural.

Later we say "complaint without correspondence".

2.4 Ambiguous cases

Although the number is small, there are cases where it was not possible to determine at the time whether there was a correspondence.

- The sound pressure level is very low, and the temporal changes may match the complainant's reaction, but there is often a time lag. It is unclear whether there is a correspondence.
- It is thought that the operating state of the sound source was identified before, but countermeasures were taken to decrease the noise source, and the complainant is now unable to perceive it. Anxiety remains as a residual effect.

2.5 Cases where there remains low-frequency noise but now no problem (only one case)

This was a complaint about low-frequency noise generated by an oil boiler. The author too could detect it. The complainant (female) was encouraged to leave the house in the daytime and do volunteer work. The complainant began volunteering. The noise situation is the same as before, but it no longer bothers her. The complainant said, "I wonder why I used to be so concerned about it."

Notes for this chapter

- There were seven complaints, who were woken up by low-frequency noise at night. As it was an old measuring device, the data recorder tape must be changed every hour. The complainant woke an author when he/she felt that the low-frequency noise woke him/her up, and the time was noted. In the morning, the author checked to see if there was any change in the noise data at that time. Of the seven cases measured, the only one case where a correspondence was confirmed. In the case where the sound changed at exactly 5:00 a.m. For the other complainants, there was no change in the sound, so they were not woken up by the low-frequency noise. It was thought that they went to bed feeling anxious before going to sleep, which caused their sleep to be shallow and woke them up.
- For complainants with no correspondence, it is very difficult to get them to understand that low-frequency noise is not a problem. They are not convinced. They believe that something is causing them to feel unwell. We present scientific ideas, but do not force them.
- With the cooperation of the noise source, it is sometimes possible to turn the machine on and off. We ask the complainant to be in the most disturbing spot in the room and listen to the sound. We ask a third party (local officer etc.) to check whether the sound source is on and off. We compare the complaint time and the time of on and off of machine.

- Even around 40 years ago, there were cases where there was no correspondence. However, there were more cases where there was a correspondence. Since the spread of the Internet, there have been more complaints where there was no correspondence.

3. Threshold difference in low-frequency sound between continuous and intermittent sounds

ISO389-7 is a threshold measured by using intermittent sounds. On the other hand, there are no intermittent sounds in the field, and most complaints are about continuous sounds. Once the sound source starts working, it continues to operate continuously for several tens of minutes. It may get weaker and stronger, but it is not an intermittent sound. Therefore, we performed a threshold measurement using continuous sounds and compared it with the threshold of intermittent sounds.

A continuous sine wave is generated, and the sound pressure level is gradually increased, and when the subject perceives it, the subject is asked to press a button. Also, the sound pressure level is set to a level that the subject can clearly hear, and it is gradually lowered. When the subject can no longer perceive it, the subject is asked to press a button and the sound pressure level is recorded. The threshold for that frequency was determined by averaging the threshold when it rises and the threshold when it falls.

The results are shown in Figure 1. The threshold of continuous sounds is the same around 20 Hz as ISO389-7, which is an intermittent sound, but as the frequency increases, the threshold for continuous sounds is higher. The threshold for continuous sounds should be considered when determining whether a complaint occurs.

In this report, unless otherwise specified, continuous sounds were used in the experiments.

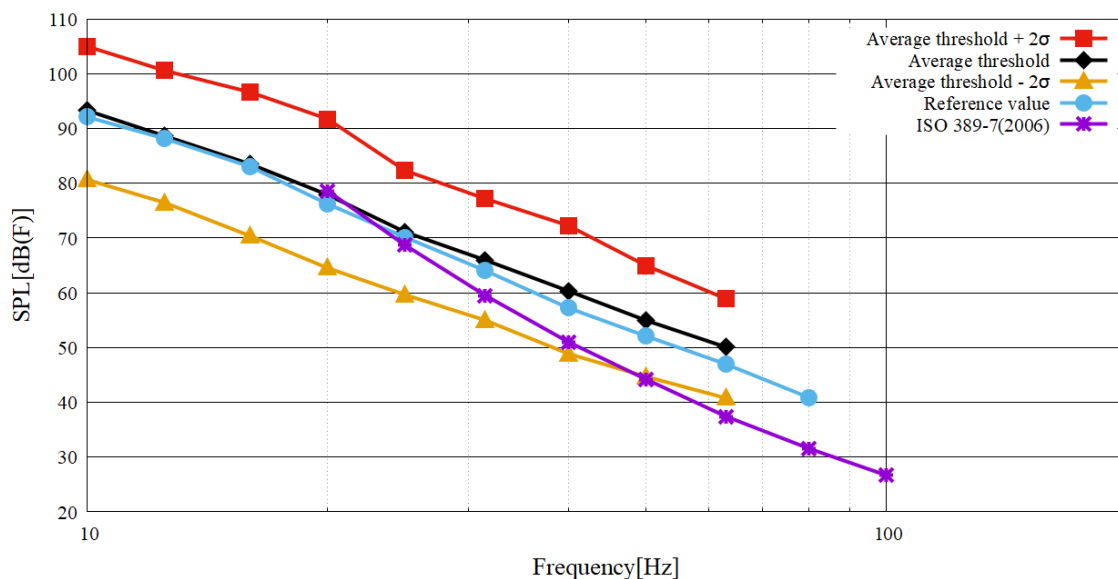


Figure 1 Threshold measured by up-down method of continuous sound (Reference value is explained in chapter 6)

Notes for this chapter

- There was a complaint about low-frequency noise generated by a large injection moulding machine that makes TV cabinets. The complainant said that he felt a low-frequency bang when the mould was closed once per minute. The author was unable to detect it. Without showing the measuring device, the complainant was asked to raise his hand when he felt the bang. This matched the movement of the meter. The sound pressure level at that time was the same as the average audible threshold of a continuous sound at 50 Hz.

4. Complainant's threshold

The author has consulted with many persons who are troubled by low-frequency noise. When the author asked complainants to measure their thresholds, they gladly cooperated. We measured the thresholds using the up-and-down method with continuous sounds. We also measured ordinary persons (mainly university students) using the same method.

The complainant's thresholds were between the maximum and minimum thresholds of the ordinary persons. The complainants are not particularly sensitive in thresholds. To date, we have measured the thresholds of several dozen complainants, but have not found any complainants who are particularly sensitive.

When they came to measure their thresholds, we asked them to take the Yatabe Guilford Personality Test. This is a psychological test to examine the subject's personality. Twelve real complainants with correspondence agreed to take the test.

*Table 1 Yatabe Guilford personality test of low-frequency noise complainants
(number of persons for each personality, total of 12 subjects)*

A	0	B	1	C	0	D	1	E	0
A'	1	B'	1	C'	0	D'	4	E'	2
A''	0	AB	1	AC	0	AD	0	AE	1

A: average type, B: unstable proactive, C: stable passive, D: stable proactive E: unstable passive

Most complainants were of the stable proactive type of Type D. From the author's perspective as a counsellor, none of them had any mental problems. Complainants are not special persons.

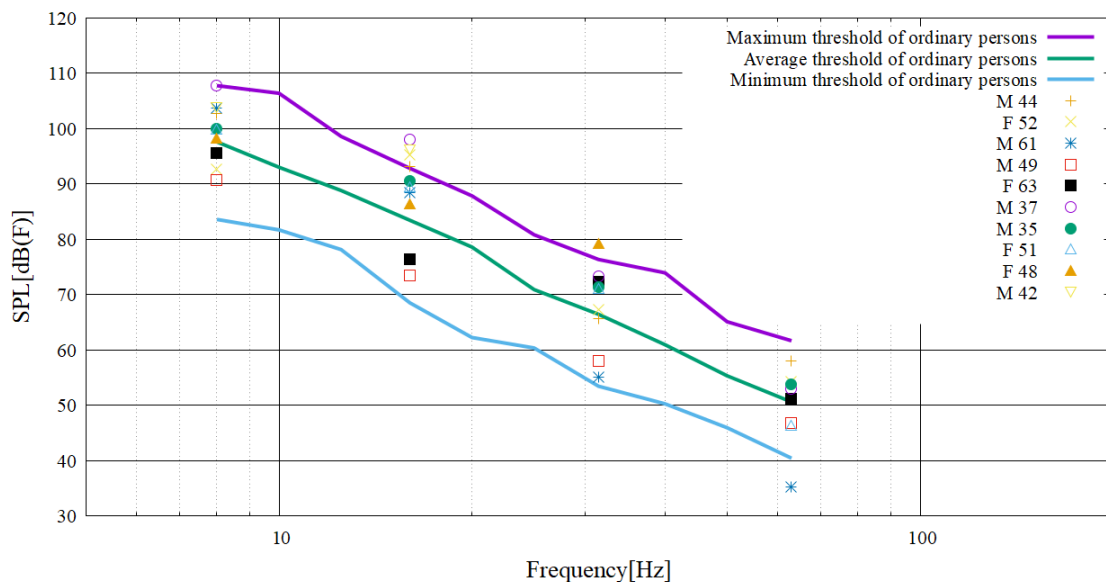


Figure 2 Threshold of complainants with correspondence

Notes for this chapter

- During the measurement of the threshold of the complainants two subjects became very anxious and unstable. The author stopped the measurement. These subjects became anxious as soon as they perceived the low-frequency noise. In order to relieve their anxiety, the author talked about pleasant subjects unrelated to sound for about 30 minutes to calm them down.

- If the problem is not resolved over time, he/she becomes more unpleasant. As a long-term effect, the discomfort occurs as soon as it is perceived. The permission level for low-frequency noise approaches to his/her hearing threshold.

5. Physiological responses by low-frequency sound (Ref. 1)

We measured the galvanic skin response, respiratory rate, heart rate, and brain waves of complainants with low-frequency noise, whom the author always consult and help. We told them only once, "Please listen to the sound as if you are at home." We told them also that they could stop the experiment at any time, but no one stopped midway.

First, there was a two-minute period without sound, and then low-frequency sound was emitted for two minutes. After that, the sound was stopped and there was a one-minute break, and then sound was generated under different conditions for two minutes. The sound pressure level presented was the same, but the frequency was changed in the experiment. At the end of the experiment, we also emitted rattling noise.

Figure 3 shows an example of a physiological reaction experiment on a complainant with correspondence (male).

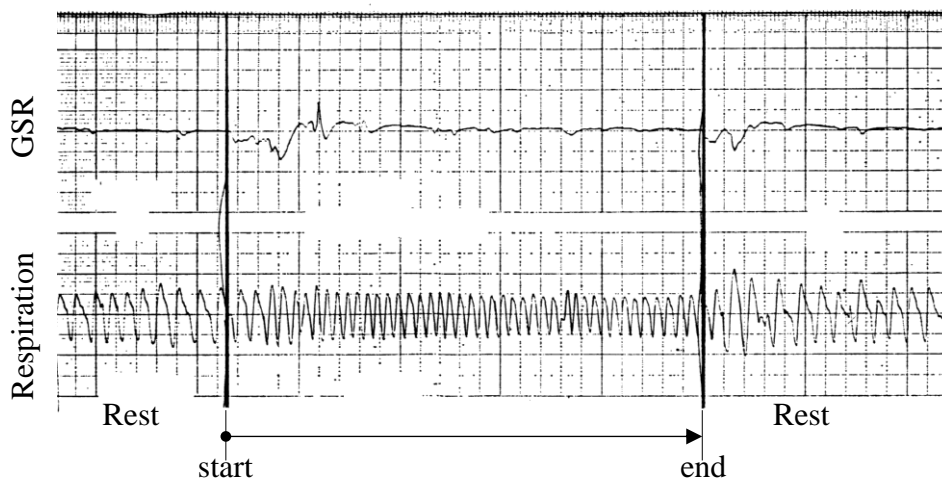


Figure 3 Response of complainant with correspondence (GSR and Respiration)

The first row of the figure shows the galvanic skin response. A downward reaction occurring immediately after the sound was emitted and immediately after it stopped. This galvanic skin responses are essentially the same as that of complainants and university students. When the sound pressure level is lowered to near the threshold, the responses disappear. Everyone has the same reaction. In other words, the perception of sound is basically the same for low-frequency noise complainants and students.

The second row shows the breathing waveform. The intervals become narrower and breathing becomes faster. The depth of breathing, represented by the height, also becomes shallower. This reaction also becomes smaller as the sound pressure level decreases. None of the university students showed a change in breathing rate. The problematic frequency at this complainant's home was 16 Hz. There is a physiological response to different frequencies from the frequency at home. There is a similar physiological response to rattling sounds, and it is thought that this is a stress response not only to low-frequency noise but to many other sounds.

Although not shown in the figure, two male subjects were found to have an increased heart rate. Although they cannot change their heart rate at will, it is thought that hearing low-frequency sound reminds them of unpleasant feelings and affects them. There was no change in the university students.

Brain waves were also collected, but no clear trends were found.

The response returned immediately after the experiment ended. This was probably because there was a trusting relationship between the experimenter and the subjects. Because women tended to be reluctant to participate in the experiment, the experiment started with a low sound pressure level.

Notes for this chapter

- One person was currently negotiating about moving their house and compensation. This person's response was completely different from the others. Maybe he thought a lot of things during the experiment. Details are omitted.
- Female complainants had fewer physiological responses.

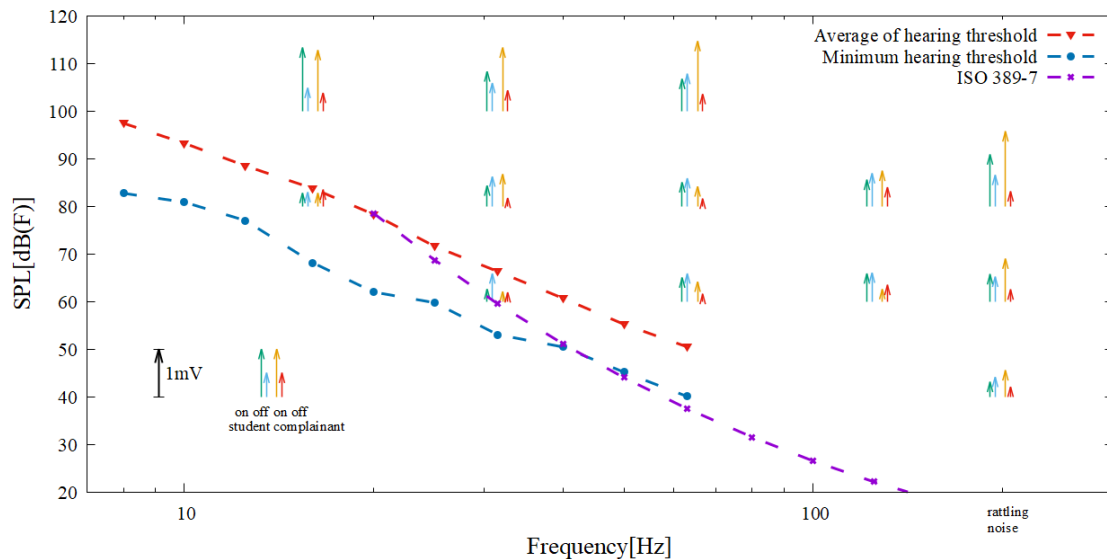


Figure 4 Average of galvanic skin responses of 9 university students and 11 low frequency noise complainants with correspondence

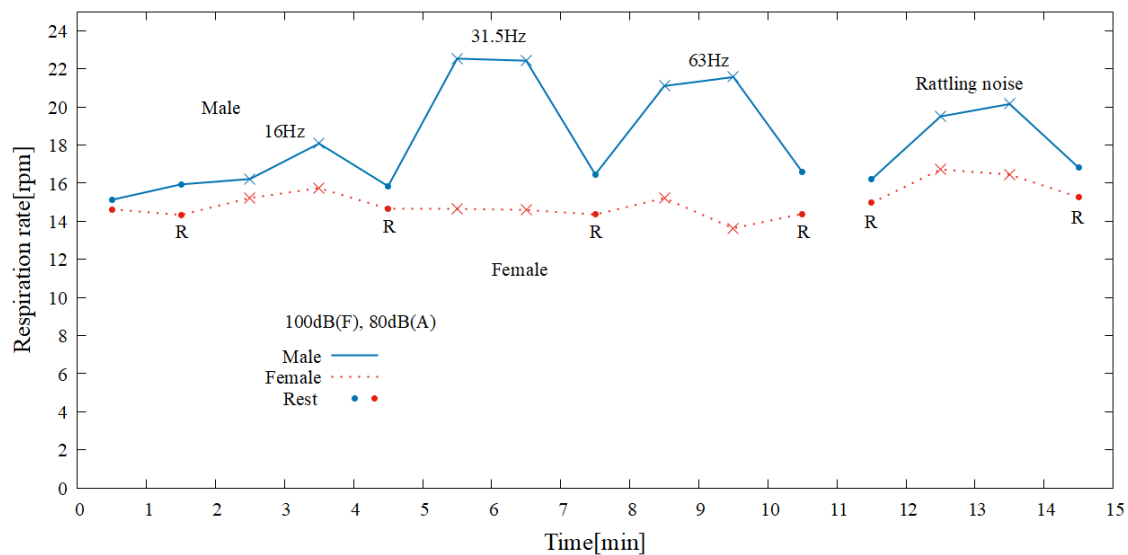


Figure 5 Respiration rate change due to low frequency noise and rattling noise (of 7 male and 4 female complainants with correspondence)

6. Guidebook for solving low-frequency noise problems in Japan (Ref. 4)

In June 2004, the Ministry of the Environment published the "Guidebook for dealing with low-frequency noise problems." It places emphasis on the correspondence between the operating state of the equipment and the response of the complainant. If there is correspondence, it judges whether the complaint is a low-frequency noise problem or a noise problem of 100 Hz or more by comparing it with a reference value.

Recently, there has been an increase in cases where there is no correspondence or the correspondence is unclear.

There are two types of low-frequency noise problems in Japan. One is the phenomenon in which the pressure of low-frequency sound makes window glass rattle. The other type is when the low-frequency sound itself is perceived indoors and becomes a complaint. The problem-solving guidebook distinguishes between the rattling sound and the phenomenon in which the low-frequency noise itself is perceived, and shows the direction for solving the problem. Here, the guidebook's thinking on the phenomenon, in which low-frequency sound itself is perceived indoors and becomes a complaint, is described.

6.1 Laboratory experiment considering the effects on the mental and physical discomfort (Ref. 3)

This experiment was conducted with intermittent sound. The tolerable sound pressure levels were measured for the ordinary persons and complainants, assuming a bedroom. Complainants were persons who self-reported that they were bothered by sound. The authors did not investigate the sites of these complainants.

For the ordinary persons, the experiment was conducted including old persons, taking into account the age of the complainants. For the ordinary persons, many persons felt that the sound pressure level was the tolerable limit in the bedroom when it was somewhat higher than the threshold. For complainants, many persons felt that the sound pressure level was the tolerable limit even if it was only slightly higher than the threshold. Complainants are more likely to feel unpleasant sensations, so they feel uncomfortable as soon as they perceive it.

The number of complainant data was small, so the stability and reliability of the data was low. The trends for each frequency were similar, so we decided to use the ordinary person's bedroom tolerance limit. Since there was a large amount of data, we determined the line that 95% of people consider to be the tolerable level in the bedroom (p05) and the line that 90% of people would tolerate (p10).

The 90% tolerance line P10 was appropriate for determining whether or not there was correspondence. Therefore, the P10 line was defined as the reference value. The reference value is appropriate for seeing approximate correspondence at low frequency noise.

The above results are shown in Figure 1 above. Threshold of ISO 389-7 is almost the same to the average thresholds at 20Hz measured by up and down method for continuous sounds but at the higher frequency ISO 389-7 is lower than the average threshold by continuous sounds. The reference value obtained is close to the average threshold value for continuous sounds.

When a complaint occurs, it is initially a sensation that some strange sound has been heard, and if the problem is not resolved over time, the sound becomes unpleasant as soon as it is perceived. As a long-term effect, since the discomfort occurs as soon as it is perceived, the sound pressure level, at which discomfort occurs, approaches the hearing threshold. The reference value obtained is a value slightly below the average hearing threshold measured with continuous sound.

Sometimes it is said that the measurement results are compared with the reference value without examining the relationship between the operation status of the sound source and the complaint, and that if it is below the reference value, it can be discarded. However, rather than discarding it at the reference value, we are seeking a careful judgment and a path to a final solution. It is not said that the sound source is bad because it exceeds the reference value, and we are of the opinion that a solution should be sought through discussion between the complainant, the sound source, the sound source's construction company, the equipment installation company, etc.

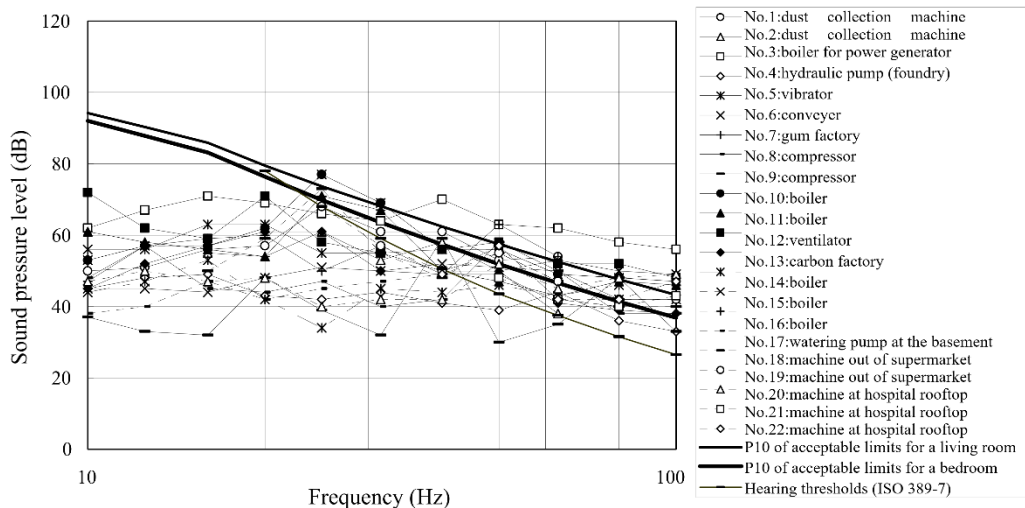


Figure 6 Measured level in rooms of 90% permission level (complainants and machine operation time and unpleasant time are correspondent)

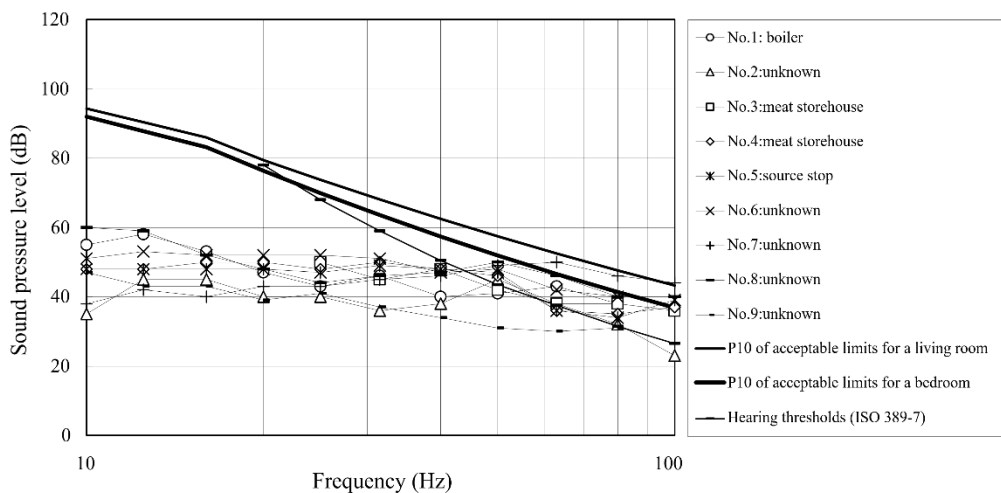


Fig. 7 Measured level in rooms of 90% permission level (complainants, but machine operation time and unpleasant time are not correspondent)

Notes for this chapter

- Laboratory experiments are short-term effects, so by applying field data, reference values are considered adaptive to long-term effects.
- This is the experience of one of the authors. The noise of a hotel cooling tower 130 meters away was 37 dBA at home. To solve the problem the methods considered included complaining directly, telling the city's environmental department, or telling a local boss. It takes courage to complain. It can destroy neighbouring relationships and make the position in the community difficult. These emotions become a great stress.
In this case, I looked into my own heart. I decided to think of it as a very effective opportunity to understand the mind of the complainant. Then, the discomfort of the noise decreased a little. I also took the courage to ask for the owner of the hotel.
- Treating the complainants and other related persons with respect as human beings, and interacting with them with feelings of fraternity, will make good relationships.

7. Guidebook for local government officials on dealing with noise generated by energy-saving water heaters, etc.

In recent years, complaints about mental and physical discomfort have been made due to low sound pressure level noise and low frequency sound generated by energy-saving water heaters installed around

homes. The Ministry of the Japanese Environment has published a guidebook on noise generated by energy-saving water heaters, etc. The problematic frequencies are about 20Hz to 500Hz or less, and the guidebook on low frequency sound is expanded to include normal noise. It also shows a way to solve the problem of noise generated by energy-saving equipment, which is a neighbourhood noise phenomenon. The method of dealing with complaints is in accordance with the guidebook (to solve low-frequency noise problems in Japan), and emphasis is placed on the existence of a correspondence between the operating status of the sound source and the complaint. When a problem occurs, the attitude is to solve the problem through discussion between local government officials, the sound source, the sound receiving side, the equipment installer, etc.

8. Sensation part of infrasound (Ref. 2)

Frequency below 20 Hz is called infrasound. However, frequencies below 20 Hz can be perceived if the sound pressure level is high. This phenomenon is the same as frequencies above 20 Hz. If the sound pressure level is lower than the threshold, it is not perceived, and if it is higher than the threshold, it is perceived. It is often said that infrasound below 20Hz cannot be heard, but it has a bad effect. The term infrasound should be reconsidered. One person has bothered by a very pure tone of 16 Hz. The complainant said that when he perceived the sound, he felt nauseous. The author also found the sound very strange. 16 Hz is not an inaudible sound.

It is often said that infrasound is felt at the abdomen. The subjects were persons who had lost their hearing from birth or as a side effect of streptomycin, and had sensorineural hearing loss, in which nerve transmission beyond the inner ear is not possible. The results are shown in Figure 8. The deaf persons have the average hearing loss of over 100 dB for a 1000 Hz sound. Although deaf persons are unable to hear, other bodily sensations remain. Many deaf persons were able to stand on one leg with his eyes closed, so his semicircular canals etc. are normal. Deaf persons say that they feel vibrations in his chest when a large truck passes by them. The perception thresholds of ordinary persons are lowered in parallel with the hearing threshold of the deaf persons up to 63 Hz, but the thresholds are 40 dB lower than deaf persons. In common life, there is no low-frequency sound with such a high sound pressure level, so the ordinary persons cannot feel vibrations in their chest. However, some persons express that they feel vibrations in their chest from low-frequency sound.

Since frequencies below 100 Hz are almost non-existent in human voices, low frequency sound is not necessary in conversation. However, tsunamis, volcanic eruptions, earthquake rumblings, etc. reach a sound pressure level that can be perceived, causing feelings of fear. It is speculated that in the general

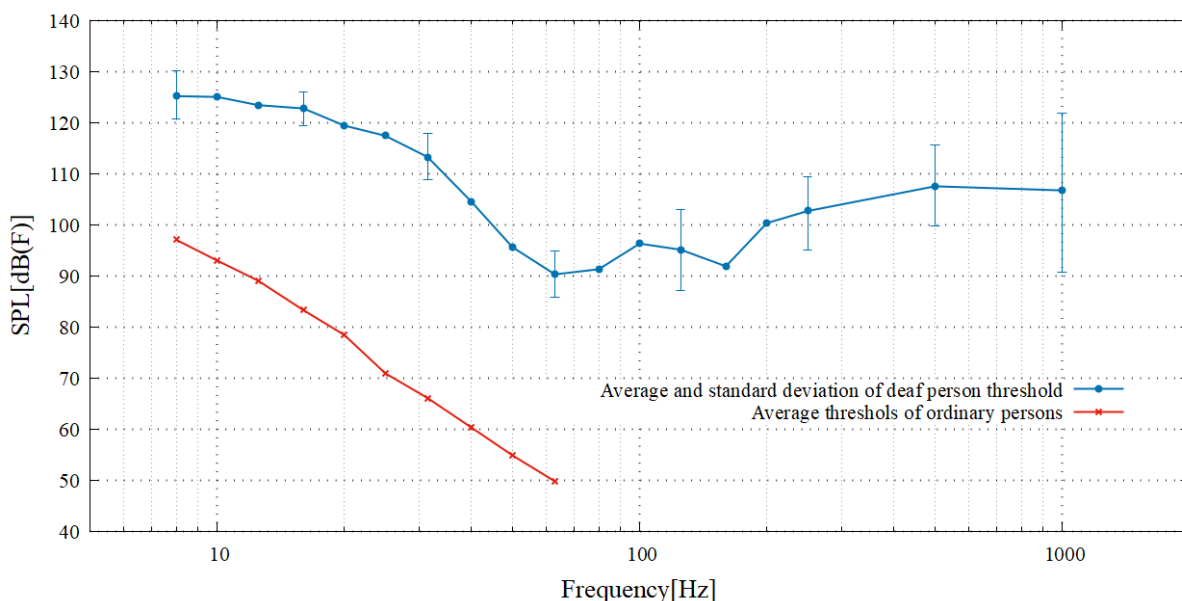


Figure 8 Average and standard deviation of deaf person threshold

public, after sound is perceived by the inner ear, it is confused with the sense of vibration in the nerve

pathway (maybe at inferior colliculus) that goes to the perception area, and it may be perceived as a sense of vibration.

Note from this chapter

- It took a year and a half to get deaf persons to participate in the experiment. An author studied sign language to communicate. The significance of having deaf persons participate in a sound experiment was not understood. After a year and a half, the author met the head of a deaf organization, who understood the significance of the experiment and he recommended the members to cooperate to the experiment. The experiment itself took only two weeks to complete. These deaf persons enjoyed Japanese drumming performance. We asked them and they performed the drumming at a conference of Acoustical Society of Japan.

9. Complaints about wind turbine installation in Japan

In Japan, there are many articles on the Internet about people becoming ill due to the low-frequency noise or infrasound generated by wind turbines. An author talked with a person at an online presentation who are opposed to the installation of wind turbines. I felt that the scientific data was not being conveyed. Concerns about the installation of wind turbines spread through the mass media and the Internet.

9.1 The Influence of Mass Media and the Internet

Newspaper articles aim to be objective, and report both the opinions of those installing wind turbines and those of residents who have concerns about the installation of wind turbines. Opinions of experts are also included. People, who have concerns, feel an affinity to negative opinions about wind turbines.

9.2 Individuality of complaints

In the research on low-frequency noise, we feel that in order to understand the reality of complaints, it is necessary to confirm individual situations through interviews as well as questionnaire surveys. Many concerns are expressed through interviews, such as land prices falling, not being able to sell land even if someone wants to move, worries about the impact on children, having to listen to noise all day and wondering how long this situation will continue. It is individuals who feel complaints. When conducting interview surveys, it is desirable for the interviews to be conducted by someone like a counsellor.

9.3 Parts of the brain related to discomfort and anxiety

The amygdala judges whether information is advantage or disadvantage to one's survival. For the residents, this phenomenon may be disadvantage to their survival. It is necessary to provide benefits to the residents as well, such as providing electricity free of charge.

Below the amygdala is an area called the hypothalamus, which controls hormones and the autonomic nervous system. In the experiment on physiological responses to low-frequency sound in Chapter 5, some complained of increased breathing rate and heart rate, and it is thought that these responses occurred through this pathway.

9.4 Examples of complaints about wind turbines

- Multiple wind turbines are installed on the ridge. The nearest wind turbine is located about 200m away from the house. The wind turbine stands behind the house. The complainant complains about low-frequency noise, but the measurement results showed that the mechanical noise of the wind turbine was predominant at 200Hz.
- The complaint was about low-frequency noise or being woken up by the sound. The wind turbine was located 700m away from the wind turbine, close to the coast. When listening to the sound in the garden of the complainant's house, it was an unpleasant rumbling sound with a strong low-frequency sound. On the day of the visit, the south wind was strong, and the waves were crashing against the water's edge, creating a sea roar. The residents said that they didn't mind this sound because it was the sea roar. Many people sleep with their windows open in the summer, so it seemed

like they were complaining. It seemed like the term low-frequency noise had come from the media, etc.

- Residents, who purchased land for vacation homes, are complaining about the 10 wind turbines on a ridge about 700 meters away. There are complaints about the mechanical noise from the wind turbines (about 160-200Hz) being annoying and causing sleeplessness and in some area, there is also the impact of shadow flicker. As the land was purchased for vacation homes, there is also the hidden problem of a decline in the land's usefulness and trading value.

Notes for this chapter

- We held information sessions on low-frequency noise for local governments and residents in areas where complaints about wind turbine noise have occurred and in areas where turbines are planned to be installed. This did not have much effect on residents who were opposed to the turbines.
- We took residents on buses or other vehicles to inspect existing wind turbine sites. This was effective in alleviating concerns for many persons. The experience device described in the next chapter was effective.

10. Low-frequency sound experience device (Ref. 5)

Many people have few opportunities to obtain correct knowledge about low-frequency noise, and therefore may feel more anxiety than necessary due to information sources that lack scientific evidence. To address this issue, we developed the Low-frequency sound experience vehicle (LFSEV) shown in Fig. 9. In the LFSEV, three people can experience various low-frequency sounds at the same time while listening to explanations from a guide with specialized knowledge. The LFSEV has the acoustic performance shown in Fig. 10. This allows participants to experience infrasound that exceeds the sensory threshold, pressure feeling and vibration feeling caused by low-frequency sound, and environmental sounds including low-frequency sound recorded in real environments.

The LFSEV has been transported to various locations, and more than 1,000 people have deepened their correct understanding of low-frequency sound at events for the general public. In an experience session for local residents around wind power plants, the loudness of the low-frequency sound contained in the wind turbine sound was confirmed with a low-frequency sound meter, and the experience was compared to the infrasound exceeding 90 dB that is generated even in everyday private cars and buses.

In a survey conducted after the experience, participants responded with comments such as, "The sound of the wind turbines was quieter than the sound inside the car," "I wanted to learn more accurate information about the health effects," and "I hope this experience will be held in other areas as well." Furthermore, from the reactions and questions of most of the participants, it was observed that their understanding had deepened and that they felt relieved after learning the actual situation. These results confirmed the importance of actually experiencing low-frequency sound. In particular, it is very useful to gain accurate knowledge through the low-frequency sound experience before anxiety or discomfort about a specific sound source builds up.

Having people gain a real understanding at the site of complaints about low-frequency noise and wind turbines is effective in solving the problem. The scenery and shadow flicker of wind turbines are images, and it is possible to show simulation results on-site using a projector. It is all a sensory issue, not an effect of chemical substances.

However, this is an experiment on short-term effects. An approach that is close to the complainants, including their human lives and human relationships, is essential. The accumulation of such experiences will likely reveal the way forward.

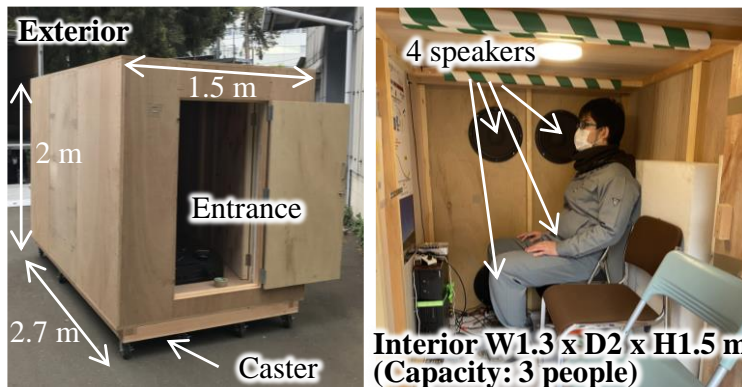
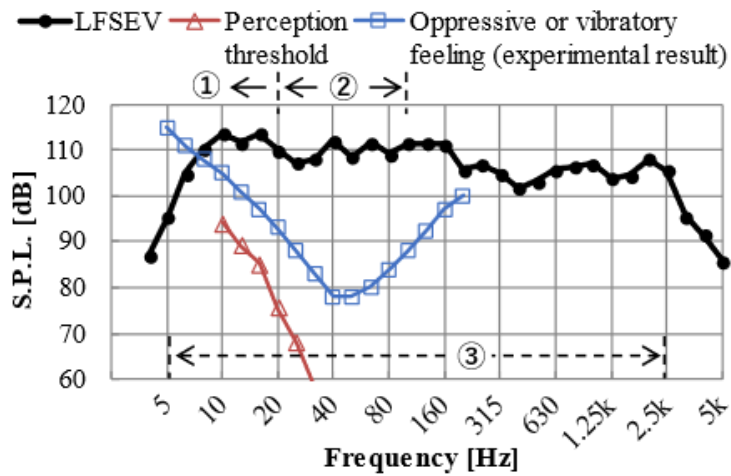


Figure 9 LFSEV



Experiential Content:

- ① Infrasound exceeding the perception threshold.
- ② Low-frequency sound with oppressive and vibratory feelings.
- ③ Low-frequency sound sources in the actual environment.

Figure 10 The maximum sound pressure level that LFSEV can reproduce

11. Conclusion

We are conducting research because there are complaints. Wind turbine noise, shadow flicker, scenery, etc. are sensory issues. Sensations cannot be grasped through logic only. Methods that appeal to the senses are effective as shown in Chapter10.

Regarding the effects of low-frequency noise, it is necessary to clarify the relationship between the operating status of the sound source and the complaints. Complaints with a corresponding relationship are important.

The sound at the site is continuous, and threshold measurements must be performed with continuous sound. The threshold for continuous sound is higher than that for intermittent sound over 20Hz.

The threshold for corresponding complainants is basically the same as that of the general public. However, in terms of the occurrence of physiological responses, university students have no responses at all, while corresponding complainants may change in respiratory rate and heart rate.

A curve has been created to separate complaints with correspondence and without correspondence. From this curve a reference value for low-frequency noise in Japan has been created. The reference value is very effective in roughly distinguishing whether there is a corresponding relationship or not.

Recommended standards for low-frequency noise are being created in many European countries. The idea of the Japanese reference value is useful, and it is effective in actual complaint situations in Japan.

Complainants' psychological responses widely spread. So, it is written as a description. If the psychological responses of complainants are accumulated in many studies, a unified view can be formed, which may lead to the development of new theories for scientifically predicting the psychology of complainants.

Complainants have a variety of problems. By treating complainants as human beings, carefully empathizing with them, listening carefully, and thinking scientifically, we can see a path to a solution that includes long-term effects.

Ideally, research should be conducted with an attitude of respect for human beings, based on the principles of humanity.

Acknowledgements

- We would like to thank the late Dr. Yukio Inukai for his great contribution to the creation of reference values.
- This paper was made possible thanks to the many complainants, students, and many others. We would like to thank many people.
- Mainly we used Google Translate when translating from Japanese to English. We are grateful.

References

- [1] S.Yamada, T.Watanabe, T.Kosaka, H.Negishi, H.Watanabe, Physiological Effects of Low Frequency Noise, J.Low Frequency Noise and Vibration, vol.5, No.1, 1986, pp.14-25
- [2] S.Yamada et al., Body sensation of low frequency noise of ordinary persons and profoundly deaf persons, J. Low Frequency Noise and Vibration, Vol.2, No.3, 1983, pp32-36
- [3] Y. Inukai, S. Yamada, H. Ochiai, Y. Tokita, Acceptable limits and their percentiles for low frequency noise in ordinary adults and complainants, 11th International Meeting on Low Frequency Noise and Vibration and its Control, Maastricht, The Netherlands, 30 August to 1 September 2004
- [4] <https://www.env.go.jp/content/900450107.pdf>, "Interpretation of Evaluation Guide" to Solve Low Frequency Noise Problems, June 2004.
- [5] K.Iwanaga and T.Doi. Development of a transportable low-frequency sound sensation chamber: Case studies of the "Low-Frequency Sound Experience Vehicle. Proceeding of autumn Meet. Acoust. Soc. Japan. pages 563-564, 2023 (in Japanese).

Paper #9 - ID: 343

Title: Perceived noise impact of transitioning towards larger wind turbines using auralisations

Author: Josephine Siebert Pockelé

11th Edition of the
International Conferences on
Wind Turbine Noise
Copenhagen, Denmark – 10th to 13th June 2025

Perceived Noise Impact of Transitioning Towards Larger Wind Turbines Using Auralisations

Josephine Siebert Pockel¹ and Roberto Merino-Martinez

Delft University of Technology, Faculty of Aerospace Engineering, Kluyverweg 1, 2629HS Delft, the Netherlands

Summary

The human perception of two wind turbines of different sizes, a small NTK turbine and a larger NREL model, was evaluated through their synthetically auralised sound. A wide range of wind speed conditions and observer locations was considered. The simulated sounds were analyzed using equivalent sound pressure levels and psychoacoustic sound quality metrics. Moreover, listening experiments were conducted to evaluate the human response to the same sounds. The least-squares models fitted to the results provided scaling laws for the different sound metrics as a function of wind speed (divided into low- and high-speed regimes) and distance to the observer. At lower wind speeds, the NREL turbine's noise and annoyance levels increase faster with increasing wind speed than the NTK turbine. The results of the NREL turbine at high wind speeds seem to indicate that turbulent boundary layer trailing-edge noise contributes more to annoyance than leading edge turbulent inflow noise. In the listening experiments, the larger wind turbine was perceived roughly 30% more annoying than the smaller one for the same conditions. The equivalent A-weighted sound pressure level and the psychoacoustic annoyance model by Zwicker were reported to closely represent the annoyance ratings reported in the listening experiment.

1. Introduction

Wind turbine noise is an important aspect of planning and permitting of onshore wind farm projects. While offshore turbines offer a compelling alternative, onshore turbines remain the majority of newly installed capacity [1]. The average size of onshore turbines has grown considerably in the last decade. In 2024, the average power rating of newly installed onshore turbines in Europe was 4.6 MW, with the average power of ordered turbines reaching 5.7 MW. Turbines exceeding 10 MW are in development for the onshore wind market at the time of writing [2]. Van den Berg *et al.* [3] showed how this increase in power rating has affected the A-weighted sound levels in a comprehensive study of noise measurements of operating turbines. The study shows little increase in A-weighted noise levels beyond a 2.0-MW rated power while suggesting that recent advances in noise-reduction technologies only affect noise in the 400 – 1600 Hz frequency range [3]. To the best of the authors' knowledge, no studies were found that quantify the effect of increasing size in terms of human sound perception.

Recently, there has been an increased interest in research about the annoyance caused by wind turbine noise, but it usually remains limited to surveys about existing installations [4]–[6]. Typical legislation and

¹Corresponding author - Email: j.s.pockele@tudelft.nl

research often focus on A-weighted sound pressure levels [7]. Nevertheless, A-weighting is known to have shortcomings in capturing the low-frequency and infrasound content of noise, while this frequency range may, in part, be one of the main causes of wind turbine noise annoyance [8], [9]. Kirkegaard *et al.* [10], [11] indicates the need for tools to enable better community engagement in the planning and mitigation of wind turbine noise.

Auralisation, the creation of sound files from simulated data [12], applied to wind turbine noise modelling, has recently emerged as a possible tool to enable the integration of noise annoyance into the wind turbine design loop [13]–[16]. It furthermore detaches annoyance research from the need for expensive measurement campaigns that were previously required for listening experiments and sound quality assessment. This paper is an application of auralisation to investigate the impact of transitioning to increasingly larger onshore wind turbines on noise perception. A listening experiment campaign was conducted to evaluate the perception of the simulated wind turbine sounds.

Section 2 explains the auralisation method employed in this study to generate the synthetic wind turbine sounds, and section 3 gathers the main inputs for the simulation setup. The analysis methods are briefly described in section 4. The results of the simulations and the listening experiments are gathered in sections 5 and 6, respectively. Lastly, the conclusions are drawn in section 7.

2. Auralisation Method

The method to auralise wind turbine noise in this paper is based on the method described by Pockelé [15]. The main difference is the replacement of the Gaussian beam tracing with a simpler image-source model for the sound propagation.

The wind turbine aeroelastic-aeroacoustic modelling is achieved with the second-generation Horizontal Axis Wind turbine simulation Code (HAWC2), developed by DTU (Technical University of Denmark) [17], [18]. The aero-noise module of HAWC2 accounts for three aerodynamic noise generation mechanisms: turbulent boundary layer trailing-edge noise (TE), turbulent inflow leading-edge noise (TI), and stall noise. In HAWC2, TE noise is modelled using the modified TNO model [19] by Bertagnolio *et al.* [20], TI noise is modelled using Amiet's theory [21], and stall noise is accounted for with the model by Bertagnolio *et al.* [22]. The aero-noise module is used to estimate the power spectral density spectrograms at the one-third-octave band central frequencies and at the selected observer locations.

Since HAWC2 only accounts for spreading losses and the Doppler effect [18], additional corrections are applied to account for ground reflections and atmospheric absorption. The received sound is only available per blade or for the full wind turbine. Hence, the corrections are applied assuming a single monopole sound source at 85 percent of each blade's span. Before applying these corrections, the HAWC2 output spectrograms are linearly interpolated to narrow-band frequencies, to match the required number of samples in the Inverse Short-Time Fourier Transform (ISTFT).

Ground effects are modelled using the approach by Embleton *et al.* [23], together with the ground impedance model by Delany and Bazley [24]. The direct and reflected spectrograms are separated at this stage to account for the difference in propagation distance when applying the atmospheric absorption. Both spectrograms are given an equal random phase, and the reflected one is supplemented with the frequency-dependent phase differences calculated in the ground reflection model. One limitation of the monopole point source assumption is the overestimation of the interference between the direct and reflected noise. In reality, the blade acts as a distributed noise source, where noise emitted from different radial positions will have different interference patterns, which results in little to no spectral dips in the measured sound on the ground [25]. In the measured spectra in [17], no clear interference patterns can be distinguished, confirming this as a modelling limitation of this method.

The noise attenuation due to atmospheric absorption is accounted for using the model in ISO standard 9613-1 by Bass *et al.* [26], [27]. A constant, frequency-dependent set of absorption coefficients $\alpha(f)$ is assumed for

all propagation paths. Similar to the ground reflections, these are calculated for the interpolated spectrogram frequencies. The attenuation spectra are then applied per blade and separately for the direct and reflected propagation paths.

Finally, the six spectrograms (for each blade: one for the direct and one for the reflected sound signal) are reconstructed into separate sound signals using the ISTFT, which are added together into the final auralised noise signal. In the ISTFT, a Hanning window is applied to smooth the transition between hops. To obtain a signal with the desired sampling frequency f_s , the spectrograms have been interpolated in the frequency domain, so they comply with the following requirement on the number of samples N_{hop} in a single STFT hop length:

$$N_{\text{hop}} = f_s \cdot \Delta t_{\text{STFT}} + 1 \quad (1)$$

where Δt_{STFT} is the time step of the spectrogram. For this paper, a reconstruction overlap of 50% is set, which means that the requirement becomes:

$$N_{f,\text{required}} = 2N_{\text{hop}} \quad (2)$$

3. Simulation Setup

3.1 Wind Turbine Simulation Models

For this work, two HAWC2 simulation models were used: (1) the *NREL 5MW reference wind turbine* (NREL)¹, and (2) the *Nordtank NTK 500/41* (NTK) wind turbine [28]. The NREL wind turbine was selected to represent the size, power rating, and control mechanism of modern onshore wind turbines since it is the only simulation model of this size, which is readily available to the authors. The NTK turbine, on the other hand, was chosen to represent older and smaller wind turbines. The size of both turbines is compared in Figure 1, while some other relevant specifications are compared in Table 1.

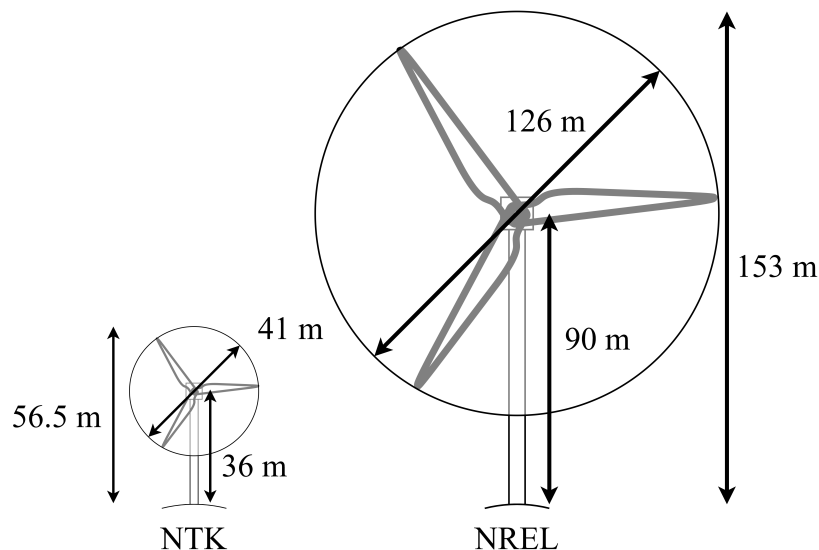


Figure 1 Size comparison of the NTK and NREL wind turbine models used in this work.

¹Available online: <https://gitlab.windenergy.dtu.dk/hawc-reference-models>

Table 1 Relevant specifications of the NREL and the NTK wind turbines.

	NTK [29]	NREL [30]
Power Rating, [MW]	0.5	5.0
Control	Passive	Active
Mechanism	Aerodynamic Stall	Collective Pitch
Rotor Speed, [rpm]	Constant (27.1)	Variable (6.9 - 12.1)

For aeroacoustic calculations in HAWC2, tabulated airfoil boundary layer parameters are required [18]. In the dataset by Bertagnolio *et al.* [28], multiple such tables are available for the NTK wind turbine. To allow for parity between both turbines, the XFOil results table with the critical amplification parameter $N_{crit} = 3$ is used. For the NREL turbine, this table is established using XFOil simulations [31], using the publicly available blade and airfoil geometries². The range of Reynolds numbers and angles of attack in this boundary layer table were determined based on the local relative inflow velocity and angle of attack, found through a series of verification simulations. The N_{crit} parameter in XFOil was set to 3, while the boundary layer was tripped at 10% of the chord length.

3.2 Simulated Operational Conditions

The auralisations were conducted under a set of common atmospheric conditions. The air temperature, pressure, and density were set to 15°C, 1013.25 hPa, and 1.225 kg/m³, respectively, based on the ground level conditions in the ISO 2533:1975 standard atmosphere [32]. The relative humidity of the air was set to 80%, based on the average air humidity in the Netherlands from the last 30 years [33]. The inflow turbulence intensity was set to 10%.

Simulations were performed for a range of wind speeds from 5.0 m/s to 25.0 m/s, in steps of 5.0 m/s. The cut-in speed of both turbines, 4.0 m/s, as well as the NREL turbine's rated wind speed, 11.4 m/s, were also simulated. Virtual microphone positions were defined upstream and downstream of the turbines, at 153 m, 500 m, 1000 m, and 2000 m, where the first distance represents the standardised measurement distance of the NREL wind turbine [34].

Pockelé and Merino-Martinez [35] showed an unfavourable relation between adding background noise and loudness-based sound quality metric results. Therefore, no ambient noise is considered, such that only the effects of the wind turbine noise are evaluated.

4. Analysis Methods

4.1 Sound Quality Metrics

Sound Quality Metrics (SQMs) describe the subjective perception of sound by human hearing, unlike the L_p metric, which quantifies the purely physical magnitude of sound based on pressure fluctuations. Previous studies [13], [36] showed that these metrics better capture the auditory behavior of the human ear compared to conventional sound metrics typically employed in noise evaluations. The four most commonly used SQMs [37] are:

- Loudness (N): Subjective perception of sound magnitude corresponding to the overall sound intensity [38]. The loudness results in this paper are expressed in loudness levels L_N in phon.
- Sharpness (S): Representation of the high-frequency sound content [39].
- Roughness (R): Hearing sensation caused by sounds with modulation frequencies between 15 Hz and

²Airfoil geometries provided by Nando Timmer, available online: <https://forums.nrel.gov/uploads/short-url/t5k5D4TrCNECxJJ7vwFKEeqaBoi.xls>

300 Hz [40].

- Fluctuation strength (FS): Assessment of slow fluctuations in loudness with modulation frequencies up to 20 Hz, with maximum sensitivity for modulation frequencies around 4 Hz [41].

These SQMs were calculated for each wind turbine noise sample. The 5% percentile values of each metric (i.e., the value of each SQM exceeded 5% of the total recording time) were combined into a global psychoacoustic annoyance (PA) metric following the model outlined by Zwicker [42]. All SQMs and the PA metric were calculated using the open-source MATLAB Sound Quality Analysis Toolbox (SQAT) v1.2 [37], [43], which is available on GitHub³.

4.2 Least-Squares Modelling

To allow for a more intuitive understanding of the results, least-squares models were fitted to the simulation outputs. As a baseline, the sound pressure levels and SQMs were related to the average wind speed (U_∞), and the distance up- and downstream (r). An interaction term between wind speed and distance was also tested for all metrics. Based on the findings of van den Berg *et al.* [3], a logarithmic relation with wind speed is assumed, while the distance term is also made logarithmic to match the general spherical spreading trend. The baseline least-squares model is described by Equation 3:

$$\text{metric} = x_1 \cdot \log_{10} \left(\frac{U_\infty}{11.4} \right) + x_2 \cdot \log_{10} \left(\frac{r}{153} \right) + x_3 \cdot \log_{10} \left(\frac{U_\infty}{11.4} \right) \cdot \log_{10} (r) + x_4 \quad (3)$$

The NREL wind turbine has two distinct modes of operation: (1) variable speed, constant pitch for low wind speeds ($U_\infty < 11.4$ m/s), and (2) constant speed, variable pitch for high wind speeds ($U_\infty > 11.4$ m/s). Similarly, the NTK wind turbine experiences partial blade aerodynamic stall at higher wind speeds. Therefore, the models were fitted separately for data where $U_\infty \leq 11.4$ m/s, and where $U_\infty \geq 11.4$ m/s. For the NREL wind turbine, the initial data analysis showed significant differences for the upstream and downstream directions in the high-wind-speed regime. Therefore, the NREL turbine results, at mean wind speeds above 11.4 m/s, are fitted to separate models for each propagation direction.

5. Simulation Results

5.1 Equivalent Sound Pressure Levels

As a baseline, the unweighted equivalent sound pressure levels $L_{p,eq}$ of the auralisations are analysed. Figure 2 presents the results for both wind turbines, side by side. The first notable difference is the wind speed slopes in the low-wind-speed region. The NREL turbine's noise levels grow considerably faster with increasing wind speed compared to the NTK turbine. In the high-wind speed regime, both turbines show a very similar increase in noise levels with wind speed. As expected, the logarithmic decrease of noise level with distance fits well to the data. For the NREL turbine, no large differences are observed between the upstream and downstream directions at high wind speeds.

The coefficients of the least-squares models are presented in Table 2 and Table 3 for the low- and high-wind speed regimes, respectively. The cross-term with wind speed and distance has been removed from the model, as this resulted in high p-values and lower adjusted R^2 values.

³Available online: <https://github.com/ggrecow/sqat>

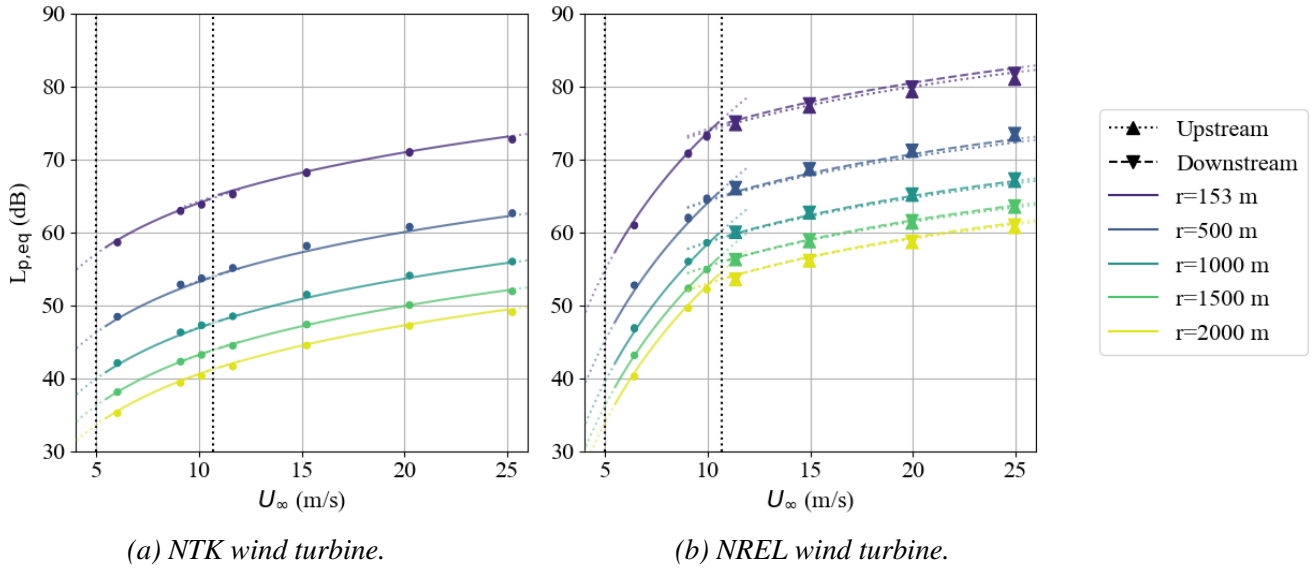


Figure 2 Equivalent sound pressure levels of the auralisations and the least-squares model curves.

The relation with distance has, as expected, a coefficient close to -20 , which corresponds to a sound power decrease with $\frac{1}{r^2}$. The differences from -20 can be explained by the ground reflections and atmospheric absorption. Because of the normalisation to $U_\infty = 11.4$ m/s and $r = 153$ m, the intercepts show the predicted sound pressure levels at this wind speed and distance. The NREL wind turbine is considerably louder, with an approximate $L_{p,eq}$ difference of 10 dB over the NTK turbine.

The initial observations of the relation with wind speed are confirmed by the wind speed slope coefficient. Interestingly, neither turbine shows the expected $50 \log(U_\infty)$ relation reported by van den Berg et al. [3]. The similar slope between both turbines in the high-wind-speed region can be explained by both turbines operating at a constant RPM. This is further supported by the slope of the NTK turbine not changing significantly between both regimes. The higher slope of the NREL turbine in the low-wind-speed regime can be explained by the significant increase of local flow velocity over the blades with increasing rotor RPM. The increase of 5.2 RPM from the minimum to the maximum RPM of the NREL turbine results in a local flow velocity increase of 34 m/s at the blade tip ($R_{blade} = 63$ m).

Table 2 Least-squares fit coefficients for $L_{p,eq}$ at low wind speeds ($U_\infty < 11.4$). All p -values are $\ll 0.05$.

	$\log_{10}(U_\infty)$	$\log_{10}(r)$	Intercept	Adjusted R^2
NTK	23.168	-21.000	65.323	0.999
NREL	62.667	-18.726	77.219	0.997

Table 3 Least-squares fit coefficients for $L_{p,eq}$ at high wind speeds ($U_\infty \geq 11.4$). All p -values are $\ll 0.05$.

	$\log_{10}(U_\infty)$	$\log_{10}(r)$	Intercept	Adjusted R^2
NTK	22.250	-21.232	65.505	0.998
NREL (upstream)	20.307	-18.671	74.983	0.995
NREL (downstream)	21.018	-18.996	75.338	0.997

5.2 A-weighted Equivalent Sound Pressure Levels

The plots of the A-weighted equivalent sound pressure levels $L_{A,eq}$ in Figure 3 show some similarities but also some major differences to the unweighted levels presented in Figure 2. In the low-wind-speed regime, the slopes with wind speed show a similar trend as the unweighted levels, with the levels of the NREL turbine increasing significantly faster than the NTK turbine. At higher wind speeds, the main difference with the unweighted levels is found for the NREL turbine. Downstream of the turbine, the A-weighted levels remain relatively constant with wind speed, whereas the upstream levels decrease. This difference between the A-weighted and unweighted levels indicates a possible change of the dominant noise generation mechanism towards lower-frequency noise.

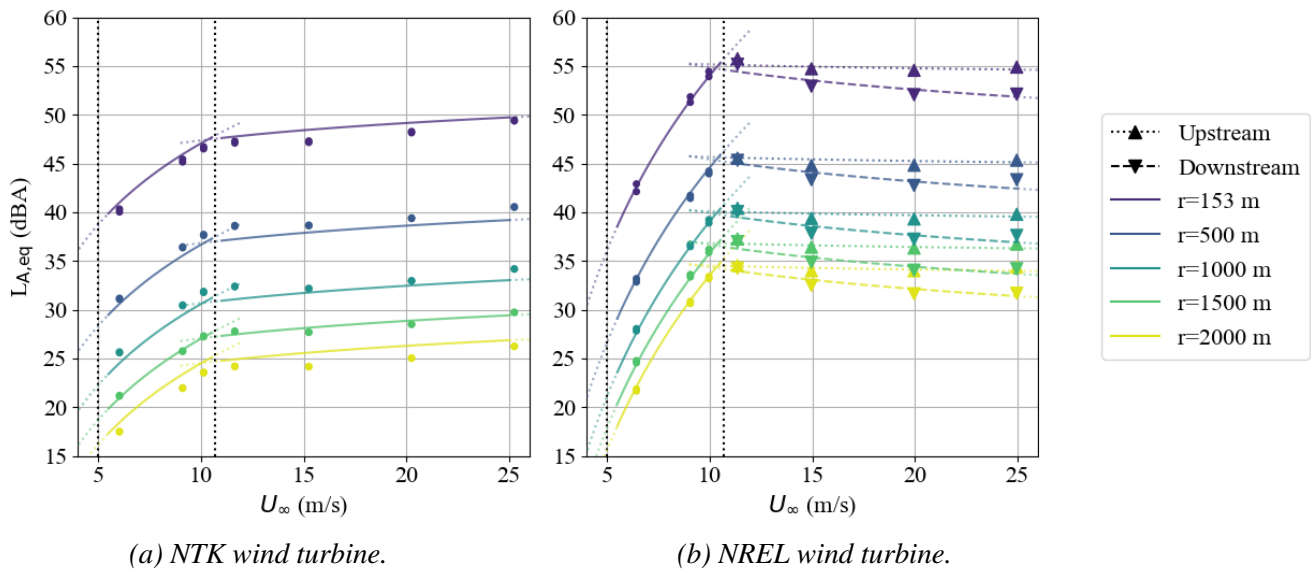


Figure 3 A-weighted equivalent sound pressure levels of the auralisations and the least-squares model curves.

Table 4 Least squares fit coefficients for $L_{A,eq}$ at low wind speeds ($U_\infty < 11.4$). All p -values are $\ll 0.05$.

	$\log_{10}(U_\infty)$	$\log_{10}(r)$	Intercept	Adjusted R^2
NTK	27.682	-20.215	48.642	0.989
NREL	59.613	-18.360	57.412	0.999

Table 5 Least squares fit coefficients for $L_{A,eq}$ at high wind speeds ($U_\infty \geq 11.4$). All p -values are $\ll 0.05$.

	$\log_{10}(U_\infty)$	$\log_{10}(r)$	Intercept	Adjusted R^2
NTK	5.923	-20.480	47.711	0.987
NREL (upstream)	-1.362	-18.495	55.102	0.997
NREL (downstream)	-7.531	-18.325	54.417	0.993

Observing the coefficients of the least-squares model fits in Table 4 and Table 5 confirms the above-noted changes. Additionally, the NTK turbine shows a decreased relation with wind speed in the high-speed regime, which creates a more distinct transition between the low- and high-wind-speed regimes than for $L_{p,eq}$. This again shows a change in the dominant noise generation mechanism when compared against the unweighted equivalent level results. Regarding the intercepts, A-weighting decreases the equivalent levels by approximately 20 dB compared to the unweighted sound pressure levels.

5.3 Loudness Level

The first psychoacoustic SQM results are those regarding the mean loudness level, $L_{N,mean}$. During the preliminary analysis, the cross-term coefficient x_3 of the least-squares model in Equation 3 was found to be highly significant, whereas the wind speed coefficient x_1 had a p-value > 0.05 . Therefore, the loudness level is fitted to the least-squares model without the x_1 term. This indicates a strong combined effect of wind speed and distance in human loudness perception.

From Figure 4, similar trends are derived compared to the A-weighted levels. In the low-wind-speed region, the loudness of the NREL turbine increases more rapidly with wind speed compared to the NTK turbine. At high wind speeds, there is once more a clear division between the upstream and downstream propagation for the NREL turbine. Visually, the loudness levels of both turbines show a closer agreement than the $L_{A,eq}$.

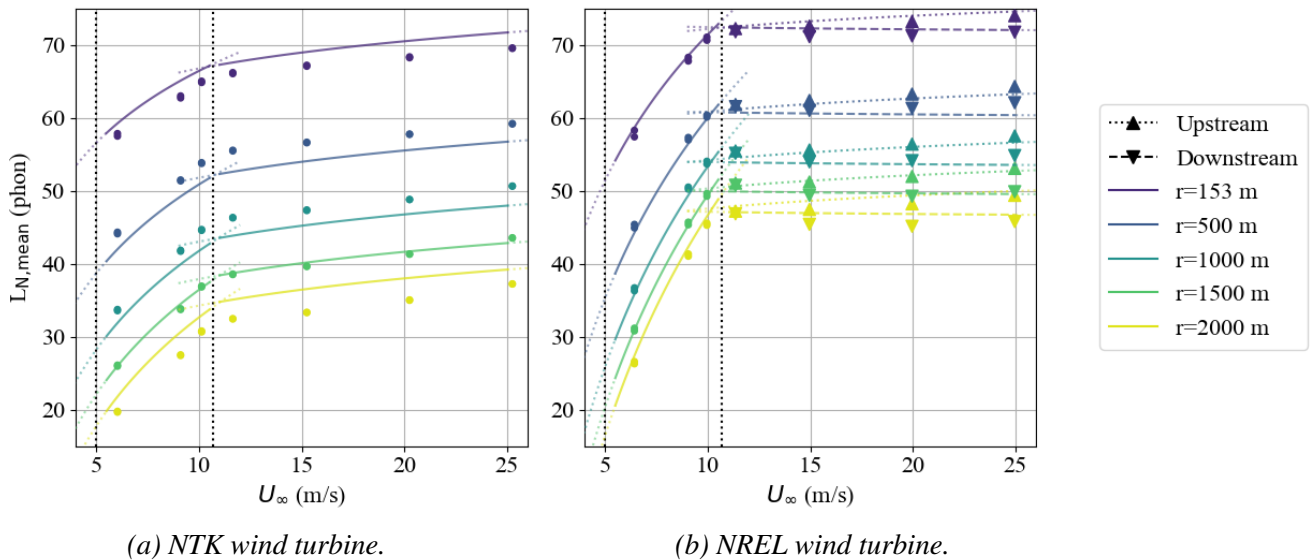


Figure 4 Mean loudness level of the auralisation results and the least-squares model curves.

The latter observation is confirmed in Table 6 and Table 7, where the intercepts are relatively closer together than those for the A-weighted levels. On the other hand, both turbines show a different relation with distance to the observer. It should be noted, based on the plots in Figure 4, that the distance fit for the NTK turbine is not as good as for the NREL turbine. The observation remains valid, however, as the data shows a larger level decrease than the model coefficient implies. One implication of this observation is that modern turbines may require larger distances to obtain an equivalent decrease in perceived loudness compared to older turbines.

Table 6 Least squares fit coefficients for $L_{n,mean}$ for low wind speeds ($U_\infty < 11.4$). All p-values are $\ll 0.05$.

	$\log_{10}(U_\infty) \times \log_{10}(r)$	$\log_{10}(r)$	Intercept	Adjusted R^2
NTK	15.009	-29.409	68.282	0.976
NREL	30.409	-20.451	75.160	0.996

Table 7 Least squares fit coefficients for $L_{n,mean}$ for high wind speeds ($U_\infty \geq 11.4$). All p -values are $\ll 0.05$, except for underlined coefficient.

	$\log_{10}(U_\infty) \times \log_{10}(r)$	$\log_{10}(r)$	Intercept	Adjusted R^2
NTK	12.408	-29.114	67.455	0.965
NREL (upstream)	6.052	-22.048	72.501	0.993
NREL (downstream)	<u>-1.011</u>	-22.676	72.366	0.988

5.4 Psychoacoustic Annoyance

For the psychoacoustic annoyance (PA) metric, the least-squares model is fit to the mean values as $10 \cdot \log_{10}(10 \cdot PA_{mean})$, since the relation with annoyance ratings in listening experiments is generally found to be logarithmic [36], [44]. The preliminary analysis also found a better adjusted R^2 when using the logarithm of PA_{mean} . Figure 5 shows a similar relation with wind speed and distance compared to the loudness levels. In previous work, loudness was found to be the primary contributing factor to the annoyance from wind turbine noise [45].

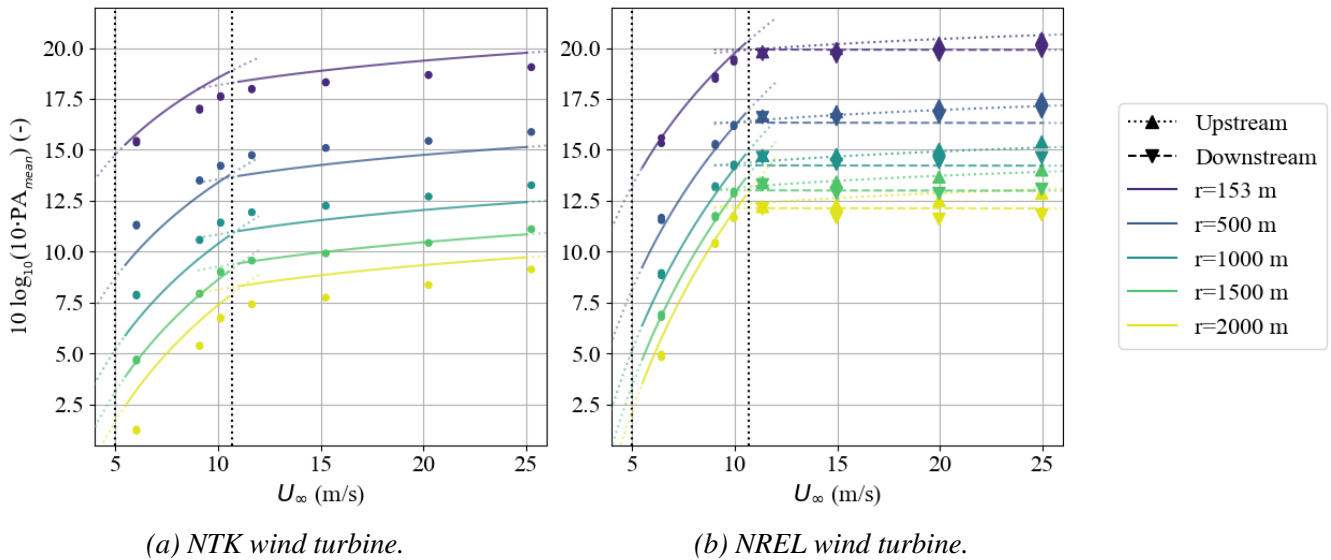


Figure 5 Mean Psychoacoustic Annoyance (PA) of the auralisation results and the least-squares model curves.

The main finding in Table 8 and Table 9 is the very similar intercepts between both turbines. Combined with the wind speed and distance relations, it can be derived that the NREL turbine is only expected to be more annoying at low wind speeds or at long distances. This is also visible in Figure 5. The main point of interest is the difference between up- and downstream PA values at high wind speeds for the NREL turbine. This finding does not line up well with the survey findings by Müller *et al.* [6], who reported higher annoyance downstream of a wind farm.

Table 8 Least squares fit coefficients for $10 \cdot \log_{10}(10 \cdot PA_{mean})$ at low wind speeds ($U_\infty < 11.4$). All p -values are $\ll 0.05$.

	$\log_{10}(U_\infty) \times \log_{10}(r)$	$\log_{10}(r)$	Intercept	Adjusted R^2
NTK	5.760	-9.675	19.251	0.951
NREL	9.916	-6.363	20.983	0.991

Table 9 Least squares fit coefficients for $10 \cdot \log_{10}(10 \cdot PA_{mean})$ at high wind speeds ($U_{\infty} \geq 11.4$). All p -values are $\ll 0.05$, except for underlined coefficient.

	$\log_{10}(U_{\infty}) \times \log_{10}(r)$	$\log_{10}(r)$	Intercept	Adjusted R^2
NTK	3.986	-8.995	18.404	0.961
NREL (upstream)	1.988	-6.774	19.957	0.993
NREL (downstream)	<u>-0.046</u>	-6.975	19.924	0.987

5.5 Low-Frequency Noise Content

Because of the previously discussed differences between the unweighted and A-weighted sound pressure levels, the low-frequency content of the wind turbine noise emissions is also investigated. For this purpose, the difference between the C- and A-weighted equivalent sound pressure levels ($L_{C,eq} - L_{A,eq}$) is used, based on the work by Vos and Houben [46]. In the preliminary analysis, the least-squares model in Equation 3 is found not to represent the data well. Therefore, based on the scatter plot in Figure 6, the second-degree polynomial in Equation 4 is fit to the data instead.

$$L_{C,eq} - L_{A,eq} = x_1 \cdot (U_{\infty} - 11.4)^2 + x_2 \cdot (U_{\infty} - 11.4) + x_3 \cdot \left(\frac{r}{153}\right)^2 + x_4 \cdot \left(\frac{r}{153}\right) + x_5 \quad (4)$$

In general, the low-frequency content of the noise emissions increases with the wind speed for all distances. A dip in low-frequency noise around 11.4 m/s is observed in Figure 6, as well as large differences between upstream and downstream for the NREL turbine at high wind speeds. In the low-wind-speed regime and upstream, both turbines show a similar trend between low-frequency noise and wind speed.

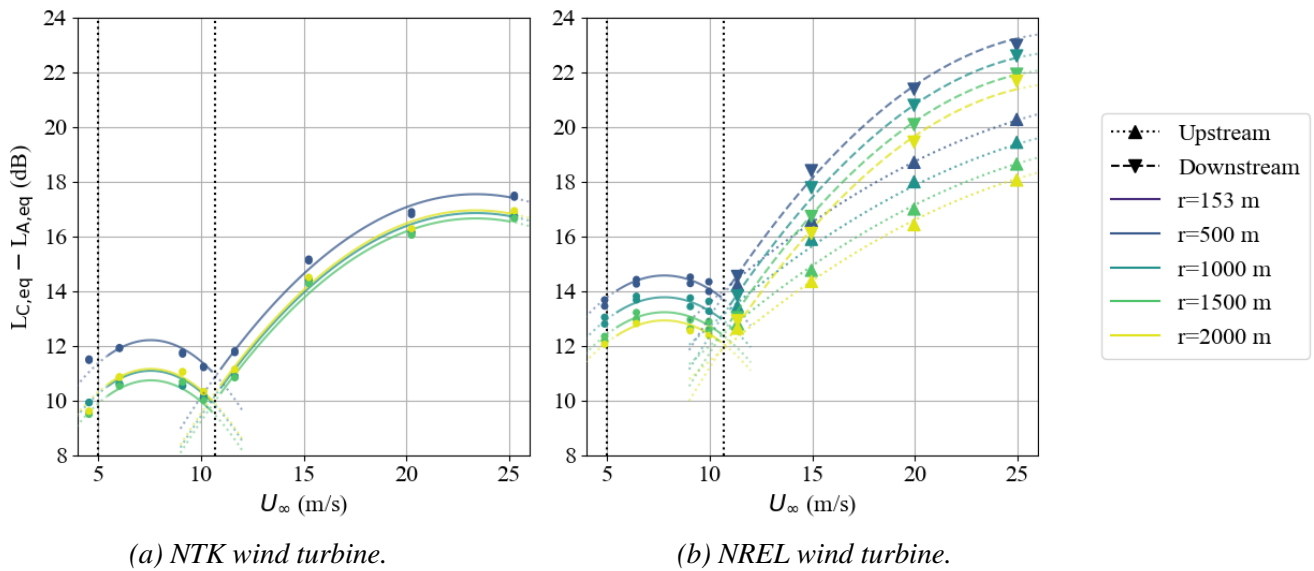


Figure 6 Difference between C- and A-weighted sound pressure levels of the auralisation results, as a measure of low frequency noise content, and the least-squares model curves.

Remarkably, the low-frequency trends of the NREL turbine match the surveyed descriptions of typical situations of wind turbine noise annoyance by Müller *et al.* [6, Sec. 3.4.3]. Their survey participants mostly describe high-wind-speed conditions and conditions where they are downstream from the turbine as situations of wind turbine noise annoyance. Given that low-frequency noise propagates better through walls and windows [47], this could partially explain annoyance in indoor situations.

Given that leading-edge turbulent-inflow (TI) noise contributes most to the low-frequency noise of wind turbines, the NREL turbine results seem to imply that a greater amount of TI noise is emitted in the downstream direction compared to upstream. With $L_{A,eq}$ showing the opposite trend, the turbulent boundary layer trailing-edge (TE) noise seems to propagate more upstream than downstream. Since the PA metric also shows larger values in the upstream direction for the NREL turbine, this implies that the TE noise of modern turbines contributes more to the annoyance than the TI noise, as expected from literature [48].

6. Listening Experiment

To validate the numerical results with human perception, a listening experiment was conducted in the Psychoacoustic Listening Laboratory (PALILA) at the Delft University of Technology [49]. This experiment combined multiple studies regarding wind turbine noise. Only the part relevant to this paper is presented.

6.1 Experimental Setup

PALILA is a box-in-box, soundproof booth with a floor plan of 2.32 m × 2.32 m, and a height of 2.04 m. The walls, floor, and ceiling are built with a modular sandwich structure of two 19 mm fibreglass panels with a 52 mm polyurethane foam core. The door is made from the same material and is acoustically sealed. The booth is connected to the floor via a vibration-damping system, and the cavity is filled with sound-absorbing foam. The walls are lined with A-B-C-D level acoustic absorbing foam to minimise reflection. Two bass traps are positioned in diagonally opposing corners to minimise low-frequency noise inside the facility. This setup provides a 0.07 s reverberation time and free-field sound propagation for frequencies higher or equal to 1600 Hz. Moreover, the facility is highly isolated from any other external influence, with a transmission loss of 45 dB and an A-weighted background noise level of only 13.4 dBA [49].

The sound reproduction equipment consists of a *Dell Latitude 7340* touchscreen-equipped laptop connected to a pair of *Sennheiser HD560s* open-back headphones. This equipment is calibrated up to 10 kHz, using a *G.R.A.S. 45BB-14 KEMAR* head-and-torso simulator with *G.R.A.S. KB5000 / KB50001 Anthropometric Pinnae*⁴. The reproduction system is accompanied by an open-source, Python-based Graphical User Interface (GUI) [50], which allows for this experiment to be self-guided and self-paced.

After a briefing by the responsible researchers, participants started the experiment with a questionnaire about their age, gender, employment, and education, as well as questions regarding their hearing health and state of well-being. This information is mainly used for reporting statistics and for bias and outlier detection. After answering these questions, participants proceeded to listen to the sound samples and were asked for each sample: "What number from 0 to 10 best describes how much you are bothered, disturbed or annoyed by the presented noise?" using an 11-point ICBEN scale. Every seven sound samples, participants are given a mandatory break from listening to alleviate fatigue.

6.2 Sample Selection

From the simulated sounds described in section 3, a subset was selected for testing in the listening experiment. To limit participant fatigue, the number of tested conditions is reduced compared to the numerical results.

Firstly, wind speed is covered by samples at simulated mean wind speeds of 5, 11.4, and 20 m/s. This wind speed range is only tested at a 153 m observer distance, upstream and downstream, and for both wind turbines. This part of the selection resulted in twelve samples. Eight additional samples are used to cover multiple distances from the wind turbine: 153, 500, and 2000 m, all simulated at a mean wind speed of 11.4 m/s. The reproduction time of all samples is limited to 20 s, as a compromise between exposure time and duration of the total experiment.

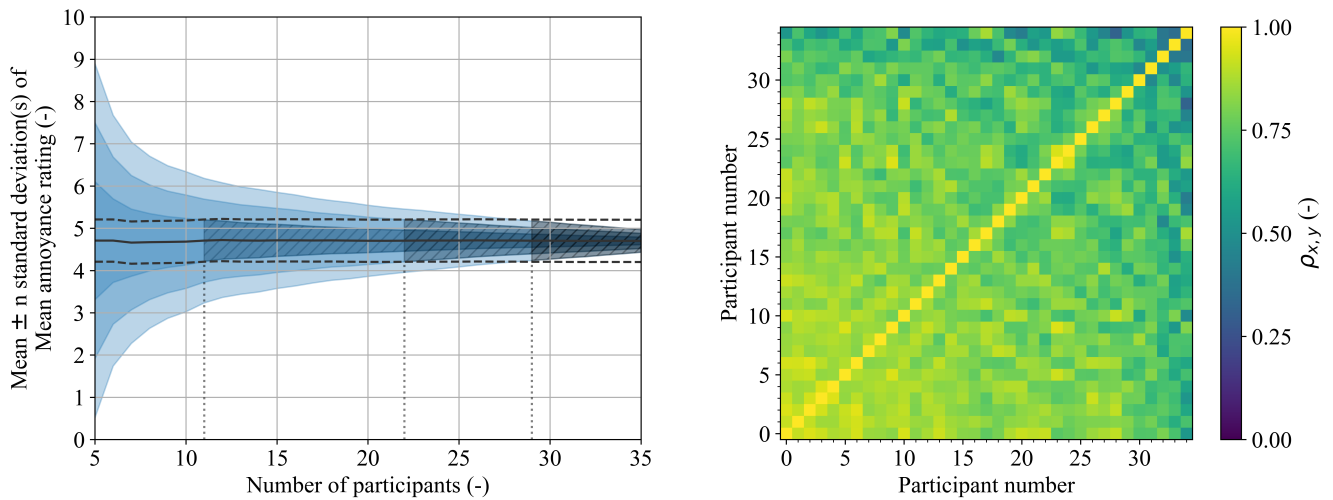
⁴Full description of the HATS available online: <https://www.grasacoustics.com/products/head-torso-simulators-kemar/kemar-for-ear-headphone-test-2-ch/product/793-gras-45bb-14>

6.3 Population Sample Statistics

Most of the participants in the experiment are a convenience sample from the Delft University of Technology, Faculty of Aerospace Engineering. The experiment had a total of 35 participants. Most participants are not directly related to research about wind turbine noise, decreasing the possibility of bias by experience.

The sample is diverse with 18 men and 17 women, with an average age of 31 years and an 8 year standard deviation. As expected from the recruitment method, most participants are employed for wages, or students, and 29 were employees or students at the university. The self-rated hearing health of the participants was generally good, with 2 "excellent", 15 "very good", 15 "good", and only 2 "fair" ratings. The only reported hearing problems were tinnitus (7 participants), or mild colds (2 participants). Furthermore, two participants indicated having had an accident affecting their hearing, and one participant reported being very tired. None of these reported hearing problems resulted in outlier values of the inter-participant cross-correlation presented in Figure 7b.

Figure 7a shows the mean annoyance rating R_{mean} has converged to $3\sigma < 0.5$, meaning the 99.7% confidence interval has converged to within the measurement error of the 11-point annoyance scale. While small, the sample size is thus considered representative of a similar population. Figure 7b shows a high level of inter-participant cross-correlation, with a mean Pearson correlation coefficient $\rho_{x,y} = 0.766$, and no significant outliers.



(a) Monte-Carlo convergence of the annoyance ratings. Dashed lines indicate mean annoyance rating ± 0.5 . (b) Inter-participant Pearson cross-correlations of the annoyance ratings.

Figure 7 Population sample analysis of the results.

To test for possible gender bias in the results, the best linear unbiased estimate of the ratio between the male and female average annoyance ratings is determined. The estimated $\hat{\frac{R_m}{R_w}} = 0.94 \pm 0.12$ indicates some gender bias. Nevertheless, the p-value of $\frac{R_m}{R_w} \neq 1$, is 0.302, indicating this bias is not statistically significant.

6.4 Listening Experiment Results

In a similar fashion to the numerical metrics, the annoyance ratings for each wind turbine were related to wind speed and distance using a least-squares model. Since the sample selection only tests the distance effect at one wind speed, the cross-term in Equation 3 is omitted, and the mean annoyance ratings are fitted to Equation 5. Similarly to the numerical results, this model is fitted separately for the low- and high-wind-speed regimes and separately for the upstream and downstream results of the NREL turbine in the high-speed region.

$$R_{mean} = x_1 \cdot \log_{10} \left(\frac{U_{\infty}}{11.4} \right) + x_2 \cdot \log_{10} \left(\frac{U_{\infty}}{153} \right) + x_3 \quad (5)$$

The results are shown in Figure 8. These plots clearly reflect the difference between both turbines in the low-wind-speed region, showing a larger annoyance increase with wind speed for the NREL compared to the NTK turbine. The difference between the up- and downstream annoyance for the NREL turbine is also clearly reflected. This difference does not look limited to the high-speed regime, however, indicating a deviation from the *PA* model. Another observation is the relatively high annoyance at a 500-m distance for the NTK turbine compared to the modelled expectation. The potential reason for the latter observation remains unclear since these noise samples are not marked as outliers in the numerical results.

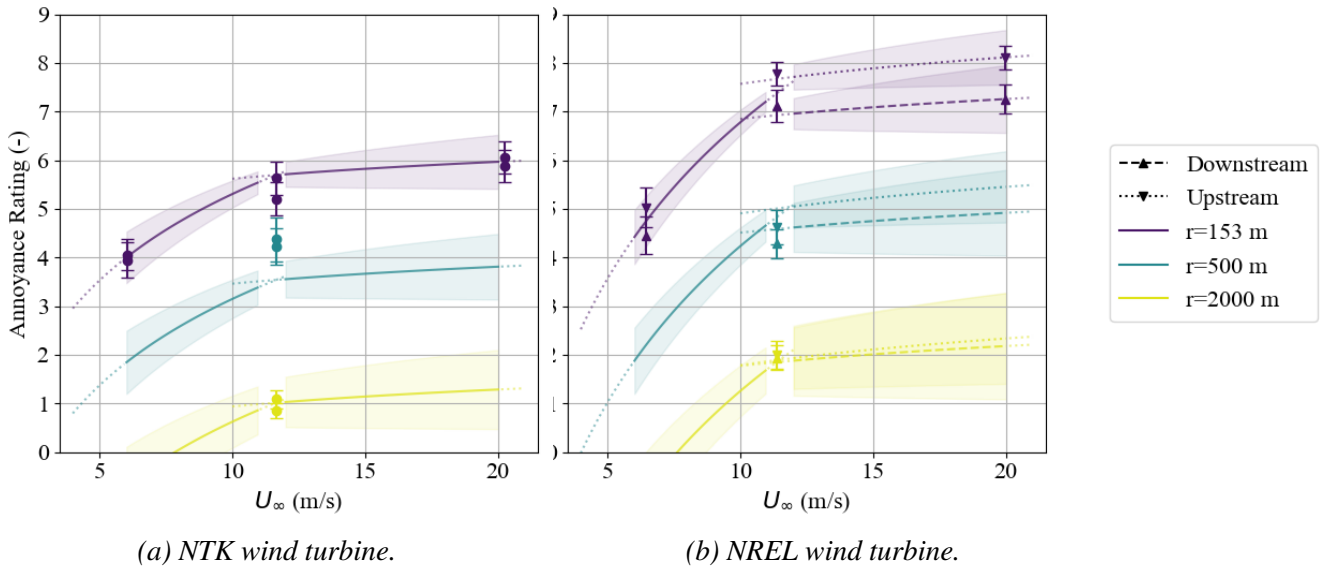


Figure 8 Listening experiment mean annoyance ratings and their standard errors, and least-squares fit curves for the NTK (left) and NREL (right) wind turbines. Shaded areas indicate the confidence intervals of the least-squares models.

The model coefficients in Table 10 and Table 11 immediately highlight the larger annoyance increase with wind speed of the NREL turbine in the low-wind-speed regime. Interestingly, both turbines show a very similar, barely significant (p -values ≈ 0.05) relation with wind speed in the high-speed region. This is different from all numerical results, where the NTK turbine generally showed a stronger relation with wind speed than the NREL turbine, except for the unweighted sound pressure levels.

Table 10 Least squares fit coefficients for the mean annoyance ratings at low wind speeds ($U_{\infty} < 11.4$). All p -values are $\ll 0.05$.

	$\log_{10}(U_{\infty})$	$\log_{10}(r)$	Intercept	Adjusted R^2
NTK	5.910	-4.194	5.641	0.907
NREL	10.693	-4.948	7.387	0.965

Table 11 Least squares fit coefficients for the mean annoyance ratings at high wind speeds ($U_\infty \geq 11.4$). All p -values are $\ll 0.05$, except for underlined coefficients.

	$\log_{10}(U_\infty)$	$\log_{10}(r)$	Intercept	Adjusted R^2
NTK	<u>1.159</u>	-4.194	5.685	0.932
NREL (upstream)	<u>1.817</u>	-5.178	7.672	0.980
NREL (downstream)	<u>1.358</u>	-4.549	6.927	0.979

The coefficients of the distance term, contrary to all numerical results, are of larger magnitude for the NREL compared to the NTK turbine. Thus, the slower decrease in noise and annoyance that was found for the PA metric is not reflected in the listening experiment.

Unlike the numerical PA metric, the intercept values of the measured annoyance ratings show significant differences between both turbines, which correspond closer to the loudness levels and the equivalent A-weighted sound pressure levels.

Similar to the PA metric and $L_{A,eq}$, at high wind speeds, the NREL wind turbine noise is more annoying upstream than downstream. This fact seems to once more support the argument that TE noise contributes more to annoyance than TI noise. While the annoyance ratings are slightly different up- and downstream at low wind speed, the overlap in standard error implies this difference is not very significant.

6.5 Correlation Between Annoyance Ratings and Sound Metrics

Lastly, the correlations between the annoyance ratings from the listening experiment and the logarithm of the mean PA metric and to $L_{A,eq}$ were evaluated, see Figure 9. A logarithmic relation was used to correlate PA since this was found to offer better fits [36], [44]. The coefficients of determination R^2 obtained in both cases are very high, with values higher than 0.95, in general. Overall, the PA metric provides marginally better fits than the $L_{A,eq}$ for both wind turbines considered.

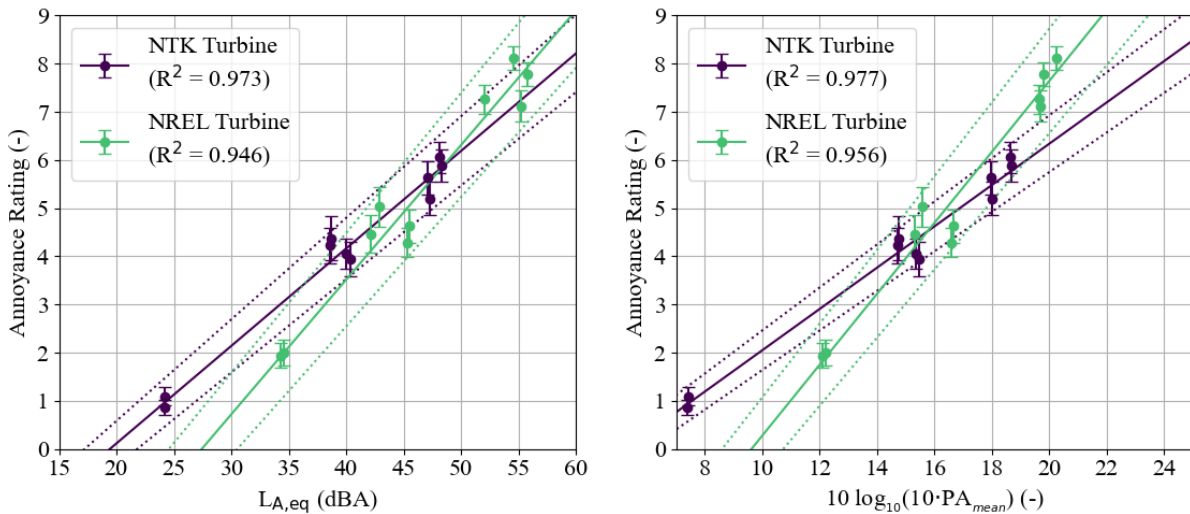


Figure 9 Correlation between the mean annoyance ratings reported in the listening experiments and $L_{A,eq}$ (left) and PA (right, in logarithmic scale). Data points show the mean annoyance ratings and their standard errors. The dotted lines show the standard errors of the Least-Squares fit curves.

On the other hand, Figure 9 shows the annoyance ratings relate differently to the noise metrics for each turbine. This shows that neither metric captures the full variability of the experienced annoyance by both turbines. Merino-Martinez *et al.* [36] commented that this relation can differ depending on the noise source and conditions under investigation. Hence, this result was not unexpected but rather interesting.

7. Conclusion

This paper investigated the variation in noise perception of wind turbines caused by transitioning towards larger wind turbines. Synthetic sound samples were auralised for two different wind turbines using a simulation-based method. A 500 kW, 41 m diameter, stall-controlled Nordtank NTK500/41 wind turbine was used to represent small, older onshore wind turbines. The NREL 5 MW reference wind turbine, with a 126 m, pitch-controlled variable speed rotor, was used to represent modern, large onshore turbines.

Results were presented in sound pressure levels, sound quality metrics (SQMs), and listening experiment annoyance ratings. All metrics show that the noise of the NREL wind turbine in the low-wind-speed regime ($U_\infty < 11.4$ m/s) has a stronger increase in noise and annoyance levels with wind speed than the NTK turbine. Based on the unweighted sound pressure level results, this is expected to be due to the variable rotor speed of the NREL turbine compared to the constant rotor speed of the NTK turbine.

In the high-wind-speed region ($U_\infty > 11.4$ m/s), the NREL turbine exhibits differences between the up- and downstream direction, unlike the NTK turbine. From the analysis of the low frequency noise content, in terms of $L_{A,eq} - L_{C,eq}$, the differences between the propagation directions seem to be driven by the low-frequency content. The lower low-frequency noise levels observed upstream, combined with higher annoyance levels than downstream, seem to imply that the low-frequency leading-edge turbulent inflow noise is less important for the annoyance of modern wind turbines than the higher-frequency turbulent-boundary-layer trailing-edge noise.

At the rated wind speed, the sound pressure levels of the NREL wind turbine is approximately 10 dB higher than for the smaller NTK turbine. The difference between the turbines at this wind speed, in terms of SQMs, is relatively smaller. The SQMs decrease less with distance for the NREL turbine than for the NTK turbine. This indicates that the distance to a modern turbine may have to be increased more to achieve a similar decrease in SQM than for an older wind turbine.

The results from a listening experiment showed similar annoyance trends as the numerical results. In general, the larger NREL turbine was perceived as roughly 30% more annoying than the smaller NTK turbine. The decrease in perceived annoyance with distance for the NREL turbine is faster than for the NTK turbine, which is the opposite of all numerical metrics. The annoyance ratings showed a good match with the Zwicker PA metric and with $L_{A,eq}$. The relations between these metrics and the annoyance ratings differ between the turbines, however, which implies that turbine size and mode of operation potentially have an influence on the human perception of wind turbine noise and the related scaling laws.

The next step in this research is to expand the set of input variables to other environmental factors, such as air temperature, pressure, and humidity, and different ground types. Based on the findings by Müller *et al.* [6], specific conditions of high annoyance will be investigated numerically. The difference between up- and downstream annoyance for the NREL turbine at high wind speeds will also be expanded upon with an investigation of the individual contributions of TE and TI noise.

Acknowledgments

We would like to acknowledge and thank the 35 participants in our listening experiment for their voluntary participation. This research would not be possible without them.

The listening experiment results of this paper were made possible by the financial support from the *Blade Extensions for Silent Turbines (BEST)* project (HER+22-02-03415120) which is supported by the Netherlands Enterprise Agency (*Rijksdienst voor Ondernemend Nederland (RVO)*), acting on behalf of the Dutch Ministry of Economic Affairs, using the Renewable Energy Transition subsidy (*subsidie Hernieuwbare Energietransitie (HER+ 2022-02)*), part of the Topsector Energy (TSE) subsidies.

This publication is also part of the *Listen to the future* project (project number 20247), a part of the Veni 2022 research programme (Domain Applied and Engineering Sciences). The latter project is granted to Roberto Merino-Martinez and is (partially) financed by the Dutch Research Council (NWO).

References

- [1] J. Lee and F. Zhao, “GWEC Global Wind Report 2024,” Global Wind Energy Council, Brussels, Belgium, Tech. Rep., 2024.
- [2] G. Costanzo, G. Brindley, and P. Tardieu, “Wind energy in Europe - 2024 Statistics and the outlook for 2025-2030,” Wind Europe, Brussels, Belgium, Tech. Rep., Feb. 2025.
- [3] F. Van Den Berg, E. Koppen, J. Boon, and M. Ekelschot-Smink, “Sound power of onshore wind turbines and its spectral distribution,” *Sound & Vibration*, vol. 59, no. 1, p. 1716, Jan. 2025. DOI: 10.59400/sv1716.
- [4] D. S. Michaud, K. Feder, S. E. Keith, *et al.*, “Exposure to wind turbine noise: Perceptual responses and reported health effects,” en, *The Journal of the Acoustical Society of America*, vol. 139, no. 3, pp. 1443–1454, Mar. 2016. DOI: 10.1121/1.4942391.
- [5] D. S. Michaud, S. E. Keith, K. Feder, *et al.*, “Personal and situational variables associated with wind turbine noise annoyance,” en, *The Journal of the Acoustical Society of America*, vol. 139, no. 3, pp. 1455–1466, Mar. 2016. DOI: 10.1121/1.4942390.
- [6] F. J. Y. Müller, V. Leschinger, G. Hübner, and J. Pohl, “Understanding subjective and situational factors of wind turbine noise annoyance,” en, *Energy Policy*, vol. 173, p. 113 361, Feb. 2023. DOI: 10.1016/j.enpol.2022.113361.
- [7] J. L. Davy, K. Burgemeister, and D. Hillman, “Wind turbine sound limits: Current status and recommendations based on mitigating noise annoyance,” *Applied Acoustics*, vol. 140, pp. 288–295, Nov. 2018. DOI: 10.1016/j.apacoust.2018.06.009.
- [8] F. Van Den Berg, “Do wind turbines produce significant low frequency sound levels?” In *11th International Meeting on Low Frequency Noise and Vibration and Its Control*, Maastricht, Netherlands, Aug. 2004.
- [9] B. Thorne, “The Problems With “Noise Numbers” for Wind Farm Noise Assessment,” en, *Bulletin of Science, Technology & Society*, vol. 31, no. 4, pp. 262–290, Aug. 2011. DOI: 10.1177/0270467611412557.
- [10] J. K. Kirkegaard, D. P. Rudolph, S. Nyborg, *et al.*, “Tackling grand challenges in wind energy through a socio-technical perspective,” en, *Nature Energy*, vol. 8, no. 7, pp. 655–664, Jun. 2023. DOI: 10.1038/s41560-023-01266-z.
- [11] J. K. Kirkegaard and D. N. Frantzen, “Learning from wind energy controversies: Listening to the noise,” en, *EU Research*, vol. Winter 2024, no. 40, pp. 32–34, 2024.
- [12] M. Vorländer, *Auralization: Fundamentals of Acoustics, Modelling, Simulation, Algorithms and Acoustic Virtual Reality* (RWTHedition), en, Second. Cham, Switzerland: Springer International Publishing, 2020, ISBN: 978-3-030-51201-9. DOI: 10.1007/978-3-030-51202-6.
- [13] R. Merino-Martínez, R. Pieren, and B. Schäffer, “Holistic approach to wind turbine noise: From blade trailing-edge modifications to annoyance estimation,” en, *Renewable and Sustainable Energy Reviews*, vol. 148, p. 111 285, Sep. 2021. DOI: 10.1016/j.rser.2021.111285.
- [14] A. Bresciani, J. Maillard, and L. d. Santana, “Perceptual evaluation of wind turbine noise,” en, in *16ème Congrès Français d’Acoustique, CFA2022*, Marseille, France: Société Française d’Acoustique; Laboratoire de Mécanique et d’Acoustique, Apr. 2022.
- [15] J. S. Pockelé, “Auralisation of Modelled Wind Turbine Noise for Psychoacoustic Listening Experiments,” M.S. thesis, Delft University of Technology and Technical University of Denmark, Delft, Netherlands, Oct. 2023.
- [16] A. P. C. Bresciani, “Physical and perceptual prediction of wind turbine noise,” English, Doctoral thesis, University of Twente, Twente, Netherlands, Mar. 2024. DOI: 10.3990/1.9789036559546.
- [17] F. Bertagnolio, H. A. Madsen, and A. Fischer, “A combined aeroelastic-aeroacoustic model for wind turbine noise: Verification and analysis of field measurements,” en, *Wind Energy*, vol. 20, no. 8, pp. 1331–1348, Aug. 2017. DOI: 10.1002/we.2096.
- [18] T. J. Larsen and A. M. Hansen, “How 2 HAWC2, the user’s manual,” DTU, Department of Wind Energy, Roskilde, Denmark, Technical Report Risø-R-1597(ver. 13.0)(EN), May 2023.

- [19] R. Parchen, “Progress report DRAW: A prediction scheme for trailing-edge noise based on detailed boundary-layer characteristics,” TNO Institute of Applied Physics, The Netherlands, TNO Report HAG-RPT-980023, 1998.
- [20] F. Bertagnolio, A. Fischer, and W. Jun Zhu, “Tuning of turbulent boundary layer anisotropy for improved surface pressure and trailing-edge noise modeling,” en, *Journal of Sound and Vibration*, vol. 333, no. 3, pp. 991–1010, Feb. 2014. DOI: 10.1016/j.jsv.2013.10.008.
- [21] R. K. Amiet, “Acoustic radiation from an airfoil in a turbulent stream,” en, *Journal of Sound and Vibration*, vol. 41, no. 4, pp. 407–420, Aug. 1975. DOI: 10.1016/S0022-460X(75)80105-2.
- [22] F. Bertagnolio, H. A. Madsen, A. Fischer, and C. Bak, “A semi-empirical airfoil stall noise model based on surface pressure measurements,” en, *Journal of Sound and Vibration*, vol. 387, pp. 127–162, Jan. 2017. DOI: 10.1016/j.jsv.2016.09.033.
- [23] T. F. W. Embleton, J. E. Piercy, and G. A. Daigle, “Effective flow resistivity of ground surfaces determined by acoustical measurements,” en, *The Journal of the Acoustical Society of America*, vol. 74, no. 4, pp. 1239–1244, Oct. 1983. DOI: 10.1121/1.390029.
- [24] M. Delany and E. Bazley, “Acoustical properties of fibrous absorbent materials,” en, *Applied Acoustics*, vol. 3, no. 2, pp. 105–116, Apr. 1970. DOI: 10.1016/0003-682X(70)90031-9.
- [25] Y. Tian and B. Cotté, “Modelling of ground and atmospheric effects on wind turbine noise,” en, Apr. 2015.
- [26] International Organisation for Standardisation (ISO), “Acoustics - Attenuation of sound during propagation outdoors - Part 1: Calculation of the absorption of sound by the atmosphere,” Geneva, Switzerland, International Standard ISO 9613-1, Aug. 1993.
- [27] H. E. Bass, L. C. Sutherland, A. J. Zuckerwar, D. T. Blackstock, and D. M. Hester, “Atmospheric absorption of sound: Further developments,” en, *The Journal of the Acoustical Society of America*, vol. 97, no. 1, pp. 680–683, Jan. 1995. DOI: 10.1121/1.412989.
- [28] F. Bertagnolio, A. Fischer, H. Aagaard Madsen, K. Enevoldsen, P. Hansen, and C. B. M. Pedersen, *NordTank NTK 500/41 Wind Turbine Definition along with Noise and SCADA Measurement Data*, 2024. DOI: 10.11583/DTU.27684813.V1.
- [29] F. Bertagnolio, H. A. Madsen, A. Fischer, and C. Bak, “Validation of an Aero-Acoustic Wind Turbine Noise Model Using Advanced Noise Source Measurements of a 500kW Turbine,” en, in *Proceedings of the 16th International Symposium on Transport Phenomena and Dynamics of Rotating Machinery*, Apr. 2016.
- [30] J. Jonkman, S. Butterfield, W. Musial, and G. Scott, “Definition of a 5-MW Reference Wind Turbine for Offshore System Development,” en, National Renewable Energy Laboratory (NREL), Golden, CO, USA, Tech. Rep. NREL/TP-500-38060, 947422, Feb. 2009. DOI: 10.2172/947422.
- [31] M. Drela, “XFOIL: An Analysis and Design System for Low Reynolds Number Airfoils,” en, in *Low Reynolds Number Aerodynamics*, T. J. Mueller, Ed., ser. Lecture Notes in Engineering, Berlin, Heidelberg: Springer, 1989, pp. 1–12, ISBN: 978-3-642-84010-4. DOI: 10.1007/978-3-642-84010-4_1.
- [32] International Organisation for Standardisation (ISO), “Standard Atmosphere,” Geneva, Switzerland, International Standard ISO 2533:1975, May 1975.
- [33] Koninklijk Nederlands Meteorologisch Instituut (KNMI), *KNMI - Klimaatviewer*, nl, 2024.
- [34] International Electrotechnical Commission (IEC), “Wind turbines - Part 11: Acoustic noise measurement techniques,” en, International Standard IEC 61400-11:2012, Nov. 2012.
- [35] J. S. Pockelé and R. Merino-Martinez, “Influence of Ambient Noise in Sound Quality Assessment of Auralised Wind Turbine Noise,” in *11th Edition of the International Conferences on Wind Turbine Noise*, Copenhagen, Denmark, Jun. 2025.
- [36] R. Merino-Martínez, R. Pieren, B. Schäffer, and D. G. Simons, “Psychoacoustic model for predicting wind turbine noise annoyance,” en, in *Proceedings of the 24th International Congress on Acoustics*, vol. A11: Psychoacoustics, Gyeongju, Korea, Oct. 2022.

- [37] G. F. Greco, R. Merino-Martinez, A. Osses, and S. Langer, “SQAT: A MATLAB-based toolbox for quantitative sound quality analysis,” in *INTER-NOISE and NOISE-CON Congress and Conference Proceedings*, Chiba, Tokyo, Japan, Aug. 2023, pp. 7172–7183. DOI: 10.3397/IN_2023_1075.
- [38] International Organisation for Standardisation (ISO), “Acoustics - Methods for calculating loudness – Part 1: Zwicker method,” Geneva, Switzerland, International Standard ISO 532-1:2017, 2017.
- [39] G. Von Bismarck, “Sharpness as an attribute of the timbre of steady sounds,” *Acta Acustica united with Acustica*, vol. 30, no. 3, pp. 159–172, 1974.
- [40] P. Daniel and R. Weber, “Psychoacoustical Roughness: Implementation of an Optimized Model,” *Acta Acustica united with Acustica*, vol. 83, no. 1, pp. 113–123, Jan. 1997.
- [41] A. Osses, R. García León, and A. Kohlrausch, “Modelling the sensation of fluctuation strength,” *Proceedings of Meetings on Acoustics*, vol. 28, no. 1, p. 050005, Sep. 2016. DOI: 10.1121/2.0000410.
- [42] H. Fastl and E. Zwicker, *Psychoacoustics: facts and models* (Springer series in information sciences 22), en, 3rd. Berlin , Germany; New York, NY, USA: Springer, 2007, ISBN: 978-3-540-23159-2.
- [43] G. F. Greco, R. Merino-Martínez, and A. Osses, *SQAT: A sound quality analysis toolbox for MATLAB*, v1.2. Zenodo. DOI: 10.5281/ZENODO.14641811, Jan. 2025.
- [44] R. Merino-Martínez, R. M. Yupa-Villanueva, B. von den Hoff, and J. S. Pockelé, “Human response to the flyover noise of different types of drones recorded in field measurements,” in *3rd Quiet Drones conference*, Manchester, UK, Sep. 2024.
- [45] J. S. Pockelé and R. Merino-Martínez, “Psychoacoustic Evaluation of Modelled Wind Turbine Noise,” English, in *Proceedings of the 30th International Congress on Sound and Vibration*, Amsterdam, Netherlands: The International Institute of Acoustics and Vibration, Jul. 2024.
- [46] J. Vos and M. M. J. Houben, “Annoyance caused by the low-frequency sound produced by aircraft during takeoff,” *The Journal of the Acoustical Society of America*, vol. 152, no. 6, pp. 3706–3715, Dec. 2022, ISSN: 0001-4966. DOI: 10.1121/10.0016596.
- [47] M. P. Norton and D. G. Karczub, *Fundamentals of Noise and Vibration Analysis for Engineers*. Cambridge, UK: Cambridge University Press, 2003, ISBN: 978-0-511-67173-9.
- [48] S. Oerlemans, M. Fisher, T. Maeder, and K. Kögler, “Reduction of Wind Turbine Noise Using Optimized Airfoils and Trailing-Edge Serrations,” en, *AIAA Journal*, vol. 47, no. 6, pp. 1470–1481, Jun. 2009. DOI: 10.2514/1.38888.
- [49] R. Merino-Martínez, B. von den Hoff, and D. G. Simons, “Design and Acoustic Characterization of a Psychoacoustic listening facility,” English, in *Proceedings of the 29th international congress on sound and vibration*, E. Carletti, Ed., Prague, Czech Republic: IIAV CZECH s.r.o., Jul. 2023, pp. 274–281, ISBN: 978-80-11-03423-8.
- [50] J. S. Pockelé, *Graphical User Interface for the Psychoacoustic Listening Laboratory (PALILA GUI)*, v1.2.0. Zenodo., Mar. 2025. DOI: 10.5281/ZENODO.15100497.

Paper #10 - ID: 344

Title: Design and Validation of Trailing-Edge Serration to achieve 3dB Reduction of Wind Turbine Noise

Author: Mohammad Kamruzzaman

11th Edition of the International Conferences on Wind Turbine Noise

Copenhagen, Denmark – 10th to 13th June 2025

Design and Validation of Trailing-Edge Serration to Achieve 3 dB Reduction of Wind Turbine Noise

**M. Kamruzzaman¹, P. Weihing, D. Bekiropoulos, J. Stenberg,
N. Noffke, C. Scheit and R. Wortelker**
**Wobben Research & Development (Enercon R&D), Borsig Str. 26, 26607 Aurich,
Germany.**

Summary

Wind turbine blade noise reduction by trailing-edge serration (TES) is an established technology for the turbine manufactures since decades. However, the overall noise reduction performance of TES for the MW class turbines varies significantly, typically 1.0 to 3.0 dB depending on the types of turbines and many other design parameters. A question remains still open to the wind turbine noise community: What is the maximum noise reduction potential of TES? Can TES deliver more than 3 dB noise reduction? This paper aims to answer above challenging questions. Hence, focuses on the enhanced TES design, optimization and validation by dedicated acoustic wind tunnel as well as full scale field measurements. TES design parameters optimization is conducted based on a semi-empirical in-house noise prediction tool and high-fidelity CFD methods. Dedicated aeroacoustic wind tunnel tests are performed to understand the sensitivity of different TES design parameters. Baseline vs TES airfoils are analysed, and an efficient serration design and optimization method consistent with turbine operation condition is developed to improve TES noise reduction performance. An enhanced method is applied to design TES for the MW wind turbine blades, and a full-scale turbine IEC standard field test is conducted for the validation purpose. Encouraging results were found. For different wind class turbines, it was found that by proper design optimization it is possible to achieve beyond 3.0 dB noise reduction, without any power/annual energy production (AEP) loss.

1. Introduction

It has long been recognised that airfoil trailing-edge noise may be reduced by modifying the trailing-edge geometry so that the efficiency by which vorticity is scattered into sound is reduced. This paper focuses on the reduction of this noise source through the introduction of trailing-edge serrations (TES) on wind turbine blades. This approach has been shown by several researchers to provide significant theoretical (Howe [1]) and experimental (Braun et. al [2], SIROCCO Project [3], Oerlemans et al [4]) reductions in self-noise radiation. A detailed theory to derive the wall pressure spectrum (WPF) for the prediction of straight and sawtooth serrated edge noise was first presented by Howe [1]. Later several extensions of this model for other types of serrations (e.g. slit) have been derived and experimentally investigated by various researchers [5]. In most cases significant noise reductions were found, except few specific situations. However, the effectiveness of serrations mainly depends on the appropriate dimension and the type of serration geometry [6].

The use of TES for wind turbine noise reduction has now become a mature technology, academic/research institutions [2], [4], [5], [3] and wind turbine manufacturers [7], [8] demonstrating its effectiveness in wind

¹ Corresponding author – Email: Mohammad.Kamruzzaman@enercon.de

tunnel and turbine tests leading to commercial products [9], [10], [11]. Since the last decades researchers from the universities performed detailed wind tunnel measurements to understand the maximum noise reduction performance of the TES by optimizing the design parameters [12], [13], [14], [15]. However, it was found that besides the acoustic measurement uncertainties, one of the key challenges is scaling of the TES design method from wind tunnel to the full-scale rotor blade. This could be one of the possible reasons why different turbine manufacturers offer dissimilar TES noise reduction performance while selling their turbines.

In the recent years, besides the classical sawtooth type of TES, many other variants of TES or aeroacoustics-addon concepts (namely “Beyond TES”) have been developed [16], [17], [12], [18], [19] and tested on full scale wind turbines [7], [20], [21], [22]. The performance of some of these technologies shows promising noise reduction outcome, compared to the standard TES. Manufacturers and many start-up companies [20], [21], [22] even claim that they can offer 3.0 dB to 6.0 dB reduction with their (Beyond) TES concepts. It is worth to mention that any such claim highly depends on the quality of the reference non-serrated blade noise level. Because the relative difference between TES vs. non-TES blades noise reduction shall be higher if the reference blade is too noisy. The design goal of turbine manufacturers is to make sure the absolute noise level of the target blade reduced significantly to comply the total turbine noise requirements. Hence, it can be easily argued that if a standard TES can reduce the same amount of noise without additional complexity or constraints, then what is the necessity of Beyond TES concepts? Another question remains open regarding the maximum performance of the standard TES: what is the upper limit of the standard TES noise reduction for wind turbine? Have we achieved it Can full potential of TES noise reduction applicable to reduce overall turbine noise?

This paper will try to answer these questions by detail optimization & enhancement of the performance of standard TES based on dedicated CFD simulation as well as wind tunnel and field measurements. To achieve best noise reduction for a given turbine and operation condition, the serration geometry is optimized consistent to the local turbulent flow characteristic based on the rotor noise simulation outcome and related wind tunnel data. Additionally, high-fidelity CFD is applied to understand the influence of different design parameters to develop an efficient Design of Experiments (DoE). Aeroacoustics wind tunnel test is performed at the Virginia Tech Stability tunnel. The enhanced method is then applied to design TES for MW wind turbine blades, and a full-scale turbine IEC standard field test is conducted for validation purposes. Section 2.1 begins with a short overview of the turbulence boundary-layer training-edge noise (TBL-TE) [23], including TES design aspects & parameter optimization in Section 2.2. Detail information of the CFD simulation methodology is described in Section 2.3. Section 2.4 describes the wind tunnel measurements setup and outcome. Section 3 focuses on field test details of the experimental setup and post processing methods. Results, validation, discussions and a conclusion are described in Section 3.2 and 4 respectively.

2. TES Design & Optimization for Wind Turbine Blade

2.1 Turbulent Boundary-Layer Training-edge Noise

There are three main aerodynamic noise sources for wind turbines, turbulence inflow noise, trailing-edge noise and separation noise. The aeroacoustics noise generation results from the interaction between vortices in the turbulent and the blade surfaces. Acoustic field tests of a full-scale turbine showed that turbulent boundary-layer trailing-edge interaction noise (TBL-TE) is the most dominant noise source for large wind turbines [4], [3], [24]. Thus, accurate prediction and reduction of this noise source is the focus for future generation wind turbine blade design. The design process principally depends on the development of an accurate theoretical model in which correct evaluation of turbulent boundary-layer (BL) structure plays a key role. The main mechanism of trailing-edge noise is the fluctuating pressure at the blade surface induced by the BL turbulent eddies, and their interaction with the sharp TE which propagates to the farfield [25], [23] (see *Figure. 1* for an overview).

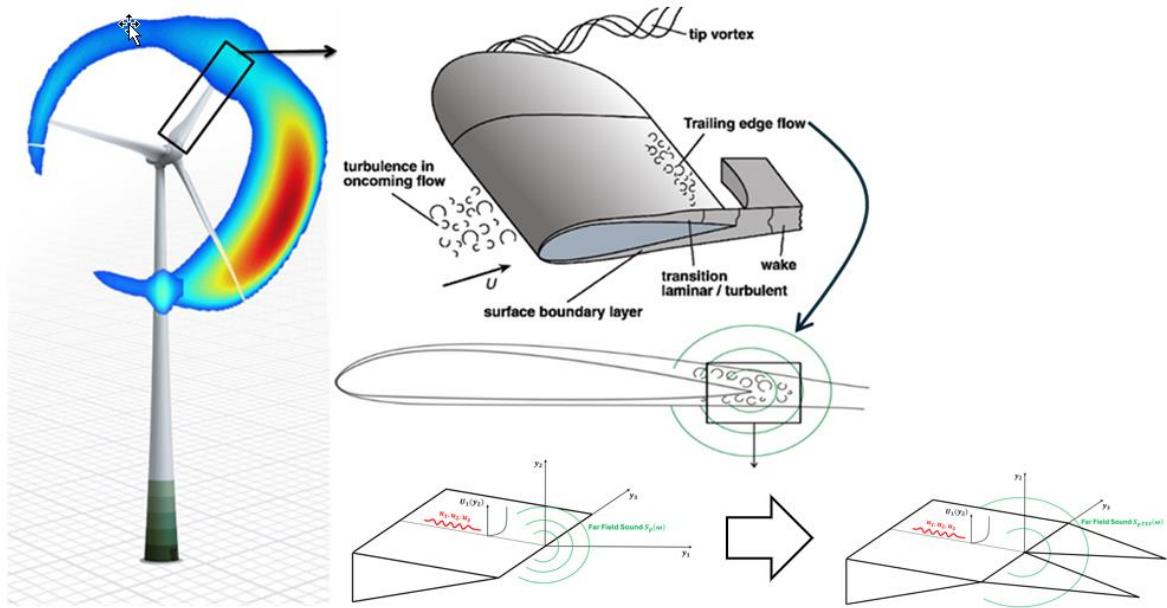


Figure 1: Wind turbine blade noise sources (left) [3] & Turbulence Boundary-Layer Trailing-edge noise (TBL-TE) characteristics (top-right & bottom) [26] [23]. Impact of serration (bottom-right).

2.2 Enhanced TES Design & Parameters Optimization

The effectiveness of serrations mainly depends on the appropriate dimensions and the type of serration geometry. From Howe's theory [1] it has been established that one of the most fundamental parameters for efficient serration design is the span-wise coherence length scale of pressure fluctuations, Λ_{p3} , [27]. The effectiveness of the serration geometry mainly relies on its appropriate dimensioning which is related implicitly to this flow dependent parameter. The most relevant design parameters for trailing-edge serrations are the length and the width of the serration and the attachment angle of the TES with respect to the chord line of the airfoil.

In general, serration length $H=2h$ and width λ have been defined based on the boundary-layer thickness calculated by empirical theory. For example, Howe [1] applied $H=10\delta$, δ being the boundary-layer thickness at the edge and found that attenuation increases rapidly when width to length ratio $\lambda/h < 5$. However, this empirical theory-based approach may not produce the optimal noise reduction. It is assumed that best results may be achieved if serration size can be designed based on the measured or predicted span-wise length scale, where $\lambda > \Lambda_{p3}$, i.e. serration length and width are greater than the average turbulence eddy size. This implies that such a design is able to diminish most energy-containing turbulence eddies.

2.3 CFD Simulation & Analysis

At Enercon, CFD simulations support the design of serrations by providing data on how the serrations alter the aerodynamic performance of the blade, including changes to aerodynamic coefficients such as lift, drag, and pitching moment. Additionally, valuable insights are provided into the local flow behavior around the serrations. In the subsequent sections, the simulation process will be outlined, and exemplary results and applications will be shown and discussed.

Process chain

The CFD process at Enercon employs the block-structured, compressible solver FLOWer. The solver features overset moving grids, well suited for the simulation of wind turbine rotors in academic research, as well as in industry [28], [29], [30], [31]. In the present study, two different turbulence models were investigated, the two-equation shear-stress transport model of Menter (SST) [32] and the one-equation strain-adaptive Spalart-Allmaras model (SALSA) [33]. However, if not otherwise stated the CFD

simulation refers to the SST turbulence model. All simulations were conducted steady state, except for operational points in the area of stall, for which transient simulations were performed using a dual-time stepping algorithm.

The laminar-to-turbulent transition in the boundary-layer is predicted by the e^N -envelope method of Drela [34]. The integral boundary-layer properties are approximated from the surface pressure distribution. A switching to turbulence occurs when the amplification rate exceeds the specified critical value $N_{crit} = 9$.

The grid setup consists of two structures, namely the background mesh of the airfoil without serrations and a grid of only the rear part of the airfoil that includes the serrations. Both are combined within the flow solver using the overset grid technique. This approach has the advantage that in the front part of the airfoil a virtually 2D grid is sufficient, which significantly reduces the number of cells. The main requirement in the industrial process is high-quality reproducible results. Therefore, meshes of all aerodynamic components are generally created automated using in-house scripts. For this purpose, an automated grid strategy was developed within the scripting environment of the meshing software Pointwise that allows for the parametrization as well as the meshing of the airfoil with the serrated trailing edge.

The meshing of the serrated part starts with the geometry parametrization for which the user needs to specify the desired planform, the flap angle, the distribution of the thickness, as well as the attachment to the airfoil. The structured grid is then generated slice by slice, starting with the point distribution on the surface, extruding the boundary layer, building the wake block and at the end extruding both towards the overset boundaries in the wall normal direction. The point distribution on the airfoil surface automatically takes into account refinements at the attachment areas and trailing edge. Special attention was given to the extrusion of the boundary layer to comply also with large flap angles. For this purpose, an in-house algorithm was developed that ensures good-quality cells for almost arbitrary flap angles. By default, a geometric extrusion with growth rates of 1.1 is applied, starting from a first wall distance that yields $y^+ < 1$ for the Reynolds number at hand. These widely established best practices led to accurate distributions of all flow variables across the boundary layer. The wake domain is aligned to an estimated direction of the wake. The cells of the boundary layer connectors and the ones on the blunt trailing edge are fanned out over a distance of around half a chord length. In the final step of the extrusion towards the overset boundaries the boundary layer and wake domains are performed to reach the specified grid resolution of the background mesh.

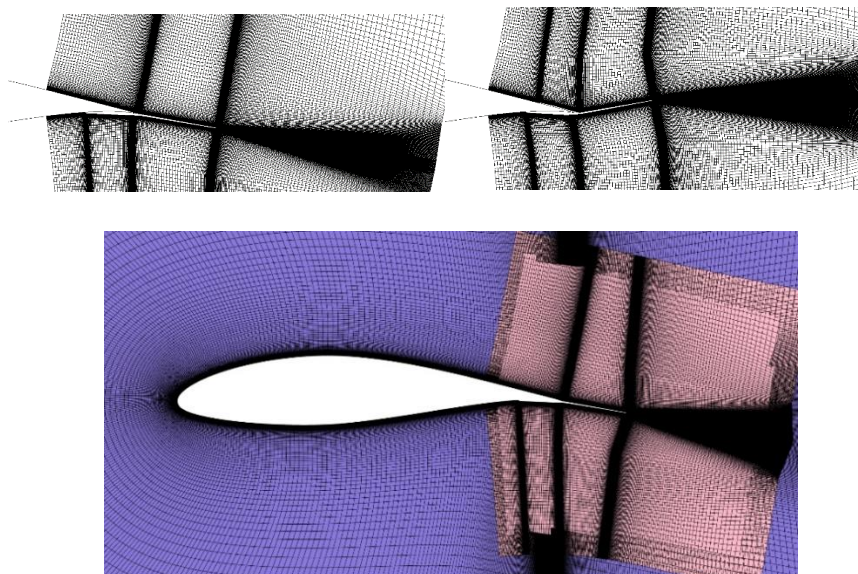


Figure 2: Computational grid around the TES. Meshing of different flap angles.

Typically, for an aerodynamic investigation outside of deep-stall events a single serration tooth is considered. Its mesh consists of 64 slices in the spanwise direction. In the final step the slices are built to blocks and automatically partitioned to the desired loading per rank. The hole definition for the background

mesh is conducted automatically. It guarantees small overlapping zones and complying grid resolutions at the interfaces. Usually, there is no manual iteration necessary to obtain a setup with less than 10 orphan points. In total, a serration setup including the background airfoil mesh contains around 7-10M grid points. *Figure 2* show examples of serration meshes for different flap angles and attachment methods to the airfoil.

CFD results

One of the most important results in the assessment of the aerodynamic performance of airfoils including trailing edge serrations are the aerodynamic polars. Therefore, it is highly important to develop a CFD process that delivers robust and accurate results on the main aerodynamic forces lift and drag as well as on the derived quantities pitching moment and aerodynamic efficiency L/D . Due to confidentiality, here only the results of L/D are shown in *Figure 3* for the baseline airfoil case without add-on (left plot) and for a representative case with serrations (right plot). The predictions are compared to measurement data from the Virginia Tech Stability wind tunnel and include both, cases with natural transition (U) and with tripped boundary layers close to the leading edge (T). Two turbulence models are compared in the baseline case. The Menter SST model yields accurate results in the linear aerodynamic region. It captures lift correctly. The slight overprediction in the L/D is due to a slight underprediction in drag. This trend is a bit more pronounced in the clean conditions, which implies the transition location to be predicted slightly too late. When approaching the non-linear regime before stall, the L/D is slightly under-predicted. Here, drag is predicted to be too low in clean conditions because the transition location moves upstream too quickly due to the adverse pressure gradient. In the stall region, the SST model reveals the typical problem of too late a prediction of stall onset. In comparison to that, the SALSA turbulence model was studied, as it remedies the latter discussed delayed stall onset prediction. The agreement with the experimental data is improved with the SALSA model that more accurately captures the stall onset and the lift breakdown. It is therefore frequently used to study sensitivities on stall onset in comparison with the SST model. On the other hand, the SALSA model has deficiencies in predicting the correct drag levels in attached flow and especially weakly loaded boundary layers. This is clearly visible in the overprediction of L/D at moderate angles of attack and particularly in clean conditions. An exemplary comparison of a CFD prediction with the SST model for a serrated case is shown in the right graph of *Figure 3*. The trends are very similar to the baseline airfoil, where L/D is slightly overpredicted in clean conditions in the rising L/D branch, due to a slight underprediction in drag. In tripped conditions the predictions are excellent in that region. However, also as for the baseline case stall onset is delayed as expected. It can be concluded that there is good agreement between CFD predictions and experimental data. This holds true also for other airfoils and many serration parameters and as such validates the developed CFD approach for the aerodynamic design of airfoils with trailing edge serrations.

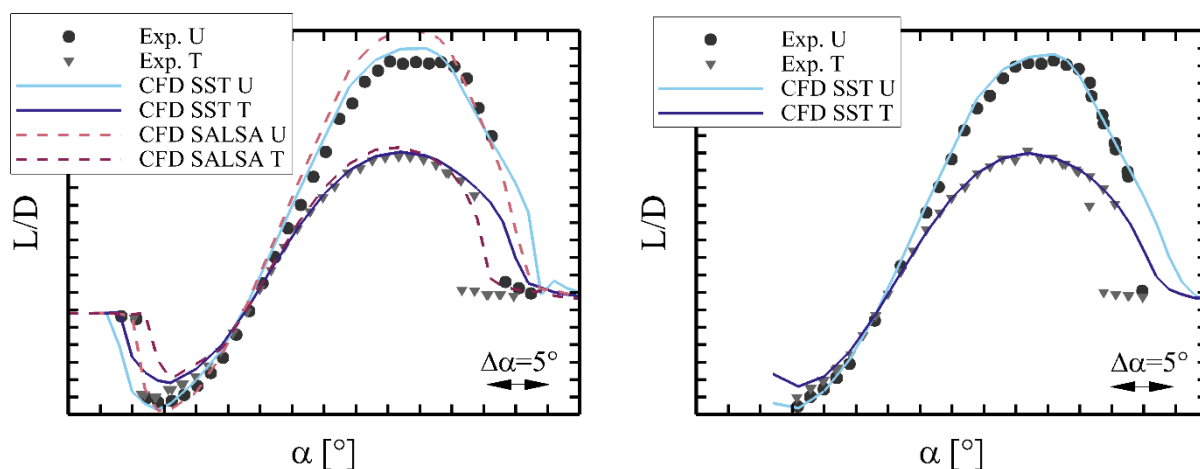


Figure 3: Comparison of predicted and measured aerodynamic efficiency, L/D , of the baseline airfoil without serrations (left) and with serrations (right) as a function of angle of attacks. Cases with natural transition (U) and tripped boundary layer (T).

The evaluation of the local flow around the serrated blade is important when defining the serration parameters during their design (i.e. lengths, widths, flap angles, thickness, materials, flow angle etc.), but also when it comes to the implementation into the blade, where the attachment method may also have an aerodynamic and aeroacoustics impact. As a standard task, CFD is therefore used to analyse the velocity field around the serrations and check for potential local separation phenomena. As an example, the velocity field shall be compared in *Figure 4* for a case of serration with large flap angle (left plot) and a serration with moderate flap angle (right plot). An iso-surface of the Q-criterion visualizes vortical structures developing around the serrations. To improve the clarity, the iso-surface is clipped at half of the span. Several slices are placed perpendicular to the inflow direction across the serration and in its wake. In case of the large flap angle, it can be observed that a trailing vortex forms around the serration side edge. This is due to the fact that a pressure difference is persistent over flapped the serration, which also means that the serrations themselves are contributing to lift. Similarly to a wing tip, a vortex rolls over from the pressure side to the suction side. This effect was similarly observed in other studies such as [35]. Apart from additional lift, however, the trailing vortex cases also induced drag. In the flow field, a spanwise non-uniform distribution of velocity emerges. The non-uniformity increases with increasing streamwise distance across the serration and becomes very prominent in its wake. In comparison to that no trailing vortex is formed when the flap angle is reduced such that the pressure difference between serration pressure and suction side diminishes. This yields a very homogeneous velocity distribution in the spanwise direction.

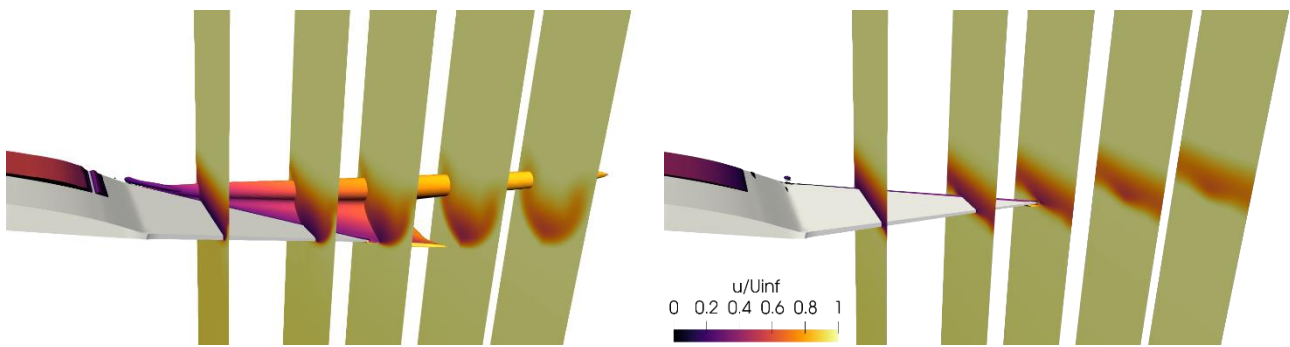


Figure 4: Comparison of the velocity field across the serration for a large flap angle (left graph) and a medium flap variant (right graph).

The corresponding boundary layer profiles of the wall tangential, the wall normal and the spanwise velocity components are depicted in *Figure 5*, plotted against the boundary layer thickness of each case, respectively. The evaluation position is at half of the serration in the streamwise direction on the suction side. Two spanwise positions are extracted. The first is located in the serration's mid plane, whereas the second one is close to the serration side edge. The cross-flow through the serration at large flap angle causes changes in the velocity profiles between the serration edge and serration centre. The vortex roll-over induces an acceleration in the tangential velocity close to the side edge compared to the baseline airfoil near the wall. At the height between $0.25 < d_w/\delta < 0.5$ a negative spanwise velocity component indicates the fluid is deflected towards the serration centre. Below of that, the wall-normal velocity is almost zero, or even slightly negative, which means that the flow is deflected towards the surface. This behaviour was very similarly also observed in PIV measurements of [36]. It can be seen, that in the midplane there is almost no wall-normal velocity below this height. Compared to the baseline airfoil the flow through the serration reduces the outwards motion of the fluid. In the region, where the spanwise velocity is largest at the serration edge, a retardation of the tangential velocity is observed in the serration's midplane. Very close to the wall, the velocity profile is slightly richer compared to the baseline airfoil. As it could be observed in the contour plots, reducing the serration flap angle may diminish the cross-flow over the serration. As a direct consequence the wall-normal and spanwise components become very small. And the profiles evaluated close to the serration edge and in the midplane almost coincide. The fact that there is no cross-flow also means that pressure equalization between both sides is shifted upstream and does not occur over the serration. This results in a less loaded boundary layer on the serration, which can

be retrieved from the acceleration of the tangential velocity close to the wall. With increasing wall distance this effect reduces, and the profiles approach the trend of the baseline airfoil.

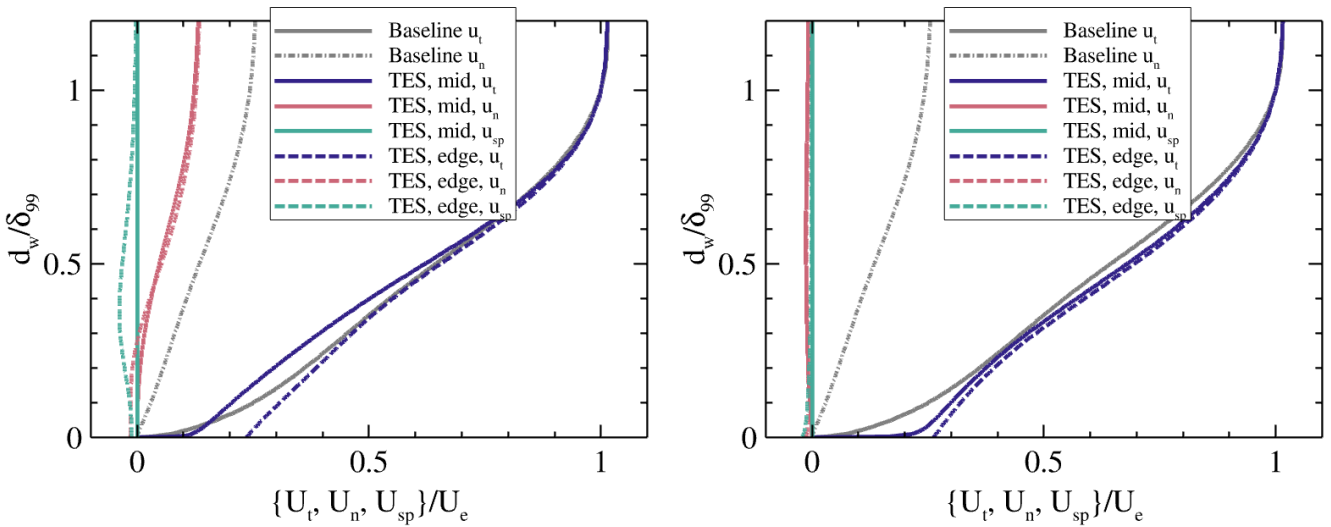


Figure 5: Boundary layer profiles of the tangential velocity u_t , wall normal normal velocity u_n and spanwise velocity u_{sp} evaluated at $x/L_{TES} = 0.5$ in the mid plane of the serration (solid lines) and close to serration side edge (dashed lines). Comparison of a serration configuration with large flap angle (left graph) with a serration of medium flap angle (right graph) as well as the baseline airfoil without add-on (grey lines).

The evaluation of turbulence parameters is important in the design of serrations, to derive the integral length and time scales of turbulence upon which the serrations are then adapted on the operating design of the turbine. As an example, the flap effect on turbulence kinetic energy shall be illustrated in a similar visualization as in the previous velocity profiles. The contours are shown in various slices over the serration and in its wake in Figure 6. A very inhomogeneous distribution is obtained in case of the serration with large flap angle, accumulating high values in two stripes around the serration edges and a bulb shaped spot in the serration centre. In the wake the magnitude k_t is dissipated in the downstream direction. In the area of the trailing vortex moderate values of k_t appear. Similarly to the velocity profiles a reduction of the flap angle yields also a very homogeneous, almost two-dimensional distribution of turbulence kinetic energy, where the turbulence peak occurs in a stripe in the middle of the boundary layer. From visual inspection it can be also seen that the boundary layer thickness is significantly thinner. In the vicinity of the serration's side edges the concentrations of k_t are also significantly less than in the case of the larger flap angle.

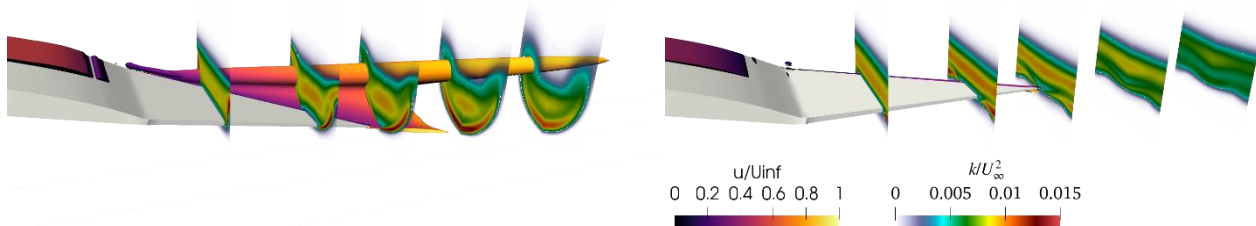


Figure 6: Comparison of turbulence kinetic energy in slices across the serration for a large flap angle (left graph) and a medium flap variant (right graph)

A closer quantification of the profiles in *Figure 7* shows that in both serration cases the peak values exceed the ones from the baseline airfoil. This overshoot is more pronounced in the case of the smaller flap angle. Besides that, as already implied from the contour plots, at small flap angle all profiles almost coincide. Hence there is not much change of the turbulence quantities occurring over the serration, neither in the spanwise direction, nor in the streamwise direction. Recalling that there is no cross-flow through it, also the changes in velocity profiles and in its gradients is small. This is different for the case of the larger flap angle, where both occurs, a slight increase of the peak values towards the serration tip and more pronounced, larger k_t values appears in the near-wall region close to the serration side edge.

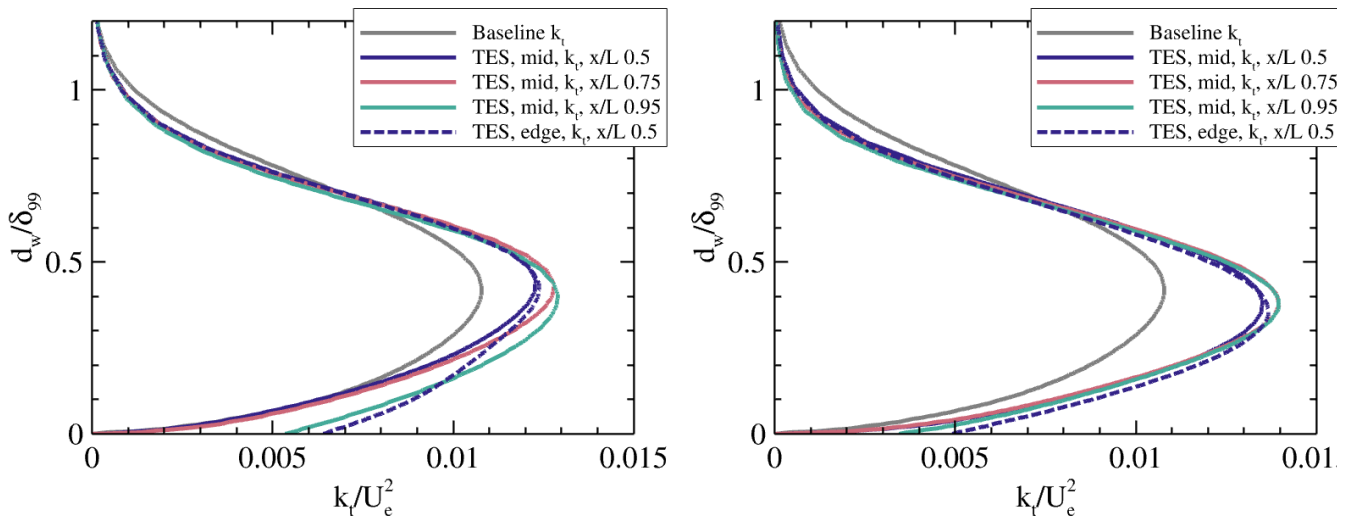


Figure 7: Development of turbulence kinetic energy profiles in the streamwise direction. Comparison of a serration configuration with large flap angle (left graph) with a serration of medium flap angle (right graph) as well as the baseline airfoil without add-on (grey lines).

The results shown are not supposed to be complete but shall serve an overview, where CFD methods at Enercon support the design of serrations, namely in the aerodynamic performance assessment to predict the effect of the add-ons on the polars, as well as in the analyses of how the respective serration configuration influences the local flow behaviour.

2.4 Wind Tunnel Test & Validation

The key discipline in validating different serration designs aerodynamically and aeroacoustically is to conduct wind tunnel experiments. For this purpose, extensive campaigns were conducted in the anechoic test section of the Virginia Tech Stability wind tunnel. The primary goal was to find more efficient trailing edge add-on geometries for noise reduction. The assumption was, that standard TES used by Enercon do not represent the optimal geometry for maximum trailing edge noise reduction and aero performance. Older serration setups only reached a sound reduction between 2 dB and 3dB compared to the baseline turbine. The aim was to find a robust TES design that reduces trailing edge sound emission of wind turbines by more than 3 dB without compromising aerodynamic performance. With the presented wind tunnel setup, it is possible to identify the best layouts and attachment methods of future TES configurations. A representative baseline outboard airfoil section was chosen to test a variety of parameters for trailing edge add-ons with a focus on aerodynamic performance and trailing-edge noise reduction.

The Virginia Tech Stability wind tunnel features a square-cut test section with a height and width of 1.84m. The full span airfoil model is supported by 88.9mm-diameter steel tubes which project 166mm from either end of the model. The tubes fit into rotatable couplings mounted in the floor and ceiling in the center of the test section. The airfoil chord length is 0.9m. The aerodynamic coefficients of the airfoil section and different add-ons are determined by integration of the surface pressure distribution. The pressure

distribution is measured by pressure transducers connected to 80 pressure taps implemented into the test wing.

The anechoic test section's port and starboard walls are made of tensioned fabric which extend 4.2 m in the streamwise direction and the full height of the test section. The starboard side chamber (suction side of the airfoil) contains a 251-channel microphone array to measure the acoustic signature of the model.

Acoustic spectra were calculated by integrating a predefined region in the acoustic source maps around the midspan section of the test wing. All parameter variations were tested for natural transition and forced transition (fully turbulent flow).

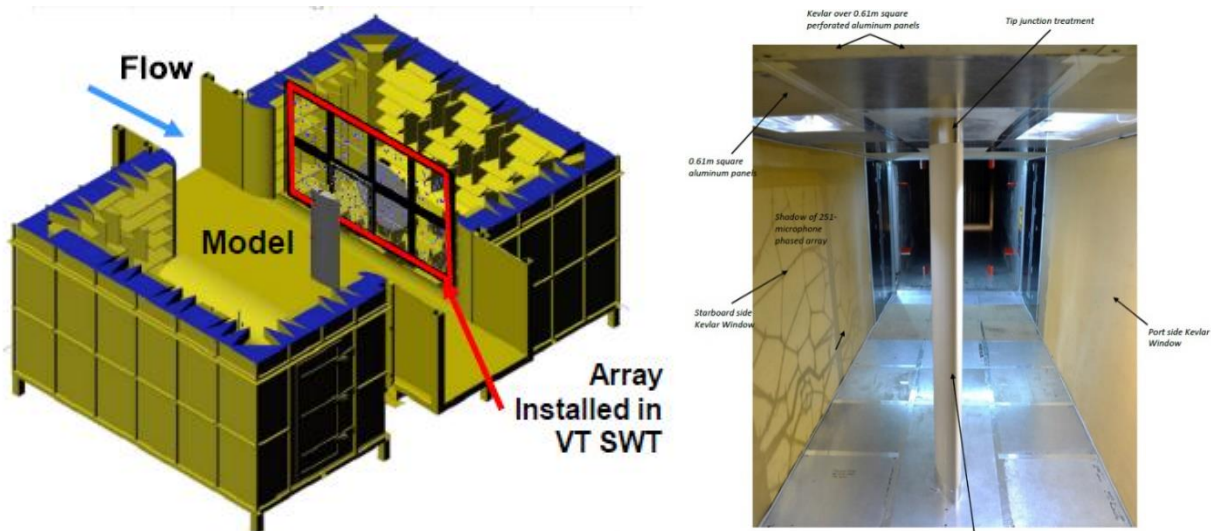


Figure 8: Schematic test setup (left) and picture of test section with installed test wing (right).

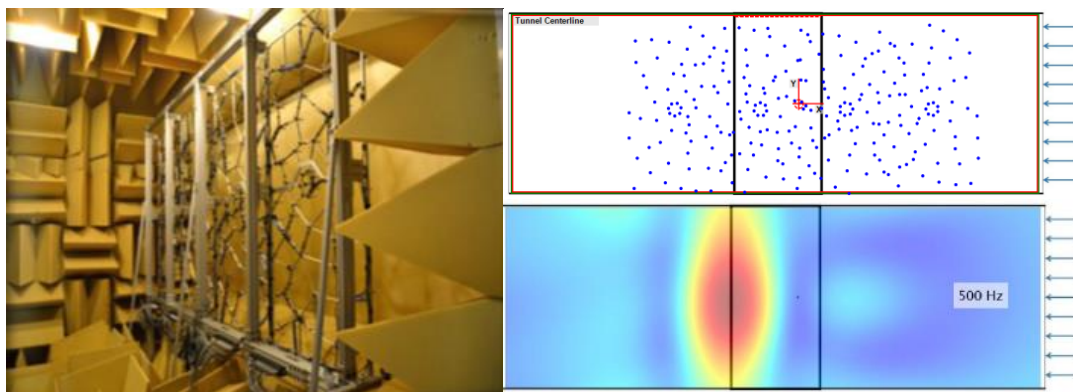


Figure 9: Picture of microphone array (left), locations of microphones relative to test wing (upper right) and example of a selected 1/12th octave band beamforming map at 500Hz (lower right).

An example on the effect of varying serration parameters such as length, width, flap angle or attachment method on the overall sound power level is shown in Figure 10, plotted vs. the angle of attack. The grey dashed line represents the baseline airfoil without serrations. It can be retrieved from the figure that careful design of the serration parameters is necessary, to achieve the greatest noise reductions in the desired lift regime. A wrong choice of a parameter can totally diminish any noise reduction as it can be observed from the yellow and rose curves. By variation of one parameter the angle of attack region in which the serrations are most effective can be adjusted left and right (compare wine colour with dark green colour). Therefore, a different optimum may be found depending on the individual blade design or actual site conditions. However, as indicated by the light blue configuration an optimum could be found that outperforms all other variants across the entire angle of attack range.

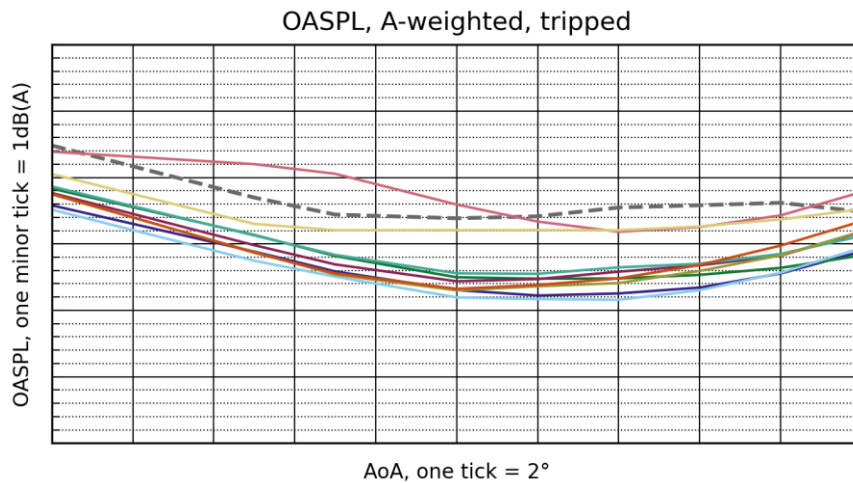


Figure 10: The effect of serration parameters (length, width, flap) on the overall sound pressure. Baseline airfoil without add-on shown in grey.

Apart from the overall sound power level, also the frequencies are important in which the serrations alter the acoustic signature. From a noise imission perspective, it is desirable to achieve large noise reductions especially in the lower frequencies. The Figure 11 and Figure 12 show one-third octave band spectra for two selected angles of attack. The former at low to moderate lift and the latter in the moderate to high lift regime. All configurations of the OASPL graph before are cross-plotted. Frequency is given non-dimensional in terms of the Strouhal number based on the suction side displacement thickness near the trailing edge, which was extracted from CFD simulations. By non-dimensionalising frequency it can be seen, that for both angles of attack, the maximum of the spectrum of the baseline airfoil lies between 0.07 and 0.1. At the lower angle of attack especially the rose, but also the yellow configuration seem to be ineffective in reducing noise at lower frequencies in that peak region. On the other hand, they induce significant additional noise at higher frequencies. The parameters in the other configurations are chosen such that they reduce noise up to a Strouhal number of ~ 0.5 . The optimized light blue variant performs up to 3 dB better than green configuration in the peak region of the baseline spectrum. There is a slight noise increase after the cross-over frequency of 0.5 compared to the other configurations. However, since the general level is already quite low this does not manifest into the OASPL. Additionally, from imission perspective it is also less important than the noise reduction at lower frequencies.

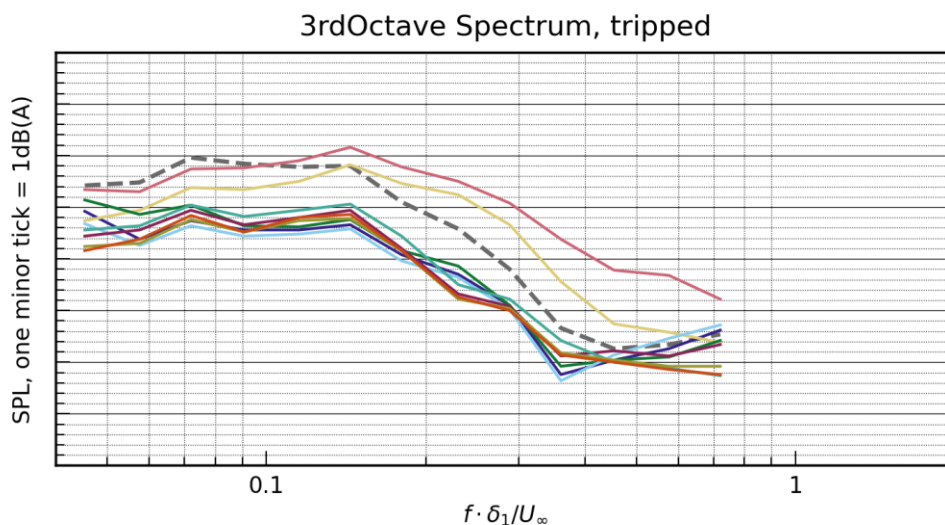


Figure 11: The effect of serration parameters (length, width, flap) on the acoustic spectrum at an angle of attack of low to moderate lift. Baseline airfoil without add-on shown in grey.

The trend in the spectrum becomes even more obvious for the angle of attack at higher lift. The spectrum of the baseline airfoil becomes steeper and is more influenced by the effect of the suction side. Here, the blue, wine and yellow color-coded configurations achieve similar noise reductions at low frequencies. However, the serration induced self-noise starts dominating. The further the optimum of the design parameter is left, the earlier the noise increase starts (from color codes: ochre, teal, orange to yellow). Again, here the dark and light blue coded configurations represent a global optimum in the parameter space, where there is an effective noise reduction at low frequencies without losing through additional sound at high frequencies.

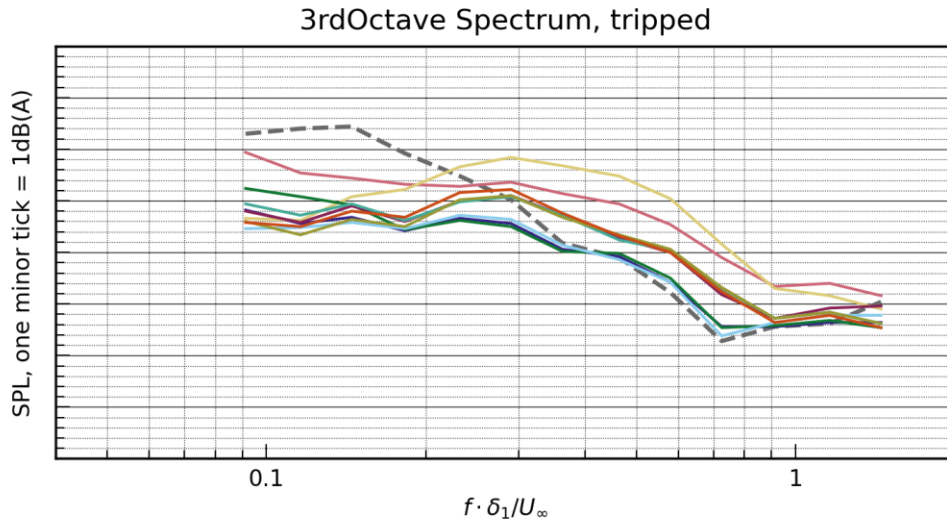


Figure 12: The effect of serration parameters (length, width, flap) on the acoustic spectrum at an angle of attack of moderate to high lift. Baseline airfoil without add-on shown in grey.

2.5 TES Design for Full Scale Wind Turbine Blade

The wind turbine blade trailing-edge noise reduction problem is complex and involves a variety of opposing constraints. A wind turbine operates over a range of wind speeds, pitch angles, and turbulent inflow conditions, resulting in a corresponding range of local flow conditions over the outboard region of the blades. This means that noise reduction techniques must be effective over a range of conditions as opposed to only for a single design point.

During the last years, trailing-edge serrations have been adapted for multiple wind turbines of the two to seven MW class. The serrations are included in the aerodynamic design of a rotor blade and the attachment is designed in such a way, that the airflow is not disturbed attached. They were applied over the outer quarter of the blade, and their length and width are designed based on the numerically predicted largest spanwise coherence length scale $\Lambda_{p,3} \equiv \ell_3$, which varies as a function of radial position along the blade (see Figure 13 and 14). The spanwise coherence length scale of the fluctuating pressure has been calculated based on a semi-empirical model as a function of the local convection velocity U_c and the peak frequency f_{peak} , where $U_c = c1 \cdot V_{eff}$. The effective or local incoming velocity V_{eff} is found via Blade Element Momentum (BEM) calculations. The BEM also provides other necessary flow parameters such as local flow Angles of Attack (AOAs), Reynolds and Mach numbers. The parameter f_{peak} is the frequency where boundary-layer trailing-edge noise spectrum has its maximum value. This parameter can be evaluated either via dedicated wind tunnel measurements of the turbulent boundary-layer Wall Pressure Fluctuation (WPF) point frequency spectrum [27] or by any theoretical noise prediction model [26], [23], [37]. In the present analysis, Enercon's in-house noise prediction tool has been applied. Figure 13 to 14 depict an example evaluation. Designing the TES geometry based on the above approach enables the identification of the most energetic turbulence eddy sizes in the flow, which should be diminished or broken up to consequently reduce noise emissions. Interestingly, the above derivation also satisfies Howe's

theoretical condition $\frac{\omega h}{u_c} \gg 1$. It must be noted that the calculation of $\Lambda_{p3}(r/R)$ via a semi-empirical model is not trivial. It can be calculated more accurately from the two-point WPF wind tunnel measurements [27].

Finally, for the definition of serration dimensions along the blade span following formula are applied. Serration length,

$$H(r/R) = c2 \cdot \Lambda_{p3}\left(\frac{r}{R}\right), \tag{0.1}$$

and width

$$\lambda = H/c3 \tag{0.2}$$

where $c2$ =empirical constant in the range 4-15 and $c3$ =0.5 to 6. To develop a continuous function along the blade span, predicted $\Lambda_{p3}(r/R)$ at different span positions have been utilized to define a 6th order polynomial function by a curve fitting method. It should be noted that $\Lambda_{p3}(r/R)$ will vary based on the local flow condition or turbine operation. *Figure 13* depicts predicted spectra and corresponding peak frequencies. *Figure 14* shows the dimension of the serrations along the radius with the respective analytical function which fit the predicted data in design and off-design conditions best. Note that, the serration length and width must be selected in a way that it is more effective in the design condition and less effective in off-design. The TES flap angle is chosen based on CFD simulations as well as aeroacoustics and aerodynamic wind tunnel tests, in order to comply with performance and loads requirements.

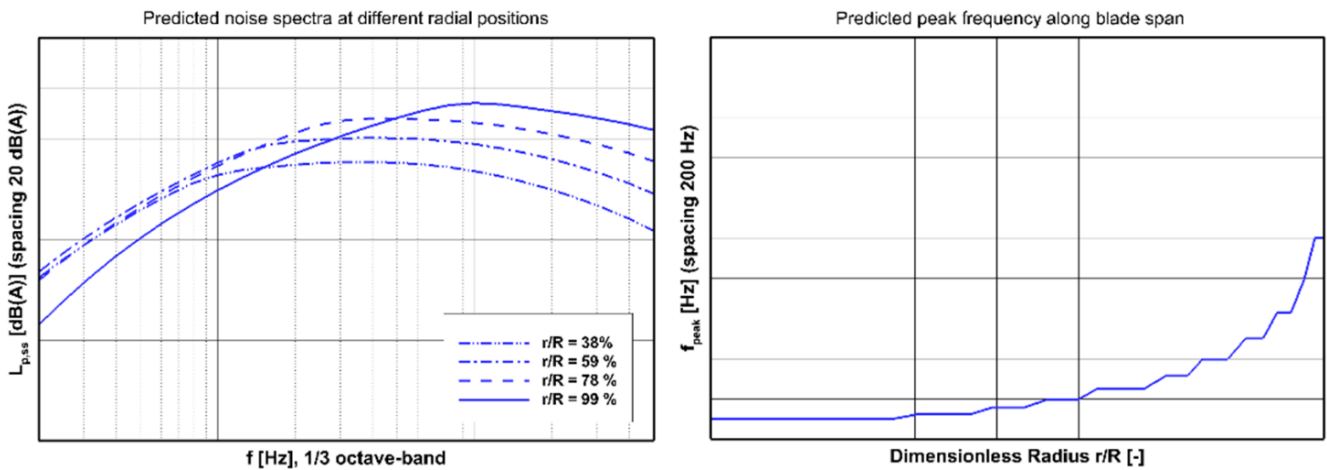


Figure 13: Predicted TE noise spectrum from four airfoil sections of the blade (left) and peak frequency, where TE noise spectrum has its maximum value (right).

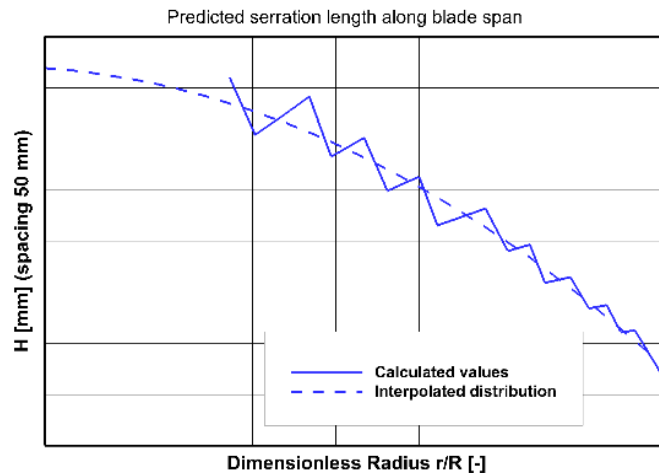


Figure 14: Applied serration length along the blade span based on the predicted spanwise length scale within design and off-design conditions.

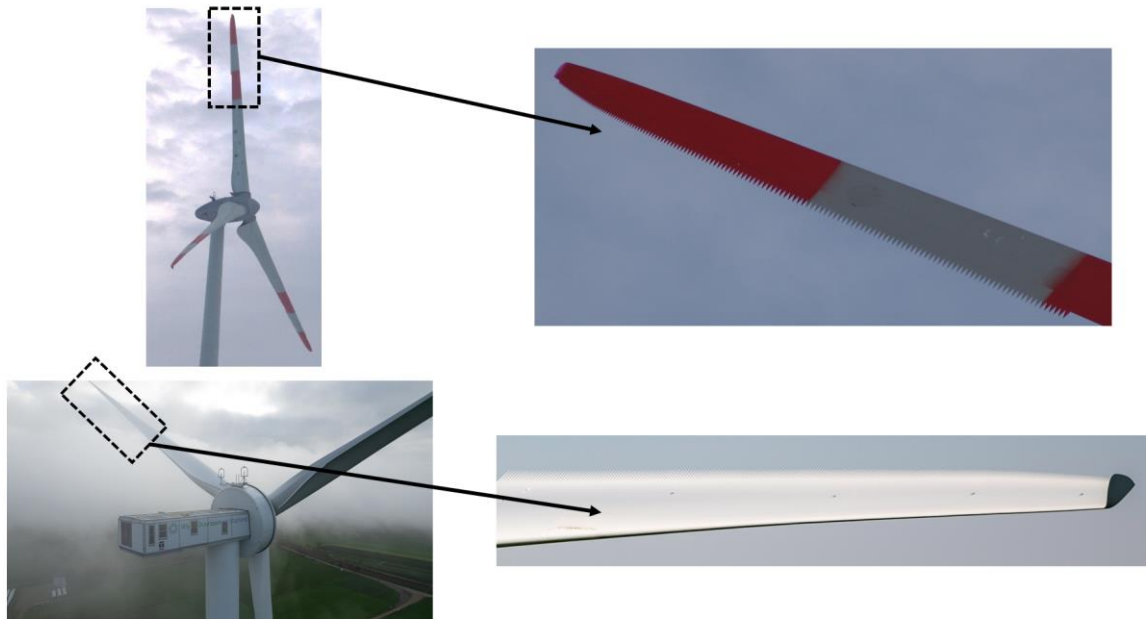


Figure 15: Trailing-edge serration on a full-scale MW class turbine (top plot: Standard Enercon design – bottom plot: Enhanced design).

2.6 Design Constraints

The primary design objective of the TES is to achieve maximum noise reduction. While the physical conditions necessary for this are well understood and detailed in Section 2.5, additional constraints must be considered to successfully integrate TES or any blade add-on into an existing blade design. These constraints can be categorized into three main groups: geometry, compliance, and manufacturing.

Geometry: The maximum relative length with respect to the local chord must not be exceeded. Additionally, the size and contour shape must adhere to Enercon's internal best practices, which impose specific constraints.

Compliance: To ensure compliance, the final product must not significantly impact loads and power production. The TES must be designed to meet the expected lifetime and maintain structural integrity under harsh conditions such as UV radiation, erosion, icing or severe gusts. Compliance with health and safety regulations is mandatory, and only qualified materials can be used for serial production. The proposed design should comply not only with the noise reduction of the standard operation mode but also with other operation modes.

Manufacturing: The TES must be easy to handle during the production process to minimize the risk of manufacturing errors. Both material and production costs should be kept low.

Given these constraints, it is evident that implementing a new TES design is a complex and demanding task, extending beyond the physical optimization itself.

3. Field Test Results, Validation & Discussions

Noise reduction performance of the optimized serration design (TES+) compared to the standard TES as well as the overall performance of the standard TES are conducted in the following section. As discussed in Section 2, serration geometry is optimized consistent to the local turbulent flow characteristic based on the rotor noise simulation outcome and corresponding wind tunnel data. IEC 61400-11:2012 ed.3.1 sound power measurements have been performed for different MW class turbines as shown in Table 1, with and

without TES, and with TES vs. TES+ designs. Turbines are pitch regulated and thus the angle of attack will vary significantly with wind speed.

3.1 Test Matrix

A dedicated validation test matrix has been developed varying turbine types, site conditions, types of serrations, attachment methods etc. as shown in Table 1. A visual overview of a general IEC compliant field measurement setup and procedures can be seen in Figure 16.

Table 1: Field measurements test cases considered for the validation study.

Test Case Name	MW Class	Approx. Rotor Diameter	Design Variant	Validation Data
EP1	< 1.0 MW	Rotor diameter 50 to 60m	TES	Blade with and w/o TES
EP2	1 to 2.x MW	Rotor diameter 70 to 100m	TES	Blade with and w/o TES
EP3 Case 1	3 to 4.x MW	Rotor diameter 101 to 140m	TES	Blade with and w/o TES
EP3 Case 2	3 to 4.x MW	Rotor diameter 101 to 140m	TES	Blade with and w/o TES
EP3	3 to 4.x MW	Rotor diameter 101 to 140m	Optimized serration (TES+)	Blade with TES vs TES+
EP4	4.0 MW to 5.x MW	Rotor diameter > 140m	Optimized serration (TES+)	Blade with TES vs TES+

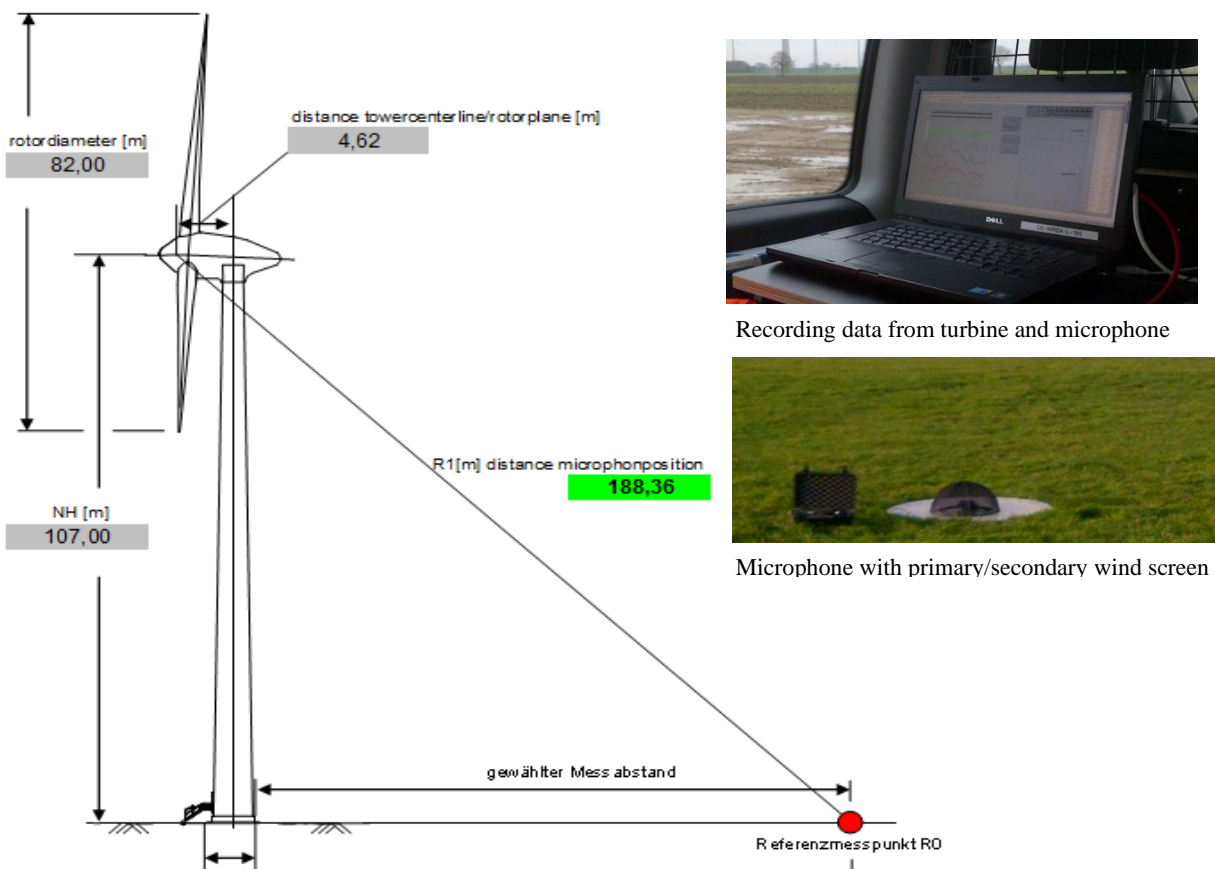


Figure 16: IEC61400-11 standard measurement setup.

3.2 Validation & Discussions

For several turbine types of platforms EP1, EP2, and EP3, the acoustical performance of the serrations has been evaluated by comparing IEC 61400-11 compliant measurement results on turbines with serrations and turbines without serrations in the same operating mode. *Figure 17* shows aggregated overall sound power level L_{WA} statistics per turbine type over all measurements for this evaluation.

While EP3 Case 1 shows quite equally dispersed data, EP1 displays a larger spread without TES and EP3 case with TES. It must be noted that the net difference between the averages of the two groups “with serrations” and “without serrations” is also depending on the choice and availability of measurements and not only the effect of the serrations themselves especially considering the available number of measurements. For the cases displayed here, the maximum sound power level difference varies for the different types and wind speeds between 1 and 3 dB.

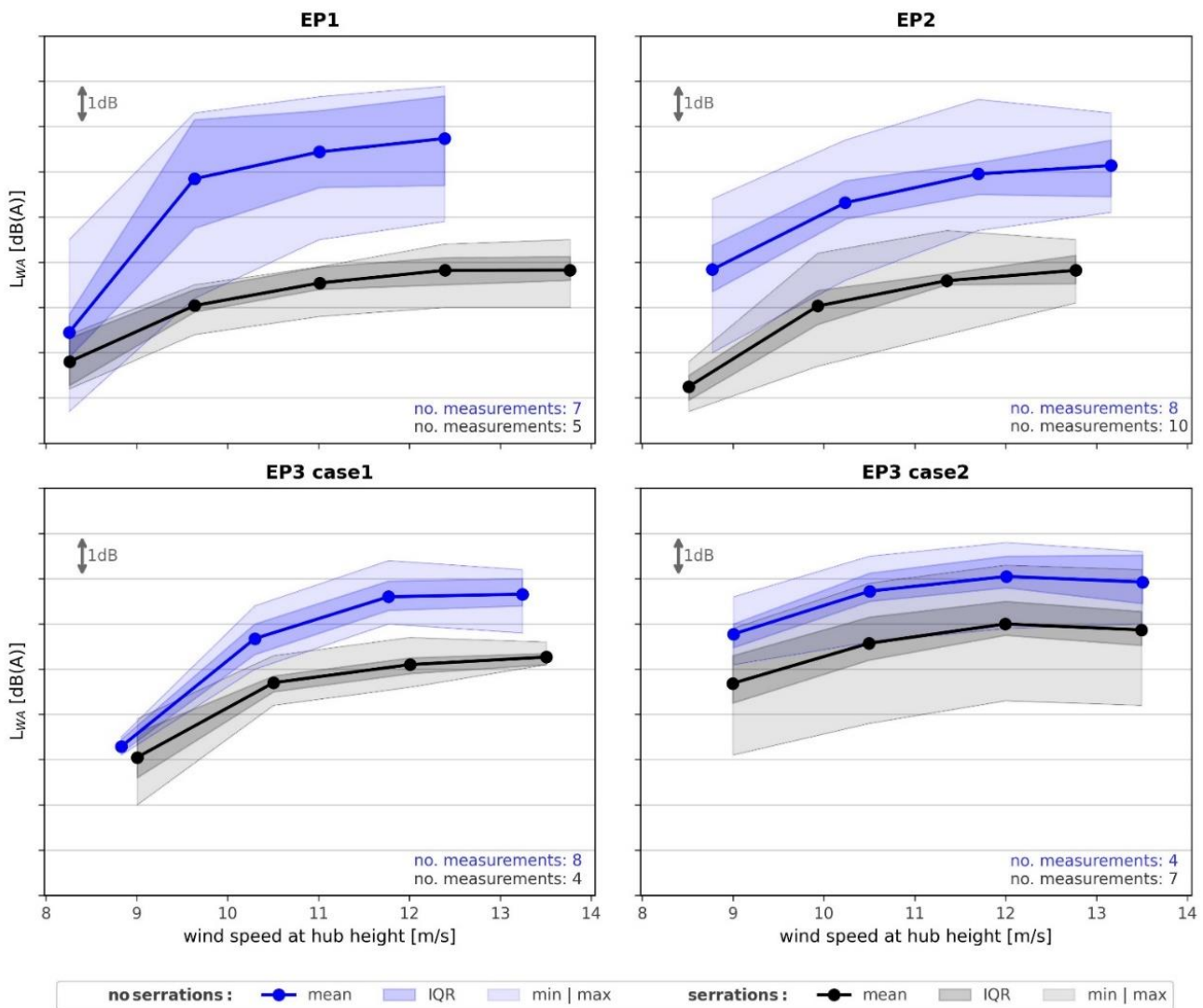


Figure 17: Overall sound power level statistics for different turbine types.

In *Figure 18*, statistics for sound power level third octave of the loudest wind bin per measurement are presented. As could be seen for the total sound power levels, the spread per state (turbine and serration / no serration) is varying and not homogenous. For EP3 Case 1 & 2, there is a frequency region of reduction and region of slight increase, as would be expected with serrations. The crossing point for both cases is between 900 Hz and 1 kHz. For EP3 Case 2, the peak levels without and with serrations seem to be comparable just shifted to higher frequencies, which is why there is less total sound power level reduction. For the EP1 case, there seems to be a broad reduction over almost the whole displayed frequency range. However, the spread is also considerable for the case without serrations. Probably there are other effects present for the case without serrations (e.g. noticeably different meteorological conditions, blade surface

conditions etc.), that contribute to the spread and therefore enlarge the difference of the means independent of the impact of the serrations.

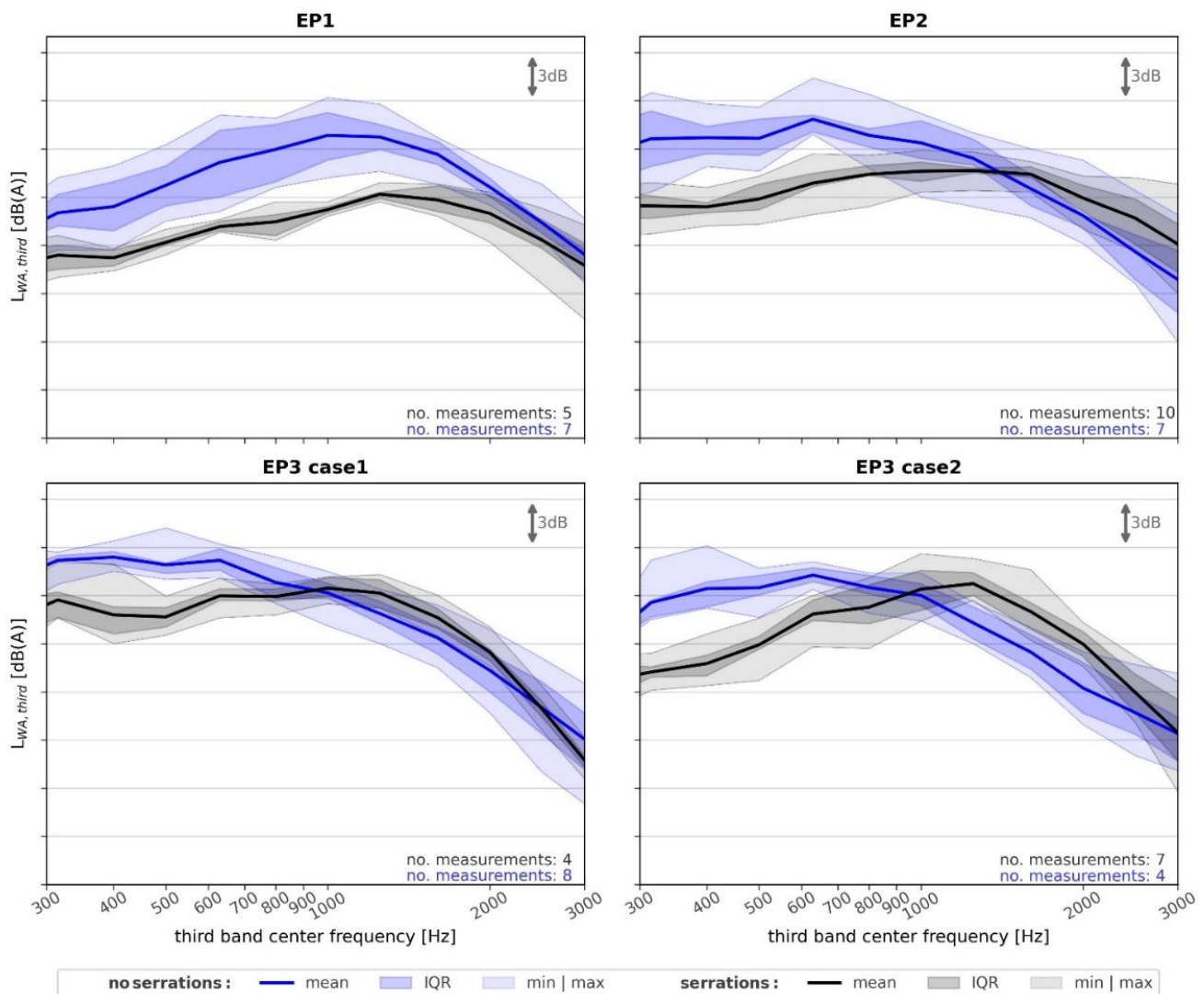


Figure 18: Sound power level statistics as third octave for the loudest wind bin of the different turbines.

In the process of serration design optimisation, both for EP3 as well as EP4 single turbines were equipped with optimized serrations, called TES+. Figure 19 shows the corresponding results of IEC 61400-11 ed 3.1 compliant measurements for turbines equipped with standard serrations (TES) and one turbine with optimized improved serrations (TES+). As there is only a single measurement available for the new TES+ design, no statistics can be made like the regular TES vs without TES validation study as shown in Figures 17 & 18. However, a one-to-one relative difference between the regular TES vs. enhanced TES+ design is conducted for two different turbine types to understand the performance of the new design. This comparison plot for the overall sound power level L_{WA} as well as the 3rd octave frequency spectra can be seen in Figures 19 and 20. The better noise reduction performance of the enhanced TES+ is clearly visible compared to the standard TES. For the EP3, it is very interesting to see that TES+ design provides the best noise reduction potential near the maximum OASPL (L_{WA}) which is the most critical position for the turbine manufacturer to comply the noise regulation/guarantee data. Moreover, compared to the group of standard TES performance as shown in Figures 17 & 18, both in sound power level sum as well as spectrally the enhanced TES+ measurement shows lower levels than all others, see Figures 19 and 20.

In addition to the IEC measurements, elaborate multi microphone measurements have been performed on a turbine equipped with both standard TES and improved TES+ serrations at the same time on different blades (results not shown here). A rotation section wise comparison around the points of largest acoustical

impact of the single blades shows better acoustical performance for the TES+ serrations in the exact same frequency range (700 Hz and above) as the difference of the single IEC measurement compared to the group of measurements in *Figure 20*. This is a strong indication that the TES+ design leads to even further sound reduction than the standard serrations. Looking at the spectra in *Figure 20*, the enhanced TES+ design is more effective at the mid frequency range where trailing-edge noise is most dominant, whereas low frequency performance remains the same. Hence, it can be concluded based on the current validation study and data analysis that one can achieve more than 3 dB noise reduction by means of trailing-edge serrations.

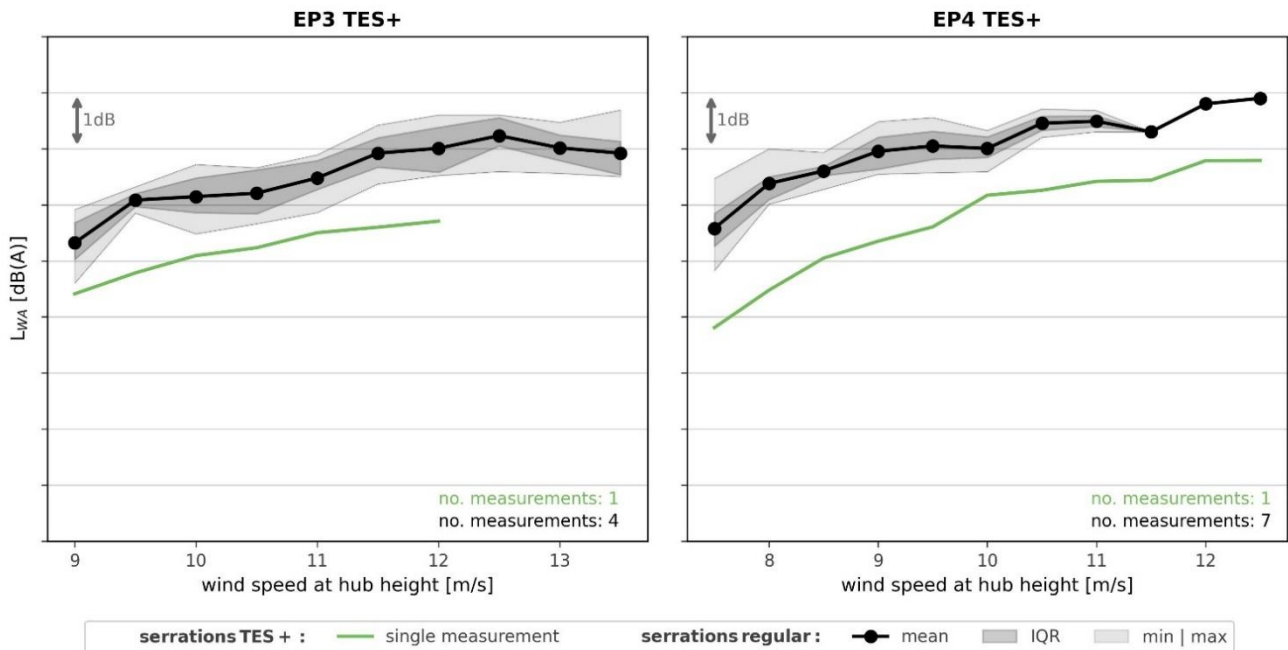


Figure 19: Overall sound power level comparison standard serration TES with enhanced TES+ measurements. For EP4 case, measurements are all on same turbine.

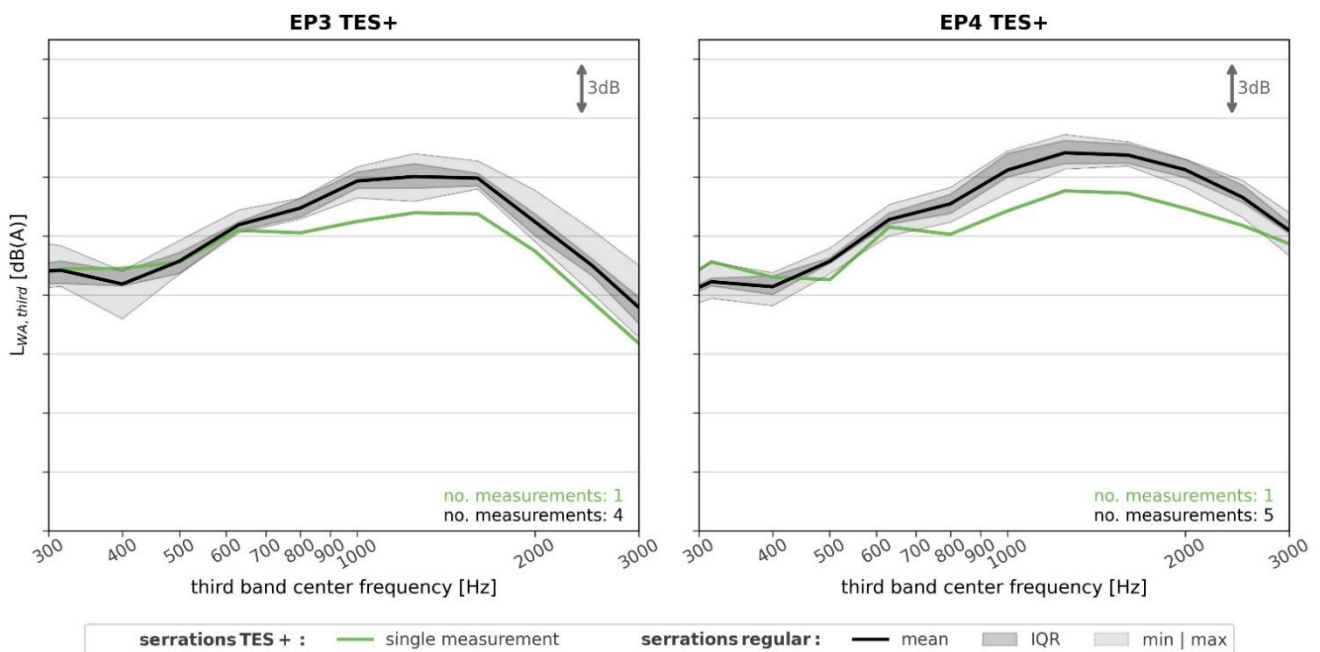


Figure 20: Sound power level as third octave comparison around loudest wind bin for standard TES vs enhanced TES+ serrations. For EP4 case, measurements are all on same turbine.

4. Conclusions

A robust trailing-edge serration design method consistent to the blade local flow condition, has been developed and validated based on the acoustics wind tunnel as well as full scale turbine field test data. The noise reduction potential of standard trailing-edge serrations (TES) across varying turbine types, site/atmospheric conditions, operation modes, attachment methods, etc., has been evaluated based on measurement data statistics. A clear variation of noise reduction of approx. 2 to 3 dB in OASPL near the rated power wind speed has been observed with the standard TES. However, the optimized serration (TES+) design which takes the detailed flow physics into account shows additional noise reduction compared to the standard TES. This confirms the robustness of the enhanced serration design methodology leading to more than 3 dB noise reduction without any power/annual energy production (AEP) loss. This also demonstrates that trailing edge serrations are an effective way of reducing noise of modern pitch regulated wind turbines. However, serration dimension, teeth shape, flow angle, blade angle, attachment method, material type, thickness etc. are the most critical design parameters to achieve the best performance. Importantly, the design geometry should be consistent with the local turbulent flow characteristics near the blade trailing-edge. High-fidelity CFD methods provide important input data for the design, such as the boundary layer state near the trailing edge of the blade. In addition, the simulations facilitate optimal implementation of the serration by eliminating unwanted interference effects that could locally disrupt the flow around the blade trailing edge. The enhanced serration design methodology has been successfully applied for the ongoing and future Enercon blade technologies to deliver low noise turbines for the noise sensitive markets.

References

- [1] M. S. Howe, *Acoustics of Fluid-Structure Interactions*, Online ISBN: 9780511662898, Hardback ISBN: 9780521633208, Paperback ISBN: 9780521054287 ed., Cambridge University Press, 1998.
- [2] K. A. Braun, R. A. Gordner, N. J. C. M. v. Borg, A. G. M. Dassen, P. Parchen and F. Doorenspleet, "Serrated Trailing Edge Noise (STENO)," in *Report No. JOR3-CT95-0073, THE EUROPEAN COMMISSION. Also in Proceedings of the European Wind Energy Conference, James and James Science, London, Oct. 1999, pp. 180–183, 1999.*
- [3] J. G. Schepers, A. Curvers, S. Oerlemans, K. Braun, T. Lutz, A. Herrig, W. Wuerz, A. Mantesanz, L. Garcillán, M. Fischer, K. Koegler and T. Maeder, "SIROCCO: Silent rotors by acoustic optimisation," in *Second International Meeting on Wind Turbine Noise, Lyon, France. Also ECN report: ECN-M--07-064., 2007.*
- [4] S. Oerlemans, M. Fisher, T. Maeder and K. Koegler, "Reduction of Wind Turbine Noise using Optimized Airfoils and Trailing-Edge Serrations," *AIAA Journal*, vol. 47(6), 2009.
- [5] M. Gruber, P. F. Joseph and M. Azarpeyvand, "Airfoil trailing edge noise reduction by the introduction of sawtooth and slitted trailing edge geometries," in *Proceedings of 20th International Congress on Acoustics, ICA 2010, Sydney, Australia, 23-27 August 2010.*
- [6] A. C. Arce-León, "Modelling of Serrated Trailing Edges to Reduce Aerodynamic Noise in Wind Turbines Using Computational Fluid Dynamics," MSc. Thesis, Uppsala University., 2010.
- [7] S. Oerlemans, "Reduction of wind turbine noise using blade trailing edge devices," in *AIAA 2016-3018, 22nd AIAA/CEAS Aeroacoustics Conference, 30 May - 1 June, Lyon, France, 2016.*
- [8] M. Kamruzzaman, J. Hurault and K. D. Madsen, "Wind Turbine Rotor Noise Prediction & Reduction for Low Noise Rotor Design," in *7th International Conference on Wind Turbine Noise, Rotterdam – 2nd to 5th May, 2017.*
- [9] VESTAS, <https://www.vestas.com/en/energy-solutions/onshore-wind-turbines>, Aarhus, Denmark.
- [10] ENERCON, "<https://www.enercon.de/en/wind-turbines/product-portfolio>," Aurich, Germany.
- [11] Siemens-Gamesa, "<https://www.siemensgamesa.com/global/en/home/products-and-services/onshore.html>," Brande, Denmark.

- [12] A. Fischer, O. Lylloff, C. Bak, A. S. Olsen, F. Bertagnolio, S. Luesutthiviboon, T. L. Pereira, D. Ragni, F. Avallone, D. Cassalino, M. Herr and C. A. a. J. M. Pereira-Gomes, “IEA Task 39: Wind tunnel serration benchmark,” IEA Task 29, 2021.
- [13] A. Celik, Y. Mayer and M. Azarpeyvand, “On the aeroacoustic characterization of a robust trailing-edge serration,” *Physics of Fluids*, vol. 33, no. 7, p. p. 075120, 2021.
- [14] J. Mathew, A. Singh, C. A. León and J. Madsen, “Serration Design Methodology for Wind Turbine Noise,” in *Journal of Physics: Conference Series 753 (2016) 022019, TORQUE*, Munich, Germany, 2016.
- [15] S. Luesutthiviboon, L. T. L. Pereira, D. Ragni and F. A. & M. Snellen, “Aeroacoustic Benchmarking of Trailing-Edge Noise from NACA 633 –018 Airfoil with Trailing-Edge Serrations,” *AIAA Journal*, vol. 61, no. 1, pp. pp. 2329-354, 2023.
- [16] M. Herr, Trailing-Edge Noise Reduction Concepts and Scaling Laws, Dissertation, Technical University Braunschweig, Germany, DLR report 2013-32, 2013.
- [17] T. P. Chong, A. Vathylakis and E. Dubois, “Aeroacoustic and flow assessments of the poro-serrated trailing edges,” in *22nd AIAA/CEAS Aeroacoustic Conference*, Lyon, France, June, 2016.
- [18] S. M. Hasheminejad, T. P. Chong and P. J. a. G. Lacagnina, “Airfoil self-noise reduction using fractal-serrated trailing edge,” in *24th AIAA/CEAS Aeroacoustics Conference, AIAA 2018-3132*, Atlanta, USA, 2018.
- [19] P. C. Woodhead, T. P. Chong, P. F. Joseph and J. G. Wissink, “On the Double-Rooted Trailing Edge Serration,” in *25th AIAA/CEAS Aeroacoustics Conference, AIAA-2019-2436*, Delft, The Netherlands, 20-23 May 2019.
- [20] BioME, “<https://www.biomerenewables.com/featheredge>”.
- [21] W. W. T. Systems, “<https://www.wts-online.eu/>”.
- [22] MuteSkin, “<https://muteskin.eu/#section-technology>”.
- [23] M. Kamruzzaman, Study of Turbulence Anisotropy and Its Impact on Flow Induced Noise Emission, Stuttgart: ISBN 978-3-8439-0490-2, Dr. Hut Verlag, Dissertation, University of Stuttgart, 2011.
- [24] M. Herr, R. Ewert, B. Faßmann, C. Rautmann, S. Martens and C.-H. R. a. A. Suryadi, “Noise Reduction Technologies for Wind Turbines,” in *Notes on Numerical Fluid Mechanics and Multidisciplinary Design*, Vol. 136, New Results in Numerical and Experimental Fluid Mechanics XI, Springer International Publishing AG, 2018.
- [25] M. Choudhari, C. Bahr, M. Khorrami, D. Lockard, L. Lopes, N. Zawodny, M. Herr, P. Pollenske, M. Kamruzzaman, T. v. d. Ven, E. Manoha, S. Redonnet, K. Yamamoto, T. Imamura and T. Ikeda, “Simulations & Measurements of Airframe Noise: A BANC Workshops Perspective.,” Proceedings of NATO STO-MP-AVT-246 Specialists Meeting on Progress and Challenges in Validation Testing for Computational Fluid Dynamics, Avila, Spain, September 26–28, 2016.
- [26] T. F. Brooks and T. H. Hodgson, “Trailing edge noise prediction from measured surface pressures,” *Journal of Sound and Vibration*, vol. 78(1), no. 69, p. 117, 1981.
- [27] A. Herrig, M. Kamruzzaman, W. Würz and S. Wagner, “Broadband Airfoil Trailing-edge Noise Prediction from Measured Surface Pressures and Spanwise Length Scales,” *Int. Journal of Aeroacoustics*, vol. 12, no. 1, pp. 53-82, 2013.
- [28] N. Kroll, C. C. Rossow, K. Becker and F. Thiele, “The MEGAFLOW project,” *Aerospace Science and Technology*, vol. 4, pp. 223-237, 2000.
- [29] L. Klein, J. Gude, F. Wenz, T. Lutz and E. Krämer, “Klein, L., Gude, J., Wenz, F., Lutz, T., & Krämer, E. (2018). Advanced computational fluid dynamics (CFD)–multi-body simulation (MBS) coupling to assess low-frequency emissions from wind turbines,” *Wind energy science*, vol. 3, pp. 713-728, 2018.

- [30] P. Weihing, J. Letzgus, G. Bangga, T. Lutz and E. Krämer, “Hybrid RANS/LES capabilities of the flow solver FLOWer—Application to flow around wind turbines,” in *Symposium on hybrid RANS-LES methods*, Strasbourg, 2016.
- [31] P. Weihing, M. Cormier, T. Lutz and E. Krämer, “The near-wake development of a wind turbine operating in stalled conditions – Part 1: Assessment of numerical models,” *Wind energy science*, pp. 933-962, 2024.
- [32] F. Menter, “Two-equation eddy-viscosity turbulence models for engineering applications,” *AIAA Journal*, 1994.
- [33] T. Rung, U. Bunge, M. Schatz and F. Thiele, “Restatement of the Spalart-Allmaras eddy-viscosity model in strain-adaptive formulation,” *AIAA Journal*, 2003.
- [34] M. Drela and M. Giles, “Viscous-inviscid analysis of transonic and low Reynolds number airfoils,” *AIAA Journal*, 1987.
- [35] P. C. Woodhead, T. P. Chong, P. F. Joseph and A. Vathylakis, “Aerofoil self-noise radiations subjected to serration flap angles,” *Experiments in Fluids*, vol. 62, 2021.
- [36] C. A. León, R. Merino-Martinez, D. Ragni, F. Avallone, F. Scarano, S. Pröbsting, M. Snellen, D. Simons and J. Madsen, “Effect of trailing edge serration-flow misalignment on airfoil noise emissions,” *Journal of Sound and Vibration*, vol. 405, pp. 19-33, 2017.
- [37] M. Kamruzzaman, D. Bekiropoulos, T. Lutz, W. Wuerz and E. Kraemer, “A Semi-empirical Surface Pressure Spectrum Model for Airfoil Trailing-edge Noise Prediction,” *Int. Journal of Aeroacoustics*, vol. 14, no. 5-6, pp. 833-882, 2015.

Paper #11 - ID: 345

Title: How do Residents Experience Wind Turbine Noise? The Results of a Two-Year Study

Author: Erik Koppen

11th Edition of the
International Conferences on
Wind Turbine Noise
Copenhagen, Denmark – 10th to 13th June 2025

How do Residents Experience Wind Turbine Noise? The Results of a Two-Year Study

Erik Koppen¹, Madelon Ekelschot-Smink and Jaap Boon

Arcadis Nederland BV, Arnhem, Gelderland, 6814 CM, The Netherlands

Summary

Noise from wind turbines is often a significant concern for nearby residents. To better understand the actual impact of wind turbine noise, an interactive app was utilized across several wind projects, allowing residents to easily report their real-time experiences with turbine noise.

One such project involves 26 wind turbines in the Netherlands, grouped into three geographically separated clusters, spread over a 26-kilometre stretch along a busy motorway. For two years, starting from the turbines' initial operation, residents could report noise-related annoyance on a 7-point scale at any time, day or night. For this project, high annoyance - defined as the top two levels on a 7-point annoyance scale - was most frequently reported during wind speeds of 8 to 13 m/s at hub height, at distances of less than 1,000 metres from the turbines, and when the wind blew towards the motorway, reducing background noise and making the turbines more noticeable. Also, high annoyance was most frequently reported during the late evening and at the start and end of the night, highlighting the influence of quieter periods on perceived annoyance.

The annoyance patterns observed for the 26-turbine project were compared with data from other wind farms where the app was implemented, offering a broader perspective. This comparison revealed significant variability in annoyance patterns across different wind farms. Although no clear seasonal trend was identified, over two years, four out of six wind farms using the interactive app showed above-average high annoyance levels in April, August, and September. The lack of a seasonal trend underscores the complexity of annoyance, which is shaped by factors such as weather, environmental conditions, and turbine operations rather than predictable seasonal patterns. These factors vary per location, emphasizing the importance of site-specific analysis.

Daily annoyance patterns were more consistent across wind farms than monthly patterns. Most wind farms showed peaks in high annoyance levels between 9 p.m. and 1 a.m., as well as between 7 a.m. and 8 a.m., corresponding to the end of the evening and the start and end of the night. While some reports submitted at the end of the night may reflect delayed responses to earlier annoyance, the findings suggest that annoyance intensifies during quieter periods when background noise is reduced.

Overall, the results highlight the importance of accounting for time-dependent factors and local environmental conditions when developing noise mitigation strategies for wind farms. Understanding the interaction between turbine noise, background noise, and specific conditions is crucial to minimize annoyance for nearby residents.

¹ Corresponding author – Email: erik.koppen@arcadis.com

1. Introduction

Noise from wind turbines is often a significant concern for nearby residents. Residents feel uncertain about what to expect and worry about the potential impact on their living environment. Involving residents in the siting process and maintaining clear communication from developers and authorities can help provide clarity and alleviate some of these concerns [1] [2]. However, the day-to-day effects of wind turbine noise remain uncertain, as they are heavily influenced by changing weather conditions. Adding to the concerns is that noise issues of operating wind farms are not always adequately addressed. The variability in both the level and character of wind turbine noise, driven by atmospheric conditions, can make it difficult for operators to fully recognize and address these concerns.

An interactive app has been developed to address both acoustic and non-acoustic factors influencing how people experience wind turbine noise [3]. This app provides residents near wind turbines a hyper-local 48-hour forecast of wind turbine noise and shadow flicker. It also estimates the perceptibility of wind turbine noise, factoring in masking effects from ambient noise like traffic or rustling leaves. Next to these forecasts, the app provides a local weather forecast, wind force and wind direction at hub height, energy production estimates, historical production data, avoided CO₂ emissions, and news updates about the wind farm and related developments. By providing transparency into wind turbine operations, the app builds trust, enhances social acceptance and strengthens the relation between residents and developers.

The app also enables residents to anonymously report, 24/7, how they experience the sound (on a 7-point scale) and shadow flicker (on a 5-point scale) of the wind turbines. This feature provides a sense of control and helps reduce irritation. With user consent, the feedback is linked to location, date and time, forecast data, weather conditions, and turbine conditions, enabling detailed analysis. Resident feedback is essential for monitoring the actual impact of the wind turbines and provides valuable insights into how weather, environmental factors, and turbine conditions affect that impact. This deeper understanding supports the development of more effective noise management strategies and communication efforts. In addition to addressing non-acoustic factors such as transparency and providing a sense of control, the app also addresses acoustic factors by continuously monitoring and optimizing the effectiveness of mitigation measures.

The noise forecast app has been applied in a variety of projects. For several projects already for over two years. For some projects detailed results may not be shared in this stage. This paper focuses on one specific project, Energie A16, where the results have already been made public. This project involves 26 wind turbines grouped into three geographically separated clusters, spanning a 26-kilometre stretch along a busy motorway. Over a two-year period, starting from the turbines' initial operation, residents were given the opportunity to report annoyance by noise on a 7-point scale at any time, day or night. They could also report annoyance by shadow flicker on a 5-point scale. Additionally, this paper briefly revisits another case study for which interim results were previously presented by Koppen et al. [3], providing a summary of findings over an extended period. The patterns in annoyance levels for the Energie A16 project are also compared with findings from other wind farms where the app has been applied, providing a broader context for understanding these trends.

2. Energie A16 wind project - A two-year study

2.1 The Project

The Energie A16 project is a collaborative initiative aimed at generating clean energy along the A16 motorway in West-Brabant, in the Netherlands. The project involves 26 wind turbines situated between the Moerdijk Bridge and the Belgian border, organized into three geographically separated clusters. A total of eight developers have contributed to the initiative [4]. The turbines include seven Nordex N149-4.5 MW, eleven Nordex N149-5.7 MW, and eight Vestas V150-4.3 MW models, all with a hub height of 135 metres. An overview of the turbine locations and the surrounding environment is shown in Figure 1.

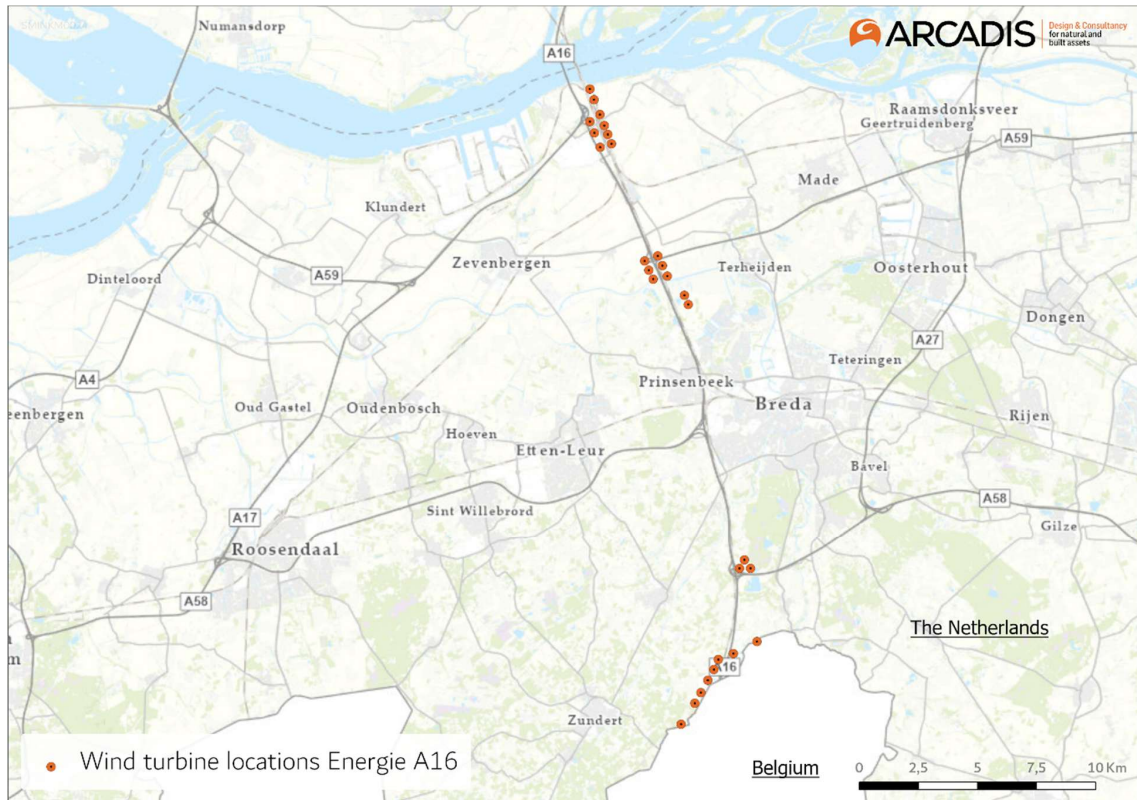


Figure 1 Overview of turbines and surrounding environment Energie A16 project.

The project aims to accelerate the energy transition by leveraging wind energy and fostering community engagement. Key aspects of the project include:

- Community involvement: Residents, organizations, developers, and governments work together to produce sustainable energy.
- Investment in local projects: A quarter of the revenue from the wind turbines is reinvested in local energy projects focused on energy saving and clean energy production.
- Support for residents: Special arrangements are made for residents living near the wind turbines, including access to tools like the interactive noise forecast app.

When, in 2016, initial discussions about the project began, many residents were already experiencing noise pollution from the nearby high-speed rail and the A16 motorway. This led to concerns about additional noise from wind turbines. The project team decided to assess the cumulative noise impact, combining expected wind turbine noise with existing noise sources, to provide a clearer picture of overall noise levels. As the wind farm plans became more detailed, noise concerns dominated discussions during public meetings and consultations with residents. Noise was a decisive factor in finalizing the plan. Residents insisted on noise monitoring once the turbines were operational, rather than relying solely on theoretical models. This commitment was made by the project team. The Environmental Service of Central and West Brabant conducted baseline measurements at 10 locations and conducted new noise measurements after the turbines started operations [5]. The post-construction measurements have not been published yet.

Besides noise measurements the province Noord-Brabant decided to apply the noise forecast app to enhance transparency and to monitor the actual impact of the turbines on the residents. The app enables residents to easily share how they experience the sound and shadow flicker of the turbines. The feedback from the residents, combined with the measurement data, provides a comprehensive understanding of the noise situation. The province committed to taking residents' concerns seriously and addressing possible issues.

2.2 Deployment area app and communication efforts

The app was made available to all residents within a radius of 2.1 km of the wind farm, which is ten times the tip height of the wind turbines. This encompassed approximately 6,900 residential addresses: 900 in the northern cluster, 5,000 in the middle cluster, and 1,000 in the southern cluster. Figure 2 illustrates the locations of the turbines and residential addresses.

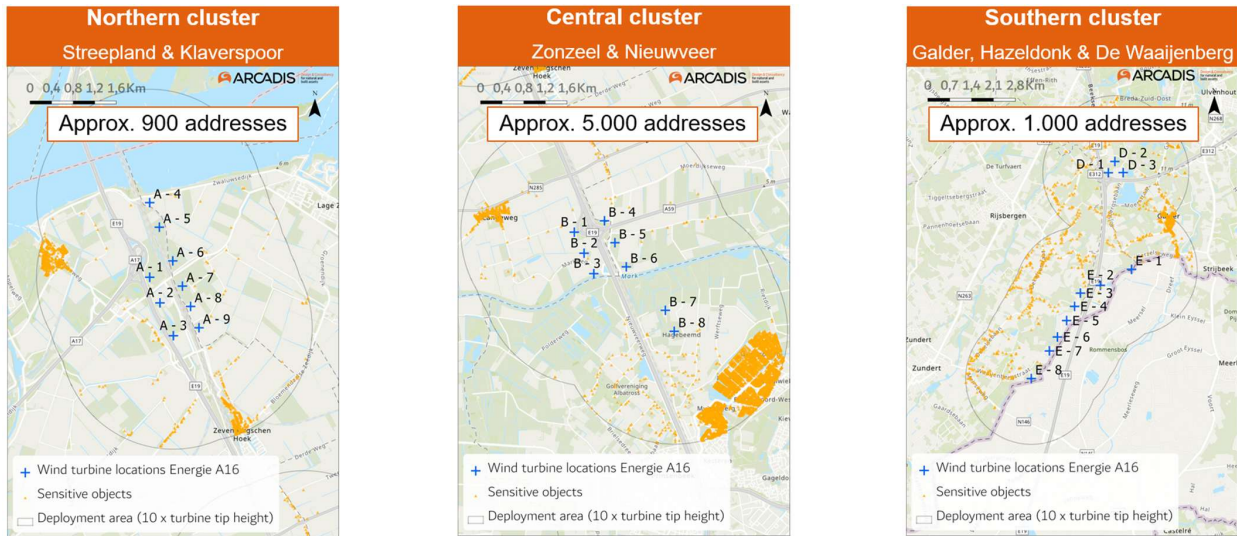


Figure 2 Deployment area noise forecast app Energie A16 project.

All residents received a letter informing them about the app and inviting them to a webinar. Additionally, information was disseminated through the Energie A16 website and a regional newspaper article. Resident feedback was regularly analysed. In 2023, results were shared through monthly reports with infographics. A sample excerpt, in Dutch, is shown in Figure 3. In 2024, an annual report for 2023 was initially published, followed by quarterly reports with infographics [6]. In 2025, a comprehensive report for 2024 was released. These reports were made available through news items in the app and on the Energie A16 website [7].



Figure 3 Sample excerpt from a monthly infographic report for residents in the Netherlands (written in Dutch). This excerpt describes the reported annoyance levels for noise and shadow flicker for May 2023, and shows how these annoyance levels vary with distance.

2.3 Users of the app and overview feedback locations

The app was launched in May 2022 to provide residents with updates on the construction activities of the wind turbines. Between May and December 2022, a total of 736 unique users accessed the app. The wind turbines became operational around January 2023. In 2023, the app had 723 unique users. In 2024, this number decreased to 305. Over the entire deployment period, the app was used by a total of 1,359 unique users. This represents 20% of the total residential addresses within a 2.1 km radius of the wind turbines². In 2023, when the turbines were operational, this percentage was 10%, and in 2024, it decreased to 4%. For comparison, in other wind farms where the app was deployed, this percentage ranges from approximately 10% to 30%. In general, when residents feel more annoyed, they use the app more frequently and the number of users increases.

The monthly number of unique users is illustrated in Figure 4, which highlights a peak of 385 users in March 2023 when a webinar on the app was held. Following this peak, user numbers gradually declined, eventually stabilizing at around 50 users per month during the second half of 2024.

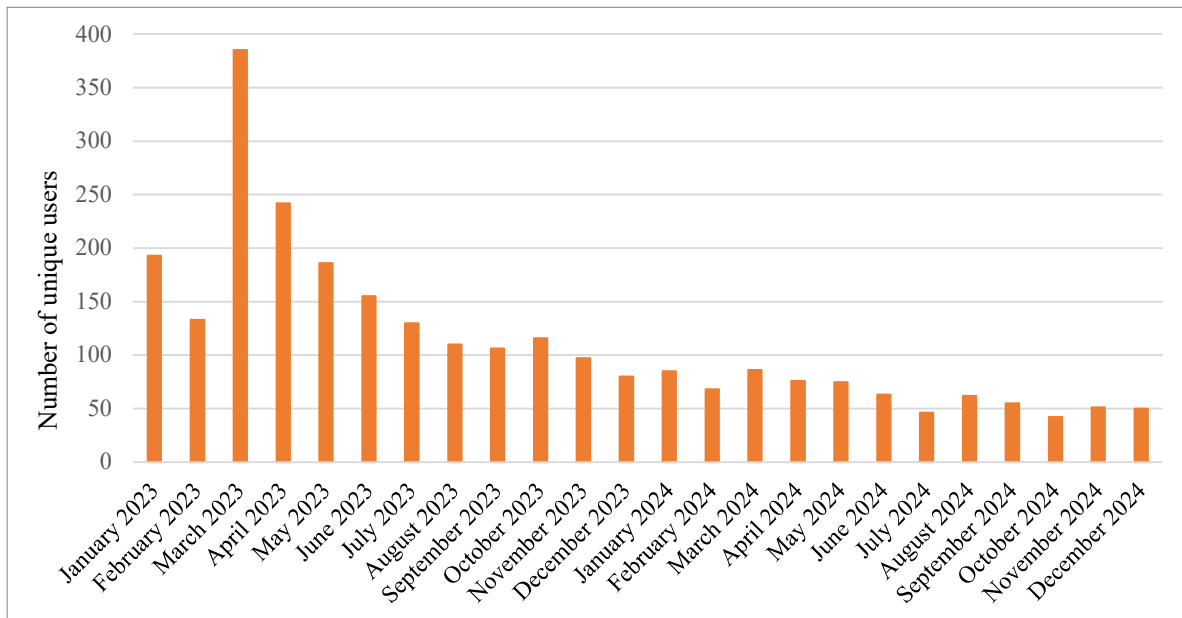


Figure 4 Monthly number of unique users Energie A16 project.

The users are quite evenly distributed across the settlements near the Energie A16 turbines, as shown in Figure 5. A significant portion of the users, 43%, reside in Breda. This is not surprising, as several residential neighbourhoods in northwest Breda fall within the influence area of the turbines located in the central cluster.

² The 2.1 km radius of the wind turbines is equivalent to ten times the turbine tip height and is considered the influential area of the wind turbines

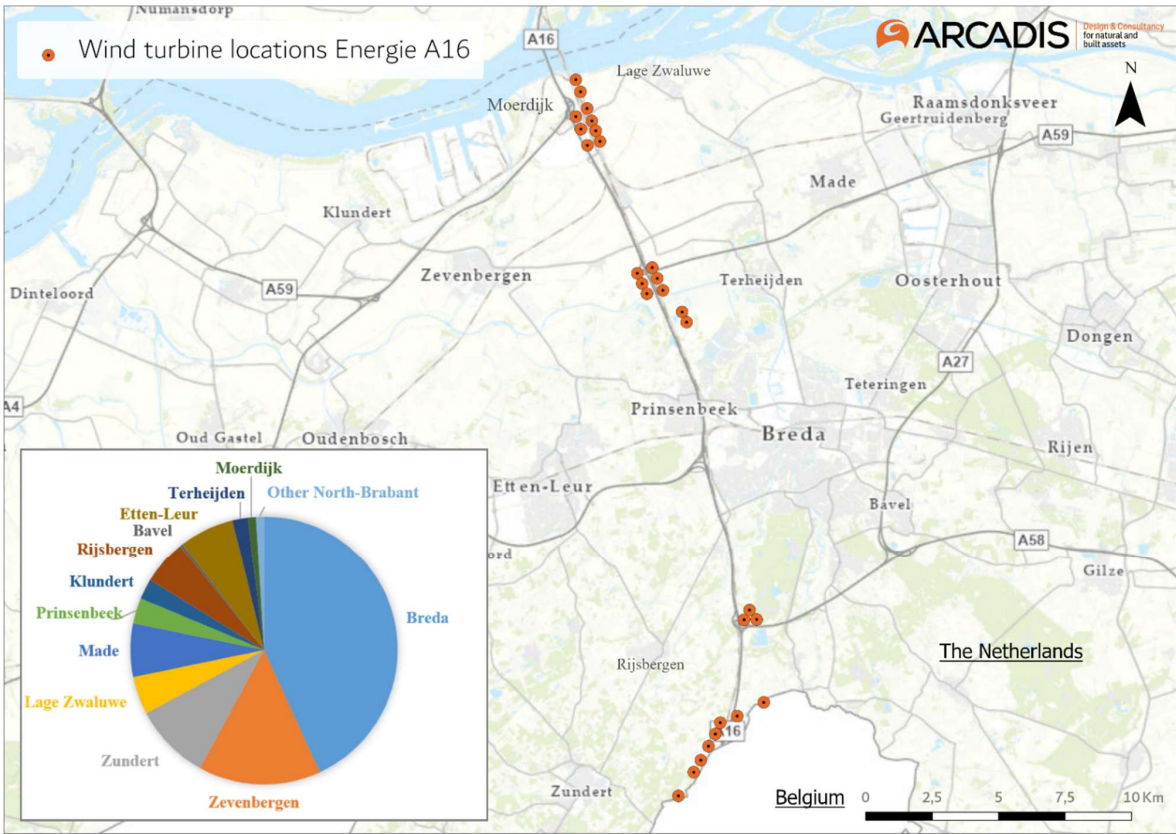


Figure 5 User distribution across various settlements near the Energie A16 turbines.

Figure 6 illustrates the distribution of residents who shared feedback on their experience with turbine noise, grouped by postal code. The visualization indicates that the residents providing feedback were evenly distributed across the area near the Energie A16 turbines.



Figure 6 Distribution of residents near the Energie A16 turbines who provided feedback on their experience with turbine noise, grouped by postal code. Larger circles represent a higher number of responses, while darker shades of red indicate more negative feedback.

2.4 How do the residents experience wind turbine noise?

2.4.1 Number of feedback responses and annoyance ratings

Figure 7 presents the number of feedback responses and annoyance ratings on a 7-point scale. Over a two-year period, residents from 53 distinct locations submitted a total of 460 feedback responses. This means that 0.8% of residences located within a 2.1 km radius³ have submitted feedback at least once. For the northern cluster, it was 1% (9 locations); for the central cluster, 0.5% (26 locations); and for the southern cluster, 1.8% (18 locations). For reference, for other wind projects where the app was used, this percentage ranged from approximately 2% to 20%. This suggests that, for the Energie A16 project, both the number of residents using the app and the number of residents providing feedback are relatively low compared to other wind projects, despite the extensive and frequent communication efforts regarding the wind project and the app.

Other wind projects have demonstrated a strong correlation between the frequency of app usage, the number of submissions, and the level of annoyance reported by residents. Typically, the more annoyed residents feel, the more actively they engage with the app. This trend is also observed in the Energie A16 project when analysing the number of residences that have submitted feedback at least once, categorized by their distance from the wind farm. Within the project area, 16.4% of the 55 residences located less than 500 metres from the wind farm provided feedback at least once. For the 196 residences situated between 500 and 1000 metres, this figure was 10.2%, while only 0.4% of the 6,694 residences located between 1 and 2.1 kilometres from the turbines submitted feedback. The feedback percentages for residences within 1000 metres of the wind turbines align more closely with results from other projects where the app was used. The relatively low rate of feedback submission overall can largely be attributed to the fact that 96.4% of all residences within a 2.1-kilometre radius are located at least 1000 metres away from the wind turbines.

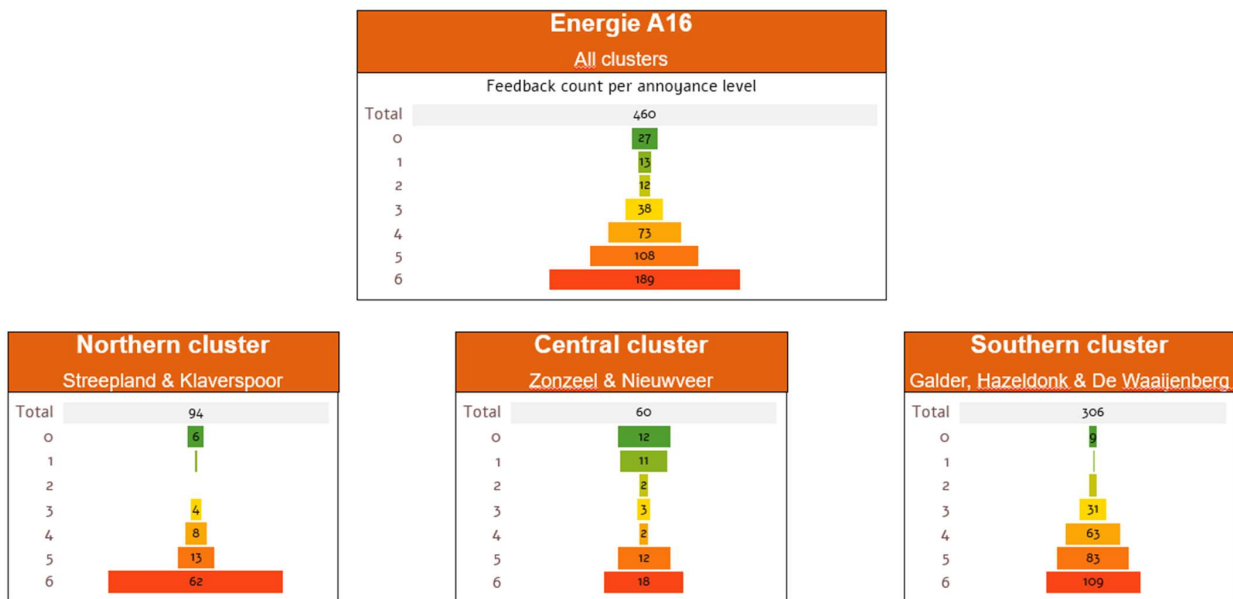


Figure 7 Number of feedback responses and annoyance ratings on a 7-point scale.

Among the feedback responses, high annoyance ratings - defined as the top two levels on a 7-point annoyance scale - were reported by residents from 31 distinct locations, while residents from 22 locations who did provide feedback never reported high annoyance. It is important to note that annoyed residents are generally more likely to provide feedback compared to those who are not annoyed, which is a typical

³ This radius, based on ten times the turbine tip height, reflects Dutch case law, which assumes that beyond this distance, no significant effects are anticipated.

human behaviour. Consequently, the 58.4% of app users reporting high annoyance cannot be considered representative of the percentage of residents within the turbines' influence area who experience high annoyance.

A more accurate estimate of the percentage of the population experiencing high annoyance can be derived from the proportion of residents who submitted high annoyance feedback at least once, compared to the total number of residential addresses within 2.1 km of the turbines. Overall, this percentage is 0.4% (31 out of 6,945 addresses). For specific turbine clusters, the percentages are as follows: 0.8% for the northern cluster, 0.2% for the central cluster, and 1.3% for the southern cluster. This indicates that the southern cluster had the highest number of annoyance reports, both in absolute terms and relative to the number of residents.

2.4.2 Monthly feedback responses and annoyance ratings

Figure 8 displays the monthly number of feedback responses and annoyance ratings on a 7-point scale for the Energie A16 project, with the blue line representing the number of distinct locations providing feedback. The figure demonstrates that the trend in the number of feedback submissions closely corresponds to the trend in the number of feedback locations. However, the figure highlights notable differences between the clusters.

For the northern cluster, the highest levels of annoyance were reported in April and June 2023, followed by a significant decrease, with a slight increase again in September and October 2024. In the central cluster, most annoyance was reported in April 2023, after which it declined steadily, with feedback ceasing entirely from September 2024 onward. In contrast, the southern cluster saw the highest levels of annoyance between July 2023 and January 2024, which later decreased, followed by an increase in April 2024 and again between August and October 2024.



Figure 8 Monthly number of feedback responses and annoyance ratings for the total Energie A16 project, the northern, central and southern clusters. The blue line indicates the number of distinct locations providing feedback.

2.4.3 Feedback responses and annoyance ratings by hour of the day

Figure 9 displays the number of feedback responses and annoyance ratings for the Energie A16 project by hour of the day, with the blue line representing the number of distinct locations providing feedback. This

figure shows that most annoyance was reported during the late evening and at the start and end of the night. The figure demonstrates that again the trend in the number of feedback submissions closely aligns with the trend in the number of feedback locations. As presented by Koppen et al. [3] in 2023, an analysis of feedback - taking into account factors such as time, location, distance from turbines, forecasted sound levels, turbine Scada data, and field sound measurements - suggests that residents generally provide honest responses. There is no evidence of intentional negative manipulation significantly affecting the overall results. Feedback generally appears logical, showing a clear correlation with input from other residents, identifiable trends, and comparisons with measured sound levels and the sound spectrum.

Figure 9 highlights notable differences between the clusters. In the northern cluster, the highest levels of annoyance were reported during the late evening and at the start of the night, with less prominent levels in the early morning. In the central cluster, most annoyance occurred during the evening and at the end of the night. Overall, annoyance was most frequently reported around the times when residents go to sleep or wake up. It must be noted that the annoyance reported at the end of the night might, in part, be attributed to delayed responses from residents who experienced annoyance during the night. In contrast, the southern cluster experienced the highest levels of annoyance between 7 a.m. and 12 p.m., with surprisingly lower levels of annoyance reported between midnight and 7 a.m.



Figure 9 Number of feedback responses and annoyance ratings for the total Energie A16 project, northern, central and southern clusters by hour of the day. Each time label represents the hour starting at the specified time.

2.4.4 Feedback responses and annoyance ratings by wind direction sector

The feedback from residents has also been categorized by wind direction sector. The left graph of Figure 10 displays the wind rose for the period between January 2023 and December 2024. The wind rose illustrates the percentage of time specific wind directions and wind speeds occurred. The graph shows that the prevailing wind direction is southwest. The right graph presents the feedback rose, which indicates the wind direction at the time feedback was submitted along with the corresponding annoyance rating. A comparison of these graphs shows that annoyance occurs relatively more frequently during northeastern to eastern wind directions.

Figure 11 presents the feedback rose for the northern, central, and southern clusters separately. The feedback rose for the northern cluster shows that most nuisance was reported for northeastern to eastern wind directions, while - for the same period - the prevailing wind direction was southwest. Figure 6 indicates that all feedback for this cluster was submitted by residents located east of the A16 motorway and south to west of the wind turbines. This indicates that most nuisance was experienced when the wind was blowing towards the A16 motorway and, to some extent, towards the wind turbines. This suggests that background noise plays an important role in how residents perceive the sound of the wind turbines. When the wind blows towards the A16 motorway, background noise levels are relatively low, and most annoyance is reported. Conversely, when the wind blows from the motorway towards the residents, background noise levels are relatively high, and fewer instances of nuisance are reported.

The feedback rose for the central cluster presents a more mixed picture. While most nuisance was reported for a south-southeastern wind direction, a relatively high level of nuisance was also reported for eastern to northeastern wind directions, though less prominently than in the northern cluster. Figure 6 shows that feedback was submitted by residents located both east and west of the A16 motorway, as well as from multiple sides of the wind turbines.

The feedback rose for the southern cluster shows that most nuisance was reported for southwestern wind directions and, to a much lesser extent, for northeastern wind directions, while the prevailing wind direction was southwest. Figure 6 indicates that most feedback was submitted by residents living west of the A16 motorway, though a substantial number of annoyance reports were also received from residents living east of the motorway. Most residents submitting feedback live west of the wind turbines, but also some live north of the turbines. Similar to the northern cluster, this suggests that most annoyance was experienced when the wind was blowing towards the A16 motorway and less when the wind was blowing from the motorway towards the residents. Once again, this highlights the role of background noise caused by the motorway in how residents perceive the sound of the wind turbines.

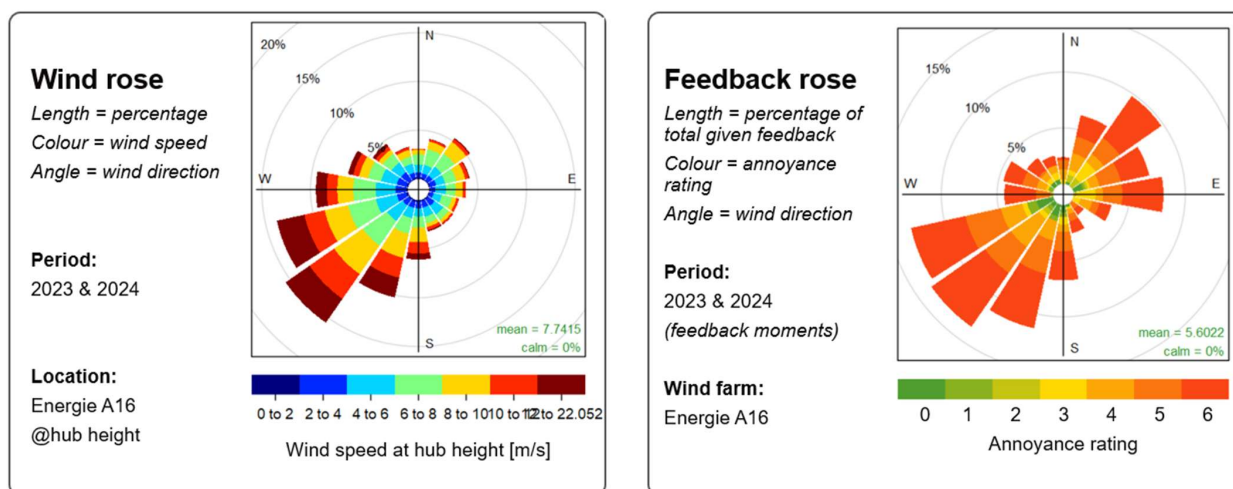


Figure 10 Wind rose for the 2023–2024 period (left graph) and the number of feedback responses and annoyance ratings for the Energie A16 project categorized by wind direction sector (right graph).

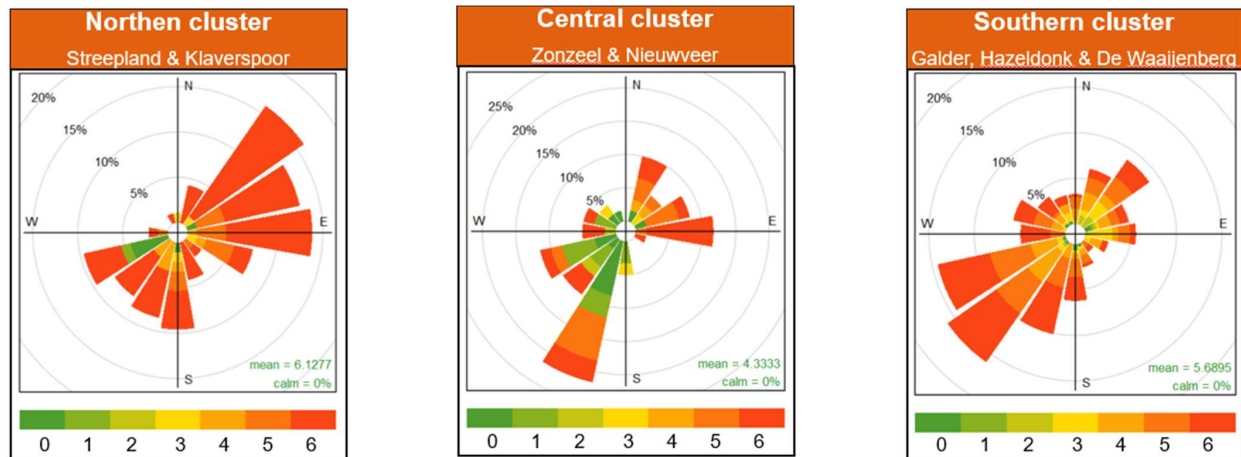


Figure 11 Number of feedback responses and annoyance ratings for the northern, central, and southern clusters categorized by wind direction sector.

2.4.5 Feedback responses and annoyance ratings by distance to the turbines

The feedback from residents has been grouped into three distance categories based on their proximity to the wind turbines. Figure 12 illustrates that for the northern cluster, residents living within 500 to 1000 meters of the wind farm most frequently reported high annoyance by the sound of the wind turbines. This feedback originated from two locations. For distances less than 500 metres or greater than 1000 metres, feedback was received from three and four locations respectively, but it was significantly less frequent compared to the 500 to 1000 metre distance category. In relation to the total number of residential addresses within the northern cluster, 11.5% of the 26 addresses located less than 500 metres from the wind farm reported high annoyance, 8.0% of the 25 addresses at a distance of 500 to 1000 metres, and 0.1% of the 864 addresses at a distance of 1 to 2.1 kilometres.

Similarly, Figure 12 shows that for the central cluster, the highest number of nuisance reports came from residents living 500 to 1000 metres away from the wind turbines, followed by those residing within 500 metres. Feedback for these distances was submitted from five and four locations respectively. When considering the proportion of residences at these distances from the wind farm, the percentage of residents reporting nuisance was highest among those living less than 500 metres away. Residents living more than 1000 metres from the wind farm submitted the most feedback overall. However, most of these reports indicated no or only slight levels of annoyance. In relation to the total number of residential addresses within the central cluster, 20.0% of the 20 addresses located less than 500 metres from the wind farm reported high annoyance, 4.2% of the 48 addresses at a distance of 500 to 1000 metres, and 0.1% of the 4,937 addresses at a distance of 1 to 2.1 kilometres.

For the southern cluster, most nuisance reports were submitted by residents living 500 to 1000 metres from the wind farms, originating from 13 different locations. Residents at a distance of less than 500 metres also reported nuisance frequently, with feedback coming from two locations. At distances greater than 1000 metres, nuisance reports were submitted by residents from three locations, but these reports were less frequent compared to those from residents living within 1000 metres of the wind farm. In relation to the total number of residential addresses within the southern cluster, 22.2% of the 9 addresses located less than 500 metres from the wind farm reported high annoyance, 9.8% of the 123 addresses at a distance of 500 to 1000 metres, and 0.2% of the 893 addresses at a distance of 1 to 2.1 kilometres.

Overall, the highest number of nuisance reports came from residents living 500 to 1000 metres away from the wind turbines. In relation to the total number of residential addresses within the Energie A16 project area, 16.4% of addresses situated less than 500 metres from the wind farm reported high levels of annoyance. This figure was 8.2% for addresses located 500 to 1000 metres away and 0.1% for those at a distance of 1 to 2.1 kilometres from the turbines.

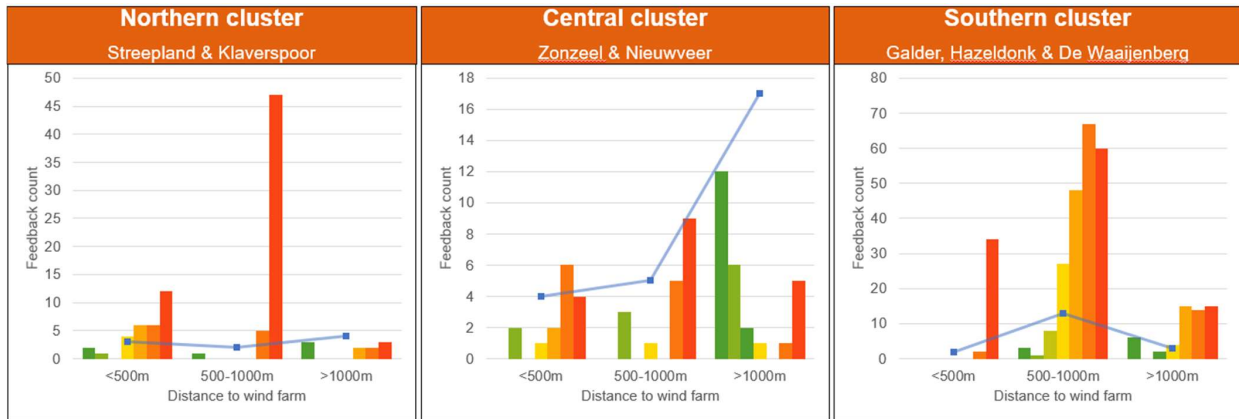


Figure 12 Number of feedback responses and annoyance ratings for the northern, central, and southern clusters as a function of the distance to the wind farm. The blue line indicates the number of distinct locations providing feedback.

2.4.6 Feedback responses and annoyance ratings by wind speed bins

Figure 13 presents the number of feedback responses and annoyance ratings categorized by wind speed bins. The dots represent the percentage of feedback received within specific wind speed bins, while the color of the dots reflects the average annoyance rating. Darker shades of red indicate more negative average annoyance ratings. The grey line in the graph represents the average wind speed distribution at hub height.

The data shows that relatively more nuisance is reported at higher wind speeds (greater than 8 m/s at hub height), while relatively less nuisance is reported at lower wind speeds (less than 8 m/s). This observation is consistent with expectations since the Vestas turbines of the Energie A16 project reach their maximum noise production at a wind speed of 9 m/s at hub height. The Nordex turbines reach their maximum noise production at 11 m/s, though at 9 m/s their noise output is only 1.1 to 1.6 dB(A) below maximum. From a wind speed of 13 m/s, the feedback distribution aligns more closely with the wind distribution. At these wind speeds, wind turbine noise will be partially masked by wind-induced background noise. A notable exception is observed in the results at a wind speed of 16.5 m/s.

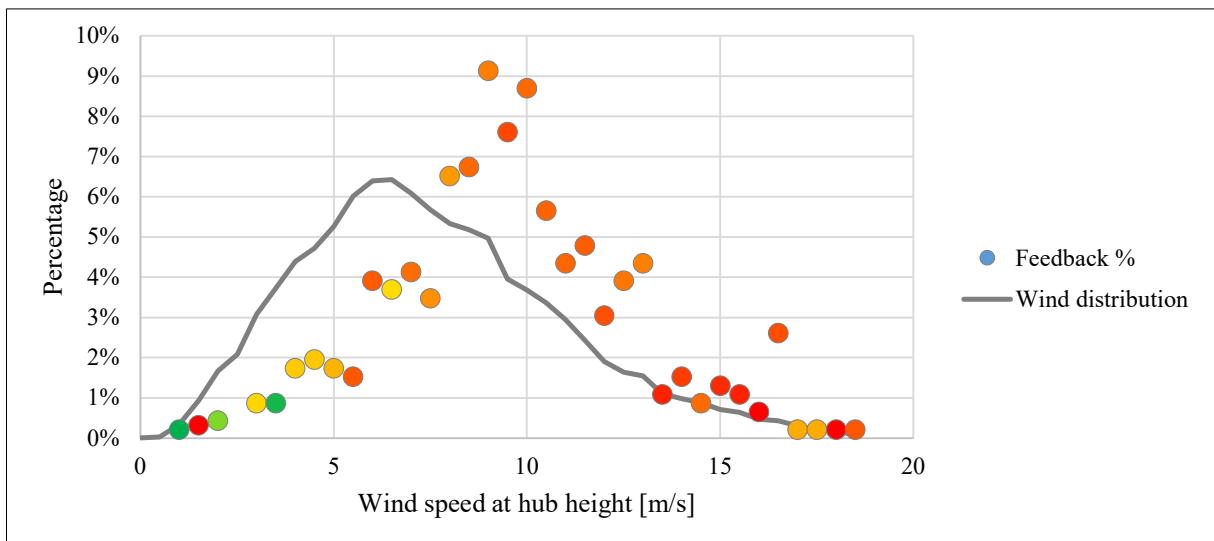


Figure 13 Number of feedback responses and annoyance ratings for the Energie A16 project categorized by wind speed class at hub height. The dots represent the percentage of feedback received within specific wind speed bins, while the colour of the dots reflects the average annoyance rating. The grey line represents the average wind speed distribution at hub height.

2.5 Characterizations of the wind turbine sound by residents

When submitting feedback about their experience with the sound of wind turbines, residents could also include comments describing their observations. A number of these comments refer to the aerodynamic noise emissions of the turbines and amplitude modulation.

Residents have described the sound of wind turbines using terms such as “loud whooshing sound,” “pulsating whooshing sound,” “rotating sound,” “thumping sound,” “scooping sound,” and “whoosh sound.” Other comments refer to sounds emitted by the drive train of the wind turbines, including descriptions like “low humming”, “buzzing sound”, “airplanes that seem to hover in the air”, and “intermittent humming sound.” These observations often point to low-frequency sounds, possibly with a tonal character.

Additional feedback compares the sound of wind turbines to background noise from the nearby motorway, with comments such as “almost no traffic and a rhythmic intermittent humming tone”, “distinct scooping sound because the motorway makes less noise”, and “a lot of noise during evening hours when there is less traffic on the A16”

Some residents also noted how wind turbine sound varies depending on wind direction and background noise, providing comments such as “audible indoors with an eastern wind, even though the house is east of the turbines”, “normally completely silent with eastern wind, but now sounds like a large fan”, and “more noise due to strong northeastern wind”.

These comments align with the findings described in Chapter 2.4.4. They demonstrate that background noise plays a significant role in how residents experience the sound of wind turbines. The comments related to wind direction are all from residents living east of the A16 motorway. It is unlikely that the reported annoyance is caused by higher wind turbine sound levels. Instead, it is more likely that residents are able to hear the wind turbines more clearly because the noise levels from the motorway are significantly reduced when the wind blows toward the motorway. The presence of the nearby motorway means that background noise near the residences is highly dependent on wind direction.

2.6 Conclusions Energie A16 wind project

This study provides valuable insights into the impact of wind turbine noise on nearby residents. Despite extensive and frequent communication efforts, the proportion of residents actively providing feedback about the wind turbines remains relatively low compared to other wind farm projects, with only 0.8% of addresses within a 2.1-kilometre radius submitting feedback. However, the results show that residents using the app for information and feedback are evenly distributed across settlements near the Energie A16 turbines. The relatively low rate of feedback submission is largely explained by the fact that 96.4% of all residences within a 2.1-kilometre radius are located at least 1000 metres from the wind turbines. When feedback is categorized by proximity to the turbines, clear patterns emerge. Within the project area, 16.4% of the 55 residences less than 500 metres from the wind farm submitted feedback at least once. Among 196 residences located 500 to 1000 metres away, the figure was 10.2%, while only 0.4% of the 6,694 residences between 1 and 2.1 kilometres submitted feedback. Feedback rates for residences within 1000 metres of the turbines are consistent with findings from other projects using the app.

High annoyance was reported by 0.4% of all residential addresses within 2.1 kilometres of the Energie A16 wind turbines. In general, residents are more inclined to provide feedback when they experience high levels of annoyance. While the overall number of affected residents is limited, certain conditions lead to severe annoyance for some, particularly those living close to the turbines or near the southern cluster of turbines. Within the Energie A16 project area, 16.4% of 55 residential addresses situated less than 500 metres from the wind farm reported high levels of annoyance at least once. This drops to 8.2% among 196 addresses located 500 to 1,000 metres away, and to 0.1% among 6,694 addresses situated 1 to 2.1 kilometres from the turbines. For addresses within 500 metres of the turbines, the percentage reporting high annoyance levels is nearly twice as high in the central and southern clusters compared to the northern cluster. The results suggest that background noise, primarily caused by the A16 motorway and heavily impacted by wind direction, plays a key role. The findings indicate that when the wind blows from the motorway toward nearby residences, the background noise often masks the sound of the wind turbines.

Over time, there was a noticeable decline in the number of reported annoyances for the northern and central clusters, but annoyance reports increased for the southern cluster. This suggests that annoyance levels are dynamic and influenced by factors such as weather conditions, environmental circumstances, and turbine operations.

The analysis highlights specific conditions under which severe annoyance is reported. The analysis indicates that the noise impact of the wind turbines is partially dependent on wind direction and the level of background noise. Most annoyance was reported:

- At the end of the evening, and the start and end of the night.
- During wind speeds between approximately 8 and 13 m/s at hub height.
- In the northern cluster during eastern and northeastern winds, and in the southern cluster during southwestern winds. In these instances, the wind blows toward the A16 motorway, reducing background noise and making the turbines more audible.
- At distances of less than 1,000 metres from the wind farm.

These findings underscore the importance of considering wind direction-dependent background noise when assessing the impact of wind turbine noise on nearby residents. While the number of reports remains limited overall, the feedback highlights specific circumstances under which annoyance is most likely to occur. This information provides valuable insights for improving future planning and implementing effective mitigation strategies.

3. Wind farm Oude Maas

In 2023, Koppen et al. [3] presented the results of applying the app to the Oude Maas wind farm in the Netherlands, using data collected until April 2023. Since then, the app has continued to monitor the impact of the wind turbines for nearly two more years. The results from the entire monitoring period are summarized below. Residents living near the Oude Maas wind farm in the Netherlands have been using the noise forecast app since March 2022. The wind farm, situated in an agricultural area along the Oude Maas river, consists of five Nordex N131-3.6 MW wind turbines with a hub height of 120 meters. The turbines became operational on July 12, 2022. Residents raised concerns about the noise impact of the turbines and requested noise measurements. In response, the municipalities of Barendrecht and Hoeksche Waard chose to use the interactive noise forecast app as an alternative method to monitor the turbines' impact.

The closest residences are 550 to 650 metres from the wind farm, with a total of 4,196 residences within a 2-kilometre radius. Residents were invited to use the app, and feedback was regularly analysed and shared. Koppen et al. [3] presented that from July 2022 to April 2023, the app had an average of 416 users per month, with 260 feedback responses regarding noise and 17 regarding shadow flicker. Most feedback indicated no annoyance. Since April 2023 the project continued to monitor and report results. The number of users gradually decreased until stabilizing at around 60 to 80 users from July 2024, two years after the wind turbines began operation. Between April 2023 and March 2025, a total of 142 feedback responses regarding noise were submitted from 28 distinct locations. High annoyance (nuisance levels 5 to 6) was reported 16 times (11%) from 4 distinct locations (14%). No annoyance (nuisance level 0) was reported 112 times (79%) from 16 distinct locations (57%). Between July 12, 2024, and March 2025, more than two and a half years after the turbines began operating, high annoyance was reported only three times by a single location.

Figure 14 illustrates the monthly number of feedback responses per nuisance level. Figure 15 shows the monthly number of unique locations that submitted feedback per nuisance level. In total, 402 feedback responses were submitted by 88 distinct locations. Of these, 290 responses (72%) indicated no annoyance, while 38 responses (9%) from 17 distinct locations (19%) indicated high annoyance (nuisance levels 5-6). Most of the negative feedback was received during the first five months of operation.

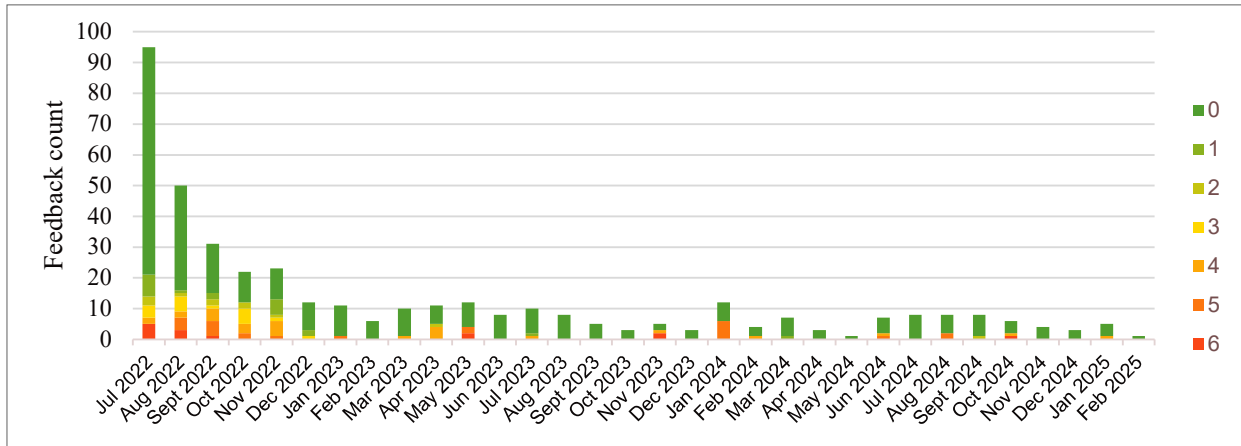


Figure 14 Number of feedback responses per nuisance level, per month.

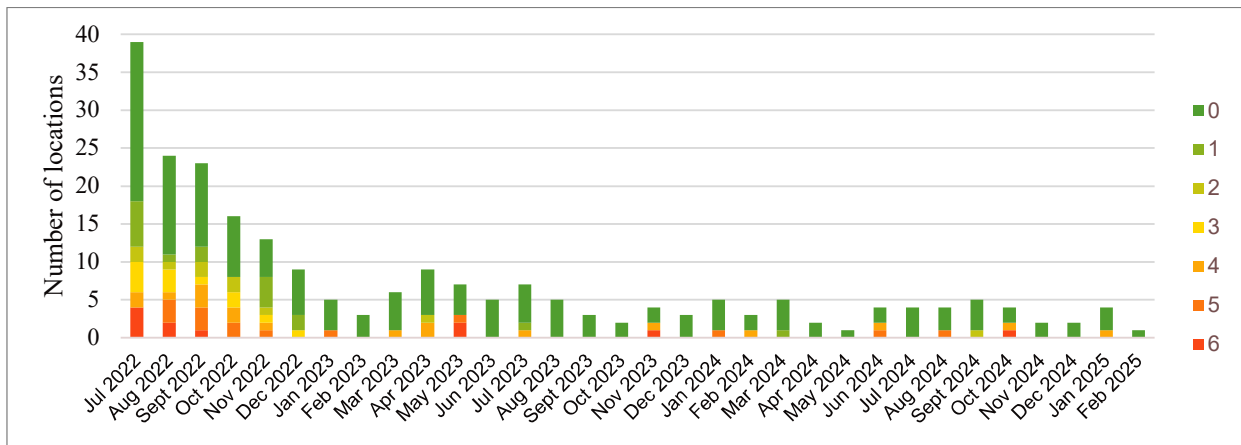


Figure 15 Number of locations submitting feedback per nuisance level, per month.

4. Pattern in annoyance levels compared to other projects

4.1 Monthly variation in high annoyance levels

The monthly number of feedback responses and annoyance ratings on a 7-point scale across the entire Energie A16 project and its three clusters - north (A), central (B), and south (C), - have been presented in chapter 2.4.2. Based on this data, the relative amounts of reported high annoyance levels by month over a two-year period were derived for these clusters. High annoyance levels are defined as the top two ratings on a 7-point annoyance scale. The results are presented in Figure 16. Additionally, a similar analysis was conducted for three other wind projects where the app was used for at least a two-year period. The results for these projects, labelled as D, E, and F, are also shown in Figure 16. While the analysis for these projects also covers exactly two years, the start and end dates of this period differ for two of the projects compared to the Energie A16 project.

Figure 16 shows that the pattern of high annoyance varies between wind farms. The data does not reveal a clear seasonal trend. However, it does show that, for four out of six wind farms, high annoyance levels are above average in April, August, and September. The absence of a seasonal trend is not surprising, as the underlying data reveal that the conditions leading to high annoyance are influenced by factors such as prevailing background noise, wind direction, and wind speed. The specific wind directions and wind speeds that lead to the highest levels of annoyance differ for each wind farm and location.

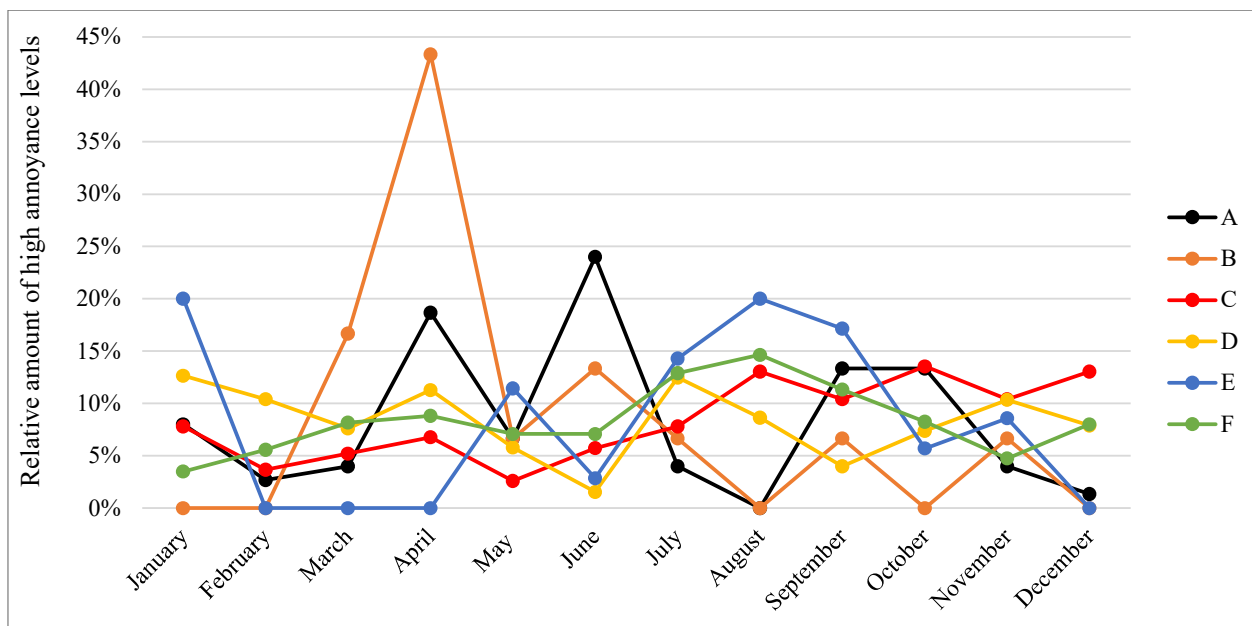


Figure 16 Relative amount of reported high annoyance levels by month for six wind projects over a two-year period, including clusters north (A), central (B) and south (C) of the Energie A16 project.

4.2 Variation in annoyance level by hour of the day

The number of feedback responses and annoyance ratings on a 7-point scale, categorized by hour of the day, across the entire Energie A16 project and its three clusters - north (A), central (B), and south (C), - have been presented in chapter 2.4.3. Based on this data, the relative amounts of reported high annoyance levels by hour of the day over a two-year period were derived for these clusters. The results are presented in Figure 17. A similar analysis was carried out for three other wind projects where the app was used for at least two years. The results for these projects, labelled as D, E, and F, are also shown in Figure 17. While the analysis for these projects also spans exactly two years, the start and end dates of this period differ for two of the projects compared to the Energie A16 project.

Figure 17 shows that most wind farms experience a peak in high annoyance levels between 9 p.m. and 1 a.m. and again between 7 a.m. and 8 a.m., corresponding to the end of the evening and around the start and end of the night. It should be noted, however, that some annoyance reports submitted at the end of the night may reflect delayed responses to annoyance experienced earlier during the night.

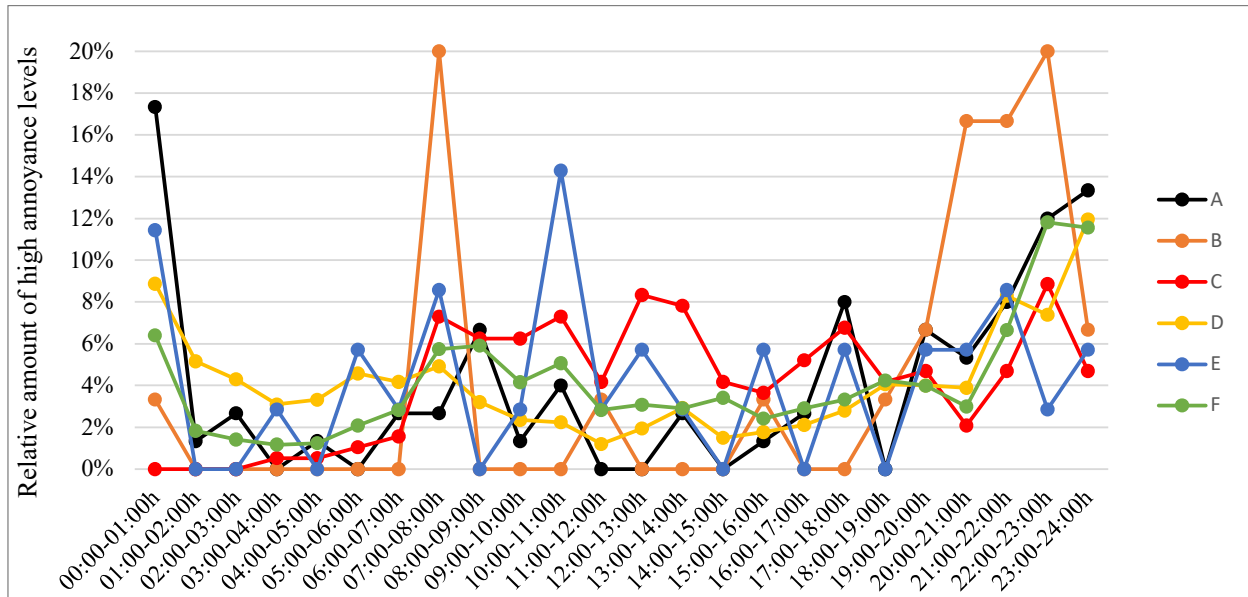


Figure 17 Relative amount of reported high annoyance levels by hour of the day for six wind projects over a two-year period, including clusters north (A), central (B) and south (C) of the Energie A16 project.

5. Conclusions

This study provides valuable insights into the impact of wind turbine noise on nearby residents, revealing significant variability in annoyance patterns across wind farms. While no clear seasonal trend is evident, two years of data show that for four out of six wind farms using the interactive app, high annoyance levels were above average in April, August, and September. The absence of a seasonal trend underscores the complexity of annoyance, which is influenced by factors such as weather, environmental conditions, and turbine operations, rather than predictable seasonal patterns. These factors vary across wind farms and locations, making site-specific analyses crucial.

For the Energie A16 project, the analysis highlights specific conditions under which annoyance is most likely to occur. High annoyance was most frequently reported during wind speeds of 8 to 13 m/s at hub height, at distances of less than 1,000 metres from the turbines, and during specific wind directions that reduce background noise (e.g. northeastern winds for the northern cluster and southwestern winds for the southern cluster). These findings emphasize the need to account for wind direction-dependent background noise when assessing the impact of wind turbine noise on nearby residents. Additionally, high annoyance levels were most frequently reported during the late evening and at the start and end of the night, further highlighting the influence of quieter periods on perceived annoyance. In relation to the number of residences near the wind turbines, high annoyance was most frequently reported by residents living within 500 metres of the wind turbines. Within this distance, the proportion of residents reporting high annoyance levels is nearly twice as high in the central and southern clusters compared to the northern cluster. The findings suggest that background noise from the A16 motorway, heavily influenced by wind direction, is a key contributing factor.

Daily annoyance patterns show greater consistency across wind farms than monthly patterns. Most wind farms using the interactive app exhibited peaks in high annoyance levels between 9 p.m. and 1 a.m. and again between 7 and 8 a.m., corresponding to the end of the evening and the start and end of the night. While some reports submitted at the end of the night may reflect delayed responses to annoyance experienced earlier, the findings suggest that annoyance is more pronounced during quieter periods when background noise is reduced.

The results stress the importance of considering *time-dependent factors* and *local environmental conditions* when designing and implementing noise mitigation strategies. The findings from this study offer valuable guidance for improving wind turbine planning and operations:

- Localized mitigation: Develop strategies tailored to site-specific conditions, such as adjusting operations during wind directions and speeds that heighten annoyance.
- Time-dependent noise curtailment: The peaks in annoyance during the late evening and the start and end of the night emphasize the importance of addressing quieter periods when turbine noise is more noticeable. In situations requiring noise curtailment, annoyance may be more effectively reduced by applying additional noise reduction at the start of the night, when residents are going to bed, rather than sustaining a lower level of noise reduction throughout the entire night.
- Long-term monitoring: Feedback patterns reveal that annoyance levels tend to stabilize over time as residents adapt to turbine operations. Long-term monitoring can help identify trends and inform mitigation measures that address persistent issues.
- Community engagement: Enhance communication and accessibility through tools like the interactive noise forecast app to gather meaningful feedback and improve interventions.

By addressing these perspectives, future wind turbine projects can better balance the need for sustainable energy production with the concerns of nearby residents, ensuring effective noise management and community satisfaction.

References

- [1] RIVM, Aarten Wind Solutions, ECN, GGD-GHOR Netherlands & EAE/RUG, “Kennisbericht Geluid van windturbines (Knowledge document wind turbine noise),” Pilot Kennisplatform Windenergie, 2015.
- [2] I. van Kamp and G. P. van den Berg, “Health effects related to wind turbine sound: an update,” RIVM report 2020-0150, 2020.
- [3] E. Koppen, M. Ekelschot-Smink and J. Boon, “Noise forecast app: positively impacting non-acoustic factors,” in *10th International Conference on Wind Turbine Noise*, Dublin, 2023.
- [4] Energie A16, “Energie A16,” [Online]. Available: <https://energiea16.nl/>. [Accessed 13 March 2025].
- [5] Energie A16, “Inlossen van een belofte: hoe zit het met het geluid van de windmolens?,” 16 November 2023. [Online]. Available: <https://energiea16.nl/inlossen-van-een-belofte-hoe-zit-het-met-het-geluid-van-de-windmolens/>. [Accessed 13 March 2025].
- [6] R. Diepenhorst, “Energie A16 in 2023: de belangrijkste conclusies van de Geluidsverwachting.nl app,” Energie Werkplaats Brabant, [Online]. Available: <https://www.energiwerkplaatsbrabant.nl/actualiteiten/nieuws+nieuwste/2741211.aspx?t=Energie-A16-in-2023-de-belangrijkste-conclusies-van-de-Geluidsverwachtingnl-app>. [Accessed 13 March 2025].
- [7] Energie A16, “Geluidsverwachting.nl app,” [Online]. Available: <https://energiea16.nl/app/>. [Accessed 14 March 2025].

Paper #12 - ID: 346

Title: Comparing Narrow-Band and 1/3-Octave Band Methods for Detecting Tonal Wind Turbine Noise

Author: Jaap Boon

11th Edition of the

International Conferences on Wind Turbine Noise

Copenhagen, Denmark – 10th to 13th June 2025

Comparing Narrowband and 1/3-Octave Band Methods for Detecting Tonal Wind Turbine Noise

Jaap Boon¹, Erik Koppen and Madelon Ekelschot-Smink
Arcadis Nederland BV, Arnhem, Gelderland, 6814 CM, The Netherlands

Summary

Residents living near wind turbines occasionally report annoyance by low-frequency tonal noise. To assess tonal characteristics, narrowband spectral measurements are critical for identifying tones and determining their audibility. These measurements require high-resolution data across both frequency and time intervals and an in-depth analysis. However, simplified survey methods are also commonly used to evaluate tonal audibility in wind turbine noise. Both the ISO 1996-2 and ANSI/ASA S12.9-2013/Part 3 standards outline methods that rely on 1/3-octave band sound level differences to assess tonality. While the standards do not specify exact level differences to use for tonal audibility assessments, they do provide a possible choice. Understanding the relationship between 1/3-octave band sound level differences and tones identified through narrowband spectral methods offers insights into the accuracy of the survey methods and the optimal level differences to be used.

This study compares tonal wind turbine noise detected using IEC 61400-11 and ISO TS 20065 narrowband analysis with the survey methods outlined in ISO 1996-2 and ANSI/ASA S12.9-2013/Part 3, which rely on 1/3-octave band spectra. The study found that ANSI/ASA S12.9-2013/Part 3 relates best with the tonal audibility as detected by the narrowband methods. The optimal threshold K_T for detecting audible tones ($\Delta L \geq 0$ dB) in the frequency range between 63 and 160 Hz was found to be approximately 4 dB(A). This approach is recommended when seeking an equally weighted balance between optimal recall and precision. If precision is prioritised over recall - ensuring that identified tones are accurate, even at the expense of missing tones - using a higher K_T , such as 6 dB(A), is recommended. For detecting prominent tones ($\Delta L \geq 5$ dB) $K_T = 8$ dB(A) would be more appropriate, or slightly higher, such as $K_T = 10$ dB(A), if precision is prioritized over recall. For measurement locations and frequencies where an ANSI/ASA level difference larger than 4 dB(A) occurs at least 20% of the time, it is reasonable to assume that audible tones might be detectable with a proper FFT-method (recall 76-97% and precision 52-91%). Precision was particularly low when most potential tones (based on ANSI/ASA) were near the threshold of 4 dB(A). Contrarily, when the energy average of all suspected tones² was at least 9 dB(A) and these suspected tones occurred more than 20% of the time, the likelihood of audible tone occurrence significantly (recall 93-97% and precision 87-91%).

While these results provide insight into the relationship between 1/3-octave band methods and proper FFT-methods on detecting tonality, it should be remarked that a 1/3-octave band method should only be used as a first indication of a potential tonal issue. Peaks observed in a 1/3-octave band spectrum are not exclusively indicative of tonal components; they may also arise from noise with a broader frequency span than tonal noise. Especially for peaks with lower average ANSI/ASA level differences one should be

¹ Corresponding author – Email: jaap.boon@arcadis.com

² Suspected tones: Occurrences when the ANSI/ASA level difference was larger than $K_T = 4$ dB(A).

cautious of assigning conclusions with regards to tonality before conducting tonality measurements with a proper narrowband method.

1. Introduction

Residents living near wind turbines occasionally report annoyance by low-frequency tonal noise [1]. To assess tonal characteristics, narrowband spectral measurements like those specified in the IEC 61400-11 [2] and the ISO TS 200065 [3] standards are critical for identifying tones and determining their audibility. These measurements require high-resolution data across both frequency and time intervals and an in-depth analysis. However, simplified survey methods are also commonly used to evaluate tonality for wind turbine noise. Both the ISO 1996-2 [4] and ANSI/ASA S12.9 [5] standards outline survey methods that rely on 1/3-octave band sound level differences to assess tonality. This approach is especially relevant since measurements at the source and at nearby residences are often conducted using 1/3-octave band spectra. While the standards do not specify exact level differences to use for tonal audibility assessments, they do provide a possible choice. Understanding the relationship between 1/3-octave band sound level differences and tones identified through narrowband spectral methods offers insights into the accuracy of the survey methods and the optimal level differences to be used.

This study compares tonal wind turbine noise detected using IEC 61400-11 and ISO TS 20065 narrowband analysis with the survey methods outlined in ISO 1996-2 and ANSI/ASA S12.9, which rely on 1/3-octave band spectra. For this analysis, simultaneous narrowband and 1/3-octave band measurements were conducted at three different locations near operating wind turbines. This paper builds upon previous papers, such as a previous study from Søndergaard and Bastasch [5], which concluded that 1/3-octave band methods may be effective, provided that the tone frequency is not near the boundary of the band.

2. Standards for assessing tonal sounds of wind turbines

2.1 Narrowband tonal audibility assessment – Engineering methods

The IEC 61400-11 standard [6] describes a narrow band method for analysing tones and their audibility in wind turbine noise emissions. Measurements must be conducted at a set distance³ from the wind turbines. The primary objective is to identify tonal noise components that could contribute to annoyance for nearby residents and evaluate their prominence relative to surrounding broadband noise. The analysis employs the Fast Fourier Transform (FFT) to convert the time-domain noise signal into a frequency-domain spectrum. A tone is considered present if its sound pressure level exceeds the average level of adjacent frequencies (masking noise) by at least 6 dB. The standard states that average tonal audibility must be reported if the tonal audibility is greater than or equal to -3.0 dB. However, tones are classified as "Not relevant tones" if they appear in fewer than 20% of at least 10 spectra with the same origin. If tones appear in more than 20% but fewer than 6 spectra, additional measurements are required. A tone is deemed audible if its tonal audibility exceeds 0 dB. The method requires measuring narrowband spectra using A-weighted energy average sound pressure levels over a 10-second period. A Hanning window with at least 50% overlap is applied during the analysis. The frequency resolution must be between 1 Hz and 2 Hz to ensure accurate identification of tonal components.

The second narrowband tonality assessment method that is used in this paper is the ISO TS 20065 standard [3]. The method is similar to IEC 61400-11 but is designed to address tonal noise in general, rather than being specific to wind turbines. There is also no set distance where the measurement has to be conducted, so it is also applicable for measurements near residents. A tone is considered present if its sound pressure level exceeds the average level of adjacent frequencies (masking noise) by at least 6 dB. The standard states that only if the audibility ΔL exceeds 0 dB a tone is present. When determining the energy average audibility for multiple timestamps, tones for all spectra where no tone is found must be assigned a value

³ For a horizontal axis wind turbine, the horizontal reference distance is equal to the hub height of the turbine plus the length of the blades

of $\Delta L = -10$ dB. The method is only applicable for frequencies starting from 50 Hz. The ISO TS 20065 method requires measuring narrowband spectra using A-weighted energy average sound pressure levels over 3-second time intervals. A Hanning window with at least 50% overlap is applied during the analysis. The frequency resolution must be between 1.9 Hz and 4 Hz to ensure accurate identification of tonal components.

2.2 1/3-Octave band tonal audibility assessment – Survey methods

The first 1/3-octave band survey method evaluated in this study is the approach described in Annex K of the ISO 1996-2:2017 standard [4]. This method provides a straightforward way of detecting prominent tones within a specific 1/3-octave band by calculating the difference between the equivalent sound pressure level of the target band and the highest equivalent sound pressure level of its two adjacent 1/3-octave bands. If the difference exceeds a specific constant threshold, it indicates the presence of a prominent tone. For the purpose of this paper this level difference is denoted as K_T , similar to the ANSI method described in the next paragraph. However, it is important to note that this K_T is not the same as the tonal adjustment K_T defined in Annex J of ISO 1996-2:2017. K_T may vary depending on frequency. Possible choices for the level difference presented in ISO 1996-2:2017 are:

- 15 dB for frequencies between 25 Hz and 125 Hz;
- 8 dB for frequencies between 160 Hz and 400 Hz;
- 5 dB for frequencies between 500 Hz and 10 kHz.

The ISO standard does not specify whether A-weighting should be applied, though it is likely this is intended as other assessments described in the ISO standard also incorporate A-weighting. Since it is not certain, the performance of this method is tested for both A-weighted as well as Z-weighted (linear) sound spectra.

The second 1/3-octave band survey method evaluated in this study is the approach described in Annex B of the ANSI/ASA S12.9-2013/Part 3 standard [5]. The ANSI/ASA method differs from the ISO method in that it uses the arithmetic average of the equivalent sound pressure levels of the two adjacent 1/3-octave bands, rather than the highest equivalent sound pressure level, for comparison with the 1/3-octave band in question. The suggested possible choices for K_T are identical to the ISO method. Again, it is not specified whether A-weighting should be applied. However, applying A-weighting only has a marginal effect on the calculated sound level differences, since the arithmetic difference balances out the effect of A-weighting on the adjacent 1/3-octave bands. For frequencies between 20 and 160 Hz, the effect of A-weighting causes a maximum difference in the ANSI/ASA level difference of 0.25 dB.

As a potential alternative to the ISO and ANSI/ASA methods, a third 1/3-octave band survey method was evaluated in this study. This method is similar to the ANSI/ASA approach, but instead of taking the arithmetic average of the two adjacent 1/3-octave bands, the arithmetic average of the *four* adjacent 1/3-octave bands is used. The reason that this method is also evaluated is twofold: Firstly, the narrow band methods take a critical bandwidth starting at roughly 100 Hz around the tone. In some cases, information within the critical bandwidth may extend beyond the immediately adjacent 1/3-octave bands and into the second adjacent bands. Secondly, tones might occur near the boundary of a 1/3-octave band. In that case, one of the adjacent bands might also have an elevated sound pressure level due to the presence of the tone. Therefore, using the arithmetic average of four adjacent frequency bands, rather than just two, could provide a more reliable result. In this paper, this last method will be referred to as ‘Alternative ANSI’.

3. Evaluating the accuracy of survey methods versus engineering methods for tonal noise assessment

3.1 Measurements

To evaluate the accuracy of 1/3-octave band survey methods for detecting tonal wind turbine sound, noise measurements were conducted near operational wind turbines in areas with relatively low background noise levels. Data were collected over 120 hours at three different locations, each with varying wind, weather and environmental conditions. At each location, measurements were performed using two type-1 sound level meters. At location 1 the two meters were placed next to each other. Due to practical constraints, the distance between the two meters at location 2 was 8 metres and at location 3 the distance was 40 metres. However, the distance to the turbines varied by less than 5%. The sound level meters were equipped with similar, though not identical, wind screens, and the measurement height was approximately 1.5 metres. One sound level meter performed continuous narrowband measurements with a frequency resolution of 1.25 Hz, while the other meter performed continuous 1/3-octave band measurements. Both meters also recorded the equivalent sound pressure level (LAeq), which is used as an indicator of the variability between the two meters. The sampling time was set to 10 seconds. However, because the meters could not align exactly at 10-second intervals, comparisons were made with resampled 10-minute data. This paper focuses on the analysis of low-frequency noise within the range of the 20 and 200 Hz 1/3-octave bands.

3.2 Determining optimal 1/3-octave threshold (K_T)

Survey methods based on 1/3-octave band data provide advantages in terms of time and cost when compared to engineering methods that rely on FFT data. Not all sound level meters are equipped with a module for FFT measurements. Moreover, FFT measurements require significantly more effort and complexity in data analysis compared to 1/3-octave band measurements. While survey methods offer clear benefits, they cannot fully replace engineering methods. Their value largely depends on the accuracy of the results compared to those obtained through engineering methods.

A survey method can serve as an initial indication of potential tonal noise issues. However, in critical situations, further investigation using an engineering method will be required. To optimize the effectiveness of a survey method, it is important to determine the optimal 1/3-octave band threshold for the level difference K_T , making it possible to predict whether an FFT-method would likely detect an audible tone ($\Delta L \geq 0$ dB) within the corresponding frequency range. For this study, an increment of 0.5 dB(A) was used whilst looking for the optimal thresholds, because smaller increment size would give a false sense of certainty. For finding the optimal threshold, the following confusion matrix classifications⁴ are defined:

True Positive (TP) = Number of times a tone was detected using the FFT-method, and a potential tone was indicated using a 1/3-octave band threshold.

False Positive (FP) = Number of times *no* tone was detected using the FFT-method, but a potential tone was indicated using a 1/3-octave band threshold.

False Negative (FN) = Number of times a tone was detected using the FFT-method, but *no* potential tone was indicated using a 1/3-octave band threshold.

True Negative (TN) = Number of times *no* tone was detected using the FFT-method, and *no* potential tone was indicated using a 1/3-octave band threshold.

An example of these classifications is provided in Figure 1.

⁴ A confusion matrix is a standard statistical tool.

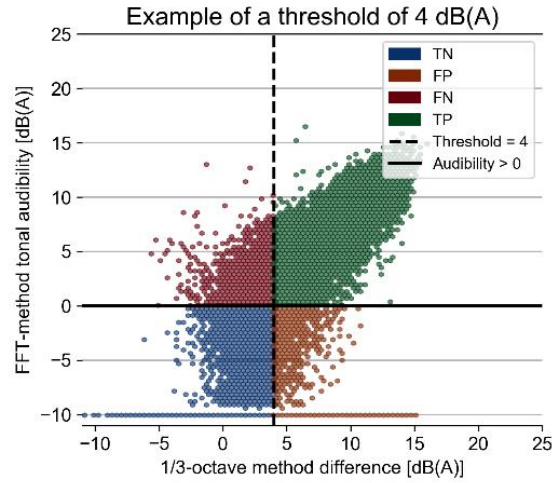


Figure 1 Example of separation of into TN/FP/FN/TP for a given threshold of 4 dB(A), as indicated by the black dashed vertical line. The audibility threshold is defined as 0 dB(A) by the FFT-standards. The data used for this example is not yet resampled to 10 minutes and thus shows a large number of outliers.

Using these classifications, the precision (minimize false tonality alarms, Eq. 1) and the recall (minimize failing to predict a tone, Eq. 2) of the threshold can be evaluated. For this paper, an evaluator called the F1-score [7] was chosen. The F1-score is a number between 0 (bad) and 1 (perfect) and it combines the precision and recall equally, as shown in Eq. 3. That means that we equally weight the importance of minimizing false alarms and minimizing failure to predict a tone. In case precision is deemed more important than recall the decibel threshold K_T would increase compared to the optimal threshold determined by the F1-score, and vice versa.

$$Precision = \frac{TP}{TP + FP} \quad 1$$

$$Recall = \frac{TP}{TP + FN} \quad 2$$

$$F1Score = 2 \times \frac{Precision \times Recall}{Precision + Recall} \quad 3$$

3.3 Comparing tones with 1/3-octave band differences

In deviation from the IEC 61400-11 standard, periods where tones occur more than 5% of the time were for the purpose of this paper also considered, in order to also determine correlations for time intervals where tones were less frequent, but with still enough samples. For the assessment according to the IEC 61400:11 method, the frequency resolution and sampling time of the narrowband dataset were set to 1.25 Hz and 10 seconds, respectively. For the analysis according to the ISO TS 20065 method the same resolution and sampling time were used. This deviates from the required frequency resolution of 1.9 to 4 Hz and the required sampling time of 3 seconds. Using a smaller frequency resolution than intended might lead to a larger number of detected tones with lower audibility, but the exact effect of this is not known. The larger sampling time should not have a large effect, since most of the tones that occur for wind turbine noise span longer time periods. ISO TS 20065 states that a *lower* sampling time than 3 seconds leads to unjustified audibility but does not state anything about longer sampling time. Furthermore, for ISO TS 20065, tones with an audibility below 0 dB were not disregarded, in order to determine better correlations for moments where tones occurred with lower audibility. This change is in line with the changes implemented to ISO TS 20065 by the IEC TS 61400-11-2 [2] standard, which mentions that “*although a potential tone with a $\Delta Lk < 0$ might not be audible by itself, (...) all tone energy within a critical band is perceived as a single tone, and therefore all tone energy is summed to account for this.*” [2].

Tones detected using a narrow band (FFT) method are grouped into 1/3-octave bands based on the lower and upper frequency bounds of the band. If no tone is detected at a given timestamp, the audibility is set to -10 dB, following the guidelines of the ISO TS 20065 and IEC TS 61400-11-2 standards (note that IEC 61400-11 does not specify this). Additionally, for ISO TS 20065, tones with audibility levels below -10 dB are clipped to -10 dB (these “tones” could occur due to the decision to not exclude tones below 0 dB). Timestamps without detected tones are assigned a value of -10 dB to ensure that these instances are included in the analysis rather than excluded. If multiple audible tones are found within the same 1/3-octave band, the highest audibility is stored at that timestamp.

Next, the grouped FFT-method dataset is merged with the 1/3-octave band dataset based on the nearest timestamp. Note that because both datasets were sampled at *roughly* 10 seconds resolution. Because of the slight temporal misalignment in the sampling time, 0 to 5 seconds mismatch could occur within a 10 second bin. To account for this temporal mismatch, the dataset was resampled to 10-minute intervals using an energetic average. This time interval corresponds to the standard time intervals of wind turbine SCADA data.

4. Results

4.1 Dataset exploration

Figure 2 shows the correlation of the A-weighted equivalent sound pressure levels (LAeq) for the three measurement locations. The horizontal and vertical axis both show the LAeq level, each measured by one of the devices. Each 10-second measurement is binned into a small hexagonal grid, with the colour of each bin corresponding to a linear increase of the amount of datapoints within that bin. As expected, the LAeq levels show very strong correlation (0.94), and the fit line indicates full agreement. The wide outliers (in purple) are most likely caused by the slight difference in sample times of approximately 10 seconds between the two sound level meters. This can result in time shifts of up to 5 seconds within the 10-second bins. As shown in Figure 3, resampling the data to 10 minutes eliminates the outliers. Figure 3 highlights that location 1 has the fewest outliers, whereas location 3 has the most. The most likely explanation is that on average the wind speeds during the measurements were higher at locations 2 and 3 than at location 1. Additionally, due to the proximity of trees and bushes, wind-induced noise likely played a more significant role at locations 2 and 3. The placement of the sound level meters may also have contributed to the outliers, since for location 2 and 3 practical constraints prevented close proximity between the sound level meters.

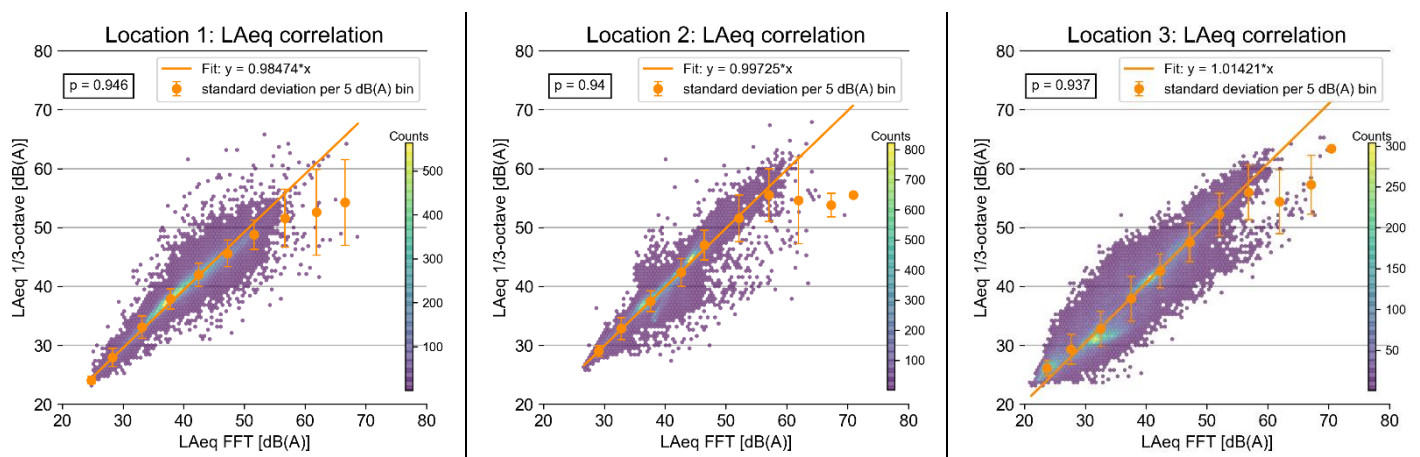


Figure 2 Three correlation plots comparing LAeq signals. The horizontal axis represents the LAeq levels obtained from FFT measurements, while the vertical axis shows the LAeq levels derived from the 1/3-octave band measurements. Each plot corresponds to a specific measurement location (locations 1, 2, and 3). The Pearson correlation coefficient is displayed in the top-left corner of each plot. A linear fit passing through the origin is shown in orange, accompanied by the standard deviation calculated for each 5 dB(A) bin. The data is visualized using hexagonal bins, with the colour indicating the number of data points within each bin on a linear scale.

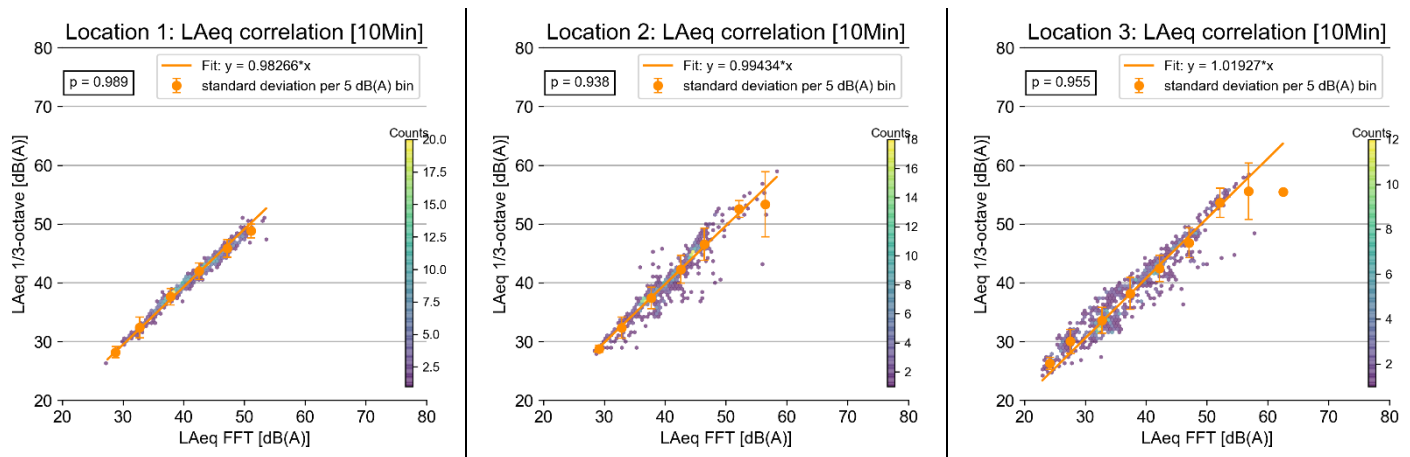


Figure 3 Identical plot as Figure 2, but with input data resampled to 10 minutes. This resampling results in a significant decrease in outliers due to slight temporal misalignment.

4.2 Comparison between tones detected by FFT-method and 1/3-octave band differences

Table 1 shows an overview of tones that were detected using the IEC 61400:11 and ISO TS narrow band tonality methods for each location. The audibility that is listed in the table is the energy average audibility of the audible tones [i.e. all tones with audibility > 0 dB] that were detected within one 1/3-octave band. Tones are only listed in the table if audible tones occurred more than 5% of the time (after resampling to 10 minutes) within a 1/3-octave band. No tones below 63 Hz and inside the 125 Hz band were detected more than 5% of the time for this dataset.

Frequencies shown in Table 1 are the centre frequencies of the 1/3-octave band in which audible tones occurred. The actual tone frequencies that were detected varied between frequency band, location, and method. The distribution of all tones detected by the IEC 61400-11 and ISO TS 20065 methods within each 1/3-octave band is shown in Figure 9 and Figure 10 in the Appendix. The axis limits are set to the lower and upper boundary of each 1/3-octave band. From the figures, it can be concluded that, especially for location 2, the audible tones within the 63 Hz 1/3-octave band occur at the centre of the frequency band, whereas the audible tones at location 1 within the 80 Hz 1/3-octave band occur near the lower boundary of the this frequency band.

IEC 61400:11 and ISO TS 20065 show quite similar results with regards to tonal audibility and tonal occurrence. In general, ISO TS 20065 is able to detect more tones, albeit that for this research it was chosen to not exclude tones below 0 dB audibility (in line with recommendations mentioned in IEC TS 20065). For frequencies where both IEC 61400:11 and ISO TS detected a similar audible tone occurrence, the average tonal audibility of all audible tones differs by a maximum of 1 dB.

Table 1 An overview of the tones that were detected using two narrow band tonality methods for each location. The tones are grouped into 1/3-octave bands according to section 3.3. Only tones (resampled to 10 minutes) with audibility of more than 0 dB that occurred more than 5 % of the time are shown in this table.

Location	Audible tones detected more than 5% of the time (after resampling to 10 minutes), noted as: [frequency*] [percentage of time detected], [energy average tonal audibility of occurring <i>audible</i> tones, i.e. all tones with audibility > 0 dB(A)]	
	IEC 61400:11 narrowband method	ISO TS 20065 narrowband method
Location 1	63 Hz : 5%, $\Delta L = 3$ dB 80 Hz : 47%, $\Delta L = 8$ dB -- 160 Hz : 14%, $\Delta L = 2$ dB	-- 80 Hz : 45%, $\Delta L = 7$ dB 100 Hz : 11%, $\Delta L = 1$ dB 160 Hz : 28%, $\Delta L = 2$ dB
Location 2	63 Hz : 39%, $\Delta L = 10$ dB 80 Hz : 8%, $\Delta L = 3$ dB -- --	63 Hz : 37%, $\Delta L = 9$ dB 80 Hz : 7%, $\Delta L = 2$ dB 100 Hz : 21%, $\Delta L = 1$ dB 160 Hz : 12%, $\Delta L = 1$ dB
Location 3	63 Hz : 40%, $\Delta L = 4$ dB -- 100 Hz : 8%, $\Delta L = 2$ dB 160 Hz : 16%, $\Delta L = 2$ dB	63 Hz : 40%, $\Delta L = 3$ dB -- -- 160 Hz : 12%, $\Delta L = 1$ dB
*The exact frequencies of the tones differ. For example, the 63 Hz frequencies at location 2 fall within the centre of the 1/3-octave band, while the exact frequencies of the 80 Hz tones at location 1 fall more towards the lower boundary (± 73 Hz).		

Figure 4 shows the correlation between the 1/3-octave band level differences in line with ANSI/ASA S12.9-2013/Part 3 and audibility of tones detected by ISO TS 20065 for the 63 Hz 1/3-octave band. Figure 5 and Figure 6 show the same information but for the 80 Hz and 160 Hz 1/3-octave bands. These figures are only shown for the comparison of ANSI/ASA S12.9-2013/Part 3 and ISO TS 20065, as these demonstrated the best correlations. Other methods are presented in a more compact form later in this chapter in Table 3 and Table 4.

In general, all figures show a positive linear trend that intersects at roughly $X = [-2 \text{ to } 2]$ dB(A) for moments when no tone was detected $Y = -10$ dB. Since there are extended periods without tone occurrences, the majority of data points cluster around this intersection. Consequently, other points appear purple on the color scale due to their relatively low count compared to the densely populated intersection point.

- Tones within 63 Hz 1/3-octave band: Location 1 and location 2 seem to be following a similar slope. The slope of location 3 is higher, indicating a lower 1/3-octave band difference for the same tonal audibility as detected by ISO TS 20065 at this location. The greater the tonal audibility observed, the stronger the correlation. This might be due to the practical constraints that resulted in a larger distance between both meters at location 3.
- Tones within 80 Hz 1/3-octave band: Location 1 is the only location with strong positive correlation ($p \geq 0.8$). Again, the greater the tonal audibility observed, the stronger the correlation. The slopes of the linear fit differ.
- Tones within 160 Hz 1/3-octave band: Location 1 is the only location with strong positive correlation ($p \geq 0.8$). Again, the greater the tonal audibility observed, the stronger the correlation.

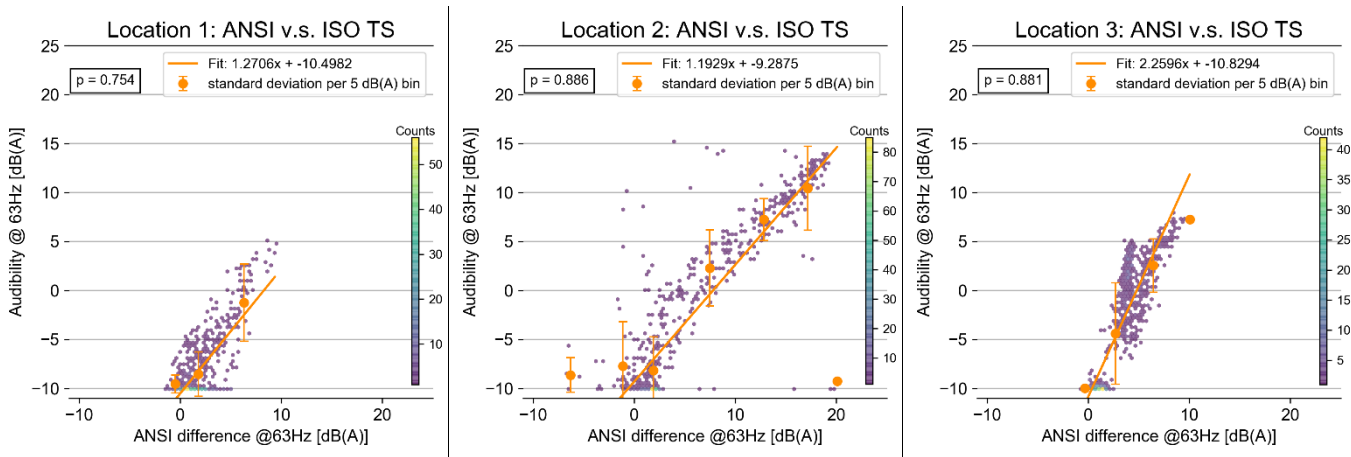


Figure 4 Three correlation plots comparing the ANSI/ASA 1/3-octave band method with the ISO TS 20065 FFT-method. Both were resampled to 10-minute bins to prevent temporal misalignment. The horizontal axis represents the 1/3-octave band differences [dB(A)], while the vertical axis shows the tonal audibility [dB] derived from the FFT-method. Each plot shows the correlation at the 63Hz 1/3-octave band and a specific measurement location (locations 1, 2, and 3). The Pearson correlation coefficient is displayed in the top-left corner of each plot. A linear fit is shown in orange, accompanied by the standard deviation calculated for each 5 dB(A) bin. The data is visualized using hexagonal bins, with the colour indicating the number of data points within each bin on a linear scale.

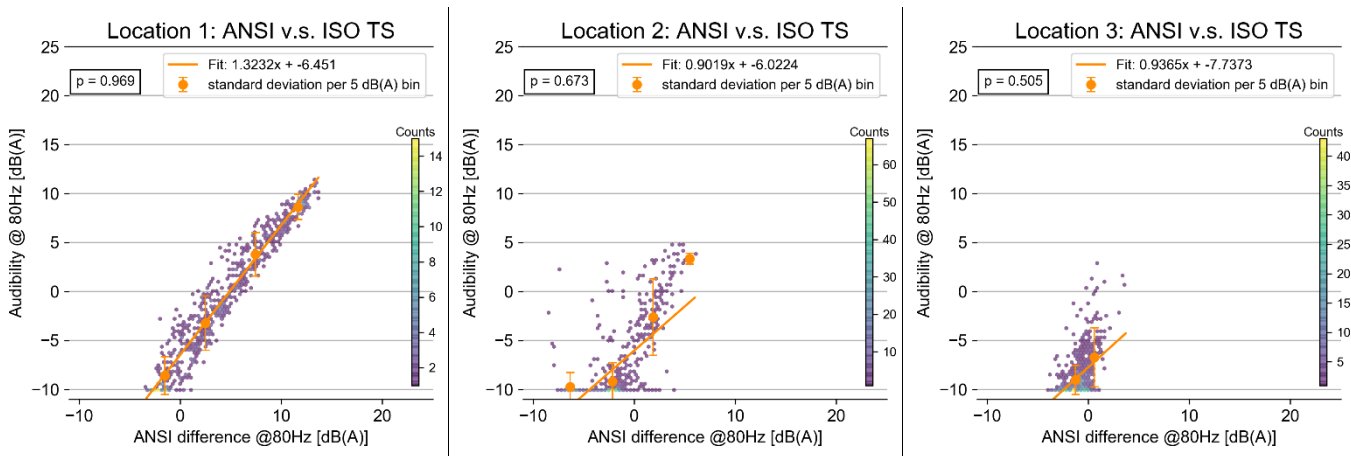


Figure 5 Identical plot as Figure 4, but for 80 Hz 1/3-octave band

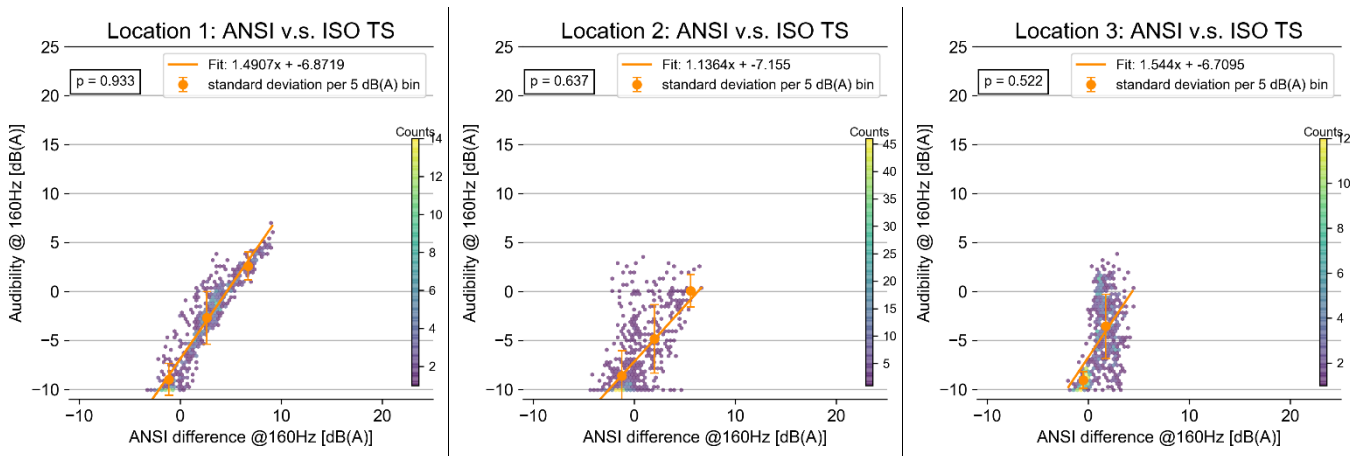


Figure 6 Identical plot as Figure 4, but for 160 Hz 1/3-octave band

Figure 7 shows a generalized picture of level differences measured at all frequencies (63, 80, 100, 125 and 160 Hz 1/3-octave bands) and all locations, for ANSI/ASA S12.9-2013/Part 3. From this figure it can be

concluded that a similar slope occurs for the different frequencies and locations, although with a larger data spread compared to the individual frequencies and locations, especially at ANSI/ASA level differences between -5 and 6 dB. This is expected, since different frequencies might have varying results, and each measurement location has other measurement conditions.

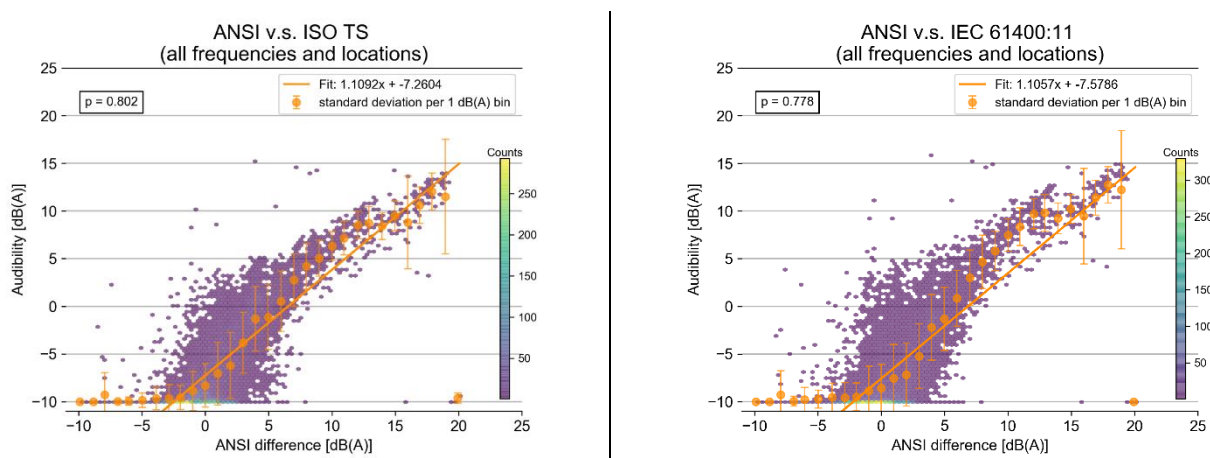


Figure 7 Identical plot as Figure 4, but for all frequencies and all locations. The error bars show the standard deviation per 1 dB(A) interval. The left figure is for a comparison between ANSI/ASA and ISO TS, the right image for ANSI/ASA and IEC 61400:11.

Table 2 shows the arithmetic average, standard deviation and 95% confidence interval of the tonal audibility for each ANSI/ASA level difference bin with 1 dB(A) width. The arithmetic average and standard deviation are identical to the error bars shown in Figure 7. It shows that on average IEC 61400:11 shows slightly higher tonal audibility, but overall the results of both FFT-methods are quite similar.

Table 2 The arithmetic average, standard deviation and 95% confidence interval of the tonal audibility for each ANSI/ASA level difference bin with 1 dB(A) width. For all frequencies and locations.

ANSI/ASA level difference	Tonal audibility according to ISO TS 20065		Tonal audibility according to IEC 61400:11	
	Arithmetic average ± std	95% confidence interval	Arithmetic average ± std	95% confidence interval
(0.5, 1.5]	-7.1 ± 3.3	[-13.5 - -0.6]	-7.5 ± 3.6	[-14.5 - -0.6]
(1.5, 2.5]	-6.2 ± 3.5	[-13.0 - 0.6]	-7.2 ± 3.3	[-13.6 - -0.7]
(2.5, 3.5]	-3.8 ± 3.2	[-10.1 - 2.5]	-5.2 ± 3.4	[-11.9 - 1.4]
(3.5, 4.5]	-1.3 ± 3.4	[-8.0 - 5.3]	-2.2 ± 3.4	[-9.0 - 4.5]
(4.5, 5.5]	-1.1 ± 3.4	[-7.8 - 5.6]	-1.3 ± 3.3	[-7.8 - 5.2]
(5.5, 6.5]	0.5 ± 3.2	[-5.7 - 6.8]	0.8 ± 2.9	[-4.9 - 6.6]
(6.5, 7.5]	2.7 ± 2.8	[-2.7 - 8.2]	3 ± 2.9	[-2.7 - 8.7]
(7.5, 8.5]	4.2 ± 2.4	[-0.6 - 9.0]	4.7 ± 2.8	[-0.9 - 10.2]
(8.5, 9.5]	5 ± 1.9	[1.3 - 8.8]	5.8 ± 2.1	[1.7 - 9.9]
(9.5, 10.5]	6.3 ± 1.5	[3.3 - 9.4]	7.5 ± 1.7	[4.0 - 10.9]

4.3 Finding the optimal threshold K_T

This chapter describes the determination of the optimal thresholds K_T for each location and 1/3-octave band. Ultimately, these thresholds are generalized for all measurement locations and all 1/3-octave bands between 63 and 160 Hz.

Figure 8 shows three examples of the process of finding the optimal threshold K_T by determining at what threshold the F1-score is maximum. The left image shows that for an ANSI/ASA S12.9-2013/Part 3 vs. ISO TS comparison at location 1 at 80 Hz. For this case, there is a clear optimal threshold at which the F1-score peaks at 95%. The centre image shows an optimal K_T of 6 dB(A) for location 2 at 63 Hz, although the F1-score is not a clear peak this time, and flatlines at 90-92% between 4 and 6 dB(A), indicating that any value between this range would result in a similar accuracy and precision ratio. The right image shows a very clear peak at a K_T of 3.5 dB(A) with an F1-score of 81% for location 3 at 63 Hz.

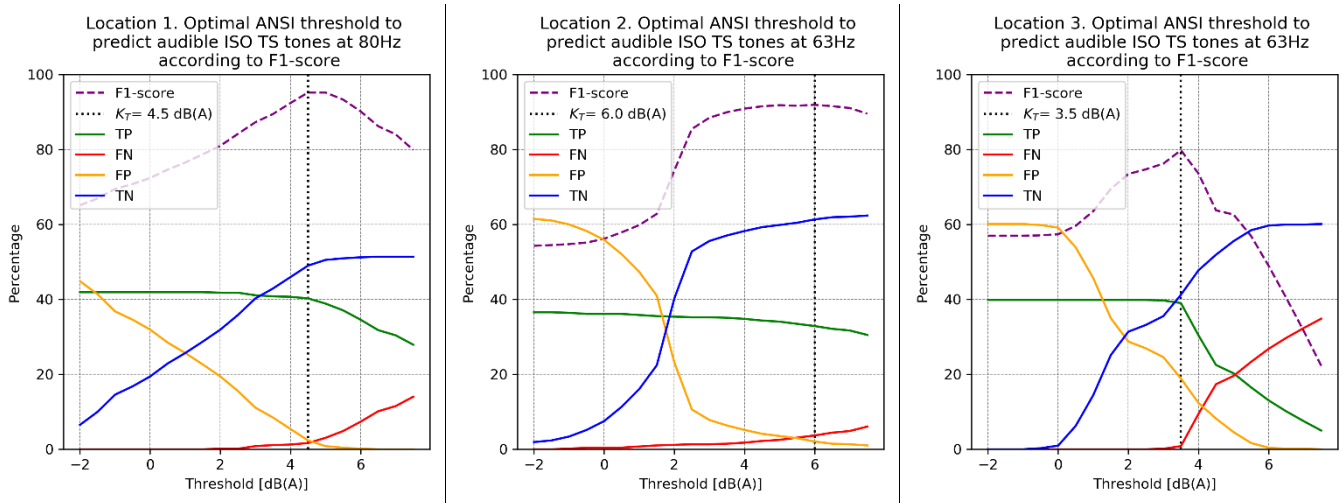


Figure 8 Three examples of several F1-scores. Left figure: 80 Hz comparison at location 1 resulted in an optimal ANSI/ASA level difference K_T of 4.5 dB(A). Center figure: 63 Hz comparison at location 2 resulted in an optimal ANSI/ASA level difference K_T of 6 dB(A), although from 4 to 6 dB(A) the difference in F1-score is marginal. Right figure: 63 Hz comparison at location 3 resulted in an optimal ANSI/ASA level difference K_T of 3.5 dB(A).

Table 3 shows a list of all the different F1-scores, together with the Pearson correlation coefficients and K_T -value, for several frequencies and measurement locations that have an occurrence of audible tones above 5%. All of these are for comparing several 1/3-octave band methods to the IEC 61400:11 FFT-method. Table 4 shows the same information compared to the ISO-TS FFT-method.

Table 3 For four combinations of 1/3-octave band methods with the IEC 61400:11 FFT-method, this table shows information on the optimal threshold K_T . Only when more than 5% of the time a tone occurred within a 1/3-octave band information is shown. The information in each cell shows for each frequency: (1) the Pearson correlation coefficient between the average tonal audibility and the 1/3-octave band differences, (2) the maximum F1-score and (3) the optimal threshold K_T .

Frequency	Measurement location	IEC 61400:11 Audible tone occurrence and mean tonal audibility	Assessment of tones for four 1/3-octave band survey methods, noted as: [Pearson correlation coefficient], [Maximum F1-score], [K_T = threshold at maximum F1-score]			
			ISO (A-weighted) vs. IEC 61400:11	ISO (Z-weighted) vs. IEC 61400:11	ANSI/ASA vs. IEC 61400:11	“Alternative ANSI” vs. IEC 61400:11
63 Hz	Location 1	5%, $\Delta L = 3$ dB	p=0.64, F1score=0.60, $K_T=1.0$ dB(A)	p=0.63, F1score=0.74, $K_T=4.0$ dB(A)	p=0.74, F1score=0.82, $K_T=6.0$ dB(A)	p=0.46, F1score=0.48, $K_T=7.5$ dB(A)

Frequency	Measurement location	IEC 61400:11 Audible tone occurrence and mean tonal audibility	Assessment of tones for four 1/3-octave band survey methods, noted as: [Pearson correlation coefficient], [Maximum F1-score], [K_T = threshold at maximum F1-score]			
			ISO (A-weighted) vs. IEC 61400:11	ISO (Z-weighted) vs. IEC 61400:11	ANSI/ASA vs. IEC 61400:11	“Alternative ANSI” vs. IEC 61400:11
	Location 2	39%, $\Delta L = 10$ dB	p=0.86, F1score=0.88, $K_T=2.0$ dB(A)	p=0.84, F1score=0.90, $K_T=3.5$ dB(A)	p=0.89, F1score=0.92, $K_T=4.5$ dB(A)	p=0.91, F1score=0.93, $K_T=5.5$ dB(A)
	Location 3	41%, $\Delta L = 4$ dB	p=0.85, F1score=0.78, $K_T=2.0$ dB(A)	p=0.87, F1score=0.82, $K_T=1.0$ dB(A)	p=0.88, F1score=0.81, $K_T=3.5$ dB(A)	p=0.91, F1score=0.81, $K_T=4.5$ dB(A)
80 Hz	Location 1	47%, $\Delta L = 8$ dB	p=0.93, F1score=0.92, $K_T=3.5$ dB(A)	p=0.83, F1score=0.83, $K_T=2.0$ dB(A)	p=0.96, F1score=0.95, $K_T=4.5$ dB(A)	p=0.96, F1score=0.95, $K_T=6.0$ dB(A)
	Location 2	8%, $\Delta L = 3$ dB	p=0.60, F1score=0.62, $K_T=0.5$ dB(A)	p=0.31, F1score=0.35, $K_T=-1.0$ dB(A)	p=0.62, F1score=0.61, $K_T=2.5$ dB(A)	p=0.73, F1score=0.64, $K_T=4.5$ dB(A)
100 Hz	Location 3	8%, $\Delta L = 2$ dB	p=0.27, F1score=0.15, $K_T=-2.0$ dB(A)	p=-0.22, F1score=0.02, $K_T=-2.0$ dB(A)	p=0.17, F1score=0.18, $K_T=-1.5$ dB(A)	p=0.15, F1score=0.19, $K_T=-2.0$ dB(A)
160 Hz	Location 1	14%, $\Delta L = 2$ dB	p=0.86, F1score=0.83, $K_T=4.0$ dB(A)	p=0.89, F1score=0.82, $K_T=1.5$ dB(A)	p=0.89, F1score=0.87, $K_T=5.5$ dB(A)	p=0.90, F1score=0.27, $K_T=7.5$ dB(A)
	Location 3	16%, $\Delta L = 2$ dB	p=0.29, F1score=0.38, $K_T=-0.5$ dB(A)	p=-0.04, F1score=0.15, $K_T=-2.0$ dB(A)	p=0.27, F1score=0.38, $K_T=0.5$ dB(A)	p=-0.70, F1score=0.28, $K_T=-2.0$ dB(A)

Table 4 For four combinations of 1/3-octave band methods with the ISO TS 20065 FFT-method, this table shows information on the optimal threshold K_T . Only when more than 5% of the time a tone occurred within a 1/3-octave band information is shown. The information in each cell shows for each frequency: (1) the Pearson correlation coefficient between the average tonal audibility and the 1/3-octave band differences, (2) the maximum F1-score and (3) the optimal threshold K_T .

Frequency	Measurement location	ISO TS 20065 Audible tone occurrence and mean tonal audibility	Correlation of tones and 1/3-octave band method, noted as: [Pearson correlation coefficient], [Maximum F1-score], [TH = threshold at maximum F1-score]			
			ISO (A-weighted) vs. ISO TS 20065	ISO (Z-weighted) vs. ISO TS 20065	ANSI vs. ISO TS 20065	“Alternate ANSI” vs. ISO TS 20065
63 Hz	Location 2	37%, $\Delta L = 9$ dB	p=0.86, F1score=0.90, TH=2.5 dB(A)	p=0.84, F1score=0.91, TH=3.5 dB(A)	p=0.89, F1score=0.92, TH=6.0 dB(A)	p=0.91, F1score=0.93, TH=7.0 dB(A)

Frequency	Measurement location	ISO TS 20065 Audible tone occurrence and mean tonal audibility	Correlation of tones and 1/3-octave band method, noted as: [Pearson correlation coefficient], [Maximum F1-score], [TH = threshold at maximum F1-score]			
			ISO (A-weighted) vs. ISO TS 20065	ISO (Z-weighted) vs. ISO TS 20065	ANSI vs. ISO TS 20065	“Alternate ANSI” vs. ISO TS 20065
	Location 3	40%, $\Delta L = 3$ dB	p=0.86, F1score=0.77, TH=2.0 dB(A)	p=0.86, F1score=0.79, TH=1.0 dB(A)	p=0.88, F1score=0.80, TH=3.5 dB(A)	p=0.92, F1score=0.81, TH=5.0 dB(A)
80 Hz	Location 1	45%, $\Delta L = 7$ dB	p=0.94, F1score=0.92, TH=3.5 dB(A)	p=0.88, F1score=0.84, TH=2.0 dB(A)	p=0.97, F1score=0.95, TH=4.5 dB(A)	p=0.97, F1score=0.96, TH=6.0 dB(A)
	Location 2	7%, $\Delta L = 2$ dB	p=0.64, F1score=0.63, TH=1.5 dB(A)	p=0.37, F1score=0.38, TH=0.0 dB(A)	p=0.67, F1score=0.68 TH=2.5 dB(A)	p=0.78, F1score=0.73, TH=4.5 dB(A)
100 Hz	Location 1	11%, $\Delta L = 1$ dB	p=0.73, F1score=0.70, TH=1.5 dB(A)	p=0.78, F1score=0.82, TH=1.5 dB(A)	p=0.83, F1score=0.79, TH=3.0 dB(A)	p=0.86, F1score=0.84, TH=4.0 dB(A)
	Location 2	21%, @1 dB(A)	p=0.79, F1score=0.67 TH=1.5 dB(A)	p=0.84, F1score=0.77 TH=2.0 dB(A)	p=0.85, F1score=0.75, TH=3.5 dB(A)	p=0.86, F1score=0.80, TH=4.0 dB(A)
160 Hz	Location 1	28%, $\Delta L = 2$ dB	p=0.91, F1score=0.87, TH=3.0 dB(A)	p=0.91, F1score=0.89, TH=0.5 dB(A)	p=0.93, F1score=0.84, TH=4.0 dB(A)	p=0.92, F1score=0.46, TH=7.5 dB(A)
	Location 2	6%, $\Delta L = 1$ dB	p=0.58, F1score=0.30, TH=2.5 dB(A)	p=0.61, F1score=0.47, TH=1.5 dB(A)	p=0.64, F1score=0.30, TH=3.5 dB(A)	p=0.56, F1score=0.13, TH=7.5 dB(A)
	Location 3	12%, $\Delta L = 1$ dB	p=0.42, F1score=0.27, TH=-1.0 dB(A)	p=0.04, F1score=0.12, TH=-2.0 dB(A)	p=0.52, F1score=0.30, TH=1.0 dB(A)	p=-0.47, F1score=0.22, TH=5.5 dB(A)

In general, an assessment according to the ANSI/ASA S12.9-2013/Part 3 standard performs better than according to the ISO 1996-2:2017 standard, showing higher correlations and higher optimal F1-scores. In some cases, the ‘alternative ANSI’ method performed marginally better than the average of the two adjacent 1/3-octave bands as stated in ANSI/ASA S12.9-2013/Part 3. However, in other cases with lower tonal occurrence, the ‘alternative ANSI’ method performed significantly worse.

For location 1, most of the audible tones occurred at a frequency of 72 to 74 Hz, which is close to 71 Hz, the lower boundary of the 80 Hz 1/3-octave band. Although this was the case, still the tonal audibility correlated very strongly ($p=0.97$) with the ANSI/ASA S12.9-2013/Part 3 1/3-octave band method, as shown in Figure 5. The other methods also showed correlation coefficients larger than 0.8. This suggest that the ANSI/ASA S12.9-2013/Part 3 method could still be effective at detecting tones somewhat close to the boundaries of the 1/3-octave band.

For ANSI/ASA S12.9-2013/Part 3, the following optimal level difference thresholds K_T were determined (omitting results with a Pearson correlation coefficient below 0.6, results are for both the comparison with ISO TS 20065 and IEC 61400:11 and for all measurement locations):

- 63 Hz: Optimal $K_T = 3.5 - 6.0$ dB(A)
- 80 Hz: Optimal $K_T = 2.5 - 4.5$ dB(A)
- 100 Hz: Optimal $K_T = 3.0 - 3.5$ dB(A)
- 160 Hz: Optimal $K_T = 3.5 - 5.5$ dB(A)

As a result, setting a K_T of 4 dB(A) for ANSI/ASA S12.9-2013/Part 3 appears a reasonable choice for detecting potential tones within the 63 until 160 Hz 1/3-octave bands. Table 5 and Table 6 list the performance of ANSI/ASA S12.9-2013/Part 3 for detecting audible tones with a K_T of 4 dB(A) compared to IEC 61400:11 and ISO TS 20065 respectively. It shows the following results:

- When the ANSI/ASA-method detected a potential audible tone more than 20% of the time:
 - Recall was between 76 and 97%, meaning that 3 to 24% of the time a tone detected by the FFT-method was missed by the 1/3-octave band method.
 - Precision was between 52 and 91 %, meaning that 9 to 48% of the time a potential audible tone was suggested based on 1/3-octave band data, but the FFT-method detected no real audible tone at that time.
 - After applying equal weighting to recall and precision, F1-score varied between 67% and 93%.
 - The energy average of all suspected tones (all ANSI/ASA level differences $\geq K_T$) was 6 to 14 dB(A). F1-score was higher for larger average ANSI/ASA level differences: For cases where the energy average of the suspected tones was larger than 9 dB(A), recall was between 93 and 97% and precision was between 87 and 91%.
- The 100 Hz and 125 Hz 1/3-octave bands at measurement location 2 showed several potential audible tones that were suggested by the ANSI/ASA method, 17 to 19 percent of the time. The number of tones detected by the FFT-methods was however minimal. In this case the recall was often still decent, but the precision was bad. That is why it is also important to look at the energy average of the suspected tones: in this case it was 5 dB(A), only 1 dB(A) above K_T . These results suggest that to avoid low precision, it is recommended to verify that the energy average of the suspected tones (all ANSI/ASA level differences ≥ 4 dB(A)) is at least 6 dB(A).
- If all frequencies and locations are generalized, the ANSI-method scored an average 70 to 72% recall and 62 to 70% precision.

Table 5 ANSI/ASA detected (TP + FP), recall, precision and F1-score for ANSI S12.9-2013/Part 3 with $K_T = 4$ dB(A), compared to ISO TS 20065. Results are listed together with the tone occurrence (as detected by FFT-method) for every frequency and location. Rows where ANSI/ASA detected a potential tone less than 20% of the time are highlighted in grey. The energy average of the suspected tones (all ANSI/ASA level differences ≥ 4 dB(A)) is also listed.

1/3-octave band	Location	Audible tone occurrence (ISO TS 20065)	ANSI/ASA detected ($K_T = 4$)	Energy average ANSI diff. (for diff ≥ 4 dB)	Recall	Precision	F1-score
63 Hz	Location 1	<5%	15%	6 dB(A)	100%	30%	46%
	Location 2	37% $\Delta L=9$ dB	40%	14 dB(A)	95%	87%	91%
	Location 3	40% $\Delta L=3$ dB	43%	6 dB(A)	76%	71%	74%
80 Hz	Location 1	45% $\Delta L=7$ dB	46%	9 dB(A)	97%	88%	92%
	Location 2	7% $\Delta L=2$ dB	2%	5 dB(A)	28%	93%	43%
	Location 3	<5%	0%	N/A	0%	0%	0%
	Location 1	11% $\Delta L=1$ dB	10%	5 dB(A)	80%	76%	78%

1/3-octave band	Location	Audible tone occurrence (ISO TS 20065)	ANSI/ASA detected ($K_T = 4$)	Energy average ANSI diff. (for diff ≥ 4 dB)	Recall	Precision	F1-score
100 Hz	Location 2	21% $\Delta L=1$ dB	19%	5 dB(A)	51%	56%	54%
	Location 3	<5%	0%	4 dB(A)	0%	0%	0%
125 Hz	Location 1	<5%	1%	5 dB(A)	57%	80%	67%
	Location 2	<5%	17%	5 dB(A)	88%	20%	32%
	Location 3	<5%	0%	4 dB(A)	0%	0%	0%
160 Hz	Location 1	28% $\Delta L=2$ dB	24%	6 dB(A)	82%	86%	84%
	Location 2	6% $\Delta L=1$ dB	5%	5 dB(A)	23%	25%	24%
	Location 3	12% $\Delta L=1$ dB	1%	4 dB(A)	1%	25%	2%
All frequencies & all locations				9 dB(A)	70%	70%	72%

Table 6 ANSI detected (TP + FP), recall, precision and F1-score for ANSI/ASA S12.9-2013/Part 3 with $K_T = 4$ dB(A), compared to IEC 61400:11. Results are listed together with the tone occurrence (as detected by FFT-method) for every frequency and location. Rows where ANSI/ASA detected a potential tone less than 20% of the time are highlighted in grey. The energy average of the suspected tones (all ANSI/ASA level differences ≥ 4 dB(A) is also listed.

1/3-octave band	Location	Tone occurrence (IEC 61400:11)	ANSI/ASA detected ($K_T = 4$)	Energy average ANSI diff. (for diff ≥ 4 dB)	Recall	Precision	F1-score
63 Hz	Location 1	5% $\Delta L=3$ dB	15%	6 dB(A)	97%	32%	49%
	Location 2	39% $\Delta L=10$ dB	40%	14 dB(A)	93%	90%	92%
	Location 3	41% $\Delta L=4$ dB	43%	6 dB(A)	77%	74%	75%
80 Hz	Location 1	47% $\Delta L=8$ dB	46%	9 dB(A)	95%	91%	93%
	Location 2	8% $\Delta L=3$ dB	2%	5 dB(A)	23%	93%	37%
	Location 3	<5%	0%	N/A	0%	0%	0%
100 Hz	Location 1	<5%	10%	5 dB(A)	63%	21%	31%
	Location 2	<5%	19%	5 dB(A)	70%	15%	24%
	Location 3	8% $\Delta L=2$ dB	0%	4 dB(A)	0%	0%	0%
125 Hz	Location 1	<5%	1%	5 dB(A)	41%	70%	52%
	Location 2	<5%	17%	5 dB(A)	84%	23%	36%
	Location 3	<5%	0%	4 dB(A)	0%	0%	0%
160 Hz	Location 1	14% $\Delta L=2$ dB	24%	6 dB(A)	94%	52%	67%
	Location 2	<5%	5%	5 dB(A)	19%	11%	14%
	Location 3	16% $\Delta L=2$ dB	1%	4 dB(A)	0%	0%	0%
All frequencies & all locations				9 dB(A)	72%	62%	67%

5. Conclusions & discussion

To address the slight temporal misalignment in the 10-second sampling of the two sound level meters used for the measurements, the measurement data was resampled to 10-minute time intervals.

When comparing 1/3-octave band survey methods to the IEC 61400:11 and ISO TS 20065 engineering methods based on FFT measurements, the following conclusions can be drawn.

The engineering methods IEC 61400:11 and ISO TS 20065 show quite similar results regarding tonal audibility and tonal occurrence. In general, ISO TS 20065 is able to detect more audible tones, albeit that

for this research it was chosen to not exclude tones below 0 dB audibility, in line with recommendations mentioned in IEC TS 20065. For frequencies where both IEC 61400:11 and ISO TS 20065 detected a similar audible tone occurrence, the average tonal audibility of all audible tones differed by a maximum of 1 dB.

In general, for survey methods, an assessment according to the ANSI/ASA S12.9-2013/Part 3 standard performs better than according to the ISO 1996-2:2017 standard, showing higher correlations and a higher optimal positive/false (F1) scores. In some cases, taking the arithmetic average of the sound pressure levels for the four adjacent 1/3-octave bands performed marginally better than the average of the two adjacent 1/3-octave bands as stated in ANSI/ASA S12.9-2013/Part 3. However, in other cases with lower tonal occurrence, it performed significantly worse. Therefore, when using a survey method to assess possible tonal wind turbine noise it is recommended to use the approach as stated in ANSI/ASA S12.9-2013/Part 3. For the frequencies that were investigated in this study, applying A-weighting of Z-weighting had negligible results on the outcome for the ANSI/ASA S12.9-2013/Part 3 method, since taking the average of the two adjacent 1/3-octave bands balances out the effect of A-weighting on the adjacent 1/3-octave bands.

For location 1, most of the audible tones occurred at a frequency of 72 to 74 Hz, which is close to 71 Hz, the lower boundary of the 80 Hz 1/3-octave band. Although this was the case, still the tonal audibility correlated very strongly ($p=0.97$) with the ANSI/ASA S12.9-2013/Part 3 1/3-octave band method. This suggests that the ANSI/ASA S12.9-2013/Part 3 method could still be effective at detecting tones close to the boundaries of the 1/3-octave band. This contrasts with what Søndergaard and Bastasch [8] found in their 2021 study.

For ANSI/ASA S12.9-2013/Part 3, the following optimal level difference thresholds K_T were determined (omitting results with a Pearson correlation coefficient below 0.6):

- 63 Hz: Optimal $K_T = 3.5 - 6.0$ dB(A)
- 80 Hz: Optimal $K_T = 2.5 - 4.5$ dB(A)
- 100 Hz: Optimal $K_T = 3.0 - 3.5$ dB(A)
- 125 Hz: Optimal $K_T =$ unknown due to very low occurrence of these tones in this dataset
- 160 Hz: Optimal $K_T = 3.5 - 5.5$ dB(A)

These level difference thresholds are considerably lower than the K_T values suggested by ANSI/ASA S12.9-2013/Part 3 of 15 dB for frequencies between 25 Hz and 125 Hz and 8 dB for frequencies between 160 Hz and 400 Hz. However, the standard states that these are, first of all, possible choices, and secondly, they are intended to identify *prominent* discrete tones. The audibility of a prominent tone would exceed the minimum of $\Delta L = 0$ dB that was used in this paper. Søndergaard et al. [9] indicate the tonal audibility of a prominent tone would be approximately 5 dB. An increased audibility criterion would also result in higher values for K_T . The results of this paper indicate that $K_T = 15$ dB can only detect tones with very high average tonal audibility ($\Delta L > 10$ dB), whereas $K_T = 8$ dB corresponds to a minimum tonal audibility of approximately 5 dB.

The authors suggest that when using a survey method to assess possible tonal wind turbines noise in the frequency range between 63 and 160 Hz, ANSI/ASA S12.9-2013/Part 3 with a threshold of $K_T = 4$ dB(A) should be applied to identify potential tones with minimum audibility of 0 dB. This approach is recommended when seeking an equally weighted balance between optimal recall and precision. If precision is prioritised over recall - ensuring that identified tones are accurate, even at the expense of missing some - using a higher K_T , such as 6 dB(A), is recommended. For detecting prominent tones $K_T = 8$ dB(A) would be more appropriate, or slightly higher, such as $K_T = 10$ dB(A), if precision is prioritized over recall.

If an ANSI/ASA level difference larger than $K_T = 4$ dB(A) occurs at least 20% of the time, it is reasonable to assume that audible tones might be detectable with a proper narrow band method. Under these conditions, recall ranged from 76% to 97%. However, precision was more variable, ranging from 52% to 91%. This variability suggests that while the 1/3-octave band data was proficient at indicating the presence of tones, false positives occurred in 9% to 48% of cases, where tones were indicated but no audible tones

were actually present. Precision was particularly low when most suspected tones (based on ANSI/ASA) were near the threshold of 4 dB(A). If the energy average ANSI/ASA level difference of the suspected tones was larger than 9 dB(A), recall and precision increased significantly: Under these conditions, recall was between 93 and 97% and precision was between 87 and 91%.

These results provide insight into the relationship between 1/3-octave band survey methods and narrowband engineering FFT-methods in detecting tonal sounds. However, 1/3-octave band methods should only be used as an initial indication of a potential tonal noise issues. Peaks observed in a 1/3-octave band spectrum are not always indicators of tonal components; they may also result from broadband noise. Especially for peaks with lower average ANSI/ASA level differences one should be cautious before drawing conclusions about tonality without conducting measurements with a narrow band engineering narrowband method.

References

- [1] L. S. Søndergaard and T. H. Pedersen, "Tonality in wind turbine noise. IEC 61400-11 ver. 2.1 and 3.0 and the Danish/Joint Nordic method compared with listening tests," in *5th International Conference on Wind Turbine Noise*, Denver, 2013.
- [2] International Electrotechnical Commission (IEC), "IEC TS 61400-11-2:2024, Wind energy generation systems – Part 11-2: Acoustic noise measurement techniques – Measurement of wind turbine sound characteristics in receptor position," 2024.
- [3] International Organization for Standardization (ISO), "ISO/TS 20065:2022, Acoustics — Objective method for assessing the audibility of tones in noise — Engineering method," 2022.
- [4] International Organization for Standardization (ISO), "ISO 1996-2:2017 Acoustics – Description, measurement and assessment of environmental noise - Part 2: Determination of sound pressure levels," 2017.
- [5] American National Standards Institute/ Acoustical Society of America (ANSI/ASA), "ANSI/ASA S12.9-2013/Part 3, Quantities and Procedures for Description and Measurement of Environmental Sound - Part 3: Short-term Measurements with an Observer Present," 2013.
- [6] International Electrotechnical Commission (IEC), "IEC 61400-11:2012+AMD1:2018, Edition 3.1, Wind turbines – Part 11: Acoustic noise measurement techniques," 2018.
- [7] C. J. Van Rijsbergen, *Information Retrieval (2nd Edition)*, Butterworth-Heinemann, 1979.
- [8] L. S. Søndergaard and M. Bastasch, "Tonality content analysed with both 1/3 octave band and narrowband methods with comparison to listening test," in *9th International Conference on Wind Turbine Noise*, Remote from Europe, 2021.
- [9] L. S. Søndergaard, C. Thomsen and T. H. Pedersen, "Prominent tones in wind turbine noise - Round-robin test of the IEC 61400-11 and ISO/PAS 20065 methods for analysing tonality content," in *8th International Conference on Wind Turbine Noise*, Lisbon, 2019.

6. Appendix

Figure 9 shows the distribution of all audible tones (10-second time intervals) by ISO TS 20065 within each 1/3-octave band.

Figure 10 shows the distribution of all audible tones (10-second time intervals) by IEC 61400:11 within each 1/3-octave band. The average audibility is higher compared to the ISO TS 20065 method, but the overall count of tones is lower.

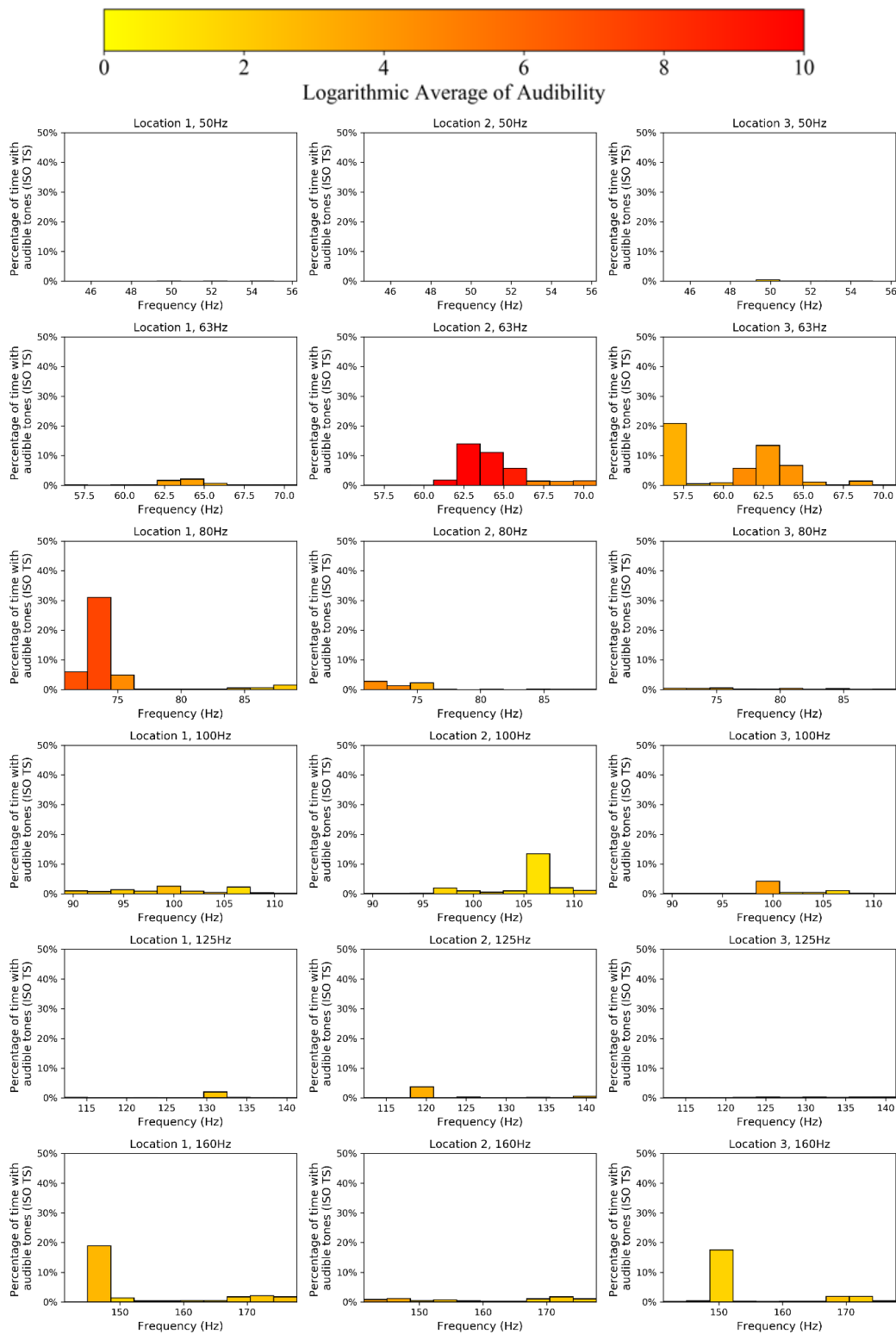


Figure 9 The distribution of tones determined by ISO TS 20065 within each 1/3-octave band. The colour indicates the energy average audibility of the bin. The horizontal axis limits are set to the lower and upper bounds of the frequency bin. The vertical axis shows the occurrence of audible tones [i.e. tones with audibility above 0].

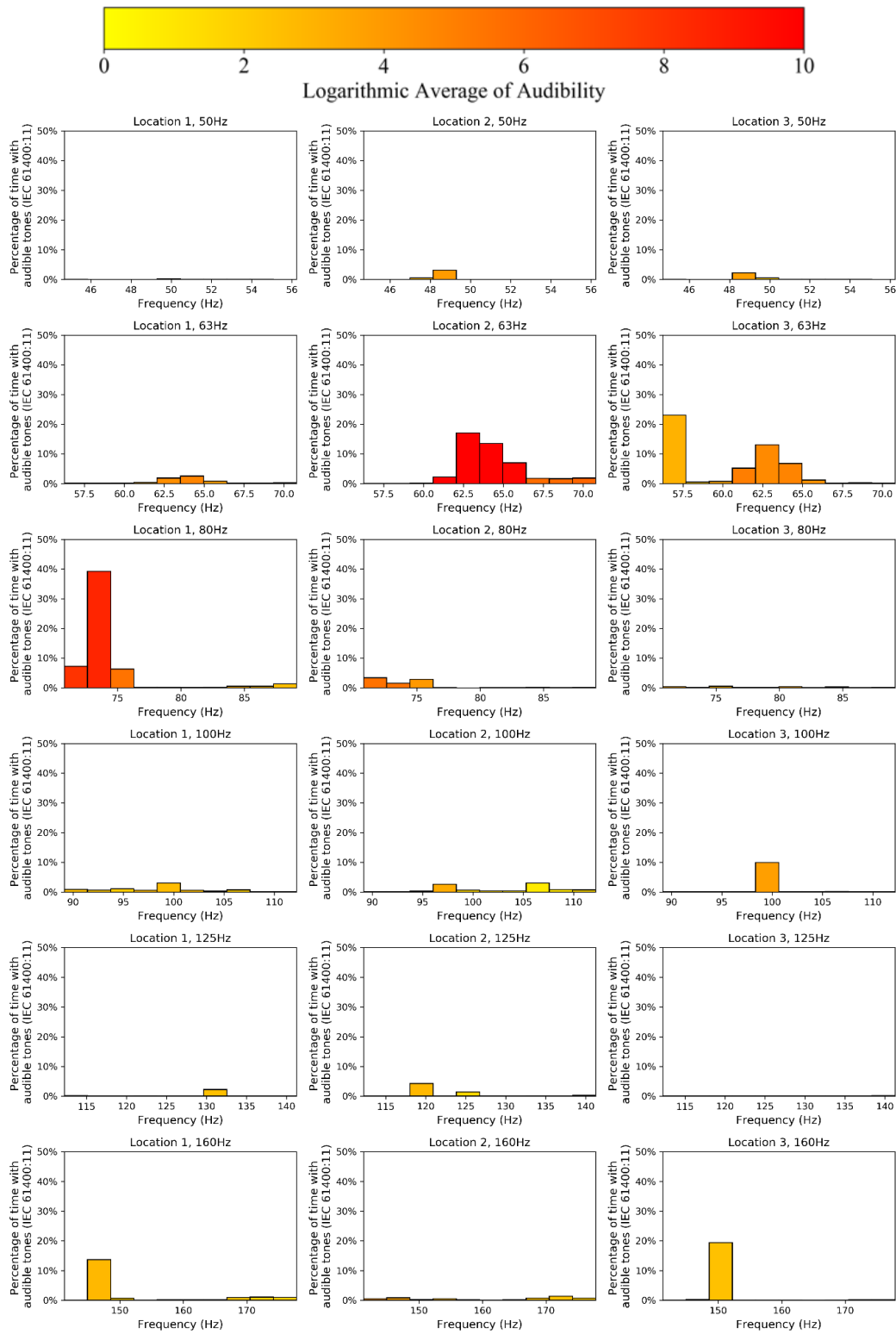


Figure 10 The distribution of tones determined by IEC 61400:11 within each 1/3-octave band. The colour indicates the energy average audibility of the bin. The horizontal axis limits are set to the lower and upper bounds of the frequency bin. The vertical axis shows the occurrence of audible tones [i.e. tones with audibility above 0].

Paper #13 - ID: 347

Title: Aeroacoustic investigation of leading edge erosion in a wind tunnel

Author: Oliver Lylloff

11th Edition of the
International Conferences on
Wind Turbine Noise
Copenhagen, Denmark – 10th to 13th June 2025

Aeroacoustic investigation of leading edge erosion in a wind tunnel

Oliver Lyloff¹ and Andreas Fischer and Anders S. Olsen

**Airfoil and Rotor Design, Wind Turbine Division, Dept. of Wind and Energy Systems,
Technical University of Denmark (DTU). Frederiksborgvej 399, Roskilde, Denmark**

Summary

Leading edge erosion (LEE) on wind turbine blades is a significant challenge for the wind turbine industry. It affects the structural integrity of the blades as well as the aerodynamic and acoustic performance. While there is a lot of research addressing structural integrity and aerodynamic performance, the effects of LEE on noise emissions remain largely unknown. The goal of this study is to analyze effects of LEE on the noise emission at airfoil level through wind tunnel testing. Aerodynamic and acoustic measurements were conducted on an FFA-W3-211 airfoil in the Poul la Cour wind tunnel at DTU Risø Campus, using various leading edge surface conditions to simulate erosion damage. Two wind tunnel configurations were utilized: hard walls for capturing aerodynamic lift and drag coefficients, and Kevlar walls for recording far-field noise with a microphone array. The combined dataset ranges from Reynolds numbers of 1.8 million to 4.5 million and angles of attack from -20 to +20 degrees, with four different leading edge surface conditions consisting of sandpaper and trip tape (zig-zag tape). The results indicate that in the attached flow regime there is a strong correlation between the measured drag and the acoustic noise emission. This suggests that the change in boundary layer properties due to an eroded leading edge is the primary driver of increased noise generation. A regression model describing the noise increase as a function of drag increase is derived. This methodology can serve as the basis for future investigations of leading edge erosion and may lead to new models for noise characterization.

1. Introduction

Leading edge erosion (LEE) on wind turbine blades not only impacts aerodynamic performance but also affects structural integrity, lifespan, and acoustic emission [1, 2]. LEE is caused by particles hitting the airfoil leading edge during operation. The effect is considered greater on offshore wind turbines than onshore due to a larger percentage of operation at maximum tip speed [3]. Keegan et al. provided a review of leading edge erosion on wind turbine blades, examining potential degradation caused by environmental variables, with a focus on raindrop and hailstone impacts [4]. The study reports that LEE can become significant after as little as two years of operation. A more recent review, which includes mitigation measures, was presented by Mishnaevsky et al. [5].

Several studies have focused on estimating annual energy production (AEP) losses at the rotor or wind farm level due to erosion. Bak et al. used computational fluid dynamics (CFD) and blade element momentum (BEM) simulations to investigate how AEP losses are influenced by LEE, rotor control, and wind climate [6]. The study estimated losses ranging from 0.5–4% AEP depending on wind climate and damage severity.

¹Corresponding author - Email: ollyl@dtu.dk

They noted that fully turbulent flow may not sufficiently model aerodynamic effects of leading-edge damage (e.g., grooves and bumps). A simplified model, SALT, was later developed to predict AEP losses due to LEE [7]. Özçakmak et al. evaluated multiple prediction models, estimating a 4.3% AEP reduction under severe erosion [8]. The SALT tool [7] and OpenFAST [9] were compared and found to produce comparable results for erosion-induced AEP losses. Furthermore, 3D CFD simulations revealed that erosion affects blade forces beyond the eroded area, highlighting the need for high-fidelity 3D models alongside 2D tools. Forsting et al. developed a spectral model to represent LEE, showing that complex surface topology can be mathematically represented as a superposition of regular waves [10]. These erosion patches were used in 2D CFD simulations, revealing sharp performance losses (reduced lift, increased drag). Gaudern et al. evaluated LEE impacts on two wind turbine airfoils in a wind tunnel, finding that all erosion configurations degraded lift and increased drag [11]. The authors noted that using leading-edge tripping as an erosion proxy fails to capture severe erosion impacts. Performance degradation also varied across airfoil designs. Sareen et al. reached similar conclusions, reporting 5%–25% AEP losses [1], however, the high end estimate of 25% has not been reported elsewhere. Maniaci et al. analyzed LEE impacts on U.S. wind turbines using power curves and uncertainty quantification, finding up to 5% AEP losses for utility-scale turbines and increased risks due to larger rotors and higher tip speeds [12]. At the wind farm level, Visbeck et al. developed a framework combining damage prediction, aerodynamic loss modeling, and wind farm flow simulations [3]. They found that single-turbine LEE modeling overestimates AEP losses by up to 7%, while wind farm-wide modeling showed an average 1.4% loss (peaking at 2.7%).

Few studies address noise emissions from LEE. Zhang et al. explored far-field acoustic measurements as a non-contact monitoring technique [13]. Wang et al. analyzed LEE effects on a 5-MW blade using CFD and the Ffowcs Williams–Hawkings (FWH) acoustic analogy, reporting higher noise levels for eroded blades (up to 8 dB increase in overall sound pressure level, OASPL) [14].

This study investigates the aeroacoustic effects of LEE on an FFA-W3-211 airfoil in a wind tunnel. By coupling aerodynamic measurements with far-field acoustic data from a microphone array, the impacts of LEE are quantified through correlations between drag and noise. Erosion is simulated using trip tape (zig-zag) and sandpaper with two different grain sizes. While these surface add-ons force turbulent transition and imperfectly model LEE [1, 11], they enable the development of a methodology for linking surface-condition changes to aerodynamic and acoustic performance by providing a dataset with a broad range of drag coefficients. Since it is well-established that the airfoil boundary layer is a primary driver of trailing edge noise [15], changes in surface conditions caused by erosion must alter the boundary layer properties and, consequently, the noise characteristics. This fact is utilized by applying a Strouhal number scaling to the acoustic results using the boundary layer displacement thickness, calculated from the wake velocity deficit measured by a wake rake in the aerodynamic tests. With this scaling, the acoustic spectra collapse for different velocities, surface conditions, and a range of angles of attack, allowing them to be systematically integrated into overall sound pressure levels (OASPL) for use in regression analysis.

This study was conducted as part of the *LERCat* project, funded by the Danish Energy Agency and in collaboration with several industry partners. The goal of the project is to establish a link between LEE inspection data and aerodynamic losses. To develop a categorization scheme, digital twins were created from surface scans of real eroded blades, which are used in flow simulations and wind tunnel measurements to assess their performance impact. The reader is referred to Ref. [16] for more details.

Ultimately, understanding the dynamics of erosion and its connection to acoustic emission will enhance turbine efficiency and reliability, ensuring optimal energy production and reducing downtime.

This paper is structured as follows: In Section 2, the experimental wind tunnel campaign is described. The airfoil model, surface conditions, and data analysis methods are presented. In Section 3, the results from the aerodynamic and acoustic test campaigns are shown and combined using the Strouhal number spectrum. The OASPL is calculated, and a linear regression analysis is presented. The methods and results are discussed in Section 4, and the study is concluded in Section 5.

2. Methods

2.1 Wind tunnel campaign

The experimental investigation was conducted in the Poul la Cour Tunnel (PLCT) at DTU Risø Campus, employing two different test section configurations to assess aerodynamic and acoustic performance under varying leading-edge surface conditions. For aerodynamic testing, a hard-wall setup was used, with wall pressure taps determining the lift coefficient (C_l) and effective angle of attack (AoA), while a wake rake was employed to calculate the drag coefficient (C_d). A schematic of the setup is shown in Figure 1. Acoustic

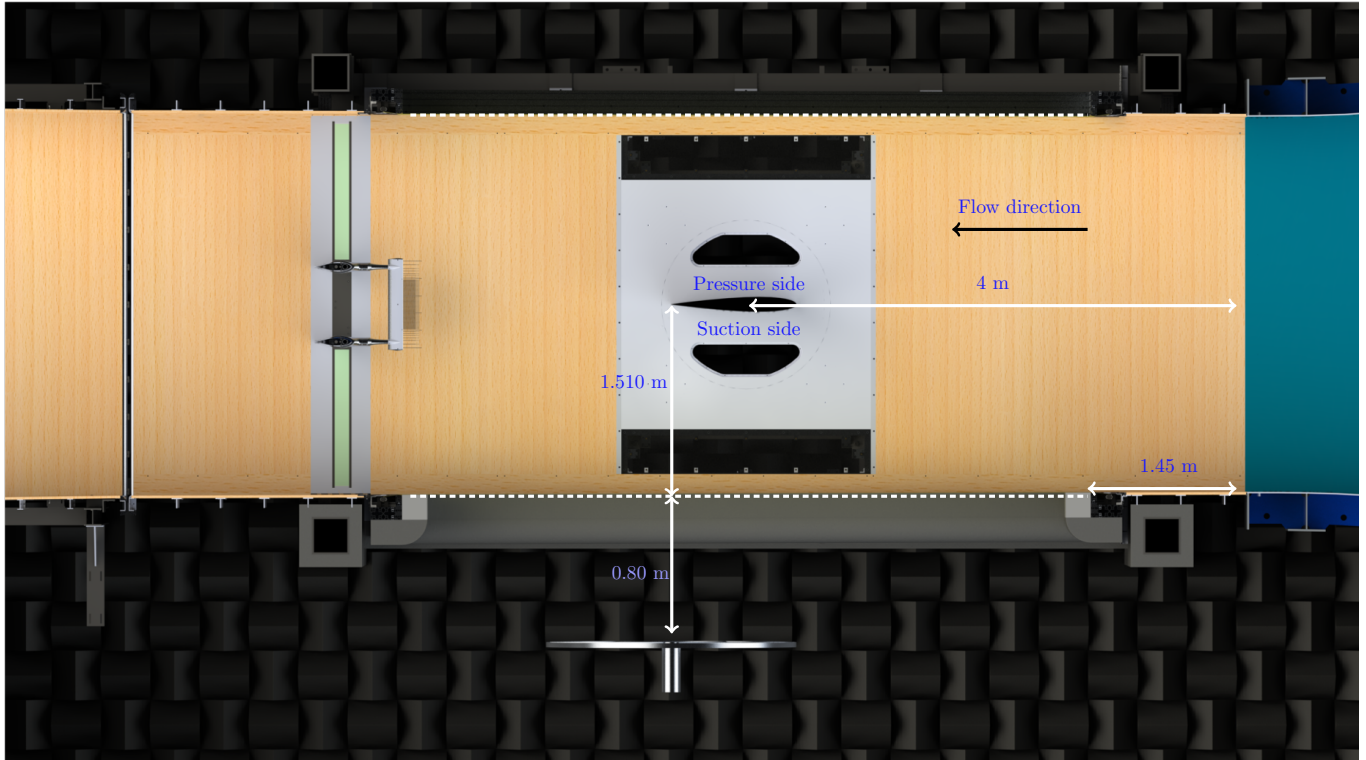


Figure 1 Test section setup in PLCT. White dashed lines mark the position of interchangeable walls; aerodynamic hard walls with pressure taps or acoustic Kevlar walls.

measurements utilized a Kevlar-wall configuration, allowing far-field noise capture via a microphone array positioned outside the flow field. Tensioned Kevlar fabric is almost acoustically transparent, confines the flow, and its high tensile strength makes it suitable for retaining the loads applied by the airfoil model inside the test section [17, 18].

The airfoil model, an FFA-W3-211 with a chord length of 0.9 m and a span of 2 m, was equipped with 140 pressure taps shown in Figure 2. Pictures of the airfoil mounted in the wind tunnel are shown in Figure 3. The model was made of aluminum and coated with paint to enable infrared imaging for boundary layer state detection.

A significant amount of pressure taps were covered by the applied sandpaper, which makes the calculation of lift coefficient uncertain. Therefore, wall pressure taps were used in calculating the lift coefficient consistently in all configurations.

The study maintained fixed Reynolds numbers ranging from 1.8 million to 4.5 million, with angles of attack spanning from -20° to $+20^\circ$, however some of the surface conditions were only tested at two Reynolds numbers, see Table 1. The two types, P40 and P400, refer to coarse and fine sandpaper, respectively, with the coarse type having fewer but larger particles, and the fine type having many smaller particles. In addition, this study relies on wake rake data for calculating the drag coefficient and displacement thickness, which further limits the angle of attack (AoA) range to approximately -8 to 11 degrees. For the comparison between

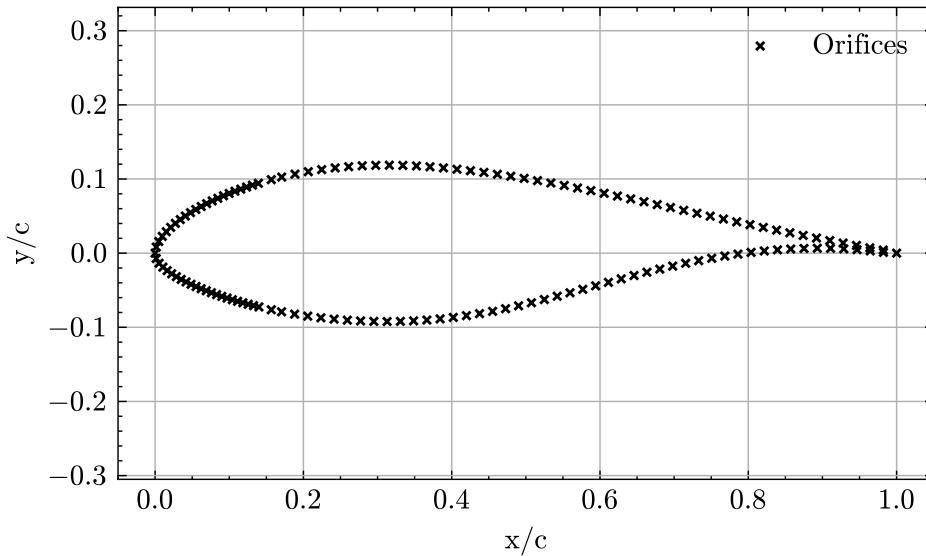


Figure 2 Pressure tap locations on the FFA-W3-211 profile.

Table 1 Experimental wind tunnel dataset

Type	Position [x/c]	Re (Aero)	Re (Acoustic)	AoA (Acoustic)
P40	4PS-3SS	3e6, 4.5e6, 6e6	3e6, 4.5e6	-15:15
P400	4PS-3SS	3e6, 4.5e6, 6e6	3e6, 4.5e6	-15:15
ZZ	10PS + 5SS	1.8e6, 3e6, 4.5e6, 6e6	1.8e6, 3e6, 4.5e6	-15:15
Clean	-	1.8e6, 3e6, 4.5e6, 6e6	1.8e6, 3e6, 4.5e6	-15:15

the two test section setups, the effective angle of attack, AoA_{eff} , was used. The calculation and validation of AoA_{eff} in the Kevlar wall setup are described in Ref. [19].

Acoustic data was acquired at sample rate 2^{14} Hz using 20-second recordings and converted into 1/12-octave band cross-spectral matrices using a Hanning window with 50% overlap. Conventional frequency-domain beamforming techniques were applied to generated acoustic images [20, 21] using the open-source software *AeroAcoustics.jl* [22]. The steering vectors were constructed to produce equivalent free field sound pressure levels by correcting for wind tunnel effects [23]. The microphone array consists of 84 1/4" B&K microphones arranged in a pseudo-random pattern and was placed at a distance of $r = 2.3$ m from the test section centerline centered at the trailing edge position. The far field noise spectra were calculated from a summation of the sound contribution within an integration region of the acoustic images covering 0.8 m in span-wise extent and 0.5 m in chord-wise extent, centered over the trailing edge, see Fig. 4. The results are then scaled to a result of 1 m span (unit: dB/m span). The trustworthy frequency range of the integrated spectra is approximately 400 Hz to 3 kHz for this particular airfoil.

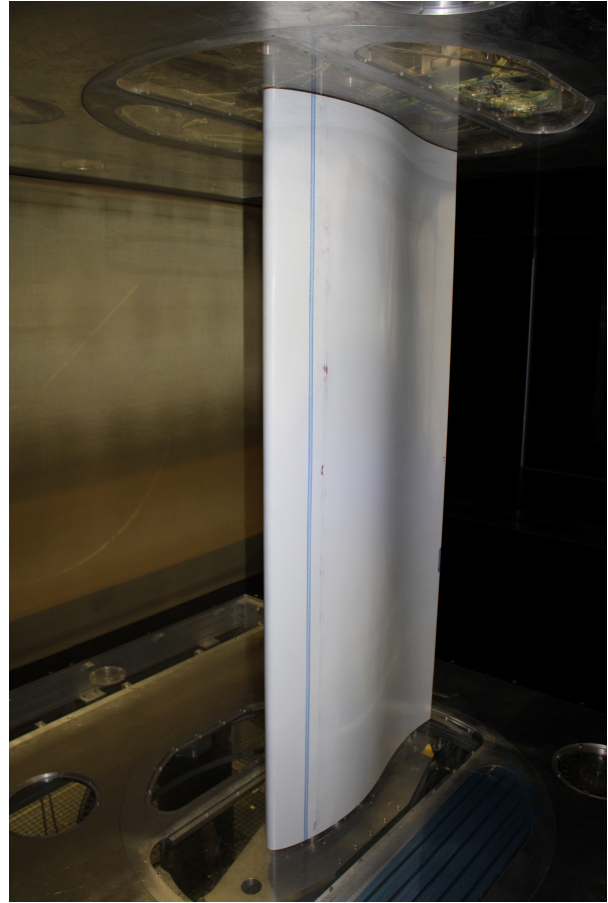
The datasets from the aerodynamic and acoustic wind tunnel campaigns were merged by the fixed Reynolds numbers, geometric angle of attack and descriptions of surface conditions, clean, zz, P40, P400. The effective angle of attack was calculated in both test section configurations and was also used to match measurement points.

2.2 Experimental data analysis

The data obtained in the aerodynamic test section setup consisted of lift from wall pressure and drag from the wake-rake. The lift was computed by integration of the difference of the wall pressure distribution on the walls facing pressure and suction side of the airfoil. The detailed procedure is described in [24].



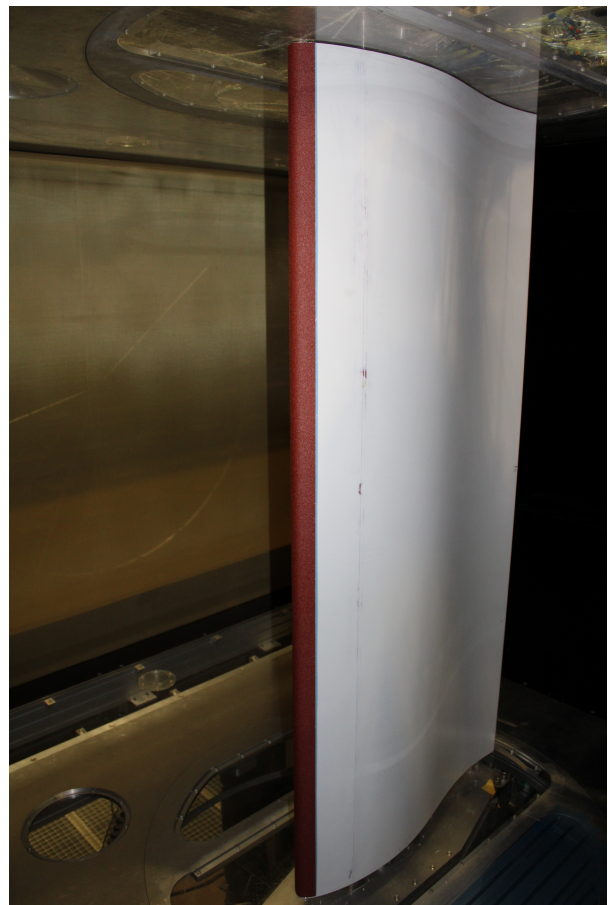
(a) Clean



(b) Tripped with Zig-Zag tape



(c) P400 sandpaper covering leading edge



(d) P40 sandpaper covering leading edge

Figure 3 Images of FFA-w3-211 airfoil with different surface conditions in Kevlar wall configuration.

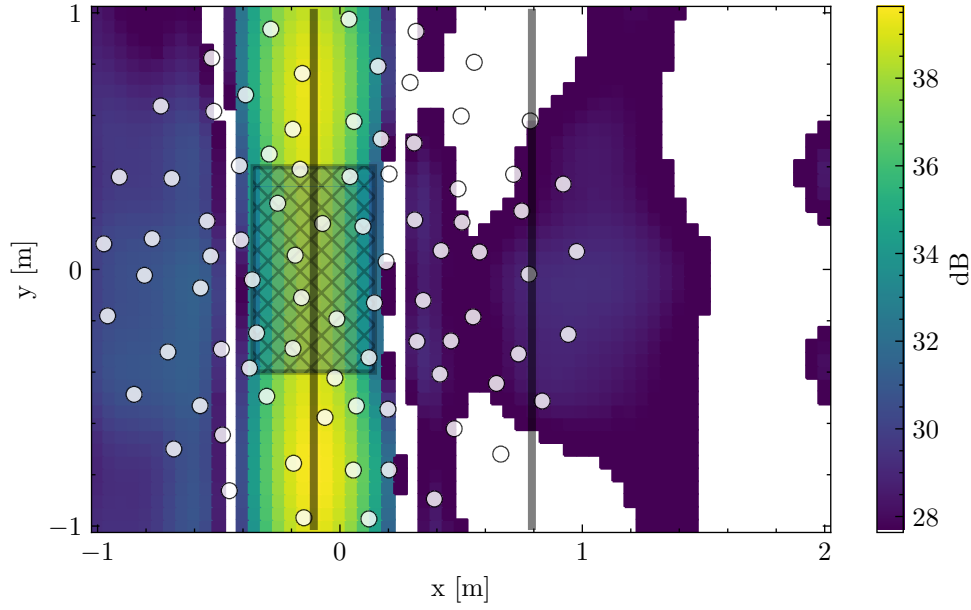


Figure 4 Acoustic image at 1000 Hz (1/12 octave band) overlaid with microphone array geometry (white dots), integration region (hatched square), airfoil leading and trailing edge (black vertical lines). Flow direction is right to left.

In the case of attached flow, the drag of the airfoil is computed using the method of integration of the wake flow deficit as proposed in Ref. [25]. At a position sufficiently far downstream of the airfoil trailing edge where the streamlines passing the edge of the wake deficit are approximately parallel to the mean flow direction, the sectional drag is computed by the expression

$$D = \rho \int_0^{y_1} u (u_e - u) dy, \quad (1)$$

where subscript e refers to the edge, $u = u(y)$ is the velocity profile of the wake deficit, and ρ is the density of the fluid, which is assumed constant over the wake rake. y is the direction normal to the tunnel mean flow and the span of the airfoil model. It is assumed that the wake flow deficit is contained in the region from $y = 0$ to $y = y_1$, ie. $u(0) \approx u_e$ and $u(y_1) \approx u_e$. The drag is related to the missing momentum flow by

$$D = \rho u_e^2 \theta_{wr}, \quad (2)$$

where θ_{wr} is the momentum thickness based on the wake flow deficit. Eq. (2) was derived by combining Eq. (1) and [26, Eq. 17.14].

The momentum thickness based on the boundary layer flow profile close to the trailing edge of an airfoil is a measure for the turbulence scales that generate trailing edge noise. Hence, it can be used to scale the spectral content of the emitted trailing edge noise. In the absence of boundary layer profile measurements, the momentum thickness based on the wake flow deficit can be used as a measure for the turbulence scales that generate trailing edge noise, because the boundary layer flow profiles are directly related to the wake flow deficit in attached flow conditions.

It is more common to use the displacement thickness for spectral scaling of trailing edge noise [27]. The displacement thickness based on the wake deficit, δ_{wr}^* , is not as directly related to the drag as the momentum thickness, but it can be computed as function of the wake flow deficit by

$$\delta_{wr}^* = \int_0^{y_1} \left(1 - \frac{u}{u_e} \right) dy. \quad (3)$$

Eq. (3) was derived from [26, Eq. 17.9] and the assumption that the density is constant in the wake flow deficit. Following the argumentation above, it is assumed that the displacement thickness based on the wake

deficit is an equivalent measure of the turbulence scales generating trailing edge noise as the displacement thickness based on boundary layer profiles. In the following δ_{wr}^* is denoted δ^* .

The acoustic far field data, acquired from acoustic images, consists of trailing edge noise spectra in 1/12-octave band levels scaled to 1 m span. To compare configurations (Reynolds number, angle of attack, and surface condition), the spectra are scaled by the Strouhal number, based on the boundary layer thickness [27],

$$L_{1/12,scaled} = L_{1/12} - 50 \cdot \log_{10}(M_{\infty}/M_{ref}) - 20 \cdot \log_{10}(r_{ref}/r) - 10 \cdot \log_{10}(\delta^*/\delta_{ref}^*) \quad (4)$$

$$St = f \cdot \delta^*/U_{\infty}, \quad (5)$$

where M_{∞} and U_{∞} are the free stream Mach number and velocity, respectively, r is the measurement distance, and the subscript *ref* refers to the chosen scaling reference values close to the mean of each variable: $M_{ref} = 0.15$, $r_{ref} = 1$ m, $\delta_{ref}^* = 0.0055$ m, and $r = 2.3$ m in all acoustic measurements.

The overall sound pressure level (OASPL) is calculated in order to reduce the data and make a simplified regression model. The integrated spectra are summed within a range of Strouhal numbers, based on the range where the scatter of the scaled sound pressure levels is less than 1 dB. Additionally, the trustworthy frequency range of the acoustic measurements are also required to find the range of summation,

$$f_{low} = (St_{low} \cdot U_{\infty})/\delta^*, \text{ if } > f_{low,trust} \quad (6)$$

$$f_{high} = (St_{high} \cdot U_{\infty})/\delta^*, \text{ if } < f_{high,trust} \quad (7)$$

$$OASPL = \sum L_{1/12}(f_{low}; f_{high}) \quad (8)$$

$$OASPL_{scaled} = OASPL - 50 \cdot \log_{10}(M_{\infty}/M_{ref}) - 20 \cdot \log_{10}(r_{ref}/r) - 10 \cdot \log_{10}(\delta^*/\delta_{ref}^*) \quad (9)$$

The noise and drag *increase* is then calculated by using the clean surface condition as reference,

$$\Delta OASPL = OASPL_{scaled,x} - OASPL_{scaled,clean} \quad (10)$$

$$\Delta Cd = \frac{Cd_x}{Cd_{clean}}, \quad (11)$$

where x denotes one of the surface conditions *zz*, *P40* or *P400*.

3. Results

3.1 Aerodynamic results

First, the traditional aerodynamic coefficients, lift Cl , drag Cd , and lift-to-drag ratio Cl/Cd is shown in Figure 5 for multiple Reynolds numbers and airfoil surface conditions. As expected, the clean airfoil attain highest max lift, lowest drag, and therefore largest glide ratio. The zig-zag tape and P400 sandpaper perform very similar and P40 sandpaper has as expected, the largest performance penalty. The wake rake velocity deficit is shown in Figure 6 for two AoAs and at fixed Reynolds number $3e6$ for the four surface conditions. Since the drag coefficient is calculated based on the velocity deficit, it is again clear, that P40 has the largest deficit area and clean has the smallest. A skewing of the deficit is also visible especially for AoA = 6 degrees. The displacement thickness δ^* calculated from the velocity deficit is shown in Figure 7. The trends observed for the drag coefficient in Figure 5 is also visible here. As expected, the displacement thickness decreases with increasing Reynolds number (seen most clearly for the clean case). It also seems that the mutual difference between surface conditions decrease with increasing Reynolds number, especially near an operational AoA of 6 to 8 degrees.

3.2 Strouhal number scaling

The Strouhal number scaling (defined in Eq. (4-5)), is used in Figure 8 to plot spectra for the four surface conditions at two Reynolds numbers $3e6$ and $4.5e6$ and angles of attack ranging from 0 to 8 degrees. For

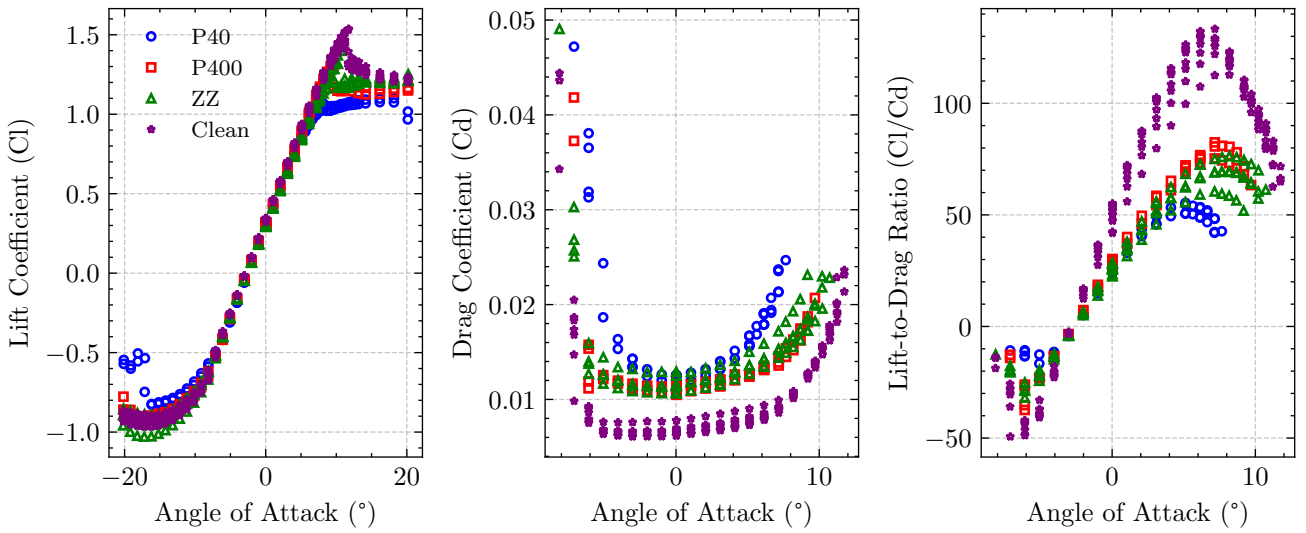


Figure 5 Aerodynamic coefficients from wall pressure data and wake rake.

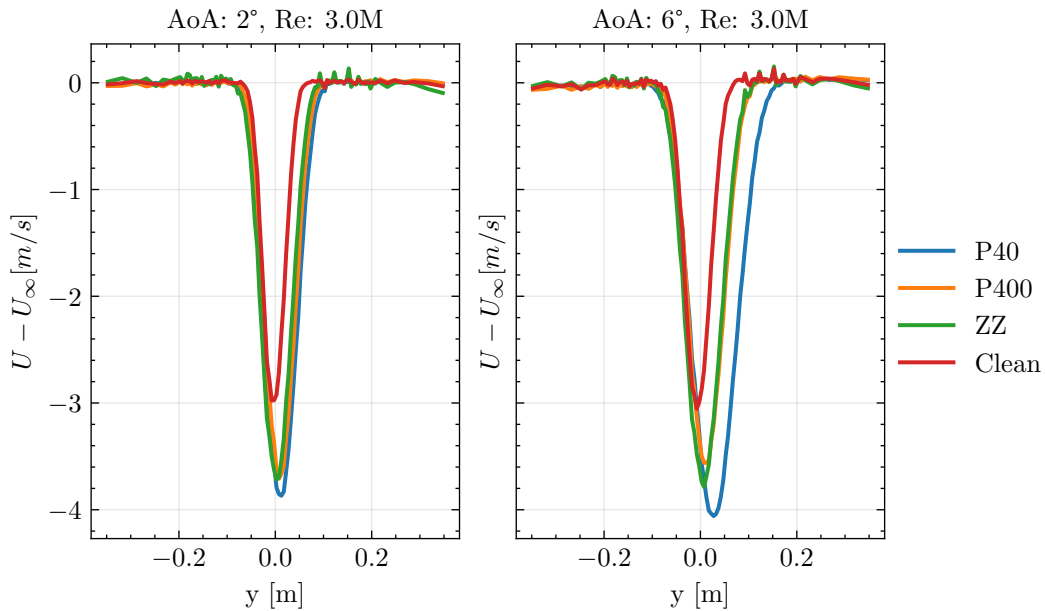


Figure 6 Velocity deficit from wake-rake.

fixed AoA, the Strouhal number is very good at capturing the scaling over two Reynolds numbers. Using a Mach number scaling of M_∞^5 , is clearly a good match, which agrees with theory and empirical studies. Using δ^* as a characteristic length scale in the Strouhal number is also good at capturing the Reynolds number dependence. It is, however, clear that there is a systematic dependence on AoA that is not captured by the scaling approach. With increasing AoA, the slope of all of the surface conditions increases, producing more acoustic energy in the low frequency end of the spectrum and less in the high frequency end. This behavior is well described in the literature and can be attributed to the increasingly thicker boundary layer at higher angles of attack, and consequently larger turbulent length scales and vortical structures. One obvious consequence is a higher overall sound pressure level, with a larger contribution coming from the low frequency end of the spectrum.

3.3 Overall Sound Pressure Level and regression analysis

Finally, the scaling of the experimental data and summation into Overall Sound Pressure Level (OASPL), facilitates a simple regression analysis. The available dataset consists of two Reynolds numbers $3e6$ and $4.5e6$ in the range $AoA_{eff} = -7 - 10$. The scaled OASPL is calculated according to Eq. (9) and shown in

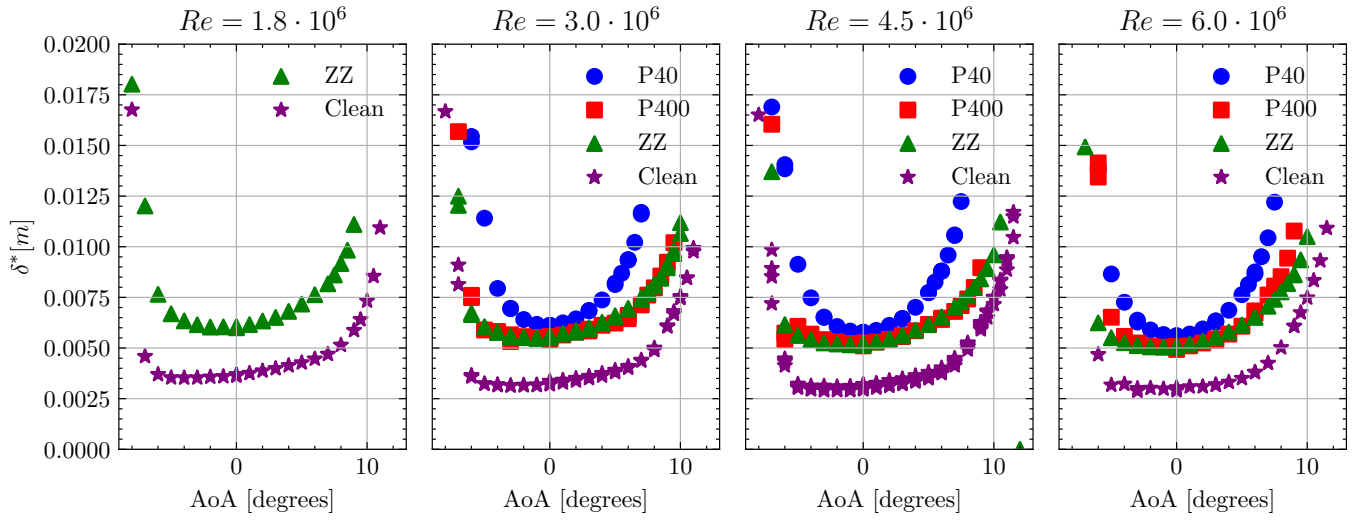


Figure 7 Displacement thickness δ^* calculated from wake rake velocity deficit

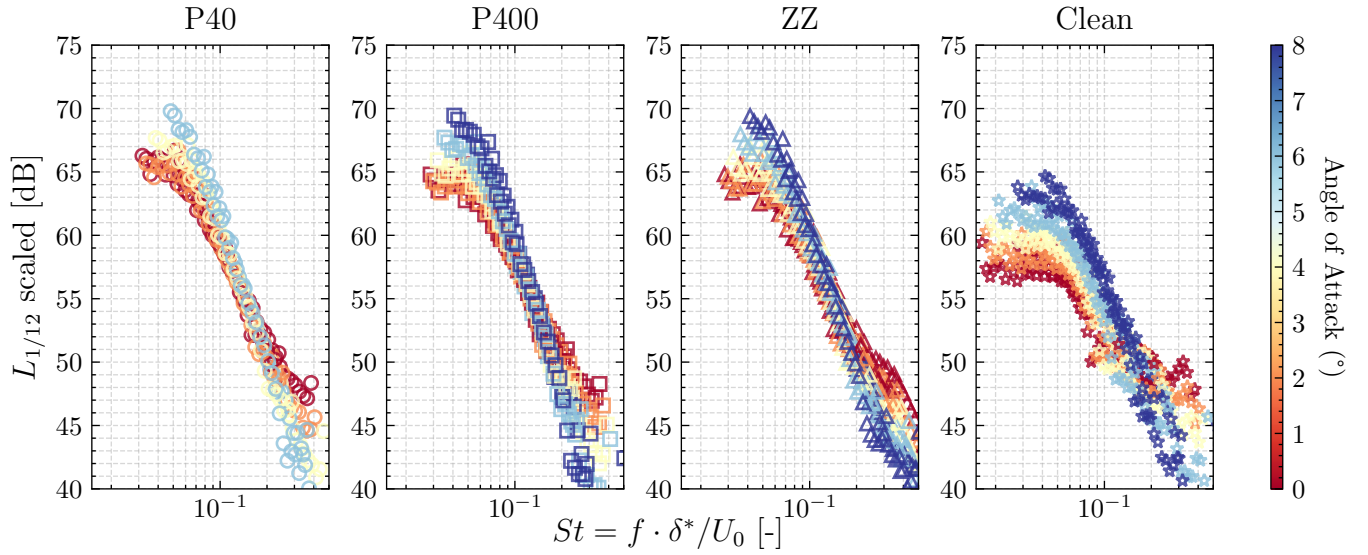


Figure 8 Strouhal plots for each surface type for Reynolds numbers $3e6$ and $4.5e6$ and positive AoAs.

Figure 9. There is a clear trend of increasing overall sound pressure level (OASPL) with increased drag, as expected. However, a group of outliers is observed, particularly for AoAs above 6 and below -5 degrees, indicating that the scaling method does not capture the physics well near flow separation conditions.

A subset of $AoA_{eff} = 5 - 9$ degrees was chosen, to focus on typical operational condition, and limit the spread observed in Figure 8 and 9. Using Eq. (10-11), a linear regression line is calculated,

$$\Delta OASPL = -6.5 + 6.75 \cdot \Delta Cd [dB] \quad (12)$$

With $R^2 = 0.833$, see Figure 10. To arrive at this equation, a subset of the original data was used, and two data points were excluded. The two points are both at a Reynolds number of $3e6$ and $AoA = 8$ degrees. Looking at Figure 8, there is a discrepancy in the clean data around $AoA = 8$, which is not observed for the other surface conditions (P40 has no data at this AoA). This suggests that the chosen range of AoAs for the regression analysis might be too large and that the scaling does not capture the physics well for AoAs nearing flow separation. One possible explanation is that the clean airfoil lacks forced tripping, and the transition point from laminar to turbulent flow changes significantly between Reynolds numbers $3e6$ and $4.5e6$ near flow separation.

Despite the potential bias and uncertainties in the analysis, an $R^2 = 0.833$ indicates a correlation between

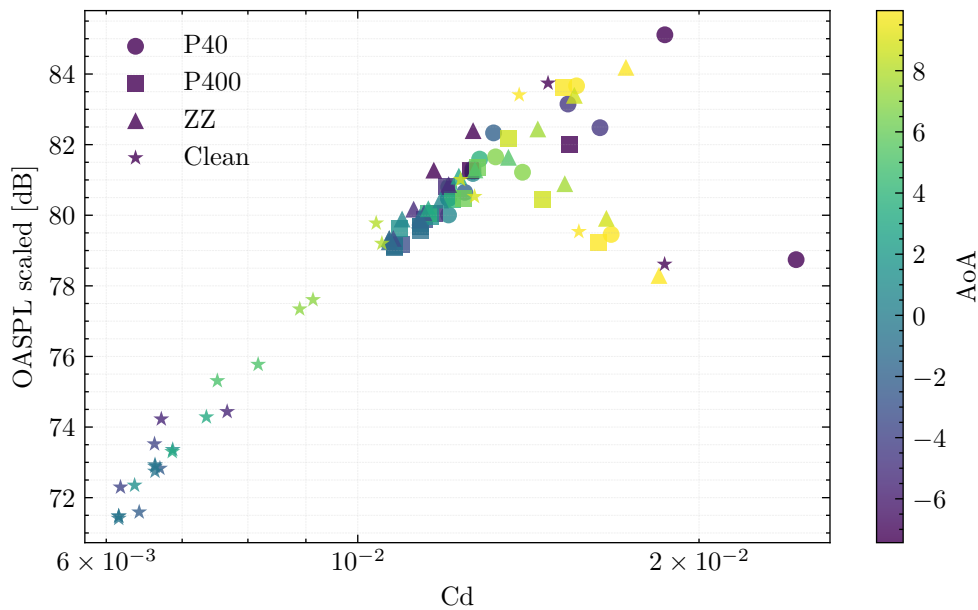


Figure 9 Scaled Overall Sound Pressure Level (OASPL) as function of drag for two Reynolds number $3e6$ and $4.5e6$.

noise and drag as expected from the initial hypothesis.

4. Discussion

A significant uncertainty in the analysis is the observed variation with angle of attack. Hutcheson et al. also observed AoA variations in their wind tunnel campaign, with an increase in low-frequency noise due to a thicker boundary layer on one side and a thinner one on the other [28]. There is an asymmetry between the boundary layers on the suction side and pressure side that is not captured by the velocity deficit and, consequently, the δ^* scaling. We observe the same effect, but scaling with the displacement thickness does not collapse all the data. This indicates that different scales of turbulence are responsible for trailing edge noise emission in different frequency ranges, but not all of them scale with the displacement thickness. The so-called BPM study [27] introduced an empirical angle of attack term to compensate for this limitation. One obvious drawback of using δ^* , or any other measure of boundary layer thickness, is the lack of information about the frequency content. It is possible to imagine two different boundary layers with the same δ^* but completely different spectra. In this domain, where there is a lack of knowledge about leading-edge erosion and noise, it would be beneficial to address and model the effects of LEE on the spectral level. This is also an issue with the overall sound pressure level metric, since it cannot be used directly to model sound emission from a wind turbine, which requires a frequency spectrum to correctly account for propagation and air absorption. The use of zig-zag tape and sandpaper as a proxy for LEE does not accurately represent actual erosion, as reported by several studies. It was observed that zig-zag tape and P400 sandpaper exhibited very similar aerodynamic and acoustic performance. Interestingly, they force flow transition in different ways; zig-zag tape has both forward-facing and backward-facing steps, while sandpaper, which covers the full leading edge, only has a backward-facing step. Is the observed drag increase a consequence of the step or the actual change in roughness, and at what limit does it change? With additional data and more realistic erosion damage, it might be possible to better answer this question.

5. Conclusion

Multiple wind tunnel campaigns using aerodynamic and acoustic test section configurations were conducted on an FFA-W3-211 airfoil at Reynolds numbers from $1.8e6$ to $6e6$, using four different surface conditions: clean, zig-zag tape, and two types of sandpaper to model leading-edge erosion. The drag was calculated

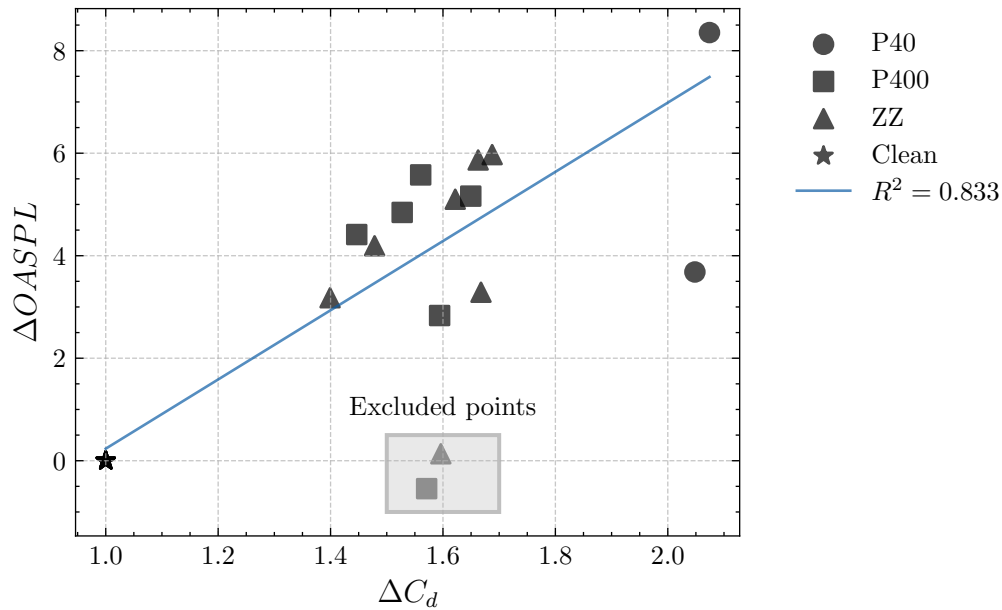


Figure 10 $\Delta OASPL$ increase as function of drag increase (relative to clean) for Reynolds numbers $3e6$ and $4.5e6$ and AoA_{eff} from 5 to 9 degrees. A linear regression line is also shown and two points excluded from the regression.

from a wake rake in the aerodynamic setup, and the far-field noise was captured using a microphone array in the acoustic setup. The combined measurement dataset was scaled by the Strouhal number, using the displacement thickness δ^* , calculated from the wake-rake velocity deficit. The presented data scales consistently according to the physical laws derived from classical aeroacoustic theory, i.e., the M_∞^5 law. The scaling provided good agreement of measurements across Reynolds numbers but failed to capture the angle of attack dependence. Using a subset of the data, a linear regression analysis was performed, revealing a simple relationship between the overall noise increase and drag increase with a correlation of $R^2 = 0.833$. This result can be used at a high level to guide the need for maintenance and calculate approximate annual energy production losses. Note that the data basis is limited to one airfoil shape, and more experimental data are needed to validate the generality of the findings. This study has provided methodological advances toward understanding the effects of leading-edge erosion on noise. Future studies can use these methods to evaluate real erosion cases, preferably with detailed information about boundary layer thickness and its spectra. Additionally, other airfoil models should be tested to validate the findings of this study.

Acknowledgments

We are grateful for the dedicated work by wind tunnel engineers Jimmie Beckerlee, Sigurd Ildvedsen, and Theis Lak Aarup, who conducted many of the wind tunnel tests needed to prepare this manuscript. We also thank Alexander M. Forsting for his valuable comments.

The present work is conducted as part of the project LERCat - Leading Edge Roughness Categorisation supported by the EUDP project Jr. nr. 64021-2027 funded by the Danish Energy Agency (Energistyrelsen).

References

- [1] A. Sareen, C. A. Sapre, and M. S. Selig, "Effects of leading edge erosion on wind turbine blade performance," *Wind Energy*, vol. 17, pp. 1531–1542, 10 2014.
- [2] R. Herring, K. Dyer, F. Martin, and C. Ward, "The increasing importance of leading edge erosion and a review of existing protection solutions," *Renewable and Sustainable Energy Reviews*, vol. 115, 11 2019.
- [3] J. Visbeck, T. Göçmen, S. Özçakmak, A. M. Forsting, Hannesdóttir, and P.-E. Réthoré, "Aerodynamic effects of

- leading-edge erosion in wind farm flow modeling,” *Wind Energ. Sci*, vol. 9, pp. 1811–1826, 2024.
- [4] M. H. Keegan, D. H. Nash, and M. M. Stack, “On erosion issues associated with the leading edge of wind turbine blades,” *Journal of Physics D: Applied Physics*, vol. 46, 9 2013.
- [5] L. Mishnaevsky, C. B. Hasager, C. Bak, A.-M. Tilg, J. I. Bech, S. Doagou Rad, and S. Fæster, “Leading edge erosion of wind turbine blades: Understanding, prevention and protection,” *Renewable Energy*, vol. 169, pp. 953–969, 5 2021.
- [6] C. Bak, A. M. Forsting, and N. N. Sorensen, “The influence of leading edge roughness, rotor control and wind climate on the loss in energy production,” *Journal of Physics: Conference Series*, vol. 1618, 9 2020.
- [7] C. Bak, “A simple model to predict the energy loss due to leading edge roughness,” *Journal of Physics: Conference Series*, vol. 2265, 5 2022.
- [8] S. Özçakmak, D. Bretos, B. Méndez, and C. Bak, “Determination of annual energy production loss due to erosion on wind turbine blades,” *Journal of Physics: Conference Series*, vol. 2767, 6 2024.
- [9] OpenFAST Developers, “Openfast,” <https://github.com/OpenFAST/openfast>, 10.5281/zenodo.6324287, 2024.
- [10] A. Meyer Forsting, A. Olsen, M. Gaunaa, C. Bak, N. Sørensen, J. Madsen, R. Hansen, and M. Veraart, “A spectral model generalising the surface perturbations from leading edge erosion and its application in CFD,” *Journal of Physics: Conference Series*, vol. 2265, 5 2022.
- [11] N. Gaudern, “A practical study of the aerodynamic impact of wind turbine blade leading edge erosion,” *Journal of Physics: Conference Series*, vol. 524, 6 2014.
- [12] D. C. Maniaci, C. Westergaard, A. Hsieh, and J. A. Paquette, “Uncertainty Quantification of Leading Edge Erosion Impacts on Wind Turbine Performance,” *Journal of Physics: Conference Series*, vol. 1618, 9 2020.
- [13] Y. Zhang, F. Avallone, and S. Watson, “Leading edge erosion detection for a wind turbine blade using far-field aerodynamic noise,” *Applied Acoustics*, vol. 207, 5 2023.
- [14] H. Wang and B. Chen, “Investigation on aerodynamic noise for leading edge erosion of wind turbine blade,” *Journal of Wind Engineering and Industrial Aerodynamics*, vol. 240, 9 2023.
- [15] R. Amiet, “Noise due to turbulent flow past a trailing edge,” *Journal of Sound and Vibration*, vol. 47, pp. 387–393, 8 1976.
- [16] A. M. Forsting, A. Olsen, N. Sørensen, A. Fischer, C. Markussen, and C. Bak, “An aerodynamic digital twin of real-world leading edge erosion: Acquisition, generation and 3d cfd,” *Journal of Physics: Conference Series*, vol. 2767, jun 2024.
- [17] W. J. Devenport, R. A. Burdisso, A. Borgoltz, P. A. Ravetta, M. F. Barone, K. A. Brown, and M. A. Morton, “The Kevlar-walled anechoic wind tunnel,” *Journal of Sound and Vibration*, vol. 332, no. 17, pp. 3971–3991, 2013.
- [18] W. Devenport, C. Bak, K. Brown, A. Borgoltz, J. Osterlund, P. Davidsson, and S. T. O, “Design and Operation of Hybrid Aeroacoustic Wind Tunnels,” in *Design and Operation of Aeroacoustic Wind Tunnel Tests for Group and Air Transport*, vol. STO-EN-AVT, 1 2017.
- [19] A. Fischer, C. Bak, O. Lylloff, A. S. Olsen, R. F. Mikkelsen, S. B. Ildvedsen, J. S. Beckerlee, A. Borgoltz, M. Kuester, and N. Intaratep, “Cross validation of the aerodynamic and acoustic measurements in two Kevlar-walled wind tunnels,” *Journal of Physics: Conference Series*, vol. 2265, 5 2022.
- [20] T. Brooks and W. Humphreys, Jr., “Effect of directional array size on the measurement of airframe noise components,” in *5th AIAA/CEAS Aeroacoustics Conference and Exhibit*, no. 99, (Reston, Virginia), American Institute of Aeronautics and Astronautics, 5 1999.

- [21] P. Sijtsma, “Phased Array Beamforming Applied to Wind Tunnel And Fly-Over Tests,” in *SAE Technical Papers*, 10 2010.
- [22] O. Lylloff, “AeroAcoustics.jl: A Julia package for aeroacoustics,” *Journal of Open Source Software*, vol. 9, p. 6390, 5 2024.
- [23] A. Fischer, O. Lylloff, E. Fernandez Grande, and C. Bak, “Analytical corrections for acoustic transmission in kevlar-walled wind tunnels,” *AIAA Journal*, vol. 61, no. 7, pp. 3119–3133, 2023.
- [24] A. S. Olsen, N. N. Sørensen, C. Bak, M. Gaunaa, R. Mikkelsen, A. Fischer, J. Beckerlee, and S. Ildvedsen, “Why is the measured maximum lift in wind tunnels dependent on the measurement method?,” *Journal of Physics: Conference Series*, vol. 1618, sep 2020.
- [25] B. Jones, *The Measurement of Profile Drag by the Pitot-traverse Method*. Aeronautical Research Committee. Reports and memoranda, H.M. Stationery Office, 1936.
- [26] J. Anderson, John D., *Fundamentals of Aerodynamics*. New York, NY: McGraw-Hill Education, 6 ed., 2017.
- [27] T. F. Brooks, D. Pope, and M. A. Marcolini, “Airfoil self-noise and prediction,” *Nasa Reference Publication*, no. 1218, 1989.
- [28] F. V. Hutcheson and T. F. Brooks, “Effects of Angle of Attack and Velocity on Trailing Edge Noise Determined Using Microphone Array Measurements,” *International Journal of Aeroacoustics*, vol. 5, pp. 39–66, 1 2006.

Paper #14 - ID: 348

Title: Overview of the results of the PIBE project (Predicting the Impact of wind turbine noise)

Author: David Ecotiere

11th Edition of the
International Conferences on
Wind Turbine Noise

Copenhagen, Denmark – 10th to 13th June 2025

Overview of the results of the PIBE project (Predicting the Impact of wind turbine noise)

D. Ecotière¹

UMRAE, Cerema, Gustave Eiffel University, 11 Rue Jean Mentelin, 67200, Strasbourg, France

B. Gauvreau

UMRAE, Gustave Eiffel University, Cerema, Allée des ponts et chaussées, 44340, Bouguenais, France

B. Cotté

IMSIA, ENSTA Paris, 91120 Palaiseau , France

M. Roger

LMFA, École Centrale de Lyon, Université de Lyon 69131 Écully, France

I. Schmich-Yamane

EDF-DTG, 38950 Saint-Martin-le-Vinoux, France

F. Junker

EDF-Renewables, 92932 Paris La Défense, France

Summary

The PIBE project aimed to improve wind turbine noise prediction methods and to explore new solutions for noise reduction. This five years project (2019-2024) brought together French experts in aeroacoustics, sound propagation, experimental noise characterization and wind engineering, and was structured around three work packages. The first one aimed to study amplitude modulation phenomena and focused particularly the characterization of dynamic stall noise. Specific aerodynamic and acoustic measurements were carried out in a wind tunnel, showing the influence of several stall regimes on noise production. The second work package focused on quantifying the uncertainties due to variabilities of environmental parameters of noise prediction methods. It developed an open-access online application (WindTUNE) that quantifies uncertainties on noise prediction of a wind farm, and a parametric and uncertainties calculation tool for the engineering application Code-TYMPAN. This work package also produced a large open-access database of a 410 days campaign of meteorological and acoustical measurements around a wind farm. The last work package investigated new noise reduction solutions based on modified leading and/or trailing edges. The efficiency of these solutions were characterized in a wind tunnel, both acoustically and

¹ Corresponding author – Email: david.ecotiere@cerema.fr

aerodynamically. The paper presents the main results obtained at the end of the project. A specific focus is made on the outcomes freely available online.

1. Introduction

Wind power is one of the energy sources contributing to the energy transition needed to combat climate change, but despite a strong growth in the sector in recent decades, it sometimes faces opposition from wind farm neighbours who often cite noise as a potential nuisance. In this context, first French collaborative research project on wind turbine noise (WTN), the PIBE project (2019-2024) aimed to improve prediction methods for WTN and to explore new solutions for noise reduction [1]. The project was structured in three work packages (WP). The first one studied the amplitude modulation phenomena of WTN, which is known to be a possible source of annoyance when they occur. The second one focused on quantifying the variability of noise predictions and its associated uncertainties. The last one aimed to study and propose new noise reducing devices, using blades with modified leading and/or trailing edges.

2. WP 1: characterizing the amplitude modulation phenomena

Local stall can occur on wind turbine blades during the upper part of the rotation when a strong wind shear or another source of inhomogeneous inflow, such as yaw or topography, occurs. Periodic separation and reattachment of the boundary layer can then appear on the wind turbine blade suction side during its rotation. Stall noise is then associated with a strong low-frequency increase that could explain the strong amplitude modulations of WTN that are commonly observed around wind farms. WP1 aimed to characterize dynamic stall noise in controlled conditions. It investigated noise created by a pitching airfoil for which the origin of the noise is not clearly identified compared to static airfoil. Some experiments were conducted in an anechoic wind tunnel on a NACA 0012 airfoil equipped with pressure taps, and NACA 633-418 airfoil, more representative of the outer part of wind turbine blades, both in the static and dynamic regimes, with synchronous acoustic and flow measurements. The airfoil was placed facing the flow at an oscillating plate (Figure 1:-a) and several microphones recorded the far-field noise radiation, while pressure sensors measured steady and fluctuating wall pressures at the airfoil surface. Figure 1-b shows an example of noise radiation for an airfoil oscillating at the frequency f_0 , a flow speed $U=50\text{m/s}$ and for reduced frequency $k=\pi f_0 c/U=0.01$. The results exhibit specific noise regimes corresponding to several types of flow boundary layer separation around the airfoil, and to an hysteretic evolution of the lift coefficient of both the oscillating airfoil and static airfoil cases (Figure 1-c). The database of experimental data (flow and acoustic measurements) is available online [2] (see [3][4] for more details about WP1 results).

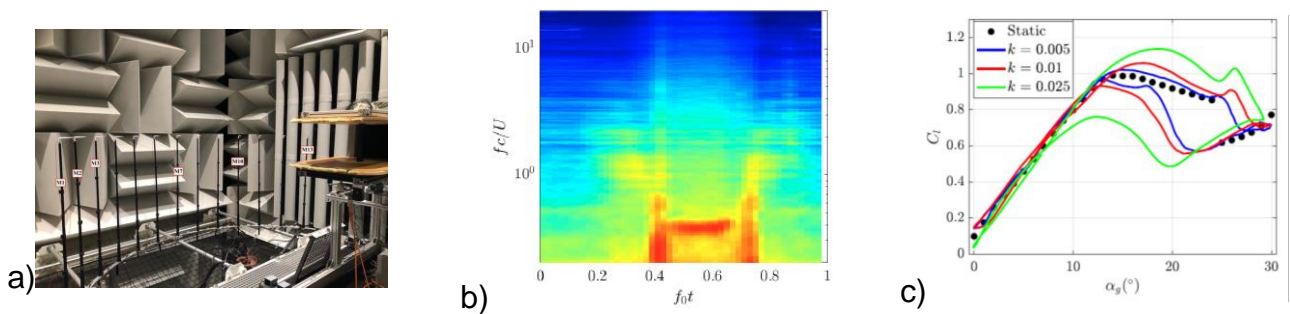


Figure 1 a) Experimental setup in an anechoic openjet facility ; b) phased-averaged spectrograms of acoustic pressure ($k=0.01, U=50\text{m/s}$) ; c) phased-averaged lift coefficient for the oscillating airfoil at different reduced frequencies k ($U=50\text{m/s}$) and angles of attack α_g .

3. WP 2: estimating the variability of wind turbine noise

Atmospheric and ground properties influence sound propagation. The aim of WP2 was to study the variability and uncertainties due to the temporal fluctuations of these phenomena on the estimation of the sound pressure level (SPL) at local residents. Two approaches were adopted in the project (more details about WP2 results can be found in [5]).

The first one consisted in collecting and building up a large experimental database thanks to a 410 days long-term measurements campaign near a French wind farm [6]. 57 million sound levels and 100ms acoustic spectra [6.3 Hz; 20kHz] have been collected at 5 locations from 350m to 1.3km to the wind farm, together with 10min meteorological data (wind, temperature, turbulence) and wind turbines operational data (production, blades settings...). Two supplementary 10 days observation periods at two seasons included additional devices. The data have been put available online [7].

The second approach was to develop two models capable of estimating the variability and uncertainties of noise prediction, one based on a precise physical model, while the other is based on an engineering model. The two methods consists in modelling noise levels at receiver for many scenarios of influent input parameters thanks to a quasi-Monte Carlo sampling that enables to build the probability density function (PDF) of the SPL induced by of uncertain or fluctuating input parameters. The physical model developed in the project results from the coupling of an emission model [8] and a Wide-Angle Parabolic Equation (WAPE) propagation model [9][10][11]. It has been experimentally validated satisfactorily against the field measurements collected during the long-term campaign [5][12]. In order to get a fast model suitable to the Monte Carlo process, that requires thousands of simulations at prohibitive calculation costs, a metamodel was trained with a set composed of SPL maps calculated from the physical model and generated via a Latin-Hypercube-Sampling design in the space of input parameters. This metamodel has been finally implemented in the web application WindTUNE [13][17] developed during the project, that allows to estimate uncertainties of WTN prediction [14][15]. The second approach to quantify SPL dispersion of WTN was done by means of a numerical design of experiment using a Parametric Calculation Tool based on an engineering open-source software of noise prediction [16].

4. WP3: reducing noise emission at the blades

WP3 focused on research of devices that minimize the aerodynamic noise emission. Trailing-edge serrations, and leading-edge modified as tubercles or wavy shape, are recognized as mitigation means for the broadband and/or tonal noise of airfoils. However, their application to large wind turbines seems to be very rare. WP3 carried out experiments to assess both technologies on a NACA-0012 in static and dynamic stall conditions, following a similar protocol as described at section 2. Various versions of the baseline and modified NACA 633-418 airfoil have been 3D-printing manufactured (Figure 2-a).

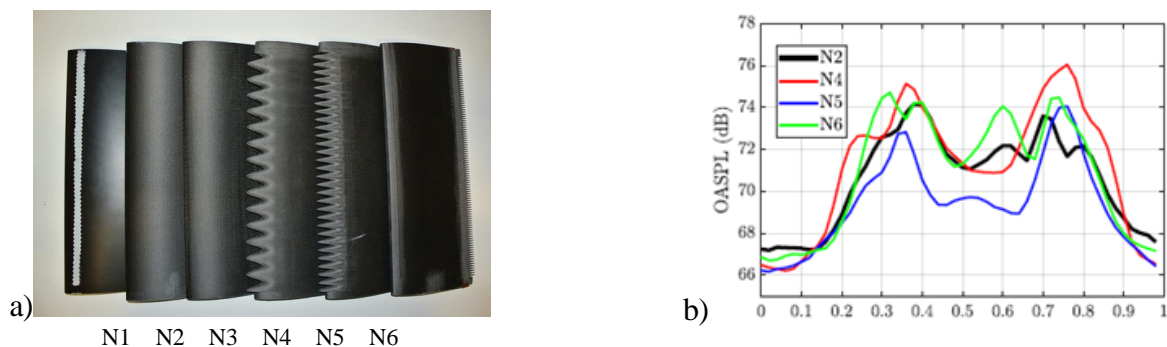


Figure 2 a) Baseline (N1) and modified versions of the NACA-0012 used in the experiment ; b) Cyclic time variations of the filtered OASPL [75 Hz-1kHz] (microphone in the orthogonal plane to the flow direction).

A clear overall reduction of the noise pattern was found (Figure 2-b) with the smaller-wavelength tubercles of the airfoil of wavy leading-edge and serration wavelength 10mm (N5), making this design a promising

candidate for noise mitigation in applications. In particular, lower-noise region is formed between the comparatively louder events at separation and at reattachment [3].

5. Conclusions

The outcomes of the projects are multiple [17] and provide a better understanding of WTN emission and propagation, and on the potentiality of new noise reducing solutions: model for predicting WTN propagation, a database of experimental data on the wind tunnel characterization of noise due to dynamic stall at blades, a database of experimental acoustical and meteorological data around a wind farm, a web application for estimating the uncertainties of WTN, a package to estimate the uncertainties of noise prediction on an engineering software, investigations of new solutions for reducing WTN emissions.

Acknowledgments

This research was funded by the French National Agency for Research (contract ANR-18-CE04-0011). The Carnot Climadapt Institute of Cerema co-funded some experimental equipments.

Many thanks to A. Alarcon, S. Bianchetti, R. Boittin, L. Brendel, V. Gary, G. Guillaume, E. Jondeau, B. Kayser, B. Lafoux, H. Lefèvre, G. Litou, D. Mascarenhas, R. Monchaux, M.C. Nessi, A. Notarantonio, D. Raus, J. Ripolles, L. Ségaud, T. Thénint, M. Tonelli, P. Souchotte and L. Sicard for their contribution to this project.

References

- [1] PIBE website. <https://www.anr-pibe.com/en>. Last accessed 2025-04-01.
- [2] <https://zenodo.org/records/10638882>, Last accessed 2025-04-01.
- [3] B. Cotté, L. Sicard, R. Monchaux, E. Jondeau, P. Souchotte, and M. Roger. Experimental characterization of stall noise on a pitching wind turbine blade section. In: Proc. Inter-Noise. Nantes, France, 2024.
- [4] D. Raus, B. Cotté, R. Monchaux, E. Jondeau, P. Souchotte, and M. Roger. Experimental study of the dynamic stall noise on an oscillating airfoil. *J. Sound Vib* 537, 117-144, 2022.
- [5] B. Gauvreau, A. Alarcon, S. Bianchetti, R. Boittin, L. Brendel, B. Cotté, V. Gary, G. Guillaume, F. Junker, B. Kayser, H. Lefèvre, G. Litou, D. Mascarenhas, J. Ripolles, I. Schmich-Yamane, and D. Ecotière, 2024. Uncertainties in numerical predictions and experimental characterization of wind farm noise. In: Proc. Inter-Noise. Nantes, France, 2024.
- [6] D. Ecotière, B. Gauvreau, I. Schmich-Yamane, A. Alarcon, M.C. Nessi, F. Junker, G. Guillaume, V. Gary, L. Brendel, G. Litou, R. Boittin, L. Segaud, and H. Lefèvre. A large-scale, long-term experimental campaign for the investigation of wind turbine noise fluctuations and amplitude modulation phenomena. In *Proceedings of Inter-Noise 2022*, Glasgow, U.K., 2022.
- [7] G. Guillaume, B. Cotté, D. Ecotière, B. Gauvreau, H. Lefèvre, F. Junker and I. Schmich-Yamane. Development and distribution of an in situ experimental wind turbine noise database. In: Proc. Inter-Noise, Nantes, France, 2024.
- [8] B. Cotté. Extended source models for wind turbine noise propagation. *J. Acoust. Soc. Am.* 145, 1363-1371, 2019.
- [9] B. Kayser, Open access of a wide-angle parabolic equation model for sound propagation in a moving atmosphere above an absorbing and rough ground. In *Proceedings of Forum Acusticum*, Torino, Italy, 2023
- [10] B. Kayser, D. Mascarenhas, B. Cotté, D. Ecotière, and B. Gauvreau. Validity of the effective sound speed approximation in parabolic equation models for wind turbine noise propagation. *J. Acoust. Soc. Am.* **153**, pages 1846–1854, 2023.
- [11] B. Kayser, D. Écotière and B. Gauvreau. Criteria for the assessment of the influence of atmospheric turbulence on wind turbine noise propagation. *Acta Acustica* **7**, 63, 2023.
- [12] B. Cotté, D. Mascarenhas, D. Ecotière, G. Guillaume, B. Gauvreau and F. Junker. Validation of a wind turbine noise propagation model against field measurements. In *Proceedings of Forum Acusticum*, Torino, Italy, 2023
- [13] Kayser, B., Bianchetti, S., Ecotière, D., Gauvreau, B., 2023. WindTUNE: a new tool for modelling wind farm noise uncertainties, in: Proc. Wind Turbine Noise, Dublin, Ireland.
- [14] B. Kayser, B. Gauvreau, B., D. Ecotière, and V. Mallet. Wind turbine noise uncertainty quantification for downwind conditions using metamodeling. *J. Acoust. Soc. Am.* **151(1)**, pages 390 – 402, 2022.
- [15] S. Bianchetti, B. Kayser, G. Guillaume, B. Gauvreau, A. Notarantonio, F. Junker, D. Ecotière. Variability and uncertainty of wind farm noise: A comparison between numerical predictions and in-situ measurements. In

Proceedings of Forum Acusticum, Torino, Italy, 2023.

[16] J. Ripolles, T. Thénint and I. Schmich-Yamane. Introducing uncertainties in acoustic engineering studies. In Proc. Inter-Noise, Nantes, France, 2024.

[17] <https://www.anr-pibe.com/projet/productions>. Last accessed 2025-01-31.

Paper #15 - ID: 349

Title: Modifications to BPM model to incorporate trailing edge noise reduction by porous add-ons

Author: Marco Caboni

11th Edition of the
International Conferences on
Wind Turbine Noise
Copenhagen, Denmark – 10th to 13th June 2025

Adjustments to Brooks, Pope, and Marcolini’s model to incorporate trailing edge noise mitigation add-ons for wind turbine blades

Marco Caboni¹, Akshay Koodly Ravishankara and Koen Boorsma
TNO, Wind Energy Technology, Westerduinweg 3, 1755 LE Petten, The Netherlands

Summary

This study introduces a straightforward modification to the widely utilized Brooks, Pope, and Marcolini model to include trailing edge noise reduction add-ons for wind turbine blades. The method involves fine-tuning specific model parameters using wind tunnel data. The findings show that this approach can accurately replicate the experimental noise spectra, including peak Strouhal number, shape, and level. Additionally, our validation against two sets of experimental measurements of conventional airfoils showed that the noise component introduced by Brooks and colleagues, which accounts for noise behavior as a function of the angle of attack, results in poorer simulation outcomes. Indeed, we observed that the experimental sets used by Brooks et al. to develop their model display different noise behavior with varying angles of attack compared to the two datasets we utilized. Including the angle of attack dependent source term led to poorer predictions across all cases in the two datasets we analyzed.

1. Introduction

Wind turbine noise is a disadvantage that hinders the deployment of onshore wind turbines. Regulations are in place to limit people’s exposure to this noise. To comply with these regulations, wind turbine operators often reduce rotor speed, which decreases noise but also lowers energy production. To enhance the commercial appeal of their turbines, manufacturers must consider noise during the design phase, balancing performance and noise emission. The boundary layer turbulence passing the trailing edge is considered the primary noise source for wind turbine applications [1]. To further improve noise reduction, various trailing edge add-ons, including serrations, brushes, fences and extensions with permeable and elastic materials, have been developed [2]. The design of wind turbine blades depends on fast engineering methods that model blade noise, including trailing edge noise reduction add-ons.

For conventional blades, noise modeling ranges from simple empirical one-equation models to computational aeroacoustic simulations that capture both the flow field and acoustic disturbances around wind turbine blade [3]. A balance between accuracy and computational effort can be achieved with semi-empirical methods, which segment wind turbine blades and treat them as two-dimensional airfoil sections that generate sound sources [4, 5]. The Brooks, Pope, and Marcolini (BPM) model [6] is the most widely used in industrial practice for predicting these sectional sources. Brooks and colleagues developed semi-empirical models to predict airfoil self-noise, utilizing both theoretical studies and acoustic measurement data. The modeled noise mechanisms encompassed turbulent boundary layer trailing edge (TBL-TE) noise, laminar boundary layer vortex shedding noise, separation stall noise, trailing edge bluntness vortex shedding noise, and tip

¹Corresponding author - Email: marco.caboni@tno.nl

vortex formation noise.

Only a limited number of studies have explored quick engineering modeling techniques for trailing edge mitigation add-ons. Notably, Mayer *et al* [7] and Lyu and Ayton [8] developed rapid noise prediction models for serrated trailing edges using new analytical formulations. Wang *et al* [9] developed a semi-empirical model for predicting rotor noise, which includes blade add-ons. The model relies on spectral corrections that were calibrated using wind and field measurements, as well as computational aeroacoustics simulations.

This paper aims to present a straightforward method for modifying the widely used BPM model to incorporate the effects of generic trailing edge noise mitigation add-ons for wind turbine blades, for which wind tunnel data is available. The methodology involves fine-tuning certain BPM parameters to align the model output with wind tunnel data.

2. Methods

2.1 Brooks, Pope, and Marcolini's model for turbulent boundary layer trailing edge noise

Brooks *et al* [6] developed shape and amplitude functions to describe the 1/3-octave spectral characteristics of the TBL-TE noise mechanism. Mirroring the behavior of the measurements shown in the example in Figure 1, the modeled spectra display a concave down, parabola-like shape, defined by a peak frequency (or Strouhal number), shape, and level. Brooks *et al* [6] empirically derived the spectral shape and amplitude functions from an extensive database of acoustic measurements conducted on various NACA-0012 airfoil blade sections with different chords, Mach and Reynolds numbers, and angles of attack.

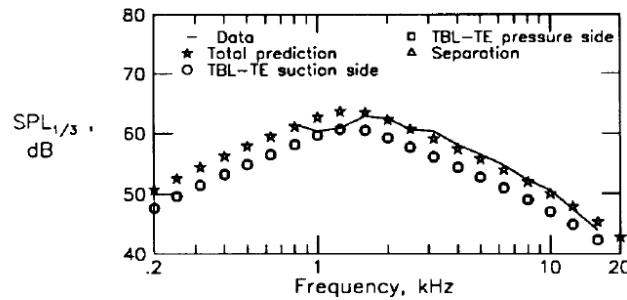


Figure 1 Example of comparison between measured and predicted spectra of turbulent boundary layer trailing-edge noise. Image reproduced from Brooks *et al* [6].

The derivation of the BPM model for turbulent boundary layer trailing edge noise, as described by Brooks *et al* [6], began with calculating a scaled sound pressure level for each experimental condition from the referenced database. This is done by subtracting a semi-empirical scaling function, which is based on the analysis by Ffowcs Williams and Hall *et al* [10], from the total sound pressure level, as follows:

$$\text{Scaled SPL}_{(1/3)} = \text{SPL}_{(1/3)} - 10 \log \left(\frac{\delta_s^* M^5 L}{r_e^2} \right) \quad (1)$$

As seen in Eq. (1), the scaling function is proportional to the fifth power of the Mach number (M), the trailing edge boundary layer displacement thickness on the suction side (δ_s^*), and the span-wise length wetted by the flow (L), while being inversely proportional to the square of the observer distance (r_e). The relationship between the scaling function and the fifth power of velocity has been confirmed in several studies Brooks *et al* [6]. Brooks and his colleagues used Eq. (1) to calculate scaled spectra for various experimental conditions, including different Mach and Reynolds numbers, as well as angles of attack. If the scaling function alone could account for noise variations due to these factors, then all the scaled levels for the different conditions would converge in a single scaled spectra. However, this was not the observed behavior.

The scaled spectra did not converge into a single profile. Therefore, Brooks et al. introduced additional shape and amplitude functions to complement the scaling function and better match the experimental results.

The derivation of the spectral shape and amplitude functions was intended to model the measured scaled spectra based on variations in the free-stream velocities, Reynolds numbers, and angles of attack. The scaled spectra, according to Eq. (1), were initially modeled for scenarios with a zero angle of attack and varying free-stream velocities and Reynolds numbers. Two equations, including the scaling function from Ffowcs Williams and Hall and tuned shape and amplitude functions, were introduced to account for equal contributions of the pressure and suction sides to the total spectrum, assuming that each side of an airfoil produces TBL-TE noise independently. However, the shape and amplitude functions developed for a zero angle of attack were found to misrepresent the scaled spectral behavior in cases with varying angles of attack. Indeed, according to the zero angle of attack shape and amplitude functions, with an increasing angle of attack, the scaled peak Strouhal number would remain constant, the scaled peak level would decrease, and the scaled spectral shape would broaden at the peak. The experiments showed the opposite behavior. To compensate for this, Brooks, Pope, and Marcolini developed an additional angle-dependent noise component, using different shape and amplitude functions, which these authors referred to as “separated boundary layer noise contribution”. Although labeled as a “separated boundary layer noise contribution”, this component was intended to be active for non-zero angles of attack, including those well below the threshold for trailing edge separation

Thus, based on the BPM model, the total TBL-TE and separation noise spectrum in a 1/3-octave presentation is calculated, as detailed in Eq. (2), by adding the noise contributions at zero angle of attack from the pressure side (Eq. (3)) and the suction side (Eq. (4)), as well as the angle-dependent noise contribution (Eq. (5)).

$$\text{SPL}_{\text{TOT}} = 10 \log(10^{\text{SPL}_\alpha/10} + 10^{\text{SPL}_s/10} + 10^{\text{SPL}_p/10}) \quad (2)$$

$$\text{SPL}_p = 10 \log\left(\frac{\delta_p^* M^5 L \bar{D}_h}{r_e^2}\right) + A\left(\frac{\text{St}_p}{\text{St}_1}\right) + (K_1 - 3) + \Delta K_1 \quad (3)$$

$$\text{SPL}_s = 10 \log\left(\frac{\delta_s^* M^5 L \bar{D}_h}{r_e^2}\right) + A\left(\frac{\text{St}_s}{\text{St}_1}\right) + (K_1 - 3) \quad (4)$$

$$\text{SPL}_\alpha = 10 \log\left(\frac{\delta_s^* M^5 L \bar{D}_h}{r_e^2}\right) + B\left(\frac{\text{St}_s}{\text{St}_2}\right) + K_2 \quad (5)$$

The individual contributions to the total noise spectrum are determined by the aforementioned scaling function derived from the analysis by Ffowcs Williams and Hall *et al* [10], spectral shape functions (A and B), and amplitude functions (K_1 , K_2 and ΔK_1). The spectral shape functions depend on the ratio of the Strouhal numbers (St_p and St_s) to their peak values (St_1 and St_2) and the Reynolds number. Figure 2 depicts the shape function A , characterized by a concave downward parabolic shape that is symmetrical around $\text{St}/\text{St}_{\text{peak}} = 1$. The width of this shape varies with the Reynolds number. Indeed, the shape functions are provided for both the maximum and minimum Reynolds numbers, as available from the experiments used to develop this function. Interpolation is required to determine the shape function for any given Reynolds number.

2.2 Parameterization of Brooks, Pope, and Marcolini’s model for turbulent boundary layer trailing edge noise

The aim of this work is to largely retain the equation structure of the BPM’s TBL-TE noise model, developed for conventional airfoil shapes, and adjust some of its parameters to model the noise of airfoils with noise mitigation add-ons. As explained in the validation section reported below, we found that better results are obtained by omitting the aforementioned angle-dependent noise contribution. Therefore, Eq. (5) was excluded from the equation structure, relying solely on Eq. (3) and Eq. (4).

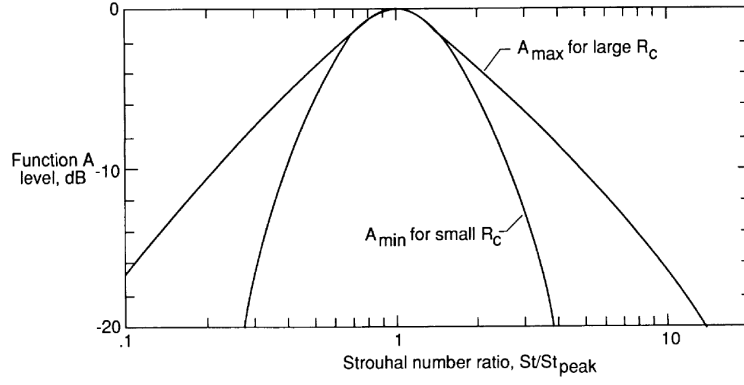


Figure 2 Spectral shapes A as functions of the ratio of the Strouhal number to its peak and Reynolds number. Image reproduced from Brooks et al [6].

The BPM's TBL-TE noise model defines the spectral shape using shape functions, such as the one shown in Figure 2. This spectral shape was empirically determined using measurements on a conventional airfoil. To capture the spectral shapes of airfoils with noise mitigation add-ons, we modified the original spectral function by defining an alternative spectral function using Eq. (6):

$$A = -20 \left(\log \left(\frac{St}{St_{peak}} \right) I^{-1} \right)^e \quad (6)$$

where I is the value of St/St_{peak} at $A = -20$ dB, and e is the function's exponent. Thus the spectral function is parameterized by means of the parameters e and I . Figure 3 compares the original spectral function to the parameterized one. As mentioned above, the original BPM's TBL-TE noise model extrapolates the spectral function for the actual Reynolds number using two empirical spectral functions, A_{max} and A_{min} , respectively determined for the maximum Reynolds number and the minimum Reynolds number. Figure 3 shows the shape functions at the maximum and minimum Reynolds numbers, the interpolated shape function at a given Reynolds number, and the parameterized shape function determined to match the interpolated function as closely as possible. The comparison demonstrates that the parametric spectral function has good flexibility and effectively captures the original function. To capture the noise of airfoils with trailing edge add-ons, the

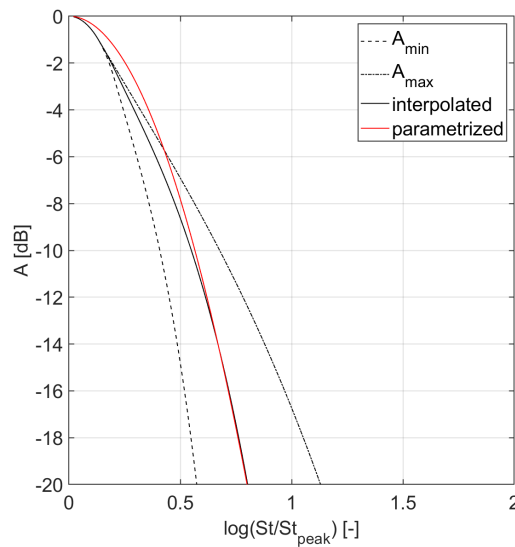


Figure 3 Spectral shape functions at the maximum and minimum Reynolds numbers, A_{max} and A_{min} , the interpolated shape function at a given Reynolds number, and the parameterized shape function.

spectral shape alone is not sufficient. The spectral peak Strouhal number and level also need to be modeled.

The spectral peak Strouhal number St_1 is directly a parameter in Eq. (3) and Eq. (4). The level is adjusted using the K_1 parameter, which in the original model is a function of the Reynolds number and also appears in Eq. (3) and Eq. (4). Since St_1 and K_1 are direct model parameters and the parametric spectral function can closely matches the original, as shown in Figure 3, the parametrization, with proper tuning of the parameters, is able to align with the original BPM model.

In summary, the proposed modification of the BPM's TBL-TE noise model is based on four parameters: e , I , St_1 and K_1 . Figure 4 illustrates the individual impact of these parameters on the predicted sound pressure level using a generic test case. The parameters e and I affect the broadness of the spectrum around its peak and the slope of the spectrum towards its peak. The parameter St_1 shifts the spectrum in the frequency direction (i.e., along the x-axis), while K_1 shifts it in the sound pressure level direction (i.e., along the y-axis).

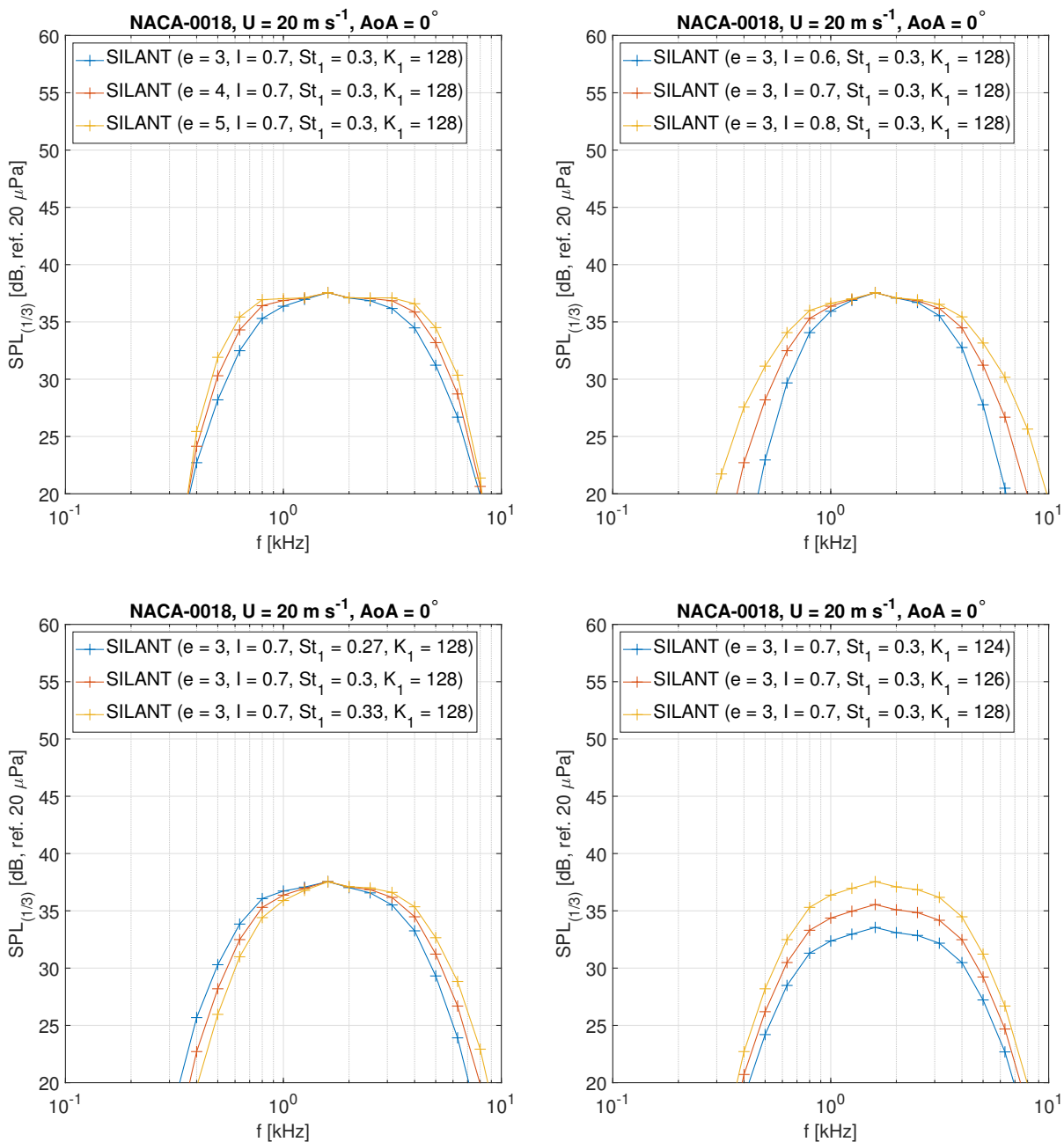


Figure 4 Individual impact of parameters e , I , St_1 and K_1 on the predicted sound pressure level.

3. Results

3.1 Validation of Brooks, Pope, and Marcolini's model for turbulent boundary layer trailing edge noise against the BANC database

The Benchmark Problems for Airframe Noise Computations (BANC) database [11–14] provides validation data for TBL-TE noise. The database include measurements from the Institute of Aerodynamics & Gas Dynamics (IAG) at the University of Stuttgart, DLR Braunschweig, the University of Florida (UFL) and Virginia Tech University (VTST). Table 1 summarizes the tested conditions. The NACA-0012 airfoil was utilized for the first four cases, the DU96-W-180 airfoil for case 5, and the NACA-64618 airfoil for cases 6 and 7. The boundary layer was tripped for cases 1 through 5, whereas cases 6 and 7 feature natural transition. Information on the tripping devices used for cases 1 through 5 is reported by Herr *et al* [11].

Table 1 Tested airfoils and conditions in the BANC testcase.

case	airfoil	U [m s ⁻¹]	AoA [°]
1	NACA-0012	56	0
2	NACA-0012	54.8	4
3	NACA-0012	53.0	6
4	NACA-0012	37.7	0
5	DU96-W-180	60.0	4
6	NACA-64618	45	-0.88
7	NACA-64618	45	4.62

Figure 5 illustrates the influence of the Mach number's power on the scaled 1/3-octave spectra for cases 1 and 4. Both cases involve the same NACA-0012 airfoil and a zero angle of attack, differing only in the free-stream velocity. The scaled levels are calculated according to Eq. (1), with the exponent of the Mach number ranging from 4 to 7. The displacement thickness on the suction side, as estimated with RFOIL [15] under experimental conditions, is used for normalization. Figure 5 illustrates that a better collapse of the scaled levels is achieved using an exponent of five, confirming the Ffowcs Williams and Hall scaling function, as used in the BPM's TBL-TE noise model, is proportional to the fifth power of the Mach number.

Figure 6 presents the scaled 1/3-octave spectra for cases 1, 2, and 3. These cases involve the same airfoil and roughly the same free-stream velocity (see Table 1) but differ in their angles of attack. The fifth power of the Mach number and the displacement thickness on the suction side, as estimated with RFOIL under experimental conditions, are used for normalization. It is observed that as the angle of attack increases, the peak Strouhal number rises, the peak level decreases, and the spectral shape broadens at the peak. This behavior is not consistent to the one observed by Brook and colleagues which they modeled with the aforementioned additional angle-dependent noise component. Indeed, Brooks and colleagues observed that as the angle of attack increases, the peak level rises, and the spectral shape becomes less broad at the peak. To emphasize once more, this analysis was performed on scaled spectra that already take into account Mach number and boundary layer thickness scaling.

Given that the behavior of scaled spectra for varying angles of attack differs between the BANC database and the BPM database, the BPM model should better align with the BANC cases when the angle-dependent noise contribution is excluded. To verify this, we examined the effect of including and excluding this contribution on the total sound pressure level using the BANC database.

Figure 7 and Figure 8 show comparisons between the experimental and simulated sound pressure levels for BANC test cases 1 through 7. Simulations are performed using two codes that implement the BPM's TBL-TE noise model: SILANT [16] and NAFNoise [17]. For both codes, we present the predicted total noise,

including and excluding the angle-dependent noise component. The results without the angle-dependent noise component are labeled as “noSPLalpha”. It is observed that the angle-dependent noise component results in an overestimation of the noise level (up to 5 dB) for the BANC cases with non-zero angles of attack. Better agreement is indeed achieved by omitting this component for cases 2, 3, and 7. In case 5, the experimental spectrum does not include the peak, making it impossible to assess whether the exclusion of the angle-dependent noise component led to better results.

Figure 9 presents the overall sound pressure levels for BANC cases 1 to 5. Omitting the angle-dependent noise component results in better agreement for all cases.

3.2 Modification of Brooks, Pope, and Marcolini’s model for trailing edge noise mitigation add-ons using the A-tunnel NACA-0018 database

In this section, we present the modification of the original BMP model to include the trailing edge noise mitigation of a confidential add-on, which was applied to the nominal NACA-0012 profile and acoustically measured in the A-tunnel at TU Delft. During the same campaign, measurements were also conducted on the nominal NACA-0012 airfoil. Figure 10 shows the scaled spectra from measurements of the nominal airfoil and one with the trailing edge noise mitigation add-ons. Because the trailing edge boundary layer displacement thickness remains unaffected by the add-ons, RFOIL is utilized to determine this thickness for both the nominal airfoil and the one with add-ons. In both cases, as the angle of attack increases, the peak Strouhal number rises, the peak level decreases, and the spectral shape broadens at the peak. This behavior is consistent with the observations reported above for the BANC cases.

Figures 11 and 12 present comparisons between the experimental and simulated sound pressure levels for angles of attack from zero to ten degrees. Simulations are performed using SILANT. The predicted total noise, both including and excluding the angle-dependent noise component, is shown. The results without the angle-dependent noise component are labeled as ‘noSPLalpha’. It is observed that the angle-dependent noise component leads to an overestimation of the noise level for cases with non-zero angles of attack. As seen with the BANC cases, better agreement is achieved by omitting this component.

The four previously mentioned parameters were adjusted to closely match the measured 1/3-octave spectra of the airfoil with trailing edge noise mitigation add-ons to the modeled spectra. Figures 11 and 12 illustrate the strong agreement between the experimental and simulated spectra for airfoils with noise mitigation add-ons, achievable through parameter tuning. Figure 13 shows the values of the model parameters as a function of the angle of attack. The experiment demonstrates that as the angle of attack increases, the spectral shape broadens, which is reflected by the rising values of e and I . The increase in peak frequency is captured by the rise in St_1 , while the reduction in level is achieved through the reduction in K_1 .

4. Conclusion

By adjusting its parameters, we successfully adapted the well-known turbulent boundary layer trailing edge noise model by Brooks et al., originally designed for conventional airfoils, to include the effects of trailing edge noise mitigation add-ons. We tuned the model parameters to match the model output with the acoustic measurement data obtained from airfoils equipped with add-ons. For airfoils with trailing edge noise mitigation add-ons, acoustic measurement data indicates that as the angle of attack increases, the scaled spectral peak Strouhal number rises, the scaled spectral peak level decreases, and the scaled spectral shape broadens at the peak. This behavior was captured by the original model through parameter adjustments. The acoustic dataset we used to adjust Brooks et al. model for trailing edge noise mitigation add-ons was limited, allowing us to investigate only variations due to changes in the angle of attack. Future work should aim to create a more comprehensive measurement dataset that includes free-stream velocity and the geometrical features of the add-ons.

Based on two acoustic measurement datasets for conventional airfoils, as the angle of attack increases, the scaled peak level decreases, and the scaled spectral shape broadens at the peak. This behavior contrasts with

the observations from the acoustic measurement dataset used to develop the original Brooks et al. model. To address this discrepancy, the Brooks et al. model was applied without the noise contribution designed to capture noise variations as a function of the angle of attack, resulting in a better match with the two aforementioned datasets. A more thorough examination is necessary to produce a guideline for the usage of this component of Brooks, Pope, and Marcolini's model.

Acknowledgments

Linked to the Blade Extensions for Silent Turbines (BEST) project, this research was supported by The Netherlands Enterprise Agency (RVO), part of the Dutch Ministry of Economic Affairs, under grant number HER+22-02-03415120.

References

- [1] S. Oerlemans, P. Sijtsma, and B. Méndez López, "Location and quantification of noise sources on a wind turbine," *Journal of Sound and Vibration*, vol. 299, no. 4, pp. 869–883, 2007.
- [2] S. Luesutthiviboon, *Assessing and improving trailing-edge noise reduction technologies for industrial wind-turbine applications*. Dissertation (tu delft), Delft University of Technology, 2022. Award date: 14 Oct 2022, Supervisors: M. Snellen, D. Ragni, Advisor: D.G. Simons.
- [3] P. J. Morris, L. N. Long, and K. S. Brentner, "An aeroacoustic analysis of wind turbines," in *42nd AIAA Aerospace Sciences Meeting and Exhibit*, (Reno, Nevada), American Institute of Aeronautics and Astronautics, January 2004.
- [4] K. Boorsma, J. Schepers, and P. N. Energy research Centre of the Netherlands ECN, "Enhanced wind turbine noise prediction tool silant," Jan. 2025.
- [5] F. Bertagnolio, H. A. Madsen, and A. Fischer, "A combined aeroelastic-aeroacoustic model for wind turbine noise: verification and analysis of field measurements," *Wind Energy*, vol. 20, no. 8, pp. 1331–1348, 2017.
- [6] T. F. Brooks, D. S. Pope, and M. A. Marcolini, "Airfoil self-noise and prediction," Tech. Rep. NASA-RP-1218, NASA Langley Research Center, 1989.
- [7] Y. D. Mayer, B. Lyu, H. K. Jawahar, and M. Azarpeyvand, "A semi-analytical noise prediction model for airfoils with serrated trailing edges," *Renewable Energy*, vol. 143, pp. 679–691, 2019.
- [8] B. Lyu and L. J. Ayton, "Rapid noise prediction models for serrated leading and trailing edges," *Journal of Sound and Vibration*, vol. 469, p. 115136, 2020.
- [9] G. Wang, J. Hurault, A. Herrig, R. Ramakrishnan, M. Canal, and C. E. Carcangiu, "Aero-acoustic prediction tool for complex wind turbine blade configurations," in *Proceedings of the 10th International Conference on Wind Turbine Noise*, (Dublin, Ireland), LM Wind Power, June 2023. Accessed: 2025-01-27.
- [10] J. E. Ffowcs Williams and L. H. Hall, "Aerodynamic sound generation by turbulent flow in the vicinity of a scattering half plane," *Journal of Fluid Mechanics*, vol. 40, no. 4, p. 657–670, 1970.
- [11] M. Herr and M. Kamruzzaman, "Benchmarking of trailing-edge noise computations: Outcome of the banc-ii workshop," in *19th AIAA/CEAS Aeroacoustics Conference*, p. 2123, American Institute of Aeronautics and Astronautics, 2013.
- [12] M. Herr, R. Ewert, C. Rautmann, M. Kamruzzaman, D. Bekiropoulos, A. Iob, R. Arina, P. Batten, S. Chakravarthy, and F. Bertagnolio, "Broadband trailing-edge noise predictions—overview of banc-iii results," in *21st AIAA/CEAS Aeroacoustics Conference*, p. 2847, American Institute of Aeronautics and Astronautics, 2015.
- [13] M. Herr, M. Kamruzzaman, and C. J. Bahr, "Fourth workshop on benchmark problems for airframe noise computations (banc-iv); category 1: Trailing-edge noise," 2014.

- [14] M. Choudhari and D. P. Lockard, "Simulations & measurements of airframe noise: A banc workshops perspective," 2016.
- [15] R. A. van Rooij, "Modification of the boundary layer calculation in RFOIL for improved airfoil stall prediction," Tech. Rep. IW-96087R, TU Delft, 1996.
- [16] K. Boorsma and J. Schepers, "Enhanced wind turbine noise prediction tool silant," in *Proceedings of the Fourth International Meeting on Wind Turbine Noise*, (Rome, Italy), Energy research Centre of the Netherlands, April 2011. Accessed: 2025-01-24.
- [17] P. Moriarty, "Nafnoise: Nrel airfoil noise." <https://www.nrel.gov/wind/nwtc/naf-noise.html>, 2005. Accessed: 2025-01-24.

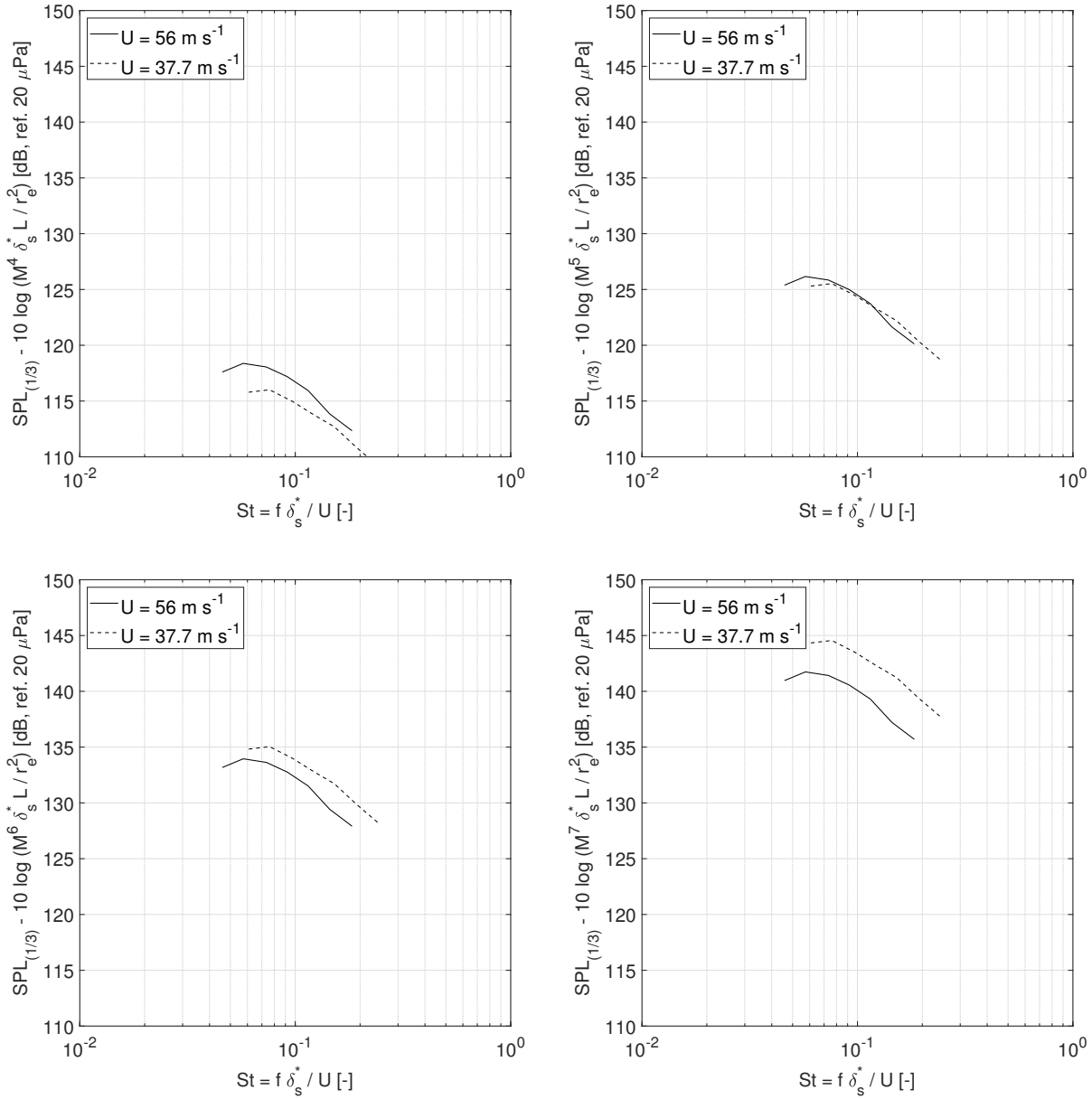


Figure 5 Scaled levels for BANC cases 1 and 4, both characterized by the same NACA-0012 airfoil and a zero angle of attack. Each plot is generated using a different scaling exponent for the Mach number (shown in the y-axis label of each plot).

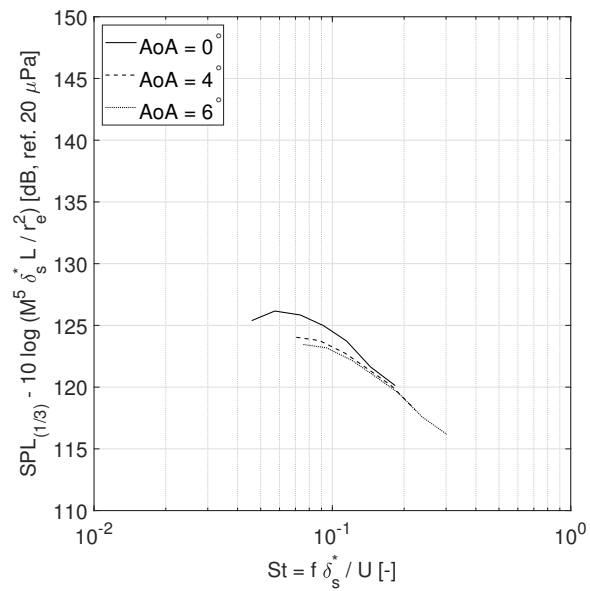


Figure 6 Scaled levels for BANC cases 1, 2, and 3, which involve the same NACA-0012 airfoil and approximately the same free-stream velocity, but with different angles of attack.

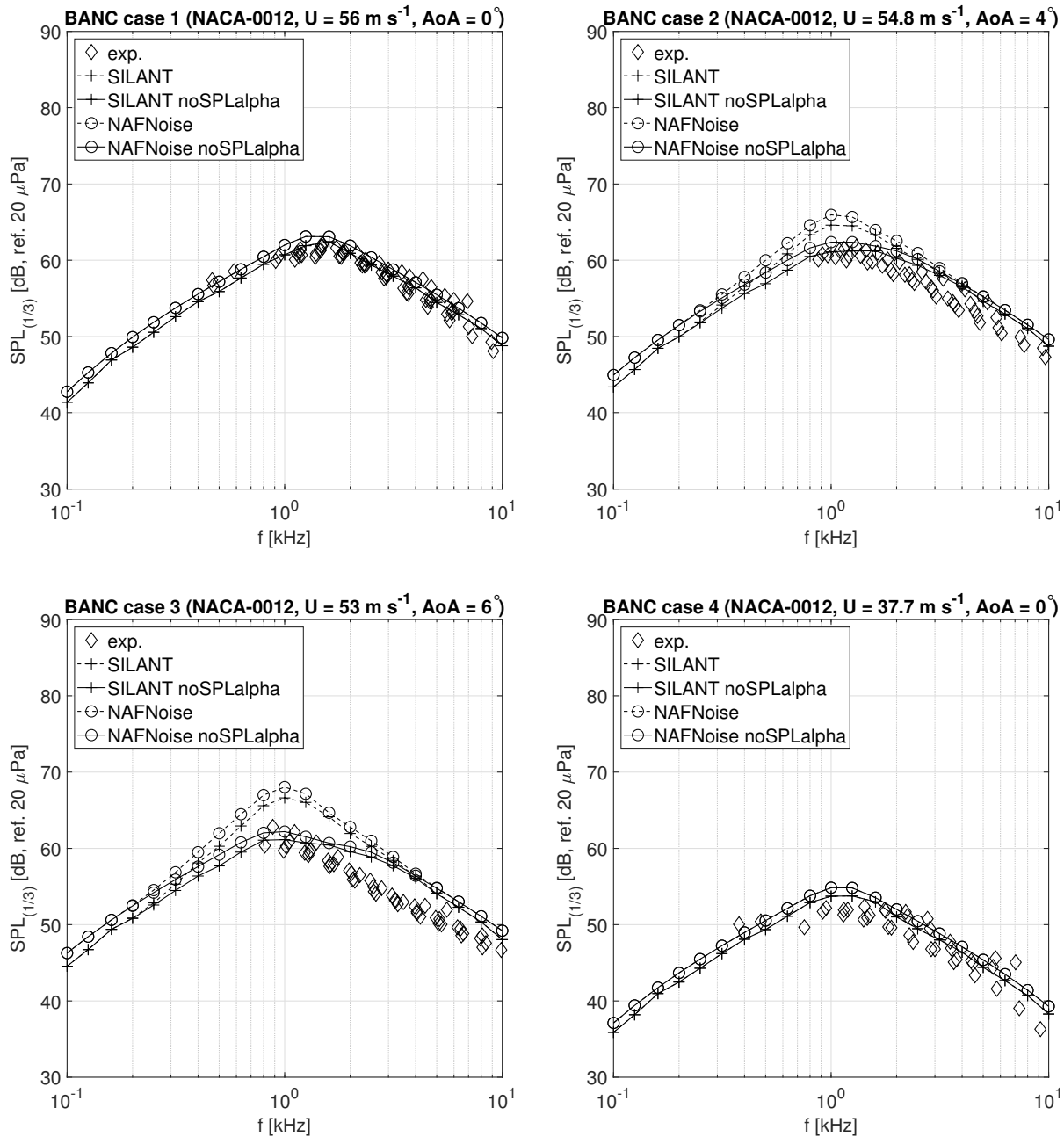


Figure 7 Comparison between experimental and simulated 1-3-octave band sound pressure level for BANC case 1, 2, 3 and 4. The figures presents measurements from IAG, DLR and UFL which were combined together.

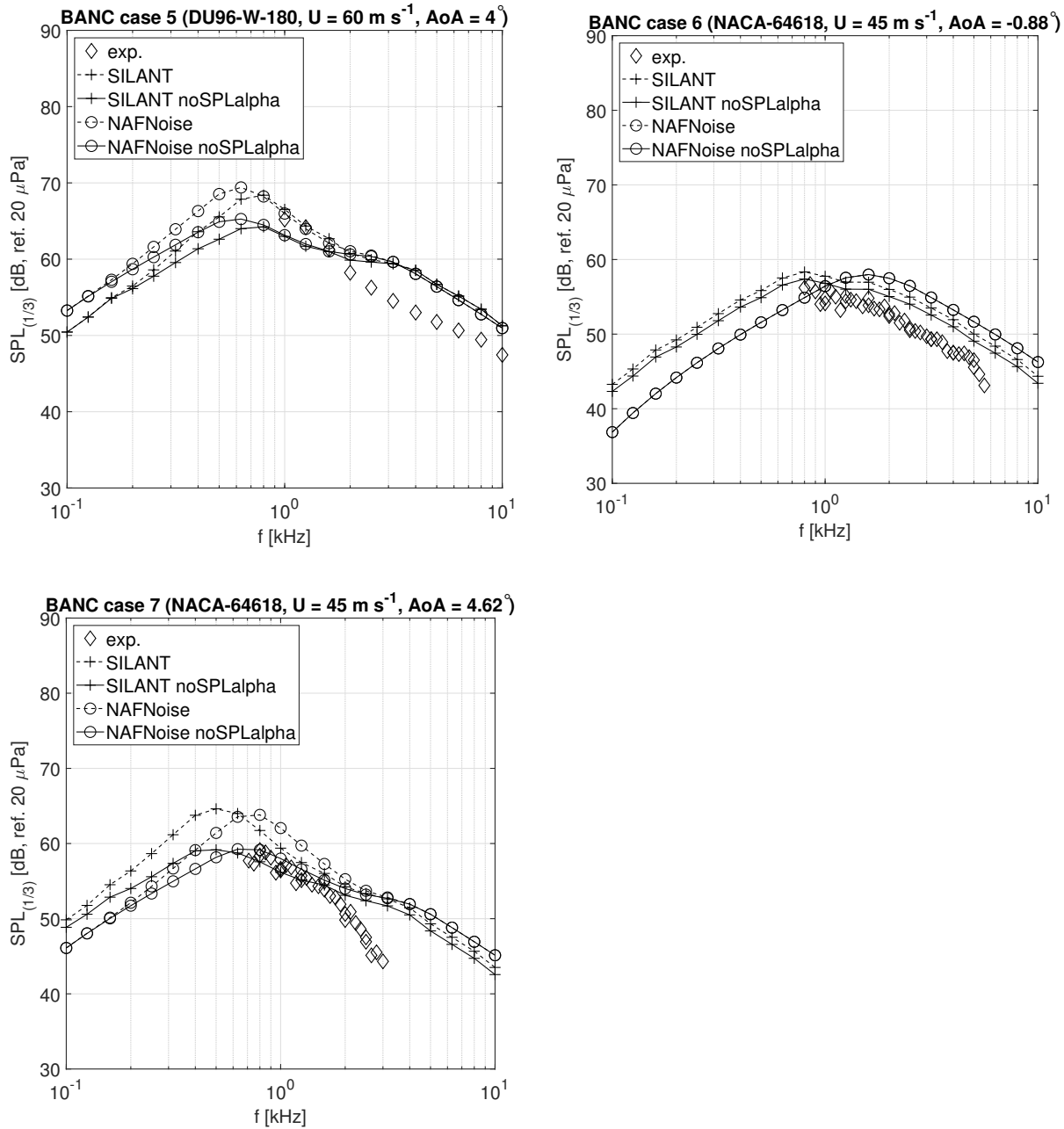


Figure 8 Comparison between experimental and simulated 1-3-octave band sound pressure level for BANC case 5, 6 and 7. The figures presents measurements from DLR for case 5 and from VTST for case 6 and 7.

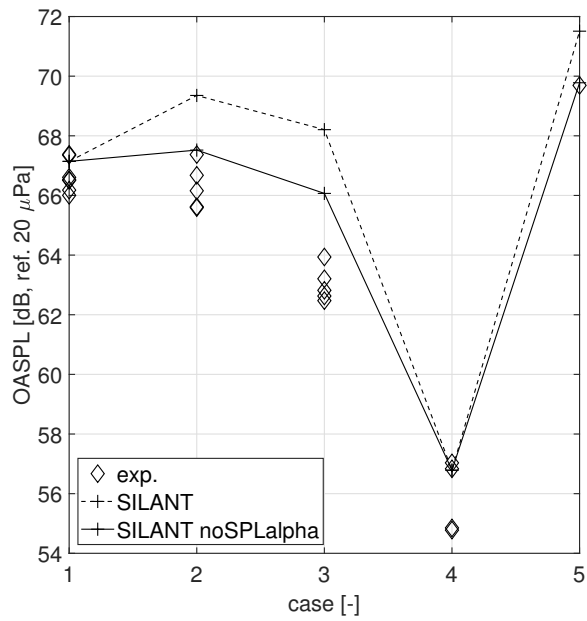


Figure 9 Overall sound pressure levels for BANC cases 1 to 5.

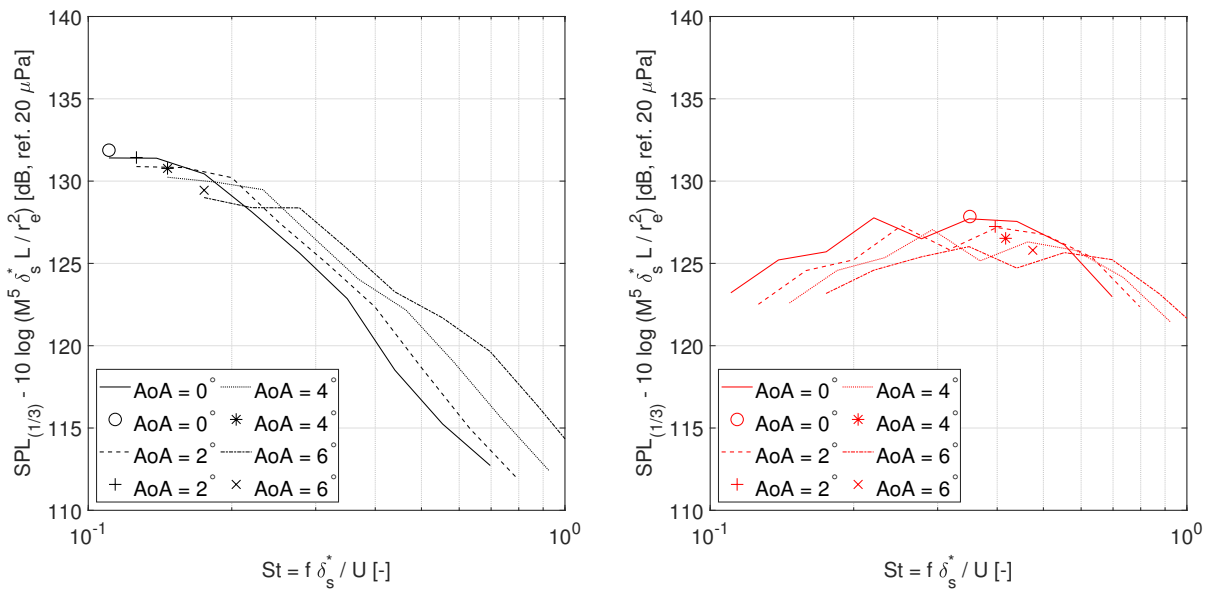


Figure 10 Scaled 1/3-octave spectra for airfoils at different angles of attack and a free-stream velocity of 20 m s^{-1} are shown for the nominal NACA-0018 airfoil (left subplot) and the NACA-0018 airfoil with trailing edge noise mitigation add-ons. Solid lines represent measured spectra, while markers indicate the approximate spectral peak locations.

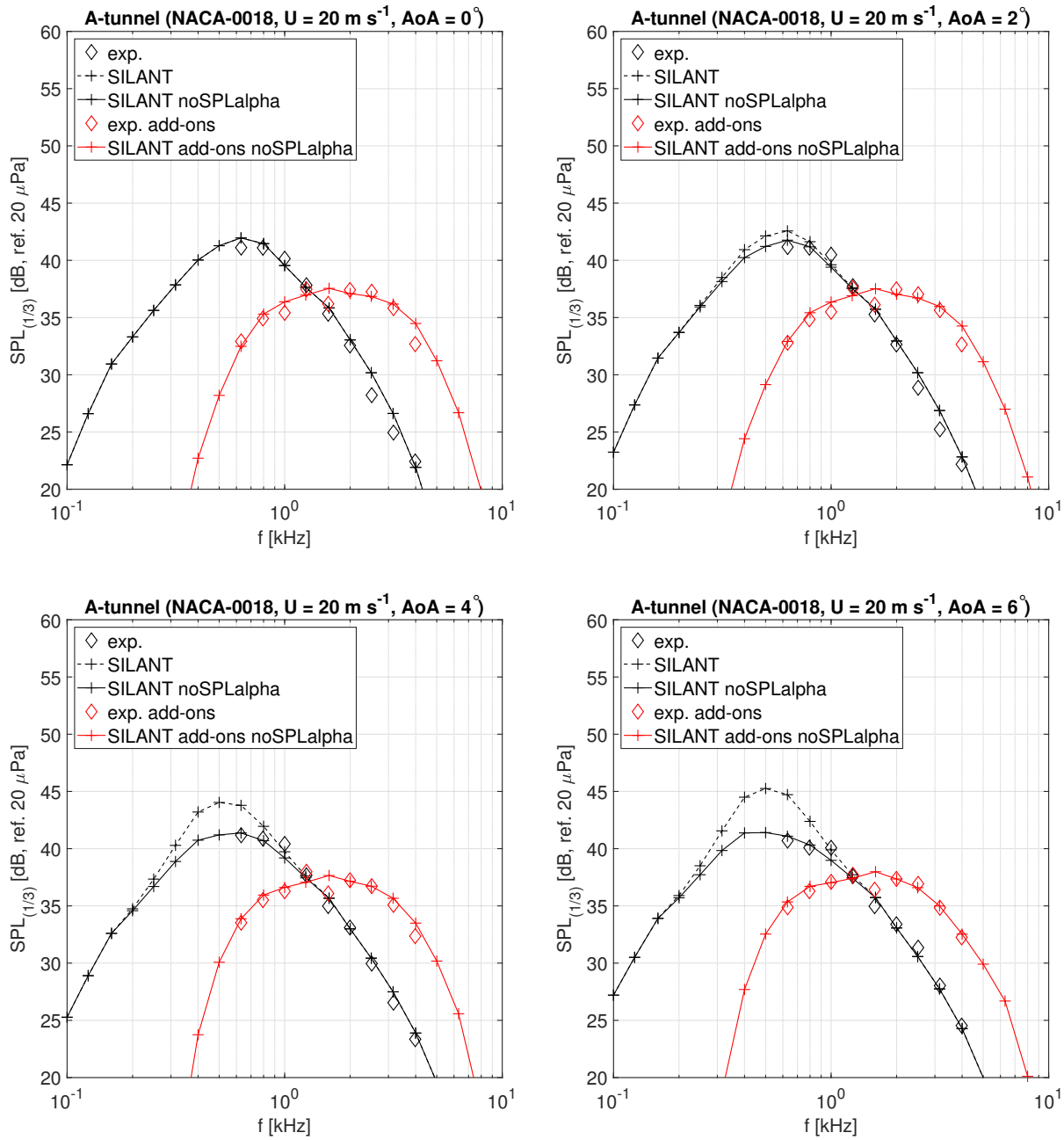


Figure 11 Comparison of measured and simulated 1/3-octave spectra for the nominal NACA-0018 airfoil and the NACA-0018 airfoil featuring trailing edge noise mitigation add-ons at angles of attack from 0° to 6° and a free-stream velocity of 20 m s^{-1} .

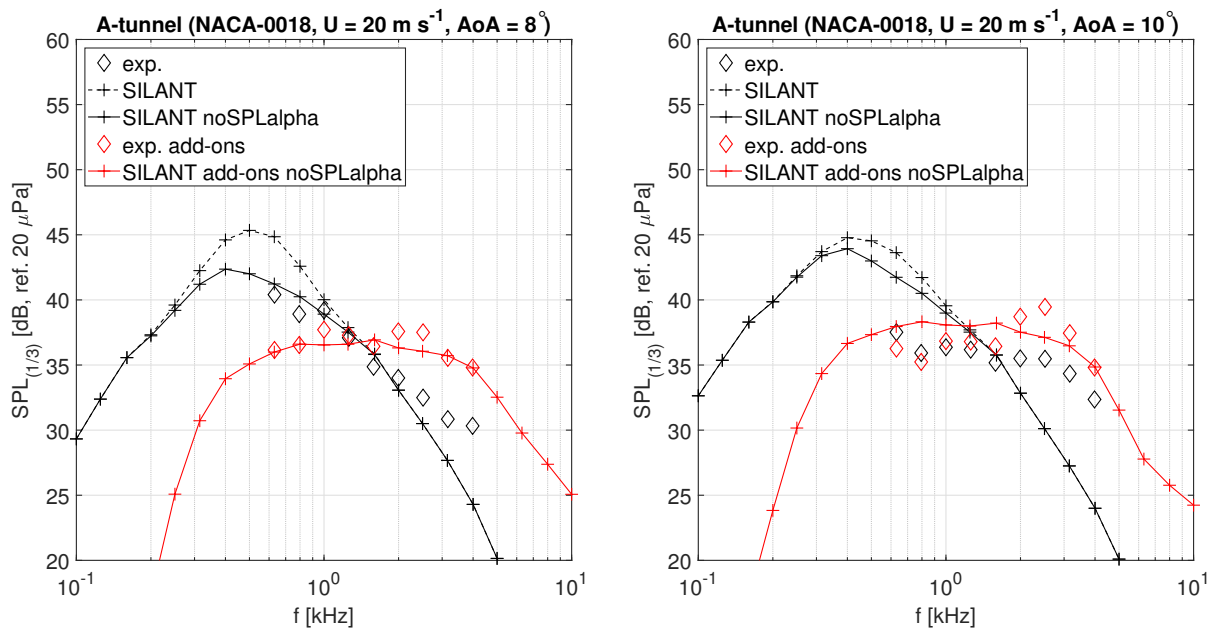


Figure 12 Comparison of measured and simulated 1/3-octave spectra for the nominal NACA-0018 airfoil and the NACA-0018 airfoil featuring trailing edge noise mitigation add-ons at angles of attack from 7.8° to 10° and a free-stream velocity of 20 m s^{-1} .

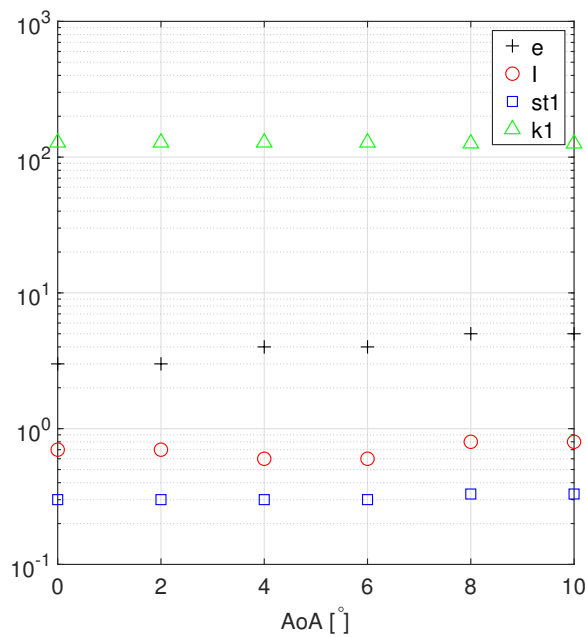


Figure 13 Values of BPM parameters as a function of the angle of attack.

Paper #16 - ID: 350

Title: Estimating wind turbine noise in Swedish national noise map over green areas

Author: Mikael Ögren

11th Edition of the
International Conferences on
Wind Turbine Noise
Copenhagen, Denmark – 10th to 13th June 2025

Wind turbine contribution in nationwide noise mapping across Sweden's green landscape

Mikael Ögren¹ and Erik Rosengren

University of Gothenburg, 405 30 Gothenburg, Sweden

Magnus Lindqvist

The Swedish Environmental Protection Agency, 120 30 Stockholm, Sweden

Manne Friman

Soniqa, Karlskrona, Sweden

Andreas Gustafson

**The Swedish National Road and Transport Research Institute (VTI),
402 78 Gothenburg, Sweden**

Summary

Mapping noise in green spaces like nature reserves or outdoor recreational areas is challenging, as it is necessary to account for distant sound sources to accurately estimate noise levels when they are comparatively low. In Sweden, we have used the Nord2000 noise prediction model to generate a national noise map for noise from wind turbines, major airports, road and railway traffic. The noise map has a spatial resolution of 500 m by 500 m, and sources were included up to 12 km from the receiver (8 km for road traffic noise).

To be able to map such extensive areas, we utilized an efficient database for propagation calculations. Weather effects were incorporated using data from the ERA5 climate database. The map shows that 57 % of Sweden's 5560 nature reserves experience an average yearly noise level (day and evening) below 25 dB over more than 90 % of their area. About 16 % of the reserves were exposed in the same manner above 35 dB. Road traffic noise was the predominant source in 82 % of the reserves, and noise from wind turbines was the dominant source in 3.7 % of them. The calculation for wind turbine noise was repeated assuming that all wind turbines under planning, both approved and awaiting approval, was built. In this theoretical case the percentage of nature reserves where wind turbines were dominant increased to 5.7 %.

¹ Corresponding author – Email: mikael.ogren@amm.gu.se

1. Introduction

Traditional noise mapping focuses on predicting the noise level from different sources where the noise level is relatively high, and often at locations where the noise level is dominated by one major source. A typical example would be a building with dwellings close to a major road. The methodology focuses on estimating the ground effect and the effects of screening and reflection by terrain, buildings and noise barriers. In our case longer propagation distances are the focus, and then the influence of weather becomes of major importance. Therefore we have used the Nord2000 method [1], and also included some improvements from the Harmonoise/Imagine projects [2], [3].

In this project we aim to estimate lower noise levels in natural areas often located relatively far from the noise sources. For a small, forested area more than 2 km from a major road, other factors are important for the prediction of the noise level than for a receiving point on a building in an urbanised residential area 50 meters from the major road. In the second case the noise level varies over time as the strength of the source itself varies (time of day, weekday, holidays...), but the noise level is almost always dictated by the traffic on the major road. In the first case, the remote natural area, the noise level does not only vary with the strength of the source, but also the wind direction, humidity and temperature are very important factors. In some weather situations the major road might not contribute to the total level at all, and instead a local road in another direction determines the noise level.

This research was funded by Naturvårdsverket, the Swedish Environmental Protection Agency, under their program for monitoring environmental effects on health (HÄMI). The calculations we used are based on a previous project which provided a method for calculating noise levels in green areas in Sweden. The method is documented in a conference paper [4] and a technical report (in Swedish) [5], and the noise map itself is openly available online [6].

2. Method

In this paper we aim to compare the impact of noise from wind turbines on natural reserves in Sweden, both in comparison to other sources such as road and railway noise, and to a theoretical case including more wind turbines based on available expansion plans. The basic method is Nord2000 [1], and in addition to wind turbines we include noise from road traffic, railway traffic and flight operations close to major airports [4].

The noise map covers Sweden including areas at sea within the Swedish exclusive economic zone, and the spatial resolution is 500 m. Our estimation of sound power of the noise sources are direct from the current Nord2000 for road and railway, and for aircraft operations we used a reverse engineering approach developed for Harmonoise / Imagine [7].

Of special interest here is of course our approach for estimating sound power for wind turbines. All underlying basic information on the turbines was extracted from the national database on wind power named Vindbrukskollen (VBK) [8]. VBK includes position and hub height for almost all wind turbines in Sweden. Although there is a possibility to voluntarily add sound power information to each turbine by the operator, most turbines are missing this information. Instead we adopted a simplified approach where each turbine was assigned a sound power based on hub height, a procedure proposed in a noise mapping project in Stockholm [9]. For a hub height of 70 m and lower we assumed an A-weighted sound power of 101 dB, which was then linearly increased up to a maximum of 105 dB for a hub height of 130 m or higher. A standard spectrum and directivity pattern was used for all turbines [9].

Wind turbine noise is normally evaluated at a specific weather case in Sweden, assuming a wind speed of 8 m/s at 10 m above ground, and with a wind direction always from the source (the turbine) and directly towards the receiver. This approach does not include any variations over time, it is a static case. For the national noise map we instead wanted to model the yearly average noise level including weather effects. We also focused on the times when natural reserves would mainly be visited, and therefore decided to use the yearly average noise level between 06 in the morning and 22 in the evening (L_{06-22}).

For long sound propagation distances it has been suggested to operate Nord2000 with 25 different weather classes divided into propagation directions of 10 degrees, but in order to reduce the calculation time needed we instead adapted the four weather classes suggested for use in Denmark [10], and used eight propagation directions (N, NE, E,...) corresponding to an angular resolution of 45 degrees. The classes are denoted M1, M2, M3 and M4, where M1 corresponds to upward refraction propagation (lowest noise levels) and M4 is strong downward refraction propagation (highest noise levels). M2 is then neutral atmosphere and M3 slight downwards refraction.

The weather statistics needed for the method was obtained from the “hourly reanalysis” ERA5 climate dataset for the ten year period 2013 – 2022 [11]. The downloaded data contained 87,648 hours in a latitude/longitude grid of 15 arcseconds (0.25 degrees), which corresponds to approximately 10 km × 28 km in the north part of Sweden and 16 km × 28 km in the south part. Using these hourly data we then calculated the weather class M1 – M4 in each of the eight directions for day, evening and night propagation. A first set of calculations was then performed for each hour in the dataset to test how much information was needed for an accurate estimation of the yearly average levels [4]. For the final mapping we used the average temperature, humidity and proportion of weather class in each propagation direction for the day, evening and night periods for every month, an example is given in Figure 1.

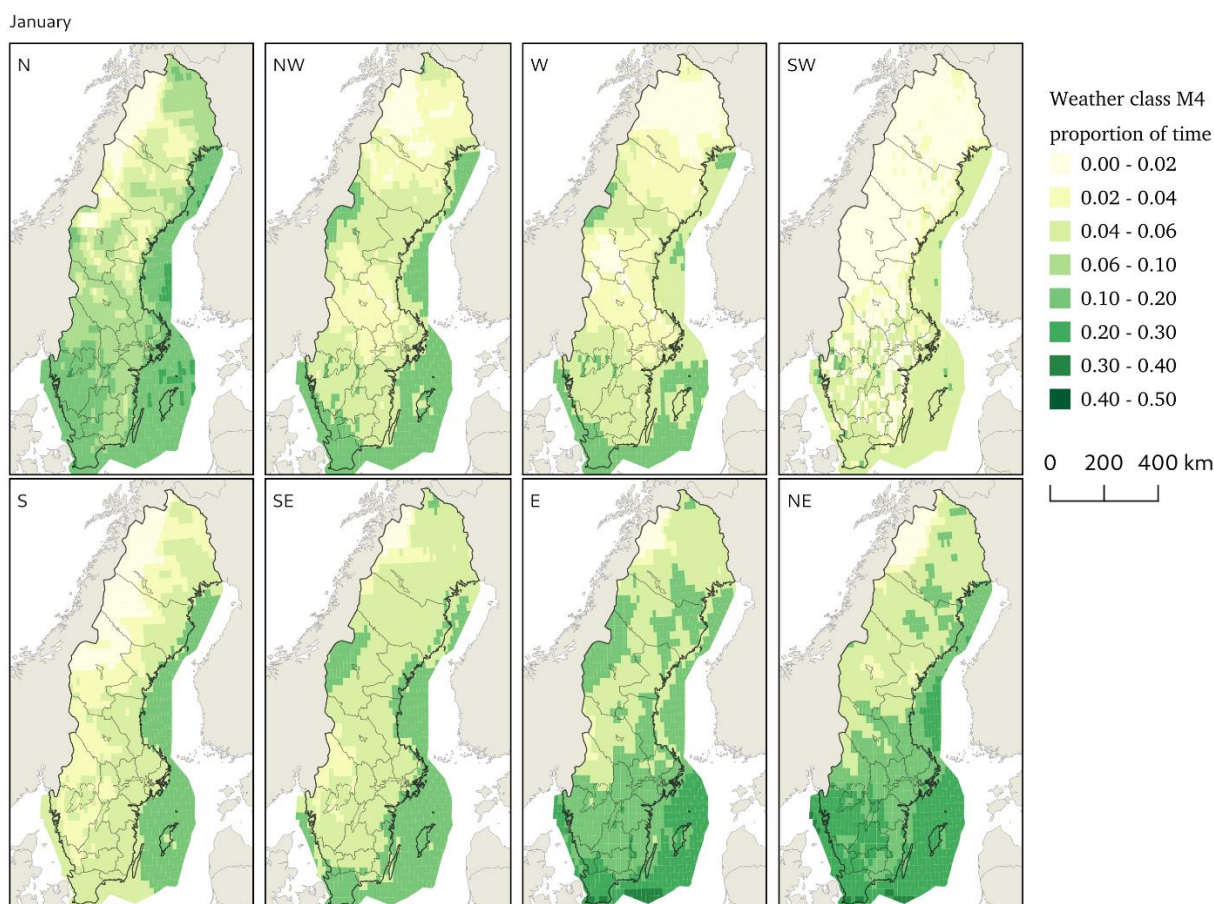


Figure 1. Proportion of time (1.0 = 100%) with weather class M4 for January, daytime (06 – 18). Each map represents a different propagation direction. Mean over ten years (2013 – 2022).

For the results presented in this paper we used the noise map as described above, and then recalculated the noise map using the same method but included not only wind turbines in operation, but also those under planning and those with final approval from the authorities but not yet in operation (either under construction or in various stages of final planning). These data were extracted from the VBK database January 1 2025, and is summarised in Table 1.

Table 1 Wind turbines in operation and under planning in Sweden January 1 2025.
Source VBK (www.vindbrukskollen.se).

	Number of wind turbines
In operation	5,587
Approved plans	1,397
Under planning	2,435

The noise exposure from our different sources were evaluated at each of the 5,560 nature reserves in Sweden. The contribution of wind turbines in each nature reserve was then determined using

$$b_{WT} = \frac{\sum 10^{L_{WT,n}/10}}{\sum 10^{L_{tot,n}/10}}, \quad (1)$$

where the proportion of exposure due to noise from wind turbines b_{WT} is calculated from the sum over all n calculation points in each area from exposure to wind turbines only L_{WT} and the total level from all sources L_{tot} . Noise from wind turbines is considered as the dominant source in a nature reserve if the contribution b_{WT} is greater than the contribution calculated for each of the other sources (road, railway and airport).

All nature reserves were also assigned a sound environment class from A to C, where A is the least affected by noise exposure from road, rail, airport and wind turbine noise. The classification used the 90-percentile for the area of the nature reserve, i.e. the yearly average equivalent level (06 – 22) that 90 % of the calculation points within the area are lower than. The classes are described in Table 2. The colours used for the classes and in the noise maps below is an adapted version of the colourmap proposed by Weninger [12].

Table 2 Classification of noise exposure in nature reserves A – C.

Class	L_{06-22} at 90% of area	Colour
A	< 25 dB	
B	25 – 35 dB	
C	≥ 35 dB	

3. Results

Our results explore the scenario where all planned wind turbines are built compared to the current situation, a 69 % increase in the number of turbines overall (see Table 1). All other calculation parameters are kept constant, such as traffic flows, weather and so on. As mentioned above the resolution of the calculated noise maps is 500 m, and the calculation covers Sweden including the exclusive economic zone at sea. The total national noise map is difficult to present meaningfully in a small figure but can be accessed online [13], and an overall picture of all nature reserves and their corresponding class is given in the map in Figure 2 below.

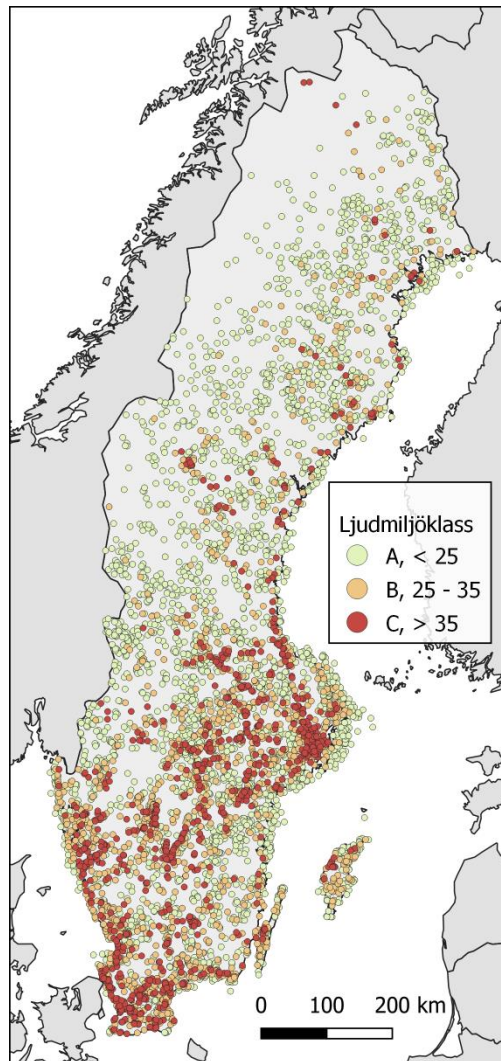


Figure 2. Map of sound environment class A – C for all nature reserves in Sweden.

From a national perspective the total area exposed above 35 dB from wind turbines (yearly average equivalent level 06-22) is 1,326 km² (projected area EPSG 3006). Adding the planned turbines increased this area to 1,987 km² (+ 50 %). In comparison, the total area exposed to road traffic noise above 35 dB is more than 24,800 km².

A zoomed in comparative example is given in the three maps in Figure 3 below, where a number of nature reserves are also indicated in green outlines. Here the increase in the number of turbines is visible comparing the left and the middle figure, but also the total combined exposure to all sources compared to wind turbines by comparing the right and the middle figure.

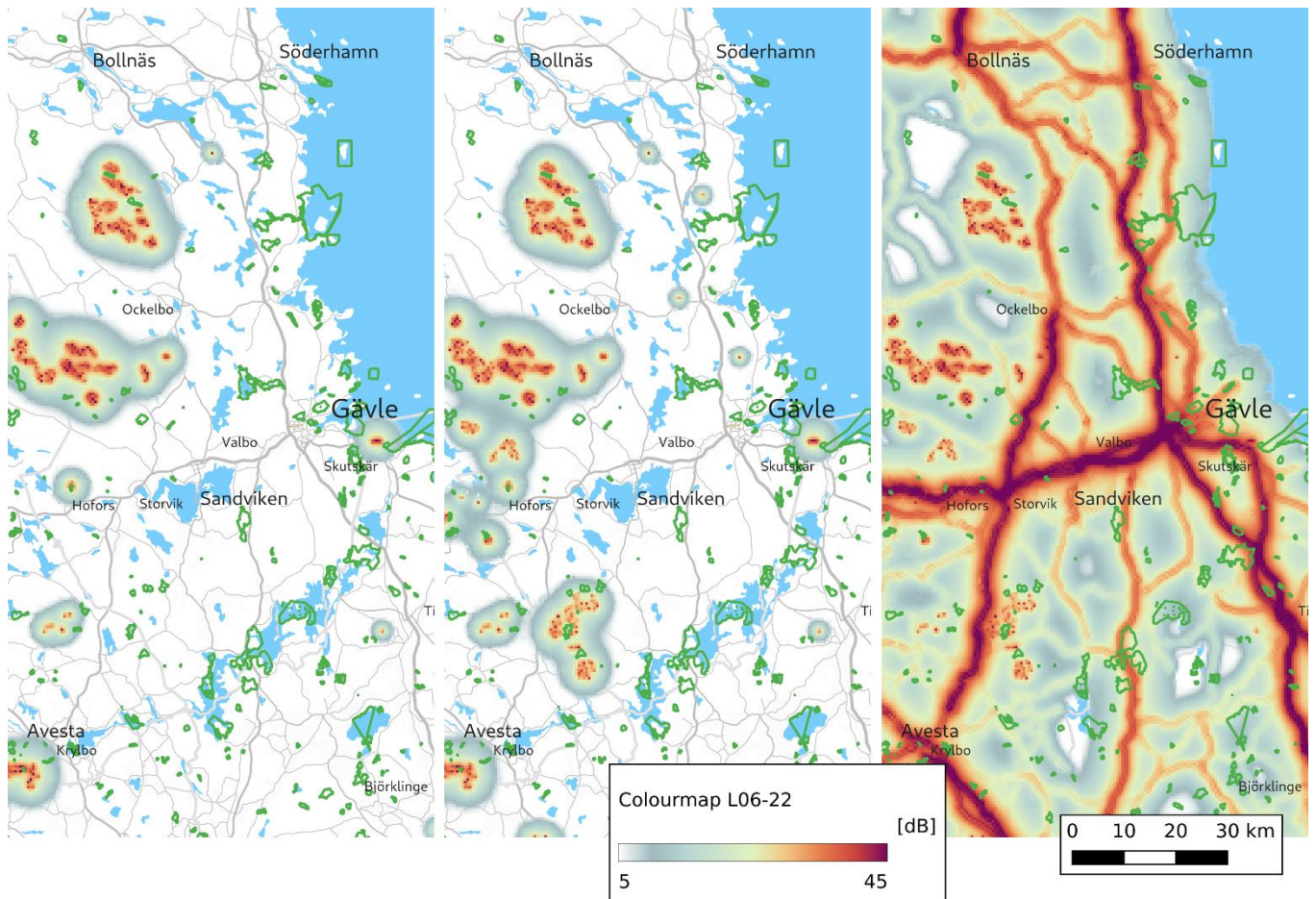


Figure 3. Map of calculated noise level (L_{06-22}) for an example area around Gävle, Sweden. Left is current wind turbines (2024), middle is including planned turbines, right is also including road, railway and airport noise. Nature reserves indicated with green outlines.

If we focus on nature reserves and their exposure we can compare the 90 percentile L_{06-22} indicator, and thus the sound environment class A, B and C. For the current situation 57.0 % of all nature reserves are classed as A, which is reduced down to 56.5 % if all planned wind turbines are added. If we further focus on areas where noise from wind turbines is the dominant source the statistics are given in Table 3. The impact of adding the turbines under planning is larger for nature reserves with less total exposure.

Table 3 Percentage of nature reserves where wind turbines are the dominant noise source for each noise environment class A – C.

	A < 25 dB	B 25 – 35 dB	C ≥ 35 dB	All
Current (2024)	4.4 %	4.0 %	0.9 %	3.7 %
Added turbines	7.0 %	5.6 %	1.2 %	5.7 %

The population living close to each nature reserve (within 5 km) was also included in the noise mapping effort in 2024 [4] as a simplified indicator of potential visits. Note that the same population may be included in the statistics for several nature reserves with this simplified measure. As expected, the areas with high population within 5 km was also often more exposed to noise. A scatterplot of the population within 5 km and the increase in noise when adding the wind turbines under planning is presented in Figure 4. Most of the 5,560 nature reserves have little or no change and are clustered over the x-axis, but those who do get increase levels show a decreasing trend as population increase.

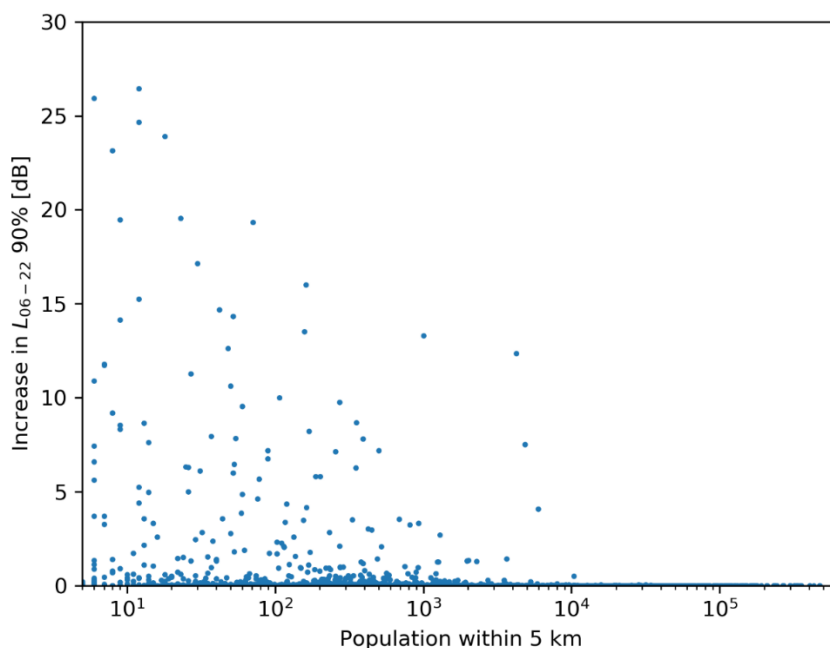


Figure 4. Scatterplot of the population within 5 km from a nature reserve and the change in noise indicator L_{06-22} (90 % of the area of the reserve) by adding wind turbines under planning.

4. Conclusions

Adding all wind turbines under planning to the current wind turbines in operation represents a theoretical scenario for noise exposure assessment. Some planned project may not result in actual turbines in operation, final planning and construction may take a long time during which other wind turbines are taken out of commission and so on. On the other hand, new plans may appear in the future and could lead to even more turbines being built, although the planning and approval process will always take time.

The noise mapping method used in this paper is not relevant for population exposure in relation to Swedish guidelines. The sound power estimation is not accurate enough, and the method is aimed at estimating the yearly average relatively far from the wind turbine. Swedish guidelines are formulated relative a standard static weather with a worst-case approach in terms of adding up the contribution of neighbouring wind turbines.

The mapping method is however relevant for nature reserves and other nature areas, and is available using the same principles and procedures for the whole of Sweden. The scenario calculations illustrate that if all planned wind turbines are built the exposure in nature reserves will increase, and the contribution relative to the other mapped sources will increase. Though in comparison to road and railway traffic noise, the overall importance of wind turbines is still low.

Adding better information such as the rated sound power and the uptime for each wind turbine could improve the accuracy of the noise map for future research, but it is unlikely that this information will be easily available unless it becomes mandatory to report the sound power to the authorities, and they in turn make the information public. Other improvements could be better and more realistic scenarios for the future and prediction of the impact of climate changes in the near future.

Acknowledgments

We gratefully acknowledge the support of Sara Persson, Hung Nguyen and Oscar Hagefalk.

References

- [1] B. Plovsing, 'Proposal for Nordtest Method: Nord2000 – Prediction of Outdoor Sound Propagation, AV 1106/07, DELTA, revised 2014', Delta acoustics, Hørsholm, Delta report AV1106/07, Jan. 2014. [Online]. Available: <https://forcetechnology.com/-/media/force-technology-media/pdf-files/projects/nord2000/nord2000-nordtestproposal-rev4.pdf>
- [2] P. de Vos, M. Beuving, and E. Verheijen, 'Harmonised Accurate and Reliable Methods for the EU Directive on the Assessment and Management Of Environmental Noise - Final Technical Report', AEA Technology Rail, Utrecht, HAR7TR041213AEAT03, 2005.
- [3] 'IMAGINE: Improved Methods for the Assessment of the Generic Impact of Noise in the Environment, Final Synthesis Report', DeltaRail, 2006.
- [4] M. Ögren, M. Lindqvist, M. Friman, S. Persson, A. Gustafson, and E. Rosengren, 'Nationwide noise mapping across Sweden's green landscape', *INTER-NOISE NOISE-CON Congr. Conf. Proc.*, vol. 270, no. 5, pp. 6704–6713, Oct. 2024, doi: 10.3397/IN_2024_3860.
- [5] M. Ögren, M. Lindqvist, A. Gustafson, M. Friman, E. Rosengren, and S. Persson, 'Ljudmiljö i naturområden', *Samhällsmedicin och folkhälsa*, Göteborgs universitet, Göteborg, Sweden, NV-07389-20, Jun. 2024. Accessed: Apr. 11, 2025. [Online]. Available: <https://www.naturvardsverket.se/4a56bf/contentassets/2b28a9e8af72478c8d429d1f5d4e57fa/slutrapp-ort-ljudmiljo-i-naturomraden.pdf>
- [6] 'Geodata nedladdningstjänst, Ljudmiljö i naturområden', Naturvårdsverket. Accessed: Jun. 25, 2024. [Online]. Available: <https://geodata.naturvardsverket.se/nedladdning/ljudmiljo/>
- [7] F. de Roo, E. Salomons, D. Heimann, and P. Hullah, 'IMAGINE - Reference and engineering models for aircraft noise sources', DeltaRail, IMAGINE D9, 2007.
- [8] 'Vindbrukskollen', Energimyndigheten. Accessed: Mar. 29, 2024. [Online]. Available: <https://www.energimyndigheten.se/fornybart/elproduktion/vindkraft/vindbrukskollen>
- [9] A. Novak, T. Gredenman, R. Fred, C. Eriksson, and G. Pershagen, 'Kartläggning av bullerfria områden. Metodbeskrivning för Stockholms län', Centrum för arbets- och miljömedicin, Stockholms läns landsting, Stockholm, 2016.
- [10] B. Plovsing, 'Noise mapping by use of Nord2000 - Reduction of number of meteo-classes from nine to four', Danish ministry of the environment, Working Report 18 2007, 2007.
- [11] C3S, 'ERA5 hourly data on single levels from 1940 to present'. 2018. doi: 10.24381/CDS.ADBB2D47.
- [12] B. Weninger, 'A color scheme for the presentation of sound immission in maps: requirements and principles for design', presented at the EuroNoise, Maastricht, 2015, pp. 439–444.
- [13] M. Ögren, 'Bullerprognosen, Ljudmiljö i naturområden', *Webbkarta ljudmiljö i naturområden*. [Online]. Available: <http://bullerprognosen.se/webmap>

Paper #17 - ID: 351

Title: Investigation of individual pitch control for infrasound noise reduction from wind turbines

Author: Anik Hirenkumar Shah

11th Edition of the

**International Conferences on
Wind Turbine Noise**

Copenhagen, Denmark – 10th to 13th June 2025

Investigation of Individual Pitch Control for Infrasound Noise Reduction from Wind Turbines

Anik H. Shah¹, Carlo R. Sucameli and Carlo L. Bottasso

Wind Energy Institute, Technical University of Munich, Garching bei München, Bavaria, 85748, Germany

Summary

Wind turbine (WT) noise remains a hindrance for onshore wind energy expansion. While most research focuses on audible noise, the health effects of infrasound noise (<20 Hz) are not fully understood. Infrasound noise spectra from WTs are dominated by tonal peaks at the blade passing frequency (BPF) and its harmonics. This study explores mitigating WT infrasound emissions by using individual pitch control (IPC), inspired by the effectiveness of IPC in reducing amplitude modulation (AM), a periodic swishing sound also caused by BPF modulation.

The study uses a computational framework that combines large eddy simulation (LES) and an aeroelastic model through the actuator line method. The Ffowcs Williams-Hawkings (FW-H) acoustic analogy captures the infrasound noise from the rotor and tower, their interactions, and near-wake turbulence effects.

An open-loop IPC approach is tested with two pitch profile strategies: one based on lift variation (ΔL_{rms}) along the blade span and another using noise predictions (AP_{rms}) from a simplified Farassat 1A formulation. Both strategies achieve a reduction of 1.5-2 decibels (dB) in the overall sound pressure levels (OASPL) by reducing the 3P peak. The study highlights the similarities and differences between IPC for infrasound and AM reduction, exploring the possibility of an optimized IPC method that effectively minimize overall noise annoyance from WTs.

1. Introduction

Onshore wind energy will remain a significant part of the renewable energy mix despite the rapid growth of offshore wind farms [1]. However, onshore projects face challenges related to environmental impacts and social acceptance, with noise being a primary concern. While regulations are in place to limit the effects of audible noise from wind turbines (WTs), infrasound emissions (<20 Hz) are not given as much attention [2]. This gap is partly due to the ongoing debate about the physiological and psychological effects of WT infrasound on humans and animals.

Several measurement studies show that infrasound emissions from wind farms are below the threshold of human hearing, as summarized in [3]. However, infrasound behaves very differently from audible sound. It travels long distances with minimal attenuation and is known to interact differently with buildings. Infrasound noise emissions from WTs are periodic and last for long durations. References [4, 5] suggest that higher indoor SPL may result from the resonance of the structure with infrasound frequencies from WTs. There is a need to investigate the effects of infrasound coupling with building structures on audible

¹ Corresponding author – Email: anik.shah@tum.de

noise [6]. Furthermore, various surveys indicate long-term health problems due to infrasound from WTs [5]. Flemmer and Flemmer, 2023 [5] summarize the phenomenology of infrasound and its effect on people, covering a vast database of infrasound research articles. They highlight the need for further research to determine the frequencies of WT sound spectra responsible for annoyance among residents. While there is a clear need to better understand the impact of infrasound on humans and animals, it is still worthwhile investigating ways to mitigate infrasound from WTs, which is the focus of this paper.

Both infrasound noise and amplitude modulation (AM) are generated from periodic aerodynamic forces caused by blade rotation. Infrasound noise emissions from WTs are characterized by tonal peaks at the blade passing frequency (BPF) and its harmonics. These are caused by the mutual interactions when blades pass in front of the tower [7]. Amplitude modulation is a periodic swishing sound caused by oscillations in the audible frequency range generated primarily by the turbulent boundary layer on the trailing edge of the blade. These oscillations are linked to the cyclic change in inflow at the blade airfoils due to the tower or a sheared, non-uniform, or misaligned inflow. Cyclic pitch control of the individual blades can reduce AM and mitigate fatigue loading due to shear [8]. The efficacy of individual pitch control (IPC) to reduce AM was investigated in [9] for different inflow velocities, shear exponents, observer positions, and blade flexibility. This study showed that optimizing IPC to eliminate AM at any targeted position comes at the expense of increasing AM at other locations. Hence, the strategy is constrained by the relative position of nearby settlements. While freestream wind speed has little effect on the optimal azimuthal pitch profile, shear exponent strongly affects how to pitch a blade. Infrasound and AM are closely linked to BPF. Since IPC shows promise in reducing AM by targeting BPF, this study also investigates IPC as a strategy to reduce infrasound from WTs.

The rest of the paper is organized as follows: section 2 describes the FW-H acoustic analogy for WTs and the development of two open-loop IPC strategies for infrasound reduction; section 3 showcases the effect of both IPC strategies on infrasound from WTs in different inflow and design conditions; section 4 discusses the similarities and differences between IPC for AM and infrasound; and finally, section 5 summarizes the main conclusions and outlines future work.

2. Methodology

2.1 FW-H acoustic analogy for wind turbines

Acoustic analogy computes the acoustic pressure field by rearranging the Navier-Stokes equations to form a wave equation using equivalent aero-acoustic sources. Ffowcs Williams-Hawkings (FW-H) generalized Lighthill's formulation by adding the possibility of modeling the sound generated by moving solid surfaces, which is crucial for WTs where blades are in motion [10]. Farassat's formulation 1A [11] of the FW-H analogy can be applied with a BEM-based aeroelastic WT model to calculate infrasound emissions [12]. It computes the noise in the far-field at a stationary observer, generated directly from the surface of the rotating blades affected by a decelerated flow due to the WT tower. While this approach is computationally efficient, it has a significant limitation: it neglects the infrasound noise emissions generated by the unsteady pressure distribution on the tower induced by the rotor. Higher fidelity mesh-resolved CFD approaches have shown that these emissions are more significant than the noise emissions from the rotor [13].

The present work uses a comprehensive yet efficient framework to capture all the relevant infrasound emissions from a WT [7]. FW-H acoustic analogy based on [14] is applied on permeable stationary integration surfaces that surround the entire WT, thereby capturing the coupled effects of the rotor, tower, and the near wake of the wind turbine, as shown in Figure 1. The flow-field and turbine response are computed by coupling the LES tools of OpenFOAM with NREL's FAST aeroelastic solver through the actuator line method (ALM) within an in-house framework based on SOWFA [15]. The use of ALM significantly reduces the number of cells compared to mesh-resolved CFD approaches. The nacelle and tower are modeled using the immersed boundary method. This work uses the DTU 10 MW reference onshore turbine [16]. This machine has a rated wind speed of 11.4 m/s and a rated rotor speed of 9.6 rpm. The pressure and flow velocity at the surfaces shown in Figure 1 are extracted from the CFD domain and

used in the FW-H acoustic analogy to calculate the noise at a far-field observer. This work does not consider sound propagation effects such as refraction, ground reflection, and absorption. A detailed description of the CFD setup and the FW-H formulation can be found in our earlier work [7].

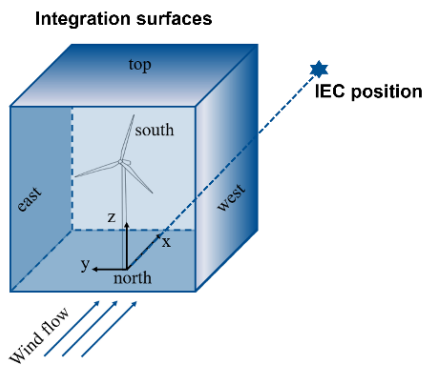


Figure 1 - FW-H analogy with permeable integration surfaces around the WT.

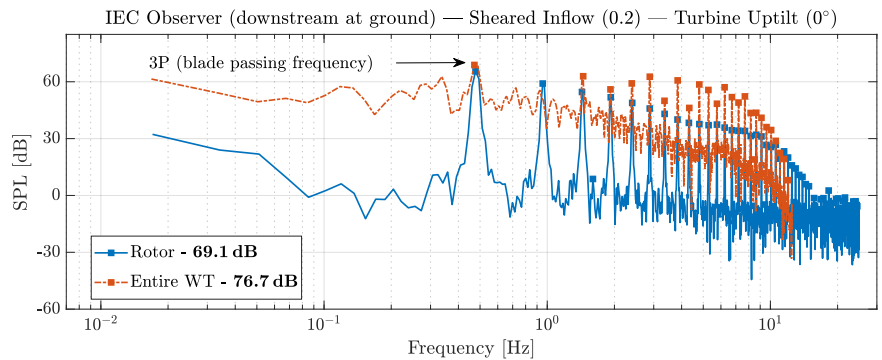


Figure 2 - SPL spectra for the DTU 10 MW WT at rated conditions in a sheared inflow.

This approach uses established, computationally efficient tools, enabling a comprehensive analysis of factors influencing infrasound noise emissions from WTs, including rotor-tower interactions, observer positions, environmental conditions, and design parameters. These analyses are discussed in detail in our previous work [7]. This study highlighted that tonal peaks generated at the BPF and its harmonics when the blades pass in front of the tower dominate the infrasound spectrum. The difference between the noise levels obtained for the “Entire WT” and just the “Rotor” is shown in Figure 2. The plot shows the unweighted SPL spectra for the two cases with an overall sound pressure level (*OASPL*) difference of approximately **8 dB** at an observer on the ground at a downstream distance $R_0 = H + D/2$, where D is the rotor diameter and H is the hub height, which is a reference position as per IEC guidelines. The significant difference in noise levels is due to rotor-tower interactions, with the broadband noise increase in the "Entire WT" case attributed to the turbulence-generated noise in the near-wake of the WT. The change of a few design parameters, such as up-tilt and overhang, was also investigated in that same study with the goal of reducing these rotor-tower interactions and infrasound emissions [7]. In the current study, IPC strategies are developed to further mitigate infrasound noise emissions from WTs.

2.2 Individual pitch control for infrasound

An IPC approach is proposed to reduce the rotor-tower interactions when blades pass in front of the tower. As a preliminary step, the change in the angle of attack (ΔA_oA) is plotted throughout a single rotation of the DTU 10 MW WT for different positions along the blade span (normalized to the radius R) in Figure 3. In this case, the WT is operating in uniform inflow at rated conditions with no up-tilt for simplification. These periodic *AoA* fluctuations are primarily caused by a reduction in the relative wind speed due to the deceleration of the flow as it approaches the tower. The blade is directly in front of the tower when the azimuth position is 180° . Figure 3 also shows the change in lift experienced over a single rotation. It can be noted that close to the root, due to stall, the change in the lift is quite abrupt, even for a uniform inflow. However, moving towards the tip of the blade, a distinct behavior appears, characterized by sharp reductions in *AoA* and lift when blades cross the tower. The hypothesis used here is that the change in lift at the blade airfoils is a good indicator of the unsteady aerodynamics experienced by the rotor. This leads to unsteady rotor-tower interactions that generate the tonal peaks observed in the infrasound noise spectrum. Figure 3 also shows the RMS value of the change in lift ΔL_{rms} calculated for each blade position, which is used as a noise indicator.

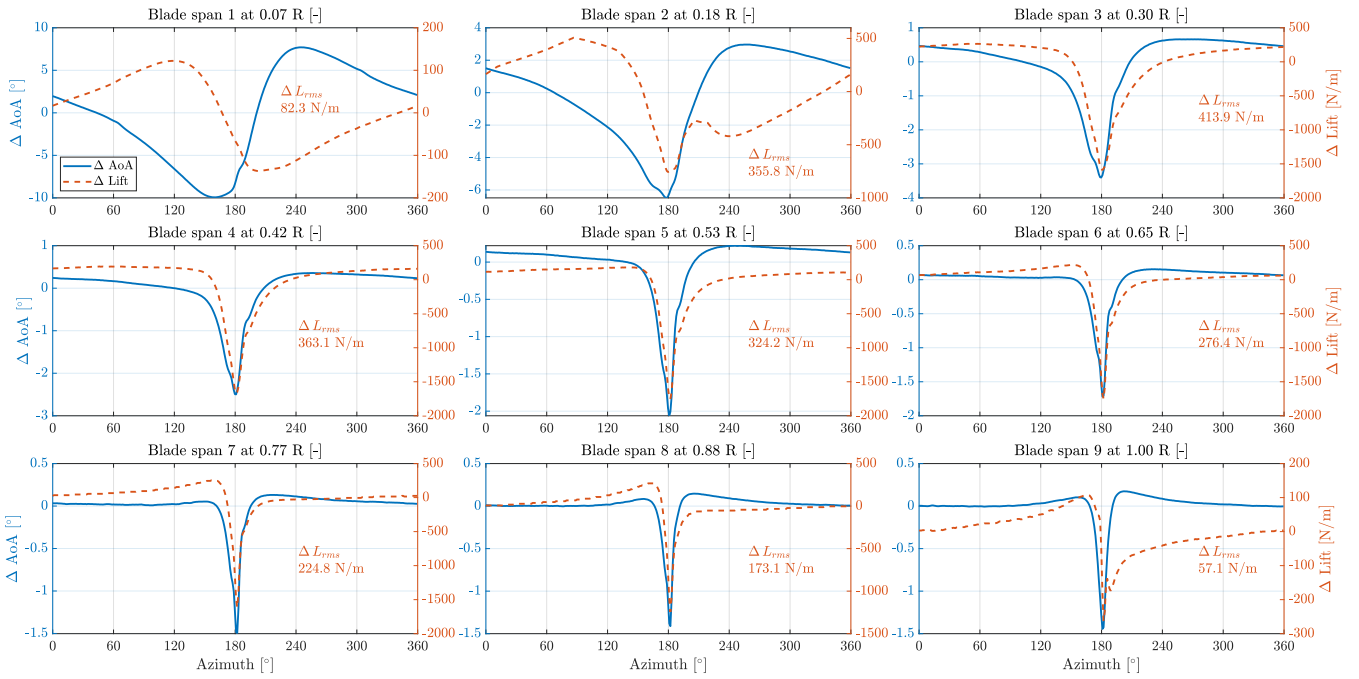


Figure 3 – Change in the angle of attack AoA ($^{\circ}$) and lift (N/m) along the blade span over a single rotation in uniform inflow at rated conditions.

Furthermore, the pressure and velocity distributions on the blade surfaces are reconstructed using the airfoil polars associated with the blade elements of the actuator line and the boundary layer software X-FOIL [17]. A BEM-based formulation of the moving FW-H analogy is applied to the rotating blades. It calculates the noise emitted from different positions along the blade span [12]. The $OASPL$ and the RMS value of the acoustic pressure signal AP_{rms} are used as indicators of emitted noise. These two quantities exhibit different sensitivities when analyzed as functions of blade position, as shown in Figure 4. Since $OASPL$ is a logarithmic measure, it smoothens the variations experienced along the blade. On the other hand, AP_{rms} is a linear measure and is more useful in highlighting localized noise emissions along the blade span.

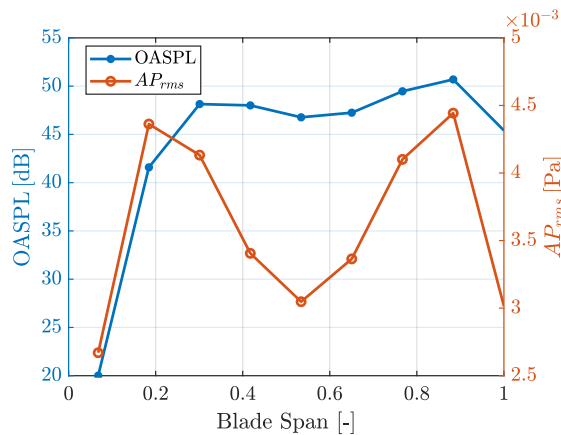


Figure 4 - Noise indicators along the blade span of the WT in uniform inflow at rated conditions using the moving FW-H analogy at an IEC observer.

The pitch control strategy utilizes ΔL_{rms} and AP_{rms} as noise indicators to apply weights on the AoA profiles along the blade span, consequently generating optimal pitch profiles as functions of the azimuth position of the blade. The weighted-mean AoA profiles are further modified to restrict the pitch rate to 7.5 $^{\circ}/s$, which is assumed to be the limit for the DTU 10 MW turbine. The pitch profiles are chosen as the opposite of the weighted-mean AoA profiles to counteract the tonality of the infrasound spectrum. A summary of the weighted-mean AoA profiles, the rate of change of the weighted-mean AoA profiles representing the blade pitch rate, and the weighting applied to the different blade stations for the two noise indicators is shown in Figure 5. The ΔL_{rms} -based weighting emphasizes the midspan of the blade, while

placing reduced importance on the root and the tip of the blade. The AP_{rms} -based weighting gives a relatively uniform importance to all nodes, with a slightly higher relevance to the midspan of the blade. The two profiles are relatively similar, with AP_{rms} slightly less sharp due to its higher weighting close to the root. Despite the pitch rate limitations, the zoomed-in inset for the weighted-mean AoA profile highlights the minimal difference between the two strategies when the blades cross the tower. The optimized pitch profiles with pitch rate limitations ($\Delta L_{rms, ltd}$ and $AP_{rms, ltd}$) are applied in open loop as functions of the azimuth to counteract the sharp fluctuations in lift observed along the blade span and reduce the unsteadiness of rotor-tower interactions.

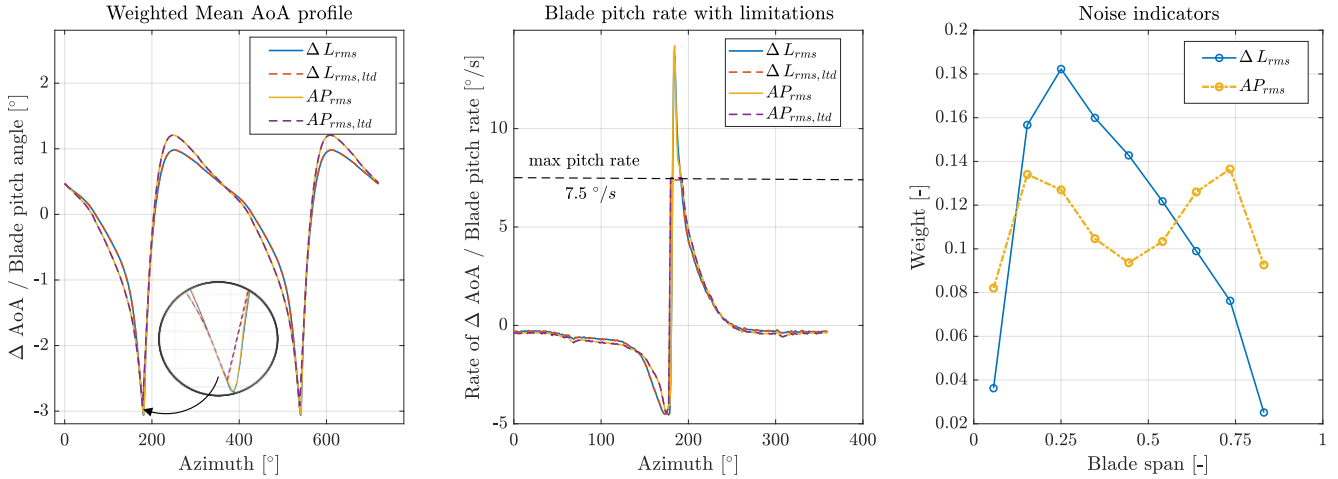


Figure 5 - Optimized individual pitch control profiles in uniform inflow at rated conditions. Weighted mean AoA profiles (left); blade pitch rates with limitations (middle); and weights for blade stations based on noise indicators (right).

3. Results

3.1 Uniform inflow with no uptilt

In this section, the effect of IPC on the infrasound emissions is evaluated for uniform inflow conditions. The DTU 10 MW WT is operated at rated conditions with no uptilt, with the blades following an IPC strategy optimized as a function of the azimuth position, as explained in the previous section. Figure 5 summarizes the two IPC profiles, $\Delta L_{rms, ltd}$ and $AP_{rms, ltd}$, with pitch rate limitations. The unweighted SPL spectra for these two IPC strategies are compared to the baseline case “No IPC” in Figure 6. The spectra show that both IPC strategies eliminate the 3P harmonic, which reduces the OASPL by **1.5-2 dB**, depending on the strategy.

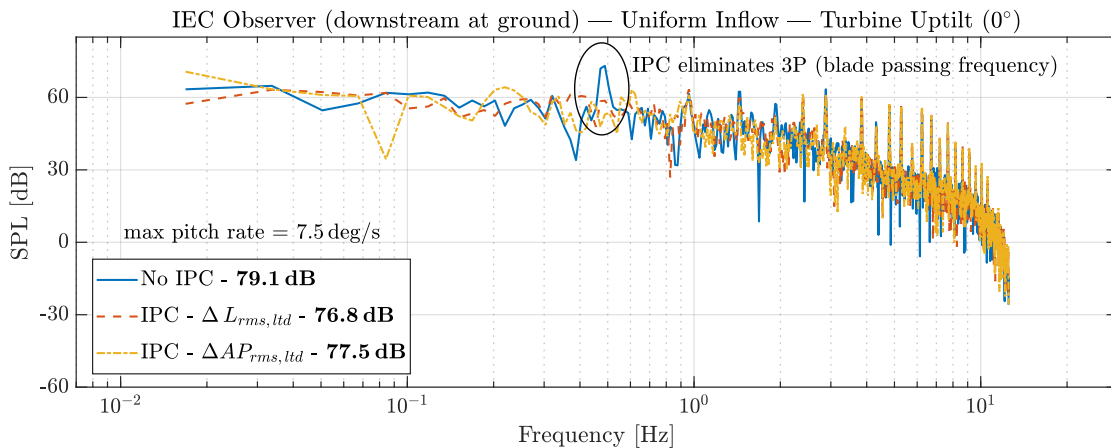


Figure 6 - Effect of individual pitch control profiles on the SPL spectra in uniform inflow at rated conditions.

The $\Delta L_{rms, ltd}$ -based strategy performs slightly better than the $AP_{rms, ltd}$ -based strategy, which can be attributed to the noise indicator targeted by the strategy. Since lift-based weighting gives higher importance to the midspan of the blade, it creates a slightly sharper pitch profile, which is more effective in reducing rotor-tower interactions. Both strategies have almost no impact on the higher harmonics of the infrasound spectra.

3.2 Sheared inflow with WT up tilt

In this section, the DTU 10MW WT is still operated at rated conditions but in a sheared inflow (0.2 power law exponent) to test the impact of IPC on infrasound emissions in a more realistic inflow, typically observed at nighttime. Sheared inflow reduces the 3P peak compared to a uniform inflow because of the lower wind speeds experienced in the bottom half of the rotor that interacts with the tower. The turbine is also configured with a 5° up tilt, which further reduces the infrasound noise emissions by increasing the distance between the blade and tower and significantly reducing rotor-tower interactions [7]. Figure 7 shows the change in the angle of attack AoA ($^\circ$) and lift (N/m) over a single rotation along the blade span.

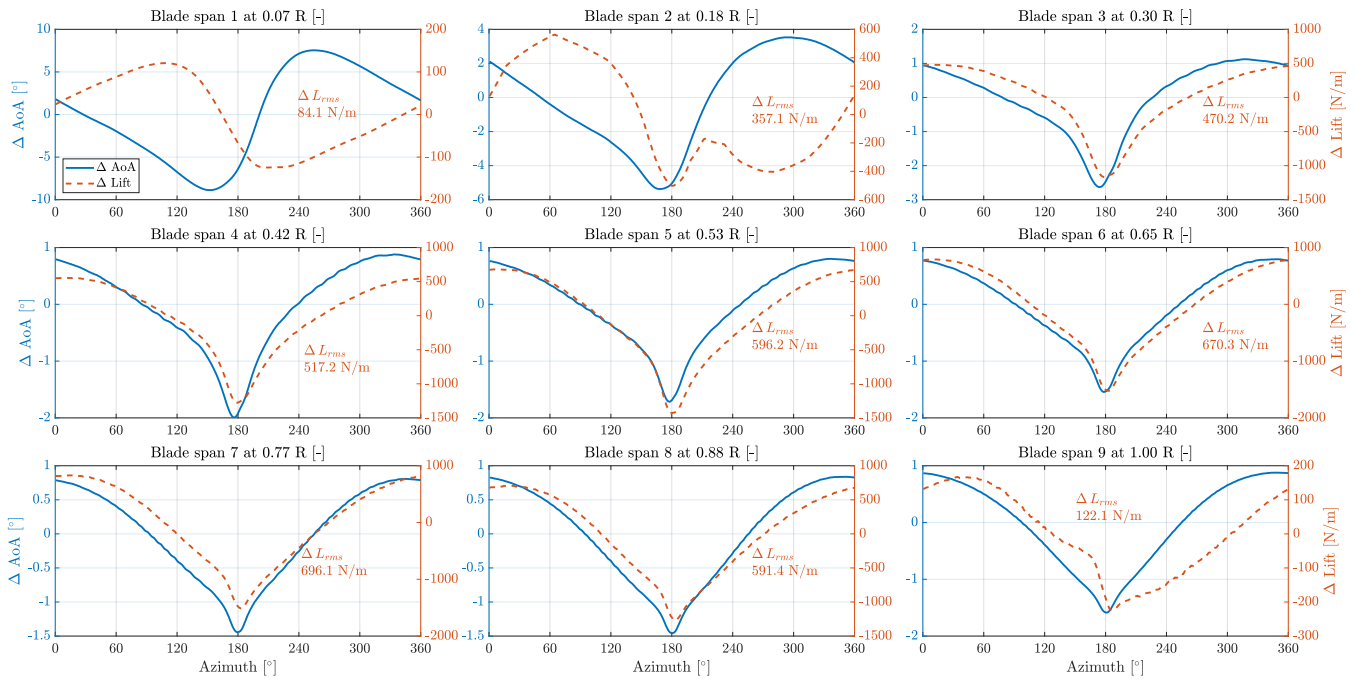


Figure 7 - Change in the angle of attack AoA ($^\circ$) and lift (N/m) along the blade span of the WT over a single rotation in sheared inflow at rated conditions.

A broader variation in AoA and lift is observed due to shear, with a slightly sharper drop observed near 180° when the blade is directly in front of the tower. The optimized pitch profile is obtained by weighting these ΔAoA profiles along the blade span based on ΔL_{rms} as the noise indicator. A summary of the weighted-mean AoA profile, the rate of change of the weighted-mean AoA profile representing the blade pitch rate, and the weighting applied to the different blade stations is shown in Figure 8. The optimized profile is much broader for this case than for the uniform inflow case, and the pitch rate is already within the limit. The weighting shifts towards the outer section of the midspan due to higher ΔL_{rms} values, but it still gives very little importance to the root and the tip of the blade. The ΔL_{rms} values in the outer section of the midspan are larger because of the higher wind speed variations experienced by these blade stations in the top and bottom parts of the rotor due to shear.

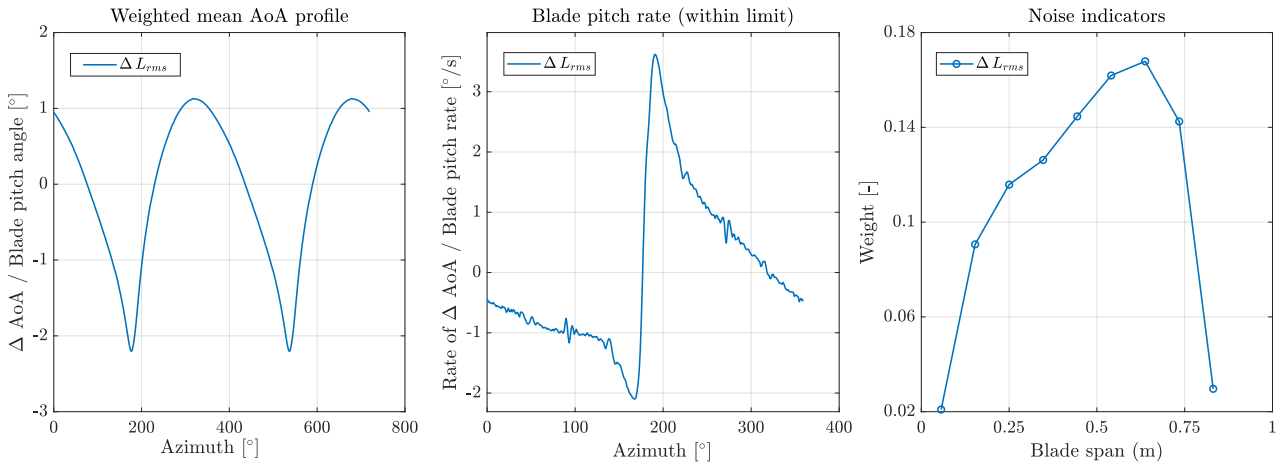


Figure 8 - Optimized individual pitch control profile for the WT with uptilt in sheared inflow at rated conditions. Weighted mean AoA profile (left); blade pitch rate (middle); and weights for blade stations based on ΔL_{rms} (right).

After applying the optimized IPC, Figure 9 compares the unweighted SPL spectra of the “IPC” case to the “No IPC” baseline case. The BPF harmonics, except for the 3P, are negligible due to uptilt. Therefore, a significantly lower OASPL (73.4 dB) is observed in this case compared to the uniform inflow case with no uptilt (79.1 dB). However, the optimized pitch profile still manages to reduce the 3P, and a reduction of **1 dB** in OASPL is achieved.

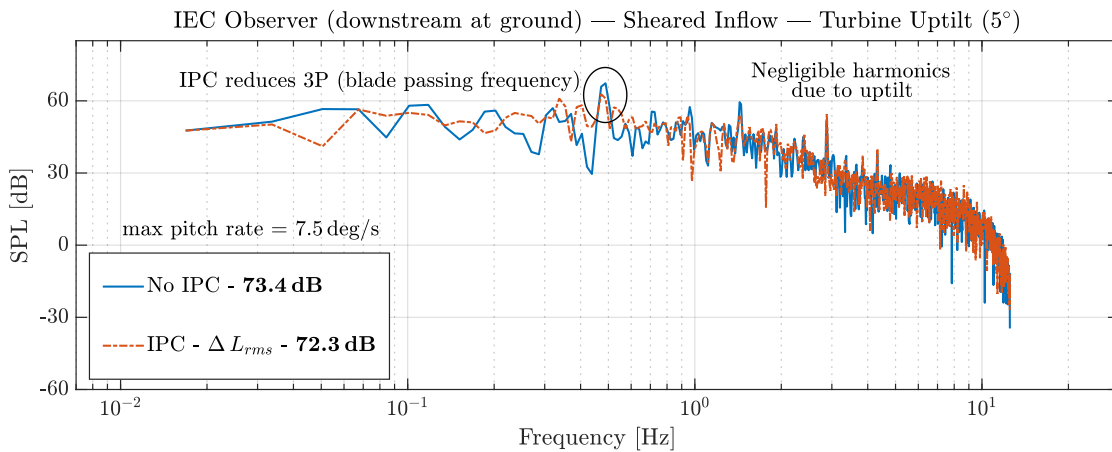


Figure 9 - Effect of IPC on the SPL spectra for WT with uptilt in sheared inflow at rated conditions.

4. Comparison between IPC for infrasound and amplitude modulation

While infrasound and AM are both characterized by cyclic variations in the aerodynamic forces due to blade rotation, subtle differences exist between the aspects that influence these WT noise phenomena. The presence of the tower dominates infrasound emissions from WTs, whereas AM is governed by periodic changes in the blade airfoil self-noise due to turbulent boundary layer trailing edge (TBL-TE) noise and turbulent inflow. In the present work, noise spectra in the audible range are calculated through the framework described in [12], where the TBL-TE noise is calculated using the BPM model [18]. While there is some dependence of WT infrasound on the observer position [7], AM is much more sensitive to the observer position due to trailing edge directivity. In [9], IPC for AM was formulated by directly optimizing the modulation depth at a particular location along with a combination of the deviation in the OASPL, blade pitch angle variations, change in the aerodynamic power output, and fatigue load. Figure 10 shows the pitch profiles developed in [9] for AM reduction as functions of azimuth for different observer positions in uniform inflow (left) and for different shear exponents at a specific observer (right). The pitch activity is highly correlated to the directivity behavior of trailing edge noise and the relative distance between the dominant blade and the observer position.

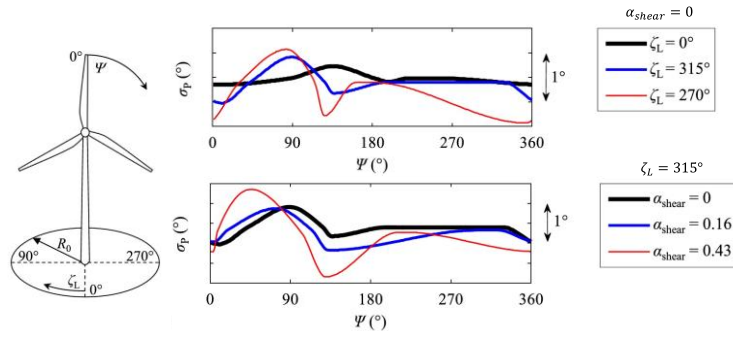


Figure 10 - Optimal azimuthal IPC curves to reduce AM depth for different observer positions in fixed shear (top-right) and for fixed observer in different shear exponents (bottom-right) [9].

On the other hand, the open-loop IPC for infrasound reduction aims to mitigate the unsteadiness of the rotor-tower interactions and reduce the infrasound emissions from WTs. Therefore, there is more pitch activity when the blades cross the tower in the lower half of the rotor. Although this strategy does not target power or fatigue loading, the aerodynamic power output is only minimally affected (<1%), and only a slight increase is observed in blade root loading. Despite the difference in the pitch profiles, it is relevant to study the effect of IPC for infrasound on AM reduction. Figure 11 shows the effect of $\Delta L_{rms, ltd}$ -based IPC on the AM depth for different observers located on the ground at IEC distance, surrounding the WT operating at rated conditions in uniform inflow with no uptilt. The AM depth is calculated as follows:

$$AM_{depth} = \frac{1}{N} \sum_{i=1}^N (OASPL_{95,i} - OASPL_{5,i}), \quad (1)$$

where N is the number of turbine rotations considered, $OASPL_{95,i}$ and $OASPL_{5,i}$ are respectively the 95th and 5th percentile of the A-weighted trailing edge OASPL time history over the i^{th} rotation.

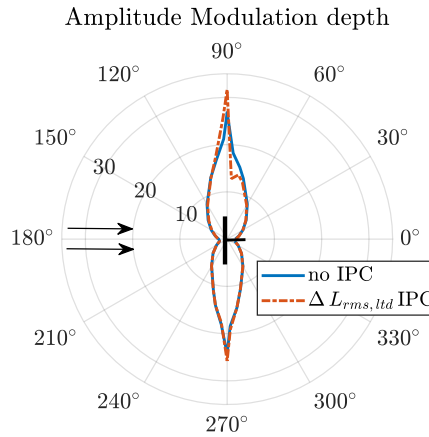


Figure 11 - Effect of IPC ($\Delta L_{rms, ltd}$) for infrasound reduction on AM depth for observers at IEC distance around the WT in uniform inflow.

As expected, the AM depth is much higher in the transverse direction than in the longitudinal one due to the directivity pattern of trailing edge noise. IPC for infrasound has a mixed effect on AM depth. While it does manage to decrease the AM depth in the 60° - 90° section, it increases significantly in the adjacent section (90° - 110°). This jump is due to the sensitivity of the trailing edge directivity model to the blade geometry and observer position. IPC for AM reduction at a specific observer is typically characterized by increased AM depth at other observer locations, generally in orthogonal directions. This study indicates that while IPC for infrasound can reduce AM depth in certain specific directions, further investigation is necessary to evaluate the feasibility of an optimized IPC that effectively minimizes overall noise annoyance from WTs.

5. Conclusions and future work

Infrasound emissions from WT's are primarily generated by rotor-tower interactions at the BPF and its harmonics. In the present work, open-loop IPC strategies are optimized to reduce these emissions by mitigating rotor-tower interactions. Two different noise indicators are used to weigh the angle of attack profiles along the blade span and optimize the pitch profile curves: one based on the lift variation along the blade span, and another using the noise predictions from a BEM-based formulation of the FW-H analogy on the rotating blades. Both strategies obtained a reduction in the 3P blade passing frequency peak and an OASPL reduction of approximately **1.5 - 2 dB** in uniform inflow conditions. Sheared inflow and turbine up-tilt naturally reduce infrasound emissions by decreasing the intensity of rotor-tower interactions. However, the optimized IPC strategy further reduced OASPL by an additional **1 dB**, even in these conditions, demonstrating its robustness.

While sheared inflow already represents a realistic environmental condition experienced by the WT, especially during the night, the addition of a turbulent boundary layer and structural flexibility could provide further insights. So far, IPC has only been developed for the DTU 10 MW WT operating at rated conditions. An extension of this study should investigate the effect of different wind speeds and shear exponents on the IPC profiles. A look-up table-based approach is envisioned as the most practical way to implement an open-loop IPC strategy to adapt dynamically to changing wind conditions. A deeper investigation of the effect of IPC for infrasound on power output and fatigue loading is critical to ensure structural integrity and annual energy production.

Infrasound and AM are linked to periodic aerodynamic forces generated by blade rotation, but the IPC profiles needed to mitigate them are quite different. The effect of blades on the tower influences IPC for infrasound, whereas IPC for AM is very sensitive to observer position and trailing edge directivity. Hence, IPC optimized for infrasound had a mixed effect on AM depth - reducing it in some locations but increasing it in others. This observation may change for a different trailing edge directivity model. Given that IPC for infrasound and AM target different periodic phenomena due to blade rotation, a superimposition of the two IPCs could be a possible way for an optimized IPC that effectively minimizes overall noise annoyance from WT's. However, the sensitivity of AM on the directivity of trailing edge noise could limit any practical solution that optimizes control strategies not only for AM but also for infrasound.

Acknowledgments

This research was supported by the German Federal Ministry for Economic Affairs and Climate Action within the Flamingo (FKZ: 03EE2011B) project.

References

- [1] IEA, "Wind," June 2023. [Online]. Available: <https://www.iea.org/energy-system/renewables/wind>. [Accessed 2025].
- [2] W. Y. Liu, "A review of wind turbine noise mechanism and de-noising techniques," *Renewable Energy*, vol. 108, pp. 311-320, August 2017.
- [3] R. Tonin, "A Review of Wind Turbine-Generated Infrasound: Source, Measurement and Effect on Health," *Acoustics Australia*, vol. 46, no. 1, pp. 69-86, 2017.
- [4] I. van Kamp and F. van den Berg, "Health Effects Related to Wind Turbine Sound, Including Low-Frequency Sound and Infrasound," *Acoustics Australia*, vol. 46, no. 1, pp. 31-57, 2017.
- [5] C. Flemmer and R. Flemmer, "Wind turbine infrasound: Phenomenology and effect on people," *Sustainable Cities and Society*, vol. 89, p. 104308, 2023.
- [6] E. Blumendeller, M. Hofsäß, A. Goerlitz and P. W. Cheng, "Impact of wind turbine operation conditions on infrasonic and low frequency sound induced by on-shore wind turbines," *Journal of Physics: Conference Series*, vol. 2265, no. 3, p. 032048, 2022.
- [7] A. H. Shah, C. R. Sucameli and C. L. Bottasso, "Development of a FW-H tool coupled with CFD for infrasound noise emissions from wind turbines," *Journal of Physics: Conference Series*, vol. 2767, no. 2, p. 022030, 2024.

- [8] F. Bertagnolio, H. A. Madsen, A. Fischer, Bak and Christian, "Cyclic pitch for the control of wind turbine noise amplitude modulation," in *Internoise 2014*, Melbourne, 2014.
- [9] L. Mackowski and T. H. Carolus, "Wind Turbine Trailing Edge Noise: Mitigation of Normal Amplitude Modulation by Individual Blade Pitch Control," *Journal of Sound and Vibration*, vol. 510, p. 116279, 2021.
- [10] J. Ffowes Williams and D. Hawkings, "Sound generation by turbulence and surfaces in arbitrary motion," *Proceedings of the Royal Society of London. Series A, Mathematical and Physical Sciences*, vol. 211, pp. 321-342, 1969.
- [11] F. Farassat, "Derivations of Formulations 1 and 1A of Farassat," NASA, Virginia, 2007.
- [12] C. R. Sucameli, P. Bortolotti, A. Croce and C. L. Bottasso, "Comparison of some wind turbine noise emission models coupled to BEM aerodynamics," *Journal of Physics: Conference Series*, vol. 1037, no. 2, p. 022038, 2018.
- [13] L. Klein, J. Gude, F. Wenz, T. Lutz and E. Krämer, "Advanced computational fluid dynamics (CFD)-multi-body simulation (MBS) coupling to assess low-frequency emissions from wind turbines," *Wind Energy Science*, vol. 3, no. 2, pp. 731-728, 2018.
- [14] G. A. Brès, F. Pérot and D. Freed, "A Ffowes Williams-Hawkings Solver for Lattice-Boltzmann based Computational Aeroacoustics," in *Aeroacoustics Conference*, 2010.
- [15] NREL, "Overview of the Simulator fOr Wind Farm Applications - SOWFA," 2012. [Online]. Available: http://www.sauvegardedubarres.com/pdf/SOWFA_tutorial_05-20-2014.pdf.
- [16] C. Bak, F. Zahle, R. Bitsche, T. Kim, A. Yde and L. C. Henriksen, "The DTU 10-MW Reference Wind Turbine," 2013. [Online]. Available: https://backend.orbit.dtu.dk/ws/portalfiles/portal/55645274/The_DTU_10MW_Reference_Turbine_Christian_Bak.pdf.
- [17] XFOIL, "XFOIL Documentation," 2017. [Online]. Available: <https://web.mit.edu/drela/Public/web/xfoil/>.
- [18] T. F. Brooks, S. D. Pope and M. A. Marcolini, "Airfoil Self-Noise and Prediction," NASA Reference Publication 1218, 1989.

Paper #18 - ID: 352

Title: Numerical investigation of noise propagation in wind farms and the influence of wind turbine layouts

Author: Jules Colas

11th Edition of the
International Conferences on
Wind Turbine Noise
Copenhagen, Denmark – 10th to 13th June 2025

Numerical investigation of noise propagation in wind farms and the influence of wind turbine layouts

Jules Colas, Ariane Emmanuelli, and Didier Dragna ¹

Ecole Centrale de Lyon, CNRS, Université Claude Bernard Lyon 1, INSA Lyon, LMFA, UMR5509, 69130, Ecully, France

Richard J.A.M. Stevens

Physics of Fluids Group, Max Planck Center Twente for Complex Fluid Dynamics, J. M. Burgers Center for Fluid Dynamics, University of Twente, P.O. Box 217, 7500 AE Enschede, The Netherlands

Summary

This study presents an analysis of noise propagation from a wind farm. Large eddy simulations are used to model the flow around the wind farm. The average flow field data is then integrated into sound source and propagation models. Sound propagation is simulated using the parabolic equation method, while wind turbine noise is modeled with an extended moving source. Initially, noise propagation from a single wind turbine is evaluated to establish a baseline. Following this, the analysis is extended to a 16-turbine aligned wind farm to examine the influence of wind farm flow on noise propagation. The analysis includes the overall sound pressure levels and amplitude modulation around the wind farm. The results highlight that the aligned wind farm layout tends to smooth out the variations in sound pressure levels, compared to an isolated wind turbine. In particular, the amplitude modulation downwind is significantly attenuated.

1. Introduction

Noise propagation due to an isolated wind turbine has been extensively investigated in the literature. In particular, numerical studies have highlighted the importance of the turbine wake for the prediction of noise levels downwind. Accurately capturing the underlying phenomena requires a detailed description of wind speed profiles, wind turbine noise sources, and propagation effects. Several propagation models have been proposed including geometrical approaches [1] and wave-based approaches (parabolic equations [2] or linearized Euler equations [3]). While the latter approaches have been mostly restricted to two-dimensional configurations, three-dimensional propagation effects due to wakes have recently been investigated by Bommidala *et al* [4] using a parabolic equation. Effects of the topography on wind turbine noise propagation have also been examined [5, 6].

Noise propagation from wind farms has received less attention. Cao *et al* [7] have highlighted that propagation of acoustic waves in a wind farm can be significantly affected by the multiple wakes of the turbines. Shen *et al* [8] have illustrated wind farm noise accounting for complex terrain. We can also mention the works

¹Corresponding author - Email: didier.dragna@ec-lyon.fr

performed by Cao *et al* [9] and Nyborg *et al* [10] for the optimization of wind farm layout using, among others, an acoustic criterion. However, there has been no systematic and detailed study investigating the effect on a wind farm on noise generation and propagation.

This study aims to address this gap by performing wind turbine noise simulations for two configurations: an isolated wind turbine and a wind farm comprising 16 turbines. In this paper, we focus on a single wind farm layout, i.e. an aligned wind farm consisting of four rows of four turbines. A detailed comparison is conducted, examining the flow characteristics, sound power levels of the turbines, and propagation effects. The sound pressure levels and the amplitude modulation around the wind farm are analyzed in relation to those around the isolated wind turbine.

The paper is organized as follows. In Sec. 2, the configurations and the methods are introduced. Sec. 3 presents the results. Finally, concluding remarks are given in Sec. 4.

2. Scenario and methods

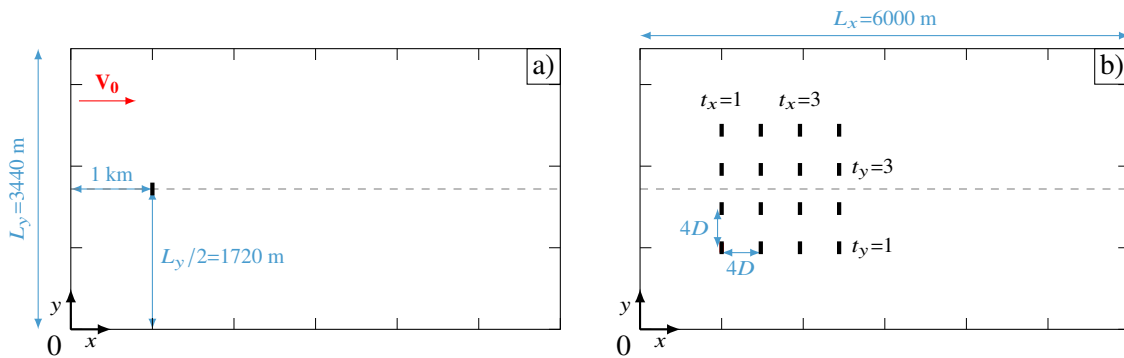


Figure 1 Sketch of the two configurations investigated: a) an isolated wind turbine and b) an aligned wind farm of 16 turbines. Wind turbines are indicated using thick lines.

Two configurations are investigated, as sketched in Fig. 1: an isolated wind turbine and a wind farm composed of 16 turbines. All turbines are the same with a hub height $z_h = 90$ m and a rotor diameter $D = 120$ m. In the wind farm, the turbines are positioned uniformly in an aligned layout, with a spacing of $4D$ in both the streamwise and spanwise directions. A neutral atmosphere is considered. The wind speed at hub height is set to 11.4 m s^{-1} . The ground is flat and absorbing.

The flow around the wind turbine is obtained through large eddy simulations (LES) using the code developed at the University of Twente (see, e.g., [11]). For the wind turbine noise source model, we use the model proposed by Tian and Cotté [12] and based on Amiet's strip theory. Each blade is split into eight segments. The source model provides the effective sound power level in free field (SWL) for each blade segment, depending on the blade orientation. Finally, the propagation model is based on a two-dimensional parabolic equation, that accounts for the influence of the mean flow on sound propagation, without relying on the effective sound speed approximation [13]. Simulations are performed for seven equivalent point sources distributed along a vertical line in the rotor plane of each wind turbine, following the approach introduced by Cotté [14]. To obtain results in a three-dimensional geometry, multiple simulations are performed in vertical slices around each turbine. The frequency range of the simulations is between 50 Hz and 1080 Hz.

The computation of the sound pressure levels follows the methodology proposed in Colas *et al* [3, 15]. First, the mean flow and the turbulent dissipation rate are extracted from the LES results. They are both used in the source model to calculate the SWL for each position of the blade segments. The mean flow from the LES is also used in the propagation model. Propagation simulations are performed for each turbine and for each equivalent point source to determine the sound pressure level relative to the free-field (ΔL). The overall sound pressure level (OASPL) due to a wind turbine is obtained by combining SWL for each blade segment position with the corresponding ΔL for the equivalent point source and integrating over the frequency range.

From this, we obtain the time-varying OASPL for the wind farm by summing the contributions of all wind turbines, accounting for the differences in the emission time. Finally, we can determine the average value of the OASPL, denoted $\overline{\text{OASPL}}$, and the amplitude modulation (AM), defined as the difference between the maximum and minimum value of the OASPL.

3. Results

3.1 Flow

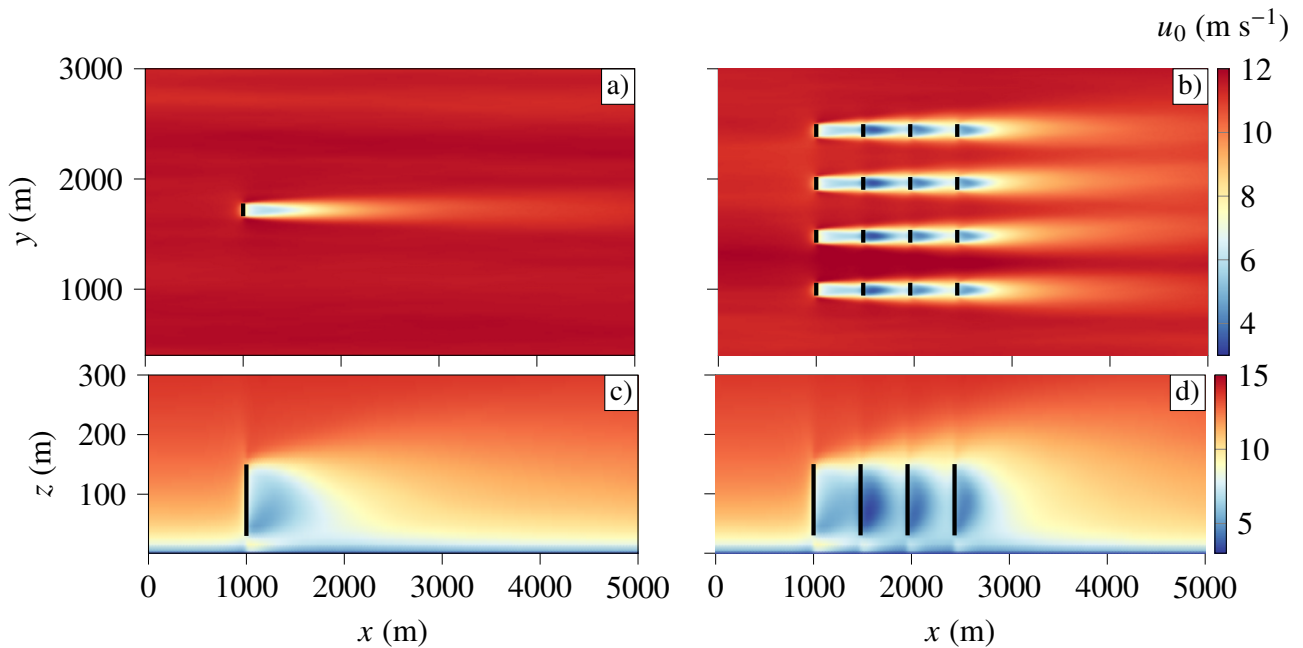


Figure 2 Streamwise wind velocity fields for an isolated wind turbine in a) and c) and for the wind farm in b) and d). In a) and b), the fields are plotted for a plane at hub height ($z = z_h$). In c) and d), the fields are plotted for a plane at $y = 1720$ m and $y = 1000$ m, respectively. Wind turbine rotors are indicated using a black line.

Figure 2 shows the streamwise component of the mean flow for an isolated wind turbine and for the wind farm. We note the wake in Fig. 2 a) and c) behind the isolated wind turbine. For the wind farm in Fig. 2 b) and d), the wake is almost identical for the wind turbines in a same row. The wake behind the turbines in the first row corresponds to that behind the isolated turbine. The highest velocity deficit is observed behind the turbines in the second row. Finally, the wakes behind the turbines in the third and fourth rows are nearly identical, with a velocity deficit falling between those of the first and second rows.

3.2 Source

We now focus on the source power of the wind turbines. First, the source model provides a source power level of 103.2 dBA for the isolated turbine. In Fig. 3, we show the relative sound power level of the turbines in the wind farm using the sound power level for the isolated wind turbine as a reference. It can be observed that the turbines in each row generate nearly the same SWL, with variations within a 1 dBA margin. The highest SWL is obtained for the first row ($t_x = 1$), corresponding to that of the isolated wind turbine. The second row ($t_x = 2$) exhibits the lowest SWL, showing a reduction of 6.5 dBA compared to the isolated wind turbine. Finally, the SWL of the third and fourth rows gradually increase but remain 4 dBA lower than that of the isolated wind turbine. Overall, these variations in SWL within the wind farm are related to those in the mean wind speed. In particular, the reduction in SWL reflects the reduction in wind speed in the rotor plane due to the wakes of the upstream turbines.

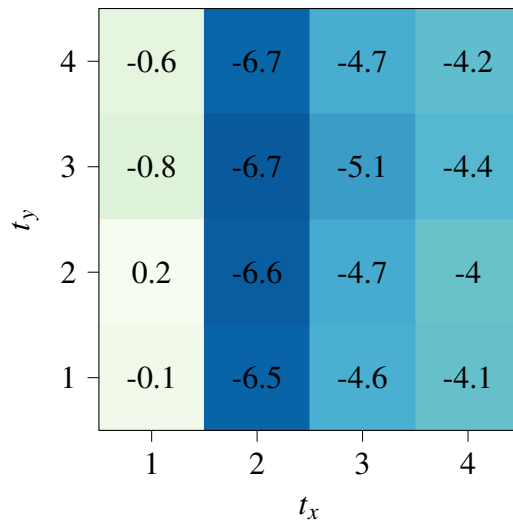


Figure 3 Relative sound power level for each turbine of the wind farm, with the reference level corresponding to that of an isolated wind turbine.

3.3 Propagation

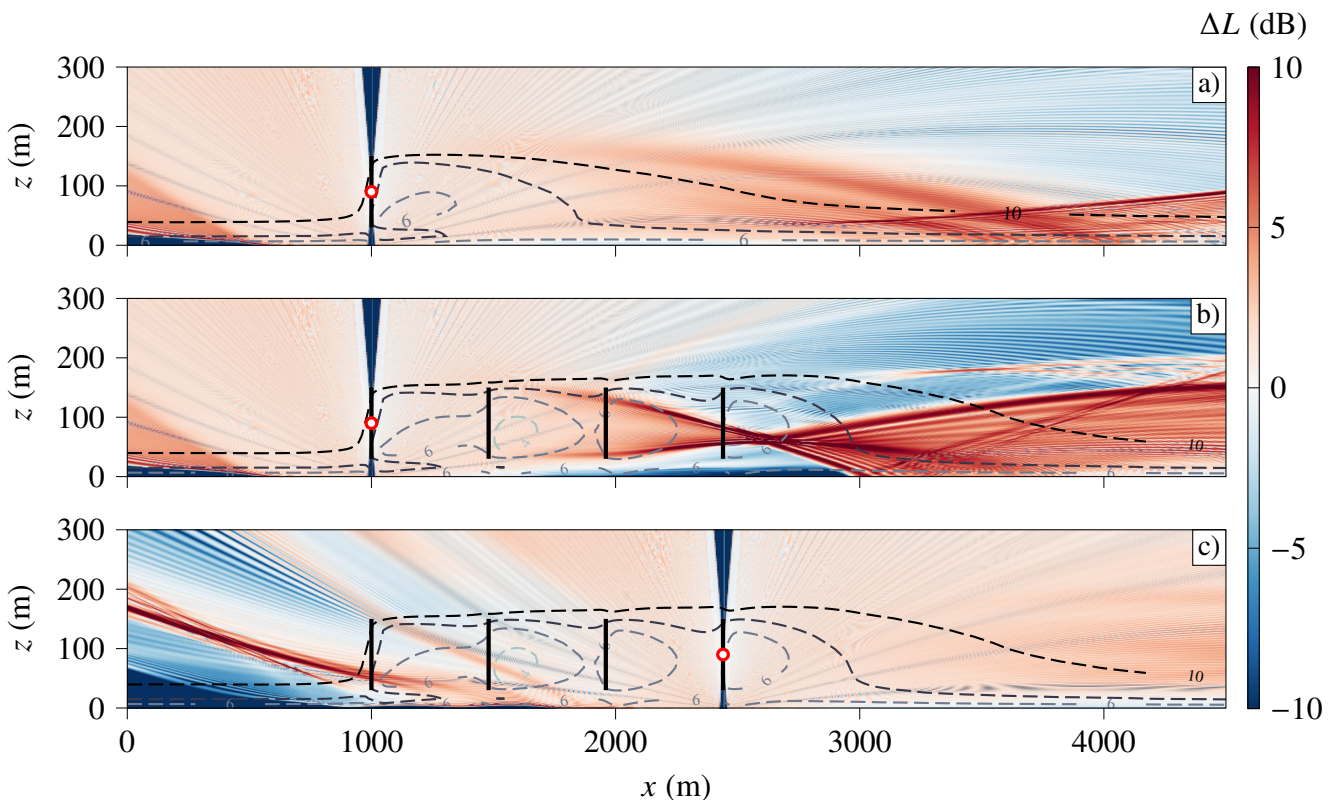


Figure 4 Propagation from a source located at hub height: a) for the isolated wind turbine in the plane $y = 1720$ m and for the b) first ($t_x = 1, t_y = 1$) and c) last ($t_x = 4, t_y = 1$) turbines of the wind farm in the plane $y = 1000$ m. The streamwise wind speed is shown with dashed contour lines. The acoustic source is indicated with a red dot.

Figure 4 illustrates the difference in propagation between an isolated wind turbine and a turbine within a wind farm. Fig. 4 a) shows the contour of ΔL for a source located at hub height of the isolated wind turbine. Upstream, we note the presence of a shadow zone close to the ground. Downstream, the presence of the wake creates focusing of acoustic waves leading to a 5 dB increase in ΔL near the ground at a distance of 2.5 km from the turbine. The corresponding contours for the wind farm are plotted in Fig. 4 b) and c). In b), the source is located at the hub of a turbine in the first row. The propagation upstream is similar to that

for the isolated wind turbine. The multiple wakes cause a large focusing of sound waves downstream, at $x = 2.7$ km and $z = 70$ m. At the ground, ΔL increases by a maximum of 10 dB at $x = 3$ km. Finally, in c), the source is located at the hub of a turbine in the fourth row. Upstream propagation is significantly affected by the crossing of the wakes. Nevertheless, a shadow zone remains visible at the ground for $x < 2$ km. Finally, we do not observe focusing due to the wake downstream, which is due to the reduced value of the velocity deficit. Focusing may still appear at greater distance but it would be less efficient than that observed for an isolated wind turbine.

3.4 Noise levels

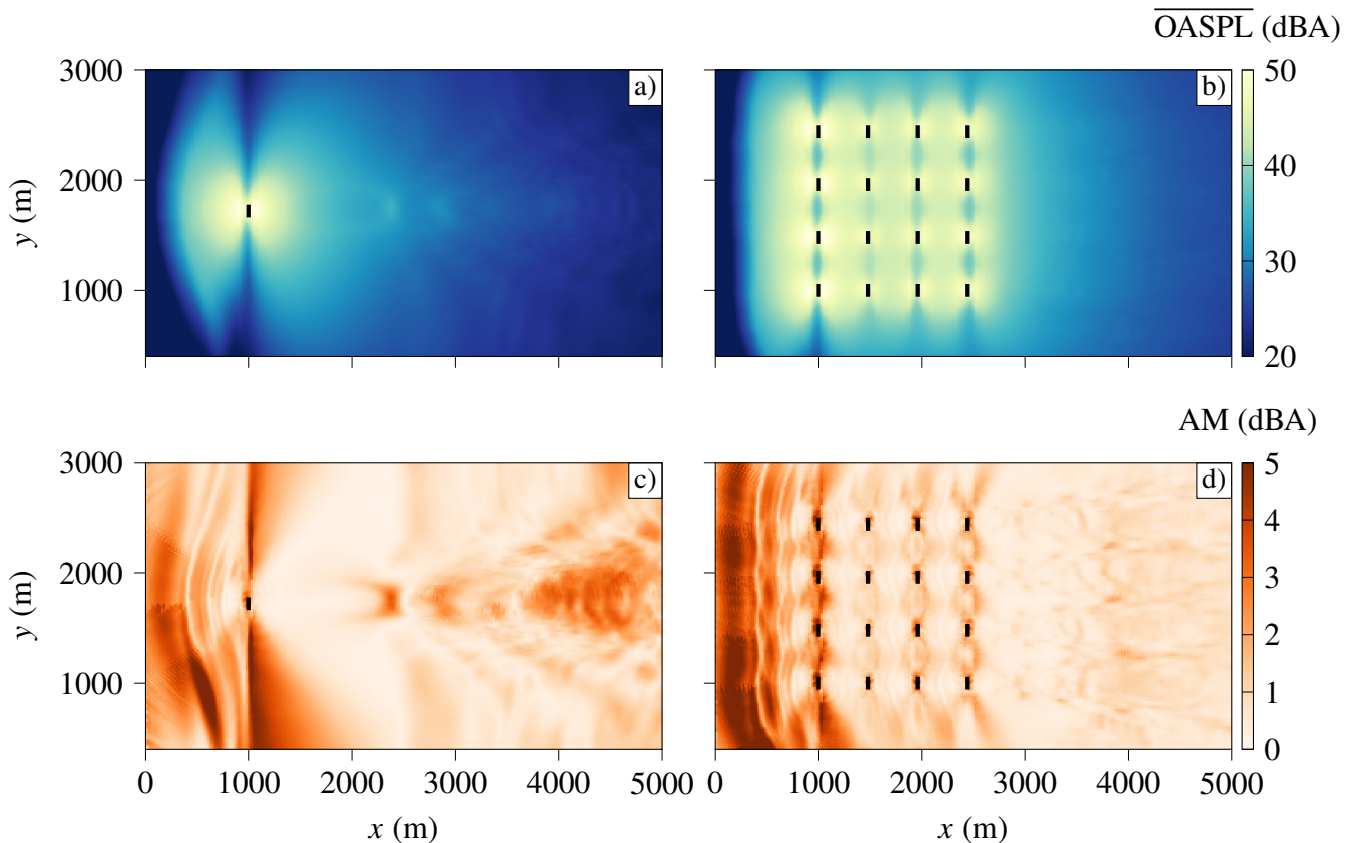


Figure 5 a), b) \overline{OASPL} and c), d) AM for a), c) the isolated wind turbine and b), d) the wind farm. The fields are plotted for a plane at $z = 2$ m. Wind turbine rotors are indicated with black lines.

Figure 5 shows the \overline{OASPL} and the AM for the isolated wind turbine and the wind farm in a horizontal plane at $z = 2$ m. Concerning the \overline{OASPL} for the isolated wind turbine in Fig 5 a), we observe the shadow zone upstream for $x < 0.5$ km and the extinction zones crosswind with a large reduction of the \overline{OASPL} . Downwind, we note for $x > 2$ km zones with increased \overline{OASPL} due to focusing by the wake. For the wind farm in Fig 5 b), the shadow zone remains visible for $x < 0.5$ m. The crosswind extinction zones are significantly smoothed out due to the surrounding turbines. Moreover, no focusing effects induced by the wakes are observed. As for crosswind extinction zones, the \overline{OASPL} generated by the surrounding turbines exceeds that of the focusing zones, effectively masking their presence. Additionally, as reported in Sec. 3.3, the wake velocity deficit behind the turbines in the fourth row is too small to generate significant focusing zones downwind.

The AM for the isolated wind turbine is shown in Fig 5 c). High values are observed upstream at the boundary of the shadow zone, within the crosswind extinction zones, and downstream for $x > 2$ km along the focusing zones induced by the wake. For the wind farm in Fig 5 d), the AM remains high upstream at the boundary of the shadow zone. However, it is significantly reduced in the crosswind extinction zones, except for the turbines in the first row. Finally, the AM downstream is close to zero, further illustrating that turbine

wakes have no noticeable influence on wind farm noise for this particular layout.

4. Conclusion

Noise propagation of an aligned wind farm has been analyzed and compared to that of an isolated wind turbine under neutral atmospheric conditions. It was shown that the sound power level of the turbines within the wind farm varies significantly due to spatial variations in the flow field. Sound propagation is also largely impacted by the presence of multiple wakes. However, in an aligned wind farm, the average sound pressure levels are more uniform and the amplitude modulations are reduced compared to an isolated wind turbine, as the contributions from the surrounding turbines tend to smooth out the variations in the sound pressure levels. In particular, the increase in levels observed in the focusing zones induced by the turbine wake for an isolated wind turbine is not noticeable for the aligned wind farm.

Acknowledgments

This work was performed within the framework of the LABEX CeLyA (ANR-10-LABX-0060) of Université de Lyon, within the program “Investissements d’Avenir” (ANR-16-IDEX-0005) operated by the French National Research Agency (ANR). This project has received funding from the European Research Council under the European Union’s Horizon Europe program (Grant No. 101124815). It was granted access to the HPC resources of PMCS2I (Pôle de Modélisation et de Calcul en Sciences de l’Ingénieur et de l’Information) of Ecole Centrale de Lyon.

References

- [1] D. Heimann and A. Englberger, “3D-simulation of sound propagation through the wake of a wind turbine: Impact of the diurnal variability,” *Applied Acoustics*, vol. 141, pp. 393–402, 2018.
- [2] E. Barlas, W. J. Zhu, W. Z. Shen, M. Kelly, and S. J. Andersen, “Effects of wind turbine wake on atmospheric sound propagation,” *Applied Acoustics*, vol. 122, pp. 51–61, 2017.
- [3] J. Colas, A. Emmanuelli, D. Dragna, P. Blanc-Benon, B. Cotté, and R. J. A. M. Stevens, “Wind turbine sound propagation: Comparison of a linearized Euler equations model with parabolic equation methods,” *Journal of the Acoustical Society of America*, vol. 154, no. 3, pp. 1413–1426, 2023.
- [4] H. Bommidala, J. Colas, A. Emmanuelli, D. Dragna, C. Khodr, B. Cotté, and R. J. A. M. Stevens, “Three-dimensional effects of the wake on wind turbine sound propagation using parabolic equation,” *Journal of Sound and Vibration*, vol. 608, no. 119036, pp. 1–22, 2025.
- [5] D. Heimann, A. Englberger, and A. Schady, “Sound propagation through the wake flow of a hilltop wind turbine - A numerical study,” *Wind Energy*, vol. 21, no. 8, pp. 650–662, 2018.
- [6] J. Colas, A. Emmanuelli, D. Dragna, P. Blanc-Benon, B. Cotté, and R. J. A. M. Stevens, “Impact of a two-dimensional steep hill on wind turbine noise propagation,” *Wind Energy Science*, pp. 1–26, 2024.
- [7] Z. Sun, W. J. Zhu, W. Z. Shen, E. Barlas, J. N. Sørensen, J. Cao, and H. Yang, “Development of an efficient numerical method for wind turbine flow, sound generation, and propagation under multi-wake conditions,” *Applied Sciences*, vol. 9, no. 1, p. 100, 2018.
- [8] W. Z. Shen, W. J. Zhu, E. Barlas, and Y. Li, “Advanced flow and noise simulation method for wind farm assessment in complex terrain,” *Renewable Energy*, vol. 143, pp. 1812–1825, 2019.
- [9] J. F. Cao, W. J. Zhu, W. Z. Shen, J. N. Sørensen, and Z. Y. Sun, “Optimizing wind energy conversion efficiency with respect to noise: A study on multi-criteria wind farm layout design,” *Renewable Energy*, vol. 159, pp. 468–485, 2020.
- [10] C. M. Nyborg, A. Fischer, P.-E. Réthoré, and J. Feng, “Optimization of wind farm operation with a noise constraint,” *Wind Energy Science*, vol. 8, no. 2, pp. 255–276, 2023.

- [11] S. N. Gadde, A. Stieren, and R. J. A. M. Stevens, “Large-eddy simulations of stratified atmospheric boundary layers: Comparison of different subgrid models,” *Boundary-Layer Meteorology*, vol. 178, no. 3, pp. 363–382, 2021.
- [12] Y. Tian and B. Cotté, “Wind turbine noise modeling based on Amiet’s theory: Effects of wind shear and atmospheric turbulence,” *Acta Acustica united with Acustica*, vol. 102, no. 4, pp. 626–639, 2016.
- [13] V. E. Ostashev, D. K. Wilson, and M. B. Muhlestein, “Wave and extra-wide-angle parabolic equations for sound propagation in a moving atmosphere,” *Journal of the Acoustical Society of America*, vol. 147, no. 6, pp. 3969–3984, 2020.
- [14] B. Cotté, “Extended source models for wind turbine noise propagation,” *Journal of the Acoustical Society of America*, vol. 145, no. 3, pp. 1363–1371, 2019.
- [15] J. Colas, A. Emmanuelli, D. Dragna, P. Blanc-Benon, B. Cotté, and R. J. A. M. Stevens, “Exploring the effect of wind farm flow on wind turbine noise propagation through numerical simulations,” in *Wind Turbine Noise 2023*, (Dublin, Ireland), pp. 131–141, INCE/Europe, 21 - 23 June 2023.

Paper #19 - ID: 353

Title: A feasibility study on Neural Networks for Rating Prominent Tones in Noise

Author: Lars Sommer Søndergaard

11th Edition of the
International Conferences on
Wind Turbine Noise
Copenhagen, Denmark – 10th to 13th June 2025

A feasibility study on Neural Networks for Rating Prominent Tones in Noise

Lars Sommer Søndergaard¹

FORCE Technology, Department of Acoustics, Noise and Vibration, Denmark

Rune Sehested & Niels Asp Fuglsang

FORCE Technology, Department of Digital Asset-Integrity Solutions, Denmark

Torben Holm Pedersen

FORCE Technology, Department of SenseLab, Denmark

Summary

Wind turbine noise primarily consists of aerodynamic noise but often also includes audible tones. The presence of audible tones in noise significantly increases annoyance compared to noise without such tones. Many countries' legislation includes a penalty of a few dB to measured noise levels to account for this increased annoyance. Various objective methods based on psycho-acoustic principles exist to determine the audibility of tones, but results can vary widely, especially since many methods assume stationary tones. Wind turbine noise, however, often features tones that vary in amplitude and frequency due to the non-stationary nature of wind speed and direction. Traditionally, the development, testing, and rating of objective tonality methods rely on listening tests, which are time-consuming and costly. SenseLab's Virtual Listener Panel™ (VLP), a machine learning-powered tool trained on expert panel data, has demonstrated efficiency in evaluating perceptual quality of audio products. This study investigates the feasibility of applying a similar approach to a dataset of audio files with tonal content, previously analysed through both listening tests and objective methods. The goal is to investigate if neural networks can provide a reliable and efficient alternative for rating prominent tones in noise. Although this feasibility study is based on a relatively small set of data, the results are promising.

1. Introduction

It is a general experience that the presence of audible tones in noise increases the annoyance relative to the same noise level without the audible tones. In the legislation of many countries, a “penalty” of 3-6 dB is added to the measured noise levels (L_{Aeq}) to compensate for the extra annoyance due to clearly audible tones in the noise [1].

The accurate assessment of tones in wind turbine noise (WTN) is a critical aspect of environmental noise evaluation. Tones, characterized by their distinct and narrow frequency content, can significantly influence the overall perception of noise. Unlike broadband noise, which is spread across a wide range of frequencies, tones are more easily detectable by the human ear and can be perceived as more annoying and intrusive.

¹ Corresponding author – Email: lss@forcetechnology.com

This heightened sensitivity to tonal noise underscores the necessity for precise and reliable assessment methods.

For instance, in a Danish opinion analysis from 2012 [2], 20% of participating neighbours chose the response “*The sound is composed of tones and sounds in different pitches*” to describe their experience of wind turbine noise. This indicates the prominence of pure tones in their perception.

Pure tones stand out against the background noise, making them more noticeable and potentially more irritating. Therefore, accurately identifying and quantifying these tones is essential for understanding and mitigating their impact on human well-being. Many environmental noise regulations (for instance the Danish [3]) impose stricter limits on tonal noise due to its higher potential for causing annoyance. Standards such as IEC 61400-11[4] provide guidelines for the measurement and assessment of tonal noise from wind turbines. Compliance with these regulations requires precise identification and measurement of pure tones to ensure that wind turbine operations do not exceed permissible noise levels.

2. Motivation

IEC 61400-11 is the widely used standard for analysing the tonal content in wind turbine noise for sound power level measurements made close to the turbine. This standard provides procedures for measuring and analysing acoustic emissions from wind turbines, including methods for assessing tonal audibility

However, various methods are used worldwide to analyse the tonal content of wind turbine noise at the receptor position (i.e., where the noise is received by humans or measuring instruments). Some of these methods include:

- ISO 1996-2:2007[5] Annex C (e.g., used in Denmark [3])
- ETSU-R-97[6] (e.g., used in UK)
- IEC TS 61400-11-2 [7]
- ISO/TS 20065[8] (referred to in ISO 1996-2:2017[9] Annex J, engineering method)
- ISO 1996-2:2017[9] Annex K, survey method (1/3 octave band method [10])

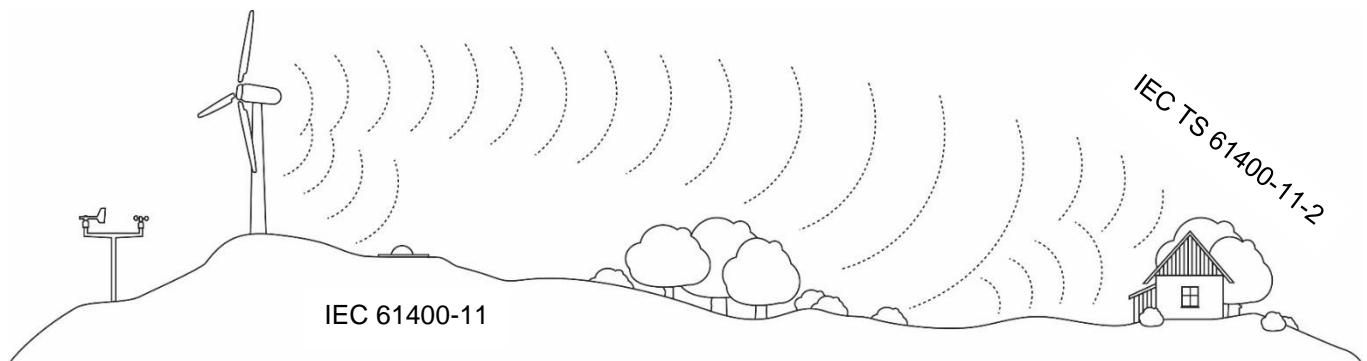


Figure 1: Typically, measurements of tonal content are either determined as part of a sound power level measurement (for example according to IEC 61400-11) relatively close to the turbine, or at receptor position (for example according to IEC TS 61400-11-2)

As an international wind turbine manufacturer, navigating measurement standards can be complex, as one method is often specified for sound power level measurements and another for receptor position measurements, and typically these differ from country to country.

Methods for measuring tonal prominence can generally be divided into two steps:

- **Analysis of a Frequency Spectrum**, which involves examining the frequency spectrum of the noise to identify tonal components.
- **Combination of Periods**, which involves combining the results from different periods to provide a comprehensive assessment of tonal audibility.

For single prominent and stationary tones, the results of different methods are reasonably comparable [11]. However, tones from wind turbines are often not stationary in amplitude and frequency because they

depend on the rotational speed of the rotor, which is influenced by wind speed and flow. Additionally, wind turbine noise often consists of multiple tones, making analysis more complex.

Proficiency tests and round robins have shown large variations in results between participants for measuring tonal prominence [11] and [12]. This indicates the need for further investigation and standardization to improve the accuracy and reliability of tonal prominence assessments.

Because of the many methods for assessing the tonal prominence (for noise sources in general) in late 2024 a new ad hoc group was established; ISO/TC 43/SC 1/AHG 2 “*Common tonal methodology*” with the task “*To determine the need, interest and scope for a common ISO tonal methodology*”.

Given the challenges posed by non-stationary tones and variations in proficiency tests, there is motivation to explore the use of neural networks for rating prominent tones. Neural networks can potentially provide more accurate and consistent assessments by learning from large datasets and adapting to complex patterns in the noise.

SenseLab’s Virtual Listener Panel™ (VLP), a machine learning-powered tool trained on expert panel data, has demonstrated efficiency in evaluating perceptual quality of audio products [13], and this feasibility study investigates if a similar approach can be used for rating prominent tones in noise.

Motivation for this study stems from the need to explore data-driven approaches versus traditional methods. We present a feasibility study demonstrating how machine learning (ML) can be used to evaluate the characteristics of wind turbine noise. By leveraging data from human assessors, we aim to develop a model that is more representative of human perception than other methods. Through analyzing the resulting model, we can identify features of audio that affect the perceived tonal prominence, potentially leading to novel insights into human sound perception.

The problem statement guiding this research is:

"Can the perceived tonal prominence of wind turbine noise be successfully modelled with machine learning?"

3. Method

In this work, we consider 31 audio stimuli representing wind turbine noise. The audio samples were presented to a total of 27 participants who were asked each to assess the tonal prominence of each sample [14]. Using this data, we now seek to formulate a machine learning regression model that predicts the perceived tonal prominence for a given audio sample of wind turbine noise. Thus, the raw input to the model is an audio sample waveform and the response is a perceived tonal prominence score. This raises the question on how to define the tonal prominence scores given the 27 tonal prominence assessments for each sample. For the purposes of this work, we define the tonal prominence score as the mean of the 27 assessments for each sample, thereby excluding assessor variation from the model. However, it should be noted that this approach can be sensitive to outliers, and it may be beneficial to account for assessor variability — potentially through alternative methods such as modelling no-reference listening tests using pairwise preference predictions, as explored in SenseLab’s VLP [13], which can help mitigate the influence of outliers.

3.1 Stimuli

The 31 audio samples were from a previous study in 2013 [14]. From several original recordings of wind turbines 24 samples of 20 second periods were selected for the listening tests. If more equally prominent tones in different critical bands were present in a sample, the least prominent were attenuated to facilitate an unambiguous and comparable assessment in the listening test and in the tone analysis. Supplementary 7 samples of stationary industrial noise with tones were added. The samples - each mono recordings and of duration of 20 seconds - were level aligned so that the A-weighted levels were the same for all samples. The intended presentation level after the level calibration was 50 dB(A).

For this study, the samples are divided into nine groups according to their origin and similarity. By separating the audio samples, we avoid potential issues in the analysis, such as data leakage. Narrowband analysis of the 31 audio samples, divided into nine groups, is shown in Figure 3.

Each audio sample's file name consists of a letter (either T for Turbine or D for non-Turbine), a number indicating the rounded tonal center frequency, and an 'A' followed by a number indicating the rounded tonal audibility (both center frequency and tonal audibility according to ISO 1996-2:2007 Annex C). Two files with no audible tone are included, designated as “no tone.” For the remaining 29 files, the tonal center frequency ranges from 70 Hz to 7 kHz, and the tonal audibility ranges from -3 to 17 dB (see Figure 2).

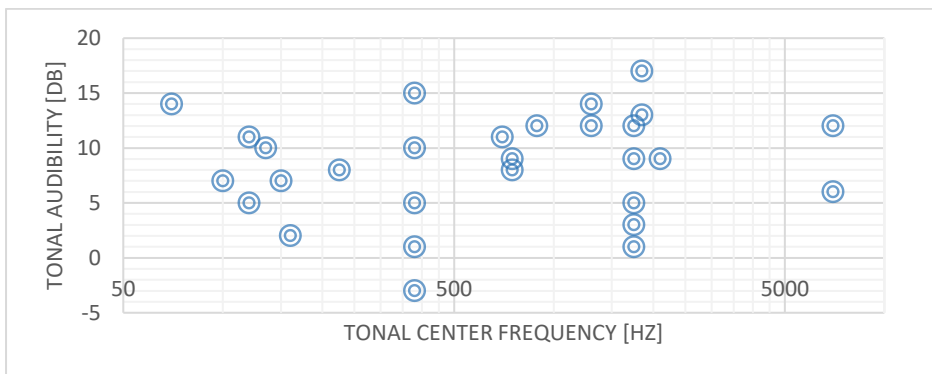


Figure 2. Tonal centre frequency and audibility for the 29 audio files with tones based on ISO 1996-2:2007 Annex C

The length of each file is 20 seconds. However, the tone amplitude and frequency of the 31 audio samples are not necessarily stationary, as shown in the spectrograms in Figure 8, Figure 9 and Figure 10. In the original listening test from 2013 [14], a better correlation with objective tonality methods was observed when only the first 5 seconds of each sample were analyzed. This suggests that listeners may make their assessments within the first part of the sample.

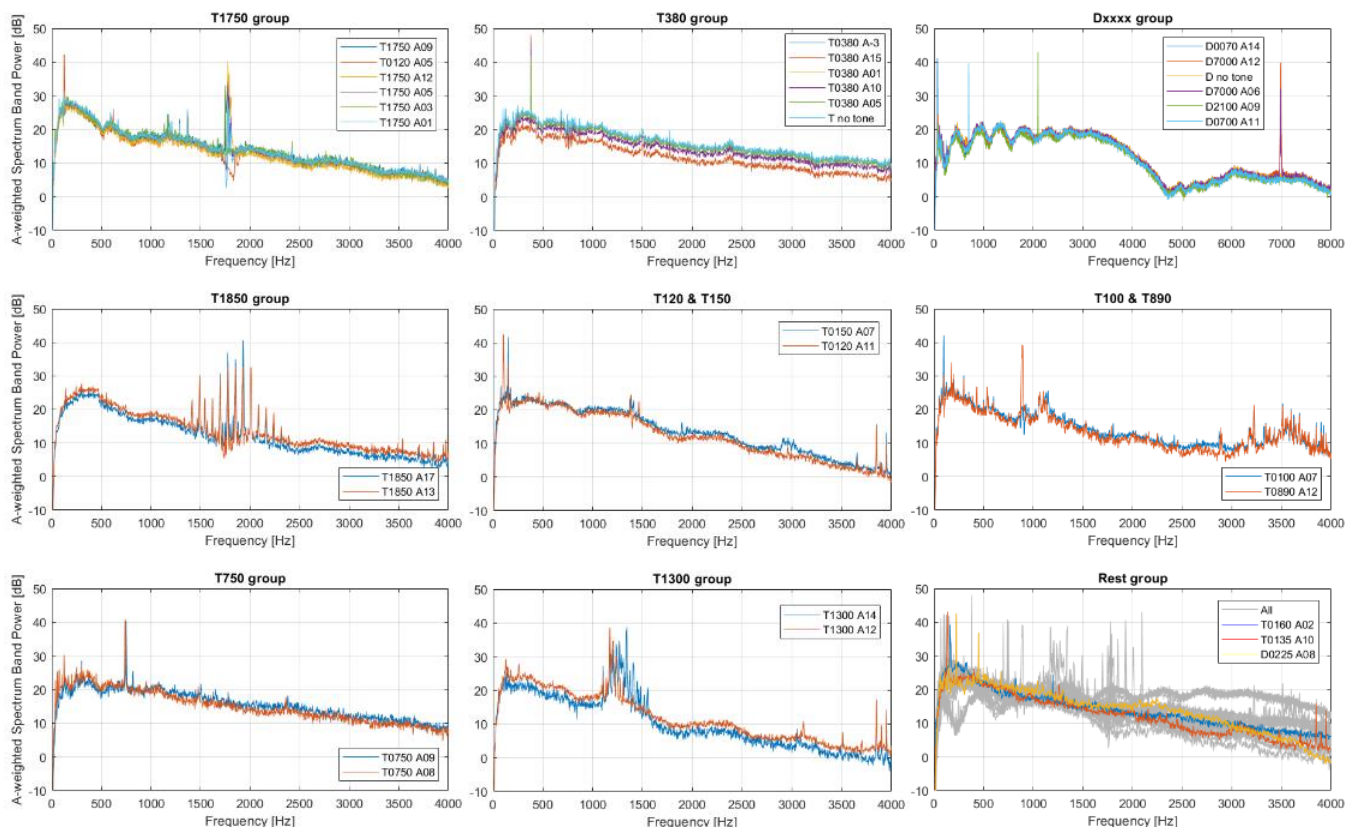


Figure 3: Narrowband analysis of the 31 audio samples, divided into 9 groups (for the ‘Rest group’ plot all 31 audio samples are show in grey for comparison). Note that the x-axis is different for the ‘Dxxxx group’ to accommodate the tones at 7kHz. The other audio samples do not have tones above 4kHz.

3.2 Feature Extraction

The proposed machine learning regression model consists of a feature extractor and a regression model. As a preprocessing step for feature extraction, the audio sample waveforms are converted to “mel scale” spectrograms in dB, such that we can treat them as images. The spectrograms cover frequencies from 0 to 22050 Hz with a resolution of 128 frequency bins, with a logarithmic frequency axis. The choice of frequency range was made to thoroughly cover the human hearing range. It could be argued that the maximum frequency should be lowered to e.g. 8 kHz to match the human hearing range more closely. This choice was not tuned for the purposes of this project and remains an area for improvement. The mel scale was chosen as it has been used for similar approaches and provides an approximated representation of the human auditory filter shapes [15]. For the feature extractor, we use a ResNet model with 18 layers, which is a convolutional neural network (CNN) [16]. The ResNet model is pre-trained on the ImageNet-1k classification dataset, which consists of ~14 million natural images [17]. Even though the model is fitted to the natural images, the feature encoding should still be useful for other domains, such as spectrograms. This is known as transfer learning. Finally, the feature encoding of the spectrograms is obtained by extracting the output preceding the classification layer of the ResNet model. The resulting encoding for each audio sample is then composed of 512 high level features.

To visualize the feature encodings of the audio samples, they are embedded into 2 dimensions using T-SNE [18]. From the visualization (except for the Dxxxx group), we observe that audio samples with similar tonal prominence scores appear clustered together, suggesting that the features are appropriate for modelling. For example, the low scoring samples, represented by blueish colours, appear centred, with the high scoring samples, represented by green, surrounding them. This does not hold for the samples in the Dxxxx group, which have visually different spectrograms from the other groups, and they appear clustered together, even with quite different tonal prominence scores. For all groups, except for the “rest“ group, the audio samples within the same group appear clustered together, confirming that samples within each group indeed are similar.

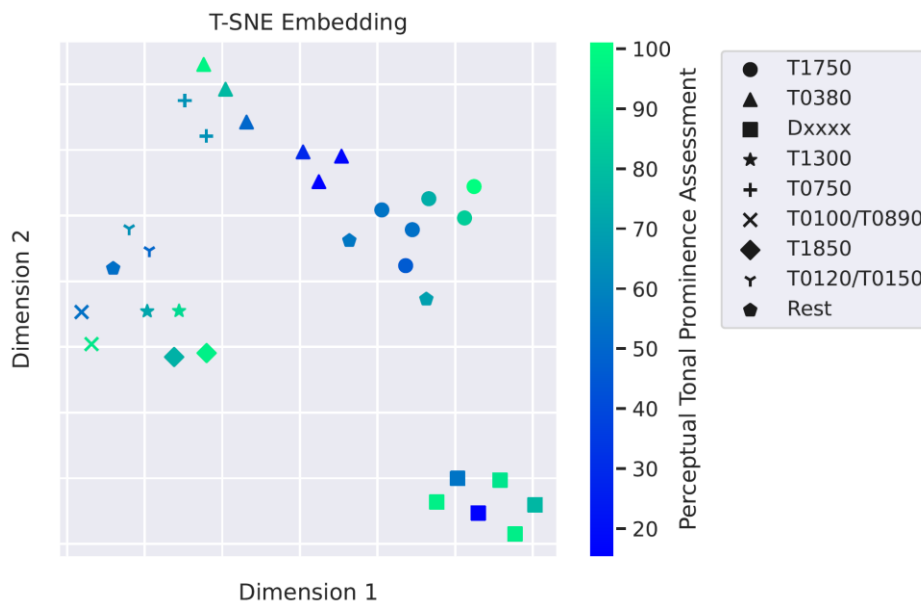


Figure 4: T-SNE embeddings of the audio feature encodings extracted by a ResNet with 18 layers pretrained on ImageNet. The embeddings are coloured by mean perceptual tonal prominence assessment.

3.3 Regression Model

Having obtained feature encodings for the audio sample, it remains to choose an appropriate regression model, mapping the feature encoding to a tonal prominence score. Our initial approach was to replace the classification layer of the ResNet model with a linear regression layer and fit it using gradient descent. However, we quickly concluded that this approach is (currently) infeasible due to the scarcity of the data. Therefore, we opted for linear regression models with and without regularization. Three linear regression

models were considered: Ordinary least squares (OLS), ridge regression, and least absolute shrinkage and selection operator (LASSO) regression.

3.4 Experiments

For model selection and testing, leave-one-group-out cross validation was chosen, setting aside the audio samples of one group for testing the models in each fold. This was done such that as much data as possible was left for fitting the regression models. To determine the optimal regularization strength for the ridge regression and LASSO model, an inner cross validation loop was used for each outer fold in the leave-one-group-out cross validation loop. Finally, for each outer fold, the three models were fitted and subsequently used for predicting the test samples in the hold out group.

4. Results

We use the R^2 measure (coefficient of determination) to assess the performance of the models.

4.1 Comparing predicted and perceptual ratings

Of the three considered models, the highest coefficient of determination was achieved by the LASSO model with $R^2 \sim 0.781$ when only observing the first quarter of the file. When observing the full length of the file the highest coefficient of determination was also achieved by the LASSO model with only $R^2 \sim 0.667$. The performance of all models for both file lengths is shown in Figure 5 and Table 1.

From the visualization of the model fit, we observe that the model is fairly accurate, when taking the uncertainty of the ground truth mean tonal prominence assessments into account. However, the model fails on a few select samples, often with low tonal prominence. Overall, these results suggest that this approach is feasible for modelling the perceived tonal prominence.

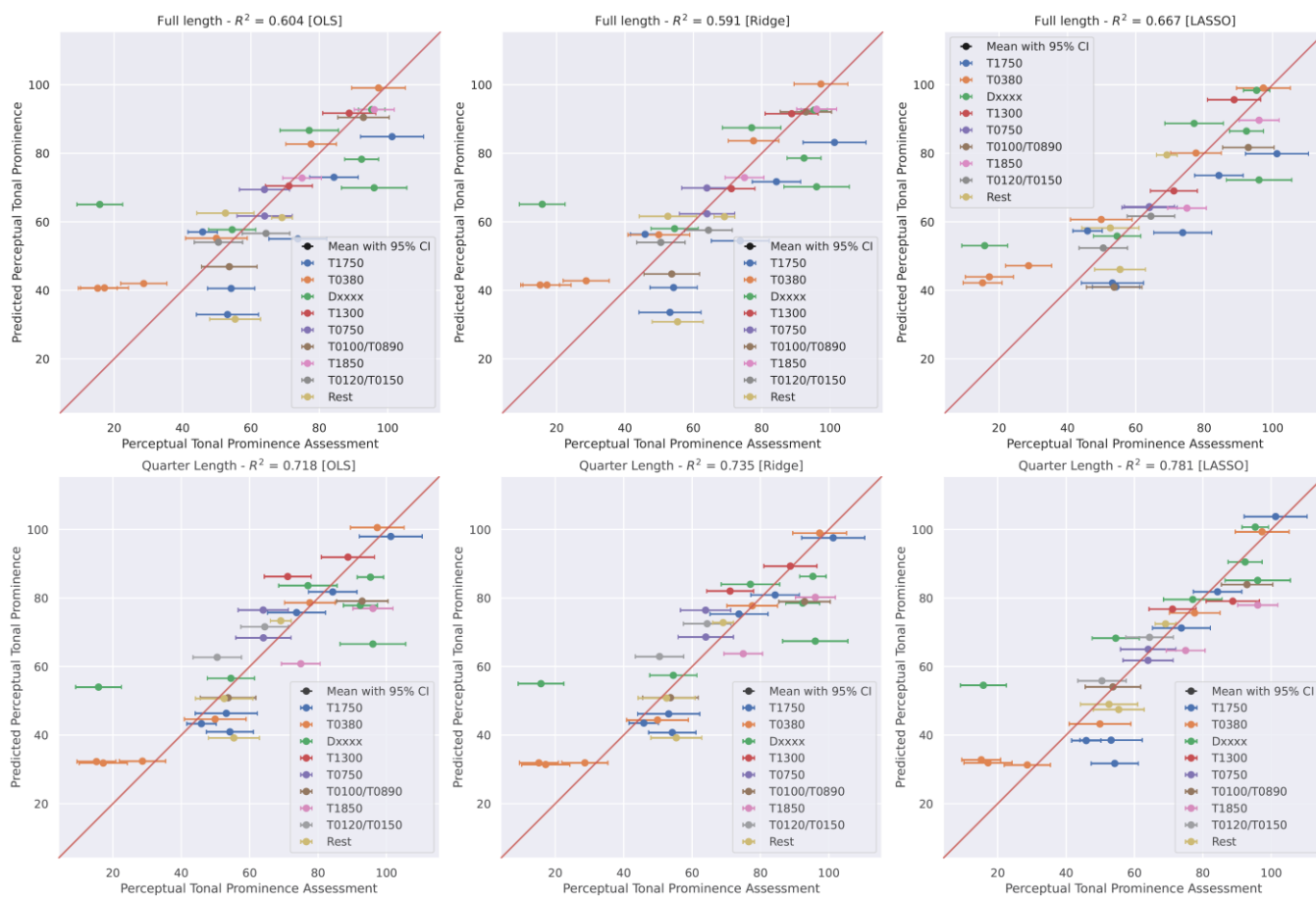


Figure 5 Mean tonal prominence assessments versus predicted tonal prominence for the three models for both full length and quarter length of the sound samples as input.

4.2 Comparing predicted and objective results

The tonal audibility for the 31 sound samples have previously been analysed using three different methods:

- **ISO 1996-2:2007 Annex C:** This method was applied to both the first 5 seconds and the full 20 seconds of each sound sample. The analysis was conducted by one person [14].
- **IEC 61400-11:** This analysis was part of a round robin test involving several laboratories. The mean value of the reported tonal audibility was used [11].
- **ISO/PAS 20065 [19]:** Like the IEC 61400-11 analysis, this was also part of a round robin test with several laboratories participating. The mean value of the reported tonal audibility was used [11].

Figure 6, Figure 7, Table 1 and Table 2 compares the results with the objective methods described above with the predicted results from the previous section, and the comparisons indicate the following:

- Respectable correlation:
 - o There is a respectable correlation between perceptual (human perception) and predicted (model predictions for the chosen model) tonal audibility [between $R^2 = 0.667$ and 0.781].
 - o There is also a respectable correlation between perceptual and objective (standardized methods) tonal audibility [between $R^2 = 0.693$ and 0.861].
- Poor correlation:
 - o The correlation between predicted and objective methods is not impressive [between $R^2 = -0.123$ and 0.453]. The best fit is with the quarter length prediction. There is no clear answer to which objective method has the best fit, since it varies depending on combinations.

Table 1: Overview of R^2 measure (coefficient of determination) for different combinations of prediction model and file length

	OLS	Ridge	LASSO
Full length prediction	$R^2 = 0.604$	$R^2 = 0.591$	$R^2 = 0.667$
Quarter length prediction	$R^2 = 0.718$	$R^2 = 0.735$	$R^2 = 0.781$

Table 2: Overview of R^2 measure (coefficient of determination) for different combinations of objective method, predicted result, perceptual rating and file length.

	IEC 61400-11:2012	ISO/PAS 20065:2016	ISO 1996-2:2007 Annex C	
	20 sec	20 sec	5 sec	20 sec
Full length prediction, LASSO	$R^2 = -0.056$	$R^2 = -0.123$	$R^2 = 0.277$	$R^2 = 0.301$
Quarter length prediction, LASSO	$R^2 = 0.432$	$R^2 = 0.139$	$R^2 = 0.453$	$R^2 = 0.255$
Perceptual Tonal Prominence	$R^2 = 0.693$	$R^2 = 0.779$	$R^2 = 0.861$	$R^2 = 0.728$

From figures 6 and 7, we observe that the model seems to demonstrate better performance in predicting a portion of the data points with high tonal audibility (perceptual tonal prominence >80) compared to the objective methods. Conversely, the objective methods are seemingly more accurate at predicting low tonal audibility (perceptual tonal prominence <40), where there are fewer data points. There is a general connection between the number of data points at different score levels and the accuracy of the model, suggesting that the performance of the model is influenced by the size and distribution of the training data. The poor correlation between the model and objective methods could be explained by the methods failing in different areas. This discrepancy results in disagreements between the model and objective methods, leading to accumulated errors during comparison.

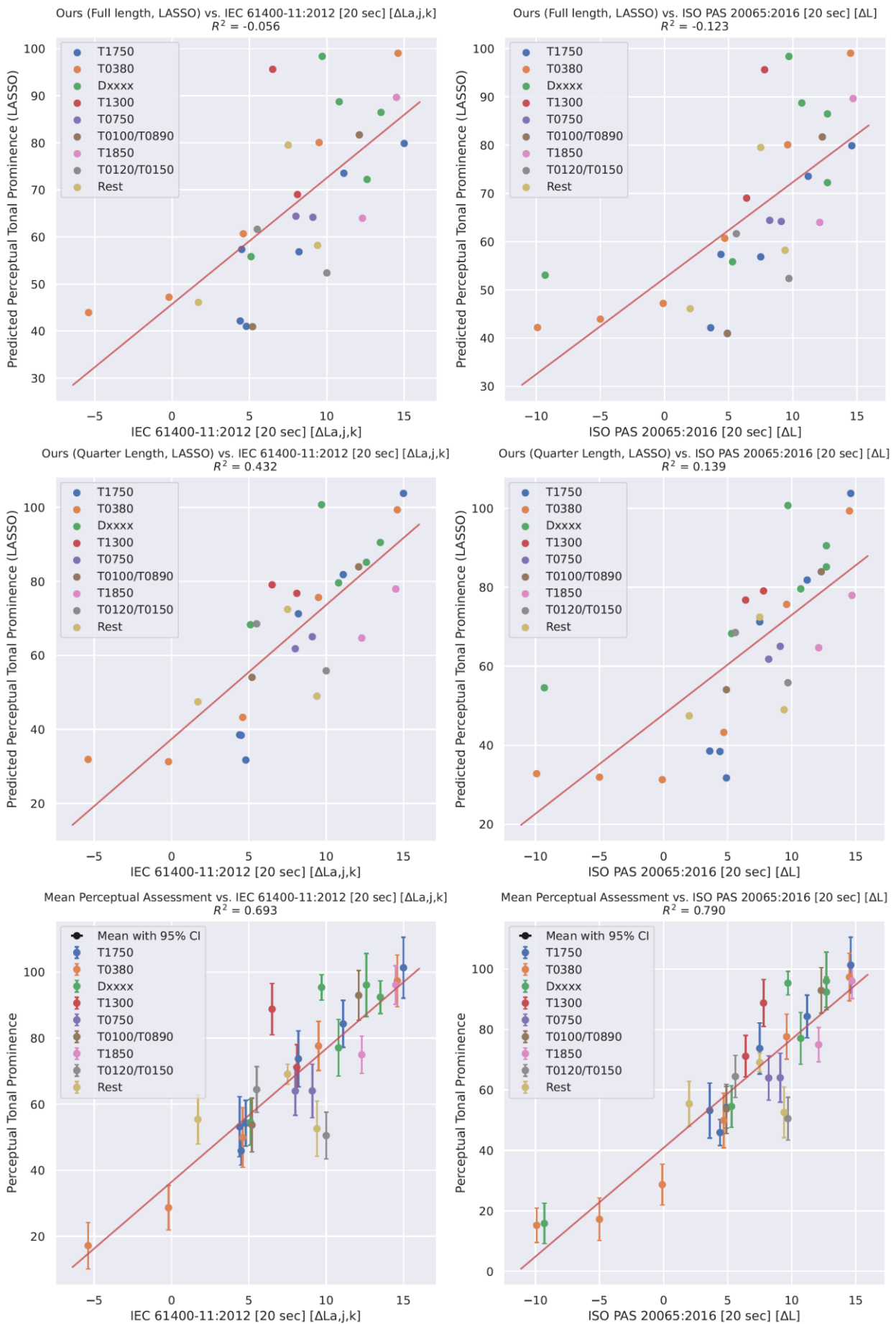


Figure 6 Comparisons between perceptual assessment, predicted prominence and tonal audibility calculated by 2 different methods: The IEC 61400-11 and ISO/PAS 20065.

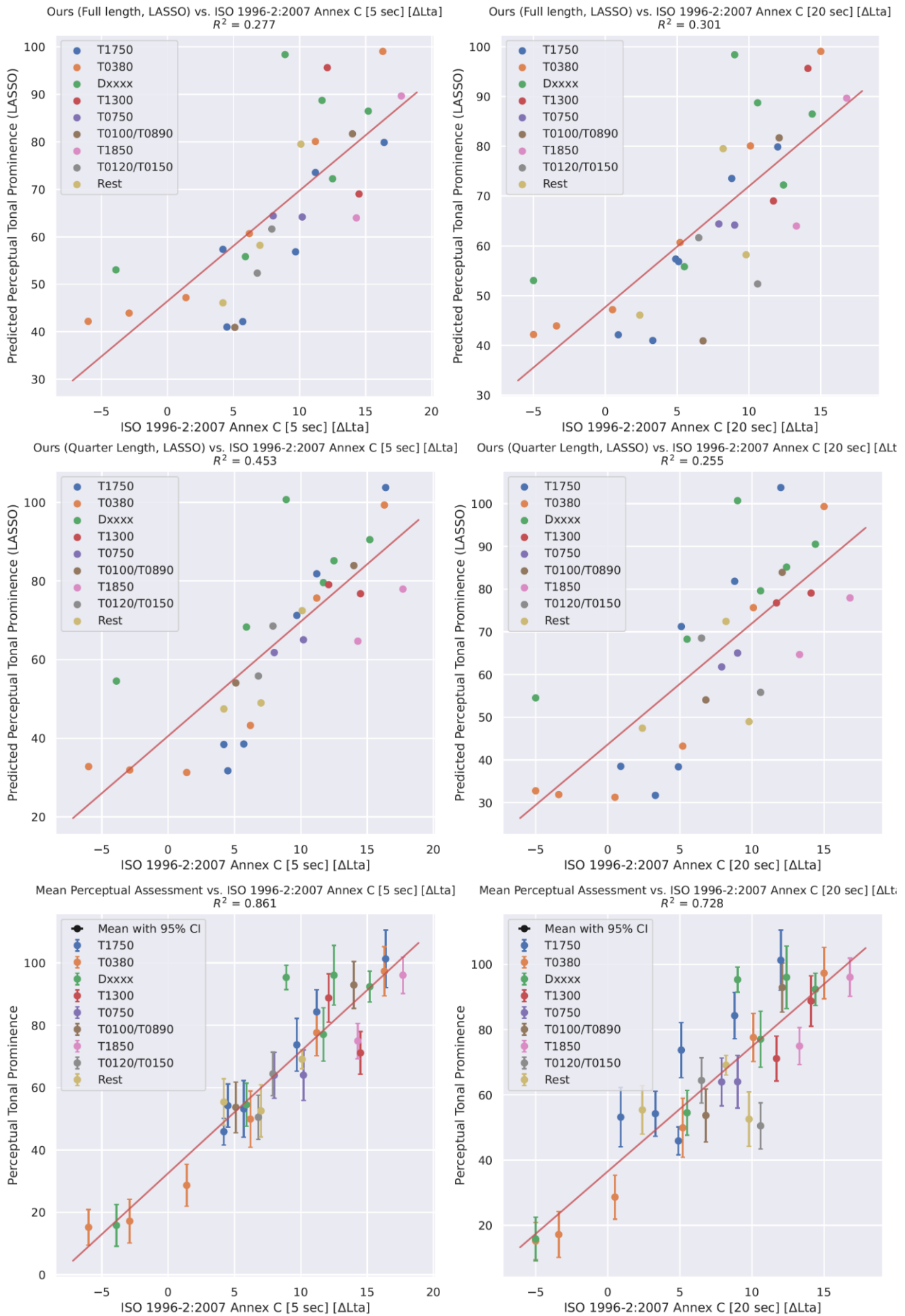


Figure 7: Comparisons between perceptual assessment, predicted prominence and tonal audibility calculated by the ISO 1996-2:2007 Annex C method (5 seconds or 20 seconds).

5. Conclusion and discussion

From the results, we conclude that a machine learning approach for predicting the perceived tonal prominence in WTN is feasible. We hypothesize that significantly better results can be achieved with more data or a more sophisticated modelling approach. In particular, CNNs such as the ResNet used in our approach are not an optimal choice for spectrograms due to their inductive biases. Furthermore, gathering more data will allow for more complex models and thereby a potentially better result. A larger and more diverse dataset would also allow us to establish a benchmark dataset for robust comparison of models.

To visualize and understand the behaviour of our model, we have produced saliency maps with SmoothGrad for each data point (see Figure 8, Figure 9 and Figure 10). The saliency maps visualize which features in the input spectrogram contribute to changes in the output prediction of the model. Overall, the saliency maps for audio containing a prominent tone suggest that the model uses information from and around the prominent tone(s) in the spectrograms to produce a prediction. This is less apparent for audio where the centre frequency of the prominent tone is low, e.g. < 512 Hz, suggesting that the model may have trouble recognizing these tones. In addition, we observe that the predictions of the model may be affected by unimportant patterns in the spectrograms, such as bird song or other unrelated signals. This is especially pronounced for audio with low tonal audibility. Improving robustness to these confounding patterns could be a key factor in developing a better model in future work. E.g. a higher number of frequency bins (better frequency resolution) will make weak tones more prominent in the analysis.

Further investigation of the differences between assessors could yield important insights into human perception of tones and noise. For instance, certain assessors may be more sensitive to tones than other assessors. Addressing this variation in future work may therefore be beneficial for both the soundness of the analysis and the potential use cases of the approach. Specifically, extending our model for prediction of the annoyance felt by human listeners may require a different modelling approach than what is presented in this work, as the scale for e.g. annoyance could be subjective to the individual listeners.

This study demonstrated an approach that leverages machine learning to create a data-driven assessment of human perception of tonal content in wind turbine noise. The proposed method can be easily extended to other annoyance factors, such as swishing, whistling, and pulsating sounds, which may lack standardized methods for impact calculation. Data-driven approaches have the potential to play a crucial role in identifying and assessing annoyance factors in a way that more accurately reflects human perception.

6. Future work

For this feasibility study, we started with an available dataset primarily based on wind turbine sounds to investigate the feasibility of this approach. Having concluded that the approach is feasible, we plan to expand the study with additional data, both within the area of wind turbine sounds and with non-wind turbine-related sounds. If you have recordings to share, we would greatly appreciate them. We are interested in good quality and preferable level calibrated files:

- Recordings with matching ratings from listening tests (preferably)
- Audio files that could potentially be perceived as annoying
- Audio files containing audible tones, impulses, amplitude modulation, low frequency sounds, etc.
- An additional file with a matching 1 kHz calibration tone (preferably)

Please let us know what you can share. We are happy to treat your contributions anonymously, but we can also acknowledge your contribution if you prefer.

Acknowledgments

FORCE Technology wishes to thank the Danish Agency for Institutions and Educational Grants for their financial support of this work as part of the Performance Contract 2025-2028 “Intelligent Sound Perception with AI: Future Acoustic Solutions for a Healthy and Safe Society”.

References

- [1] T. H. Pedersen, “Prominent tones in noise - Proficiency testing among 30 laboratories of the ISO 1996-2 Annex C method and its predecessors,” in Acoustic 08 Paris, 2008, p. 5. doi: 10.1121/1.2934274.
- [2] J. Analyse, “Vindmøllenaboers opfattelse af vindmøller,” 2012.
- [3] *Bekendtgørelse om støj fra vindmøller, no. 135*. Denmark: Miljø- og Fødevareministeriet, 2019, pp. 1–24.
- [4] IEC, “IEC 61400-11 Wind turbines - Part 11: Acoustic noise measurement techniques,” 2012.
- [5] ISO, “ISO 1996-2:2007 Acoustics — Description, measurement and assessment of environmental noise — Part 2: Determination of environmental noise levels,” 2007.
- [6] “The Assessment & Rating of noise from Wind Farms,” ETSU-R-97. 1996.
- [7] IEC, “IEC TS 61400-11-2 Wind energy generation systems – Part 11-2: Measurement of wind turbine noise characteristics in receptor position”. 2024.
- [8] ISO, “ISO/TS 20065:2022 Acoustics - Objective method for assessing the audibility of tones in noise – Engineering method,” 2022.
- [9] ISO, “ISO 1996-2:2017 Acoustics – Description, measurement and assessment of environmental noise – Part 2: Determination of sound pressure levels,” 2017.
- [10] L. S. Søndergaard and M. Bastasch, “Tonality content analysed with both 1/3 octave band and narrowband methods with comparison to listening test,” in 9th International Conference on Wind Turbine Noise 2021, Remote from Europe, 2021, pp. 402–431.
- [11] L. S. Søndergaard, C. Thomsen, and T. H. Pedersen, “Prominent tones in wind turbine noise - Round-robin test of the IEC 61400-11 and ISO/PAS 20065 methods for analysing tonality content,” in 8th International Conference on Wind Turbine Noise, 2019, pp. 1–12.
- [12] J. E. Laursen, “Proficiency tests on environmental noise,” in INTER-NOISE 2012, the 41st International Congress and Exposition on Noise Control Engineering, 2012.
- [13] M. Herlufsen and N. A. Fuglsang, “Establishing a Virtual Listener Panel for audio characterisation,” in AES International Conference on Machine Learning and Artificial Intelligence for Audio, 2025. [Online]. Available: <http://www.aes.org/e-lib>
- [14] L. S. Søndergaard and T. H. Pedersen, “Tonality in wind turbine noise . IEC 61400-11 ver. 2.1 and 3.0 and the Danish / Joint Nordic method compared with listening tests,” in 5th International Meeting on Wind Turbine Noise, 5th International Meeting on Wind Turbine N, 2013, pp. 2–10.
- [15] K. Kumar et al., “MelGAN: Generative Adversarial Networks for Conditional Waveform Synthesis,” Oct. 2019, [Online]. Available: <http://arxiv.org/abs/1910.06711>
- [16] K. He, X. Zhang, S. Ren, and J. Sun, “Deep Residual Learning for Image Recognition,” Dec. 2015, [Online]. Available: <http://arxiv.org/abs/1512.03385>
- [17] J. Deng, W. Dong, R. Socher, L. J. Li, K. Li, and L. Fei-Fei, “ImageNet: A Large-Scale Hierarchical Image Database,” in 2009 IEEE Conference on Computer Vision and Pattern Recognition, CVPR 2009, IEEE Computer Society, 2009, pp. 248–255. doi: 10.1109/CVPR.2009.5206848.
- [18] L. Van Der Maaten and G. Hinton, “Visualizing Data using t-SNE,” *Journal of Machine Learning Research*, vol. 9, pp. 2579–2605, 2008.
- [19] ISO, “ISO/PAS 20065:2016 Acoustics – Objective method for assessing the audibility of tones in noise – Engineering method,” 2020.

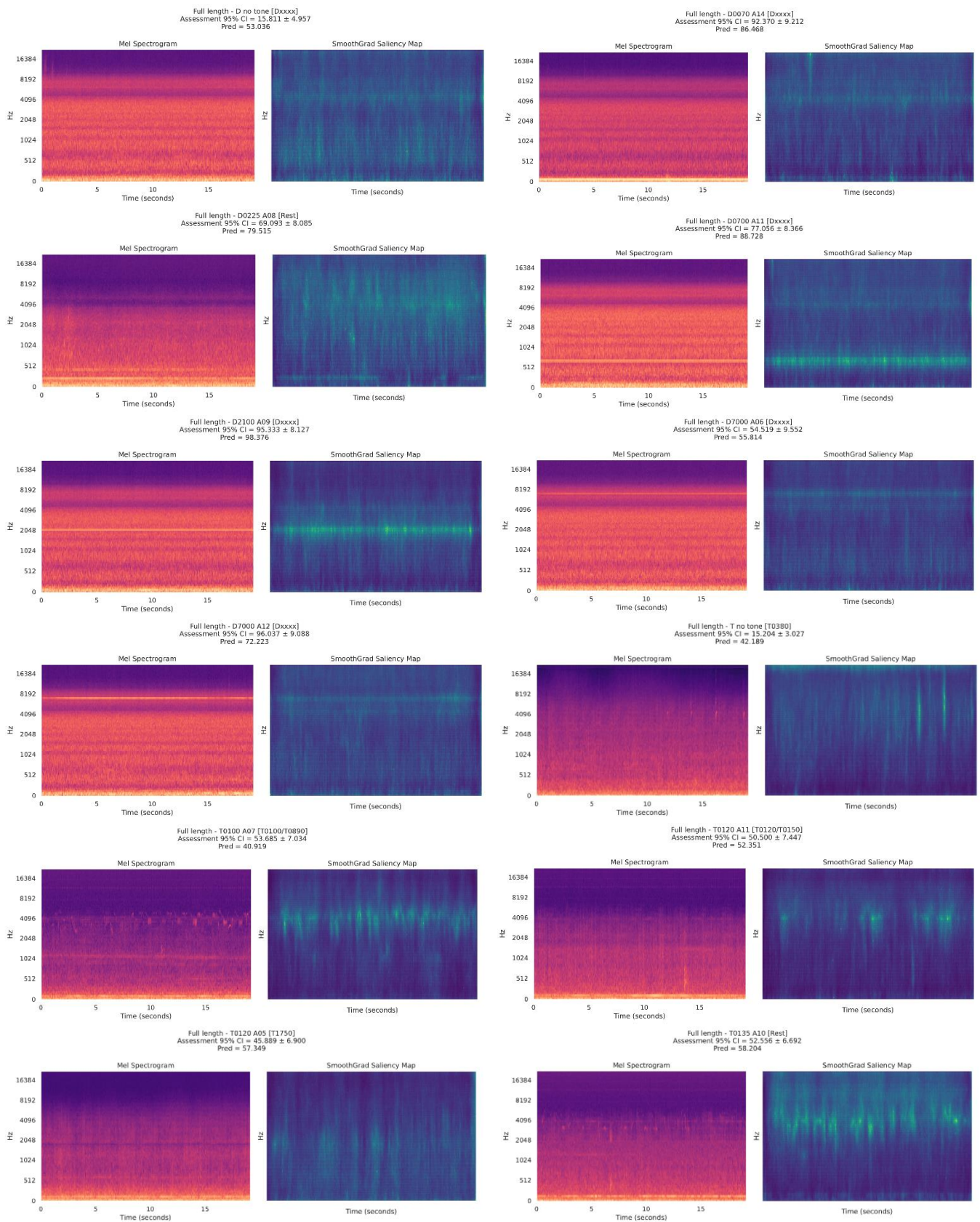


Figure 8: Mel scale spectrograms in dB (left) and corresponding SmoothGrad saliency maps (right) for the first 12 sound samples. Light colours in the saliency maps indicate higher saliency scores on an arbitrary scale. A high saliency score for a feature in the spectrogram can be interpreted as a high importance of that feature for prediction of the tonal prominence by the model.

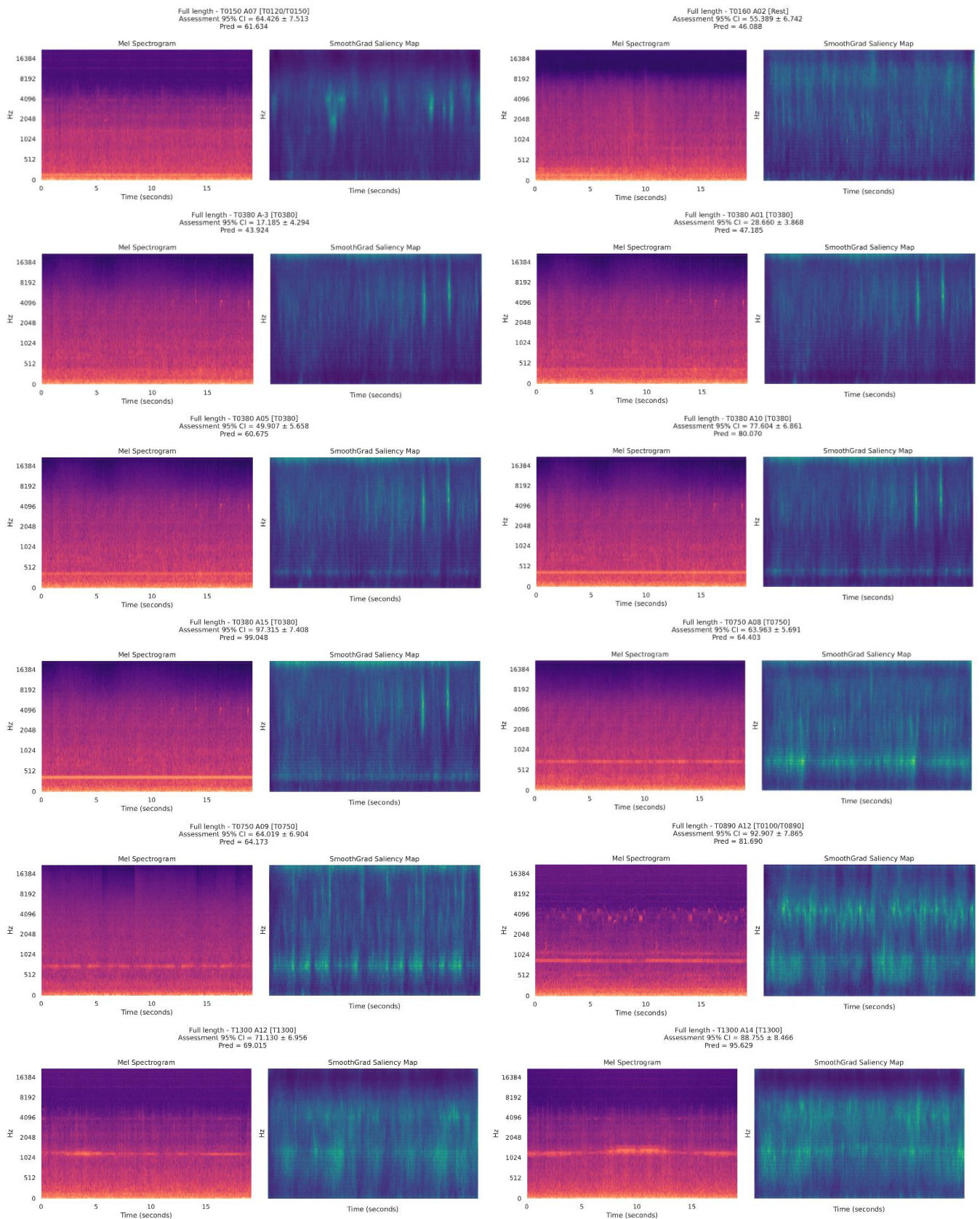


Figure 9: Mel scale spectrograms in dB (left) and corresponding SmoothGrad saliency maps (right) for the next 12 sound samples. Light colours in the saliency maps indicate higher saliency scores on an arbitrary scale. A high saliency score for a feature in the spectrogram can be interpreted as a high importance of that feature for prediction of the tonal prominence by the model.

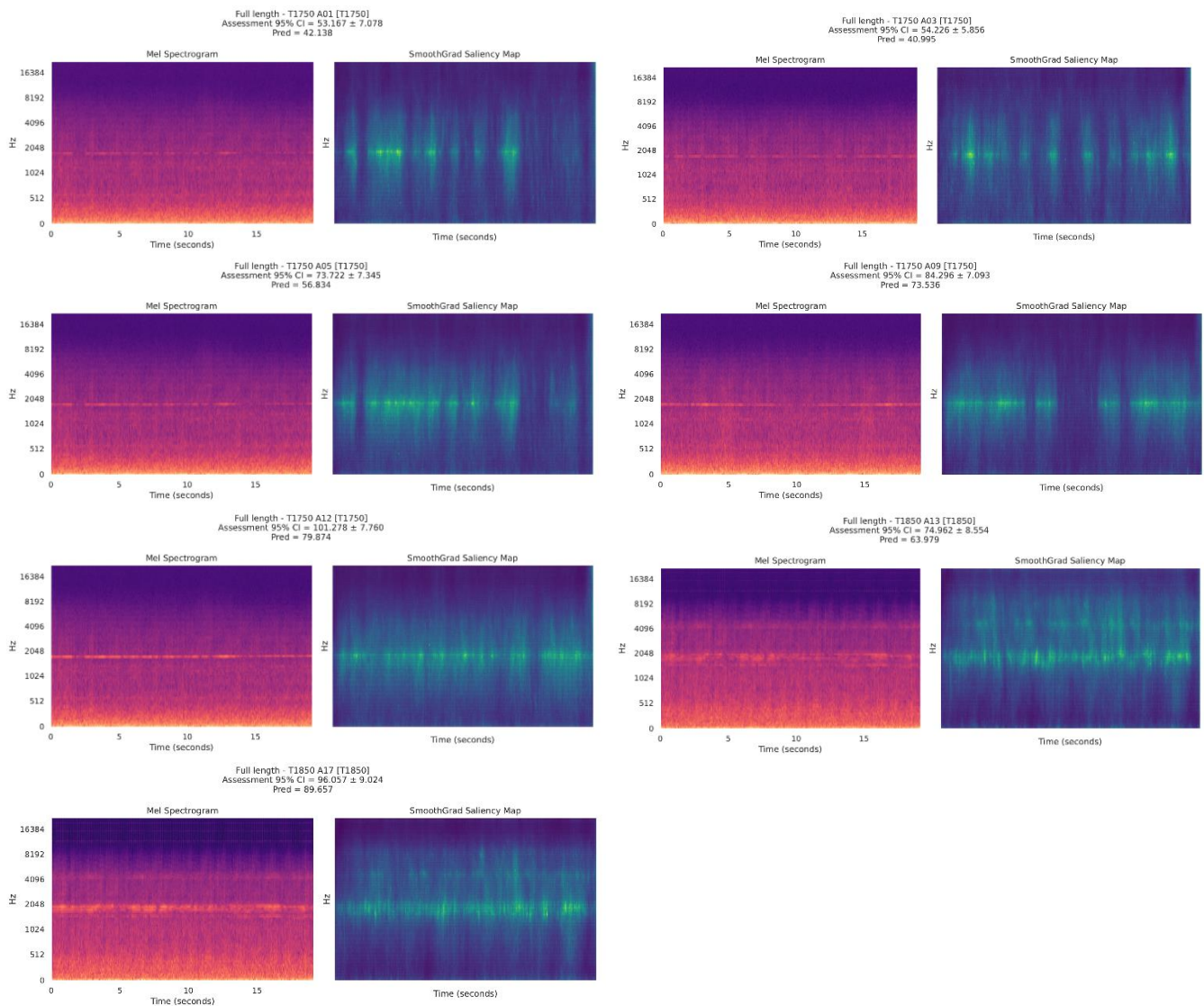


Figure 10: Mel scale spectrograms in dB (left) and corresponding SmoothGrad saliency maps (right) for the last 7 sound samples. Light colours in the saliency maps indicate higher saliency scores on an arbitrary scale. A high saliency score for a feature in the spectrogram can be interpreted as a high importance of that feature for prediction of the tonal prominence by the model.

Paper #20 - ID: 354

Title: Measurement of directivity patterns of a commercial wind turbine under yaw offset

Author: Arthur Finez

11th Edition of the
International Conferences on
Wind Turbine Noise

Copenhagen, Denmark – 10th to 13th June 2025

Measurement of directivity patterns of a commercial wind turbine under yaw offset

A. Finez¹ and T. Duc

ENGIE Green, 6 Rue Alexander Fleming, 69007 Lyon, France

C. Le Bourdat

ENGIE Green, 11, Rue Arthur III, TSA 11450 44262 Nantes Cedex 2, France

Summary

Effects of the observation angle on wind turbine noise levels are today only partly understood. It is clear that positions close to the rotor plane fall within generally low levels area, with a ~ -4 dB offset compared to downstream positions. However asymmetries and complex lobes patterns have been observed but not fully explained. To provide additional experimental material, a novel measurement campaign is conducted within the framework of the TWAIN European research project. A commercial wind turbine is fully surrounded by 24 microphones to analyse the change in both sound magnitude and directivity. OASPL patterns are observed and analysed in general agreement with the literature, together with variations of the spectral content. An assessment of the validity of the omnidirectionality assumption used in the IEC61400-11 standard is proposed using the microphone circle measurements, indicating that this hypothesis may not lead to very large deviations in the sound power estimates. Another part of the experiment consists in testing the turbine under yaw offset with the perspective of wind farm control. Observed effects of yaw angle on the directivity boils down to a rotation of the directivity pattern with the turbine orientation, but also to a general variation in noise levels. In yawed configurations, the microphone circle allows to partially counteracts the pattern rotation to estimate variations of sound power levels. In the case of a positive yaw of $+20^\circ$, we observe a slight increase of 1 to 2 dB.

1. Introduction

Acoustic impact studies of wind farm projects most often involve monopole point noise sources located at the nacelle centre of the wind turbines. However, numerous scientific studies challenge the source omnidirectionality assumption. For instance, Oerlemans and Schepers [1] equipped a 2.3 MW 90 meter diameter wind turbine with 8 on ground microphones arranged in circle around the turbine mast. They draw OASPL² directivity patterns and compare them to several analytical predictions. Basically, they observed two 6 dB “noise dips” in the crosswind directions, which are well understood and correctly captured by analytical models. But the measured directivity patterns also show a more complex multi-lobe structure, with upstream/downstream and upstroke/downstroke asymmetries than can only be partially explained by the models. Similarly, in his study on turbulence impact noise, Buck [2] experimentally highlights a listener angle dependence with 12 microphones. Upwind/downwind asymmetry of a few dB is also observed and a link is made to the core directivity of broadband trailing edge and leading edge noise

¹ Corresponding author – Email: arthur.finez@engie.com

² Over All Sound Pressure Level

and their relative weight. But an upstroke/downstroke asymmetry is also consistently observed and this could not be reproduced by models from the literature, which use the asymptotical high frequency formulation for trailing edge noise. Okada [3] used 6 microphones close to a 1.5 MW 70.5 m diameter upwind wind turbine and observed a 4 dB noise dip in the rotor plane. He fitted a simple empirical omni + bidirectional model to the measurements with a dependence on the frequency range and rotor speed. It is assumed in the model that there is no difference between upwind and downwind direction as well as between symmetrical positions relatively to the vertical plan containing the rotation axis. Finally, Bresciani [4], studying the effects of blade deflection on wind turbine noise directivity, also presents large angle variations for certain frequencies using analytical models. The precise dependence of wind turbine noise emission on the observer angle appears to be only partly understood and there is a need for additional well equipped directivity measurements on industrial turbines.

This work presents the implementation of a novel field campaign involving a single commercial wind turbine fully surrounded by 24 microphones in order to analyse the changes in both sound magnitude and directivity in various conditions and to provide new experimental material for model validation. It is also to be noted that the dependence of fine directivity effects on wind turbine model is unclear but may play an important role, so additional field directivity measurements may be beneficial for the understanding.

The experiment was conducted in the context of the TWAIN European research project which aims at providing a framework for multi-objective Wind farm control (WFC): increase in power production, reduction in turbine loading, complying with grid requirements or environmental regulations (acoustics, wildlife and social consciousness). Among the WFC strategies, wake steering consists in misaligning the upstream turbines to deflect the wake away from the downstream turbines [5]. It has shown high potential for power improvements, with a track record of many full scale field tests showing significant energy gains (see e.g. [6] [7]); the acoustic impact of yaw misalignment is thus a matter of concern in the project.

Actually the effect of wake steering on noise remains an open question, with only two full scale experiments either pointing toward a reduction of the noise emission due to the application of extreme yaw misalignment [8] or showing no hearable impact [9]. As a consequence, the present experiment includes some intentional yaw misalignment conditions. Apart from novel WFC strategies, a wind turbine can also operate temporarily under yaw misalignment when a change in wind direction is too sudden for the adaptation of the nacelle orientation.

2. Experimental setup

The measurements were carried out from March 25 to 28, 2024, on an industrial wind turbine ($D = 110$ m, $P = 2.2$ MW, and $HH = 80$ m) in a wind farm operated by ENGIE Green and located in northern France. *Figure 1* below summarizes the experimental setup implemented for the measurement.

Twenty four microphones surrounding the wind turbine were placed at a distance of approximately one blade tip height from the wind turbine (135 m), and a far-field microphone (#25) at ~400 m downstream. Used microphones are from different manufacturers but all class I, so level deviations shall not exceed ± 0.8 dB. A 10 m mast and Windcube lidar on the ground are installed at ~100 m and ~320 m from the wind turbine, respectively. In addition to the sensors visible in the figure, a 4-beam lidar mounted on the nacelle was installed at the top of the test turbine E12. High-frequency SCADA data (sampling period of 1 second) were collected during the test for the most important variables (electrical power, wind speed, nacelle position, rotor speed, etc.). The temporal synchronization and calibration of all acoustic sensors were checked each morning before starting new measurements. Overall acoustic pressure levels and third-octave band spectra were recorded with a sampling period of 1 s.

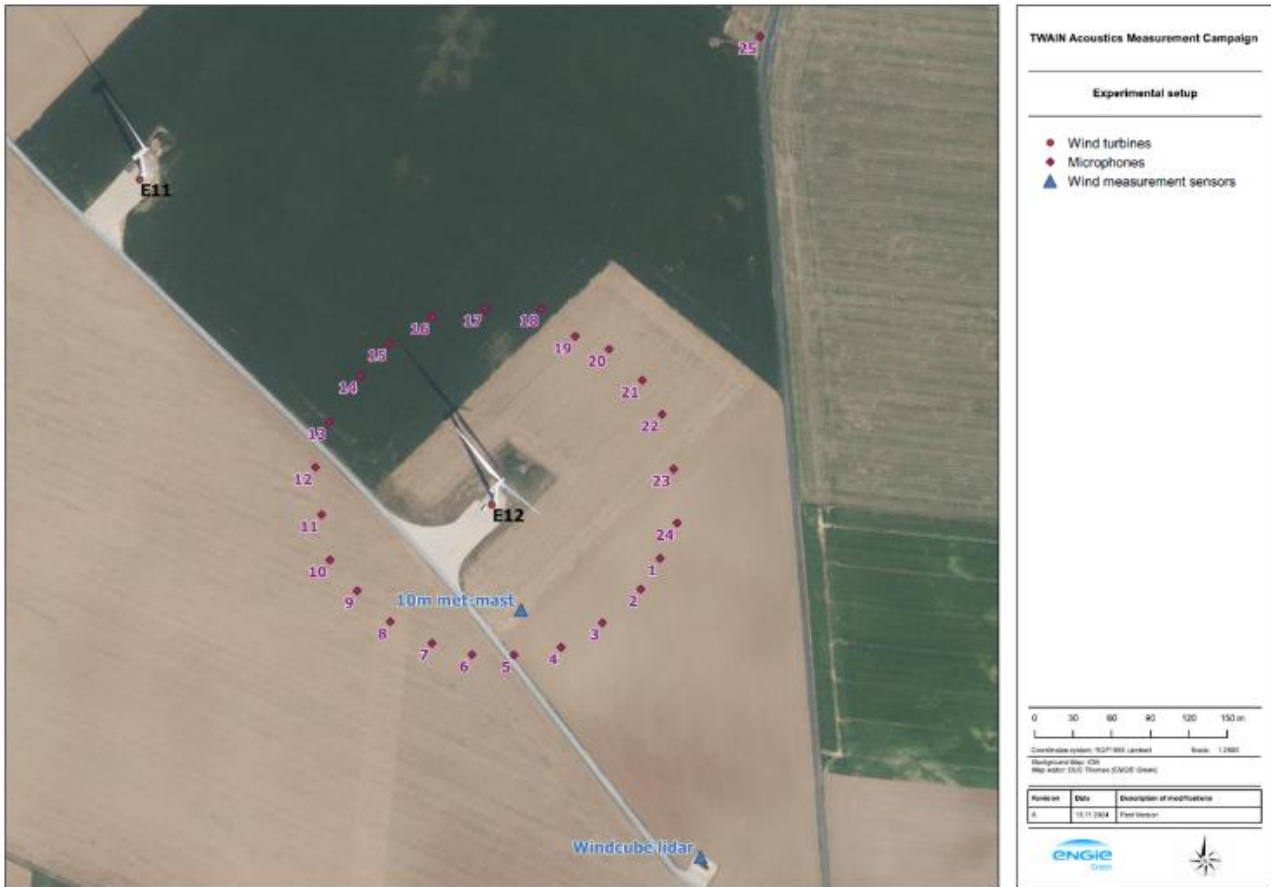


Figure 1: Experimental setup of the TWAIN measurement campaign.

The experiment consisted of 6 rounds of measurements that were conducted over the 4 days. During each round the turbine was alternatively yawed from -20° to $+20^\circ$ by steps of 10° , and also regularly toggled on and off to measure the background noise. The two closest wind turbines in the farm, E10 and E11, were stopped for the entire duration of the test to obtain a satisfactory signal-to-noise ratio. The wind conditions observed during the campaign were very favourable, allowing the collection of a sufficient number of data points for all yaw misalignment cases within the wind speed range of interest, from 5 to 13.5 m/s.

The data collected during the campaign were processed in accordance with the noise measurement standard IEC 61400-11, as much as possible. However, the specificity of this installation required some adjustments concerning the standard. While the standard only considers a single microphone located downstream of the wind turbine, 24 microphones had to be controlled here and their data processed. A specific procedure was therefore implemented to clean the dataset.

3. Data cleaning

3.1 Wind direction and speed

The ground-based lidar and the nacelle-mounted lidar were used as data sources for wind speed and direction. They are indeed considered more reliable than the measurements from nacelle anemometers and wind vanes when the wind turbine is stopped or yawed, and introduce less speed error at hub height V_{HH} than the 10 m mast currently recommended by the IEC61400-11 standard. Figure 2 presents a comparison of the measurements taken by the two lidars with the wind turbine's SCADA data used as a reference when it is operating without yaw misalignment. Each point represents data averaged over 1 minute. It is observed that the best correlation is obtained with the nacelle lidar for wind speed and with the ground-based lidar for wind direction. Therefore, these data sources will be used in the following.

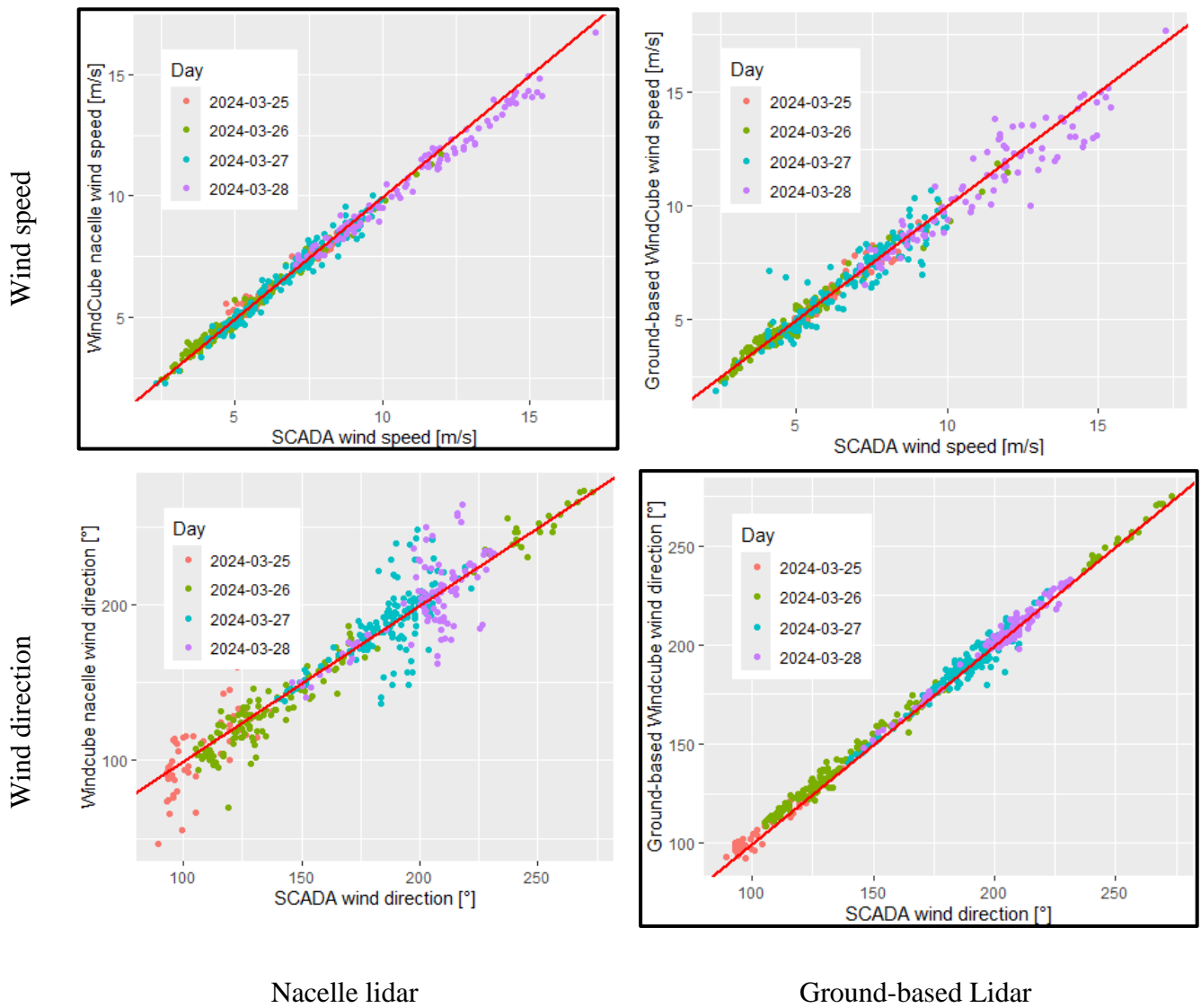


Figure 2 : Measured wind speed (upper half) and direction (lower half) of nacelle lidar (left hand side) and ground-based lidar (right hand side) compared to nacelle wind vane and anemometers when the turbine is running.

3.2 Time offset of noise levels

Despite the care taken in timestamping the sound level meters during the measurement, a time shift of several minutes was observed on some microphones. This is visible, for example, in *Figure 3*, where a sound event corresponding to an airplane passing was detected on most microphones at the black arrow (around 17:56:30). The same event is detected around 17:52:30, 17:53:15, and 17:57:15 on the data from three microphones, as indicated by coloured arrows. These time shifts varied by several seconds over the four days of measurement; their origin is unknown. It was decided to introduce a numerical compensation by resynchronizing the microphone data with the wind turbine's electrical production time series. This results in a correction per day of measurement and per microphone, which is added to the affected measurements.

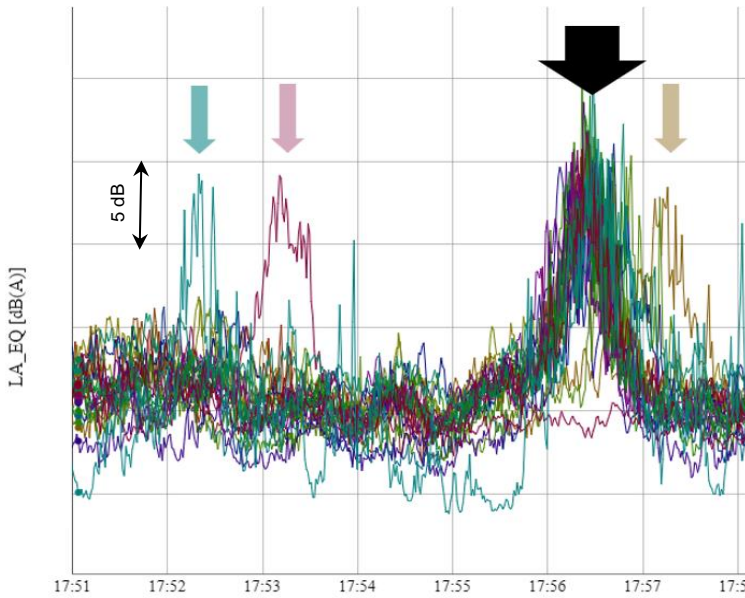


Figure 3 : Example of a plane passing-by event identified on the raw OASPL time series of 25 microphones

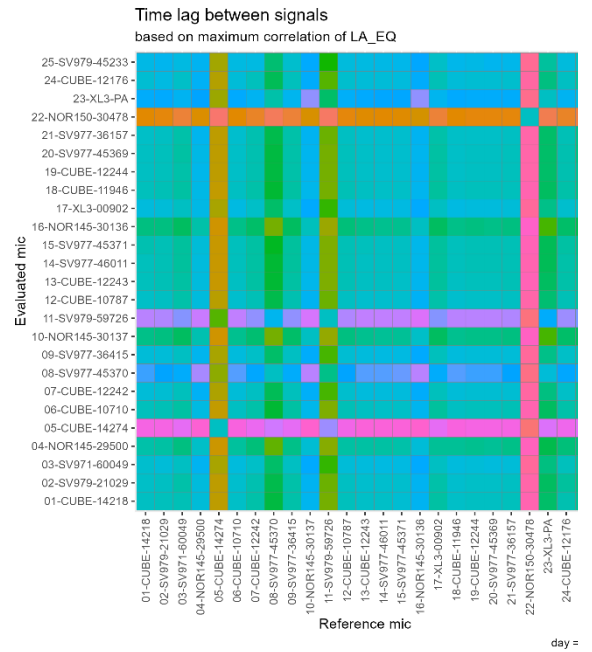


Figure 4 : Relative time lags matrix between microphone on the last measurement day, between -241 seconds (orange), +241 seconds (pink). The 0 second value is turquoise.

To estimate the value of the time realignment, cross-correlation curves were calculated for each day between the time series of each pair of microphones. The time delay corresponding to the maximum of the cross-correlation curve is identified and inserted into the matrix of relative delays presented in Figure 4 for the last day of measurement. It can be seen in this figure that a small number of microphones (namely #5, #11, and #22) show a significant delay with most other microphones, which supports the example in Figure 3.

A unique delay for each microphone relative to the average level is estimated by solving a linear optimization problem. Finally, all microphones are realigned with the wind turbine's electrical production using the same procedure of identifying the maximum of the cross-correlation curve between the average level time series and the electrical production time series. The final corrections are presented in Figure 5. Each colour corresponds to a different measurement day.

The resynchronization of acoustic measurements with electrical production is allowed by the fact that the aspects of acoustic propagation time are not the subject of this study, which focuses more on energetical aspects. However, it is beneficial to correctly synchronize the data on events related to the turbine to retain as much relevant data as possible in subsequent filtering.

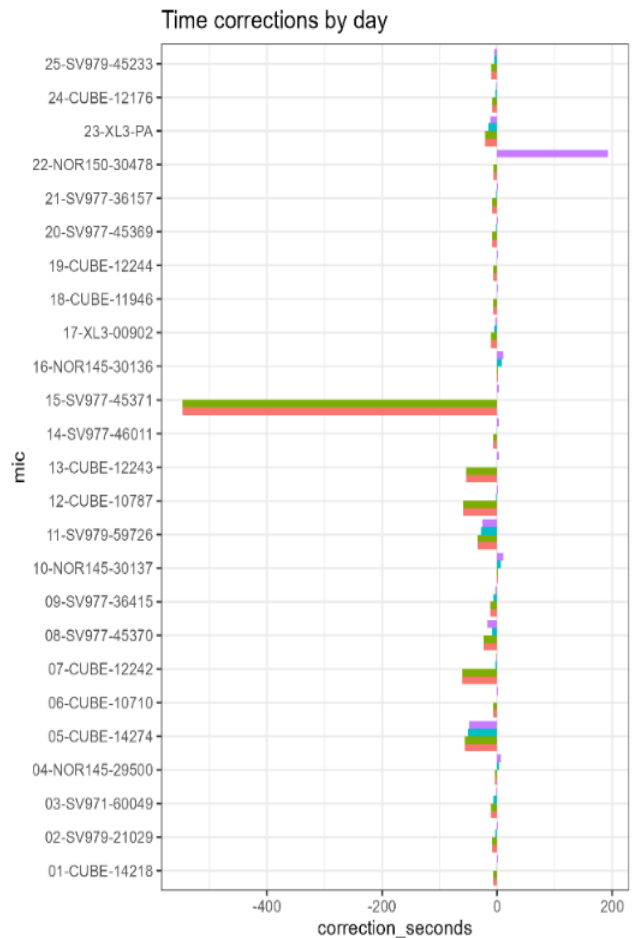


Figure 5 : Time corrections applied to microphones.

The distance between the main acoustic sources (blade tips for aerodynamic noise and the nacelle for mechanical noise) is at most around 300 m, so the dispersion of acoustic propagation times remains on the order of a second. Finally, the introduced correction is less than 10 seconds for 43% of the microphones, as presented in Figure 5.

3.3 Deletion of noisy outliers

To exclude measurements related to high noise level events (such as the passage of an airplane or a car) unrelated to the wind turbine noise, a two-pass cleaning process is established. Firstly, an operator was constantly present on site to keep track of noisy events so they could be properly filtered. Secondly, and in addition to this "manual" cleaning, an automatic cleaning process is implemented: for each microphone, a time series of sliding median is calculated from the raw time series of the overall sound pressure level (OASPL). Exceedances of more than 10 dB from the sliding median define the outlier events. Data within the vicinity of each of these events (± 20 seconds) are ignored. An example of the identification of these outliers is presented in Figure 6. The decrease in noise level during the 21:40 - 21:50 time slot is related to a wind turbine shutdown.

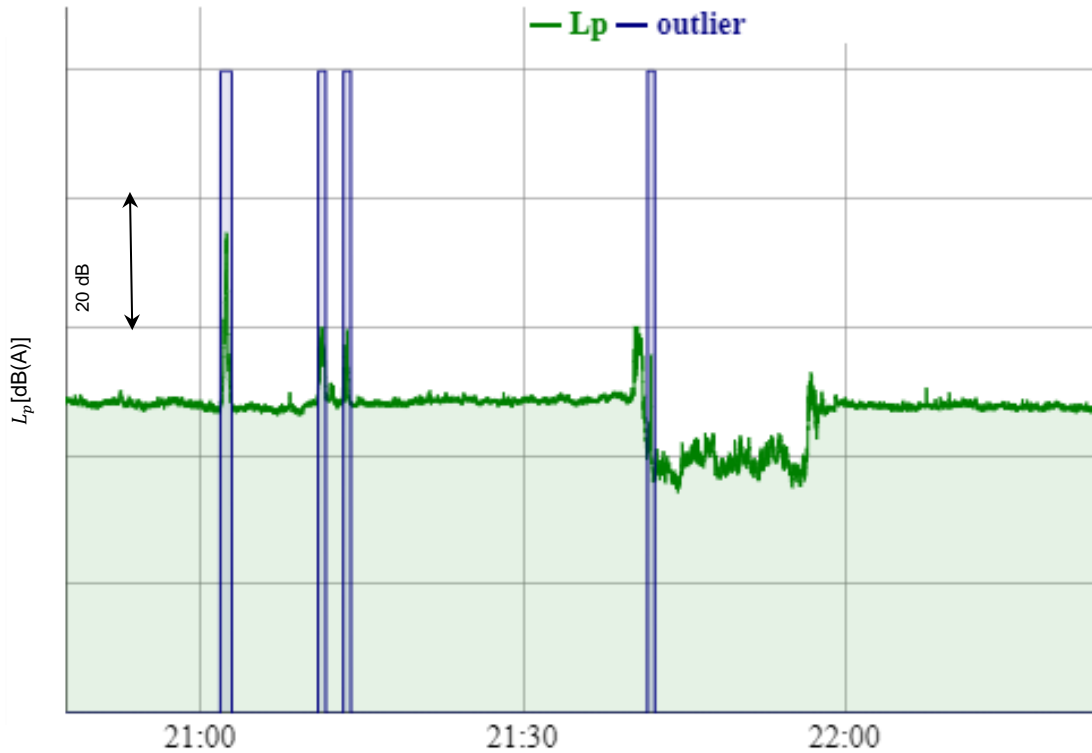


Figure 6 : Identification of noisy events (blue) from a OASPL time series measured on an example microphone (green)

Ultimately, we have a dataset of 25 microphones where outlier levels have been excluded, temporally realigned with the wind turbine's electrical production. Wind speed is provided by the nacelle-mounted lidar, wind direction by the ground-based lidar, and electrical production information directly from the wind turbine's SCADA system.

In accordance with the IEC standard, the data were then grouped into 10-second intervals and classified by wind speed in 0.5 m/s increments. This allows for the comparison of total noise level and background noise indicators, as presented in Figure 7 for the downstream position in the axis.

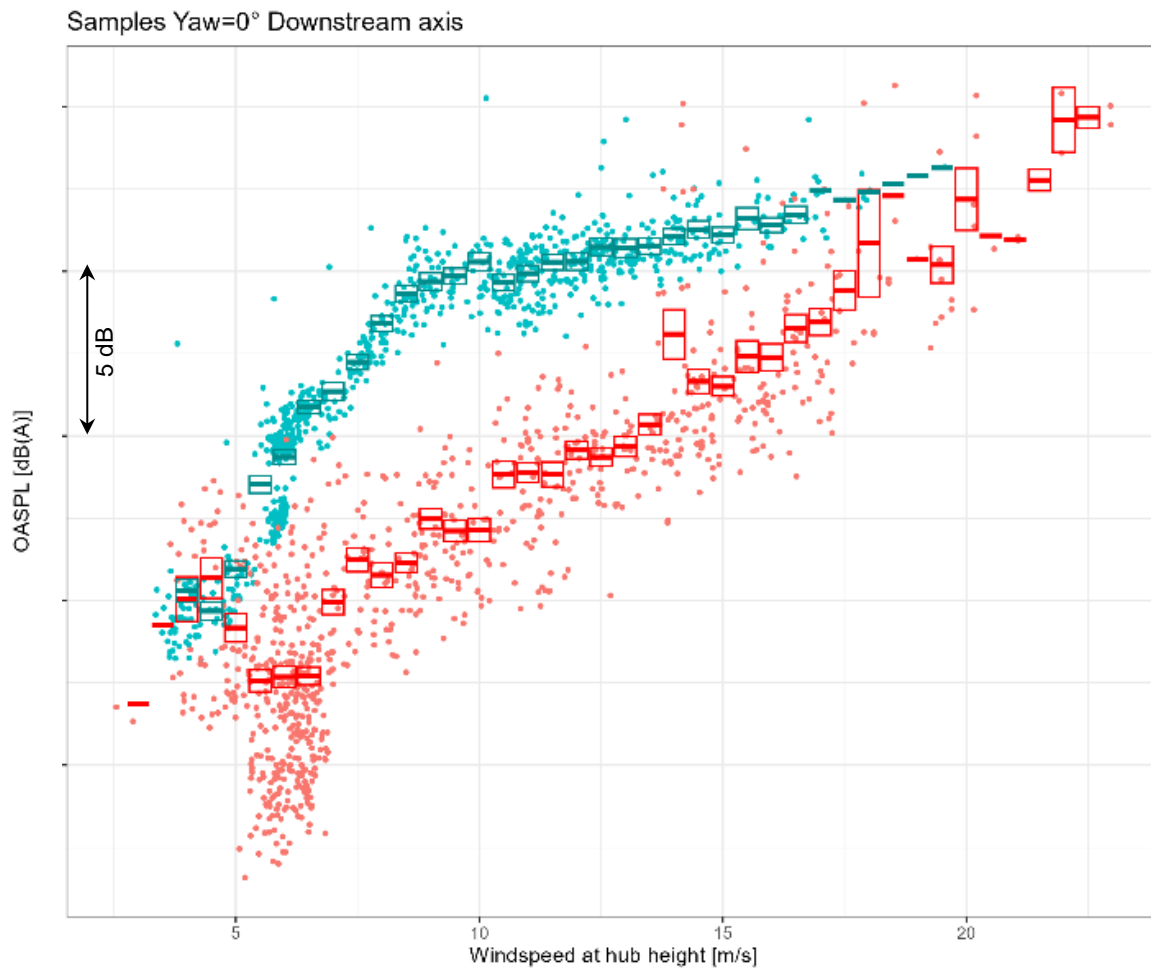


Figure 7 : Samples of total noise (turquoise) and background noise (red) obtained for the downstream position. Each point represent a 10 second sample, boxes shows the noise level indicated as computed following IEC 61400-11 with the associated uncertainty.

4. Analysis of non-steered directivity

4.1 Overall level directivity

An example of a directivity diagram obtained at the end of the data processing step is shown in Figure 8 for a wind speed of 11.5 m/s. For information the nominal electrical power of this wind turbine is reached at 12 m/s. The coloured ribbon indicates the range of values within one uncertainty value of the indicator, with uncertainty calculated according to the IEC 61400-11 standard.

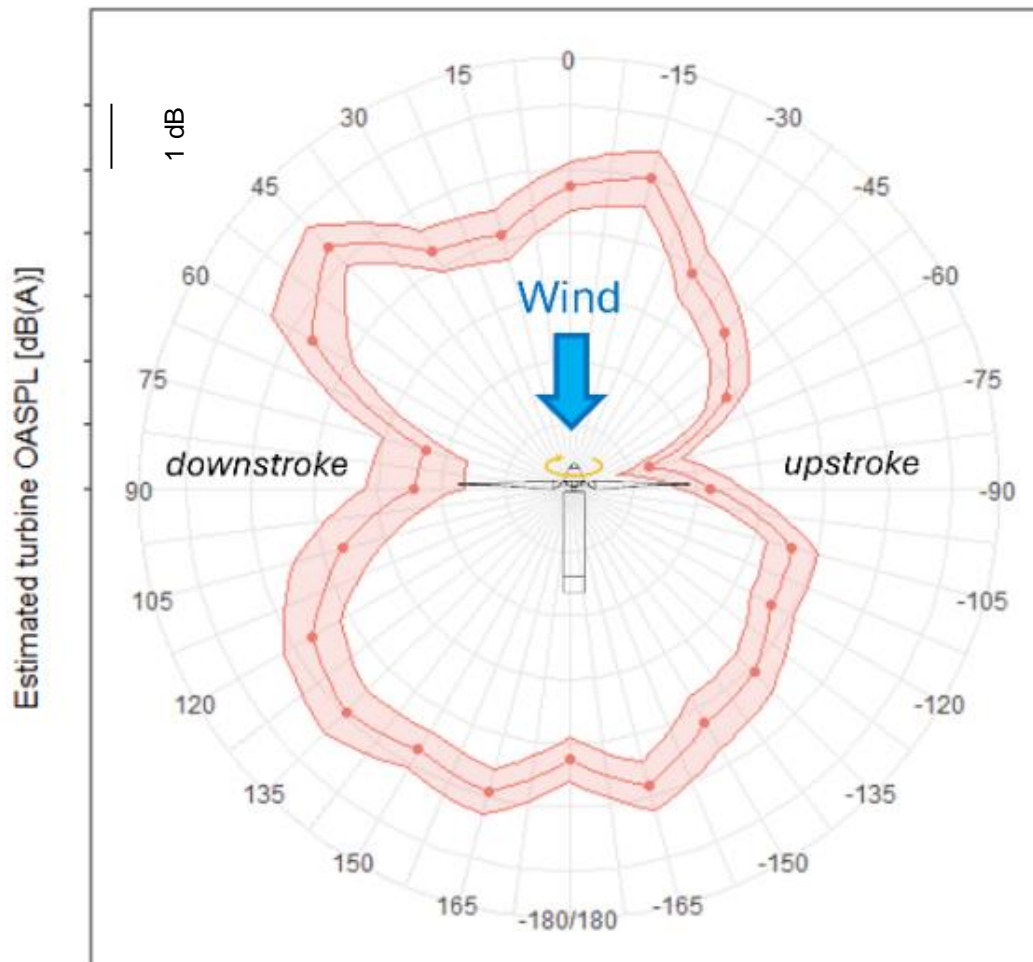


Figure 8 : Wind turbine OASPL measured on ground as a function of the observation angle θ , with $V_{HH} = 11.5$ m/s. Cercles are equally spaced by 1 dB(A).

A two-lobe configuration oriented in the wind direction can be observed. A reduction of approximately 4 dB is measured in the rotor plane compared to the position in the nacelle axis which is compatible with the literature [1] [2]. An asymmetry between the upstream and downstream diagrams is also noted, consistent with the observations of Buck [2] and Bresciani [4]. Buck attributed this effect to the tilt angle in combination with source directivity and convective amplification while Bresciani mentioned the effect of flapwise deflection of the blade. In the downstream region $|\theta| > 90^\circ$, a slight asymmetry between the two sides is also observed: on the descending blade side (left in Figure 8), the acoustic levels are slightly higher (about +1 dB(A)) than those on the ascending blade side (right in Figure 8) for the same absolute observation angle, particularly for $120 \leq \theta \leq 150^\circ$. This behavior has also been noted by Buck [2], but a comprehension of this phenomenon is still to provide. In the upstream region $|\theta| < 90^\circ$, an asymmetry also appears, particularly in the direction $\theta_1 = 45^\circ$ on the descending blade side, where a difference of +2 dB(A) is obtained compared to the symmetric point $\theta = -45^\circ$. For this wind speed, this angle θ_1 is the one of maximum acoustic emissivity. A second directivity lobe towards $\theta_2 = -15^\circ$ is also observed. The above observations remain valid for neighboring speeds, except that the values of θ_1 and θ_2 slightly depend on the wind speed (by 15° or 30°).

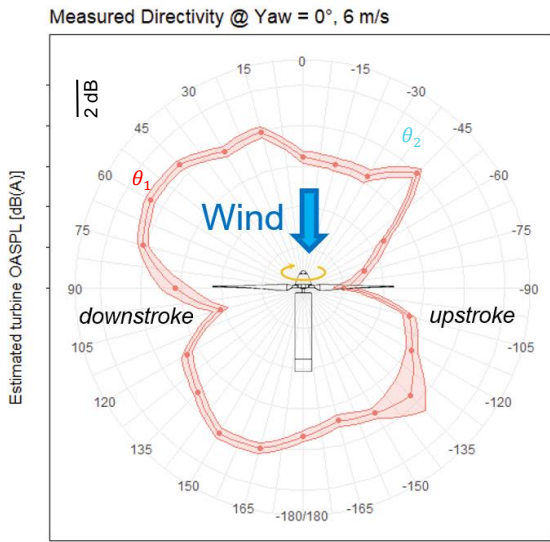


Figure 9 Wind turbine OASPL measured on ground as a function of the observer angle θ , with $V_{HH} = 6 \text{ m/s}$. Cercles are equally spaced by 2 dB(A).

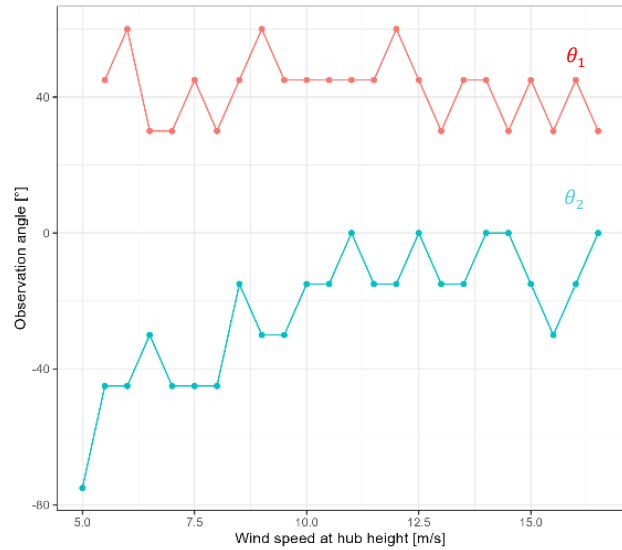


Figure 10 : Angular position of the upstream directivity lobe maximum, for the downstroke quarter, $0 < \theta_1 \leq 90$ in red and for the upstroke quarter $-90 < \theta_2 \leq 0$ in turquoise.

A second directivity diagram is presented at a wind speed $V_{HH} = 6 \text{ m/s}$ in Figure 9. At this speed, the electrical power delivered by the wind turbine is about a quarter of the nominal active power. The two-lobe structure is maintained, the 4 dB(A) level reduction in the rotor plane, the upstream/downstream and left/right asymmetries of 1 dB(A) in the downstream region are approximately found. θ_1 appears to have shifted to 60° and θ_2 to -45° .

To evaluate the shift of the directivity lobes from the upstream sector to the angles θ_1 and θ_2 with wind speed, a tracking of the angular position of the maximum level measured in the 90° sectors is plotted in Figure 10. Given the 15° angular discretization of the setup, it can be inferred that the angle θ_1 varies little with wind speed. However, the upstream emissivity lobe on the ascending blade side appears closer to the rotor plane for low wind speeds ($\theta_2 \approx -45^\circ$ for $V_{HH} \approx 7 \text{ m/s}$) than for high wind speeds ($\theta_2 \approx -15^\circ$ for $V_{HH} > 10 \text{ m/s}$).

In the two examples of Figure 8 and Figure 9, and indeed for all cases encountered in the studied wind speed range $5.5 \leq V_{HH} \leq 16 \text{ m/s}$, the downstream direction in the axis ($\theta = 180^\circ$) does not correspond to the direction of maximum acoustic emissivity.

4.2 Spectral content

Spectral analysis allows for a deeper examination of the third-octave band frequency content at various points of interest. For example, Figure 11 presents the spectra at $V_{HH} = 11.5 \text{ m/s}$ on the descending blade side.

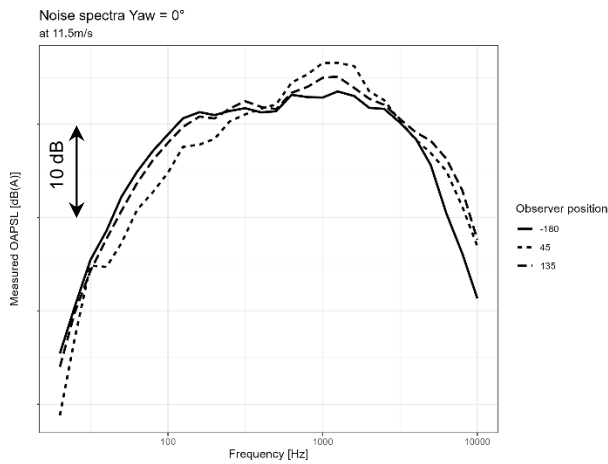


Figure 11 : Noise spectra measured at 11,5 m/s downstream (-180°), at maximum level direction θ_1 (45°) and at downstream maximum (135°), downstroke side.

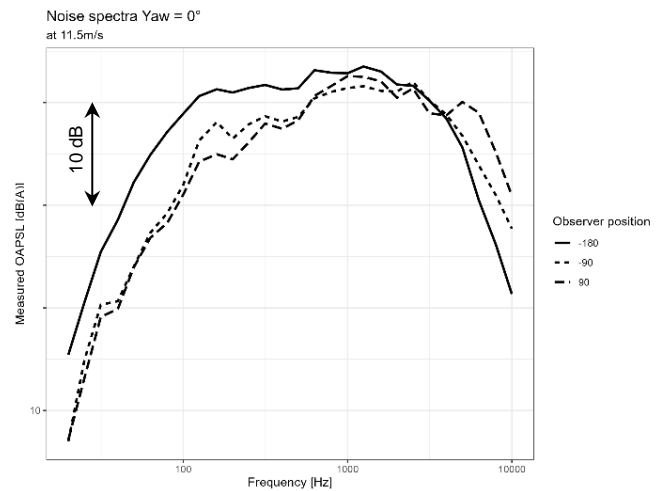


Figure 12 : Noise spectra measured at 11,5 m/s in the rotor plan, and downstream (-180°), -90° (upstroke) et $+90^\circ$ (downstroke).

The downstream spectrum at $\theta = -180^\circ$ serves as a reference. At the point of maximum upstream emissivity $\theta_1 = 45^\circ$, the spectral profile generally contains more high frequencies than the reference: the spectral level is increased by 5 dB(A) at 1000 Hz, and the very high frequencies are also higher (+7 dB for $f > 5$ kHz). Conversely, the low-frequency levels are lower (-4 dB(A) at 100 Hz). At the maximum of the downstream lobe at $\theta = 135^\circ$, the low-frequency spectral profile is similar to the reference. However, the 1 kHz component stands out by 3 dB, and the very high frequencies are more present than in the downstream spectrum.

Two other measurement points for the same flow speed are presented in Figure 12, where the spectra in the rotor plane are compared to the downstream measurement point in the axis. The low frequencies are much less pronounced (-10 dB(A) at 100 Hz), but an increase in very high-frequency content is observed, particularly on the descending blade side.

4.3 Spectral directivity

It is possible to plot directivity diagrams for specific third-octave bands as proposed in Figure 13. It is observed that the two-lobe directivity diagram is more pronounced at 200 Hz than at 2000 Hz, which presents a more complex and asymmetrical diagram, again in agreement with the literature.

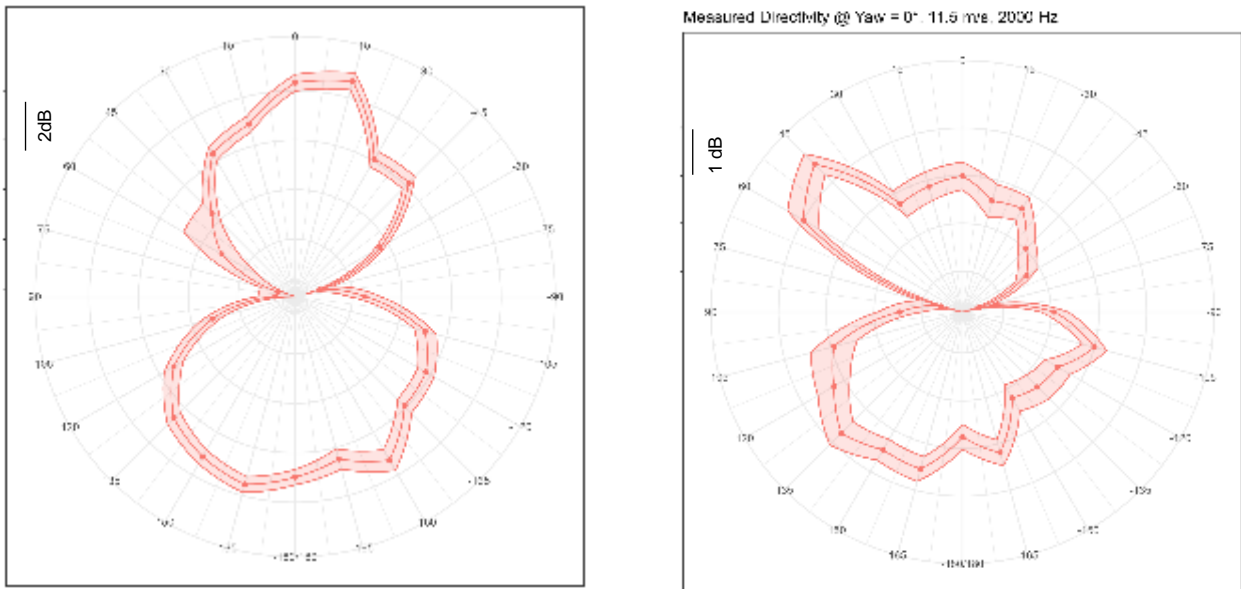


Figure 13 : Spectral directivity pattern at $V_{HH} = 11,5 \text{ m/s}$ for the 200 Hz third octave band on the left and 2000 Hz on the right.

5. Steered configuration

In this section, an illustrative example of the turbine operating under yaw offset is presented. The wind speed is 11.5 m/s, the yaw offset angle of the turbine is $\beta = +20^\circ$. A positive yaw value means that the up going blade hits the flow at an more upstream position than the down going blade. The noise directivity footprint of the turbine is plotted on Figure 14 and compared to the non-steered configuration ($\beta = 0^\circ$).

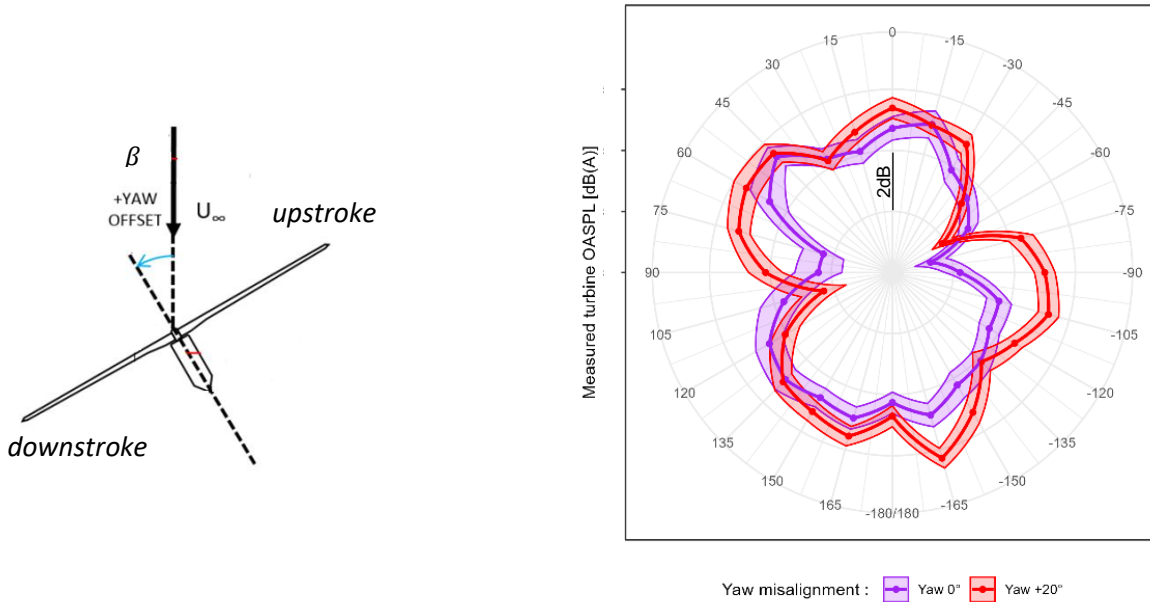


Figure 14: Influence of the yaw on the OASPL directivity pattern at 11.5m/s and yaw angle $\beta = 20^\circ$.

A first observation is that the footprint pattern is generally rotated with the turbine: the noise dips are mostly visible at -60° and $+105^\circ$. The complex multilobe pattern is preserved but appear more pronounced. On this illustrative example with $\beta = 20^\circ$, apart from the pattern rotation, the yaw misalignment appears the increase slightly the OASPL compared to the non-steered case, in particular in the downstream direction. It has also an effect on the spectral content as drawn in Figure 15 with the third octave noise spectra at two specific positions:

- at $\theta = -105^\circ$ (left of Figure 15), where there is a significant increase of the lobe level (+2 dB). In this configuration, the increase in noise level appears homogeneously distributed over the range [500 Hz-5000 Hz],
- at $\theta = 45^\circ$ (right of Figure 15), where the global level is unchanged but not the spectral content : the yawed case presents a higher frequency content than the non-steered case.

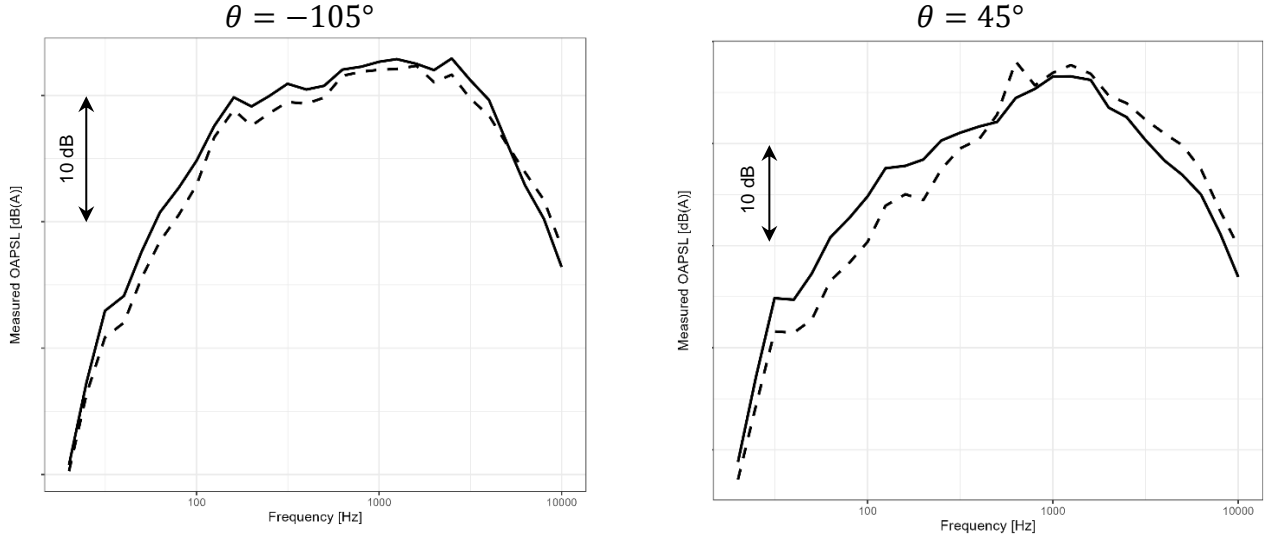


Figure 15: Spectral content of the measured noise levels in the non-steered case (solid line) and with a yaw of $+20^\circ$ (dashed). Left plot: $\theta = -105^\circ$, right plot: $\theta = 45^\circ$, $V_{HH} = 11.5$ m/s.

6. Acoustic power

The characterization of acoustic power generally involves measuring and integrating acoustic intensity over a surface encompassing the sound source, using for the acoustic intensity technique [10]. In the case of wind turbines, this operation is made very complex by the size of the turbine. To still provide an estimate for acoustic impact studies, the IEC 61400-11 standard [11] proposes a procedure based on a single measurement point downstream in the axis of the wind turbine under specific conditions. The evaluation of acoustic power relies on several simplifying assumptions, such as the wind turbine being acoustically reduced to a monopolar omnidirectional source located at the hub centre. Thus, assuming L_p represents the acoustic pressure level measured at this point $\theta = -180^\circ$ at a given frequency, the apparent acoustic power with the omnidirectionality assumption is written as:

$$\tilde{L}_{w,omni} = L_p - 6 + 10 \log_{10} \left(\frac{4\pi R_1^2}{S_0} \right) \quad (1)$$

The -6 dB factor is a compensation for the supposedly perfectly reflective surface on which the microphone is positioned, R_1 is the direct distance between the microphone and the assumed source position (the hub center), and $S_0 = 1 \text{ m}^2$.

The measurements from the present study allow testing the omnidirectionality hypothesis. Indeed, the arrangement of the 24 microphones surrounding the wind turbine introduces a notion of azimuthal dependance that can be accounted for in the estimation of acoustic power. For this, the contributions of each microphone are summed, assuming that the acoustic level is constant over a slice of the hemisphere. The assumption that the source is positioned at the hub center is still maintained. The apparent acoustic power under the homogeneity by slice hypothesis can be opposed to Eq. (1):

$$\tilde{L}_{w,slice} = 10 \log_{10} \left(\sum_{\theta_i} 10^{0,1(L_v(\theta_i)-6)} \times \frac{4\pi R_1^2}{S_0} \times \frac{\Delta\theta}{360^\circ} \right) \quad (2)$$

$L_v(\theta_i)$ represents the pressure level measured by microphone i for the listening angle θ_i and $\Delta\theta = 15^\circ$ in our setup. Thus, we can compare these two approximate estimators, the second taking into account azimuthal variability ignored by the first, as shown in Figure 16 for all available wind speeds.

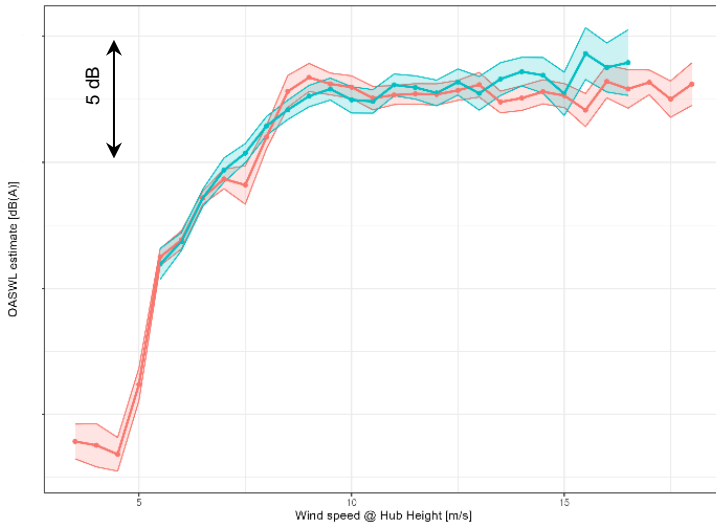


Figure 16 : Apparent OASWL³ as calculated by Eq. (1) for $\tilde{L}_{w,omni}$ in red and Eq. (2) for $\tilde{L}_{w,slice}$ in turquoise. Colored ribbons show the 1- σ uncertainty range

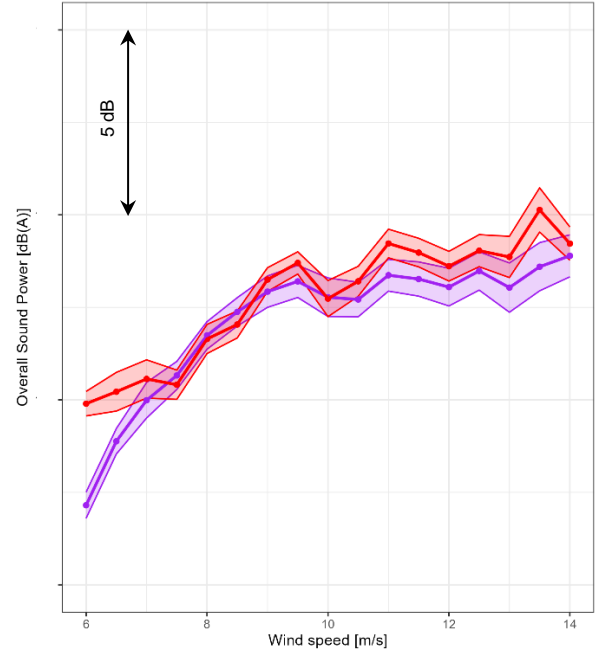


Figure 17: Apparent OASWL $\tilde{L}_{w,slice}$ without Yaw $\beta = 0^\circ$ (purple) and with yaw $\beta = 20^\circ$ (red)

The levels of apparent acoustic power differ on average by 0.5 dB, sometimes positively, sometimes negatively, with a maximum deviation of 2 dB, without any clear trend emerging. This observation can be related to the fact that the downstream position in the axis is not the direction of maximum emissivity; thus, there is no systematic overestimation of acoustic power by $\tilde{L}_{w,omni}$. The curve of the estimator $\tilde{L}_{w,slice}$ appears less erratic than that of $\tilde{L}_{w,omni}$, possibly because the operation involves a larger number of sensors and is therefore less sensitive to measurement errors. At this stage, it is not possible to assert from these measurements that the omnidirectionality hypothesis induces a systematic bias on $\tilde{L}_{w,omni}$ compared to the actual acoustic power.

A proper comparison of apparent acoustic power with and without yaw cannot be made using $\tilde{L}_{w,omni}$ because of the rotation of the directivity pattern with the wind turbine axis. A positioning of the measurement point in an acoustic dip would attribute a global effect to a local cause. Instead the $\tilde{L}_{w,slice}$ indicator may partially account for the pattern rotation⁴. A comparison of apparent OASWL is presented on Figure 17 using Eq. 2 between $\beta = 0^\circ$ and $\beta = 20^\circ$ cases. It indicates that in the lowest speed range $V_{HH} \leq 7 \text{ m/s}$ and in the highest range (above rated power), the yaw tends to increase the estimated power by 1 to 2 dB. This hypothesis based on a partial observation has to be tested against other measured yaw set points and possibly turbine models. However it departs from conclusions of Hamilton [8] which observed a *reduction* of measured noise level under positive yaw operations with another turbine model and measurements limited to the downstream sector with a $\sim 120^\circ$ aperture.

7. Conclusion

This study presents a unique acoustic directivity field campaign at 24 points regularly spaced around an industrial wind turbine at a blade tip height distance, based on the international IEC 61400-11 standard. This original setup highlights significant variations in sound level with listening direction, rising to 4 dB

³ Over All Sound Power Level

⁴ at least in the lower frequency range where the number of lobes is reduced and the observer angle discretization is sufficient.

between the downstream direction and the rotor plane. An asymmetry of the diagrams relative to the rotation plane is observed, consistent with the literature.

In the downstream sector, a sound level increase of about 1 dB is observed on the descending blade side. The standard position does not correspond to the point of maximum emission. Additionally, other upstream directivity lobes are highlighted, the first at 45° on the descending blade side, which is the direction of maximum emissivity in several configurations. A second upstream lobe on the ascending blade side is identified. It is also located at 45° for low wind speeds but gradually approaches the axis with increasing V_{HH} until it reaches 15° as the rated electrical power is approached. The spectral content of the measurements shows that at the maximum of the directivity lobes, mid frequencies around 1 kHz are very present, as well as very high frequencies > 5 kHz. In the rotor plane, low frequencies are very weak.

Application of a yaw offset of $+20^\circ$ indicates that the directivity pattern is globally rotated with the turbine axis, and lobes are reinforced under yaw. The spectral content is also affected in places.

The impact of these directivity effects on apparent acoustic power has been evaluated. A modification of the omnidirectionality hypothesis to a slice homogeneity has been taken into account. At this stage, the measurements do not allow for a conclusion of a marked effect, which supports the omnidirectionality hypothesis chosen in the IEC 61400-11 standard. Under a moderate yaw offset, a slight increase of 1 to 2 dB is observed compared to the non-yawed case. Comparison with different yaw set points and numerical simulations may be valuable to gauge the validity of this statement.

Acknowledgments

The TWAIN acoustics campaign is realized under the TWAIN project, funded by the European Union's Horizon Europe research and innovation program with grant agreement no. 101122194.

The authors would like to thank Echopsy for their great support in setting up and conducting the field test.

Références

- [1] S. Oerlemans and J. Schepers, "Prediction of Wind Turbine Noise and Validation against Experiment," *International Journal of Aeroacoustics*, vol. 8, pp. 555-584, August 2009.
- [2] S. Buck, S. Oerlemans and S. Palo, "Experimental characterization of turbulent inflow noise on a full-scale wind turbine," *Journal of Sound and Vibration*, vol. 385, pp. 219-238, 2016.
- [3] Y. Okada, K. Yoshihisa, K. Higashi and N. Nishimura, "Horizontal directivity of sound emitted from wind turbines," *Acoustical Science and Technology*, vol. 37, pp. 239-246, 2016.
- [4] A. Bresciani, U. Boatto, S. Le Bras, P. Bonnet and L. Santana, "Influence of blade deflections on wind turbine noise directivity," 2022.
- [5] S. Boersma, B. M. Doekemeijer, P. M. O. Gebraad, P. A. Fleming, J. Annoni, A. K. Scholbrock, J. A. Frederik and J.-W. van Wingerden, "A tutorial on control-oriented modeling and control of wind farms," in *2017 American Control Conference (ACC)*, 2017.
- [6] P. Fleming, J. Annoni, J. J. Shah, L. Wang, S. Ananthan, Z. Zhang, K. Hutchings, P. Wang, W. Chen and L. Chen, "Field Test of Wake Steering at an Offshore Wind Farm," *Wind Energy Science*, vol. 2, p. 229-239, 2017.
- [7] E. Simley, P. Fleming, N. Girard, L. Alloin, E. Godefroy and T. Duc, "Results from a wake-steering experiment at a commercial wind plant: investigating the wind speed dependence of wake-steering performance," *Wind Energy Science*, vol. 6, p. 1427-1453, 2021.
- [8] N. Hamilton, P. Bortolotti, D. Jager, Y. Guo, J. Roadman and E. Simley, *Aeroacoustic Assessment of Wind Plant Controls*, 2021.

- [9] I. Bonsma, N. Gara and B. Howe, "Intentional Yaw Misalignment and the Effects on Wind Turbine Noise," *Canadian Acoustics*, vol. 47, p. 66–67, October 2019.
- [10] ISO3744, "Acoustics — Determination of sound power levels and sound energy levels of noise sources using sound pressure — Engineering methods for an essentially free field over a reflecting plane," *ISO standard*, 2010.
- [11] IEC61400-11, "Wind turbines - Part 11: Acoustic noise measurement techniques," 2018.

Paper #21 - ID: 355

Title: Investigation of acoustics inside wind turbine blades and how it effects the outside

Author: Lukas Schneider

11th Edition of the
International Conferences on
Wind Turbine Noise
Copenhagen, Denmark – 10th to 13th June 2025

Investigation of acoustics inside wind turbine blades and how it effects the outside

Lukas Schneider¹

ESM Energie- und Schwingungstechnik Mitsch GmbH, Heppenheim, Germany

Massimiliano Calloni, Rabah Hadjit, Oliver Goy

ESI Group, a part of Keysight Technologies, Bagneux, France

Benjamin Fischer

Amperax Energie GmbH, Itzehoe, Germany

Summary

Wind turbine blades emit tonal and broadband noise in the far field due to air flow around the blade but also due to structural vibration coming from generator, gear box or transformer. So far, the acoustic behaviour of the air inside the blade is neglected assuming that it has no amplifying effect on the outside. In this study measurements of transversal and longitudinal standing waves, its wavelength, frequencies and reverberation times for a 57m blade are presented. It is shown that strong longitudinal standing waves are excited between the webs of the blade. The waves even excite the soft webs and with them the whole blade vibrates and can emit noise. It is also shown with structural and acoustic excitation that damping measures inside the blade (absorber mats and resonators) have an effect on the outside. Numerical investigations with boundary element - and finite element methods of a generic blade submerged in an acoustic field help to understand and confirm the effect of these countermeasures.

1. Introduction

On the European market the noise of wind turbines is a key selling point, i.e. it has strong influence on the decision for or against a wind turbine. The sound power level is determined by the broadband noise coming from the aerodynamics of blades (see e.g. [1]) but also from the tonal noise that is generated in the generator and gear box and that is emitted through tower, nacelle and/or blades (see [2]). The emission of tonal noise by the blades is demonstrated by the Doppler frequency shift measured on the ground (see [3]).

The blades play an important role in the acoustics of wind turbines. First the air flow around the blade generates broadband noise and second the blade is a large resonance body that turns structural vibrations into pressure fluctuations on a very large area. The surface structure of the blade is usually a thin shell that has low eigenfrequencies and that can easily be excited by structural vibrations but also by external or internal sound pressure. It is the goal of this investigation to show that the effect of the blade internal sound effects the surrounding acoustics.

¹ Corresponding author – Email: Lukas.Schneider@esm-gmbh.de

The aerodynamic noise imposes strong restriction on blade design and in particular on the blade tip (see [4]). It also limits the rotor speed and therefore the energy production of the turbine. Counter measures against noise are welcome that do not affect the air flow around the blade.

2. Blade-internal acoustics

The inside of a blade is a closed room that is framed by thin shells and that includes one, two or three webs going straight from blade root to the blade tip (see Figure 1). Also, the inner side of the foil consists of smooth surfaces that can be considered as acoustically hard walls. The thickness of the walls varies a lot but in general they can be considered as shells with thin thickness (so that the sun is shining through it as can be seen in Figure 1). By design, the blade reduces its diameter from 2-4m at the blade root to zero at the blade tip. It therefore has a conical shape in the longitudinal direction and round/oval shape in a cross section.



Figure 1: Inside of 45m blade of an ESM-owned turbine with two webs.

The acoustics inside the blade show the following characteristics:

1. The round and smooth inner walls of the blade allow good reflection of sound waves with small diffusion.
2. The room modes in the transvers direction of the blade depend on the diameter of the respective cross section. In a blade with 3m root diameter for example the room mode was measured to be 69Hz (see Figure 2) which fits quite well to the calculated room mode frequency in the round cross section.

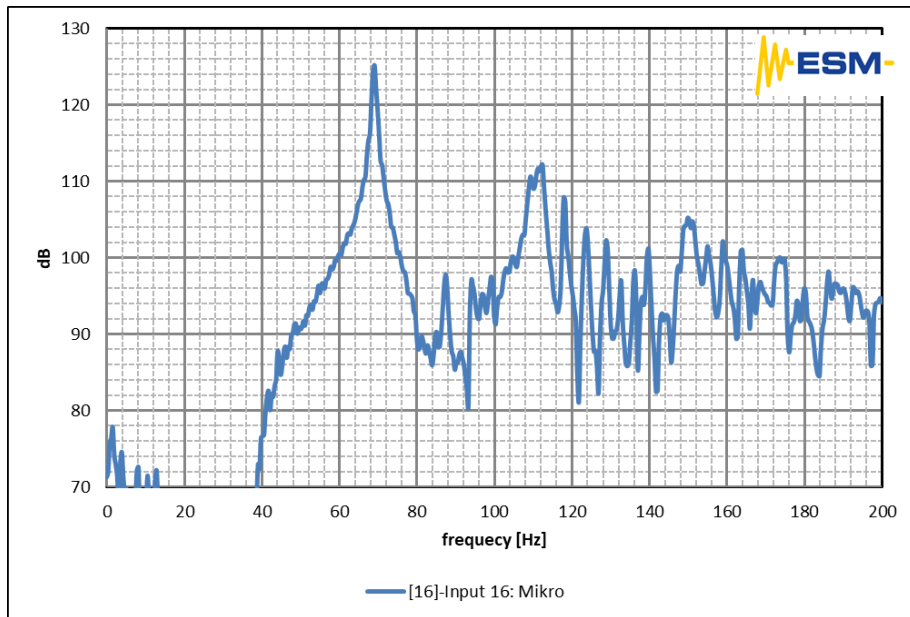


Figure 2: sound power vers. excitation frequency measured with a microphone at 3m diameter root inside a blade excited by a 30Hz-200Hz frequency sweep with a vibration isolated loudspeaker standing inside the blade at the root.

Also, the trend of the transvers room modes along the blade fits well to the calculated room modes (see Figure 3). In a single degree of freedom sound wave the relation between sound frequency f , wave speed c and the wave length λ is:

$$f = \frac{c}{\lambda} \tag{1}$$

A room mode or standing wave in a closed room is present if a half wavelength of the sound fits between the walls of the room.

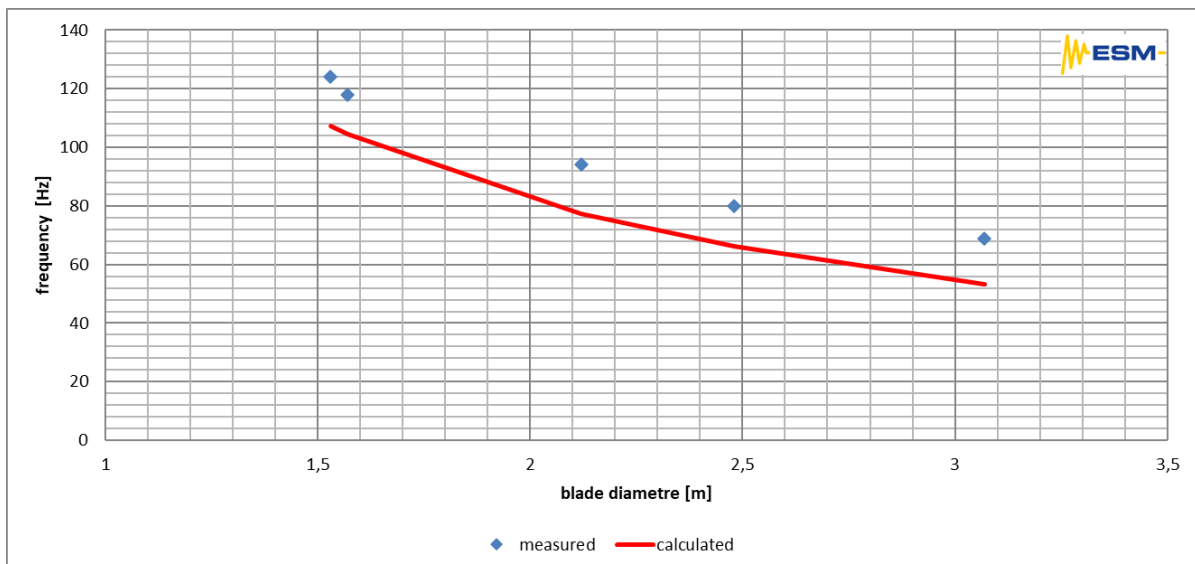


Figure 3: room mode frequency vers. blade diameter at the measured position (blue dots) and the calculated frequencies for the different blade diameters using equation (1).

3. The room mode along the blade axis between two webs (see Figure 1) start at much lower frequencies because in a blade of e.g. 60m a sound wave with frequency 2.75Hz fits between the root and the blade tip. As the harmonics to this sound wave also fit into the same blade length also the harmonics show up in the measurements (see Figure 4). The room modes along the blade axis move more air mass then in the transvers direction and therefore much more kinetic energy is active

in room modes along the blade axis. In addition, the space between the webs is a long equidistant channel with no disturbance in the width direction and conical shape in the height direction (see Figure 1). This geometry reduces the dispersion of sound waves and increases the capacity to store vibrational energy.

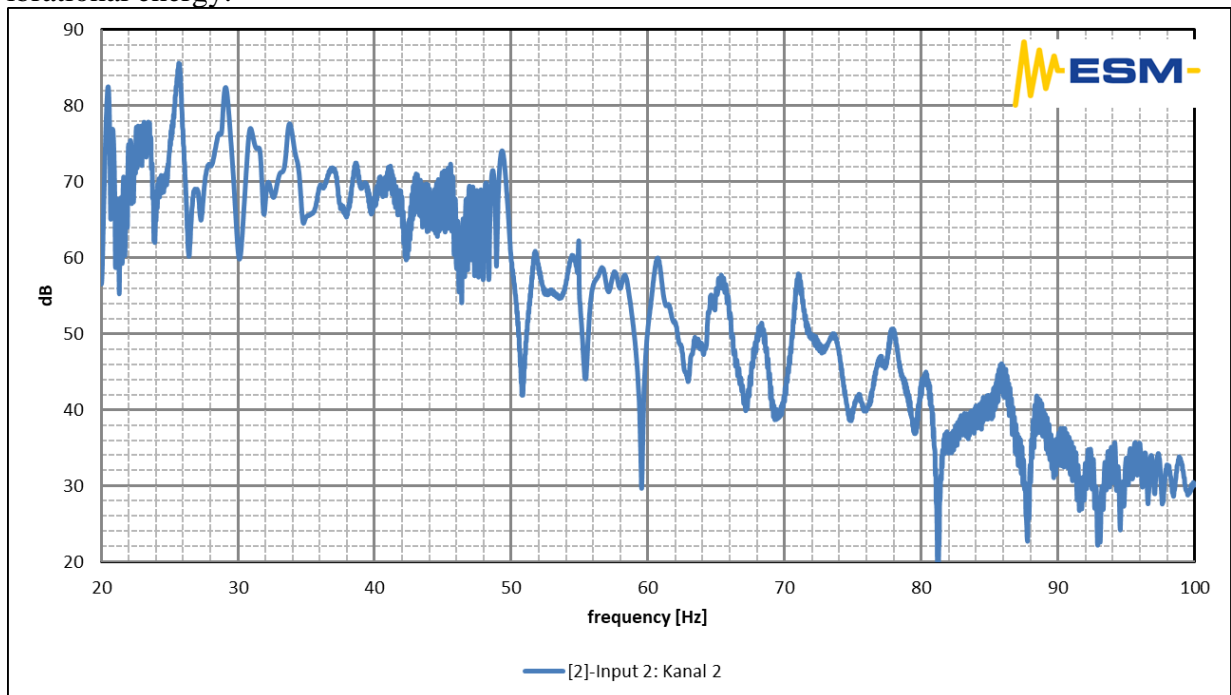


Figure 4: sound power vers. excitation frequency measured with a microphone between two webs excited by a 20Hz-100Hz frequency sweep with a vibration isolated loudspeaker standing at the blade root.

4. The damping ratio of a 30Hz room mode along the blade axis is measured to be 0,005 which corresponds to a reverberation time of $T_{60} = 6s$ (see Figure 5). This small damping allows large kinetic energies in the longitudinal room modes because only a small amount of energy is dissipated. The reason for the low damping ratio is the absence of sound dispersion and the acoustically hard walls.

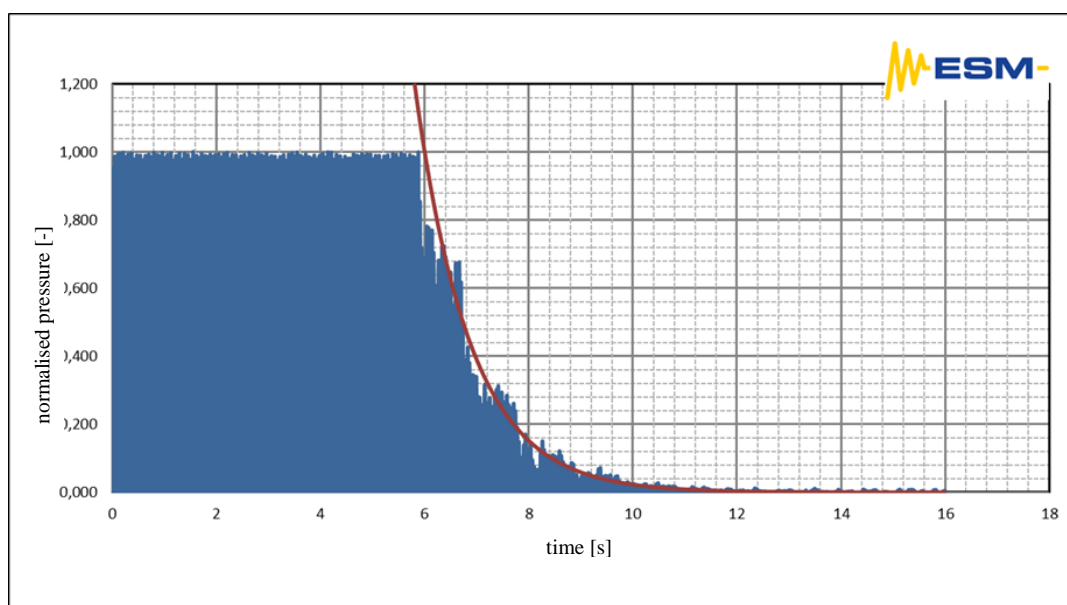


Figure 5: normalised pressure decay curve (blue line) measured with a microphone between two webs excited by a vibration isolated loudspeaker at 30Hz standing at the blade root; exponential decay curve (red line)

Room modes have the property that the velocity of the air molecules is zero at the walls but the pressure amplitude is maximum there. Consequently, the walls of the blade experience the room modes as strong pressure oscillations. From the above analysis it is therefore expected that especially the longitudinal room modes lead to strong pressure fluctuations on the blade walls, because due to low damping and high vibrating masses the kinetic energy in these type of room modes is high.

5. At higher frequencies (above the Schröder frequency [5]) room modes cannot be identified anymore but the above results for high kinetic energy in the longitudinal direction of the blade remains true.

The above analysis of the acoustics in blades neglects the structural eigenmodes of the blades. As the used loudspeaker is isolated from the structure it does not directly excite the structural eigenmodes but the thin shells of the blade can easily be excited by the in-blade acoustics. In this case a structural eigenmode can give a sound amplification back into the room. Consequently, the amplification in Figure 4 can also be structural eigenmodes instead of room modes. Here and in the following study a differentiation between room modes and structural modes can only be done by exciting the structure with a loudspeaker or a mobile shaker. Removing the blade internal sound using noise-absorbent mats or resonators also helps to differentiate between structural eigenmodes and room modes in the blade.

3. Effect of acoustics inside the blade on the outside for frequencies higher than 500Hz

To show the effect of the inner acoustic of a blade on the outside, noise-absorbent mats are positioned at the inside of a 57m blade close to the blade root (see Figure 6).



Figure 6: 12m² noise-absorbent mats of 5cm thickness at the blade root of 57m long blade.

The blade is excited by a loudspeaker inside the blade and by structural shaker at the root. The sound is measured with a microphone outside the blade. The comparison of outside sound power with and without noise-absorbent mats results in the following observations:

1. Exciting the inside of the blade with a loudspeaker and measuring the sound power outside the blade for both configurations, i.e. with and without noise-absorbent mats, shows that in the frequency range where the noise-absorbent mats are active (above 500Hz), the sound power reduces up to 6dB (see Figure 7). This observation demonstrates that the blade shell is not an acoustically

isolating structure, but it can transfer the inner acoustic to the outside of the blade. As the noise-absorbent mats are only active for frequencies above 500Hz this observation holds only true in the frequency range the noise-absorbent mats are active.

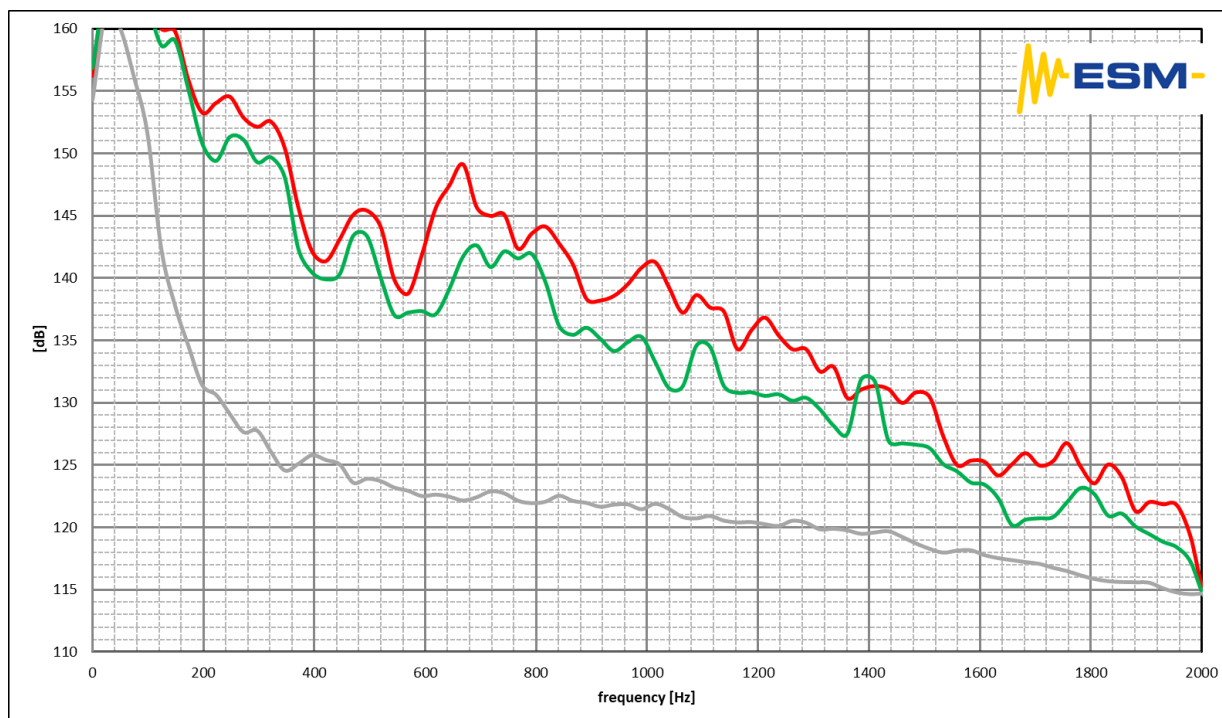


Figure 7: sound power vers. frequency measured with a microphone outside the blade excited by 70Hz-2000Hz frequency sweep using a vibration isolated loudspeaker inside the blade without noise-absorbent mats (red line) with noise-absorbent mats (green line) and without excitation (grey line).

2. Exciting the blade structure with a structural shaker at the blade root gives a less pronounced result compared to the excitation of loudspeaker but still a reduction of up to 2dB can be observed (see Figure 8). The reason for the reduced effect of the noise-absorbent mats on the outside acoustic – compared to the loudspeaker excitation – is that with shaker excitation two transfer paths exist to the outside microphone. The direct transfer path through the blade structure into the outside air is the most obvious one that is usually expected to be the only one. With this measurement it is shown that there is also a second transfer path where the vibrations go from the shaker into the structure, into the inside air of the blade, back into the structure and only then into outside air. The later path is not obvious, but it exists because of the large area of inner blade walls, because of the low damped air acoustic inside the blade that collects a lot of kinetic energy (see section 2) and because of the low stiffness walls of the blade that easily transfer the inner sound to the outside.

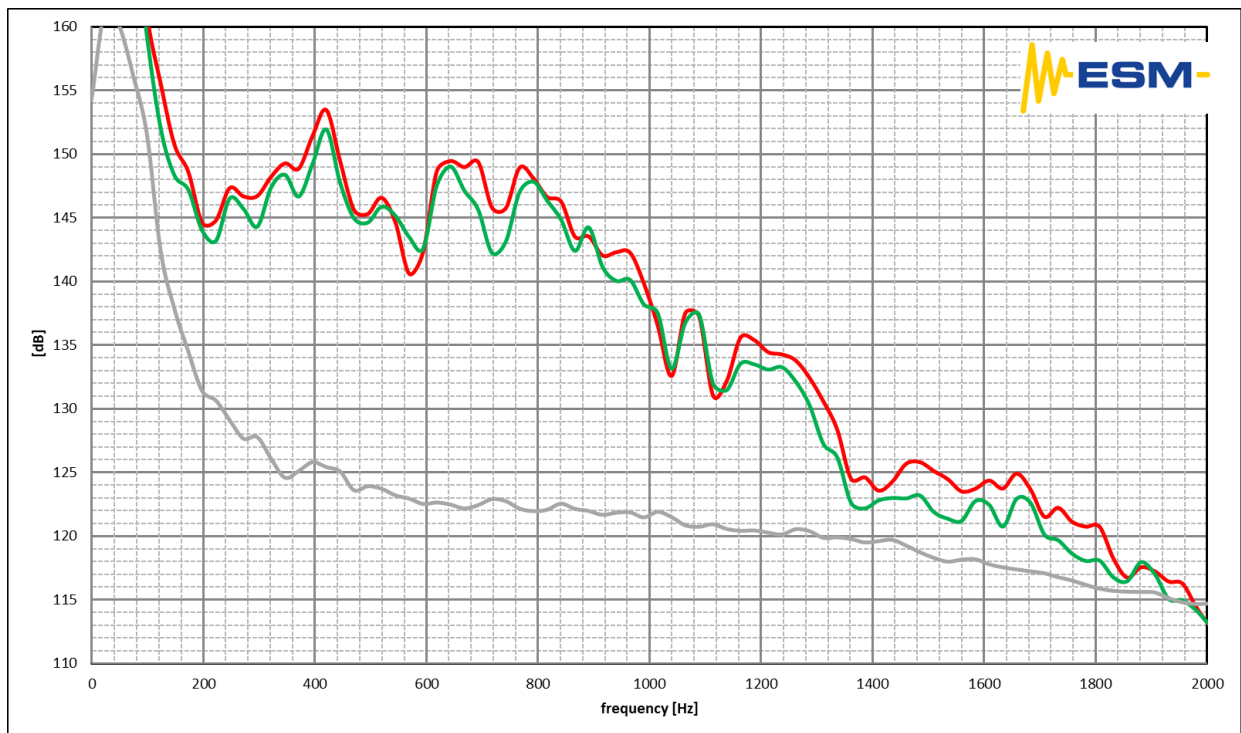


Figure 8: sound power vers. frequency measured with a microphone outside the blade excited by 70Hz-2000Hz frequency sweep using a structural shaker at the blade root without noise-absorbent mats (red line), with noise-absorbent mats (green line) and without excitation (grey line).

The above analysis also shows that noise-absorbent mats can be used to reduce emission of broadband noise coming from blades because it reduces the second transfer path. Noise-absorbent mats can be positioned close to the blade root because due to the conical shape of the blade the sound energy is concentrated at the blade root. They also have the advantage that they don't effect the flow around the blade as for example serrations or vortex generators do.

In operating wind turbines the broadband noise is generated in the air flow at the tip and at the trailing edge (see [1]). It is commonly assumed that the noise is directly emitted to the far field. The above evidences allow the hypothesis that there is another transfer path from the noise generation, via the blade structure, into the blade internal air, back into the blade structure and from there into the surrounding air towards the far field. This hypothesis needs to be proven by future tests on operating turbines. It is expected that this more complicated path is only possible because of the large blade emitting areas towards the inside and the outside air, because of the low damped room modes and acoustics inside the blade and because of the thin shells of the blade.

4. Effect of low frequency room modes inside the blade on the outside

To show the effect of low frequency room modes inside the blade on the outside, frequency tuned and damped resonators are distributed in a lying blade so that room modes are damped. The effect of the resonator is checked by loudspeaker excitation in the blade. In Figure 9 it is observed that in the frequency range between 85Hz and 105Hz the sound power is reduced by up to 10dB using the resonators. This observation demonstrates that the room modes can also have an effect on structural vibrations coming from the generator and gear box and being amplified by the standing waves in the blade.

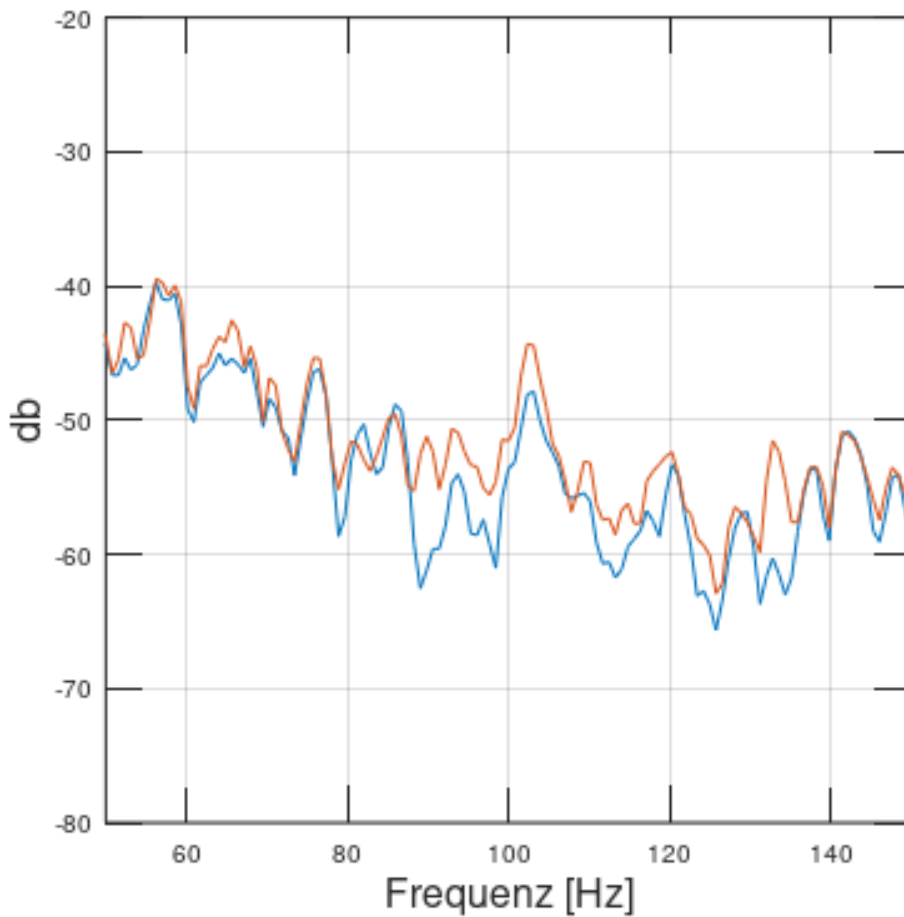


Figure 9: sound power vers. frequency measured with a microphone outside of the blade without resonators (orange) and with resonators (blue).

5. Numerical investigation of internal blade acoustics

The Simulation plays a crucial role in understanding the dynamic behavior of wind turbine blades, enabling optimized designs from the outset and correlation with test data. This approach not only ensures efficient performance but also helps achieve compliance with external noise regulations.

A vibroacoustic simulation model of a generic single wind turbine blade has been developed in ESI VA One 2024 (see [6]) to highlight the importance of incorporating noise control treatments, consequently, additional damping to reduce noise emissions, particularly under structural loads. The wind turbine blade is 27 meters long and its weight is 3000kg (Figure 10).

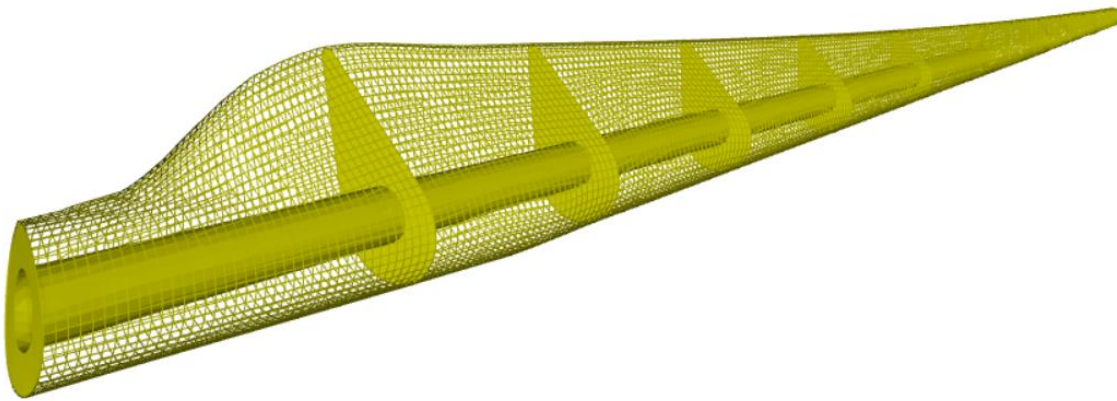


Figure 10 – Wind Turbine Blade Finite Element Model

The vibroacoustic model consists of a structural finite element (FE) representation comprising 14184 elements, acoustic FE representation for eight interior cavities with a total of 222947 elements (*Figure 11*), unit structural loads applied in three directions at the hub connection, and a semi-infinite fluid (SIF) (*Figure 12*) domain to enable exterior noise radiation analysis.

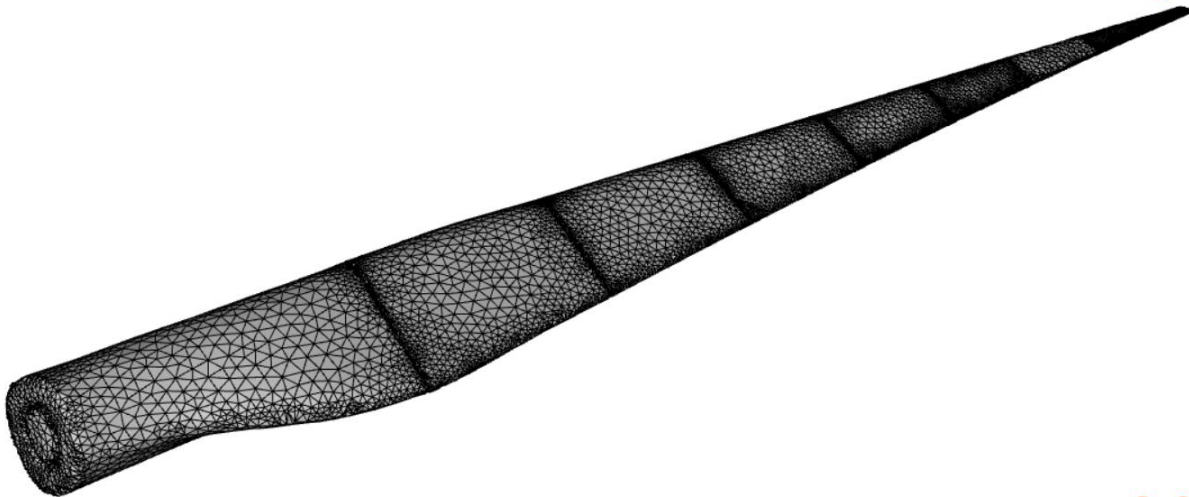


Figure 11 - Acoustic Finite Element Model

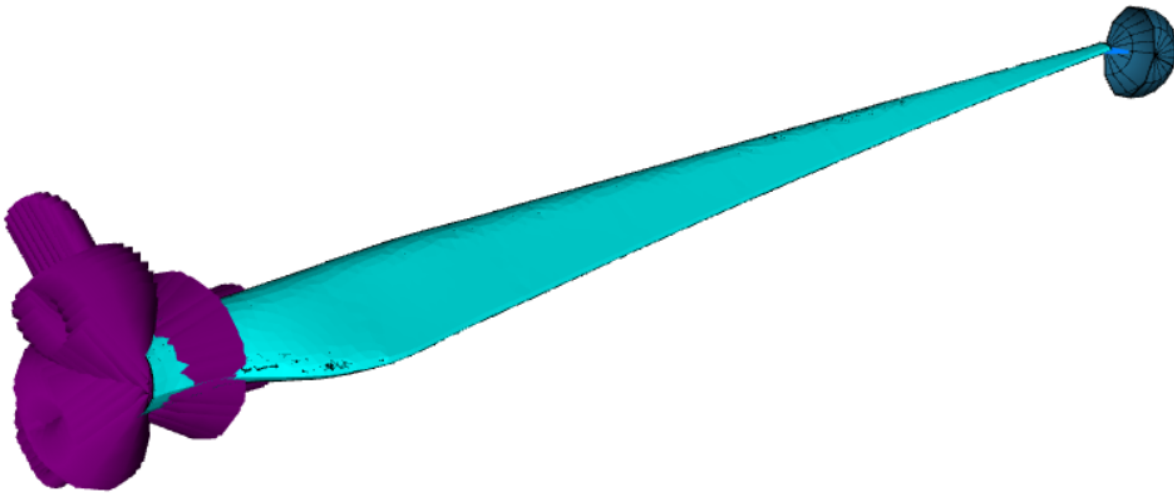


Figure 12 - Vibroacoustic Model with Loads and SIF

Structural and acoustic normal modes (*Figure 13* and *Figure 14*) have been computed using ESI VPS solver, ensuring the model's validity within a frequency range of 300 Hz. The analysis has been conducted in narrowband with a resolution of 1 Hz. If an extended frequency range is required, Statistical Energy Analysis (SEA) method available in ESI VA One is recommended.



Figure 13 - First Structural Bending Mode

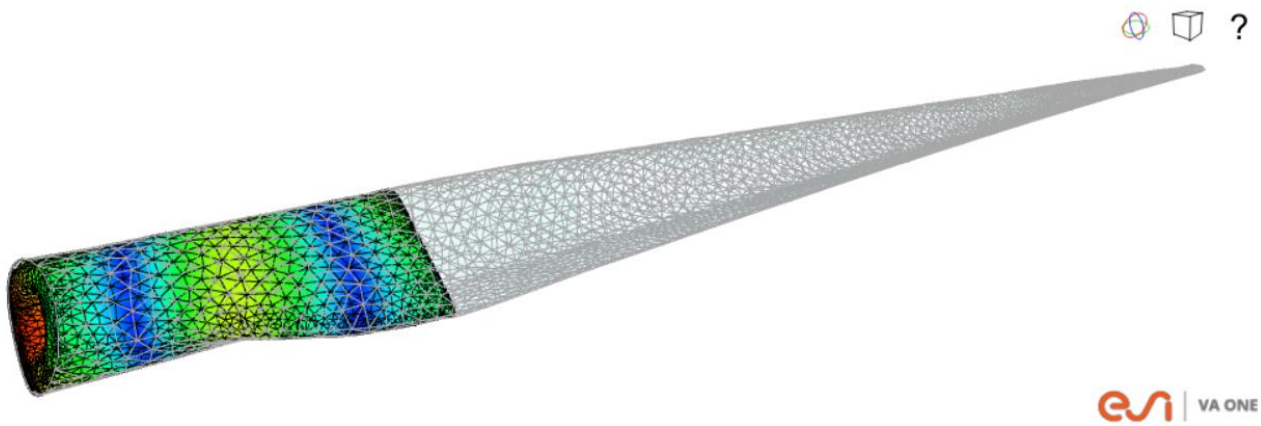


Figure 14 - Acoustic Mode of the First Cavity

Additionally, a second model has been developed where the interior of the blade has been treated with 5 cm noise control treatment of a low-density foam (8 kg/m³) to introduce absorption and damping (Figure 15). Figure 16 presents a comparison of the sound power emitted by the blade with empty cavities versus the blade with poroelastic (foam) material applied to it. The results indicate that the addition of foam leads to a reduction in noise emission across the entire frequency range, attributed to both increased absorption and additional damping. However, it is important to note that incorporating foam increases the blade's weight by 39 kg, about 1.3% of the total weight of the blade, which could impact other performance factors. Therefore, selecting the appropriate poroelastic material is critical to balancing all key performance criteria under operational conditions.

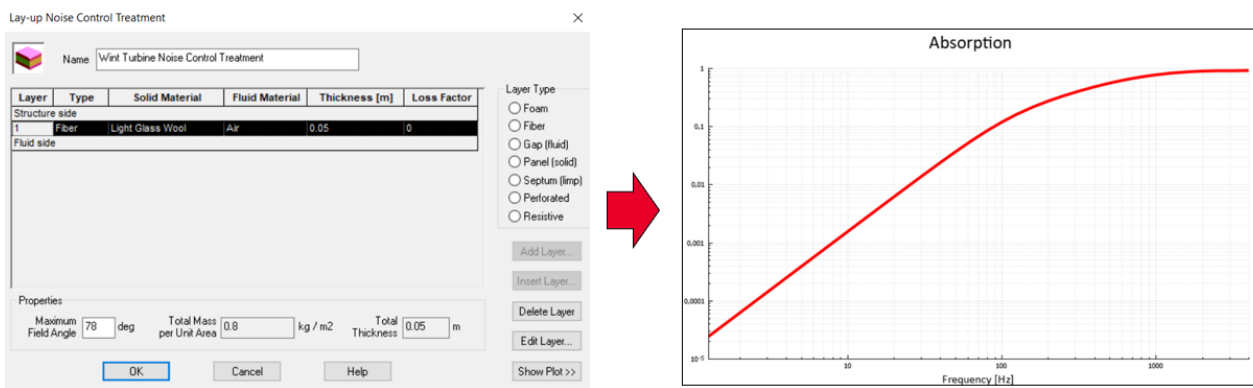


Figure 15 - Poroelastic Model (PEM) properties

Power Inputs to Semi Infinite Fluid

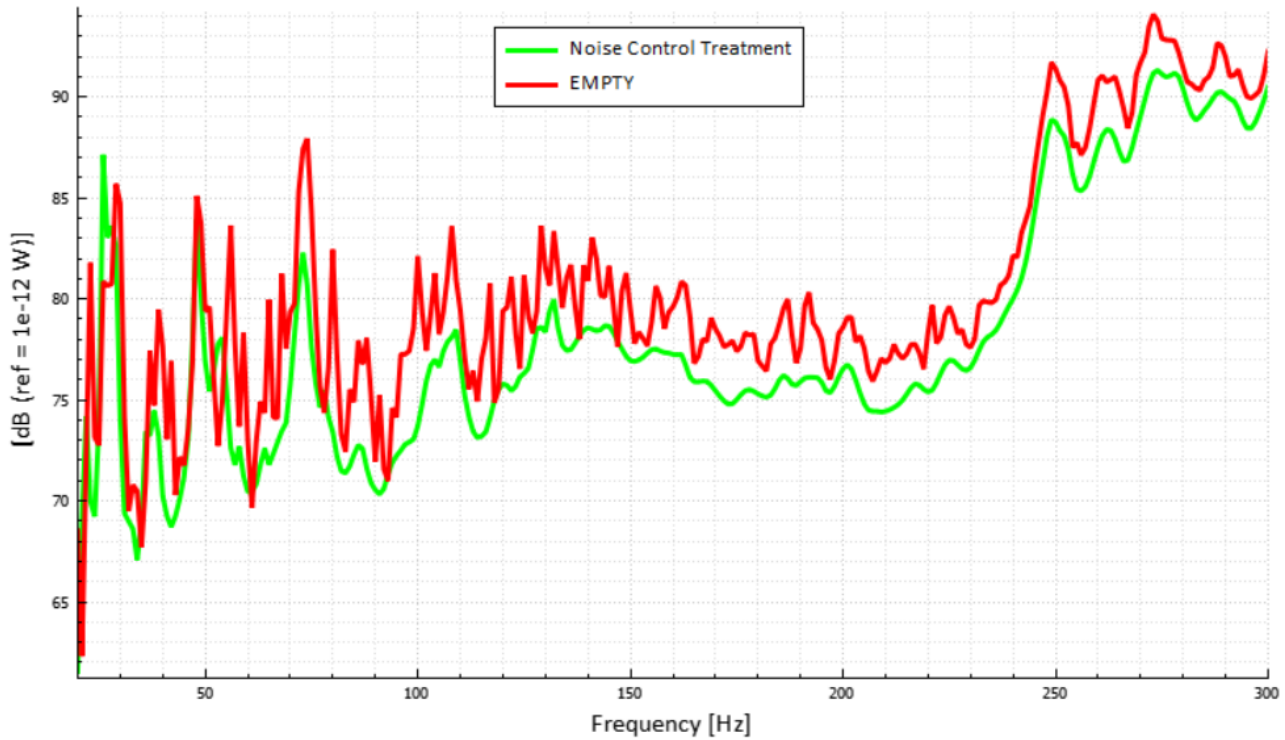


Figure 16 - Acoustic Power Emitted

For the peak at 74 Hz, as an example, the SIF models were converted into boundary element models (BEM) to gain deeper insights into blade radiation (see Figure 17). Furthermore, four virtual microphone planes were integrated into the model to analyze radiation patterns, confirming that the blade with noise control treatment applied exhibits superior vibroacoustic performance, as evidenced by reduced noise emissions (see Figure 18).

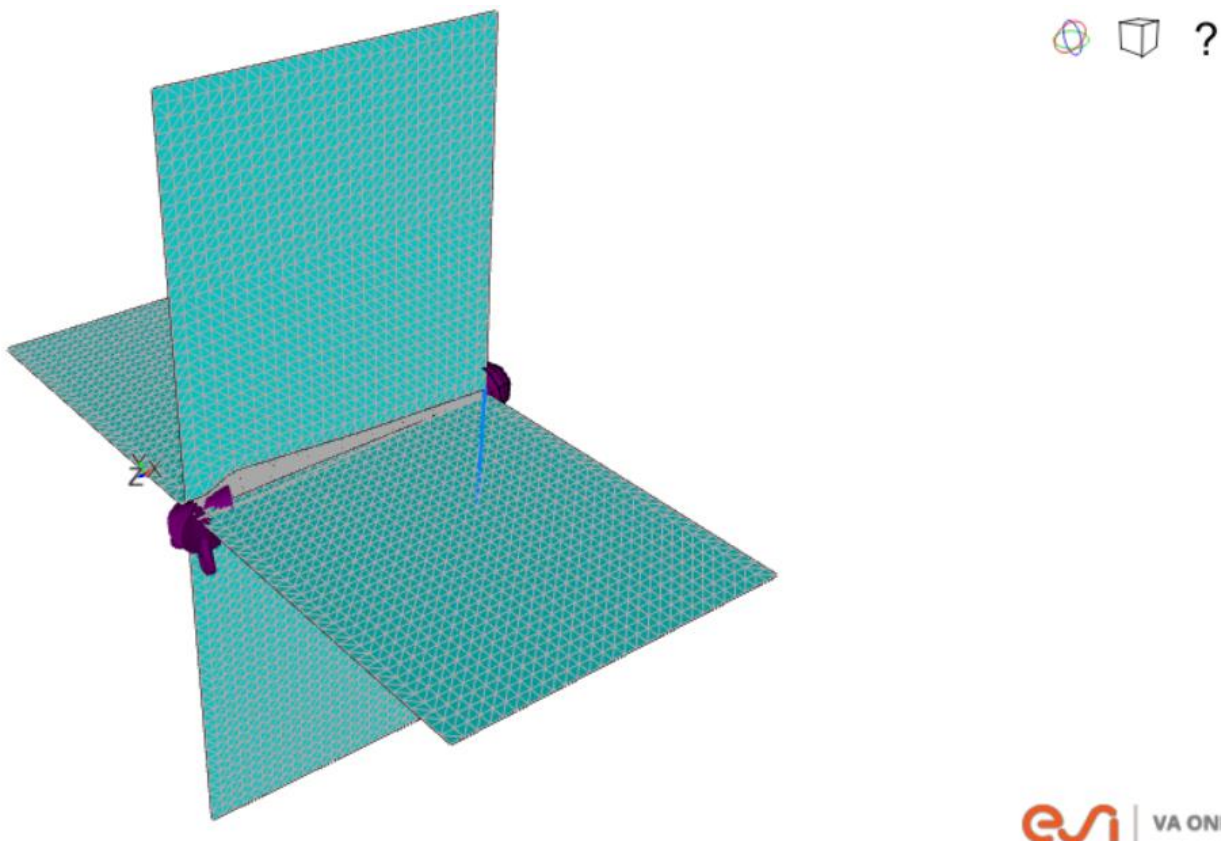


Figure 17 - Boundary Element model (BEM)

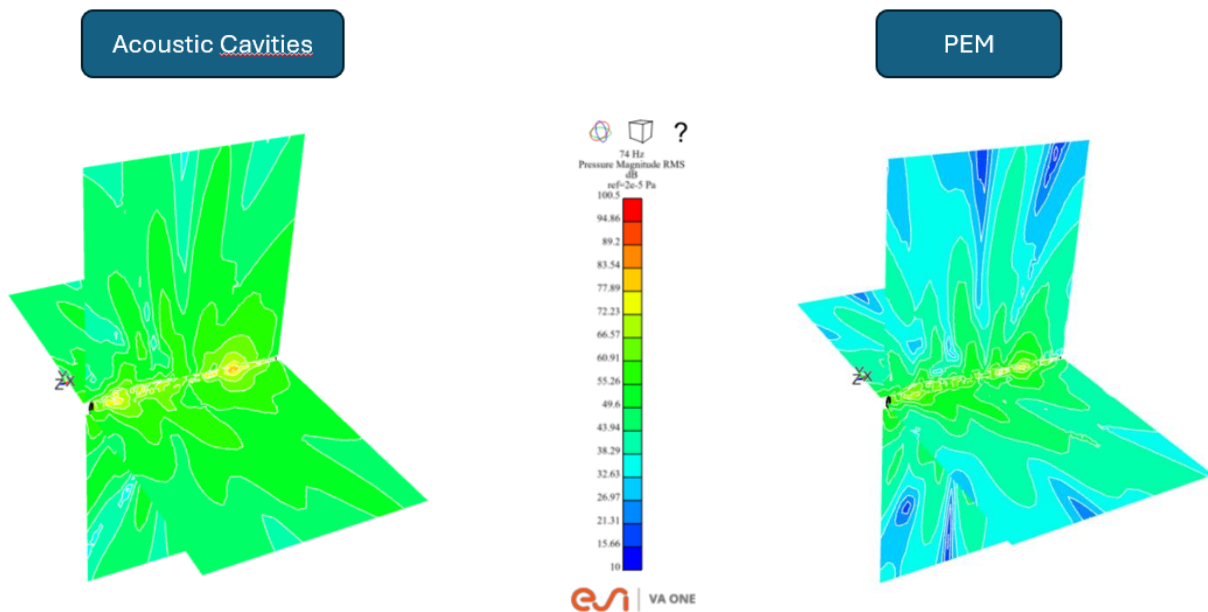


Figure 18 - Comparison between the model with noise control treatment (PEM) and the one with air in the cavities at 74 Hz

6. Conclusions

Experimental and numerical investigations give strong evidence that the acoustic of the room inside the blade has an effect on the far field acoustic of a wind turbine. It is also shown that noise-absorbent mats at the blade root and resonators distributed in the blade have a positive effect on the broadband and tonal noise behaviour of a blade. Sound measurements on an operating turbine and numerical investigation of the corresponding blade are planned to complete this analysis.

References

- [1] Deshmukh et. al., “Wind turbine noise and its mitigation techniques: A review” 2nd International Conference on Energy and Power, ICEP2018 *Internation Conference on Energy and Power ICEP2018, Sydney, Australia*, 13-18 December 2018.
- [2] Lukas Schneider, Karl-Heinz Hanus, “Origin, Transfer and Reduction of Structure-Borne Noise in Wind Turbines” 7th *Intern. Conf. on Wind Trubine Noise*, Rotterdam, 2nd-5th May 2017.
- [3] Xavier Falourd et. al. “Low Frequency Amplitude Modulation related to Doppler frequency shift: an experimental study of a 101m diameter wind turbine in a swiss valley” 6th *Intern. Conf. on Wind Trubine Noise, Glasgow*, 20-23 April 2015.
- [4] Colin G. Anderson, “Wind Turbines Theory and Praticce”, 2nd edition, Cambridge University Press, 2025.
- [5] Helmut V. Fuchs, “Schallabsorber und Schalldämpfer“, 3rd eddition, Springer, 2010.
- [6] ESI VA One 2024 User Manual – ESI Group, part of Keysight Technologies.

Paper #22 - ID: 356

Title: Prediction Based Noise Limits and Why They Should Not Be Used When Consenting Wind Farms

Author: Jason Baldwin

11th Edition of the
International Conferences on
Wind Turbine Noise
Copenhagen, Denmark – 10th to 13th June 2025

Issues Relating to Predictions Based Limits

Jason Baldwin¹

TNEI Ireland, Dublin, County Dublin, D24 A386, Ireland

Andrew Birchby²

TNEI Services Limited, Glasgow, G2 5UB, UK

Summary

Whilst noise limits in the UK and Ireland are typically set in accordance with the relevant national guidance, there have been instances where sites have been conditioned to predicted noise levels for the candidate turbine presented in the planning application. This paper considers the benefits and weaknesses of adopting prediction based noise limits (Prediction Limits).

With regards to the benefits; noise limits in the UK and Ireland can be considered to be a ‘noise budget’ so setting an individual schemes limits based on predicted levels ensures that spare budget is available for future development (rather than being allocated to projects which do not need it). It would also offer more protection for residents as there will be little headroom available to increase noise output from a given wind farm.

When Predicted Limits are used, the operational wind farm noise levels that are being measured will often be very near to or at the limit. This results in practical issues in demonstrating compliance due to the uncertainties inherent in both the prediction and measurement of wind farm noise.

The use of Predicted Limits often results in limits which are below the existing background noise levels. This also creates practical issues in demonstrating compliance and can lead to protracted monitoring campaigns involving turbine shutdowns and an associated loss of renewable energy.

The use of Predicted Limits can also influence the selection of the final turbine model, potentially leading to the deployment of sub-optimal turbines and the need for curtailment over and above that needed to meet the relevant national guidance.

Planning conditions are required to meet certain standards and the use of Predicted Limits raises questions around whether the resulting conditions are enforceable and reasonable.

Whilst some practical methods which can be used to assist when making compliance assessments against Predicted Limits are suggested, the paper concludes that Predicted Limits should not be used when consenting wind farms due to the issues identified.

¹ Jason Baldwin – Email: jason.baldwin@tneigroup.com

² Andrew Birchby – Email: andrew.birchby@tneigroup.com

1. Introduction

Wind farm noise limits in the UK and Republic of Ireland are typically set in accordance with ETSU-R-97 'The assessment and rating of noise from wind farms' [1] and the 'Wind Energy Development Guidelines' 2006 (WEDG2006) [2], respectively. The UK Institute of Acoustics document 'A good practice guide to the application of ETSU-R-97 for the assessment and rating of wind turbine noise' (IOA GPG) [3] is used to supplement the guidance in ETSU-R-97 and WEDG2006. Both documents establish noise limits based on background noise levels at noise sensitive dwellings, subject to fixed minimum limits when background noise levels are low.

In some cases, noise limits for developments are conditioned based on the predicted noise levels reported as part of a planning application (Predicted Limits), regardless of whether the appropriate guidelines highlighted above (ETSU / WEDG2006) were followed. This is a practice common to Northern Ireland in particular, and more recently, in parts of Scotland.

Whilst setting noise limits based on predictions seems logical, due to the inherent difficulties in demonstrating compliance with Predicted Limits (as outlined below), it is sometimes suggested that such limits are not reasonable, practical, or appropriate to condition developments with them.

Issues relating to demonstrating compliance with Predicted Limits include;

- How to account for uncertainty inherent in measurements / predictions, in addition to dealing with measurements that are based on measured averages;
- The need to account for the influence of background noise and cumulative noise (resulting in lost renewable energy through unnecessary turbine shut downs); and,
- Accounting for potential changes in wind turbine models from the planning stages, potentially resulting in the need for curtailment due to the change in sound power curve.

There are also questions in relation to enforceability as a result of the above, in terms of meeting the requirements for planning conditions set out in relevant policy / guidance.

The results of the above can be costly; both financially, from a renewable energy point of view, and from a residents point of view as compliance surveys are generally protracted as a result.

This paper explores the highlighted issues and considers the merits of the use of Prediction Limits in noise conditions.

2. Relevant Guidance / Methods to Conditioning Noise limits

When using both ETSU-R-97 in the UK and the WEDG in the Republic of Ireland, noise limits are typically set 5 dB(A) above background noise levels, subject to fixed minimum limits (FMLs) which apply when background noise levels are low. The choice of FML depends on the time of day, or in the case of ETSU-R-97, can also be increased depending on whether a property has financial interest, or should there be sufficient justification, i.e. due to the size of development, the cumulative situation etc.

The limits established in accordance with ETSU-R-97 and WEDG2006 are sometimes referred to as 'Total Noise Limits' (TNL) which should not be exceeded by the combined operation of all wind farms in an area. The TNL can be considered to represent a 'noise budget'. To account for the presence of proposed, consented or operational wind farms in an area it is sometimes necessary to set limits for an individual wind farm at levels below the TNL (to account for the situation where a proportion of the TNL has been allocated to, and can realistically be used by, other wind farm developments). A noise limit allocated to a specific wind farm is sometimes referred to as a 'Site Specific Noise Limit' (SSNL). The need to consider cumulative noise continues to increase as more wind farms are proposed / consented and the use of SSNLs is therefore likely increase in the future.

Councils, particularly in Northern Ireland, and more recently in certain parts of Scotland, have pushed for noise limits to be set based on predictions. Restricting a development using Predicted Limits will offer;

1. Higher protection to residents as often there will be little margin for operators to work around meaning noise levels will be required to stick very closely to those originally reported; and,

2. Increased headroom for other cumulative developments to operate in should they be proposed in the future.

Protection of residents is an important consideration, it can be argued that the higher the level of noise, the higher the likelihood of complaint, and restricting operators to the predicted levels of noise that they reported as part of their planning application results in lower noise limits.

With relation to (2), it is considered that penalising a project that is at the consenting stage may not be justified as you are considering a future scenario that may not materialise. For future projects sufficiently along the development path, a number of options to apportion already existing noise limits are available which seek to demonstrate that other cumulative developments do not require all the existing noise budget set at locations. This is explained and rationalised in detail in the IOA GPG, and using this method is considered sufficient to protect residents as the combined operation will, in theory, never exceed the originally established TNL.

The various methods are highlighted graphically in figure 1 below, and illustrates five different noise limits which could be applied to a single proposed wind farm;

1. The development could be allocated the entire TNL;
2. It could be allocated an SSNL (which may be appropriate if another wind farm is also proposed in the area);
3. It could be allocated a limit which is based upon the predicted noise levels plus a margin, in this case 2 dB has been added;
4. It could be allocated a limit which is based upon the predicted noise levels with no additional margin;
5. It could be allocated a flat limit which is based upon the maximum noise prediction (plus a margin of 2 dB) across the wind speed range.

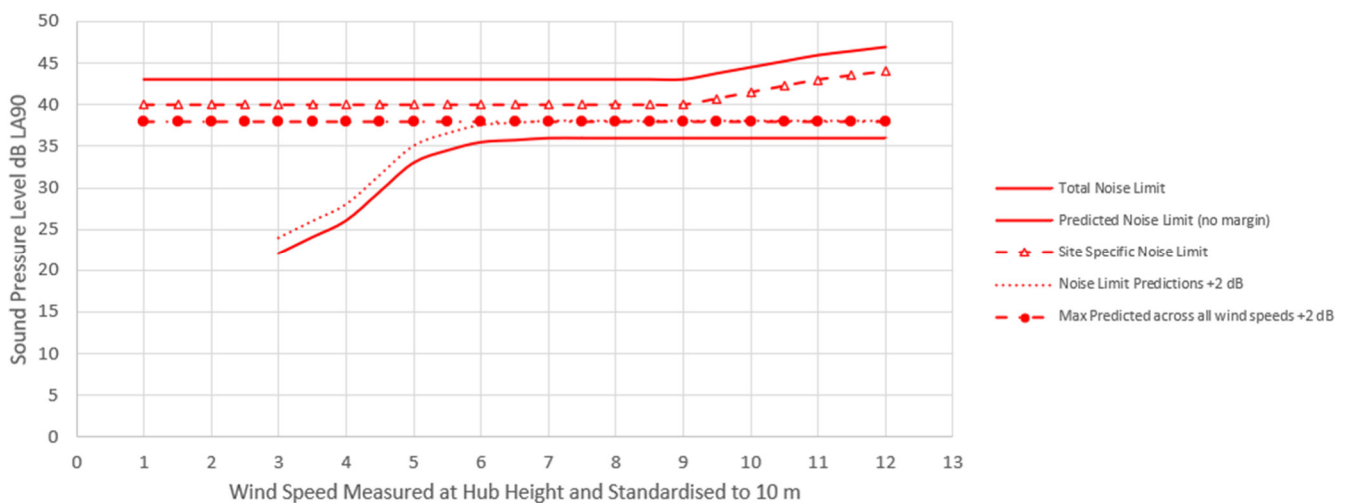


Figure 1 Example noise limit types

The range of margins between the various types of limit is large – there is no margin at all should Predicted Limits with no additional margin be conditioned. It can also be seen that where limits are set relative to predicted levels noise limits tend to reduce, sometimes quite significantly, at lower wind speeds. Margin is a very important consideration with regards to compliance monitoring, as due a host of complexities (including measurement uncertainty, the influence of background, differences in wind speed measurement location [which can shift data left or right on the graphs] etc) it can be very difficult to demonstrate compliance without some margin for error. The margin can therefore have a significant influence on the complexity of any noise compliance monitoring, should it be required.

3. Issues to consider when predicted noise levels are conditioned

As highlighted above, there are several issues relating to demonstrating compliance with Predicted Limits that need to be considered. These have been detailed in the following paragraphs.

3.1 Prediction and Measurement Uncertainty

In the UK and Ireland, predictions are undertaken in accordance with ISO 9613-2 ‘Acoustics — Attenuation of sound during propagation outdoors’ as recommended in the IOA GPG. The standard is considered a robust method for predicting the propagation of noise outdoors, and is widely used in the acoustics industry. Measurements undertaken in the near field, including those undertaken by the author, also indicate predictions can correlate very closely with each other. There are however levels of uncertainty to consider when using the standard, and ISO 9613-2 indicates that uncertainty levels of up to 3 dB can be expected at larger distances of >100 m - the overall level of which is proportionate to the source receiver distance. Generally the closer the source receivers are to each other, the lower the level of uncertainty, with distances up to 100 m there can be an associated uncertainty of 1 dB.

Should Noise Sensitive Receptors (NSRs) with big separation distances be conditioned based on predictions, then there is increased potential of inaccuracy (not accounting for increased background noise influence, and weaker signal to noise ratios as discussed in Section 3.2).

Equally there is an associated level of uncertainty in the instruments used to measure noise levels, and this level of uncertainty can come into play both in;

1. IEC 61400-2 Wind Turbine Sound Power Level testing [4]; and,
2. Compliance noise survey assessments.

Regarding (1), the measured octave band and overall sound power levels undertaken in accordance with IEC 61400-2 are used to undertake noise predictions. The IOA GPG Supplementary Guidance Note 3 [5] states that uncertainty can arise from ‘*measurement uncertainties, production tolerances and design differences*’, and as such the guidance recommends that additional uncertainty be applied to the measured values to account for them. Manufacturer documentation and independent test reports³ will all generally indicate the level of uncertainty that should be considered before using the data for noise prediction purposes. Should no measurement uncertainty be recommended then the IOA GPG suggests that an additional 2 dB should be included. In some cases, and after several years of working in the field reviewing other acousticians reports, it has been seen that varying levels of uncertainty have been seen applied to manufacturer data, and indeed no uncertainty being applied on some occasions. This can particularly be the case with older assessments undertaken pre publication of the IOA GPG.

Should no uncertainty be applied to the measured sound power levels during the prediction modelling stages, then this will lead to even less margin for error should Predicted Limits be conditioned.

In addition to the above, it should be considered when sound power tests are undertaken in accordance with IEC61400-11, they are based on 10 second LAeq measurements, following which a polynomial, or line of best fit is used to fit the data; the method is therefore based on averages. The conditions associated with the testing of wind turbines in accordance with IEC 61400-11 are very controlled, i.e. testing sites are used with flat terrain, little influence of background, testing of single turbines only, resulting in very clean datasets, such as that in Figure 2 below [6];

³ The more test reports that are available for a particular turbine model, the better indication of uncertainty that can be applied to the data, it may be that several reports indicate very similar levels, and therefore the level of uncertainty can be reduced.

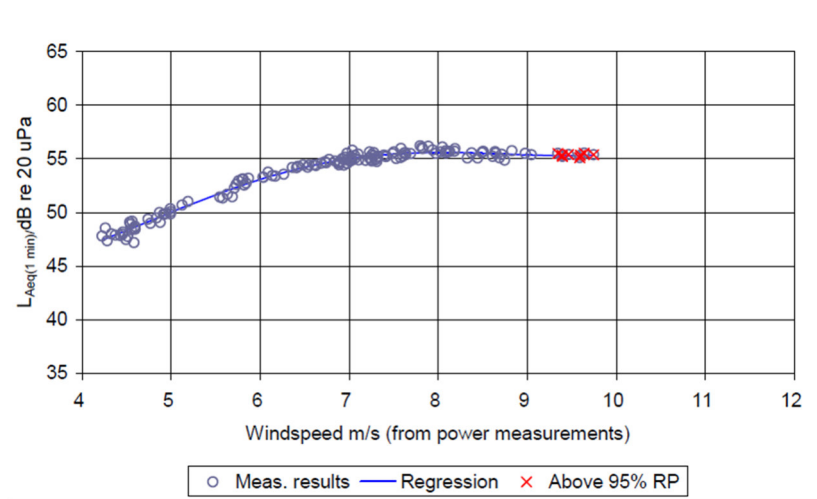


Figure 2 Typical IEC61400-11 Measurement Result (Delta, 2009)

As can be seen in Figure 2, the datapoints will sit above and below the regression trend. In a compliance noise monitoring exercise data will need to be collected in near perfect conditions to emulate this, i.e. whereby ~50 % of datapoints are above the ‘trend’, and ~50 % below it. In reality, measuring this ideal scenario out in rural areas, in variable conditions, is difficult.

When the potential for margin to be very small or non-existent for a given development consented with Predicted Limits, the potential uncertainty associated with the above will all count to a higher chance of exceedance during any compliance exercise.

3.2 Influence of Background Noise

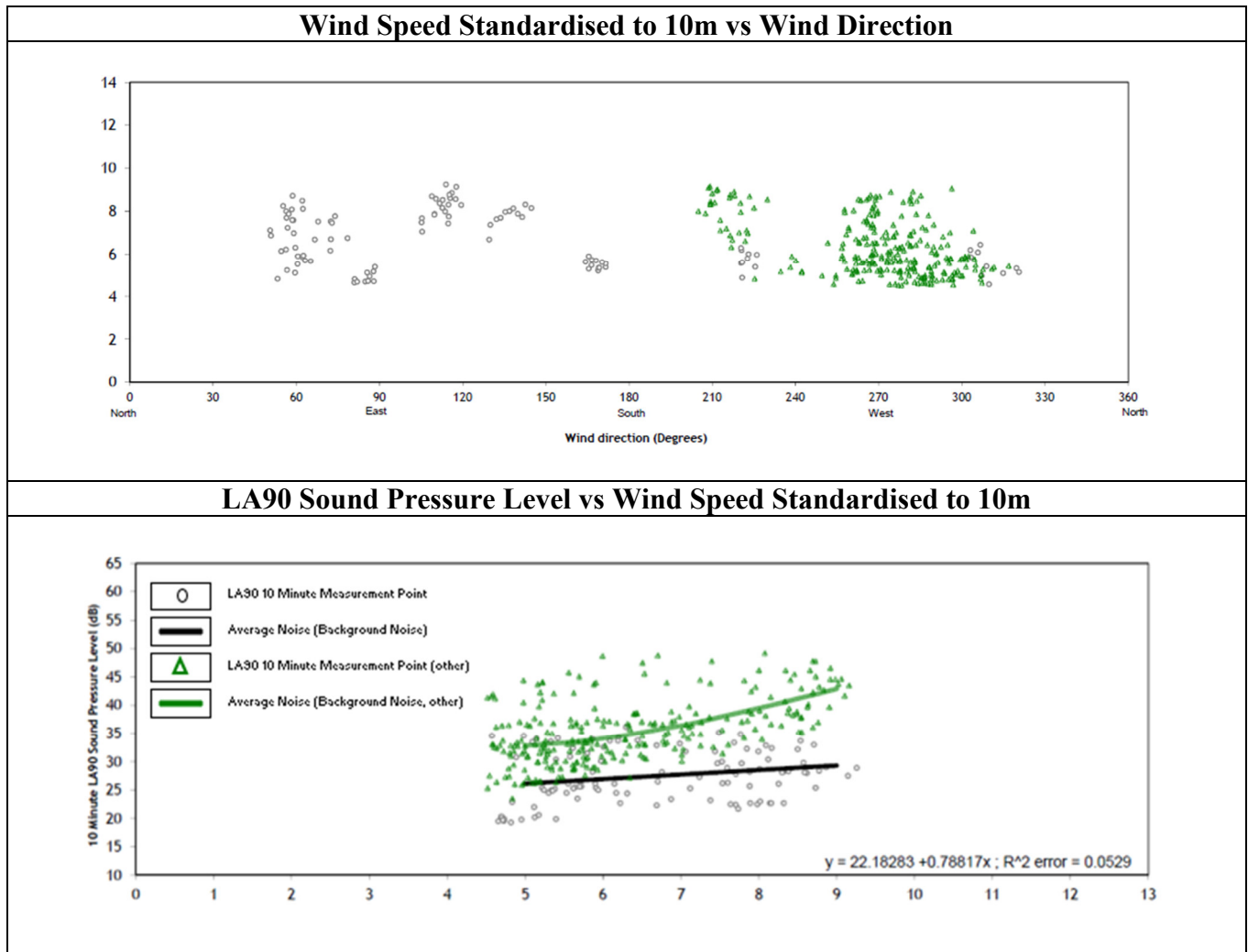
The influence of background noise is a key consideration in any compliance noise survey, but particularly so in determining compliance with Predicted Limits with little margin. In this case even the slightest background influence has the potential to lead to an exceedance during compliance exercises.

Typically as a first step during a compliance assessment the ‘Total Noise Levels’ are measured during downwind conditions, to consider a worst case. The Total Noise Levels comprise both the source (the wind farm) and the Background Noise Levels at a given location. Should this pass the noise limits then compliance can be concluded. Where this is not the case, Background Noise Levels will then need to be subtracted from the Total Noise Levels to derive the Specific Noise Levels, or noise from the wind farm only. Determining the Background Noise Level can either be done by;

1. Referencing back to the measured levels made during the planning stages;
2. Measuring the levels through any pre construction monitoring; or,
3. By undertaking turbine shutdowns.

Using (1) and (2) would be more straightforward options, however issues arise if the monitoring data is not like for like in terms of wind speeds and directions collected. An example is highlighted below in Table 1, where for a given survey TNEI collected data during periods of turbines off (grey datapoints). Later during the same project, data from a previous survey was made available (green datapoints); it was considered that combining would make for a more robust assessment. It was found on comparison that both datasets measured noise from opposite wind directions (one in upwind conditions, and one in downwind conditions), and the difference was notable by several dB. In this case the TNEI measured levels were made in upwind directions and the other dataset in downwind conditions, indicating noise levels were already much higher in downwind conditions without the wind farm operating;

Table 1 – Comparison of Measurements in Different Wind Sectors

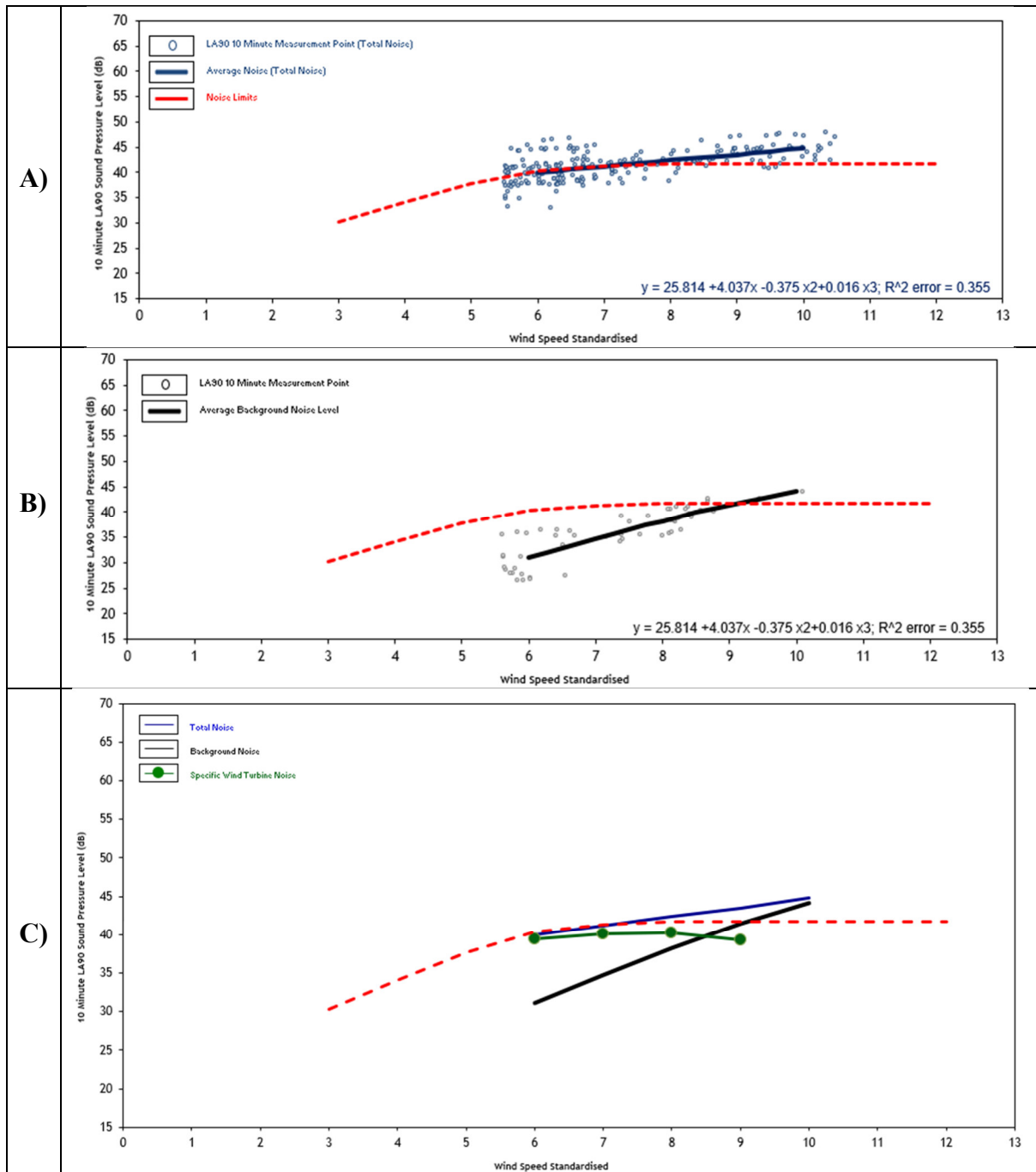


Generally it is considered that option (3) is the best way to measure Background Noise, as periods of shutdown can be planned according to weather forecasts such that like for like comparisons can be made. The measurements will also be up to date, and measured during a similar period as the Total Noise measurements. Of course shutting down turbines is costly, and will inevitably result in lost renewable energy. Noise kits are generally installed and it can be a prolonged period waiting for the ideal conditions to occur before shutting turbines down resulting in a longer noise survey.

The effect of background noise on Total Noise levels can also be significant, as the following example shows. (A) in the Table 2 below shows Total Noise measurements taken at a property. The levels were measured in downwind conditions and during periods of normal wind farm operation. The levels can be seen to **exceed** the Predicted Limits, and so Background noise levels were made during periods of turbine shutdowns, as shown in (B). In this case the influence of background is high; and when (B) is subtracted from (A) to produce (C) (the green dotted line, or the Specific Noise Level), the Specific Noise Level meets the Predicted Limits. There is some degree of headroom and due to the small difference between Total and Background at the higher wind speeds (>9 m/s) no correction can be made. In this case the IOA GPG SGN 5 states;

‘It should be noted, however, that where the shut-down noise approaches the operational noise, the level of shut-down noise has an increasing effect on the calculated turbine noise such than when the difference between the two is 3 dB or less, it may no longer be appropriate to use this correction with any degree of accuracy’

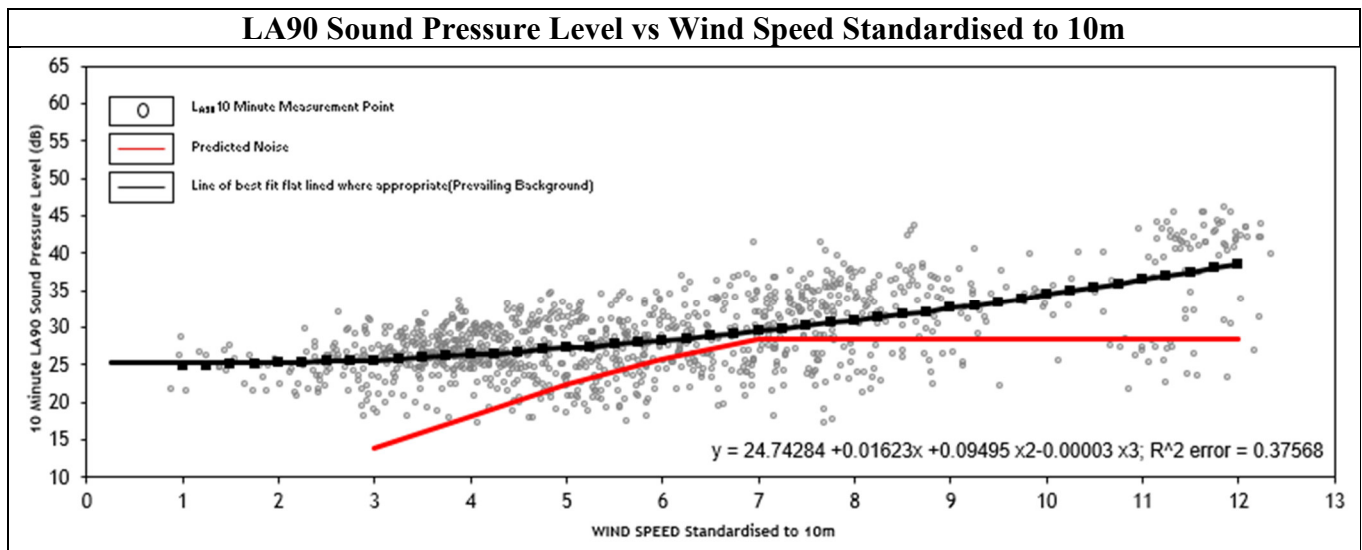
Table 2 – Effects of Background Noise on the Total Noise



In this case the Specific Noise Level is close to exceeding the lower wind speeds of 6-7 m/s whilst there is more headroom at the higher wind speeds.

Of course background will play a key role in trying to demonstrate compliance at NSR’s consented with low Predicted Limits from a wind farm – this would be a nigh on impossible exercise as background noise has the potential to already be exceeding the Predicted Limits in the first place, as seen in Table 3 below;

Table 3 Example of Background Noise being Higher than Predicted Limits



The example above is an extreme case but shows why in some circumstances Predicted Limits would be unnecessarily restrictive, and difficult to demonstrate compliance with. In these situations other options should be considered, one of which is highlighted in Section 4.2 Use of Proxy Noise Monitoring Locations, though their use is not always considered practical.

3.3 Influence of Other Wind Turbine Schemes

Similar to background noise considerations, accounting for other cumulative noise schemes on measurements can be challenging and complicated. The assessor will need measure noise over the course of several scenarios as below;

1. Measure **Total Noise Levels** (noise from all cumulative schemes);
2. Measure 1 again but in the absence of the development of interest (through turbine shutdowns);
3. Subtract 2 from 1 to derive the **Specific Noise + Background Noise** from the development of interest;
4. If background noise data is available from a previous survey then this can potentially be subtracted the resulting level; deriving the **Specific Noise** from the development of interest.

Whilst this is an option, the level of accuracy will be lower (considering the like for like examples above, measurement uncertainties, other turbine operation etc) and using this to demonstrate compliance to a Predicted Limit with little to no margin could be challenging. Use of Proxy Monitoring Locations here would also be a useful other option.

3.4 Change in candidate turbine

As noted in the IOA GPG (section 4.1.6), it is standard practice to select a candidate turbine on which to base the acoustic impact assessment for a planning application. The candidate should be representative of the range of turbines which may be installed on site to provide an appropriate estimate of the noise levels at nearby properties. For the majority of sites, the candidate will not end up being the final turbine model that is installed on site, with the suitability of the final turbine model being secured through the imposition of adequate planning conditions.

The final turbine model may differ from the candidate for various reasons including:

- A more detailed assessment of site conditions e.g. wind speed and turbulence intensity, may show that a different turbine type is more suitable.
- The candidate turbine may no longer be offered by the turbine manufacturer due to the time elapsed between the application being made and consent being granted.

- A deal may have subsequently been struck with a different turbine manufacturer making the use of their turbines more economic.

Predicted Limits can restrict the ability to change from the candidate turbine if the final turbine model that the developer would like to deploy is constrained by these noise limits. Whilst potentially being able to meet Predicted Limits by operating some turbines in reduced noise mode, this results in energy loss which reduces the value of the project and makes it less likely to progress with the preferred final turbine model.

Predicted Limits may equal the limits that would be imposed by relevant national guidance, should predicted noise levels from the candidate turbine be right up to the limit, but are often lower. If the preferred final turbine model has to be curtailed we can therefore distinguish between any curtailment that is required to meet the relevant guidance and any additional curtailment that is required to bridge the gap between the guidance and the Predicted Limits, as illustrated by Figure 3 below. This additional curtailment is unnecessary in order to meet the relevant guidance and is only required due to the method used to set noise limits in the planning conditions.

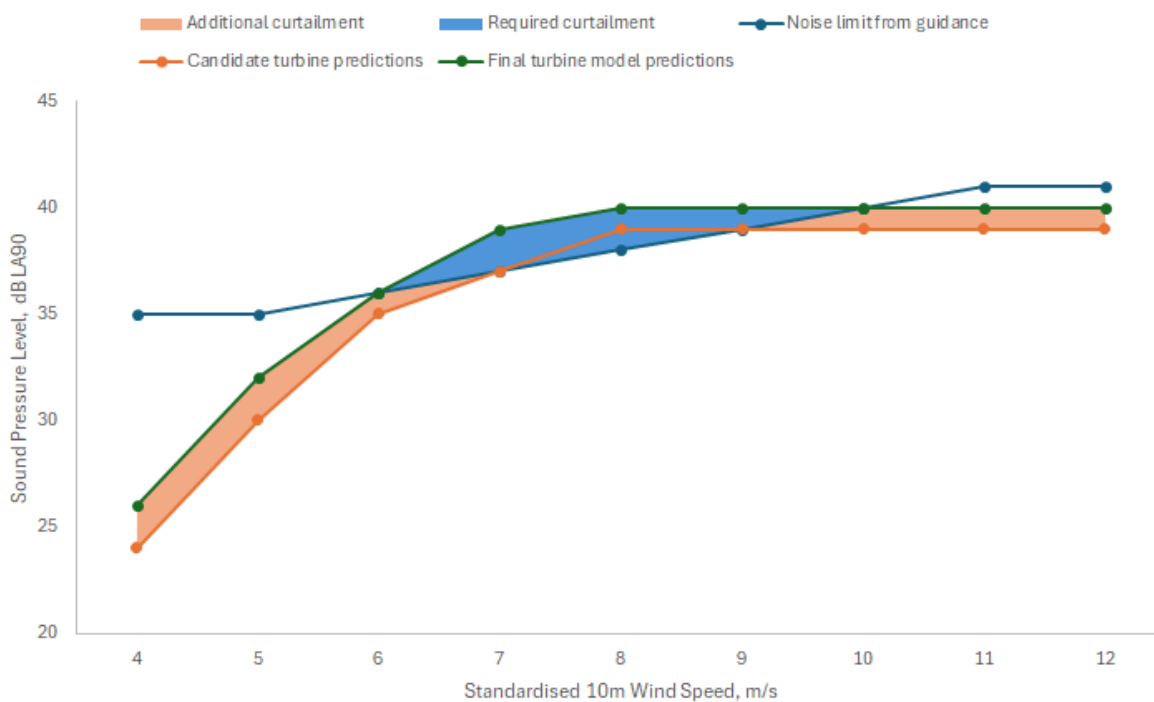


Figure 3 Curtailment Requirement due to Candidate Change

The use of Predicted Limits can therefore unnecessarily restrict the ability of the developer to select the most appropriate turbine for the site from both a technical and commercial perspective. Furthermore, the final turbine model that is selected could require curtailment over and above that necessary to meet the limits specified in relevant guidance, resulting in additional, unnecessary energy loss and reducing the contribution of the project towards meeting national greenhouse gas emission reduction targets.

3.5 Meeting the tests for a planning condition

The requirements for planning conditions in the UK are set out in the relevant policy / guidance including the National Planning Policy Framework (for England and Wales) [6], the Development Management Guidelines (for Ireland) [7] and Circular 4/98 (for Scotland) [8]. All three documents require planning conditions to be: necessary, relevant to planning, relevant to the development, enforceable, precise and reasonable in all other respects.

The following guidance is provided in Circular 4/98 with regard to enforceability:

“Sometimes a condition will be unenforceable because it is in practice impossible to detect an infringement. More commonly it will merely be difficult to prove a breach of its requirements.”

The difficulties that can be posed by noise from other sources, whether background noise or noise from adjacent wind farms, during compliance testing has already been discussed above. Where Predicted Limits are low relative to the noise levels from other sources in the vicinity, they may be unenforceable as it would be difficult to prove whether any breach of the limit is due to the project or another noise source.

With regards to reasonableness:

“A condition may be unreasonable because it is unduly restrictive, Although a condition may in principle impose a continuing restriction on the use of land (provided that there are good planning reasons for that restriction), such a condition should not be imposed if the restriction effectively nullifies the benefit of the permission.”

An argument could be made that it is unreasonable to constrain the turbines beyond meeting the noise limits specified by relevant national guidance and that any additional curtailment, over and above this, to meet Predicted Limits is disproportionate. This additional curtailment reduces the benefits, i.e. the amount of renewable energy generated, associated with the permission and could nullify them if it results in the project becoming uneconomic.

The use of Predicted Limits within planning conditions could therefore potentially be challenged on the basis of both enforceability and reasonableness.

4. Potential Ways to Account for Predicted Limits

There are several options that can be considered to give a more successful chance of demonstrating compliance with Predicted Limits, these are detailed in the following paragraphs.

4.1 Cross referencing with ETSU-R-97 / WEDG2006 derived limits at lower windspeeds

It will be the case that Predicted Limits at lower windspeeds will be low, as this is when turbines will kick-in and begin to operate. In this instance it would be considered appropriate to cross reference back to the original ETSU / WEDG limits such that these lower wind speeds can be scoped out, as trying to demonstrate compliance at these wind speeds will be difficult when accounting for the influence of background. The IOA GPG specifies that;

‘If the proposed wind farm produces noise levels within 10 dB of any existing wind farm/s at the same receptor location, then a cumulative noise impact assessment is necessary’

Whilst the text relates to determining whether a cumulative scheme requires to be included in an assessment at the proposed stages, by the same logic, where predicted noise for a given wind speed is > 10 dB below that of the ETSU / WEDG noise limit then this would give suitable justification to scope out the requirement of demonstrating compliance at this wind speed, as noise levels at these wind speeds would not influence other developments to meet the noise limit (in the case of a cumulative situation). Table 4 highlights an example at a particular NSR, where the NSRs guidance based noise limit is compared to its predicted noise level;

Table 4 Wind speeds >10 dB between ETSU-R-97 Limits and Predictions

Standardised 10m Wind Speed	4	5	6	7	8	9	10	11	12
ETSU-R-97 Noise Limit	37.5	37.5	37.5	38.1	39	39.7	40.4	41	41.4
WF Predicted Noise Level	20.2	26.5	31.5	33.6	33.7	33.7	33.7	33.7	33.7
Difference	-17.3	-11	-6	-4.5	-5.3	-6	-6.7	-7.3	-7.7

It can be seen that the difference between the predictions and the guidance based noise limits is > 10 dB at wind speeds of 4 & 5 m/s and could subsequently be scoped out of the need for assessment.

4.2 Use of Proxy Noise Monitoring Locations

Due to the reduction in the signal to noise ratio from a wind farm as a result of higher background influence at a particular NSR, it is recommended that the use of Proxy Noise Monitoring Locations (PNMLs) supplement, or even replace⁴ Noise Monitoring Locations (NMLs) at dwellings. PNMLs can be installed on wind farms sites, allowing a much greater signal to noise ratio, and much less influence from background. The PNML location would be intended to be in an open location, away from background influencing noise generating objects typically found at dwellings (e.g. wind generated in buildings / sheds, fence rattle, wind chimes, human activity etc).

An Equivalent Noise Limit (ENL) would be derived, accounting for the difference between the predicted noise level at the PNML, and the NSR it is serving to demonstrate compliance for. Should this be met then this would be considered sufficient to report compliance at the NSR. A simple example is provided below of where a PNML would be located with relation to the NSR;

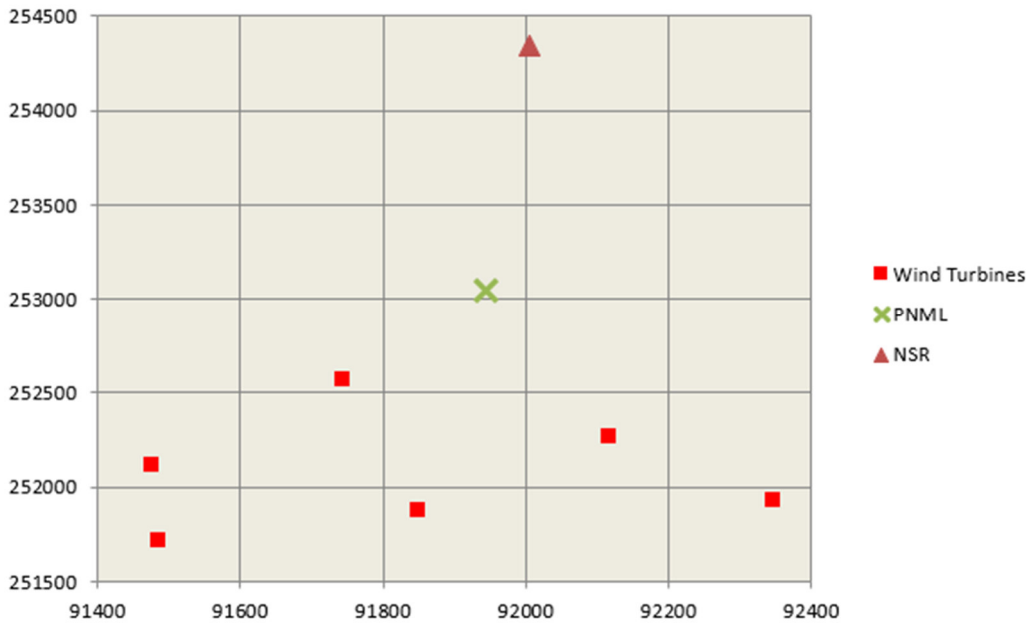
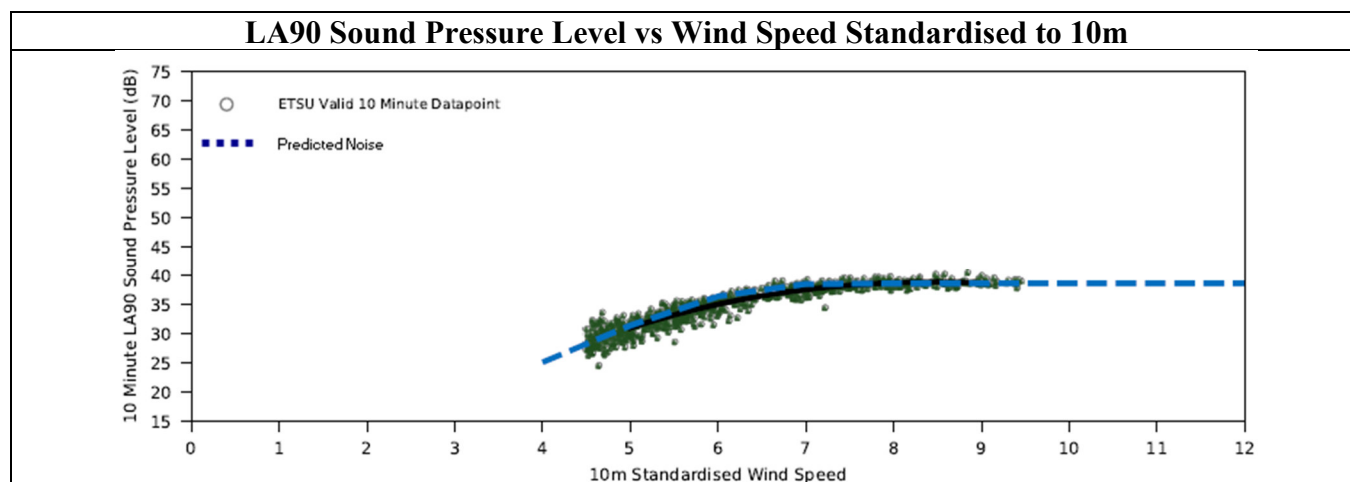


Figure 4 Example PNML Location with Relation to NSR

The approach allows measurements to be made where the wind turbines will be dominant, reducing the influence of background noise on measurements, in addition to other cumulative schemes. Table 5 below demonstrates measurements undertaken at a PNML on a wind farm site that meet the Predicted Limit (shown as a blue dashed line). The signal to noise ratio is high giving a very strong correlation with the Predicted Limit;

⁴ It should be noted that it is not normally possible to consider noise character at proxy locations so where consideration of this is required it may be necessary to measure at the NSR (to consider noise character) and the proxy location (to consider levels)

Table 5 PNML Compliance Noise Measurement



The measurements in this case meet the Predicted Limits, though it can be seen that there is little margin for error available.

It is recommended that PNMLs are installed should locations around a wind farm be suitable, i.e. not forested, close to streams / rivers, where the influence of background and cumulative turbine schemes is low. Their use is considered advantageous given the very strong signal to noise ratio that will be available closer to the wind farm that will not be seen further away.

5. Conclusions

This paper has considered the benefits and weaknesses of adopting prediction based noise limits for conditioning wind farms. Whilst the reasoning behind why they are being used to condition wind farm sites is clear, e.g. they provide potentially better protection for residents, and allow margin for more cumulative sites to be developed etc; they are notably difficult to demonstrate compliance with for several reasons;

- Due to the influence of background noise on measurements (especially in locations where noise prediction values are low, or similar in value to background noise);
- Due to the requirement to deal with the effects of uncertainty – both on measurements and those inherent within predictions;
- Due to the complexities associated with other cumulative developments on measurements; and,
- Due to the potential for the candidate turbine to change post consent, resulting in potentially different prediction curves to those originally reported.

In addition the following reasons highlight other consequences that result in the use of noise limits based on predictions;

- They can prevent the most optimal turbine model being deployed as slight changes to the sound power curve could result in exceedances;
- They can result in curtailment (loss of energy) over and above that needed to meet the limits specified by the guidance; and,
- They can result in planning conditions which can be challenged on the grounds of enforceability and reasonableness.

As a result of any compliance assessment, there is higher potential for renewable energy to be lost through requirement of turbine shut downs (to determine the influence of background noise / cumulative noise). Whereas this may not be required if the guideline limits are used, as more margin is available (for use by all cumulative schemes). Compliance surveys can also be protracted, due to the requirement to measure background noise, and, if exceedances are observed, due to the requirement for multiple surveys as curtailment strategies are developed and programmed into control systems.

It would not be recommended that prediction based limits are used, but where they are being considered at the conditioning stages, they should be conditioned with suitable additional margin (conventionally 2 dB is used), such that some margin for uncertainty / allowance for challenges associated with compliance monitoring / allowance for the use of alternative turbine models post consent is allowed for. In addition, to prevent issues related to demonstrating compliance at the lower wind speeds (where the sound power drops off significantly) adoption of a flat limit equal to the max predicted level + 2 dB would be recommended. If prediction based limits are conditioned, an additional margin should be added and the options for demonstrating compliance detailed in Section 4 should be allowed.

References

- [1] ETSU for the DTI (Department of Trade and Industry, “The Working Group on Noise from Wind Turbines ETSU-R-97 The Assessment and Rating of Noise from Wind Farms’,” 1996.
- [2] H. a. L. G. (. Department of Environment, “<https://www.gov.ie/en/publication/f449e-wind-energy-development-guidelines-2006/>,” 2006. [Online]. [Accessed 09 04 2025].
- [3] UK Institute of Acoustics, “Good Practice Guidance on the application of ETSU-R-97 for wind turbine noise assessment,” 2013.
- [4] BS EN 61400-11:2013: Wind turbine generator systems — Part 11: Acoustic noise measurement techniques.
- [5] UK Institute of Acoustics, “A Good Practice Guide to the Application of ETSU R 97 for the Assessment and Rating of Wind Turbine Noise SGN3: Sound Power Level Data,” 2014.
- [6] Department for Levelling Up, Housing and Communities, “National Planning Policy Framework,” 07 02 2025. [Online]. Available: <https://www.gov.uk/government/publications/national-planning-policy-framework--2>. [Accessed 09 04 2025].
- [7] Department of the Environment, “Development Management Practice Note - Use of Planning Conditions,” 04 2015. [Online]. Available: https://www.infrastructure-ni.gov.uk/sites/default/files/publications/infrastructure/dmpn-20-use-of-planning-conditions-v1-april-2015_0.pdf . [Accessed 09 04 2025].
- [8] Scottish Government, “Planning Circular 4/1998: the use of conditions in planning permissions,” 1998.

Paper #23 - ID: 357

Title: Influence of Ambient Noise in Sound Quality Assessment of Auralised Wind Turbine Noise

Author: Josephine Siebert Pockelé

11th Edition of the
International Conferences on
Wind Turbine Noise
Copenhagen, Denmark – 10th to 13th June 2025

Influence of Ambient Noise in Sound Quality Assessment of Auralised Wind Turbine Noise

Josephine Siebert Pockelé¹ and Roberto Merino-Martinez

**Delft University of Technology, Faculty of Aerospace Engineering, Kluyverweg 1,
2629HS Delft, the Netherlands**

Summary

The influence of ambient noise in the perception of wind turbine noise is evaluated in this exploratory study. For this purpose, experimental field measurements of an NTK wind turbine at different wind speeds and background noise levels are considered. Synthetic wind turbine noise auralizations are then computed to replicate the weather and operational conditions during the experiments. Different background noise recordings were then synthetically added to the simulated auralizations to investigate the effect in sound quality metrics, such as loudness, roughness, or the psychoacoustic annoyance model by Zwicker. A least-squares analysis was applied to the resulting sound signals. It was found that adding background noise to the auralisations notably reduced the differences in metrics between simulations and experiments. However, the behaviour with respect to the A-weighted signal-to-noise ratio then becomes background-noise dependent and, hence, more challenging to predict. Therefore, for perceptual studies, it is recommended to use experimental recordings with low background noise as a ground truth.

1. Introduction

In the onshore wind energy sector, noise remains a prevalent issue for the social acceptance of new installations [1]. Whereas offshore wind is on the rise, the majority of current new installations are still onshore [2], [3]. Since current research on noise annoyance due to wind turbines is mostly limited to surveys of inhabitants around existing installations [4], [5], it is important to bridge the knowledge gap between human noise perception and wind turbine design.

For human perception research, sound signals are required [6], [7], which are normally not available during the early design stages of wind turbines. Merino-Martinez *et al.* [8] proposed one method involving auralisation (i.e. the creation of sound files from simulated data) to integrate noise annoyance within the design loop [8]. Auralisation using simulated data has recently shown promising results in research about human perception [9]–[11].

One issue highlighted by Pockelé [10] in the validation of fully synthetic auralisations is quantifying the influence of ambient or background noise (BGN) in the perception of the evaluated sounds. At the time of writing, the only established methods for dealing with ambient noise in the analysis of wind turbine noise consist simply of its subtraction (in the frequency domain) from experimental recordings aiming to isolate the wind turbine noise contribution. None of these methods are based on the exact ambient noise during the

¹Corresponding author - Email: j.s.pockele@tudelft.nl

measurements of the turbine, which is a known limitation [12]. While acceptable for spectral analysis in research and permitting, wind turbine noise in the time domain (for human perception research) can only be isolated in sound signals if the exact background noise during the recording is known. This is, however, very challenging to achieve in practice.

This exploratory study proposes two different methods for dealing with background noise in human perception research of auralised wind turbine noise: (1) accounting for background noise by adding representative sample signals to the auralisations, or (2) not adding background noise and considering recordings with low ambient noise levels as a ground truth. A preliminary analysis comparing both methods is therefore presented to explore the establishment of a best practice for future research. The sound analysis in this study is conducted using sound quality metrics (SQMs) from the field of psychoacoustics, which are expected to represent human perception more accurately than conventional sound metrics [13].

The experimental measurements of wind turbine noise considered for this study are described in section 2. Section 3 introduces the employed auralisation methodology, as well as the wind turbine model and operating conditions. The descriptions of the SQMs considered for the acoustic analysis of the wind turbine sounds are briefly explained in section 4, as well as the main results per metric. Lastly, concluding remarks are given in section 5.

2. Experimental Noise Measurements

Noise measurements of a *Nordtank NTK 500/41* wind turbine, conducted at the Technical University of Denmark (DTU) Risø campus are used. The dataset [14] contains simultaneous noise, met mast, and SCADA (Supervisory Control And Data Acquisition) data of the turbine. These measurements span 15, 16, and 23 October 2015, with varied wind and climatic conditions, and multiple background noise levels [15].

2.1 Measurement Setup

The wind turbine noise is measured using eight microphones, evenly distributed along a circle of 45-m radius centered at the turbine tower. The microphones are manufactured by *BSWA Technology Co.* (ref. MPA 261 combining a 1/2" microphone and a pre-amplifier) and are configured according to the IEC 61400-11:2012 measurement standard [16], without a secondary windshield [15]. Their respective positions are shown in Figure 1. The sampling frequencies employed for the acoustic recordings were 50 kHz on 15 October and 25 kHz on 16 and 23 October.

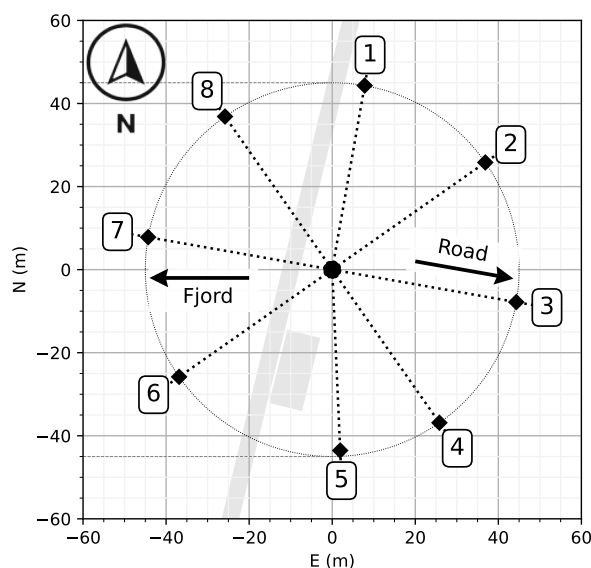


Figure 1 Microphone positions in the noise measurement dataset. Adapted from Pockelé, Figure 8.2 [10].

The SCADA data of the turbine covers the rotor RPM, power output, yaw, and other operational parameters, as well as wind speed and direction measured by the nacelle's anemometers. The met mast data contains wind measurements at different heights and measurements of air temperature and pressure at sea level. All these data are recorded at 35 Hz on a 16-bit data acquisition system [15].

2.2 Wind Turbine Noise Measurement Selection

The data from 15 October is used to represent high-level, road-related background noise, whereas the data from 23 October is used to represent low-level background noise from the fjord. Henceforth, the 15 October data is referred to as "road", while the 23 October data is referred to as "fjord".

For both dates, a selection of 30 second measurement segments is made. To limit the scope of this work, the selection is limited to the four microphones that most closely represent the IEC 61400-11:2012 standardised measurement positions [16], considering the mean wind direction on each date. The selected microphone numbers are given in Table 1:

Table 1 Microphones used to represent the positions from the IEC 61400:11-2012 standard [16]. The microphone numbers refer to Figure 1.

IEC position	1	2	3	4
15 October	6	7	2	5
23 October	3	4	7	2

Firstly, an initial selection is made using the local minimum wind speed fluctuations, based on the 30-second moving standard deviation. These segments are sorted into 1 m/s mean wind speed bins. Since the noise measurements are to be used for listening experiments, clipping beyond a 1.0 Pa amplitude should be accounted for, as clipping results in audible disturbing artefacts. Since no intervals are found with no clipping, a selection criterion is set up, which combines the deviation of the mean wind speed from the bin wind speed and the amount of clipping. This criterion is defined in Equation 1, where the second term is the integral of all sound signal peaks where the pressure magnitude goes beyond 1.0 Pa (representing the amount of clipping).

$$\text{criterion} = |U_{\infty, \text{bin}} - U_{\infty, \text{mean}}| + \int_0^{30} \left(|p(t)|_{|p(t)| > 1} - 1 \right) dt \quad (1)$$

After this selection, one 30-second segment remains per wind speed, per measurement data. To limit the scope of this work to steady background noise conditions, the sound files are manually inspected for audible disturbances such as aircraft flyovers, bird noises, and other impulsive noises. If such a disturbance is found, the segment is excluded, and the above selection process is repeated. A short summary of the final selection is provided in Table 2. The $L_{A, \text{eq}}$ of the selected 30-second wind turbine noise measurements ranges from 55 dBA to 60 dBA.

Table 2 Summary of the final selection of noise recording segments.

BGN condition	Road	Road	Road	Road	Road	Road	Fjord	Fjord	Fjord	Fjord
$U_{\infty, \text{bin}}$, [m/s]	5	6	7	8	9	10	6	7	8	9
$U_{\infty, \text{mean}}$, [m/s]	4.51	6.32	6.97	7.90	9.02	10.10	6.41	7.01	7.83	8.62
$\sigma_{U_{\infty}}$, [m/s]	0.54	0.73	0.79	0.88	0.90	0.98	0.21	0.29	0.35	0.35
Criterion	0.56	0.33	0.03	0.18	0.12	0.20	0.41	0.01	0.17	0.45

2.3 Background Noise Selection

For the first proposed method (adding representative ambient noise to auralised signals), a selection is made of the background noise (BGN) recordings in the NTK turbine measurements. For each operational interval, per microphone position, a 30-second background noise sample is selected from the background recordings before the turbine was started. The selection is based on a manual inspection to eliminate audible disturbances, such as aircraft flyovers, birds, or other impulsive sounds. These are excluded for the same reason as for the case of the wind turbine noise measurements.

3. Setup of Wind Turbine Auralisations

3.1 Auralisation Methodology

A simplified version of the method presented by Pockelé [10] is used. In the current work, the Gaussian beam tracing is replaced with a simpler image-source model.

The aeroelastic-aeroacoustic simulations are handled with the HAWC2 code developed by DTU, and the attached aeroacoustics module [17]. These simulations model the wind turbine dynamics and the following noise sources: (1) leading-edge turbulent inflow noise, (2) turbulent boundary layer trailing-edge noise, and (3) flow separation/stall noise [15].

Ground reflections are calculated using the model by Embleton et al. [18] and Delany and Bazley [19]. Atmospheric absorption losses are determined using the model in ISO standard 9613-1 by Bass et al. [20], [21]. To use the latter two models, the HAWC2 noise results per blade are used and are assumed to propagate from three moving monopole sources at 85% of the blade span.

The result of the above method is six spectrograms (for each blade: one for the direct and one for the reflected sound signal). These spectrograms are individually reconstructed into sound signals, using the Inverse Short-Time Fourier Transform (ISTFT). In order to meet the requirement for STFT sample points in time and frequency, the HAWC2 spectrogram outputs are interpolated using a piecewise-linear method in the frequency axis. Before the ISTFT, a randomised phase is added to the spectrogram. The direct and reflected signals are assigned the same random phase. The six resulting sound signals are summed to obtain the final auralised wind turbine noise signal.

3.2 Wind Turbine Model Description

The above auralisation method is applied to the validated simulation model of the *Nordtank NTK 500/41 wind turbine* developed by DTU [14], [22], [23]. In the available model, the XFOil boundary layer data, with a critical amplification parameter $N_{crit} = 3$ is used to represent a workflow with low computational cost. The properties of the NTK turbine are summarised in Table 3:

Table 3 Relevant specifications of the NTK 500/41 wind turbine [23].

Power Rating	0.5 MW
Rotor Diameter	41.1 m
Hub Height	36 m
Control	Passive
Mechanism	Aerodynamic Stall
Rotor Speed	Constant (27.1 RPM)

3.3 Simulation Input Conditions

The simulated operational conditions are obtained from the above-described measurements to match the conditions during the selected recording intervals. The simulations span the full intervals in the measurements where the turbine is operating to avoid any transient effects of the simulation start-up. From the resulting sound signals, the selected intervals are extracted for the analysis.

The wind measurements from the met mast, at multiple heights, were input in HAWC2, using the *met_mast_wind* input parameter. The necessary wind time series file is built from the measurements of the south-facing cup anemometers as they are the least disturbed by the met mast structure. The turbulence intensity for the noise calculations is derived from the sonic anemometer at 34.5 m height. The air temperature and pressure are set as the mean of the respective operational intervals. Since the humidity is not available in the dataset, it is derived from the Danish Meteorological Institute's open data [24] based on the date and time of the noise measurements.

4. Sound Quality Metric Results

4.1 Sound Quality Metrics

Sound Quality Metrics (SQMs) describe the subjective perception of sound by human hearing, unlike the sound pressure level L_p metric, which quantifies the purely physical magnitude of sound based on pressure fluctuations. Previous studies [8], [13] showed that these metrics better capture the auditory behavior of the human ear compared to conventional sound metrics typically employed in noise evaluations. The four most commonly used SQMs [6] are:

- Loudness (N): Subjective perception of sound magnitude corresponding to the overall sound intensity [25]. The loudness results in this paper are expressed in loudness levels L_N in phon.
- Sharpness (S): Representation of the high-frequency sound content [26].
- Roughness (R): Hearing sensation caused by sounds with modulation frequencies between 15 Hz and 300 Hz [27].
- Fluctuation strength (FS): Assessment of slow fluctuations in loudness with modulation frequencies up to 20 Hz, with maximum sensitivity for modulation frequencies around 4 Hz [28].

These SQMs were calculated for each wind turbine noise sample. The 5% percentile values of each metric (i.e., the value of each SQM exceeded 5% of the total recording time) were combined into a global psychoacoustic annoyance (PA) metric following the model outlined by Zwicker [29]. All SQMs and the PA metric were calculated using the open-source MATLAB Sound Quality Analysis Toolbox (SQAT) v1.2 [6], [7], which is available on GitHub¹.

4.2 Analysis Method

The differences between the measured wind turbine noise recordings and the auralised sound samples are quantified in terms of the differences of the analysed metric under consideration. These differences are analysed against the estimated A-weighted signal to noise ratio SNR_A . The SNR_A for each sample is estimated with the synthetic wind turbine noise auralisations and the corresponding background noise sample. In general, the cases with road background noise present relatively low (and even negative) SNR_A , whereas the cases with fjord background noise, the SNR_A is generally higher than 10 dBA.

The difference, per metric, between simulation and recording are quantified with and without background noise added to the synthetic wind turbine noise signals. For each case, both least-squares models in Equation 2 and Equation 3 are fitted to the data:

¹Available online: <https://github.com/ggrechow/sqat>

$$\Delta_{\text{metric}} = \begin{cases} (x_{1,\text{fjord}} + \Delta x_1) \cdot \text{SNR}_A + x_{2,\text{fjord}} + \Delta x_2 & \text{if road} \\ x_{1,\text{fjord}} \cdot \text{SNR}_A + x_{2,\text{fjord}} & \text{if fjord} \end{cases} \quad (2)$$

$$\Delta_{\text{metric}} = \begin{cases} x_{1,\text{road}} \cdot \text{SNR}_A + x_{2,\text{road}} & \text{if road} \\ (x_{1,\text{road}} - \Delta x_1) \cdot \text{SNR}_A + x_{2,\text{road}} - \Delta x_2 & \text{if fjord} \end{cases} \quad (3)$$

While both models give identical results, they are fitted to determine the p-values and confidence intervals of the slopes and intercepts for the road and fjord BGN separately.

4.3 Psychoacoustic Annoyance

The differences in the mean psychoacoustic annoyance between the measurements and simulations are analysed in terms of $\Delta 10 \cdot \log_{10}(10 \cdot \text{PA}_{\text{mean}})$. The base 10 logarithm of the PA metric is used, as it typically shows a better fit with listening experiment data [13], [30]. Figure 2 shows that the auralisations without added background noise have a similar slope with respect to the SNR_A for both the road and fjord background cases. The samples with added BGN show a significantly different trend between the two BGN conditions. It is expected that differences in annoyance get masked by the ambient noise at lower SNR_A values, which is reflected by the insignificant slope for the road BGN case for low SNR_A .

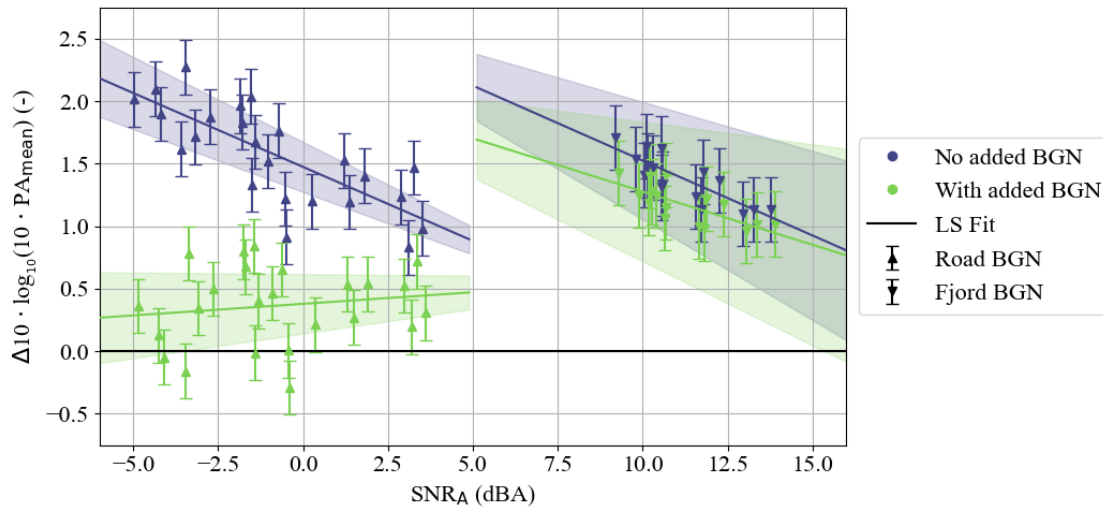


Figure 2 Difference in the mean PA metric between the experimental recording and synthetic auralisation, with and without added background noise, as a function of the A-weighted signal-to-noise ratio (SNR_A). Mean difference values and their least-squares estimated standard errors are shown per measurement sample.

For the road case, adding BGN to the auralized sounds make their differences with respect to the experimental data considerably smaller (closer to the $y = 0$ line). However, for the evaluation of auralised wind turbine noise, the behaviour observed for the cases without added background noise is more desirable, since a constant relation with SNR_A in different BGN conditions can be more easily compensated for than a background-noise-dependent relation with SNR_A . The coefficients of the least-squares model are shown in Table 4. Without added background noise, the slope of the difference with SNR is essentially constant, with only an offset in the intercept between the two BGN conditions. For the cases with added BGN, on the other hand, the intercept offset remains similar, while the slope with SNR_A becomes significantly different between the road and fjord ambient noise.

Table 4 Least-squares regression coefficients of Equation 2 and Equation 3 for the differences in the PA metric between recording and simulation. All p -values are $\ll 0.05$, except for the underlined coefficients.

BGN Condition	Slope (x_1)			Intercept (x_2)			Adjusted R^2
	Road	Fjord	Δ	Road	Fjord	Δ	
No added BGN	-0.118	-0.120	<u>0.002</u>	0.880	2.120	1.240	0.570
With added BGN	<u>0.019</u>	-0.085	0.104	0.472	1.702	1.230	0.692

4.4 Loudness Level

The difference in mean loudness levels $L_{N,mean}$ between the recorded and synthesised noise in Figure 3 shows a similar behavior as the PA metric. Previous findings with this dataset [10], [31] showed that the loudness results of the NTK wind turbine noise had a dominant influence on the PA metric.

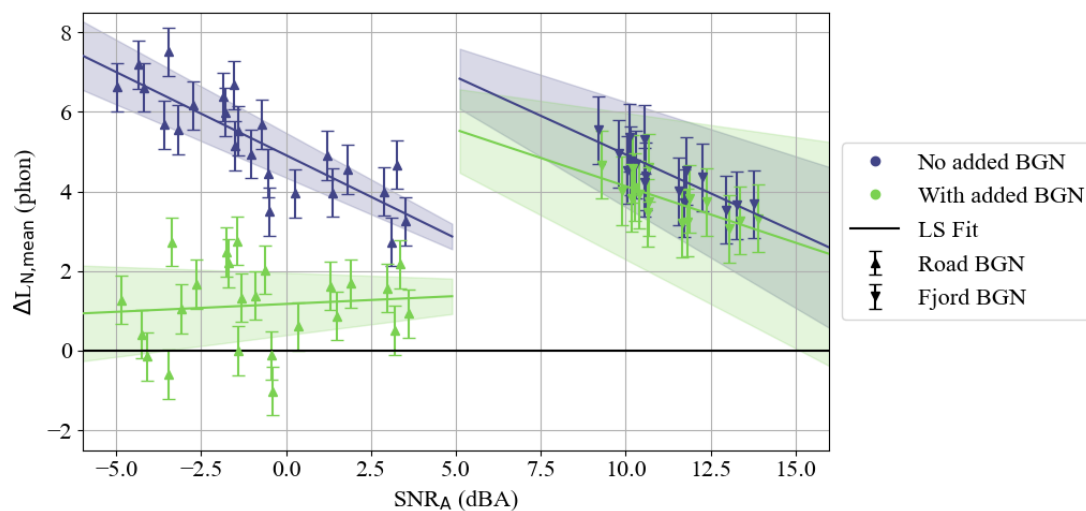


Figure 3 Difference in the mean loudness level $L_{N,mean}$ between the experimental recording and synthetic auralisation, with and without added background noise, as a function of the A-weighted signal-to-noise ratio (SNR_A). Mean difference values and their least-squares estimated standard errors are shown per measurement sample.

The coefficients in Table 5 confirm the observations from Figure 3. Once more, the slope with respect to SNR_A is similar between the road and fjord BGN when no ambient noise is added to the simulations. The slope is significantly different between these two BGN conditions when the background noise is added to the simulations. The change in intercept between these two cases is again similar and independent of adding ambient noise to the simulated noise sample.

Table 5 Least-squares regression coefficients of Equation 2 and Equation 3, for the differences in the loudness level $L_{N,mean}$ between recording and simulation. All p -values are $\ll 0.05$, except for the underlined coefficients.

BGN Condition	Slope (x_1)			Intercept (x_2)			Adjusted R^2
	Road	Fjord	Δ	Road	Fjord	Δ	
No added BGN	-0.418	-0.390	<u>0.028</u>	2.821	6.874	4.054	0.689
With added BGN	<u>0.040</u>	-0.284	0.323	1.369	5.550	4.180	0.687

4.5 Roughness

The differences in mean roughness between the measurements and auralisations are plotted in function of the signal-to-noise ratio in Figure 4. The mean roughness metric is converted to a log-scale as $10 \cdot \log_{10}(10 \cdot R_{\text{mean}})$ before taking the difference, as it was done for the PA metric. In the preliminary analysis, this logarithmic conversion resulted in better p-values and adjusted R^2 values.

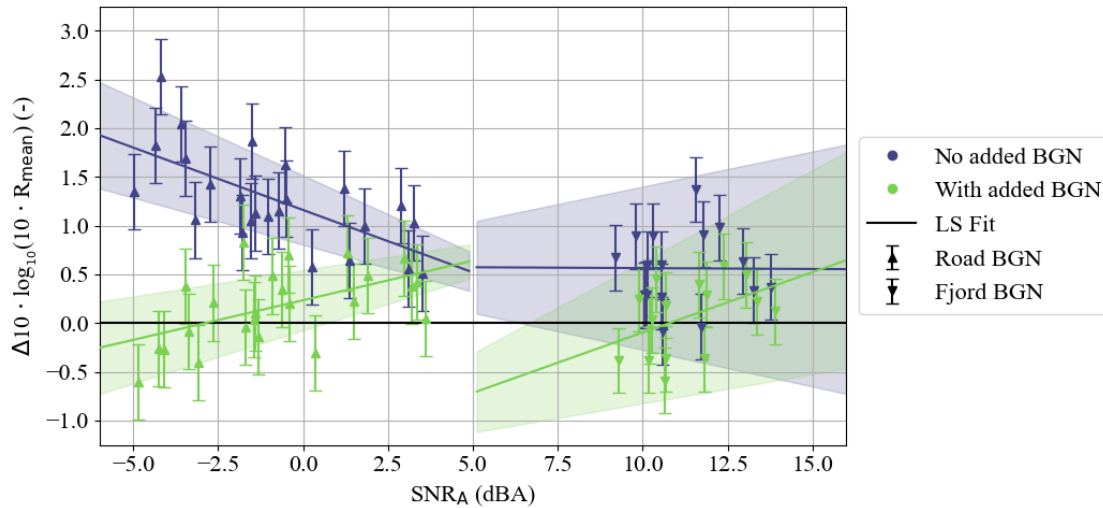


Figure 4 Difference in the mean roughness between the experimental recording and synthetic auralisation, with and without added background noise, as a function of the A-weighted signal-to-noise ratio (SNR_A). Mean difference values and their least-squares estimated standard errors are shown per measurement sample.

Roughness shows a very different behaviour to loudness and PA. In the roughness differences, the addition of background noise to the simulations results in a similar slope with respect to SNR_A between the two types of background noise, which the coefficients in Table 6 confirm. Adding no background noise, on the other hand, results in a different slope between the road and fjord noise. The analysis of the roughness differences should only be considered indicative since the adjusted coefficients of determination for the least-squares fits are very low. Especially for high SNR_A , the spread in the data points in Figure 4 is very large, which is reflected by the large confidence intervals of the least-squares functions.

Table 6 Least-squares regression coefficients of Equation 2 and Equation 3, for the differences in roughness R_{mean} between recording and simulation. All p-values are $\ll 0.05$, except for the underlined coefficients.

BGN Condition	Slope (x_1)			Intercept (x_2)			Adjusted R^2
	Road	Fjord	Δ	Road	Fjord	Δ	
No added BGN	-0.128	<u>-0.002</u>	0.126	0.520	<u>0.573</u>	<u>0.053</u>	0.507
With added BGN	0.081	0.124	<u>0.043</u>	0.641	-0.716	1.357	0.169

5. Conclusions

Ambient noise is an important factor in the investigation of the perceived annoyance due to wind turbine noise. This exploratory work presented acoustic measurements and auralised simulations to investigate two proposed methods for dealing with ambient noise in sound quality metric assessments. The first method involves adding representative background noise to the simulations, whereas the second method consists of using measurements with low BGN as ground truth instead of adding ambient noise to the simulations.

Based on the presented results, it can be recommended not to add background noise to auralised wind turbine noise signals and, instead, to use experimental recordings with high A-weighted signal-to-noise ratios (i.e. with low background noise) as a ground truth. When investigating loudness-based metrics and the overall PA metric, a consistent relation between the difference in metrics between simulated and recorded noise and the SNR_A is observed. At high SNR_A , the addition of background noise has little effect on the perceived differences.

For modulation-based metrics, such as roughness, the presented data gives no clear indication of which method for handling ambient noise results in the most desirable result. The results seem to indicate that the addition of ambient noise may be required to obtain consistent results for modulation-based metrics, such as roughness and fluctuation strength.

Acknowledgments

This publication is a part of the *Listen to the future* project (project number 20247), a part of the Veni 2022 research programme (Domain Applied and Engineering Sciences). The latter project is granted to Roberto Merino-Martinez and is (partially) financed by the Dutch Research Council (NWO).

References

- [1] J. K. Kirkegaard and D. N. Frantzen, “Learning from wind energy controversies: Listening to the noise,” en, *EU Research*, vol. Winter 2024, no. 40, pp. 32–34, 2024. [Online]. Available: https://issuu.com/euresearcher/docs/digital_magazine_eur40.
- [2] J. Lee and F. Zhao, “GWEC Global Wind Report 2024,” Global Wind Energy Council, Brussels, Belgium, Tech. Rep., 2024. [Online]. Available: https://gwec.net/wp-content/uploads/2024/05/GWR-2024_digital-version_final-2.pdf.
- [3] G. Costanzo, G. Brindley, and P. Tardieu, “Wind energy in Europe - 2024 Statistics and the outlook for 2025-2030,” Wind Europe, Brussels, Belgium, Tech. Rep., Feb. 2025.
- [4] D. S. Michaud, S. E. Keith, K. Feder, *et al.*, “Personal and situational variables associated with wind turbine noise annoyance,” en, *The Journal of the Acoustical Society of America*, vol. 139, no. 3, pp. 1455–1466, Mar. 2016. DOI: 10.1121/1.4942390.
- [5] F. J. Y. Müller, V. Leschinger, G. Hübner, and J. Pohl, “Understanding subjective and situational factors of wind turbine noise annoyance,” en, *Energy Policy*, vol. 173, p. 113 361, Feb. 2023. DOI: 10.1016/j.enpol.2022.113361.
- [6] G. F. Greco, R. Merino-Martinez, A. Osses, and S. Langer, “SQAT: A MATLAB-based toolbox for quantitative sound quality analysis,” in *INTER-NOISE and NOISE-CON Congress and Conference Proceedings*, Chiba, Tokyo, Japan, Aug. 2023, pp. 7172–7183. DOI: 10.3397/IN_2023_1075.
- [7] G. F. Greco, R. Merino-Martínez, and A. Osses, *SQAT: A sound quality analysis toolbox for MATLAB*, v1.2. Zenodo. DOI: 10.5281/ZENODO.14641811, Jan. 2025.
- [8] R. Merino-Martínez, R. Pieren, and B. Schäffer, “Holistic approach to wind turbine noise: From blade trailing-edge modifications to annoyance estimation,” en, *Renewable and Sustainable Energy Reviews*, vol. 148, p. 111 285, Sep. 2021. DOI: 10.1016/j.rser.2021.111285.
- [9] A. Bresciani, J. Maillard, and L. d. Santana, “Perceptual evaluation of wind turbine noise,” en, in *16ème Congrès Français d’Acoustique, CFA2022*, Marseille, France: Société Française d’Acoustique; Laboratoire de Mécanique et d’Acoustique, Apr. 2022. [Online]. Available: <https://hal.science/hal-03847876>.
- [10] J. S. Pockelé, “Auralisation of Modelled Wind Turbine Noise for Psychoacoustic Listening Experiments,” M.S. thesis, Delft University of Technology and Technical University of Denmark, Delft, Netherlands, Oct. 2023. [Online]. Available: <https://resolver.tudelft.nl/uuid:cc9e67b4-6bde-4114-97c0-43b11b4a48ef>.
- [11] A. P. C. Bresciani, “Physical and perceptual prediction of wind turbine noise,” English, Doctoral thesis, University of Twente, Twente, Netherlands, Mar. 2024. DOI: 10.3990/1.9789036559546.

- [12] C. Hansen and K. Hansen, “Recent Advances in Wind Turbine Noise Research,” en, *Acoustics*, vol. 2, no. 1, pp. 171–206, Mar. 2020, Number: 1 Publisher: Multidisciplinary Digital Publishing Institute. doi: 10.3390/acoustics2010013. [Online]. Available: <https://www.mdpi.com/2624-599X/2/1/13> (visited on 01/20/2025).
- [13] R. Merino-Martínez, R. Pieren, B. Schäffer, and D. G. Simons, “Psychoacoustic model for predicting wind turbine noise annoyance,” en, in *Proceedings of the 24th International Congress on Acoustics*, vol. A11: Psychoacoustics, Gyeongju, Korea, Oct. 2022.
- [14] F. Bertagnolio, A. Fischer, H. Aagaard Madsen, K. Enevoldsen, P. Hansen, and C. B. M. Pedersen, *NordTank NTK 500/41 Wind Turbine Definition along with Noise and SCADA Measurement Data*, 2024. doi: 10.11583/DTU.27684813.V1.
- [15] F. Bertagnolio, H. A. Madsen, and A. Fischer, “A combined aeroelastic-aeroacoustic model for wind turbine noise: Verification and analysis of field measurements,” en, *Wind Energy*, vol. 20, no. 8, pp. 1331–1348, Aug. 2017. doi: 10.1002/we.2096.
- [16] International Electrotechnical Commission (IEC), “Wind turbines - Part 11: Acoustic noise measurement techniques,” en, International Standard IEC 61400-11:2012, Nov. 2012.
- [17] T. J. Larsen and A. M. Hansen, “How 2 HAWC2, the user’s manual,” DTU, Department of Wind Energy, Roskilde, Denmark, Technical Report Risø-R-1597(ver. 13.0)(EN), May 2023. [Online]. Available: <http://tools.windenergy.dtu.dk/HAWC2/manual/>.
- [18] T. F. W. Embleton, J. E. Piercy, and G. A. Daigle, “Effective flow resistivity of ground surfaces determined by acoustical measurements,” en, *The Journal of the Acoustical Society of America*, vol. 74, no. 4, pp. 1239–1244, Oct. 1983. doi: 10.1121/1.390029.
- [19] M. Delany and E. Bazley, “Acoustical properties of fibrous absorbent materials,” en, *Applied Acoustics*, vol. 3, no. 2, pp. 105–116, Apr. 1970. doi: 10.1016/0003-682X(70)90031-9.
- [20] International Organisation for Standardisation (ISO), “Acoustics - Attenuation of sound during propagation outdoors - Part 1: Calculation of the absorption of sound by the atmosphere,” Geneva, Switzerland, International Standard ISO 9613-1, Aug. 1993.
- [21] H. E. Bass, L. C. Sutherland, A. J. Zuckerwar, D. T. Blackstock, and D. M. Hester, “Atmospheric absorption of sound: Further developments,” en, *The Journal of the Acoustical Society of America*, vol. 97, no. 1, pp. 680–683, Jan. 1995. doi: 10.1121/1.412989.
- [22] P. Vølund and S. M. Petersen, “Validation of aeroelastic model of Nordtank 500/37,” Risø National Laboratory, Roskilde, Denmark, Technical Report Risø-R-1006(EN), 1997.
- [23] F. Bertagnolio, H. A. Madsen, A. Fischer, and C. Bak, “Validation of an Aero-Acoustic Wind Turbine Noise Model Using Advanced Noise Source Measurements of a 500kW Turbine,” en, in *Proceedings of the 16th International Symposium on Transport Phenomena and Dynamics of Rotating Machinery*, Apr. 2016. [Online]. Available: <https://hal.science/hal-01891317>.
- [24] Danmarks Meteorologiske Institut (DMI), *Observationer*, da, 2023. [Online]. Available: <http://www.dmi.dk/friedata/observationer/>.
- [25] International Organisation for Standardisation (ISO), “Acoustics - Methods for calculating loudness – Part 1: Zwicker method,” Geneva, Switzerland, International Standard ISO 532-1:2017, 2017.
- [26] G. Von Bismarck, “Sharpness as an attribute of the timbre of steady sounds,” *Acta Acustica united with Acustica*, vol. 30, no. 3, pp. 159–172, 1974.
- [27] P. Daniel and R. Weber, “Psychoacoustical Roughness: Implementation of an Optimized Model,” *Acta Acustica united with Acustica*, vol. 83, no. 1, pp. 113–123, Jan. 1997.
- [28] A. Osses, R. García León, and A. Kohlrausch, “Modelling the sensation of fluctuation strength,” *Proceedings of Meetings on Acoustics*, vol. 28, no. 1, p. 050005, Sep. 2016. doi: 10.1121/2.0000410.
- [29] H. Fastl and E. Zwicker, *Psychoacoustics: facts and models* (Springer series in information sciences 22), en, 3rd. Berlin, Germany; New York, NY, USA: Springer, 2007, ISBN: 978-3-540-23159-2.

- [30] R. Merino-Martínez, R. M. Yupa-Villanueva, B. von den Hoff, and J. S. Pockelé, “Human response to the flyover noise of different types of drones recorded in field measurements,” in *3rd Quiet Drones conference*, Manchester, UK, Sep. 2024.
- [31] J. S. Pockelé and R. Merino-Martínez, “Psychoacoustic Evaluation of Modelled Wind Turbine Noise,” English, in *Proceedings of the 30th International Congress on Sound and Vibration*, Amsterdam, Netherlands: The International Institute of Acoustics and Vibration, Jul. 2024.

Paper #24 - ID: 358

Title: Validation of a wind turbine noise high-frequency prediction tool

Author: Andres Gimeno Garcia

11th Edition of the
International Conferences on
Wind Turbine Noise
Copenhagen, Denmark – 10th to 13th June 2025

Validation of a wind turbine noise high-frequency prediction tool

Andrés V. Gimeno-García^a,

Dominik Krug^{1a}, and

Wolfgang Schröder^{2a}

^aRWTH Aachen University, Chair of Fluid Mechanics and Institute of Aerodynamics, Wüllnerstrasse 5a, 52062 Aachen, Germany

Summary

The validation process of the first simulation chain, SC-I, of WEAcoustics, an aeroacoustics prediction tool developed under a Simulink environment to predict sound power and pressure levels at a high-frequency output rate, is discussed in detail. The outcoming signal, interpreted by a control algorithm, can lead to quieter, yet more efficient wind turbine operation. SC-I consists of two computational blocks: a flow field solver and an acoustic analysis module. The flow field solver combines Alaska/Wind and XFOIL to extract incoming flow properties and boundary-layer data essential for the aeroacoustics prediction. Alaska/Wind is a state-of-the-art wind turbine multi-dynamics simulation software blade with a blade element momentum (BEMT) -based flow field solver. XFOIL is a two-dimensional airfoil analysis tool. The subsequent acoustic block applies the semi-empirical Brooks, Pope, and Marcolini (BPM) method to predict turbine noise emissions based on the aerodynamic data from the previous block. The validation of WEAcoustics is primarily achieved through direct comparison with experimental data (two-dimensional) and real-world field measurements (three-dimensional). The accuracy range is under 2.5 dB with respect to the reference data.

1. Introduction

Balancing power maximization with the reduction of rotor blade noise emissions remains a key challenge in the development of wind turbine operating strategies. In countries such as Germany, strict legal noise limits [1] impose constraints on the placement of onshore wind turbines. To comply with these regulations -particularly at night- wind turbines are often operated in conservative modes that reduce noise but also limit power generation, thereby impacting economic viability. Various studies have explored strategies to enhance noise-reduced turbine operation through numerical optimization methods. For instance, Leloudas *et al.* [2] propose wind speed-dependent operating points that satisfy a maximum noise threshold while optimizing power output. Shaltout *et al.* [3] extend this concept by computing the control commands necessary to realize these optimized strategies. However, many such approaches rely on offline optimization, which assumes steady-state conditions and does not account for real-world turbulence and environmental variations.

¹Corresponding author - Email: d.krug@aia.rwth-aachen.de

²Corresponding author - Email: w.sch@aia.rwth-aachen.de

In practice, wind turbines operate in dynamic and unpredictable conditions, necessitating control algorithms that adapt in real time through online optimization. The design and validation of such algorithms require efficient tools capable of accurately predicting rotor blade noise with minimal computational cost. To address this need, *WEAcoustics* has been developed, a wind turbine noise prediction framework able to predict wind turbine noise at high frequency rates. *WEAcoustics* employs the blade element momentum theory-based (BEMT) [4, 5] flow solver from Alaska/Wind [6]. The extracted information is then processed using a trailing edge noise model based on XFOIL [7–9] and a semi-empirical aeroacoustics algorithm derived by Brooks *et al.* [10, 11] and later refined by Moriarty *et al.* [12, 13]. Using this hybrid approach, *WEAcoustics* enhances noise prediction accuracy while maintaining computational efficiency. This makes it a valuable tool for real-time wind turbine control applications.

2. WEAcoustics

WEAcoustics is designed with computational time as the primary constraint. As a complementary tool for a predictive control algorithm, it generates output data at a rate sufficient to enable real-time optimization of the efficiency-noise trade-off in wind turbines [14, 15].

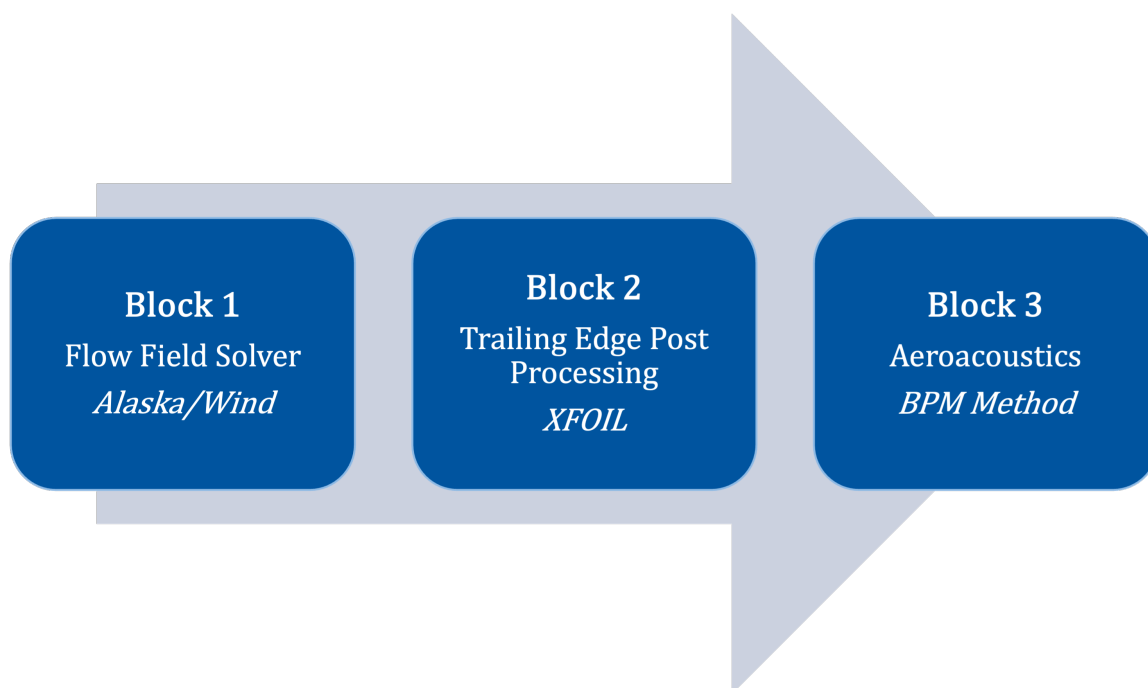


Figure 1 Block diagram of WEAcoustics.

The tool has been designed in a three block configuration (see Figure 1): the flow field solver block, which examines the interaction between airflow and turbine blades; the trailing edge block, which processes flow field data to extract relevant trailing edge information, including the boundary-layer thicknesses; and the acoustic block, which utilizes the collected aerodynamic data to predict the wind turbine blade noise output. This specific configuration allows for isolated modifications of each section towards a better acoustics prediction depending on the problem conditions.

2.1 Block 1: Flow field solver

The main new input to *WEAcoustics* belongs into this block. The flow field solver model is integrated in Alaska/Wind, a validated, holistic wind turbine simulation software based on multi-body dynamics. It is structured around a blade element momentum theory (BEMT) framework. It provides flow field information at rates below 1 Hz, fulfilling the input rate requirements of active control algorithms.

The flow field is assumed to be uniform and follows a power-law profile with increasing velocity as a function

of height above the ground. This relationship reads:

$$U_{\text{hub}} = U_g \left(\frac{h_{\text{hub}}}{h_g} \right)^E \quad (1)$$

where:

- U_{hub} : Wind speed at the hub height (m/s)
- h_{hub} : Hub height (m)
- U_g : Wind speed at reference height (m/s)
- h_g : Reference height (m)
- E : Power law exponent ($-$)

This formulation, commonly used in wind energy applications, provides an approximation of the vertical wind shear profile and is particularly useful when more complex atmospheric models are unavailable [16].

Blade Element Momentum Theory (BEMT) offers a computationally efficient method for evaluating wind turbine performance. However, it is based on simplifying assumptions that limit its ability to capture complex flow physics. Specifically, BEMT models each radial blade section as a quasi-two-dimensional element, thereby neglecting key three-dimensional aerodynamic effects such as tip vortices and spanwise flow.

To compensate for these limitations, Alaska/Wind incorporates empirical corrections. However, these corrections can introduce inaccuracies in non-ideal conditions, such as yawed inflow or turbulence generated by the wake of an upstream turbine within a wind farm. In such cases, the inherently three-dimensional nature of the flow becomes dominant and cannot be ignored. Additionally, the BEMT-based approach assumes the flow field to be orthogonal to the rotor blade plane and linear, which may not adequately represent real-world aerodynamic interactions.

2.2 Block 2: Post processing algorithm

boundary-layer information along the wingspan of the rotor blades is key for the acoustic algorithm to provide reliable prediction results. The information matrix determined by the flow field solver block does not provide the characteristics of the flow around the airfoil; instead, it calculates lift and drag forces, the power coefficient (C_p), and the thrust coefficient (C_t) based on local flow conditions. The local flow conditions at the leading edge of the airfoil are post-processed to obtain the required boundary-layer data at the trailing edge for noise prediction.

To extract the boundary-layer data from the local flow conditions, XFOIL [7–9], a well-known open-source simulation tool for two-dimensional geometries, is used. In XFOIL, boundary-layer thicknesses around a two-dimensional airfoil are computed by coupling an inviscid potential flow solver with an integral boundary-layer formulation. First, a panel method determines the external velocity distribution at a certain distance from the airfoil surface, $u(y)$, along the airfoil. The panel method grid is refined through the Grid>Pane XFOIL configuration menu in the areas of the leading and trailing edges, where the most sensitive data is calculated. Then, for each chord-wise location, the displacement thickness (δ^*) and momentum thickness (θ) are obtained by solving the integral boundary-layer equations [17]. The nominal boundary-layer thickness is typically defined by the displacement and momentum thicknesses using a corrective factor depending on the flow. For laminar flow in XFOIL, the definition is:

$$\delta = \theta(3.15 - 1.72/H_k) + \delta^* \quad (2)$$

where:

- δ : boundary-layer thickness (m)
- δ^* : displacement thickness (m)
- θ : momentum thickness (m)
- H_k : Shape factor ($-$)

By refining the inviscid flow solution and the boundary-layer characteristics in each iteration, XFOIL achieves a converged estimate of boundary-layer thicknesses.

WEAcoustics uses the output data from the information matrix coming from block 1 as input to the XFOIL module, which calculates the boundary-layer information along the blade. This process has also been optimized using a script that calculates the boundary-layer information for the first and last section of a particular airfoil geometry, as well as critical sections (e.g., maximum angle of attack). Then, an interpolation algorithm calculates the intermediate sections along the whole wingspan.

2.3 Block 3: Aeroacoustics prediction

Brooks et al. [10] introduced a semi-empirical approach for predicting airfoil noise in a flow field, known as the BPM method. This simplified technique integrates analytical models with empirical data to estimate noise generated at the trailing edge of an airfoil. This method involves determining blade element velocities and forces, calculating the sound pressure level (SPL) for each blade segment using empirical relations based on local flow conditions, and summing these contributions to derive the overall SPL of the turbine rotor blade. The specific SPL term for noise emitted by a two-dimensional section at a 1-meter distance from the trailing edge -orthogonal to the chord line and co-planar with the airfoil- is referred to as sound power level (SPwL) [13]. Both SPwL and SPL are expressed in decibels (dB), with contributing sources being logarithmically combined.

This method offers key advantages such as computational efficiency and simplicity. Unlike Computational Fluid Dynamics (CFD) or Computational Aeroacoustics (CAA) simulations, it requires significantly less computational effort, making it a practical tool for preliminary design and acoustic optimization studies. However, its simplified nature means limitations. The approach assumes a uniform, two-dimensional flow field, potentially overlooking important noise generation mechanisms. It does not account for factors such as turbulence, blade surface roughness, non-uniform inflow, or the three-dimensional effects of rotating flow, which may lead to inaccuracies, especially for wind turbines operating under off-design conditions. Due to its two-dimensional framework, SPL values must be determined sectionally along the wingspan of the blade. Their summation yields the overall sound pressure level (OASPL) for the three-dimensional blade.

2.4 Noise terms

The BPM method distinguishes five noise sources. These are considered independent from one another and are calculated separately. Their contribution to the final noise spectra is added as non-correlated noise sources. They have been included in *WEAcoustics* as follows. For further information, you can refer to the work of Brooks et al. [10] and Moriarty et al. [12].

Turbulent boundary-layer trailing edge (TBL-TE)

The turbulent boundary-layer (TBL) noise is considered one of the major noise sources in aerodynamic systems. It is generated by the turbulent boundary-layer passing over the trailing edge of the airfoil, on both the pressure side and the suction side of the blade. The total TBL noise is a combination of the SPL generated on the pressure side and the suction side of the blade, described by:

$$SPL_p = 10 \log \left(\frac{\delta_p^* M^5 L \bar{D}_h}{r_e^2} \right) + A \left(\frac{St_p}{St_1} \right) + (K_1 - 3) + \Delta K_1 \quad (3)$$

where:

- δ_p^* : Pressure side displacement thickness (m)
- M : Mach number ($-$)
- L : Span of the airfoil section (m)
- \bar{D}_h : High frequency limit directivity function ($-$)
- r_e : Observer effective distance (m)
- A : TBL-TE spectral shape function ($-$)
- St_p : Pressure side Strouhal number ($-$)
- St_1 : TBL-TE Strouhal number ($-$)
- K_1 : Constant ($-$)
- ΔK_1 : Constant ($-$)

$$SPL_s = 10 \log \left(\frac{\delta_s^* M^5 L D \bar{h}}{r_e^2} \right) + A \left(\frac{St_s}{St_1} \right) + (K_1 - 3) \quad (4)$$

where:

- δ_s^* : Suction side displacement thickness (m)
- St_s : Suction side Strouhal number ($-$)

As the angle of attack increases beyond the flow separation threshold, the boundary-layer on the suction side of the blade grows significantly. This phenomenon introduces an additional term into the final TBL trailing-edge (TBL-TE) noise equation, referred to as the separation flow term, denoted by SPL_α :

$$SPL_\alpha = 10 \log \left(\frac{\delta_s^* M^5 L D \bar{h}}{r_e^2} \right) + B \left(\frac{St_s}{St_2} \right) + K_2 \quad (5)$$

where:

- B : Separation noise spectral shape function ($-$)
- St_2 : TBL-TE Strouhal number ($-$)
- K_2 : Constant ($-$)

Finally, all terms are added in Equation (6).

$$SPL_{TBL-TE} = 10 \log \left(10^{SPL_p/10} + 10^{SPL_s/10} + 10^{SPL_\alpha/10} \right) \quad (6)$$

Laminar boundary-layer vortex shedding (LBL-VS)

Laminar vortices leaving the trailing edge generate pressure waves that travel upstream in subsonic flow, amplifying boundary-layer instabilities. As these instabilities reach the trailing edge, similar frequency vortices are formed, generating an interference loop.

This source of noise manifests mostly on the pressure side with a tonal nature due to the quasi-homonymous frequency present inside the interference loop.

$$SPL_{LBL-VS} = 10 \log \left(\frac{\delta_p M^5 L \bar{D}_h}{r_e^2} \right) + G_1 \left(\frac{St'}{St'_{peak}} \right) + G_2 \left(\frac{Re_c}{(Re_c)_0} \right) + G_3(\alpha) \quad (7)$$

where:

- δ_p : Pressure side thickness (m)
- St' : LBL-VS Strouhal number ($-$)
- St'_{peak} : Peak LBL-VS Strouhal number ($-$)
- Re_c : Reynolds number based on chord length ($-$)
- $(Re_c)_0$: Reference Reynolds number based on chord length ($-$)
- α : Angle of attack ($^\circ$)
- G_1 : LBL-VS Spectral shape function ($-$)
- G_2 : Re_c dependence for G_1 ($-$)
- G_3 : Angle dependence for G_2 ($-$)

Trailing edge bluntness vortex shedding (TEB-VS)

The bluntness of the trailing edge in a traditional wind turbine airfoil geometry can lead to vortex shedding downstream. Under certain flow conditions, this shedding can evolve into a vortex street, contributing to turbulence in the wake. This noise source can become dominant when the bluntness dimension exceeds the boundary-layer thickness, as defined in Equation (8).

$$SPL_{TEB-VS} = 10 \log \left(\frac{\delta_p^* M^5 L \bar{D}_h}{r_e^2} \right) + G_4 \left(\frac{h}{\delta_{avg}^*}, \Psi \right) + G_5 \left(\frac{h}{\delta_{avg}^*}, \Psi, \frac{St''}{St''_{peak}} \right) \quad (8)$$

where:

- h : Trailing edge bluntness (m)
- δ_{avg}^* : Average displacement thickness (m)
- Ψ : Surface slope parameter ($^\circ$)
- St'' : TEB-VS Strouhal number ($-$)
- St''_{peak} : Peak TEB-VS Strouhal number ($-$)
- G_4 : Peak level function ($-$)
- G_5 : TEB-VS Spectral shape function ($-$)

Tip Vortex

This noise source differs from the previous ones as it is a three-dimensional noise source generated by the interaction of the blade tip vortex and the trailing edge. Brooks et al. [10] defined it for an untwisted, constant-chord blade:

$$SPL_{Tip} = 10 \log \left(\frac{M^2 M_{max}^5 \mathcal{L}^2 \bar{D}_h}{r_e^2} \right) - 30.5 \left(\log St''' + 0.3 \right)^2 + 126 \quad (9)$$

where:

- M_{max} : Maximum Mach number ($-$)
- \mathcal{L} : Spanwise extent of tip vortex (m)
- St''' : Tip vortex Strouhal number ($-$)

Turbulent Inflow

Turbulent inflow is the single leading-edge-related noise source. It is generated by the interaction of the free-stream with the leading edge of the blade. It is predominant at low frequencies and is influenced by the leading edge radius and the turbulence length scale. The turbulence length scale is a measure of the size of the largest eddies in a turbulent flow representing the characteristic distance over which velocity correlations persist and energy is transferred from larger to smaller scales before dissipation occurs [18, 19].

WEAcoustics uses the Amiet's theory [20] derived by Lawson [21] to predict turbulent inflow noise:

$$SPL_{Inflow} = SPL_{Inflow}^H + 10 \log \left(\frac{LFC}{1 + LFC} \right) \quad (10)$$

The noise term generated by the incoming flow consists of high-frequency (11) and low-frequency corrective terms (12).

$$SPL_{Inflow}^H = 10 \log \left(\frac{\rho_o^2 c_o^2 l L}{2r_e^2} M^3 U_\infty^2 I^2 K^3 (1 + K^2)^{-7/3} \bar{D}_l \right) + 58.4, \quad \text{where: } K = \pi f C / U \quad (11)$$

where:

- ρ_o : Air density (kg/m^3)
- c_o : Speed of sound (m/s)
- U_∞ : Wind mean velocity (m/s)
- l : Turbulence length scale (m)
- I : Turbulence intensity (%)
- f : Frequency ($Hz = 1/s$)
- C : Local chord length (m)
- U : Local flow velocity (m/s)
- K : Local wave number (-)
- \bar{D}_l : Low frequency directivity factor (-)

The low-frequency correction factor (LFC), including the Sears term [12, 22] reads:

$$LFC = 10S^2(1 - 9\alpha^2)MK^2\beta^{-2}, \quad \text{where: } \beta^2 = 1 - M^2, \quad S^2 = \left(\frac{2\pi K}{\beta^2} + \left(1 + 2.4 \frac{K}{\beta^2} \right)^{-1} \right)^{-1} \quad (12)$$

where:

- S^2 : Compressible Sears function (-)

Several improved models exist; WEAcoustics incorporates the Guidati model [23, 24] shown in equations (13) and (14).

$$SPL_{Inflow} = SPL_{Amiet} + SPL_{Guidati} + 10dB \quad (13)$$

$$SPL_{Guidati} = -(1.123(D_{rel,1\%} + D_{rel,10\%}) + 5.317(D_{rel,1\%} + D_{rel,10\%})^2)(2\pi f C / U + 5) \quad (14)$$

where:

- $D_{rel,1\%}$: Relative thickness at 1% chord (m)
- $D_{rel,10\%}$: Relative thickness at 10% chord (m)

3. Validation

The first simulation chain of *WEAcoustics*, SC-I, has been successfully validated against two- and three-dimensional experimental data, establishing it as a useful tool for wind turbine active control. Next, the validation of the implementation of its different block packages and the tool as a whole are presented.

3.1 boundary-layer postprocessing and aeroacoustics blocks implementation

Through comparison against experimental and numerical data using different airfoil geometries, namely the NACA0012 and the SANDIA 13.2MW airfoil family, the validation of the two-dimensional implementation of the BPM method algorithms contained in the acoustic block has been possible.

The experimental data for the NACA0012 are taken from the study conducted by Brooks et al. in 1989 [10, 11], who investigated aerodynamic noise generation mechanisms. The experimental setup was based on a three-dimensional anechoic wind tunnel where acoustic measurements were made for a two-dimensional airfoil under various flow conditions. This setup allowed the detailed analysis of the aerodynamic noise at different frequencies, and the investigation of the impact of factors like Mach number, Reynolds number, and angle of attack. The measurements were performed by placing microphones in the vicinity of the airfoil to capture the radiated sound across a range of frequencies.

The numerical predictions presented for the NACA0012 and the SANDIA airfoil family are obtained using the validated tool NREL NAFNoise [25]. This tool combines the acoustic analogy theory with the turbulent flow solutions provided by XFOIL. NAFNoise also predicts the broadband noise generated by turbulent flows interacting with the airfoil surface, using an algorithm that includes the empirical models for sound generation based on the work of Brooks et al. [10] and Moriarty [12, 13].

Figure 2 depicts the validation of *WEAcoustics* at different velocities for constant angle of attack [12]. The tool shows a smooth fit with the numerical data, keeping an X-axis translational displacement towards smaller frequencies compared to the experimental data as the velocity decreases. This can be due to the fact that at lower velocities the flow can interact easier in the wingspan direction, especially in the wind tunnel, producing effects not only in the tonality, but also slightly reducing the maximum SPL due to a partially destructive effect of the sound waves interaction.

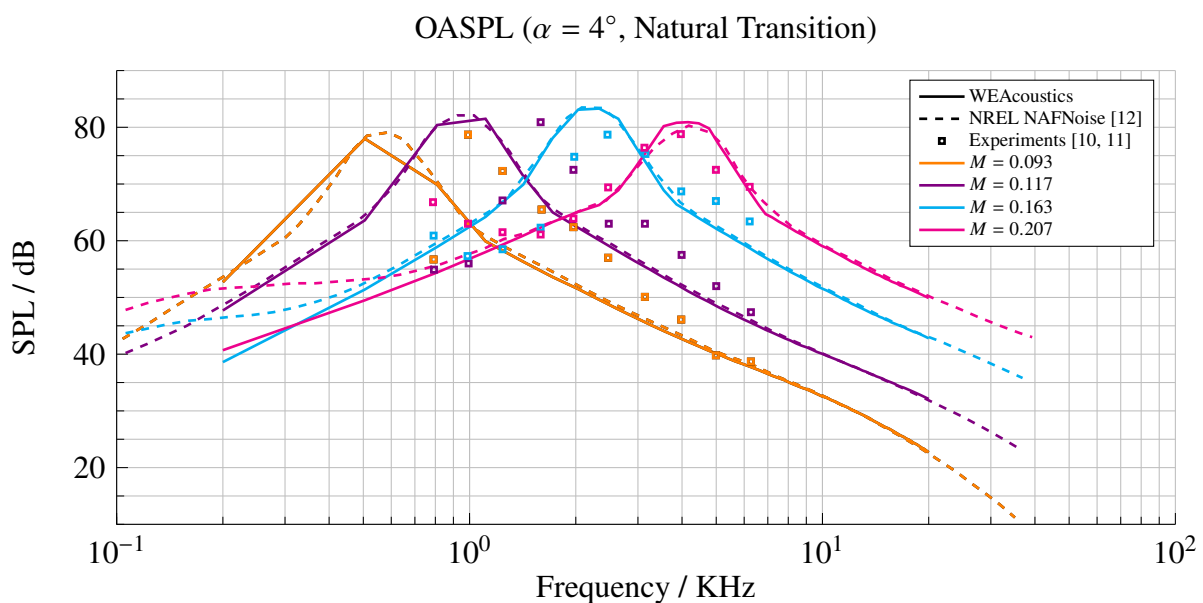


Figure 2 *WEAcoustics* two-dimensional validation against experimental [10, 11] and numerical [12] data for a NACA0012 airfoil at several Mach numbers.

The influence of the different aerodynamic noise generation mechanisms is extremely sensitive to variations of the boundary-layer thickness. Due to the turbulent and rotational nature of the flow, XFOIL is not able to

accurately predict its natural tripping position, resulting in significant translations in tonality when compared with those in Figure 2. Delays of the separation position in the radial direction result in over-predicted overall sound pressure levels, OASPL. It is also possible that the estimation of the Strouhal number (Equation 15) is affected by the three-dimensional effects of the turbulent flow. This creates an effective chord value, c_{eff} , corresponding to the specific length, L , which is larger than the chord, c .

$$St = \frac{fL}{U} \quad (15)$$

where:

- St : Strouhal number (-)
- f : Characteristic frequency of the flow (Hz)
- L : Characteristic length (m)
- U : Flow velocity (m/s)

All these phenomena lead to the increasing mismatch in Figure 3 as the angle of attack increases.

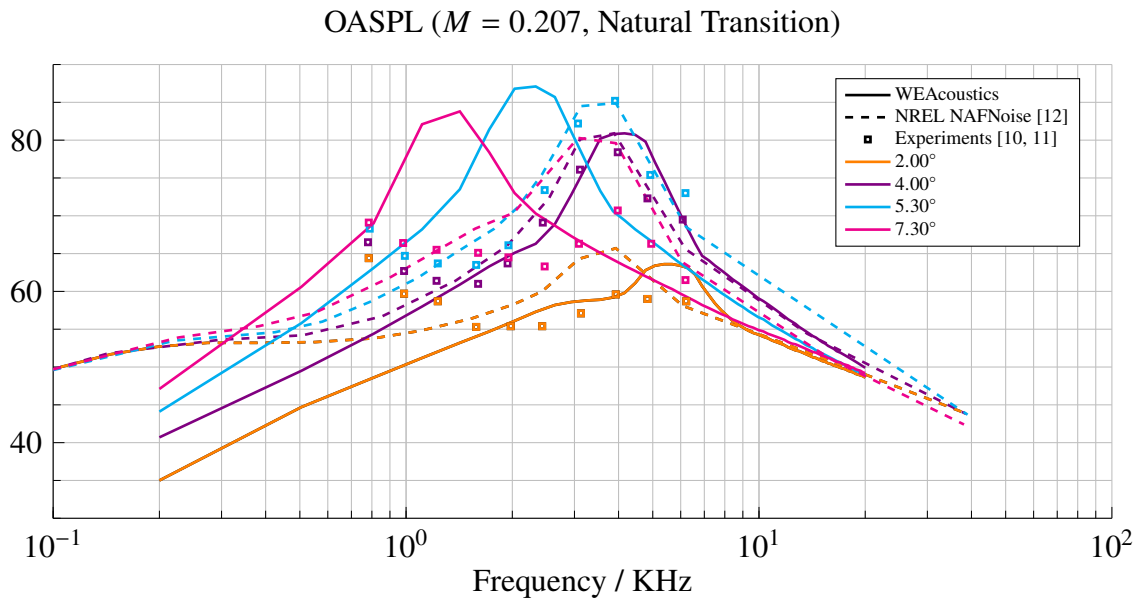


Figure 3 WEAcoustics two-dimensional validation against experimental [10, 11] and numerical [12] data for a NACA0012 airfoil at several angles of attack.

Note that there is not a severe change in the absolute values of the sound pressure level predicted by NAFNoise and WEAcoustics. Nevertheless, for increasing angle of attack, separation occurs and therefore the self-noise output strongly diminishes due to the noise mechanism modification. If the tool was able to detect separation, the code could no longer estimate the noise, since there is no boundary-layer thickness information to rely on. NAFNoise and WEAcoustic force a wrong attached flow condition over the airfoil, providing an overprediction of almost 15dB. Previously both numerical prediction models were showing similar tonality discrepancies with the experimental data. In Figure 3, however, NAFNoise performs better, withstanding tonality similarities with the reference data while WEAcoustics maintains the trend shown in Figure 2. Matching the tonality performance of NAFNoise would require modifying geometrical parameters.

To re-ensure the correct implementation of WEAcoustics, and to validate its use for wind turbine airfoil geometries other than the NACA0012, simulations were carried using NAFNoise and WEAcoustics for the SANDIA 13.2 MW airfoil family. Figures 4, 5, and 6 show the distributions of overall sound pressure level (OASPL), turbulent boundary layer trailing edge (TBL-TE), and laminar boundary layer vortex shedding

(LBL-VS) of both codes at a tip speed ratio (TSR) of 7 and inflow velocity of 10 m/s at a 50 meter wingspan position from the blade root. The test was also repeated in a tip section -at 95 meters from the blade root- showing similar results. The inner sections were not computed as the naturally shaped high angles of attack do not allow attached flow in these sections.

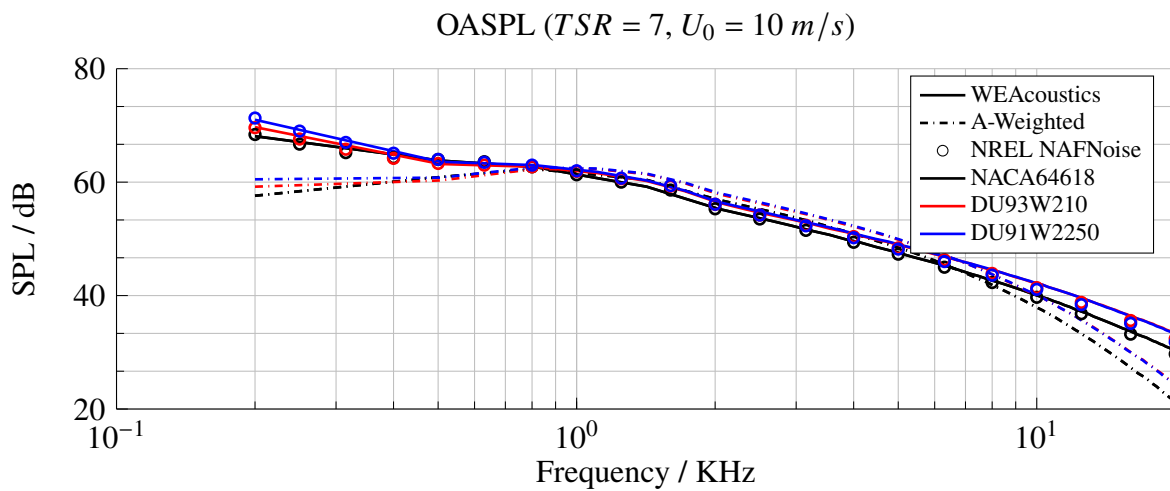


Figure 4 WEAcoustics two-dimensional validation against numerical data for the SANDIA 13.2 MW turbine airfoil family.

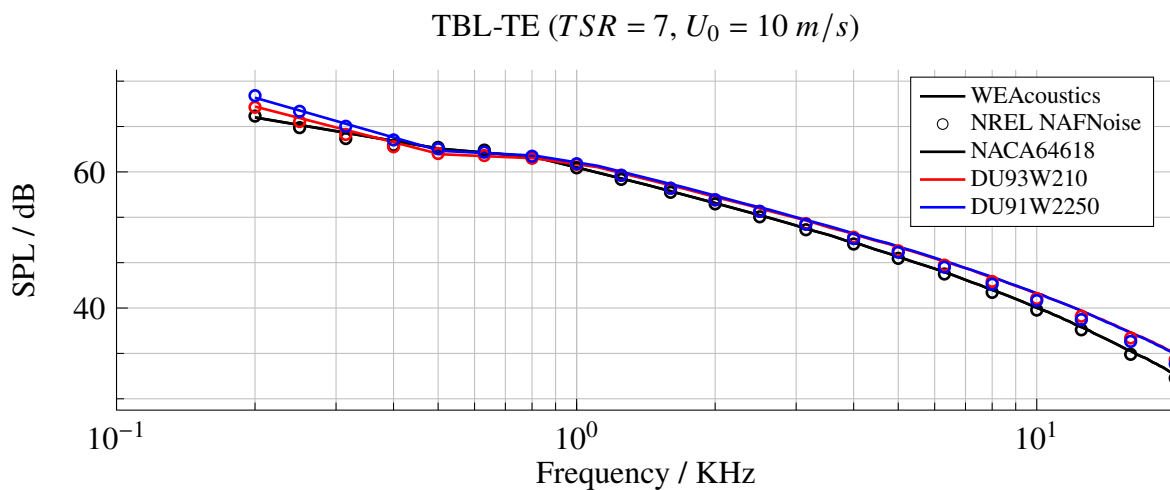


Figure 5 WEAcoustics two-dimensional validation against numerical data for the SANDIA 13.2 MW turbine airfoil family.

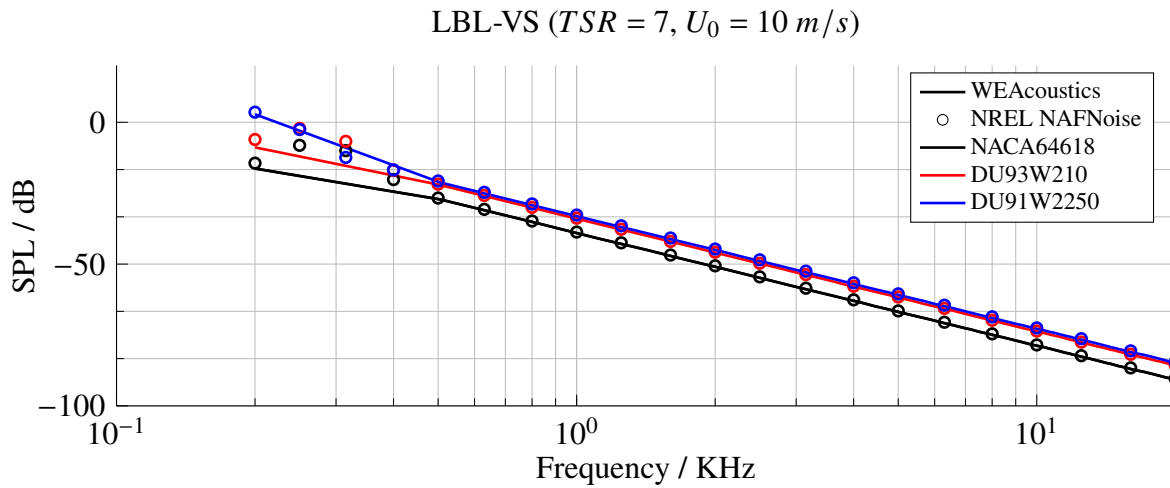


Figure 6 *WEAcoustics* two-dimensional validation against numerical data for the SANDIA 13.2 MW turbine airfoil family.

3.2 *WEAcoustics* implementation

The aerodynamic noise generated by rotor blades is primarily influenced by the interaction of turbulent boundary-layers with the blade surface. The noise generation in the outer sections of the rotor blade is predominantly driven by high-speed flow, high Reynolds number conditions, and low angles of attack. These conditions are ideal for efficient noise production due to the steady, coherent turbulence that interacts with the blade surface. In contrast, the inner sections, where flow separation occurs, contribute much less to the overall noise due to the lower intensity of the turbulence and the irregular flow structure [26, 27].

The prediction of aerodynamic noise in the BPM semi-empirical model relies on the boundary-layer thickness as an indicator of the turbulence intensity, which is directly linked to noise generation mechanisms. However, the high angles of attack in the inner sections introduce significant flow detachment, leading to unsteady, chaotic turbulent structures that cannot be modeled by the algorithm implemented in *WEAcoustics*. This leads to the low quality of semi-empirical models for these regions.

Nevertheless, sound pressure level (SPL) is measured logarithmically and the addition of smaller noise contributions from the inner blade sections is less significant when summed with the larger contributions from the outer sections. Mathematically, the logarithmic addition of sound pressure levels ensures that contributions from regions with lower noise output are negligible compared to those from the outer blade sections, where noise levels are much higher [28]. Therefore, omitting the inner blade sections from the noise calculation leads to an acceptable error in the prediction of the overall sound pressure level. The logarithmic nature of SPL means that small differences in noise contributions do not have a substantial impact on the final value. This justifies the omission of the inner sections.

For the final validation of the complete *WEAcoustics* blockchain, it must be tested against high-fidelity or experimental aeroacoustic data. To achieve this, data from the certification report of a commercial onshore turbine in the 3 MW range was utilized.

The reference measurements have been taken following the noise-measuring setups and techniques established by the IEC 61400-11 standard [29] for wind turbine certification. Nevertheless, the information in the report includes several margins and uncertainties that have influenced the validation process: the flow field orthogonality to the rotor plane considers $\pm 15^\circ$ reading margins, the measurements have a tolerance of $\pm 2\text{dB}$, and the distance from the microphone to the tower allows for $\pm 20\%$ variations. Together with the assumptions made regarding flow field data, i.e., steady flow, orthogonal to the rotor plane, the use of a BEMT-based flow field solver, which does not capture the three-dimensional nature of the rotor blade flow, and the impossibility for XFOIL to identify separated flow conditions when its iterations converge, lead to variations of $\pm 2.5\text{dB}$ through the noise predictions in the reference test cases. These variations

are considered valid within the semi-empirical application framework of the *WEAcoustics* tool and can be regarded as acceptable margins for a validated tool defined by the aforementioned assumptions.

Figure 7 shows the comparison of the sound power level, SPwL, data of the certification report and *WEAcoustics*. The error bars for *WEAcoustics* represent the upper and lower limits in the 10-measurement bin calculated for each one of the test cases. Since the bin information was only available as an average value for the experimental data, the $\pm 2\text{dB}$ measurement error margin set in the IEC report has been included for reference.

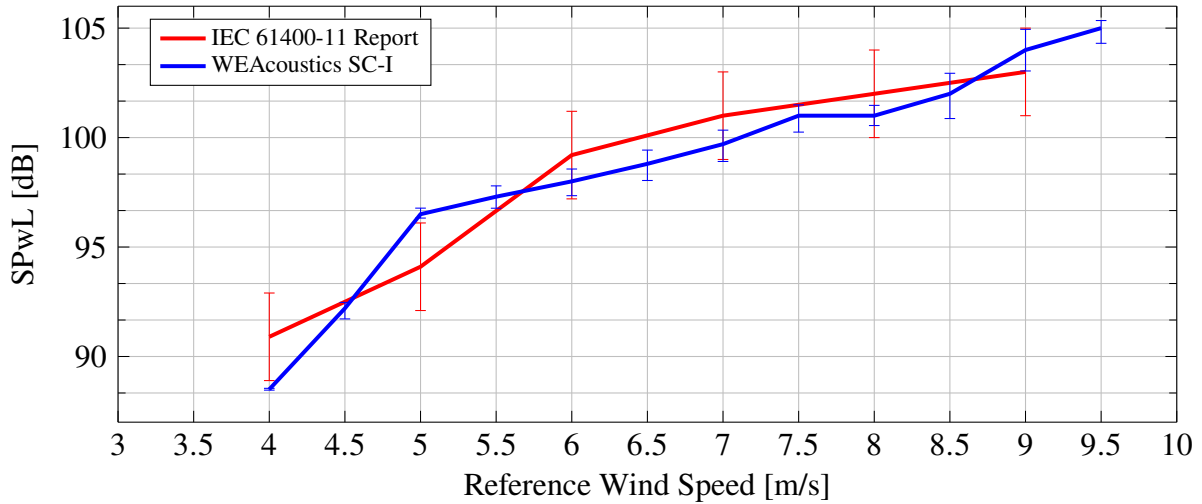


Figure 7 *WEAcoustics* sound power level (SPwL) three-dimensional validation against measurements of the acoustic certification report of a wind turbine in the 3 MW range.

The experimental and *WEAcoustics* data for the available flow conditions and microphone setup conditions for the sound pressure level (SPL) are shown in Figure 8. Compared to measurements away from the turbine, an overprediction along the whole measured spectra is observed. This is due to the previously mentioned measuring margins in the IEC report, but also the lack of a propagation algorithm.

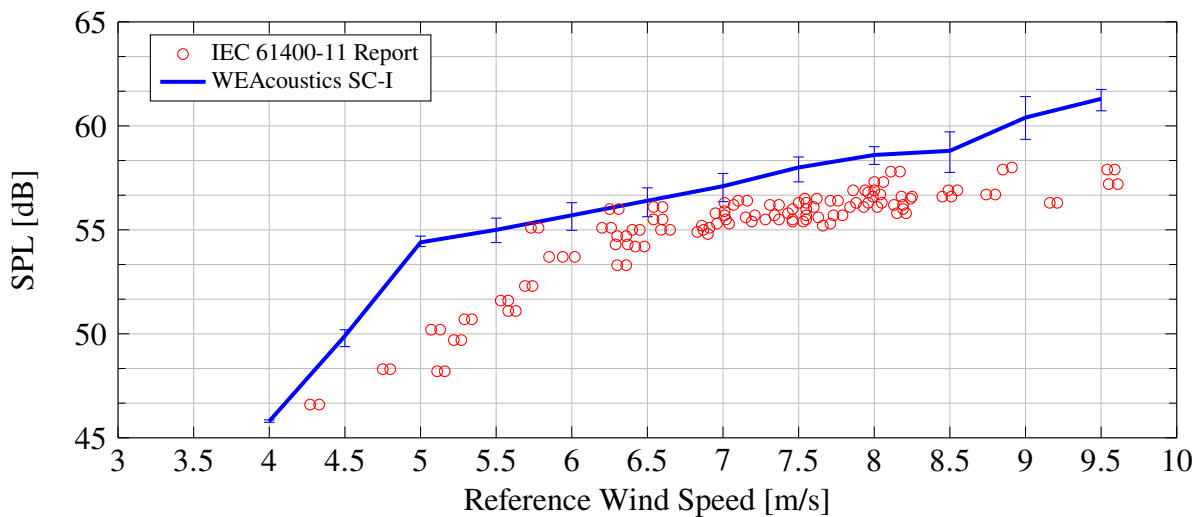


Figure 8 *WEAcoustics* sound pressure level (SPL) three-dimensional validation against measurements of the acoustic certification report of a wind turbine in the 3 MW range. Measured with a microphone 94 m behind the turbine base in the orthogonal direction with respect to the rotorplane.

4. Conclusion

The partial implementation of the boundary-layer and acoustic blocks has been validated for a two dimensional application for various airfoils and configurations. Furthermore, the comparison of *WEAcoustics* data against empirically measured data from a commercial turbine in the 3 MW range, proved the three-dimensional application of the tool to be reliable with tolerances ranging ± 2.5 dB. These tolerances are acceptable since *WEAcoustics*:

- 1) Utilizes a BEMT-based flow field solver and the accuracy limitations this solver inherently carries when solving the potentially three-dimensional flow in a wind turbine rotorblade.
- 2) Features an XFOIL algorithm that is not always capable of accurately predict the natural laminar-turbulent transition (tripping) of the flow over the bladespan.
- 3) Uses an algorithm based in the BPM semi-empirical model that omits the inner sections of the turbine blade as it is not capable to predict the aerodynamic noise without boundary-layer information.

The current research focuses on enhancing the tool by altering the flow field solver and acoustic modeling blocks. These advancements aim to enable more accurate predictions of wind turbine noise emissions, even under challenging off-design conditions characterized by rapidly changing flow fields, yaw effects, and turbulence. In the present phase of the project, an LLM based flow field solver is being implemented. In the future, we will substitute the XFOIL-based algorithm by another algorithm based on the MIT collection of programs for analysis and design of single- or multi-element airfoils (MSES). A sound propagation algorithm will also be coupled to the code.

References

- [1] D. Bundesregierung, "Technische anleitung zum schutz gegen lärm - ta lärm," tech. rep., Die Bundesregierung, 1998.
- [2] G. Leloudas, "Control of large wind energy systems," *Springer International Publishing*, 2022.
- [3] M. e. Shaltout, "Tradeoff analysis of energy harvesting and noise emission for distributed wind turbines," *Sustainable Energy Technologies and Assessments*, 10, 12-21 Elsevier Ltd., 2015.
- [4] W. J. M. Rankine, "On the mechanical principles of the action of propellers," *Trans. Roy. Inst. Naval Arch.*, 6:13-30, 1865.
- [5] W. Froude, "On the elementary relation between pitch, slip and propulsive efficiency," *rans. Roy. Inst. Naval Arch.*, 19(47):47-57, 1878.
- [6] H. Freudenberg, "Der einsatz von alaska bei der entwicklung von windkraftanlagen," tech. rep., Institut für Mechatronik e.V., Chemnitz, Germany, 2016.
- [7] M. Drela, "Viscous-inviscid analysis of transonic and low reynolds number airfoils," tech. rep., MIT Dept. of Aeronautics and Astronautics, Cambridge, Massachusetts, 1987.
- [8] M. Drela, "Xfoil: An analysis and design system for low reynolds number airfoil," tech. rep., MIT Dept. of Aeronautics and Astronautics, Cambridge, Massachusetts, 1989.
- [9] M. Drela, "Integral boundary layer formulation for blunt trailing edges," tech. rep., MIT Dept. of Aeronautics and Astronautics, Cambridge, Massachusetts, 1989.
- [10] T. F. Brooks, W. J. Pope, and J. Marcolini, "Aeroacoustic measurements of airfoil noise in a wind tunnel," *Journal of Sound and Vibration*, vol. 137, no. 3, pp. 499-509, 1989.
- [11] W. J. Pope, T. F. Brooks, and J. Marcolini, "Numerical simulation of turbulent flow and its influence on airfoil noise," *Journal of Fluids Engineering*, vol. 111, no. 2, pp. 225-233, 1989.

- [12] P. Moriarty *et al.*, “Semi-empirical acoustic noise prediction code for wind turbines,” tech. rep., National Renewable Energy Laboratory (NREL), 2003.
- [13] P. J. Moriarty *et al.*, “Prediction of turbulent inflow and trailing-edge noise for wind turbines,” in *26th AIAA Aeroacoustics Conference*, 2005.
- [14] M. O. L. Hansen and S. K. Voutsinas, “Wind turbine noise: A review of the reduction of noise levels in modern wind turbine designs,” *Renewable and Sustainable Energy Reviews*, vol. 12, no. 5, pp. 1242–1256, 2008.
- [15] S. Scherer and S. Schreiber, “Noise and power trade-offs in modern wind turbine designs,” *Wind Energy*, vol. 16, no. 3, pp. 357–373, 2013.
- [16] J. F. Manwell, J. G. McGowan, and A. L. Rogers, *Wind Energy Explained: Theory, Design and Application*. John Wiley & Sons, 2nd ed., 2009.
- [17] T. von Kármán, “„Über laminare und turbulente reibung, 1921“ (on laminar and turbulent friction),” tech. rep., National Advisory Committee on Aeronautics, 1946.
- [18] S. B. Pope, *Turbulent Flows*. Cambridge University Press, 2000.
- [19] P. A. Davidson, *Turbulence: An Introduction for Scientists and Engineers*. Oxford University Press, 2004.
- [20] R. K. Amiet *et al.*, “Acoustic radiation from an airfoil in a turbulent stream,” *Journal of Sound and Vibration*, 1975.
- [21] M. V. Lowson, “Assessment and prediction of wind turbine noise,” Tech. Rep. 92/19, Flow Solutions, Bristol, England, 1992.
- [22] W. R. Sears, “Some aspects of non-stationary airfoil theory and its practical application,” *Journal of the Aeronautical Sciences*, vol. 8, no. 3, pp. 104–108, 1941.
- [23] G. Guidati *et al.*, “Simulation of aerodynamic sound generation on airfoils in low mach-number flows,” *Proc., Fifth International Congress on Sound and Vibration*, 1997.
- [24] G. Guidati *et al.*, “Simulation and measurement of inflow-turbulence noise on airfoils,” *AIAA Oaoaer 97-1698*, 1997.
- [25] N. R. E. Laboratory, “Nafnoise: A computational aeroacoustic tool for broadband noise prediction,” 2005.
- [26] C. Chong, H. Lee, and S. K. Lele, “Aerodynamic noise from rotors: theory and models,” *Progress in Aerospace Sciences*, vol. 51, pp. 1–22, 2012.
- [27] S. de Lang, J. P. C. P. DeGraaff, and D. L. R. Luchtenburg, “Aerodynamic noise prediction for helicopter rotors,” *Journal of Sound and Vibration*, vol. 333, no. 24, pp. 6672–6689, 2014.
- [28] A. Michaels and B. Green, “The impact of boundary layer turbulence on aerodynamic noise generation,” *AIAA Journal*, vol. 48, no. 6, pp. 1191–1203, 2010.
- [29] I. E. Commission, “International standard, wind turbine generator systems - part 11, iec 61400-11,” tech. rep., International Electrotechnical Commission, 2012.

Paper #25 - ID: 359

Title: Impact of a Novel Flexible Serrated Trailing Edge in the Reduction of Far-Field Wind Turbine Noise

Author: Ryan Church

11th Edition of the
International Conferences on
Wind Turbine Noise
Copenhagen, Denmark – 10th to 13th June 2025

**Impact of a Novel Flexible Serrated Trailing Edge in the Reduction of Far-Field
Wind Turbine Noise**

Ryan Church¹

BiomeRenewables Inc. 150 King Street West Suite 262, Toronto, Ontario, Canada

Matthew Cand

Hoare Lea LLP. 155 Aztec West, Bristol, BS32 4UB, United Kingdom

Duncan Halstead

Aercoustics Engineering Ltd. 1004 Middlegate Rd Suite 1100, Mississauga, Ontario, Canada

Summary

In this paper, we investigate the impact of a novel flexible serrated trailing edge device on the reduction of far-field broadband noise through reductions in sound energy in the low- to mid-frequency spectrum (< 1000 Hz) on two contrasting sizes of MW-class wind turbines. The impact of far-field noise, particularly at distances of 500 m or more at typical receptor locations around the turbines, is becoming a larger and more pertinent topic of investigation as wind farm development occurs closer to communities. As such, understanding the impact of novel technologies that have the potential to reduce the impact of noise at far-field locations is of interest for the industry. In this study, before and after sound power measurements in accordance with IEC 61400-11 ed.3 were taken on a 2 MW and 6 MW turbine respectively, both with and without installation of the FeatherEdge® serration technology described. A corresponding 1/3 octave band analysis and propagation using the standard ISO 9613-2 methodology was completed for broadband impact at distances of 500 m, 800 m, 1100 m and 1500 m. The results from both turbines were compared to assess the differences. In addition, far-field measurements according to IEC TS 61400-11-2:2024 were conducted on the 6 MW turbine at similar distances to compare to the output of the ISO 9613-2 method. A discussion on refinement of numerical methods follows, to be concluded by areas for further research.

1. Introduction

The topic of wind turbine noise has become a pressing topic in recent years in many areas around the world. The development of new wind power facilities balances the pursuit of open areas with optimal wind resources with a desire to minimize transmission losses by situating these facilities closer to areas of higher population. Consequently, there has been a gradual encroachment of wind development around populated areas, which have tighter constraints on land availability, community setback requirements, and regulations on noise emissions, especially at night. Even geographies that were not previously considered to be noise-

¹ Corresponding author – Email: rchurch@biomerenewables.com

sensitive areas, like India, are now facing regulations. These factors underscore a compelling need for noise-reducing technologies in wind turbines. Nowhere is this need more acutely felt than Europe.

In Germany for example, the Federal Immission Control Act states that noise emissions must not be above 50 dB(A) during the day and 35 dB(A) at night for residential areas [1]. At the same time, the trend for new wind turbines considered for these developments has been an increase in nominal output, rotor size, tip speed and noise generation. These two combining factors place increasing limitations on wind developers, who try to maximize the output of these projects, while staying compliant with regulations.

The advent of variable speed, pitch-regulated wind turbine technology has led to an efficient design in terms of noise emissions from modern turbines, leading to low noise emissions at low wind speeds and then increasing to a noise emission peak at or close to the turbine rated power, with noise emissions then either staying constant or decreasing at the highest wind speeds. Noise emissions are now dominated by the trailing edge of the turbine blade.

As the main source of noise is aerodynamic in nature, there are two strategies that wind developers can take. The first is to select wind turbines that have the lowest noise profile, which often come equipped with blades with trailing edge serrations (TEEs), typically providing an extra 2 dB(A) reduction at source at no energy cost (or marginal energy gain), and these are now available as standard on most commercial turbine models. This noise reduction has compensated for the potential increases in noise which may have been the consequence of the increasing size of modern turbines with rotor diameter in excess of 100 m. TEE blades represented the state-of-the-art, and further reductions in source noise levels were generally thought to only being obtained in practice through the use of noise-reduced operational sound modes (OS modes), which reduce the tip speed and limit the output of the generator. For many projects, operating in one or more OS modes can be their only path to project reality. There is, however, a negative financial impact in doing this. Van den Berg *et al.* looked at 19 different modern wind turbines and noted that “the reduction in rated power is 4.8% per dB noise reduction, and for reductions up to 5 dB both are strongly correlated [2].”

The influence of different noise assessments on the viability, risk and generating capacity of wind farm developments is frequently underestimated. Seemingly small changes to environmental noise limits or assessment methodologies can translate into substantial lost renewable energy generation and development opportunities. Where noise is a constraint due to proximity to noise-sensitive locations, even a difference of 2 or 3 dB, which is unlikely to be perceptible in a controlled test, could translate up to a 40% reduction or enhancement of the energy generating potential of a scheme. This is because increased separation distance is often the main mitigation measure available and, where development area is limited, this will translate into a reduced project scale.

To meet the challenge of increased noise reduction, Biome Renewables (Biome) has developed the next evolution in serration technology, which is known commercially as FeatherEdge® (FE). Inspired by the silent flight of the owl, it is applied to the trailing edge of the outer 1/3 of the rotor blade. Each section is roughly 500mm wide, and a unique collection of up to 9 different sizes are specified and tailor-engineered for each blade type. The technology is both an after-market add-on, and available for integration into the OEM blade supply chain, suitable for onshore and offshore. FE exhibits passive-adaptive characteristics and enhanced technical specificity for every rotor blade in the market. The technology has been designed to target the low-frequency spectrum, given the commercial importance of seeing increased noise reduction at receptor locations, which is where the realization of noise occurs in the permitting process and where the impact is felt by dwellings. To say this another way, what occurs at the receptor locations is more important than what occurs at the source.



Figure 1. An aerial shot of the FeatherEdge® technology installed on the ENERCON E160 EP5 E3 at Hämelhausen, Germany (Credit: Schierloh Engineering GmbH).

2. IEC Testing

2.1 Method and parameters

Under study was the effect of FES on the Overall Sound Power Level (OASPL) and its impact on the frequency spectrum. The effect of the FES on the sound profile of a wind turbine was evaluated by conducting tests in line with the third edition of the IEC 61400-11 [3] to determine the apparent sound power level of the turbine before and after the installation of the FES. Two test turbines are evaluated in this study, discussed below.

2.1.1 Senvion MM92

Sound power testing was undertaken on a Senvion MM92 wind turbine located in at the Nergica Research institute in Gaspé, Quebec, Canada. The environment around the test turbine is generally hilly, with large, forested areas surrounding much of the turbine location. This turbine has an installed hub height of 80 m, a rotor diameter of 92 m, and a nominal rated power output of 2.05 MW. The tests were undertaken in line with the third edition of the IEC 61400-11 [3] sound power test standard, with a deviation in the location of the anemometer required to mitigate the impact of a forested area around the

turbine, which placed the microphone closer to the turbine and just on the edge of the acceptable parameter (Fig. 2). The turbine was first tested in its normal configuration in September and October 2023, by Nergica staff with technical support provided by Aercoustics. The LM blade was equipped with standard blade vortex generators, which were considered to represent the current state of the art when the turbine was designed.



Figure 2: Picture of the microphone board used for the IEC 61400-11 test of the Senvion MM92 turbine.

Subsequently, FeatherEdge® serrations (FES) were installed on the test turbine. A similar sound power test was undertaken on the turbine in October 2024. A pitch alignment was completed prior to the baseline test in 2023, but not on the subsequent FES test. In both cases, the turbine operated in the same standard mode with a rated power of 2.05 MW.

2.1.2 Enercon E160 EP5 E3

Separate sound power tests were undertaken on one specific Enercon E-160 EP5 E3 wind turbine located in Hämelhausen, Lower Saxony, Germany, both with and without the blade additions described in the present paper. This turbine has an installed hub height of 166.6m and rotor diameter of 160 m. The tests were undertaken in line with the third edition of the IEC 61400-11 [3] sound power test standard. The turbine was first tested in its normal configuration in February 2024, by Deutsche WindGuard GmbH, an accredited test company. The turbine blade was equipped with standard blade additions: vortex generators, “T-Spoiler” and Serrated Trailing Edge (STEs) of LM, which are considered to represent the current state of the art in terms of blade add-ons.

Subsequently, FES were installed on the test turbine to replace the standard STE. Similar sound power tests were undertaken on the turbine by T&H Ingenieure GmbH, an accredited test company, following installation of the FES in March 2025. In both cases, the turbine operated in the same standard power-optimized mode with a rated power of 5.6MW. In both cases, the microphone location was in the same position, exactly in-line with the standard (Fig. 3). Additionally, in both cases, the pitch alignment was ensured to be the same to manufacturer specifications, noting the impacts that pitch misalignment can have on noise generation.



Figure 3: Picture of the microphone board used for the IEC 61400-11 test of the Enercon E160 turbine.

2.2 Results

2.2.1 Senvion MM92

The overall sound power levels of the baseline test case and the FES case are summarized in Figure 4, with the combined uncertainties of the OASPL shown in the error bars. While the minimum IEC 61400-11 reportable wind bins for this turbine range from 8-13 m/s, the baseline test had poor data quality due to high ambient noise in the four highest windspeed bins. As such, comparisons are made at wind speeds of 8 m/s to 11 m/s only.

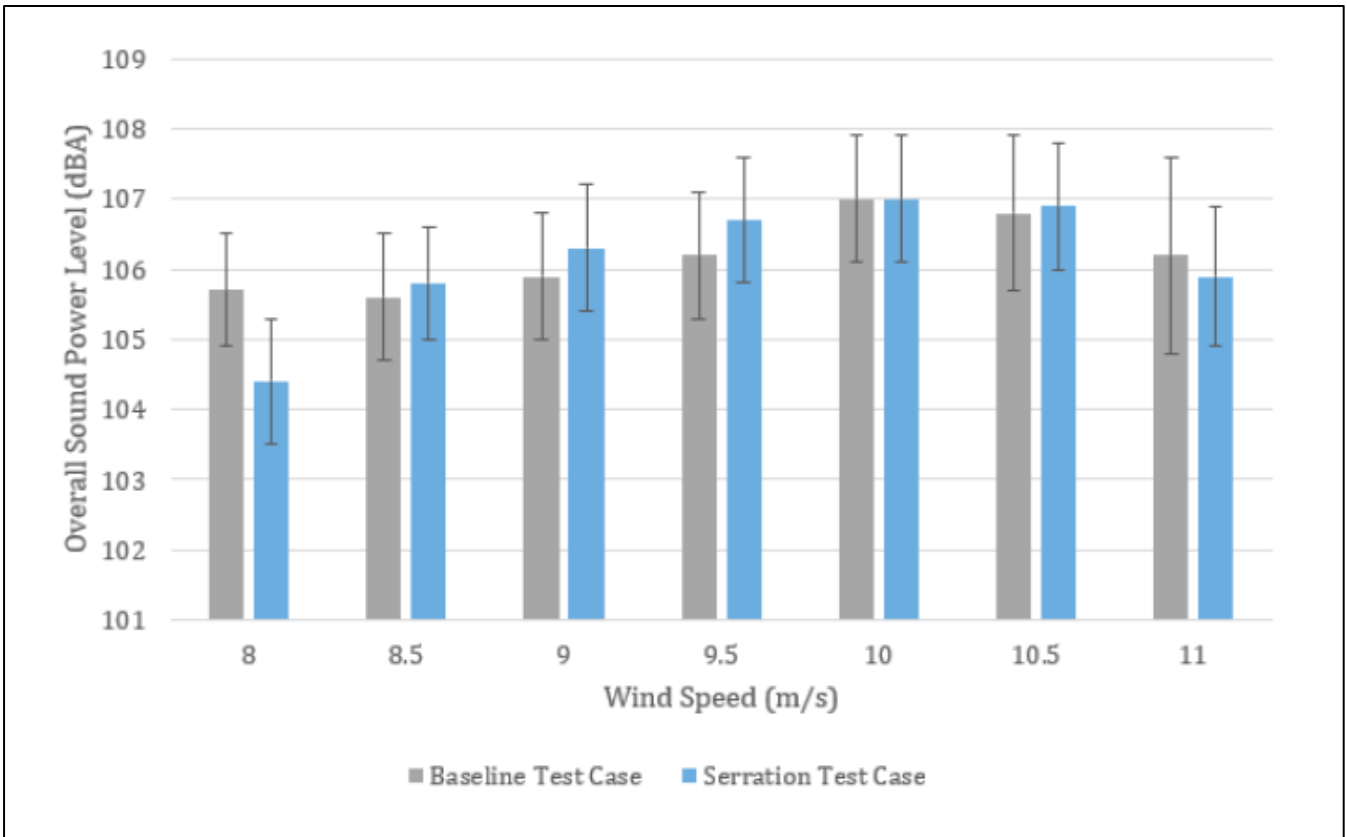


Figure 4 Comparison of A-weighted sound power test results for a Senvion MM92 turbine with standard blade add-ons (Baseline Test Case) and the FES technology (Serrations Test Case) – vertical bars represent test uncertainty U_c .

Comparing with the baseline test case, the serration test case resulted in similar OASPL for wind speed bins of 8.5 m/s to 11 m/s. The overall sound power level for the serration test case at 8 m/s was found to be lower than the baseline test case by 1.3 decibels (dB), although from 8.5-9.5 m/s the OASPL is slightly higher with the FES add-ons. At 10 m/s, corresponding to the maximum tested sound power level, there is virtually no difference between Baseline and FES case.

While the OASPLs between the baseline and the serration test case were generally similar, the FES did have a notable effect on the spectral sound levels of the test turbine. Specifically, there was found a notable reduction in the low to mid frequencies (100 to 800 Hz), of up to 7 dB in some 1/3 octave bands in this frequency range, and a notable increase in sound level at higher frequencies (1000 to 2500 Hz), of up to 7 dB in some 1/3 octave bands in this frequency range. As an example, Figure and Figure 5 plot the 1/3 octave sound power levels between the baseline test case and the serration test case at the wind speed of 8.5 and 10 m/s, respectively.

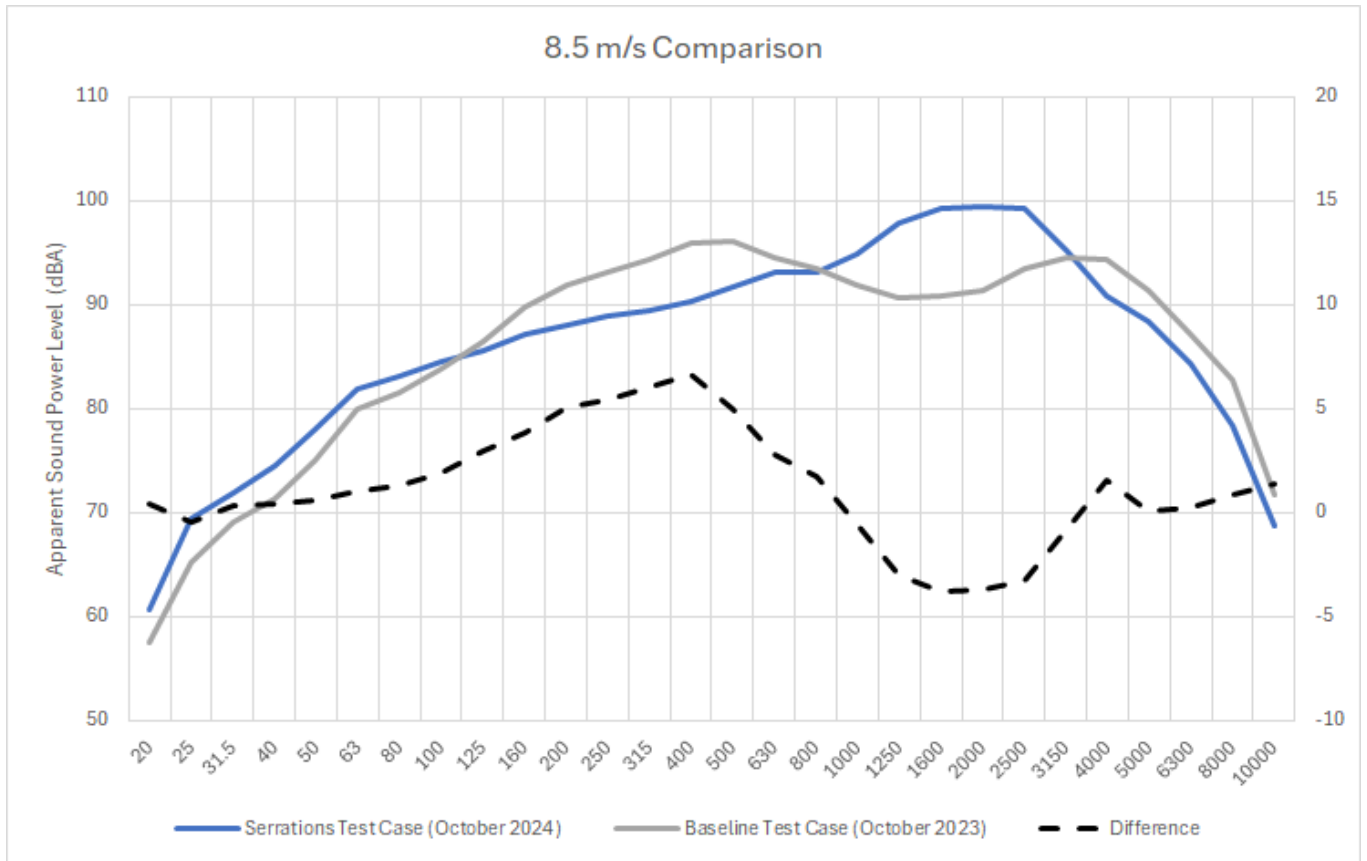


Figure 5 Comparison of measured 1/3 octave sound power levels for a Senvion MM92 turbine with standard blade add-ons (Baseline) and the FES technology (Serrations) – 8.5 m/s hub height wind speed.

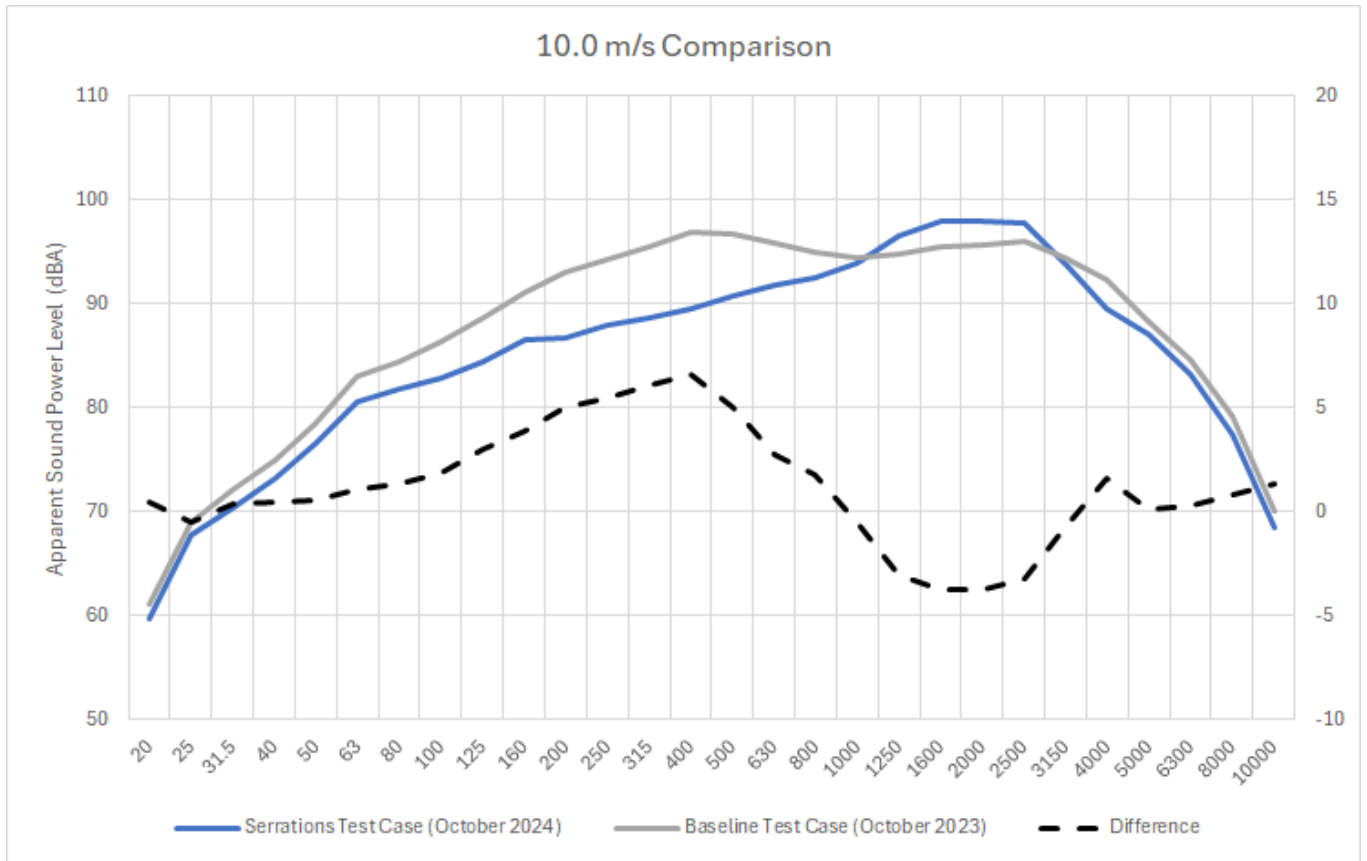


Figure 6 Comparison of measured 1/3 octave sound power levels for a Senvion MM92 turbine with standard blade add-ons (Baseline) and the FES technology (Serrations) – 10 m/s hub height wind speed.

From these results, it appears that the effect of the FES was to shift the acoustic energy from lower to higher frequency bands. As higher frequencies are more quickly attenuated through the atmosphere, the net result is expected to reduce the noise level at surrounding points of reception, despite the limited impact on the apparent sound power emissions of the turbine. No reportable tones were found with the test turbine during the Baseline test case, nor for the serration test case.

Table 1 sets out the resulting octave band spectra at the same three representative wind speeds to illustrate the noise reductions obtained.

Table 1 Comparison of octave sound power spectra for a Senvion MM92 turbine with standard blade add-ons (Baseline) and the FES technology.

Hub-Height WS	63 Hz	125 Hz	250 Hz	500 Hz	1000 Hz	2000 Hz	4000 Hz	8000 Hz	dB(A)	Reduction
Baseline 8.5 m/s	84.4	92.1	98.0	100.3	96.9	96.8	98.4	88.6	105.6	
Baseline 10 m/s	87.4	93.9	99.1	101.2	99.4	100.5	97.1	85.8	107.0	
FeatherEdge 8.5 m/s	84.9	89.6	92.6	95.5	99.4	102.6	95.8	84.3	105.8	-0.2
FeatherEdge 10 m/s	86.2	90.7	93.6	96.6	100.5	104.1	97.2	85.4	107.0	0.0
Average reduction	0.3	2.8	5.5	4.7	-1.8	-4.7	1.3	2.4		

2.2.2 Enercon E160 EP5 E3

The comparison of the tested data between the baseline case with standard STE on the blades and the FES shows first a clear reduction in the source noise levels: see Figure and Table 2. For the model tested, this showed a reduction of 1 to 2 dB(A) in the OASPL, with the highest reductions at medium wind speeds (8 to 10 m/s at hub height). The reduction is clear relative to the test uncertainties also represented in Figure . A relatively reduced performance is observed at higher wind speeds in this case (11 m/s and above).

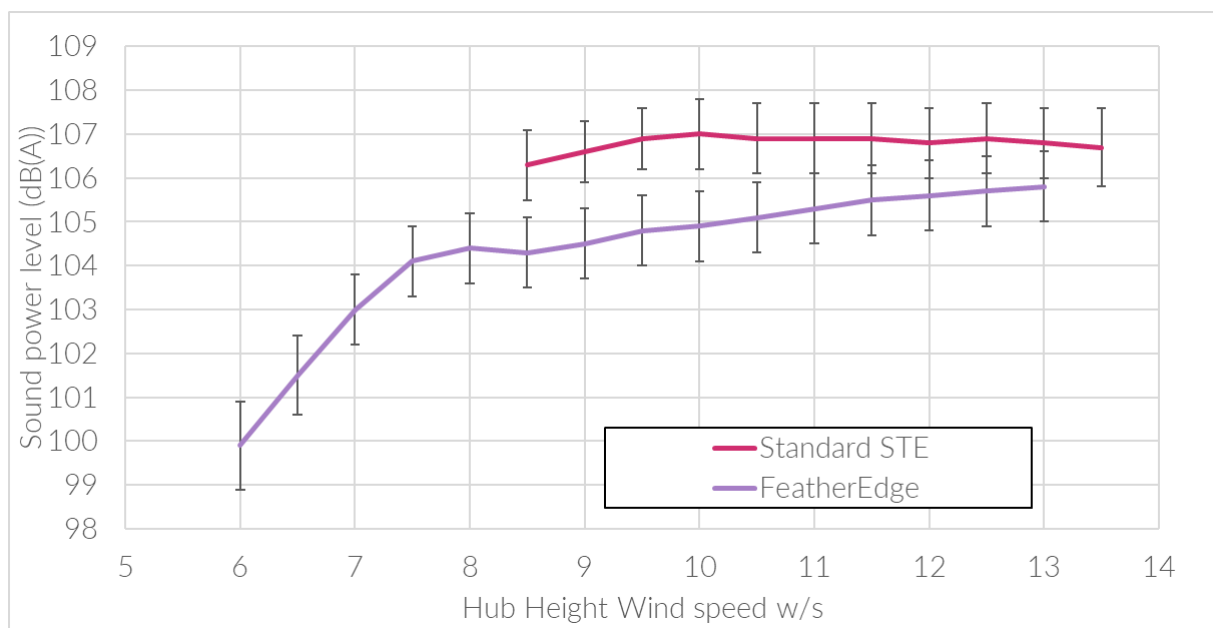


Figure 7 - Comparison of A-weighted sound power test results for an Enercon E-160 EP5 E3 turbine with standard blade add-ons and the FES technology – vertical bars represent test uncertainty U_c .

Figure 8 to Figure 10 show a more detailed comparison of the tested 1/3 octave noise spectra, both before and after the blade modifications. This shows that a key performance feature of the change is a strong

broadband reduction in noise emissions over a wide range of low to medium frequencies between 50 and 500 Hz, with typical reductions between 3 and 5 dB over that range, although this is less pronounced at higher wind speeds. This is also compounded by an even stronger decrease at the higher frequency range of 2 to 6 kHz (up to 10 dB). Only the highest frequencies of 8 kHz and above do increase, although these will be strongly absorbed by the atmosphere during propagation as set out later in this paper. This will likely change the subjective perception of the wind turbine noise although this is harder to quantify. The implications on noise propagation with distance are considered in section 3.

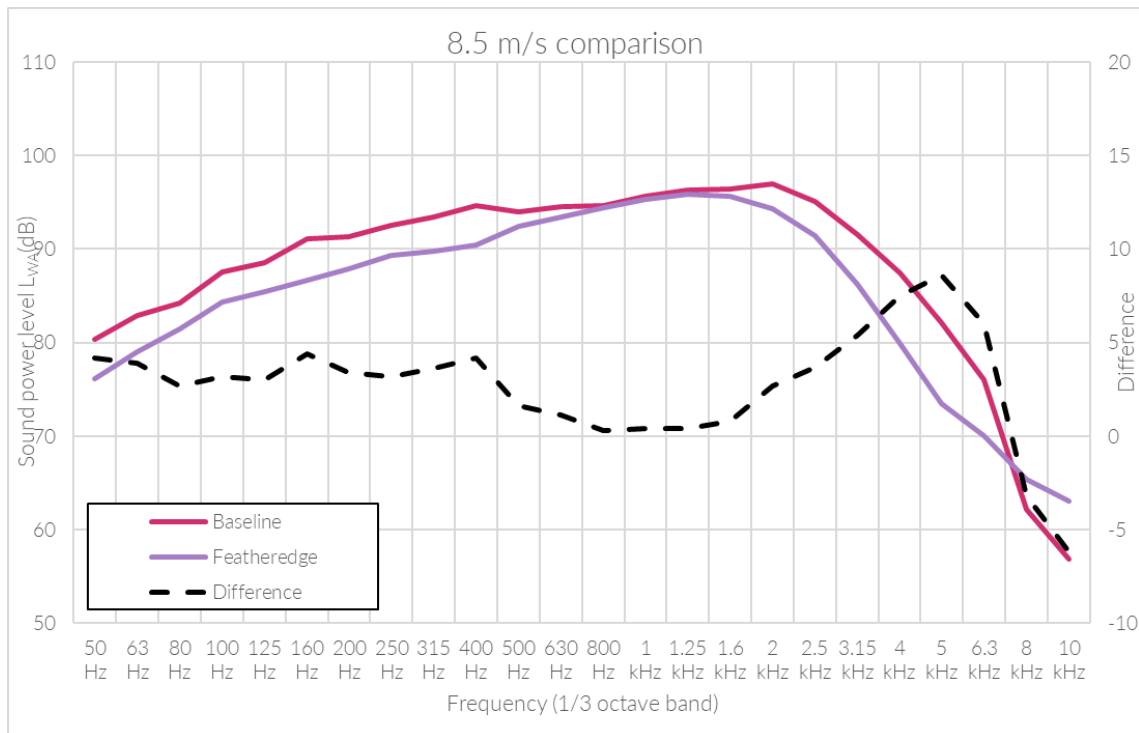


Figure 8 - Comparison of measured 1/3 octave sound power levels for an Enercon E-160 EP5 E3 turbine with standard blade add-ons (baseline) and the FES technology – 8.5 m/s hub height wind speed bin.

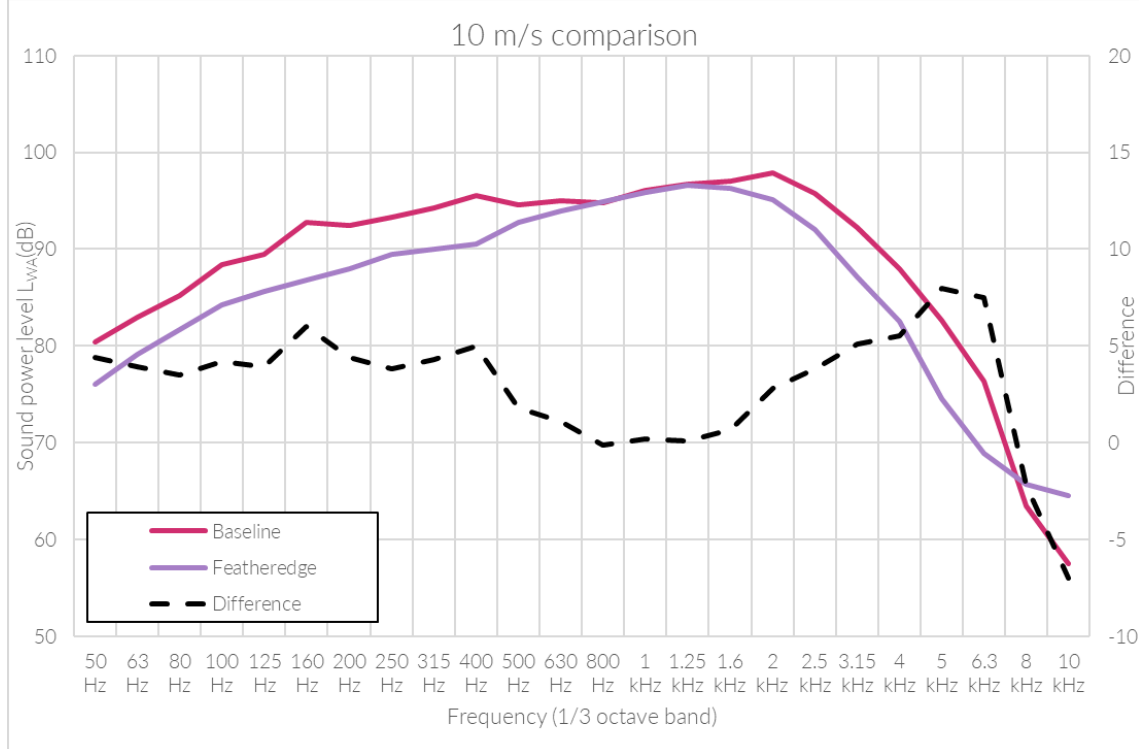


Figure 9 - Comparison of measured 1/3 octave sound power levels for an Enercon E-160 EP5 E3 turbine with standard blade add-ons (baseline) and the FES technology – 10 m/s hub height wind speed bin.

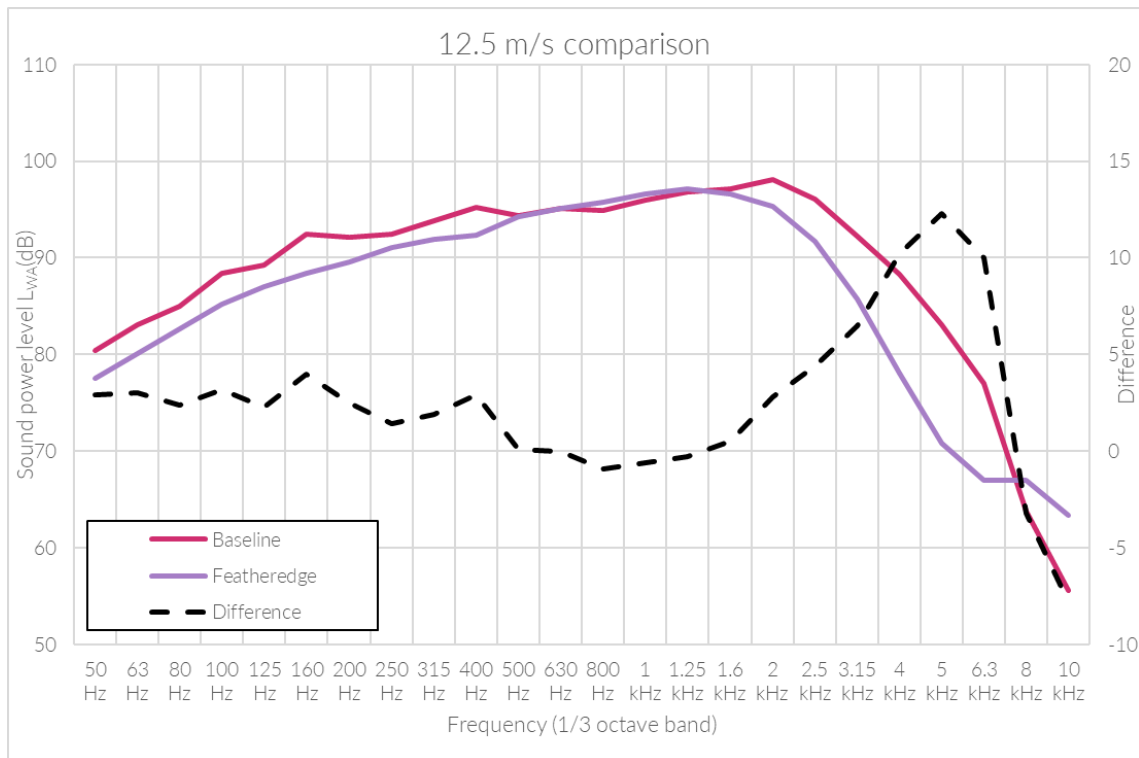


Figure 10 - Comparison of measured 1/3 octave sound power levels for an Enercon E-160 EP5 E3 turbine with standard blade add-ons (baseline) and the FES technology – 12.5 m/s hub height wind speed.

Table 2 then sets out the resulting octave band spectra at the same three representative wind speeds to illustrate the noise reductions obtained.

Table 2 Comparison of octave sound power spectra for an Enercon E-160 EP5 E3 turbine with standard blade add-ons (baseline) and the FES technology.

Hub-Height WS	63 Hz	125 Hz	250 Hz	500 Hz	1000 Hz	2000 Hz	4000 Hz	8000 Hz	dB(A)	Reduction
Baseline 8.5 m/s	87.5	94.1	97.3	99.2	100.4	101.0	93.3	76.2	106.3	
Baseline 10 m/s	88.1	95.4	98.2	99.8	100.7	101.8	93.9	76.7	107.0	
Baseline 12.5 m/s	88.0	95.2	97.6	99.7	100.7	102.0	94.1	77.2	106.9	
FeatherEdge 8.5 m/s	84.2	90.4	93.8	97.0	100.0	98.9	87.3	71.9	104.3	2.0
FeatherEdge 10 m/s	84.3	90.4	94.0	97.4	100.6	99.6	88.6	71.6	104.9	2.1
FeatherEdge 12.5 m/s	85.3	91.8	95.7	98.8	101.3	99.8	86.5	70.9	105.6	1.3
Average reduction	3.3	4.0	3.2	1.8	0	2.2	6.3	5.2		

3. Propagation

The reductions in A-weighted sound emission levels (at source), set out above in Section 2, do not represent the full picture of the effect of the blade addition at typical separation distances where noise-sensitive residential neighbours of the wind turbines may be located (500 to 2000 m or more depending on the circumstances). Over this distance, the effect of air absorption in particular means that high frequency sounds above 2 kHz dissipate strongly whereas lower frequency sounds attenuate less. This means that the effect of the FES technology frequency shift will be much larger in practice than suggested by the sound emission testing once the frequency dependent attenuating effect of atmospheric propagation over larger distances is accounted for.

3.1 Method and parameters

Noise propagation was modelled using the ISO 9613-2 standard [4], recognised as a practical engineering method which is effective at modelling sound propagation over typical distances.

Different turbine layout configurations were modelled to simulate the relative propagation effect with distance of different turbine layout situations. For example, the rate of reduction of noise levels with distance will change depending on a single turbine scenario and one with 5 turbines in a row perpendicular to the direction of propagation (it was assumed the turbines were separated by a distance equivalent to 3 rotor diameters). Figure 11 illustrates the two representative layouts considered in this paper and the increased propagation of noise with distance which occurs in the 5-turbine layout. Predictions were made at a height of 4 m, assuming flat ground 50% hard, with an adjustment of +2dB for all source data [4], in downwind conditions.

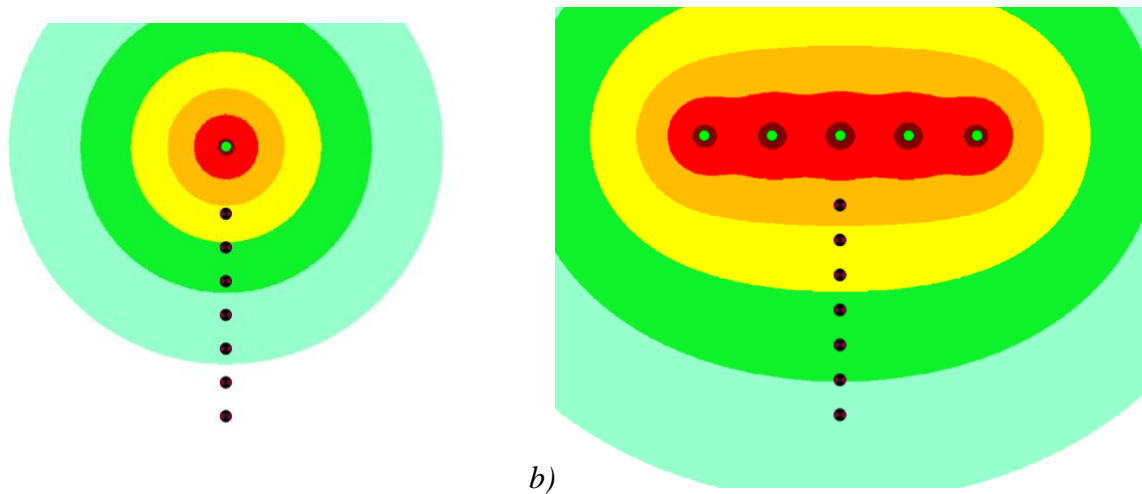


Figure 11 - Comparison of predicted noise propagation for a single turbine (a) and 5 turbines (b) perpendicular to the row of turbines – noise contours in 5dB increments. Points shown represent receptors from 500 to 2000 m distance from the nearest turbine in 250 m increments.

3.2 Results

3.2.1 Senvion MM92

Using the methodology described in Section 3.1, a comparative prediction of the sound propagation between Baseline and FES was modelled for the case of a single turbine and five turbines in a row. The resulting sound levels show a relative reduction introduced by the FES technology that increases with distance from the wind turbine(s). This reduction at a distance – despite the relatively unchanged overall sound power levels in Figure 4 – is due to the strong reductions observed in the range below 500 Hz, combined with the increased attenuation over the propagation distance of the higher frequencies by the atmosphere.

Sound levels in tabular format are provided in Table 3 and Table 4.

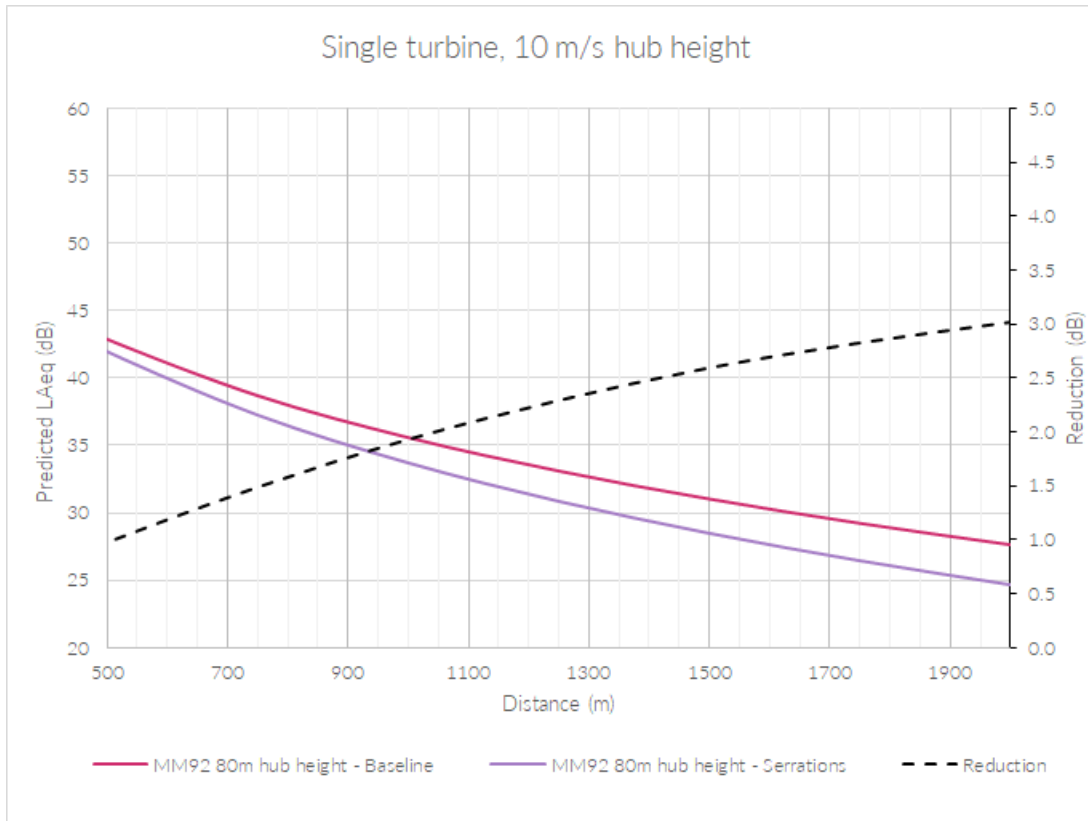


Figure 12: Comparison of predicted L_{Aeq} levels at different distances for the Senvion MM92 turbine, Baseline and FES – 10 m/s hub height wind speed – single turbine.

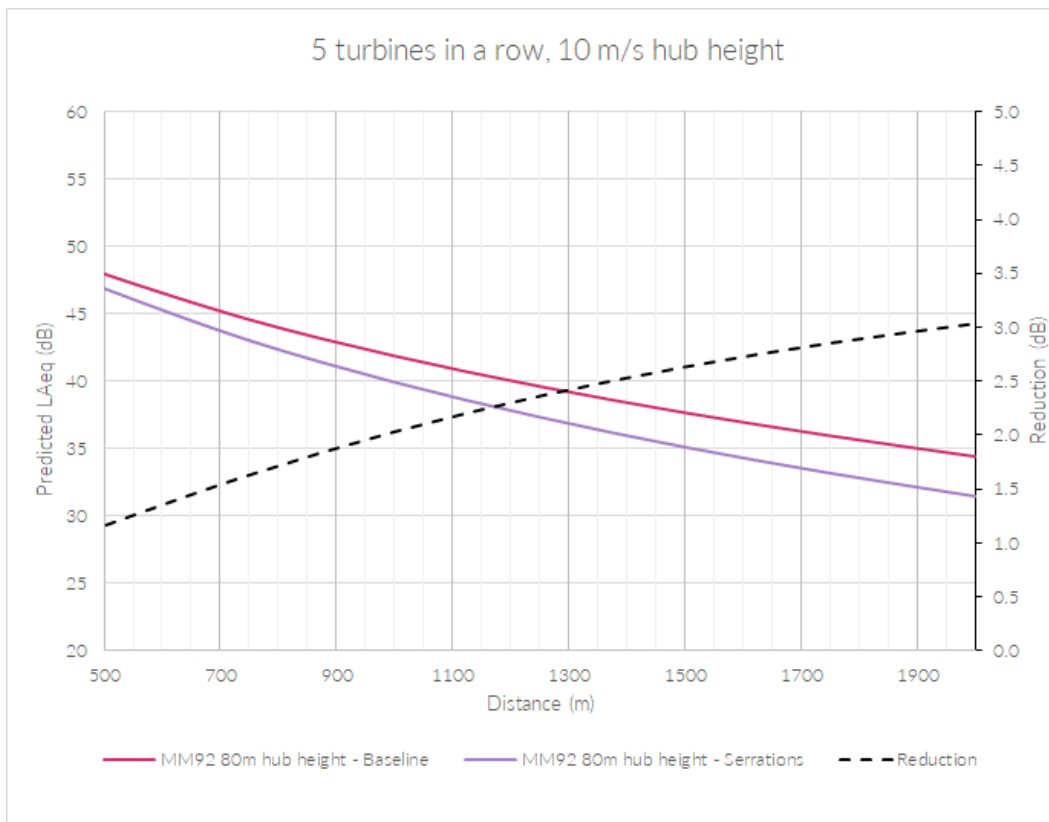


Figure 13: Comparison of predicted L_{Aeq} levels at different distances for the Senvion MM92 turbine, Baseline and FES – 10 m/s hub height wind speed – five turbines row.

Table 3: Propagation results of predicted LAeq levels at different distances for the Senvion MM92 turbine with different blade additions – 8.5 m/s.

Receptor Distance (m)	Single turbine: Baseline	Single turbine: FeatherEdge	Difference	5 turbines in a row: Baseline	5 turbines in a row: FeatherEdge	Difference
500	41.3	40.7	-0.6	46.4	45.6	-0.8
800	36.5	35.2	-1.3	42.5	41.1	-1.4
1000	34.2	32.5	-1.7	40.5	38.7	-1.8
1100	33.1	31.3	-1.8	39.5	37.6	-1.9
1500	29.7	27.4	-2.3	36.3	33.9	-2.4
2000	26.3	23.6	-2.7	33.1	30.3	-2.8

Table 4: Propagation results of predicted LAeq levels at different distances for the Senvion MM92 turbine with different blade additions – 10 m/s.

Receptor Distance (m)	Single turbine: Baseline	Single turbine: FeatherEdge	Difference	5 turbines in a row: Baseline	5 turbines in a row: FeatherEdge	Difference
500	42.9	41.9	-1.0	48.0	46.8	-1.2
800	38.0	36.4	-1.6	44.0	42.3	-1.7
1000	35.6	33.7	-1.9	41.9	39.9	-2.0
1100	34.6	32.5	-2.1	41.0	38.8	-2.2
1500	31.1	28.5	-2.6	37.7	35.1	-2.6
2000	27.7	24.7	-3.0	34.5	31.4	-3.1

3.2.2 Enercon E160 EP5 E3

Figure 14 and Figure 15 show a comparative prediction of propagation based on the tests with different blade additions with distance, for the case of a single turbine or five turbines in a row respectively. This first shows that propagation effects mean that the relative reduction introduced by the FES technology increases from 2 dB(A) at source to around 3 dB(A) at 2 km, due to the relative attenuation of higher frequencies and the relative importance of the strong reductions observed in the range below 500 Hz. This represents a substantial reduction in noise levels over the current state of the art.

Comparison of the two propagation trends, for a fixed noise level, shows that, to obtain a comparable reduction in noise levels, an increased distance of approximately 200 m or more would be required in the case of a single turbine. For situations where a receptor faces several turbines in a row, as represented by the scenario in Figure 15, the same reduction in noise levels corresponds to almost doubled increase in distance (almost 400 m). This illustrates the scale of the implications of the reductions in noise offered by this technology.

Figure 16 shows that this effect is less pronounced at higher wind speeds due to the reduced performance at lower frequencies. However, higher wind speeds can in some cases correspond to conditions of reduced disturbance and relaxed regulatory limits due to the increased levels of background noise which would occur, in the absence of wind turbines, in these windier conditions.

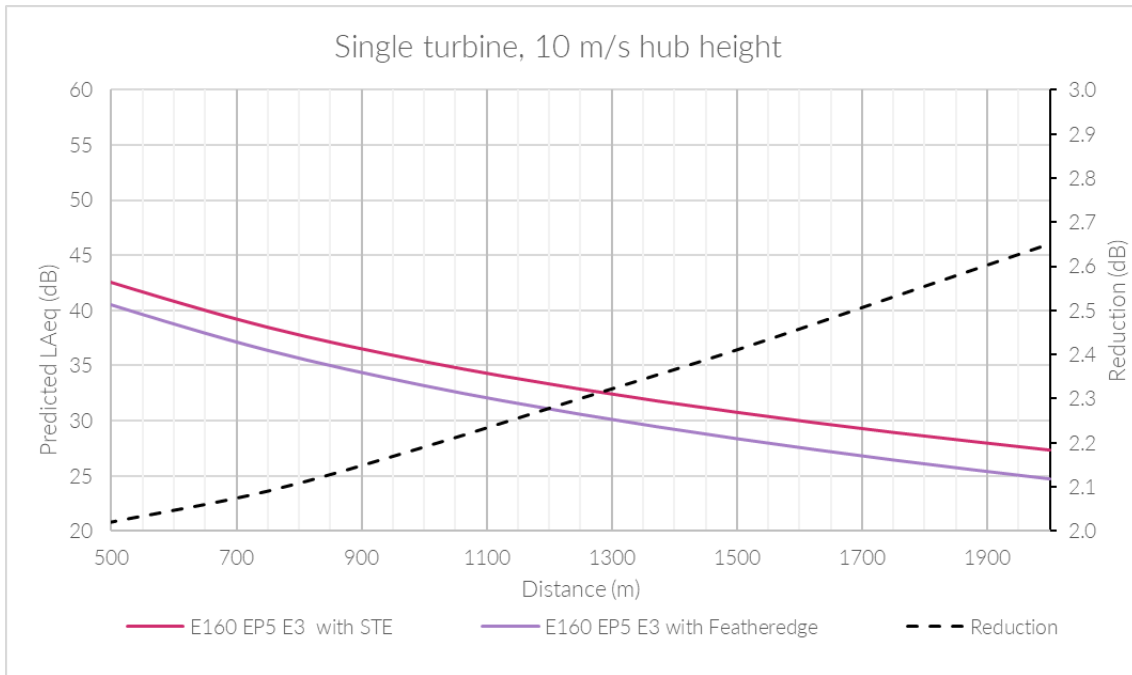


Figure 14 - Comparison of predicted L_{Aeq} levels at different distances for the Enercon E-160 EP5 E3 turbine with different blade additions – 10 m/s hub height wind speed – single turbine.

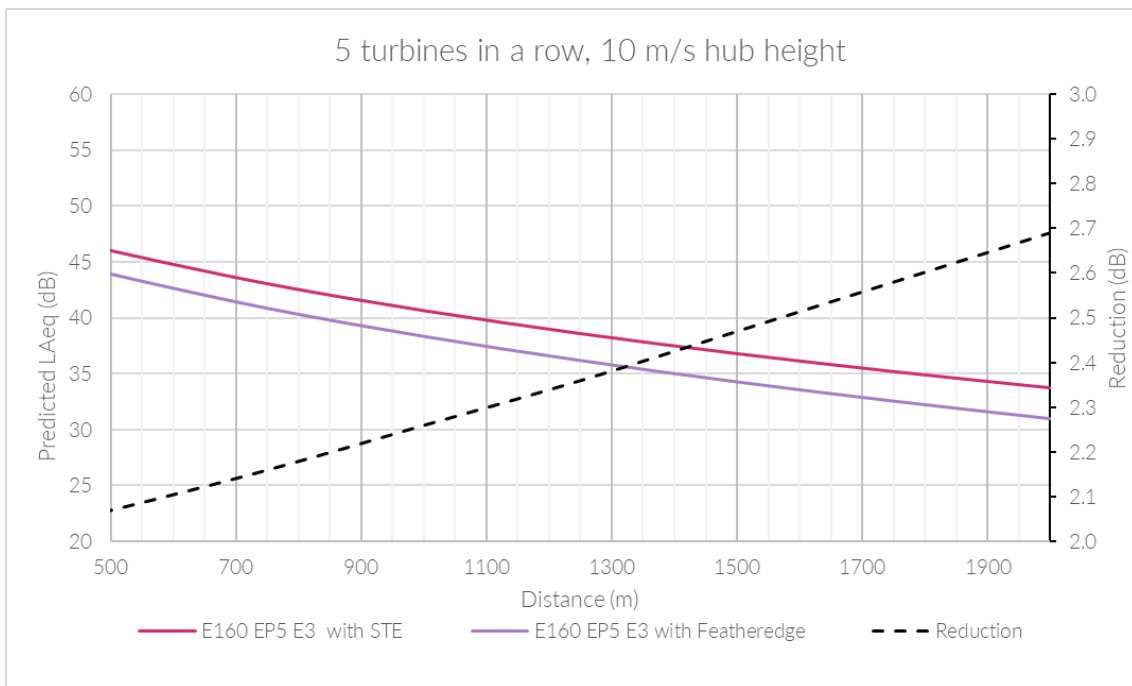


Figure 15 - Comparison of predicted L_{Aeq} levels at different distances for the Enercon E-160 EP5 E3 turbine with different blade additions – 10 m/s hub height wind speed – five turbines row.



Figure 16 - Comparison of predicted L_{Aeq} levels at different distances for the Enercon E-160 EP5 E3 turbine with different blade additions – 12.5 m/s hub height wind speed – single turbine.

Noting the publication by van den Berg *et. al.* [2], a noise reduction of 2 to 3 dB(A) could represent further energy gains of 10 to 15% based on reducing or eliminated noise mitigation if it is required in some cases. The same publication also highlights that, in some cases, the spectral effect of traditional serrations (with a marginal increase in low-frequency content) is such that their effectiveness (in terms of decrease of A-weighted levels) can actually reduce with distance from the turbine due to the same propagation effects. The following tables show the differences of propagation impact with varying distances and simulation setup.

Table 5: Propagation results of predicted L_{Aeq} levels at different distances for the Enercon E-160 EP5 E3 turbine with different blade additions – 8.5 m/s.

Receptor Distance (m)	Single turbine: Baseline	Single turbine: FeatherEdge	Difference	5 turbines in a row: Baseline	5 turbines in a row: FeatherEdge	Difference
500	41.9	40.0	-1.9	45.3	43.4	-1.9
800	37.2	35.2	-1.9	41.9	39.9	-2.0
1000	34.7	32.7	-2.0	39.9	37.9	-2.1
1100	33.7	31.6	-2.0	39.1	37.0	-2.1
1500	30.0	27.9	-2.2	36.0	33.8	-2.2
2000	26.6	24.3	-2.3	32.9	30.6	-2.4

Table 6: Propagation results of predicted L_{Aeq} levels at different distances for the Enercon E-160 EP5 E3 turbine with different blade additions – 10 m/s.

Receptor Distance (m)	Single turbine: Baseline	Single turbine: FeatherEdge	Difference	5 turbines in a row: Baseline	5 turbines in a row: FeatherEdge	Difference
500	42.5	40.5	-2.0	46.0	43.9	-2.1
800	37.8	35.7	-2.1	42.5	40.4	-2.2
1000	35.4	33.2	-2.2	40.6	38.4	-2.3
1100	34.4	32.1	-2.2	39.8	37.5	-2.3
1500	30.8	28.4	-2.4	36.8	34.3	-2.5
2000	27.3	24.7	-2.7	33.7	31.0	-2.7

Table 7: Propagation results of predicted L_{Aeq} levels at different distances for the Enercon E-160 EP5 E3 turbine with different blade additions – 12.5 m/s.

Receptor Distance (m)	Single turbine: Baseline	Single turbine: FeatherEdge	Difference	5 turbines in a row: Baseline	5 turbines in a row: FeatherEdge	Difference
500	42.4	41.4	-1.0	45.8	44.9	-1.0
800	37.6	36.7	-1.0	42.3	41.4	-1.0
1000	35.1	34.2	-1.0	40.4	39.4	-1.0
1100	34.1	33.1	-1.0	39.6	38.5	-1.0
1500	30.5	29.4	-1.1	36.5	35.4	-1.1
2000	27.1	25.8	-1.2	33.4	32.2	-1.2

Some measurements at different distances from 500 to 1500 m from the turbine are being tested, further than the sound power test in accordance with IEC 61400-11 described in Section 2. At the time of writing, these measurements were not complete and ready to analyse as work is ongoing. Further results may however be produced in due course. What will follow is an analysis of the measured far-field values with those produced in Section 2 and a discussion.

4. Conclusions

The present study investigated the acoustic impact of the FeatherEdge® technology of Biome Renewables on two turbines with different rotor sizes, generator outputs, and initial blade conditions. The Senvion MM92 is a 2.05MW turbine with 92m rotor diameters and 80m hub height, displaying an older blade profile and no initial OEM serration, whereas the Enercon E160 EP5 E3 is a modern wind turbine of 5.6MW, a rotor diameter of 160m, hub height of 166m and a modern blade profile equipped with the standard OEM state-of-the-art serrations. Between the two machines, one can notice the frequency peak at full load (10m/s) of the Senvion machine to be at 500Hz (101.2 dB), whereas the Enercon machine has a frequency peak at 2000Hz (101.8 dB). One can compare the two IEC results at

full load (HH 10m/s) to conclude that the Enercon test outperformed the Senvion test campaign, giving in this case 2.1 dB(A) reduction compared to virtually no gain, especially considering that standard OEM serrations give 2.0 dB(A) of benefit. The reasons for this are potentially due to microphone location differences, blade misalignment, and environmental differences in the two tests. But this doesn't tell the whole story, as the frequency shift and reductions seen in the lower frequency bands (below 1000Hz) are more pronounced on the Senvion MM92 test campaign with FES. As such, the impact at far-field locations is made up to a certain degree. The reduction at 2km is 3.1 dB(A) in the five-turbine simulation for the MM92 test, whereas the same Enercon simulation delivers 2.7 dB(A) (4.7 dB(A) if compensated for starting from a bare blade). This underscores the importance of reducing noise in frequencies below 1000Hz, and especially around 125-500Hz, which has historically been hard to achieve. The FES technology achieves this in both cases, signalling broad applicability for the market in reducing noise at the all-important location of the receptor.

Acknowledgments

The authors would like to thank Nergica Test Center and Schierloh Engineering GmbH for hosting the test campaigns.

References

- [1] https://www.verwaltungsvorschriften-im-internet.de/bsvwvbund_26081998_IG19980826.htm.
- [2] F. van den Berg, E. Koppen, J. Boon, M. Ekelschot-Smink, "Sound power of onshore wind turbines and its spectral distribution," *Sound & Vibration*, p. 17 59(1): 1716. 2025.
- [3] International Electrotechnical Commission (2018), IEC 61400-11:2021+A1:2018: Wind turbines - Part 11: Acoustic noise measurement techniques.
- [4] International Standards Organisation (2024), ISO 9613-2:2024 'Acoustics – Attenuation of sound during propagation outdoors – Part 2: Engineering method for the prediction of sound pressure levels outdoors'.

Paper #26 - ID: 360

Title: Acoustic and SCADA data for the wind turbine noise level estimation

Author: Abdelazyz Rkhiss

11th Edition of the
International Conferences on
Wind Turbine Noise
Copenhagen, Denmark – 10th to 13th June 2025

Impact of environmental data on wind turbine noise level estimation

A. RKHISS¹, A. FINEZ, J-R. GLOAGUEN.

Engie Green, Lyon, 69007, France

G. VASIELE

GIPSA-Lab, Grenoble-INP UGA, Grenoble, 38000, France

J. MAILLARD

CSTB, Grenoble, 38000, France

Summary

Wind energy is one of the most widely used renewable energy sources in the world and has grown rapidly in recent years. However, wind turbines generate noise that is often perceived as a disturbance by nearby residents. So, developing tools to assist wind farm developers and regulatory authorities is essential. This study focus on the impact of environmental data on wind turbine noise (WTN) level estimation using recurrent neural networks (RNNs). We compare the performance of an architecture which is based on long-short term memory cells (LSTM). LSTM model trained using only acoustic features in the frequency range of 31.5 Hz to 2 kHz with those incorporating additional environmental features, such as wind speed and wind turbine power accorded to each wind speed value. The results highlight the influence of these factors on noise characterization and demonstrate the extent to which environmental data enhances WTN level estimation.

1. Introduction

The noise generated by wind turbines has raised concerns among residents living near wind farms, as it can negatively impact sleep quality and overall well-being [1]. With the increasing size of modern wind turbines, noise issues have become more significant, prompting several countries, including France, to implement strict regulatory standards to control wind turbine noise (WTN) emissions. These regulations define emergence as the difference between the total noise level during wind turbine operation and the background noise level when the turbines are inactive. Compliance requires that emergence does not exceed 5 dB(A) during the day and 3 dB(A) at night if the total noise is exceeding 35 dB(A).

An on/off strategy for wind turbines is commonly used to verify a curtailment plan employed to reduce noise emissions. This plan is implemented to limit the noise impact of wind farms and ensure regulatory conformity. During the operational phase, it is verified through measurements taken during start/stop cycles of the wind farm. However, these measurements have several drawbacks. Their limited duration does not always reflect the variability of residual noise. They are also costly, as they require shutting down the

¹abdelazyz.rkhiss@grenoble-inp.fr

turbines. Additionally, depending on the situation, they may lead to excessive or insufficient curtailment of the wind farm.

Several methods have been explored to address this issue. For instance, Gloaguen et al. [2] proposed a non-negative matrix factorization (NMF)-based approach to estimate WTN levels. Despite promising results in some cases, the uncertainty of the method prevents its deployment on an industrial scale. Consequently, we are moving towards the use of deep neural networks, given their success in the field of source separation [3], sound classification [4] and sound event detection [5]. Anicic et al. [6] applied Support Vector Regression (SVR) to predict WTN levels from acoustic and wind speed data, confirmed the importance of integrating environmental data, such as wind speed, to increase the accuracy of prediction models.

The method presented in this paper uses Recurrent Neural Networks (RNNs) for WTN level estimation from total noise monitoring. RNNs proved their effectiveness in extracting features from acoustic scenes[7], and handling long-term dependencies in sound patterns. These models are well-suited for capturing the temporal dynamics and sequential nature of acoustic data, making them good candidates for extracting WTN level from total noise.

Section 2 provides a comprehensive overview of the methodology, beginning with the dataset construction process, from background noise measurements and WTN synthesis, and environmental data description. Section 3 then outlines the data preprocessing steps, provides an explanation of the LSTM cell, and introduces the proposed architecture along with the evaluation metrics and optimization algorithm. The experimental results are discussed in the final section, Section 4.

2. Dataset

To train the supervised LSTM model, it is crucial to have an appropriate training dataset. The dataset includes the time series of the total noise level, L_{TN} as input, while the overall sound pressure level of wind turbine noise, L_{WTN} , serves as the output (label). Both time series consist of one-second equivalent noise levels, measured in third-octave bands ranging from 31.5 Hz to 2 kHz. The levels are expressed in A-weighted decibels (dB(A)).

Measuring L_{WTN} during recordings presents a challenge due to the presence of background noise from various sources that cannot be isolated. To create realistic soundscapes, a hybrid approach combining measurement and sound synthesis is adopted. This method used a background noise measured at a development site during an initial state (2.1), ensuring consistency with wind measurements taken at a height of 81 meters. This background noise combines with a generated WTN based on wind speed measurements and machine specifications (see Subsection 2.2).

2.1 Background noise measurements

Background noise levels were measured in third-octave bands, sampled at a one-second resolution to provide a detailed representation of the sound environment, in line with the capabilities of sound level meters. These measurements are accompanied by wind speed data recorded over 10-minute intervals. Fig. 1 presents a sample of the measured Background noise levels in dB(A).

2.2 Wind turbine noise synthesizing

The estimation of sound power levels (L_W) for wind turbines relies on the Machine Specifications (MS) document, which provides octave-band values in dB(A) for various wind speeds, typically following the ISO 61400-11 standard procedure. As a choice for this study, a 2 MW industrial turbine with a 90 m diameter is used, with L_W values specified for wind speeds ranging from 3 to 25 m/s. To obtain time-varying L_W values, the recorded 10-minute wind speed measurements are used to linearly interpolate the corresponding

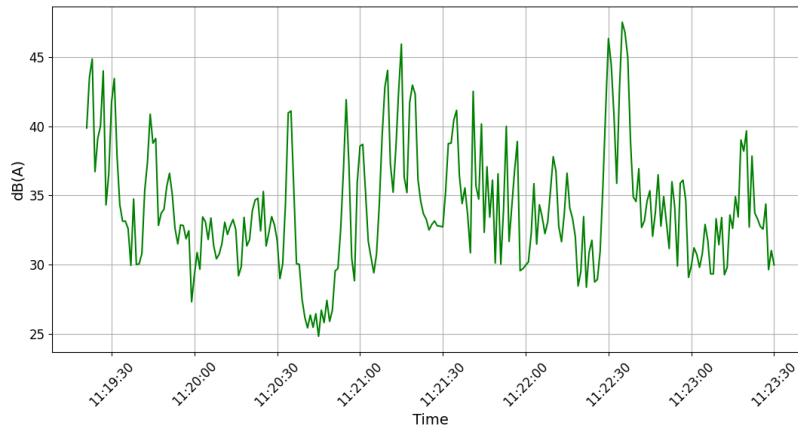


Figure 1 The overall SPL of the measured background noise sample (L_{BN}).

sound power levels from the MS. This process allows for obtaining $L_w(F, T)$ in octave bands (F) for each 10-minute interval (T). An up-sampling procedure is then applied to convert these results ($L_w(F, T)$) into third-octave bands (f), yielding $L_w(f, T)$. This conversion simply serves to bring different data sources onto the same frequency basis. The next step involves adjusting the sampling frequency of the signal from 10-minute intervals to one second by applying zero-padding. This ensures compatibility with the desired sampling frequency using an up-sampling ratio of 1/600, ultimately obtaining $L_w(f, t)$ in third-octave bands per second (t). Fig. 2 illustrates the complete process for generating time series of acoustic power for the WTN component.

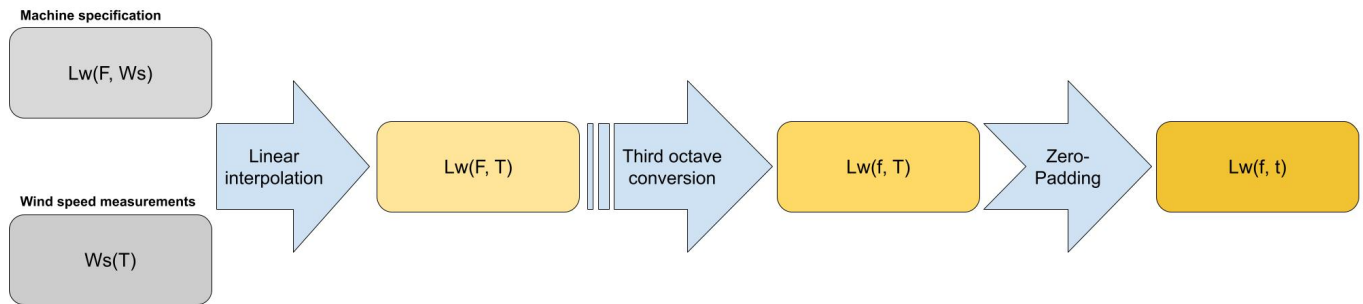


Figure 2 Flowchart illustrating the step-by-step process for obtaining time series of acoustic power levels. The process starts with machine specifications and wind speed measurements, followed by linear interpolation to estimate $L_w(F, T)$. A third-octave conversion, and zero-padding is applied to resample the data to a third octave bands and one-second resolution, resulting in $L_w(f, t)$.

The sound pressure level of the WTN (L_{WTN}) is computed for a simplified scenario in which a wind farm consists of a single wind turbine. This level is determined at the receiver point by applying an acoustic propagation filter. The filter is based on solving the parabolic equation, a physical propagation model that accounts for various parameters such as ground impedance, sound speed gradient, geometric divergence, atmospheric absorption, and an extended wind turbine source model [8]. These filters were previously used in a study by Gloaguen et al. [2]. Fig. 3 illustrates attenuation filters for three different distances, based on a simplified assumption and moderately favorable propagation conditions. However, these propagation assumptions are highly simplified, as in reality, propagation filters continuously vary due to factors such as atmospheric turbulence.

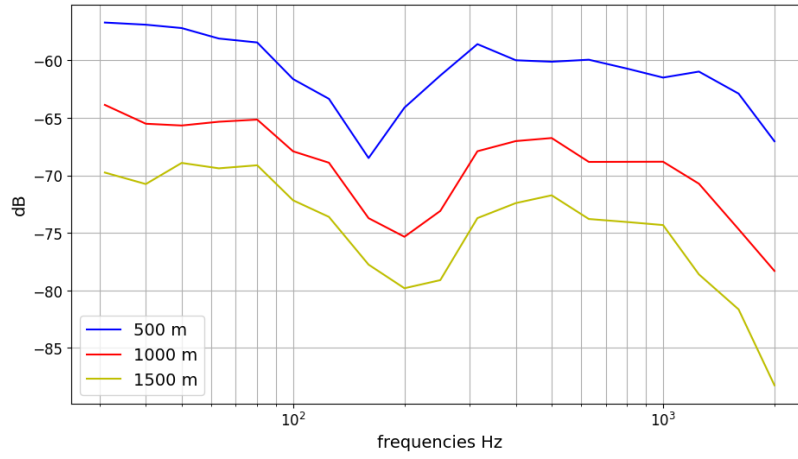


Figure 3 Attenuation filters corresponding to distances of 500 m, 1000 m, and 1500 m between the receiver (at a height of 1.5 m) and the wind turbine under moderately favorable propagation conditions.

2.3 Total noise

The total noise SPL (L_{TN}) is obtained by summing the synthesized L_{WTN} with the background noise L_{BN} , as follows:

$$L_{TN} = L_{WTN} \oplus L_{BN}, \quad (1)$$

where \oplus represents the energetic summation of decibels. Finally, a dataset is produced, consisting of time series of L_{TN} and L_{WTN} for each location at 3 distances from the turbine.

2.4 Environmental data

For simplification purposes, we have defined the electrical production data and wind speed as environmental variables. The wind speed is interpolated with a temporal resolution of one second and integrated as an input into the LSTM model. The wind turbine's electrical production, which depends on wind speed, is used alongside acoustic data for model training. This integration accounts for the impact of wind speed on generated noise and considers the correlation between energy production and wind conditions. Fig. 4 presents a sample of wind speed recorded per second, derived from measurements taken every 10 minutes. It also displays the corresponding electrical production in kW over time, illustrating the correlation between wind speed variations and power generation.

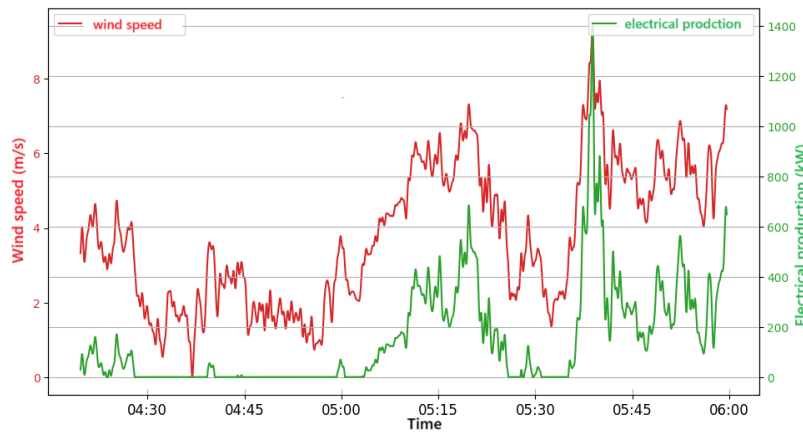


Figure 4 Time series of wind speed (in m/s, red) and electrical production (in kW, green) over a period of approximately 1.5 hours. The wind speed data is interpolated at a resolution of one second, while the electrical production corresponds to the turbine's response to varying wind speed.

3. Methodology

3.1 Data preprocessing

The features used for training include total noise (31 Hz to 2 kHz in dB(A)), electrical production, and wind speed, which have significantly different scales (0-25 m/s for wind speed and 0-2000 kW for production). Normalization is required to harmonize the amplitudes, prevent certain variables from dominating, and enhance the model's convergence, and stability.

To ensure optimal convergence and prevent the disproportionate influence of features with large dynamic ranges, Z-score normalization [9] is applied. This technique scales all features to the same range, promoting balanced and efficient learning.

The input data, denoted as $X_{i,k}$, are standardized using Z-score normalization to produce $X_{i,k}^{\text{std}}$:

$$X_{i,k}^{\text{std}} = \frac{X_{i,k} - \mu_k}{\sigma_k}, \quad (2)$$

where:

- $\mu_k = \frac{1}{N} \sum_{i=1}^N X_{i,k}$ is the mean of feature k ,
- $\sigma_k = \sqrt{\frac{1}{N} \sum_{i=1}^N (X_{i,k} - \mu_k)^2}$ is its standard deviation,
- N is the total number of samples.

Fig. 5 illustrates the impact of Z-score normalization on the wind speed feature (m/s) for our LSTM model. The original wind speed distribution (left plot) shows characteristic right-skewness (mean = 4.89 m/s). Normalization successfully transforms the data to zero mean and unit variance (right plot).

The persistence of skewness post-normalization suggests the feature retains non-Gaussian characteristics, which is inconsequential for RNNs—as they do not assume input normality—but ensures stable gradient updates during training by mitigating scale disparities across features (wind speed, electrical production, acoustic data), without altering the physically meaningful distribution shape of wind speeds. Values extending beyond $Z = +3\sigma$ (corresponding to wind speeds $> \sim 10$ m/s in the original scale) represent high-wind events. While these could be considered statistical outliers, that the LSTM's activation functions and sequential processing can inherently handle such deviations. This preprocessing step is essential to harmonize feature scales without distorting temporal patterns.

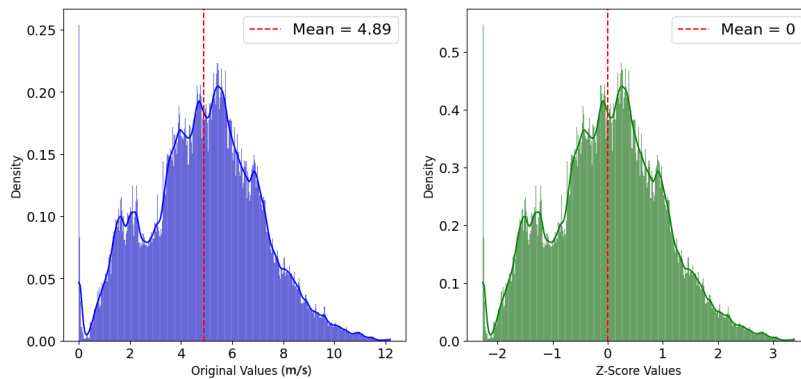


Figure 5 Density distributions of original wind speed values (in m/s) and their z-score normalized ($\mu = 0$, $\sigma = 1$).

3.2 Neural networks

Given the temporal nature of the dataset—comprising total noise, wind speed, and electrical production—where each row represents a specific time step t and the next row corresponds to the following time step $t + 1$, it is beneficial to use Recurrent Neural Networks (RNNs), such as LSTM [10].

3.2.1 LSTM cell

A standard LSTM cell includes three *gates*: the forget gate f_t which determines how much of the previous data to forget; the input gate i_t which evaluates the information to be written into the cell memory; and the output gate o_t which decides how to calculate the output from the current information, calculated from input data x_t and previous hidden state h_{t-1} by a sigmoid function, see Fig. 6.

$$\begin{aligned} i_t &= \sigma(W_i x_t + R_i h_{t-1} + b_i) \\ f_t &= \sigma(W_f x_t + R_f h_{t-1} + b_f) \\ o_t &= \sigma(W_o x_t + R_o h_{t-1} + b_o). \end{aligned} \quad (3)$$

Here, the W , R , and b variables represent the matrices and vectors of trainable parameters. The LSTM unit is defined by

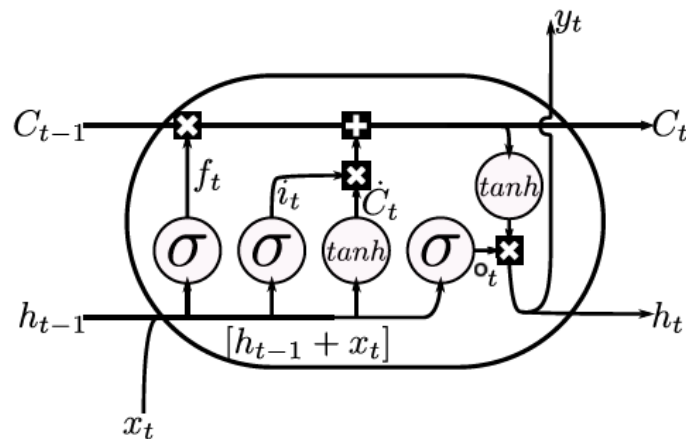


Figure 6 Illustration of a LSTM cell. The diagram represents the flow of information within the cell.

$$\begin{aligned} \dot{C}_t &= \tanh(W_c x_t + R_c h_{t-1} + b_c) \\ C_t &= f_t \odot C_{t-1} + i_t \odot \dot{C}_t \\ h_t &= o_t \odot \tanh(C_t) \\ y_t &= \sigma(W_y h_t + b_y). \end{aligned} \quad (4)$$

In words, the candidate cell state \dot{C}_t is calculated using the input data x_t and the previous hidden state h_{t-1} . The cell memory or current cell state C_t is calculated using the forget gate f_t , the previous cell state C_{t-1} , the input gate i_t and the candidate cell state \dot{C}_t . The Hadamard product \odot is simply the element-wise product of the involved matrices. The output y_t is calculated by applying the corresponding weights (W_y and b_y) to the hidden state h_t .

3.2.2 proposed architecture

In this study, we propose a regression architecture, illustrated in Fig. 7, based on a stack of LSTM layers to predict the global sound pressure level (OASPL) of WTN from the total acoustic spectrogram. The input to the model is a time-frequency representation of the total noise, computed over third-octave bands from 31 Hz to 2 kHz. Each time step contains 19 spectral features, forming a sequence that encodes the acoustic context.

The model begins with two sequential unidirectional LSTM layers, each designed to learn temporal dependencies in the acoustic data. These layers extract relevant sequential features that capture the dynamics of the wind turbine's acoustic behavior. Following the LSTM stack, a non-linear dense layer with ReLU activation is introduced to model complex relationships within the extracted temporal features.

To prevent overfitting and enhance generalization, a dropout layer with a rate of 20% is added. Finally, a custom non-linear output layer with a scaled tanh activation function is employed: $f(x) = 60 \cdot \tanh(x)$. This function constrains the output within a plausible acoustic range, centered on 0. It enables predictions up to 60 dB(A), and allows negative values approaching -60 dB(A), representing situations with no WTN contribution, such as when the turbine is shut down.

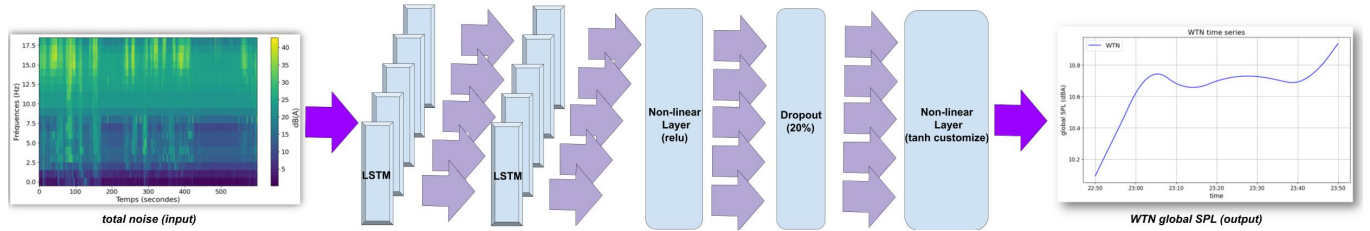


Figure 7 RNN architecture used for the estimation of the OASPL of WTN from total noise spectrograms.

3.3 Evaluation Metrics and Optimization

The Mean Absolute Error (MAE) is selected as the evaluation metric for assessing the performance of the RNN model during training. The MAE quantifies the average magnitude of the errors between the predicted particular noise level \hat{L}_{WTN} and the actual value L_{WTN} in dB(A), and is defined as follows:

$$MAE = \frac{1}{N} \sum_{i=1}^N |L_{WTN_i} - \hat{L}_{WTN_i}|. \quad (5)$$

To improve robustness against outliers (highly variable noise conditions), the Huber loss function is adopted as the objective function for training, which combines Mean Squared Error (MSE) for small residuals and Mean Absolute Error (MAE) for larger residuals:

$$L_{\delta}(L_{WTN}, \hat{L}_{WTN}) = \begin{cases} \frac{1}{2}(L_{WTN} - \hat{L}_{WTN})^2, & \text{for } |L_{WTN} - \hat{L}_{WTN}| \leq \delta \\ \delta(|L_{WTN} - \hat{L}_{WTN}| - \frac{1}{2}\delta), & \text{otherwise} \end{cases} \quad (6)$$

where δ is a threshold controlling the transition between quadratic and linear behavior.

The derivative of the Huber loss with respect to the model predictions \hat{L}_{WTN} is quadratic for small residuals and linear for larger ones. This ensures smooth and stable gradients in the presence of clean data, while limiting the influence of outliers through a reduced gradient response for large errors. Such behavior facilitates efficient and robust optimization using gradient-based algorithms. To minimize the loss function, we use the Adam optimizer, which updates the model parameters θ iteratively as follows:

$$\theta = \theta - \eta \cdot \nabla_{\theta} \mathcal{L}_{\delta}. \quad (7)$$

Here, $\nabla_{\theta} \mathcal{L}_{\delta}$ denotes the gradient of the Huber loss with respect to the model parameters θ , and η is the learning rate.

4. Results and Discussion

This section presents the experimental results obtained on the test set using two distinct architectures. The first architecture relies solely on acoustic data (19 features), while the second includes two additional variables—wind speed and power generation—bringing the total number of input features to 21.

The prediction performance of both input configurations is evaluated on the test set using the *MAE*, as presented in Table 1. The results highlight the impact of including environmental variables (wind speed and power generation) on the model’s accuracy.

Table 1 Comparison of prediction performance (*MAE*) and loss function (*Huber*) on the test set with and without environmental data.

Test Set Configuration	Loss function dB(A)	MAE dB(A)
Without environmental data	1.86	0.72
With environmental data	0.84	0.26

The results present a significant improvement in prediction accuracy when environmental variables, wind speed and power generation, are included in the model. Both MAE and loss function show substantial reductions, from an MAE of 0.72 dB(A) to 0.26 dB(A), and from a loss of 1.86 dB(A) to 0.84 dB(A). This indicates that the addition of environmental data enhances the model’s ability.

Fig. 8 compares the predicted WTN results obtained using two input configurations: with (left) and without (right) environmental data. The real WTN levels (L_{WTN}) and the predicted ones (\hat{L}_{WTN}) are plotted alongside the real and predicted background noise levels (L_{BN} and \hat{L}_{BN}), with the total noise (L_{TN}) in red.

The left panel shows that when wind speed and power generation are incorporated into the model, the predicted WTN signal closely aligns with the actual measurements. The predicted \hat{L}_{WTN} almost perfectly overlaps with the real L_{WTN} , confirming the model’s ability to accurately capture WTN dynamics. This also enables precise estimation of background noise (\hat{L}_{BN}) through decomposition from the total noise.

In contrast, the right panel shows the model performance using only acoustic features. Here, slight deviations between predicted and real WTN are visible, particularly during fluctuations in total noise. These discrepancies propagate to the estimated background noise, as seen in the divergence between real and predicted L_{BN} .

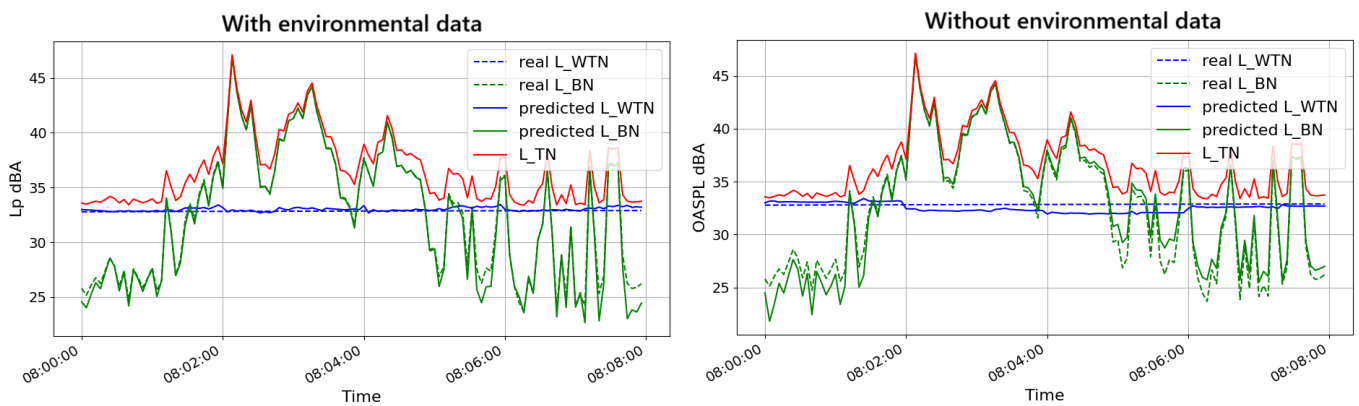


Figure 8 Comparison of predicted wind turbine noise with and without environmental data. Left: model using acoustic and environmental features. Right: model using only acoustic features.

To better visualize the impact of including environmental data, we compare the ground truth WTN OASPL with the predicted WTN using two model configurations. As shown in Fig. 9, the blue curve represents the ground truth, while the red and black curves correspond to the model predictions with and without environmental data, respectively.

The model incorporating environmental inputs (red curve) demonstrates a strong ability to follow the underlying trend of the ground truth. It closely captures both the gradual rise and the eventual plateau of the WTN signal.

In contrast, the model without environmental data (black curve) exhibits higher variance and abrupt fluctuations that deviate significantly from the actual trend. This erratic behavior—especially noticeable during the mid and late intervals—highlights the model’s limited capacity to infer WTN characteristics based only on acoustic features in this test set sample, with an observed error trend of approximately ± 0.5 dB(A).

This comparison reinforces the earlier observation that environmental data leads to more stable and reliable predictions of WTN.

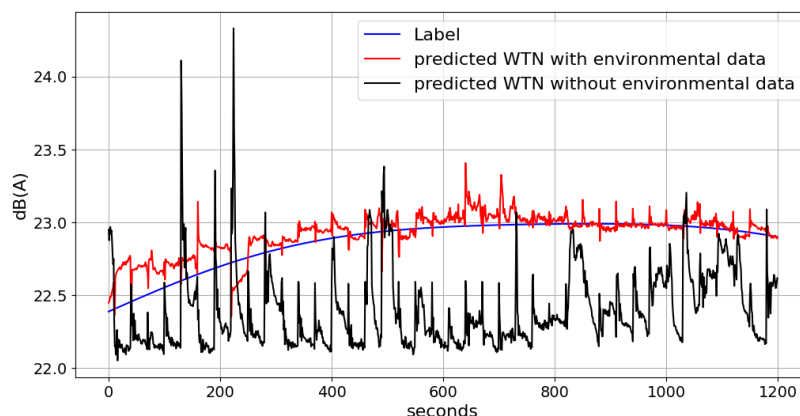


Figure 9 Comparison of WTN OASPL prediction using models with (red) and without (black) environmental data. The blue curve shows the ground truth label.

5. Conclusion

In this work, we proposed and evaluated an LSTM-based sequence-to-sequence (seq2seq) model for estimating wind turbine noise (WTN) levels from acoustic measurements, with particular attention to the role of environmental data. Our findings demonstrate the capability of recurrent neural networks (RNNs) to learn meaningful patterns from acoustic signals, yielding robust performance even under challenging conditions with high WTN levels. While both model configurations showed promising results, the inclusion of environmental variables led to significantly more accurate predictions. This performance gap highlights the importance of contextual information in capturing the temporal and spectral dynamics of WTN signals. To improve robustness, a customized output activation function was adopted along with the Huber loss, which effectively handles outliers and stabilizes training.

For future work, we aim to develop more realistic and diverse simulated WTN datasets to better train and evaluate the models. This includes incorporating additional environmental variables, generating complex and varied acoustic scenes using advanced wind turbine noise models, and leveraging more sophisticated deep learning architectures such as attention mechanisms and convolutional neural networks (CNNs). These enhancements are expected to enable a deeper investigation and comparison of existing deep learning techniques applied to WTN level estimation from acoustic input data.

References

- [1] A. Freiberg, C. Schefter, M. Girbig, V. C. Murta, and A. Seidler, “Health effects of wind turbines on humans in residential settings: Results of a scoping review,” *Environmental Research*, vol. 169, pp. 446–463, Feb. 2019.
- [2] J.-R. Gloaguen, D. Ecoti re, B. Gauvreau, A. Finez, A. Petit, and C. Bourdat, “Automatic estimation of the sound

- emergence of wind turbine noise with nonnegative matrix factorization,” *The Journal of the Acoustical Society of America*, vol. 150, pp. 3127–3138, Oct. 2021.
- [3] P.-S. Huang, M. Kim, M. Hasegawa-Johnson, and P. Smaragdis, “Deep learning for monaural speech separation,” in *2014 IEEE International Conference on Acoustics, Speech and Signal Processing (ICASSP)*, pp. 1562–1566, May 2014.
- [4] C. Zhang, H. Zhan, Z. Hao, and X. Gao, “Classification of Complicated Urban Forest Acoustic Scenes with Deep Learning Models,” *Forests*, vol. 14, p. 206, Jan. 2023.
- [5] A. Gorin, N. Makhazhanov, and N. Shmyrev, *DCASE 2016 Sound Event Detection System Based on Convolutional Neural Network*. Sept. 2016.
- [6] O. Anicic, D. Petković, and S. Cvetkovic, “Evaluation of wind turbine noise by soft computing methodologies: A comparative study,” *Renewable and Sustainable Energy Reviews*, vol. 56, pp. 1122–1128, Apr. 2016.
- [7] S. Mun, S. Shon, W. KIM, D. Han, and H. ko, “A Novel Discriminative Feature Extraction for Acoustic Scene Classification Using RNN Based Source Separation,” *IEICE Transactions on Information and Systems*, vol. E100.D, pp. 3041–3044, Dec. 2017.
- [8] B. Cotté, “Extended source models for wind turbine noise propagation,” *The Journal of the Acoustical Society of America*, vol. 145, pp. 1363–1371, Mar. 2019.
- [9] J. Han, M. Kamber, and J. Pei, *Data Mining: Concepts and Techniques*. Elsevier, 3rd ed., June 2011.
- [10] S. Hochreiter and J. Schmidhuber, “Long short-term memory,” *Neural computation*, vol. 9, no. 8, pp. 1735–1780, 1997.

Paper #27 - ID: 361

Title: Aeroacoustic investigation into the X-Rotor vertical-axis wind turbine using lattice-Boltzmann very large eddy simulation (LB-VLES)

Author: Yan Wu

11th Edition of the
International Conferences on
Wind Turbine Noise
Copenhagen, Denmark – 10th to 13th June 2025

Aeroacoustic investigation into the X-Rotor vertical-axis wind turbine using lattice-Boltzmann very large eddy simulation (LB-VLES)

Yan Wu, Daniele Ragni, Damiano Casalino, and Frits de Prenter¹
Delft University of Technology, Faculty of Aerospace Engineering, The Netherlands

Francesco Avallone
Polytechnic University of Turin, Department of Mechanical and Aerospace Engineering, Italy

Summary

In this contribution, we present the results of an investigation into the aeroacoustic performance of the X-Rotor concept. High-fidelity numerical computational fluid dynamic (CFD) simulations have been carried out using the Lattice-Boltzmann Very Large Eddy Simulation (LB-VLES) solver 3DS PowerFLOW. The assessment initially focused on aerodynamic performance and surrounding flow fields to validate the numerical model. Subsequently, the aeroacoustic performance at various observer locations was determined using the solid formulation of the Ffowcs Williams & Hawkings (FW-H) acoustic analogy. Results suggest that the tonal noise originating from interactions between the lower blades and the secondary rotor dominates the low-frequency noise emitted by the X-Rotor. Additionally, the broadband noise generated by the secondary rotors is the primary source of high-frequency noise. The considerably high noise level generated by the current baseline concept of X-Rotor suggests the need to optimize the current design to mitigate noise in the future.

1. Introduction

The X-Rotor (X-shaped Radical Offshore wind Turbine for Overall cost of energy Reduction) is an offshore wind turbine concept developed in a Horizon 2020 project with participants: University of Strathclyde, Norwegian University of Science and Technology, Delft University of Technology, University College Cork, Fundacion Cener National Renewable Energy Centre, and GE Renovables España [1]. This document is largely based on deliverable D2.9 [2].

As the impacts of climate change become increasingly apparent, offshore wind energy is a crucial factor in reducing CO₂ emissions. However, to reach the CO₂ reduction goals, the cost of offshore wind energy must be lowered. The X-Rotor concept offers a direct approach to significantly cutting offshore wind energy's capital and operational costs.

The X-Rotor is a large-scale vertical-axis wind turbine concept, designed to reduce both the capital and operating costs of energy from offshore wind. As illustrated in Fig. 1, it comprises two primary blades forming an approximate x-shape (which extract power from the wind similar to standard vertical-axis wind

¹Corresponding author - Email: F.dePrenter@tudelft.nl

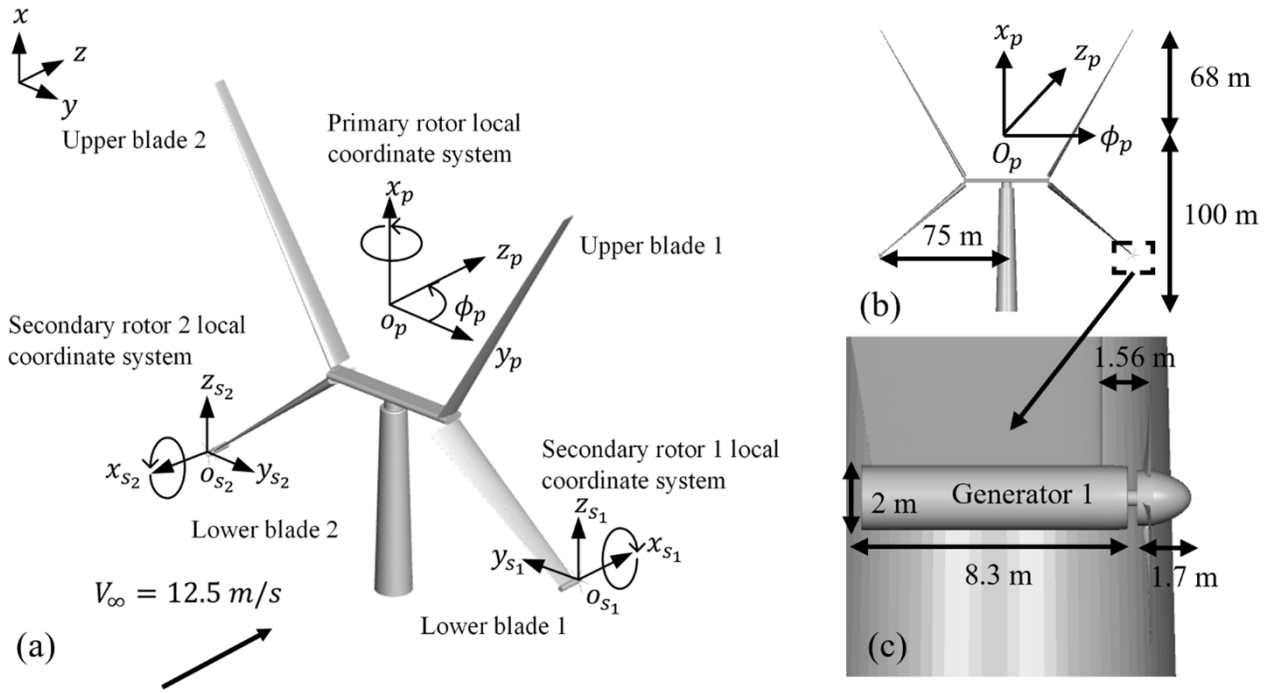


Figure 1 The baseline concept of the X-rotor, with reference frames, coordinate systems, and dimensions.

turbines) and two secondary horizontal-axis rotors placed at the lower ends of these primary blades. Instead of a generator connected to the vertical axis, energy is harvested from these secondary rotors, which are powered by the induced velocity of the primary blades. These secondary rotors are directly coupled to a generator, which omits the requirement of a gearbox. Furthermore, compared to conventional designs, maintenance-intensive components (such as moving parts/bearings/generators) are placed closer to the sea level to reduce the cost of maintenance. More information about the X-Rotor can be found [1].

This contribution presents a high-fidelity CFD study of the aerodynamics and a first investigation into the aeroacoustics of the X-Rotor concept. The document is structured as follows: Section 2 provides a detailed description of the simulation setup. Section 3 presents the simulation results. Section 4 summarizes and concludes the work.

2. Geometry and numerical setup

2.1 Wind-turbine Geometry

Fig. 1 illustrates the baseline concept of the X-rotor. The primary rotor forms an "X"-shape, and two secondary rotors are fixed 1.56 m in front of the leading edge at the bottom of the primary blades. Both secondary rotors are directly connected to a generator inside the primary rotor blade. The primary rotor has a radius $R_t^{(p)} = 75$ m. It consists of upper and lower blades of, respectively, 100 m and 65 m long, coning angles of 30° and 50° , NACA 0025 and NACA 0008 airfoil profiles, and no twist or pitch angles for either primary blades. From the blade roots to the tips, the chords of the primary blades reduce linearly: from $c_p^{(u)} = 10$ m to 5 for the upper blade and from $c_p^{(l)} = 14$ m to 7 m for the lower blade. The secondary rotor employs five blades with a FFA-W3-241 airfoil profile, has a radius $R_t^{(s)} = 4.69$ m, and a twist angle and chord length (c_s) given in Fig. 2.

As indicated in Fig. 1, three rotating coordinate systems (Local Reference Frames, LRF) are employed. First, a LRF is employed for the primary rotor, which rotates around the x_p -axis at a (fixed) speed of $\Omega_p = 0.833$ rad/s (tip Mach number of 0.19). The rotational center is denoted by O_p and is set 100 m above sea level.

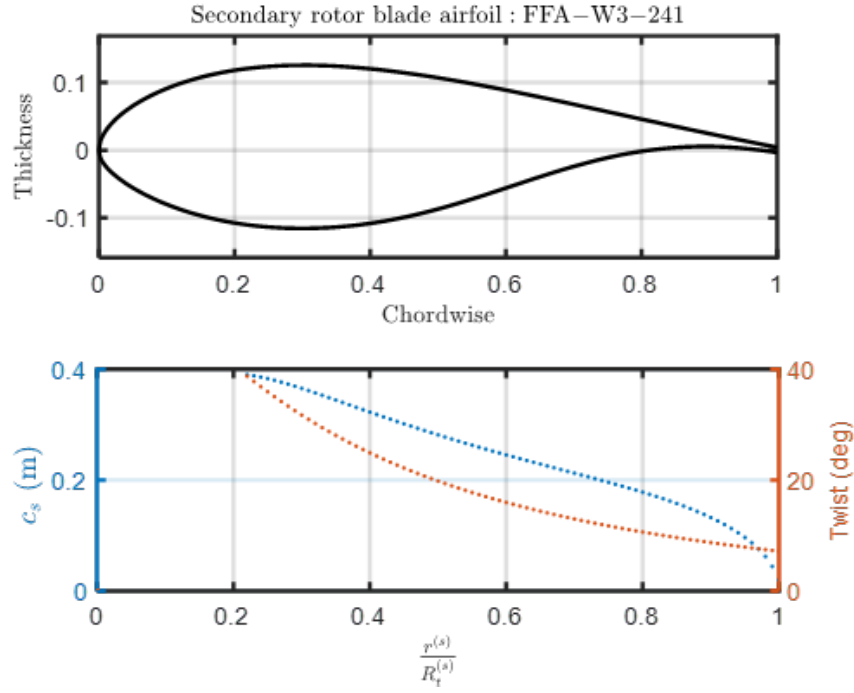


Figure 2 Secondary rotor.

Second, two LRFs are placed inside the primary LRF for the secondary rotors, which rotate around the x_{s_1} and x_{s_2} -axes, respectively. The secondary LRFs rotate with a (fixed) speed of $\Omega_s = 43.06$ rad/s (tip Mach number of 0.59). The freestream velocity in the direction of the z-axis of the global coordinate system is $V_\infty = 12.5$ m/s.

2.2 Simulation domain

Fig 3 presents the simulation domain. The center of the primary LRF (O_p) is $18.5R_t^{(p)}$ from the inlet and $37R_t^{(p)}$ from the sides and the outlet. A spherical-shaped acoustic sponge is implemented, which (artificially) gradually increases the fluid's bulk viscosity starting at $4.7R_t^{(p)}$, in order to minimize the backward reflection of the acoustic waves from the outer boundary. An inflow velocity V_∞ , turbulent intensity $I = 10.2\%$, and turbulent length scale $L = 145$ m are applied as boundary conditions at the inflow (see [3] for the details of evaluating the turbulence parameters). Slip wall boundary conditions are applied at the sides, and an ambient pressure $p_\infty = 1.00125 \cdot 10^5$ Pa is applied as boundary condition at the outflow.

Fig. 4 shows the 15 different Variable Resolution (VR) regions employed (the grid size varies a factor 2 between subsequent regions), with the coarsest resolution VR0 ($\delta x = 156$ m) far away from the turbine and with the finest resolution VR14 ($\delta x = 9.525 \cdot 10^{-3}$ m) employed as an offset of the secondary rotor blades. The mesh size of VR14 generates approximately 50 voxels along the mean chord (c_s) of the secondary rotor blade, and results in a time step in the finest VR of $6.4 \cdot 10^{-6}$ s and a y^+ value of approximately = 1000. The fine equivalent number of voxels of the complete setup is 23.5 million. While the fine equivalent number of voxels is not excessively large, the relatively long physical simulation time required to cover the rotation of the primary rotor still results in a computational cost of $4.9 \cdot 10^4$ CPU hours/revolution on a 480 cores cluster (Linux Xeon® Gold 6148 2.4GHz Platform). Two coarser meshes are similarly created to perform a convergence study. Table 1 provides the details of these meshes.

The fine and the medium resolution simulations are initialized with the result of the coarse resolution simulation. Fig. 5 presents the time-averaged tangential force during a rotation for subsequent rotations of the primary rotor. From this result, it is concluded that the flow reaches a converged state after 7 rotations. After these 7 revolutions, the sampling of pressure starts on the solid surfaces. The surface pressures are sampled for 2 rotations of the primary rotor to calculate far-field acoustics. The far-field acoustics are

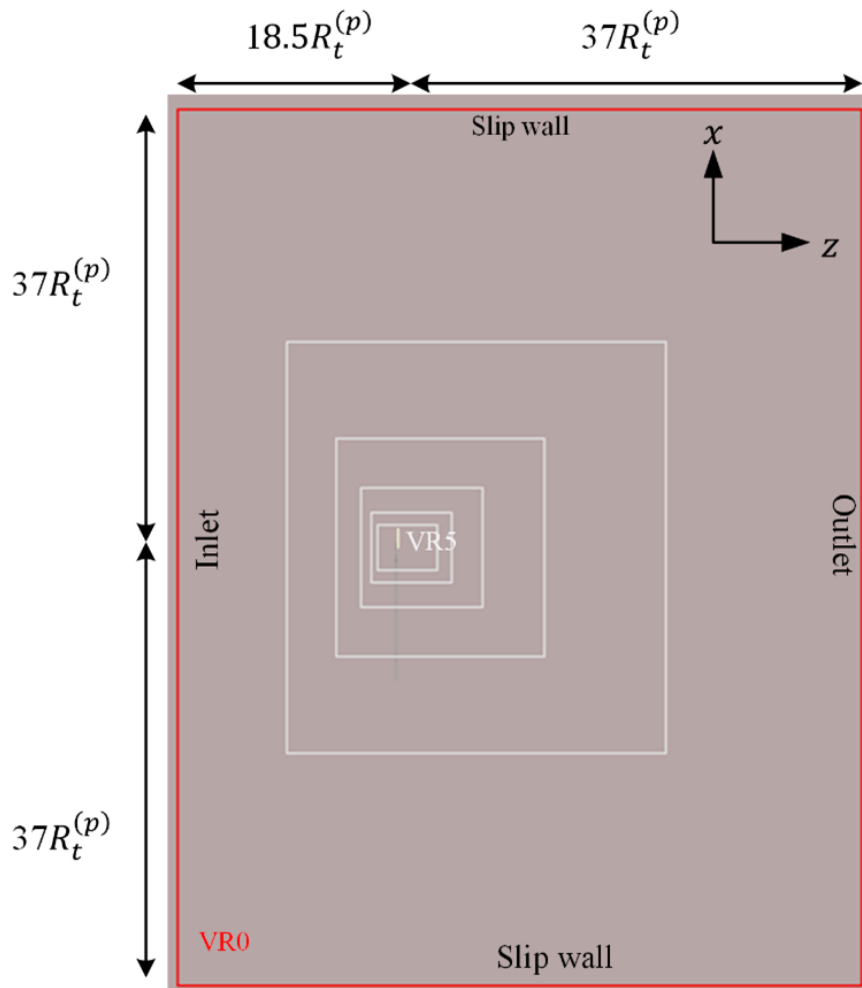


Figure 3 Side view of the simulation domain.

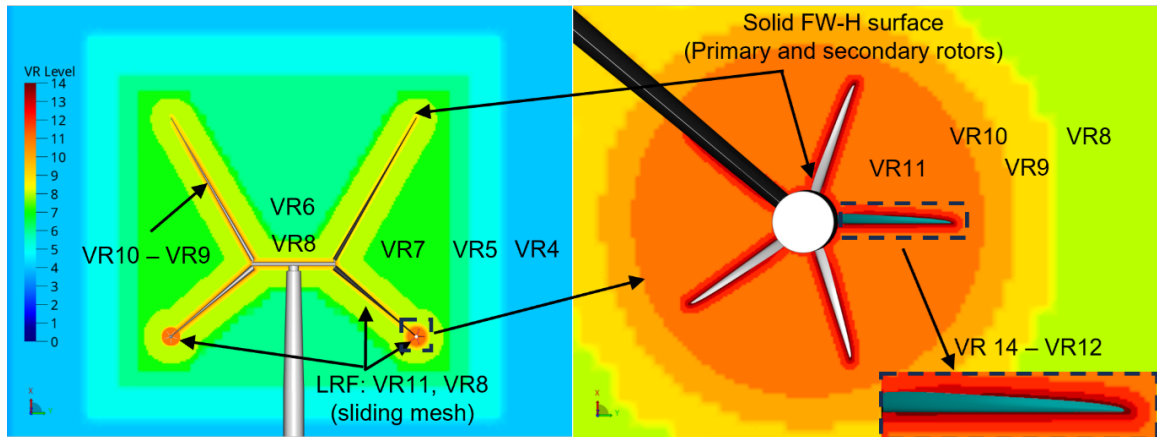


Figure 4 Distribution of VR regions.

Table 1 Employed meshes.

Type	Resolution $c_s/\delta x, y^+$	Fine equivalent voxels	CPU hours per revolution
Coarse	25, $y^+ = 2000$	8.2 million	9.57×10^3
Medium	35, $y^+ = 1410$	14.5 million	2.33×10^4
Fine	50, $y^+ = 1000$	23.5 million	4.88×10^4

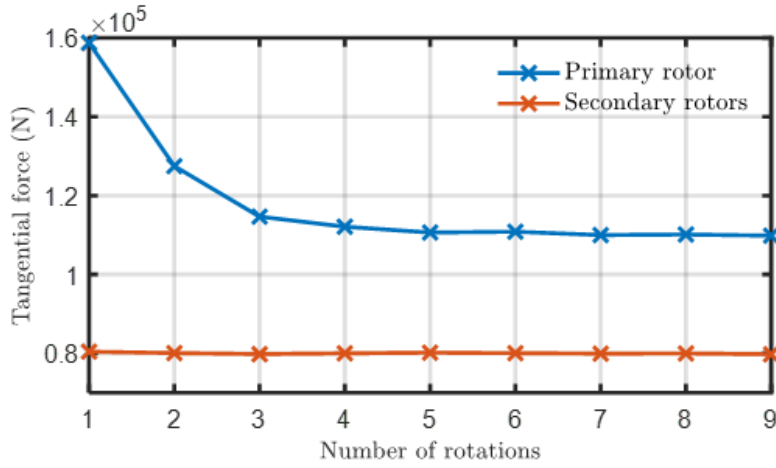


Figure 5 Time-averaged forces on the primary and secondary for each (primary rotor) revolution.

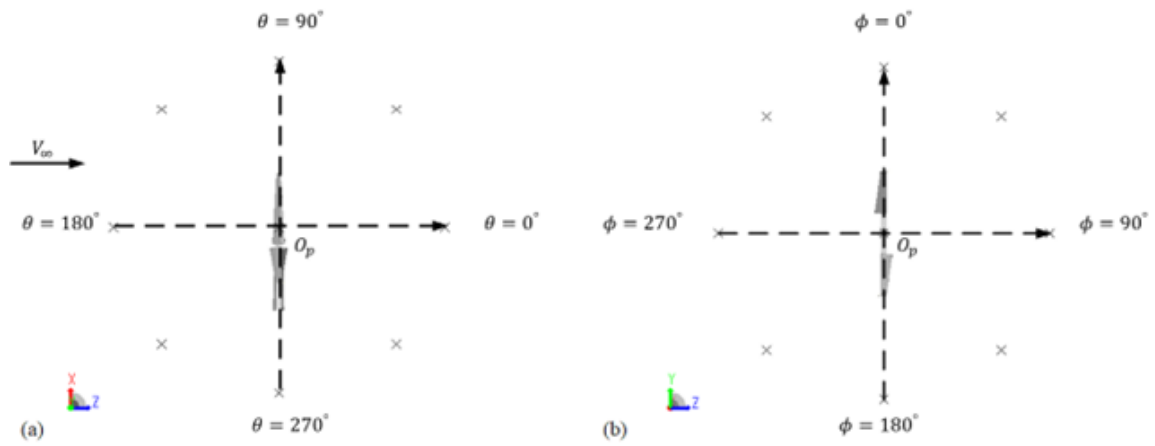


Figure 6 Microphones placed at 200 m in the (a) x-z plane (polar), and (b) y-z plane (azimuthal).

calculated using the Ffowcs Williams & Hawkins (FW-H) acoustic analogy with formulation 1A solved in forward-time [4–6]. For the primary rotors, this is done with SIMULIA PowerACOUSTICS, while for the secondary rotors, OptydB-PFNOISESCAN is applied [7]. The sampling of the surface pressure is done with a frequency of 24.5 kHz and spatial resolution of 0.019 m, resulting in the generation of a 5 TB solid FW-H surface results dataset. The flow field is sampled for only 1 revolution of the primary rotor, starting after 8 rotations.

2.3 Noise measurements

Two rings of 8 virtual microphones are considered in both the x-z plane (polar) and the y-z plane (azimuthal). The rings are placed at, respectively, 200 m ($2.6R_t^{(p)}$) and 400 ($5.3R_t^{(p)}$) from the rotational center O_p . Fig. 6 illustrates the ring at 200 m.

3. Results

3.1 Grid-independence study

A grid-independence study is performed using three resolutions (coarse, medium, and fine) with a refinement ratio of $M = \sqrt{2}$. Table 1 provides details of the different resolutions. For the evaluation of the rotor performance, the pressure coefficient is defined as:

$$C_p = \frac{p - p_\infty}{0.5\rho_0 V_\infty^2}, \quad (1)$$

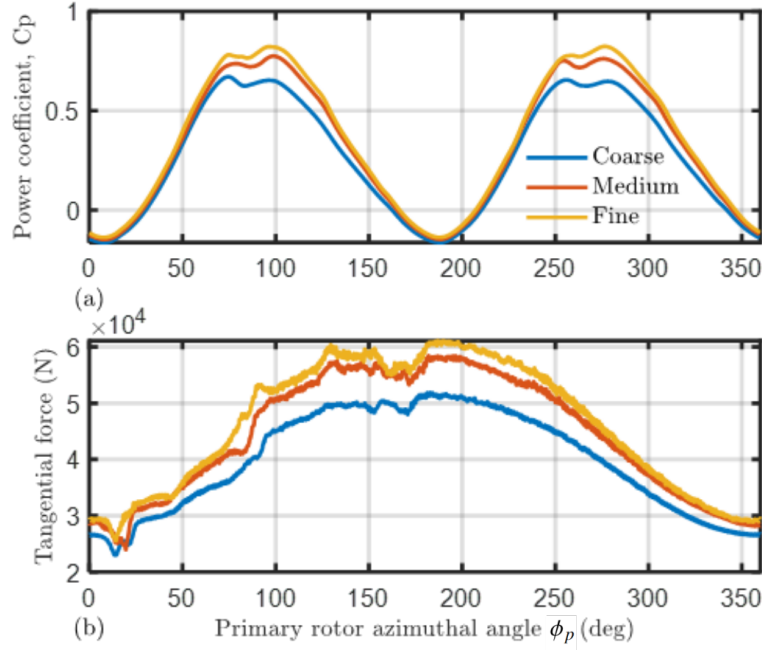


Figure 7 Phase averaged results plotted against the primary rotor azimuthal positions ϕ_p : (a) primary rotor power coefficient (b) secondary rotor thrust.

and the power coefficient as:

$$C_P = \frac{P}{0.5\rho_0 A_{\text{rot}} V_\infty^3}, \quad (2)$$

with ρ_0 is the ambient density, A_{rot} is the swept area of the rotor, p the static pressure, and P the power.

Fig. 7 presents phase-averaged results for the different meshes, which show a converging trend. Fig. 8 further investigates this trend and presents time-averaged values plotted against a dimensionless mesh size, ranging from 2 (coarse) to 1 (fine). The value of 0 is a hypothetical converged result obtained by Richardson extrapolation. A Grid Convergence Index (GCI) is computed to assess the convergence [8]:

$$\text{CGI} = \frac{\text{GCI}_{1.4,2}}{M^N \text{GCI}_{1,1.4}}. \quad (3)$$

For the primary rotor C_P in Fig. 8(a): $\text{GCI}_{1,1.4} = 10.19\%$ and $\text{GCI}_{1.4,2} = 22.07\%$. With $N = 1$ and $M = \sqrt{2}$, this gives a CGI ratio of 1.087, indicating we are within the asymptotic range of convergence. Extrapolation results in $C_P = 0.39$ represented by the red square [9], which aligns very well with the value of 0.39 to 0.4 for which the design was made using QBLADE. For the secondary rotor average thrust in Fig. 8(b): $\text{GCI}_{1,1.4} = 3.37\%$ and $\text{GCI}_{1.4,2} = 8.67\%$. This gives a CGI ratio of 1.0413, which is also very close to one and indicates asymptotic convergence.

Fig. 9 presents acoustic results for the different meshes. The Overall Sound Pressure Level (OSPL) in (a) and (b) again show a converging trend. Additionally, it can be observed from this figure that there is only a minor dependence of the OSPL on the direction, with a maximal difference of 1.7 dB between the maximum and minimum value in the azimuth. The averaged OSPL over the rings at 200 m and 400 m differs by 5.9 dB and 6.2 dB in the polar and azimuthal planes, respectively, which agrees with the theoretical squared dependence on the distance. Panel (c) presents the Sound Pressure Level (SPL) spectrum at 400 m distance in the upwind direction. The peak at 34 Hz, corresponding to the Blade Passing Frequency (BPF) of the secondary rotor, has the same value for all meshes. Up to 300 Hz, the broadband is similar for the medium and fine grid but is underpredicted by the coarse mesh. Furthermore, a frequency shift in the broadband noise is observed from coarse to medium to fine, after which the noise at frequencies above approximately 1000 Hz is underpredicted. This can be explained by the lack of resolution, which does not sufficiently resolve small turbulent structures to predict noise at these frequencies. Similar results are observed in [10].

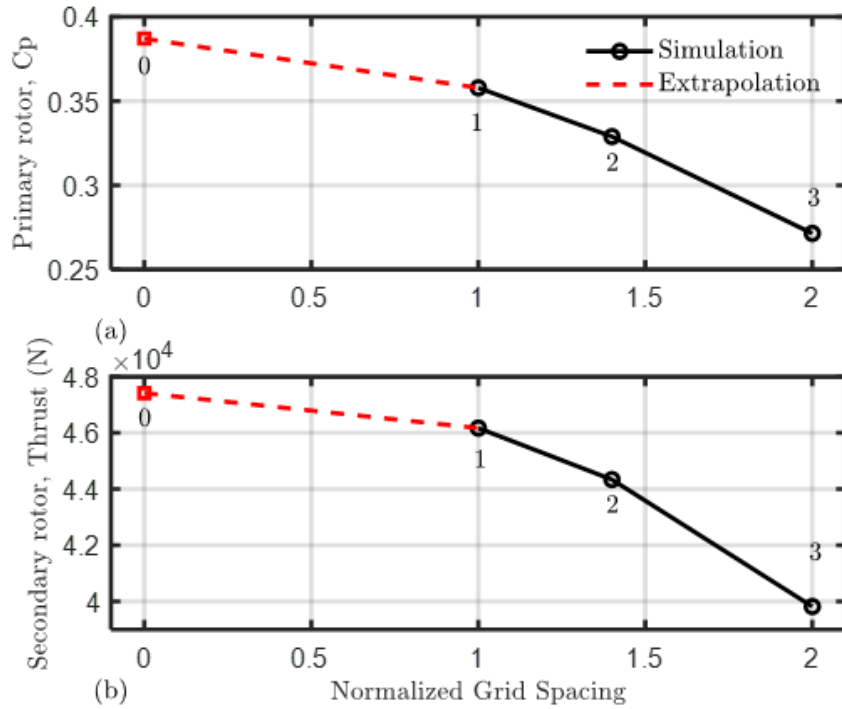


Figure 8 Convergence trends and extrapolated values of (a) time-averaged primary rotor C_p , and (b) time-averaged secondary rotor thrust. The grid size is normalized with the finest grid equal to 1, the medium grid equal to $\sqrt{2}$, and the coarse grid equal to 2. The grid size 0 is the result of Richardson extrapolation.

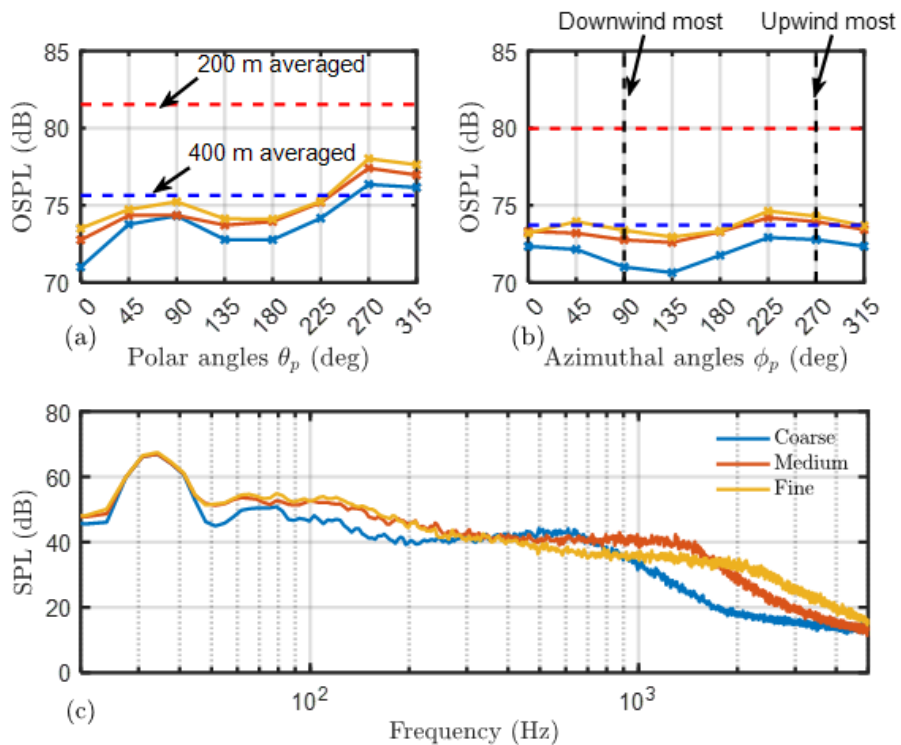


Figure 9 Acoustic results from the different meshes at the observer distance of 400 m. Subplots (a) and (b) present OSPL at different angles. Subplot (c) presents the spectrum at $\phi_p = 270^\circ$ (the most upwind location).

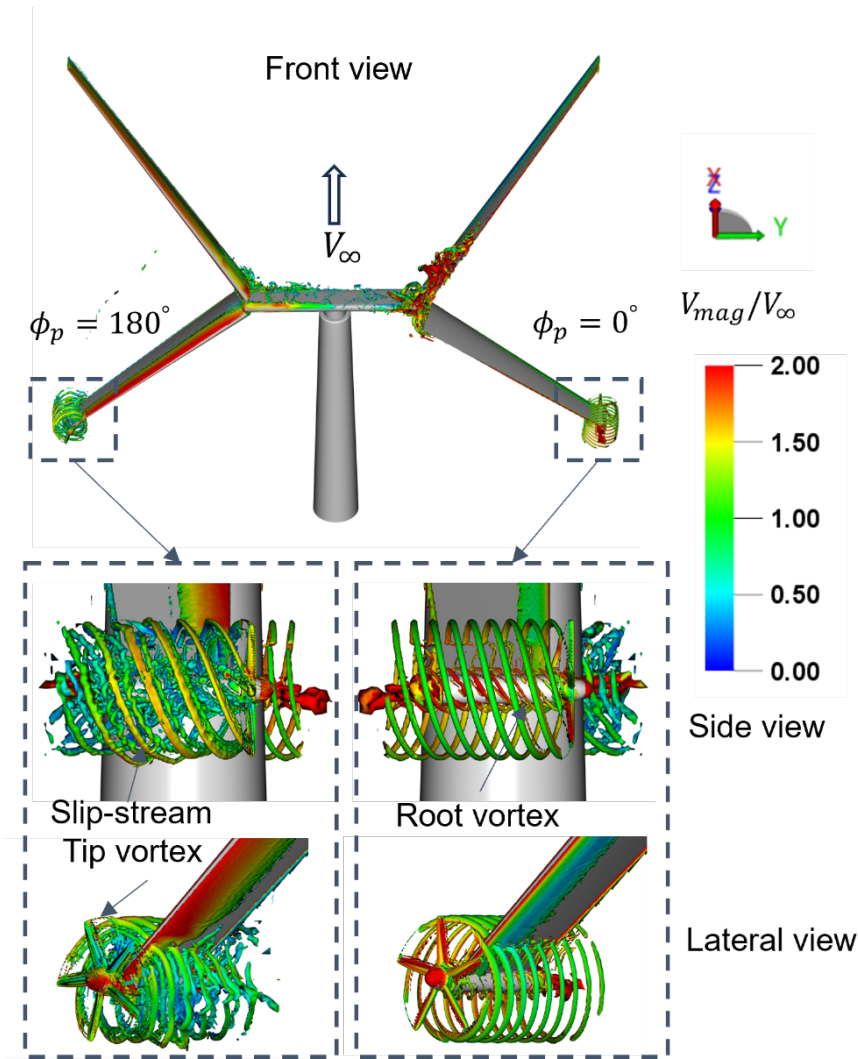


Figure 10 Iso-surface of λ_2 visualization ($\lambda_2 = -300 \text{ s}^{-1}$). Colors indicate dimensionless velocity.

3.2 Aerodynamic investigation

From here on, only the results of the finest mesh are considered. Fig. 10 visualizes the instantaneous turbulent flow structures generated by the X-Rotor using the iso-surface of the λ_2 -criterion, with the colors indicating the velocity magnitude V_{mag}/V_∞ . An interaction between the slipstream of the secondary rotor and the lower primary blade is visible. Besides the distortion of the slipstream, it can also be observed that the downstream expansion of the slipstream is faster at the $\phi_p = 180^\circ$ side. This is caused by the higher relative inflow velocity caused by the freestream. Finally, some vortices are shed from the root of the upper blade, which will also be visible in Fig 12.

The (instantaneous) flow field around the turbine in the y - z plane at the height of the secondary rotors at different azimuthal positions is presented in Fig. 11. The colors represent a normalized vorticity magnitude ω_{c_s}/V_∞ . Multiple rotor-wake interactions are visible. At $\phi_p = 15^\circ$, 125° , and 180° , in (a), (c), and (e), respectively, the wake of one of the secondary rotors impinges on the other secondary rotor. At $\phi_p = 155^\circ$ in panel (d), a secondary rotor interacts with its own wake. These interactions cause fluctuations in the thrust in Fig. 7(b). Additionally, a Von Kármán vortex street is formed at the tower, which impinges on the rotor at $\phi_p = 90^\circ$ and 270° , which causes the fluctuations at those angles in Fig. 7.

Fig. 12 presents the (instantaneous) x -vorticity $\omega_x c_s/V_\infty$ in the y - z plane at two different heights. Subplots (a-c) correspond to a plane at 10% of the vertical distance from the root to the tip of the upper blades, while subplots (d-f) correspond to a plane at 10% of the vertical distance from the root to the tip of the lower blades. As visible in (a) and (d), the flow is attached on the surface of both the upper and lower blades at azimuthal

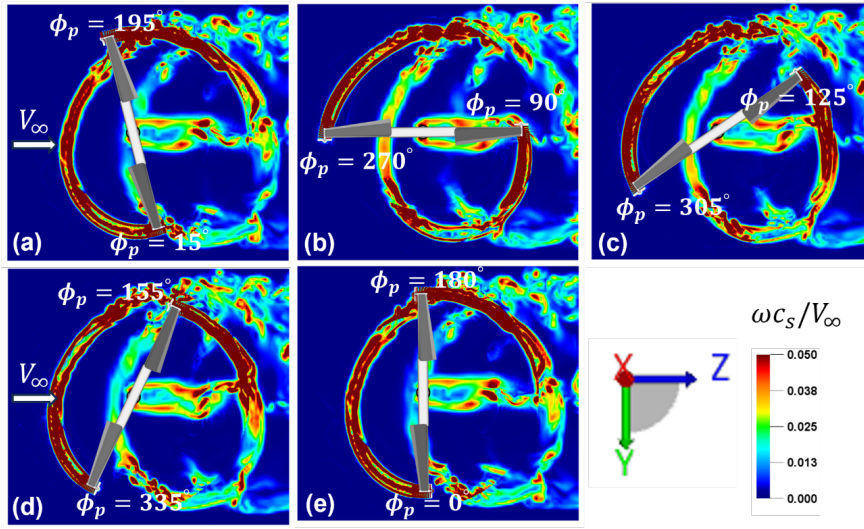


Figure 11 The (instantaneous) non-dimensional vorticity magnitude $\omega c_s/V_\infty$ in the plane through the centers of the secondary rotors.

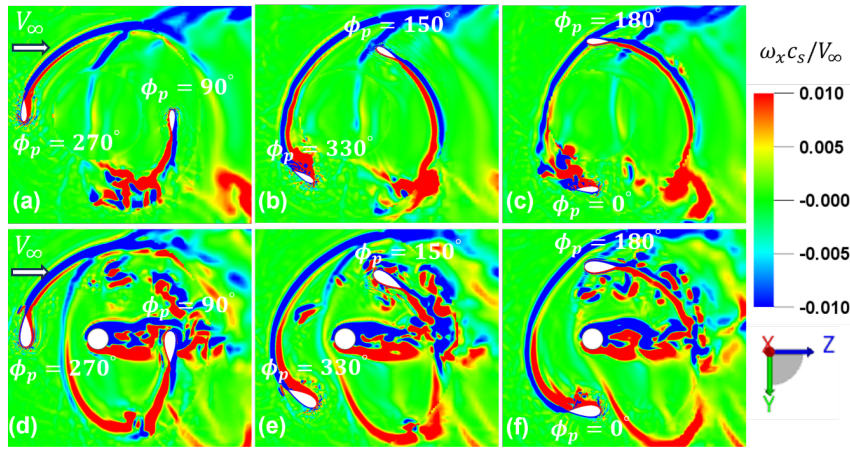


Figure 12 The (instantaneous) non-dimensional x-vorticity $\omega_x c_s/V_\infty$. Panels (a-c) and (d-f) correspond to planes at 10% of the vertical distance from the root to the tip of the upper blades and lower blades, respectively. Contours (a, d), (b, e), and (c, f) have been extracted at the same time instance.

positions $\phi_p = 90^\circ$ and 270° . Later in the rotation at $\phi_p = 330^\circ$, a separation can be observed on the inner surface of the upper blade, characterized by the opposing x-vorticities. This is even more pronounced at $\phi_p = 0^\circ$, where the shedding of vortex pairs is also visible. Conversely, the flow remains attached to the lower blade, yet several minor disturbances can be observed on the inner surface of the lower blade.

The deviation from the (time-averaged) pressure coefficient, $C_{p_{dev}}$, on the tip of the lower blade is illustrated in Fig. 13, for three time instances close to the azimuthal angle $\phi_p = 0^\circ$. The subplots correspond to these three moments during the passage of a secondary rotor blade in front of the leading edge of the lower primary blade. Pressure fluctuations caused by the tip vortex of the secondary rotor are clearly visible on both sides of the lower blade, with a larger magnitude on the inside due to the direct impingement. Additionally, at the moment of passage, an increase in $C_{p_{dev}}$ close to the leading edge of the inner side can be observed, which we expect to be the effect of potential field interactions[11, 12].

Fig. 14 presents the power spectral density (PSD) of the lower blade forces F_x , F_y and F_z . Peaks are visible at harmonics of the secondary rotor blade passing frequency (BPF). Particularly in the axial direction of the second rotor, F_x , peaks up to the fourth harmonic are visible. These force fluctuations are attributed to the interactions between the secondary rotor and the tip of the lower blade and may result in low-frequency tonal noise in the far field [11, 13].

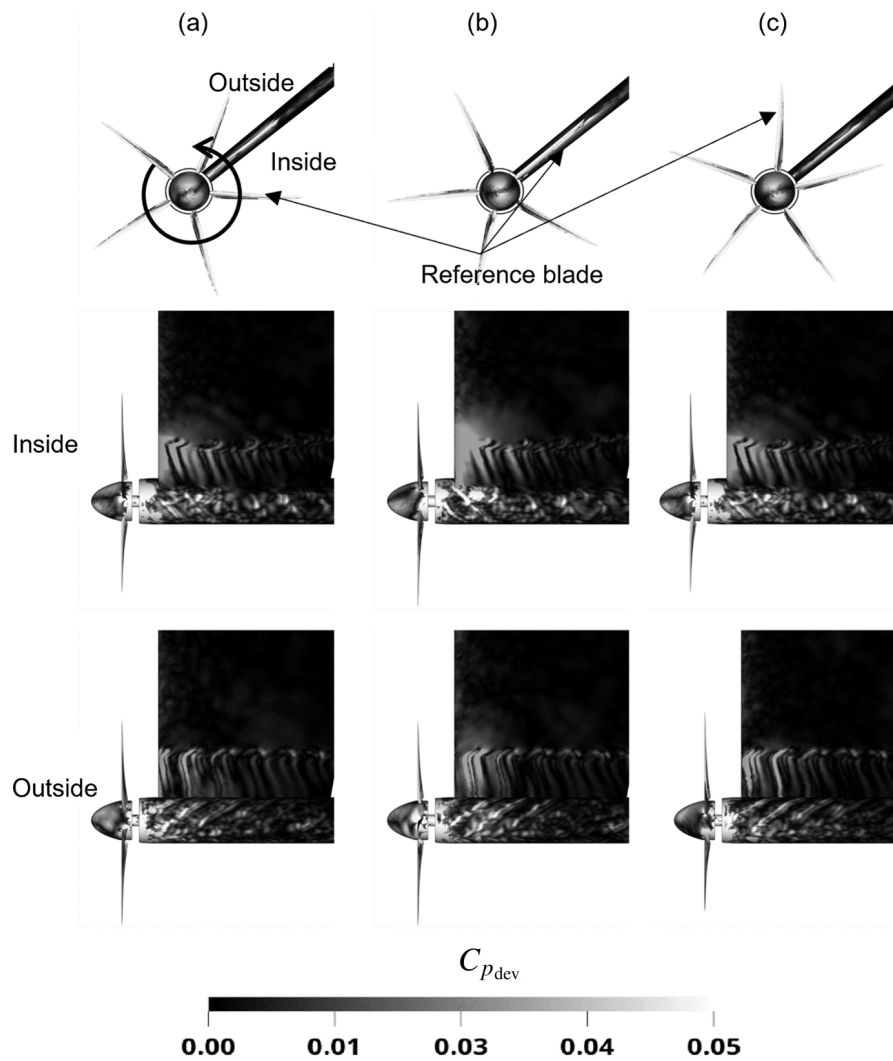


Figure 13 Deviation from time-averaged pressure coefficients at the tip of the lower blade around an azimuthal angle of $\phi_p = 0^\circ$. Subplots (a) to (c) present different moments during the passage of a reference blade in front of the lower blade leading edge at $\phi_{\text{offset}}^{(s)} = -36^\circ, 0^\circ, \text{ and } 36^\circ$.

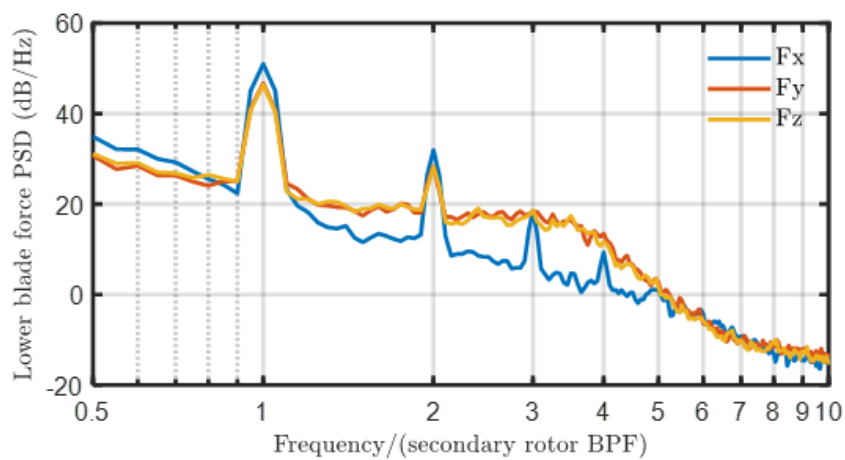


Figure 14 PSD of the lower blade force in the directions of its reference system.

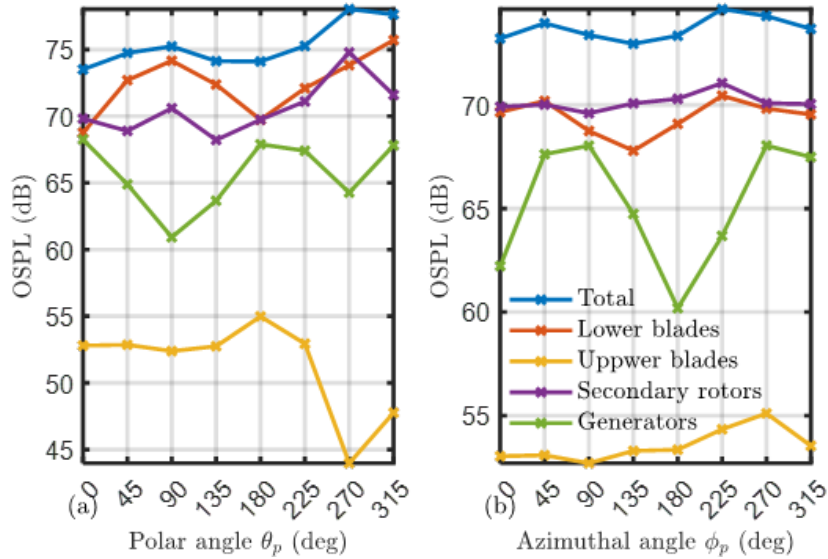


Figure 15 OSPL contributions from different components at a 400 m distance from the primary rotor rotational center O_p . For (a) in the polar direction and (b) in the azimuthal direction.

3.3 Aeroacoustic results

Fig. 15 plots the separate OSPL contributions from subcomponents at 400 m distance from the primary rotor rotational center O_p . The results are integrated from 20 Hz to 5000 Hz. The OSPL contributions of the lower blades and secondary rotors are generally at similar levels and primarily compose the total noise. Additionally, the generators also make notable contributions at specific observer locations, such as the upwind most ($\phi_p = 270^\circ$) and downwind most ($\phi_p = 90^\circ$). Conversely, the contribution of the upper blades can be neglected, with an average of 20 dB less than the total.

Figs. 16 and 17 depict the spectra of the different components at various polar and azimuthal angles. The data was processed using the pwelch function of MATLAB with a Hanning window, an overlap of 50%, and a bandwidth of 3.42 Hz (equivalent to one-tenth of the secondary rotor BPF). In the lower-frequency regime, the results again indicate the lower primary blades and secondary rotors as the primary noise source, with the secondary rotors and the generators dominating at higher frequencies. The tonality in the lower-frequency regime clearly indicates the interactions between the primary blades and the secondary rotors as the main noise source, which is also supported by the force spectra in Fig. 14. The broadband contribution from the primary blades seems negligible compared to the secondary rotors and the generators across all observer locations. The results furthermore suggest that the generators form a significant noise source in specific directions in frequencies below 200 Hz and above 2000 Hz. In this regard, it should be mentioned that the generators are modeled as simple 2 m diameter cylinders, which could be further optimized in the future.

A band-pass filtered Power Spectrum of Pressure (PSP) is integrated over different frequency ranges to visualize how noise sources are distributed over the subcomponents. This calculation considers the unsteady pressure during one entire rotation of the primary rotor. Fig. 18 presents the results with six different frequency ranges: 25—75 Hz, 75—125 Hz, 150—250 Hz, 500—1500 Hz, 1500—2500 Hz, and 2500—3500 Hz, denoted by the average of the range f_c . The results clearly illustrate the distribution of noise sources, characterized by higher PSP values at specific parts of the rotors.

Fig. 18 clearly indicates the secondary rotor as the primary noise source. For frequencies up to 200 Hz, high values are obtained over the secondary rotor's entire surface. For higher frequencies, substantial contributions are visible at both the leading and trailing edges near the blade tips and at the suction side trailing edge near the root. The former can be attributed to either the high relative velocities experienced by the tips or to a tip vortex interaction. The latter can be correlated with the vortex shedding visible in Fig. 10. The lower blade only has surfaces with high values at frequencies below 500 Hz, as was expected

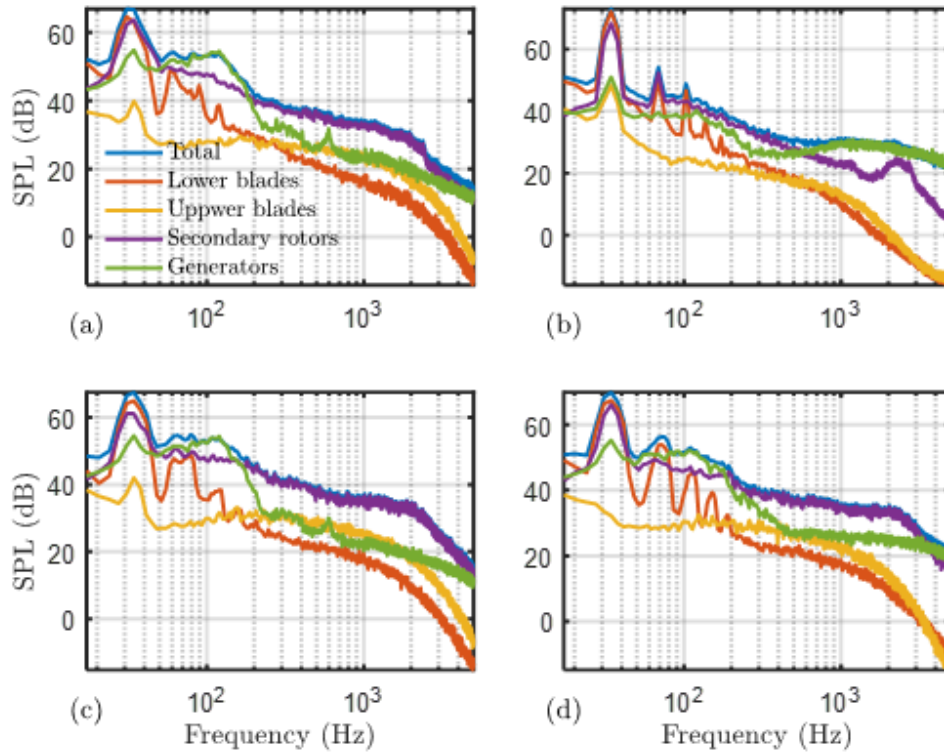


Figure 16 SPL spectra from different components at different polar angles. For (a) $\theta_p = 0^\circ$, (b) $\theta_p = 90^\circ$, (c) $\theta_p = 180^\circ$, and (d) $\theta_p = 225^\circ$.

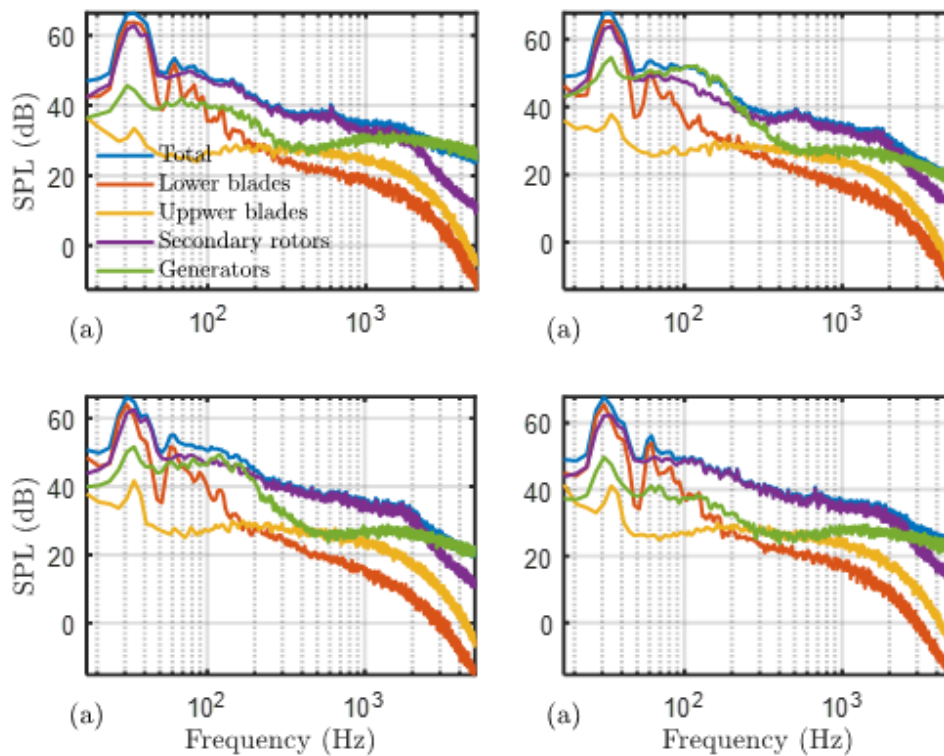


Figure 17 SPL spectra from different components at different azimuthal angles. For (a) $\phi_p = 0^\circ$, (b) $\phi_p = 45^\circ$, (c) $\phi_p = 135^\circ$, and (d) $\phi_p = 225^\circ$.

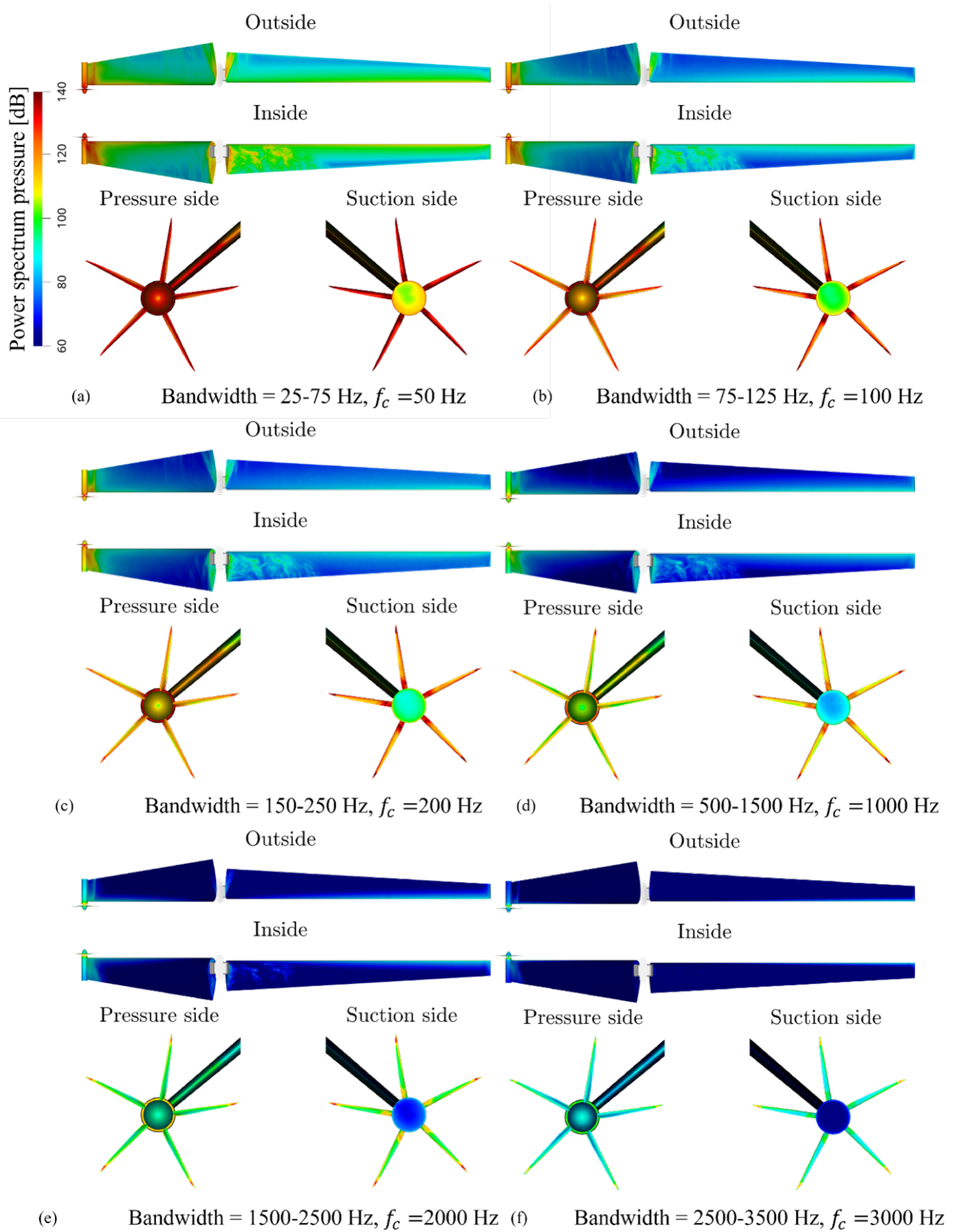


Figure 18 Integrated Power Spectra of Pressure (PSP) over different bandwidths.

from Figs. 16 and 17. The high-value concentration near the leading edge and close to the tip of the lower primary blades indicates that the interaction with the secondary rotor mainly causes these fluctuations. It can also be noted that the direct impingement of the secondary rotor tip vortex on the inside of the lower blade results in a broader distribution on the inside part compared to the outside part of the blade. Finally, a relatively weaker contribution is visible at the inside of the upper blade root region, which is attributed to vortex shedding resulting from flow separation, as shown in Fig. 12.

Fig. 19 displays a time-frequency analysis of the acoustic pressure generated by the secondary rotor and observed 400 m directly above the X-Rotor center O_p ($\theta_p = 90^\circ$). The reception time is converted to emission time and reported in the azimuthal position of the rotor, such that the observed noise can be correlated with the flow features causing it. The spectrum is calculated with a Hanning window, 75% overlap, and a bandwidth of 6.85 Hz (equivalent to one-fifth of the secondary rotor BPF). An increase in both the tonal noise at the BPF harmonics and the broadband noise is visible between approximately $\phi_p = 90^\circ$ to $\phi_p = 270^\circ$, as the secondary rotor moves from downstream to upstream, increasing the relative velocity and loading, with a peak at approximately $\phi_p = 180^\circ$. Additionally, acoustic pressure fluctuations are noted at several angles where the secondary rotor interacts with a wake, as visualized in Fig. 11.

The A-weighted sound power level (SWL) (calculated by averaging the results in azimuthal and polar directions) is reported in Fig. 20 to put the X-rotor in perspective with conventional turbines. Due to a lack of reliable data for offshore turbines, results for onshore turbines reported in [14] are utilized for comparison. The SWL from the X-Rotor is significantly higher than that from the other three types of wind turbines, particularly in the higher frequency regime. As previously discussed, this higher noise level is primarily attributed to the secondary rotors.

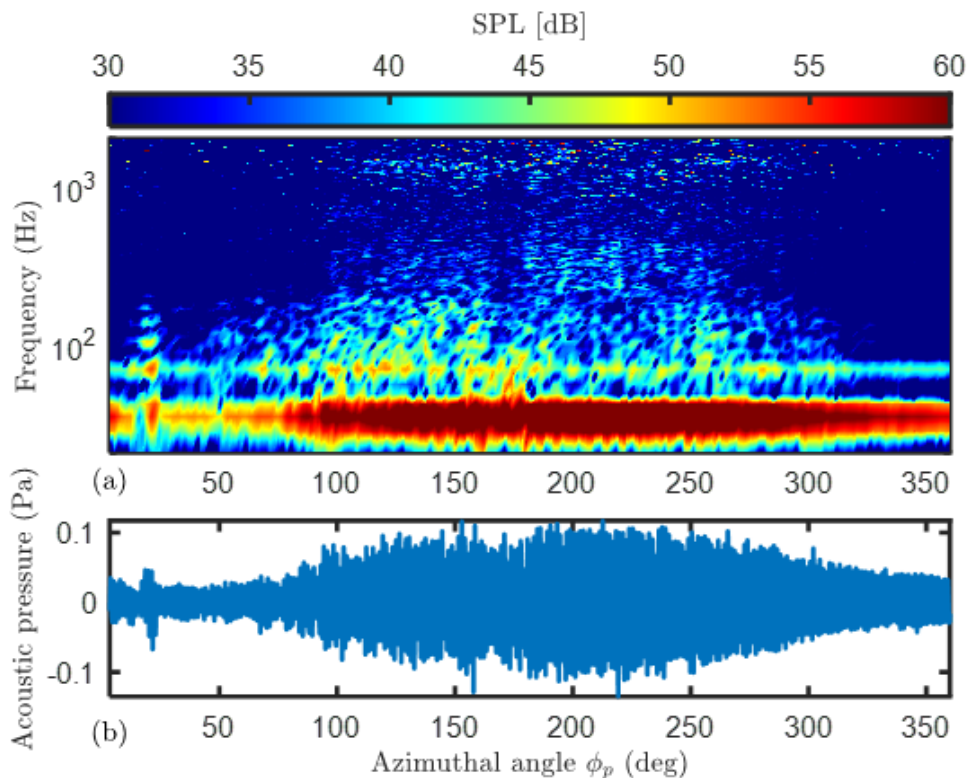


Figure 19 (a) time-frequency analysis of the acoustic pressure observed at 400 m directly above the X-Rotor, (b) acoustic pressure. Time is converted to emission time and azimuthal positions.

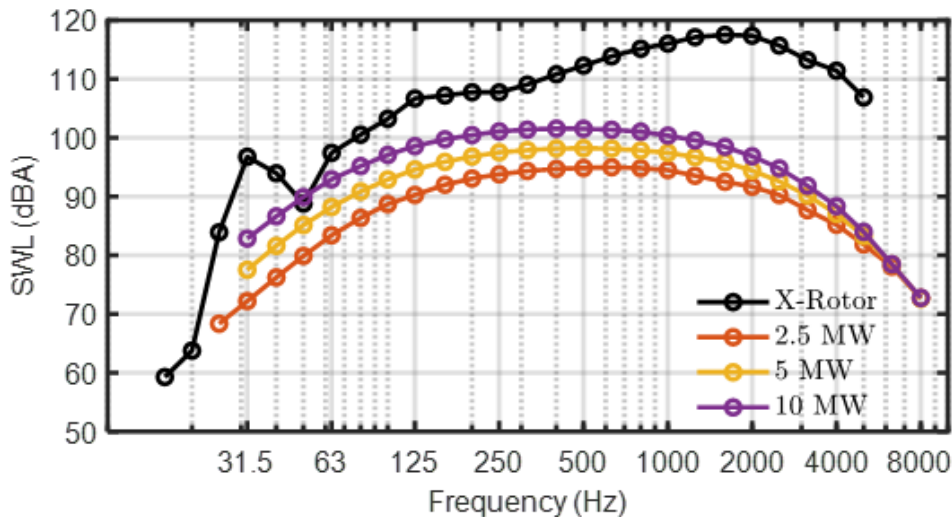


Figure 20 A-weighted sound power level (SWL) in one-third octave bands. Results of conventional 2.5, 5, and 10 MW wind turbines are added as reference.

4. Summary and conclusion

This contribution presents the results obtained from high-fidelity numerical simulations of the baseline concept for the X-Rotor operating at maximum power extraction conditions. The approach uses a high-fidelity CFD simulation based on the LBM/VLES method, and the far-field acoustics are computed using the solid FW-H approach. The results give an overview of both the aerodynamic and the aeroacoustic performance.

The analysis starts with a convergence study considering multiple grids. Convergence trends are assessed via GCI values, with the GCI ratio indicating convergence within the asymptotic regime. The extrapolated primary rotor power coefficient C_p aligns closely with the expected value from QBLADE software. The flow field reveals predominant interactions between the secondary rotor and the lower primary blade, particularly in the downwind section. Interactions between the tower and rotor and between two secondary rotors are also observed at specific azimuthal positions.

The OSPL results indicate minimal variation across observer locations, with only a 1.7 dB difference between the lowest and highest values. Secondary rotors are primary sources of noise in basically all frequency regimes. The lower primary blades form a significant noise source due to the interaction with the secondary blades, which creates a tonal noise that dominates the low-frequency regime. The generator substantially contributes to the broadband noise, particularly between 100 Hz and 200 Hz and above 1000 Hz at specific observer locations. Noise from the upper blades is comparatively negligible. Visualizations of the Pressure Power Spectrum (PSP) in different frequency regimes over the surfaces of the different components again confirm the interaction between the secondary rotor and the lower primary blade as the dominant source at low frequencies and the secondary rotor as the dominant contribution at higher frequencies.

A comparison of A-weighted Sound Power Level (SWL) between the X-Rotor and three different conventional horizontal wind turbines finally indicates that the X-Rotor is significantly higher, exceeding other turbines by over 20 dB above 2000 Hz. This is mainly attributed to the secondary rotor's higher tip speed. The considerably high noise level generated by the current baseline concept of X-Rotor suggests the need to optimize the current design to mitigate noise in the future, mainly by reducing the noise from the secondary rotor.

Acknowledgments



This project has received funding from the European Union's Horizon 2020 research and innovation program under grant agreement no 101007135 (X-Rotor).

References

- [1] “X-rotor.” <https://xrotor-project.eu>, Accessed: 17-3-2025.
- [2] Y. Wu, F. Avallone, D. Ragni, and D. Casalino, “3d cfd simulations of noise from a full x-rotor concept,” *X-ROTOR H2020 Project*, 2024. <https://doi.org/10.5281/zenodo.11395455>.
- [3] W. Zhu, N. Heilskov, W. Shen, and J. N. Sørensen, “Modeling of aerodynamically generated noise from wind turbines,” *Journal of Solar Energy Engineering*, vol. 127, no. 4, pp. 517–528, 2005.
- [4] J. Ffowcs Williams and D. Hawkings, “Sound generation by turbulence and surfaces in arbitrary motion,” *Philosophical Transactions of the Royal Society of London. Series A, Mathematical and Physical Sciences*, vol. 264, no. 1151, pp. 321–342, 1969.
- [5] F. Farassat, “Derivation of formulations 1 and 1a of farassat,” *NASA Technical Report, NASA/TM-2007-214853*, 2007.
- [6] D. Casalino, “An advanced time approach for acoustic analogy predictions,” *Journal of Sound and Vibration*, vol. 261, no. 4, pp. 583–612, 2003.
- [7] D. Casalino, E. Grande, G. Romani, D. Ragni, and F. Avallone, “Definition of a benchmark for low reynolds number propeller aeroacoustics,” *Aerospace Science and Technology*, vol. 113, no. 106707, 2003.
- [8] P. Roache, *Verification and validation in computational science and engineering*. Hermosa Publishers, 1998.
- [9] P. Roache, “Quantification of uncertainty in computational fluid dynamics,” *Annual review of fluid mechanics*, vol. 29, no. 1, pp. 123–160, 1997.
- [10] D. Lockard, M. Choudhari, and P. Buning, “Grid sensitivity study for slat noise simulations,” *20th AIAA/CEAS Aeroacoustics Conference*, no. AIAA 2014-2627, 2014.
- [11] B. Zajamsek, Y. Yauwenas, C. Doolan, K. Hansen, V. Timchenko, J. Reizes, and C. H. Hansen, “Experimental and numerical investigation of blade–tower interaction noise,” *Journal of Sound and Vibration*, vol. 443, pp. 362–375, 2019.
- [12] Y. Wu, M. J. Kingan, and S. T. Go, “Propeller–strut interaction tone noise,” *Physics of Fluids*, vol. 34, no. 5, 2022.
- [13] Y. Yauwenas, B. Zajamšek, J. Reizes, V. Timchenko, and C. Doolan, “Directivity of blade-tower interaction noise,” *JASA Express Letters*, vol. 1, is. 6, no. 063601, 2021.
- [14] H. Møller and C. Pedersen, “Low-frequency noise from large wind turbines,” *The Journal of the Acoustical Society of America*, vol. 129, no. 6, pp. 3727–3744, 2011.

Paper #28 - ID: 362

Title: Frequency Content of Measured Wind Farm Noise Levels and Band-Limited Regressions

Author: Tom Levet

11th Edition of the

International Conferences on Wind Turbine Noise

Copenhagen, Denmark – 10th to 13th June 2025

Frequency Content of Measured Wind Farm Noise Levels and Band-limited Regressions

Tom Levet¹

Hayes McKenzie Partnership Ltd, Lodge Park, Tre'r-ddol, Machynlleth, Powys, SY20 8PL, UK

Summary

A wind farm noise assessment is usually carried out based upon overall A-weighted broadband noise parameters, such as L_{A90} or L_{Aeq} . In the UK, compliance measurements often involve periods where the wind farm is periodically paused, so that the background noise component can be measured alongside the operational periods of total noise levels measured in other periods of the survey. Regression analyses are then performed on the total and background datasets and a logarithmic subtraction is undertaken upon these broadband levels to quantify the wind farm component.

Some examples are shown where, instead of basing the analysis on a broadband L_{A90} , regression analyses are performed on noise levels that are band-limited to particular frequency bands, mostly in the low-mid frequency range below 800 Hz. The resulting regressions generally demonstrate less scatter, and a reasonable correlation with a predicted noise level (using ISO 9613-2) is usually achieved.

By concentrating the assessment on a frequency range where there is a large signal-noise ratio, arguably more certainty is achieved in the level attributable to the wind farm, than if a logarithmic subtraction is applied on standard broadband levels where there is a smaller signal-noise ratio. However, sensible results are dependent upon the availability of reliable source spectrum information, and a lower frequency range may not be suited to all turbine models and local circumstances.

1. Introduction

For a typical wind farm compliance measurement in the UK, periods of total noise levels (when the wind farm is operating) are interspersed by scheduled periods of background noise levels (when the wind farm is temporarily paused). This is done so that the noise level specifically attributable to the wind farm can be calculated, by logarithmically subtracting the background noise level from the total noise level. The measurements are undertaken using an overall broadband $L_{A90,10min}$ parameter, and polynomial regression relationships with wind speed are derived for the operational and background datasets. Due to the nature of local background noise sources, and sometimes due to the distances involved, the wind farm component may be relatively low compared to other things in the environment.

Consequently, there can be considerable scatter to these regression relationships, and sometimes only a small difference in the measured broadband noise level between the wind farm being on or being off. These factors can arguably call into question the reliability of undertaking a logarithmic subtraction upon

¹ Email: tom@hayesmckenzie.co.uk

broadband L_{A90} noise levels, in order to derive an accurate measure of the wind turbine noise level. Instead of using the broadband L_{A90} parameter, the following analyses explore the effect of deriving alternative regressions based on a limited lower frequency range, potentially where there is a greater signal-noise ratio, and potentially where there is smaller uncertainty due to the reduced scatter.

2. General method

The following noise measurements have been undertaken at residential receptor locations, located in the broad vicinity of fully operational wind farms (e.g. at approximate distances in the range 500 – 1600 m). Measurements were undertaken using double-layer wind shields at 1.5 m height, usually in the centre of an outdoor amenity area such as a garden, facing the wind farm.

The analyses have been referenced to a standardised 10m wind speed, where this wind speed has been derived from the average hub height wind speed measured on the nacelle of each turbine. In each instance, the worst-case downwind sector has been analysed, where this generally corresponds to a 90° sector centred on the closest turbine. For both operational and background datasets, obvious extraneous events, such as rainfall, lawn-mowing, or dawn choruses, have been excluded from the analyses.

To derive a band-limited $L_{A90,10min}$ level here, this has been simply calculated by a summation of the measured $L_{90,10min}$ levels of the relevant third-octave frequency bands, after applying A-weighting. It is acknowledged that this approach is not, strictly speaking mathematically correct. Therefore, a possible improvement would be to calculate the relevant frequency band on a 100ms basis, then derive the L_{A90} of the 10-minute period, from the measured band-limited 100ms values.

In terms of the presented noise predictions, these have been undertaken using ISO 9613-2:1996 [1]. Propagation assumptions included: a $G=0.5$ mixed ground assumption, 10 °C and 70 % relative humidity, point sources at either hub or tip+10 m height, and 4 m high receptor heights. A difference of 2 dB was assumed between L_{Aeq} and L_{A90} . The assumed sound power levels were based upon manufacturer supplied specified noise levels for the turbine model in question, with the addition of 1-2 dB uncertainty. The frequency spectra assumed in the predictions were based upon either a test report or that suggested by the manufacturer.

3. Examples

The below section details some examples of noise measurements where a band-limited approach has been undertaken.

3.1 Example 1: sheltered location near a watercourse

The measurements at Example 1 were undertaken in the garden area of a residential location approximately 500 m from the nearest turbine. The hilly topography of the site means that the measurement location is relatively sheltered, but still has a clear line-of-sight up towards the closest turbines. There is a watercourse that runs along the side of the garden, approximately 15 – 20 m from the measurement location. There is also various sized vegetation that grows throughout the garden.

Measured broadband noise levels at this location were significantly affected by noise from the watercourse. Figure 1 below shows an example waterfall plot of one particular day of the noise survey. Here the measured A-weighted third-octave band $L_{A90,10min}$ values are shown as a function of time. Consideration of the SCADA data indicates that the turbines were not operating between 06:50 – 15:20 and 21:50 – 00:00 (the latter of which was a scheduled shut-down). At these times, for frequencies in the 50 – 500 Hz range, there is an obvious reduction in measured noise levels as the turbines pause operation. For frequencies above approximately 1 kHz, measured noise levels tend to remain relatively constant, which is partially replicated in the measured overall broadband L_{A90} level. In this situation, it seems noise generated by the watercourse is predominantly focussed in the mid-high frequency range, with only a small contribution

below approximately 500 Hz. For a lower frequency range, it appears there is a larger signal-noise ratio for the noise generated from the wind farm. Therefore in this scenario, compared to a broadband measure, a lower frequency range arguably provides for a more accurate determination of noise levels from the wind farm.

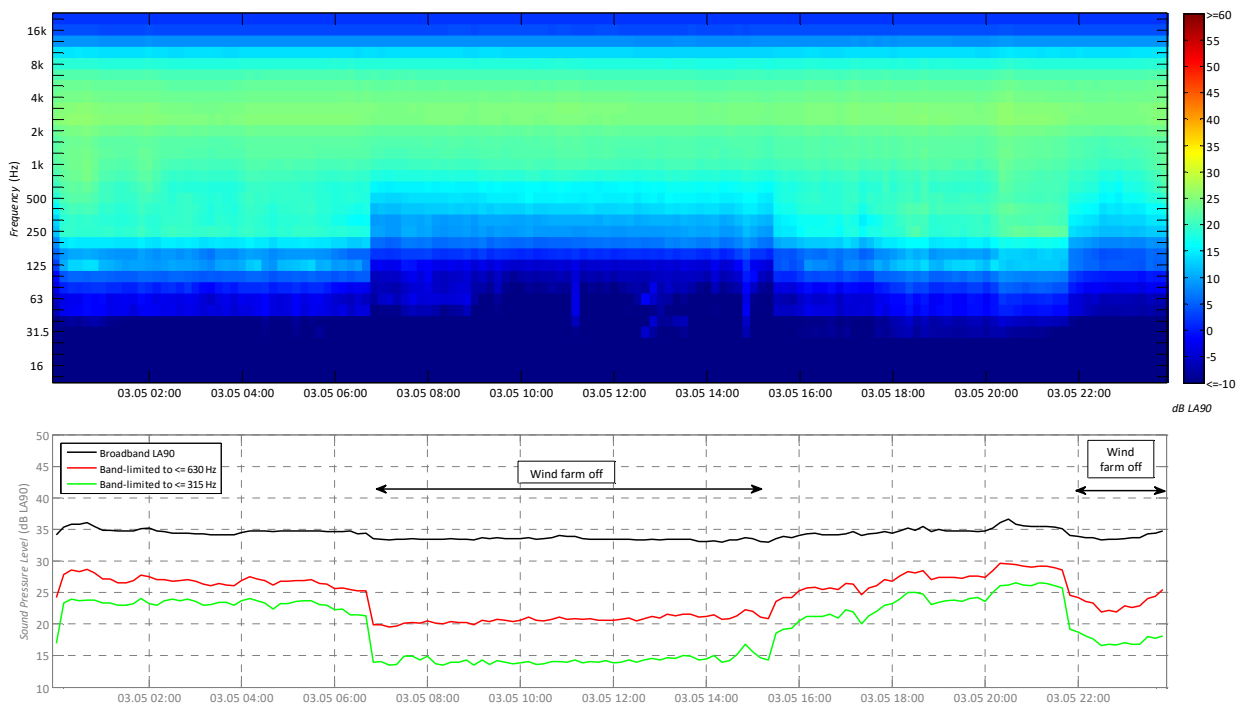


Figure 1: Waterfall plot of one day of measured noise levels at Example 1 location.

Figure 2 below shows regression analyses of the measured noise levels as a function of wind speed, for the downwind sector. Panel a) shows the broadband results, panel b) shows results band-limited to ≤ 630 Hz, panel c) shows results band-limited to ≤ 315 Hz. The broadband results exhibit a large amount of scatter for a given wind speed. The scatter becomes less for the band-limited results shown in panels b) and c), as the analysis is focused on progressively lower frequencies. The polynomial regression lines that represent the datasets are therefore less uncertain for the band-limited options.

Also shown for comparison in Figure 2, is the predicted noise levels of the wind farm, undertaken using ISO 9613-2:1996. In addition to the broadband prediction, the relevant band-limited prediction is also shown, where this is derived by addition of the relevant octave band levels predicted by ISO 9613-2:1996. It can be seen that in this instance, by limiting the measurements to ≤ 630 Hz, there is a vastly improved correlation with wind speed, and a reasonable agreement with the predicted noise level. For the ≤ 630 Hz option, there is only a 1.0 dB predicted difference due to the loss in higher frequencies. For the measurements ≤ 315 Hz there is again a good agreement with the equivalent band-limited predicted noise level, in this instance at the cost of a predicted 3.8 dB loss in higher frequencies.

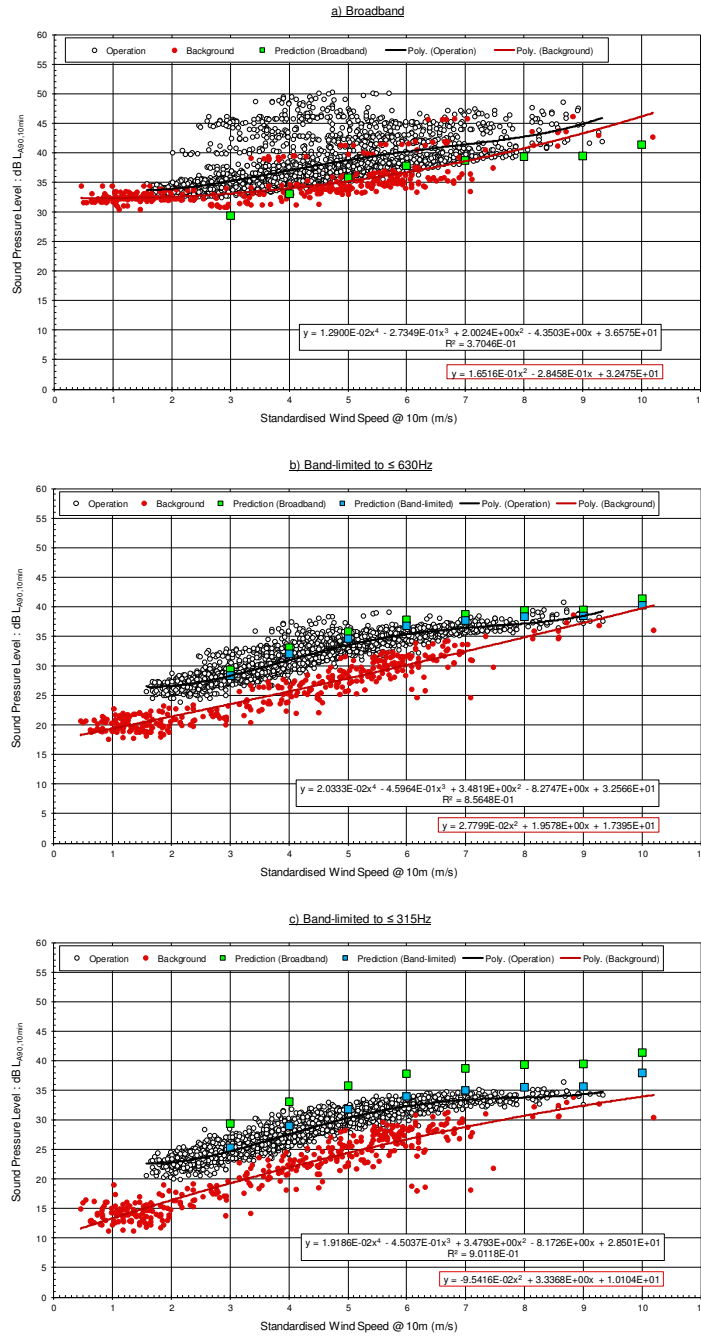


Figure 2: Noise regression results for different frequency band-limits at Example 1 location, a) broadband, b) band-limited to ≤ 630 Hz, c) band-limited to ≤ 315 Hz.

Table 1 below provides a quantification of the uncertainty of the polynomial regressions of the operational datasets, by way of a ‘Type A’ uncertainty estimation at each integer wind speed. Here this is the standard deviation of the residuals of the measured 10-minute values, compared to the polynomial regression curve, as detailed in Equation (1). This is also akin to how the U_A uncertainty component was previously calculated in sound power level tests according to the previous version of the IEC 61400-11 standard [2].

$$U_A = \sqrt{\frac{\sum_{i=1}^N (L_{A90,10min}(i) - L_{A90,poly})^2}{N-2}} \quad (1)$$

Table 1: Type A uncertainty estimation of operational regressions.

	R ² value of operational regression	Type A uncertainty U _A [dB]					
		3 m/s	4 m/s	5 m/s	6 m/s	7 m/s	8 m/s
Broadband	0.37	2.7	3.6	3.3	2.7	2.7	2.4
Band-limited to ≤ 630 Hz	0.86	1.3	1.6	1.3	1.0	0.7	0.8
Band-limited to ≤ 315 Hz	0.90	1.1	1.3	1.1	1.0	0.7	0.7

Table 1 suggests for example, that at wind speeds 4 – 7 m/s, there may be approximately ± 3 – 4 dB uncertainty associated with how appropriately the broadband regression represents the dataset. Whereas for the band-limited regressions, the uncertainty is estimated to be more than halve that of the broadband regression, at approximately ± 1 – 2 dB. The correlation coefficient R² value also reflects the improved correlation with wind speed of the band-limited regressions, increasing from approximately 0.4 for the broadband analysis, to approximately 0.9 for the band-limited options.

3.2 Example 2: location near some vegetation

The Example 2 measurement is a residential location, located approximately 500 m from the nearest turbine (at a different wind farm site and turbine model to Example 1). The sound level meter was located in a garden area facing the wind farm. In this instance there is a small watercourse approximately 50 m from the microphone location, that does occasionally contribute some energy to the background noise levels. But generally, the main source of background noise levels are the medium-large sized trees (approximately 15 m from the microphone) whose leaves rustle when the wind blows through the location.

Figure 3 shows a waterfall plot of the measured third-octave frequency band L_{A90,10min} noise levels applicable for one day of the noise survey. The wind farm had a scheduled shut-down of operation at 00:00 – 02:00, and also slowed operation as the wind speed dropped towards cut-in at around 17:00. Outside those times the wind farm was fully operational. The lower panel details the overall broadband L_{A90} noise levels, and band-limited levels to ≤630 Hz and ≤315 Hz. It can be seen for the first two hours, background noise levels are predominantly in the 300 – 3 kHz range centred around 1 kHz, but after that the higher noise levels are more centred around 400-500 Hz with all the lower frequencies generally exhibiting an increase. At 02:10 when the wind farm comes back on, the broadband level increases by approximately 5 dB, whilst the band-limited results for ≤630 Hz and ≤315 Hz increase by approximately 7 dB and 10 dB respectively. That is, there is a larger signal-noise ratio shown in the lower frequency range.

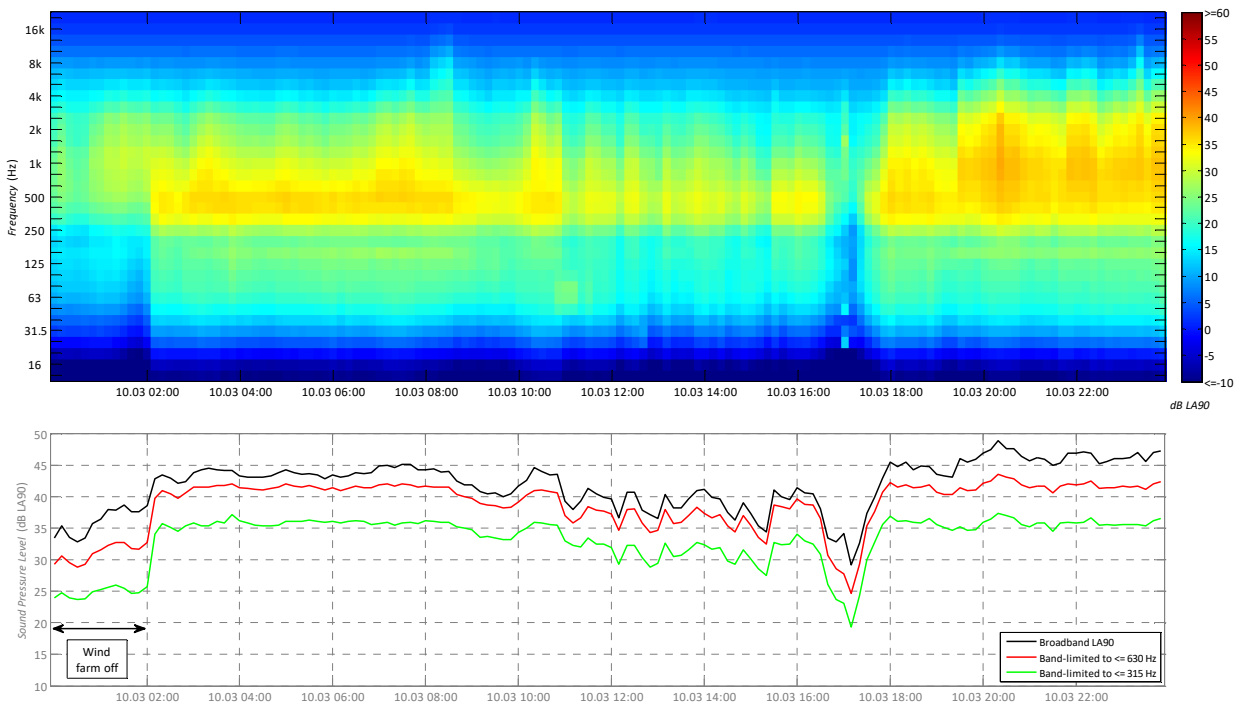


Figure 3: Waterfall plot of one day of measured noise levels at Example 2 location.

Figure 4 below shows regression analyses of the measured noise levels as a function of wind speed at Example 2, for the downwind sector of this location. Panel a) shows the broadband results, panel b) shows results band-limited to ≤ 630 Hz, panel c) shows results band-limited to ≤ 315 Hz. It is apparent that the operational curves of the lower frequency options show slightly better correlation with wind speed. These analysis options also exhibit a larger margin above the background curves, especially in the medium wind speed range.

Also shown is the equivalent ISO 9613-2 predicted noise level. It can be seen that the ≤ 630 Hz band-limited prediction shows relatively good agreement with the measured operational curve, for wind speeds 3 – 10 m/s. It is suspected that for higher wind speeds, background noise wind effects (from either wind blowing through vegetation or wind-induced noise on the microphone) have more of an influence on the measured noise levels. For this distance and turbine model, compared to a broadband prediction, for the ≤ 630 Hz option there is only a 0.5 dB predicted difference due to the loss in higher frequencies. This loss could be added back in to arrive at a broadband result. For the ≤ 315 Hz option there is a predicted 2.5 dB loss in higher frequencies.

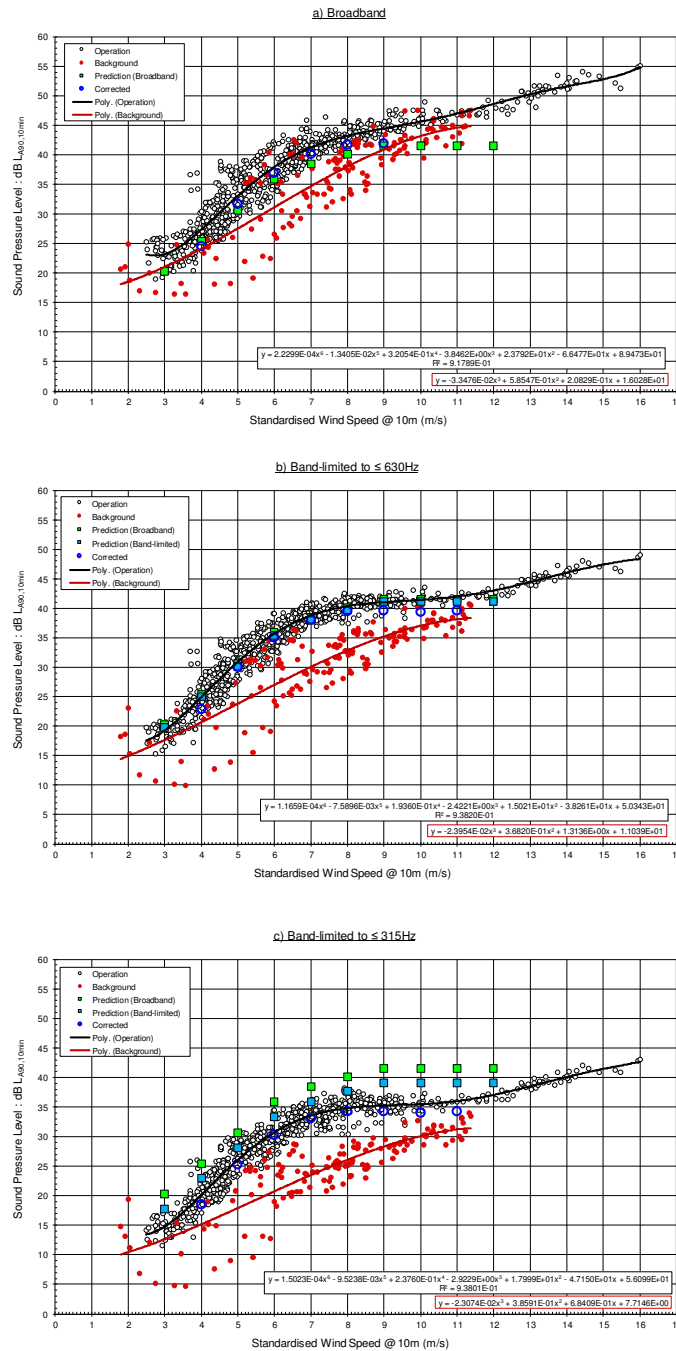


Figure 4: Noise regression results for different frequency band-limits at Example 2 location, a) broadband, b) band-limited to ≤ 630 Hz, c) band-limited to ≤ 315 Hz.

Also shown on Figure 4 are the corrected noise levels, which are a result of a logarithmic subtraction of the two polynomial regressions (shown only when there was at least 3 dB signal-noise ratio). This should be the level attributable to the wind farm for that frequency option. Figure 5 below shows those corrected noise levels, plus the addition of the amount of high frequencies predicted to be missing due to the band-limiting approach. It may be expected that, if the overall measurement/analysis approach is reasonable, and the predictions are representative, then the band-limited results would broadly overlap each other, and these would correspond with a broadband prediction. It is apparent that in this instance the ≤ 630 Hz result has the best agreement with the broadband prediction. The fact that the ≤ 315 Hz result is somewhat lower may be for a variety of reasons.

One reason may be that the source sound power level spectrum assumed in the predictions may not be exactly realistic compared to what is actually installed and measured on-site. That is, even though the

modelled overall broadband sound power levels represent what would be warranted, the manufacturer does not warrant the frequency spectrum shape, and in reality there may be relatively less low frequencies (and vice versa), than is generally specified. That is, in this instance the modelled spectrum may be slightly too low frequency biased, and for the 315 Hz option, one actually has to add back in, slightly more high frequencies.

Additionally, within the predictions the same frequency spectrum shape has been assumed for all wind speeds, which has then been normalised to the relevant broadband sound power level for the relevant wind speed. It is likely that in reality there is a change in spectrum shape as the wind speed changes, and that the modelled frequency shape is likely to be more appropriate for one wind speed bin more than the others.

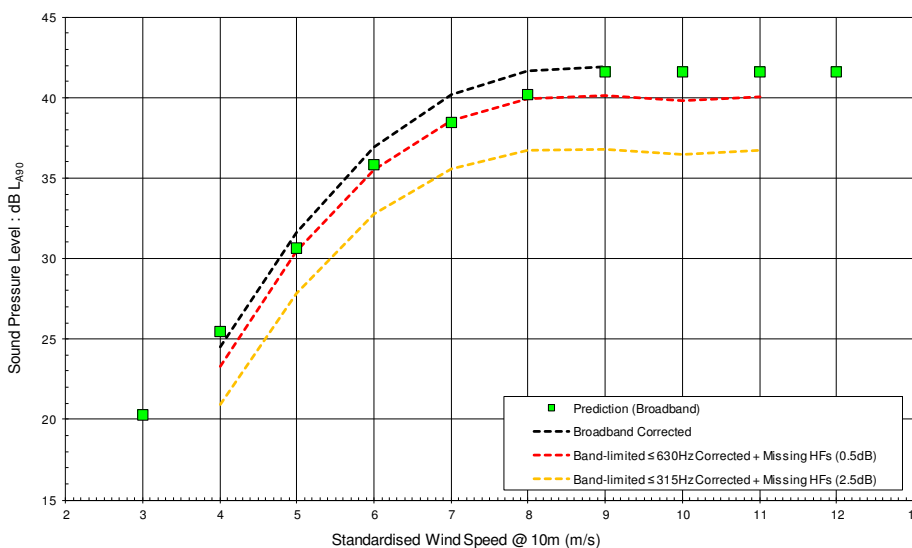


Figure 5: Corrected noise levels at Example 2 location, including the addition of predicted missing high frequencies.

Figure 6 below shows the average (A-weighted) third-octave frequency band spectra measured for the 7 m/s wind speed bin, for the downwind sector, calculated by an arithmetic average. It can be seen that the operational and background levels are relatively comparable for frequencies above approximately 1 kHz. For frequency bands below 800 Hz the signal-noise ratio is in the 5 – 10 dB range, with the largest value occurring in the 315 Hz band.

The ISO 9613-2 octave band prediction is shown for comparison (adjusting for the equivalent third-octave bandwidth). Given that the ≤ 630 Hz band-limited regression levels are quite comparable, in this instance the slight under prediction at around 400 – 500 Hz would seem to be balanced out by a somewhat over-prediction of the lower frequencies.

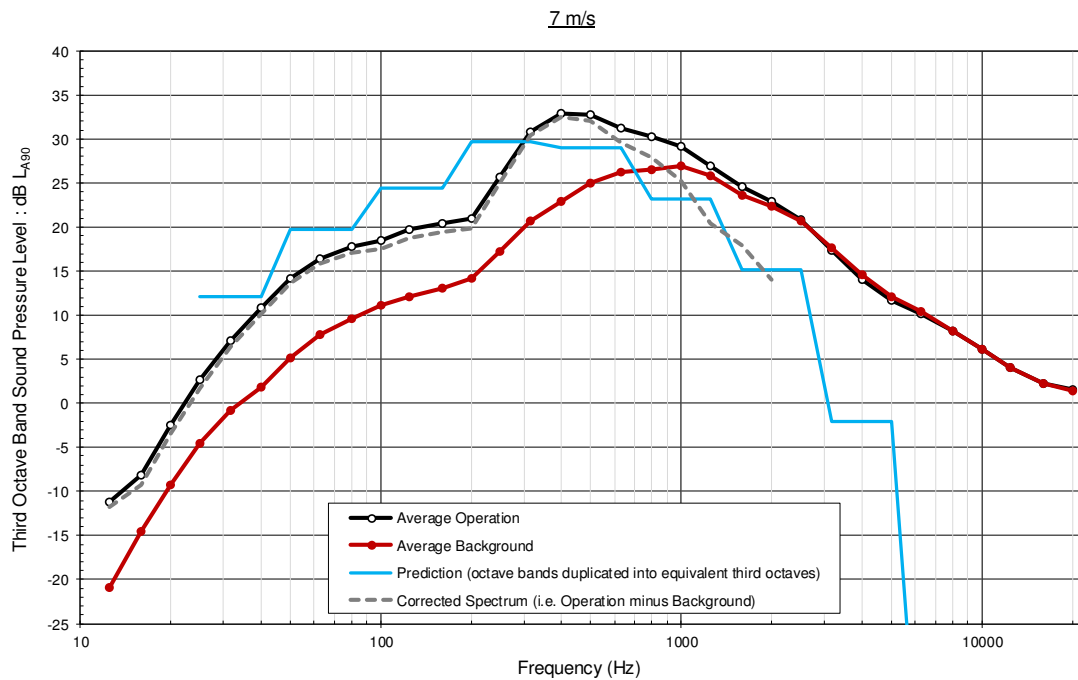


Figure 6: Average third octave band frequency spectra measured at Example 2 location, 7 m/s.

3.3 Example 3: location near some vegetation, at larger propagation distance

The Example 3 measurement is a residential location, located at a larger propagation distance of approximately 1.6 km away from the wind farm (at a different wind farm site and model to the previous examples). The sound level meter was located in a garden area facing the wind farm. At this location, there was not any watercourse nearby, and most of the audible background noise originated from medium sized trees on the edge of the garden approximately 20 m away. In this instance, unfortunately it was not possible to measure any background periods when the wind farm was not operating.

Figure 7 below shows regression analyses of the measured total noise levels (that are inevitably a combination of wind farm and background) as a function of wind speed at Example 3, for the downwind sector of this location. Panel a) shows the broadband results, panel b) shows results band-limited to ≤ 630 Hz, panel c) shows results band-limited to ≤ 315 Hz. The predicted noise level according to ISO 9613-2 is also shown for comparison. It can be seen that in particular, the prediction result for the ≤ 315 Hz band-limited option corresponds reasonably well with the measured average noise level, for wind speeds 4 – 7 m/s. For this distance and turbine model, compared to a broadband prediction, for the ≤ 630 Hz option there is a 1.4 dB predicted difference due to the loss in higher frequencies. For the ≤ 315 Hz option there is a predicted 3.9 dB loss in higher frequencies.

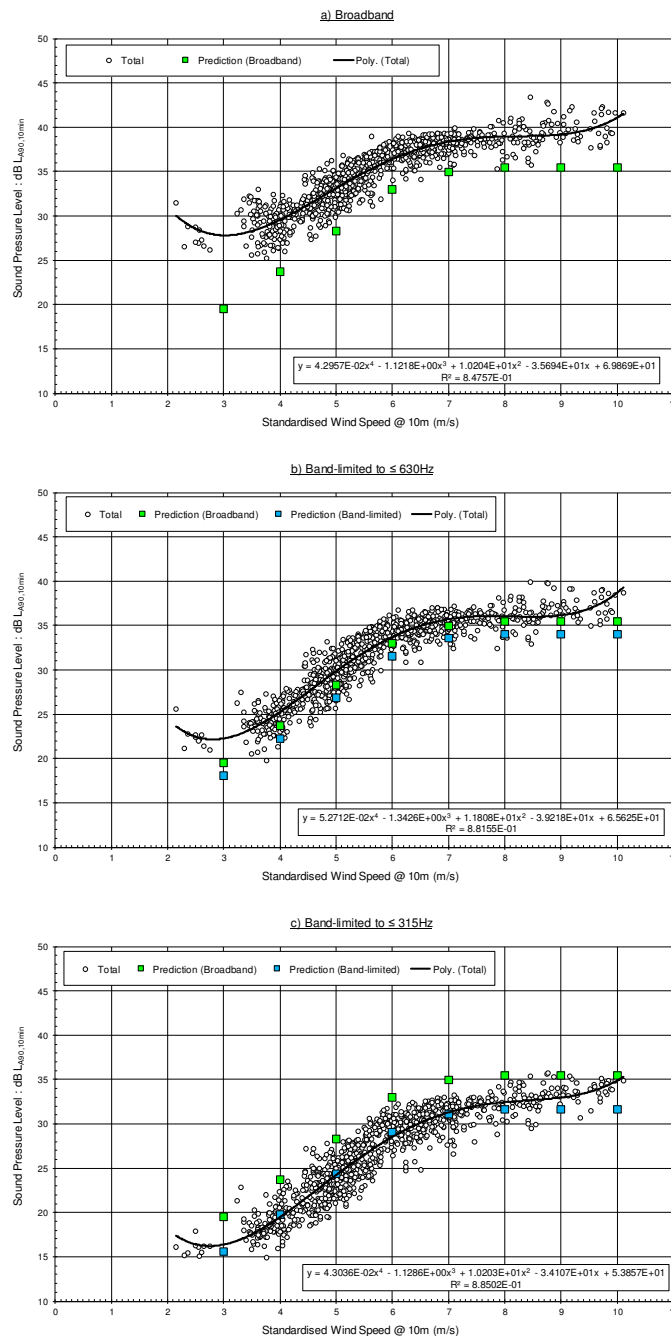


Figure 7: Noise regression results for different frequency band-limits at Example 3 location, a) broadband, b) band-limited to ≤ 630 Hz, c) band-limited to ≤ 315 Hz.

3.4 Example 4: another location near some vegetation, at larger propagation distance

The Example 4 measurement is a residential location, located at a propagation distance of approximately 1.1 km from the wind farm. This is again at a different wind farm site and model to the previous examples, with this turbine model including serrated trailing edges. The sound level meter was located in a garden area facing the wind farm. The main source of background noise originated from wind blowing through the medium sized trees approximately 20 – 30 m from the microphone location.

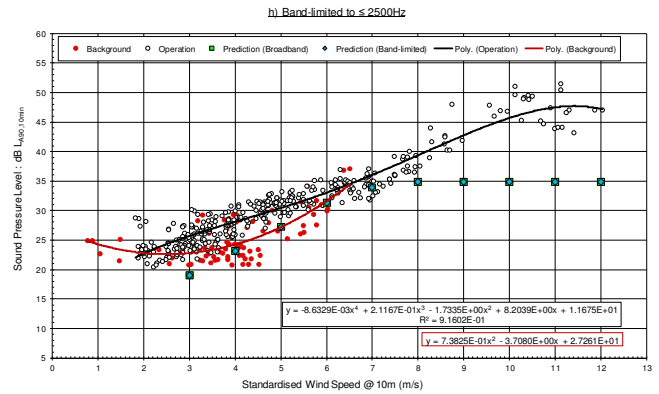
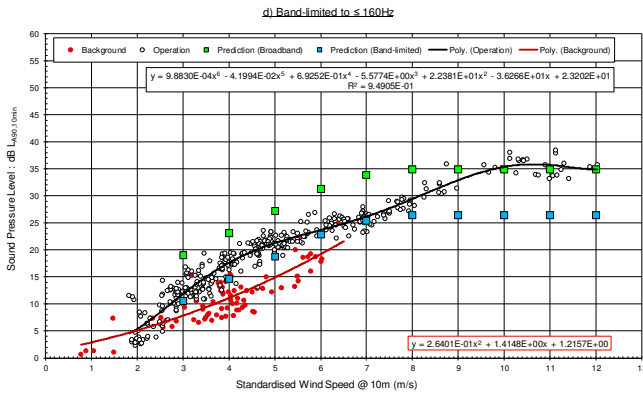
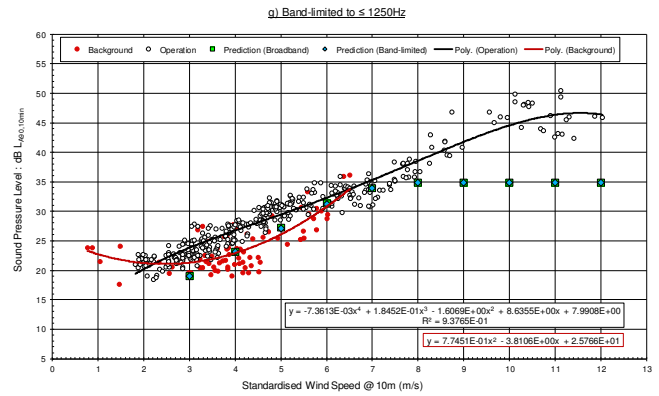
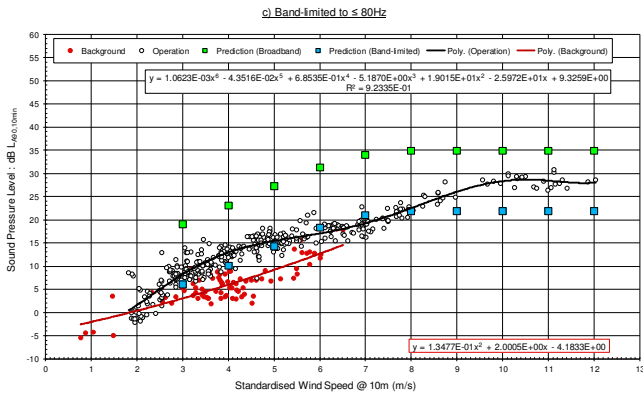
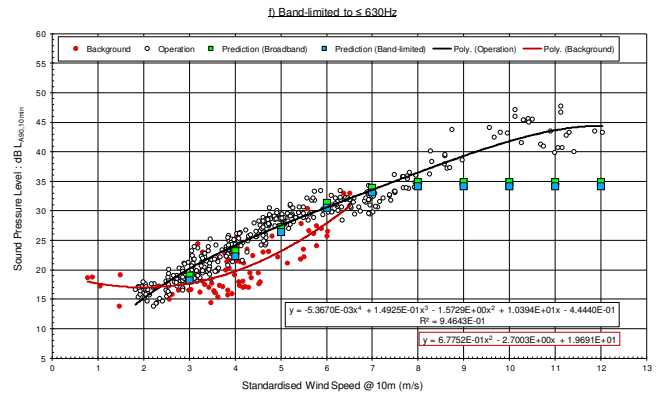
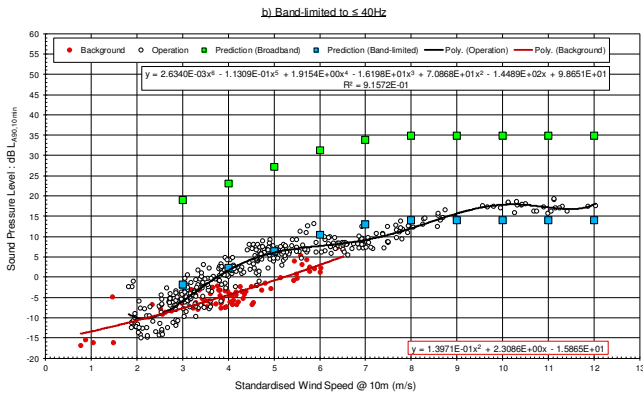
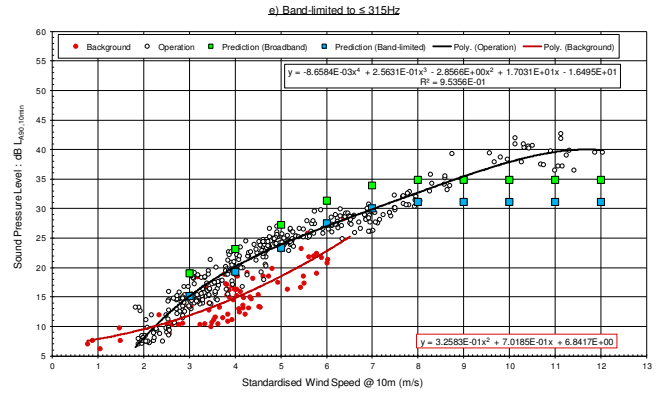
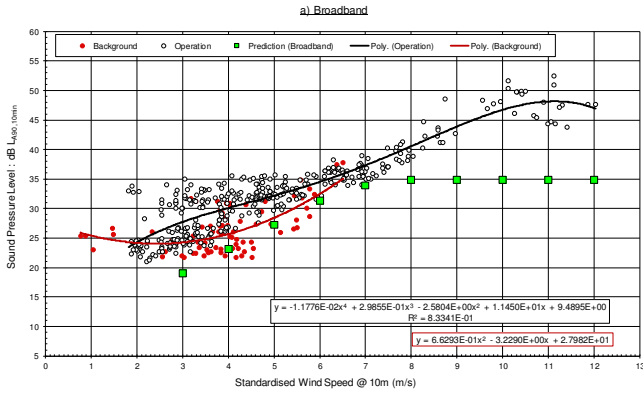


Figure 8: Noise regression results for different frequency band-limits at Example 4 location, a) broadband, and then band-limited to: b) ≤ 40 Hz, c) ≤ 80 Hz, d) ≤ 160 Hz, e) ≤ 315 Hz, f) ≤ 630 Hz, g) ≤ 1250 Hz, h) ≤ 2500 Hz.

Figure 8 above shows a variety of regression analyses of the measured operational and background noise levels, for the downwind sector at this location. These levels are limited to a progressively wider lower frequency range, such that panels b) – h) show band-limited results from: b) ≤ 40 Hz, c) ≤ 80 Hz, d) ≤ 160 Hz, e) ≤ 315 Hz, f) ≤ 630 Hz, g) ≤ 1250 Hz, h) ≤ 2500 Hz, and panel a) shows the broadband result in comparison. Compared to the broadband option, most of the lower frequency options provide a tighter regression curve and somewhat of an improvement in signal-noise ratio. In comparison to the equivalent predicted noise level, for most lower frequency options there is reasonable agreement between the measured and predicted noise level for wind speeds 3 – 7 m/s, with probably the best agreement shown for the ≤ 315 Hz and ≤ 630 Hz options. It is suspected that for higher wind speeds, measured noise levels become increasingly more affected by background wind effects, either from wind-induced noise on the microphone, or from wind blowing through the local vegetation. Unfortunately, the periods of non-operation were limited in this survey, such that it was not possible to measure background noise levels for wind speeds above approximately 7 m/s.

Table 2 below provides a summary of the prediction and measurement results for the 6 m/s wind speed bin. This details the possible trade-off that one may encounter with the band-limited approach. The analysis is generally improved via a greater signal-noise ratio and more certain polynomial, but a certain amount of higher frequencies are omitted from the measurement, that would need to be added back in to arrive back at a broadband wind farm result. For example at this location, compared to the broadband result, the ≤ 630 Hz and ≤ 315 Hz options result in an approximate 1 – 2 dB improvement in signal-noise ratio (with the R^2 correlation coefficient increasing from ~ 0.8 to ~ 1.0), but this is predicted to be at the expense of missing 0.8 dB and 3.8 dB of higher frequencies, respectively. For some locations and some wind turbine spectra, the amount missing from the measurement may be small enough to be acceptable, in order to achieve an arguably more certain assessment of the wind farm component of the noise.

Table 2: Summary of results at 6 m/s.

	Broadband [dB(A)]	Band-limited to:						
		≤ 40 Hz	≤ 80 Hz	≤ 160 Hz	≤ 315 Hz	≤ 630 Hz	≤ 1250 Hz	≤ 2500 Hz
Predicted L_{A90} noise level	31.3	10.5	18.3	22.9	27.5	30.5	31.3	31.3
Difference in level vs broadband		-20.9	-13.0	-8.5	-3.8	-0.8	0.0	0.0
Signal-noise ratio	2.0	4.6	4.4	4.5	4.2	2.7	1.5	1.4
R^2 value of operational regression	0.83	0.92	0.92	0.95	0.95	0.95	0.94	0.92
Improvement in signal-noise ratio		2.6	2.3	2.4	2.2	0.7	-0.6	-0.6
Improvement in R^2 value		0.08	0.09	0.12	0.12	0.11	0.10	0.08

Figure 9 below summarises the resultant corrected noise levels, relevant to the various band-limited regression options detailed above in Figure 8. The corrected noise level is the result of a logarithmic subtraction of the two polynomial regressions in each instance, derived only when there was a least 3 dB signal-noise ratio. Figure 9 shows those corrected noise levels, plus the addition of the amount of high frequencies predicted to be missing due to the band-limiting approach.

The broadband corrected result (derived from Figure 8a) may arguably be the most uncertain result, given this exhibits the smallest signal-noise ratio and greatest scatter of the majority of options. This is not surprising given the wind farm noise level, e.g. at 4 – 5 m/s, is expected to be around 23 – 27 dB L_{A90} , whilst at these wind speeds broadband background noise levels when the wind farm was off, was measured in the range 22 – 32 dB L_{A90} . That is, in an A-weighted broadband context, especially at low wind speeds, the wind farm is relatively low in the mix compared to other things in the local environment. The band-limited results shown in Figure 9 are closer to a predicted noise level than the broadband result, and to some extent overlay each other. If considering just the ≤ 160 Hz, ≤ 315 Hz, and ≤ 630 Hz options, the results are within 2.6 dB of each other and partially centred around the broadband prediction.

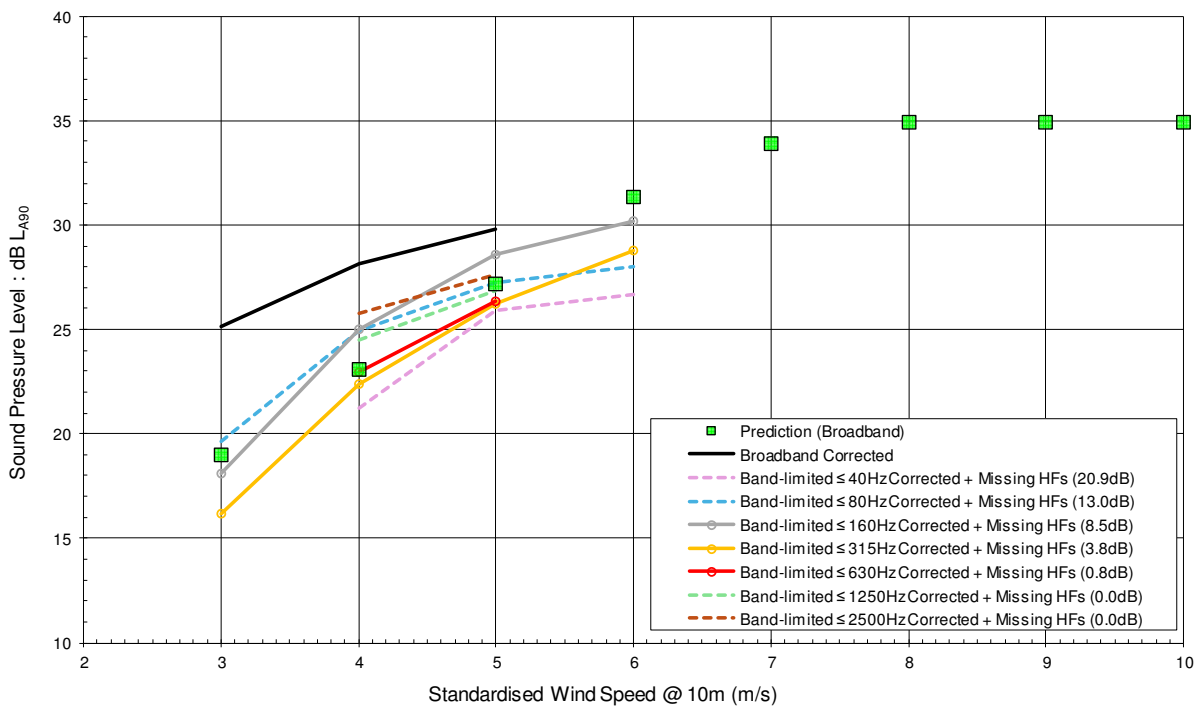


Figure 9: Corrected noise levels at Example 4 location, including the addition of predicted missing high frequencies.

Figure 10 below shows the average (A-weighted) third-octave frequency band spectra measured for the 6 m/s wind speed bin, for the downwind sector at this location, calculated by an arithmetic average. It can be seen that the operational and background levels are relatively comparable for frequencies above approximately 800 Hz. For frequency bands 31.5 – 500 Hz the signal-noise ratio is in the 4 – 6 dB range, with the largest value occurring in the 125 Hz band. For these frequency bands where there is good signal-noise ratio, there is reasonable agreement between the predicted and measured noise levels.

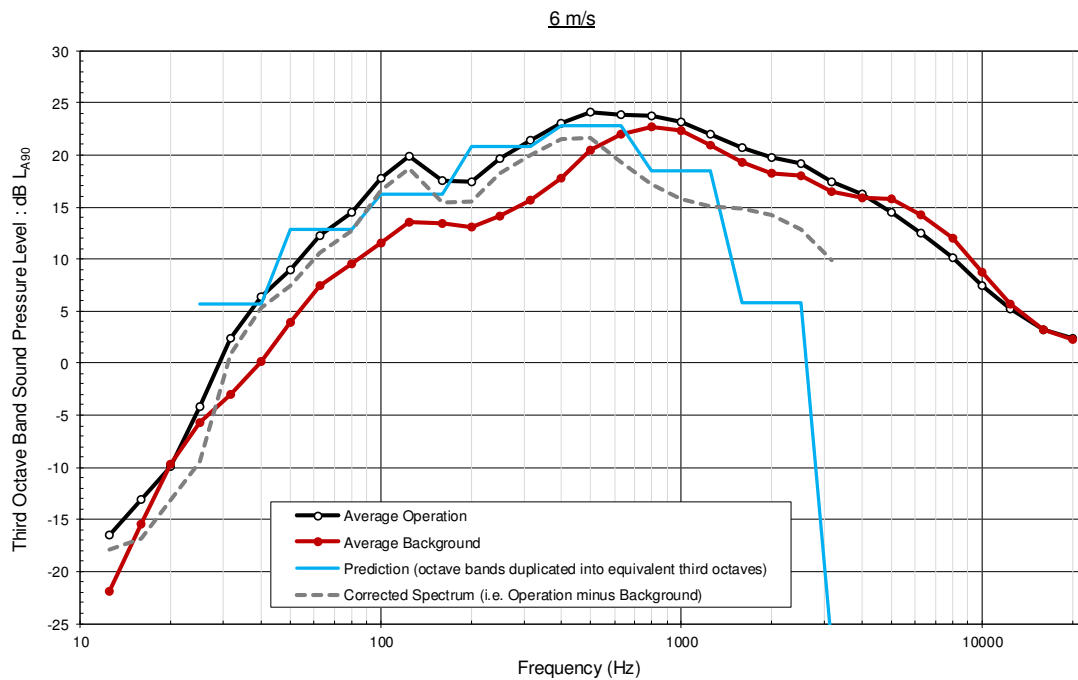


Figure 10: Average third octave band frequency spectra measured at Example 4 location, 6 m/s.

4. Conclusions

Regression analyses performed upon low-mid frequency band-limited data have been undertaken on noise measurements of operating wind farms at a sample of receptor locations.

In comparison to an analysis on broadband measured levels, the band-limited regressions of operational noise have generally demonstrated less scatter, resulting in less uncertainty in the derived polynomial that represents the dataset.

A larger signal-noise ratio has usually been achieved by discounting higher frequencies and limiting the regression analysis to a low-mid frequency range such as ≤ 315 Hz or ≤ 630 Hz. This arguably provides for a more accurate measure of the wind farm component of the total noise. A reasonable agreement with predicted noise levels according to ISO 9613-2 has usually been achieved.

The downside of the approach is that the higher frequencies are missing from the measurement. However, for the wind farm frequency spectra predicted, this may be a relatively small value compared to the overall broadband level. The gain achieved by having a tighter regression and a larger signal-noise ratio may be worth that trade-off. For example, if limiting the regressions to ≤ 630 Hz, the amount missing that would need to be added back in to arrive at a broadband result, is predicted to be of the order of 1 dB for the examples investigated.

References

- [1] *Acoustics - Attenuation of sound during propagation outdoors - Part 2: General method of calculation*, ISO 9613-2:1996, International Organization for Standardization, 1996.
- [2] *Wind turbine generator systems - Part 11: Acoustic noise measurement techniques*, IEC 61400-11:2006, 2.1 ed., International Electrotechnical Commission, 2006.

Paper #29 - ID: 363

Title: A comparison of turbine mitigation methods to achieve an 'n' decibel reduction in sound power level

Author: Kira Marshall

11th Edition of the
International Conferences on
Wind Turbine Noise

Copenhagen, Denmark – 10th to 13th June 2025

A comparison of turbine mitigation methods to achieve an ‘n’ decibel reduction in sound power level.

Kira Marshall and Merlin Garnett¹

Green Cat Renewables Ltd, Glasgow, Scotland.

Cameron Sutherland

Green Cat Renewables Ltd, Glasgow, Scotland.

Summary

Where noise mitigation is required for a turbine to meet a specified limit or achieve a sound power reduction to address a complaint, operating the turbine in a reduced power mode is a common method to limit the sound power level. This paper compares the effectiveness of reduced power modes, with an alternative method using blade pitch angle settings, to limit the power output such that a specific dB reduction requirement is achieved.

Following a desktop analysis of predictions using manufacturer’s data, field measurements were conducted in the vicinity of a 2.35MW turbine operating in each mitigation method. An overview of each method is provided with discussion on predictions, limiting factors in practice, and the results of each mitigation method.

1. Introduction

A complaint about wind turbine noise was raised in relation to a small wind farm in Scotland. A compliance test was conducted that demonstrated the turbine was operating within the approved noise limits. With agreement from the resident, a noise diary was kept and analysed to determine the range of wind speeds and directions on which to focus further investigation. The results of this demonstrated the most common complaints arose during windspeeds of 6.5m/s – 9m/s and in directions of 220° – 265°. The operator of the project indicated that they were willing to have mitigation applied to the dominant turbine in order to achieve a sound reduction at the resident’s property in the conditions of greatest concern. Owing to the resident’s reluctance to have further measurements conducted at their property, the local Environmental Health department agreed that material reductions in sound level demonstrated at the turbine would indicate that mitigation had been successful. The target level reduction was selected to be 3dB for hub height wind speeds and would activate at 7m/s and 8m/s (bin centres) and 247° +/- 30°.

¹ Corresponding authors – Email: kira.marshall@greencatrenewables.co.uk and merlin@greencatrenewables.co.uk

Following a desktop review of predictions and initial survey results, the proposed mitigation was to operate the turbine in ‘Alternative Power Modes’ (APMs) of 500kW at wind speeds up to 7.5m/s and 1000kW at windspeeds 7.5m/s – 8.5m/s. At windspeeds greater than 8.5m/s the turbine would operate in the standard mode of operation, Mode 0, with power peaking at 2,350kW in this case. As the windspeed range being targeted was narrow, it was decided that operating the turbine in the 500kW mode would smooth the transition of the turbine changing modes of operation at the lower windspeeds and the power curve did not vary greatly at the lower windspeeds, as shown below in Figure 1.

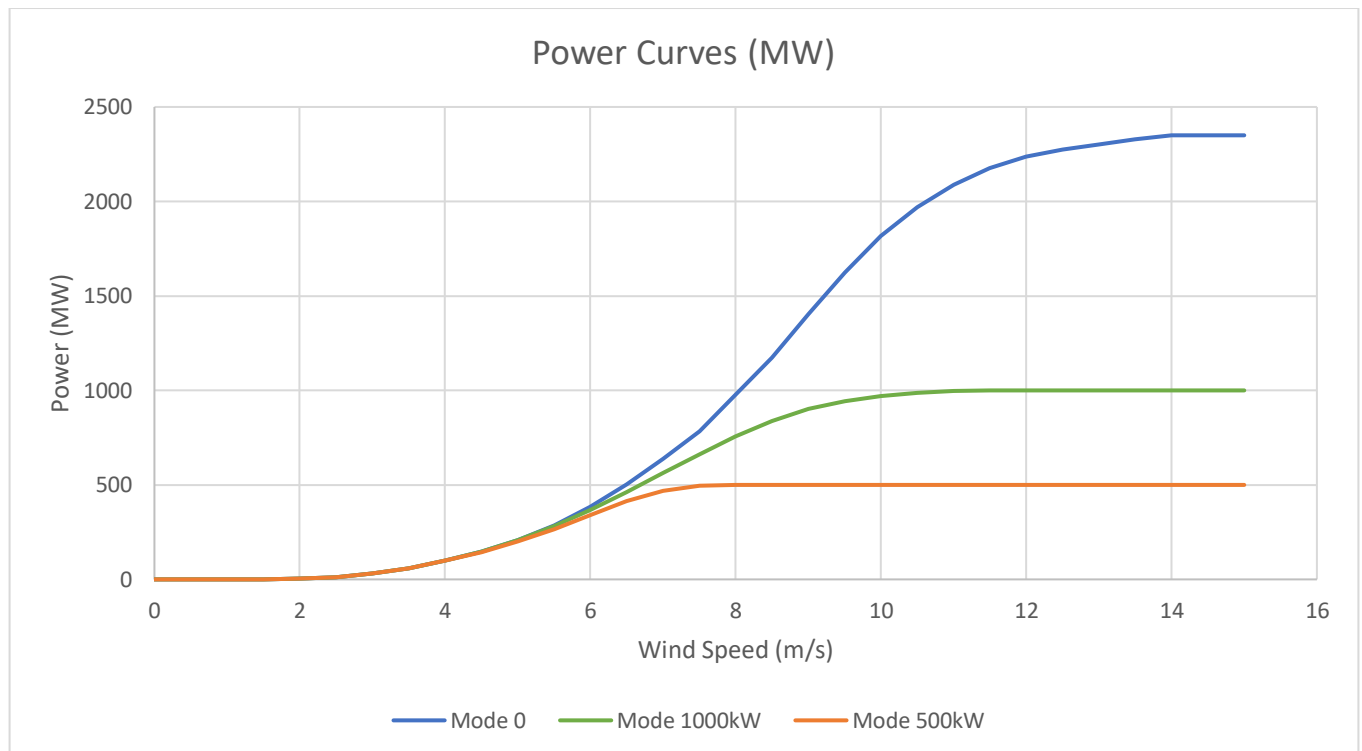


Figure 1 Comparison of power curves for alternative power modes

This mitigation operated to the satisfaction of the council for approximately one year with no further complaints from the resident. Following blade issues due to a lightning strike and subsequent repairs on the turbine, the complaint resurfaced in late 2024 with new diary entries suggesting slightly higher windspeeds contributing to annoyance than previously.

If the current mitigation was to be enhanced and/or extended to a wider windspeed range, the already significant impacts to the energy yield of the project would be increased. Therefore, an investigation into alternative mitigation in the form of pitch angle settings was conducted to assess the effectiveness of sound power reduction while balancing the resulting impact on the operation of the turbine.

Field work, in the form of IEC 61400 turbine sound power measurements [1], was undertaken to confirm the level of reduction the current APM mitigation was providing in comparison to the unmitigated baseline operation. Sound power measurements were then conducted for minimum blade pitch angle settings of 3°, 4° and 5°. The results of the measurement data were then compared, and comment is provided on the effectiveness of each scenario and observations regarding weather conditions and turbine operation. Additionally, the theoretical yield impact for each scenario was assessed to provide comment on the overall impact to the development.

2. Methodology

2.1 Determining Target Mitigation Conditions

The analysis of the resident’s noise diary correlated frequency and intensity of complaints with hub height wind speeds and directions. The results of this demonstrated the most common complaints arose during

windspeeds of 6.5m/s – 9m/s and in directions of 220° – 265°, which are the downwind conditions for the receptor. This provided the target conditions to apply mitigation as shown below in Figure 2.

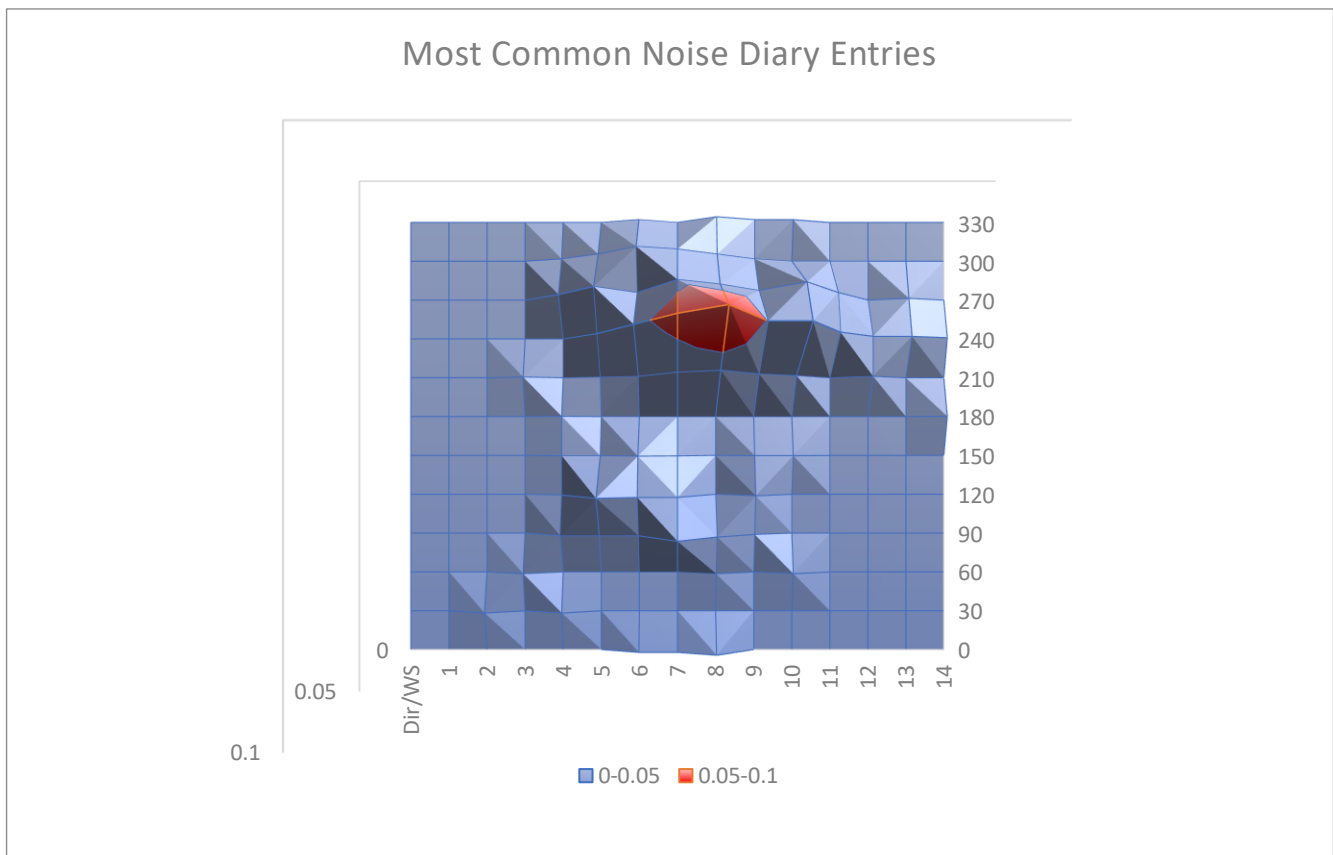


Figure 2 Spread of noise diary entries in relation to hub height wind speed and direction

Figure 2 plots the percentage of complaints recorded for each windspeed and direction for the duration of the noise diary.

2.2 Fieldwork Methodology

The aim of the survey was to measure sound power levels for the following operating conditions:

- Mode 0 (Unmitigated)
- Current Mitigation (500kW up to 7.5m/s, 1000kW up to 8.5m/s)
- 3° minimum blade pitch angle
- 4° minimum blade pitch angle
- 5° minimum blade pitch angle

The pitch angles to be tested were chosen based on the expected power curve and how that compared to Mode 0 and the current mitigation. As can be seen below in Table 1, the power output values at lower wind speeds are comparable or marginally lower across all settings than Mode 0. At 7-8m/s, the blade pitch settings reduce the power output in comparison to Mode 0 but are slightly higher than the APM mitigation. This is the critical area of balancing power output and reducing sound levels.

Table 1 Power Curve (kW) for each operating mode

Hub Wind Speed (bin centre)	Mode 0	Current Mitigation	3°	4°	5°
4	98	98	90	86	78
5	208	200	201	196	181
6	384	340	372	355	330

Hub Wind Speed (bin centre)	Mode 0	Current Mitigation	3°	4°	5°
7	637	470	602	573	533
8	976	757	903	857	799
9	1404	1404	1249	1186	1112
10	1818	1818	1593	1517	1433

Initial testing was conducted for 4° and 5° with the decision to either increase or decrease the angle depending on the outcome of those measurements. As the results of 4° were only marginally different to 5°, it was decided to test 3° to see how this compared to 4°.

To gain an understating of the current mitigation in practice, the windspeed and direction parameters were kept in place. For the mitigation to activate, the conditions would need to be present for 1-minute before the turbine switches mode of operation. For the blade pitch setting tests, windspeed and direction limitations were not applied to allow measurement of the setting without interruption.

The measurement, data reduction, and calculations for each test scenario were carried out in accordance with IEC 61400 Edition 3.0, 2012 “Wind turbine generator systems – Part 11: Acoustic noise measurement techniques” [1] Concurrent data were recorded from the turbine SCADA output and an IEC 61672-1 Class 1 sound level meter (SLM) in 10 second increments. For periods of turbine shutdown, meteorological data at hub height was measured from a LiDAR unit installed on site. Determination of the acoustic performance of the wind turbine (WT) was achieved through measurements during operation (total sound level) and non-operation (background sound level). To establish the co-variance of sound levels with wind speed, sound levels were plotted against hub height wind speeds as measured by the turbine or LiDAR.

Having established sound levels for each half-integer wind speed bin with the turbine switched on and off, sound pressure levels attributed to the test turbine were calculated by logarithmic subtraction of the background noise levels from operational noise levels. A level difference not less than 6dB was found to occur between operational and background sound levels. Where there was less than 10 data points in a wind speed bin, the value has not been included in the analysis.

To compare the impact each mitigation scenario has on the potential energy yield of the turbine, a theoretical calculation of yield using the manufacturer’s power curve for each setting was produced.

To obtain sufficient data in the target meteorological conditions, measurements were conducted across four separate days. Details of each measurement position, instrumentation and test turbine are provided below in Tables 2, 3 and 4.

Table 2 Measurement Geometry

Parameter	13/01/2025	14/01/2025	25/02/2025	06/03/2025
1.) Horizontal distance noise source – measurement position				
Measuring distance (R0)	101.8 m	113.2 m	114.6 m	115.5 m
Distance rotation plane of the rotor – centre line of the tower	2.65 m	2.65 m	2.65 m	2.65 m
2.) Vertical distant noise source – measurement position				
Hub height	69 m	69 m	69 m	69 m
Microphone height	0 m	0 m	0 m	0 m
Height Difference (Altitude)	2 m	2 m	2 m	4 m
Total Vertical height	67 m	67 m	67 m	65 m
Distance noise source – measurement position (R1)	124.1 m	133.8 m	135.0 m	134.8 m

Parameter	13/01/2025	14/01/2025	25/02/2025	06/03/2025
Ø	32.7°	30.0°	29.8°	28.8°

Table 3 Details of Instrumentation

Instrument	Make	Model	Serial No.	Calibration Date
Logger (Turbine)	CampbellSci	CR1000	E8868	-
Logger (LiDAR)	ZX LiDAR	ZX 300	856	04/07/2024
Sound Level Meter (IEC 61672-1 Class 1)	Rion	NL-52	01032465	29/02/2024
Microphone	Rion	UC-59	05860	29/02/2024
Pre-amplifier	Rion	NH-25	32493	29/02/2024
Acoustic Calibrator (IEC 60942 Class 1)	Rion	NC-74	34494275	08/05/2024

Table 4 Turbine Details

Operating Details	
Vertical or horizontal axis wind turbine	Horizontal
Upwind or downwind rotor	Upwind
Hub height	69 m
Horizontal distance from rotor centre to tower axis	2.65 m
Diameter of rotor	92 m
Tower type (lattice or tube)	Tube
Passive stall, active stall, or pitch controlled turbine	Full pitch control
Constant or variable speed	Variable
Rotational speed at wind bins	Max 17 rpm
Rated power output	2350 kW
Gearbox	Direct drive (no gearbox)
Rotor Details	
Rotor control devices	Pitch/ Annular generator
Presence of vortex generators, stall strips, serrated trailing edges	Serrated Trailing Edges
Number of blades	3

The measurement equipment set-up in relation to the turbine under test is shown in Figure 3.



Figure 3 Measurement equipment in relation to the turbine

3. Results

The calculated sound power results for each measurement conducted is provided in Table 5.

Table 5 Sound Power Level Results

Test Setting	Hub Height Wind Speed (m/s)	5.5	6	6.5	7	7.5	8	8.5	9	9.5	10
Mode 0 (25/02/2025)	Number of Values	25	31	56	61	63	53	45	42	21	16
	Average value (LAFeq)	96.3	97.3	98.9	100.2	101.5	102.4	103.1	103.5	103.5	103.8
Mode 0 (06/03/2025)	Number of Values	-	17	28	36	58	79	129	166	206	221
	Average value (LAFeq)	-	98.8	99.0	101.2	102.3	103.7	104.2	104.5	104.8	105.0

Test Setting	Hub Height Wind Speed (m/s)	5.5	6	6.5	7	7.5	8	8.5	9	9.5	10
Current Mitigation (13/01/2025)	Number of Values	13	34	45	36	33	23	38	20	34	34
	Average value (LAFeq)	99.9	100.8	100.9	100.9	101.8	104.2	104.3	105	105.9	106.6
Current Mitigation (14/01/2025)	Number of Values	-	16	49	48	38	23	12	-	-	-
	Average value (LAFeq)	-	99.8	99.5	99.6	99.7	100.8	100.0	-	-	-
3 degrees (25/02/2025)	Number of Values	32	57	69	58	55	34	22	17	-	-
	Average value (LAFeq)	96.0	96.6	97.6	99.2	100.4	100.6	101.7	102.2	-	-
3 degrees (06/02/2025)	Number of Values	-	-	-	-	-	-	22	33	42	55
	Average value (LAFeq)	-	-	-	-	-	-	103.8	103.9	103.9	104.0
4 degrees (14/01/2025)	Number of Values	11	16	27	35	36	59	44	36	19	-
	Average value (LAFeq)	98.4	98.0	99.2	100.0	101.4	102.0	102.3	102.7	102.9	-
5 degrees (14/01/2025)	Number of Values	36	34	31	36	48	46	41	41	27	31
	Average value (LAFeq)	94.5	96.9	97.5	99.5	100.6	101.5	102.0	102.6	103.2	103.3

Due to the variability in wind conditions Mode 0, Current Mitigation, and 3 degrees were measured on two different days. The range of windspeeds experienced on each measurement day is shown in Figure 4.

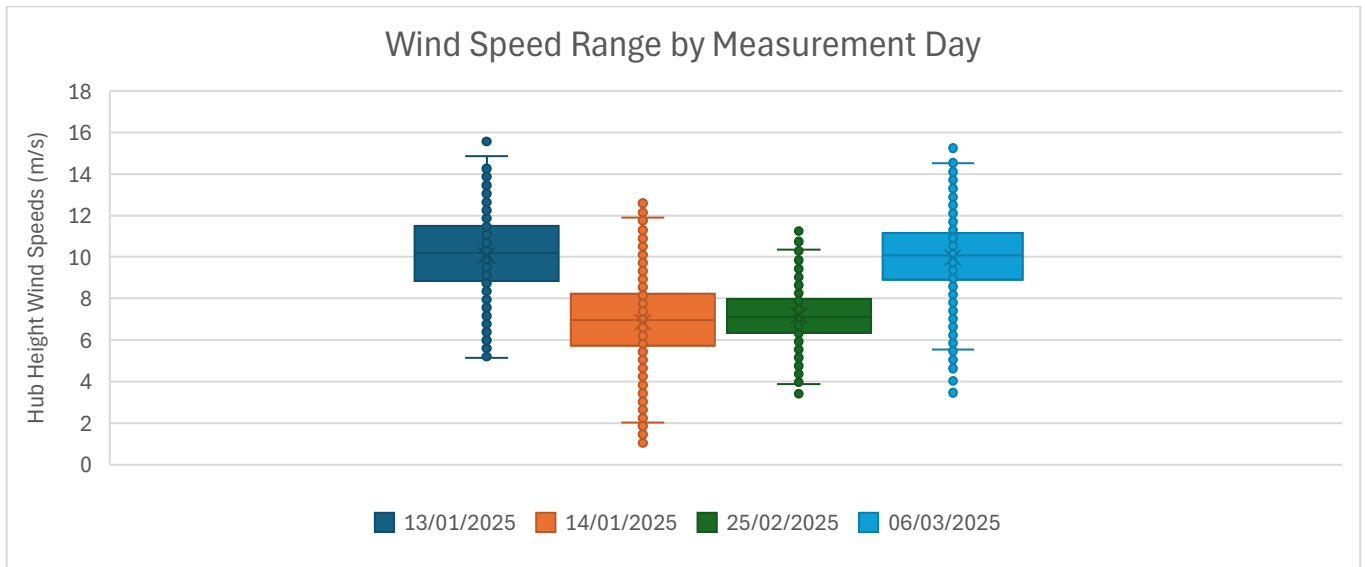


Figure 4 Range of windspeeds on each measurement day

The box for each day highlights the wind conditions that the turbine was generally operating within for each day. This graph demonstrates that while each day experienced the full range of target windspeeds, the overall conditions were higher on the 13th January and 6th March. This impacts the amount of time the APM mitigation is actually active as the turbine changes in and out of mitigation throughout the measurement period. Turbine status data was reviewed to confirm which mode the turbine was operating in and the duration.

Additionally, the Mode 0 data measured on 25/02/25 and 06/03/25 showed higher variances than expected. Conditions on the 25th February were very stable and as shown in Figure 4, a narrower range of windspeeds were experienced. By comparison, the windspeeds on the 6th March covered a wider range. The number of data points was significantly lower on the 25th February and may be a contributing factor to the lower levels recorded. While the measured sound power levels on the 6th March are higher, these are in closer alignment with the expected maximum output as the turbine has a maximum sound power of 105dB(A) according to the manufacturer’s datasheet. A comparison of both measurement days is shown below in Figure 5.

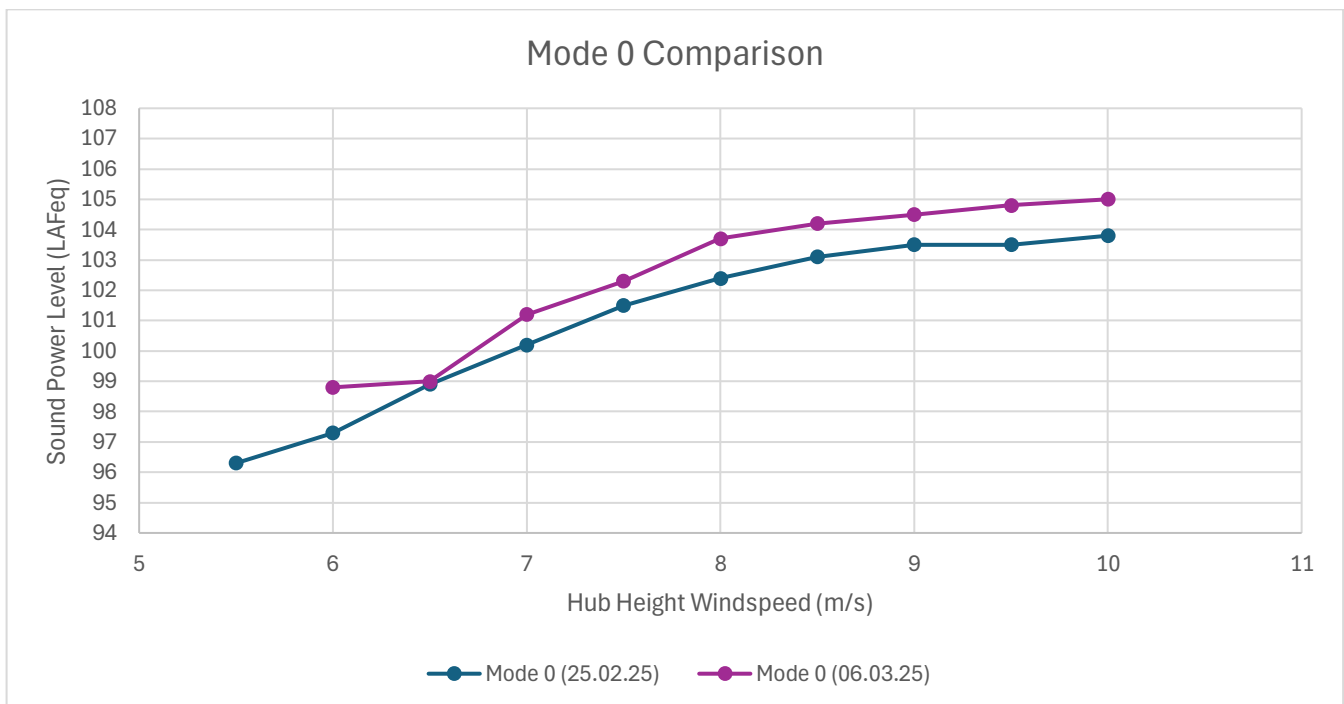


Figure 5 Comparison of Mode 0 Measurements

As the primary targeted windspeed is 8m/s, which occurs during both low-mid range wind conditions and mid-high range conditions, on days with wide variation in wind conditions this windspeed bin consists of both unmitigated and mitigated levels. This means that there will be data points at 8m/s where the time window/conditions for activating the mitigation have not been triggered yet. The standard time hysteresis before triggering mitigation is 2 minutes. During test measurements of the APM mitigation during 2023 it was decided to reduce this to 1 minute to increase the frequency of mitigation being active.

As can be seen from Figure 6, the results from the 13th January, where wind conditions were generally higher and the mitigation was not always active, the desired reduction in sound level was not achieved. In comparison, during stable conditions on the 14th January where the turbine remained in the reduced power modes, the current mitigation does provide the expected reductions, with the target 3dB being met at 8m/s. This shows that while the APM mitigation can achieve the desired sound power reduction, on days where the operating mode changes regularly between Mode 0 and reduced power, or wind conditions result in the mitigation not triggering often enough, the expected reductions are not seen in the data.

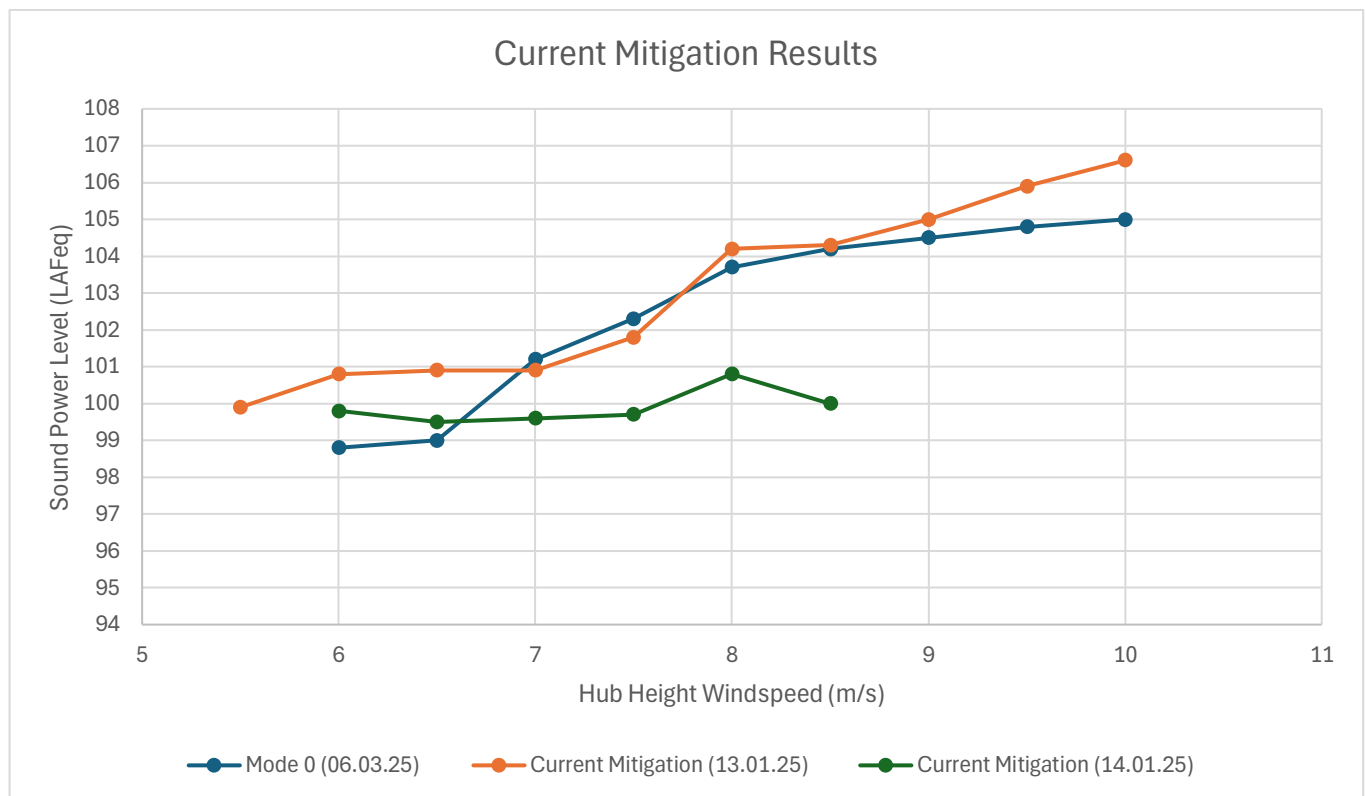


Figure 6 Current Mitigation Results

On the 14th January, 4° and 5° minimum pitch angle settings were tested. It was expected that, depending on the outcome of these measurements, the minimum pitch angle would either be increased or decreased for further testing. Shown below in Figure 7, the level reduction was similar for both settings and a consistent 2dB reduction for 7-9m/s was measured for 5°.

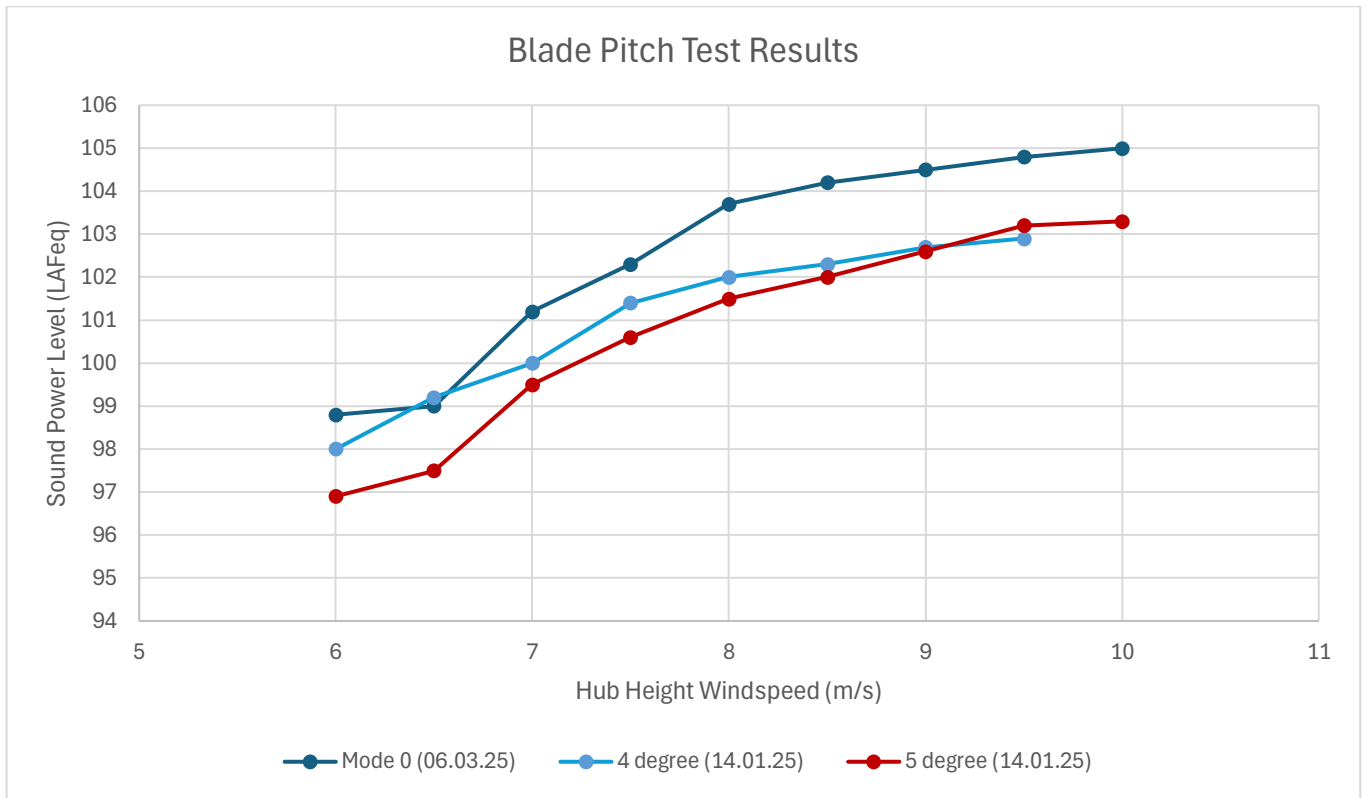


Figure 7 Blade Pitch Test Results

As the results of 4° did not vary greatly from 5°, and both degree settings evened out at 9m/s, it was decided to test 3°. If similar results were found at wind speeds 9m/s and above, then this would provide an option for extending the mitigation range with less impact on project energy yield. On this test day (25/02/25), the wind conditions were stable and did not increase above 8m/s consistently. The results shown below, demonstrate a 2dB reduction at 8m/s before trending towards the baseline, as expected, although still providing a lower level.

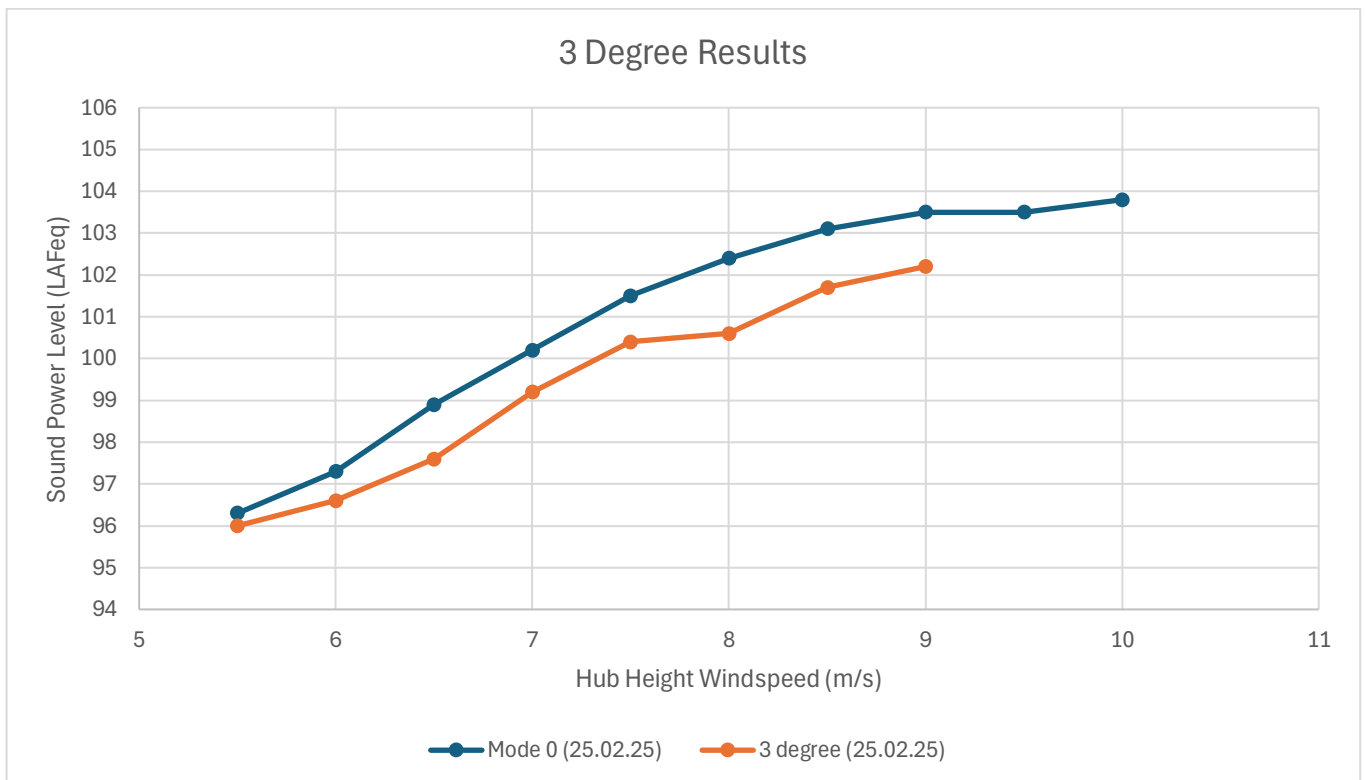


Figure 8 3 Degree Results

Due to the 3° results being unexpectedly lower in level than the 4° and 5° results, it was planned to re-take the measurements. However, the wind conditions at the time of re-testing did not drop below 8.5m/s, and so a further comparison is yet to be made.

4. Discussion

The results of the current mitigation show that when consistently active, the target level of sound reduction can be achieved at the main windspeed bin of 8m/s. However, on days where the turbine is fluctuating in and out of mitigation settings, mitigation is not always active during the key complaint windspeed of 8m/s. To improve this, it is likely that extending the mitigation over a wider windspeed range would be needed to ensure the mitigation is triggered frequently enough during the most common complaint conditions. By extending the mitigation up to 10.5m/s, a significant impact on energy yield would occur. To compare the mitigation scenarios from this perspective, a theoretical calculation of yield using the manufacturer’s power curve for each setting has been produced. The results were then compared to the theoretical maximum of the turbine operating without noise curtailment, and Figure 9 below shows the resulting impact for each scenario. The blue represents mitigation being applied up to the current parameter of 8m/s (bin centre) and the red shows the impact if this were to be extended to 10m/s (bin centre). These calculations assume the mitigation is only applied during down wind conditions of the receptor +/-30°.

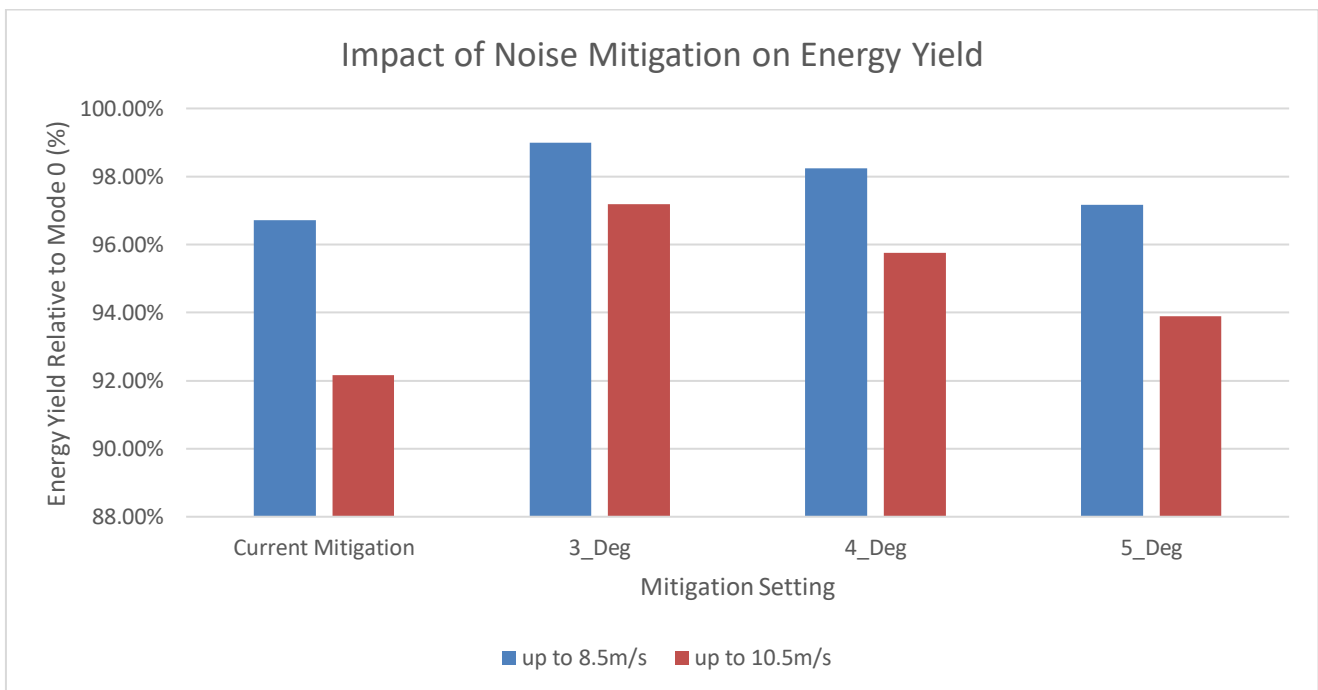


Figure 9 Comparison of Impact on Energy Yield

It can be seen that the current method of using APMs would result in a significant impact on yield were this to be extended to a wider range of windspeeds. By comparison, the blade pitch angle settings wouldn’t lose as much energy even under extended conditions. This is a promising result as both 3° and 4° could be trialled in a wider range without significant difference to the current impact. Even if a 3dB reduction is not met by applying minimum blade pitch settings, decreasing the levels over a wider range could improve the overall perception of the turbine noise.

Additionally, results at windspeeds lower than 7m/s show that it is difficult to get a 3dB reduction owing to the fact the power curves do not vary significantly under these conditions for any setting. The greatest reductions are therefore found between 7-10m/s where the difference in efficiency of Mode 0 compared to either form of mitigation is largest. While this does not impact this specific complaint investigation, it is worth noting for other sites.

Visits to site and analysis of data have shown that the general meteorological conditions can have an impact on results at the mid-range windspeeds. The analysis would benefit from increased number of data points

for each windspeed bin and/or multiple measurements days to confirm results. This would ensure results reported for any windspeed bin are representative of the turbine in those conditions rather than being influenced by a high deviation in wind speed captured by the high resolution 10-second measurements. Ideally, Mode 0 would be measured on each test day for direct comparison, however, this was not always possible due to the duration the target wind conditions were present on each test day.

5. Conclusions

An investigation into turbine noise mitigation methods comparing alternative power modes and blade pitch angle settings has been conducted. The turbine under test has been the subject of a noise complaint and a target level reduction of 3dB was agreed with the EHO.

The measurement results demonstrated the difficulty with targeting a narrow range of windspeeds as the level of reduction varied depending on the stability of the windspeeds at the time of surveying. To improve the frequency of mitigation activating in these conditions, the windspeed range could be extended. However, the APM method of mitigation results in a significant impact on potential energy yield of the project.

The minimum blade pitch angle tests demonstrated that a consistent level reduction could be achieved in the target range of windspeeds. By adjusting the minimum blade pitch angle, intervention from the control system to limit power is removed, which results in less unintended impact on adjacent windspeeds of the targeted range. Additionally, this method of mitigation would have a less severe impact on energy yield, providing a better balance between reducing overall sound levels and affecting the yield potential of the development.

References

- [1] International Standard, "IEC 61400-11:2012 Wind turbines - Part 11: Acoustic noise measurement techniques," 2012. [Online]. Available: <https://webstore.iec.ch/en/publication/5428>.

Paper #30 - ID: 364

Title: An investigation of immission spectrum resulting from increasing turbine rotor diameter

Author: Merlin Garnett

11th Edition of the
International Conferences on
Wind Turbine Noise

Copenhagen, Denmark – 10th to 13th June 2025

Spectral Variability in Wind Turbine Noise Immissions: Effects of Rotor Size, Design, and Trailing Edge Serrations.

Justin Lee and Merlin Garnett¹

Green Cat Renewables Canada, Calgary, Canada

Green Cat Renewables Ltd, Glasgow, Scotland.

Kira Marshall and Cameron Sutherland

Green Cat Renewables Ltd, Glasgow, Scotland.

Summary

This study was undertaken to better understand how noise immissions vary between different types and sizes of wind turbines. The goal is to support more informed design and siting decisions in wind energy projects, particularly in areas where wind energy development is relatively new. Specifically, the analysis focused on the one-third octave band immission spectra produced by individual wind turbines of varying rotor diameter, tip height, and generating capacities. The study used predictive modelling based on manufacturer-provided data at maximum sound power, simulating conditions typical of wind farm planning where compliance with a specific noise limit is required.

A total of forty turbine models from various manufacturers were analysed, including both standard configurations and models equipped with trailing edge serrations (TES); small ridges added to the blade's trailing edge to reduce noise. Each turbine was modelled such that an immission level of 37 dBA L_{eq} was achieved at the receptor location, representing a level likely to be audible above typical rural background under moderate wind conditions. This setup enabled a consistent basis for comparing spectral content across turbine types.

The analysis revealed that, across all 40 turbines, the frequencies between 315 Hz and 1 kHz consistently emerged as the most prominent contributors to the total immission level at the receptor, regardless of differences in turbine size or design. While a weak positive correlation between rotor diameter and low frequency energy was observed, this relationship was not strong. Turbines equipped with TES exhibited consistent spectral redistributions at both low and high frequencies, indicating that the perceived sound at the receptor may differ noticeably from non-TES variants, even when overall A-weighted sound levels are equal. This finding could be particularly relevant in contexts where low-frequency sensitivity is a concern.

¹ Corresponding authors – Email: Justin.Lee@greencatrenewables.ca and merlin@greencatrenewables.co.uk

These results challenge the common perception that larger turbines inherently produce fundamentally different noise characteristics, particularly in the low-frequency range. While it was intuitively expected that larger rotors would result in increased low-frequency emissions, the study found that spectral differences were more closely tied to manufacturer-specific design decisions – such as blade shape, hub and nacelle design, tower design, and mechanical noise sources – than to general turbine parameters like size or rated power output.

By highlighting both the relative spectral similarities and subtle distinctions across a wide range of turbine models – including modern large-rotor designs and older, smaller turbines – this study offers valuable insights into how turbine type and design may influence community noise perception. This is particularly relevant in regions new to wind energy development, where public understanding of turbine acoustics may be limited. The receptor-focused approach used in this study, and its alignment with how turbine noise is evaluated during permitting processes, mirrors assessment frameworks applied in practice and offers useful context for regulators and developers evaluating potential noise impacts from different turbine configurations.

1. Introduction

Wind energy has become a key component of the global transition toward sustainable energy solutions. However, concerns regarding wind turbine noise remain a notable consideration in project development and community engagement – particularly in regions where turbines are a relatively new presence, such as Alberta, Canada. In such areas, residents may have limited experience with the audible characteristics of wind turbines, and uncertainty about what turbines will sound like and how that sound may affect them can be a major source of concern.

The acoustic characteristics of wind turbines may be influenced by multiple factors, including rotor diameter, manufacturer, and aeroacoustic treatments (e.g., serrations). Exploring how these variables relate to noise emissions and immissions may help improve understanding of what future wind farms sound like to nearby communities—and, in turn, support more informed dialogue and potentially greater acceptance of wind energy developments.

A resident near a potential wind farm may assume that the immission spectrum from a large, modern wind turbine would exhibit a different sound character than that produced by smaller turbines. Larger rotors typically operate at lower maximum revolutions per minute (rpm), potentially affecting the frequency content of the sound experienced at nearby receptors. This study explores whether, from the perspective of a wind project neighbour, the immission spectrum of a modern, large-rotor wind turbine differs significantly from that of legacy turbine models from the last 20 years or so, that used smaller diameter rotors. The goal is to provide a clearer picture of any variation in turbine sound character and how these differences may influence design and siting decisions for wind energy projects.

2. Methodology

This study included a total of 40 different wind turbine models, 18 with TES and 22 without TES, representing various manufacturers and turbine sizes. The key steps in the analysis are outlined below:

2.1 Noise Modelling

Noise models were developed for each candidate turbine using sound power data provided by the turbine manufacturer. The lowest hub height listed on the manufacturer's datasheet was used, and the lowest hub height wind speed at which the sound level reaches its maximum was considered. To account for uncertainty regarding the sound power data used in the modelling, three approaches were applied:

- Where the manufacturer did not specify an uncertainty value, an additional 2 dB was added to the sound power levels.
- Where the manufacturer included uncertainty in the data, no extra uncertainty was added.
- Where the manufacturer specified a margin of uncertainty, that value was incorporated in the sound power levels.

Using these parameters, noise propagation simulations were performed using CadnaA, assuming a ground attenuation factor of 0.5 and receptor height of 4m, in accordance with the ISO 9613-2 (2024) [1]. The setback distance at which the receptor would receive a predicted immission L_{eq} of 37 dBA was determined. Topography was not included in the models.

2.2 Turbine Selection and Data Collection

The data set consisted of turbines from multiple manufacturers and included a broad range of rotor diameters and generating capacities. For each turbine, both TES (if available) and non-TES sound power levels were considered, including relevant uncertainty. Where available, third-octave band data was used as input to the model, otherwise, octave band data was used.

2.3 Analysis of Distance and Frequency Content

The relationship between rotor diameter and the predicted distance at which a receptor would experience a 37 dBA immission level was assessed. Furthermore, the immission spectrum at the receptor location was examined to identify trends in frequency content distribution.

2.4 Low frequency analysis

An indication of low frequency content for each candidate turbine was derived by subtracting 'A' weighted from 'C' weighted immission values, expressed as an integer dB difference. This method is commonly used for quantifying low-frequency sound in Canada [2].

2.5 Comparative Evaluation

Additional turbine characteristics, including broadband sound power level and power generation capacity, were analysed to identify potential correlations with immission spectra. Detailed comparative analyses were conducted between:

- Turbines with similar sound power levels but differing rotor diameters and generating capacities.
- Turbines with similar rotor diameters but from different manufacturers.

3. Results

Overall Statistics

Table 1 presents the maximum and minimum range of key parameters included in the analysis.

Table 1 – Maximum and Minimum Range of Single Figure Parameters for Assessed Turbines

	Rotor Diameter (m)	Hub Height (m)	Setback Distance (m) for 37 dBA	Capacity (MW)	Maximum Sound Power (dBA) ²	dBC-dBA (dB)
Minimum	52	40	427	0.5	100.7	9
Maximum	175	120	1140	6.8	111.3	18

Figure 1 shows the included rotor diameters.

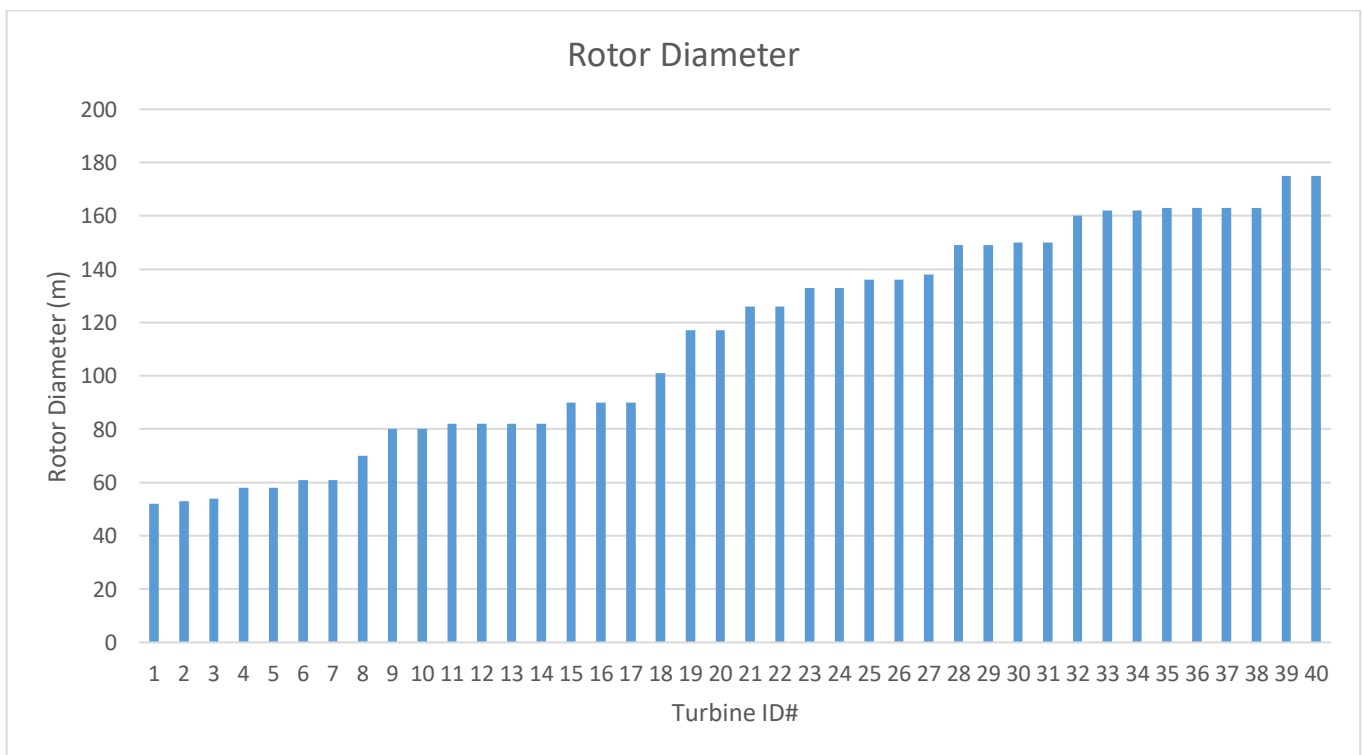


Figure 1 – Rotor Diameters for All 40 Turbines

Figure 2 shows the 37 dBA setback distance for the turbines included in the analysis, corresponding to the same Turbine ID as shown in Figure 1.

² Inclusive of uncertainties described in section 2.1

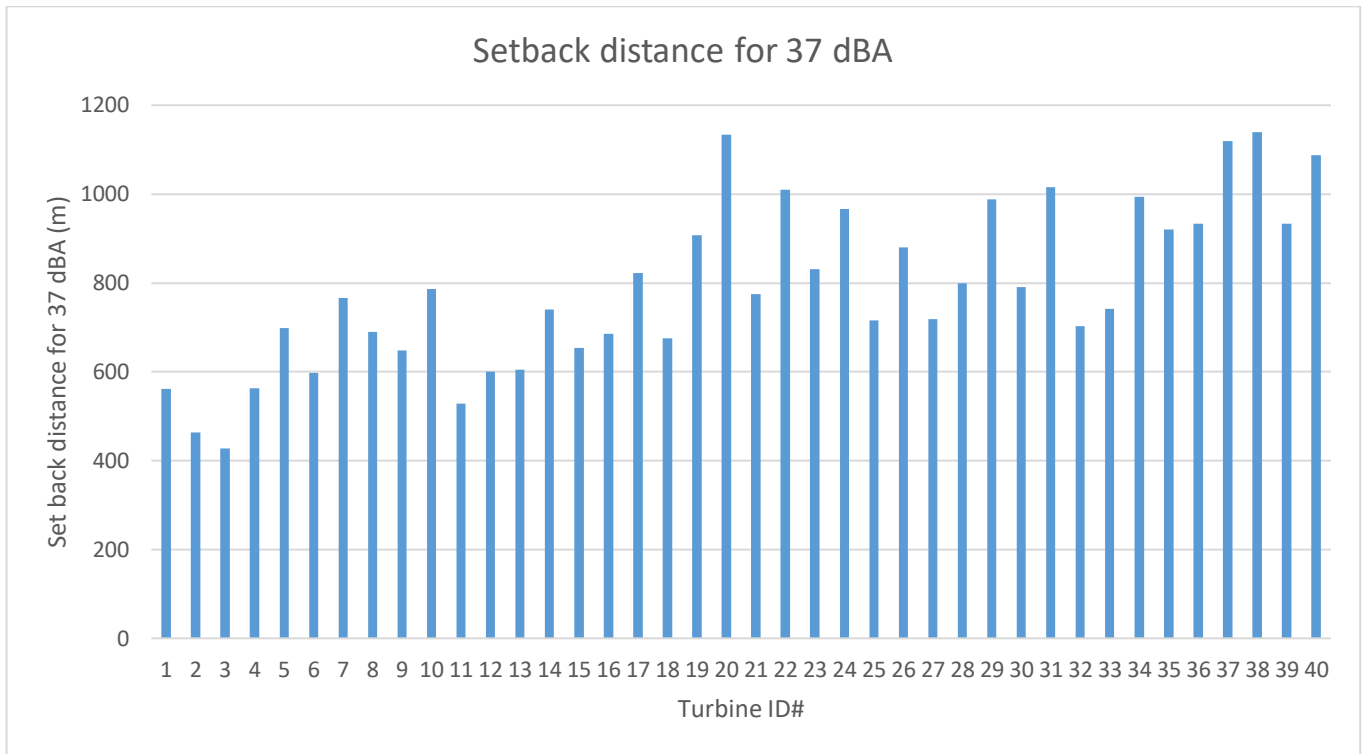


Figure 2 – 37 dBA Setback Distance for All 40 Turbines

Figure 3 shows the resulting immission spectra at the receptor location as one-third octave bands. A larger version of this figure can be found in Appendix A.

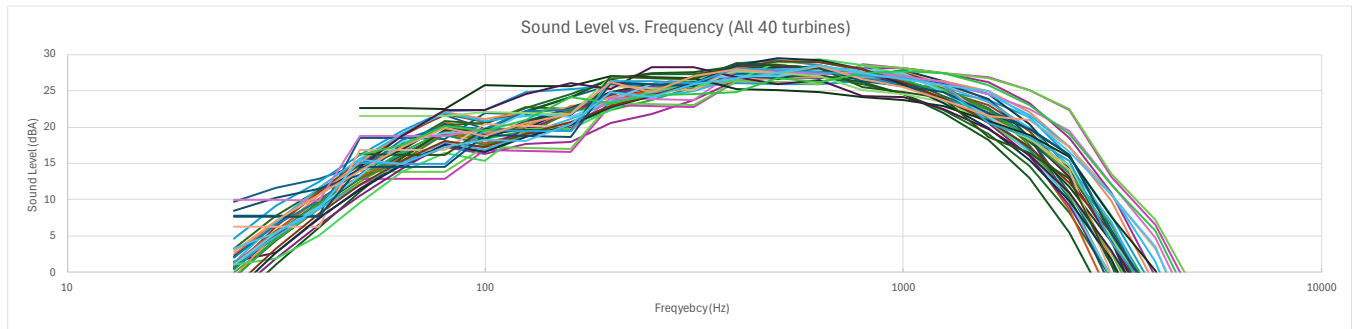


Figure 3 – 1/3 Octave Band Frequency Spectra for All 40 Turbines at the Receptor Location

The calculated minimum, maximum, average, and standard deviation for the frequency content of the sound levels received at the receptor location for each of the 40 turbine models are provided in Table 2.

Table 2 – Summary of Sound Level Frequency Spectra at the Receptor Location (All 40 Turbines)

Frequency (Hz)	50	63	80	100	125	160	200	250	315	400	500	630	800	1k	1.25k	1.6k	2k
Min (dBA)	9.6	12.9	12.9	15.4	16.7	16.6	20.6	21.8	22.8	24.8	25.1	24.8	24.2	23.7	21.9	18.2	13.0
Max (dBA)	22.6	22.6	22.5	25.8	25.7	26.1	27.0	28.3	28.3	28.8	29.5	29.4	28.7	28.2	27.5	26.9	25.1
Average (dBA)	14.3	16.8	19.0	19.1	20.5	21.6	24.4	25.3	26.0	27.4	27.5	27.6	27.1	26.4	25.0	22.4	18.9
S.D. (dBA)	2.7	2.1	2.4	2.1	2.0	2.2	1.5	1.3	1.2	0.9	1.0	1.0	1.0	1.1	1.4	2.2	2.7

Low frequency content

To assess low-frequency sound of the turbines, broadband dBC – dBA values at the receptor location were recorded for each of the 40 turbine types and plotted against their rotor diameters as shown in **Figure 4** below.

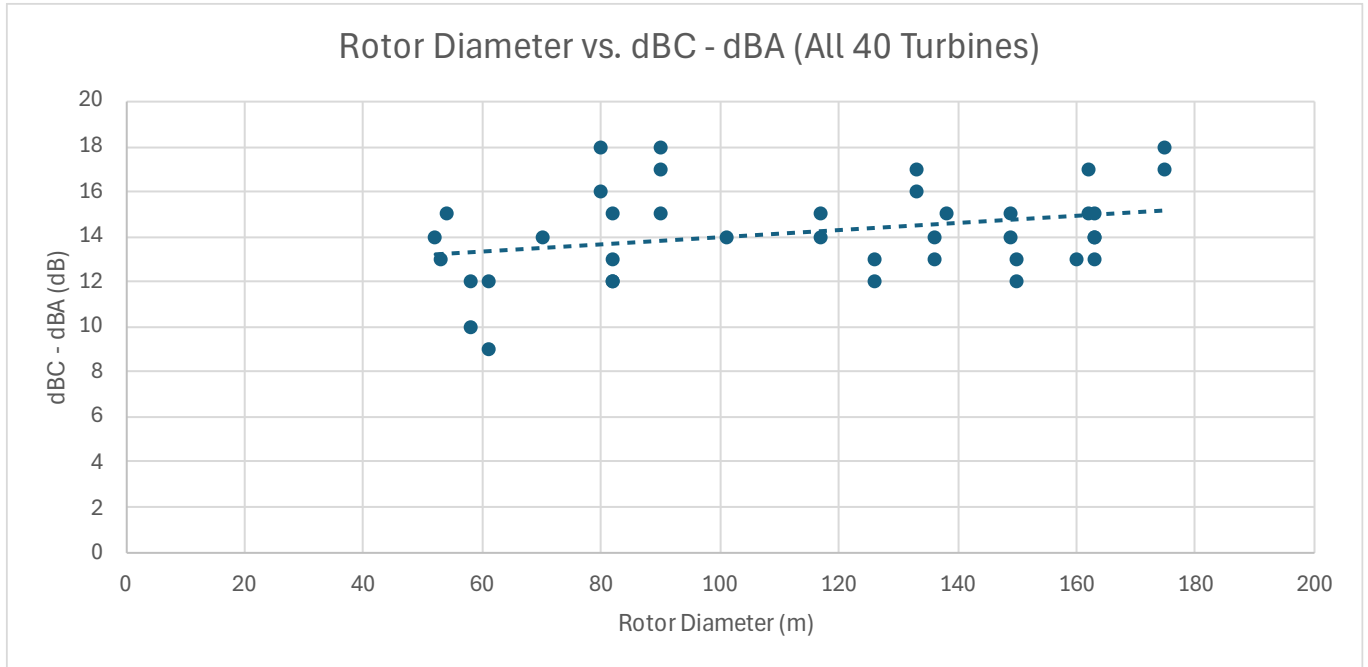


Figure 4 – Rotor Diameter vs. dBC-dBA (All 40 Turbines)

While a slight positive trend is visible, this trend is largely influenced by two smaller turbines that exhibit lower levels of low-frequency content. When these two outliers are removed, as shown in **Figure 5** below, the trend flattens, suggesting that rotor diameter has only a weak correlation with low-frequency sound emissions.

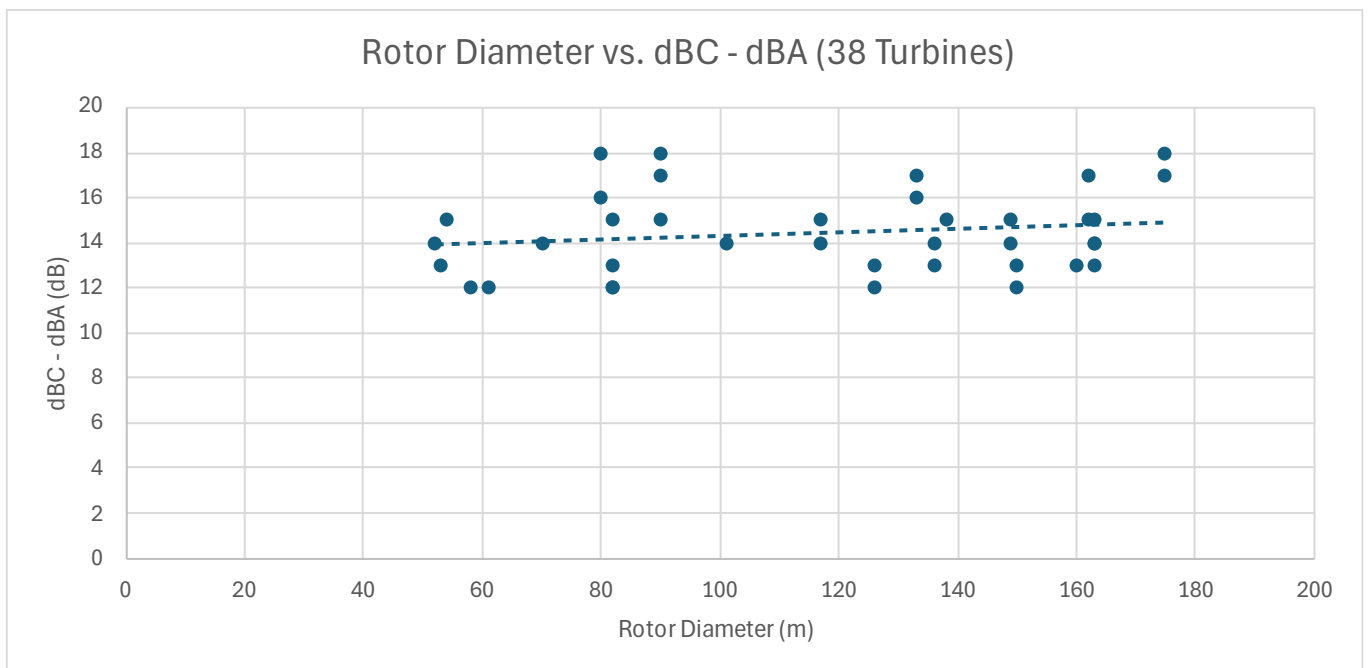


Figure 5 – Rotor Diameter vs. dBC-dBA (38 Turbines with the Outliers Removed)

Influence of TES on spectra statistics

Where applicable, comparisons were made between turbines with and without TES.

Table 3 summarises the calculated average and standard deviation of the frequency content of the sound levels received at the receptor location for all 18 turbines with TES and all 22 turbines without TES.

Table 3 Summary of Sound Level Frequency Spectra at the Receptor Location (18 Turbines with TES and 22 Turbines without TES)

Frequency (Hz)	50	63	80	100	125	160	200	250	315	400	500	630	800	1k	1.25k	1.6k	2k
Average TES (dBA)	14.1	16.9	19.4	19.2	20.6	21.6	24.0	24.9	25.6	27.3	27.4	27.5	27.3	26.7	25.4	23.2	19.9
S.D. TES (dBA)	1.7	1.9	2.7	1.9	2.2	2.4	1.5	1.4	1.3	0.8	0.9	0.9	0.7	1.0	1.4	2.2	2.8
Average Non-TES (dBA)	14.5	16.7	18.6	19.1	20.5	21.6	24.8	25.6	26.2	27.6	27.7	27.8	27.0	26.2	24.7	21.6	18.1
S.D. Non-TES (dBA)	3.3	2.3	2.2	2.2	1.9	2.0	1.5	1.1	1.0	1.0	1.0	1.1	1.2	1.2	1.4	1.9	2.4

The figures below illustrate the frequency content at the receptor location for turbine models with various rotor diameters, comparing those with and without TES from the same manufacturer (Manufacturer #1). For each case, the distance between the turbine and receptor location, at which 37 dBA was received, is also provided for both TES and Non-TES variants.

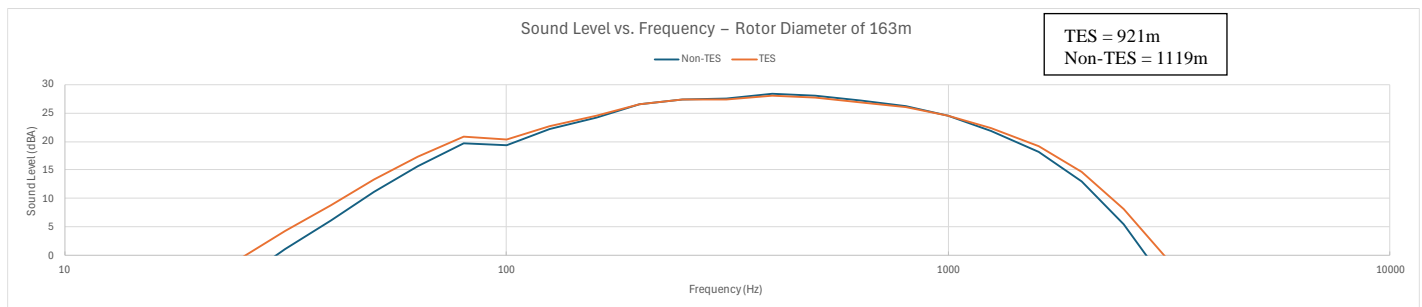


Figure 6 – 1/3 Octave Band Frequency Spectra for a 163m RD turbine (TES and Non-TES)

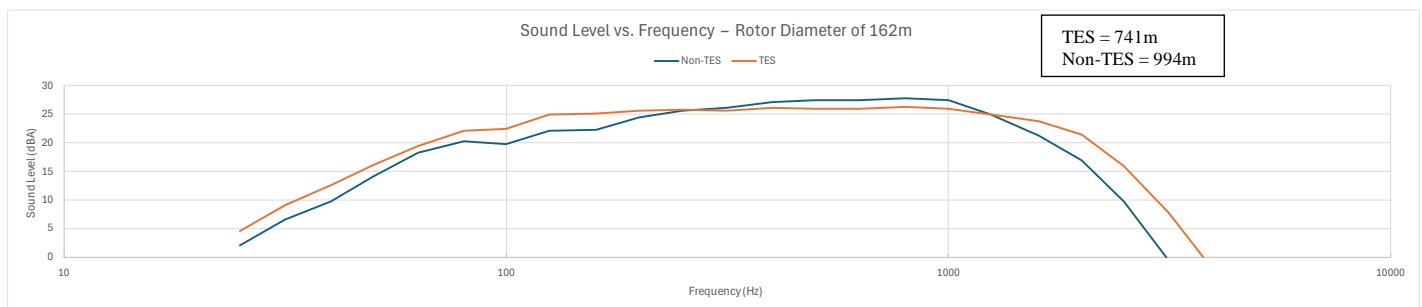


Figure 7 – 1/3 Octave Band Frequency Spectra for a 162m RD turbine (TES and Non-TES)

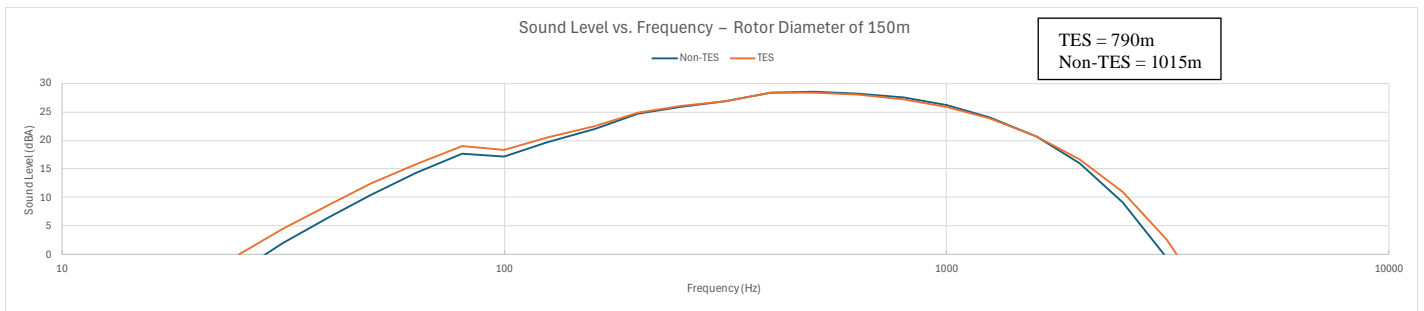


Figure 8 – 1/3 Octave Band Frequency Spectra for a 150m RD turbine (TES and Non-TES)

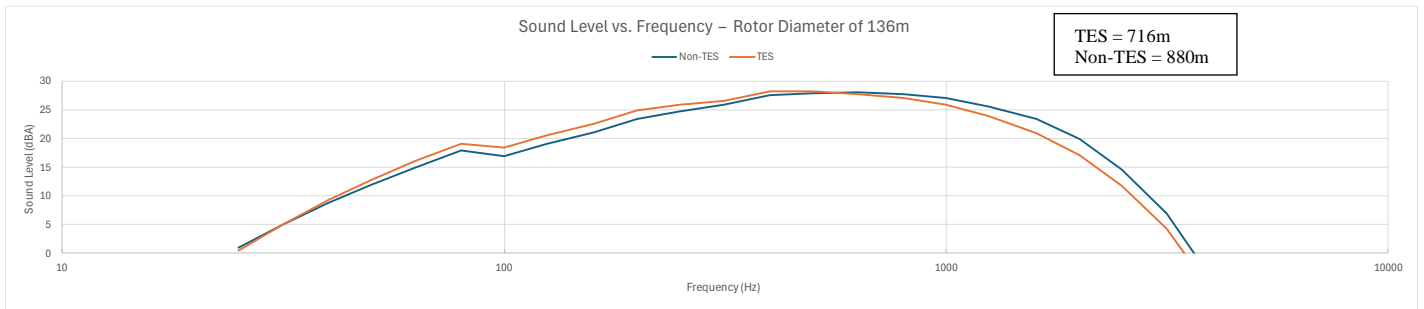


Figure 9 – 1/3 Octave Band Frequency Spectra for a 136m RD turbine (TES and Non-TES)

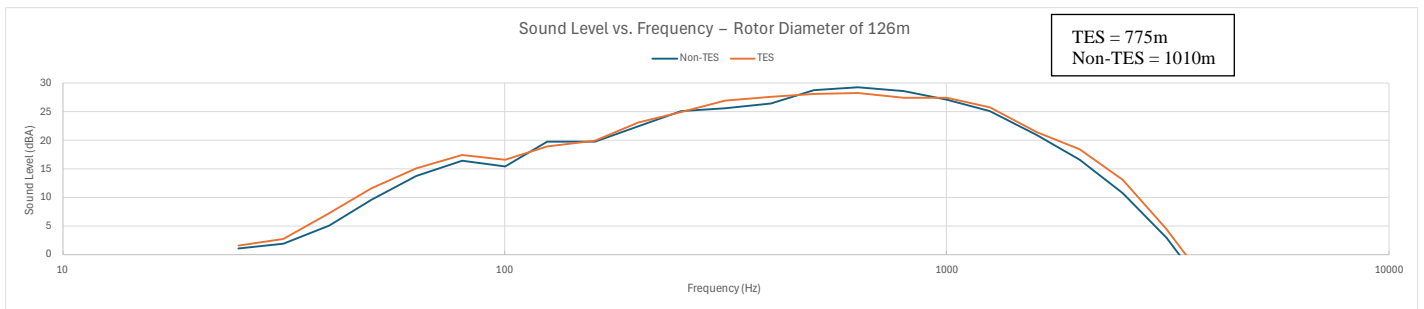


Figure 10 – 1/3 Octave Band Frequency Spectra for a 126m RD turbine (TES and Non-TES)

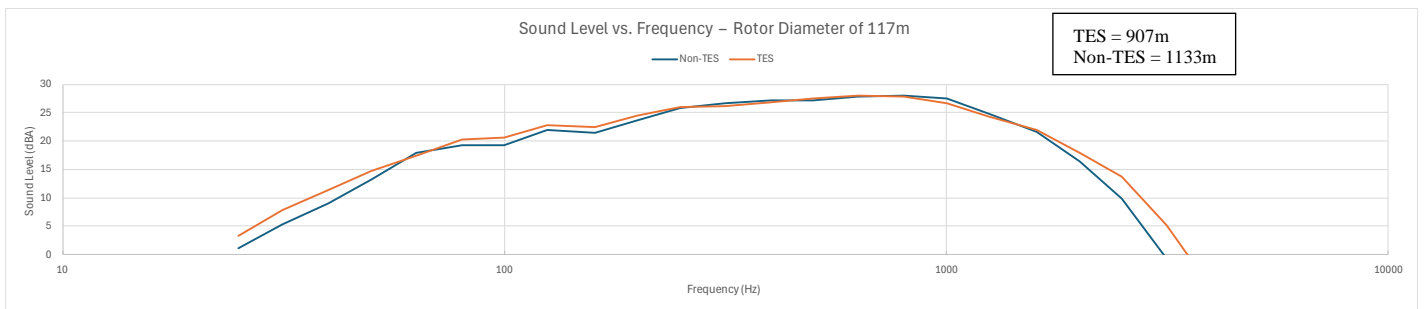


Figure 11 – 1/3 Octave Band Frequency Spectra for a 117m RD turbine (TES and Non-TES)

Figure 12 and **Figure 13** illustrate this comparison for two turbine models from Manufacturer #2 and **Figure 14** for a smaller turbine model from Manufacturer #3

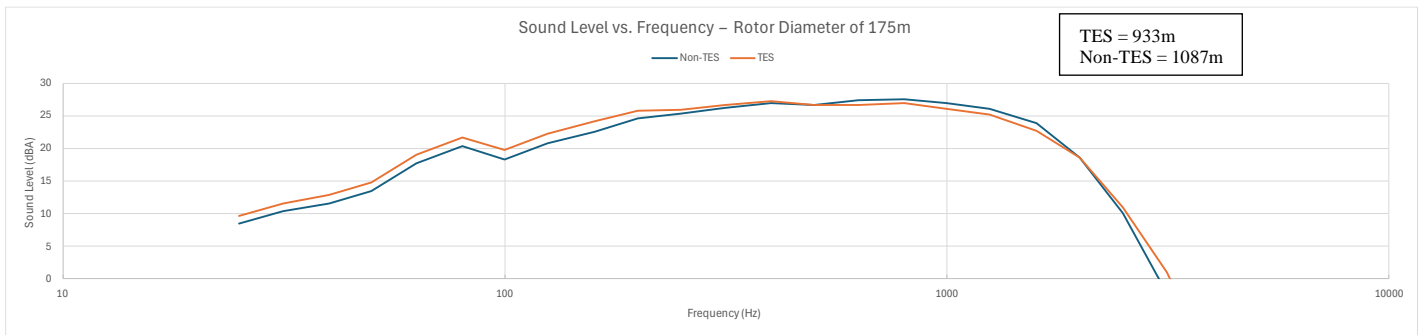


Figure 12 – 1/3 Octave Band Frequency Spectra for a 175m RD turbine (TES and Non-TES)

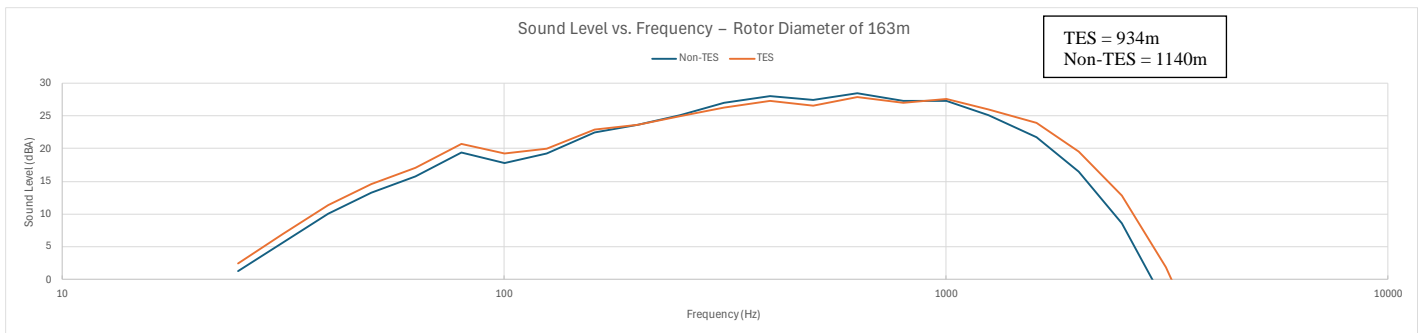


Figure 13 – 1/3 Octave Band Frequency Spectra for a 163m RD turbine (TES and Non-TES)

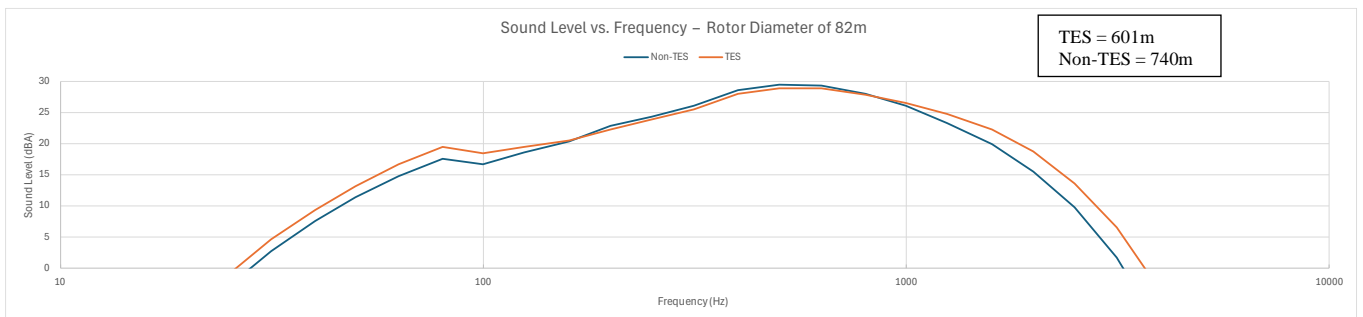


Figure 14 – 1/3 Octave Band Frequency Spectra for an 82m RD turbine (TES and Non-TES)

Note that a similar comparison for smaller turbines could not be conducted due to limited data availability and the general absence of TES as an option for these smaller turbine models.

Influence of Manufacturer-specifics on spectra statistics

A comparison was made between turbines with similar rotor diameters but from different manufacturers. **Figure 15** through **Figure 17** present the 1/3 octave band frequency spectra at the receptor location for turbine models with rotor diameters around 160m, 135m, and 50m, respectively, allowing for a direct comparison of manufacturer-specific effects.

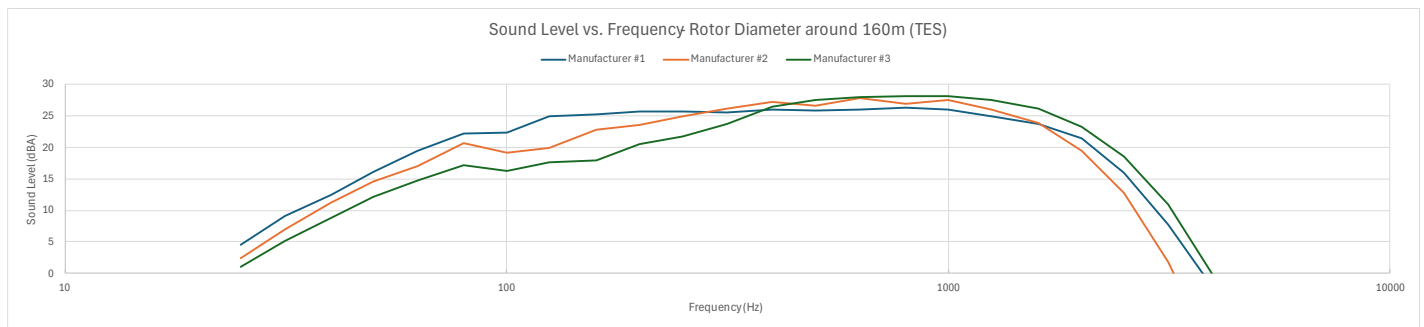


Figure 15 – 1/3 Octave Band Frequency Spectra at the Receptor Location – Turbines with RD of around 160m

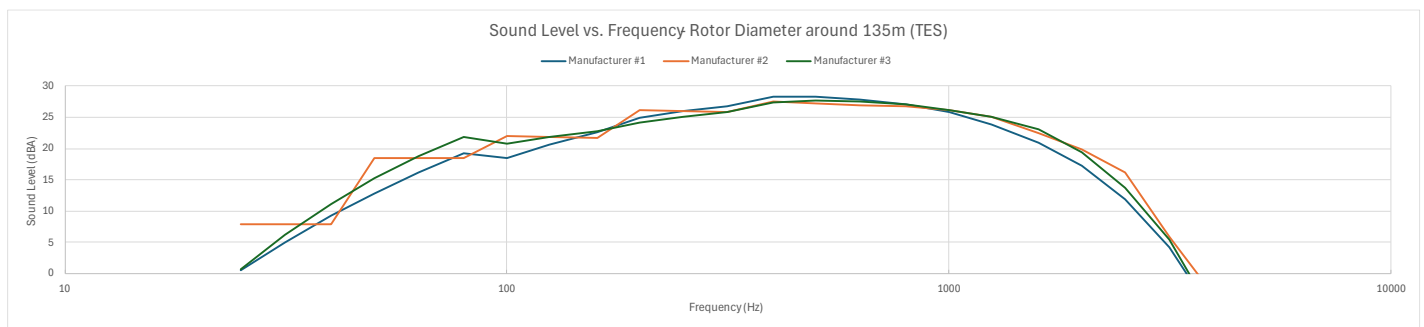


Figure 16 – 1/3 Octave Band Frequency Spectra at the Receptor Location – Turbines with Rotor Diameter of around 135m

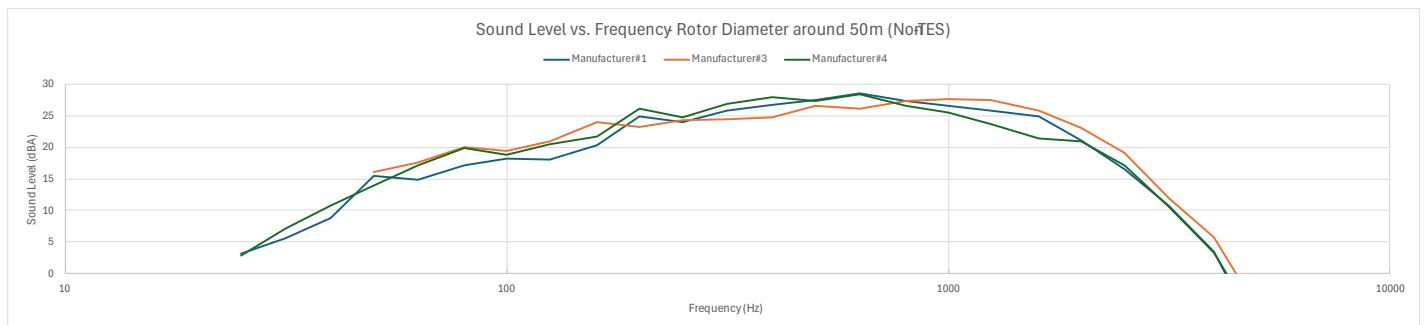


Figure 17 – 1/3 Octave Band Frequency Spectra at the Receptor Location – Turbines with Rotor Diameter of around 50m

4. Discussion

This study revealed that turbines with larger rotor diameter do not necessarily result in higher immission levels at the receptor, which contrasts with common perceptions in regions where wind farm developments are relatively new. In fact, similar overall sound power levels resulted in comparable distances where 37 dBA L_{eq} was received, regardless of rotor diameter or generating capacity, or other factors such as TES or manufacturer. Despite variation in these factors, frequencies between 315 Hz and 1 kHz consistently emerged as the most prominent contributors to the total immission level of at the receptor.

Although the receptor distance for each turbine model was adjusted to achieve a total immission level of 37 dBA L_{eq} , the distribution of sound energy across frequency bands varied between turbine models. Some frequency bands – particularly between 315 Hz and 1 kHz, where turbine noise is most prominent – showed relatively low variability (standard deviations around 1 dBA). In contrast, bands below 200 Hz and above 1.6 kHz, exhibited higher variability, with standard deviations up to 2.7 dBA. These spectral differences may meaningfully influence how turbine noise is perceived, even when overall A-weighted immission levels are identical.

While it was hypothesized that turbines with a larger rotor diameter would contribute more low-frequency content at the receptor, the analysis did not reveal a strong correlation between rotor diameter and low-frequency content at the receptor. Although a slight positive trend was observed (**Figure 4**), it was primarily driven by a few small turbines with distinctly lower low-frequency emissions. When these outliers were removed in **Figure 5**, the trend largely disappeared, suggesting that rotor diameter alone is not a strong predictor of low-frequency emissions.

As expected, turbines equipped with TES generally exhibit a lower overall sound level, allowing turbines to be placed closer to receptors without exceeding 37 dBA L_{eq} . As shown from **Figure 6** through **Figure 14**, the difference in distance between turbine and the receptor, at which 37 dBA was reached, for TES and Non-TES variants ranged from 139m to 253m across the three manufacturers compared. However, while all turbines were modelled to produce the same overall A-weighted sound level at the receptor (37 dBA), the frequency content of the received sound differed between TES and non-TES models. Specifically, TES-equipped turbines tended to exhibit greater sound energy in both low frequencies (below 160Hz) and high frequencies, compared to their non-TES counterparts. This trend was observed across most turbine pairs studied, with the exception of the 136m rotor diameter model (**Figure 9**), which showed less high frequency energy in the TES variant. This indicates that the influence of TES on the spectral characteristic of sound received at the receptor location is not unique to a specific manufacturer or rotor diameter but may represent a broader trend across turbine designs.

The higher frequency energy observed for TES-equipped turbines may be partly attributed to their closer proximity to the receptor. Since high-frequency sound attenuates more rapidly with distance due to atmospheric absorption, non-TES turbines – being further away – may lose more high-frequency energy before reaching the receptor. Conversely, given that low-frequency sound attenuates less efficiently over distance, the relatively higher low-frequency content observed in TES-equipped turbines suggests that TES may alter the spectral balance in a way that increases the relative presence of low-frequency content at the receptor. This spectral shift implies that while TES can reduce overall noise, it may also subtly reshape the spectral profile of the sound at the receptor, which may be relevant in areas sensitive to low-frequency noise.

Additionally, comparison between turbines with similar rotor diameters but from different manufacturers revealed notable differences in spectral characteristics at the receptor location. These variations highlight the influence of manufacturer-specific design choices – such as blade shape, hub and nacelle design, tower design, and mechanical component noise – on the turbine noise received at the receptor. As a result, it is important to recognize that factors other than rotor diameter or generator size may have a more significant impact on turbine noise emissions. These factors should be carefully considered when selecting a turbine for a specific location and context.

This study considers a specific scenario where turbines are modeled based on manufacturer-provided sound power data at maximum power output and a single hub height (the lowest listed in the manufacturer

datasheet). While this approach provides valuable insights, it has limitations. Manufacturer data may not fully represent real-world operating conditions, potentially introducing some uncertainty in the accuracy of the findings. Additionally, by focusing on a single operating scenario (maximum power output), the study does not account for variation in turbine noise emissions under partial load conditions or different wind speeds, which may influence noise profiles in practice. Additionally, only one receptor immission level (37 dBA L_{eq}) at 4m height was considered for comparison across all turbine models. This simplification does not account for the potential variation in receptor height or environmental conditions that could influence the actual immission levels at different receptor locations.

5. Conclusions

This study examined how wind turbine immission spectra vary across a diverse set of turbine models, using predictive modeling to simulate A-weighted sound levels of 37 dBA L_{eq} at a receptor location. Despite wide variation in rotor size, generating capacity, manufacturer and other features such as TES, a common characteristic among the turbines was that frequencies between 315 Hz and 1 kHz consistently dominated the immission spectra.

Contrary to initial expectations, larger rotor diameters were not strongly correlated with greater low frequency immission. Instead, spectral variability was found to be more strongly influenced by manufacturer-specific acoustic design choices. These findings highlight the importance of using detailed, turbine-specific sound power data in noise impact assessments to accurately evaluate the potential noise impact of wind turbines at receptor locations.

While TES can effectively reduce overall noise levels, it may also alter the spectral balance in a way that increases the relative presence of low-frequency content at the receptor compared to non-TES variants – potentially affecting perceived audibility at receptors.

Considering the limitations of the study, future research should include a broader range of turbine models and incorporate field measurements under varying atmospheric and operational conditions. Additionally, accounting for terrain, long-term performance, and real-world variability will further refine noise prediction models and help improve wind farm siting strategies.

As wind energy expands into regions that are relatively unfamiliar with turbine developments, misconceptions about turbine noise often arise, particularly when developers switch turbine models or manufacturers during the permitting process. While maintaining overall noise limits remain essential for regulatory compliance, this study underscores the importance of understanding the frequency content of wind turbine sound and how it influences perception in nearby communities. By providing insights into these factors, the study may help reduce concerns stemming from common misconceptions and foster greater community acceptance of wind farms.

References

- [1] International Standard, “ISO 9613-2:2024 Acoustics — Attenuation of sound during propagation outdoors — Part 2: Engineering method for the prediction of sound pressure levels outdoors,” 2024. [Online]. Available: <https://www.iso.org/standard/74047.html>.
- [2] Alberta Utilities Commission, “AUC Rule 012: Noise Control,” 2024. [Online]. Available: <https://www.auc.ab.ca/rules/rule012/>.

Appendix A

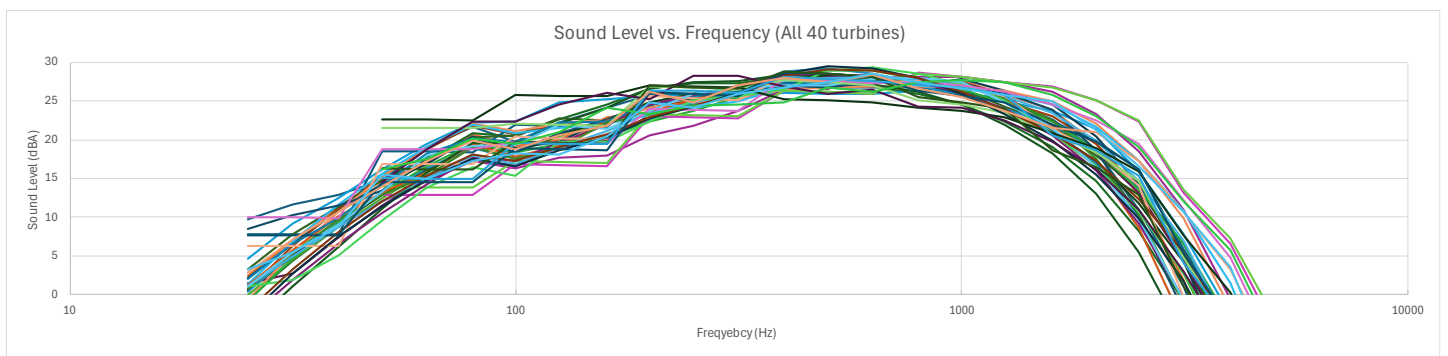


Figure A1 – 1/3 Octave Band Frequency Spectra for All 40 Turbines at the Receptor Location

Paper #31 - ID: 365

Title: Multi-Scale Turbulence Structures in Grid-Generated Turbulence for Leading Edge Noise Prediction

Author: Sparsh Sharma

11th Edition of the
International Conferences on
Wind Turbine Noise
Copenhagen, Denmark – 10th to 13th June 2025

Multi-Scale Turbulence Structures in Grid-Generated Turbulence for Leading Edge Noise Prediction

Sparsh Sharma¹, Alexandre Suryadi and Michaela Herr
German Aerospace Center (DLR), 38108 Braunschweig, Germany

Summary

This study investigates multi-scale turbulence characteristics and their impact on leading-edge noise generation in controlled wind tunnel conditions. Using a turbulence grid mounted in the Acoustic Wind Tunnel Braunschweig (AWB), the inflow turbulence is experimentally characterised and numerically reproduced via large eddy simulations (LES) in OpenFOAM. The analysis focuses on the spatial evolution of turbulence intensity, integral length scales, and energy spectra upstream and downstream of a NACA0012 airfoil. Comparisons between LES and experimental measurements show excellent agreement across key metrics, validating the simulation's fidelity. Vortical structure visualisation and spectral analysis reveal how turbulence decays, distorts, and regenerates through airfoil interaction. These flow dynamics are directly linked to the observed sound pressure level (SPL) spectra and far-field directivity patterns. The findings confirm that grid-generated turbulence drives leading-edge noise through coherent-structure interactions, consistent with classical theories and modern computational predictions.

1. Introduction

Leading-edge noise arises from the unsteady interaction between turbulent inflow structures and the leading edge of an airfoil. In wind energy applications, this mechanism is a major contributor to aeroacoustic emissions, affecting both operational efficiency and environmental compliance. Understanding and predicting leading-edge noise is therefore critical to improving rotor blade designs and reducing turbine noise footprints.

The theoretical basis for leading-edge noise was established by Amiet [1], who developed a semi-empirical model assuming homogeneous, isotropic turbulence interacting with an incompressible flat-plate airfoil. This formulation has been widely adopted in noise prediction frameworks. However, recent studies have shown that real-world turbulence—particularly in wind energy scenarios—is often anisotropic, intermittent, and structured across multiple scales [2, 3]. These deviations from idealised assumptions significantly impact noise generation and radiation characteristics.

To study airfoil-turbulence interaction under controlled and repeatable conditions, researchers frequently employ turbulence-generating grids in wind tunnel experiments. These grids produce defined turbulence intensities and length scales, allowing systematic investigation of how turbulence properties affect noise. Experimental studies consistently report that increased turbulence intensity raises overall noise levels, while larger integral length scales shift dominant noise frequencies to lower ranges [4, 5].

Complementing experimental approaches, high-fidelity numerical simulations—particularly large eddy

¹Corresponding author - Email: sparsh.sharma@dlr.de

simulation (LES)—offer a powerful means of resolving the spatial and temporal evolution of turbulent structures. LES has demonstrated superior capability in reproducing flow dynamics and associated noise mechanisms compared to lower-fidelity methods. Recent work [6, 7] highlights the importance of capturing turbulence intermittency, anisotropy, and coherent structures to accurately model leading-edge noise.

Despite progress, several open questions remain regarding the predictive capability of numerical simulations for leading-edge noise. One key challenge is to assess how well LES-based simulations reproduce turbulence and noise characteristics when compared directly with experimental data. Additionally, it is important to understand how turbulence evolves as it convects from the grid towards and through the airfoil, and how this evolution influences noise generation mechanisms.

This study addresses these questions using a combined numerical and experimental approach. Controlled inflow turbulence is generated in the Acoustic Wind Tunnel Braunschweig (AWB) using a passive turbulence grid. A series of LES calculations are performed in OpenFOAM to reproduce the same setup, resolving turbulence evolution and airfoil interaction in detail. The analysis focuses on turbulence intensity, integral length scales, energy spectra, coherent structures, and acoustic radiation. By comparing LES predictions with hot-wire and microphone array measurements, we evaluate the fidelity of turbulence resolution and its acoustic relevance.

The remainder of this paper is structured as follows. Section 2 outlines the numerical methodology and computational setup used in the large eddy simulations (LES), while Section 3 describes the experimental configuration in the Acoustic Wind Tunnel Braunschweig (AWB). Section 4 presents a comparative analysis of turbulence intensity, integral length scales, vortical structures, velocity spectra, and far-field sound pressure levels obtained from both LES and experimental data. Finally, the conclusions are summarised in Section 5.

2. Numerical Setup

Large Eddy Simulation (LES) is used to model near-field turbulence, with a subgrid scale model (SGS) accounting for unresolved eddies, while larger scales are directly resolved. The governing equations are derived by spatial filtering of the incompressible Navier-Stokes equations, incorporating the Smagorinsky SGS model with a dimensionless time step of $\Delta t^* = 0.012$. The computational framework, numerical schemes, and boundary conditions closely follow our previous work [8], where further implementation details can be found.

The numerical domain is designed to replicate the AWB, with grid-generated turbulence introduced upstream of the airfoil. The three-dimensional computational domain extends six airfoil chord lengths ($6D$) upstream to the velocity inlet and 28 chord lengths ($28D$) downstream to the pressure outlet. The upper and lower boundaries are set as symmetry planes, located $3D$ away from the airfoil chord line. The NACA 0012 airfoil is modelled with a no-slip condition, while the turbulence grid is also treated as a solid boundary.

The freestream velocity in the simulations was initially varied as $U_\infty \in [20, 30, 40]$ m/s. However, in the present study, we focus exclusively on the case of $U_\infty = 20$ m/s. A refined mesh is applied near the airfoil to resolve the viscous sublayer, ensuring a dimensionless wall distance $y^+ < 1$. The spanwise direction is treated with periodic boundary conditions across 100 parallel planes spanning $4D$, enabling an efficient representation of the inflow turbulence. The computational grid consists of 80 million cells, ensuring adequate resolution of the turbulent structures.

Unlike the experimental setup, the numerical model omits the physical wind tunnel nozzle and its contraction ratio, as its primary focus is on simulating the airfoil-turbulence interaction.

3. Experimental Setup

The experimental investigations were carried out in the Acoustic Wind Tunnel Braunschweig (AWB) at DLR. The AWB is a closed-loop, anechoic open test section wind tunnel designed to minimise sound reflection above 200 Hz.

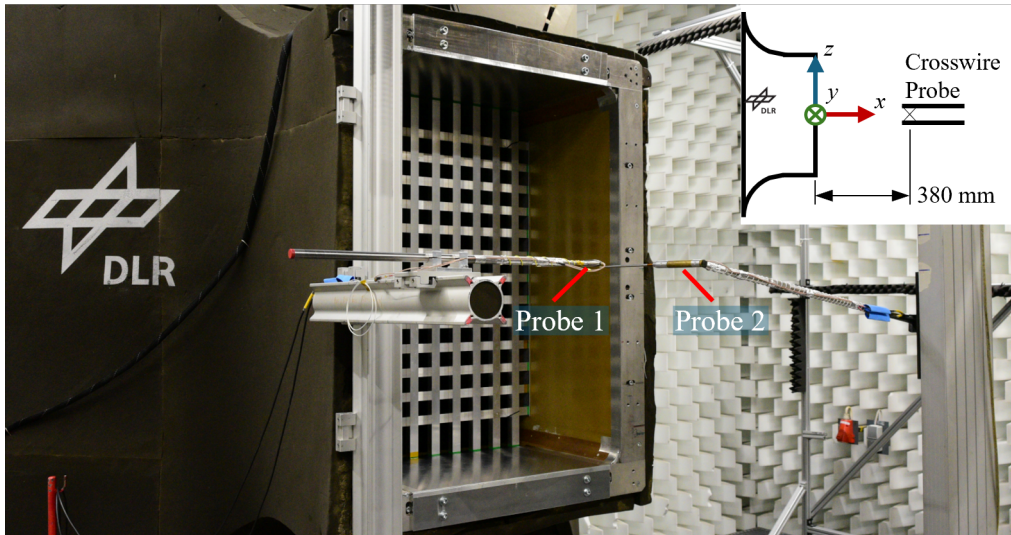


Figure 1 The AWB equipped with a turbulence grid and 2 cross-wire probes for flow measurements.

The wind tunnel operates at velocities up to 65 m/s, with a relatively low turbulence intensity of 0.3%. The flow is introduced into the test section through an 800 mm span and 1200 mm high rectangular nozzle, as shown in Fig. 1, along with the turbulence grid and two cross-wire velocity probes placed 380 mm downstream of the nozzle.

To produce varying inflow turbulence intensities, the AWB was equipped with a turbulence grid generator. The grid is made of rectangular profile bars with dimensions $d = 20$ mm and the distance between the bars is $M = 60$ mm. It should be noted that the maximum freestream velocity, U_∞ , decreases to below 40 m/s as the blockage ratio exceeds 33%, limiting the Reynolds number range that can be studied. The grid is installed 495 mm upstream of the nozzle, 875 mm from the velocity probes, ensuring a minimum development distance of $10M$ for the turbulence to develop into isotropic turbulence.

The leading-edge noise was analysed using the coherent output power technique introduced by Brooks and Hodgson [9] and was applied for the investigation of leading-edge noise by Hutcheson and Brooks [10]. Two sets of line-array consisting of Bruel&Kjær microphones were installed with 6 1/4-inch microphones 746 mm above the model and 8 1/4-inch microphones 1244 mm below. After factoring refraction of sound by the test section's shear layer, the difference of the distance between the model's edge and the respective microphones was compensated for by delaying one of the two measured signals. The time delay was determined from the cross-correlation of two measurement signals from the microphones above and below the model. The predominant noise source position was determined by cross-correlating two microphones from either above or below the model. In this manner, the leading-edge noise will have a shorter path to the upstream microphone, and vis-a-vis, the trailing-edge noise will have shorter path to the downstream microphone. Namely, the leading-edge noise will have a time-lag and the trailing-edge noise a time-lead. It was with the turbulence grid generator, the predominant noise source is radiating from the leading edge position. The COP analysis produces a cross-spectrum and a phase-spectrum that is out-of-phase as a result of measuring the edge radiated noise at opposite directivity angles. If the conditions of out-of-phase spectrum and phase-lag cross-correlation are considered, the cross-spectral density is taken to be representative of the power spectral density of the leading-edge noise eliminating the incoherent noise sources inside the test section.

4. Results and Discussion

In this section, we analyse the turbulence characteristics from both numerical and experimental perspectives. The discussion follows a structured approach, beginning with turbulence intensity and integral length scales, followed by intermittency analysis, coherence decay, and energy spectra. The trends observed are compared

with previous research findings to highlight their significance.

4.1 Turbulence Intensity and Integral Length Scale

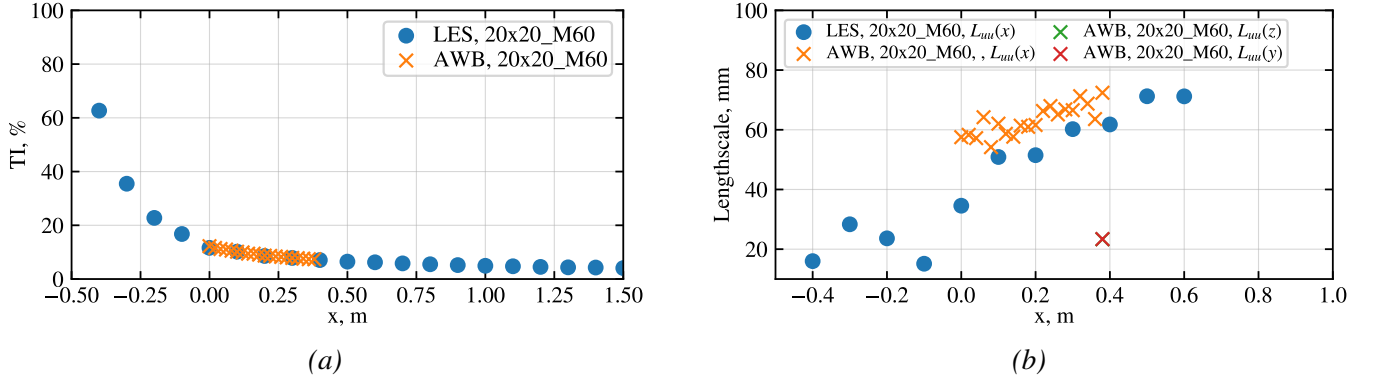


Figure 2 (a) Turbulence intensity and (b) integral length scales at different locations in the streamwise direction for a NACA0012 airfoil at $U_\infty = 20$ m/s with a turbulence grid of $M = 60$ mm.

Figure 2a compares the decay of turbulence intensity (TI) predicted by LES (blue dots) with experimental AWB wind tunnel measurements (orange crosses). Turbulence intensity is defined as the ratio of the root-mean-square (RMS) of velocity fluctuations to the mean free-stream velocity:

$$TI = \frac{\sqrt{\frac{1}{3} (\overline{u'^2} + \overline{v'^2} + \overline{w'^2})}}{U_\infty}. \quad (1)$$

Here, u' , v' , and w' are the components of the instantaneous velocity fluctuations and U_∞ is the mean freestream velocity. Both datasets exhibit the expected power-law decay typical of grid-generated turbulence [11]. Immediately downstream of the grid ($x \approx -0.5$ m), turbulence intensities are highest, consistent with strong wake-induced turbulence reported by Liu et al. [12]. LES predictions closely align with experimental results near the airfoil leading edge ($x = 0$ m), indicating reliable modelling of turbulence dissipation processes crucial for aeroacoustic studies [13].

Further downstream ($x > 0$ m), the experimental TI values plateau slightly, reflecting open-jet effects such as ambient air entrainment, as also observed by Bowen et al. [14]. Conversely, LES continues a mild decay, suggesting boundary condition limitations or numerical dissipation in the far field [12]. Overall, the strong qualitative and quantitative agreement confirms the validity of the LES setup, aligning well with classical [15] and recent computational studies [13, 16], while highlighting minor aspects for simulation refinement.

Figure 2b compares the streamwise integral length scale $L_{uu}(x)$ derived from LES (blue dots) with experimental measurements (orange crosses) from the AWB wind tunnel. The integral length scale in the streamwise direction is defined based on the autocorrelation function $R_{uu}(r)$ of the velocity fluctuations u' :

$$L_{uu}(x) = \int_0^\infty R_{uu}(r) dr, \quad \text{where} \quad R_{uu}(r) = \frac{\overline{u'(x, t)u'(x+r, t)}}{\overline{u'^2(x, t)}}. \quad (2)$$

Both datasets reveal a clear trend of increasing integral length scales downstream of the turbulence grid, indicating a progressive aggregation of turbulent structures as smaller eddies merge into larger coherent motions. This behaviour contrasts classical turbulence theories [17, 18], which typically predict monotonic decay of length scales due to continuous energy dissipation.

Recent literature increasingly supports this transient growth in integral length scales. Burton et al. [19] and Wang et al. [7] reported similar downstream growth, attributing it to vortex merging mechanisms transferring

energy to larger-scale structures. The excellent agreement between LES and experimental data near the airfoil ($x = 0$ m) further validates the simulation's fidelity, consistent with high-quality LES validations presented by Trascinelli et al. [13].

Minor discrepancies between LES and experiments downstream ($x > 0.5$ m) may arise from differences in boundary conditions, mesh resolution limitations, or numerical dissipation in LES [12]. Nonetheless, the overall consistency confirms that the LES reliably captures the dynamic evolution of turbulence structures, essential for accurate aeroacoustic predictions.

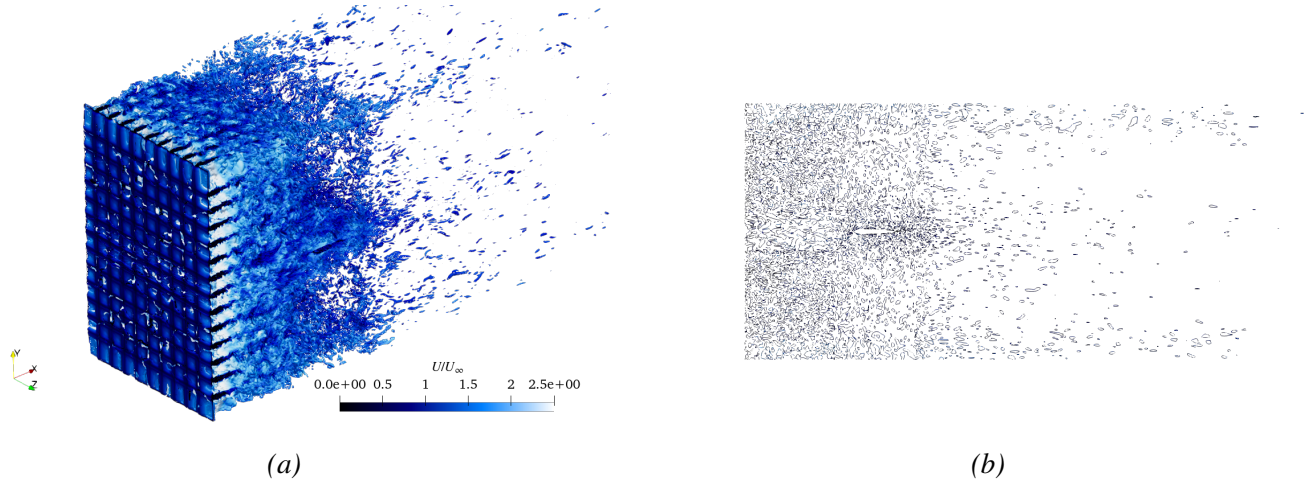


Figure 3 (a) Isosurfaces of Q -criterion visualizing coherent vortical structures downstream of the M60 turbulence grid, coloured by instantaneous velocity magnitude and (b) streamwise-parallel slice of the instantaneous Q -criterion field taken at the mid-span $y/D = 0$.

Figure 3a visualises the vortical structures using the Q -criterion at the final simulation timestep for the M60 grid and freestream velocity of 20 m/s. The Q -criterion is defined as:

$$Q = \frac{1}{2} \left(\|\mathbf{\Omega}\|^2 - \|\mathbf{S}\|^2 \right), \quad (3)$$

where $\mathbf{\Omega}$ is the asymmetric part of the velocity gradient tensor (vorticity tensor), and \mathbf{S} is the symmetric part (rate-of-strain tensor). A positive Q value indicates regions where rotation dominates over strain, marking coherent vortex structures.

Immediately downstream of the grid, dense small-scale vortical filaments dominate the flow field. These are indicative of wake breakup and shear-layer roll-up due to strong velocity gradients through the mesh openings. This region correlates with the peak turbulence intensity (TI) observed earlier (cf. Figure 2a), where small eddies with high vorticity lead to elevated velocity fluctuations. Such intense vortex activity agrees with findings from Liu et al. [12] and Trascinelli et al. [13], who observed similar structure densities near grids in LES and experiment.

Further downstream, the vortical structures appear more spatially coherent and larger in scale. This evolution supports the increasing trend in the streamwise integral length scale $L_{uu}(x)$ (cf. Figure 2b), consistent with the vortex merging mechanisms discussed in Burton et al. [19] and Wang et al. [7]. As turbulence transitions from highly intermittent to more organised, larger energy-containing eddies emerge. This observation aligns with theoretical perspectives on turbulence structure evolution (Meneveau & Marusic, 2011; Frisch, 1995).

Finally, in the far wake as seen in Figure 3b, the vortex density decreases, and the structures elongate, indicating reduced rotational intensity and overall turbulence decay. This spatial transition aligns with the downstream drop in TI and the levelling of the integral scales. Despite the decay, persistent coherent eddies suggest that large-scale turbulence continues to influence the flow field at significant distances downstream, which is particularly relevant for aeroacoustic source modelling.

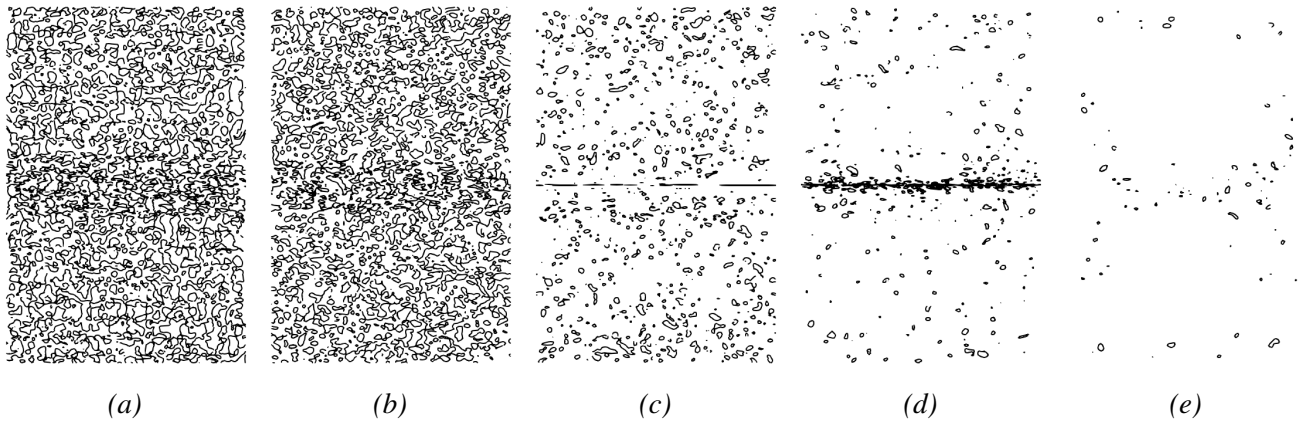


Figure 4 Cross-sectional Q -criterion contours at five streamwise locations relative to the airfoil leading edge ($x = 0$ m), progressing from upstream to downstream: (a) $x = -0.8$ m (closest to the turbulence grid), (b) $x = -0.5$ m, (c) $x = 0$ m (leading edge), (d) $x = 0.5$ m, and (e) $x = 1.0$ m.

To complement the three-dimensional visualization of vortical structures in Figure 3a, Figure 4 shows two-dimensional cross-plane Q -criterion contours at five streamwise locations: $x = -0.8$, -0.5 , 0 , 0.5 , and 1.0 m. These slices illustrate the spatial development of vortical structures from the turbulence grid towards and beyond the airfoil’s leading edge ($x = 0$). Closest to the grid ($x = -0.8$ m), the flow exhibits densely packed and highly disordered small-scale structures, indicative of the initial turbulent field populated with energetic eddies. Moving downstream toward the leading edge ($x = -0.5$ and $x = 0$ m), the vortex cores begin to organize, with enhanced concentration near the airfoil midplane—suggesting compression and distortion of incoming turbulence by the stagnation region [20, 21]. At $x = 0.5$ m and further downstream at $x = 1.0$ m, the structures become more filamentary and spatially dispersed, consistent with progressive vortex stretching and dissipation. This streamwise evolution supports the presence of a turbulence cascade and energy redistribution following the airfoil interaction, consistent with classical turbulence theory [22, 23] and with recent LES-based studies of grid-generated turbulence interacting with airfoil geometries [13].

4.2 Energy Spectra of Streamwise Velocity Fluctuations

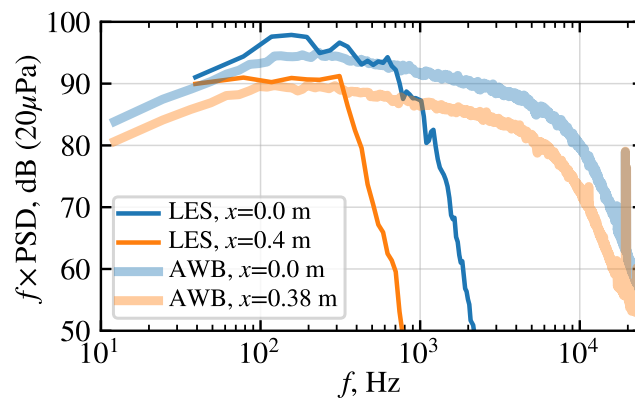


Figure 5 Premultiplied energy spectra of streamwise velocity fluctuations, $E_{uu}(f)$, comparing LES (solid lines) and AWB wind tunnel measurements (opaque lines) at $x = 0$ m and $x = 0.4$ m.

Figure 5 compares premultiplied energy spectra of streamwise velocity fluctuations from LES (darker lines) and AWB experiments (lighter lines) at $x = 0.0$ m and $x \approx 0.4$ m. LES captures the low-frequency peak accurately, reproducing energy-containing motions essential for realistic inflow conditions. In the mid-frequency range, both LES and experimental spectra exhibit an approximate $-5/3$ slope, consistent with Kolmogorov’s inertial subrange [24, 25]. This agreement indicates adequate LES resolution to capture the turbulent cascade. At high frequencies, LES shows a steeper decay than experiment, attributable to

subgrid-scale dissipation and finite mesh resolution [26]. Notably, spectral distortion near the airfoil leading edge manifests as an elevated low-frequency plateau and suppressed high-frequency content, in line with observed physical behavior [27]. These effects are relevant for aeroacoustics, as the turbulence spectrum directly influences leading-edge noise prediction models [1, 20]. Overall, the LES reproduces key spectral features with high fidelity, supporting its reliability in both turbulence resolution and broadband noise modeling.

4.3 Farfield noise

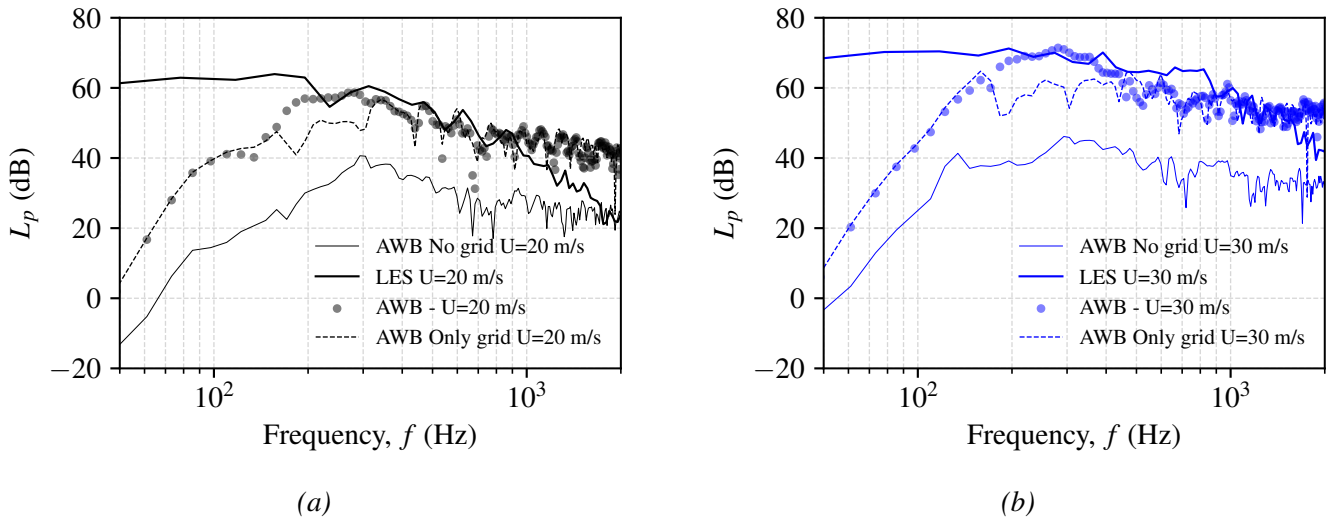


Figure 6 Sound pressure level (SPL) spectra at 90° above the leading edge of a NACA0012 airfoil at (a) $U_\infty = 20$ m/s and (b) $U_\infty = 30$ m/s. Comparison includes LES predictions, AWB experimental measurements, and baseline cases with and without the turbulence-generating grid. The AWB No Grid case represents background and self-noise; the AWB Only Grid case isolates grid-induced turbulence noise.

Figures 6a and 6b show narrowband sound pressure level (SPL) spectra measured at 90° above the NACA0012 leading edge for $U_\infty = 20$ m/s and 30 m/s, comparing four configurations: *AWB No Grid*, *AWB Only Grid*, LES, and AWB experiments. The sound pressure levels in the LES were computed using the Ffowcs Williams–Hawkings (FWH) acoustic analogy formulation, following the approach detailed in our previous works [28, 29]. The *AWB No Grid* case reflects self-noise and background levels in smooth inflow, consistent with findings that airfoil trailing-edge noise is relatively low in laminar or low-turbulence conditions [30]. In contrast, the *AWB Only Grid* configuration shows increased broadband noise due to vortex shedding from the grid bars, aligning with observations by Geyer et al. [31], who reported characteristic humps in grid-induced noise spectra associated with bar wake Strouhal numbers.

The LES and AWB spectra of the NACA 0012 with grid both exhibit broadband features typical of leading-edge turbulence-interaction noise, with good agreement in spectral shape and peak regions. The SPL rises through the mid-frequency range where turbulent eddies with scales comparable to the leading-edge radius interact efficiently with the airfoil [1, 32]. The observed plateau corresponds to the inertial subrange of turbulence, where energy-containing eddies dominate the unsteady surface loading [24]. At higher frequencies, the LES SPL rolls off slightly faster than the experiment, likely due to grid resolution limits and numerical dissipation, as discussed by Roger and Moreau [20] and Pope [26].

The increase in flow speed from 20 to 30 m/s leads to a broadband SPL rise of approximately 8–10 dB, matching the expected U^5 scaling law for dipole-like sources as predicted by Ffowcs Williams and Hall [33]. Additionally, spectral features shift to higher frequencies due to convective scaling of eddy passage frequency ($f \propto U/\ell$), a behavior confirmed in experimental studies by Devenport et al. [34] and numerical studies by Lyu and Azarpeyvand [21]. This trend is especially apparent in the *AWB Only Grid* and LES spectra, where the grid wake shedding hump translates upward with increased U_∞ .

The influence of turbulence scale and intensity on spectral shape is also evident. The presence of the grid introduces larger turbulence intensity (u'/U) and defines a dominant integral length scale Λ , both of which affect SPL amplitude and peak location. As shown by Hutcherson et al. [35], even moderate turbulence levels can raise leading-edge noise well above self-noise. The turbulence length scale controls the spectral peak frequency; larger eddies generate lower-frequency sound, while smaller eddies shift energy higher [36]. Amiet's theory [1] and later refinements by Roger and Moreau [20] quantify this dependency via turbulence spectra and spanwise coherence.

Finally, the close agreement between LES and experimental spectra validates the simulation's turbulence fidelity. The correct reproduction of turbulence intensity, integral length scale, and spectral energy content—supported by matching velocity spectra [13]—ensures that the LES input to aeroacoustic models is physically meaningful. Discrepancies in the high-frequency tail are expected and reflect practical resolution trade-offs [26, 37]. Overall, the results are consistent with modern understanding of leading-edge noise mechanisms in multi-scale turbulence environments [27].

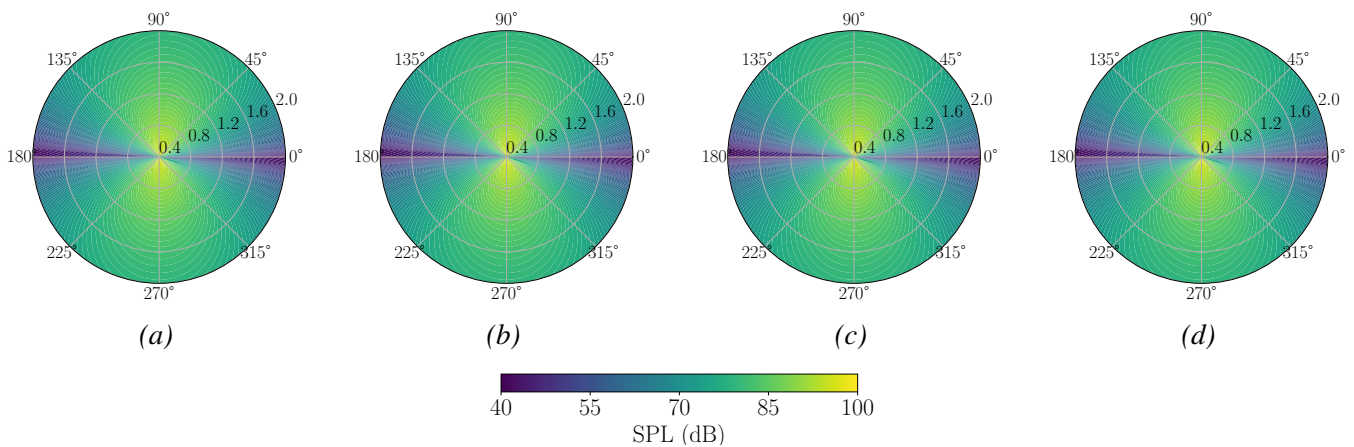


Figure 7 Polar heatmaps of sound pressure level (SPL) measured at a 1 m radius from the leading edge of a NACA0012 airfoil at four frequencies: (a) 100 Hz, (b) 200 Hz, (c) 500 Hz, and (d) 1000 Hz.

Figure 7 presents polar heatmaps of the sound pressure level (SPL) at four representative frequencies (100 Hz, 200 Hz, 500 Hz, and 1000 Hz), plotted over a 1 m radius arc centered above the airfoil. As expected for leading-edge interaction noise, the SPL peaks around 90° , perpendicular to the flow direction, and displays dipole-like behavior [1, 33]. These plots validate that the noise source exhibits a classical dipolar pattern.

5. Conclusion

This study has examined the spatial and spectral evolution of grid-generated turbulence and its role in leading-edge noise generation under controlled wind tunnel conditions. By combining large eddy simulations (LES) with experimental measurements in the AWB facility, a comprehensive characterisation of turbulence properties—including intensity, integral length scale, and energy distribution—was achieved.

The LES captured the downstream decay and structural reorganisation of turbulent eddies with high fidelity, showing excellent agreement with experimental data. Integral length scales were found to increase downstream due to vortex merging, while turbulence intensity decayed in a manner consistent with classical and modern turbulence theories. The Q-criterion analysis revealed how coherent vortical structures interact with the airfoil leading edge and evolve downstream, supporting theoretical models of turbulence-induced acoustic forcing.

Spectral comparisons confirmed that LES accurately reproduces both the shape and amplitude of streamwise velocity spectra in the energy-containing and inertial subranges. Narrowband SPL spectra and polar directivity patterns validated the aeroacoustic response of the simulated flow, including the classical dipole-like radiation and frequency-dependent directivity.

Taken together, these findings demonstrate that LES, when carefully validated against experimental data, can serve as a robust tool for predicting inflow turbulence and its acoustic implications in wind tunnel configurations.

6. Acknowledgment

The authors gratefully acknowledge the scientific support and HPC resources provided by the German Aerospace Center (DLR). The HPC system CARO is partially funded by "Ministry of Science and Culture of Lower Saxony" and "Federal Ministry for Economic Affairs and Climate Action".

References

- [1] R. K. Amiet, "Acoustic radiation from an aerofoil in turbulent flow," *AIAA Journal*, vol. 14, no. 4, pp. 547–558, 1975.
- [2] D. Moreau and C. Doolan, "Grid-generated turbulence for experimental aeroacoustic research," *Applied Acoustics*, vol. 179, p. 108063, 2021.
- [3] F. Bertagnolio, A. Fischer, and N. Sørensen, "Computational and experimental investigation of turbulence characteristics for wind turbine aeroacoustics," *Wind Energy*, vol. 23, pp. 1121–1138, 2020.
- [4] K. B. M. Q. Zaman and M. Samimy, "Decay of turbulence in wind tunnel shear layers: An experimental perspective," *Physics of Fluids*, vol. 34, no. 5, p. 054103, 2022.
- [5] Y. Liu, R. Maryami, and X. Zhang, "Aeroacoustic characteristics of turbulence grids in wind tunnels," *Journal of Sound and Vibration*, vol. 550, p. 117889, 2023.
- [6] P. Spalart, M. Strelets, and M. Shur, "Large-eddy simulation of airfoil noise: State of the art and challenges," *Annual Review of Fluid Mechanics*, vol. 54, pp. 353–385, 2022.
- [7] M. Wang, J. Freund, and S. Lele, "Effect of turbulence scales on leading-edge noise," *AIAA Journal*, vol. 59, no. 3, pp. 1009–1023, 2021.
- [8] S. Sharma, A. Suryadi, and M. Herr, "Assessment of turbulence modeling in navier-stokes simulations for grid-generated turbulence and airfoil interaction," in *30th AIAA/CEAS Aeroacoustics Conference*, AIAA, June 2024.
- [9] T. F. Brooks and T. H. Hodgson, "Trailing edge noise prediction from measured surface pressures," *Journal of Sound and Vibration*, vol. 78, no. 1, pp. 69–117, 1981.
- [10] F. V. Hucheson, T. F. Brooks, and D. J. Stead, "Measurement of the noise resulting from the interaction of turbulence with a lifting surface," *International Journal of Aeroacoustics*, vol. 11, no. 5-6, pp. 675–700, 2012.
- [11] M. S. Mohamed and J. C. LaRue, "The decay power law in grid-generated turbulence," *Journal of Fluid Mechanics*, vol. 219, pp. 195–214, 1990.
- [12] Y. Liu, R. Maryami, and X. Zhang, "Aeroacoustic characteristics of turbulence grids in wind tunnels," *Journal of Sound and Vibration*, vol. 390, pp. 91–106, 2017.
- [13] M. Trascinelli, T. Pagliaroli, and R. Camussi, "Validation of les for aeroacoustic predictions of grid turbulence interactions with naca airfoils," *AIAA Journal*, vol. 61, no. 5, pp. 2017–2029, 2023.
- [14] W. Bowen, S. Lee, and D. Burton, "Experimental studies of turbulence intensity decay in open-jet wind tunnels," *Experiments in Fluids*, vol. 63, no. 3, p. 55, 2022.
- [15] G. Comte-Bellot and S. Corrsin, "Simple eulerian time correlation of full and narrow-band velocity signals in grid-generated, 'isotropic' turbulence," *Journal of Fluid Mechanics*, vol. 25, no. 4, pp. 657–682, 1966.

- [16] S. Sharma and M. Herr, "Efficient prediction of turbulent inflow and leading-edge interaction noise using a vortex particle method with look-up table approach," in *Journal of Physics: Conference Series*, vol. 2767, p. 022059, IOP Publishing, June 2024.
- [17] G. Taylor, "Statistical theory of turbulence," *Proceedings of the Royal Society A*, vol. 151, pp. 421–444, 1935.
- [18] G. Batchelor, *The Theory of Homogeneous Turbulence*. Cambridge University Press, 1953.
- [19] D. Burton, M. Thompson, and A. Smits, "Grid-generated turbulence and its decay mechanisms," *Physics of Fluids*, vol. 32, no. 10, p. 105102, 2020.
- [20] M. Roger and S. Moreau, "Analytical modeling of broadband noise mechanisms for airfoil–turbulence interaction," *Journal of Sound and Vibration*, vol. 329, no. 4, pp. 4380–4397, 2010.
- [21] B. Lyu and M. Azarpeyvand, "Numerical investigation of leading-edge noise reduction using porous materials," *Journal of Fluid Mechanics*, vol. 817, pp. 512–535, 2017.
- [22] W. K. George, "Classical theory of homogeneous turbulence revisited," *Philosophical Transactions of the Royal Society A: Mathematical, Physical and Engineering Sciences*, vol. 371, no. 1982, p. 20120346, 2013.
- [23] T. Kurian and J. H. Fransson, "Grid-generated turbulence revisited," *Fluid Dynamics Research*, vol. 39, no. 10, pp. 675–694, 2007.
- [24] A. Kolmogorov, *Local structure of turbulence in incompressible viscous fluid at very large Reynolds numbers*, vol. 30. 1941.
- [25] S. G. Saddoughi and S. V. Veeravalli, "Universal spectrum of the one-dimensional velocity components in turbulent shear flows," *Journal of Fluid Mechanics*, vol. 268, pp. 333–372, 1994.
- [26] S. Pope, *Turbulent Flows*. Cambridge University Press, 2000.
- [27] R. Camussi, "Trailing-edge noise: Classical theories and recent developments," *Journal of Sound and Vibration*, vol. 489, p. 115640, 2021.
- [28] S. Sharma, T. F. Geyer, and J. Giesler, "Effect of geometric parameters on the noise generated by rod-airfoil configuration," *Applied Acoustics*, vol. 177, p. 107908, 2021.
- [29] S. Sharma, T. F. Geyer, and E. J. Arcondoulis, "On the influence of porous coating thickness and permeability on passive flow and noise control of cylinders," *Journal of Sound and Vibration*, vol. 549, p. 117563, 1 2023.
- [30] M. R. Fink, "Trailing edge and inflow noise—experimental evaluation of theory," *AIAA Journal*, vol. 13, no. 4, pp. 442–443, 1975.
- [31] T. F. Geyer and E. Sarradj, "Grid-generated inflow turbulence and airfoil trailing edge noise: Experimental investigations using different types of grids," *Experiments in Fluids*, vol. 60, no. 3, p. 43, 2019.
- [32] R. W. Paterson and R. K. Amiet, "Acoustic radiation from a turbulent boundary layer with arbitrary pressure gradient," *AIAA Journal*, vol. 14, no. 9, pp. 1231–1237, 1976.
- [33] J. E. Ffowcs Williams and L. H. Hall, "The generation of sound by turbulence and surfaces in arbitrary motion," *Philosophical Transactions of the Royal Society of London. Series A, Mathematical and Physical Sciences*, vol. 255, no. 1064, pp. 469–503, 1970.
- [34] W. J. Devenport, A. Borgoltz, and M. C. Rife, "Airfoil self-noise and turbulent inflow noise: Experiments and predictions," *Journal of Sound and Vibration*, vol. 329, no. 9, pp. 1517–1530, 2010.
- [35] F. V. Hucheson, T. F. Brooks, and W. M. Humphreys, "Airfoil leading edge noise reduction using porous treatments," *AIAA Journal*, vol. 50, no. 5, pp. 1080–1091, 2012.
- [36] S. Moreau, "Aeroacoustics of wall-bounded flows," *Advances in Applied Mechanics*, vol. 45, pp. 151–244, 2011.

- [37] V. Evely and G. Albanez, "Application of amiet's model with correction for the dissipation range to predict airfoil leading-edge noise," *Experiments in Fluids*, vol. 52, no. 1, pp. 75–89, 2012.

Paper #32 - ID: 366

Title: Psychological and physiological responses to amplitude-modulated low-frequency sounds

Author: Hiroshi Matsuda

11th Edition of the

International Conferences on Wind Turbine Noise

Copenhagen, Denmark – 10th to 13th June 2025

Psychological and physiological responses to amplitude-modulated low-frequency sounds

Hiroshi Matsuda¹ and Nobuo Machida

College of Science and Technology, Nihon University, Funabashi City, Chiba, 274-8501, Japan

Summary

The amplitude-modulated low-frequency sounds examined in this study consist of a pure tone with a carrier frequency ranging from 20 to 100 Hz, in which the sound pressure levels fluctuate continuously. This study aims to develop a quantitative indicator for evaluating the psychological and physiological effects of amplitude-modulated low-frequency sounds. This paper reports the psychological and physiological responses of participants exposed to amplitude-modulated low-frequency sounds in a low-frequency sound chamber. Psychological responses were assessed through questionnaires, focusing on three specific sensations associated with low-frequency sounds: vibratory sensation, oppressive sensation, and annoyance, which were rated on a seven-point scale. The loudness and fluctuation sensation of the sounds were measured using the magnitude estimation method. Physiological responses, including electrocardiograms and salivary amylase activity, were measured to assess autonomic nervous system activity. This paper discusses the relationships between the physical parameters of amplitude-modulated low-frequency sound and psychological and physiological responses.

1. Introduction

Wind turbine noise primarily originates from aerodynamic sounds generated by the rotation of blades [1]. The noise contains low-frequency components ranging from 20 Hz to 100 Hz [2] and is characterized by amplitude modulation, where the sound pressure level undergoes periodic fluctuations.

Focusing on this amplitude modulation characteristic, Fukushima et al. [3] proposed the amplitude modulation depth (AM depth) indicator to quantitatively understand the amplitude modulation sound in wind turbine noise. AM depth is a method for estimating the extent of AM using sound levels obtained by FAST and SLOW dynamic characteristics. Yokoyama et al. [4] created artificially synthesized sounds modeling the wind turbine noise and investigated the fluctuation sensation by changing the AM depth. As a result of the experiment, the fluctuating sensation was confirmed under the condition that AM depth was higher than 1.7 dB. Pörschmann et al. [5] created an amplitude-modulated model sound with a nominal value for AM depth of 0 to 8 dB in 2 dB increments and a 1.2 ± 0.1 s fluctuation cycle from actual wind turbine noise. They investigated the model sound effect on annoyance through listening experiments using headphones. The experimental results showed that annoyance increased with increasing AM depth and reached a maximum between 0 and 2 dB.

On the other hand, regarding the psychological effects of steady low-frequency sound (S-LFS), whose

¹ Corresponding author – Email: matsuda.hiroshi@nihon-u.ac.jp

sound pressure level does not vary over time, Nakamura and Tokita [6] conducted a laboratory experiment using steady sinusoidal tones with 5 to 80 Hz and one-third octave band noise with center frequencies ranging from 10 to 630 Hz. They exposed participants to whole-body exposure to S-LFS and asked them to rate the eight items: annoyance, oppressive sensation, vibratory sensation, displeasure, etc. As a result, they reported the presence of vibratory and oppressive sensations as sensations specific to low-frequency sound and identified the frequency that these sensations appeared preferentially [6, 7].

In addition to such psychological effects, there is growing interest in the physiological effects of low-frequency sounds. Previous studies have investigated the effects of auditory stimuli on physiological indices such as heart rate and brain activity [8]. However, most of these studies have focused on mid- to high-frequency sounds or music, and relatively few have examined low-frequency sounds or wind turbine noise specifically. Maijala et al. [9] investigated the effects of low-frequency sound (infrasound) from wind turbines on human physiological responses. In their experiment, they measured heart rate, heart rate variability, and skin conductance in response to wind turbine sounds. The study found no significant impact of the presence or absence of infrasound on these physiological responses. Walker et al. [10] investigated the effects of low-frequency noise (31.5–125 Hz) on cardiovascular and stress responses in healthy male participants. The results showed that exposure to low-frequency noise led to a decrease in heart rate variability (HRV) and an increase in blood pressure, indicating activation of stress responses. Nevertheless, differences in target frequency ranges, sound pressure level conditions, and physiological indicators used across studies have limited the consistency of their findings. Given this background, a comprehensive understanding of human responses to low-frequency sounds—including those emitted by wind turbines—requires evaluation that incorporates both psychological and physiological indices.

This study focuses on amplitude-modulated low-frequency sound (AM-LFS) based on pure tones at carrier frequencies ranging from 20 to 100 Hz. This study aims to develop a quantitative indicator to evaluate the psychological and physiological effects of AM-LFS. This paper describes the results of the dose-response relationship between the physical quantities (carrier frequency, equivalent sound pressure level, and amplitude-modulated level) and psychological and physiological response quantities of AM-LFS.

2. Creation of amplitude-modulated low-frequency sound

AM-LFS was created by amplitude-modulating a pure tone carrier wave. The sound stimulus conditions of the AM-LFS were a combination of the carrier frequency, the equivalent sound pressure level, the fluctuation cycle of the sound pressure level, and the amplitude-modulated level of the fluctuation depth of the sound pressure level. Figure 1 illustrates the sound pressure level waveforms of the AM-LFS used in the experiment.

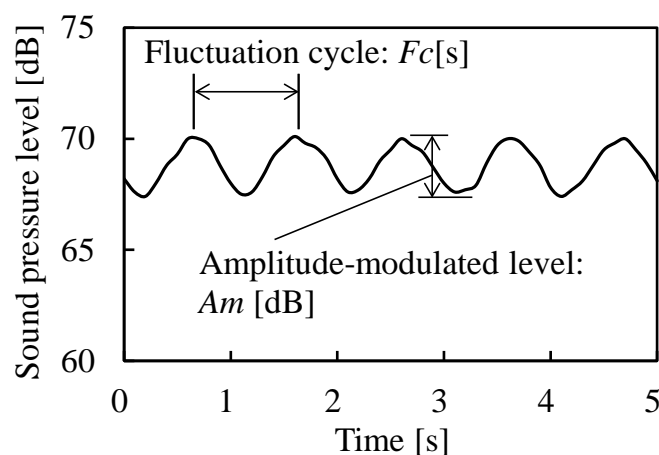


Figure 1 Sound pressure level fluctuation of AM-LFS (Carrier frequency 40 Hz, Equivalent sound pressure level 67 dB, Fluctuation cycle 1 s, Amplitude-modulated level 2.5 dB)

3. Experimental method

3.1 Experimental environment and system

Figure 2 provides an overview of the experimental system. The low-frequency chamber has a floor space of 2.7 m², a ceiling height of 2.2 m, a wall panel thickness of 45 mm, and four speakers of 380 mm diameter. A sound level meter designed for low-frequency sound (NL-62, RION Co., Ltd.) was used to measure both AM-LFS and S-LFS. Due to the long wavelength and high energy of low-frequency sound, the chamber was considered a uniform pressure field. Participants were exposed to low-frequency sound through whole-body exposure while seated in the low-frequency chamber. The S-LFS was generated using a sine-wave oscillator. The AM-LFS was produced using a PC-controlled function synthesizer, with the synthesized signals amplified through a power amplifier and output through the speakers.

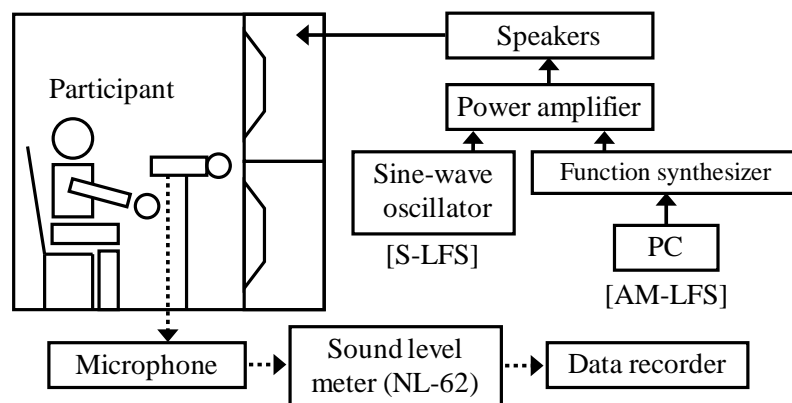


Figure 2 Diagram of the experimental system

3.2 Sound stimulus conditions and experimental protocol

Table 1 shows sound stimulus conditions used in this study. The equivalent sound pressure levels of AM-LFS were set based on the hearing thresholds for pure tone S-LFS previously measured by the authors. 2σ and 3σ mean that a sound pressure level two or three times the standard deviation σ dB of the hearing threshold for S-LFS is added to the hearing threshold for S-LFS. The sound pressure level of S-LFS was set to match the equivalent sound pressure level of AM-LFS for comparison with AM-LFS.

Each experimental condition lasted for 10 minutes. The baseline rest period lasted 5 minutes and 30 seconds, the AM-LFS or S-LFS exposure period lasted 3 minutes, and 1 minute and 30 seconds were allotted for completing the psychological questionnaire. Psychological responses were measured using Stevens' magnitude estimation (ME method) and a psychological questionnaire with a 7-point rating scale. Physiological responses were measured using salivary amylase activity (SAA) and electrocardiogram (ECG). SAA was measured twice: first, 3 minutes and 30 seconds after the start of the experiment, and second, immediately after the end of the sound stimulus exposure. ECG was recorded continuously throughout the experiment. The participants were 18 normal-hearing college students aged between 21 and 24. Each participant was exposed to either AM-LFS or S-LFS under randomly assigned sound stimulus conditions.

Table 1 Sound stimulus conditions

Carrier frequency C_f [Hz]	Equivalent sound pressure level $L_{P_{eq, 180s}}$ [dB]	Fluctuation cycle F_c [s]	Amplitude-modulated level A_m [dB]
20	81 (+2 σ), 83 (+3 σ)	0 (S-LFS)	0 (S-LFS)
40	67 (+2 σ), 71 (+3 σ)		
80	47 (+2 σ), 51 (+3 σ)		
100	35 (+2 σ), 37 (+3 σ)		
		1	2.5
		3	7.5

4. Measurement and evaluation of psychological and physiological responses to amplitude-modulated low-frequency sound

4.1 Method for measuring and evaluating psychological responses

The loudness and fluctuating sensation caused by AM-LFS and S-LFS were measured using the ME method. The participants rated the loudness and fluctuating sensation on a scale from 1 to 100. Annoyance, oppressive, and vibratory sensations were measured using a seven-point rating scale, as shown in Table 2. All statistical analyses were conducted using BellCurve for Excel.

Table 2 Psychological questionnaire using a 7-point rating scale

	Not at all	Almost not at all	Not much	Somewhat	Feel	Quite	Very much
Annoyance	1	2	3	4	5	6	7
Oppressive sensation	1	2	3	4	5	6	7
Vibratory sensation	1	2	3	4	5	6	7

4.2 Measurement and evaluation method of physiological responses

The purpose of measuring physiological responses is to investigate the effects of low-frequency sound on the autonomic nervous system (ANS). The physiology of the human body is under the influence of ANS. Sympathetic and parasympathetic nervous systems are the two subdivisions of ANS, and they are antagonistic to each other [11]. Studies have shown that sound perceived as annoying leads to an increase in sympathetic nervous system (SNS) activity and suppression of parasympathetic nervous system (PNS) activity [12]. In this study, we used changes in ANS activity as an indicator to examine whether low-frequency sound induces a physiological stress response. We measured SAA, heart rate (HR), and the low-frequency to high-frequency power ratio (LF/HF) as physiological indicators.

SAA is used as an indicator of sympathetic nervous system activity and psychological stress [13]. A disposable test strip designed explicitly for saliva collection was placed under the tongue for 30 seconds to measure SAA. The strip was then inserted into a measuring device (Cocoro Meter, NIPRO Corp.) and analyzed for approximately 20 seconds. The ratio of SAA immediately after sound stimulus exposure to the baseline (resting) level was calculated. A ratio greater than one indicated dominant SNS activity in response to the sound stimulus.

Electrocardiogram (ECG) signals were recorded using lead II configuration with electrodes attached to the participant's body surface. The acquired signals were transmitted via Bluetooth to a PC outside the low-frequency sound chamber using a small wearable device (Intercross-415, INTERCROSS Corp.) and continuously recorded. These data calculated the average HR and LF/HF values at rest and during exposure to sound stimuli. HR was defined as the number of heartbeats per minute, while LF/HF represented the power spectral density ratio derived from the frequency analysis of heart rate variability [14]. The relative HR and LF/HF changes during sound stimulus exposure (Δ HR, Δ LF/HF) were calculated using the resting state as a reference. Δ HR or Δ LF/HF greater than one indicated dominant SNS activity in response to the sound stimulus.

5. Experimental results

5.1 Loudness and fluctuating sensation

Figure 3(a) illustrates the relationship between carrier frequency and loudness, while Figure 3(b) illustrates the relationship between carrier frequency and fluctuating sensation. Each plot presents the geometric mean of the same sound stimuli conditions at the equivalent sound pressure level and the same carrier frequency. Figure 3(a) shows that both S-LFS and AM-LFS show a slight increase in loudness between 20 and 40 Hz, followed by a decrease at carrier frequencies above 40 Hz. A Student's t-test ($p < 0.05$) was performed to compare the mean loudness between AM-LFS and S-LFS under conditions with identical carrier frequency and equivalent sound pressure level. No statistically significant differences were observed at any of the

carrier frequencies. Figure 3(b) shows that the fluctuating sensation for AM-LFS remains relatively constant between 20 and 80 Hz, with a notable decrease observed at 100 Hz. In contrast, S-LFS shows a relatively stable trend across all carrier frequencies. A Student's t-test ($p < 0.05$) revealed statistically significant differences between AM-LFS and S-LFS at carrier frequencies of 20, 40, and 80 Hz. These results indicate that no significant difference in loudness was observed between AM-LFS and S-LFS when the carrier frequency was below 100 Hz. Regarding fluctuating sensation, distinct characteristics were observed between AM-LFS and S-LFS at carrier frequencies below 80 Hz.

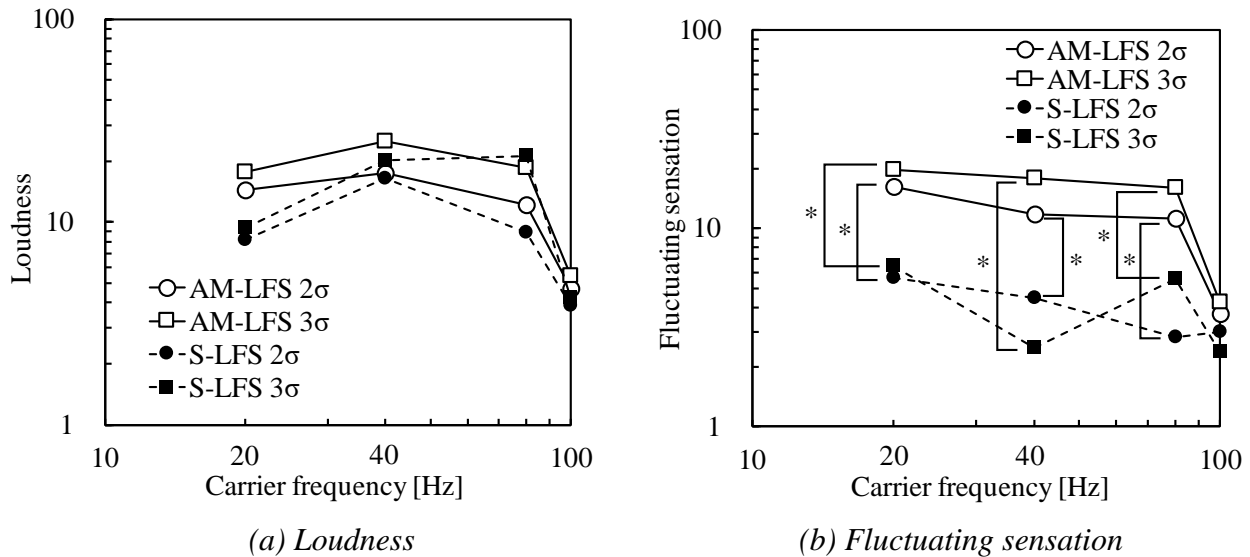


Figure 3 Relationship between carrier frequency and loudness, fluctuating sensation (*: $p < 0.05$)

5.2 Annoyance, oppressive sensation, and vibratory sensation

Figures 4(a) and 4(b) show that both S-LFS and AM-LFS show a slight increase in annoyance and oppressive sensation between 20 and 40 Hz, followed by a decrease at carrier frequencies above 40 Hz. The annoyance and the oppressive sensation ranged from 2 (almost not at all) to 4 (somewhat), suggesting that neither S-LFS nor AM-LFS is much annoyed or has an oppressive sensation at the equivalent sound pressure level of the hearing threshold plus 2σ to 3σ . Figure 4(c) shows that vibratory sensation decreased with increasing carrier frequency for both S-LFS and AM-LFS. A strong negative correlation was observed between vibratory sensation and carrier frequency, with a correlation coefficient exceeding 0.9. The vibratory sensation at the carrier frequency of 20 Hz ranged from 4 (somewhat) to 5 (feel) for both S-LFS and AM-LFS. The vibratory sensation at the carrier frequency of 20 Hz tended to increase compared to the vibratory sensation at other carrier frequencies. Statistical analyses in Figures 4(a)-(c) were performed by ANOVA with Dunnett's multiple comparisons of the means test, and $p < 0.05$ was considered significant. The control group consists of the three sensations of the S-LFS with the same carrier frequency and an equivalent sound pressure level (hearing threshold plus 2σ or 3σ). The comparison groups comprise these sensations of the AM-LFS. There was a statistically significant difference in the three sensations of the carrier frequency of 20 Hz, as shown in Figures 4(a)-(c).

5.3 Results of physiological responses

Figure 5 shows the relationship between the carrier frequency and three physiological response indices: ΔSAA , $\Delta LF/HF$, and ΔHR . Figures 5(a) and 5(b) show that ΔSAA and $\Delta LF/HF$ were equal to or greater than one under almost all conditions. This result suggests that exposure to low-frequency sound at an equivalent sound pressure level above the auditory threshold may enhance sympathetic nervous system activity. In contrast, Figure 5(c) shows that ΔHR remained close to one across all conditions, indicating no significant change compared to the resting state. All three physiological response indices exhibited approximately constant trends regardless of the carrier frequency. A t-test was conducted to compare S-LFS and AM-LFS under conditions with the same carrier frequency and equivalent sound pressure level. The results showed no statistically significant differences in any of the physiological indices. Therefore, no difference in physiological responses was observed between S-LFS and AM-LFS.

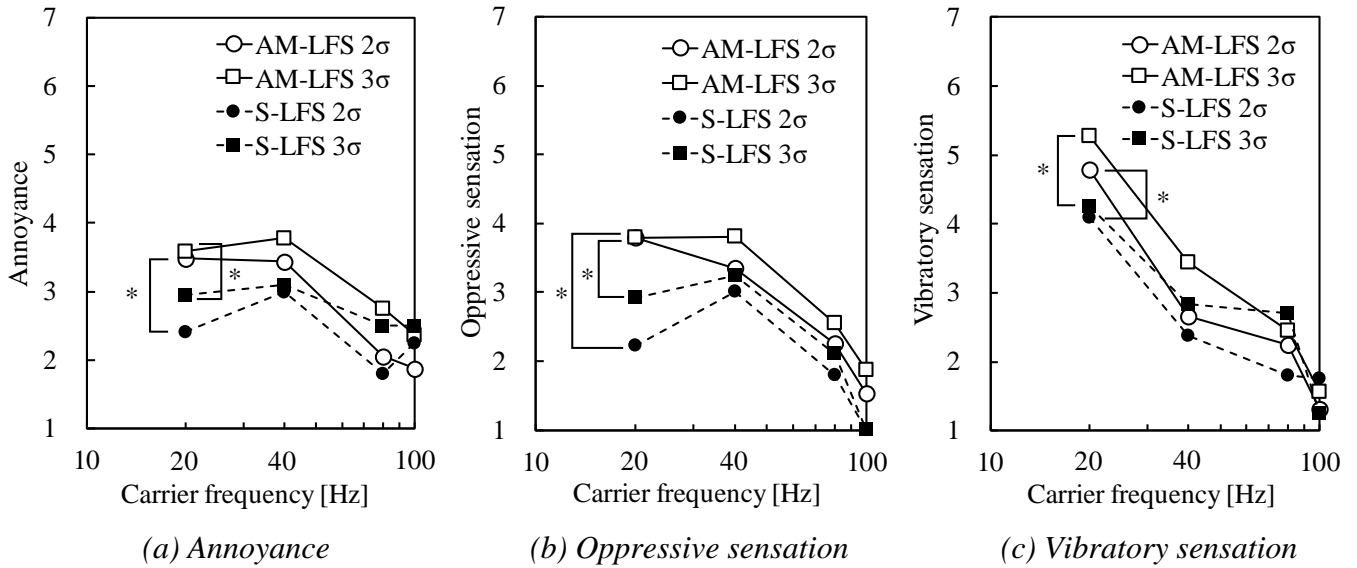


Figure 4 Relationship between carrier frequency and three sensations peculiar to low-frequency sound (*: $p < 0.05$)

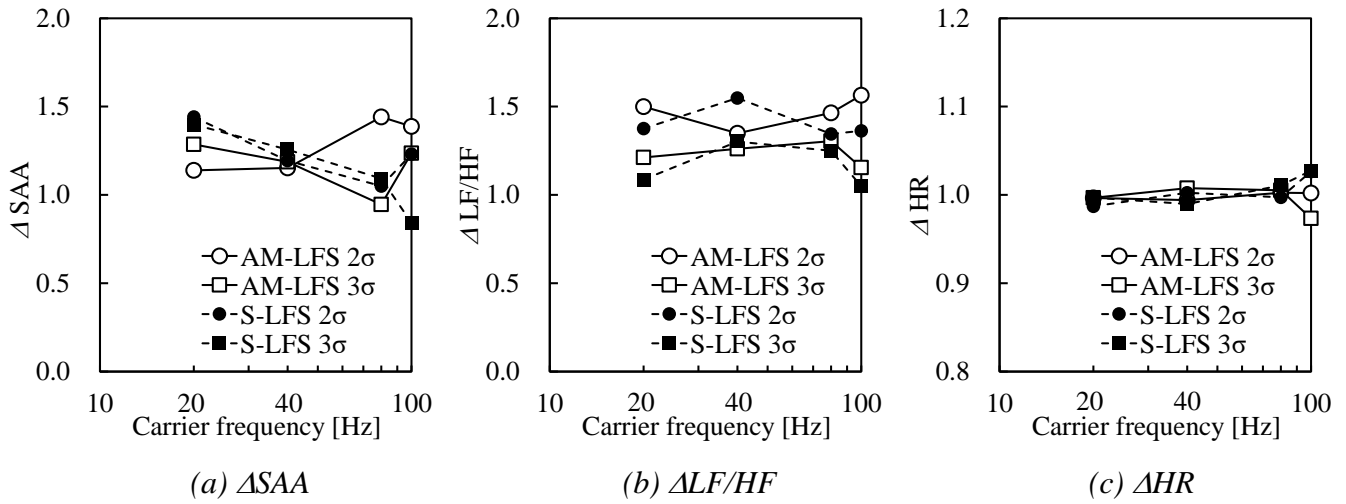


Figure 5 Relationship between carrier frequency and three physiological indicators

6. Discussion

In previous studies by Nakamura and Tokita [6] and Morinaga et al. [15], it has been reported that the perceptual thresholds for oppressive and vibratory sensations caused by S-LFS pure tones, expressed in terms of sound pressure level, tend to decrease as the carrier frequency increases, as illustrated in Figure 6. The equivalent sound pressure levels of the sound stimuli used in this study are marked with symbols such as circles and squares in Figure 6, and all fall within the 10 to 20 phon range of the equal-loudness contours defined in ISO 226: 2023 [16]. These values are lower than the perceptual thresholds for oppressive and vibratory sensations reported in [6] and [15].

This study evaluated oppressive and vibratory sensations using subjective rating scales. A tentative perceptual threshold was defined as the midpoint between rating scale values of 2 ("almost not at all") and 3 ("not much"). Based on this assumption, for carrier frequencies of 80 Hz and 100 Hz, rating scale values for both AM-LFS and S-LFS remained below this tentative perceptual threshold under almost all conditions, indicating that participants barely perceived oppressive and vibratory sensations. In contrast, at a carrier frequency of 20 Hz, the mean oppressive sensation rating exceeded 3, while the vibratory sensation rating exceeded 4 ("somewhat"), suggesting that perceptible sensations were elicited even at the equivalent sound pressure levels used in this study. At a carrier frequency of 40 Hz, both oppressive and vibratory sensations tended to exceed the defined perceptual threshold. These results suggest that at 20 Hz

and 40 Hz, participants subjectively experienced oppressive and vibratory sensations, even though the equivalent sound pressure levels were lower than the perceptual thresholds reported in [6] and [15]. This discrepancy may be attributed to differences in evaluation criteria, individual differences among participants, the experimental environment, and stimulus characteristics (e.g., presence of amplitude modulation). Further investigations are warranted to elucidate the unique perceptual characteristics of AM-LFS.

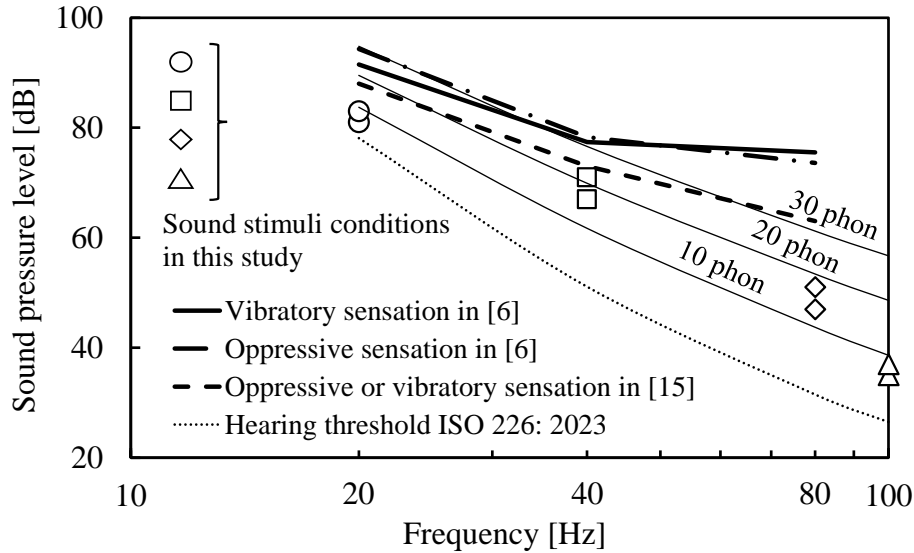


Figure 6 Comparison of oppressive and vibratory sensation in reference [6,15], hearing thresholds in ISO 226: 2023, and sound stimulus conditions set in this study

7. Conclusions

This study measured psychological and physiological responses to whole-body exposure to AM-LFS and S-LFS above the hearing threshold set at the same equivalent sound pressure level. The main results obtained are shown below.

The loudness of AM-LFS and S-LFS showed no significant differences across the measured range of carrier frequencies. However, statistical differences in fluctuating sensation were observed between AM-LFS and S-LFS at carrier frequencies below 80 Hz.

The annoyance and oppressive sensation caused by AM-LFS and S-LFS show a slight increase between carrier frequencies of 20 Hz and 40 Hz, followed by a decrease at carrier frequencies above 40 Hz. Vibratory sensation decreased with increasing carrier frequency for both S-LFS and AM-LFS. Annoyance, vibratory sensation, and oppressive sensation caused by AM-LFS at the carrier frequency of 20 Hz tended to be greater than these sensations of S-LFS.

AM-LFS and S-LFS at equivalent sound pressure levels above the auditory threshold enhance sympathetic nervous system activity, as shown by Δ SAA and Δ LF/HF. However, HR remained unchanged across all conditions, indicating no significant physiological change.

References

- [1] D. Bowdler and G. Leventhall, "Wind turbine noise," Multi-Science Publishing Co., Ltd, 2011.
- [2] K. Bolin and G. Bluhm, "Infrasound and Low Frequency Noise from Wind Turbines: Exposure and Health Effects," *Environmental Research Letters*, vol. 6, 2011.
- [3] A. Fukushima and K. Yamamoto, et al., "Study on the amplitude modulation of wind turbine noise: Part 1 – Physical investigation," in *Proceedings of INTER-NOISE 2013*.
- [4] S. Yokoyama and S. Sakamoto, et al., "Study on the amplitude modulation of wind turbine noise: Part 2 – Auditory experiments," in *Proceedings of INTER-NOISE 2013*.
- [5] C. Pörschmann and S. Großarth, et al., "Amplitude modulations increase annoyance due to wind turbine noise immission," in *Proceedings of INTER-NOISE 2021*.

- [6] S. Nakamura and Y. Tokita, "Frequency characteristics of subjective responses to low frequency sound," in *Proceedings of INTER-NOISE 81*, pp. 735-738, 1981.
- [7] Y. Tokita and S. Nakamura, "Frequency weighting characteristics for evaluation of low frequency sound," in *Proceedings of INTER-NOISE 81*, pp. 739-742, 1981.
- [8] E. H. Idrobo-Ávila and H. Loaiza-Correa, et al., "Different types of sounds and their relationship with the electrocardiographic signals and the cardiovascular system - Review," *Front Physiol*, vol. 9, no. 525, 2018.
- [9] P. P. Majjala and I. Kurki, et al., "Annoyance, perception, and physiological effects of wind turbine infrasound," *Journal of Acoustical Society of America*, vol. 149, no. 4, pp. 2238-2248, 2021.
- [10] E. D. Walker and A. Brammer, et al., "Cardiovascular and stress responses to short-term noise exposures-A panel study in healthy males," *Environ Res.*, vol. 150, 2016.
- [11] R. Tiwari and R. Kumar, et al., "Analysis of heart rate variability and implication of different factors on heart rate variability," *Current Cardiology Rev.*, vol. 17, 2021.
- [12] D. Dmitri and I. Olga, et al., "The effect of auditory stimulation on the nonlinear dynamics of heart rate: The impact of emotional valence and arousal," *Noise and Health*, vol. 25, no. 118, pp. 165-175, 2023.
- [13] M. Yamaguchi and T. Kanemori, et al., "Performance evaluation of salivary amylase activity monitor," *Biosensors and Bioelectronics*, vol. 20, no. 3, pp. 491-497, 2004.
- [14] W. V. Rosenberg and T. Chanwimalueang, et al., "Resolving ambiguities in the LF/HF ratio: LF-HF scatter plots for the categorization of mental and physical stress from HRV," *Sec. Clinical and Translational Physiology*, vol. 8, no. 360, 2017.
- [15] M. Morinaga, S. Yokoshima, et al., "A laboratory investigation into the threshold of the oppressive or vibratory feeling to low-frequency pure tone," in *Proceedings of INTER-NOISE 2022*.
- [16] ISO 226, "Acoustics – Normal equal-loudness-level-contours," 2023.

Paper #33 - ID: 367

Title: Experimental validation of a prediction model of wind turbine noise variability

Author: Bill Kayser

11th Edition of the
International Conferences on
Wind Turbine Noise
Copenhagen, Denmark – 10th to 13th June 2025

Experimental validation of a prediction model of wind turbine noise variability

B. Kayser¹

UMRAE, Cerema, Université Gustave Eiffel, 11 Rue Jean Mentelin, 67200, Strasbourg, France.

D. Ecotièrè

UMRAE, Cerema, Université Gustave Eiffel, 11 Rue Jean Mentelin, 67200, Strasbourg, France.

B. Gauvreau

UMRAE, Université Gustave Eiffel, Cerema, Allée des ponts et chaussées, 44340, Bouguenais, France.

Summary

Wind turbine noise assessment is a crucial aspect of environmental impact studies, particularly due to the variability of environmental parameters influencing sound propagation. This paper presents the validation of the online application WindTUNE designed to estimate the sound pressure level (SPL) distribution at a receiver position around a wind farm. The tool, which is freely accessible, allows users to define distributions of key environmental parameters such as wind speed, temperature, and ground absorption. It then computes the resulting SPL variability, both globally for the entire wind farm and individually for each turbine contribution. The application is built upon a metamodel integrating an emission model based on Amiet's theory and a propagation model using the parabolic equation method. The use of a metamodel considerably reduces computing costs while maintaining fidelity to complex physical models. This approach ensures an efficient and accurate estimation of noise levels under varying environmental conditions (atmosphere, ground). The results obtained from the application are compared against in situ measurements conducted during the French PIBE project. This experimental campaign provides a useful database for assessing the reliability of the modeled SPL distributions. The comparison highlights the strengths and potential limitations of the approach, offering insights into its practical applications in wind turbine noise prediction and regulatory assessments. By making this tool freely available online, we aim to provide researchers, policymakers, and industry professionals with a user-friendly and scientifically-based resource for wind farm noise evaluation. The application contributes to more comprehensive noise impact assessments.

¹Corresponding author - Email: bill.kayser@cerema.fr

1. Introduction

Accurate prediction of wind farm noise at long range requires a detailed understanding of both aerodynamic noise generation and outdoor sound propagation mechanisms. Although source and propagation models are now well established [1–3], comparing their predictions to experimental measurements remains a challenging task, as it requires accounting for numerous environmental and operational variables that influence outdoor sound level.

To address this, the present study uses WindTUNE , an innovative and user-friendly online application that offers a streamlined, turnkey solution for predicting wind turbine noise. WindTUNE estimates sound level variations at microphone locations using advanced modeling approaches, including Amiet’s theory for noise emission and the wide-angle parabolic equation (WAPE) for sound propagation [4]. To reduce computational time and enable fast predictions, a metamodel was developed based on this reference model [5], and it is this surrogate model that powers the WindTUNE application.

The aim of this paper is to assess the accuracy and robustness of WindTUNE by comparing its sound level estimation against a dataset of long-term field measurements. The comparison spans a range of operational and environmental conditions encountered during the experimental campaign, illustrating the tool’s ability to account for real-world variability on sound pressure level. Through this study, we seek to contribute to ongoing efforts in enhancing the reliability of wind farm noise prediction models, with the broader goal of improving noise impact assessments.

2. WindTUNE modelling tool

The WindTUNE application, previously introduced and detailed in earlier studies [6, 7], is a modeling tool designed to provide rapid and accurate predictions of wind turbine noise variability at receiver locations.

WindTUNE considers a representative onshore wind turbine with a nominal electrical power of 2.3 MW, a rotor diameter of 93 m, a hub height of 80 m, and three blades, each 45 m in length. The rotational speed increases linearly from 6 rpm at the cut-in wind speed of 4 m/s (measured at hub height) to 16 rpm at a wind speed of 12 m/s.

WindTUNE allows the user to modify the value of seven key input parameters that influence the predicted sound levels:

- Wind speed at reference height: U_{ref} (from 3 to 13 m/s)
- Wind direction: θ (from 0 to 360°)
- Shear exponent: α (from 0.05 to 0.6)
- Atmospheric turbulence intensity: γ_T (from 1E^{-7} to 1E^{-5})
- Ground-level temperature: T_0 (from -20 to 40 °C)
- Logarithmic temperature gradient coefficient: T_{log} (from -0.5 to 0.25 °C/m)
- Ground resistivity: σ (from 50 to 5000 kN·s·m⁻⁴)

Each of these parameters can be defined as a fixed value or drawn from a statistical distribution to reflect variability in experimental conditions. Supported distributions include uniform, normal, Weibull, log-normal, and exponential. Sampling from these distributions can be performed using either random or quasi-random methods, such as Monte Carlo, Sobol sequences, or Latin Hypercube Sampling (LHS), depending on the desired properties.

3. Experimental campaign

The measurement campaign took part in the PIBE project [8], as described in previous publications [9, 10]. It was conducted at a wind farm comprising eight wind turbines, each with a nominal power of 3 MW, a rotor diameter of 90 m, and a hub height of 80 m. The turbines are aligned in nearly a straight line, positioned at an approximate 60° angle to North, and are designated WT1 to WT8 from right to left, as

shown in Figure 1. During the campaign, five sound level meters, labeled “Long duration points” in Figure 1, collected continuous data over a span of 410 days from February 2020 to April 2021. These meters were placed at a height of 1.5 m, except for L4-N2, which was located at 2.6 m. Additionally, nine sound level meters, marked as “POI acoustic points” in Figure 1, recorded data during a focused 10-day observation period from June 23, 2020, to July 2, 2020. Two additional sound level meters were placed at ground level near WT1 at the IEC measurement position. For the comparison with model predictions in Section 4, both meteorological and acoustic data were averaged over 10-minute periods.

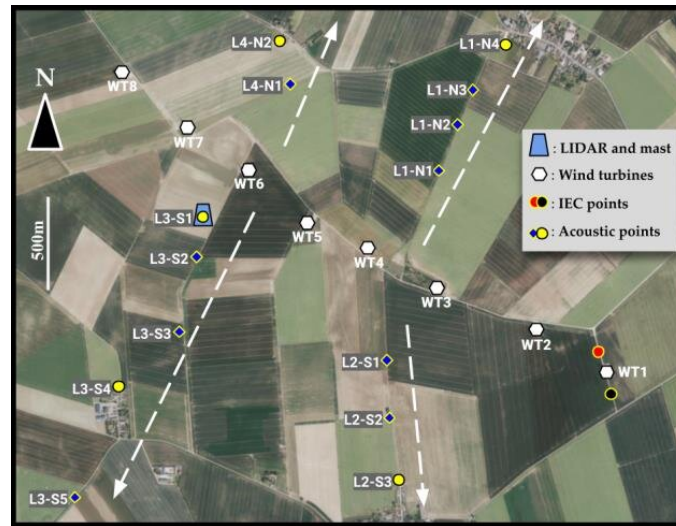


Figure 1 Experimental protocol of the PIBE campaign

4. Comparison between WindTUNE predictions and field measurements

In this section, we compare the sound level distributions predicted by WindTUNE with those measured in the field. WindTUNE allows for estimating the variation in sound levels around a normalized sound level value. Our focus is solely on the variability of the predicted and measured levels. In this sense, WindTUNE serves as a complementary tool, providing a probabilistic approach to the traditionally deterministic predictions of sound levels used in the industry. While this paper presents a single case study, more complete comparisons will be discussed during the conference.

We focus here on data from the L2-S3 point, located approximately 1 km from the nearest wind turbine. This microphone was mounted on a mast at a height of 1.5 m. The figure 2 shows the measured SPL distributions (LA50), compared with the simulations from WindTUNE, for downwind propagation conditions.

5. Conclusion

This study demonstrates the ability of WindTUNE to provide rapid and accurate predictions of wind turbine noise, with a focus on the variability in sound levels. The comparison between WindTUNE predictions and field measurements highlights the tool’s effectiveness in capturing real-world fluctuations while complementing traditional engineering methods. Future work will explore additional case studies across different wind farm sites and operational conditions, further validating the robustness and adaptability of WindTUNE. These ongoing efforts aim to refine the tool’s predictive capabilities and contribute to better noise impact assessments for wind energy projects.

Acknowledgments

This research was funded by the French National Agency for Research (contract ANR-18-CE04-0011).

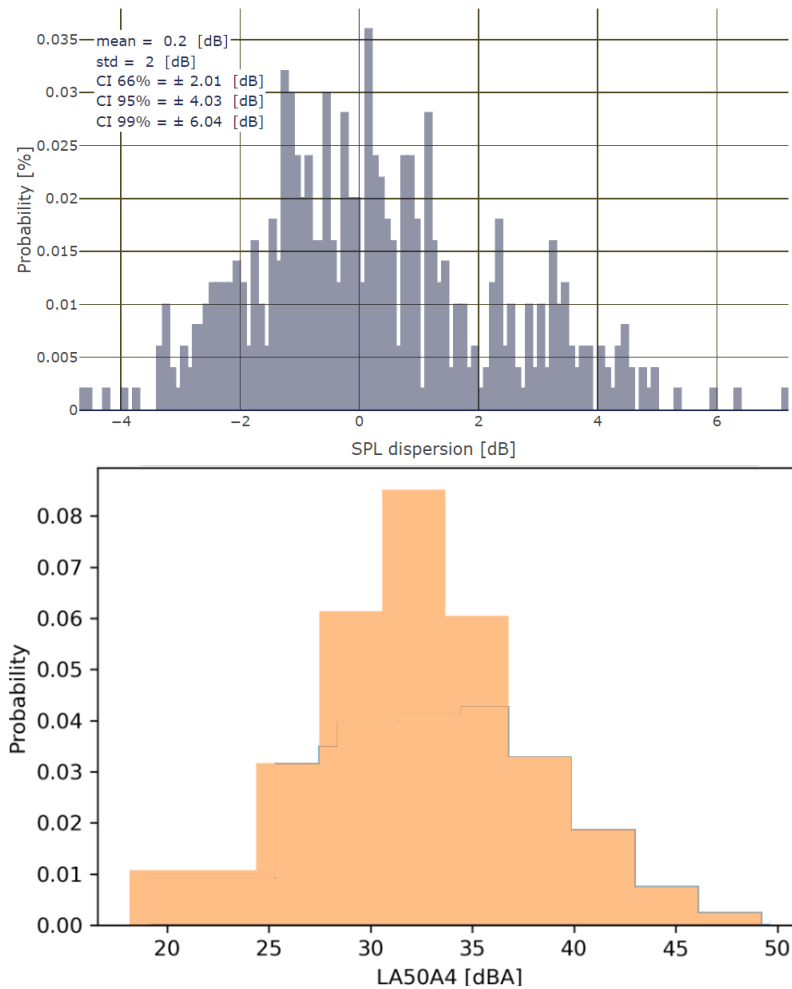


Figure 2 Comparison of SPL distributions obtained using the WindTUNE tool (top) and from the experimental campaign at point L2-S3 (bottom).

References

- [1] E. Barlas, W. J. Zhu, W. Z. Shen, K. O. Dag, and P. Moriarty, “Consistent modelling of wind turbine noise propagation from source to receiver,” *The Journal of the Acoustical Society of America*, vol. 142, no. 5, pp. 3297–3310, 2017.
- [2] B. Kayser, D. Mascarenhas, B. Cotté, D. Ecotière, and B. Gauvreau, “Validity of the effective sound speed approximation in parabolic equation models for wind turbine noise propagation,” *The Journal of the Acoustical Society of America*, vol. 153, no. 3, pp. 1846–1854, 2023.
- [3] J. Colas, A. Emmanuelli, D. Dragna, P. Blanc-Benon, B. Cotté, and R. JAM Stevens, “Wind turbine sound propagation: Comparison of a linearized euler equations model with parabolic equation methods,” *The Journal of the Acoustical Society of America*, vol. 154, no. 3, pp. 1413–1426, 2023.
- [4] B. Cotté, “Coupling of an aeroacoustic model and a parabolic equation code for long range wind turbine noise propagation,” *Journal of Sound and Vibration*, vol. 422, pp. 343–357, 2018.
- [5] B. Kayser, B. Gauvreau, D. Écotière, and V. Mallet, “Wind turbine noise uncertainty quantification for downwind conditions using metamodeling,” *The Journal of the Acoustical Society of America*, vol. 151, no. 1, pp. 390–401, 2022.
- [6] S. Bianchetti, B. Kayser, G. Guillaume, B. Gauvreau, A. Notarantonio, F. Junker, and D. Ecotière, “Variability and uncertainty of wind farm noise: A comparison between numerical predictions and in-situ measurements,” in *Proc.. Forum Acusticum*, pp. 11–15, 2023.

- [7] B. Kayser, S. Bianchetti, D. Ecoti re, and B. Gauvreau, “Windtune: a new tool for modelling wind farm noise uncertainties,” in *Proc. 10th International Conference on Wind Turbine Noise, Dublin, Ireland, 2023*.
- [8] PIBE Website, “Pibe website.” <https://www.anr-pibe.com/>. Last accessed: April 08, 2025.
- [9] D. Ecoti re, B. Gauvreau, I. Schmich-Yamane, A. Alarcon, M.-C. Nessi, F. Junker, G. Guillaume, V. Gary, L. Brendel, G. Litou, *et al.*, “A large-scale, long-term experimental campaign for the investigation of wind turbine noise fluctuations and amplitude modulation phenomena.,” in *INTER-NOISE and NOISE-CON Congress and Conference Proceedings*, vol. 265, pp. 6678–6684, Institute of Noise Control Engineering, 2023.
- [10] D.  coti re, B. Gauvreau, B. Cott , M. Roger, I. Schmich-Yamane, and F. Junker, “Predicting the impact of wind turbine noise: general overview and results of the pibe project,” in *INTER-NOISE and NOISE-CON Congress and Conference Proceedings*, vol. 270, pp. 9251–9262, Institute of Noise Control Engineering, 2024.

Paper #34 - ID: 368

Title: Examining the Effects of Atmospheric Parameters on Sound Power Level Measurements from Wind Turbines: Findings from Parallel Measurements in the IEC 61400-11 Reference Position and Extended Distances

Author: Niels Frederik Christensen

11th Edition of the
International Conferences on
Wind Turbine Noise

Copenhagen, Denmark – 10th to 13th June 2025

Examining the Effects of Atmospheric Parameters on Sound Power Level Measurements from Wind Turbines: Findings from Parallel Measurements in the IEC 61400-11 Reference Position and Extended Distances

Niels Frederik Christensen¹.

Sweco Denmark A/S, Aarhus, Midtjylland, 8200, Denmark

Irene Ortega²

Sweco Denmark A/S, Aarhus, Midtjylland, 8200, Denmark

Gustav Juul³

Sweco Denmark A/S, Aarhus, Midtjylland, 8200, Denmark

Summary

This paper investigates the effect of varying atmospheric parameters on sound power level determinations based on IEC 61400-11, focusing on the effect of air absorption. Given the considerable distances from many modern wind turbines to the reference position, atmospheric conditions can have a significant influence on the determined sound power levels since no correction is made to account for air absorption. This study involves simultaneous measurements at the IEC reference position and extended distances. By comparing the measurements, the paper aims to quantify the effects of atmospheric conditions on air absorption as a function of distance for three measurement campaigns, and to examine the influence this would have on the sound power level determination.

The findings indicate that atmospheric conditions can significantly impact sound power level determinations by affecting the measured sound pressure levels, especially at extended distances from the turbine. The data reveal that lower temperatures result in greater level differences above 400 Hz between the IEC reference position and extended distances, which is assumed to be caused by increased air absorption. Similarly, increased air absorption is indicated for higher atmospheric pressure. The air density is estimated based on the measured temperature and atmospheric pressure to evaluate its influence on air absorption, indicating that higher air density leads to higher air absorption.

¹ Niels Frederik Christensen – E-mail: nielsfrederik.christensen@sweco.dk

² Irene Ortega – E-mail: irene.ortega@sweco.dk

³ Gustav Juul – E-mail: Gustav.juul@sweco.dk

1. Introduction

As wind turbines are getting larger, so are the distances at which noise levels are being measured, when following the IEC 61400-11 ed. 3.1 (IEC) standard. This may result in atmospheric conditions having a significant influence on the determined sound power levels, since no corrections are made to account for air absorption.

By performing simultaneous sound pressure level measurements at different distances, including the IEC position as reference, and comparing the results, the effects of atmospheric conditions on air absorption as a function of distance are evaluated.

Air absorption is estimated based on measured level differences in different extended microphone positions for three measurement campaigns.

For commercial reasons, no turbine specific details are provided in this paper. For the same reason, only level differences are shown.

2. Environment and measurement conditions

Three measurement campaigns were carried out on a wind turbine at the Wind Turbine Test Centre Østerild, Denmark. The site is in flat, rural land, surrounded by forest, far from major roads and other noise sources. The closest neighbouring turbines were stopped during the measurements.

Table 1 shows the dates for each measurement campaign and measured meteorological parameters.

Table 1: Measurement campaign dates and measured ranges of atmospheric parameters.

Campaign	Date	Ambient temperature [°C]	Relative humidity [%]	Atmospheric pressure [kPa]
Campaign 1	04-12-2024	2 – 3	87 – 95	101.5 – 102.5
Campaign 2	16-12-2024	6 – 8	86 – 97	100.8 – 101.5
Campaign 3	19-01-2025	-2 – 0	86 – 93	101.9 – 102.3

3. Measurements

3.1 Measurement setup

Four microphones were placed downwind of the turbine, one in the standard IEC reference measurement position, two at 500 m from the turbine (relatively close together, as seen in the photo at the bottom of figure 1, so that they are comparable) and one at 800 m. Two of the microphones were placed on reflective boards on ground level, and two were placed on tripods at a 1.5 m height, as seen in Table 2 and Figure 1.

Table 2: list of microphone positions with distances to the turbine tower centre and a description of the setup.

Measurement position	Distance from turbine	Description
Position 1 (IEC reference)	235 m	On reflective ground board
Position 2a	500 m	On reflective ground board
Position 2b	500 m	On tripod at 1.5 m height
Position 3	800 m	On tripod at 1.5 m height

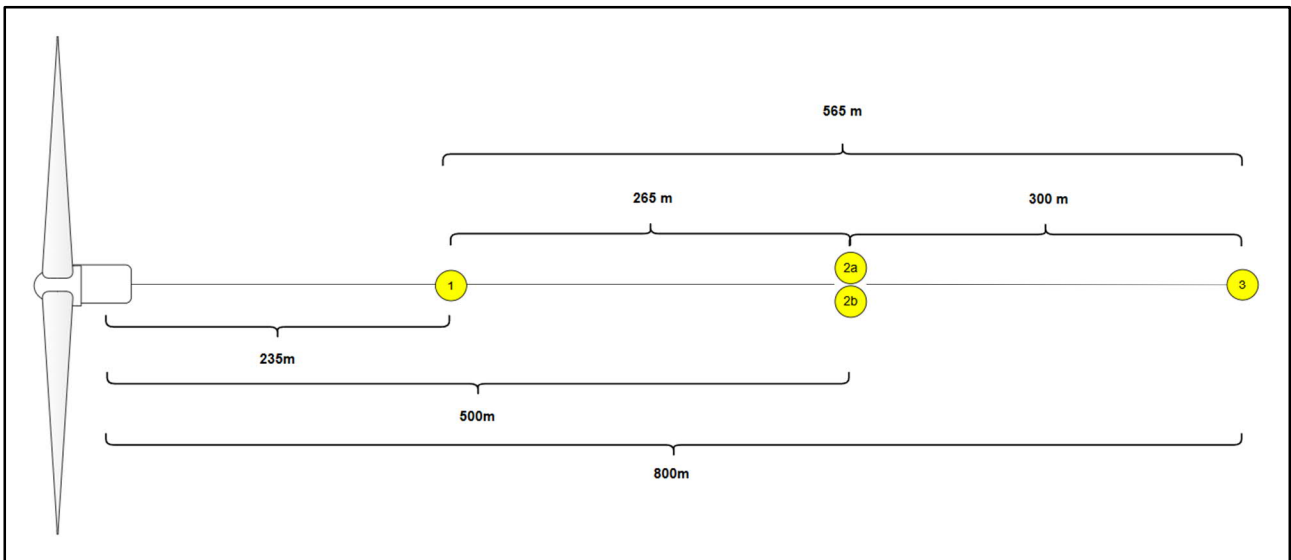


Figure 1: diagram with microphone positions and distances



Figure 2: Microphone positions and setup. On the top left is the IEC reference position, on the top right is the tripod at 800 m and on the bottom, the two microphones at 500 m.

3.2 Measured data

All data was averaged over 10 seconds periods and all sound pressure levels are A-weighted.

3.2.1 Acoustic data

The equivalent continuous sound pressure levels, L_{Aeq} , were measured for the total noise, as well as the background noise, and used to determine the normalized 1/3-octave band spectra for each 10 second period, according to the IEC standard. The 1/3-octave band spectra were corrected for the influence of their respective secondary wind screens.

3.2.2 Meteorological data

Ambient temperature, relative humidity and atmospheric pressure at 1.5 m height were measured using a Gill Instruments GMX300 weather station.

The wind speed was measured at 11.8 m height using a Gill WindSonic ultrasonic anemometer and determined at hub height using the power-based wind speed and the nacelle anemometer.

4. Methods

To estimate the air absorption, it is assumed that the sound pressure level from the turbine, L_{pA} , at a distance from the turbine can be described using a simple prediction method such as that described in the Danish Statutory Order 995 for wind turbine noise according to the below formula for land-based turbines.

$$L_{pA} = L_{WA,ref} - 10 \log(l^2 + h^2) - 11dB + \Delta L_g - \Delta L_{air} \quad (1)$$

where:

l : is the horizontal distance from the turbine tower to the calculation point

h : is the hub height of the wind turbine

11dB: $10 \cdot \log 4\pi$, sound power level to sound pressure level assuming a point source in free field

ΔL_g : is the terrain correction

ΔL_{air} : is the air absorption

The terms $L_{WA,ref}$ and $10 \cdot \log 4\pi$ are identical for all positions, so the measured level differences, $L_{pA,m1-m2}$, between two measurement positions m_1 and m_2 , then becomes:

$$\Delta L_{pA,m1-m2} = 10 \cdot \log \left(\frac{l_{m1}^2 + h^2}{l_{m2}^2 + h^2} \right) + \Delta L_{g,m1-m2} - \Delta L_{air,m1-m2} \quad (2)$$

where:

l_{m1} : is the horizontal distance from the turbine tower to the calculation point m_1

l_{m2} : is the horizontal distance from the turbine tower to the calculation point m_2

$\Delta L_{g,m1-m2}$: is the difference in terrain correction between point m_1 and m_2

$\Delta L_{air,m1-m2}$: is the difference in air absorption between point m_1 and m_2

By accounting for the difference in horizontal distances between measurement positions and any potential difference in terrain correction, it is possible to estimate the difference in air absorption, $\Delta L_{air,m1-m2}$. The difference in air absorption along with the difference in propagation distance can then be used to estimate the average air absorption per meter.

4.1.1 Data handling and Normalization

Data was normalized according to the below description to allow comparison between the different measurement positions, with the aim of highlighting the effect of the air absorption on the measured values.

- Background noise

The 1/3-octave band total noise spectra, $L_{V,T,I,k}$, are corrected for background noise, for each microphone position, to obtain the background noise corrected 1/3-octave band spectra $L_{V,c,I,k}$, following the procedure in the IEC standard.

- Distance normalization

Since measurements were done at different distances, the background noise corrected 1/3-octave band spectra, $L_{V,c,I,k}$, from the 500 m and 800 m positions was normalized to the reference IEC position distance of 235 m from the turbine using the distance term in eq. (2). The sound propagation distance for each microphone position was determined as the slant distance from the wind turbine hub to the microphone. The difference between the sound propagation distance to the 500 m and 800 m positions relative to the IEC position was calculated.

- Tripod/board effect

Having simultaneous measurements at the same distance from the turbine on both a board and a tripod, allows to estimate the effect of the board by subtracting the levels, $L_{V,c,I}$, of the tripod measurement from the levels of the ground board, $L_{V,c,I}$. This corresponds to the difference in terrain correction $\Delta L_{g,m1-m2}$ in eq. (2). This is used as a correction to the results of the tripod measurements and is applied to the 500 m and 800 m tripod measurement to allow comparisons. The correction, named board effect, is shown in Figure 3.

At low frequencies, the difference between the sound measured at the ground board and the tripod is minimal. The ground effect for the tripod is small since the phase delay from the direct sound and the sound reflected by the ground is negligible.

The peak seen around 200 Hz is likely due to the ground interference dip caused by the microphone being at 1.5 m above the ground.

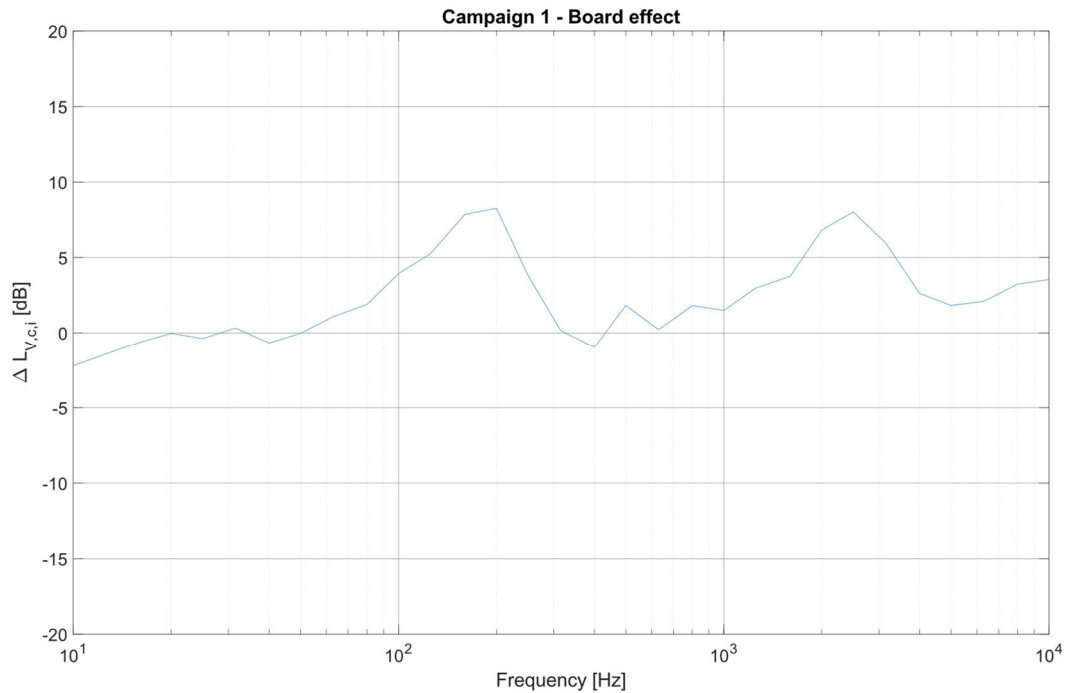


Figure 3: level difference between the sound pressure levels measured on the tripod and those measured on the ground board, both at 500 m.

It was seen that the signal-to-noise-ratio (SNR) of the measurements done on the ground board is higher than that for the measurements done on the tripod, both at 500 m. The data from the microphone on the tripod at 500 m is therefore only used to describe the effect of the board, while that captured with the microphone on the board, is the one used for comparisons with levels measured at the IEC reference and used in the remaining investigations. It is assumed that the difference in terrain correction is zero, $\Delta L_{g,m1-m2} = 0$, when comparing measurements done on ground board at IEC reference and the ground board at 500 meters. This does not consider that the angle of incidence of the sound field is slightly different between the two positions.

It is assumed that after doing the described corrections and normalizations, the resulting level differences relates only to the air absorption term, $\Delta L_{V,m1-m2} = \Delta L_{air,m1-m2}$.

4.2 Frequency range of interest

The air absorption is calculated according to ISO 9613-2:2024 (ISO) for reference and shown in Figure 4 (red line), for the average weather conditions during one of the measurement campaigns. The calculated air absorption drops off at low frequencies and becomes negligible below around 400 Hz.

Up to around 110 Hz, the differences in the background noise corrected and normalised levels for all microphone positions were found to be small.

Figure 4 shows that the differences between the reference IEC position and the microphone at 500 m are relatively low up to 250 Hz, after which the difference starts increasing until 4 kHz. Above 4 kHz, the

measurement at the 500 m position is highly influenced by background noise, leading to a poor SNR and making comparisons based on the measured level differences unfeasible.

To study the frequency range where air absorption is significant and where the SNR is decent, it was decided to limit the frequency range of the investigations from 400 Hz to 4 kHz.

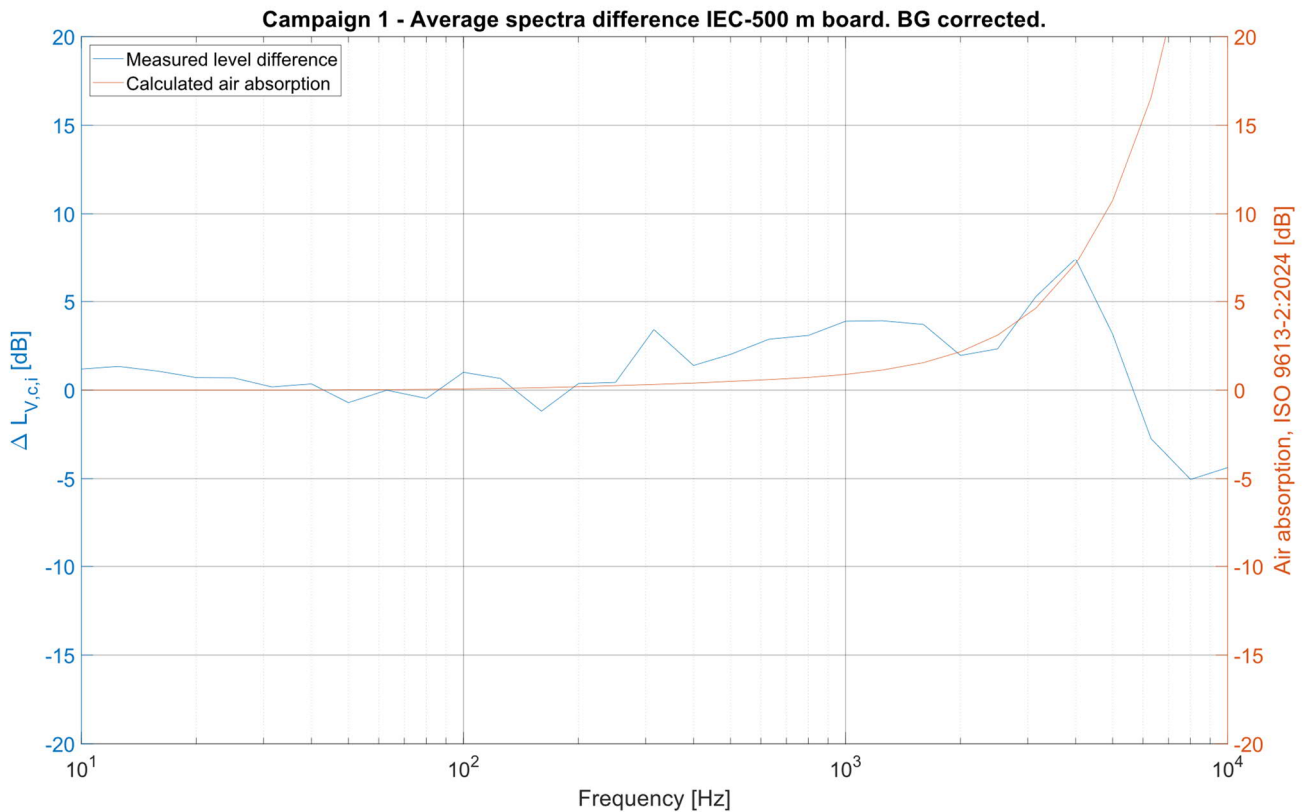


Figure 4: Sound pressure level differences between IEC and 500 m positions and calculated air absorption, as a function of frequency.

Due to the low signal-to-noise-ratio at 500 m, and knowing that sound pressure as a function of distance follows the inverse square law⁴, the data from the microphone at 800 m was excluded in the following evaluations.

4.3 Air density

According to ISO, the air absorption depends strongly on the frequency of the sound, temperature and relative humidity of the air, and to a lesser extent on the ambient pressure. Since temperature and pressure both fluctuate during the measurements, the measured values at 1.5 m height were used to calculate the air density, using the ideal gas law, to study the influence of this single combined parameter on air absorption.

It is important to note that while the ideal gas law provides a good approximation for air density under normal conditions, outside high pressure and low temperature cases, it may not accurately predict the behaviour of air at high relative humidity levels. As the air approaches water vapor saturation, which is the case for the measurements presented here, condensation may occur—a phenomenon the ideal gas law does not account for.

⁴ The inverse square law states that the intensity of sound decreases proportionally to the square of the distance from the source, corresponding to approximately 6 dB decrease in the sound pressure level per doubling of distance.

5. Results

Results were initially pooled in wind speed bins. However, since no trend was found in the level differences as a function of wind speed bin for any of the three campaigns, it was chosen to pool the data together across all wind speeds to get a larger data set for the investigations on the effect of the other meteorological parameters.

The relative humidity only had small variations around a limited range of 86-97 % across the campaigns and was therefore not of much interest for examining the effect of changing humidity levels.

The following figures show the impact of temperature and atmospheric pressure in the level differences between the IEC and 500 m position.

Figure 5 shows that the lower the temperature, the larger the level difference between the two positions, which indicates a higher air absorption.

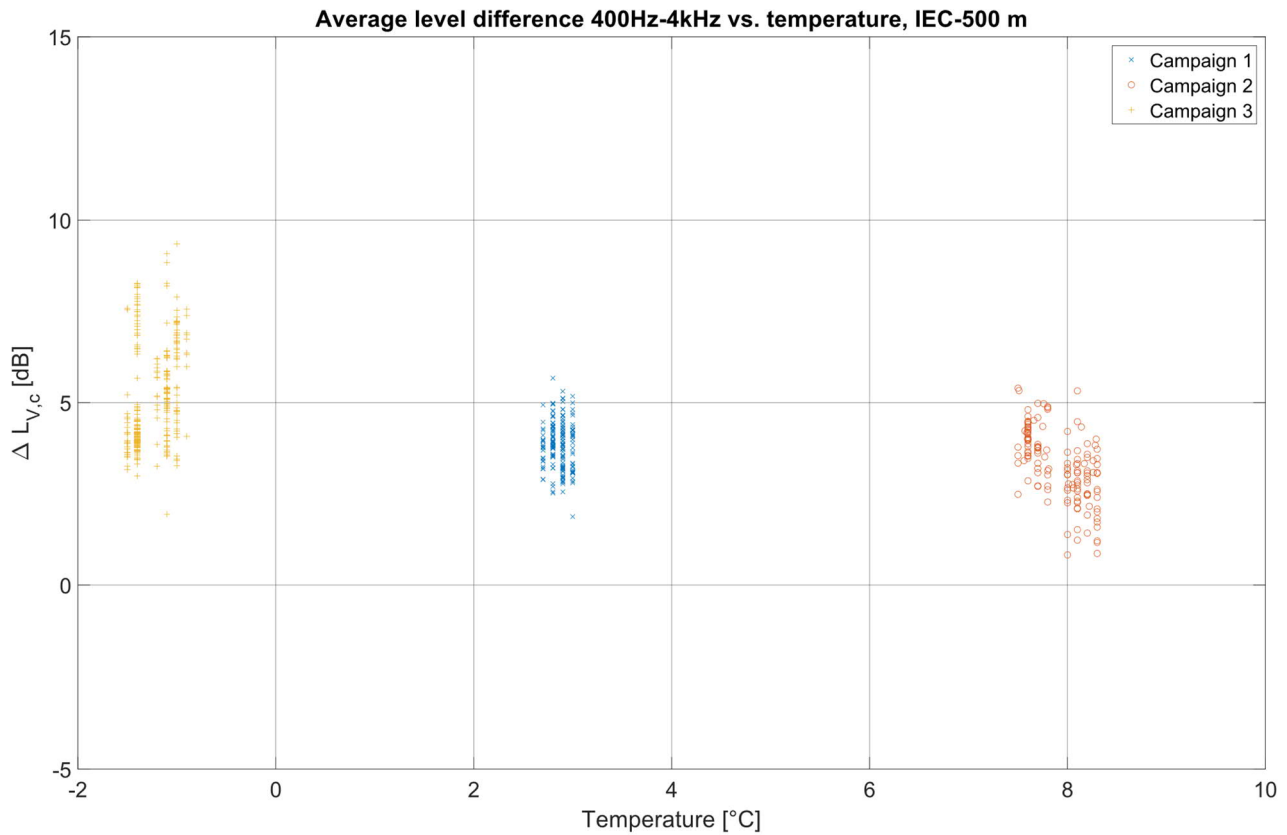


Figure 5: level difference between IEC and 500 m positions as a function of temperature for each measurement campaign.

Figure 6 presents the level differences as a function of atmospheric pressure, with a small trend indicating that the higher the pressure, the higher the higher air absorption. The effect of changing atmospheric pressures is less significant than changing temperatures, as expected.

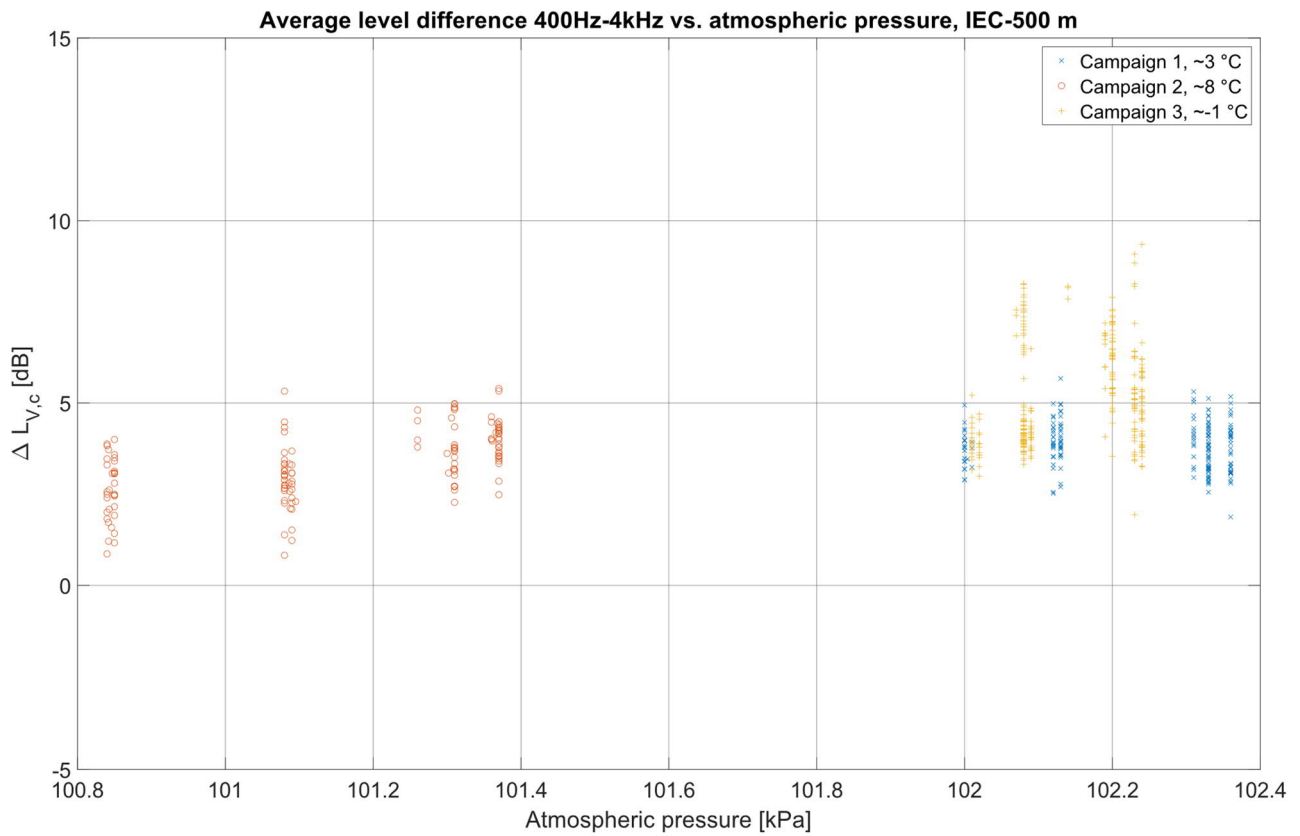


Figure 6: level difference between IEC and 500 m positions as a function of atmospheric pressure for each measurement campaign.

Figure 7 further points towards the influence of these two parameters, showing that the higher the air density (corresponding to lower temperature), the higher the air absorption.

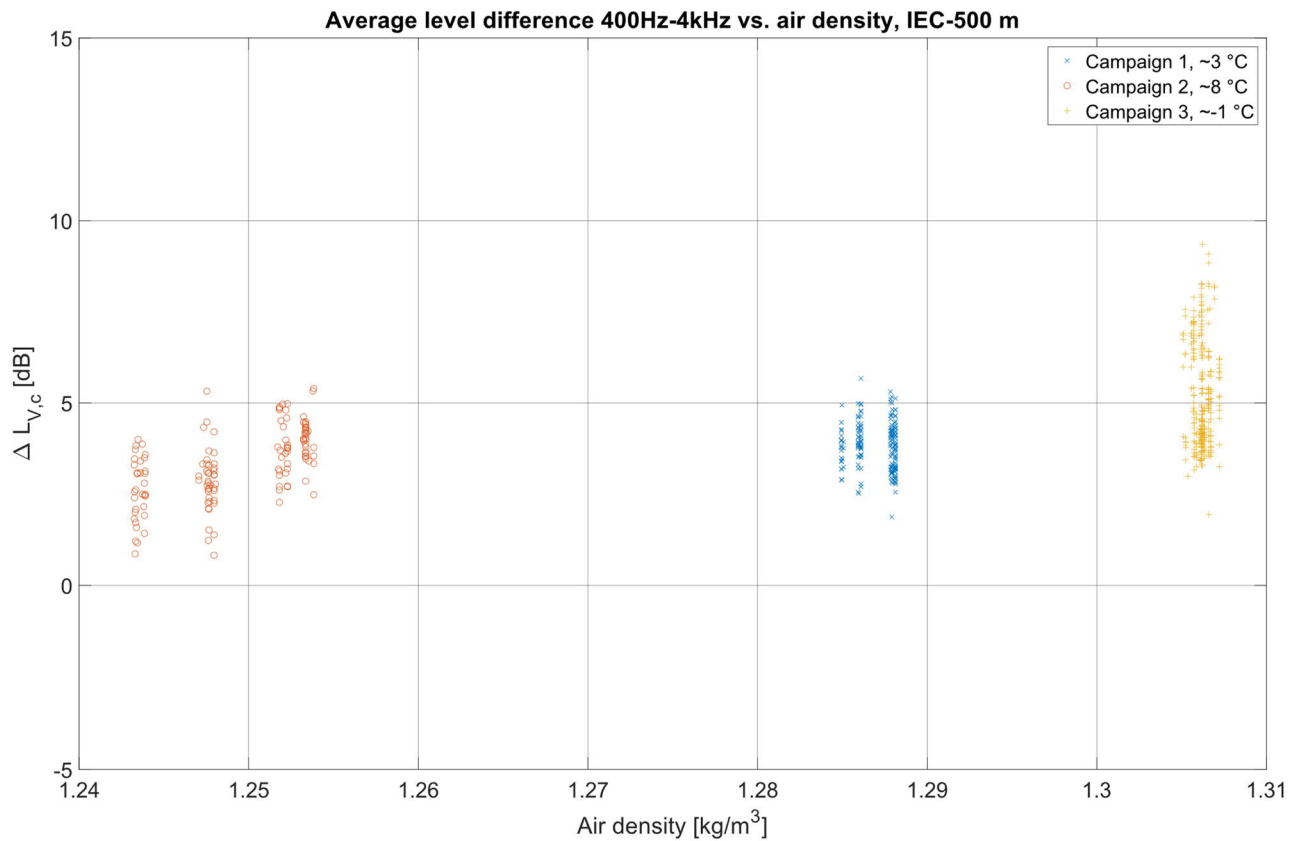


Figure 7: level difference between IEC and 500 m positions as a function of air density for each measurement campaign.

6. Conclusions

This paper provides analysis of the effects of atmospheric parameters on sound power level measurements from wind turbines. The study involved simultaneous measurements at the IEC 61400-11 reference position and extended distances, focusing on the influences of temperature, relative humidity, and atmospheric pressure on air absorption.

The findings indicate that atmospheric conditions can significantly impact the measured sound pressure levels at extended distances from the turbine. The results show that lower temperatures result in greater level differences as a function of distance, which is thought to be caused by increased air absorption. Similarly, the results indicate higher air absorption with higher atmospheric pressure.

These results suggest that applying corrections to the measured sound pressure levels based on atmospheric conditions is important for achieving more accurate sound power level determinations. If such corrections were applied, accounting for the specific atmospheric conditions at the time of the measurements, it would allow more reproducibility in sound power level determinations, particularly at high frequencies and for larger wind turbines.

Acknowledgments

We would like to thank Vestas Wind Systems A/S for allowing us to use data from the measurement campaigns.

References

- [1] IEC 61400-11 edition 3.1, “Wind turbines – Part 11: Acoustic noise measurement techniques”, 2018-06.
- [2] The Danish EPA, 2024 BEK nr. 995, “Bekendtgørelse om støj fra vindmøller” (Statutory Order on Noise from Wind Turbines; Statutory Order no. 995).
- [3] ISO 9613-2:2024, “Acoustics - Attenuation of Sound During Propagation Outdoors.”

Paper #35 - ID: 369

Title: Planning conditions - what should they cover?

Author: James Mackay

11th Edition of the
International Conferences on
Wind Turbine Noise
Copenhagen, Denmark – 10th to 13th June 2025

Planning conditions – what should they cover?

James Mackay¹

TNEI Services Limited, Newcastle upon Tyne, Tyne and Wear, NE1 3PA, UK

Jim Singleton²

TNEI Services Limited, Glasgow, G2 5UB, UK

Summary

Planning conditions are attached to wind farm consents in the United Kingdom and the Republic of Ireland to control wind farm noise emissions and to provide a mechanism to trigger compliance assessments, where required. Whilst example planning conditions have existed for well over 10 years, the matters considered within noise related conditions vary significantly between individual consents and in different countries. This paper considers the guidance that is in place in relation to planning conditions, which require conditions to be necessary, relevant to planning, relevant to the development, enforceable, precise and reasonable in all other respects (the six tests). The paper then presents a comparison of a number of noise conditions attached to wind farms consented in Scotland and Ireland between January 2024 and April 2025. Trends and patterns are identified, and discussion is included as to whether the conditions that are routinely applied, comply with the six tests.

1. Introduction

The wind farm industry spends a significant amount of time and effort designing wind farm developments to comply with the relevant noise regulations. Whilst many developments go on to be built and operate without any noise issues, it is sometimes necessary to rely on noise controls included within the developments planning consent to resolve issues, including noise complaints. In the United Kingdom (UK) and Republic of Ireland (ROI), the first line of control is in the form of planning conditions.

When a consenting body in the UK or the ROI (e.g. a Local Authority (Council) or the Government) grants planning permission they have the option to apply conditions to control the development (e.g. restricting the hours when construction activities can occur, setting out additional information that needs to be agreed by the Council prior to operation of the development etc). Conditions imposed within a planning permission can enable many development proposals to proceed where it would otherwise have been necessary to refuse planning permission. Whilst consenting bodies have the power to impose planning conditions on a variety of topics, this power needs to be exercised in a manner which is fair, reasonable and practicable.

This paper explores which topics are typically covered within wind farm noise related planning conditions and considers how well such conditions align with wider guidance regarding the use of planning conditions.

¹ james.mackay@tneigroup.com

² jim.singleton@tneigroup.com

Whilst conditions are sometimes included to cover noise during the construction and decommissioning phases, this paper focuses on conditions relating to operational wind turbine noise only.

2. Guidance regarding the use of planning conditions

Whilst the planning systems used to consent wind farm developments differ slightly across the UK (England, Scotland, Wales and Northern Ireland) and the ROI, consents in all regions can be issued with a series of planning conditions. Separate guidance regarding the use of these conditions is available across the UK and the ROI, specifically in the *'National Planning Policy Framework'* (for England and Wales) [1], *'Circular 4/98 The Use of Planning Conditions in Planning Permissions'* (for Scotland) [2], *'Development Management Practice Note 20 – Use of Planning Conditions'* (for Northern Ireland) [3] and the *'Development Management Guidelines'* (for Ireland) [4]. The guidance documents adopt many of the same principles including when and why conditions should be adopted whilst all four documents also require planning conditions to be:

- Necessary;
- Relevant to planning;
- Relevant to the development;
- Enforceable,
- Precise; and,
- Reasonable in all other respects

These six requirements are sometimes referred to as 'the tests'.

Whilst it is noted that guidance regarding planning conditions may vary significantly elsewhere in the world, alignment with the six tests may be desirable (for example most stakeholders would want a planning condition to be precise rather than being vague and open to interpretation), and it is therefore hoped that the contents of this paper will also prove to be of interest to acousticians working in other regions.

3. The evolution of wind farm noise related planning conditions in the UK and ROI

The current UK wind farm noise guidance *'The assessment and rating of noise from wind farms'* (ETSU-R-97) [5] was written in 1996. The Authors noted, on page 15, that in the absence of direct guidance on the use of planning conditions for wind farms, several methods have evolved to control wind farm noise immission levels.

ETSU-R-97 did set out, as noted on page iii, a methodology to establish noise limits which were:

'presented in a manner that makes them a suitable basis for noise-related planning conditions or covenants within an agreement between a developer of a wind farm and the local authority.'

The Authors did also note, on page x, that:

'The Noise Working Group thought that it would be beneficial to present its recommendations in a form which might be useful to developers and planners. We therefore considered drafting planning conditions, but came to the conclusion that the necessary definitions of terms which would be required would make planning conditions too complicated.'

Notwithstanding the guidance in ETSU-R-97, wind farm noise planning conditions continued to be drafted in a variety of ways some early conditions contained technical errors and, it could be argued, a number of the conditions failed to meet the six tests.

In 2013, the UK Institute of Acoustics published *'A good practice guidance to the application of ETSU-R-97 for the assessment and rating of wind turbine noise'* (IOA GPG) [6] which included an example planning condition that was built on the guidance in ETSU-R-97 but had been developed, iterated and

refined to reflect current best practice. This example planning condition had been used for several larger scale wind farm developments and has also been examined in detail in wind farm planning appeals³.

The example condition included in the IOA GPG is shown below as Figure 1; it was five pages of A4 text long. Clearly the text in the figure is not intended to be readable but is has been included to highlight the amount of detail that was included in the example condition, the full condition can be viewed on the IOA website⁴.



Figure 1 The example condition in the IOA GPG

The use of the IOA GPG was endorsed by all of the regional Governments in the UK, for example, the Scottish Government noted in the Onshore Wind Turbines Planning Advice guidance [7] that:

‘The document provides significant support on technical issues to all users of the ETSU-R-97 method for rating and assessing wind turbine noise, and should be used by all IOA members and those undertaking assessments to ETSU-R-97. The Scottish Government accepts that the guide represents current industry good practice.’

Whilst the IOA GPG is almost universally referenced and used within wind turbine noise assessments in Scotland, the example condition was not as widely adopted. Even though the example condition met the tests it was often considered to be highly technical and some decision maker felt its use required specialist input from acousticians who were familiar with wind farm noise. The example condition contained extensive cross referencing (e.g. ‘in accordance with Guidance Note 2(b)’ or ‘as made under paragraph (c)’) meaning that it was easy to introduce errors if changes were made by someone who was not familiar with the structure, whilst the length and complexity of the conditions meant that consenting authorities often preferred to adopt much more succinct conditions (even if these did not meet the tests).

In 2017, McKenzie *et al* [8] jointly drafted an article, which was published in the Acoustics Bulletin magazine, that set out an alternative noise condition built on much of the original text in the IOA GPG example condition but also included consideration of Amplitude Modulation (AM)⁵. Whilst the approach suggested in the Acoustics Bulletin article was used in some consents it was not incorporated back into the IOA GPG (as no updates have been published since 2013) and its use was not endorsed by the IOA or any Government departments in the UK or the ROI.

In February 2025 the Scottish Government issued standard onshore wind planning conditions [9] for Section 36 Consents⁶ and an operational noise condition was included which is very similar in function to the IOA GPG example condition. This does not consider AM.

³ A planning appeal can be triggered in several ways (e.g. refusal of an application by a Local Authority). The most high-profile form of appeal is a Public Inquiry where evidence is given, and expert witnesses are called to give evidence. The example condition included in the IOA GPG was based on versions discussed in detail at a number of Public Inquiries (so had been subject to detailed examination by acousticians, lawyers and planning experts).

⁴ Available at <https://www.ioa.org.uk/publications/wind-turbine-noise> (last accessed 24-04-2025)

⁵ Amplitude modulation is a term used to describe periodic fluctuations in the level of audible noise from a wind turbine (or wind turbines), the frequency of the fluctuations being related to the blade passing frequency of the turbine rotor(s).

⁶ Applications for wind farms with a rated capacity of over 50 MW are made directly to the Scottish Governments Energy Consents Unit (ECU) who consider the applications in accordance with Section 36 of the Electricity Act 1989.

4. Matters covered in wind farm noise conditions

Despite the presence of the IOA GPG example condition for over ten years, there continues to be a range of planning conditions that are applied in both the UK and the ROI, and developers, consultants, consenting authorities and residents often disagree on what should be included and what should not.

The IOA GPG example condition and the 2025 standard condition provided by the Scottish Government both include the following⁷:

- A. Tables of noise level limits (which usually vary with wind speed) for the nearest noise sensitive receptors for daytime and night time periods;
- B. A requirement to submit for approval, a list of consultants who can perform compliance assessments in accordance with the noise conditions;
- C. A requirement to log certain data (e.g. on-site wind speed and wind direction) to enable compliance with the conditions to be tested;
- D. A requirement for the operator to undertake compliance monitoring and an assessment in the event that a complaint is received;
- E. Guidance on how limits should be selected (from the noise limit table(s)), for a property that is not listed in those tables;
- F. Timescales that should be followed for any compliance monitoring / the submission of the associated compliance assessment report;
- G. A methodology to measure tonal noise (if present) and a system to be used to determine a tonal penalty (if required) to inform the calculation of a Rating Level;
- H. A requirement to submit a detailed noise assessment procedure (sometimes referred to as a 'protocol' or a 'programme') prior to the commencement of any compliance monitoring;
- I. Guidance notes that explain in detail how the assessment should be undertaken (which usually cover matters such as how much data needs to be collected, how to determine if data is valid, the process to determine the specific noise (by undertaking a background noise correction) and how to apply a tonal penalty (where required)); and
- J. Submission of data collected as part of the compliance assessment to the Council.

Over and above the matters listed above, there are several other topics that are discussed intermittently in the UK and the ROI, which are sometimes incorporated into planning conditions, despite not always meeting the tests. These include:

- K. Noise limit principles (as opposed to specifically detailing noise limit values) e.g. 'The limit is set at background noise + 5 dB', but background noise is not specified;
- L. Consideration of AM;
- M. A requirement for mandatory post commissioning compliance monitoring (to be undertaken automatically regardless of whether complaints are received);
- N. A requirement for permanent, or regular noise monitoring covering the lifetime of the wind farms operation;
- O. Use of 'proxy' noise monitoring locations situated between receptors and the wind turbines to improve the signal to noise ratio;
- P. Cumulative noise limits⁸;
- Q. Noise limits relating to Low Frequency Noise;
- R. Text requiring submission of details regarding the operation of the wind turbines (e.g. exact modes adopted, sound power levels etc);

⁷ A detailed comparison has not been made with the condition included in the Acoustics Bulletin as it was not intended to represent a complete condition. The authors of the article noted that: *'It is acknowledged that there may be other parts of the current IOAGPG conditions which require inclusion here'*

⁸ Such limits effectively make the operator of a given wind farm responsible for the noise immissions from the combined effects of their development and other wind farm(s) in the area. This approach is discussed in the IOA GPG as a potential method to resolve cumulative constraints but it is acknowledged in the GPG that the approach places considerable risk on the operator and can present challenges in relation to meeting the tests.

- S. A requirement for turbines to be individually controllable to enable the reduction of noise levels in the future, if required;
- T. Consideration of impulsivity; and,
- U. A requirement to share data collected during compliance monitoring with residents.

To consider how frequently each of the matters above are included within wind farm noise conditions, a review has been undertaken of a selection of wind farm consents⁹ issued up to April 2025, since the start of 2024 in Scotland by the DPEA¹⁰ and the Energy Consenting Unit (ECU)¹¹ and decisions issued in the ROI by An Bord Pleanála (ABP)¹². The review has considered Scotland, which is the area of the UK with the most wind farm developments, and ROI, where neither ETSU-R-97 or the IOA GPG have any official standing (with the current guidance in the ROI being contained within the ‘Wind Energy Development Guidelines’ (WEDG2006) [10].

Table 1 below lists each of the consents that have been identified, then notes for each of matters listed above as A to U, whether they have been considered in the conditions.

Table 1 Summary of matters included in wind farm consents..

Wind Farm Reference / Location	A	B	C	D	E	F	G	H	I	J	K	L	M	N	O	P	Q	R	T	S	U
Mains of Cairnbrogie Farm, PPA-110-2452, Scotland	Y	Y	Y	Y	Y	Y	Y	Y	Y	Y	N	Y	Y	Y	N	N	N	N	Y	N	N
Cornharrow, PPA-170-2177, Scotland	N	Y	Y	Y	Y	Y	Y	N	Y	Y	Y	N	N	N	N	N	N	N	N	N	N
St John's Town of Dalry, PPA-170-2178, Scotland	Y	Y	Y	Y	Y	Y	Y	N	Y	Y	N	N	N	N	N	N	N	N	Y	N	N
Manquhill, PPA-170-2179, Scotland	N	Y	Y	Y	N	Y	Y	N	Y	Y	Y	N	N	N	N	N	N	N	N	N	N
Strath Oykel, WIN-270-18, Scotland	Y	Y	Y	Y	Y	Y	Y	Y	Y	Y	N	N	N	N	N	N	N	N	N	N	N
Garvary, WIN-270-20, Scotland	Y	Y	Y	Y	Y	Y	Y	Y	Y	Y	N	N	N	N	Y	N	N	N	N	N	N
Ourack, ECU00001999, Scotland	N	Y	Y	Y	Y	Y	Y	Y	Y	Y	Y	N	N	N	Y	N	N	N	N	N	N
Lethans Extension, ECU00002221, Scotland	Y	Y	Y	Y	Y	Y	Y	Y	Y	Y	N	Y	N	N	Y	N	N	N	Y	N	N
Bunloinn, ECU00003304, Scotland	Y	Y	Y	Y	N	Y	Y	Y	Y	Y	N	N	N	N	Y	N	N	N	N	N	N
Tom na Clch, ECU00003453, Scotland	Y	Y	Y	Y	Y	Y	Y	Y	Y	Y	N	N	N	N	N	N	N	N	N	N	N
Claichaig Glen, WIN-130-7, Scotland	Y	Y	Y	Y	Y	Y	Y	N	Y	Y	N	N	N	N	N	N	N	N	N	N	N

⁹ Planning conditions are only attached when consent is granted, they are not provided when a proposal is refused.
¹⁰ The Planning and Environmental Appeal Division who determine certain appeals against decisions made by planning authorities and other bodies across Scotland.
¹¹ The ECU determine applications for developments of over 50 MW submitted under Section 36 of the Electricity Act 1989.
¹² An Bord Pleanála is Ireland’s national independent planning body that decides appeals on planning decisions made by local authorities as well as direct applications.

Wind Farm Reference / Location	A	B	C	D	E	F	G	H	I	J	K	L	M	N	O	P	Q	R	T	S	U
Cairn Duhie, ECU00003225, Scotland	Y	Y	Y	Y	N	Y	Y	Y	Y	Y	N	N	N	N	Y	N	N	Y	N	N	N
Rowan, ECU00003230, Scotland	Y	Y	Y	Y	Y	Y	Y	N	Y	Y	N	N	N	N	N	N	N	Y	N	N	N
Wind Standard III, WIN-170-2003, Scotland	Y	Y	Y	Y	Y	Y	Y	Y	Y	Y	N	N	N	N	Y	Y	N	N	N	N	N
Creag Rhiabach, ECU00004487, Scotland	N	Y	Y	Y	Y	Y	Y	Y	Y	Y	N	N	N	N	Y	N	N	N	N	N	N
Hollandmey, ECU00003353, Scotland	Y	Y	Y	Y	Y	Y	Y	Y	Y	Y	N	N	N	N	Y	N	N	N	N	N	N
Inchamore, ABP-319216-24, Ireland	N	N	N	N	Y	N	Y	Y	N	N	Y	Y	Y	Y	N	Y	N	N	N	Y	N
Kilcash, ABP-319800-24, Ireland	N	N	N	N	Y	N	N	Y	N	N	Y	N	Y	Y	N	Y	N	Y	N	N	N
Dundalk, ABP-320542-24, Ireland	N	N	N	N	Y	N	N	Y	N	N	Y	N	Y	Y	N	N	N	Y	N	N	N
Lissanore, ABP-317459-23, Ireland	N	N	N	N	Y	N	N	Y	N	N	Y	N	Y	N	N	Y	N	Y	N	N	N
Knockastanna, ABP-315865-23, Ireland	N	N	N	N	Y	N	N	Y	N	N	Y	N	Y	N	N	Y	N	Y	N	N	N
Kilgarven repowering, ABP-319741-24, Ireland	N	N	N	N	Y	N	N	Y	N	N	Y	N	Y	Y	N	Y	N	N	N	N	N
Sheskin, ABP-315933-23, Ireland	N	N	N	N	Y	N	N	Y	N	N	Y	N	Y	N	N	Y	N	Y	N	N	N
Fehy Beg, ABP-317227-23, Ireland	N	N	N	N	Y	N	N	Y	N	N	Y	N	Y	N	N	Y	N	Y	N	N	N
Knockanarragh, ABP-319448-24, Ireland	N	N	N	N	Y	N	Y	Y	N	N	Y	Y	Y	Y	N	Y	N	N	N	Y	N
Cush, ABP-318816-24, Ireland	N	N	N	N	Y	N	N	Y	N	N	Y	N	Y	N	N	Y	N	Y	N	N	N
Glenard, ABP-312659-22, Ireland	N	N	N	N	Y	N	Y	Y	N	N	Y	Y	Y	Y	N	Y	N	N	N	Y	N
Ballinagree, ABP-312606-22, Ireland	N	N	N	N	Y	N	N	Y	N	N	Y	N	Y	N	N	Y	N	Y	N	N	N
Gortyrhilly, ABP-314602-22, Ireland	N	N	N	N	Y	N	N	Y	N	N	Y	N	Y	Y	N	Y	N	Y	N	N	N
Oweninny Phase 3, ABP-316178-23, Ireland	N	N	N	N	Y	N	N	N	N	N	Y	N	N	N	N	Y	N	N	N	N	N
Carrowleagh, ABP-317560-23, Ireland	N	N	N	N	Y	N	Y	Y	N	N	Y	N	Y	N	N	Y	N	Y	N	N	N
Ballivor Bog, ABP-316212-23, Ireland	N	N	N	N	Y	N	N	Y	N	N	Y	N	Y	N	N	Y	N	Y	N	N	N
Borrisbeg, ABP-318704-23, Ireland	N	N	N	N	Y	N	N	Y	N	N	Y	N	Y	N	N	Y	N	Y	N	N	N

Wind Farm Reference / Location	A	B	C	D	E	F	G	H	I	J	K	L	M	N	O	P	Q	R	T	S	U
Inchamore, ABP-317889-23, Ireland	N	N	N	N	N	N	N	N	N	N	N	N	N	N	N	N	N	N	N	N	N
Knockranny, ABP-318723-23, Ireland	N	N	N	N	Y	N	N	Y	N	N	Y	N	Y	N	N	Y	N	Y	N	N	N
Boolyvannanan, ABP-318295-23, Ireland	N	N	N	N	Y	N	N	Y	N	N	Y	N	Y	N	N	Y	N	Y	N	N	N

Table 2 summarises the results of the review by setting out the % of the decisions where matters were included for Scottish decisions, then for decisions in the ROI, and then for overall numbers.

Table 2 Matters included in conditions by region.

Matter	Inclusion in Scottish consents (%)	Inclusion in consents in ROI (%)	Inclusion overall in consents (%)
A. Inclusion of a table of noise limits	75%	0%	33%
B. Requirement to approve a list of consultants	100%	0%	44%
C. Requirement to log wind farm data	100%	0%	44%
D. Complaints driven compliance assessments	100%	0%	44%
E. Selection of limits for additional properties	81%	95%	89%
F. Timescales for monitoring and reporting	100%	0%	44%
G. Methodology to account for tonal noise	100%	20%	56%
H. Requirement to submit an assessment protocol	69%	90%	81%
I. Inclusion of guidance notes attached to the condition	100%	0%	44%
J. Requirement to submit the collected data to the Council	100%	0%	44%
K. Noise limit principles (rather than a table of limits)	19%	95%	61%
L. Consideration of Amplitude Modulation	13%	15%	14%
M. Requirement for a mandatory compliance assessment	6%	90%	53%
N. Requirement for permanent / repeat compliance assessments	6%	35%	22%
O. Allowance for the use of 'proxy' noise monitoring locations	50%	0%	22%
P. Inclusion of cumulative noise limits	6%	90%	53%
Q. Noise limits relating to Low Frequency Noise	0%	0%	0%
R. Requirement for the operational modes of the turbines to be submitted	13%	70%	44%
S. Requirements for the turbines to be individually controllable	19%	0%	8%
T. Consideration of the impulsivity of the noise	0%	15%	8%
U. Requirement to share data collected with the residents	0%	0%	0%

5. Discussion and consideration of the tests

Clearly there is a significant difference in the way that wind farms are conditioned between Scotland and ROI, and a detailed discussion of how each of the matters A – U are considered would require a very lengthy paper, however, some of the key findings are discussed here, grouped into three broad categories of i) Setting Noise Limits ii) Compliance Monitoring and Complaints Investigations; and, iii) Noise Characteristics. Specific matters are detailed in square brackets, for reference.

5.1 Setting Noise Limits

In Scotland, nearly all of the consents include site specific, tabulated noise level limits [A], in line with the recommendations of the IOA GPG and the recently published Scottish standard Section 36 condition. This means that the limits are precise and relevant to the development. In contrast, nearly all of the ROI limits were presented using descriptive text, such as ‘background +5dB’, which is ambiguous and open to interpretation i.e. not precise. Furthermore, nearly all of the ROI consents include cumulative noise limits [K], with wording such as;

Noise levels generated by the wind farm following commissioning by itself or in combination with other existing or permitted wind energy development in the vicinity, when measured externally at noise sensitive locations, shall not exceed.....

It is usually impossible for a wind farm operator to have complete control over the cumulative noise immission levels at noise sensitive locations, as they can only control their own development and have no influence on any neighbouring developments. In fact, there could easily be a situation where a windfarm with a cumulative noise limit is operating at relatively low levels, yet, the noise limits are being exceeded due to a neighbouring, noisy development. Accordingly, these types of conditions are not relevant to the development.

5.2 Compliance Monitoring and Complaints Investigations

In Scotland, only one wind farm had conditions requiring mandatory compliance monitoring. In that instance, the compliance survey was required within the first 12 months of operation and every two years thereafter, until the Local Authority determines that further monitoring is no longer required. In contrast, 18 of the 20 ROI developments have a compliance monitoring requirement.

No developments in ROI have a requirement for the operator to undertake compliance monitoring in the event of a complaint, however, all developments in Scotland have this requirement. So in ROI, compliance requirements are much more onerous but are likely to be less effective, requiring all developments to undertake monitoring (usually within six months of operation), but having no requirement to investigate complaints after this initial survey.

Interestingly, nearly all developments across both countries also have a requirement to submit some form of compliance monitoring and / or complaints investigations protocol for approval by the Local Authority. This requirement [H] is, in fact, one of a small number matters included within the IOA GPG condition that appears to be universally adopted.

As more wind farm developments become operational, identifying the specific contribution is becoming more complex, particularly at properties located in between multiple windfarms. Whilst not included in the IOA GPG example conditions the use of ‘proxy’ measurement locations was discussed in the IOA GPG itself and this has started to be incorporated into conditions in Scotland ([O] was included in 50% of conditions). Whilst the practice is used on some sites in Ireland it is not referenced in any conditions.

5.3 Noise Characteristics

All developments in Scotland had a requirement to consider tonality [G] when assessing compliance (through the use of a Rating Level)¹³. Three conditions in Ireland did mention tonal noise but details of how to calculate a Rating Level were not specified.

For both Scotland and Ireland, requirements to consider other noise characteristics is generally low, with 0% considering low frequency noise [Q], 0% in Scotland and 15% in ROI considering impulsivity [T], and 14% considering AM [L].

¹³ Where a Rating Level is used to define the noise limits, this requires that certain character corrections or penalties, are added to the measured noise level to account for particular characteristics, that might be present in the noise received at the dwelling, such as tonality.

6. Conclusions

It is clear that there is a significant difference in how conditions are drafted within the UK and the ROI. The example condition included in the IOA GPG is adopted relatively consistently in the UK and conditions in Ireland are considerably shorter and less detailed. There are a number of matters which are sometimes included (particularly in Ireland) which, it can be argued, do not meet the tests set out in the relative guidance. Generally speaking the conditions attached to consents in Scotland do tend, on the whole, to meet the tests.

It should be noted that updated versions of ETSU-R-97, the IOA GPG and the WEDG2006 are currently being considered. It may be that any future updates will provide further guidance in relation to noise related planning conditions. It is noted that a ‘one size fits all’ approach is unlikely to be suitable, and conditions will often need to be drafted with input from a suitably qualified acoustician to ensure that they are appropriate to the individual site being considered. Nevertheless, to ensure that conditions provide suitable protection to wind farm neighbours without placing undue burdens on wind farm operators, any updated guidance may benefit from example conditions (built on previous work incorporating changes to reflect best practice) and they should be drafted carefully to ensure they comply with the tests.

Acknowledgments

Thanks is given to the wider team at TNEI who regularly track and review planning consent information, including Megan Barrie, Florence Usher, Sarang Choudary, James McBride and Conall McDonald. The contribution of Faolán Ly and George Ball (who helped review the consents to populate Table 1), is also gratefully acknowledged.

References

- [1] Department for Levelling Up, Housing and Communities, “National Planning Policy Framework,” 07 02 2025. [Online]. Available: <https://www.gov.uk/government/publications/national-planning-policy-framework--2>. [Accessed 09 04 2025].
- [2] Scottish Government, “Planning Circular 4/1998: the use of conditions in planning permissions,” 1998.
- [3] Department of the Environment, “Development Management Practice Note - Use of Planning Conditions,” 04 2015. [Online]. Available: https://www.infrastructure-ni.gov.uk/sites/default/files/publications/infrastructure/dmpn-20-use-of-planning-conditions-v1-april-2015_0.pdf. [Accessed 09 04 2025].
- [4] Department of Housing, Local Government and Heritage, “Development Management Guidelines,” 2020.
- [5] ETSU for the DTI (Department of Trade and Industry, “The Working Group on Noise from Wind Turbines ETSU-R-97 The Assessment and Rating of Noise from Wind Farms,” 1996.
- [6] Institute of Acoustics, “Good Practice Guidance on the application of ETSU-R-97 for wind turbine noise assessment,” 2013.
- [7] Scottish Government, “Web Based Renewables Advice: ‘Onshore Wind Turbines’,” 28 05 2014. [Online]. Available: <https://www.gov.scot/publications/onshore-wind-turbines-planning-advice/>. [Accessed 09 04 2025].
- [8] Institute of Acoustics, “A planning condition for wind turbines,” *Acoustics Bulletin*, vol. 42, no. 6, pp. 56-60, November/ December 2017.
- [9] Scottish Government, “Standard onshore wind conditions – section 36 consent and deemed planning permission: form and guidance,” 25 02 2025. [Online]. Available: <https://www.gov.scot/publications/standard-onshore-wind-conditions-section-36-consent-and-deemed-planning-permission-form-and-guidance/>.
- [10] Department of Housing, Local Government and Heritage, “Wind Energy Development Guidelines,” 2006. [Online]. Available: <https://www.gov.ie/pdf/?file=https://assets.gov.ie/111145/93cd5b8e-e0d5-4369-8d41-45b9738a7b4d.pdf#page=null>. [Accessed 09 04 2025].

Paper #36 - ID: 371

Title: A Native GPU CFD solver to predict trailing edge noise of wind turbine blades

Author: Hauke Reese

11th Edition of the
International Conferences on
Wind Turbine Noise

Copenhagen, Denmark – 10th to 13th June 2025

Addressing time constraints in the design of serrated trailing edges

H. Reese¹

Ansys Germany GmbH, Darmstadt, 64295, Germany

Summary

The investigation of trailing edge noise in wind turbines is of great importance to increase the acceptance of wind energy. In this study, the trailing edge noise of wind turbines is simulated using Computational Fluid Dynamics (CFD), with calculations performed on Graphics Processing Units (GPUs). The use of GPUs enables a significant acceleration of the simulations, allowing for higher resolution of the flow fields and the investigation of various design parameters in realistic time frames. A finite volume method is employed to solve the transient compressible Navier-Stokes equations. A Large Eddy Simulation (LES) method is used to resolve turbulent fluctuations in the boundary layer of the aerofoil, which is essential to capture the noise sources. The Far-field noise is calculated using the acoustic analogy of Ffowcs Williams and Hawkings (FWH).

The approach is demonstrated using a NACA 64-618 aerofoil of the AIAA BANC-V Workshop. The predictive capability of the simulation approach is demonstrated by considering blunt and serrated trailing edge configuration.

1. Introduction

Trailing edge noise, a significant concern in aeroacoustics, exhibits broadband characteristics due to the turbulent boundary layer interactions with the trailing edge of aerofoils [1]. This type of noise is particularly critical for low-speed propellers [2], where it constitutes a major portion of the overall noise emissions [1].

Different trailing edge noise mitigation solutions have been proposed over the past years. Among these solutions the noise reduction due to trailing edge serration is established by wind turbine manufacturers.

The analytical model developed by Howe offers a theoretical framework for predicting noise from serrated trailing edges [3]. This model has been instrumental in understanding the noise reduction mechanisms associated with serrated designs. Additionally, semi-empirical methods have been developed for academic studies, providing a balance between computational efficiency and prediction accuracy [4].

To predict the effect of complex serration shapes in detail on the noise emissions, a high-fidelity scale resolved simulation method e.g. LES is needed to resolve turbulent scales in the boundary layer.

The required time and space resolution needed for running those simulations without compromising accuracy beyond the acceptable range do hardly fit engineering requirements in the design cycle when using CPU-based computer hardware resources. In addition to computational speed, the monetary and energy costs of computer hardware and infrastructure are increasingly coming into focus, both from budget limitation and environmental footprint perspectives. The costs associated with either acquiring computing

¹ Corresponding author – Email: Hauke.reese@ansys.com

hardware for engineering analysis or performing computations on cloud services are ever increasing. Consequently, an attractive strategy is to reduce both run-time and energy consumption by utilizing Graphical Processing Unit (GPU) clusters for CFD simulations [5] [6].

The commercial Ansys® Fluent GPU solver [7] is a newly designed code with the ability to utilize multiple GPU units for handling larger and more complex models, achieving substantial speedups compared to traditional CPU-based solvers [8]. This solver employs the well-established Finite Volume Method (FVM) to solve both compressible and incompressible flows.

The paper is organized as follows: The next section describes the test case and the setup of the simulations. Before detailing the variation of the trailing edge, a mesh variation demonstrates the quality of the setup. In the third section, the two different trailing edge designs are compared. Before the conclusion, an overview of the numerical effort is provided.

2. Example case

The presented work is based on a NACA 64-618 profile with a chord length of 600 mm. The geometry is shown in figure 1. To investigate the impact of trailing edge serration, two trailing edge designs—a shark tooth and a blunt edge were created. The thickness of the trailing edge is set to 1 mm for both designs. The dimensions of the shark tooth are 5% of the chord in span and 10% of the chord in the streamwise direction. The flap angle of the serration is zero degrees relative to the chord.

The operational points are aligned with the AIAA BANC-V workshop of Case 6 and Case 7. Both cases are set up for a Reynolds number of 1.43 million. The difference between the cases is the angle of attack: Case 6 has a slightly negative angle of -0.88° , while Case 7 has a positive angle of 4.62° . For both cases, no forced transition due to boundary layer tripping is applied.

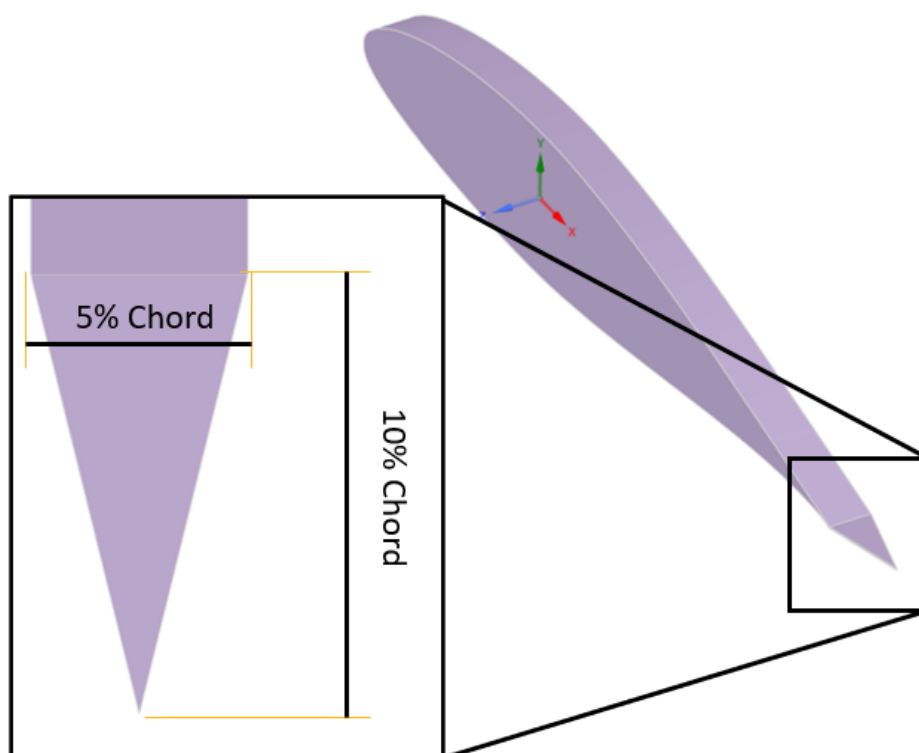


Figure 1 Aerofoil geometry NACA 64-618 with trailing edge serration

2.1 Computational domain and meshing

The computational domain, shown in figure 2, is divided into a far-field and a near-field domain. The boundaries of the far-field domain are 66.7 chord lengths away from the aerofoil to avoid any blockage effects on the results. The near-field domain, which contains the aerofoil, has a radial dimension of 5 chord lengths. This dual-domain approach offers advantages in space discretization and automated workflow. Using an interface approach, two different meshing strategies can be applied, and for design variations, only the inner domain needs to be updated. For the spanwise dimension, 5% of the chord is used. This dimension is determined by the periodicity of the serration and the boundary layer thickness to avoid correlation effects.

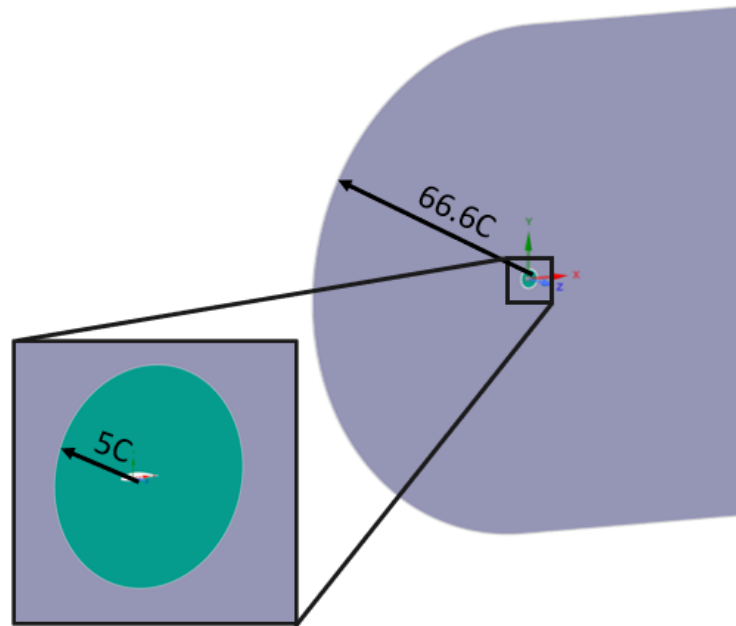


Figure 2 Simulation domain.

Typical structured meshes are well-established for profile simulation based on the finite volume method. Such meshes are less dissipative and allow for aspect ratios that minimize cell count. However, meshing complex serrations, such as those shown in [8], is challenging with a structured approach. Considering automation, these approaches are complex to automate and often more error-prone.

For the present work, an unstructured meshing approach using polyhedral elements is employed. Snapshots of the computational mesh are shown in figure 3. To meet the requirements of the LES simulation, the near-wall region is meshed with 25 prismatic layers. The first cell height is set to 0.002 mm, corresponding to a y^+ value below 1 over the entire blade geometry. For the surface mesh resolution, a value between 0.125 mm near the trailing edge and 0.25 mm is used. This value is a compromise between effort and accuracy. The impact of finer mesh resolution is investigated and discussed later in the paper. The maximum cell size is set to 1mm in the near-field and wake region. The overall maximum cell size is limited to 4 mm for the near-field domain.

The outer domain is meshed using a sweep approach. Eight cell layers are used in the spanwise direction. Close to the boundaries and the interface with the near field, the mesh size is limited to 8 mm for a smooth transition. The maximum cell size is limited to 500 mm. The overall cell count of the blunt case is 28.5 million for the inner domain and 0.7 million cells for the outer domain. The cell count of the serrated design increase up to 31.7 million elements.

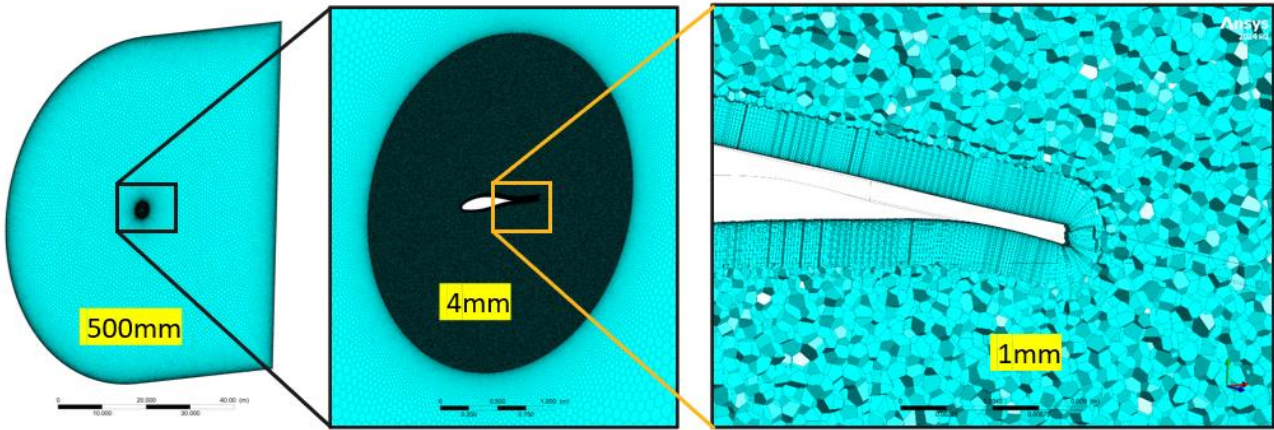


Figure 3 Computational mesh.

2.2 Physical models and boundary conditions

In this study, we perform a compressible transient simulation using the ideal gas law to model the flow around the aerofoil. A sub-grid scale model, the WALE (Wall-Adapting Local Eddy-Viscosity) model [9], is employed. The WALE model is an algebraic model that accounts for both the strain rate and the rotational rate of the flow. This dual consideration allows the WALE model to produce minimal eddy-viscosity in wall-bounded laminar flows, making it highly effective in accurately simulating near-wall turbulence. The WALE model calculates the eddy-viscosity based on the local velocity gradients, ensuring that the model adapts to the varying flow conditions near the wall. This adaptability is crucial for capturing the natural transition from laminar to turbulent flow, which is essential for this study.

To calculate the sound pressure at receiver points in the far field the acoustical analogy according to Ffowcs Williams and Hawkings [10] [11] is applied. Although a compressible approach is used the dipole noise due to the interaction of the unsteady pressure field with walls is taken for this work into account only. The whole aerofoil is considered as source region. The solver exports the surface pressure values during the simulation. The sound pressure calculation is done as a post step after the simulation [7].

A periodic condition in spanwise direction is applied. A pressure outlet condition with a gauge pressure of 0 is applied at the downstream boundary. A velocity inlet is applied on the upstream boundary. Next to the temperature the velocity magnitude and a direction vector is used. The direction vector determines the angle of attack. All input values are summarised in the table 1. Due to a higher reference pressure the inlet density deviates by around 9% to the experimental data of the AIAA BANC-V workshop.

Table 1 Boundary conditions.

Version	Velocity [m/s]	Temperature [K]	Angle [°]	Density [kg/m ³]	Ambient Pressure [Pa]
Case 6	45	317.6	-0.88	1.11354	101325
Case 7	45	317.6	4.62	1.11354	101325

2.3 Numerical method and solution strategy

A so called “optimized” set of LES numerical scheme have been developed and evaluated for the native GPU Solver [7] [11]. These setting are summarised in the table 2 below.

Table 2 Numerical setting.

Settings	Pressure Velocity Coupling	Spatial Discretization		Transient Formulation	Underrelaxation factors		
		Pressure	Momentum		Pressure	Density	Momentum
Optimized LES Numerics	SimpleC	3.0	100	2 nd Order Implicit	1	2	0.95

The transient simulation is initialized from a steady state solution. At the beginning of the transient mode a time steps size of 0.0005s is used and ramped down over 8000-time steps to the sampling time step size of 2e-6s. Additional 30,000 timesteps are solved to eliminate any initial effects. This period corresponds to a flow over of 4.5 chord length. The sampling of the flow field is done for another 60,000 timesteps. Local scaled residuals with a target of 1e-5 is used to determine convergence within a time step. This convergence criteria yields to 5 sub-iterations per time step for the smallest time step size. The simulations are done in double precision.

3. Results

In the following section the results of the simulation with and without a serrated trailing edge are presented and discussed. The figure 4 shows a snapshot of Case 6 and Case 7. The velocity plot shows a typical flow pattern. From the stagnation point a laminar boundary layer develops and transitions to a turbulent layer. The turbulent structures of are passing the trailing edge and damped out further downstream. Both cases do not show any significant separations near the trailing edge. The turbulent structure inside the wake of case 7 seems larger compared to Case 6.

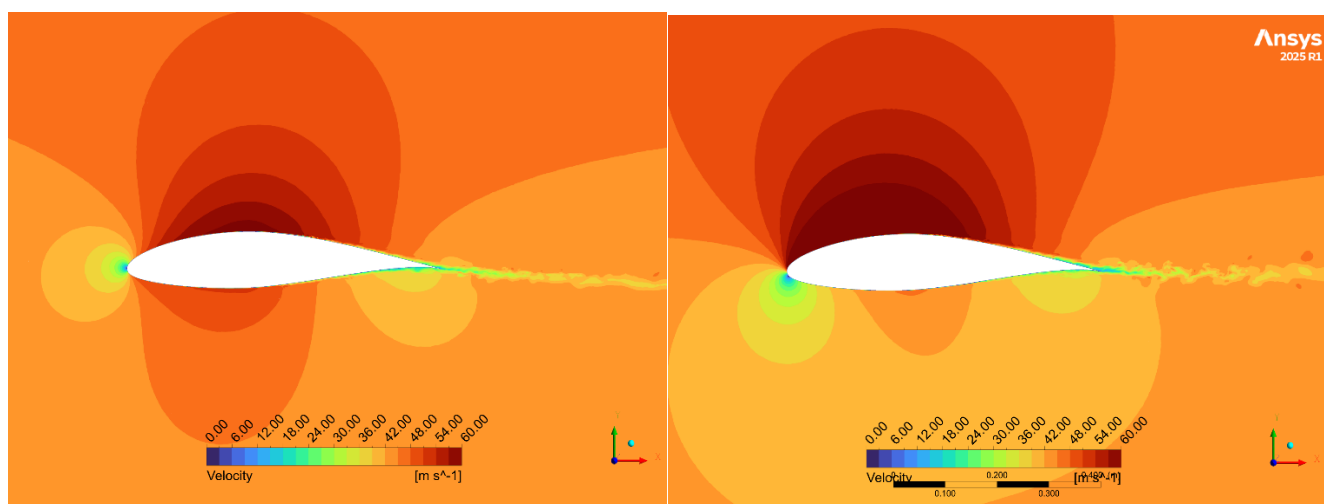


Figure 4 Velocity snapshot, left: Case 6, right: Case 7

Before going into details, a mesh sensitivity is investigated by a variation of the surface resolution. The shown experimental data is taken from the AIAA BANC V workshop in this section.

3.1 Mesh sensitivity

A mesh sensitivity investigation is done for the Case 6. The study bases on a variation of the surface mesh resolution. The surface mesh resolution is reduced by 25% from 0.25mm to 0.2mm. All other setting has been kept the same. Due to the finer surface mesh the cell counts increases by 39% from 29.1 to 40.5 million elements.

The figure 5 shows the time averaged velocity and streamwise Reynolds stress profile at 97.5% of the chord length. Both meshes slightly overestimate the mean flow velocity outside of the boundary layer, The profile itself is well aligned with the experimental data. The mean flow overestimation is also observed in the numerical study of Romani et al. [12].

The Reynolds stress at the inner boundary layer is underpredicted. The finer mesh fits well with the experimental data for the outer boundary layer.

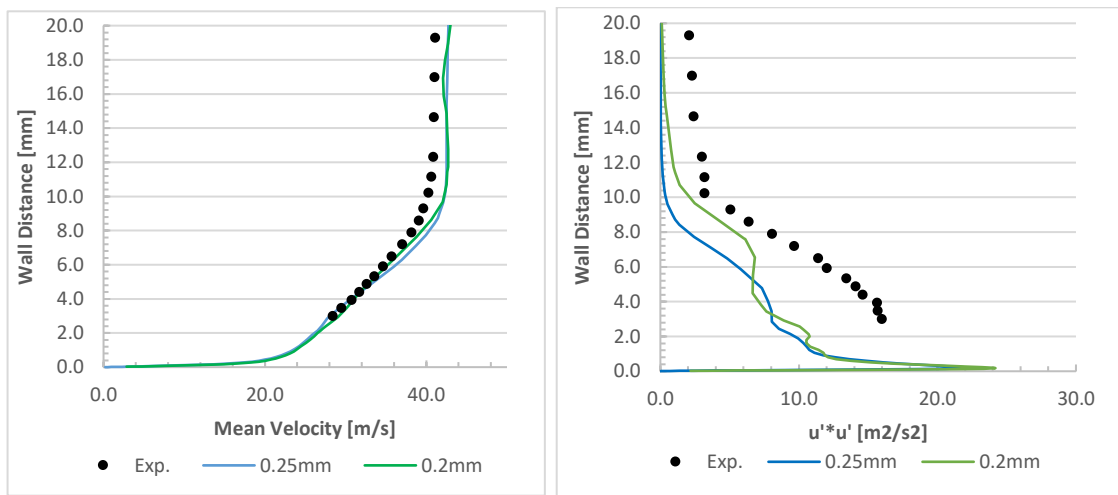


Figure 5 Case 6, Boundary profile on 97.5% chord, suction side.

A comparison of the surface pressure coefficient C_p is shown in figure 6. The version with 0.25mm surface mesh shows a slightly overprediction of the C_p on the suction side. With finer mesh resolution this gap could be closed.

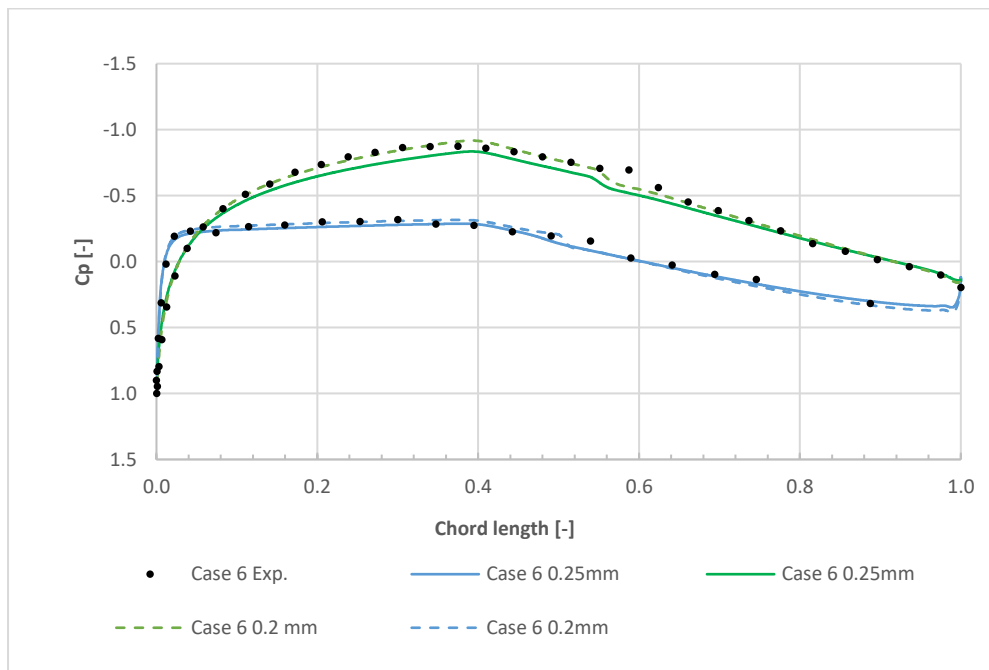


Figure 6 Case 6, surface pressure and skin friction coefficient for different mesh resolutions.

Focus of this work is to demonstrate the capturing of the air born noise emission due to the flow around the aerofoil. A comparison of the sound pressure level in 1/3 Octave band is shown in figure 7. Because of

the different dimension in Span wise direction, the CFD results are scaled according to the following equation [13].

$$L_p(1/3)(f_c)_{b_2} = L_p(1/3)(f_c)_{b_1} + 10 \log_{10} \frac{b_1}{b_2} \quad (1)$$

This procedure bases on assumption of non-coherent noise sources which is a valid assumption for broadband noise.

Both meshes show good alignment with the experimental data. The results of the finer surface mesh, except for one point, fall within a band of 3 dB. The coarser surface mesh shows an offset compared to the finer mesh but remains within a band of 5 dB relative to the experimental data. Due to a 39% increase in effort, the investigation of different trailing edges is conducted using the coarser surface mesh resolution.

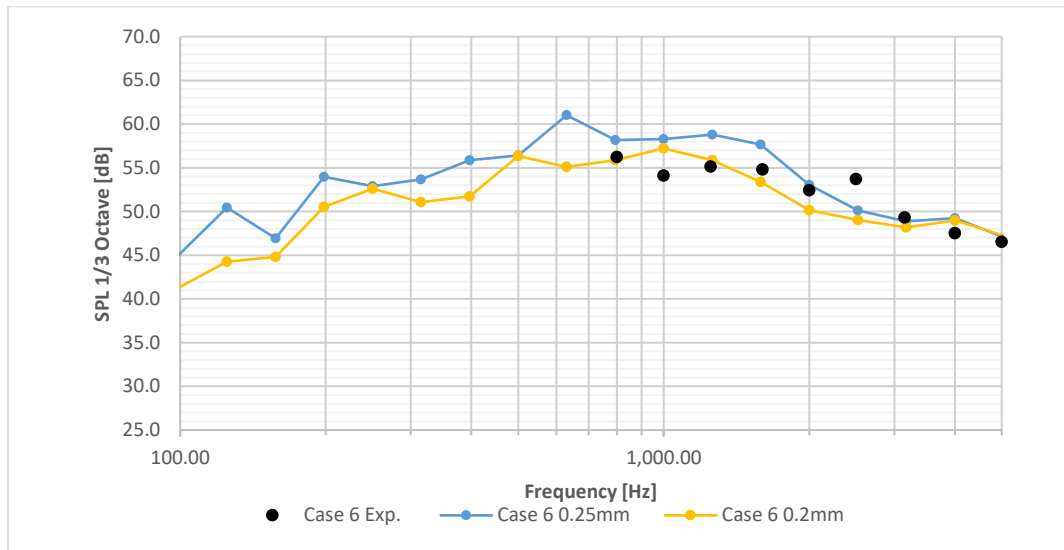


Figure 7 Case 6, sound pressure level 1m above the trailing edge, scaled to 1m span

3.2 Natural transition

Figure 8 shows the averaged pressure coefficient (C_p) and friction coefficient (C_f). The CFD results show good alignment for the pressure coefficient with the experimental data. Compared with Case 6, Case 7 shows better alignment with the experiments.

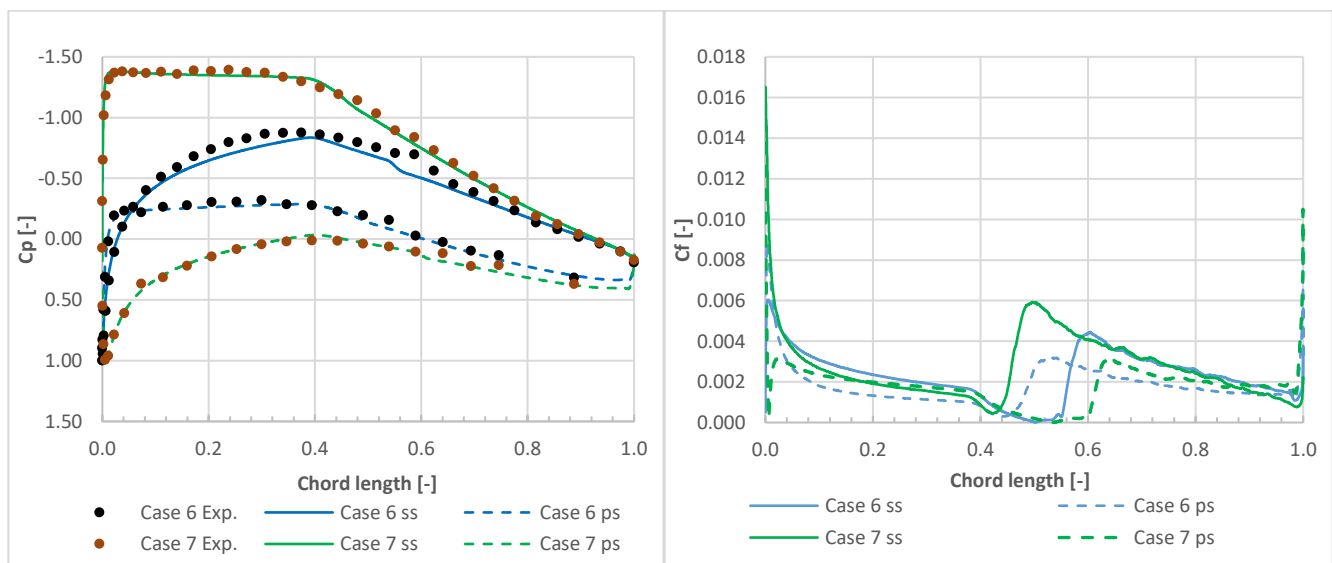


Figure 8 Pressure and skin friction coefficient of the blunt trailing edge design

The natural effective transitional point of the CFD simulation is determined from the skin friction coefficient. The values are compared with experiments in table 3. The CFD results indicate the transitional

point nearly 5% to 6% earlier on the suction side. This might still be an indication of the mesh resolution. To overcome this behaviour, a WMLES approach that allows transitional effects could help achieve better results. The development of such a model is in progress for the GPU solver.

Table 3 Comparison of the effective natural transition points as relative position of the chord.

Type	Experiment		CFD	
	Suction side	Pressure side	Suction side	Pressure side
Case 6	0.65	-	0.61	0.52
Case 7	0.56	-	0.50	0.64

3.3 Results of the trailing edge variation

Figure 9 shows a snapshot of the velocity for all four cases at the middle plane. Due to the flap angle of 0° to the chord, a small separation at the kink in the transition from the suction side to the flap can be detected for Case 6 and Case 7. The surface pressure spectrum for a point at 98% of the chord length is plotted in figure 10. Due to the separation, the serrated design of Case 6 shows a higher surface pressure level than the non-serrated design below 1 kHz. The surface pressure spectrum of Case 7 does not show any significant changes between the serrated and the blunt design.

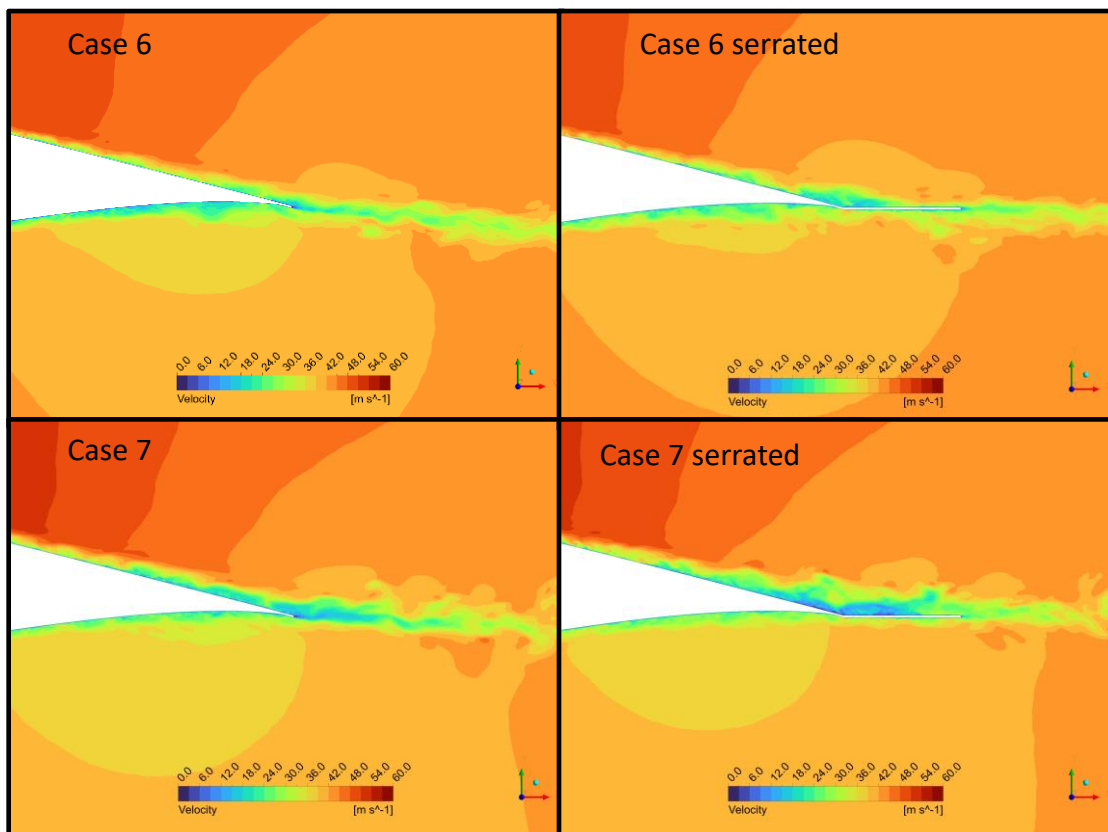


Figure 9 Snapshot of the velocity field near the trailing edge

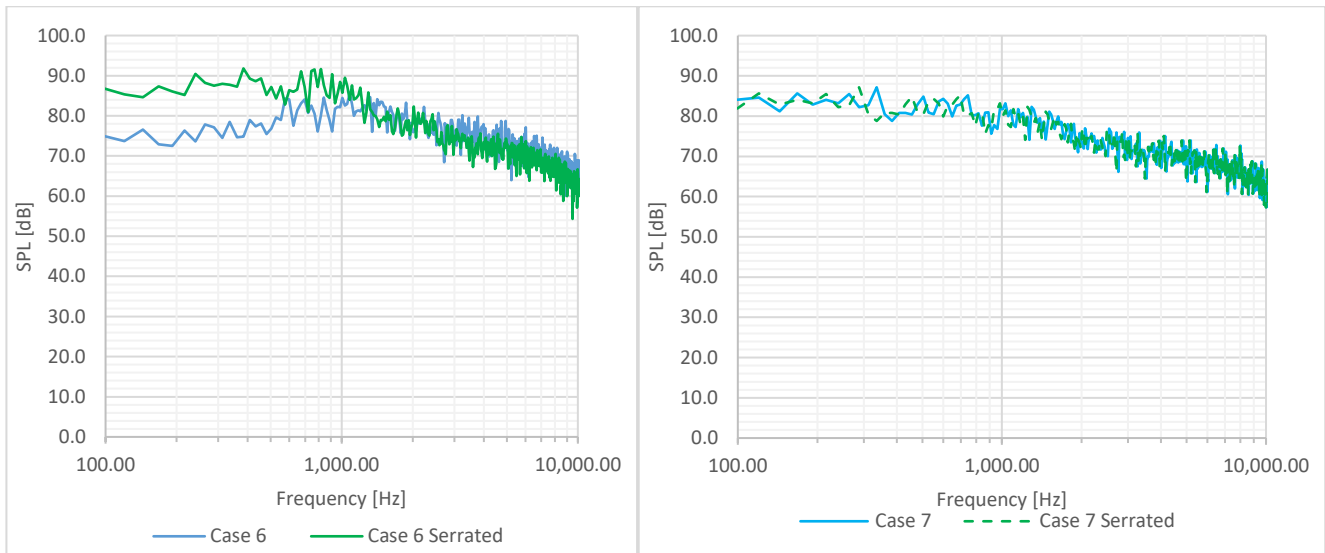


Figure 10 Normalized small band surface pressure spectrum at 98% chord on the suction side, left: Case 6, right: Case 7

Figure 11 shows cut planes with the mean velocity at the wake of the aerofoil. Surface streamlines are plotted on the planes. The serration leads to a vortex structure for both cases on the pressure side of the serration.

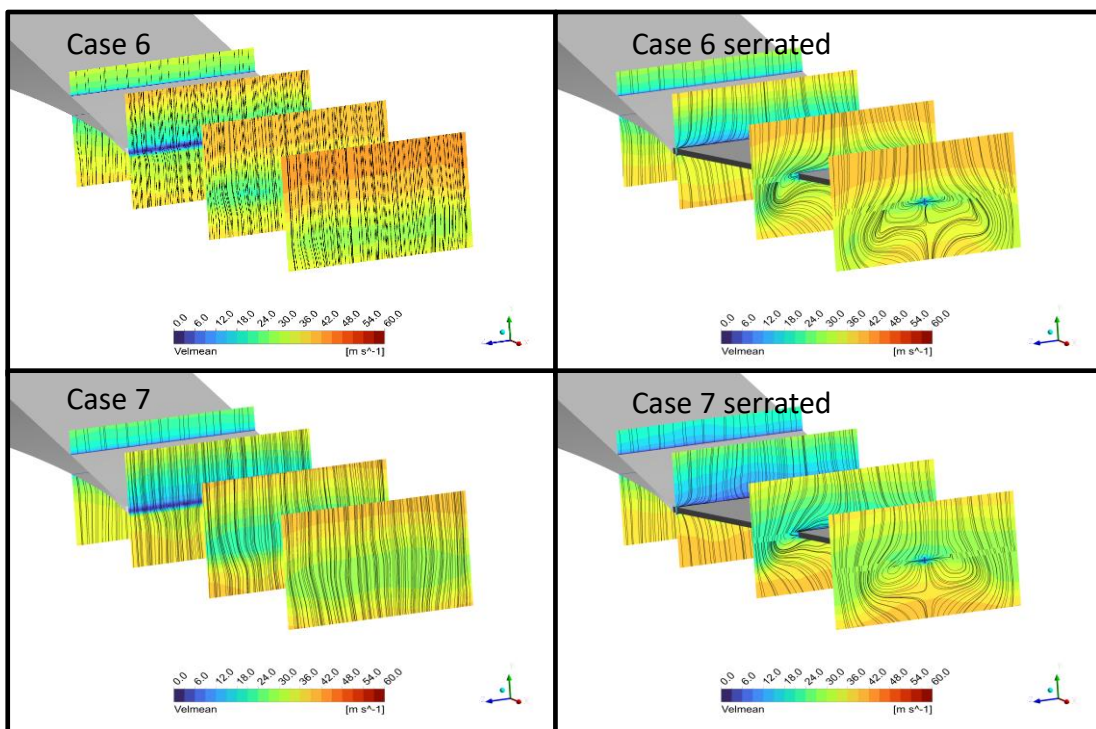


Figure 11 Averaged velocity field near the trailing edge

The impact of the noise level at a receiver 1 m above the trailing edge is shown in figures 12 and 13. Case 6 shows a small impact on the noise level due to serration. A noise reduction can be detected below 200 Hz and from 500 Hz to 2 kHz. Compared to Case 7, where the flap is not as aligned with the mean flow, the noise reduction is significantly higher. In this case, the noise level is reduced in the frequency range from 300 Hz up to 2 kHz.

The predicted trends are aligned with the experimental investigation of Luesutthiviboon et al. [14]. This work experimentally investigated different serration designs on a NACA633-018 aerofoil at various Reynolds numbers.

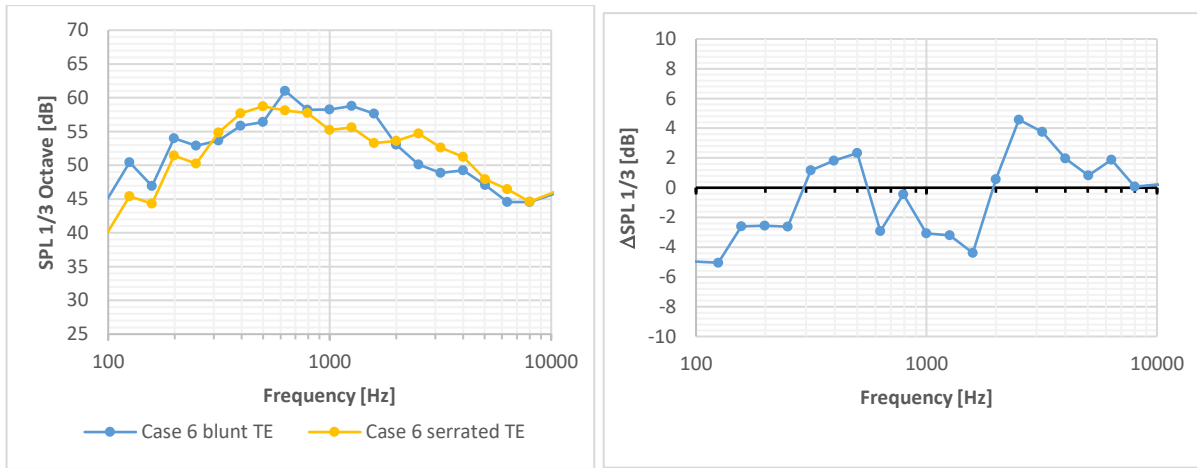


Figure 12 Case 6, noise level at receiver 1m above the TE, left: SPL spectrum, right: difference between the TE designs

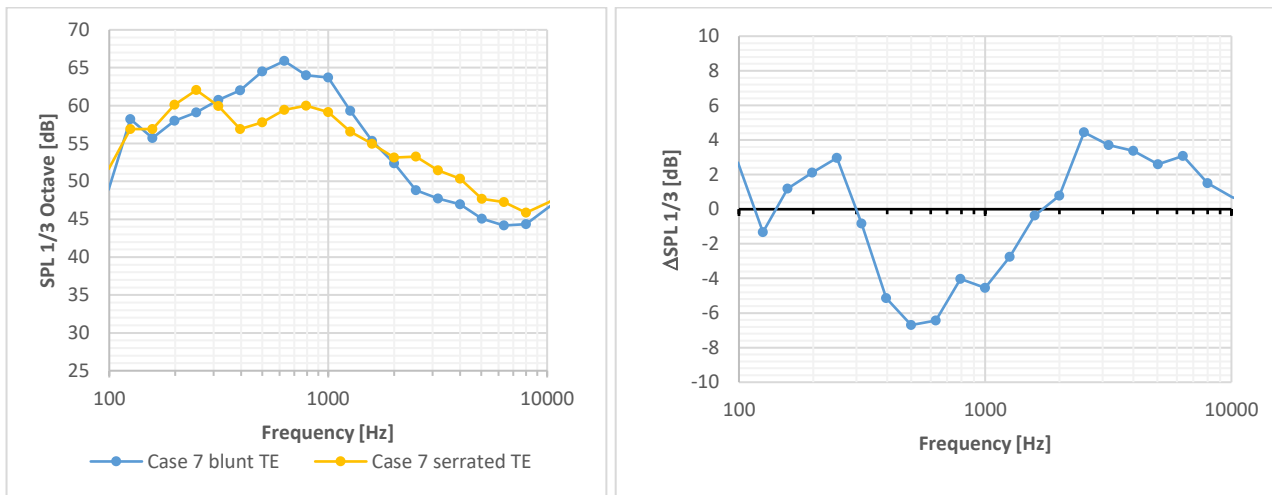


Figure 13 Case 7, noise level at receiver 1m above the TE, left: SPL spectrum, right: difference between the TE designs

3.4 Computational speed

The computational speed and scalability performance of the Ansys® Fluent GPU solver have been evaluated. The evaluation is done for two different hardware setups. The first setup of compute nodes has 4 NVIDIA® QuadL 40 cards in combination with AMD® EPYC 9124 16 Cores. The second setup uses 2 NVIDIA® H100 cards in combination with INTEL® XEON® Gold 6542Y Cores. The number of CPU cores is kept the same as the number of used GPU cards for the simulation. The runtime is evaluated for the sampling phase and shown in table 4. The simulations are done in double precision mode, the sound source data is exported, and the transient mean values of the flow field are sampled. The values are based on the blunt trailing edge design with a cell count of around 28.5 million elements. This setup uses an average of 5 sub-iterations per time step.

Using 8 QuadL 40 GPU cards, the whole simulation from initialization to data sampling can be finished within 24 hours. Comparing the newer hardware of H100 cards with QuadL 40 cards, a speedup of nearly 4 can be achieved. The H100 cards drop in parallel efficiency faster than the QuadL 40 cards. However, with 12 QuadL 40 cards or 4 H100 cards, a parallel efficiency of above 70% is reached.

Table 4 Computational effort and parallel efficiency

Hardware	NVIDIA® QuadL 40			NVIDIA® H100	
	4	8	12	2	4
Number of cards	4	8	12	2	4
Run time for 0.1s [h]	29.0	16.3	12.5	16.8	11.7
Parallel efficiency	100%	89%	77%	100%	72%

4. Conclusions

The investigation of trailing edge noise has yielded two exemplary outcomes, demonstrating the robustness of the simulation in aligning closely with experimental data. The simulation has proven to be sensitive enough to accurately capture design trends, ensuring reliable predictions for future designs. An unstructured meshing strategy is applied to overcome challenges in automation.

The change of the GPU cards from quadL40 to a newer H100 points out an acceleration factor of nearly four. Continuous hardware developments are expected in future and with it the simulation time in a design cycle can be reduced to few hours in future. This development also enhances the precision of the simulation by employing finer mesh configurations like octree approaches and longer sampling times.

Moreover, the implementation of Wall-Modelled Large Eddy Simulation (WMLES) techniques, particularly with forced transition or upcoming WMLES models that can predict natural transition, holds promise for further improving the accuracy and reliability of the results.

Acknowledgments

The author thanks Yuri Egorov and Wolfgang Bauer from Ansys, for all their kind help and discussion.

References

- [1] T. F. Brooks, D. S. Pope and Marcolini, „Airfoil self-noise and prediction,“ Tech. rep., NASA Reference Publication, 1989.
- [2] H. H. Hubbard, „Aeroacoustics of Flight Vehicles,“ *Theory and Practice, Tech. rep., NASA*, Bd. Volume 1: Noise Sources, 1991.
- [3] M. S. Howe, „Aerodynamic noise of a serrated trailing edge,“ *Journal of Fluids and Structures*, No. 1, Vol. 5, p. 33–45, 1991.
- [4] O. F. Gasch, S. Oerlemans, F. Bertagnolio, A. W. Fischer, B. Arnold, T. Lutz, B. W. Fassmann and M. Herr, „Trailing Edge Noise Prediction of Wind Turbine Airfoils: A Benchmark Exercise,“ in *25th AIAA/CEAS Aeroacoustics Conference, AIAA Paper 2019-2675*, 2019.
- [5] J. S. Park, F. D. Witherden und P. E. Vincent, „High-Order Implicit Large-Eddy Simulations of Flow over a NACA0021 Aerofoil,“ *AIAA Journal*, No. 7 vol. 55, p. 2186–2197, 2017.
- [6] S. P. Vanka, A. F. Shinn and K. C. Sahu, „Computational Fluid Dynamics Using Graphics Processing Units: Challenges and Opportunities,“ *Fluids and Thermal Systems; Advances for Process Industries*, Bd. Volume 6, Nr. Parts A and B, pp. 429-437, 2011.
- [7] Ansys, Inc, „Ansys Fluent User’s Guide. Release 2025R1,“ Canonsburg, PA, USA, 2025.
- [8] Ansys Inc., 2022. [Online]. Available: <https://www.ansys.com/de-de/blog/unleashing-the-power-of-multiple-gpus-for-cfd-simulations> .

- [9] L. T. L. Pereira, F. Avallone, D. Ragni and F. Scarano, „A parametric study of serration design for trailing-edge broadband noise reduction,“ *Applied Acoustics*, Nr. Volume 211,109470, August 2023.
- [10] F. Nicoud und F. Ducros, „Subgrid-Scale Stress Modelling Based on the Square of the Velocity Gradient Tensor.Flow,“ *Turbulence, and Combustion*, No. 62(3), pp. 183-200, 1999.
- [11] J. E. Ffowcs-Williams and D. L. Hawkings, „Sound Generation by Turbulence and Surfaces in Arbitrary Motion,“ *Proc. Roy. Soc London* , No. A264, pp. 312-342, 1969.
- [12] Ansys, Inc, „Ansys Fluent Theory Guide. Release 2025R1,“ Canonsburg, PA, USA, 2025.
- [13] G. Romani, W. v. d. Velden and D. Casalino, „Deterministic and Statistical Analysis of Trailing-Edge Noise Mechanisms with and without Serrations,“ in *24th AIAA/CEAS Aeroacoustic Conference*, Atlanta, Georgia, 2018.
- [14] W. Blake, „Mechanics of flow-induced sound and vibration,“ Academic Press, 1986.
- [15] S. Luesutthiviboon, L. T. L. Pereira, D. Ragni, F. Avallone and M. Snellen, „Aeroacoustic Benchmarking of Trailing-Edge Noise from NACA 633-018 Airfoil with Trailing-Edge Serrations,“ *AIAA Journal*, No. 1, Volume 61, <https://doi.org/10.2514/1.J061630>, January 2023.

Paper #37 - ID: 372

Title: Blade-tower interaction noise prediction using a simplified 2D vortex model

Author: Franck Bertagnolio

11th Edition of the
International Conferences on
Wind Turbine Noise
Copenhagen, Denmark – 10th to 13th June 2025

Blade-Tower Interaction Noise Prediction Using a Simplified 2D Vortex Model

F. Bertagnolio¹

**DTU Wind Energy, Technical University of Denmark, Frederiksborgvej 399,
Roskilde, DK-4000, Denmark**

Summary

A simplified model for calculating the wind turbine aerodynamic noise generated by blade-tower interaction, including the tower as a noise source, is proposed. This model is based on a geometric assumption for the blade spanwise sections' spatial displacement and 2D potential flow theory. The blade sections are modelled as moving vortices, and the resulting fluctuating pressure on the tower (a cylinder in 2D) surface can be calculated using the above theoretical framework, together with the unsteady Bernoulli equation. From the tower surface pressure, the radiated noise can be estimated using Ffowcs Williams-Hawkings analogy, and its solution according to Farassat formulation 1A. The relative contributions of different low-frequency noise mechanisms are investigated and compared with existing high-fidelity simulations on the same turbine model.

1. Introduction

Low-Frequency Noise (LFN) from wind turbines and wind farms is a topic of public concern when considering their environmental impact. Infra-Sound (IS) falls into the category of LFN, but is usually understood as acoustic waves with a frequency below 20 Hz. The impact of IS may be an even more sensitive topic for public acceptance, as it is in principle not audible to the human ear and travels easily over large distances [1–4]. The present paper is concerned with the relative contributions of various aerodynamic noise mechanisms to IS.

As far as aerodynamic noise is concerned ², the two main generating mechanisms are:

- Turbulence-blade interaction
- Blade-tower interaction

The first one originates from the atmospheric turbulent vortices impacting the moving blades. These generates pressure fluctuations on the blade surfaces, which in turn radiate noise. This mechanism is relatively well-understood. It is broadband in nature because of the turbulence energy cascade in the atmosphere, that creates vortices of all sizes from the turbine rotor size itself (and larger) down to the dissipation scales (a few millimeters or less). However, in order to be accurately predicted, it requires a good definition of the atmospheric turbulence statistical properties, and a model for the scattering effects when looking at higher frequencies [5]. At lower frequencies, the noise sources (understood here as the blade surfaces) can be

¹ Corresponding author - Email: frba@dtu.dk

² It should be noticed here that mechanical noise may also produced LFN and IS.

considered as acoustically compact and that simplifies considerably the noise predictions [6–8].

Blade-Tower Interaction (BTI) gives rise to two distinct (however related) noise generation mechanisms. In the case of an *upwind* rotor, the wind inflow impacting the moving blades is affected by the presence of the tower, which slows down and deflects the mean flow upstream of itself. This creates pressure fluctuations on the blades as they convect through these disturbances, and thereby noise as described earlier. In the case of a *downwind* rotor, the impact is even greater because of the wake of the tower that, on top of creating a stronger deceleration of the mean flow, also contains strong vortices from the Von Kármán street flow created by the tower in its wake [9]. In the two above scenarios, only the noise emission from the blades is usually considered. However, if the flow deflections and its turbulent content affect the blade and its surface pressure field, the tower is also affected temporarily by the passage of the blades and will emit noise through its own surface pressure fluctuations resulting from this interaction.

A few research works have been published on the topic of LFN/IS noise emissions from the tower itself when considering wind turbine BTI. Yauwenas *et al* [10] investigated both experimentally and numerically a small rotor configuration and concluded that the blade and tower noise emissions behave as dipole and monopole, respectively. Klein *et al* [11] conducted numerical investigations of the NREL 5MW reference wind turbine [12] using a high-fidelity model. They concluded that the BTI dominates the acoustic emission associated with the blade-passage frequency harmonics and that the tower can be the main contributor to these emissions. In the present work, a simplified model is proposed and the above findings are tested.

The paper is organized as follows. The next Section 2 describes the new model for BTI and the prediction of tower noise emissions. It is also explained how this model is integrated into an existing framework for wind turbine noise predictions. Section 3 shows some comparisons with earlier results using a high-fidelity model applied to the above-mentioned multi-MW turbine. Conclusions are drawn in the last section.

2. A 2D vortex model for tower noise emission from blade-tower interaction

In this section, the concepts of the model and their implementation into an aeroelastic code are introduced. A simplified model for the BTI noise is derived using:

- an approximation for the spatial displacement of the individual blade spanwise sections when interacting with the tower,
- 2D vortex/potential flow theory for the resulting flow field created by the atmospheric wind around these blade sections and the tower,
- a classical theory for the aerodynamic noise generation by acoustically compact objects.

2.1 Geometric and flow physics assumptions

The first approximation consists in assuming that the individual spanwise blade sections' spatial displacement relatively to the tower is *horizontal*. In reality, each blade section follows a circular motion around the wind turbine rotor axis¹, as illustrated by the red circles in Fig. 1. In order to provide an analytical solution for the flow field affecting the pressure on the tower (see below), the spanwise blade section displacements are vertically projected onto an horizontal band as illustrated in blue in Fig. 1. The width of this vertical band associated with a given spanwise blade section is equal to the considered blade section span length, and its height relatively to the rotor center corresponds to the considered blade section radius. This geometric assumption may appear as very crude. However, it can be argued that, when the blade and tower are closest to each other and most of the noise is produced by their mutual interaction, the blade section horizontal displacement is a good approximation of its actual kinematics, as illustrated in Fig. 1d.

It should be noted here that the issue of numerical discretisation has not been introduced yet. The terminology

¹ The circular motion of the blade sections is strictly valid if neglecting aeroelastic deflections of the blades. Note that these deflections are included in the present model, although projected on the 2D plane where the displacement of the blade sections is assumed to take place.

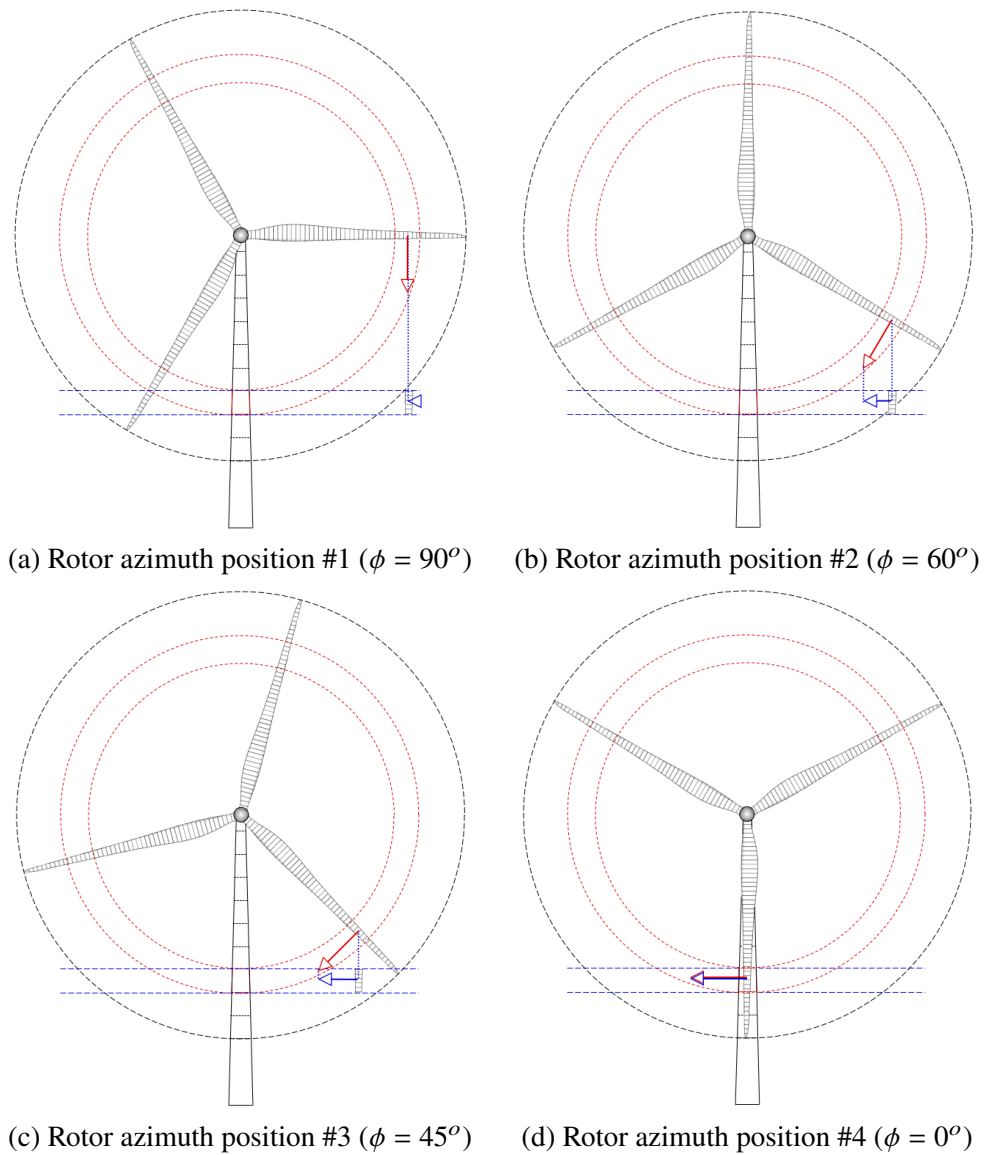


Figure 1 Sketch of a rotating wind turbine rotor and the tower. The red circles delimit a blade span section and its actual displacement during a rotor revolution. The horizontal blue lines delimit the fictitious displacement of this blade section according to the proposed model. The real blade section of interest is the one from which the red vector, indicating its rotational velocity, originates. The blue vector indicates the displacement velocity of the fictitious blade section in the projected plan of the present 2D model.

‘spanwise blade section’ is used here to conceptualise a part of the blade span which kinematics (as well as aerodynamic characteristics as it will be introduced below) can be considered as uniform along its length.

The above approximation for the kinematics of the individual spanwise blade sections yields to a two-dimensional (2D) conceptualisation of the interaction between the blades and the tower. The air flowfield around the blades and tower is thereby assumed to occur in a 2D horizontal plane as illustrated in Fig. 2.

In the context of inviscid 2D potential flow theory, the perturbation of the main wind inflow field created by a lifting body (here, the blade) combined with the effect of the presence of a cylinder (the tower) can be handled analytically [13]. Furthermore, it is possible to recover the unsteady pressure on the tower surface using the unsteady Bernoulli equation. Finally, the Ffowcs-Williams Hawking analogy [14] can be used to compute the noise radiated by the tower. These different steps of the model derivation are detailed later in Section 2.3. Before that, the overall computational framework used for the wind turbine simulation is presented in the next section.

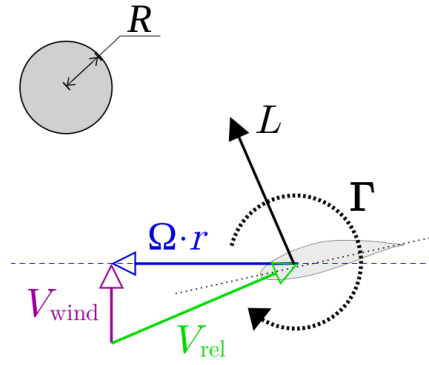


Figure 2 Sketch of the two-dimensional horizontal plane into which the displacement of a spanwise blade section relatively to the tower cylindrical section is approximated. The classical velocity triangle of a rotating airfoil section in the incoming wind flow (where Ω is the rotational velocity, r the radius, V_{wind} the incoming wind speed, and V_{rel} the relative velocity impacting this blade section), the lift L and the resulting airfoil vortex Γ are also displayed.

2.2 HAWC2 aeroelastic model for calculating the blade and tower aerodynamics

The present BTI noise model is implemented as an integrated part of the HAWC2 aeroelastic model dedicated to the prediction of aerodynamics and structural loads on wind turbines [15]. HAWC2 is a simulation software based on a multibody approach combined with Timoshenko beam element theory for describing the structural dynamics of the blade, tower and drive train. Rotor aerodynamics is handled using Blade Element Momentum (BEM) theory [16].

The blades are discretised spanwise and the BEM analysis applies differently on each of these blade sections depending on the local wind conditions, including wind shear, turbulence, etc, and more importantly here, the mean inflow deflection created by the tower. Note that the case of a downwind turbine where the wake of the tower interacting with the blade can also be modelled. The associated noise impact have been investigated previously using the present modelling framework [9]. The impact of the turbulence on the LFN emission using HAWC2 has also been investigated [8]. The model derived below re-uses many of the features already implemented in the HAWC2 code.

The resulting set of structural and aerodynamic equations are solved in the time-domain. A numerical scheme and associated time-step are defined to compute the time-series of the physical variables of interest. A typical time-step for a multi-MW turbine is of the order of $\Delta t = 0.01$ s, which theoretically allows for computing acoustic phenomena at frequencies lower than 50 Hz (considering the associated Nyquist frequency).

2.3 BTI noise model derivation

As part of HAWC2 and the BEM theory implementation (see previous section), the local inflow wind speed on the rotor disk, including the induction from the rotor itself, can be computed in conjunction with the aerodynamic loading on the blades in the form of lift (and drag which is not used in the present model). The local wind inflow conditions along the tower height are then readily available. These also yield the relative velocity impacting the blade along its span, using the classical velocity triangle as illustrated in Fig. 2.

From the above calculated lift and relative velocity, 2D vortex theory predicts that each blade span section can be modelled as a vortex with intensity Γ given by the formula:

$$\Gamma = -\frac{L}{\rho V_{rel}}$$

where L is the norm of the lift force, ρ the fluid density, and V_{rel} the relative velocity impacting the blade section. These are readily available numerical quantities from the HAWC2 code as explained above. Note here that the above 2D vortex theory is assumed to be valid (at each time-step of the HAWC2 simulation) in a plane perpendicular to the blade axis. Since, the final model is based on 2D potential flow theory in a

plane perpendicular to the tower axis, as described in the previous section, the Γ component is projected onto the latter axis to obtain an ‘effective’ vortex intensity as:

$$\Gamma_{\text{eff}} = \Gamma \cos(\phi)$$

where ϕ is the azimuthal angle between the blade and tower axes, associated with the rotation of the blade. It is equal to 1 when both axes are aligned with the blade pointing downward (see Fig. 1d), and 0 when they are perpendicular (see Fig. 1a). When the blade is pointing upward (i.e. its axis spans above the hub height), the BTI mechanism is assumed to vanish and Γ is always set to 0. For the sake of conciseness, the effective vortex intensity is still denoted as Γ in the following.

Using 2D potential flow theory, the flow field around each blade element is given by the complex flow potential Φ defined as:

$$\Phi(z) = U_{\infty} \left(z e^{-i\alpha_{\infty}} + \frac{R^2 e^{-i\alpha_{\infty}}}{z} \right)$$

where z is the spatial variable in the complex plane, U_{∞} and α_{∞} are the mean flow speed and direction at the considered blade element height, respectively, and R is the tower element radius (assumed cylindrical, even if it is conical in reality) at the considered height. Note that the tower center in the complex plane is considered located at the origin, i.e. $z = 0$. The complex velocity $U = u - i v$, where u and v are the cartesian velocity components in the complex plane, is given by:

$$U(z) \equiv \frac{\partial \Phi}{\partial z} = U_{\infty} \left(e^{-i\alpha_{\infty}} - \frac{R^2 e^{-i\alpha_{\infty}}}{z^2} \right)$$

The above derivations account only for the mean wind flow field. By linearity of potential flow theory, the contribution from the blade vortices, for the blade sections located at the same height as the considered tower element, must be added to the above results. This flow potential contribution reads:

$$\Phi(z) = \frac{i\Gamma}{2\pi} \left(-\log(z - z_G) + \log\left(\frac{R^2}{z - z_G^*}\right) \right)$$

and the velocity contribution is:

$$U(z) \equiv \frac{\partial \Phi}{\partial z} = \frac{i\Gamma}{2\pi} \left(-\frac{1}{z - z_G} - \frac{R^2/z^2}{R^2/z - z_G^*} \right)$$

where z_G is the position of the considered blade section vortex, and the star $*$ denotes the complex conjugate.

As the blades rotate, they are passing close to the tower with a varying loading. Therefore, the associated vortices (with ‘effective’ strength Γ) positions z_G also vary in time. In the numerical implementation of the model, some geometric calculations are needed in order to monitor the vortex positions for all blade sections relatively to the tower elements in time.

Furthermore at each time step t , a complex flow potential and velocity can be defined at any position z in the 2D plane, corresponding to each tower element, as:

$$\Phi(z, t) \quad \text{and} \quad U(z, t)$$

Applying the unsteady Bernoulli’s equation, the pressure field time-series at any position in the 2D plane can also be calculated as:

$$P(z, t) = P_{\infty} + \frac{1}{2} \rho U_{\infty}^2 - \frac{1}{2} \rho |U(z, t)|^2 - \rho \frac{\partial \Re(\Phi(z, t))}{\partial t} \quad (1)$$

where the operator \Re denotes the real part of a complex value.

The time-series of the pressure on the tower surface can be calculated using the above formula. Thereby, the acoustic pressure in the far-field is obtained using Farassat F1A formulation [7]. It provides the acoustic pressure p_a at any receiver/listener location using the following integral over the entire tower surface S emitting noise:

$$p_a(t) = \frac{1}{4\pi C_0} \int_S \left[\frac{\dot{\vec{l}} \cdot \vec{r}}{r (1 - M_r)^2} \right]_{\text{ret}} dS \quad (2)$$

where C_0 is the speed of sound, $\vec{l} \equiv P(z, t) \vec{n}$ is the pressure force vector applied on the elementary tower surface dS , \vec{n} being the vector normal to the tower surface pointing outward, and the upper dot denotes a time derivative. \vec{r} is the vector between the elementary tower surface where the pressure is applied and the listener location in the far-field where the acoustic pressure is calculated pointing toward the receiver, r is its norm, and M_r is equal to $\vec{M} \cdot \vec{r}$ where $\vec{M} = \vec{v}/C_0$ with \vec{v} being the velocity of the elementary surface dS relative to the listener (which should be zero in the present case if the tower and receiver are not moving). The integration is conducted over the whole tower surface S .

2.4 Integration of the BTI model in the aeroelastic code and numerical model of the NREL 5MW turbine

As mentioned earlier, the BTI noise model is implemented as part of an aeroacoustic module, which is itself already integrated in the wind turbine aeroelastic code HAWC2. In the latter code, the blades are discretised along their span for calculating the aerodynamic loading from the incoming wind flowfield (see Section 2.2). This same discretisation is used in the aeroacoustic modelling of the blades and their interaction with the atmospheric turbulence [8].

Independently, the model proposed in the previous Section 2.3 requires a discretisation of the tower surface in order to conduct the numerical integration of Eq. (2). Firstly, the tower is discretised into tower sections along its height, as illustrated in Fig. 1. In each of these sections, the 2D potential flow and vortex dynamics of the passing blades is calculated as described in the previous section. Secondly, each tower section is discretised along its circumference into angular segments onto which the fluctuating pressure can be calculated locally according to Eq. (1), before being used in the surface integration of Eq. (2).

Note that in the calculations of the NREL 5MW turbine conducted in the following Section 3, the tower is discretised into sections of 0.6 m along its height and 24 angular segments, resulting in circular arc lengths of approximately 0.6 m depending on the position along the tower height. Indeed, the actual tower diameter varies from 6 m at its base to 3.87 m at the hub, with a tower height of 87.6 m. This conical shape of the tower is included in the model.

Finally, the HAWC2 aeroelastic calculations are conducted in the time-domain (see Section 2.2). The present model uses the same time discretisation and a time-step of 0.01 s, giving access to frequencies up to 50 Hz.

3. Model predictions and comparisons for the NREL 5MW turbine

In the present section, the proposed model is applied to the NREL 5MW turbine and its results are investigated. Selected results are compared with the high-fidelity computations conducted by Klein *et al* [11]. The latter use a full 3D-CFD model for the flow impacting the turbine, including the atmospheric turbulence, and over the blades. The acoustic emissions are modelled using a solver for the Ffowcs-Williams Hawkins analogy for calculating the contributions of the rotor blades and tower surfaces, neglecting the volume contributions which are negligible at low Mach numbers, similarly to the present model.

3.1 Test-case definition

The NREL 5MW reference turbine is defined by Jonkman *et al* [12]. The operational conditions for the considered test-case are those defined by Klein *et al* [11] and are reported in Table 1. Three inflow conditions are considered:

- “Uniform”: Uniform and steady inflow as a function of height (i.e. no shear and no turbulence).
- “Shear”: Steady inflow with shear, using a power law with an exponent equal to 0.19 (no turbulence).
- “Turbulent”: A synthetic turbulent inflow is superimposed on the above mean inflow wind shear using the Mann model [17].

The noise levels are computed at two receptor locations on the ground, each located at 1 km from the turbine tower base. The first position (denoted as ‘A’) is located directly downwind of the turbine. The second one (denoted as ‘B’) is located in the plane transverse to the mean wind direction and to the left of the turbine when looking from upstream.

Table 1 Test-case definition for the NREL 5MW calculations.

Parameters	Unit	Value
Hub wind speed	m/s	11.3
Rotor speed	RPM	11.7
Pitch (positive nose up)	deg.	-2.29
Atmospheric turbulence intensity	%	16
Atm. turb. integral length scale	m	42

3.2 Comparisons of the rotor and tower relative contributions

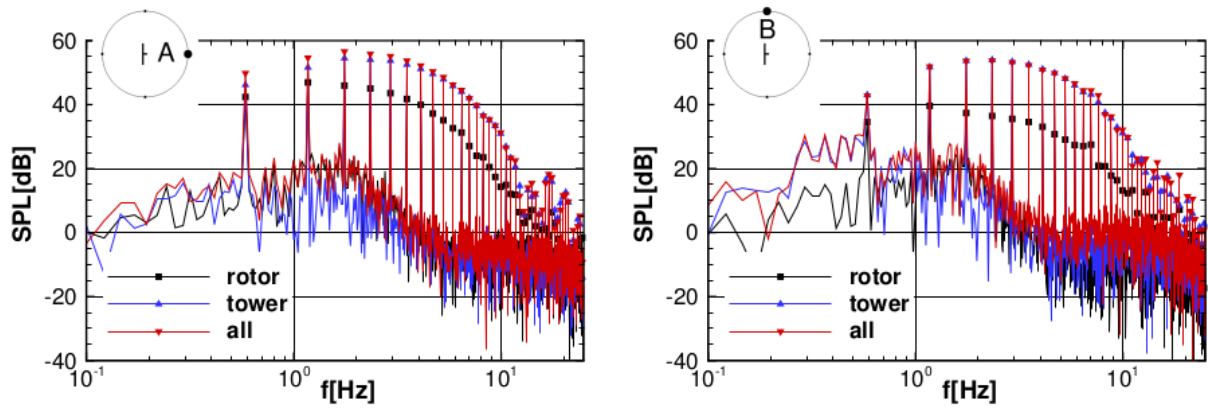
In this section, the relative contributions of the rotor and tower are compared to the overall noise emission at locations A and B. Only the “Uniform” inflow case is considered.

3.2.1 Sound pressure levels

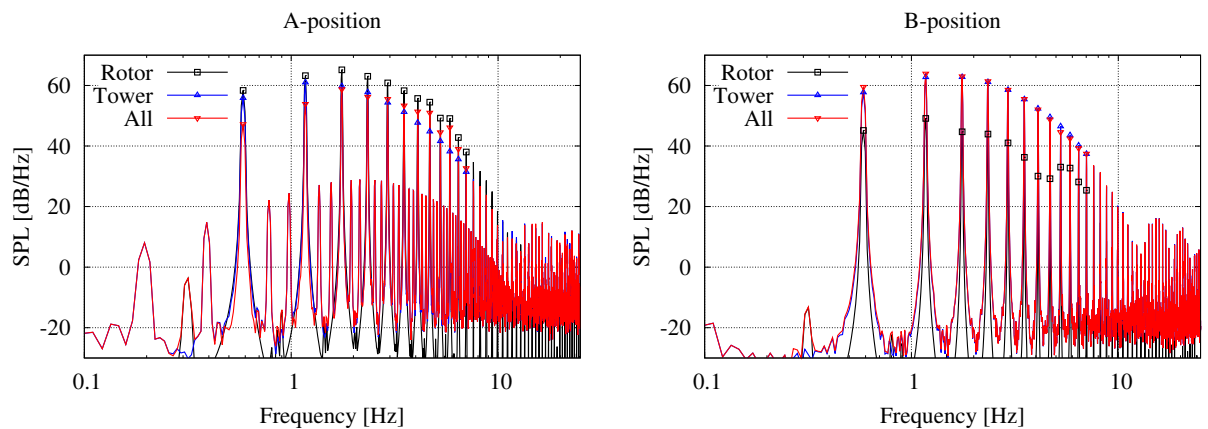
The results obtained with the high-fidelity model by Klein *et al* [11] are compared with those from the present model in Figs. 3a and 3b, respectively.

Qualitatively, the two models produced similar results. However, when looking closer at the quantitative values, discrepancies in the acoustic energy levels are observed. The tonal spectral peaks for the main blade passage frequency (approximately equal to 0.585 Hz) and its harmonics coincide well in frequency, but their energy contents are higher for the present model. Note that the ranges for the vertical axes in Figs. 3a and 3b are identical, but a shift is applied for the plots with the present model in order to accommodate for the higher peak values. It is noticeable that, at the receptor location A, the present model predicts higher tonal peak energy levels for the rotor as a noise source than the tower, while the model by Klein *et al* [11] predicts an opposite trend. However, at location B, the two models are in better agreement. Furthermore, between the tonal peaks, the predicted acoustic spectra obtained by Klein *et al* [11] contain higher broadband energy levels, while the present model predicts a much lower broadband energy content. The latter discrepancy might be attributed to the fact that the high-fidelity model includes more physical features of the noise generation mechanisms, like the vibration of the blades.

An striking discrepancy is the fact that the present model predicts tonal spectral peaks for the combined contributions of rotor and tower (denoted as ‘All’ in the figure legends) that are less energetic than the rotor and tower contributions alone for the receptor at location A (see 3b, left plot). This is not predicted by the high-fidelity model (see 3a, left plot). In contrast, at location B (see right plots in the above mentioned figures), both models predict a combined contribution dominated by the tower emission. As far as the present model is concerned, the lower peak levels for the combined contributions at location A are explained by an interference phenomenon. This is illustrated in Fig. 4 which displays a short interval of the time-series of the predicted acoustic pressure contributions. At location A, the passage of the blade near the tower is clearly observable at regular periodic time-intervals (corresponding to the blade passage frequency). It is also observed that the respective acoustic pressure contributions of the rotor and tower have opposite signs, significantly reducing the overall acoustic levels. At location B, the rotor contribution is rather small



(a) Reproduced with permission from Klein *et al* [11]



(b) Present model

Figure 3 Case “Uniform” - Narrow-band sound pressure spectra on the ground at 1 km from the turbine tower base (Left: Location A downwind of turbine; Right: Location B in transverse plane relative to the wind direction and to the left of the rotor when looking from upstream) - The markers on the spectra represent the peaks associated with the harmonics of the blade passage frequency.

(because of the directivity pattern of this specific noise source, see below), and the overall acoustic pressure is clearly dominated by the tower noise emission.

3.2.2 Noise directivity

In this section, the directivity patterns of the different acoustic noise sources (here the blade and the tower) are investigated. Polar plots of the noise levels predicted by the present model at receptor locations distributed on a circle around the turbine at ground level are displayed in Fig. 5. The displayed noise levels are computed by isolating the spectral peak energy level at the blade passage frequency for the different receptor locations.

The rotor noise present a clear dipole-like directivity pattern which can be expected from the interaction of a moving blade with a change in flow conditions (i.e. angle of attack) at low frequencies. Note also that the dipole axis is slightly rotated clockwise by a few degrees when looking from above the turbine, which is in accordance with the predictions of Klein *et al* [11].

The noise directivity pattern from the tower is much more like a monopole, in accordance with Klein *et al* [11] and Yauwenas *et al* [10] findings. The circular shape of the monopole is here slightly elongated into an ellipsoid in the direction transverse to the wind, and rotated clockwise by around 20° .

It should be noted that the above monopole and dipole directivity patterns are observed on the ground. Therefore, these do not necessarily reflect the overall three-dimensional directivity features of the turbine noise emission. Furthermore, only IS emission (at a given frequency) has been investigated and different directivity patterns may be expected for higher frequencies.

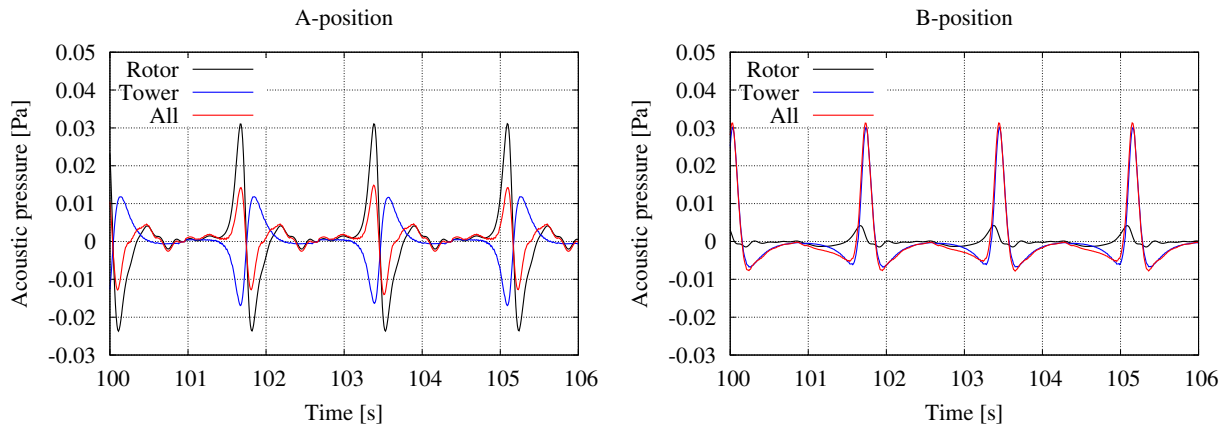


Figure 4 Case “Uniform” - Time-series excerpt of acoustic pressure (See caption in Fig. 3 for differences between left and right plots).

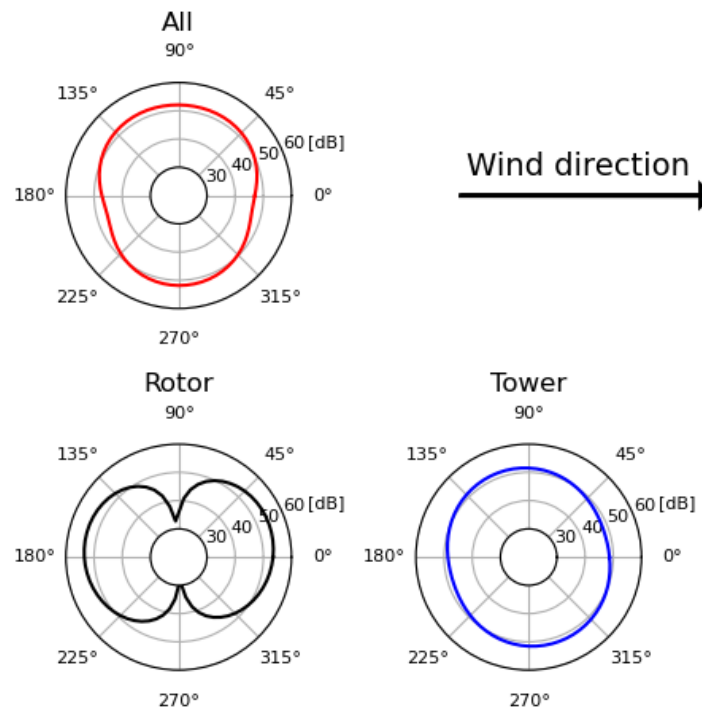


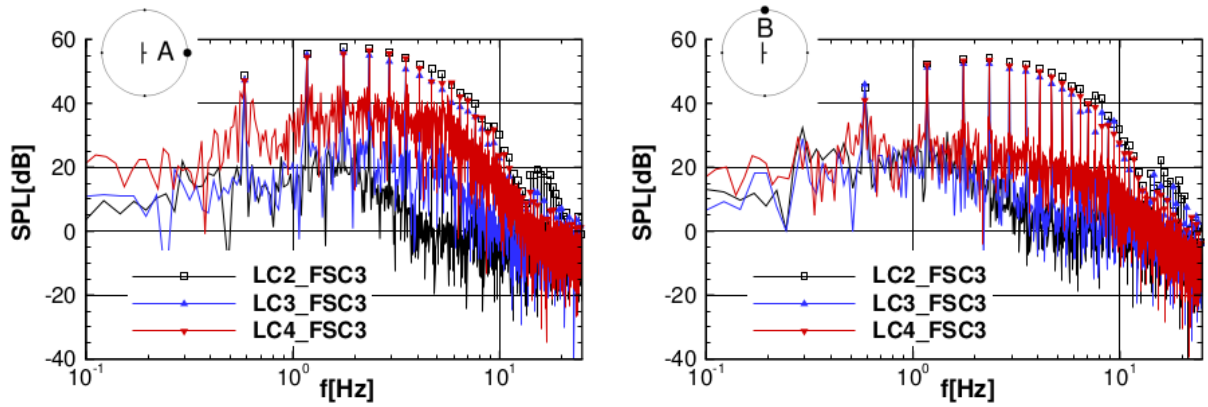
Figure 5 Case “Uniform” - Noise directivity plot for the tonal peak corresponding to the blade passage frequency (as seen from above the turbine).

3.3 Comparisons of the all contributions for different inflow conditions

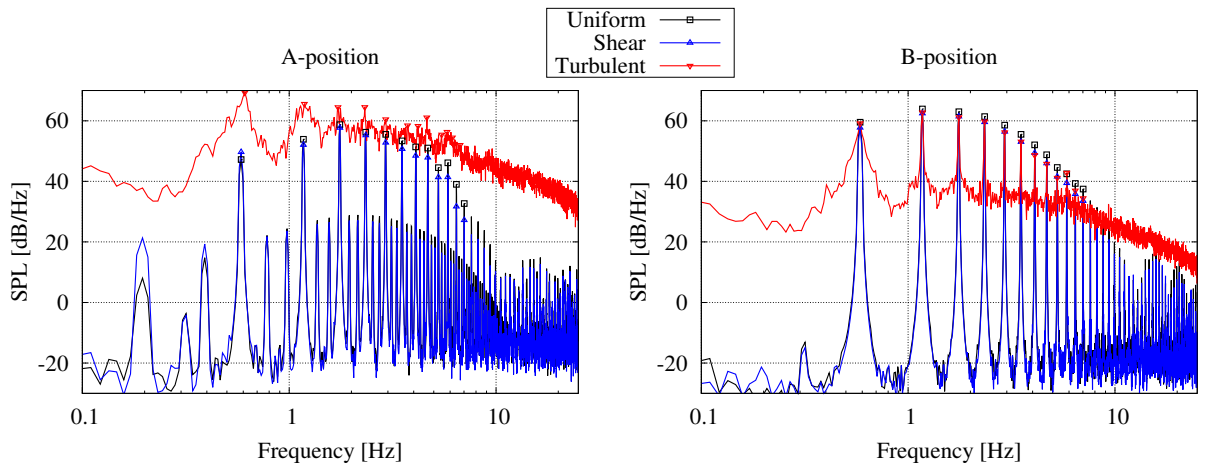
The differences between the “Uniform”, “Shear” and “Turbulent” inflow cases are now investigated. The results of the high-fidelity model by Klein *et al* [11] are compared with those of the present model in Figs. 6a and 6b, respectively.

From these two figures, it stands out that the broadband energy content from the atmospheric turbulence interaction with the blades (the “Turbulent” case) is much higher for the present model than the prediction of Klein *et al* [11] calculations. Similar conclusions as those drawn in Section 3.2.1 for the “Uniform” case apply here. It appears that the “Uniform” and “Shear” cases give very similar results using the present model, while the latter case exhibits a higher broadband energy content in the calculations of Klein *et al* [11].

In order to investigate further the discrepancy observed for the “Turbulent” case, calculations were conducted with the present wind turbine noise model using lower turbulence intensities. If using a turbulence intensity of 2%, broadband noise levels similar to those of Klein *et al* [11] are recovered as illustrated in Fig. 7. The reason for these discrepancies is still unclear.



(a) Reproduced with permission from Klein *et al* [11]. Cases “Uniform”, “Shear” and “Turbulent” are tagged “LC2_FSC3”, “LC3_FSC3” and “LC4_FSC3” in the legend, respectively.



(b) Present model

Figure 6 Comparisons of “Uniform”, “Shear” and “Turbulent” inflow cases for all contributions (Blades and tower) (See caption in Fig. 3 for differences between left and right plots, and markers definition).

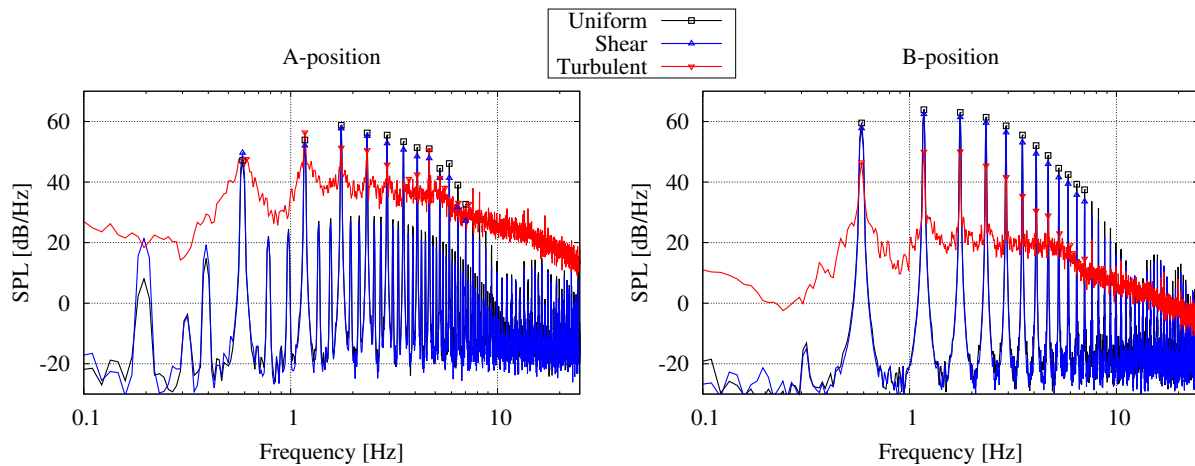


Figure 7 Comparisons of “Uniform”, “Shear” and “Turbulent” inflow cases for all contributions (Blades and tower). The “Turbulent” case is calculated with a turbulence intensity of 2% (See caption in Fig. 3 for differences between left and right plots, and markers definition).

4. Conclusion

A model for the blade-tower interaction (BTI) noise from wind turbines is proposed. It is based on geometrical simplifications of the turbine dynamics, more precisely the motion of the individual spanwise blade sections relatively to the tower and the associated aerodynamics. Using these assumptions, 2D potential flow and vortex theory is applied to compute the fluctuating pressure on the blades. The resulting noise emission is calculated using a classical acoustic analogy.

The model is tested by comparing its results with a high-fidelity model from the literature. Qualitative comparisons show relatively good agreement, but a number of quantitative discrepancies are also observed.

Noise directivity patterns observed in the two simulation frameworks indicate that the two models capture the same noise generation mechanisms.

A first important discrepancy is the existence of an acoustic interference between the blade and tower noise emissions that is predicted by the present model and not by the high-fidelity model. The second one is the difference in noise emission levels when including the atmospheric turbulence in the calculations.

At this stage, there is no explanation for the observed discrepancies. Further numerical investigations could help better understand the models as many input parameters are involved, and the present model involves a lot of approximations. Ideally, comparisons with wind turbine noise field measurements would help validate the models.

Acknowledgments

The present benchmark is conducted as a sub-task of the IEA Wind TCP research Task 39 (Quiet Wind Turbine Technology). It was partly supported by the EUDP project Jr.nr. 134-21022 funded by the Danish Energy Agency (Energistyrelsen).

The author is grateful to Thorsten Lutz for giving the permission to reproduce the figures from Klein *et al* [11].

References

- [1] G. Leventhall, “What is infrasound?,” *Progress in Biophysics and Molecular Biology*, vol. 93, no. 1, pp. 130–137, 2007.
- [2] C. J. Doolan, “A Review of Wind Turbine Noise Perception, Annoyance and Low Frequency Emission,” *Wind Engineering*, vol. 37, no. 1, pp. 97–104, 2013.

- [3] D. S. Michaud, K. Feder, S. E. Keith, S. A. Voicescu, L. Marro, J. Than, M. Guay, A. Denning, T. Bower, P. J. Villeneuve, E. Russell, G. Koren, and F. van den Berg, “Self-reported and Measured Stress Related Responses Associated with Exposure to Wind Turbine Noise,” *Journal of the Acoustical Society of America*, vol. 139, no. 3, pp. 1467–1479, 2016.
- [4] B. Zajamsšek, K. L. Hansen, C. J. Doolan, and C. H. Hansen, “Characterisation of Wind Farm Infrasound and Low-Frequency Noise,” *Journal of Sound and Vibration*, vol. 370, no. 1, pp. 176–190, 2016.
- [5] R. K. Amiet, “Acoustic Radiation from an Airfoil in a Turbulent Stream,” *J. Sound Vib.*, vol. 41, no. 4, pp. 407–420, 1975.
- [6] L. A. Viterna, “Method for Predicting Impulsive Noise Generated by Wind Turbine Rotors,” in *Second DOE/NASA “Wind Turbine Dynamics” Workshop*, Conference Proceedings, (Cleveland (OH)), 24-26 Feb. 1981.
- [7] F. Farassat and G. P. Succi, “A Review of Propeller Discrete Frequency Noise Prediction Technology with Emphasis on Two Current Methods for Time Domain Calculations,” *J. Sound Vib.*, vol. 71, no. 3, pp. 399–419, 1980.
- [8] F. Bertagnolio, H. A. Madsen, and A. Fischer, “A Temporal Wind Turbine Model for Low-Frequency Noise,” in *InterNoise17*, INTER-NOISE and NOISE-CON Congress and Conference Proceedings, (Hong Kong, China), pp. 5025–5033, INCE (publisher), August 2017.
- [9] F. Bertagnolio and H. A. Madsen, “A Tower Wake Model for Low-Frequency Noise of Downwind Turbine Rotors,” in *9th International Conference on Wind Turbine Noise*, Conference Proceedings, (Online), May 2021.
- [10] Y. Yauwenas, B. Zajamsšek, J. Reizes, V. Timchenko, and C. Doolan, “Directivity of Blade-Tower Interaction Noise,” *JASA Express Letters*, vol. 1, p. 063601, June 2021.
- [11] L. Klein, J. Gude, F. Wenz, T. Lutz, and E. Krämer, “Advanced CFD-MBS coupling to Assess Low-Frequency Emissions from Wind Turbines,” *Wind Energy Science*, vol. 3, pp. 713–728, 2018.
- [12] J. Jonkman, S. Butterfield, W. Musial, and G. Scott, “Definition of a 5-MW Reference Wind Turbine for Offshore System Development,” Tech. Rep. NREL/TP-500-38060, National Renewable Energy Laboratory, Golden (CO), Februar 2009. (Contract No. DE-AC36-08-GO28308).
- [13] J. Katz and A. Plotkin, *Low-Speed Aerodynamics (2nd edition)*. Cambridge Aerospace Series, Cambridge University Press, 2001.
- [14] J. E. Ffowcs Williams and D. L. Hawkings, “Sound Generated by Turbulence and Surfaces in Arbitrary Motion,” *Philosophical Transactions of the Royal Society*, vol. A264, no. 1151, pp. 321–342, 1969.
- [15] T. J. Larsen and A. M. Hansen, “How 2 HAWC2, The User’s Manual,” Tech. Rep. RISØ-R-1597(ver.3-1), Risø-DTU, Roskilde, Denmark, December 2007. Available at <http://www.hawc2.dk/download/hawc2-manual> (Accessed: 2021-03-11).
- [16] H. Glauert, *Airplane Propellers*, vol. In: *Aerodynamic Theory Volume IV*. Springer, Berlin, Heidelberg, 1935.
- [17] J. Mann, “The Spatial Structure of Neutral Atmospheric Surface-layer Turbulence,” *Journal of Fluid Mechanics*, vol. 273, pp. 141–168, 1994.

Paper #38 - ID: 374

Title: The role of the planning process for wind turbine noise annoyance – results from multiple cross-sectional and longitudinal field studies

Author: Florian J. Y. Müller

11th Edition of the

International Conferences on Wind Turbine Noise

Copenhagen, Denmark – 10th to 13th June 2025

The role of the planning process for wind turbine noise annoyance – results from multiple cross-sectional and longitudinal field studies

Florian J. Y. Müller¹, Valentin Leschinger and Gundula Hübner
MSH Medical School Hamburg, Hamburg, 20457, Germany

Summary

The expansion of renewable energy technologies leads to an increasing number of people living in the vicinity of wind turbines (WT). Therefore, acceptance of these residents is of central interest. One major acceptance factor are worries about WT emissions, like sounds [1]. In a series of studies in the USA (2016, n = 1407) as well as Central Europe (northern Germany, 2012, n = 212, to 2018, n = 130, and southern Germany, 2020, n = 149, to 2023, n = 80) residents of wind farms were surveyed. While the USA survey was cross-sectional, both European studies had a longitudinal design. In all three studies, objective data (e.g., distance to WTs, number of visible turbines) were compared to subjective data (e.g., attitude towards the energy transition). Among these, the strongest relations to WT noise annoyance were related to the planning process. The results show that the basis is laid for annoyance often even before the WTs are in operation. They emphasize the importance of participation and considering the perspective of residents early on.

Acknowledgments

These studies were founded by Wind Energy Technologies Office of the DOE's Office of Energy Efficiency and Renewable Energy, under Contract No. DE-AC02-05CH11231, by Deutsche Bundesstiftung Umwelt (German Federal Environmental Foundation, support code 28754-24/01, /02) and by the Federal Ministry for Economic Affairs and Climate Action on the basis of a decision by the German Bundestag (grants 0325839F and 03EE2023A).

References

- [1] G. Hübner, V. Leschinger, F. J. Y. Müller and J. Pohl, "Broadening the social acceptance of wind energy - An integrated acceptance model," *Energy Policy*, p. 113360, 2023.

¹ Corresponding author – Email: florian.mueller@medicalschooll-hamburg.de

Paper #39 - ID: 375

Title: Long-term Wind Farm Noise assessment over different meteorological conditions

Author: Krispian Lowe

11th Edition of the International Conferences on Wind Turbine Noise

Copenhagen, Denmark – 10th to 13th June 2025

Long-term Wind Farm Noise assessment over different meteorological conditions

Krispian T. E. Lowe¹, Mikel Amatriain², Markus Buße³ and Sylvia Broneske⁴
RWE Renewables Europe & Australia

Summary

Recently European Court of Auditors (ECA) recommended introducing EU noise-reduction targets and noise limits in the Environmental Noise Directive. The ECA approach would be aligning the noise exposure reporting thresholds, as closely as possible, with the guideline levels in the 2022 update report by the World Health Organization (WHO) in urban areas. WHO Guidelines provide guideline L_{den} and L_{night} levels for specific noise sources. For wind turbines, they provide a guideline level of 45 dB L_{den} with no L_{night} guideline determined. For long term assessment relevant factors must be defined, as the calculation method for yearly L_{den} may be affected by different meteorological conditions, operational states of the turbines, relative position of the source and receptor, background noise and masking levels or applicable daily night-time and short time limits. The determination of how to determine compliance with an L_{den} will be explored.

The present work's aim is the identification of the environmental parameters necessary for sound propagation and the reasonable evaluation time for long term wind farm noise assessment. A detailed knowledge and understanding of the emission and propagation characteristics can allow an optimised noise levels and energy yield, which can be achieved by adapting the operation of the turbine.

1. Introduction

European Union Directive 2002/49/EC (END) [1] was published to define a common approach intended to avoid, prevent or reduce on a prioritised basis the harmful effects, including annoyance, owing to exposure to environmental noise. Noise indicators L_{den} and L_{night} were selected for the preparation and revision of strategic noise mapping. Day-evening-night level L_{den} in decibels (dB) is defined by the A-weighted long-term average sound pressure level as defined in ISO 1996-2:1987 [2] and the updated to ISO 1996-2:2017 [3]. The equation for the day-evening-night weighted sound pressure level, L_{den}, for the equivalent continuous sound pressure level for day-time, L_{day}, evening-time, L_{evening}, and night-time, L_{night}, with the weightings of 0 dB, 5 dB and 10 dB, respectively, is shown in the equation below [4]. The time, in hours, for the day-time, t_{day}, evening-time, t_{evening}, and night-time, t_{night}, are normally 12, 4 and 8 hours, respectively. These times may vary for different countries⁵.

¹ RWE Renewables UK Limited, Reading, krispian.lowe@rwe.com

² RWE Renewables Iberia S.A.U. mikel.amatriain@rwe.com

³ RWE Renewables Europe & Australia GmbH, Hanover, markus.busse@rwe.com

⁴ RWE Renewables UK Limited, Swindon, sylvia.broneske@rwe.com

⁵ The typical values are day-time of 0700 to 1900, evening time of 1900 to 2300 and night-time 2300 to 0700.

$$L_{den} = 10 \log_{10} \left[\frac{t_{day} 10^{0.1L_{day}} + t_{evening} 10^{0.1(5+L_{evening})} + t_{night} 10^{0.1(10+L_{night})}}{24} \right]$$

European Environment Agency collects official noise data reported every five years by EEA member countries under the Environmental Noise Directive (END) with last available noise country fact sheets of 2021, including road, rail, aviation and industry sound sources.

The WHO Regional Office for Europe developed environmental noise guidelines for the European Region in 2018 [5], proposing an updated set of public health recommendations on exposure to environmental noise. The guidelines presented recommendations on reducing noise levels for road, railway, aircraft, wind turbine and leisure noise sources.

A compendium of WHO and other UN guidance on health and environment update of 2022 refers to L_{den} and L_{night} indicators for noise monitoring and exposure assessment adding $L_{Aeq,T}$ for measuring leisure noise exposure. For average noise exposure, sound pressure levels <45 dB L_{den} for wind turbine noise are recommended. There is no reference for night noise exposure or $L_{Aeq,T}$ for wind turbine noise.

Recently, the European Court of Auditors (ECA) [6], published a special report about urban pollution in the EU, giving the recommendation of prioritising actions against noise pollution to The European Commission, to assess the feasibility of introducing EU noise-reduction targets in the Environmental Noise Directive and aligning the noise exposure reporting thresholds as closely as possible with those recommended by the World Health Organization with a target implementation date of 2029. The referred indicators are L_{den} and L_{night} without any reference to $L_{Aeq,T}$ levels. The noise sources are focused on road, aircraft and railway noise.

1.1 World Health Organisation 2018

World Health Organisation (WHO): Regional Office for Europe (ROE) provided Environmental Guidelines for the European Region for the following noise sources: Road Traffic, Railway, Aircraft, Wind Turbines and Leisure Activities. The recommended level for wind turbine noise is an L_{den} value of 45 dB. This latest report works in conjunction with WHO 1999 [7] and WHO 2009 [8] where those guidelines levels also apply, in particular 45 dB $L_{Aeq,8hour}$ outside a bedroom with a window open, and 40 dB $L_{night,outside}$, respectively.

The wind turbine guideline level was given a **conditional** recommendation and would require substantial debate amongst stakeholders, since the quality of the evidence used to derive the rating was **low quality**. It was marked as **low-quality** owing to heterogeneity, inconsistency and imprecision. No guidelines for L_{night} were produced since the evidence consisted of study limitations, inconsistent results and imprecision.

The WHO themselves state that the L_{den} and L_{night} is a poor acoustic measure for wind turbines in section 3.4.2.3, an excerpt is quoted below:

“Even though correlations between noise indicators tend to be high (especially between L_{Aeq} -like indicators) and conversions between indicators do not normally influence the correlations between the noise indicator and a particular health effect, important assumptions remain when exposure to wind turbine noise in L_{den} is converted from original sound pressure level values. The conversion requires, as variable, the statistical distribution of annual wind speed at a particular height, which depends on the type of wind turbine and meteorological conditions at a particular geographical location. Such input variables may not be directly applicable for use in other sites. They are sometimes used without specific validation for a particular area, however, because of practical limitations or lack of data and resources. This can lead to increased uncertainty in the assessment of the relationship between wind turbine noise exposure and health outcomes.”

“Based on all these factors, it may be concluded that the acoustical description of wind turbine noise by means of L_{den} or L_{night} may be a poor characterization of wind turbine noise and may limit the ability to observe associations between wind turbine noise and health outcomes.”

It is important to note that the WHO does not provide methodology, procedure or detailed information on how to predict, measure and assess an L_{den} for wind turbines.

1.2 Compendium of WHO and other UN guidance on Health and Environment 2022 update

The compendium of WHO and other UN guidance on Health and Environment report, chapter 11, provides a short summary of the guideline levels to achieve for a range of sources such as: road traffic noise, railway noise, aircraft, wind turbine, leisure sources [9]. The compendium states an average level of less than 45 dB L_{den} is recommended. There is no other guidance or other information provided for wind turbines in the compendium document.

1.3 Special report 02/2025

The European Court of Auditors (ECA) provides a review of the European Green Deal and the Zero Pollution Action Plan to reduce air and excessive noise on human health with respect to the END [6]. The special report found that there are no EU limit values or reduction targets for noise, and provides recommendations for limits for road, rail and aircraft. There is no mention of wind turbines in the report; however, the ECA special report should assess the feasibility of aligning the reporting thresholds as closely as possible with those recommended by the WHO by 2029. Therefore, wind turbine levels could be passed through without careful consideration.

2. Regulation on long-term assessment

The application of the calculation and enforcement of short-term and long-term sound levels from wind turbines varies from country to country owing to noise prediction, noise modelling, legislative frameworks and evidence at the time of the law and/or supplementary guidance creation. Countries such as Spain, Lithuania and Poland may have stated annual limits, but have short-term L_{Aeq} levels that are more stringent. Therefore, in practice, the annual levels are not generally calculated or assessed.

2.1 Netherlands

The Netherlands published a law to assess the annual levels for 47 dB L_{den} and 41 dB L_{night} [10]. The Law sets out the source level for which measurements should be done according to the method in the law or NEN-EN-IEC 61400-11 (2002). These methods determine the sound power level of the wind turbine per wind speed bin at hub height from cut-in to rated power. For sound power levels at wind speeds greater than the rated power, then the sound power level at the rated power can be used for these higher wind speeds.

The wind speed distribution for day, evening and night from a long-term wind statistics should be obtained from KNMI⁶. The annual average sound power level per octave band is calculated for each period of day. The predicted immission level is then determined from subtracting following attenuation terms: geometric divergence, atmospheric attenuation⁷, reflecting objects, screening, vegetation, industrial, ground, housing and meteorological corrections. It should be noted that though the propagation methods and parameters are similar to ISO 9613-2:1996 [11] and ISO 9613-2:2024 [12], but the ground attenuation is less in the Netherlands Law. The immission level is then modified for each turbine-receptor pair based on the relative bearing, owing to the long-term meteorological effects. However, this only comes into effect at a distance 10 times the combined receptor and source heights. Once the immission has been calculated for each period, it is combined into the L_{den} . The receptor height is 5 m.

Compliance with the limits is determined by a sound power level measurement, since it is not possible to measure an annual level at a receptor location. This is owing to the dominant influence of the background noise on measurements at receptors [10].

⁶ www.windenergie.nl

⁷ 10 degrees Celsius and 80 per cent relative humidity

The ruling on Dutch wind farms means that the Law no longer be applied, but a temporary bridging scheme is in place until new rules are in place [13]. The publication of the new draft law and consultation period were in October 2023 to November 2023, whilst the new law will come into force in 2025 or 2026 [13].

2.2 Norway

The guideline for noise is specified in T-1442/2021 as an L_{den} of 45 dB [14]. The prediction of the immission level is according to NORD2000, assuming that the turbines are operating 100 per cent of the time, and the sound power level at wind speed of 8 m/s, at 10 m standardised height, shall be used. There are no set parameters for NORD2000 calculations and it is dependent on the experience of the practitioner; however, the following parameters are typically used:

- Receptor height of 4 m,
- Ground is a uniform class D⁸,
- Temperature of 10 degrees Celsius and relative humidity of 70 per cent, and
- Wind speeds at 10 m standardised height.

3. Factors affecting long-term assessments

3.1 Source Sound Power Levels

The sound power level of a turbine should be determined using the IEC 61400-11:2012+AMD1:2018 CSV [15], where the sound power level is determined with respect to hub height wind speeds and third octave frequency. The wind speed bins are centred on the integer and half integer. The sound level index should be expressed as an L_{Aeq} . Depending on the regulatory context, further processing of the measured sound power levels should be used, or the warranted levels - usually issued by the manufacturer - or declared sound power levels using IEC TS 61400-14:2005 [16]. A comparison of different representations of sound power levels are shown in Institute of Acoustics (IOA) Good Practice Guide (GPG) Supplementary Guidance Note (SGN) 3 [17].

The sound power level should be declared between cut-in to cut-out wind speeds. If the sound power level is not declared for wind speeds above the rated power wind speed, then the rated power sound power level should be used. If the sound power level is unknown for wind speeds between cut-in and the 68 per cent of the rated capacity⁹, then care should be taken in extrapolating these data. An example is given in Figure 1. Any omission of sound power levels, at wind speeds where the turbine can generate, will reduce the calculated annual average sound power level.

A larger rotor size for the same rated power would increase the swept area, energy yield and capacity factor¹⁰. Increasing the energy yield would typically involve shifting the power curve, and sound power level curve, to lower wind speeds. This would increase the L_{den} and L_{night} values, but maximum sound power level, L_{Aeq} , of the turbine would remain the same. Increasing the rotor size does not necessarily increase the sound power level, owing to the tip speed being the limiting speed.

3.2 Wind Speed

The wind speed for calculating the annual average should be measured at the same resolution as the sound power level measurements. The introduction of binning data to a lower resolution or interpolating to a higher resolution, will introduce systematic errors and additional uncertainty. The wind speed should be measured at hub height or at points above and below the proposed hub height. Therefore, care should be taken to ensure that the correct wind speeds are used with the correct hub heights for all turbines. Typically, wind turbines with a lower hub height will see lower wind speeds compared to turbines with a higher hub height. When converting wind speeds from one height to another, wind shear must be taken into account,

⁸ 2000 kPas/m² - Normal uncompacted ground (forest floors, pasture field)

⁹ 0.8 times the 85 per cent of the maximum power as per section 5 in IEC 61400-11.

¹⁰ Capacity factor is the actual or predicted energy yield divided by the maximum potential energy yield.

guidance is provided within IEC 61400-11 [15], IEC 61400-11-2 [18] and the IOA GPG [19] and the IOA GPG SGN 4 [20]. When using wind speed measurements with lower anemometers on a mast, care should be taken to account for the mast wind shadow. When using a LiDAR, data quality and signal to noise must be considered, either by filtering, infilling or omitting some data.

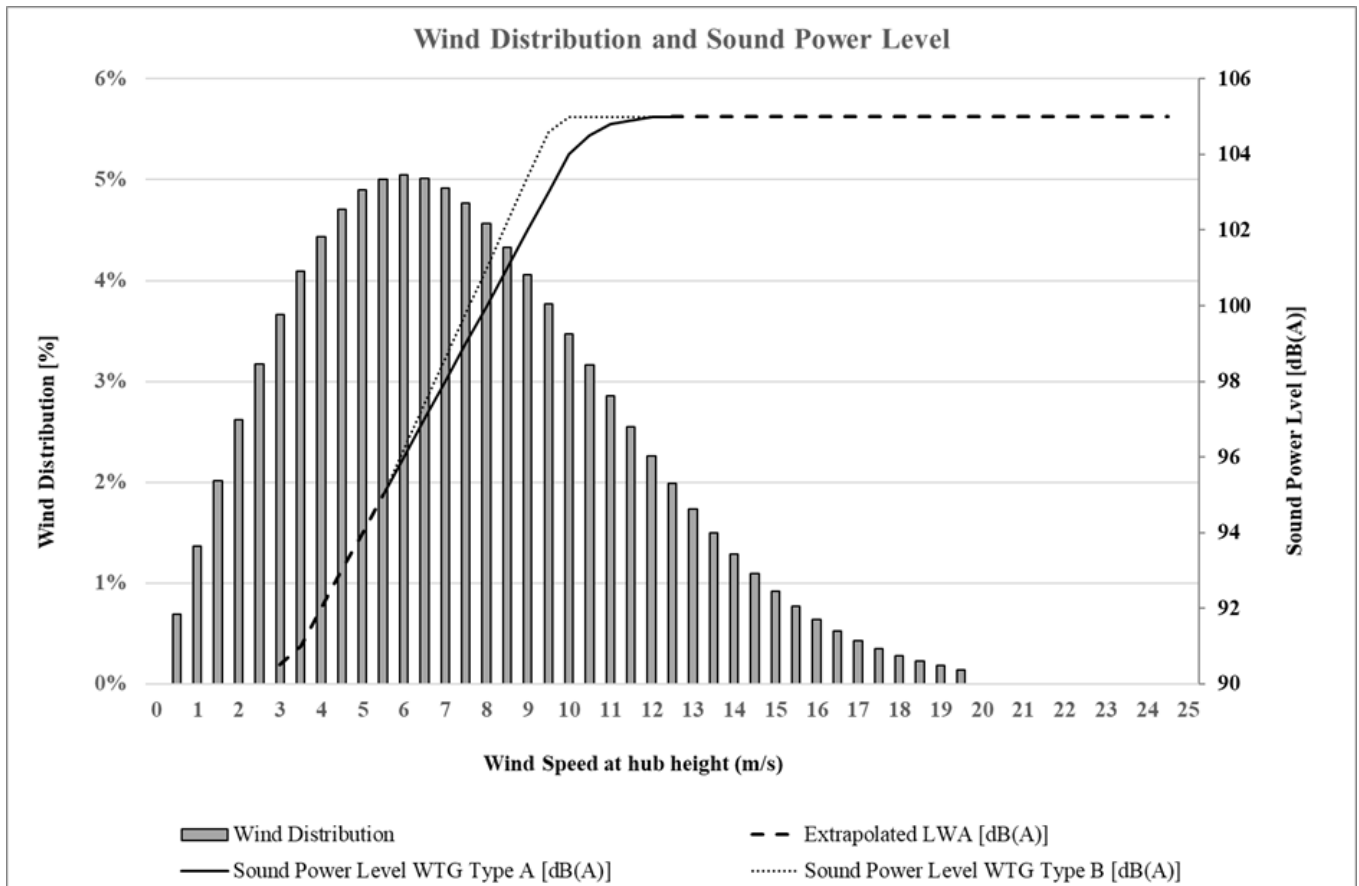


Figure 1 showing an example of sound power level (right y-axis), for Turbine Type A, with respect to hub height wind speed (x-axis) showing the solid black line as the declared sound power level and the dashed black line is the extrapolated level. Turbine Type B is shown as dotted lines. The wind distribution percentage of occurrence (left y-axis) at hub height wind speeds. The maximum sound power level for Turbine Type A and B is 105 dB(A), whilst the average sound power level is 100.8 dB(A) and 101.3 dB(A), respectively. If the wind speed distribution is the same for day, evening and night, then the L_{den} value would be 107.2 dB and 107.7 dB for turbines Type A and B, respectively.

Each site will have its own wind speed and wind direction distributions. In the case of wind measurements, a metrological mast and/or LiDAR should follow to the IEC 61400-50 series, and a robust long-term wind catalogue can be used. Wind speed measurements conducted on the development site may be limited to 1 or 2 years. These “shorter” measurements could be correlated with longer-term wind measurements from a national or international wind catalogue. Wind speed distribution will vary year by year; therefore, the annual average sound power level of the turbine will vary year by year. The wind speed distribution can be approximated to a Weibull distribution. The wind speed distributions and power curves are used to calculate representative wind energy yield(s). The calculated energy yield can be considered as the maximum potential. In real-life power output is likely to be slightly below these values owing to downtimes: maintenance, grid outages, sector managements and others (see section 3.4).

Wind speed distribution should be grouped for the day-time, evening-time and night-time periods. These time periods may vary for different countries or regions, and that the hour change to and from summer-time should also be taken into account. Therefore, the average sound power level, for a period of day, per octave band, $L_{W,period,j}$, is the logarithmic sum between cut-in and cut-out wind winds speeds for the frequency of occurrence of the wind speed bin, V_i , for the corresponding sound power level per octave and wind speed bin, $L_{W,i,j}$,

$$L_{W,period,j} = 10 \log_{10} \left[\sum_{i=v_{cut-in}}^{v_{cut-out}} V_i 10^{(0.1L_{W,i,j})} \right]$$

The sum of V_i may not equal 1 owing to wind speeds outside of the cut-in and cut-out region.

For simple flat sites it may be appropriate to use a single point for the entire wind farm, but for larger wind farms or those with complex terrain, multiple wind speed measurement locations may be needed. In addition, when a wind turbine is downwind of another turbine, the wind speed may be lower.

Determining the “mean” sound power level from the arithmetic mean wind speed is an incorrect method this is owing to (1) the wind speed distribution follows a Weibull distribution rather than a Gaussian distribution, and (2) the annual average is based on weighted logarithmic average.

3.3 Wind direction

Wind direction will have an effect on the sound pressure level at the receptor location owing to the shadow zone for the upwind and close to cross wind positions [19 and references within]. The prevailing wind direction may change owing to the season and time of day, in particular for regions in coastal or areas close to large bodies of water. Treatment of the effect of wind direction on the sound propagation is discussed further in ISO 9613-2:2024 Annex C [12] and the IOA GPG section 4.4 [19].

The distribution of wind directions is important for the siting of wind turbines in a wind farm. A wind rose shows probability of a wind from a certain sector. In addition, the wind speed distributions can be different for these wind direction sectors.

Higher wind speeds may be associated with the prevailing wind directions, whilst lower wind speeds for the non-prevailing wind directions. The wind direction may vary across the site, especial for site with complex terrain and inter- and intra-wind farm turbulence.

When assessing the directional effects, it is prudent to create an attenuation matrix of wind speed, wind direction and period for each receptor turbine pair.

According to the IEC TS 61400-14, the apparent sound power level shall be declared by combining the mean sound power level and the confidence level. Aerodynamic sound theories and experiments have demonstrated that the sound pressure levels in the crosswind direction are lower than those in the up- or downwind direction [21] [22]. There is no definition of emission directivity in the manufacturer’s sound power declaration.

3.4 Turbine Operation

The operation of the turbines on a wind farm will affect the annual average owing to, but not limited to, the following:

- Availability of the turbine, where turbines are subject to maintenance, expected levels of stoppages owing to faults and grid outages. The availability of a wind farm will not be 100 per cent but is expected to be greater than 95 per cent.
- The wind farm may be constrained by the grid restriction based on capacity load, where the wind farm may have to run a reduced power mode or shutdown owing to oversupply or other restrictions by the grid operator.
- Individual turbines operate in curtailed modes or shut down at specified wind speeds, wind directions and time of day owing to turbine wakes, turbulence from the terrain, noise mitigation to existing national laws, bat and bird protection, shadow flicker, intra-wind farm grid constraint, loading, etc.

These operational constraints may be known for the development under assessment but may be unknown for neighbouring wind farms that are not under the operator’s control.

Assuming that the wind farm will be operational 100 per cent of the time would often lead to an over estimation of the annual average.

3.5 Propagation

The depending on the propagation model (NORD2000, ISO 9613-2 etc) some of the attenuation parameters may vary over the year. The predicted levels according to ISO 9613-2 is for downwind conditions under a moderate ground-based temperature inversion, such as commonly occur on clear and calm nights.

Geometric divergence should be the same irrespective of the time and date. However, the parameters for atmospheric absorption and ground attenuation will vary. Ambient temperature, temperature gradient, relative humidity and atmospheric pressure will change throughout the day and through each season. Wind farms coexist with agricultural activities and the ground factor may change over the course of the year depending on the land use. For example, there may be crops in the summer, bare ground in winter and spring, frozen, snow or flooded during the winter. Therefore, full evaluation of temperature, relative humidity and ground conditions should be used; however, a pragmatic approach could be to use average values.

If turbine rotors are obscured by landforms relative to the receptor location, the screening attenuation for that turbine at the receptor, is limited to 3 dB according to ISO 9613-2:2024 Annex D or 2 dB according to the IOA GPG Section 3¹¹. Where a concave ground occurs between the source and the receptor, then an additional 3 dB can be added to the contribution of that turbine at that receptor according to ISO 9613-2:2024 and IOA GPG Section 3. However, it should be noted that the calculation of the mean propagation height and the trigger criteria are different in ISO 9613-2 and the IOA GPG.

3.6 Receptor Locations

The receptor location for the predicted levels should be carefully selected. Country specific requirements such as prediction on the façade closest to the wind farm or in free field conditions should be used. Care also needs to be taken, as national legislation could mandate the precise location for measurements, such as in Germany, where the immission level should be measured 0.5 m in front of the open window, outside, of the most affected room in need of protection, such as bedrooms [23].

4. Measurement and Enforcement

Measurement of an annual average at receptor locations will be impracticable owing to the effect of background noise, road, rail, aircraft, industry or other anthropogenic sources. Therefore, it will be impracticable to determine the specific sound level of the wind farm or wind turbine at receptor locations, owing to the unknown contribution of the other sounds. Also, the presence of measurement equipment in at receptor locations will have a disruptive effect on inhabitants of the dwelling and affect their subjective response to the source of noise.

To implement long-term (annual) immission measurements at several receptor positions around a wind farm, during the development and operation, will increase the cost of energy production and the security of supply, owing to the number and complexity of the measurements and precision instrumentation needed for the task. In addition, a clear description of uncertainties in any methodology will have to be calculated and stated.

In shorter term measurements, assessed against L_{Aeq} , L_{A50} , L_{A90} indices, it is a proper approach to perform shutdowns and logarithmically subtract the shutdown levels from the total levels, to give the specific sound pressure level owing to the source [18] [24]. However, it is impracticable to have regular shutdowns, over a year, for the wind farm, since this will impede the generation of electricity. In addition, neighbouring

¹¹ If the landform is close to the receptor, then a reduction of 10 dB can be used.

wind farms that are stopped for various reasons throughout the year will provide an incorrect picture of the cumulative noise exposure.

The Netherlands and Norway laws, where the L_{den} index is used, state that measurements at receptor locations are impracticable. They state that compliance is assessed with sound power level measurements with a prediction of immission levels at receptor locations [10] [14]. Therefore, given the multiple meteorological effects on propagation it is more logical to use receptor measurements to compare to L_{Aeq} , L_{A50} , L_{A90} or other similar indices for sound level limits, rather than attempt to measure an annual average.

The annual average sound level indicators do not reflect the neighbours experience of sound at their dwelling. The human experience of sound is not one of annual averages, but of a shorter nature. For example, the character or level of the sound that is transient and only occurs under specific conditions could lead to a complaint. Would a complaint be resolved if the annual average was complied with?

There are a number of challenges unresolved with regards to showing compliance with the annual limit under the following circumstances:

- The nature of the annual average implies that the short-term immission level can be greater than the annual average limit. Therefore, if a limit was X dB L_{night} , then the source could remain at $X+3$ dB L_{Aeq} for 50 per cent of the year, and then shutdown for the rest of the year and meet the limit.
- If the annual average is calculated from the operational data¹², would the wind turbine(s) or wind farm have to cease operating, or would the operator be subject to penalties, if they reach the annual limit before the 12 months? Would it be a fixed 12 months or a rolling 12 months?

5. Summary

The EU Directive 2002/49/EC aims to mitigate harmful effects of environmental noise using indicators like L_{den} and L_{night} for strategic noise mapping. The WHO European Region issued noise guidelines in 2018, recommending guideline levels for various noise sources including wind turbines. However, the WHO guidelines levels in 1999 and 2009 are still extant. The WHO guidelines level was given a conditional recommendation and still requires substantial debate, since the quality of evidence used to derive this guideline level was low quality. In addition, the WHO 2018 report states that the L_{den} and L_{night} is a poor acoustic measure for wind turbines.

A 2022 guidance update references L_{den} and L_{night} for noise monitoring, recommending $L_{den} < 45$ dB for wind turbine noise, with no L_{night} or $L_{Aeq,T}$ reference for wind turbines. The ECA recommended prioritising noise pollution actions and assessing EU noise-reduction targets within the END. These targets should align with WHO recommendations by 2029, focusing on indicators L_{den} and L_{night} for road, aircraft, and railway noise.

The Netherlands has set annual sound limits at 47 dB L_{den} and 41 dB L_{night} , assessing turbine sound power levels with NEN-EN-IEC 61400-11 and KNMI wind statistics for immission predictions. Currently, a temporary bridging scheme is active whilst the Netherlands' wind farm laws are under review, with new regulations anticipated by 2025 or 2026. Norwegian guideline T-1442/2021 sets a 45 dB L_{den} limit for noise prediction using NORD2000, with turbines assumed to operate continuously. Sound power level is based on 8 m/s wind speed at 10 m height. Norway and Netherlands calculate the L_{den} in different ways and therefore a direct comparison is not advised. Both countries do not recommend receptor measurements for the determination of the annual levels, but a sound power level measurement with a prediction to the receptor is required to determine compliance.

¹² Using power curve and an IEC 61400-11 test report to determine the sound power level, then a propagation prediction model to the receptor.

Sound power levels must be declared from cut-in to cut-out wind speeds, using rated levels if not specified above rated speeds. Extrapolation outside of measured levels requires caution to avoid reducing the annual average sound power level.

The resolution of wind speed measurements for calculating annual averages shall be the same as the sound power levels, avoiding errors from binning or interpolating. Measurement of wind speeds should be at hub height or appropriate heights, considering wind shear to convert between heights, guided by IEC standards and good practice guides.

Wind direction affects the immission at receptor locations, especially in shadow zones, with variations owing to season and time, notably near coasts and large water bodies. Wind direction distribution, illustrated by wind roses, is crucial for turbine siting in farms, with differing wind speed distributions across these sectors.

Prediction of annual levels at the receptor will have to take account the wind statistics, meteorological conditions, operational conditions and variations in the propagation attenuation over the year and lifetime of the wind farm. Assuming the turbines are operating at full rated capacity would be an overestimation of the annual averages.

Annual average sound levels may not reflect the neighbours' experience, as long-term averages often miss short-term variations, character and specific disruptive conditions.

Measuring annual average sound levels at receptor locations are impracticable owing to background noise and the long-term presence of measurement equipment, which will disrupt inhabitants and affect their response to wind farm noise. Long-term immission measurements around a wind farm increase costs of energy production and complexity, requiring precision and clear methodology, whilst trying to minimise uncertainties in the result.

Challenges in meeting annual sound limits include potentially exceeding short-term immission levels and unknown background noise levels. If they are too high, regularly wind farm shutdowns will be required to show compliance, which is complex to organise and increases the cost of energy production. Questions arise about operations ceasing and penalties if limits are reached within a shorter period than a year, whether on a fixed or rolling 12-month basis.

6. References

- [1] European Parliament and of the Council, Directive 2002/49/EC of the European Parliament and of the Council of 25 June 2002 relating to the assessment and management of environmental noise, EUR-Lex, 2002.
- [2] ISO, "Acoustics — Description and measurement of environmental noise Part 2: Acquisition of data pertinent to land use," ISO, Geneva, 1987.
- [3] ISO, "Acoustics - Description, measurement and assessment of environmental noise - Part 2: Determination of sound pressure levels," ISO, Geneva, 2017.
- [4] ISO, "Acoustics - Description, measurement and assessment of environmental noise - Part 1: Basic quantities and assessment procedures," IOA, Geneva, 2016.
- [5] World Health Organization (WHO):ROfe, "Environmental Noise Guidelines for the European Region," World Health Organization, Copenhagen, 2018.
- [6] European Court of Auditors, "Special report: Urban pollution in the EU - Cities have cleaner air but are still too noisy," Publications Office of the European Union, Luxembourg, 2025.
- [7] World Health Organisation (WHO), "Guidelines for Community Noise," WHO, Geneva, 1999.
- [8] World Health Organisation (WHO), "Night Noise Guidelines for Europe," WHO Regional Office for Europe, Copenhagen, 2009.
- [9] World Health Organization, "Compendium of WHO and other UN guidance on health and environment 2022 update," Geneva, 2022.

- [10] Secretary of State for Infrastructure and the Environment, “General rules for environmental management establishments (calculation and measurement of noise impact of wind turbines),” STAATSCOURANT, The Hague, 2010.
- [11] ISO, “Acoustics - Attenuation of sound during propagation outdoors - Part2: General method of calculation,” ISO, Geneva, 1996.
- [12] ISO, “Acoustics — Attenuation of sound during propagation outdoors — Part 2: Engineering method for the prediction of sound pressure levels outdoors,” ISO, Geneva, 2024.
- [13] IPLO, “Environmental impact assessment and new general environmental rules for wind farms,” Living Environment Information Point, [Online]. Available: <https://iplo.nl/regelgeving/regels-voor-activiteiten/gevolgen-nevele-arrest/mer-nieuwe-regels-windparken/>. [Accessed 05 03 2025].
- [14] Milø-direktoratet, “Guidelines on the treatment of noise in land-use planning,” Oslo, 2021.
- [15] IEC, “Wind Turbines - Part 11: Acoustic Noise Measurement Techniques,” IEC, Geneva, 2012.
- [16] IEC, “Wind Turbines - Part 14: Declaration of apparent sound power level and tonality values,” IEC, Geneva, 2005.
- [17] Institute of Acoustics, “SUPPLEMENTARY GUIDANCE NOTE 3: SOUND POWER LEVEL DATA,” IOA UK, St. Albans, 2014.
- [18] IEC, “Wind Energy Generation Systems - Part 11-2: Acoustics noise measurement techniques - Measurement of wind turbine sound characteristics in receptor position,” IEC, Geneva, 2024.
- [19] Institute of Acoustics, “A Good Practice Guide to the Application of ETSU-R-97 for the Assessment and Rating of Wind Turbine Noise,” Institute of Acoustics, St. Albans, 2013.
- [20] Institute of Acoustics, “Supplementary Guidance Note 4: Wind Shear,” IOA, St Albans, 2014.
- [21] S. Oerlemans and J. G. Schepers, “Prediction of wind turbine noise and validation against experiment,” National Aerospace Laboratory NLR, Amsterdam, 2009.
- [22] C. Rautmann, “Numerical Simulation Concept for Low-Noise Wind Turbine Rotors,” Deutsches Zentrum fuer Luft- und Raumfahrt, 2017.
- [23] Sechste Allgemeine Verwaltungsvorschrift zum Bundes- Immissionsschutzgesetz (Technische Anleitung zum Schutz gegen Lärm - TA Lärm, 01.06.2017).
- [24] Institute of Acoustics, “Supplementary Guidance Note 5: Post Completion Measurements,” Institute of Acoustics, St. Albans, 2014.

Paper #40 - ID: 376

Title: Unwanted event removal and background noise characterization in wind turbine noise

Author: Luca Fredianelli

11th Edition of the

International Conferences on Wind Turbine Noise

Copenhagen, Denmark – 10th to 13th June 2025

Unwanted event removal and background noise characterization in wind turbine noise

Luca Fredianelli, Geremia Pompei, Gaetano Licitra
Institute for Chemical-Physical Processes of the Italian Research Council, Via
Moruzzi 1, 56100 Pisa, Italy

Andac Akbaba, Gino Iannace
University of Campania “Luigi Vanvitelli”, Borgo San Lorenzo, 81031 Aversa, Italy

Francesco D’Alessandro
iPOOL S.r.l., Via Antonio Cocchi 3, 56121 Pisa, Italy

Francesco Artuso, Francesco Fidecaro
University of Pisa - Physics Department, Largo Bruno Pontecorvo 3, 56127 Pisa,
Italy

Summary

In environmental acoustic measurements it is necessary to separate the contribution of the source under investigation from the background noise by means of ambient noise measurements. Source separation is a complex task, especially for wind turbine noise, where long-term measurement campaigns are required. Although data analysis techniques are already in use to perform this task, they all require a preliminary step to remove anomalous events, i.e. events that are not characteristic of the standard residual noise. This step can be complex and time consuming depending on the duration of the measurements and the location. Depending on the specific site and source under evaluation, the variety of sounds that can be considered undesirable for compliance with environmental acoustic regulations is heterogeneous, ranging from road vehicles, trains and aircraft to human and animal sounds and more. Nowadays, it is possible to extrapolate from an audio source the features that describe its semantics using machine learning. The approach presented in this paper aims at locating a specific event in time within a measurement containing several acoustic events, in order to label it and then to remove the spurious events from the measurement.

1. Introduction

In the context of environmental acoustic measurements, a pivotal task is the separation of the contribution of the sound source under investigation from the residual or background noise. In fact, environmental noise measurements typically comprise numerous sounds from various sources that contribute to the emitters that an operator wishes to evaluate.

The most diffused and impacting sources, required noise mapping and monitoring for assessment by European Noise Directive are road traffic, railways, airports and industries. The necessity of such

monitoring, prevention and mitigation is vital in order to safeguard the population well-being [1-5]. Additionally, noise impact assessments are conducted for each type of craft or commercial activity to prevent effects on neighborhood and recreational noise [6-7]. Specific sound level measurements are also required for the characterization of sound power levels and spectra of machinery [8,9].

While international and/or national standards do exist for each type of measurement, all involve the removal of anomalous and spurious events. Notably, weather events such as rain and wind speeds exceeding 5 m/s should invariably be excluded from consideration. Depending on the specific type of measurement and the investigated source, additional events, such as animal sounds, voices and human activities, along with other non-investigated emitters, may also need to be removed in the aim of highlighting the contribution of predominant source from background noise.

Wind turbines merit comparable levels of consideration to other sources of noise and it has been well documented that they require monitoring. If the duration of all other sound sources can vary in terms of both duration and persistence, depending on the source, the intrinsic variability inherent in wind turbine noise necessitates a prolonged monitoring duration. For instance, in accordance with Italian legislation [10], a minimum of three weeks of continuous data is typically mandated. The procedure, based on 10' data, starts with a large amount of data that needs to be cleaned of unwanted events. This operation represents a bottleneck operation that requires significant effort from acousticians that currently perform this by manually removing anomalous events from the sound time history or from the spectrogram. The events that are removed are those which are not characteristic of standard residual noise. However, with the growth of artificial intelligence and enhanced computer calculation power, there is a pressing need to prioritize the automation and enhancement of this process.

The advent of machine learning has led to the development of automated processes that can be enhanced and expedited. Machine learning, a subfield of artificial intelligence, employs sophisticated algorithms to analyze data and derive insights. Machine learning models are able to perform complex tasks due to their training to understand the correlations that exist between patterns in input data and their respective outputs. Deep learning [11] is a subfield of machine learning that uses deep artificial neural networks as models to automatically extract different degrees of abstraction from input data. This enables the solving of complex tasks that deal with noisy data.

The specific task is referred to as Sound Event Detection (SED), the aim of which is twofold: firstly, to identify the class of the event, and secondly, to determine its onset and offset within a longer audio recording. In this article, the focus is on a preliminary step in this process, commonly referred to as Sound Event Classification (SEC), where audio segments are pretrimmed to contain only the sound event to be classified. This classification step provides a foundation for building a model capable of accurately recognizing sound classes, which can then be integrated into a more complex pipeline to perform event detection.

A significant challenge in this undertaking pertains to the markedly heterogeneous nature of these anomalous occurrences, which renders their identification a complex process. The following macro-categories of identifiable sources have been identified: i) anthropogenic sounds; ii) transportation infrastructure noise; iii) natural and animal-generated sounds; and iv) agricultural machinery and industrial operations. However, even this macro-level classification does not fully capture the variability found within individual categories, highlighting the need for adaptable classification approaches.

The conventional approach to address these tasks entails the conceptualization of a neural network architecture and its subsequent training from the fundamental stage to differentiate between a predetermined set of target classes. While this method is effective in scenarios with a limited scope, it lacks generalization capability. Specifically, if the initial set of target classes were to be extended, the model would require complete retraining to accommodate the new classes. Furthermore, in order to achieve optimal classification performance, particularly in the context of heterogeneous and complex datasets, such as in this case, it is essential to train the neural network on a substantial volume of data. This ensures that the model can learn a comprehensive representation of the wide variability in data and scenarios it will be required to recognize. The necessity for a solution that is both adaptable to diverse contexts and trained on sufficiently varied data has led to the recent widespread use of pre-trained models. These models have

already acquired knowledge of the general features that are typical of the tasks for which they were designed, such as image recognition, natural language processing, or audio classification.

These models can be used either directly or as a starting point to develop specialized models tailored to a specific set of classes or more targeted tasks. In this context, the Contrastive Language Audio Pretraining (CLAP) model has been developed. This is a deep learning model designed to learn joint representations of audio and text. To achieve this, CLAP transforms both an audio measurement and its corresponding textual description into vectors of the same dimension, termed embeddings. During the training phase, the model employs a process of contrastive learning, whereby it aligns the embeddings of matching audio-text pairs, while simultaneously distancing those of unrelated pairs. This contrastive learning enables the model to capture semantic relationships, organizing the embedding space so that similar sounds and descriptions are near each other. In [12], it is demonstrated that CLAP outperforms the classic features Mel-Frequency Cepstral Coefficients and Gammatone Frequency Cepstral Coefficients in clustering and classification tasks on a subset of five classes extracted from the ESC-50 dataset [13].

This paper presents an explanation of the transfer learning approach adopted, along with the preliminary outcomes obtained with the fine-tuned model. The results of the original CLAP model on the same dataset will be compared with the findings.

2. Transfer learning

The CLAP model is composed of two encoders: an audio encoder and a text encoder. These encoders are designed to extract two embeddings of equal dimensionality d from the audio measurement and its corresponding textual description. The objective of CLAP is to compare these embeddings and optimize the representation space such that audio and text embeddings with similar semantic content are pulled closer together, while those with differing semantics are pushed farther apart.

Once trained, the CLAP model generates a latent space in which elements are arranged according to their semantic relationships. This configuration enables the utilization of the model for classification tasks without necessitating further training. In order to employ the original model for the classification of novel sounds, it is necessary to provide a set of potential class labels. The model's classification process involves evaluating the similarity between audio and text embeddings, with the objective of aligning these embeddings to represent the same concept. Specifically, it computes the similarity score between the audio embedding and each of the class label embeddings, selecting the class with the highest score as the predicted output. The employment of a pre-trained model for classification offers distinct advantages, including its capacity to recognize a broad spectrum of classes.

However, it should be noted that the performance on an arbitrary set of classes cannot be guaranteed to be optimal. As the objective of this study is not to ensure applicability to an unlimited set of categories, but rather to achieve high performance on a well-defined subset, a transfer learning strategy was adopted. The strategy involves leveraging the robust foundational knowledge of the CLAP model and fine-tuning it to specialize in the selected subset of classes. The objective is to enhance the accuracy within a constrained set of sound classes, in comparison to the broader but less specialized performance of the original model. To this end, the initial portion of the CLAP architecture was retained, specifically the component responsible for embedding extraction. A new linear layer was then trained to project the resulting embeddings of dimension $d = 1024$ into a lower-dimensional space corresponding to the number of target classes of dimension 22. The output of this layer is a value representing the predicted likelihood that the input sound belongs to one of the predefined categories.

3. Dataset

The principle of realism is one of the primary guiding principles that guided the construction of the dataset. Due to the variability inherent in environmental sounds, the dataset aims to capture realistic soundscapes while remaining descriptive in terms of unwanted noise events. The overarching objective of this realism is to ensure that the models which are trained on this specific dataset are optimally prepared for the purpose of evaluating environmental noise and analogous contexts. These datasets are instrumental in the

development of CLAP models for the purpose of detecting and classifying real-world environmental sound events. The categorization process was meticulous, thereby enhancing the model's capacity to identify and classify sounds encountered in real-world noise measurement scenarios.

All audio samples are authentic recordings, devoid of synthetic sounds, and were obtained from four primary sources: (1) the ESC-50 dataset; (2) Freesound.org [14], a collaborative Creative Commons repository of audio clips; (3) YouTube, in that video files were converted to audio clips; and (4) measured from field recordings created by the authors.

The primary objectives of the dataset are to maintain its public availability and free distribution, to encompass a comprehensive and substantial array of environmental sound data, and to facilitate the incorporation of additional data volumes and vocabularies over time. In order to achieve these objectives, audio files were meticulously selected from 22 predetermined categories within the domain of environmental acoustics. The authors proceeded to download the audio files and implemented a stringent protocol to ensure the highest standards of data quality and relevance. To maintain consistency, all audio files that were not in wav format were converted to wav. Each sound sample was then subjected to a manual assessment process, during which the authors listened to the sound files. Following this, the sound files were standardized to a sampling rate of 44.1 kHz, a mono-channel configuration, and the wav file-type was converted to ensure consistency across recordings.

The pretraining dataset consists entirely of single-event audio samples collected from real-world recordings, as described above in the selection process. In order to enhance clarity and to place greater emphasis on the target acoustic events, all files were preprocessed to eliminate silences and to cut away unnecessary parts (e.g. irrelevant background activity or overlapping sounds). Following this preprocessing step, the subsequent audio recordings were systematically organized into category-specific folders based on the 22 environmental acoustics classes that had been pre-identified. The audio files were then renamed according to a naming convention that followed the format of "category name - 001", "category name - 002" and so on, allowing easy tracking and retrieval of files during model training.

The single-event audio files, which have been rigorously established, are stored in the manner described above. The dataset was provisioned in a format that could provide unambiguous acoustic events; as such, it was ideal for training models such as CLAP. The dataset's meticulous organization, including the isolation of individual events and the implementation of a systematic naming procedure, ensures its efficacy for machine learning workflows. This enhancement of workflow efficiency is particularly advantageous in the processes of feature extraction and alignment with text descriptions during model training.

The 22 selected classes are listed in Table 1. It has been observed that varying the segment lengths within the same dataset during classification can result in different accuracy outcomes. Consequently, multiple versions of the dataset were created, with measurements segmented into durations ranging from 1 to 10 seconds in 1-second increments. For each version of the dataset, four distinct sets were constructed: the training set, the validation set, the early stopping set, and the test set. The early stopping set is of particular significance in preventing overfitting, as training is halted when the accuracy on the early stopping set does not improve for 10 consecutive epochs. Each version of the dataset was comprised of 500, 100, 100, and 100 measurements for the training, validation, early stopping, and test sets, respectively. In instances where the total duration of the dataset for a given segment length was inadequate to meet these criteria, data augmentation was implemented through the incorporation of Gaussian noise.

Table 1. Classes of sounds chosen for the dataset.

Classes of Sounds			
Bells	Birds	Cat fights and moans	Chicken coop
Cicadas and crickets	Crows, seagulls and magpies	Dog barking and howlings	Glass breaking
Horn	Jet aircrafts	Lawn mower, brush cutter and olive shaker	Music
Propeller aircrafts	Sirens and alarms	Thunder, fireworks and gunshot	Train
Vacuum cleaner, fan and hairdryer	Vehicle idling	Vehicle pass-by	Voices
Wind turbine noise		Workshop	

4. Results

The results are evaluated by comparing them with those obtained using the CLAP pretrained model directly, and with the results obtained with the fine-tuned model. The duration of the measurement in seconds has been shown to have a significant impact on the classification performance. It has been observed that varying the lengths of the segments from the same dataset during classification can lead to different accuracy results. This variation is likely attributable to the structural differences in the spectrograms. To accurately capture recurring patterns in a sound's spectrogram, a minimum duration may be required. In this study, the impact of hyperparameters on classification accuracy was investigated, with lengths ranging from 1 to 10 seconds, in 1-second increments. The results presented in Table 2 demonstrate the impact of varying input audio lengths on the accuracy and loss of the original pre-trained model on the validation set. Subsequent experiments were conducted using the fine-tuned model, with various hyperparameters adjusted during the training process. The optimal result is documented in Table 3.

Table 2. Accuracy and Loss results of the original CLAP model on the validation set at varying of the audio length hyperparameter.

Audio length	Accuracy	Loss
7 s	75.91 %	2.84
8 s	74.55 %	2.85
10 s	74.18 %	2.85
9 s	74 %	2.85
6 s	72.31 %	2.85
5 s	68.58 %	2.86
4 s	67.84 %	2.86
3 s	65.84 %	2.86
2 s	65.41 %	2.87
1 s	57.03 %	2.89

Table 3. Accuracy and Loss result of the fine-tuned model on the validation set.

Audio length	Accuracy	Loss
7 s	95.08 %	0.23

Figures 1 and 2 show the confusion matrices of the two best cases obtained using the original and the fine-tuned model, respectively. As can be seen by these figures, these matrices allow us to evaluate the performance for each class.

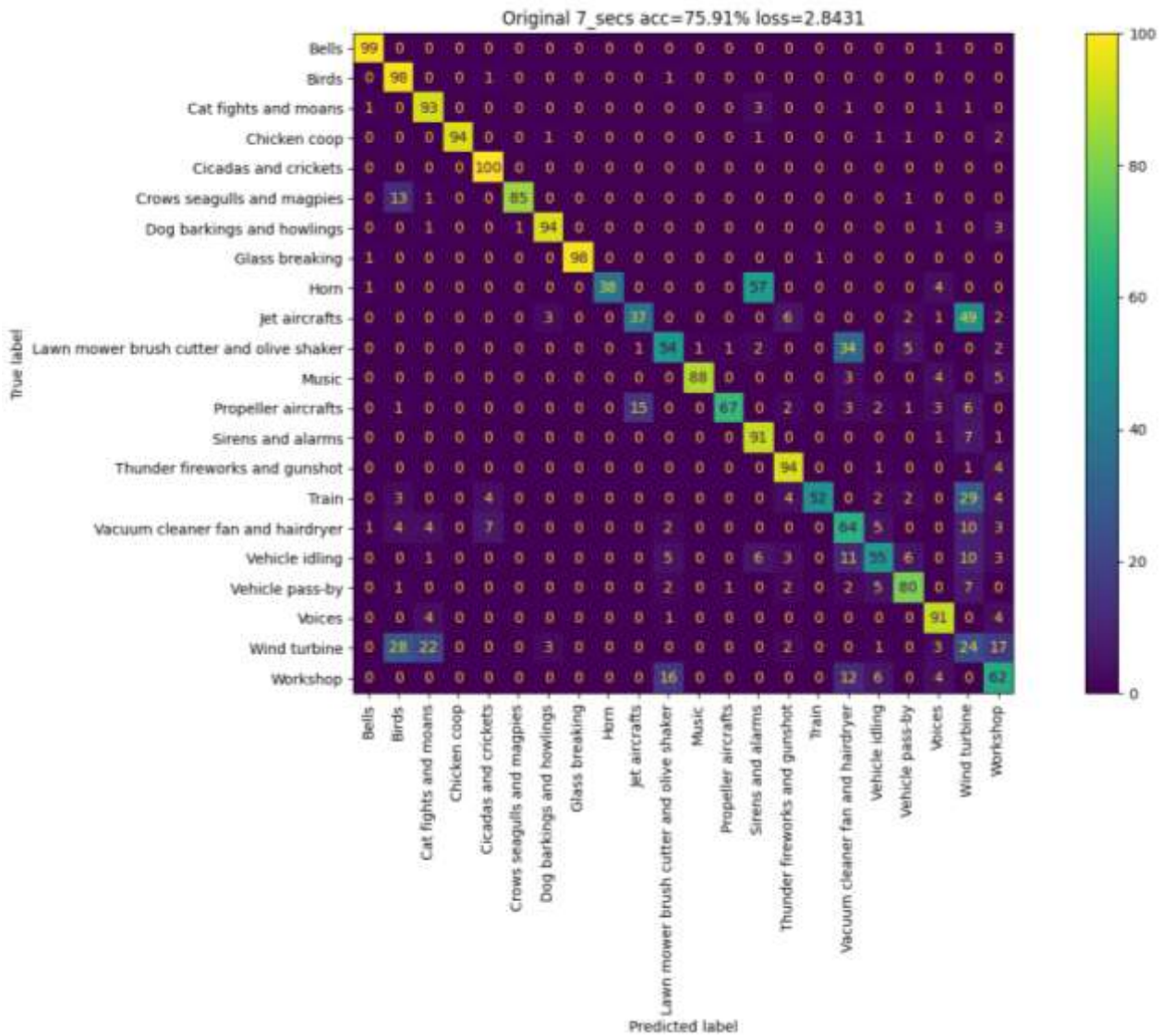


Figure 1. Confusion matrix for each class in the best case obtained with the original CLAP.

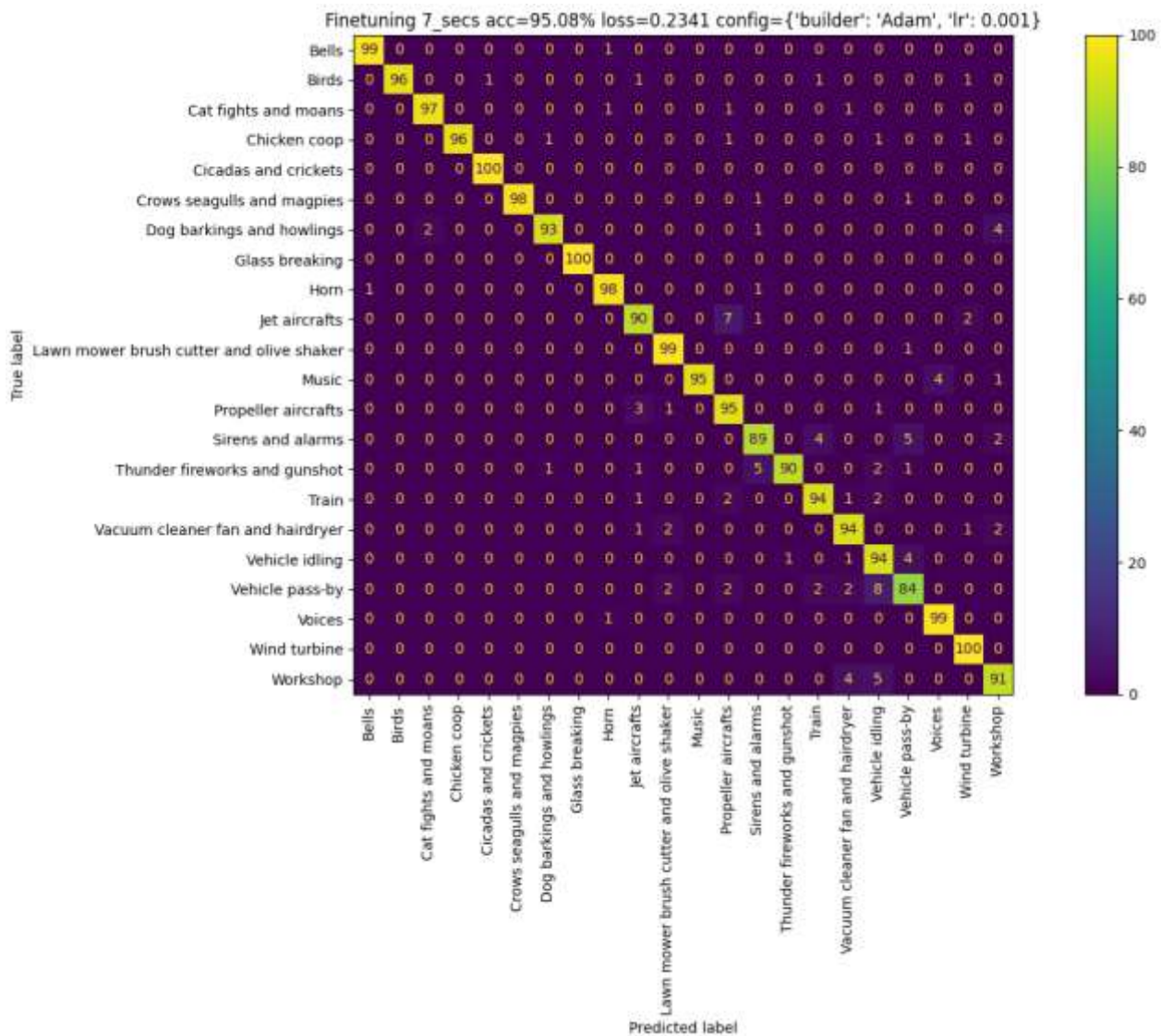


Figure 2. Confusion matrix for each class in the best case obtained with the fine-tuned model.

5. Conclusions

This study introduces the Contrastive Language-Audio Pretraining (CLAP) model, which integrates inputs from multiple domains into a shared space where their vector representations can be compared and manipulated. The model was fine-tuned using a Transfer Learning approach to perform Sound Event Classification (SEC) on a specific dataset, with a focus on key environmental sources relevant to noise monitoring. A linear layer was applied to the sound embeddings generated by the original model to adapt it for the classification task. The findings demonstrate a substantial enhancement in accuracy, with a rise from 75.91 % (the highest performance attained by the original model) to 95.08 % (the highest performance achieved by the fine-tuned model) on the validation set. The improvement on Wind Turbine Noise is impressive, a sign that the original CLAP is unaware of it.

These findings underscore the efficacy of the fine-tuned model in the classification task, showcasing a substantial enhancement in performance relative to the original model. Further analysis and exploration of additional fine-tuning strategies are warranted to continue improving these results. The subsequent stage of this research will entail the integration of the fine-tuned model into a detection pipeline for Sound Event Detection (SED), which is the ultimate objective in real-world scenarios.

Acknowledgments

The paper was supported by the PRIN 2022 project 20223LMSZN, COMBINE "Sustainable condition monitoring of wind turbines using acoustic signals and machine learning techniques" funded by the Italian Ministry of University and Research in the context of NextGenerationEU.

References

- [1] E. M. Andersson, M. Ögren, P. Molnar, D. Segersson, A. Rosengren, and L. Stockfelt. Road traffic noise, air pollution and cardiovascular events in a Swedish cohort. *Environmental research*, 185, 109446, 2020.
- [2] F. Bunn, P. Henrique Trombetta Zannin. Assessment of railway noise in an urban setting. *Applied Acoustics*, 104, 16-23, 2016.
- [3] M. Espey and H. Lopez. The Impact of Airport Noise and Proximity on Residential Property Values. *Growth and Change*, 31(3), 408-419, 2000.
- [4] P. C. Eleftheriou. Industrial noise and its effects on human hearing. *Applied Acoustics*, 63(1), 35-42, 2002.
- [5] D. Petri, G. Licitra, M. A. Vigotti and L. Fredianelli. Effects of Exposure to Road, Railway, Airport and Recreational Noise on Blood Pressure and Hypertension. *International Journal of Environmental Research and Public Health*, 18(17), 9145, 2021.
- [6] G. Iannace, A. Trematerra and I. Lombardi. Effects of nightlife noise in a city center. *Noise Mapping*, 8(1), 228-235, 2021.
- [7] A. Dzhambov and D. Dimitrova. Neighborhood noise pollution as a determinant of displaced aggression: A pilot study. *Noise and Health*, 16(69), 95, 2014.
- [8] L. Fredianelli, T. Gaggero, M. Bolognese, D. Borelli, F. Fidecaro, C. Schenone and G. Licitra. Source characterization guidelines for noise mapping of port areas. *Heliyon*, 8(3), e09021, 2022.
- [9] U. Papa, G. Iannace, G. Del Core and G. Giordano. Sound power level and sound pressure level characterization of a small unmanned aircraft system during flight operations. *Noise Vibration Worldwide*, 48(5-6), 67-74, 2017.
- [10] Ministero Della Transizione Ecologica. (2022) Decreto 1 giugno 2022 - Determinazione dei criteri per la misurazione del rumore emesso dagli impianti eolici e per il contenimento del relativo inquinamento acustico. (22A03580) (GU Serie Generale n.139 del 16-06-2022). Retrievable (in Italian) at: <https://www.gazzettaufficiale.it/eli/id/2022/06/16/22A03580/sg>
- [11] Y. LeCun, Y. Bengio, & G. Hinton. Deep learning. *Nature*, 521(7553), 436-444, 2015.
- [12] F. Artuso, F. Fidecaro, F. D'Alessandro, G. Iannace, G. Licitra, G. Pompei, and L. Fredianelli, "Identifying optimal feature sets for acoustic signal classification in environmental noise measurements," in INTER-NOISE and NOISE-CON Congress and Conference Proceedings, vol. INTER-NOISE24, (Nantes, France), pp. 7540–7549, Institute of Noise Control Engineering, 2024.
- [13] K. J. Piczak, "ESC: Dataset for Environmental Sound Classification," in Proceedings of the 23rd ACM international conference on Multimedia, (Brisbane Australia), pp. 1015–1018, ACM, Oct. 2015.
- [14] Freesound Team, "Freesound." <https://freesound.org>, 2024.

Paper #41 - ID: 380

Title: Procedure for predicting noise impact of new and repowered wind farms

Author: Marco Bernardini

11th Edition of the
International Conferences on
Wind Turbine Noise
Copenhagen, Denmark – 10th to 13th June 2025

Propagation models comparison in predicting noise impact of new and repowered wind farms

Marco Bernardini¹, Francesco D'Alessandro, Samuele Schiavoni
iPOOL S.r.l., Pisa via Cocchi 3, 56121, Italy;

MariaLuisa Ariza Alvarez
Institute of Marine Engineering of the Italian Research Council (CNR-INM), Roma (RM), Via di Vallerano 139, 00128, Italy;

Maria Josè Marsano
Department of Physics, University of Pisa, Pisa, Largo Bruno Pontecorvo 3, 56127, Italy;

Giacomo Bai
MOPI S.r.l., Pisa via Cocchi 7, 56121, Italy;

Luca Fredianelli, Gaetano Licitra
Institute for Chemical-Physical Processes of the Italian Research Council (CNR-IPCF), Pisa Via Moruzzi 1, 56100, Italy;

Summary

Wind farms are still growing or undergoing massive repowering to meet the European climate targets for 2030, which are still far to be reached. This process of modernizing installations makes it possible to increase energy production while reducing the number of turbines. All of this has a significant impact on the noise produced on the surrounding areas and on citizens. However, although a specific decree on the noise assessment of wind turbines was issued in Italy on 1st June 2022, there are still significant gaps or issues in the legislation for the predictive assessment of both new and repowered projects. Most importantly, no specific noise limits have been set for wind turbines and the predictive noise impact assessment for both new and repowering farm is only mentioned in the Decree, but no procedure is given. This document presents an operational proposal for drafting predictive acoustic impact assessments for both new and repowering projects, ensuring compliance with the measurement criteria established in the Italian decree. The objective of the procedure outlined in this article is to provide a detailed analysis of the acoustic impact of the wind farm on each receptor located within a 1500 m radius of the wind turbines, a distance defined by the decree as potentially affected by noise emissions from the installations. If issues are identified at one or more receptors, alternative solutions are proposed, considering different operational

¹ Corresponding author – Email: marco.bernardini@i-pool.it

modes of the wind farm, to bring the acoustic impact within legal limits. This article presents the proposed procedure applied to a real-world case study involving five wind farms, four of which consist of a single turbine and one with two turbines. A fundamental step in the predictive assessment of a wind farm's acoustic impact is the acoustic modelling phase, which can be carried out using different models for outdoor noise propagation. The results obtained using three different internationally recognized propagation models are compared in the evaluation of acoustic impact at the receivers located within the study area of the selected real case.

1. Introduction

The global energy transition and the increasingly ambitious climate goals set by the European Union for 2030 are driving the development of new wind farms and the repowering of existing ones. This evolution, while crucial for reducing greenhouse gas emissions and promoting energy independence, has raised concerns regarding its impact on the acoustic environment. In particular, the replacement of older wind turbines with newer, more powerful models, although reducing the number of units installed, without a proper planning may significantly alter the noise exposure experienced by nearby populations.

In Italy, the acoustic impact of wind farms is regulated by the Decree issued by the Ministry of Ecological Transition on June 1, 2022 [1], which establishes criteria for measuring noise emissions from wind power plants. However, the decree does not provide a dedicated predictive methodology, nor does it define specific immission limits for wind turbine noise. This regulatory gap leaves considerable room for interpretation in the development of acoustic impact assessments, especially for repowering projects.

Given the growing number of installations and the complexity of their acoustic interaction with the surrounding environment, there is a strong need for a standardized and technically robust procedure to evaluate noise impact during the design phase. Such a procedure must account for the variability of local meteorological conditions, terrain morphology, land use, and existing background noise levels.

The present work proposes a methodological framework for the predictive acoustic assessment of both new and repowered wind farms. The procedure includes five main phases: analysis of plant design, acoustic characterization of the study area, measurement campaign, acoustic modelling using different propagation models, and assessment of compliance with national regulations. Mitigation strategies are proposed where exceedances are identified.

A comparison is presented between three propagation models—CNOSSOS-EU [2] [3], ISO 9613-2:1996 [4], and the newly updated ISO 9613-2:2024 [5]—applied to five real-world case studies in Italy. The objective is to evaluate the influence of propagation model choice on predicted noise levels and to identify the most appropriate modelling approach for accurate and conservative assessment of wind farm noise impact.

Before the upgrading of the ISO9613-2, a study carried out in 2022 suggest the use of the older version of this method in substitution of the CNOSSOS one for wind farms noise modelling, because the latter does not have a known official document with the necessary adaptations [6]. Another comparative study between CNOSSON and the older version of ISO9613-2 focused on low frequencies noise modelling was carried out in 2023 [7]; which shows that the differences between the levels calculated using the two propagation models and the measurements taken can reach up to 25 dB. The authors of this other comparative study in 2023 identify several possible factors contributing to these differences, such as the height of the source being well above the limit defined by the models, the value of the ground factor related to the angle of incidence of the sound wave on the terrain, inaccuracies in the ground and air absorption coefficients, and the inability to directly account for wind speed and direction in the models. They also noted that the results obtained using the CNOSSOS-EU method are 3 dB lower than those obtained using the ISO 9613-2 method [7]. Section 2 illustrates, step by step, the proposed procedure for the predictive assessment of acoustic impact. Section 3 outlines the main characteristics of the propagation models used in this study. Section 4 presents the real case study under investigation. Section 5 reports and discusses the results, while Section 6 addresses the conclusions and future perspectives.

2. Predictive acoustic assessment of a wind farm

Even if the Decree issued by the Ministry of Ecological Transition on June 1, 2022 does not provide any indication for the predictive assessment of acoustic impact of wind farms, this section reports a procedure that tries to be as compliant as possible to the criteria defined by the decree. A similar approach was introduced by D'Alessandro et al. in 2024 [8]. The procedure consists of five main steps, applicable to both new installations and those undergoing repowering:

- Analysis of the plant design,
- Acoustic characterization of the project area,
- Measurement campaign,
- Acoustic modelling,
- Compliance check with regulatory limits and potential mitigation measures

2.1 New wind farm

The first step in the predictive assessment of the acoustic impact of a new wind farm involves a thorough analysis of the project, with particular focus on the characteristics of the proposed turbines, local wind variability, and the features of the installation area, defined within a 1500-meter buffer zone around the turbines. This requirement is specified by Italian legislation in the Decree of the Ministry of Ecological Transition dated June 1, 2022 which sets out the criteria for measuring noise generated by wind farms. In particular, it is essential to obtain the following information for each turbine:

- Hub height,
- Rotor diameter,
- Acoustic emission characteristics

It is well known that the acoustic emissions of wind turbines are strongly dependent on wind speed at hub height. In order to account for the varying emissions as a function of wind speed, it is essential to analyse the historical wind speed distribution, which is commonly described by the Weibull distribution. This distribution is characterized by two parameters: the scale factor (A [m/s]) and the shape factor (k). Such data are generally available to the companies responsible for the design of the wind farms.

As for the installation area, all buildings located within the buffer zone must be identified, along with their intended use, to select those buildings for which acoustic exposure must be assessed, hereafter referred to as receptors. A detailed understanding of the local topography is also useful for developing the digital ground model (DGM), which is created during the acoustic modelling phase.

The second step concerns the acoustic characterization of the project area. The goal of the predictive acoustic impact assessment for a wind farm is to verify compliance with legal noise limits. However, Italian legislation currently does not define specific absolute emission limits for noise from wind turbine sources, nor does it establish special buffer zones with dedicated thresholds.

Therefore, the applicable limits are those defined by the acoustic zoning plans of the municipalities within the study area. These zoning plans divide the municipal territory into six acoustic classes, based on the land use of each zone. Prime Minister's Decree dated Novembre 14, 1997 [9] specifies the permissible noise levels for each class, distinguishing between daytime and nighttime periods, respectively from 6 a.m. to 10 p.m. and from 10 p.m. to 6 a.m. The noise levels considered in this study are immission levels, defined as the total environmental noise levels measured in the vicinity of the receivers, i.e., the dwellings of residents affected by acoustic emissions from sources present in the area.

The six acoustic classes are reported in Table 1, with immission limits expressed in dBA for both daytime and nighttime periods.

Table 1 Acoustic classes definitions and limits, from Italian Prime Minister's Decree dated Novembre 14, 1997

Acoustic classes	Definition	Daytime limit [dBA]	Nighttime limit [dBA]
Class I	Particularly protected areas	50	40
Class II	Predominantly residential areas	55	45
Class III	Mixed-use areas	60	50
Class IV	Areas of intense human activity	65	55
Class V	Predominantly industrial areas	70	60
Class VI	Exclusively industrial areas	70	70

It is therefore essential to obtain the acoustic zoning maps of all municipalities located within the study area.

Exceedances of absolute emission limits are rare in the case of noise generated by wind farms. However, differential emission limits often present a more significant issue. The differential limit is defined by Italian legislation in the cited Prime Minister's Decree dated Novembre 14, 1997, as the arithmetic difference between the environmental noise level and the residual noise level, the latter being the level measured in the ante operam scenario, i.e., in the absence of the wind farm. The differential emission limit must not exceed 5 dBA during the daytime and 3 dBA during the nighttime. The Italian legislation establishes an applicability threshold of 50 dBA during daytime and 40 dBA during nighttime, below which the differential limit is not applied.

Almost all cases of limit exceedance associated with wind farms involve differential limits during nighttime hours.

The third step concerns the measurement campaign, which must provide three types of data:

- Sound level measurements,
- Meteorological data,
- Road traffic data (where necessary).

The objective of the sound level measurements is to estimate the typical background noise within the project area in the absence of any acoustic emissions from the wind farm.

In order to obtain data representative of the entire area, the project site is divided into acoustically homogeneous zones, which are characterized by similar soundscape conditions, due to the presence of uniformly impacting sources in the area and territorial continuity, i.e., absence of morphological obstacles to sound propagation. Appropriate measurement points are identified to characterize each zone. Sound level measurements should preferably have a minimum duration of 24 hours and must be conducted in dry weather conditions and with wind speeds below 5 m/s at microphone height, as defined by Italian legislation in the Decree of the Ministry of the Environment dated March 16, 1998 [10]. Microphone is commonly placed at 4 meters from the ground.

The purpose of the meteorological measurements is to identify the time intervals that must be excluded due to precipitation or wind speeds exceeding 5 m/s. These measurements are taken at a height approximately equal to that of the microphone.

If the study area is interested by road traffic noise, road traffic measurements provide flow rate and speed data by vehicle category, which are required as input for the acoustic modelling of road infrastructures within the project area. This allows for an accurate estimation, at the facade of each receptor, of the contribution from road traffic noise.

The fourth step concerns the acoustic modelling of the wind farm and the road infrastructures located within the study area.

The modelling is carried out using an acoustic simulation software (in the present case SoundPLAN 9.1 was used) and consists of the following steps:

- Geographical characterization of the area,
- Definition and localization of noise sources and receptors,
- Acoustic characterization of the sources,
- Execution of the calculation,
- Validation of the acoustic model

For the geographical characterization of the area, the following cartographic data must be included: the infrastructure network, existing buildings, contour lines, and elevation points. The creation of the Digital Ground Model (DGM) from these cartographic inputs represents the first geographic input for the acoustic model. A subsequent review and possible correction of elevation points affected by errors is applied to the DGM, with the aim of aligning it as closely as possible to the actual morphology of the territory. This step is essential for accurately modelling sound propagation, considering natural obstacles as realistically as possible.

The analysis of cadastre data allows the identification of buildings where the noise levels after the realization of the proposed wind farms needs to be simulated. The following step involves the characterization of the noise sources. Specifically, for each wind turbine, the following information is required:

- Exact location,
- Hub height,
- Rotor diameter,
- Acoustic emission data in 1/3 Octave bands, both for standard operating mode and for any reduced-noise operating modes.

The acoustic emission data must be provided as a function of wind speed at hub height. This approach allows to consider that the noise power level depends from the wind velocity. It is worth noting that all the wind turbines work between a minimum (cut-in) and a maximum (cut-off) wind speed.

The acoustic emission data must be provided as a function of wind speed at hub height, to associate each turbine with its noise emission level for all wind speeds from cut in to cut off.

As for the road infrastructure, traffic flow and vehicle speed data by category, required as input for the model, are obtained through road traffic measurements lasting at least 24 hours.

The calculation phase provides the noise level emitted by wind farms and road infrastructures; then the following values are estimated:

- Background noise: noise levels obtained from noise measurements without the impact of the existing roads, object of a devoted simulation;
- Residual Noise Level (*Residuo* in Italian): Energetic sum of the Background noise and of the noise simulation of the existing roads object of a devoted simulation. The Residual noise is an indicator of the noise climate in the area *without* the realization of the studied wind-farm;
- Environmental Noise Level (*Ambientale* in Italian): Energetic sum of the Residual Noise and of the Wind farm noise contribution. The Environmental Noise Level is an indicator of the noise climate in the area after the realization of the studied wind farm.

Model validation can be carried out in the post-operational phase through a new measurement campaign.

The fifth and final step concerns the verification of compliance with legal noise limits, both in terms of absolute and differential immission limits.

In the event of exceedance of the limits, mitigation measures are proposed to reduce immission levels to values within legislation thresholds. These measures may include the activation of reduced-noise operating modes at specific wind speeds at hub height. If the project does not foresee such operating modes, mitigation strategies may involve the shutdown of specific turbines at critical wind speeds or, where feasible, the operation of turbines at reduced rotational speed, corresponding to the typical behaviour observed at lower, non-critical wind speeds.

2.2 Repowering of wind farms

Repowering of a wind farm involves replacing existing turbines with new, higher-efficiency turbines, thereby increasing the total energy output of the installation while simultaneously reducing the overall number of turbines.

About the predictive acoustic impact assessment in the case of repowering, the procedure is the same as that described in section 2.1 for new installations.

The only substantial difference lies in the pre-operational scenario, as the turbines of the existing plant—those that are to be replaced—must remain shut down during the measurement campaign, to exclude their acoustic contribution from the background noise level of the project area. The Decree issued by the Ministry of Ecological Transition on June 1, 2022 also provides a measurement methodology to obtain background noise (along with the emission levels) without shutting down the wind turbines; however this methodology is too time and cost consuming to be applied with the only scope of obtaining the background noise.

During the measurement campaign, it is necessary to identify, for each measurement point, the impacting turbines of the existing installation, defined as those located within a 1500-meter radius of the measurement point.

When planning the measurement campaign in the context of a repowering project, the selection of measurement points must take this additional parameter into account, with the objective of minimizing the number of wind turbines that need to be shut down during measurements, so reducing as much as possible the economic loss for the wind farm owner.

3. Noise model propagation

As previously discussed in Section 2, the noise emitted by wind turbines has a significant impact over long distances, typically up to 1500 meters. As a result, sound propagation in the surrounding environment is of critical importance for accurate acoustic modelling.

A more in-depth analysis of the propagation mechanisms of noise generated by wind turbines is detailed in *Handbook of Wind Energy Aerodynamics* [11].

This article considers three models for outdoor noise propagation:

- CNOSSOS-EU: Standardized European method establishing common noise assessment methods according to Directive 2002/49/EC;
- ISO 9613-2:1996: International Standard general method of calculation for attenuation of sound during propagation outdoors;
- ISO 9613-2:2024: update of ISO 9613-2.

Table 2 presents the meteorological conditions considered by the three investigated propagation models.

Table 2 Meteorological conditions considered by the three investigated propagation models

Propagation model	Meteorological conditions
CNOSSOS EU	Favourable conditions: positive vertical gradient Homogeneous conditions: null gradient (also used to approximate negative gradient) Long-term noise level: computed as the energy-weighted sum of the previous two, weighted according to the percentage p of time during which favourable conditions occur.
ISO 9613-2:1996	Short-term downwind noise level: wind direction within a 45° angle relative to the source–receiver axis (with wind blowing toward the receiver), and wind speed between 1 m/s and 5 m/s at heights between 3 m and 11 m. The model also applies under positive vertical gradient conditions. Long-term noise level with meteorological correction C_{met} : correction term dependent on source and receiver heights and their mutual distance is applied for the calculation of the long-term sound level, which also accounts for propagation-unfavourable conditions.
ISO 9613-2:2004	Meteorological correction based on the angular direction of the wind

In addition to meteorological conditions, ISO 9613-2:2024 introduces the following substantial updates compared to ISO 9613-2:1996:

- Revisions in ground effect modelling,
- Revisions in barrier effect modelling,
- Reflections from curved surfaces,
- Revision in attenuation due to vegetation,
- Meteorological correction based on the angular direction of the wind,
- Introduction of Annex D, specifically dedicated to the propagation of noise generated by wind power plants

Annex D defines the equivalent wind source as a point source located at the centre of the rotor. It limits the barrier attenuation to 3 dBA and restricts the Ground Factor to values lower than 1. It requires the calculation of C_0 (factor, in decibel, which depends on local meteorological statistics for wind speed and direction, and temperature gradient, present in C_{met} formula) at rotor height, and specifies ground attenuation also for concave surface topographies.

4. Real case study for new wind farm

The procedure described in Section 2 was applied to five new wind farms plans, four of which consist of a single turbine, and one consisting of two turbines. The wind farms are referred to as WF1, WF2, WF3, WF4 and WF5.

Table 3 reports the turbine characteristics for each site, along with the Weibull distribution parameters (scale factor A [m/s] and shape factor k) representative of the respective areas.

Table 4 shows the total number of buildings, the number of receptors identified and the acoustic zoning classes within each of the five project areas.

Table 3 Turbine characteristics and Weibull parameters for the wind farms used as case studies

Farm	Hub height [m]	Rotor diameter [m]	Nominal power [MW]	A [m/s]	k
WF1	61	99.5	1	6.9	1.83
WF2	78.3	82	3	9.1	1.98
WF3	61	99.5	1	8.1	1.98
WF4	132.5	175	6	7.5	1.70
WF5	69	61	1	7.0	1.85
	74.5	71	1		

Table 4 Number of building, receptors and acoustic classes for each wind farm

Wind farm	Buildings	Receptors	Acoustic classes
WF1	548	548	I,II,III,IV,V
WF2	93	73	V
WF3	7	7	V
WF4	85	26	II,III
WF5	480	480	II,III,IV

The total number of receptors across the five wind farms is 1134, located within acoustic classes I,II,III,IV,V, which correspond to permissible limits from 50 dBA to 70 dBA for daytime and from 40 dBA to 60 dBA for nighttime.

4.1 Noise citizen exposure assessment

The assessment of background noise in the project areas is essential to evaluate the future acoustic exposure of residents due to wind farm operations. For this purpose, a measurement campaign was conducted in each area, dividing the territory into acoustically homogeneous zones. For each area, five measurement points were selected to provide representative spatial coverage, ensuring at least one point per homogeneous zone.

Where road infrastructures with non-negligible noise emissions were present, traffic measurements were carried out using radar instruments, to characterize traffic noise for use in the acoustic modelling phase.

Table 5 reports the number of measurement points, the number of homogeneous zones, and the monitored road infrastructures for each wind farm. Figure 1 shows an example of the measurement points and homogeneous areas for the WF5 wind farm.

Anomalous events, rainy or characterized by a wind velocity higher than 5 m/s were excluded to the noise measurements. After realizing this filter operation, at each building existing in the assessment areas were assigned the corresponding background level. Then the *Residuo* and *Ambientale* noise level were calculated as reported in section 2.1. The predictive acoustic impact assessment was carried out for all five wind farms using the CNOSSOS-EU common European method as the propagation model.

Section 5 presents the results obtained for each site, the comparison with the legal limits set by Italian regulations, and any mitigation measures proposed in cases where exceedances were identified.

Table 5 Number of measurement points, homogeneous zones and monitored road infrastructures for each wind farm

Wind Farm	Measurement points	Homogeneous zones	Measured road infrastructures
WF1	5	3	2
WF2	5	2	2
WF3	5	1	1
WF4	5	1	1
WF5	5	2	1

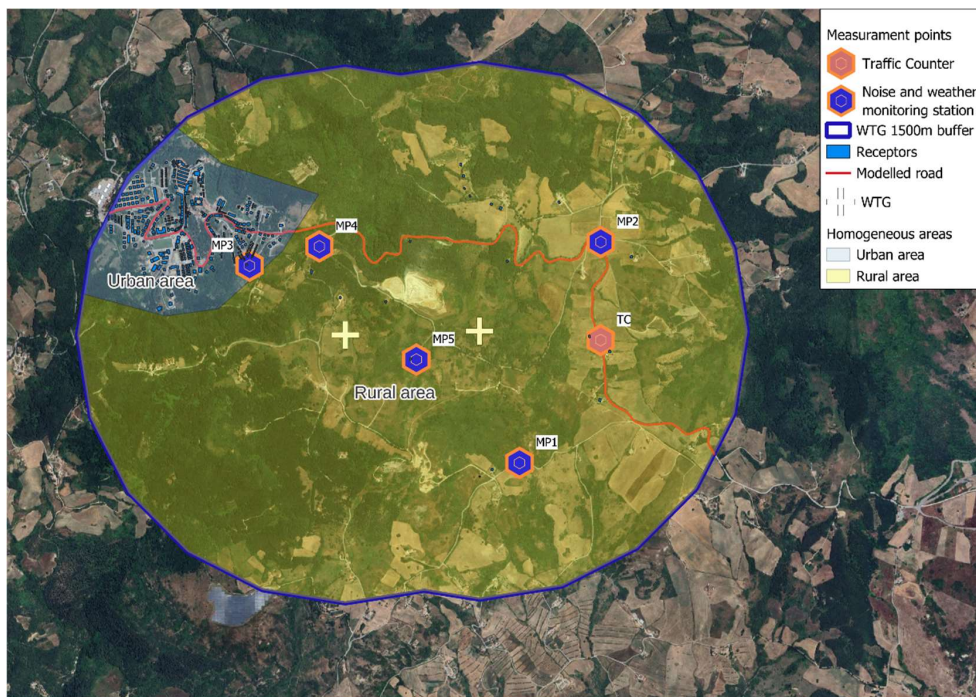


Figure 1 Measurement points and homogeneous areas for WF5

4.2 Noise model propagation comparison

The three propagation models described in Section 3 were applied to the five wind farms examined in this study.

The comparison was conducted separately for the daytime and nighttime periods and was limited to receptors with noise levels exceeding 45 dBA during daytime and 35 dBA during nighttime.

The following parameters were evaluated:

- Number of calculation points for which each model yields the highest predicted noise level,
- Mean differences between the models as a function of the Ground Factor (GF 0, GF 0.5, GF 1)

The parameters listed in the second point were subsequently evaluated using a 40 dBA threshold during the daytime period.

5. Results and discussion

The results illustrate the noise exposure of residents in the real case studies using the CNOSSOS propagation model. If needed, mitigation measures are proposed to reduce the levels below the regulatory thresholds.

In addition, the results obtained using the three propagation models CNOSSOS-EU, ISO9613-2:1996 and ISO9613-2:2024 are also evaluated and compared.

5.1 Real case study citizen exposure

The acoustic modelling carried out for the wind farms analysed in this study produced facade-level results for each building identified as a receptor. In compliance with Italian legislation, noise levels were calculated at one meter from the façade. The assessment was carried out for each facade and each floor of the building; the studies investigate 1134 receptors and 16582 calculation points.

Table 6 reports, for each wind farm, the total number of receptors and facade points, the number of receptors and facade points exceeding the limits set by Italian regulations, the time period (daytime or nighttime) in which the exceedance occurred, and the type of limit violated (absolute or differential).

Table 6 Summary of legal threshold exceedances across wind farms

Wind Farm	N°receptors	N°façade points	N°Receptors exceeding limits	N°Façade points exceeding limits	Limit exceedance period	Limit violated
WF1	548	7497	2	15	Nighttime	Differential
WF2	73	4296	2	11	Nighttime	Differential
WF3	7	96	1	1	Nighttime	Differential
WF4	26	276	1	3	Nighttime	Differential
WF5	480	4417	1	6	Nighttime	Differential

Out of a total of 1134 receivers, exceedances of legal noise limits were identified in 7 receivers, specifically in 36 calculation points. All exceedances refer to the nighttime period and the differential limit. No exceedances were observed for the absolute immission limit, nor for the differential immission limit during the daytime period.

Figure 2 shows, as an example, the two receptors that exceed the differential limits during the nighttime period in the case of the WF1 wind farm.

Table 7 reports, for each wind farm, the maximum exceedance recorded, the period and type of limit exceeded, the arithmetic mean of the noise levels corresponding to all exceedances, and the standard deviation.

At the 7 receivers where legal thresholds were exceeded, differential noise levels during the nighttime period ranged from 12.1 dBA to 3.6 dBA, in comparison with the maximum differential level of 3 dBA permitted by Italian law during the nighttime period. For each wind farm, mitigation scenarios were evaluated through acoustic modelling, including reduced-emission operating modes and the installation of turbines equipped with a TES system. In the most critical case, recorded at the WF1 site with a differential level of 12.1 dBA, no mitigation measures at the source were considered. Instead, mitigation solutions with direct intervention at the receiver have been agreed upon.

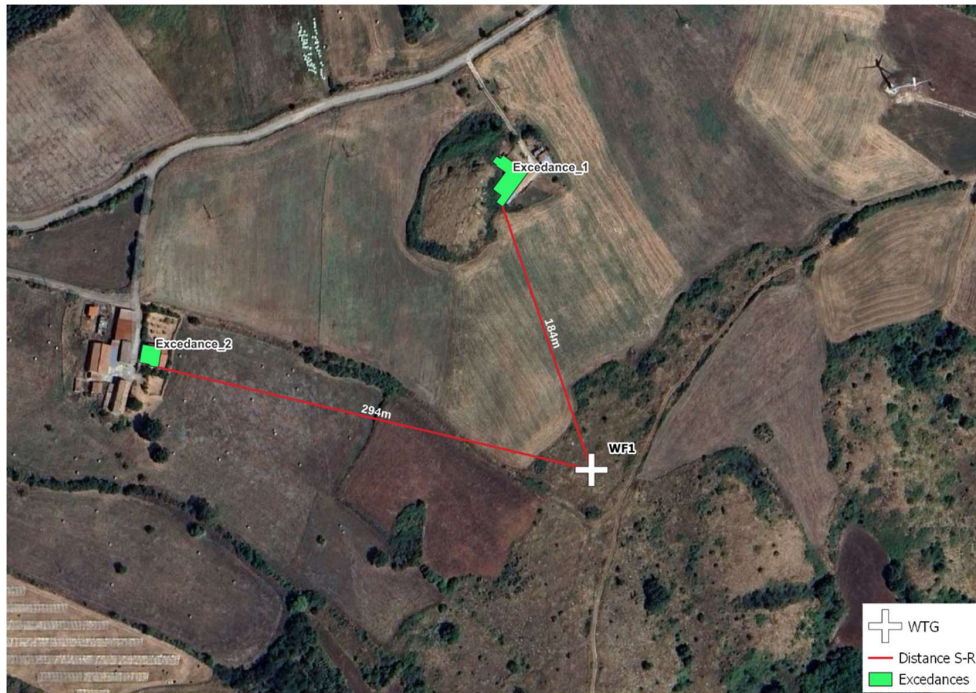


Figure 2 Receptors that exceed the differential (Differenziale) limits during nighttime period in WF1

Table 7 Exceedance parameters for each wind farm

Wind Farm	Maximum exceedance [dBA]	Average exceedance [dBA]	Standard deviation Exceedance [dBA]	Exceedance period and limit violated
WF1	12.1	7.4	2.2	Nighttime differential limit
WF2	3.7	3.4	0.2	Nighttime differential limit
WF3	3.6	3.6	-	Nighttime differential limit
WF4	5.2	5.2	0	Nighttime differential limit
WF5	4.2	3.8	0.3	Nighttime differential limit

5.2 Proposal noise mitigation

The proposed mitigation measures were derived by analysing the results of acoustic simulations carried out considering reduced operational emission modes and the installation of turbines equipped with TES system. The proposed mitigation measures include:

- Use of reduced-noise operating modes at specific wind speeds during the nighttime period,
- Shutdown of the wind farm above certain wind speeds during the nighttime period,
- Installation of turbines equipped with Trailing Edge Serration (TES),
- Receiver-targeted interventions (i.e. replacement of existing windows with sound insulating ones).

Table 8 presents the mitigation strategies planned for each of the five wind farms, along with the pre-mitigation and post-mitigation noise levels for the highest differential level, except for the case of WF1 and WF4, where mitigation measures allow the environmental noise level to be reduced below 40 dBA for the nighttime period, making the differential limit not applicable.

Table 8 Proposed mitigation measures for each wind farm

Wind Farm	Proposed mitigation measures	Pre-mitigation differential [dBA]	Post-mitigation differential [dBA]
WF1	Installation of turbines equipped with Trailed Edge Serration (TES) Receiver-targeted interventions	7.7	Environmental noise < 40 dBA
WF2	<i>Option 1</i> - Reduced noise operating for wind speed equal to 9 m/s	3.7	2.9
	<i>Option 2</i> - Installation of turbines equipped with Trailed Edge Serration (TES)	3.7	2.6
WF3	<i>Option 1</i> - Shutdown of the wind farm for wind speed higher than 10 m/s during the nighttime period	3.6	2.8
	<i>Option 2</i> - Installation of turbines equipped with Trailed Edge Serration (TES)	3.6	2.0
WF4	Reduced noise operating for wind speed higher than 8 m/s	5.2	Environmental noise < 40 dBA
WF5	Installation of turbines equipped with Trailed Edge Serration (TES)	4.2	2.5

In the case of receiver-targeted interventions in WF1, the pre-mitigation and post-mitigation levels is not reported, as extent of exceedance must be verified during the post-operational phase, to determine the most appropriate and site-specific mitigation approach.

In the cases of WF2 and WF3, two mitigation options have been proposed: one involving the use of the TES, and the other based on reduced operational modes with lower acoustic emissions at certain wind speeds. Both options bring the differential limit below 3 dBA; however, the use of a turbine equipped with TES results in a more effective reduction of acoustic impact in both farms.

5.3 Noise model propagation difference in citizen exposure

A comparative analysis was carried out to investigate the difference of the outcome of three simulation model (CNOSSOS, ISO9613-2:1996 and ISO 9613-2:2004) in the five real case studies. The comparison was limited to the calculation points where the noise impact of the wind turbines was considered significant:

- higher than 45 dB(A) in the daytime;
- higher than 35 dB(A) in the nighttime.

Consequently, the comparative analysis considered 4365 calculation points. The first object of the work was to understand which noise simulation model is more conservative among the others. At this purpose, Table 9 reports the number of calculation points for which each of the three tested models simulate the highest noise level, in both daytime and nighttime. It is worth noting that these results were obtained without varying noise emissions, receivers and source position or other factors that may interfere with noise propagation. These results were all obtained considering a ground factor of 0 (reflective ground).

Table 9 Daytime and Nighttime calculation points with highest level for propagation model

Propagation model	Daytime number of highest calculation points	Nighttime number of highest calculation points
CNOSSOS EU	87	101
ISO 9613-2:1996	33	33
ISO 9613-2:2004	4245	4231

The results shown in Table 9 identify ISO 9613-2:2024 as the propagation model that yields the highest noise levels for most of the calculation points considered, both in daytime and nighttime.

The second step of the work is to define how the ground factor influences the results of the comparative analysis. Table 10 shows the average difference between the outcomes of the three noise simulation models varying ground factor and time period. It is worth noting that the analysis was limited to the 4365 calculation points where the noise impact of the wind farms was considered relevant.

The second and third columns of Table 10 reports respectively, for ground factor equal to 1, 0.5 and 0, the average difference of the noise levels calculated using CNOSSOS-EU and ISO9613-2:1996 propagation models in daytime and nighttime. For this set of data, ISO 9613-2:1996 noise propagation model tends to estimate higher sound pressure levels compared to the CNOSSOS-EU. The difference between the two models is greater in the nighttime and for high-reflective ground.

The fourth and fifth columns of Table 10 reports respectively, for ground factor equal to 1, 0.5 and 0, the average difference of the noise levels calculated using CNOSSOS-EU and ISO 9613-2:2024 propagation models in daytime and nighttime. The comparison shows that the effect of the ground factor is more relevant in the ISO 9613-2:2024 than in the CNOSSOS-EU. In nighttime the new ISO model causes higher level compared to the CNOSSOS-EU, while in the daytime we observed the opposite behaviour.

The sixth and seventh columns of Table 10 reports respectively, for ground factor equal to 1, 0.5 and 0, the average difference of the noise levels calculated using ISO 9613-2:1996 and ISO 9613-2:2024 propagation models in daytime and nighttime. Except for ground factor equal to 0 case, in the daytime the older propagation model tends to estimate higher level compared to the more recent one. In the nighttime, we observed that for ground factor equal to 0.5 and 0, the more recent model estimates higher level compared to the 1996 one.

It is worth noting that practically in all the daytime scenarios with ground factor equal to 0, the difference among the outcomes of the three noise propagation models is minimal.

The difference between the outcomes of these models is influenced by how these simulation models compute the effect of the ground factor and the meteorological conditions.

Specifically, both versions of ISO 9613-2 consider wind directions within a 45° angle relative to the source–receiver axis, while CNOSSOS makes no such assumption. As a result, CNOSSOS tends to predict lower noise levels.

The difference between the outcomes of the new and old ISO-9613-2 are caused by several aspects:

- the most recent one fixes a limit of the sound attenuation of elements that obstruct noise propagation of noise emitted by a wind farm;
- the most recent one considers the effect of concave-shaped ground.

Table 10 Average difference between propagation models as a function of Ground Factor, with threshold level of 45 dBA in daytime and 35 dBA in nighttime

Ground Factor	CNOSSOS EU - ISO9613-2:1996		CNOSSOS EU - ISO9613-2:2024		ISO9613-2:1996 - ISO9613-2:2024	
	Daytime [dBA]	Nighttime [dBA]	Daytime [dBA]	Nighttime [dBA]	Daytime [dBA]	Nighttime [dBA]
1	-3,0	-3,7	1,2	-3,3	4,2	0,4
0.5	-1,5	-2,1	0,7	-3,5	2,2	-1,4
0	0,0	-0,5	0,1	-3,9	0,0	-3,4

The comparative analysis was repeated by lowering the daytime threshold from 45 dBA to 40 dBA, to examine the behaviour of the propagation models over a broader range of environmental noise levels. Data about the new comparative analysis are reported in Table 11. The main observed consequence is that the outcomes in the daytime period with reflective ground are not comparable as observed in Table 10.

Except for the ground factor equal to 1 case, the ISO 9613-2:2024 noise simulation model tends to estimate higher level compared to the other ones. Nevertheless, the norm established that for wind farm assessment the condition GF=1 should be always excluded.

The new model tends to limit the sound attenuation compared to the other noise models; this is the cause of the difference between data reported in Table 10 and Table 11 for daytime.

Lowering the assessment thresholds, also the difference from the outcome of all the ISO models from the CNOSSOS one increases. Nevertheless, the following behaviour was observed:

- considering the older ISO 9613-2 method, the higher the ground factor, the higher the noise impact on receivers compared to CNOSSOS;
- considering the new ISO9613-2 method, the lower the ground factor, the lower the noise impact on receivers compared to CNOSSOS. The difference remains negative, so in average the noise impact calculated with the new ISO9613-2 is higher compared the CNOSSOS.

Table 11 Average difference between propagation models as a function of Ground Factor, with threshold level of 40 dBA in daytime and 35 dBA in nighttime

Ground Factor	CNOSSOS EU - ISO9613-2:1996		CNOSSOS EU - ISO9613-2:2024		ISO9613-2:1996 - ISO9613-2:2024	
	Daytime [dBA]	Nighttime [dBA]	Daytime [dBA]	Nighttime [dBA]	Daytime [dBA]	Nighttime [dBA]
1	-3,7	-3,7	-2,7	-3,3	1,0	0,4
0.5	-2,1	-2,1	-3,0	-3,5	-0,9	-1,4
0	-0,5	-0,5	-3,4	-3,9	-2,8	-3,4

Figure 3 shows an example of the difference in predicted levels between the CNOSSOS-EU and ISO 9613-2:2024 models for the WF5 1–2 wind farm, which consists of two turbines, for the nighttime periods. Figure 4 shows the same difference map in 3D version. In the two figures the following scale was used:

- The coloured areas represent areas where the noise levels calculated with ISO 9613-2:2024 are higher compared to CNOSSOS-EU ones;
- White areas where the difference between the outcomes of the two models are not relevant;
- Grey-scaled areas where the noise levels calculated with CNOSSOS-EU are higher compared to ISO 9613-2:2024 ones.

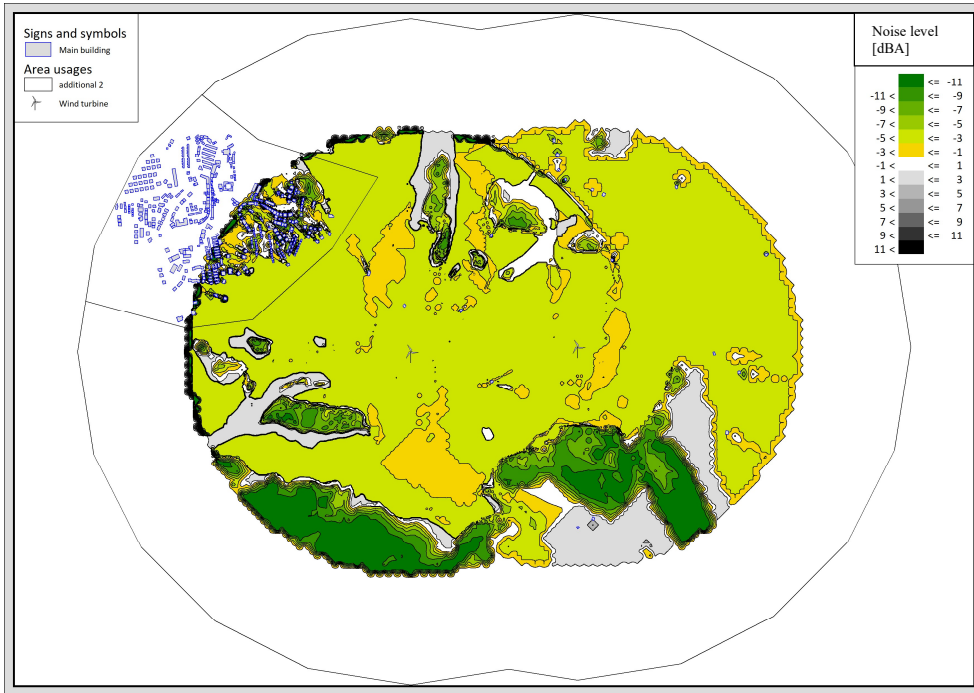


Figure 3 Difference in predicted level between CNOSSOS EU and ISO 9613-2:2004 for WF5, 2D version

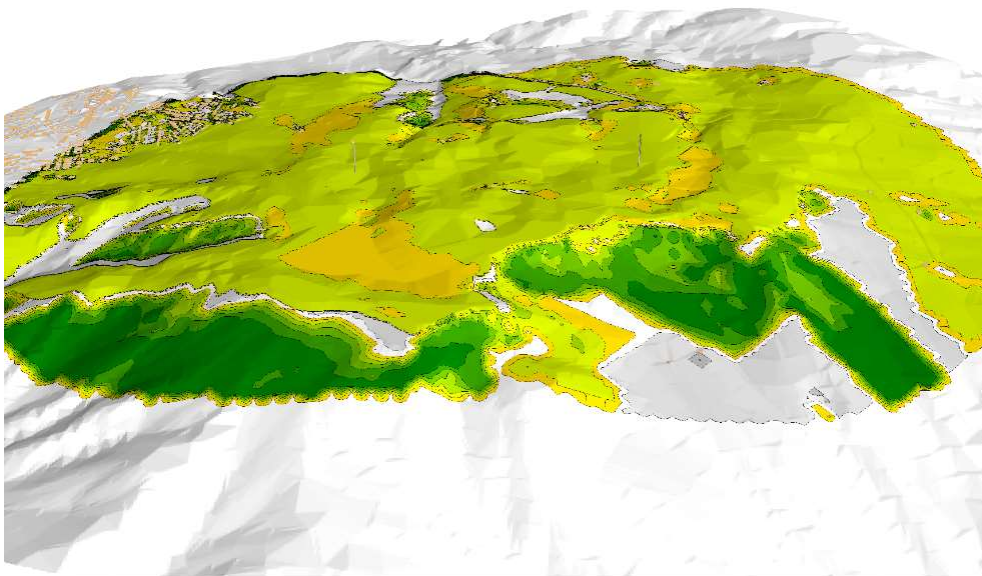


Figure 4 Difference in predicted level between CNOSSOS EU and ISO 9613-2:2004 for WF5, 3D version

As expected, the Figure 3 and Figure 4 graphically show that differences increase at the edges of the 1500-meter buffer zone around the turbines, where the noise levels are lower. The impact of CNOSSOS-EU tends to be higher over some shadowing ground or building geometries, particularly where the concave

correction of the new ISO96-13:2024 is not applicable. Similar results were obtained for all the five real case studies.

It is worth noting that the cases where CNOSSOS-EU tends to estimate higher levels compared to the ISO9613-2:2024 are not relevant for what concern a noise impact assessment. Where the highest noise impact occurs (close to the wind farm and without shadowing object) the noise impact calculated using the ISO9613-2:2024 propagation methods is practically always higher than the CNOSSOS one. Nevertheless, the difference between the outcome of the two models are less relevant close to the wind farm or in absence of elements working as noise propagation barriers.

6. Conclusions

This article describe a methodology for the assessment of noise impact from new wind power plants and repowered installations compliant with Italian legislative framework. The approach includes the collection of technical design data, the analysis of the morphological, residential, and acoustic characteristics of the study area, and the execution of a measurement campaign to determine the existing background noise levels. It also involves the acoustic modelling of noise emissions from wind turbines using the CNOSSOS-EU propagation model, as well as from other potential transport infrastructures, followed by a comparison with the legal limits established by Italian regulations, and the proposal of appropriate mitigation measures.

Moreover, a comparative analysis based on a real-world case study involving five wind farms is presented. The analysis is focused on defining the difference in terms of noise impact assessment of three different acoustic propagation models, CNOSSOS-EU, ISO 9613-2:1996, ISO 9613-2:2024. The study was carried out considering three different values of the ground factor, in daytime and nighttime period.

The study identified 7 buildings where the Italian legislative limits were overtaken. The exceedance occurred in the nighttime only for the differential noise level (*differenziale*). Mitigation measures were proposed and evaluated; the measures allowed to keep the noise impact compliant to the Italian legislation. The proposed mitigation strategies included the use of reduced-emission operational modes or turbine shutdown at certain wind speeds during the nighttime, the implementation of turbines equipped with TES systems, or direct intervention at the receivers.

The comparative analysis between the different acoustic propagation models shows that the ISO 9613-2:2024 tends to estimate higher noise levels on receivers compared to the older ISO 9613-2:1996 and the CNOSSOS-EU. Nevertheless, the difference between the outcomes of the new ISO 9613-2 method with the CNOSSOS-EU is limited where the highest noise impacts happen. However, it is evident that the characteristics of the updated ISO 9613-2 reduce the influence of elements acting as noise barriers and estimate that the noise is more able to propagate compared to the other two models. This phenomenon is more evident for reflective grounds.

The methodology presented in this article opens the way for future developments. Of particular interest will be the comparison between modelled results and actual measured noise levels at receiver locations following turbine installation, to evaluate the performance of the three propagation models in real-world scenarios. Further validation involving other models such as NORD2000 and CONCAWE is also foreseen. About the proposed procedure for noise impact assessment, the most relevant direction for future development concerns the integration of the wind farm's electricity production into the evaluation of mitigation measures. The objective is to identify those mitigation strategies that allows to obtain noise impact compliant with legal limits and maximize energy production.

References

- [1] *DM 1 June 2022. Determinazione dei criteri per la misurazione del rumore emesso dagli impianti eolici e per il contenimento del relativo inquinamento acustico.*, Italy: Decree of the Ministry of Ecological Transition.
- [2] *COMMISSION DIRECTIVE (EU) 2015/996 establishing common noise assessment methods according to Directive 2002/49/EC of the*, 2015.
- [3] S. Kephalopoulos, M. Paviotti, F. Anfosso-Lédée, D. Van Maercke, S. Shilton and N. Jones, *Advances in the development of common noise assessment methods in Europe: The CNOSSOS-EU framework for strategic environmental noise mapping*, ELSEVIER, 2014.
- [4] *ISO9613-2 first edition. Acoustic-Attenuation of sound during propagation outdoors Part 2: General method of calculation*, 1996.
- [5] *ISO9613-2 second edition. Acoustics-attenuation of sound during propagation outdoors- Part 2: Engineering method for the prediction of sound pressure levels outdoors*, 2024.
- [6] V. Rosão, R. Leonardo and P. Santos, “Necessary adjustments in ISO 9613-2 and CNOSSOS (industries),” in *euronoise 2021*, Madeira, Portugal, 2021.
- [7] B. Stepień, T. Wszolek, D. Mleczko, P. Małeck, M. Kłaczyński and P. Pawlik, “Modelling low-frequency noise of wind turbines,” in *forumacousticu 2023*, Torino, 2023.
- [8] F. D'Alessandro, F. Artuso, G. Bai, M. Bernardini, A. Esposito and G. Pitò, “PROPOSTA PER UNA PROCEDURA PER LA VALUTAZIONE PREVISIONALE DI IMPATTO ACUSTICO DI IMPIANTI EOLICI IN CONFORMITÀ AL D.M. 01/06/2022,” in *50° Convegno Nazionale Associazione Italiana di Acustica*, Taormina, 2024.
- [9] *DPCM 14 November 1997. Determinazione dei valori limite delle sorgenti sonore.*, Italy: Decree of the President of the Council of Ministers, 1997.
- [10] *DM 16 March 1998. Tecniche di rilevamento e di misurazione dell'inquinamento acustico.*, Italy: Decree of the Ministry of the Environment, 1998.
- [11] B. Stoevesandt, G. Schepers, P. Fuglsang and Y. Sun, in *Handbook of Wind Energy Aerodynamics*, Springer, 2022, pp. 1397-1426.

Paper #42 - ID: 382

Title: Developing a coastal sound speed profile for propagation models

Author: Eugene McKeown

11th Edition of the
International Conferences on
Wind Turbine Noise

Copenhagen, Denmark – 10th to 13th June 2025

Developing a coastal sound speed profile for propagation models

Eugene McKeown¹ University of Galway, Galway, H91 TK33, Ireland

James Grogan Irish Centre for High-End Computing, Galway, H91 TK33, Ireland

Basanta Samal Irish Centre for High-End Computing, Galway, H91 TK33, Ireland

Denis O’Hora University of Galway, Galway, H91 TK33, Ireland

Darius Ceburnis Mace Head Atmospheric Research Station, Co. Galway, H91 N2R2, Ireland

Colin O’Dowd Mace Head Atmospheric Research Station, Co. Galway, H91 N2R2, Ireland

Eoin King University of Galway, Galway, H91 TK33, Ireland

Summary

Modelling wind turbine noise propagation for offshore wind turbines is a developing science. Engineering or empirical models for sound propagation modelling, such as ISO 9613-2 [1], have been advanced by the Danish Executive Order BEK 995 of 2024 [2] which describes a method that takes multiple reflections from the sea surface and the atmosphere into account. In specific weather conditions the lower part of the planetary boundary layer and the sea surface can form a sound channel with enhanced sound propagation. This lower section of the planetary boundary layer (the surface layer) depth may range from 30 m in static stability conditions to a few hundred metres in convective conditions. The depth is dynamic on a daily and seasonal basis and determines the sound speed profile.

Numerical methods such as Parabolic Equation modelling are more computationally intensive and can calculate propagation for specific atmospheric conditions. The accuracy of numerical models is however limited by the imperfect knowledge of the full range of atmospheric and ground conditions along the

¹ Corresponding author – Email: e.mckeown4@universityofgalway.ie

propagation path. In practice numerical methods are not used for environmental impact assessments, and impact is assessed based on empirical base methods.

Empirical sound propagation modelling is based on measurements of sources located close to the ground. With offshore wind turbine tip heights in excess of 300m this approach may need refinement. In order to address part of this knowledge gap, a meteorological measurement campaign is underway at Mace Head Atmospheric Research Station on the Irish west coast.

The dataset is being analysed on differing timescales and for statistical estimates of the variation around calculated central tendencies. It is planned that the resulting dataset will be used to validate specific propagation conditions to refine and validate noise propagation models. This paper outlines the instrumentation setup, the data collection and work completed to date.

1. Introduction

Wind turbine noise and amplitude modulation (AM) effects in particular, have been attributed to variations in wind speed (including wind shear effects) or wind direction (veer) over the rotor plane, or a combination of both. With increased rotor diameter of offshore turbines, the variation over the swept area could give rise to enhanced source variability. Increased turbine height may also have a significant role to play in how the noise propagates from the turbine to the receiver locations. Empirical approaches (based on sources near the ground) may not adequately consider some meteorological effects. As outlined by Attenborough and van Renterghem [3] noise propagation calculations require information on wind speed, direction, temperature, relative humidity and barometric pressure as a function of height near to the propagation path.

This paper outlines a study of meteorological influences on offshore wind turbine noise at a coastal site in Ireland. Mace Head Atmospheric Research Station is located west of Carna, County Galway Ireland as shown in **Figure 1**.

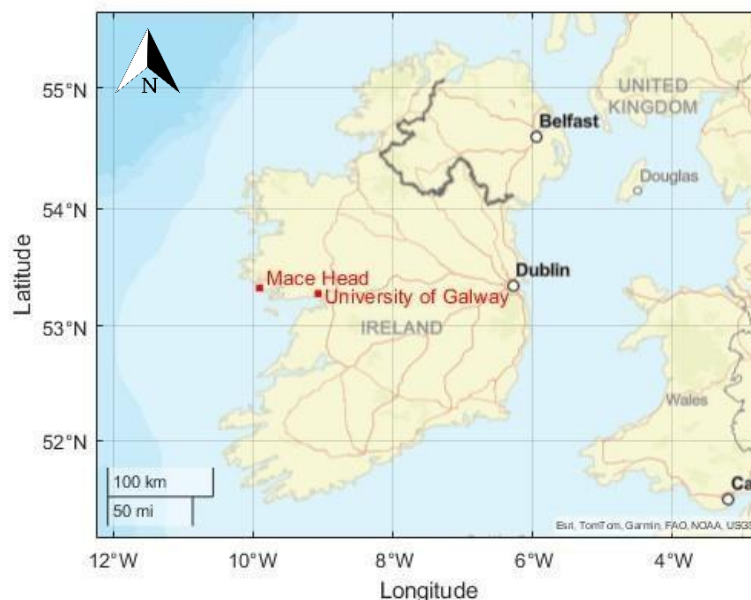


Figure 1 Mace Head Atmospheric Research Station and University of Galway Locations.

The research station site is co-located with a national weather service (Met Eireann <http://www.met.ie>) automatic weather station. A Marine Institute (<http://www.marine.ie>) ocean monitoring buoy is located to the west of the site. This provides a cluster of meteorological instruments at a coastal site on the west coast of Ireland.

The Mace Head Atmospheric Research Station near Carna, County Galway has been a site for atmospheric measurements since 1958. The location is unique in Europe, offering westerly exposure to the North Atlantic Ocean and a clean sector of South (180 degrees) through West to 300 degrees.

2. Instrumentation

Instrumentation on site includes a Vaisala-Leosphere LIDAR wind profiler (Lidar), a RPG-HATPRO infrared (IR) radiometer (Hatpro) and a Cloud Height Sensor/Ceilometer, CHM 15k. Data from these instruments will be combined with data from the weather station and the monitoring buoy. **Figure 2** shows a view of the instrumentation looking to the West.



Figure 2 Wind Profiler (Left,) IR Radiometer (Right) and Offshore Buoy (Central Red Dot)

2.1 Vaisala-Leosphere LIDAR wind profiler

The scanning Doppler lidar system is a Vaisala (formerly Leosphere) S200 unit. It measures atmospheric velocity and backscatter with high precision and a high sampling rate. The lidar has a maximum range of 9 km at low range resolution. The setup has now been optimised for scanning to the Atmospheric Boundary Layer (ABL) at high resolution. Standard scanning is a Directional Beam Swing (DBS) scan which comprise of a vertical beam and four beams at 70 degrees above the horizontal. Range Height Indicator (RHI) scans at fixed azimuth angles providing a vertical cross-section out over water and inland are carried out occasionally.

Table 1 Leosphere S200 setup parameters

Wavelength	1.5 μm (fully eye-safe)
Pulse energy	$\sim 50 \mu\text{J}$
Pulse rate	10 kHz
Range Resolution	25 m
Time Resolution	2 Hz (5000 pulse averages)
Velocity Precision	$\sim 5 \text{ cm/s}$
Minimum range	50 m
Maximum range	2.2 km (typically $\sim 1 \text{ km}$)
Platform	ground

The minimum measurement height is 50m above the Lidar measurement base.

2.2 RPG-HATPRO infrared radiometer

The HATPRO instrument is a stand-alone system for automated weather-station use. The system is passive with two frequency reception bands: 22-31 GHz (7 channel filter bank humidity profiler and Liquid Water Path radiometer) and 51-58 GHz (7 channel filter bank temperature profiler). The unit is fitted with a blower and a heater to minimise rain and condensation effects on the measurements.

Table 2 RPG-HATPRO setup parameters

Radiometric resolution	0.3 – 0.4 K RMS at 1.0 s integration time
Vertical resolution (RH)	800 m (range 5000-10000 m)
Accuracy (RH)	0.4 g/m ³ RMS (absolute hum.) 5% RMS (rel. humidity)
Minimum range	50 m
Maximum range	10 km
Radiometric resolution	0.3 – 0.4 K RMS at 1.0 s integration time
Platform	Ground

The Hatpro provides temperature, humidity and liquid water profiles to a height of 10 km. Higher resolution data is available in the 0-2 km range. The minimum measurement height is 50m above the Lidar measurement base.

2.3 Cloud Height Sensor/Ceilometer CHM 15k

The LUFFT (OTT HydroMet Fellbach GmbH) CHM 15k is a single-shaft backscatter Lidar cloud height sensor or ceilometer. It has a measuring range of up to 15 km (in 150 metre intervals). It detects cloud layers, cirrus clouds and aerosol layers and can be used to detect the boundary layer height. The lidar wavelength is 1064 nanometres and the high-resolution (5 metre intervals) data range is 5-155 metres.

2.4 Met Eireann automatic weather station

Met Eireann, Ireland's National Meteorological Service, operate an Automatic Weather Station at Mace Head since 2003. Observations are available in one-minute intervals for Air Temperature, Wind Speed and Direction, Rainfall, Atmospheric Pressure and Relative Humidity. Wind speed and direction are measured using a cup anemometer located approximately 10 metres above the Lidar measurement base.

2.5 Marine Institute oceanographic buoy

The Marine Institute, the State agency responsible for marine research, technology development and innovation in Ireland, operate a surface buoy approximately 2.3 km West-Northwest of the Lidar measurement base. Sea level is approximately 20 metres lower than Lidar Measurement base. The buoy provides data on the surface sea temperature which can be compared with the air temperature measured at the Met Eireann site.

3. Wind Turbine Noise Modelling

The Institute of Acoustics Good Practice Guide (IoAGPG) [4] was published in 2013 to present good practice in the application of the original 1996 guidance [5]. The modelling approach, based on ISO 96132, was refined to reflect the results of research carried out and experience gained in the 17 years since the original guidance was published. The 1996 guidance remains in place and a Supplementary Guidance Note [6] states that the guidance does not cover noise propagation for offshore wind farms.

The Danish Executive Order on noise from wind turbines, BEK 995, is the only statutory guidance on offshore wind turbine noise modelling. The empirical modelling approach is similar to ISO 9613-2 with a correction for multiple reflections for offshore turbines.

The turbine sound power levels (and therefore the predictions) and the background noise data (and associated noise limits) both refer to a standardised wind speed which is derived from the hub height wind speed using a simplified logarithmic roughness length formula. The formula is based on the Monin Obukhov similarity theory [7] but simplified for statically neutral conditions (windy, overcast negligible temperature advection).

Empirical models generally determine propagation losses based on ‘favourable propagation conditions’ such as downwind or under a thermal inversion. Statically neutral conditions do not coincide with worst case conditions. The simplified logarithmic relationship, when it is applicable, only applies to the Surface Layer (10-100 metres above ground level). With offshore wind turbine tip heights exceeding 300 metres the blades may be subjected to a range of sound speeds in each rotation cycle. In such circumstances a more advanced computational modelling approach may be required.

4. The Atmospheric Boundary Layer

Near-surface weather is determined in the part of the atmosphere called the (ABL). The ABL is the lower part of the atmosphere in which surface friction and surface heating effects vary considerably. Above the ABL is the ‘free atmosphere’ where such effects are less influential. Stull [7] defines the ABL as:

‘that part of the troposphere that is directly influenced by the presence of the earth's surface and responds to surface forcings with a timescale of about an hour or less’.

The boundary layer typically extends to a height of 1,000 metres but depth/thickness varies considerably. The boundary layer is thinner in high-pressure regions than in low-pressure regions and also changes with temperature variations near the ground. Rotach and Holtslag [8] further divide the lower part of the ABL into the Surface Layer and the Canopy Layer. They describe the Surface Layer as having a thickness of ~100m and the Canopy Layer as having a thickness of ~10 Metres. The thickness of the Canopy Layer is determined by vegetation, trees and buildings and is related to the roughness length.

Empirical calculation methods for wind turbine noise such as ISO 9613-2 and BEK 135 are derived from research where the source and receiver are located close to the ground i.e. within the Canopy Layer. Only a few studies have examined source heights in the 100-metre range or at distances greater than five kilometres [9], [10].

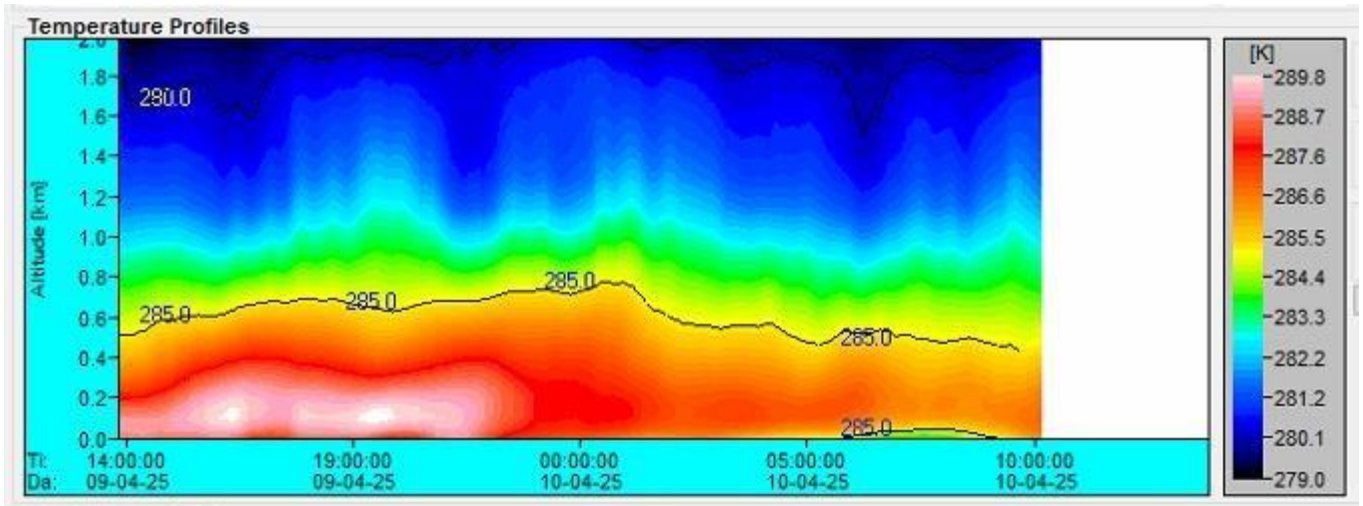


Figure 3 24-hour temperature profile showing a temperature inversion centred around turbine hub height

Waddington and Yam [11] described the importance of meteorological effects on long-distance (in their case 1008metres) as: ‘Measured sound pressure levels owe as much to near-surface weather as to ground shape and impedance and factors such as source and receiver heights and locations.’

5. Sound Speed

The earth’s atmosphere is a system driven by the heating and cooling of the sun and obeys the Gas Laws. A gas allowed to expand becomes cooler; the same volume of gas compressed into a smaller space becomes warmer. Pockets of air tend to rise and fall adiabatically in the atmosphere i.e. without an exchange of heat or mass. The composition and properties of the air determine the sound speed profile in the atmosphere. Over short distances in the Surface Layer, the speed of sound is considered as a constant. At greater heights however, the speed of sound changes and must be considered in propagation models.

The speed of sound in the atmosphere has been researched scientifically for air and space travel. Current practice is to calculate the speed of sound in dry air and then extrapolate this standard value for different heights in the atmosphere. This is generally calculated from a ‘standard’ mixture of gas components. With increasing accuracy of instrumentation and more frequent sampling of the atmosphere we now have extensive knowledge of how it changes.

5.1 Calculating sound speed

The speed of sound in the constituents of a standard atmosphere has been found to vary with temperature and humidity. The effects of humidity on the speed of sound in air at various temperatures were calculated [12] and the maximum uncertainty is estimated to be about 400 ppm or 0.136 m/s from the speed of sound in dry air in ISO 2533 [13].

The equation used by Wong and Embleton is the same as that used in ISO 2533:

$$c = \sqrt{\left(\frac{\gamma}{M} \times RT_0\right)} \quad (1)$$

Where: c is the speed of sound;
 γ is the specific heat ratio = 1.4;
M is the molar mass = 28.964420 kg·kmol⁻¹;

R is the universal gas constant = $8314.32 \text{ J}\cdot\text{K}^{-1}\cdot\text{kmol}^{-1}$;

and T_0 is the absolute temperature (in Kelvin)

From equation (1) it is clear that the temperature profile is the dominant parameter in calculating sound speed in the atmosphere.

6. Work to date

A measurement campaign was commenced in June 2024 with the objective of obtaining two years of high-resolution weather data. The Lidar is collecting DBS (vertical) scans continuously but is reprogrammed to collect two and three-dimensional data in specific weather conditions, e.g. when temperature inversions, stable and unstable atmospheric conditions arise. The two-kilometre range of the Lidar permits data to be obtained both onshore and offshore during the scan cycle.

Historical data for both the Lidar and Hatpro are available, but the Lidar data is for a longer distance range at lower resolution. Work is underway using the resources available through the Irish Centre for High End Computing (ICHEC) to integrate the historical Lidar, Hatpro, Met Eireann and Marine Institute data and interrogate the large dataset for specific weather events and statistical analysis of the combined data.

7. Preliminary results

Work is underway to compile the dataset so limited results are available at present. Preliminary results are showing the occurrence of temperature inversions in different seasons. We have also found some significant variations in wind speed and direction in the rotor plane zone.

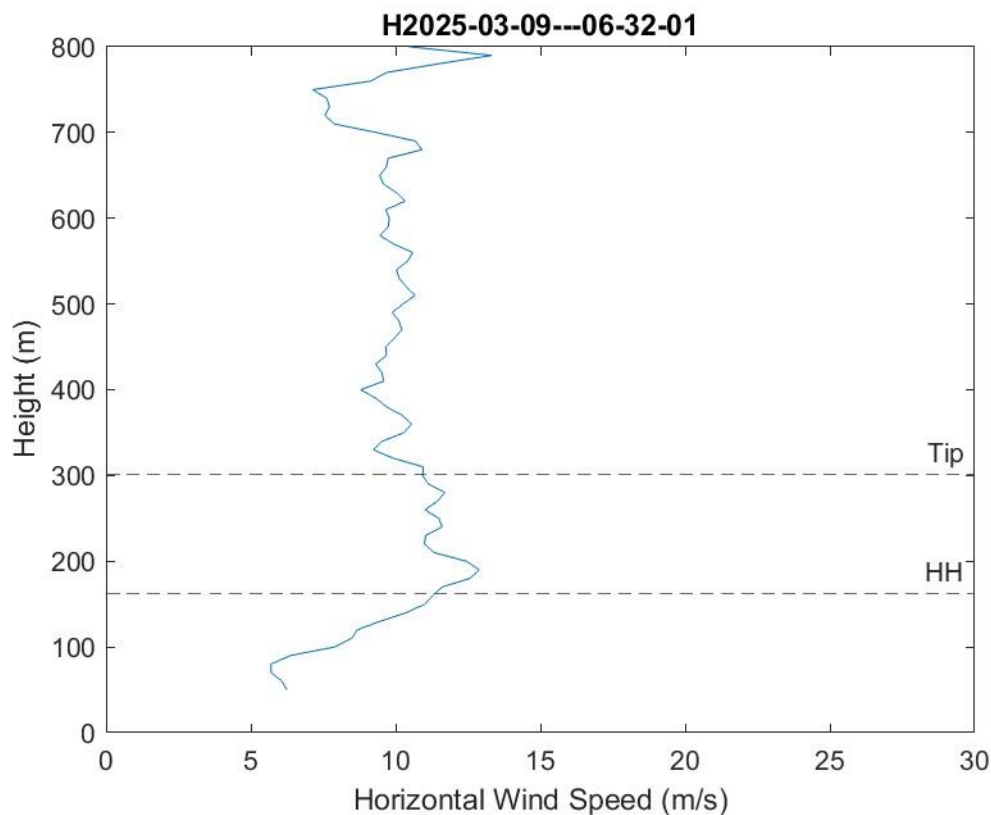


Figure 4 Horizontal wind speed recorded 9th March 2025
(HH = typical hub height, Tip = typical tip height for offshore wind turbines)

From Figure 3 it can be seen that the temperature (and sound speed) vary considerably in the rotor plane zone (0.05-0.3 kilometres). Figure 4 shows significant changes in horizontal wind speed in the lower portion of the rotor plane. This data shows the occurrence of conditions that cannot be addressed in empirical modelling calculations.

The measurement campaign is going well with high data recovery rates. Due to the large volume of data this will need to be carefully collated and quality checked prior to detailed analysis.

8. Conclusions

Preliminary results from the measurement campaign underway at Mace Head indicate significant variation in near surface weather. The variations are beyond the capability of current empirical modelling techniques. It is necessary to collate longer term datasets to determine the probability of occurrence and intensity of such events.

Further research and modelling are required to determine if such events could lead to acoustic features such as enhanced amplitude modulation at receiver locations on shore.

Acknowledgments

This research was supported by the Environmental Protection Agency through Taighde Éireann – Research Ireland grant number GOIPG/2023/4631.

References

- [1] *ISO 9613-2:2024 Acoustics - Attenuation of sound during propagation outdoors*, 2024.
- [2] *BEK nr 995 af 26/08/2024 Bekendtgørelse om støj fra vindmøller*, <https://www.retsinformation.dk/eli/lt/2024/995>, 2024.
- [3] K. Attenborough and T. van Renterghem, *Predicting Outdoor Sound*, CRC Press, Taylor & Francis, 2021.
- [4] Institute of Acoustics, “A Good Practice Guide to the application of ETSU-R-97 for the assessment and rating of wind turbine noise,” 2013.
- [5] ETSU, “Assessment & Rating of Noise from Wind Farms,” UK Department of Trade and Industry, 1996.
- [6] Institute of Acoustics, “Supplementary Guidance Note 6: Noise propagation over water for onshore wind turbines,” 2013.
- [7] R. Stull, “An introduction to boundary layer meteorology,” Kluwer Academic Publishers, 1988.
- [8] M. Rotach and A. Holtstag, *Ideal and Real Atmospheric Boundary Layers*, Elsevier Science & Technology, 2025.
- [9] K. Bolin and et al, “Long term estimations of low frequency noise levels over water from an offshore wind farm,” *The Journal of the Acoustical Society of America*, vol. 135, no. 3, pp. 1106-1114, 2014.
- [10] K. Konoshi and Z. Maekawa, “Interpretation of long term data measured continuously on long range sound propagation over sea surfaces,” *Applied Acoustics*, vol. 62, no. 10, pp. 1183-1210, 2001.
- [11] D. Waddington and Y. Lam, “The effect of weather conditions on the propagation of sound,” *Proceedings of the Institute of Acoustics*, vol. 24, no. 3, 2002.
- [12] G. Wong and T. Embleton, “Variation of the speed of sound in air with humidity and temperature,” *Journal of the Acoustical Society of America*, vol. 77, no. 5, pp. 1710-1712, 1985. [13] *ISO 2533:1975 Standard Atmosphere*, 1975.

Paper #43 - ID: 385

Title: Acoustic Profiling of Infrasound and Audible Emissions from Wind Turbines: Field Measurements in Northern Sweden

Author: José Chilo

11th Edition of the

**International Conferences on
Wind Turbine Noise**

Copenhagen, Denmark – 10th to 13th June 2025

**Acoustic Profiling of Infrasound and Audible Emissions from
Wind Turbines: Field Measurements in Northern Sweden**

Per Ängskog

**Department of Electrical Engineering Mathematics, and University of Gävle, Gävle,
SWEDEN per.angskog@hig.se**

Kourosh Tatar

**Department of Industrial Management, Industrial Design and Mechanical
Engineering, University of Gävle, Gävle, SWEDEN, kourosh.tatar@hig.se**

José Chilo¹

**Department of Electrical Engineering Mathematics, and University of Gävle, Gävle,
SWEDEN, jco@hig.se**

Summary

This study presents a comprehensive analysis of infrasound and low-frequency acoustic emissions from high-power horizontal-axis wind turbines (HAWTs) at four wind farm sites in northern Sweden: Bergvind Lingbo, Vindpark Jädraås, Hästkullen, and Björnlandhöjden. Located in the municipalities of Ockelbo and Härnösand, these sites vary in scale and operational status, comprising 41 to 73 turbines and annual energy outputs ranging from 590 to 1,051 GWh. Field measurements employed a dual-microphone setup using a Lidström infrasound microphone, optimized for detecting acoustic signals below 20 Hz, alongside a ZealSound USB condenser microphone for audible frequencies. This configuration enabled the simultaneous capture of infrasound and audible noise data, supporting detailed spectral and time-frequency analyses. Measurements at four wind farm sites show that infrasound levels are notably higher compared to a reference site without turbine activity. Recordings were conducted both outdoors and inside a stationary vehicle. In addition to elevated infrasound, broadband audible signals were observed, linked to blade swishing and wind interactions, producing harmonics and turbulence-related features. The results improve our understanding of wind turbine acoustics and provide valuable data for noise assessment and policy development

1. Introduction

The expansion of wind energy as a sustainable power source has raised concerns about its acoustic emissions. Wind turbines produce both audible noise and low-frequency infrasound (below 20 Hz), which, though often inaudible, may have physiological and psychological effects that require further investigation.

Previous studies confirm that wind turbines are significant sources of both audible and infrasonic noise. Infrasound is primarily generated by blade-tower interactions and atmospheric turbulence. Sugimoto et al. [1] demonstrated a strong correlation between infrasound levels and rotor speed, highlighting the need for

¹ Corresponding author – Email: jco@hig.se

sensitive measurement systems capable of detecting frequencies below 1 Hz. Pierzga and Boczar [2] analyzed infrasound emissions from low-power vertical-axis wind turbines (VAWTs), showing notable impacts even at smaller scales. Similarly, Malec and Boczar [3] examined high-power horizontal-axis wind turbines (HAWTs), finding that infrasound emissions vary with wind speed and are influenced by resonant and median frequencies.

Despite growing awareness, standardized methods for measuring and evaluating wind turbine infrasound are limited, particularly in non-industrial settings. Further research is essential to characterize these emissions and inform guidelines for wind farm development.

This study investigates the infrasound and audible noise generated by high-power HAWTs in Northern Sweden. Using a Lidström infrasound microphone and a high-precision microphone, we conducted simultaneous measurements to analyze the acoustic environment under varying meteorological conditions.

2. Measurement setup and wind farm sites

In this study, a Lidström infrasound microphone—specifically designed to capture acoustic signals below 20 Hz—was used in combination with a 16-bit USB-1608G analog-to-digital converter, enabling high-resolution data acquisition with adequate sampling frequency and dynamic range for infrasound analysis. Real-time data collection and monitoring were carried out using LabVIEW, which also applied digital filtering to enhance the signal-to-noise ratio within the target frequency range. Both raw and filtered data were stored continuously for further processing. Subsequently, the recorded signals were analyzed offline in MATLAB, where spectral and time-frequency analyses were performed to characterize the infrasound components and acoustic patterns generated by the wind turbines.

Audible sound from wind turbines was recorded using a ZealSound USB condenser microphone (electret type), featuring a cardioid polar pattern, 16-bit/48kHz digital resolution, and integrated analog gain control. The microphone offers a frequency response range of 40 Hz to 18,000 Hz, allowing for accurate capture of the full range of audible turbine emissions.

Systematic field measurements of infrasound were conducted in the vicinity of the wind farms to investigate the levels and spectral characteristics of turbine-generated infrasound. Table 1 summarizes the key characteristics of each measurement site, including location, number of turbines, estimated energy output, and commissioning date.

Table 1: Four wind farm locations in northern Sweden

Wind Farm Sites	Municipality	Number of Turbines	Estimated Annual Production (GWh)	Commissioning
Bergvind Lingbo	Ockelbo	58	748	June 1, 2020
Vindpark Jädraås	Ockelbo	66	689	Jan 21, 2013
Hästkullen	Härnösand	73	1,051	October 1, 2021
Björnlandhöjden	Härnösand	41	590	April 1, 2022

Additionally, we conducted a comparative measurement by placing the infrasound microphone inside a closed vehicle (see Figure 1). This setup was implemented alongside standard outdoor measurements to explore how effectively a car cabin attenuates infrasound generated by nearby wind turbines. By isolating the microphone from direct wind exposure and environmental noise, this configuration enabled an evaluation of the transmission characteristics of low-frequency acoustic signals through the vehicle’s structure. The comparison between outdoor and in-vehicle recordings offers further insight into the propagation of infrasound and its potential perceptibility in enclosed environments, such as cars or buildings—spaces commonly encountered in everyday life. Similar investigations have been conducted in residential contexts near wind farms, where infrasound levels recorded indoors were found to be significantly attenuated and well below hearing thresholds [4].



Figure 1 Measurement vehicle positioned with the wind farm visible in the background.

3. Field Infrasound Measurements

Figure 2 presents the field measurements. In this study, infrasound measurements were conducted at Wind Farm Sites – Bergvind Lingbo, Vindpark Jädraås, Hästkullen, and Björnlandhöjden – as well as at a reference site without nearby wind turbine activity. At each location, measurements were performed using an infrasound microphone placed both outdoors and inside a stationary vehicle. This setup allowed for a direct comparison between open environmental exposure and the infrasound levels that penetrate into the interior of a vehicle. The reference site, serving as a control, showed consistently low and stable infrasound levels in both environments, indicating minimal influence from external sources. In-vehicle levels at the reference location were slightly lower than those recorded outdoors, demonstrating the vehicle's capacity to attenuate ambient infrasound to some extent.

In contrast, the Wind Farm Sites exhibited varying degrees of elevated infrasound levels, depending on their respective exposure and proximity to turbines. At Bergvind Lingbo, infrasound levels outdoors were slightly above the baseline, and the in-vehicle data displayed reduced amplitude but retained some minor peaks. This suggests a relatively low, yet detectable, impact from wind turbines. Vindpark Jädraås presented a much higher degree of infrasound variability, with pronounced peaks in the outdoor measurements and similar, though somewhat dampened, fluctuations inside the vehicle. The parallel structure between outdoor and in-vehicle time series in Jädraås points to significant infrasound penetration despite enclosure.

At Hästkullen, outdoor infrasound levels were also notably high and variable, while the corresponding in-vehicle measurements showed clear signal similarity, but with reduced amplitude. This again illustrates that low-frequency sound waves generated by wind turbines are partially transmitted into the vehicle cabin. Björnlandhöjden displayed moderate outdoor variability with several pronounced peaks, and while in-vehicle measurements were attenuated, they retained the temporal pattern observed outdoors, confirming partial transmission.

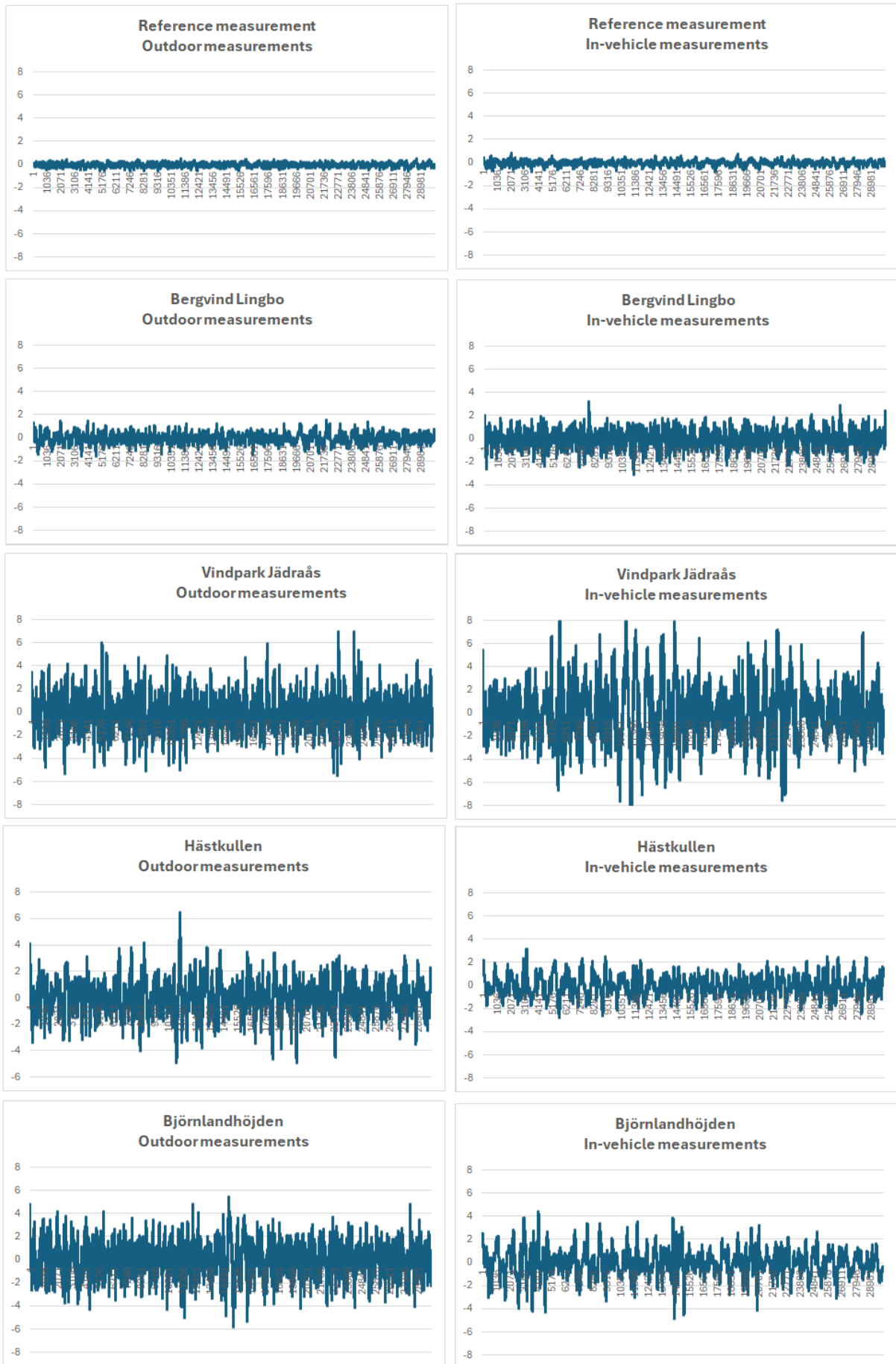


Figure 2 Infrasound Signals from Wind Turbines. The x-axis represents samples, and the y-axis is in arbitrary units.

4. Measurements in the audible range

Figure 3 displays time-domain waveforms representing audible range signals recorded at the four wind farm sites: Bergvind Lingbo, Vindpark Jädraås, Hästkullen, and Björnlandhöjden. These signals are shown primarily to illustrate the presence and temporal structure of acoustic events in the audible frequency range, rather than to support direct quantitative comparison across sites.

Across all locations, the waveforms show clear time-varying fluctuations, including both low-amplitude background modulations and occasional higher-amplitude transients. These may correspond to swishing or amplitude-modulated sounds, commonly associated with rotating turbine blades and the interaction of wind with blade surfaces. Previous studies have described such sounds as characteristic of wind turbine operation (e.g., swish or thump phenomena linked to blade–tower interaction and atmospheric turbulence) [5].

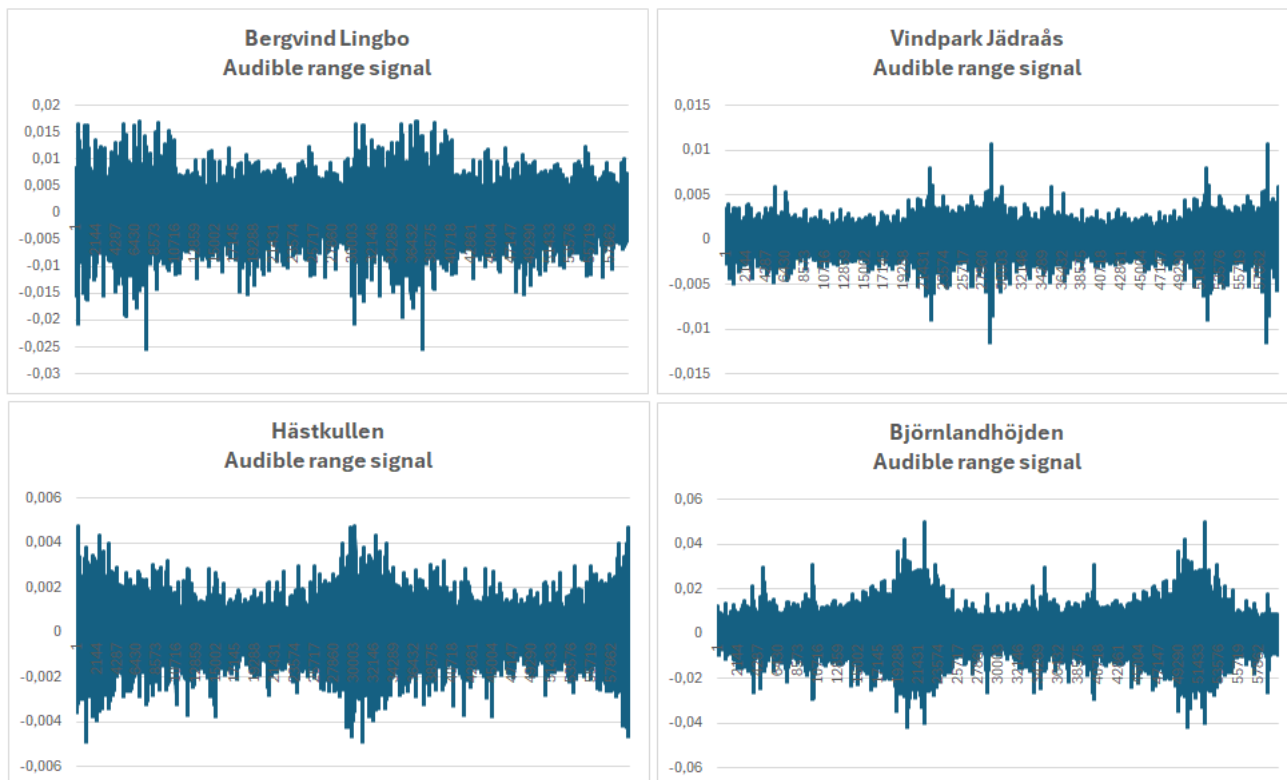


Figure 3 Audible range measurement. The x-axis represents samples, and the y-axis is in arbitrary units.

Figure 4 shows the audible range spectra measured at four wind farm sites: Bergvind Lingbo, Vindpark Jädraås, Hästkullen, and Björnlandhöjden. The x-axis represents frequency in Hz, covering the full audible range, and the y-axis shows relative sound pressure level in dB. As the absolute levels depend on the source–receiver distance, the focus is on spectral distribution.

All sites exhibit broadband acoustic content, with energy spread across the entire audible spectrum, indicating that the sound environment is not limited to discrete tonal components but includes continuous frequency content. This likely results from a combination of aerodynamic, mechanical, and environmental sources related to turbine operation.

Bergvind Lingbo and Björnlandhöjden display prominent high-frequency components (up to ~18 kHz), while Hästkullen shows stronger low- and mid-frequency peaks, potentially related to tonal mechanical emissions. Vindpark Jädraås presents a relatively flat spectrum, with more uniform energy distribution across frequencies

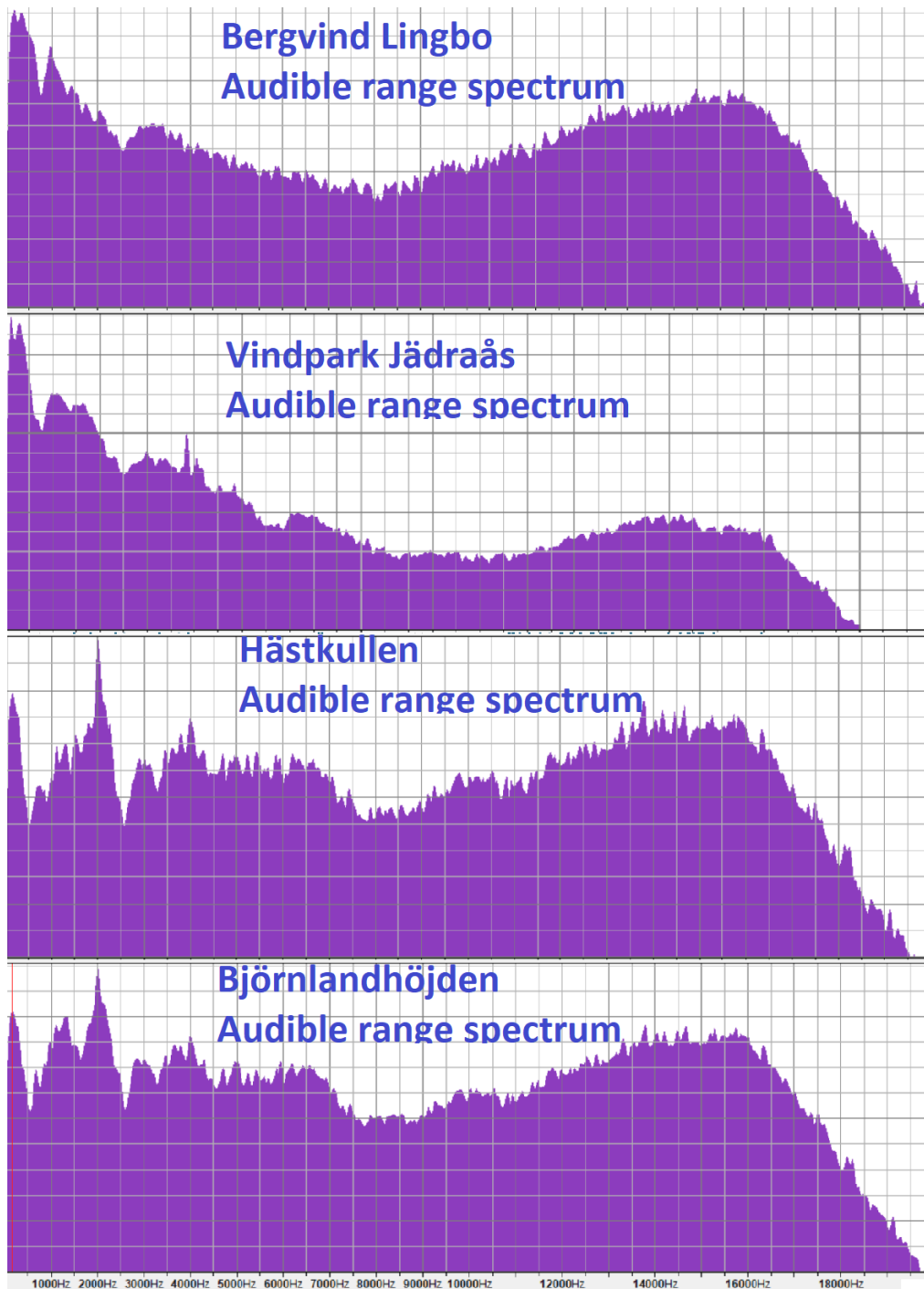


Figure 4 Audible range measurement spectrum. The x-axis represents frequency domain, and the y-axis is in arbitrary units.

5. Conclusions

Using simultaneous measurements with a Lidström infrasound microphone and a ZealSound USB condenser microphone, the research highlights the presence of infrasound components below 20 Hz and the characteristic swishing sounds within the audible range.

The comparison between outdoor and in-vehicle infrasound measurements across all sites indicates that while the vehicle provides measurable infrasound attenuation, it does not fully shield the interior from external low-frequency noise. The reference site data validate that the elevated infrasound levels observed at wind power sites are not part of the natural background, strengthening the conclusion that wind turbines

significantly contribute to infrasound in the surrounding environment. These findings support the notion that infrasound exposure may persist even in enclosed spaces such as vehicle cabins, warranting further investigation into its transmission dynamics and potential health implications. These findings contribute to a better understanding of the acoustic environment surrounding wind turbines and provide valuable data to inform future research, standardization efforts, and policy development for sustainable wind energy deployment.

The audible spectral measurements from all four wind farms reveal broadband acoustic signatures that span the full range of human hearing. The spectral shapes vary by site, possibly due to differences in turbine models, layout, topography, wind conditions, and measurement positions. These findings reinforce the need to consider the full audible range—not just tonal components or low frequencies—when assessing wind turbine noise impact and designing mitigation strategies.

References

- [1] **Sugimoto, T., Koyama, K., Kurihara, Y., & Watanabe, K.** (2008). *Measurement of infrasound generated by wind turbine generator*. In *Proceedings of the SICE Annual Conference 2008* (pp. 5-10). The University of Electro-Communications, Tokyo, Japan. Society of Instrument and Control Engineers (SICE).
- [2] **Pierzga, R., & Boczar, T.** (2013). *Analysis of low-frequency acoustic signals emitted by low-power vertical axis wind turbine (VAWT)*. In *Proceedings of the 2013 IEEE International Conference on Condition Monitoring and Diagnosis* (pp. 978-1-4673-3059-6). Opole University of Technology, Opole, Poland. IEEE. ISBN: 978-1-4673-3059-6.
- [3] **Malec, T., & Boczar, T.** (2013). *Analysis of infrasound noise emitted by high power wind turbine with asynchronous generator for selected resonant and median frequencies*. In *Proceedings of the 2013 IEEE International Conference on Condition Monitoring and Diagnosis* (pp. 978-1-4673-3059-6). Opole University of Technology, Opole, Poland. IEEE. ISBN: 978-1-4673-3059-6.
- [4] **Gastmeier, W.J., & Howe, B.** (2008). Recent Studies Of Infrasound From Industrial Sources. *New Zealand Acoustics*, 21(4).
- [5] **Møller, H., & Pedersen, C. S.** (2011). *Low-frequency noise from large wind turbines*. *Journal of the Acoustical Society of America*, 129(6), 3727–3744. <https://doi.org/10.1121/1.3543957>.

Paper #44 - ID: 387

Title: Turbulent boundary layer trailing-edge noise reduction with permeable blade extensions at full-scale conditions

Author: Friso Hartog

11th Edition of the
International Conferences on
Wind Turbine Noise
Copenhagen, Denmark – 10th to 13th June 2025

Turbulent boundary layer trailing-edge noise reduction with permeable blade extensions at full-scale conditions

Friso H. Hartog¹, Tjeu A. Gehlen, and Michiel van Nesselrooij
MuTech B.V., Delft, 2629 HS, The Netherlands

Summary

Serrations are the current industry standard for reducing turbulent-boundary-layer trailing-edge noise, which is typically the main noise source for wind turbine rotor blades. Unfortunately, these well-known devices have little room for improvement, putting the growth of onshore wind energy need to reach climate and energy independence goals at risk. This accentuates the need for next-generation technologies for broadband noise reduction such as permeable trailing-edge extensions.

The present work covers wind tunnel experiments conducted in the Poul la Cour Tunnel (PLCT) at the Technical University of Denmark (DTU). Different designs for permeable blade extensions were produced using additive manufacturing, measured on a 900 mm FFA W3-211 airfoil model using an 84-microphone array, and compared against reference serrations. Results show improved performance at typical operating conditions ($\alpha = 8^\circ$, $U_\infty = 80$ m/s), with maximum reductions of 15 dB in sound pressure level (SPL) and 8 dB(A) in A-weighted overall sound pressure level (O(A)SPL) compared to an untreated blade, and up to 3 dB(A) improvement in O(A)SPL over serrations. Furthermore, unified empirical length scaling laws are introduced that address different aeroacoustic mechanisms. This enables tailored designs for different blade geometries and operational regimes to maximise overall noise reduction.

These findings represent a significant step toward translating permeable trailing-edge extensions from laboratory concepts into commercially viable solutions. With demonstrated robust acoustic performance at full scale, permeable extensions offer a highly promising path forward for reducing wind turbine noise and supporting the broader deployment of onshore wind.

1. Introduction

Wind turbine noise presents a multifaceted impact: it contributes to environmental pollution and restricts the growth of onshore wind energy, putting climate goals and energy independence needs at risk. Among the various noise sources, turbulent boundary-layer trailing-edge (TBL-TE) noise dominates for modern, large-scale wind turbines [1]. Trailing-edge serrations have become the industry standard for mitigating this noise [2–4], but their potential for further optimization is limited. To unlock further noise reductions that enable broader public acceptance and further the adoption of onshore wind, new approaches are needed. Permeable trailing-edge extensions have emerged as a promising candidate for next-generation noise abatement.

¹Corresponding author - Email: f.hartog@muteskineu

Research in the past decade has demonstrated that permeable trailing edges can significantly reduce TBL-TE noise [5–16]. Various implementations, ranging from metal foam inserts [5–8, 12] to perforated add-ons [9–11, 13–15], have shown promising results in experiments and high-fidelity simulations. They can achieve broadband noise reductions of over 10 dB at low-to-moderate frequencies when properly designed [10, 11, 13, 14]. This reduction has been attributed to several mechanisms, such as the pressure release process [8, 12, 13, 15], breaking of turbulence coherence [15], and distributed scattering [12, 13, 15]. A secondary, mild noise-increasing effect occurs at higher frequencies due to the introduced surface roughness [8, 15]. Additionally, for certain designs, pore-induced vortex shedding can generate extra quasi-tonal peaks [15, 16]. The net result of these three effects typically ranges from 4 to 6 dB reduction in overall sound pressure levels (OSPL) at low Reynolds numbers [10, 11].

Despite promising results at scaled conditions, a critical gap remains in translating this technology to industrial applications. To our knowledge, no full-scale data is available in the literature, and key practical aspects — such as aerodynamic performance, manufacturability, and durability — remain largely unaddressed. These unknowns are further compounded by the vast design space and the resulting challenges in scaling to operational conditions of wind turbine rotor blades. As a result, a technology with clear promise was at risk of remaining "in the lab", unable to contribute meaningfully to the much needed expansion of wind energy.

This work aims to move permeable blade extensions closer to becoming a viable technology for wind turbine noise reduction. We present the first publically available, full-scale acoustic results of permeable blade extensions, measured in the Poul la Cour Tunnel (PLCT). These add-ons achieve an additional 3 dB(A) reduction in overall noise levels compared to serrations and can be manufactured and applied using industry-standard methods and materials. We also introduce scaling laws that enable design tailoring to different blade geometries and operational conditions. Proprietary constraints limit data disclosure; however, key findings and trends are shared to highlight the important advancements in this area.

2. Methodology

The present work covers an experimental wind tunnel campaign at full-scale conditions, measuring rotor blade trailing-edge noise with different noise-reducing trailing-edge devices. The wind tunnel and test section are described in Section 2.1, followed by more details on the models and conditions in Section 2.2, and an explanation of the data acquisition and processing procedure in Section 2.3. Given the use of established, standardized procedures — common for commercial testing at this facility — method descriptions are kept concise. Where relevant, references to more detailed documentation are provided.

2.1 Wind tunnel and test section

Tests were performed in the Poul la Cour Tunnel (PLCT), on the Risø Campus of the Technical University of Denmark (DTU) in Roskilde, Denmark. It is a state-of-the-art facility dedicated to aerodynamic and (aero)acoustic measurements for wind turbine applications, in particular rotor blade sections. The wind tunnel operates as a closed-loop system powered by a 2.4 MW fan to reach maximum flow speeds of up to 105 m/s. The test section measures 2 m × 3 m × 9 m (H × W × L) and has interchangeable sidewalls, which are solid and tensioned Kevlar in the aerodynamic and acoustic configurations, respectively. The test section is contained within a larger, acoustically treated anechoic room, while the rest of the system also contains acoustic absorbent treatments. This allows for acoustic measurements that approach ideal free-field conditions. For the present study, the acoustic configuration was used. More details on the facility can be found in Ref. [17].

2.2 Models and conditions

2.2.1 Blade model

A 900mm chord FFA W3-211 [18] airfoil model was used, with a 0.4 mm ZZ-trip at 5% and 10% x/c on the suction side and pressure side, respectively. The set geometric angle of attack α_{geom} was translated into an effective angle of attack α_{eff} by matching the pressure distribution curves as measured in the wind tunnel and simulated with XFOIL [19], following the procedure outlined in [11]. The airfoil and α -matching curve are shown in Figure 1. The global fit agrees well with the matching of individual cases and provides confidence in the accuracy of the estimated α_{eff} , which is used as α from hereon in presenting and discussing the results.

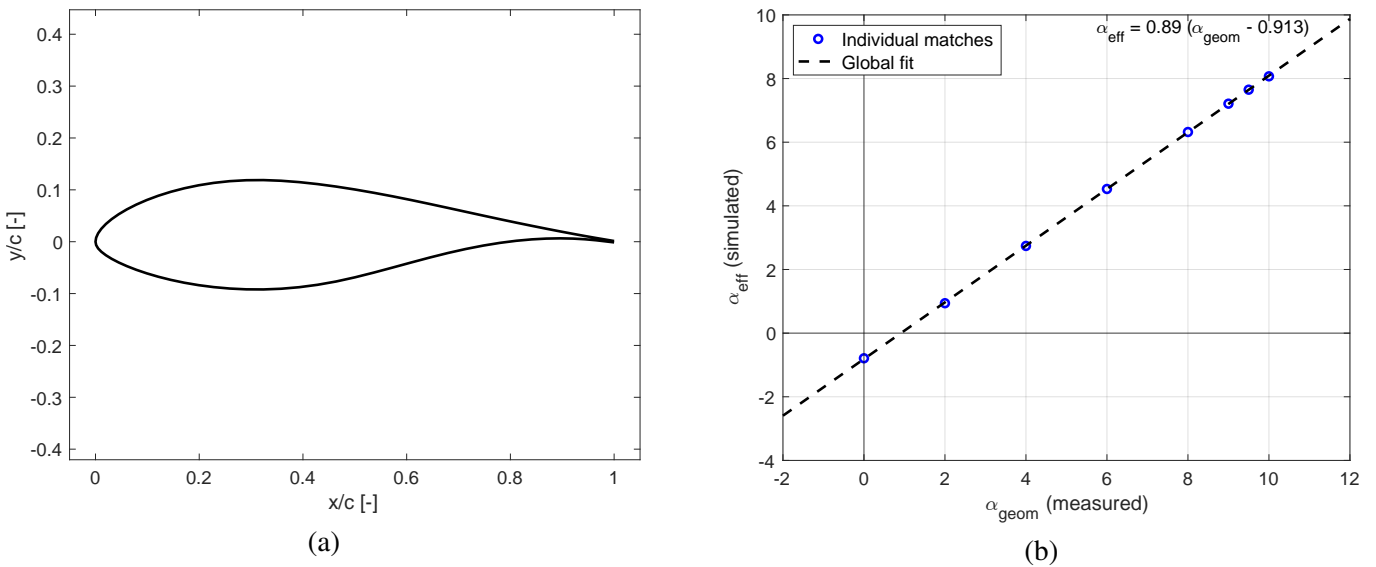


Figure 1 Blade model setup. (a) FFA W3-211 cross-sectional shape. (b) Translation of geometric to effective angle of attack.

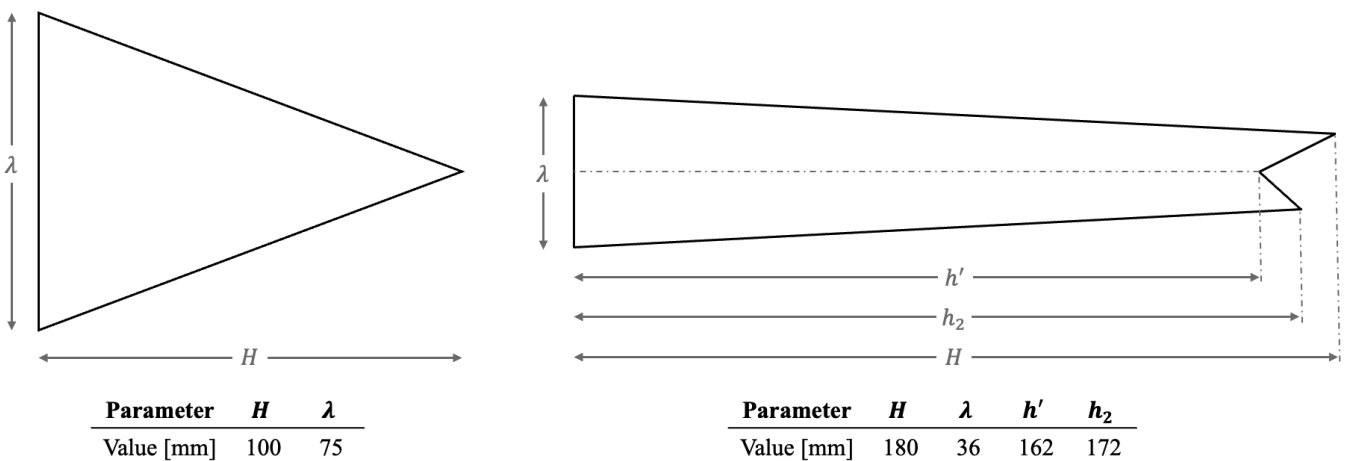


Figure 2 Reference serrations: conventional sawtooth (left) and double-rooted (right).

2.2.2 Trailing-edge models

Two serrated add-on models were selected as references for known noise-reducing technologies. The first model has a conventional sawtooth serrated geometry and is made of industrial-grade material. The second model has a double-rooted geometry and is based on input provided by Brunel University - see Ref. [20] for their work. These two models were selected to represent the status quo (former model) and a potential evolution (latter model) in serrations. Their planforms are visualised in Figure 2, and they are hereafter referred to as serrations and double-rooted trailing-edge serrations (DRootTES), respectively.

The permeable blade extension models covered variations in key design parameters, such as extension length (l_{ext}) and flap angle (β). While the focus of this study is on acoustic performance, aerodynamic considerations were taken into account during the design process. Previous campaigns have shown that well-designed permeable extensions have a limited influence on lift, drag, and stall behaviour, with β being the dominant governing parameter. By tuning β , load-neutral behavior — defined as 0% change in lift at a target design α — was achieved within 0.5° of the predicted neutral-load β . Notably, this condition typically aligns closely with β that yields optimal noise reduction, forming a natural design point for the presented results. Minor increases in drag (typically under 10%) can be compensated by small, controlled increases in lift of approximately 2%, maintaining overall aerodynamic efficiency. All add-ons in this study were designed with this balance of acoustics and aerodynamics in mind, ensuring that the optimised acoustic results reported are representative of aerodynamically viable configurations.

The add-ons measured in this campaign were produced using additive manufacturing methods to allow for many design variations and extensive parameter sweeps in testing. In addition, the most challenging design from a manufacturing perspective was successfully produced using injection moulding with standard materials commonly applied in add-ons such as vortex generators and serrations. This trial production demonstrated the feasibility of manufacturing permeable add-ons using industry-accepted methods and materials. Specific geometric details and parameter values are omitted due to confidentiality requirements.

2.2.3 Test conditions

Measurements were conducted at a range of angles of attack and flow velocities typical for operating conditions. For some designs, more resolution was provided in the angles of attack and/or velocities to collect additional data for scaling purposes. Also, for some designs, the case of natural transition was measured. Lastly, the constraints in the available testing time required abbreviated testing and hence a limited number of conditions for some models. A summary is provided in Table 1.

Table 1 Test conditions for different cases. Some permutations (e.g. joint high resolution sweeps of α and U_∞) are not explicitly included.

Test cases	α_{geom} [°]	U_∞ [m/s]	$Re_{c,max}$ [–]	Transition [–]
All	-4, 0, 4, 6, 8, 10, 11	55, 70, 85	5.5×10^6	Forced
Some	-8:2:6, 7:1:11	55, 70, 85	5.5×10^6	Forced
Some	-4, 0, 4, 6, 8, 10, 11	55, 70, 75, 80, 85	5.5×10^6	Forced
Some	-4, 0, 4, 6, 8, 10, 11	55, 70, 85	5.5×10^6	Natural

2.3 Data acquisition and processing

Acoustic measurement data was collected with an 84-channel microphone array located in the anechoic room outside the test section at a 2.3 m distance from the blade trailing-edge. Acoustic source maps were computed with conventional frequency-domain beamforming, an example of which is shown in Figure 3a. Subsequent source levels were obtained from the depicted integration window in the form of span-normalised spectra as shown in Figure 3b. Overall levels are calculated within the 200 – 5000 Hz domain. More details on the post-processing procedure can be found in Ref. [21].

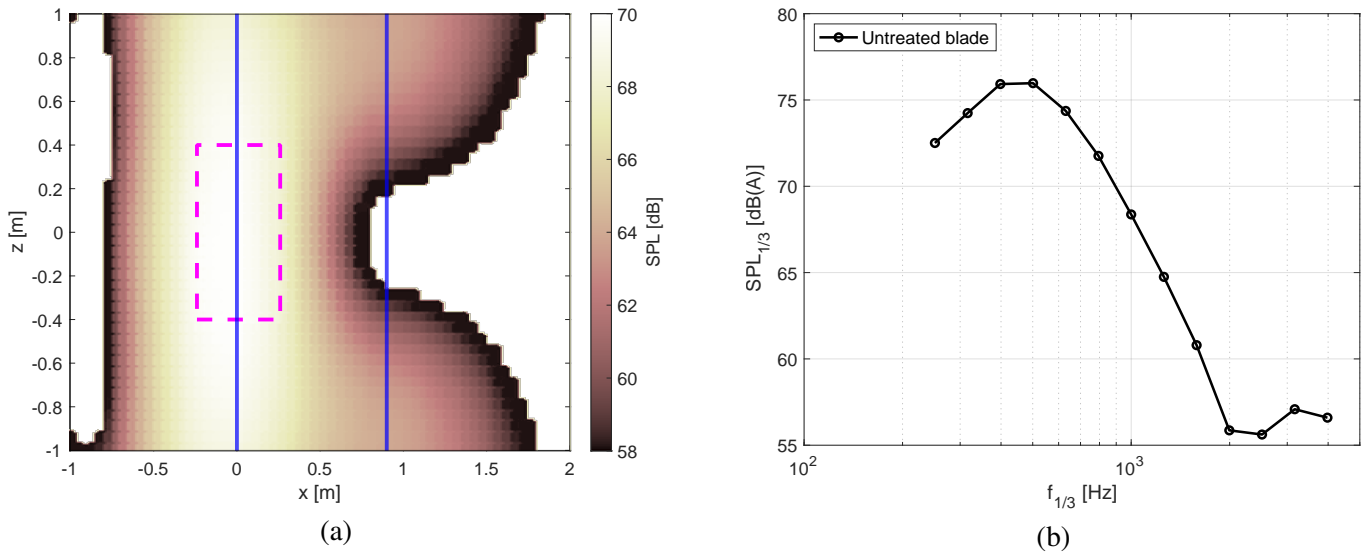


Figure 3 Beamforming results for untreated case at $U_\infty = 80$ m/s, $\alpha = 8^\circ$. (a) Source map at $f_{1/12} = 527$ Hz. Flow from right to left. Blue indicates airfoil LE and TE, magenta indicates integration window. (b) Integrated spectrum.

3. Results and discussion

This section presents the key acoustic results from the wind tunnel campaign. General acoustic performance for a specific permeable blade extension design is compared to that of the reference serrations in Section 3.1. Subsequently, Section 3.2 discusses the abatement of quasi-tonal humps for particular designs of permeable extensions. Lastly, Section 3.3 presents relevant scaling laws for permeable extensions.

3.1 General acoustic performance

The acoustic performance of the tested add-ons is evaluated relative to the untreated blade to quantify their noise reduction capacity. Figure 4a presents the difference in sound pressure level (Δ SPL) at the target design condition of $U_\infty = 80$ m/s and $\alpha = 8^\circ$, comparing the serrations, DRooTES, and permeable extension. While both the serrations and DRooTES achieve a maximum reduction of around 7 dB, the permeable extension delivers a significantly larger reduction, reaching up to 14 dB. The stronger reduction compared to scaled tests reported in the literature suggests that permeable trailing-edge extensions benefit from scaling effects, which increase their effectiveness as blade chord, flow velocity, and absolute noise levels increase. Additionally, this superior performance spans a broad frequency range from approximately 250-300 Hz up to 1,500-2,000 Hz, effectively covering the frequencies of primary relevance for wind turbine noise emission.

The robust performance of the permeable extension across varying α is illustrated in Figure 4b. The magnitude, center frequency, and width of the noise reduction region ('bucket') remain relatively stable with α . At higher frequencies, a slight increase in noise is observed, attributable to surface roughness effects. The cross-over frequency at which this occurs shows a subtle dependence on α , especially between 5° and 10° , where aerodynamic loading effects become more pronounced. This spectral behaviour of the permeable extension highlights its strong potential for operational wind turbine applications. First, its robustness to variations in α ensures effective noise reduction across the full range of operating wind speeds and radial positions along the blade. Second, the dominance of noise reduction at low-to-medium frequencies aligns favourably with real-world conditions, where atmospheric absorption disproportionately attenuates higher frequencies before reaching ground-level observers.

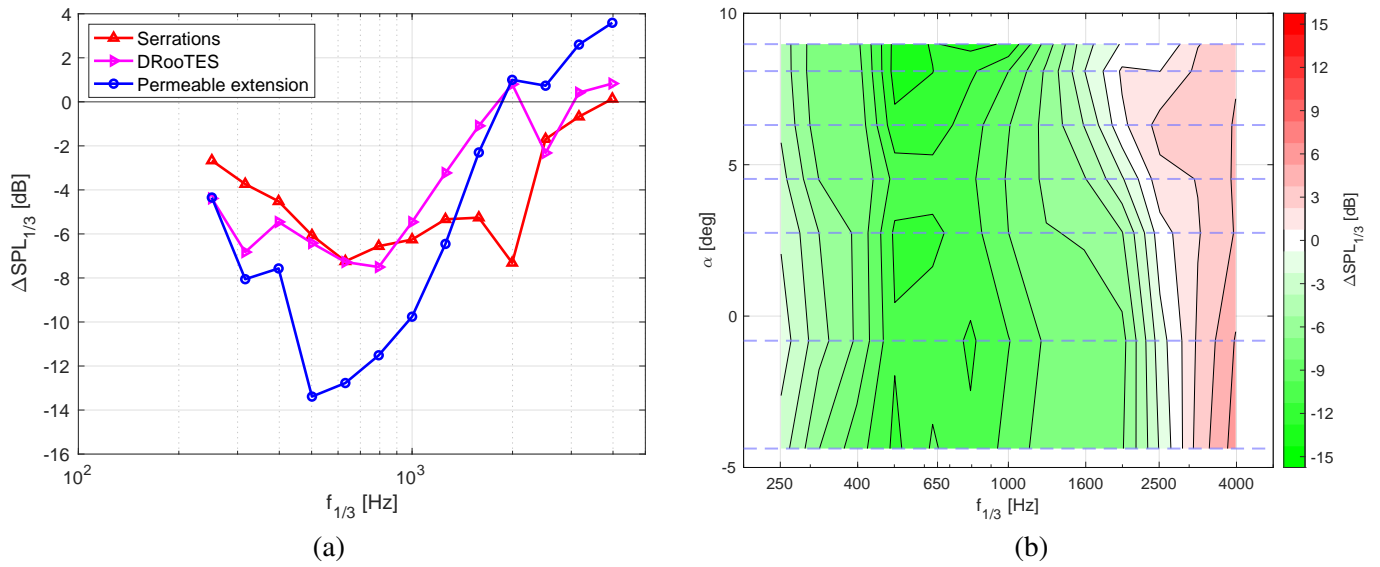


Figure 4 Difference in sound pressure level compared to an untreated blade at $U_\infty = 80$ m/s. (a) Different devices at $\alpha = 8^\circ$. (b) Permeable extension at different α . Blue lines indicate α with available data, between which values are interpolated to generate the map.

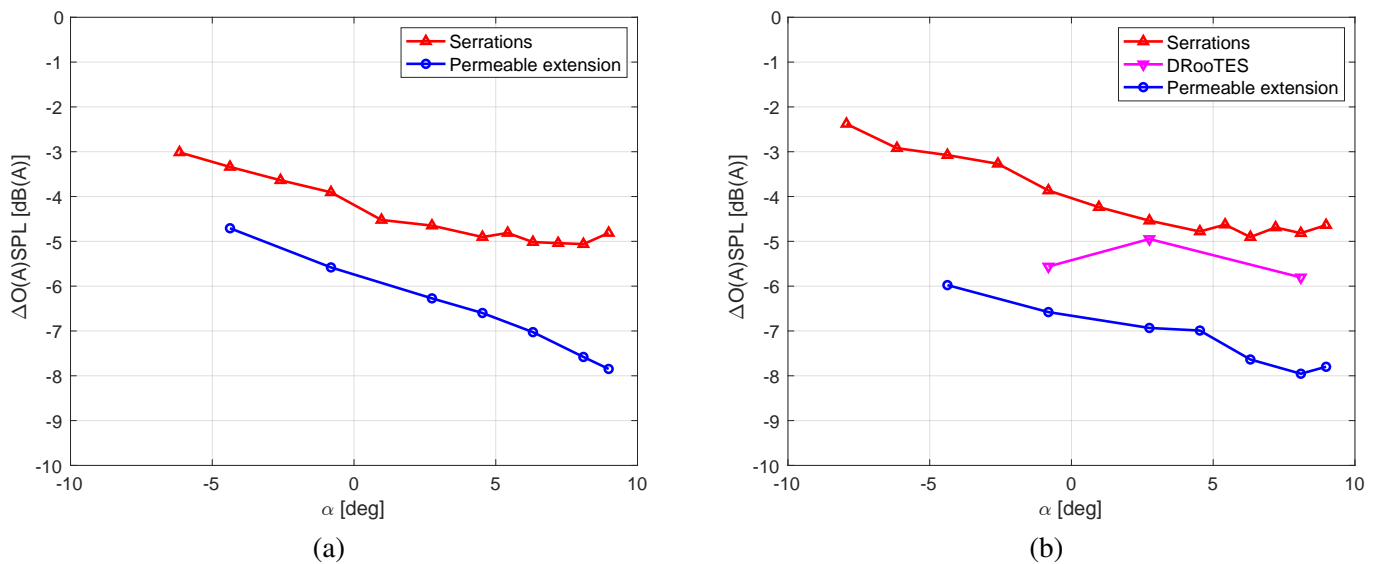


Figure 5 Difference in overall A-weighted sound pressure level compared to an untreated blade. (a) $U_\infty = 70$ m/s (b) $U_\infty = 80$ m/s.

The improved performance of the permeable extension across the key frequency range also translates into a significantly lower overall sound pressure level (OSPL). Figure 5 presents the results at 70 m/s and 80 m/s. Testing at full-scale conditions warrants the use of A-weighted levels, in line with the IEC standard for field measurements [22]. Compared to the DRooTES and serrations, the permeable extension achieves an additional reduction in O(A)SPL of up to 2–3 dB(A), with relatively stable performance across the range of α . This improvement results in a maximum overall noise reduction of 8 dB(A) at the target design condition, representing a substantial step in performance over the state-of-the-art.

3.2 Abatement of quasi-tonal humps

Flow over permeable trailing-edge extensions can induce local vortex shedding, leading to the generation of tonal peaks in the acoustic spectrum [15, 16]. This phenomenon is expected to become more pronounced at larger scales, due to increased flow velocity and blade chord length. Figure 6 shows that for certain designs, quasi-tonal humps appear as localized discontinuities within the broadband noise reduction bucket. These features were found to scale with velocity in accordance with a Strouhal-type relationship, suggesting an aeroacoustic origin such as vortex shedding at different characteristic length scales.

Targeted design modifications were implemented to suppress these tonal features without compromising the broadband noise reduction performance, which is particularly clear at the lowest frequencies where the spectra remain identical. The successful mitigation of these local effects was achieved consistently across different extension geometries, indicating that the underlying physical phenomenon can be effectively controlled through appropriate design strategies, regardless of the specific extension configuration.

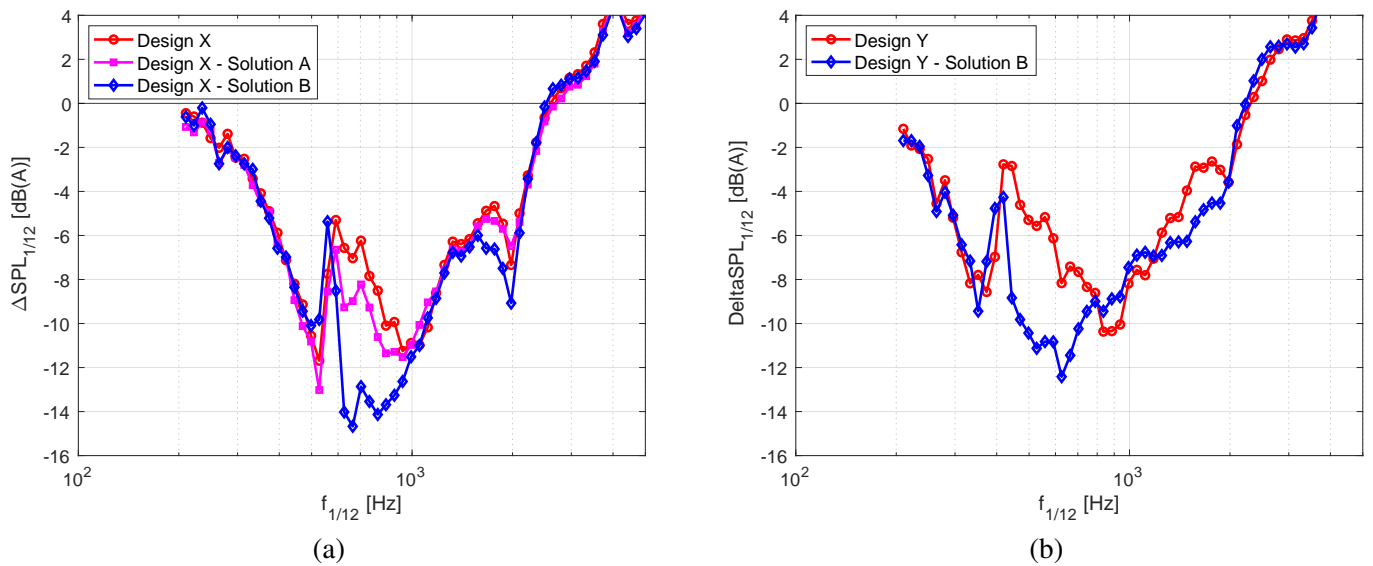


Figure 6 Difference in sound pressure level compared to an untreated blade at $U_\infty = 80$ m/s and $\alpha = 2.7^\circ$. (a) Baseline design X. (b) Baseline design Y.

3.3 Extension length scaling

To demonstrate the ability to tailor permeable extension designs to different blade geometries and operational conditions, we introduce scaling laws for a key design parameter: the extension length, l_{ext} . Figure 7a shows the unscaled noise reduction curves for five different extension lengths. Not all lengths included targeted modifications to suppress quasi-tonal humps. Therefore, for the purpose of this analysis, the spectra were corrected to omit these humps, similar to the demonstrated effects of such modifications as discussed in Section 3.2.

The data show a clear trend: longer extensions perform better at lower frequencies, while shorter extensions provide greater noise reduction at higher frequencies. However, the dependence on l_{ext} differs in magnitude between the two frequency regimes, as illustrated in Figures 7b and 7c. In the lower frequency range, noise reduction curves collapse when the frequency is scaled linearly with l_{ext} , consistent with a Strouhal-type scaling typical of TBL-TE noise. In contrast, the higher frequency range collapses when scaled with $l_{ext}^{1/2}$. This corresponds to the roughness-induced noise increase mechanism, which can be shown — see Equations (1) and (2) — to follow an approximate square-root dependence of f on l_{ext} based on Amiet's theory [23] and a change in displacement thickness (δ^*) due to the add-on [24]. The distinct empirical scaling laws — linear with l_{ext} at lower frequencies and proportional to $l_{ext}^{1/2}$ at higher frequencies — explain why longer extensions achieve broader noise reduction across a wider range of turbulent eddy scales.

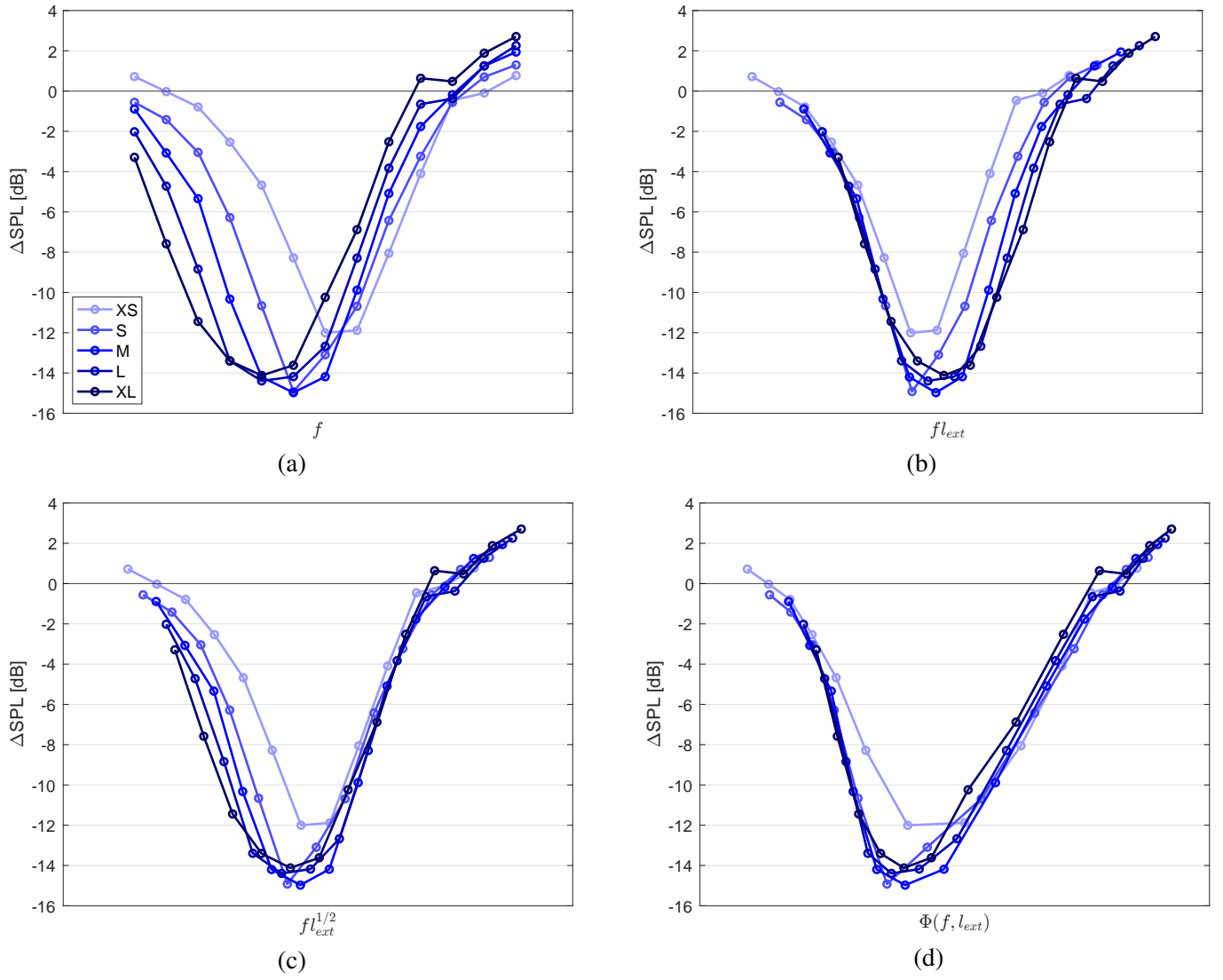


Figure 7 Noise reduction for different extension lengths at $U_\infty = 80$ m/s and $\alpha = 8^\circ$. (a) Unscaled (b) Scaled for collapse at lower frequencies. (c) Scaled for collapse at higher frequencies. (d) Unified scaling.

$$\frac{\delta^*}{x} \approx \frac{1.83}{Re_x^{1/2}} \rightarrow \delta^* \approx 1.83x \left(\frac{\nu}{Ux} \right)^{1/2} \rightarrow \Delta\delta^* \propto \Delta x^{1/2} \quad (1)$$

$$f_{TBL-TE} \propto (\delta^*)^{-1} \rightarrow \Delta f \propto \Delta x^{-1/2} \rightarrow f l_{ext}^{1/2} \approx \text{Constant} \quad (2)$$

The two scaling behaviors can be combined into a unified function, $\Phi(f, l_{ext})$, as shown in Figure 7d. A good collapse is obtained across both frequency regimes, with the largest deviations occurring near the center of the noise reduction bucket. This is attributed to two factors: first, the center region represents a blend of the two distinct scaling mechanisms; second, the absolute sound levels are lowest in this region, leading to relatively higher measurement uncertainty. Furthermore, deviations are most pronounced for the shortest design (XS). This can already be seen in the unscaled curve, where its point of maximum noise reduction ($f_{peak}, \Delta SPL_{peak}$) diverges from the general trend of ($f_{peak}, \Delta SPL_{peak}$) with l_{ext} . This suggests that the proposed scaling laws are generally accurate for effective add-ons above a certain threshold l_{ext} and that the tested range in this study satisfied this criterion for all but the shortest design. The findings from this analysis were verified for conditions (U_∞, α) outside the target design point as well. Overall, these scaling laws provide a practical framework for tailoring permeable extension designs to specific blade geometries and operational conditions, allowing optimization based on the characteristics of the relevant noise spectra.

4. Conclusion

This work presents the first publicly available full-scale acoustic measurements of permeable trailing-edge extensions for wind turbine blades. Testing was conducted under operationally relevant conditions in the Poul la Cour Tunnel (PLCT), using add-ons designed for standardised industry-grade production methods and materials while maintaining aerodynamic efficiency. Compared to the current status quo in serrations, the permeable extensions demonstrated an additional noise reduction of up to 3 dB(A) in overall sound pressure levels, with a maximum reduction of 8 dB(A) relative to an untreated blade.

The results confirm that permeable extensions not only maintain their noise reduction performance at full-scale conditions but benefit from scaling effects associated with increased blade chord and higher flow velocities. The extensions provided robust broadband reductions across a wide range of angles of attack, particularly at low-to-medium frequencies which typically cause the most problems as they travel furthest through the atmosphere. Secondary effects such as potential quasi-tonal, vortex shedding related humps, can be effectively controlled with targeted design strategies. Additionally, we introduced scaling laws for a key design parameter — extension length — linking the frequency-dependent noise-reducing characteristics to the underlying physical mechanisms. These results offer a practical framework for tailoring permeable trailing-edge designs to different blade geometries and operational regimes.

Overall, the findings represent a significant step toward translating permeable trailing-edge extensions from laboratory concepts into commercially viable solutions. By combining validated robust acoustic performance and clear empirical scaling laws, permeable extensions offer a highly promising path forward for reducing wind turbine noise and enabling broader acceptance and further adoption of onshore wind energy.

Acknowledgments

This work is part of the Blade Extensions for Silent Turbines (BEST) project (HER+22-02-03415120) which is supported by the Netherlands Enterprise Agency (Rijksdienst voor Ondernemend Nederland (RVO)), acting on behalf of the Dutch Ministry of Economic Affairs, using the Renewable Energy Transition subsidy (subsidie Hernieuwbare Energietransitie (HER+ 2022-02)), part of the Topsector Energy (TSE) subsidies.

The authors gratefully acknowledge the staff of the Poul la Cour Tunnel for their support throughout the preparation, execution, and follow-up of the experimental campaign. We also thank Professor Chong (Brunel University) for his support in making the DRooTES model available for this study.

References

- [1] S. Oerlemans, P. Sijtsma, and B. Méndez López, “Location and quantification of noise sources on a wind turbine,” *Journal of Sound and Vibration*, vol. 299, no. 4, pp. 869–883, 2007.
- [2] S. Oerlemans, M. Fisher, T. Maeder, and K. Kögler, “Reduction of wind turbine noise using optimized airfoils and trailing-edge serrations,” *AIAA journal*, vol. 47, no. 6, pp. 1470–1481, 2009.
- [3] F. Avallone, W. Van Der Velden, D. Ragni, and D. Casalino, “Noise reduction mechanisms of sawtooth and combed-sawtooth trailing-edge serrations,” *Journal of Fluid Mechanics*, vol. 848, pp. 560–591, 2018.
- [4] S. Oerlemans, “Wind turbine noise mitigation,” in *Handbook of Wind Energy Aerodynamics*, pp. 1–16, Springer, 2021.
- [5] T. Geyer, E. Sarradj, and C. Fritzsche, “Measurement of the noise generation at the trailing edge of porous airfoils,” *Experiments in fluids*, vol. 48, pp. 291–308, 2010.
- [6] T. Geyer, E. Sarradj, and C. Fritzsche, “Porous airfoils: noise reduction and boundary layer effects,” *International journal of aeroacoustics*, vol. 9, no. 6, pp. 787–820, 2010.
- [7] M. Herr, K.-S. Rossignol, J. Delfs, N. Lippitz, and M. Mößner, “Specification of porous materials for low-noise trailing-edge applications,” in *20th AIAA/CEAS aeroacoustics conference*, p. 3041, 2014.

- [8] A. Rubio Carpio, R. M. Martínez, F. Avallone, D. Ragni, M. Snellen, and S. van der Zwaag, “Experimental characterization of the turbulent boundary layer over a porous trailing edge for noise abatement,” *Journal of Sound and Vibration*, vol. 443, pp. 537–558, 2019.
- [9] A. Rubio Carpio, F. Avallone, D. Ragni, M. Snellen, and S. van der Zwaag, “3D-printed perforated trailing edges for broadband noise abatement,” in *25th AIAA/CEAS aeroacoustics conference*, p. 2458, 2019.
- [10] A. Rubio Carpio, F. Avallone, D. Ragni, M. Snellen, and S. van der Zwaag, “Quantitative criteria to design optimal permeable trailing edges for noise abatement,” *Journal of Sound and Vibration*, vol. 485, p. 115596, 2020.
- [11] S. Luesutthiviboon, D. Ragni, F. Avallone, and M. Snellen, “An alternative permeable topology design space for trailing-edge noise attenuation,” *International Journal of Aeroacoustics*, vol. 20, no. 3-4, pp. 221–253, 2021.
- [12] C. Teruna, F. Manegar, F. Avallone, D. Ragni, D. Casalino, and T. Carolus, “Noise reduction mechanisms of an open-cell metal-foam trailing edge,” *Journal of Fluid Mechanics*, vol. 898, p. A18, 2020.
- [13] C. Teruna, F. Avallone, D. Ragni, A. Rubio-Carpio, and D. Casalino, “Numerical analysis of a 3-D printed porous trailing edge for broadband noise reduction,” *Journal of Fluid Mechanics*, vol. 926, p. A17, 2021.
- [14] C. Jiang, D. Moreau, J. Fischer, and C. Doolan, “Additively manufactured sound-absorbing porous structures for airfoil trailing-edge noise control,” *Journal of Aerospace Engineering*, vol. 34, no. 5, p. 04021068, 2021.
- [15] C. Jiang, D. Moreau, C. de Silva, and C. Doolan, “Noise generation mechanisms of a micro-tube porous trailing edge,” *Journal of Sound and Vibration*, vol. 571, p. 118085, 2024.
- [16] M. Zhang and T. P. Chong, “Experimental investigation of the impact of porous parameters on trailing-edge noise,” *Journal of Sound and Vibration*, vol. 489, p. 115694, 2020.
- [17] C. Bak, A. S. Olsen, A. Fischer, O. Lylloff, R. Mikkelsen, M. Gaunaa, J. Beckerlee, S. Ildvedsen, T. Vronsky, F. Grasso, *et al.*, “Wind tunnel benchmark tests of airfoils,” in *Journal of Physics: Conference Series*, vol. 2265, p. 022097, IOP Publishing, 2022.
- [18] F. Bertagnolio, N. N. Sørensen, J. Johansen, and P. Fuglsang, “Wind turbine airfoil catalogue,” 2001.
- [19] M. Drela, “Xfoil: An analysis and design system for low reynolds number airfoils,” in *Low Reynolds Number Aerodynamics: Proceedings of the Conference Notre Dame, Indiana, USA, 5–7 June 1989*, pp. 1–12, Springer, 1989.
- [20] P. C. Woodhead, T. P. Chong, P. Joseph, and J. Wissink, “On the double-rooted trailing edge serration,” in *25th AIAA/CEAS Aeroacoustics Conference*, p. 2436, 2019.
- [21] A. Fischer, C. Bak, O. Lylloff, A. S. Olsen, R. F. Mikkelsen, S. B. Ildvedsen, J. S. Beckerlee, A. Borgoltz, M. Kuester, and N. Intaratep, “Cross validation of the aerodynamic and acoustic measurements in two Kevlar-walled wind tunnels,” in *Journal of Physics: Conference Series*, vol. 2265, p. 022103, IOP Publishing, 2022.
- [22] “Wind turbines – part 11: Acoustic noise measurement techniques,” 2012. IEC 61400-11:2012.
- [23] R. K. Amiet, “Noise due to turbulent flow past a trailing edge,” *Journal of sound and vibration*, vol. 47, no. 3, pp. 387–393, 1976.
- [24] H. Y. Hafeez and C. E. Ndikilar, “4 - boundary layer equations in fluid dynamics,” in *Applications of Heat, Mass and Fluid Boundary Layers* (R. Fagbenle, O. Amoo, S. Aliu, and A. Falana, eds.), Woodhead Publishing Series in Energy, pp. 67–94, Woodhead Publishing, 2020.